



Department of Electrical and Computer Engineering
University of Coimbra

STRATEGIES TO IMPROVE THE PERFORMANCE OF THREE-PHASE INDUCTION MOTOR DRIVEN SYSTEMS

VOLUME I

Ph. D. Thesis

Dissertation submitted for obtainment of the degree of
Doctor in Electrical Engineering

by

Fernando José Teixeira Estêvão Ferreira

Supervised by

Prof. Doctor Aníbal Traça de Almeida
Full Professor at the University of Coimbra

Coimbra
2008

Abstract

Electric motor driven systems (EMODS) account for over 40% of global electrical energy demand, i.e., 7400 TWh per year, and for about 70% of the demand for industrial electrical energy, being by far the most important electrical load. Furthermore, EMODS offer today large efficiency improvement potential, on average within 20% to 30%. If the energy saving potential associated with EMODS becomes effective, the consumption of a huge amount of fossil fuels can be avoided. The greenhouse gas emissions can significantly be reduced at zero or even negative costs, since the efficiency improvement measures in EMODS are, in general, cost-effective. Therefore, EMODS can play a key role in helping many countries' efforts to meet the post-Kyoto targets. This can strongly contribute to combat climate change and fossil fuel dependency of modern economies, providing that, at the same time, other measures are implemented, namely the promotion of renewable energies. If all EMODS were optimized, energy cost savings could reach 65-100 G€ per year worldwide and a huge amount of greenhouse gas emissions could be avoided. Nowadays, in the scope of world energy issues, the importance of the performance improvement of EMODS is evident. However, in most cases, the investment in energy efficiency is not yet a major concern in new plants or during refurbishment.

This thesis is meant to be a contribution on that scope, offering several comprehensive overviews and novel contributions on different EMODS-related topics. Briefly, recent developments and strategies to improve the performance of EMODS integrating three-phase induction motors, which account for the largest majority of the industrial electric motors, are addressed, including technical, economical, and policy aspects. The focus is on the efficiency and reliability of EMODS, being discussed several related topics such as motor performance, variable-speed drives, power quality, mechanical transmission, and system design. The end-use or mechanical-load devices are not analysed in terms of intrinsic performance, although the speed variation impact on the respective required power is taken into account. Motor efficiency and life-cycle cost related aspects are analysed, and information regarding motor standards, eco-design and market transformation, is presented. The impact of motor speed variation and inverters on EMODS efficiency and reliability is also addressed, including a comparison between 2-level and 3-level voltage-source inverters. Regarding three-phase induction motors, useful methods for in-field motor load estimation are analysed, being proposed a number of improvements in some well-known methods. Novel considerations on stator winding specifications and connection-mode change, as a function of the motor actual operating conditions, for both two-connection (delta or star) and multi-connection motors, are presented, including the discussion of theoretical, simulation (motor models), and implementation issues. Regarding the stator winding connection-mode management, besides the general proposed methodology, it is also proposed a novel electronic device for that purpose. Methodologies for stator winding optimization and/or customization, particularly useful for the rewinding process, including a tutorial and a user-friendly stator winding redesign software to help rewinders to improve motor performance for each particular situation, are proposed. Due to its present relevance, power quality impact on line- and inverter-fed motors is also discussed. A number of considerations on motor and EMODS reliability, including a comprehensive and extensive analysis on bearing currents and on voltage transients associated with inverter-fed motors, are presented.

The most important contributions were previously published in national and international journals and/or conference proceedings. Some of the topics addressed in this thesis are still under research and future publications on them are expected.

Acknowledgments

First of all, I would like to thank my girlfriend, family, friends and colleagues for the uncountable and precious support in the last years, in every way.

For the profound knowledge transfer, constructive opinions, unending learning, trust and unconditional academical support and friendship, my sincere acknowledgment to Prof. Dr. Aníbal T. de Almeida.

A very special acknowledgment to Prof. Dr. Sérgio A. Cruz for the friendly and academical support, including excellent suggestions and a careful revision of this thesis.

To Prof. Dr. Mihail Cistelecan, whose opinions and advices contributed significantly to the improvement of some parts of this thesis, my cordial recognition.

I am also grateful to some of my students, whose work in the scope of the graduation projects was an important contribution to several parts of this thesis.

For the manufacturers and maintenance companies that cooperate with me, offering technical knowledge, documentation and equipment, my sincere gratitude.

My acknowledgment to the Institute of Systems and Robotics and to the Department of Electrical and Computer Engineering of the University of Coimbra, as well as to the Department of Electrical Engineering of the Engineering Institute of Coimbra, for the laboratories and equipments provided during the experimental tasks.

Lastly, I want to thank the Portuguese Science and Technology Foundation (Fundação para a Ciência e a Tecnologia) for the scholarship provided.

Many thanks to all!

Contents

- VOLUME I -

<i>Chapter 1 – Introduction</i>	1
1.1 – Preamble	1
1.2 – The Importance of Three-Phase Induction Motors	9
1.3 – Motivation and Main Goals of the Thesis	19
1.4 – Organization of the Thesis	19
1.5 – Original Contributions and Publications	20
1.6 – References	22
<i>Chapter 2 – Motor-Driven System Performance</i>	27
2.1 – Considerations on Motor Efficiency Testing Standards	27
2.2 – High-Efficiency Three-Phase Induction Motors	36
2.3 – Minimum Energy Performance Standards	39
2.4 – Study on Eco-Design of Electric Motors	50
2.5 – Automatic Systems for Motor Efficiency Measurement	55
2.6 – Motor System Efficiency Improvement	56
2.7 – Conclusions	66
2.8 – References	67
<i>Chapter 3 – Motor Speed Adjustment</i>	71
3.1 – Introduction	71
3.2 – Technical Barriers to the Use of VSDs	76
3.3 – Comparison between Two-Level and Three-Level Voltage-Source Inverters	78
3.4 – Considerations on PWM Strategies	115
3.5 – Considerations on Steady-State Efficiency Improvement Strategies	117
3.6 – Ride-Through Capability of VSDs	129
3.7 – Economical Advantages Associated with VSDs	131
3.8 – Comparison of Motor Speed Adjustment by means of VSDs and Voltage Regulators	132
3.9 – Considerations on Mechanical Transmission	134
3.10 – Motor Selection for Variable-Speed Applications	137
3.11 – VSDs Market Characterization	139
3.12 – VSDs Savings Potential	140
3.13 – Actions to Promote VSDs	141
3.14 – Conclusions	142
3.15 – References	145
<i>Chapter 4 – In-Field Motor Load Estimation</i>	149
4.1 – Introduction	149
4.2 – Motor Load and Motor Load Factor	152
4.3 – Data Available from Manufacturers	153
4.4 – Useful Accuracy, Tolerances and Instrumentation Accuracy	154
4.5 – Motor Experimental Data and Public Databases	164
4.6 – Slip-Based Motor Load Estimation Method	164
4.7 – Current-Based Motor Load Estimation Method	177
4.8 – Power Factor-Based Motor Load Estimation Method	194
4.9 – Input Power-Based Motor Load Estimation Method	198
4.10 – Temperature-Based Motor Load Estimation Method	208
4.11 – Air-Gap Torque-Based Motor Load Estimation Method	210
4.12 – Other Relevant Motor Load Estimation Methods	212
4.13 – Multiparametric Motor Load Estimation Methods	214
4.14 – Considerations on Motor Oversizing	217
4.15 – Conclusions	219
4.16 – References	221
<i>Chapter 5 – Stator Winding Connection Change</i>	223
5.1 – Introduction	223
5.2 – Star-Delta Connection Management	224
5.3 – Multi-Connection Motor	248
5.4 – Proposed Device versus Other Voltage Regulation Techniques	293
5.5 – Conclusions	296
5.6 – References	298

<i>Chapter 6 – Main Conclusions and Recommendations for Future Work</i>	301
6.1 – Main Conclusions	301
6.2 – Recommendations for Future Work	304
6.2 – References	306
 - VOLUME II - 	
<i>Appendix 1 – Symbols, Acronyms and Constants</i>	309
A1.1 – List of the Main Symbols, Acronyms and Subscripts	309
A1.2 – List of the Main Constants and Unit Conversions	313
A1.3 – References	314
<i>Appendix 2 – Simulation Models</i>	315
A2.1 – Insulated Gate Bipolar Transistors	315
A2.2 – Three-Phase Voltage-Source Inverters	316
A2.3 – Diode Rectifiers and DC Bus	318
A2.4 – Three-Phase Cage Induction Motors	319
A2.5 – References	330
<i>Appendix 3 – Stator Winding Improvement and Motor Repair</i>	333
A3.1 – Introduction	333
A3.2 – Considerations on Stator Windings	339
A3.3 – Winding Design Software Tool	371
A3.4 – Replacement of Faulty Windings	380
A3.5 – Motor Condition Diagnosis	385
A3.6 – Large-Scale Motor Customizing Scheme	388
A3.7 – Conclusions	391
A3.8 – References	395
<i>Appendix 4 – Power Quality Impact on Motor-Driven Systems</i>	397
A4.1 – Introduction	397
A4.2 – Motor Derating Analysis	398
A4.3 – Mathematical Representation of Motor Derating	457
A4.4 – Motor Efficiency, Torque, Speed and Lifetime Derating	459
A4.5 – Effective or Thermal Motor Load	475
A4.6 – Impact of Sags on IMs	475
A4.7 – Impact of Voltage Sags and Continuous Unbalance on VSDs	477
A4.8 – DC-Bus Capacitance Influence on the Input Current Distortion of VSDs	487
A4.9 – Motor Deceleration	490
A4.10 – Considerations on Mitigation Methods	492
A4.11 – Conclusions	494
A4.12 – References	496
<i>Appendix 5 – Reliability of Motor-Driven Systems</i>	499
A5.1 – Introduction	499
A5.2 – Motor and Motor-Driven Systems Reliability	502
A5.3 – Considerations on Bearing Currents	510
A5.4 – Considerations on Voltage Transients	559
A5.5 – Conclusions	601
A5.6 – References	604
<i>Appendix 6 – Complementary Notes and Figures</i>	609
A6.1 – Complement to Chapter 1	609
A6.2 – Complement to Chapter 2	614
A6.3 – Complement to Chapter 3	625
A6.4 – Complement to Chapter 4	664
A6.5 – Complement to Chapter 5	668
A6.6 – Complement to Appendix 3	677
A6.7 – Complement to Appendix 4	686
A6.8 – Complement to Appendix 5	693
A6.9 – References	698
<i>Appendix 7 – Extra Pictures on Motor Applications</i>	701

1. Introduction

Overview – In this chapter, the importance of electric motor driven systems worldwide is evidenced, and an overview on the European electric motor market is presented. Explanations regarding scope, contributions and organization of the thesis are provided.

1.1 Preamble

The accelerated climate changes in our planet forced Humankind to reflect seriously on the way our society is developing. One of the major challenges for the Humanity is to achieve sustainable energy consumption, including the reduction of greenhouse gases emission, in order to guarantee a safe and healthy future for the next generations. Currently, one of the major environmental concerns is the greenhouse gases (GHG) emissions (CO₂, N₂O, etc.) associated with the use of fossil fuels. After signing the Kyoto protocol¹ in 1997, the European Union (EU) committed itself to reduce its overall greenhouse gases emissions over the period 2008 to 2012 by roughly 8% compared to 1990 levels, i.e., a reduction of 336 Mt/yr of CO₂ equivalent² (CO_{2eq}) [27], [67]. The efforts to fulfil the Kyoto agreement are shared by all EU members, and Portugal agreed to limit the increase of their emissions in 27% until 2010, which are promoting and investing in strategic energy-related measures and technologies. It should be noted that the United States of America (USA) declined to ratify the protocol [67]. This cannot be achieved without serious efforts in all areas of the economy, including the generation and use of electrical energy³. Although the continuous technological development, industrialization and human life quality improvement (at least in the developed countries), energy consuming and production systems, in a wide sense, should be urgently optimized. It is necessary to act in a way that contradicts the actual increasing trend of emissions, in order to ensure a sustainable development, considering the increasing energy consumption over the last decades, expected to be maintained in next decades.

Due to its flexibility⁴, cleanness, and easy-to-use, among all the energy forms available in the market, the electrical energy is the most suitable for the vast majority of the applications in

¹ Kyoto commits industrial countries to collectively cut their emissions roughly 5% from 1990 level by 2008-2012 [67].

² CO₂ equivalent is a metric measure used to compare the emissions from various greenhouse gases based upon their global warming potential (GWP). Carbon dioxide equivalents are commonly expressed as “million metric tonne of carbon dioxide equivalents (MMTCDE)”. The carbon dioxide equivalent for gas is derived by multiplying the mass of the gas (in tonne) by the associated GWP. In 2004, the average CO_{2eq} emission factor for EU-15 was 0.435 kg/kWh, and for the new ten accession countries it is 1 kg/kWh [27]. GWP depends on the used energy production technology, e.g., coal-, oil-, gas combined-cycle-, biomass-, multi-crystalline silicon photovoltaics-, cadmium telluride (thin film) photovoltaics -, nuclear (USA)-, wind-based technologies lead to a GWP of 900, 850, 400, 45, 37, 18, 24, and 11 g/kWh of CO_{2eq} (greenhouse gases) [84].

³ According to figures released in December 2007 by the United Nations Framework Convention on Climate Change (UNFCCC), in the period 1990-2005, the changes in greenhouse-gas emissions were +16.3% in USA, and –10.2% in EU-25 (not counting Cyprus and Malta). In Portugal there was an increase of +48.2%. These figures show the overall effectiveness of all the measures carried out to cut aggregate emissions. In the period 2000-2005, the changes in greenhouse-gas emissions were +1.6% in USA and +1.8% EU-25 (not counting Cyprus and Malta). In Portugal increased of +4.0%. The emissions of many individual EU countries have gone up far more than USA emissions have. The individual countries that have been most vocal in support of Kyoto protocol have especially reduced their emissions (France, Finland, The Netherlands, Germany, Sweden, United Kingdom, Denmark, etc.), while emissions have been increased sharply among many of the newer EU members in Southern (Portugal, Spain, Italy, Greece, etc.) and Eastern (Lithuania, Romania, Estonia, Slovenia, etc.) Europe [67].

⁴ Can be produced from different primary energy sources, namely, mechanical (e.g., hydroelectric), thermal (e.g., fossil, nuclear, and solar), chemical (e.g., fuel cells), and/or solar (photovoltaic), and converted in the end-use to all these primary energy forms. According to [89], in 2005, the electricity production worldwide was produced from hydroelectric (16%), coal (40.3%), nuclear (15.2%), gas (19.7%), and oil (6.6%) power plants, and a small part (2.2%) from other energy sources.

industrial and tertiary sectors. In spite of all the inherent advantages, electrical energy is one of the most expensive energy forms, being desirable to minimize the waste associated with it. Therefore, users should be focused on the state-of-the-art of rationalising and optimizing strategies technologies for electric motor-driven systems.

According to the International Energy Agency (IEA) projections [70], improved end-use efficiency accounts for about $\frac{2}{3}$ of avoided emissions in 2030 in the alternative policy scenario, as it can be seen in Fig. 1.1. Regarding the reduction of electrical energy related CO_{2eq} emissions, four major strategies could be pointed out to achieve such goal. First, increasing the use of renewable or clean energy sources. Second, increasing the use of nuclear power. Third, increasing cogeneration and power plants efficiency (e.g., by using other fuels). Fourth, and last, increasing systems efficiency and improve energy rational use or management in order to reduce energy losses or useless energy. The first three strategies can only be achieved in the medium-long term. The last two strategies play a key role⁵, and can be implemented in the short term with fast results, currently offering the largest potential at the lowest cost [27], [70].

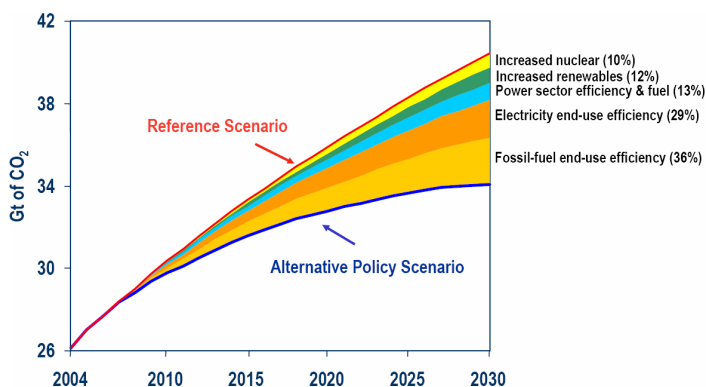


Fig. 1.1. Alternative policy scenario: key policies for CO₂ reduction (Source: IEA - International Energy Agency) [70].

For example, according to [32], Portugal is only using 43% of the hydroelectric potential, having a goal of producing 45% of the electrical energy from renewable energies in 2010⁶, in order to, taking into account bio-fuels, produce 18% of its primary energy.

Due, in part, to the generalized increase of the share of the renewable energy production, an increase in the energy price is likely to happen in the next decades. Actually, in the EU, the electrical energy average price for Industry increased, in the 2004-2006 period about 21%⁷ [92]. These facts, associated to the increasing competitiveness in the industrial and commercial fields,

⁵ The energy consumption worldwide is increasing (see Appendix 6). In 2005, the global power consumption was approximately 11.4 Gtoe, but, nowadays, is approximately 12.3 Gtoe/yr. Most of this energy comes from fossil fuels. In that year, about 81% of total energy produced in the world was provided by oil, natural gas and coal. Excessive consumption of fossil fuels in recent years led to intensive shrinking of these mineral reservations and arising concern about future energy crises. Besides that, there is worldwide worry regarding environmental issues, such as air pollution and global warming due to the emissions associated with the burning of fossil fuels (19.7%, 39.5%, 40.5%, and 0.3% of the worldwide emissions of CO₂ are associated with gas, oil, coal, and other fuels). Since renewable energy sources are not sufficient to provide the energy required worldwide, increasing energy efficiency is a critical issue for the coming years [70], [89].

⁶ According to [85], in Portugal, the electricity consumption increased 3.2% and 2.4% in 2006 and 2007, respectively. In 2007, 39% of electricity (≈ 50 TWh) was produced from renewable energies (20% hydroelectric), 46% from thermoelectric plants, and 15% imported.

⁷ According to [92], in Portugal, the electrical energy average price for Industry increased about 19%, 26%, and 5% in the 2004-2006, 2004-2007, and 2006-2007 periods, respectively.

are leading the users in the industrial and tertiary sectors to focus their attention and invest more and more in energy optimization of the electrical motor driven systems (EMODS), because of their high share in the total electrical energy consumption, as well as in improved energy management strategies.

Regarding the last mentioned strategy (electricity end-use efficiency increase), it offers CO_{2eq} emission reduction at low or negative cost, energy security and reliability benefits, enhanced business competitiveness and social welfare [70]. As it can be seen in Fig. 1.1, improved electricity end-use efficiency accounts for about 1/3 of avoided emissions in 2030 in the alternative policy scenario.

On average, EMODS use between 2/5 and 1/2 (≈ 1/3 for industrial applications) of the generated electrical energy worldwide⁸, being by far the most important electric load, particularly in Industry, as it can be seen in Fig. 1.2. According to [70], presently, there is a stock of 300 million EMODS worldwide, being sold 20-30 million new EMODS per year and repaired 60-90 million old EMODS per year. The average motor load factor is around 60%. The EMODS consumption worldwide reaches 7400 TWh/yr, with an electric peak load of 1.6 to 2.3 TW (electrical power), with associated emissions of 4.3 Gt/yr of CO₂. The associated savings potential is around 20-30%, which can be translated into 68-100 G€/yr cost savings [70].

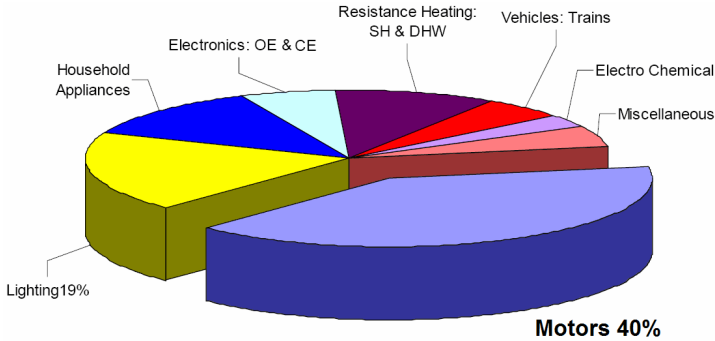


Fig. 1.2. Worldwide electricity consumption by end-use (Source: IEA - International Energy Agency) [70].

EMODS account for approximately 2/3 and 1/3 of the electricity consumed by EU industrial and tertiary (non-residential buildings) sectors, respectively. In Portugal, the share is about 3/4 and 1/3, respectively, which can be translated into 11.7 TWh/yr (total electrical energy 15.3 TWh/yr) [23]. In 2005, Germany⁹, which is one of the most industrialized EU countries, consumed about 536 TWh/yr of electrical energy¹⁰, of which about 1/2 was used for industrial applications. Of that, over 2/3 were used by EMODS [87], [88]. It is their wide use that makes EMODS particularly attractive for the application of efficiency improvements.

⁸ According to [68], EMODS in pumps, fans, compressors, and mechanical traction use 40% of the global electricity and have a savings potential of 20% to 30% within the next decade.
⁹ In Germany, there are approximately 30 million low-voltage electrical motors installed [88].
¹⁰ In 2004, the consumed electrical energy in the EU-15 was 528 TWh/yr (about 15% of the total final energy consumption in Germany). All other industrial electricity consumption goes into heat and lighting [88].

In 2000, the total electricity consumption in the EU-15¹¹ was 2574 TWh, of which 951 TWh was used in Industry. Of these, about 614 TWh, or 65%, was consumed by EMODS. European studies¹² calculated the economical savings potential¹³ of those industrial EMODS¹⁴ to 181 TWh (EU-15), or 29%¹⁵, corresponding to an emission reduction potential of 79 Mt/yr CO_{2eq} (24% of Kyoto gap, i.e. the difference between expected emissions and 2010 Kyoto target emissions).

This means a savings potential of more than 7% of the overall electrical energy consumption in the EU (roughly one ¼ to ⅓ of these savings come from the improved efficiency of the motor).

Apart from CO₂, the burning of fossil fuels for electricity generation produces also non-GHG emissions, being the main offenders the SO₂ and NO_x¹⁶, which contribute to the acidification of the environment. These pollutants have long-range transborder effects and have therefore become a major concern for most European countries. Additionally, emissions also contain heavy metals (nickel, zinc, chrome, copper, mercury, etc.) and dust. Although they can be substantially reduced by using the latest flue gases cleaning techniques, a small amount will always escape into the environment. Burning fossil fuels also produces fly ashes and solid ashes.

In EU-15, it is estimated that, in 2015¹⁷, the EMODS will be using 721 TWh/yr and 224 TWh/yr in the industrial and tertiary sectors, respectively [25], [26]. In Industry, the majority part of the EDMOS consumption (62%) is associated with pump systems (21%), fan or ventilation systems (16%) and compressed-air systems (25%). In the tertiary sector (non-residential sector), the majority part of the EMODS energy consumption (82%) is associated with pump systems (16%), fan systems (24%), refrigeration systems (25%), air-conditioning systems (17%) and lifts, conveyors and escalators (11%)¹⁸ [25], [27].

The estimated economical savings potential for industrial and tertiary sectors, in the EU-15, in 2015, associated with cost-effective application of high-efficiency motors (HEMs) and variable-speed drives (VSDs), is 89.6 TWh/yr, which can be translated into CO_{2eq} emission

¹¹ In the EU-25, a total motor annual electricity consumption of 650 TWh/yr for the industrial sector was estimated for the year 2000, of which 2, 7, 18, 16, 21, and 36% is consumed by conveyors, cooling compressors, air compressors, fans, pumps, and other applications, respectively. For the tertiary sector, these values are 209.7 TWh/yr, of which 16, 24, 26, 17, 11, and 7% is consumed by pumps, fans, refrigeration, air conditioning conveyors, and other applications, respectively [31].

¹² S.A.V.E. Studies [23], [24], [25], [26], [28], [29], [30].

¹³ The economical savings potential is related to cost-effective measures, i.e., measures with a reasonable payback time, typically up to 2 and 3 years, or with the cost of the saved energy (CSE) over a period (normally the lifetime), which has to be lower than the average price of electricity [25]. Its calculation is based on 2004 electricity prices and can therefore vary with time. The technical energy savings potential is the energy that would be saved by implementing all existing technical measures, without concern for economic efficiency, being, of course, higher than the economic savings potential.

¹⁴ The industrial energy consumption does not include transport, tertiary sector, district heating and residential consumption. The tertiary sector uses many motor systems due to the use of fans, pumps and compressors in HVAC systems. The total electricity consumption in the tertiary sector in the EU-25 was 652 TWh in 2000 [27].

¹⁵ It is interesting to look at the perspective for the year 2020. Indeed, energy policies are made based on long-range projections. Building new power stations, as well as introducing successful energy savings programmes, takes several years. The report "European energy and transport – trends to 2030" estimates the industrial energy consumption in the EU-25 by 2020 to be 1432 TWh. If the percentage of industrial motor systems' consumption, compared to the total consumption, remains the same, those systems are expected to use 859 TWh by 2020 if no action is taken. If, by then, the EU attains all the economically efficiency energy savings on those motor systems, the result would be an annual saving of 270 TWh (31% of 859 TWh), equivalent to the total electricity consumption of Spain in 2000.

¹⁶ NO_x is not a greenhouse gas. It should not be confused with N₂O, which is indeed a greenhouse gas.

¹⁷ Assuming an average growth rate of 1.2% and 1.0% for industrial and tertiary sectors, respectively [25].

¹⁸ In USA, in 1997, it was estimated that more than 60% of the electrical energy being used is consumed by motors. Roughly 65% of the electricity consumed by AC motors is associated with pumps, compressors, and fans/blowers [68].

reduction of 35.8 Mt/yr¹⁹ and in savings of 5.9 M€/yr²⁰. Regarding, high-quality repair/maintenance of induction motors, assuming that original efficiency is guaranteed, the estimated savings in the industrial and tertiary sectors in the EU-15, in 2015, is estimated to be 5.6 TWh/yr, which can be translated into savings of 378 M€/yr and into CO_{2eq} emission reduction of 2.3 Mt/yr, assuming that ⅓ of the motors in operation are repaired [24], [25], [26], [33], [50].

In 2000, the EU-15 electricity use in Industry was about 80, 100, 212 and 222 TWh/yr for compressors (e.g., air and cooling compressors), fans, pumps and other systems, with an estimated savings potential for the system application, without including HEMs and VSDs, of 23, 18, 42 and 29 TWh/yr, respectively [27]. Table 1.1 specifies the energy savings potential in Industry in the EU associated with the use of HEMs, high-quality motor repair, VSDs and optimising the application part of the drive system. The mechanical transmission improvement is not included.

TABLE 1.1
ESTIMATED ECONOMICAL ELECTRICAL ENERGY
SAVINGS POTENTIAL FOR EU-15 AND EU-25 IN 2015 [24]–[27], [33], [50].

Measure	Industrial Sector		Tertiary Sector	
	EU-15	EU-25	EU-15	EU-25
High-Efficiency Motors, TWh/yr	24.1	27	11.5	12.9
High-Quality Motor Repair, TWh/yr	4.2	4.7	1.4	1.6
Variable Speed Drives, TWh/yr	44.9*	50	9.1**	10.1
Driven Load Improvement (pumps, fans, compressors) TWh/yr	112	125	53.4	59.6
Total Energy Savings, TWh/yr	185.2	206.7	75.4	84.2
Total Motor Consumption, TWh/yr	721	780	224	275
Savings Potential of the Overall Motor Consumption in EU (%)	26%	27%	34%	31%
Total Electricity Consumption, TWh/yr	1144	3283	828	951
Savings Potential of the Overall Electricity Consumption in EU (%)	16%	6%	9%	29%
Total CO ₂ emissions, 0.4 kg CO _{2eq} /kWh, Mt/yr	74.1	82.7	30.2	33.7
Total Savings Value, M€/yr	10186	11369	7540	8420

* Considering 5%/yr price decrease. Considering fixed prices, it estimated in 39 TWh/yr. Technical savings potential is estimated in 71 TWh/yr (5%/yr price decrease).
** Considering 5%/yr price decrease. Considering fixed prices, it estimated in 8 TWh/yr. Technical savings potential is estimated in 24.6 TWh/yr (5%/yr price decrease).

It should be emphasized that the energy savings potential associated with VSDs and HEMs strongly depends on the motor system rated power. In general, VSD-associated savings potential increases with rated power and HEM-associated savings decreases with rated power.

In 2015, improving the industrial EMODS in EU-25 could result in an annual energy saving of 206.7 TWh/yr, corresponding to an emission reduction potential of 82.7 Mt/yr CO_{2eq}²¹ corresponding to around ¼ of the EU’s Kyoto target. This would eliminate the need for adding approximately 45 GW of power generation capacity to the European electricity system²², over the

¹⁹ Considering 0.4 kg de CO₂ per each generated kWh.

²⁰ Considering 0.05 €/kWh and 0.1 €/kWh average electricity prices for industrial and tertiary sectors, respectively.

²¹ This is an annual amount of CO_{2eq} that 298 million solar roofs would save, or that an average European forest of 294000 km² (approximately 87% of the size of Finland) transforms into oxygen. If Industry is allowed to trade these emission reductions based on energy saved, this would generate a revenue stream of about 1.65 T€/yr [27]. According to [70], avoiding 1 Gt/yr of CO_{2eq} is equivalent to replace 300 conventional, 500-MW coal power plants with “zero emission” power plants. It is also equivalent to install 100 Sleipner CO₂ sequestration plants, to 200 times the current USA wind generation, 1300 times the current USA solar generation, to build 150 1-GW power plants, or to replace roughly 95% of incandescent lighting (i.e., phase out).

²² The power generation capacity is the maximum capacity of power stations. To know the annual electrical energy production, this figure (45 GW) should be multiplied by the calculated number of full-load operating hours (the average European power station is running 4500 h/yr) [27].

next 15-20 years. This is equivalent to 45 nuclear power plants (with approximately 1-GW power generation) and 130 fossil fuel power plants (with approximately 0.35-GW power generation capacity). The 206.7 TWh electricity amount is equivalent to about five times the annual electricity production of all wind power units in EU-25 in 2003 (approximately 5 times 40 TWh). The electricity that can be saved by optimizing industrial EMODS (combining VSDs and HEMs) means a reduction of 6 to 7% in the overall European electricity production (more than 1/3 corresponds to savings come from the improved efficiency of the motors), so it will lead to an equivalent reduction of all the emissions mentioned above. A similar percentage is estimated for worldwide electrical energy savings [27]. According to [70], 1 € invested in more efficient electrical appliances saves approximately 2.2 € in investment in power plants and networks, evidencing the potential cost effectiveness of energy-efficiency related policies.

The fuel cycle externalities are the costs imposed on society and the environment that are not included in the market price, for example, the effects of air pollution, influences on public health, occupational diseases and accidents. The environmental cost of a European kWh is calculated at around 0.03 €/kWh. This needs to be added to the typical industrial market electrical energy price of 0.05-0.07 €/kWh. Current eco-taxation schemes in the EU member states do not internalise the full external costs of electricity generation. Therefore, saving 206.7 TWh/yr in electricity also means a reduction of 10.3-14.5 G€/yr in operating costs for Industry, as well as a saving of about 6.2 T€ in environmental costs for society [27].

EU needs to add 320 GW of new base load capacity in the next 30 years to cope with increasing electrical energy demand. This expansion will cost Europe between 200 T€ and 300 T€, and a similar additional amount of investment in transmission and distribution systems. The improvement of the EDMOS efficiency would reduce this expansion need by more than 10% and would save Europe around 50 T€, or 5 T€/yr of capital cost²³ [27].

In general, the payback period for most investments in energy-efficient EMODS is relatively short, ranging from 3 months to 3 years. The non-energy benefits of higher efficiency systems are, for example, better process control, reduced disruption (downtime) and improved product quality. Sometimes reliability is improved, but not always (e.g., the introduction of a variable speed drive can lead to a less reliable motor system). The overall cost savings associated with these benefits can be in the same order of magnitude as the energy cost savings itself. Therefore, companies or organizations that invest on motor systems also improve profit in an indirect way.

Moreover, using energy as efficiently as possible is a crucial requirement to maintain the competitiveness of the European economy. Since motor systems account for 65% of all industrial electrical energy use, they are the most important area of attention for cutting energy costs.

²³ Considering 10% discount rate.

Additionally, investments in high-efficiency EMODS can have direct effect of creating jobs in different activities such as energy services, energy-efficient equipment manufacturing, and energy and maintenance departments inside organizations. Investing to reduce the energy use of EDMOS payback over a relatively short period, after which the energy cost savings are pure profit. Therefore, investing in high-efficiency EMODS does not divert money from other essential areas. On the contrary, it even creates more money for new investments and, consequently, new jobs.

Furthermore, saving 206.7 TWh/yr improves Europe's security of supply and reduces dependency on fossil-fuel imports. It represents 43.5 Mt/yr of oil equivalent, reducing imports of primary fuel by 6%²⁴. Therefore, saving energy on EMODS would allow more time to develop alternatives for fossil fuels. On the basis of this argument, it would be defensible to look beyond the current economic savings potential associated with improved EMODS (calculated with current energy price), and encourage technology that can make them as energy efficient as possible. In other words, in the long run, a large portion of today's technical savings potential could become tomorrow's economic savings potential [27].

To achieve those goals, measures and programmes are being carried out in Europe, such as the Motor Challenge Programme (MCP) [72], which is a voluntary programme promoted by the European Commission to help companies improve the energy efficiency of their EDMOS, including electric drives, compressed air, fan and pump systems, for which it has been demonstrated that there exists a large technical and economic potential for energy saving. Several other projects were and are being carried out for assessment of the European situation in terms of EDMOS and study of new efficient technologies, to improve their overall efficiency and reliability (over the lifetime), and, more recently, of their life-cycle cost (LCC) and environmental impact. The LCC of IMs is by far dominated by energy costs during use phase (typically higher than 95%²⁵).

New products and techniques hold great promise for large electricity savings. Implementing high-efficiency EDMOS, or improving existing ones, could save a significant amount of electrical energy, which can significantly reduce the need for new power plants and hence free up capital and resources. It would also reduce the production of greenhouse gases and push down the total environmental cost of electricity generation. High-efficiency EMODS can reduce maintenance costs and improve operations in industry.

Nevertheless, adoption of high-efficiency EMODS has been limited by a number of factors, including their higher purchase cost and the lack of knowledge in the market place about their energy savings potential. Few people know that, in the majority of cases, investments in high-

²⁴ 206.7 TWh energy savings converts to 17.4 Mt oil equivalent (Mtoe). Assuming an average conversion efficiency of European power plants of 40%, this converts to a primary energy equivalent of 43.5 Mtoe, or 3% of Europe's primary energy consumption. Since Europe imports about half of its primary energy, this reduces imports by 6% [27].

²⁵ In compressed air and pumping systems the initial, energy, and maintenance costs are typically 5-16%, 78-85%, and 5-16%, respectively [29], [30].

efficiency EMODS have a short payback time. Research on improved technologies and optimizing strategies (including power quality issues) and effective regulation, combined with information campaigns, are important to help stimulate change and bring significant benefits to the European economy and environment. This would increase the competitiveness of European manufacturing industry.

From the policies perspective, according to a number of European studies (e.g., [25], [26], [28], [29], and [30]), the best strategy is a mix of information campaigns, financial incentives and regulation (e.g., mandatory minimum electrical performance standards, MEPS). A particularly promising concept is the emission-trading scheme in the EU, which could be broadened to enable companies to claim emissions credits for investments that reduce energy consumption.

An EMODS typically integrates a power supply, an electric motor, a mechanical transmission, a driven load, and, in some cases, a variable-speed drive²⁶ (VSD). Compressed air, pumping or ventilation systems (including refrigeration and air-conditioning systems) represent the majority of the motor loads (in number of units). Other important applications include materials processing (mills, mixers, centrifugal machines, lathes, saws, presses, etc.) and materials/persons handling/transport applications (conveyors, hoists/cranes, elevators, baggage handling systems, escalators, etc.). The relevance of each end-use device or load depends on the sector and on the type of activity (e.g., in the EU tertiary sector, pumps, fans and compressors account for about 83% of the total motor electricity consumption [25]). The efficiency of a EDMOS depends on several factors, including motor efficiency, motor speed control, proper sizing, power supply quality, distribution losses, mechanical transmission, maintenance practices, end-use equipment (total or part of it) efficiency and proper utilization control, leading to synergetic effects when interacting together.

Nowadays, three-phase, squirrel-cage induction motors (Fig. 1.3), hereafter denoted as IMs, are manufactured in the vast majority of the countries around the world and used in more than 90% of industrial EMODS. Systems integrating IMs are very important from the energy consumption perspective, having associated a significant energy savings potential. In Industry, depending on several factors²⁷, an electrical motor consumes on average an annual electricity amount corresponding to 5-10 times its purchase price, which, over its lifetime (on average from 12 to 20 years²⁸), translates into approximately 60-200 times its purchase price. In a number of cases, for low-medium power motors, after only four to six weeks of continuous operation, the power consumption costs can already have equalled their purchase price. In other words, the electrical

²⁶ At this point it is important to refer that “Variable-Speed Drive - VSD” is used in this thesis to denominate the frequency converter unit, which typically integrate an AC/DC conversion module (or rectifier) and a DC/AC conversion module (or inverter). In many technical texts, “VSD” is used to denominate the converter plus motor system.

²⁷ Motor rated power, load factor, electrical energy price, efficiency, etc.

²⁸ Depending on motor rated power, load profile, maintenance/repair quality, operating conditions (e.g., ambient temperature, power quality, etc.), manufacturing defects, etc.

energy consumption cost of electrical motors represent 98-99.5% of the initial investment, which have low relevance in the motor LCC, particularly if the maintenance/repair costs are taken into account (being lower for HEMs since they are likely to have extended useful lifetime). Moreover, besides the promising electric motor technologies emerging in the global market, the IM is a dominating product, technologically mature and globalized, being its position in the market granted for the next decades, particularly in industrial applications, since its performance is still being improved by means of the use of better materials (e.g., copper-cage rotors, addressed in Chapter 2) and manufacturing and design techniques, as well as by means of advanced control techniques. In fact, in recent decades, electronic controls have allowed IMs to be used in high demanding applications requiring accurate torque and/or speed control.



Fig. 1.3. Low-voltage, three-phase, squirrel-cage induction motor [73].

1.2 The Importance of Three-Phase Induction Motors

As previously shown, electric motors, and particularly IMs represent one of the most important electric loads. In spite of the wide sort of electric motors presently available in the market, as it can be seen in Fig. 1.4, IMs represent, by far, the vast majority of the electric motors' market. Its invention in the end of the 19th Century, has given a strong impetus for the transition from DC to AC in the field of generation, transmission and distribution of electrical energy. Its main advantage is the elimination of all sliding contacts, resulting in an exceedingly simple and rugged construction. IMs are built in a variety of designs with ratings from a few watts to many megawatts. Presently, IMs cover almost all industrial power ranges, as it can be seen in Fig. 1.5, and are the most widely used electrical drive motor type. Traditionally, for variable speed applications, DC brushed motors have been used for decades, but AC motors have been catching up lately (since 1990). In fact the DC/AC motors market ratio was roughly 40%/60% in 1990, 30%/70% in 1995, and 25%/75% in 2000. This rapid market shift is mainly due to the rapid progress in power electronic converters for AC motors [17]. IM efficiency-related standards (national and international) are developing at a fast pace in terms of number and revisions, but significant work has to be done in the future, requiring the collaboration of all developed countries [31], [36].

IMs are rotating electric machines designed to operate from an AC power source. Like other electric motors, they have typically a fixed part, called the stator, and a rotor that spins with a

carefully engineered air-gap between both parts. Stator windings are properly embedded in stator core slots. Similarly, IMs with short-circuited bars (die-cast or mounted) or windings embedded in the rotor core slots with accessible leads in the frame by means of brushes, can be found, called short-circuited rotors IMs in the first case, and wound rotor IMs in the last case. Since die-cast rotor circuits (bars plus end-rings), when seen without rotor core, seem like a squirrel-cage, short-circuited rotors are commonly known as squirrel-cage rotors. There are different types of squirrel-cage rotor designs, influencing the torque-speed curve. Nowadays, wound-rotors are still used, but only for very-high power ranges, being the small-medium power IMs market dominated by squirrel-cage rotors. In order to reduce core losses, both stator and rotor cores are a stack of steel sheets, insulated from each other.

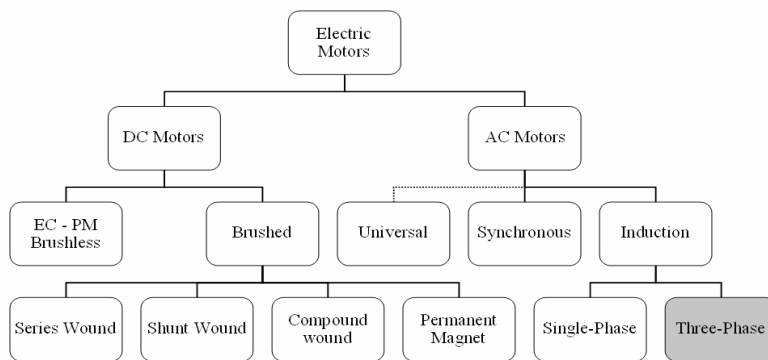


Fig. 1.4. Categorization of low-voltage electric motors [31].

Regarding IMs operation principle, it can be shortly explained as follows. When a three-phase power supply is connected to the stator windings with three per-phase sets of coils distributed over stator core slots (spatially displaced from each other by 120 electrical degrees), a rotating magnetic field is produced, inducing currents in the rotor circuits (which, interact with the rotating field, producing a torque), if rotor angular speed is different from rotating magnetic field angular speed (synchronous speed), i.e., is an asynchronous speed. This principle is behind the commonly used names for this kind of electric motor – induction or asynchronous motor. Interaction between the rotating magnetic field and the rotor currents generates the motor torque. As a result, the motor rotates in the direction of the resultant torque. The synchronous speed depends on the frequency of the power supply and on the pole-number of the motor. Particular information on IM theory is given in each chapter, when required. Complete information on IMs operating principles and control can be found, for example, in [1]–[21].

When compared with other relevant motor technologies, the success of IMs is due to their relative low cost (lowest cost per kW), construction simplicity, high reliability (no brush wear, very robust), and medium-high efficiency for small motors (around 70%) and high efficiency for large motors (over 95%), depending on the motor design. Additionally, they can be driven directly

by the grid and present low electromagnetic interference (EMI). Efficient speed and/or torque control is possible using VSDs. The speed of line-fed IMs cannot be continuously varied without additional equipment or without incurring heavy power losses. The problems of efficiently controlling the speed of IMs have been investigated for decades, and, until one and half decade ago, all doable solutions were unsatisfactory with regards to complexity, efficiency, dynamic performance, and cost. It is only due to the progress of semiconductor technology in the last 30 years that suitable VSDs can now be built at acceptable cost, making IMs the most advantageous adjustable speed drive for many applications.

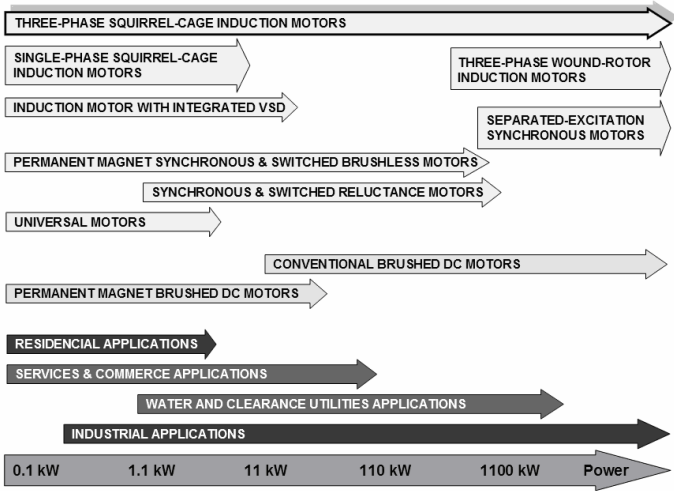


Fig. 1.5. Application range of electric motors.

Motors with 2, 4 and 6 poles represent the vast majority of the motor market, in which 4-pole motors dominate.

General purpose is a common type of IM constituting the large majority of the market (they represent 80-85% of the IM market), whose main characteristics are standardised. This standardisation allows motors to be easily exchanged around the world, by motors made by different manufacturers meeting the same requirements. There is a huge variety of special-purpose IMs, in general, custom-made for specific applications. In some applications, this sort of motors may have to comply with strict requirements (e.g., fire-proof or explosion-proof motors) in which safety is an overriding concern.

Motor efficiency is generally defined by the quotient between output mechanical power (i.e., useful or shaft power) and input electrical power (i.e., real or active power). The difference between the output mechanical power and the input electrical power is due to four different kinds of losses occurring in IMs machine, namely electrical losses (also known as copper, ohmic, Joule or I^2R losses), magnetic (or core) losses, mechanical (or windage and friction) losses and stray load losses (SLLs) [52], [62], [63].

Electrical losses (load dependent) are the Joule effect losses or the heat generated by the electrical current that flows in the stator and rotor conductors, being proportional to I^2R . These losses increase rapidly with the motor load. Magnetic or core losses (approximately constant losses for fixed frequency motors), are the losses occurring in active iron and other metal parts, i.e. in the steel laminations of the stator and rotor, due to hysteresis and eddy (or Foucault) currents, increasing approximately with the squared flux-density. Mechanical or friction and windage losses (approximately constant losses for fixed frequency motors), are the losses due to friction (occurring in bearings and seals) not including any losses in a separate lubricating system, and the losses due to the power absorbed in integral fans (external and/or internal), and in auxiliary machines, if any, forming an integral part of the machine. Stray (or additional) load losses (load dependent) are the losses introduced by the load in active iron and other metal parts other than the conductors, and eddy current losses in primary or secondary winding conductors caused by current dependent flux pulsation, and are due to leakage flux, harmonics of the air gap flux density, non-uniform and inter-bar currents distribution, mechanical imperfections in the air gap, and irregularities in the air gap flux density. Complete information on IM losses and efficiency can be found, for example, in [1]–[12], [31], [33], [47], [62], [63], as well as in a number of technical papers published in international journals and conference proceedings. Fig. 1.6 shows the typical distribution of the losses, efficiency and power factor, as a function of the load, for IMs. Fig. 1.7 shows average values for rated slip, power factor, speed and efficiency, as a function of rated power, for IMs (data extracted from [64]). In Fig. 1.8, the relation between part-load and full-load efficiency for 60-Hz IMs (data extracted from [65]) is shown.

Motor efficiency depends on load, power quality (e.g., voltage distortion, voltage unbalance, and voltage magnitude deviation, as shown in Appendix 4), ambient temperature, altitude, maintenance, etc. Motor efficiency is measured and classified according to different efficiency testing standards around the world, which can lead to quite different results depending on the accuracy of the procedures used to evaluate losses and/or input/output power. These differing standards are a market barrier to global trade, and currently there is work being undertaken, particularly by the International Electrotechnical Commission (IEC), to move towards common efficiency testing standards and efficiency level classification. These issues are addressed in the next chapter.

The IM torque is the rotational force exerted by the shaft of the motor. Four points in the torque load curve can be identified, namely, full-load torque (rated continuous torque that the motor can support without overheating), starting or locked-rotor torque (torque produced by the motor when it is energized at full voltage and with the shaft locked in place, or the amount of torque available

when power is applied to start accelerating it up), breakdown or pull-out torque (maximum torque that a motor can produce), as it can be seen in Fig. 1.9.

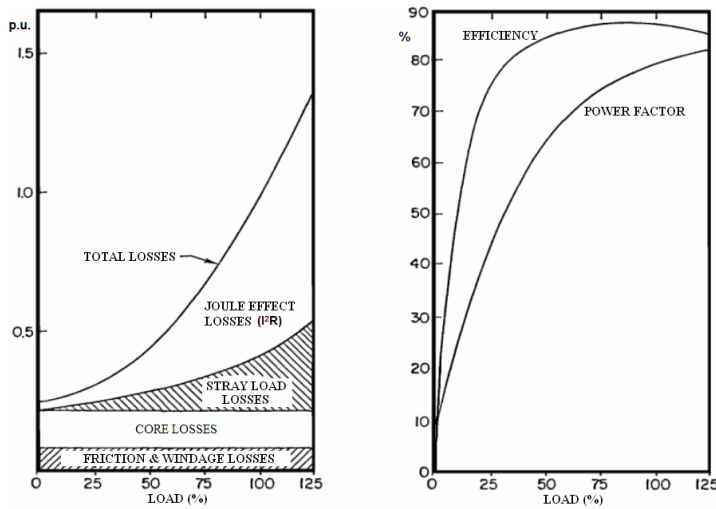


Fig. 1.6. Typical losses, efficiency, and power factor, as a function of the load, for IMs.

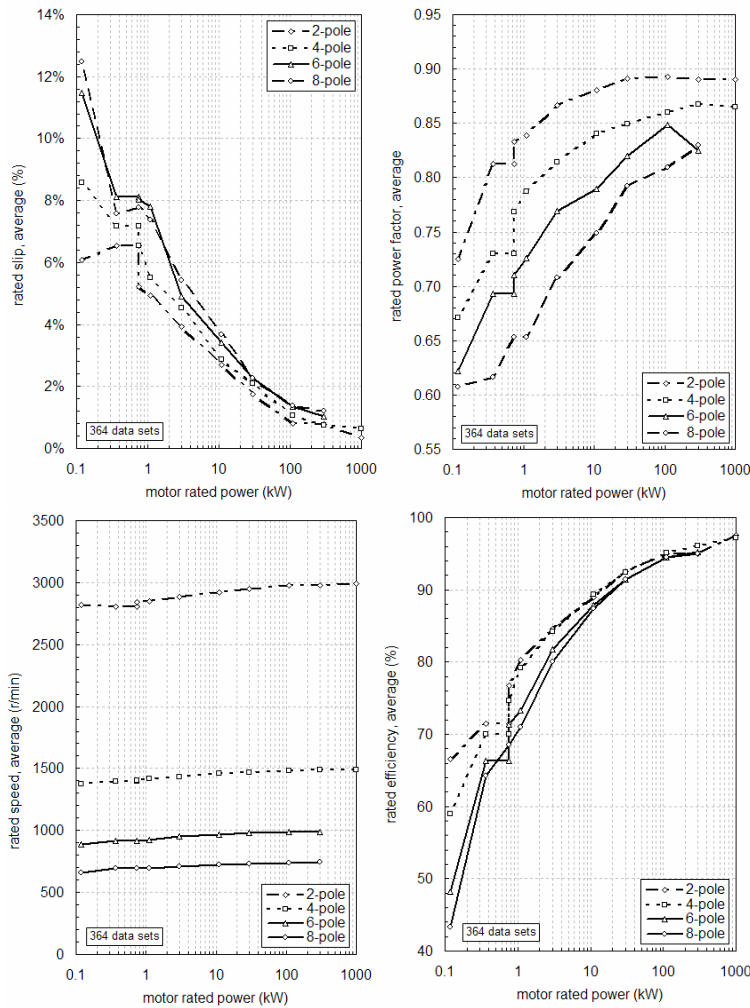


Fig. 1.7. Average values for rated slip, power factor, speed and efficiency as a function of rated power (data extracted from [64]).

The torque-speed curve shape depends on the rotor design (according to the North American National Electrical Manufacturers Association (NEMA), four types of rotors defined, namely, A, B, C, and D (see Appendix 6) [1], [11]. The IEC defines motor design N (in general, with

operating characteristics comparable to NEMA design B or A), which are the most commonly used types in Industry. The design H is nearly identical to NEMA design C.

Wound-rotor IMs are inherently less efficient than squirrel-cage rotor IMs, due to friction and ohmic losses associated with the three brush-ring contacts (static brushes and rotating rings), and require extra maintenance, being presently used mainly in applications above 0.5 MW, but they are being progressively replaced by VSD-fed squirrel-cage rotor IMs.

In Appendix 6, some short notes on the other relevant motor technologies are presented, including the single-phase induction motors, universal motors (AC commutator motors), conventional brushed DC motors (DCMs), brushless permanent-magnet motors (PM motors), and reluctance motors. Information on these machines can be found in [1]–[17], [22], [31], [66], [74], [76], [77]. However, these technologies are not analysed in this thesis. Therefore, no further consideration will be made on this sort of motors.

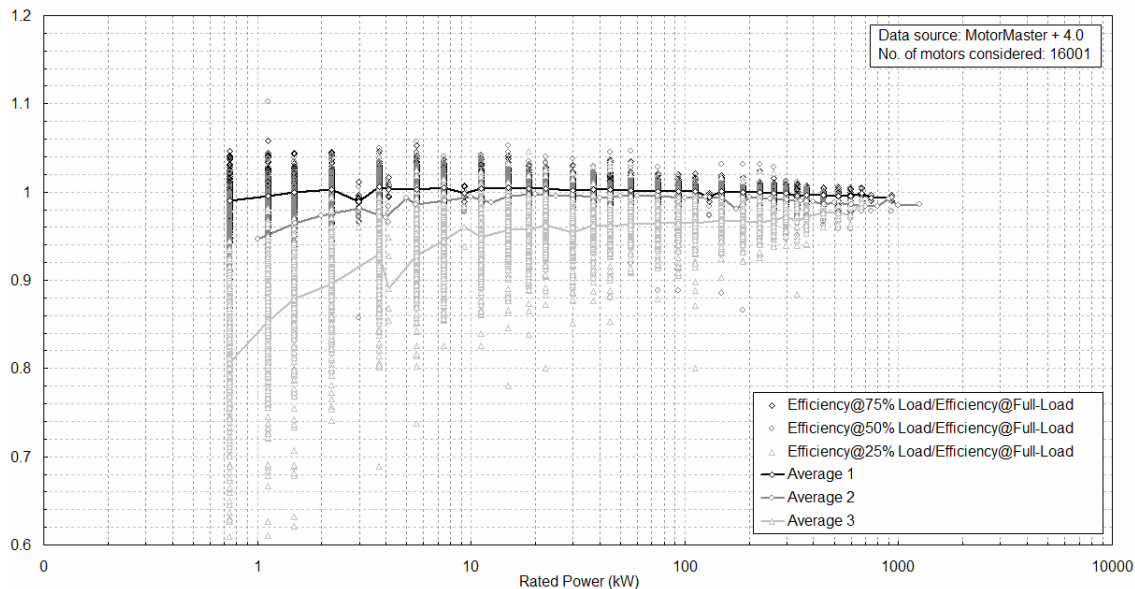


Fig. 1.8. Relation between part-load and full-load efficiency for 60-Hz IMs (16001 data sets extracted from [65]).

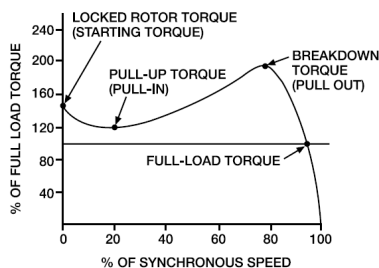


Fig. 1.9. Typical torque-speed curve for IMs.

Nevertheless, it should be emphasized that the developments in power electronics in the last decades allowed IMs to achieve the same torque/speed performance of DCMs in high demand applications, but with much higher reliability leading to a strong decline in market share of DCMs

[31]. Moreover, in the scope of high-efficiency motors, the PM and reluctance technologies should be considered, since they have a significant savings potential, ranging from 5 to 10% [66].

In the remaining part of this section, relevant information on the evolution and present electric motor market is presented, focusing the EU, including market forecast for integral horsepower motors (all motors with a power rating in excess of one horsepower). This survey includes market data from EU-25²⁹ countries.

It is also possible to estimate the integral motors market share in Europe by their type, which is presented in Fig. 1.10a. It is possible to conclude that AC integral motor sales are largely dominated by AC motors, representing more than 96% of units sold. This translates into around 9 million AC motors sold against only 350 thousand DC motors (including brushless) sold. In units, the AC integral motors market is dominated by motors in the 0.75-37 kW power range (Fig. 1.10f). IMs largely dominate AC motor market, accounting for about 87% of the revenues of the integral motors in EU-25 (Fig. 1.10b). Remain part of that market (by comparison, only account for a total of 16% of sales by value) is characterised by a wide diversity of designs, many custom made for particular original equipment manufacturers (OEMs) products, although detailed market statistics on these products are not currently available. Single-phase motors represent less than 5% of the total integral AC motors in Europe. Currently, detailed market statistics on these products are not available. IMs are generally used over single-phase induction motors in applications with a large number of operating hours due to their superior efficiency, robustness and overall cost-effectiveness. In the few cases in which single-phase integral horsepower motors have relevant electricity consumption, such as air conditioners and heat pumps, efficiency policies are directed at whole equipment and not just the motor, which is customized for each type of equipment. Regarding IM pole number, market information for EU-15 and EU-25 shows that 2-, 4-, 6-, 8-pole IM represent 15-35%, 50-70%, 7-15%, and 1-7% of the market, respectively, showing that the market is dominated by 4-pole IMs [31].

DC motor market share is about 3.8% (Fig. 1.10a). DC integral horsepower motors market is dominated by shunt wound motors (Fig. 1.10d). As referred before, the developments in power electronics in the last decades allowed IMs to achieve the same torque/speed performance of DC motors in high demand applications, but with much higher reliability. The typical short lifetime and/or large maintenance requirements of DCMs, limit its use in applications with a small number of operating hours. Therefore, DCMs are experiencing a strong sales decline. The 0.75-7.5 kW power range is the largest market of DC motors, accounting for about 87% of shipments (Fig. 1.10e), in 2002, remaining a key market for DC motors, but has seen the shift towards AC technology. It should be noted that the respective AC market is more than 21 times the size of the

²⁹ In this section, EU-25 refers to all EU-25 countries except Malta, and includes Switzerland.

DC market at these power ratings showing the shift away from DC solutions in Industry as a whole. The trends show that the DCMs market share is projected to see a decline in the next few years (VSD-fed IM sets can have a high dynamic performance, cost less and require much less maintenance). The number of DCMs sold is projected to drop sharply at a 10-15% rate per year. Large manufacturers have stopped new developments in these motors for several years. All of the DC motor types are expected to see a decline in sales, except for brushless PM motors, which have high efficiency and overcome the reliability limitations of DCMs, but are more expensive (due to the cost of PMs and of the electronic controls), being mostly used in premium motion control applications. However, due to the increasing production, their cost has been decreasing and may become a key player particularly in the low power range. Innovative approaches are being undertaken in brushless PM motors, using low-cost magnetic materials for applications not requiring high torque/weight ratio (e.g., fans) [31].

In the AC motor market, a slight increase in the demand for IMs is expected as customers continue to upgrade old technologies taking into account the more favourable economic climate. All other AC motor types are expected to maintain their market share, as they are much more specialized items, except for single-phase integral motors which will face a decrease in demand due to the increased use of electronic speed controls. These controls allow a single-phase supply to feed a cheaper and comparatively more efficient IM [31].

The generic economic data of the low-voltage AC motor market in the EU-15 (2006) is shown in Table 1.2. It is important to notice that motor trade is mainly between European countries. Only 15% to 25% of imports are from outside Europe.

TABLE 1.2
EU-15 AC MOTOR MARKET INFORMATION, 2006 [31].

Item	Motor Power Range (kW)				Total
	0.75-7.5	7.5-37	37-75	75-200	
Production (10 ⁶ Units)	6.3	1.4	0.3	0.08	8.08
Exports (10 ⁶ Units)	3.1	0.7	0.2	0.075	4.075
Imports (10 ⁶ Units)	4.0	0.8	0.2	0.1	5.1
Market (10 ⁶ Units)	7.2	1.5	0.3	0.1	9.1
Market share (%)	79.1	16.5	3.3	1.1	100
Capacity (GW)	22.5	30	15.6	11.6	79.7
Capacity share (%)	28.2	37.6	19.6	14.6	100

Fig. 1.11 shows the evolution of IMs' stock, for the EU-15, based on the installed base and on the expected evolution of electricity consumption in the respective sectors. Fig. 1.12 shows the EU-25 revenue forecast for integral horsepower motors. The integral horsepower motor market is quite mature, with expected slight growth in the near future. A rise in demand in Eastern Europe countries will be the major driver for this growth.

Regarding electric motor installed power and consumption in EU, in Industry, more than 1/2 of the motor electrical energy consumption and more than 2/3 of the motor installed capacity is associated with motors up to 130 kW, particularly concentrated in the 10-70 kW power range.

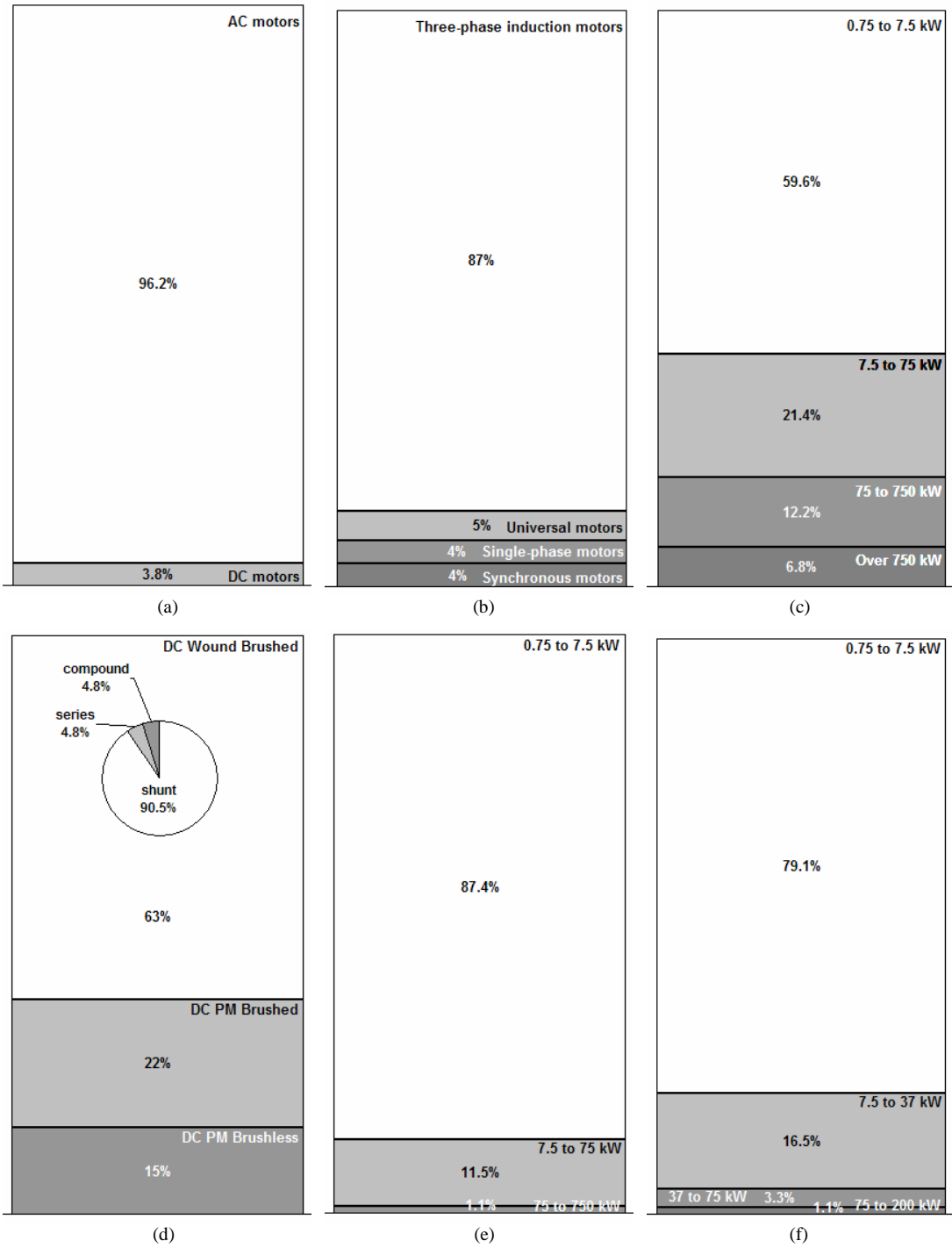


Fig. 1.10. Electric motor market data [31]:
 (a) Share of integral motor shipments by motor type in EU-25, 2002.
 (b) Projected revenues share of integral AC motors in EU-25, 2006.
 (c) Shipments share of AC integral motors by size in EU-25, 2006.
 (d) Revenues share of integral DC motors in EU-25, 2002.
 (e) Shipments share of DC integral motors by size in EU-25, 2002.
 (f) Market share of AC integral motors in units by size in EU-15, 2005.

The average number of operating hours increases consistently with the rated power, from 2000 h/yr to 8000 h/yr. However, these figures can be significantly different when analysed individually for particular industrial activities [25]. In the tertiary sector, motors up to 30 kW are responsible for more than ¾ of the total motor consumption and of the motor installed capacity, particularly concentrated in the 0.75-30 kW power range. The average number of operating hours decreases consistently up to 10-30 kW power range, from 2500 h/yr to 1000 h/yr [25].

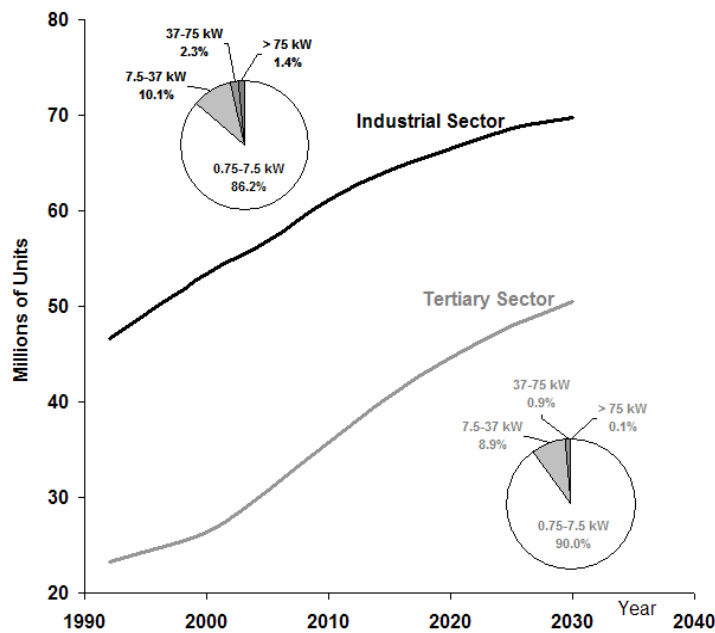


Fig. 1.11. Estimated evolution of IMs' stock and AC motor market share by power range, for EU-15 (based on the installed base and on the expected evolution of electricity consumption in the respective sectors) [31].

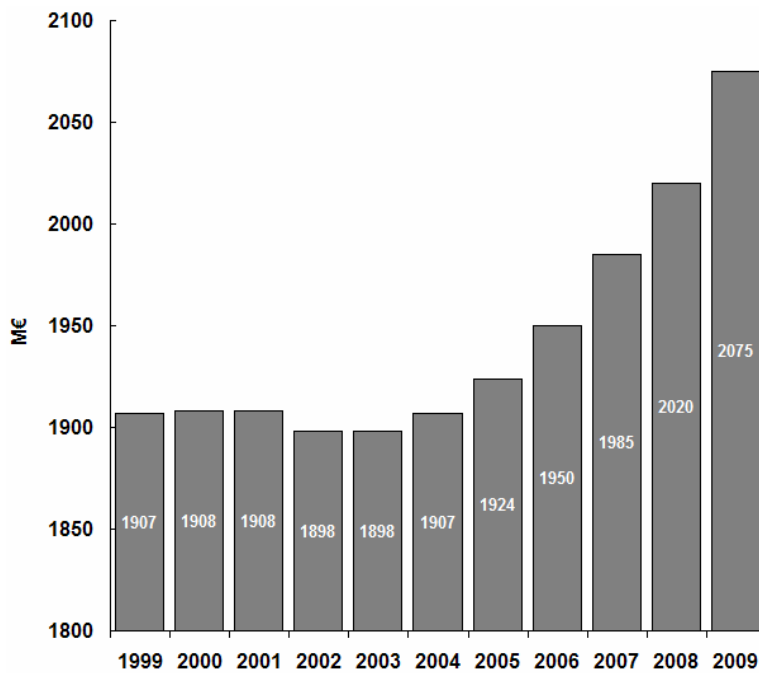


Fig. 1.12. Revenue forecast for integral motors in EU-25 (excluding Malta and including Switzerland) [31].

From the foregoing analysis, it can be concluded that IMs are the most dominant motor technology, particularly in Industry. On the basis of the actual trends, that scenario will be

probably maintained in the next 2-3 decades, making sense the research efforts to improve the performance and reliability of IM-driven systems. IMs in the 0.75-150 kW power range dominate the respective market (in units), justifying a reinforced attention in the technologies typically used in that range. Due to their significant electrical energy consumption worldwide, even modest efficiency improvements can lead to significant energy savings, contributing significantly to a better use of electrical energy and to the reduction of CO₂ emissions, being an important measure for the climate change combat, which rely, in part, upon the improvement of energy efficiency and energy management.

1.3 Motivation and Main Goals of the Thesis

The foregoing information, clearly justifies the importance of the scope of this thesis, which is focused on the improvement of the performance of EMODS. In fact, the unquestionable importance of the EMODS from the energy consumption and savings potential perspective, evidenced in previous section, was the main motivation of this thesis. Since modest improvements in the EMODS efficiency and reliability would translate into significant technical, economical and environmental benefits from a macro (world, countries) and micro (companies, users) perspective, this thesis is focused on those systems, particularizing for the case of IM-driven systems (excluding the other above mentioned electric motor technologies), representing the vast majority of in-use EMODS.

Therefore, strategies, methods and technology assessment to improve the steady-state efficiency and reliability of IM-driven systems are the main goals of this thesis, including aspects related to efficiency-related standards, eco-design and market transformation of electric motors.

It should be emphasize that the objective was not to investigate only a particular technology or solution, but, instead, to analyse and optimize the overall system from a wider perspective, since direct relation between all the modules that can constitute an EDMOS exist. Moreover, motor dynamic responses and control techniques, although slightly addressed in some chapters, are excluded from the scope of this thesis, being widely discussed in a number of technical books (e.g., [7], [12], [13], [16], [17], and [19]–[22]) and papers, and they represent a minor issue in the energy-efficiency scope, being particularly important for applications requiring accurate speed and/or torque control (e.g., automation and robotics), from a technical perspective.

1.4 Organization of the Thesis

This thesis is divided into 6 chapters. In the first two chapters, in which this chapter is included, IM efficiency and LCC related aspects, as well as existing efficiency related standards, are addressed. These chapters evidence the high importance of IMs in the scope of world energy

issues, and offer an overview on EMODS. In particular, novel information is presented with respect to motor eco-design analysis and market transformation. In Chapter 3, motor speed adjustment issues and VSDs impact on EMODS efficiency and reliability are addressed. In Chapter 4, several useful methods for in-field IM load estimation are discussed, being proposed a number of improvements in some of them. In Chapter 5, several considerations on stator winding connection change, both for conventional and multi-connection IMs, are presented. An electronic device and a method to properly manage stator-winding connections are also proposed. Chapter 6 resumes the main conclusions within this thesis and presents some recommendations for future work. In all chapters, some background theory is provided, but well-known theory and concepts are not included being only indicated some related published references. Due to the inherent extension, and for the sake of clearness, the state-of-the-art related to each topic is properly introduced in the respective sections. Therefore, a state-of-the-art chapter is not included.

Although some important topics were excluded from the main body of this thesis, since original research work was carried out on them, they are presented as appendixes, complementing the information presented in the chapters.

In Appendix 3, stator winding improvement and motor repair issues are discussed, including an overview and practical methods for stator winding optimization and/or customization, as well as a software for stator winding (re)design. In Appendix 4, the power quality impact on IMs and VSDs is analysed in detail. In Appendix 5, the reliability of EMODS is addressed, including investment decision related issues and a deep discussion on bearing currents and voltage transients associated with VSD-fed IMs. In Appendix 6, complementary notes and figures to all the previous mentioned chapters and appendixes are presented, including explanatory demonstrations. In Appendix 2, a description of the simulation models used is presented. Lastly, in Appendix 1, the main symbols, acronyms and constants are shown.

To facilitate the reading, references cited in each chapter are located in the end it. Therefore, the same reference can be listed in different chapters and appendixes.

1.5 Original Contributions and Publications

Part of the material presented in this thesis results from several European projects in which the author was directly involved as a member of the respective research teams, whose main outcomes were published in [24]–[26], [31], [35], [36], [50]–[51]. Some of the studies, prototypes and software presented, although originally proposed, designed and/or created by the author, involved the collaboration and work of many graduate students and/or of other researchers/colleagues. The articles related to the topics discussed in this thesis and published in international technical journals/magazines and conference proceedings are the base of a number of sections.

Regarding original contributions, an analysis of IM technologies, with and without VSDs, including a LCC analysis from an economical and ecological perspective, an assessment of the recent motor efficiency related standards, and considerations on market transformation, are offered, which were in part published in [35] and [36]. As concerns motor efficiency testing standards, an extensive study on stray load losses was carried out, published in [52] (this paper received a best paper award), and a user-friendly, high-efficiency test bench for automatic application of the main efficiency standards was developed (still being improved), partially described in [47].

A study on the technical and economical advantages/disadvantages associated with the use of VSDs was carried out, including a comparison between two-level and three-level voltage-source inverters in terms of their impact on the efficiency and reliability of IMs, whose main results were published in [34] and [37].

A method for star-delta winding connection management is proposed, including an electronic device for automatic connection change, described in [45], [46] and [91], which was awarded in a Portuguese contest of innovation for young engineers, having a patent pending, since it will be commercialized by a company dealing with energy management and power quality issues. An IM with multiple stator-winding connections is proposed, published in [39] and [40]. Further work on this matter will be presented in [78], [79] and [80].

An assessment of in-field IM load-evaluation methods is presented, and some particular improvements proposed (part of the principles proposed will be presented in [82]). Considerations on variable-speed IM sizing are also presented, on the basis of [60].

Considerations on stator windings (re)design from the motor efficiency and reliability perspective are presented, including a software specially developed for an optimized redesign of stator windings (presently being used by one motor manufacturer and three motor maintenance companies), partially published in [41], [48] and [50]. For the sake of completeness, considerations on motor maintenance and repair are also presented, being a tutorial mainly based on the Master Science thesis of the author and on [24], [33], [50] and [53]. The work presented in [53] is being extended to the acquisition and fusion of additional motor data, to allow bearing currents and insulation system ageing evaluation, and will be presented in [81].

A study on the power quality impact on the line-fed and VSD-fed IM performance is also presented, whose main results were partially published in [38]. A tutorial on VSDs impact on power quality is also offered, mainly based on [61] (this paper received a best paper award). The author, using additional experimental results, is still investigating these issues. Voltage transients and bearing currents issues associated with VSD-fed IMs are also analysed and a comprehensive review with some novel results is offered, partially published in [43], [58] and [59].

In part of the studies concerning the steady-state performance of IMs, a motor simulation model with thermal compensation proposed by the author in [42] was used.

Lastly, an integrated system analysis with experimental and theoretical examples is presented, mainly based on previously published work co-authored by the author, namely [25], [26], [34] and [44].

In the scope of the discussed topics, the author of this thesis is co-author of five papers in IEEE Transactions, twelve papers in international conferences, and twelve articles in Portuguese technical magazines. As referred above, some of the offered contributions were rewarded in technical and scientific events.

To carry out the presented work, the author dealt with a number of software and programming languages, e.g., MATLAB, SIMULINK, FEMLAB, PSPICE, LABVIEW, C++, and DELPHI, as well as with a number of different hardware, such as measurement equipment, motors (including stator winding design), VSDs, PCBs (including their design), etc.

Other work was (and is being) developed during the working period of this thesis (published in [54]–[57], [83], [86] and [90]), but, although related to electric machines, it is considerably out the main stream of the thesis, thus not being included. Additional on-going research work on motors (e.g., [78]–[81]) is being carried out, part of it to be published in coming international conferences, but it is not included in this thesis.

1.6 References

- [1] Chapman, S.: “*Electric Machinery Fundamentals*”, 4th Edition, McGraw-Hill, New York, 2004.
- [2] Nadel, S.; Shepard, M.; Greenberg, S.; Katz, G.; de Almeida, A.: “*Energy-Efficient Motor Systems – A Handbook on Technology, Program, and Policy Opportunities*”, American Council for an Energy-Efficient Technology, Washington D.C., 2nd Ed., 2002.
- [3] Chalmers, B.; Williamson, A.: “*A.C. Machines – Electromagnetics and Design*”, John Wiley & Sons Inc., New York, 1991.
- [4] Guru, B.; Hızıroğlu, H.: “*Electric Machinery and Transformers*”, 3rd Edition, Oxford University Press, New York, 2000.
- [5] Alger, P.: “*Induction Machines – Their Behavior and Uses*”, Gordon and Breach Publishers, 3rd Edition, New York, 1995.
- [6] Hughes, A.: “*Electric Motors and Drives*”, 2nd Edition, Newnes, Oxford, 1993.
- [7] Leonhard, W.: “*Control of Electric Drives*”, 2nd Completely Revised and Enlarged Edition, Springer-Verlag, Berlin, 1997.
- [8] de Almeida, A.; Bertoldi, P.; Leonhard, W.: “*Energy Efficiency Improvements in Electric Motors and Drives*”, Springer-Verlag, Berlin, 1997.
- [9] Beaty, H.; J. Kirtley: “*Electric Motor Handbook*”, McGraw-Hill, New York, 1998.
- [10] de Almeida, A.; Bertoldi, P.; Falkner, H.: “*Energy Efficiency Improvements in Electric Motors and Drives*”, Springer-Verlag, Berlin, 2000.
- [11] Fitzgerald, A.; Kingsley, C.; Umans, S.: “*Electric Machinery*”, 6th Edition, McGraw-Hill Higher Education, New York, 2003.
- [12] Sen, P.: “*Principles of Electric Machines and Power Electronics*”, 2nd Edition, New York, John Wiley & Sons, 1997.
- [13] Slemon, G.: “*Electric Machines and Drives*”, Addison-Wesley Publishing Company, 1992.
- [14] Chatelain, J.: “*Machines Électriques*”, Tome I & II, Presses Polytech. Romandes, Dunod, 1983.
- [15] Hindmarsh, J.: “*Electrical Machines and their Applications*”, Butterworth-Heinemann; 4th Edition, 1995.
- [16] Dubey, G.: “*Fundamental of Electrical Drives*”, 2nd Edition, Alpha Science, New York, 2008.
- [17] Boldea, I.; Nasar, S.: “*Electric Drives*”, CRC Press, 2nd Edition, New York, 2006.
- [18] Phipps, C.: “*Variable Speed Drive Fundamentals*”, 3rd Edition, The Fairmont Press, Prentice Hall PTR, 1999.
- [19] Mohan, N.; Undeland, T.; Robbins, W.: “*Power Electronics - Converters, Applications, and Design*”, 2nd Edition, John Wiley & Sons, Inc., New York, 1995.
- [20] Rashid, M.: “*Power Electronics, Circuits, Devices, and Applications*”, 2nd Ed., Prentice-Hall, Inc., Englewood Cliffs, 1993.
- [21] Bose, B.: “*Power Electronics and Motor Drives – Advances and Trends*”, Elsevier, Academic Press, New York, 2006.
- [22] Bose, B.: “*Modern Power Electronics and AC Drives*”, Prentice Hall PTR, New Jersey, 2005.
- [23] “*Actions to Promote Energy-Efficient Electric Motors*”, Report prepared for the European Commission, DGXVII, Motors Study Group, Edited by ISR-University of Coimbra, 1996.

- [24] de Almeida, A.; Ferreira, F.; Walters, D.; Parasiliti, F.: “*Barriers Against Energy-Efficient Electric Motor Repair*”, Report prepared for the European Commission, DGXVII, Edited by ISR-University of Coimbra, 1999.
- [25] de Almeida, A.; Fonseca, P.; Ferreira, F.; Guisse, F.; Diop, A.; Previ, A.; Russo, S.; Falkner, H.; Reichert, J.; Malmose, K.: “*Improving the Penetration of Energy-Efficient Motors and Drives*”, Report prepared for the European Commission, DG TREN, SAVE II Programme, Edited by ISR-University of Coimbra, 2000.
- [26] de Almeida, A.; Ferreira, F.; Fonseca, P.; Chretien, B.; Falkner, H.; Reichert, J.; West, M.; Nielsen, S.; Both, D.: “*VSDs for Electric Motor Systems*”, Report prepared for the European Commission, DG TREN, SAVE II Programme, Edited by ISR-University of Coimbra, 2001.
- [27] Keulenaer, H.; Belmans, R.; Blaustein, E.; Chapman, D.; de Almeida, A.; Watcher, B.; Radgen, P.: “*Energy Efficient Motor Driven Systems*”, Motor Challenge Programme, European Copper Institute, 2004.
- [28] “*Study on improving the energy efficiency of pumps*”, European Commission, DG TREN, 2001.
- [29] Radgen, P.; Blaustein, E.: “*Compressed air systems in the European Union*”, European Commission, DG TREN, 2002.
- [30] Radgen, P.: “*Market study for improving energy efficiency for fans*”, European Commission, DG TREN, 2002.
- [31] de Almeida, A.; Ferreira, F.; Fong, J.; Fonseca, P.: “*Ecodesign Assessment of Energy-Using Products - EuP Lot 11 Motors*”, Final Report for the European Commission, ISR-University of Coimbra, February 2008.
- [32] Pinho, M.: “*Portugal deixará de importar electricidade*” in “*O futuro da energia*”, Confrontos, Jornal Sol, N.º 44, 13 de Julho de 2007, pp. 5.
- [33] Ferreira, F.: “*Técnicas Avançadas de Manutenção Curativa e Reabilitação de Motores de Indução Trifásicos de Baixa Tensão/ Curative Maintenance and Rehabilitation Advanced Methods for Low-Voltage, Three-Phase, Induction Motors*”, Tese de Mestrado/Master Science Thesis (available in Portuguese only), Universidade de Coimbra/University of Coimbra, 2002.
- [34] de Almeida, A.; Ferreira, F.; Both, D.: “*Technical and Economical Considerations to Improve the Penetration of Variable-Speed Drives for Electric Motor Systems*”, IEEE Trans. on Industry Applications, Vol. 41, No. 1, pp. 188-199, Jan./Feb. 2005.
- [35] de Almeida, A.; Ferreira, F.; Fong, J.: “*Ecodesign of Electric Motors*”, 5th Inter. Conf. on Energy Efficiency in Motor Driven Systems (EEMODS’07), Conf. Proc., Vol. I, pp. 27-38, Beijing, 2007.
- [36] de Almeida, A.; Ferreira, F.; Fong, J.; Conrad, B.: “*Electric Motor Ecodesign and Global Market Transformation*”, IEEE Industrial & Commercial Power Systems Conf. (ICPS’08), Conf. Proc., Florida, USA, May 4-8, 2008.
- [37] Ferreira, F.; de Almeida, A.; Baoming, G.: “*Comparative Study on 2-Level and 3-Level Voltage-Source Inverters*”, 5th Inter. Conf. on Energy Efficiency in Motor Driven Systems (EEMODS’07), Conf. Proc., Vol. II, pp. 581-602, Beijing, China, 2007.
- [38] Ferreira, F.; de Almeida, A.; Deprez, W.; Belmans, R.; Baoming, G.: “*Impact of Steady-State Voltage Supply Anomalies on Three-Phase Squirrel-Cage Induction Motors*”, Inter. Aegean Conf. on Electric Machines and Power Electronics (ACEMP’07) and Electromotion Joint Conf., Conf. Proc., pp. 607-615, Bodrum, Turkey, 10-12 Set. 2007.
- [39] Ferreira, F.; de Almeida, A.: “*Novel Multi-Flux Level, Three-Phase, Squirrel-Cage Induction Motor for Efficiency and Power Factor Maximization*”, IEEE Trans. on Energy Conversion, Vol. 23, No. 1, pp. 101-109, March 2008.
- [40] Ferreira, F.; de Almeida, A.: “*Novel Multi-Flux Level, Three-Phase, Squirrel-Cage Induction Motor for Efficiency and Power Factor Maximization*”, IEEE Inter. Conf. on Industrial Technology (ICIT’06), Conf. Proc., Mumbai, India, December 2006, paper selected for oral presentation and invited for publication in a special issue of IEEE Trans. on Industrial Electronics.
- [41] Ferreira, F.; de Almeida, A.: “*Considerations on the Custom Design of the Stator Winding of Low-Voltage, Three-Phase, Cage Induction Motors to Improve their Efficiency and Reliability*”, 17th Inter. Conf. on Electric Machinery (ICEM’06), Conf. Proc., September 2006.
- [42] Ferreira, F.; de Almeida, A.; Baoming, G.: “*Three-Phase Induction Motor Simulation Model Based on a Multifrequency Per-Phase Equivalent Circuit Considering Stator Winding MMF Spatial Harmonics and Thermal Parameters*”, 17th Inter. Conf. on Electric Machinery (ICEM’06), Conf. Proc., September 2006.
- [43] Ferreira, F.; Pereirinha, P.; de Almeida, A.: “*Study on the Bearing Currents Activity in Cage Induction Motors using Finite-Element Method*”, 17th Inter. Conf. on Electric Machinery (ICEM’06), Conf. Proc., September 2006.
- [44] de Almeida, A.; Ferreira, F.: “*Advanced motors, VSDs, transmissions, and systems design*”, Improvement potentials and barriers, Industrial Electric Motor Systems Workshop, Paris, France, May 2006.
- [45] Ferreira, F.; de Almeida, A.: “*Method for In-Field Evaluation of the Stator Winding Connection of Three-Phase Induction Motors to Maximize Efficiency and Power Factor*”, IEEE Trans. on Energy Conversion, Vol. 21, No. 2, pp. 370-379, June 2006.
- [46] Ferreira, F.; de Almeida, A.; Baoming, G.; Faria, S.; Marques, J.: “*Automatic Change of the Stator-Windings Connection of Variable-Load Three-Phase Induction Motors to Improve the Efficiency and Power Factor*”, IEEE Inter. Conf. on Industrial Technology (ICIT’05), Conf. Proc., Hong Kong, 2005.
- [47] de Almeida, A.; Ferreira, F.: “*User-Friendly High-Precision Electric Motor Testing System*”, 4th Inter. Conf. on Energy Efficiency in Motor Driven Systems (EEMODS’05), Conf. Proc., Vol. I, pp. 149-157, Heidelberg, Germany, Sept. 2005.
- [48] Ferreira, F.; de Almeida, A.: “*Electric Machinery Winding Design Software for Teaching and Rewinding*”, 16th Inter. Conf. on Electric Machinery (ICEM’04), Conf. Proc., Krakow, Poland, September 2004;
- [49] de Almeida, A.; Ferreira, F.: “*Actions to Promote VSDs*”, in *Energy Efficiency in Motor Driven Systems*, Springer-Verlag, 2003.
- [50] de Almeida, A.; Ferreira, F.: “*Actions to Promote Energy-Efficient Electric Motor Repair*”, Inter. Journal of Energy Technology and Policy, Vol. 1, No. 3, pp. 302-314, 2003.
- [51] de Almeida, A.; Fonseca, P.; Ferreira, F.: “*Carbon Savings of Energy-Efficient Motor Technologies in Central and Eastern Europe*”, Inter. Journal of Energy Technology and Policy, Vol. 1, No. 3, pp. 262-277, 2003;
- [52] de Almeida, A.; Ferreira, F.; Busch, J.; Angers, P.: “*Comparative Analysis of IEEE 112-B and IEC 34-2 Efficiency Testing Standards Using Stray Load Losses in Low-Voltage Three-Phase, Cage Induction Motors*”, IEEE Trans. on Industry Applications, Vol. 38, No. 2, March/April 2002 (2001 Committee Prize Paper Award of the Energy Systems Committee, IEEE).
- [53] Santos, F.; Trovão, J.; Ferreira, F.; Coelho, D.: “*Three-Phase Induction Motor Condition Evaluation by means of Combined Current and Vibration analysis Using Artificial Neural Networks*”, 2nd Inter. Conf. on Electrical Engineering (CEE’07), Conf. Proc., November 2007.

- [54] Baoming, G.; de Almeida, A.; Ferreira, F.: “*Flexible Neural Network Based Torque Control for Switched Reluctance Motor*”, Lecture Notes in Computer Science, Springer-Verlag GmbH, ISSN: 0302-9743, Vol. 3498/2005, pp. 173-178, 2005.
- [55] Baoming, G.; de Almeida, A.; Ferreira, F.: “*Supercapacitor-based Optimum Switched Reluctance Drive for Advanced Electric Vehicles*”, 8th IEEE Inter. Conf. on Electrical Machines and Systems, Nanjing, China, 27-29 Sept. 2005, pp. 822-827;
- [56] Baoming G., de Almeida, A., and Ferreira, F.: “*Estimation of Primary Current in Saturated Current Transformer using Flexible Neural Network*”, Trans. of the Institute of Measurement and Control, No. 28, Issue 1, London, 2006, pp. 81-91.
- [57] Baoming, G.; de Almeida, A.; Ferreira, F.: “*Design of Transverse Flux Linear Switched Reluctance Motor*”, Inter. Symposium on Power Electronics, Electrical Drives, Automation and Motion (SPEEDAM’06), Conf. Proc., Taormina, 23-26 May 2006.
- [58] Ferreira, F.; Sá, C.; Carvalho, J.: “*Análise e Técnicas de Atenuação da Passagem de Correntes Eléctricas nos Rolamentos dos Motores de Indução Trifásicos*”, Revista Manutenção, N.º 91, 2007.
- [59] Ferreira, F.; Sá, C.; Carvalho, J.: “*Técnicas de Atenuação da Ocorrência e dos Efeitos dos Transitórios de Tensão em Motores de Indução Trifásicos de Baixa Tensão*”, Revista Manutenção, N.º 85, 2005.
- [60] Ferreira, F.; Sá, C.: “*Considerações sobre a Selecção de Motores de Indução Trifásicos para Accionamentos de Velocidade Variável*”, Revista Kéramica, N.º 277, 2006.
- [61] Trovão, J.; Ferreira, F.: “*Distorção Harmónica no Sector Industrial - Causas, Efeitos e Soluções*”, Revista Manutenção, N.º 88, 2006 (2006 Best Paper Award from the Portuguese and Brazilian editions of the technical magazine “Manutenção”, edited by the Portuguese Association of Industrial Maintenance (APMI – Associação Portuguesa de Manutenção Industrial).
- [62] IEEE 112 Std., 2004: “*Test Procedure for Polyphase Induction Motors and Generators*”.
- [63] IEC 60034-2-1, Ed. 1, Sept. 2007: “*Methods for determining losses and efficiency of rotating electrical machinery from tests - excluding machines for traction vehicles*”.
- [64] EuroDEEM, The European Database of Efficient Electric Motors Motor Database, <http://sunbird.jrc.it>, 2007.
- [65] MotorMaster, An energy-efficient motor selection and management tool (motor database), <http://www1.eere.energy.gov>, 2007.
- [66] Doppelbauer, M.: “*Saving Energy and Costs in Electrical Drive Systems*”, SEW-Eurodrive, 2007.
- [67] Sweet, W.: “*Greenhouse Gas Trends – A tale of two perspectives*”, Section “The Data”, IEEE Spectrum, The Magazine of Technology Insiders, January 2008, pp. 60.
- [68] Wallace, A. et al.: “*A Laboratory Assessment of In-Service Motor Efficiency Testing Methods*”, IEEE 1997, WC1-7.1-7.3.
- [69] European Initiative SEEM – Standards for Energy Efficiency of Electric Motor Systems, 2008.
- [70] Waide, P.: “*The Global Energy Consumption of Electric Motor Systems – Challenges and Opportunities*”, Inter. Conf. on Energy Efficiency in Motor Systems (EEMODS’07), Plenary Session, Presentation Slides, Beijing, China, June 2007.
- [71] Mollet, J.: “*Energy Efficiency - Motors*”, Inter. Conf. on Energy Efficiency in Motor Systems (EEMODS’07), Plenary Session, Presentation Slides, Beijing, China, June 2007.
- [72] Budin, J.; Beaugrand, R.: “*The European Motor Challenge – The results of DEXA-MCP Project, a Consortium of 11 Countries*”, Inter. Conf. on Energy Efficiency in Motor Systems (EEMODS’07), Conf. Proc., Vol. I, pp. 309-317, Beijing, China, June 2007.
- [73] Fuchsloch, J.; Noltman, J.; Peters, D.; Brush, E.; Cowie, J.: “*Systematic Design Approach for a New Series of Ultra-NEMA Premium Copper Rotor Motors*”, Inter. Conf. on Energy Efficiency in Motor Systems (EEMODS’07), Conf. Proc., Vol. II, pp. 529-541, Beijing, China, June 2007.
- [74] Boglietti, A.; Pastorelli, M.: “*Energetic Comparison between Induction Motors and Synchronous Motors*”, Inter. Conf. on Energy Efficiency in Motor Systems (EEMODS’07), Conf. Proc., Vol. II, pp. 475-482, Beijing, China, June 2007.
- [75] Petro, J.: “*High Efficiency Motors: A New Motor Technology Option*”, Inter. Conf. on Energy Efficiency in Motor Systems (EEMODS’07), Conf. Proc., Vol. II, pp. 572-577, Beijing, China, June 2007.
- [76] Trevisiol, L.; Rossi, T.: “*Permanent Magnet Synchronous Motor for Pump Application*”, Inter. Conf. on Energy Efficiency in Motor Systems (EEMODS’07), Conf. Proc., Beijing, China, June 2007.
- [77] Bartos, F.: “*Forward to the Past’ with SR Technology*”, Control Engineering Inter., Nov./Dec. 1999.
- [78] Cistelean, M.; Ferreira, F.; Cosan, B.: “*Generalized MMF Space Harmonics and Performance Analysis of Combined Multiple-Step, Star-Delta, Three-Phase Windings Applied on Induction Motors*”, 18th Inter. Conf. on Electrical Machines (ICEM’08), Conf. Proc., Vilamoura, Portugal, Sept. 2008.
- [79] Ferreira, F.; Cistelean, M.; Baoming, G.: “*Simple Strategy to Recovery Energy During Stopping Period in Large High-Inertia Line-Fed Induction Motor Driven Systems*”, 18th Inter. Conf. on Electrical Machines (ICEM’08), Portugal, Sept. 2008.
- [80] Ferreira, F.; Cistelean, M.: “*Simulating Multi-Connection, Three-Phase, Squirrel-Cage, Induction Motors by means of Changing Per-Phase Equivalent Circuit Parameters*”, 18th Inter. Conf. on Electrical Machines (ICEM’08), Conf. Proc., Vilamoura, Portugal, Sept. 2008.
- [81] Ferreira, F.; Trovão, J.; de Almeida, A.: “*Motor Bearings and Insulation System Condition Diagnosis by Means of Common-Mode Currents and Shaft-Ground Voltage Correlation*”, 18th Inter. Conf. on Electrical Machines (ICEM’08), Conf. Proc., Vilamoura, Portugal, Sept. 2008.
- [82] Ferreira, F.; de Almeida, A.: “*Considerations on In-Field Induction Motor Load Estimation Methods*”, 18th Inter. Conf. on Electrical Machines (ICEM’08), Conf. Proc., Vilamoura, Portugal, Sept. 2008.
- [83] Trovão, J.; Pereirinha, P.; Ferreira, F.: “*Comparative Study of Different Electric Machines in the Powertrain of a Small Electric Vehicle*”, 18th Inter. Conf. on Electrical Machines (ICEM’08), Conf. Proc., Vilamoura, Portugal, Sept. 2008.
- [84] Upson, S.: “*How Free is Solar Energy*”, IEEE Spectrum International, February 2008, pp. 56.
- [85] “*Electricidade - Dados Técnicos, Valores Provisórios 2007*”, Redes Eléctrica Nacional (REN), 2007.
- [86] Baoming, G.; de Almeida, A.; Ferreira, F.: “*Design of transverse flux linear switched reluctance motor*”, to be published in the IEEE Trans. on Magnetics, 2008.
- [87] Reinert, J.; Karlsson, P.: “*Improving performance and energy consumption of industrial processes by using variable speed drives*”, Emotron – Dedicated Drive, European Center for Power Electronics e.V. (ECPE) Seminar, “Towards Energy Gain and Savings – Emerging Drives and Generator Systems”, 15-16 April 2008, Warsaw, Poland.
- [88] “*Saving Energy with Electrical Drives*”, German Electrical and Electronic Manufacturers Association, Division Automation/Electric Drive Systems (ZVEI – Automation), Frankfurt, April 2006.
- [89] “*Key World Energy Statistics*”, International Energy Agency, 2007.

- [90] Ferreira, F.; de Almeida, A.; Moreira, L.: “*Impacto Energético e Ambiental Associado à Aplicação das Células de Combustível nos Veículos Eléctricos*”, II Jornadas de Engenharia Electrotécnica, Tecnologia em Movimento, DEE, Instituto Politécnico de Tomar, Tomar, Actas, pp. 81-138, 20-22 Abril de 2004.
- [91] Ferreira, F.; de Almeida, A.: “*Three-Phase Induction Motor Stator Winding Connection Type In-Field Evaluation Method for Efficiency Maximization*”, 4th Inter. Conf. on Energy Efficiency in Motor Driven Systems (EEMODS’05), Conf. Proc., Vol. II, pp. 128-137, Heidelberg, Germany, Sept. 2005.
- [92] EUROSTAT, <http://epp.eurostat.ec.europa.eu>, Feb. 2007.

2 Motor-Driven System Performance

Overview – In this chapter, a survey on the most relevant electric motor efficiency-related standards is presented, and some relevant issues pointed out, including the differences between the most relevant efficiency-testing standards, focusing stray load losses, the new proposed efficiency-testing international standard IEC 60034-2-1, the new efficiency classification international standard IEC 60034-30, and minimum energy performance standards impact on motor market transformation in the European Union, being all important tools to reduce the energy consumption of electric motor systems. High-efficiency motors are briefly addressed. The final results and conclusions of a European study to identify and recommend ways to improve the life-cycle environmental performance of electric motors at their design phase are presented, focusing life-cycle cost assessment of standard and best available electric motor technologies, using a well-known analysis methodology for the assessment of environmental impact and eco-design of energy-using products. System performance improvement issues are discussed, including considerations on investment share optimization. Most of the information presented in this chapter was published in [1]–[4], [6], [14] and [15].

2.1 Considerations on Motor Efficiency Testing Standards

A short background on the scope of this section is presented next. Detailed information on this matter can be found in standards [16], [17], [18], [19], and in a number of technical books and papers. Motor efficiency, η , is given by (2.1) and (2.2) for direct (or input-output) and indirect methods, respectively, where P_{out} is the motor useful (shaft or mechanical) power, P_{in} is the input real power, P_{loss} is the total power loss, P_{cl} the constant (approx.) loss component, P_{ll} load-dependent loss component, P_{sll} the stray load losses (SLLs, also known as additional load losses), and $K_{1,2}$ constants. Assuming (2.2), the variation of efficiency with the SLLs is given by (2.3), both considering fixed P_{in} and fixed P_{out} . For fixed P_{in} , according to (2.3), if SLLs, expressed as a percentage of P_{in} (which is common), increase 1 percentage point (p.p.) the efficiency decreases 1 p.p. [1]. Both methods can be applied to calculate motor efficiency but, of course, direct method is inherently more accurate. The old standard IEC 60034-2 [17] rely upon the indirect method, and the new standard IEC 60034-2-1 [19], as well as the IEEE 112-B [16], rely both upon the direct method. To calculate P_{out} a dynamometer is needed (torque and speed measurement required).

$$\eta_{dir} = \frac{P_{out}}{P_{in}} \quad (2.1)$$

$$\eta_{ind} = 1 - \frac{P_{loss}}{P_{in}} = 1 - \frac{P_{cl} + P_{ll} + P_{sll}}{P_{in}} \quad (2.2)$$

$$\left. \frac{d\eta_{ind}}{dP_{sll}} \right|_{P_{in}=K_1} = -\frac{1}{K_1} \quad \left. \frac{d\eta_{ind}}{dP_{sll}} \right|_{P_{out}=K_2} = -\frac{K_2}{(K_2 + P_{cl} + P_{ll} + P_{sll})^2} \quad (2.3)$$

The relative importance of the five different kinds of motor losses, namely, stator Joule (or I^2R) losses, rotor Joule losses, iron (or core) losses, friction and windage losses, and SLLs, depends on motor size or rated power, as it can be seen in Fig. 2.1. The relevance of SLLs, as a percentage of

total losses, increases with motor rated power. In general, the percentage total losses decrease with motor rated power.

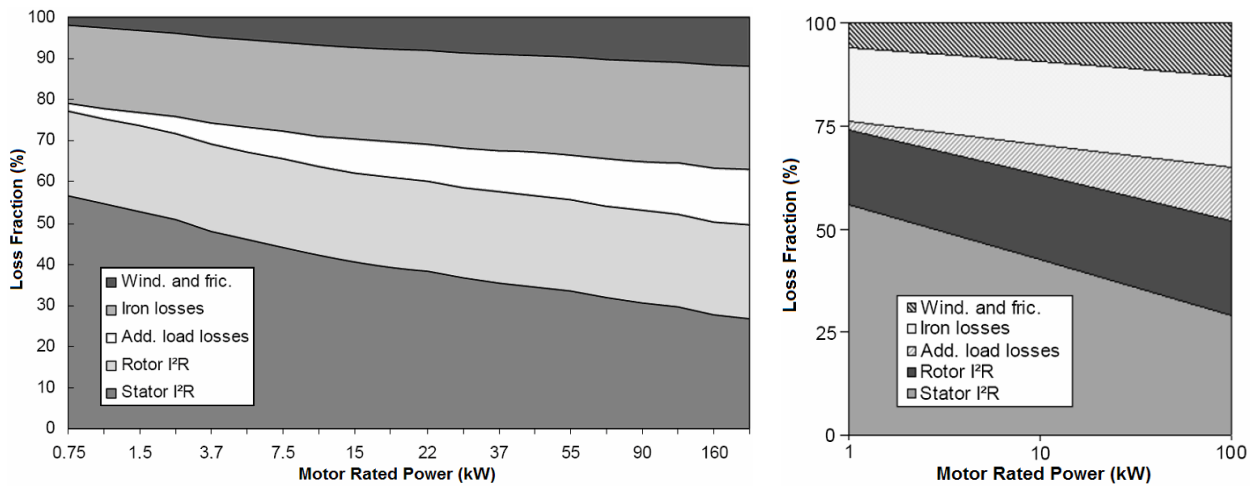


Fig. 2.1 Typical fraction of losses in 4-pole IMs (add. load losses = SLLs): (left) from [2]; (right) from [51].

The influence of poor power quality (voltage unbalance, voltage distortion, etc.) on motor performance is a main issue. The effects of power quality on motor efficiency, as well as on motor starting torque, are far greater than initially thought. In fact, poor power quality can more than wipe out the beneficial effects of deploying HEMs, and amplify the difference between motors in the different energy-efficiency classes. These issues are addressed in Appendix 4.

2.1.1 Impact of Stray Load Losses

As shown in first chapter, HEMs generally represent one of the largest opportunities for cost-effective electricity savings around the world. As a pre-condition to the development of motor market transformation strategies, such as labelling programs, motor minimum efficiency standards, and large-scale demand-side management (DSM), there is a need for assessing the efficiency of motors sold in the market using a uniform yardstick. Motor efficiency testing protocols differ around the world, and applying them to any given motor can lead to significantly different efficiency values, as it can be seen in Table 2.1. However, the higher the motor power ranges, the lower the differences in the efficiency values. Many countries with no or limited domestic motor manufacturing capacity import motors from a variety of countries using different testing procedures [1].

The motor efficiency and/or loss measurement should be measured according to standards, to allow its correct comparison in different brand motors. However, the results can differ significantly when different standards are used, as it can be seen in Table 2.1.

In order to demonstrate the impact of the error for the user, an example is presented. Considering two 50-Hz, 75-kW motors, one with a full-load efficiency tested by IEEE 112-B (or equivalent) of

91.5% and the other with a full-load efficiency tested by the old IEC 60034-2 (Ed. 2) of 93.7%, both to be operated 8000 h/yr at full-load at a 0.07 €/kWh electricity price, the estimated operating cost is 45902 €/yr and 44824 €/yr, respectively, being the difference 1078 €/yr. For such motors, and assuming they have the same price, the user will naturally choose the IM with the higher catalogue rated efficiency, corresponding to that tested according to the standard IEC 60034-2 (Ed. 2). However, the selected motor will actually have an operating cost 1078 €/yr higher. This example illustrates why it is so important to harmonize efficiency testing methods in a global motor market.

TABLE 2.1
EXAMPLES OF THE FULL-LOAD EFFICIENCY EXPERIMENTALLY OBTAINED FROM DIFFERENT STANDARDS [52], [54].

Efficiency Standard	Method	Region	Motor Rated Power								
			4 kW	5.5 kW	7.5 kW	11 kW	11 kW	15 kW	15 kW	50 kW	75 kW
IEC 60034-2, Ed. 2	Indirect	Internacional/EU	84.6%	82.3%	86.5%	90.5%	86.4%	85.5%	89.4%	92.8%	93.7%
JEC 37 ¹	Indirect	Japan	85.4%	85.0%	86.7%	90.7%	87.1%	85.5%	90.4%	93.3%	94.2%
IEEE 112-B/CSA C390	Direct	North America	82.9%	80.3%	85.9%	89.2%	86.1%	84.9%	86.9%	92.9%	91.5%

Note: CSA C390 [21], IEC 61972 [18] and IEC 60034-2-1 [19] standards include a method equivalent to IEEE 112-B standard.

Up-to-date, the efficiency data presented in the IM nameplate, given by the manufacturer, has been measured or calculated according to two main methods – IEEE 112-B and IEC 60034-2 (Ed. 2, indirect method) [17], which use different SLLs evaluation methods. In the old IEC 60034-2 standard, these losses were not measured and were arbitrarily estimated to be equal to 0.5% of the full-load input power. In the IEEE 112-B and the new IEC 600-34-2-1 (direct method with loss segregation) standards, SLLs are the losses not covered by the other three loss terms (I^2R losses, core losses, and friction and windage losses), after the measurement of the total losses, by the direct method². Due to the adopted procedures, the efficiency obtained from the two standards can differ significantly.

Due to the lack of accurate results, the IEC standard was reviewed, namely, in the SLLs estimation process, in order to become technically equivalent to the other proven national standards that compute SLLs, e.g., IEEE 112-B (USA) and CSA C390 (Canada), where the SLLs are determined by means of measurement of the output power. A few years ago, the standard IEC 61972 [18] was proposed, but it was not adopted as a European standard (EN), The IEC 61972 direct method is similar to the IEEE 112-B. The IEC 61972 indirect method, determines the SLL from assigned values in a predefined curve, which depend on motor rated output power and allocates a percentage value at the rated load (the SLL value at 1 kW is 2.5% of the full-load input power, dropping at 10 kW to 2%, at 100 kW to 1.5%, at 1000 kW to 1% and at 10 MW to 0.5%).

¹ In the Japanese motor testing standard JEC 37, SLLs are ignored.

² In the standard IEEE 112-B, SLLs are considered zero at no load. The obtained SLLs versus squared load torque curve are diagrammed. These values have to be smoothed using a linear regression. If the slope of the linear regression line is negative or the correlation factor is less than 0.9, the worst point has to be deleted and the regression has to be repeated. If this operation increases the correlation factor to 0.9 or higher, the second regression can be considered valid. If not, or the slope still negative, the test is unsatisfactory and has to be repeated.

The IEEE 112-B standard, estimates the efficiency by the direct method (according to (2.1)), i.e., P_{in} is measured using a high-accuracy wattmeter and P_{out} is measured using a speed sensor (e.g., encoder, tachometer) and a high-accuracy torque sensor. SLLs, given by the difference between the total losses and the sum of copper, core, windage, and friction losses, are corrected (using regression analysis), yielding the corrected total losses and, based on that value, corrected direct-method-based efficiency load curve. This is an accurate method, if the instrumentation has the desired accuracy and the test procedure is followed rigorously. The old IEC 60034-2 standard (indirect method), estimates the efficiency using the indirect method, in which the summation of losses is calculated, and then the efficiency according to (2.2). The copper, core, windage, and friction losses are calculated using no-load and load tests. SLLs are assumed to have a fixed value (0.5% of the rated full-load input power). Additionally, this method has a significant degree of uncertainty, because of the instrumentation lower accuracy specifications and the uncorrected winding losses in relation to the temperature. In Table 2.2 it is presented a summary of the main differences between both mentioned standards.

On the basis of data collected in 1998-2001 period in 6 countries, which use different frequencies, namely, Brazil (60 Hz), Belgium (50 Hz), France (50 Hz), Taiwan (60 Hz), U.K. (50 Hz), USA (60 Hz) and Canada (60 Hz), an analysis of the losses and efficiency values resulting from the application of both IEC 60034-2 and IEEE 112-B standards, was carried out. Of the 817 test motor data sets used, 650 (about 80%) came from independent motor test laboratories. Large motor manufacturers supplied the remaining motor data sets. The total number of 60 Hz test data sets is 781, in the range of 0.75-370 kW, all of which have been tested with IEEE 112-B (or equivalent CSA C390 Method 1), including the computation of the SLLs. Of the 60 Hz motors, 89 motors had the efficiencies tested both with IEC 60034-2 and IEEE 112-B standards. The total number of 50-Hz test data sets is 36, in the range of 2.2-75 kW. The efficiency of all the 50-Hz motors was computed both according to the IEEE 112-B (including SLL in % of full-load input power) and to the IEC 60034-2 (indirect method) standards.

These motor data are also separated in 2-, 4-, 6- and 8-pole motors. The number of 50-Hz motors used in the study is small due to the fact that 50-Hz motor manufacturers around the world only carried out efficiency testing with IEC 60034-2. It is possible to obtain a much larger number of 50-Hz motors efficiency data, whose efficiency is tested only with the IEC 60034-2 method, but the SLLs are not measured. Therefore for the purpose of this study such data is not useful. The results of the analysis are presented next.

IEEE 112-B SLL trend lines for 50 Hz and 60 Hz are presented next. In Appendix 6, the SLL (as a % of full-load input power) variation with motor rated power for 50 Hz, for 4- and 6-pole motors, can be seen. For 6-pole motors only 55 kW motors data was available. From the obtained figures,

it can be seen that the 50-Hz SLL values are on average about 1.5% of full-load input power, 90% of which fall in the range of 0.6% to 2.3%, reaching 3% in one case. This clearly shows that the old IEC 60034-2 (Ed. 2) test method can lead to gross errors in the estimation of the motor efficiency. Other statistical values are presented in Table 2.3.

TABLE 2.2
SUMMARY OF THE MAIN DIFFERENCES BETWEEN IEC 60034-2 (ED. 2), IEEE 112-B AND IEC 61972 [1].

		IEC 60034-2 (Indirect Method)	IEEE 112-B	IEC 61972 (Dir. Method)
Type of measurement		Summation of losses	Direct	Direct
Segregation of losses		Yes	Yes	Yes
Core loss with voltage drop compensation		No	No	Yes
SLL using regression analysis		No	Yes	Yes
Temperature corrected I^2R losses in the rotor and stator		No	Yes	Yes
Thermal equilibrium at rated load		No	Yes	Yes
Stabilization of no-load losses		No	Yes	Yes
Dynamometer torque correction		No	Yes	Yes
Instrumentation accuracy (+/- % of full scale)	Electrical	1.0	0.2	0.2
	Instrument transformer	1.0	0.2	0.2
	Frequency	1.0	0.1	0.1
	Speed	1.0	1 r/min	0.1
	Torque	1.0	0.2	0.2
	DC Resistance	0.5	0.2	0.2

In Appendix 6, the SLL variation with input power for 8-, 6-, 4-, and 2-pole for all 60-Hz motors, respectively, with measurements made with IEEE 112-B, can also be seen.

A frequency curve was constructed, that presents the number of points in a specific range of SLL values. This result is shown in the Fig. 2.2, in which, for the 50-Hz motors, the maximum of the 6th order polynomial used trend line is the range of 1.4% to 1.5% of P_{in} . Based on this curve and on the values presented in Table 2.3, it can be concluded that the value of SLL (% of P_{in}) that has the highest probability of occurrence is about 1.5%, and that the expected average error of the old IEC 60034-2 in the estimation of SLL is -1.0% leading to an overestimation of the motor efficiency.

In the obtained figures, it was found that SLLs are scattered around an average value of about 1.3%.

When considering all 60-Hz data, a slight decrease of the SLL (% of P_{in}) with increasing motor power was found. The average SLL (% of P_{in}) value is 1.3%, with a probability of 90% that the SLL (% of P_{in}) is in the range of 0.4-2.2%. The statistical values of the SLL distribution for 60-Hz motors can be seen in Table 2.3.

In Fig. 2.2, the 60-Hz motor data frequency of the SLL distribution can be seen including the polynomial trend line. On the basis of the values presented in Table 2.3, when compared with the IEEE 112-B method, the expected average error of the SLL predefined value according to the old

IEC 60034-2 test method is -0.8% , which will lead, once again, to an overestimation of the motor efficiency.

TABLE 2.3
STATISTICS OF SLL (% OF P_{in}) DATA [1].

No. Data Sets	Motor Frequency	Average	Standard Deviation	Max. Value	Min. Value
36	50 Hz	1.5	0.6	3.0	0.4
781	60 Hz	1.3	0.6	5.3	0.1

In the global 60-Hz data distribution, a slight decrease of the error with higher motor power values was found. For large motors, the SLL average value approaches 1%. In general, the higher the rated power, the lower the error of the IEC 60034-2 efficiency computation.

In Fig. 2.3, the influence of the motor number of poles in the average SLL for each frequency can be seen. SLLs present small variation with the number of poles and with the frequency.

In Fig. 2.4, the SLL average values as function of total losses are presented, for each motor rated power. The trend lines have similar slopes.

Although the SLLs as a percentage of full-load input power are typically higher in 50-Hz than in 60-Hz motors, the percentage of the SLL as a function of the total motor losses is smaller in 50-Hz than in 60-Hz motors.

It is important to note that 60-Hz motor data includes a majority of HEMs (motors sold in North America), whose total losses are typically 30-50% lower than those of standard motors.

The efficiency measurements made with both standards for the same motors are now compared. It was shown above that SLLs vary significantly as compared to the IEC fixed allowance (0.5% of the rated input power). This is the main reason for the observed differences in the corresponding efficiency data that is presented next.

Figs. 2.5 and 2.6 show trend lines of motor efficiency using the IEEE 112-B and IEC 60034-2, for 50- and 60-Hz motors, respectively.

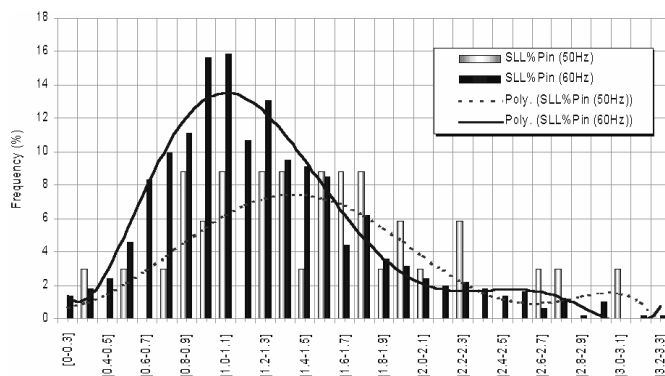


Fig. 2.2. Percentage of data frequency in different ranges of SLL (% of P_{in}) and respective 6th order polynomial trend lines.

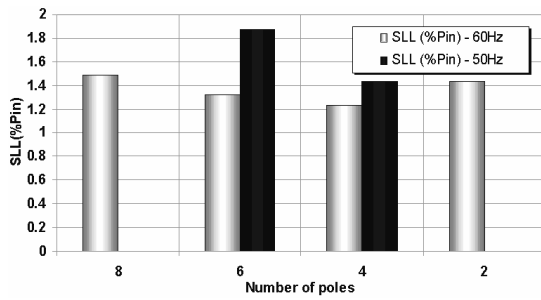


Fig. 2.3. SLL (% of P_{in}) behavior with number of poles and frequency (SLL values computed with IEEE 112-B).

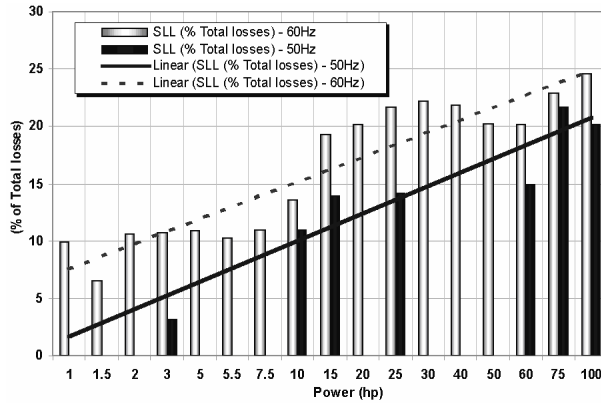


Fig. 2.4. SLL (as a % of total losses) average values, by motor rated power, for 50 Hz and 60 Hz.

Fig. 2.7 presents, the efficiency differences between IEC 60034-2 and IEEE 112-B test standards, for 50- and 60-Hz motors, plotted against motor rated power. Table 2.4 presents the average values of the efficiency data, by motor rated power.

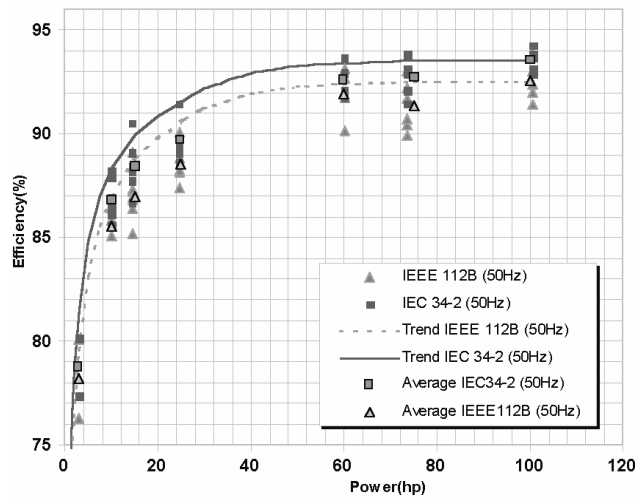


Fig. 2.5. Motor efficiency trend lines for 50-Hz motors, using the IEEE 112-B and the IEC 60034-2 standards.

Table 2.4 confirms that the IEC 60034-2 efficiency test method overestimates the efficiency values. The difference between the efficiency estimated by IEC and IEEE methods is about 1 p.p., as expected.

Table 2.5 presents a summary of the efficiency data analysis with the motors, which were tested both with IEEE 112-B and the old IEC 60034-2, considering the discrepancies between the SLL and the efficiency measurements.

Considering the average difference between the efficiency measurements using both standards in the same motors, the IEC 60034-2 efficiency overestimation is about 0.9 p.p. for 60-Hz motors and 1.2 p.p. for 50-Hz motors. These values are very similar to the observed differences in the SLL values. This is not surprising due to way in which the efficiency is computed.

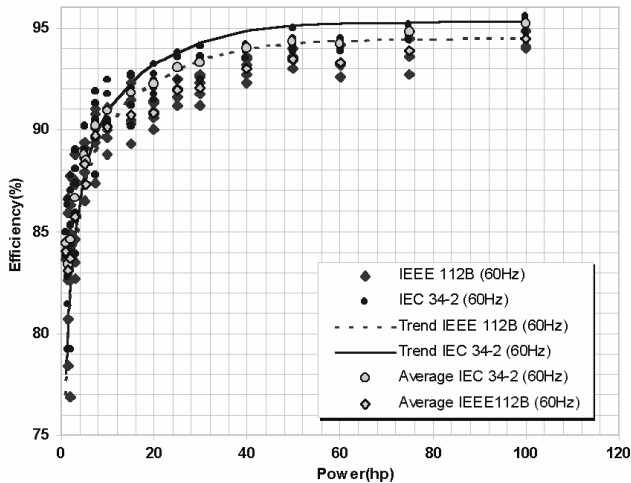


Fig. 2.6. Motor efficiency trend lines for 60 Hz, using the IEEE 112-B and IEC 60034-2 standards.

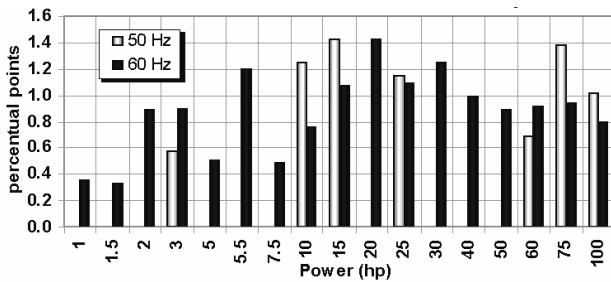


Fig. 2.7. Average difference between IEC 60034-2 and IEEE112-B efficiency average values, for 50 Hz and 60 Hz.

Concluding, a large sample of motor efficiency measurements has been collected around the world (the largest sample to the author’s knowledge) and has been analysed. On the basis of this analysis it can be stated that the efficiency determination according to the IEC 60034-2 standard is not accurate. One critical flaw of this test method is the use of a grossly underestimated value for the SLLs. Ideally, the SLLs should be computed, and cannot be replaced by a fixed allowance as the difference between motors of the same rating is significant and cannot be ignored.

On the basis of the average values of the analyzed sample, it was demonstrated that the difference in SLLs determination from one standard to another is about 1.0 p.p. and 0.8 p.p., for 50 Hz and 60 Hz, respectively. Considering the average difference between the efficiency measurements using both standards in the same motors, the IEC 60034-2 efficiency overestimation is about 1.2% for 50-Hz motors and 0.9% for 60-Hz motors. These values are very similar to the observed differences in the SLL values. The results are particularly significant in the 60-Hz sample (almost 800 motors analysed).

TABLE 2.4
AVERAGE EFFICIENCY VALUES, FOR IEC AND IEEE STANDARDS, BY MOTOR POWER AND BY FREQUENCY [1].

Motor Rated Power (hp)	50 Hz		60 Hz	
	IEC 60034-2, Ed. 2 36 motors	IEEE 112-B 36 motors	IEC 60034-2, Ed. 2 89 motors	IEEE 112-B 89 motors
1	---	---	84.4	84.1 (-0.3)
1.5	---	---	83.4	83.1 (-0.3)
2	---	---	84.6	83.7 (-0.9)
3	78.7	78.2 (-0.5)	86.6	85.7 (-0.9)
5	---	---	88.8	88.3 (-0.5)
5.5	---	---	88.5	87.3 (-1.2)
7.5	---	---	90.2	89.7 (-0.5)
10	86.8	85.6 (-1.2)	90.9	90.1 (-0.8)
15	88.4	87.0 (-1.4)	91.8	90.7 (-1.1)
20	---	---	92.3	90.8 (-1.5)
25	89.7	88.5 (-1.2)	93.1	92.0 (-1.1)
30	---	---	93.3	92.1 (-1.2)
40	---	---	94.0	93.0 (-1.0)
50	---	---	94.4	93.5 (-0.9)
60	92.6	91.9 (-0.7)	94.2	93.3 (-0.9)
75	92.7	91.3 (-1.4)	94.8	93.9 (-0.9)
100	93.5	92.5 (-1.0)	95.3	94.5 (-0.8)

TABLE 2.5
STATISTICS OF DISCREPANCIES (IN PERCENTAGE POINTS) BETWEEN THE IEC 60034-2 AND IEEE 112-B EFFICIENCY VALUES.

Motor frequency	Statistical Value	$SLL_{IEEE} (\% \text{ of } P_{in}) - SLL_{IEC} (\% \text{ of } P_{in})$	$\eta_{IEC} - \eta_{IEEE}$
60 Hz SLL: 89 data η : 781 data	Average	0.8	0.9
	Standard deviation	0.6	0.6
	Maximum value	4.8	2.4
	Minimum value	-0.4	-0.2
50 Hz SLL: 36 data η : 36 data	Average	1.0	1.2
	Standard deviation	0.6	0.6
	Maximum value	2.5	2.5
	Minimum value	-0.1	-0.1

Therefore it seems possible to compute with a good degree of approximation what would be the IEC 60034-2 efficiency result, based on the efficiency and SLL measurements made with the IEEE 112-B standard. The opposite conversion (IEC 60034-2 into IEEE 112-B equivalent values) cannot accurately be done, due to the arbitrary value of the SLL. In the large sample of measurements analysed there is, on average, an overestimation of the efficiency of around 1 p.p. when using the IEC 60034-2 standard, although with a large variance.

In a market in which the available motors come from different areas of the world and are tested with different standards (e.g., motors produced in North America and in Europe), it is recommended that the efficiency values are compared based on the same yardstick. For the reasons pointed before the IEC 60034-2 efficiency values together with the “translated“ IEEE 112-B values into IEC 60034-2 equivalent values, allow a level playing field comparison to perform a more cost-effective motor selection or the implementation of large-scale motor transformation programs.

An important conclusion that can be extracted from the SLL analysis is the irregularity of its values, which means that a fixed allowance can have a significant error. The IEC 61972 standard (direct method), although not accepted as a European standard, was a positive step towards the improvement of motor efficiency testing, and the new recently approved IEC 60034-2-1 (direct method with loss segregation) [19] end up the discrepancies between European and North American motor testing standards. On the basis of the presented results, it can be stated that, in general, the use of the indirect method of the IEC 61972 or of the old IEC 60034-2 standards, leads to an underestimation of the motor efficiency. This fact has been an incentive for the progressive avoidance of the indirect testing method around the world.

2.1.2 New Motor Efficiency Testing Standard

The new IEC 60034-2-1 standard³ [19] includes four major method groups (direct, total losses, summation of losses with & without load test, and summation of losses without load test) and information on “preferred methods” and “level of uncertainty”. For example, “low-uncertainty” indicates that all loss-components are determined from tests; “medium-uncertainty” indicates that it is based in a simplified physical model of the motor; “high-uncertainty” indicates that all loss-components are not determined by tests. For IMs up to 1 kW, the preferred method is the direct method with torque measurement, requiring a torquemeter/dynamometer for full load, being considered as a low-uncertainty method. For IMs larger than 1 kW up to 150 kW, the preferred method is the summation of losses with load test, in which SLLs are determined from the residual loss, a procedure equivalent to that used in the IEEE 112-B standard. The older method of the standard IEC 60034-2 (Ed. 2) [17] – derives SLL from assigned values, is still widely used in Europe, Japan, India, Australia, China, etc. – leads to medium-high uncertainty, and is no longer recommended, due to its inherent error, as demonstrated in previous section.

2.2 High-Efficiency Three-Phase Induction Motors

After the 70’s petroleum crises, and the consequent increase of the electrical energy price, high-efficiency IMs were introduced into the market. Since then, the IMs efficiency has evolved significantly. For example, for a 11-kW/14-hp IM, the efficiency started with a value lower than 88% in 1975, increased to 91.5% (EPAAct efficiency level) and to 93% (present Premium efficiency level), having a potential increase to 93.1-93.6% (using copper-cage rotor), to 94.1-94.5% (using amorphous-steel laminations), and to 98.5-99% (using super-conductors), being the last case values close to the impossible limit of 100% efficiency [51].

A large number of technical texts have been published on energy-efficient or high-efficiency motors (EEMs and HEMs), either written by independent researchers or by manufacturers. Given

³ IEC has started working on a new standard for specific test methods for determining losses and efficiency of converter-fed AC machines [20].

the overall orders of magnitude of motor energy consumption, shown in previous Chapter, it is well worth thinking about how efficiency can be improved, irrespective of the size of the motor, since the consumption is large practically in all power ranges, and despite the fact that improvements to an individual motor or drive might appear negligible at first sight.

The preferential consideration given to the efficiencies of large motors is justified to the extent that, on average, large motors tend to live longer than smaller ones (e.g., 0.75-7.5 kW power range, 12-yr lifetime; 7.5-75 kW power range, 15-yr lifetime; higher than 75 kW power range, 20-yr lifetime [14], [15]). Nevertheless, the lifetime of a small motor is similar to that of an average car, the difference being that at the end of its service life, in general, it will have racked up more than twenty times the number of operating hours of the car. Clearly, efforts to reduce the power consumption of small electric motors by 1% is, in principle, more worthwhile than attempts to lower fuel consumption in cars by 10%. IMs can consume an amount of energy over lifetime equivalent to 30-150 times its purchase price, depending on motor power, operating time and electricity cost. On average, motor energy cost represents 96-98% of its LCC, and initial investment and maintenance represent only 1.4-2.5% and 0.6-1.5% of its LCC, respectively. An example is presented in Fig. 2.8.

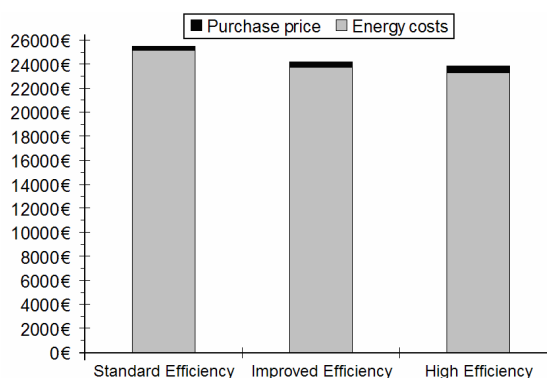


Fig. 2.8. Relation between purchase and energy costs for a 11-kW motor with different efficiency classes: standard efficiency (EFF 3 class), improved efficiency (EFF 2 class) and high efficiency (EFF 1 class). Assumptions: 0.066 €/kWh and 30000-h service life at full-load [10].

There are still a number of elements that can be designed differently to achieve higher efficiency levels in IMs⁴, namely, increased amount of active materials⁵ (limited due to frame size standardization), lower motor temperature level/class⁶, improved fan assembly design⁷ (or efficiency) and low-friction bearings use (reduces friction and windage losses and noise level),

⁴ In Appendix 2, experimental per-phase equivalent circuit parameters for several 7.5-kW, 4-pole motors with identical cross-sectional geometry but different cage materials (aluminium and copper), core magnetic steels (standard and premium), and core lengths, evidencing the impact of the quality and quantity of material used on the IM performance.

⁵ Simultaneously improving diameter to length relation of core (higher outer diameter, dimensions for the next frame size), stator in-slot copper amount increase (possible reduction of motor reliability), and rotor bar area increase [51]. Design tools became very accurate in calculating efficiency and optimizing diameter to length ratio, in order to maximize efficiency including maximum possible diameter to length ratio still meeting standardized mounting dimensions.

⁶ Increases motor reliability but has modest impact on motor efficiency, e.g., less 10°C leads to less ≈3% in resistance and less ≈1.5% in losses, leading to < 0.1% increase in a 95% efficiency motor [52].

⁷ Here, unidirectional fans can be considered [51], [52].

improved steel lamination properties⁸ and reduced thickness (lowers losses and reducing magnetizing current), reduced coil-heads and more in-slot copper (reduces copper losses and operating temperature), rotor thermal treatments and large and/or better bars and end-rings material (e.g., copper, reducing rotor losses), optimized/precision air-gap (reduces SLLs and magnetizing current), optimized stator/rotor geometries (e.g., using finite-element analysis) and slightly longer core design (improving efficiency and power factor [39]), increased heat transfer rate between active parts and housing (reduces operating temperature and, thus, stator windings and rotor losses), limited manufacturing tolerances and optimized processes, optimized lamination punching and stacking process to prevent cross currents and harmonics (reduces SLLs and burrs⁹), just to name a few, as it can be seen in Figs. 2.9 and 2.10 [10], [51]. The consequent lower motor operating temperature also contributes to extend its lifetime.

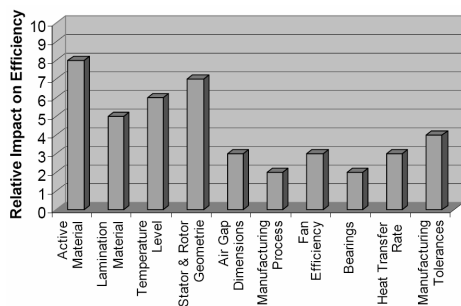


Fig. 2.9. Areas of improvement in IMs [51].

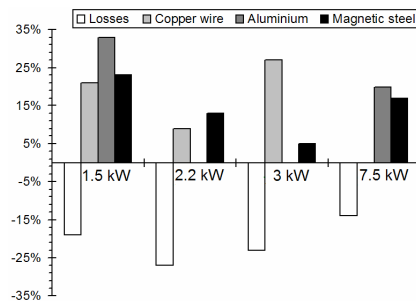


Fig. 2.10. Variation of losses as a function of the used material in IMs [10].

For VSD-fed IMs, there is also the possibility of increasing the number of phases in order to improve IM efficiency. In fact, as demonstrated in [46], the use of more than 3 phases will increase motor efficiency without increasing motor cost. However, careful study is required to assess the impact that the multi-phase design has on the cost of the inverter. Theoretically, the stator copper loss can be reduced up to 8.8% (e.g., 6-phases leads to a 6.7% copper loss reduction; 12-phases 8.3% copper loss reduction; infinite phases leads to 8.8% copper loss reduction). Estimated losses and efficiency are presented in Appendix 6.

Due to the increase of the energy cost, the use of new or previously considered technologies, which were considered too expensive, has now become practical. In fact, a new line or ultra NEMA Premium copper-rotor HEM was recently introduced into North American market [51]. Additional considerations on copper-cage¹⁰ rotors are presented in Appendix 6. The EFF 1 and Premium equivalent motors are clearly cost-effective for most applications. However, care should

⁸ High-performance lamination materials mean improved permeability, reduced losses, better interlaminar insulation quality, and/or heat treatment application [51]. Some manufacturers are using amorphous steel laminations for IMs designed to operate at frequencies higher than 200 Hz [45]. The investigations into more efficient active materials for stators and rotors are centred on lamination materials, winding materials and rotor cage materials [51].

⁹ Burrs can short out laminations, increasing core losses [51], [52].

¹⁰ Constructed/assembled copper cages have been typically used in the rotors of medium/large IMs. However, rotors with die-cast copper cage are a recent technology.

be taken when replacing EFF 3-class or EFF 2-class IMs by EFF 1-class IMs, since, in some cases, the improvement in efficiency cannot overcome the increase in the mechanical power required by the load due to the typical speed increase (i.e., slip reduction). In fact, a typical strategy to increase motor efficiency is reducing rotor resistance, R_r . However, it leads to the increase of the slope of the quasi-linear zone of the motor torque-speed curve (Fig. 2.11). Except for constant power loads, the power required by the load can increase significantly. This should be taken into account when calculating the savings. Additional considerations on this topic are presented in Appendix 6.

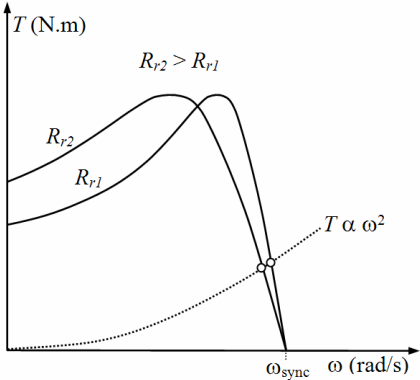


Fig. 2.11. Simplified torque-speed curves for IMs with different rotor resistances (R_r).

2.3 Minimum Energy Performance Standards

Motor efficiency improvement has associated a significant savings potential, particularly in the low-medium motor power ranges, as can it be seen in Fig. 2.12. Therefore, technical and political efforts to promote more efficient motors are very important.

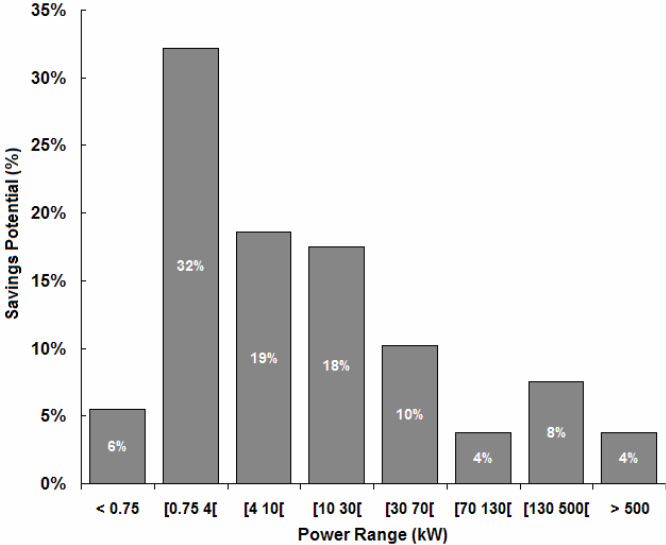


Fig. 2.12. Allocation of the savings potential by installed motors in the European Industry (installed capacity multiplied by the average efficiency improvement). Source: CEMEP.

2.3.1 New Proposed Motor Efficiency Classification Standard

Many different energy efficiency standards for IMs are currently in use (e.g., NEMA¹¹ and EPAct¹² in USA, CSA in Canada, CEMEP/EU¹³ in Europe, AS/NZ in Australia and New Zealand, JIS in Japan, and GB in China) with new classes currently being developed in several countries around the world. It becomes increasingly difficult for manufacturers to design motors for a global market and for customers to understand differences and similarities of standards in different countries. In order to overcome those undesirable situations, a new international standard is being developed by the IEC, IEC 60034-30¹⁴ [33], which is intended to globally harmonize motor energy-efficiency classes in general-purpose, line-fed¹⁵, IMs covered¹⁶ by the standard IEC 60034-1, used in stationary applications (main characteristics shown in Table 2.6). The standard also applies to motors rated for two or more voltages and/or frequencies. Motors in the 0.75-370 kW power range make up the vast majority of installed motor population and are covered by this standard. For the application of IEC 60034-30 standard, motor efficiency and losses shall be tested in accordance with IEC 60034-2-1 using a “low uncertainty” method, such as the “summation of losses” test procedure with stray load losses (SLLs) determined from residual loss, a procedure similar to the method used in the standard IEEE 112-B.

Four motor efficiency classes are proposed, namely, Standard Efficiency (IE1)¹⁷, High Efficiency (IE2)¹⁸, Premium Efficiency (IE3), and Super-Premium Efficiency (IE4). The efficiency rated value and class shall be durably marked on the nameplate. In a motor with dual frequency rating, both 50-Hz and 60-Hz efficiencies shall be marked for each rated voltage/frequency combination. IMs with full-load efficiency below the IE1 boundary are considered of being below standard efficiency. Motors with a full-load efficiency equal to or exceeding an efficiency class lower boundary/limit are classified in that efficiency class. IE1, IE2 and IE3 classes are normative, and IE4 class is intended to be informative (provided in an annex), as more experience with such products is required before standardization. As of now, no sufficient market and technological information is available to allow IE4 standardization. It is expected that advanced technologies will enable manufacturers to design motors for this efficiency class with mechanical dimensions or frame sizes (e.g., shaft heights) compatible to those of the existing motors of lower efficiency classes (as defined in standards EN 50347 and NEMA MG1).

¹¹ NEMA – National Electrical Manufacturers Association.

¹² EPAct – Energy Policy Act.

¹³ CEMEP/EU – Agreement between the EU and the European Committee of Manufacturers of Electrical Machines and Power Electronics.

¹⁴ Rotating electrical machines - Part 30: Efficiency classes of single-speed, three-phase, cage induction motors (IE-code), Second draft, July 2007.

¹⁵ Direct on-line (D.O.L.) connection.

¹⁶ Degree of protection IP 2x, 4x, 5x, or 6x, according to IEC 60034-5; Cooling method IC 0Ax, 1Ax, 2Ax, 3Ax, or 4Ax, according to IEC 60034-6.

¹⁷ The designation of the energy efficiency class consists of the letters “IE” (short for “International Energy Efficiency Class”), directly followed by a numeral representing the classification.

¹⁸ Efficiency levels equivalent to those defined in the EPAct.

TABLE 2.6
SINGLE-SPEED IM CHARACTERISTICS FOR DIFFERENT MOTOR EFFICIENCY RELATED STANDARDS [2].

Min. Efficiency Standard or Voluntary Agreement	Pole Pairs	Duty Type	Power Range	f_N (Hz)	U_N (V)	Design Type	Efficiency Testing Standard
CEMEP-EU	1, 2	S1 ^a	1.1-90 kW	50	400	N ^c	IEC 60034-2, Ed.2 ^e
IEC 60034-30	1-3	S1, S3 ^b	0.75-370 kW	50/60	≤ 1k	N ^c	IEC 60034-2-1 ^f
EPAct	1-3	S1	1-200 hp	60	460	A, B ^d	IEEE 112-B
NEMA MG 1 - 2003 & 12-6C	1-3	S1	1-500 hp	60	≤ 600	A, B ^d	IEEE 112-B
AS 1359.5	1-4	S1	0.73-185 hp	50	≤ 1k	--	AS 1359.102 ^g
GB 18613, 2006	1-3	--	0.55-315 kW	50	≤ 690	N ^h	GB/T 1032 ^e

Notes:

^a S1 - Continuous duty/rated.

^b S3 - Intermittent periodic duty, with an operation time of 80% or more.

^c According to IEC 60034-12 Standard.

^d According to NEMA.

^e Summation of losses, SLLs assumed 0.5% of input power.

^f Summation of losses, SLLs determined either from residual loss test.

^g Two methods allowed: AS 1359.102.3 (similar to IEEE 112-B) and AS 1359.102.1 (similar to IEC 60034-2, Ed. 2).

^h According to GB 755-2000 Std.

It should be noted that, in this standard, nominal motor efficiency is defined as the typical efficiency for a motor population of the same rating. Variations in materials, manufacturing processes, and testing result in motor-to-motor efficiency variations for a given motor design. The full-load efficiency for a large population of motors of a single design is not a unique value but rather a band of efficiency. Therefore, the full-load energy-efficiency limits given in IEC 60034-30 standard are nominal. The full-load efficiency of any individual motor, when operating at rated voltage and frequency, shall be not less than rated efficiency minus a percentage calculated on the basis of the allowed tolerance of the total losses stated in the standard IEC 60034-1¹⁹.

Motors covered by this standard may be used in variable-speed drive applications (IEC 60034-17), but, in these cases, the marked efficiency of the motor shall not be assumed to apply due to the increased losses resulting from the typical harmonic content of the voltages produced by VSDs. Motors specifically built for operation in explosive atmospheres²⁰ (according to IEC 60079-0 and IEC 61241-1) and motors with gears and/or brakes, are also covered by this standard. However a lower classification may be required.

Clearly excluded are motors specifically designed to be fed by VSDs with reinforced insulation (according to IEC 60034-25), motors completely integrated into a machine (pump, fan, compressor, etc.), which cannot be separated from the machine, and all other non-general-purpose motors (like smoke-extraction motors built for operation in high ambient temperature environments according to EN 12101-3, etc.). Additionally, special motors designed for applications with a large number of start/stops cycles are also not covered by this standard. The full-load continuous-duty efficiency of these special motors is typically below standard efficiency due to the requirement to reduce rotor inertia.

¹⁹ 15% tolerance on losses up to 150 kW and 10% above that power level.

²⁰ It should be noted that some design constraints associated with explosion proof motors (like increased air-gap, reduced starting-current, and enhanced sealing) have a negative impact on motor efficiency.

The relative importance of the different kinds of motor losses depends on motor size, as it can be seen in Fig. 2.1. In small-medium IMs, I^2R losses are dominant. Since I^2R losses remain constant for 50 Hz and 60 Hz, as long as the torque is kept constant, the output power is 20% higher for the 60-Hz motors, and although windage, friction and iron losses increase with frequency, they play a minor role in IMs. Therefore, most IMs develop a better efficiency at 60 Hz compared to that at 50 Hz, becoming easier to reach a higher motor efficiency levels when the motor is designed for and operated at 60 Hz instead of 50 Hz. The difference in efficiency between 50 Hz and 60 Hz varies with the number of poles and the size of the motor. In general, the 60-Hz efficiency of IMs in the 0.75-370 kW power range is 2.5% (small motors) to less than 0.5% (large motors) greater when compared to the 50 Hz efficiency. Only large 2-pole IMs may experience a lower efficiency at 60 Hz due to the higher relevance of windage and friction losses²¹.

In some countries 8-pole motors are included in energy-efficiency regulations (Table 2.6). However, their market share is already very low (1% or less). Due to the increasing acceptance of VSDs and the low cost associated with 4-pole and 6-pole standard motors, it is expected that 8-pole motors will even further disappear from the general market in future, thus this standard excludes provisions for 8-pole motors.

The 50-Hz values for IE3 class are newly designed and set above the value for IE2 class, considering about 15% reduced losses. The 60-Hz values were derived from the 50-Hz values taking the influence of supply frequency on motor efficiency into account, resulting in the levels presented in Fig. 2.13, for 4-pole, 50-Hz IMs. This approach will enable manufacturers to build motors for dual rating (50/60 Hz).

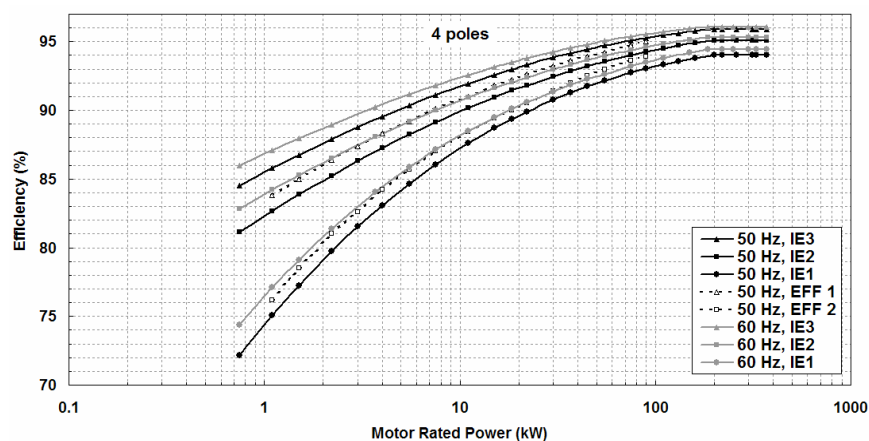


Fig. 2.13. Efficiency levels defined by IEC 60034-30 standard and by CEMEP/EU agreement for 4-pole, 50-Hz IMs [2], [33].

The approved IEC 60034-30 efficiency classification standard, currently under final discussion, will harmonize the currently different requirements for IMs efficiency levels around the world, hopefully ending the difficulties manufacturers encounter when producing motors for a global

²¹ For example, the core losses, friction & windage losses, stator I^2R losses, rotor I^2R losses, and SLLs represent 19%, 25%, 26%, 19%, and 11% of the total losses for a 2-pole, 37-kW IM, and 21%, 10%, 34%, 21%, and 14% of the total losses for a 4-pole 37-kW IM [55].

market. Additionally, customers will benefit by having access to a more transparent and easier to understand information.

2.3.2 Minimum Motor Efficiency Requirements Around the World

Minimum efficiency requirements or minimum energy performance standards (MEPS) are a powerful tool to force market transformation, as it can be seen in Figs. 2.14 and 2.15. In this scope, it is first necessary to define nominal efficiency (statistical average of a sample; in the USA a sample includes five equal motors), which is the base for setting MEPS, versus the rated efficiency of one single motor that can have a tolerance not larger than the standard prescribes. In Table 2.7, an overview of minimum efficiency requirement agreements and regulation around the world, can be seen, in which four efficiency classes of IMs, according to IEC 60034-30 can be found: a) IE3 (similar to NEMA Premium); b) IE2 (similar to EPAct or Europe EFF 1); c) IE1 (similar to Europe EFF 2); d) < IE1 (low efficiency, similar to Europe EFF 3).

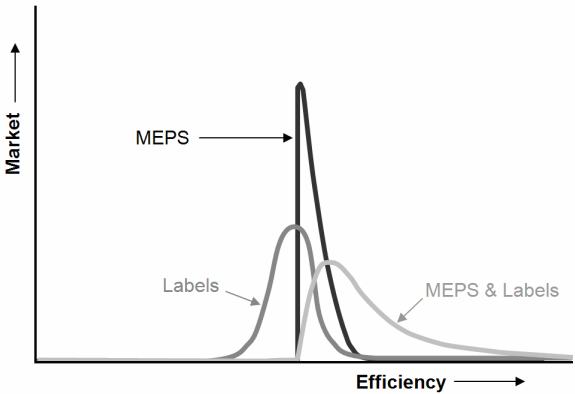


Fig. 2.14. Effects on motor market of mandatory MEPS and efficiency class labelling [2].

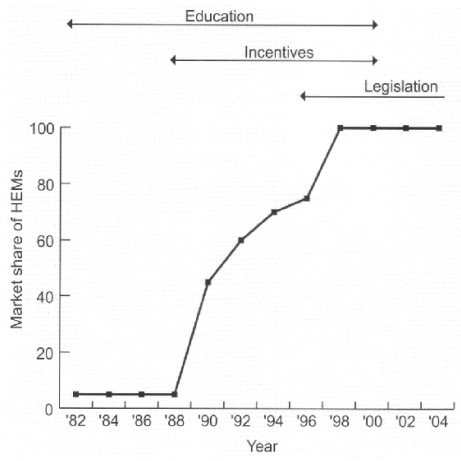


Fig. 2.15. Example of successful market transformation in Canada (British Columbia Hydro Project) [33].

In 1992, the US Congress approved the Energy Policy Act (EPAct), which granted the USA Department of Energy (DoE) the authority to set MEPS for electric motors to be manufactured or imported for sale in the USA. These mandatory standards became effective in October 1997. At the time, market sales for the EPAct level of efficiency are estimated at around 20%. In 2005,

EPAct motors constituted 54% of the integral horsepower IM market share, as it can be seen in Fig. 2.16a. Other motors include premium efficiency and non-general purpose motors. EPAct scheme applies to TEFC & ODP, single-speed IMs, with the characteristics presented in Table 2.6 [4].

TABLE 2.7
OVERVIEW OF MOTOR EFFICIENCY VOLUNTARY AGREEMENTS AND REGULATION AROUND THE WORLD [2].

Region	Mandatory Agreement & Year of Implementation	Voluntary Agreement & Year of Implementation	Market Share*
USA ^a	EPAct/High Eff./IE2, 1997; NEMA Prem./IE3, 2011.	NEMA Prem., 2001.	NEMA Prem.: 20%; EPAct: 55%. ^a
Canada ^b	EPAct/High Eff./IE2.	NEMA Prem., 2001.	NEMA Prem.: 16%; EPAct: 54%. ^b
Mexico ^b	EPAct/High Eff./IE2, 1998.	NEMA Prem., 2003.	n.a.
EU ^c	IE2, 2011 (?).	Eff. classification scheme & EFF3 market reduction, 1998.	EFF1: 9%; EFF2: 87%. CEMEP agreement members. ^c
Australia ^b	High Eff./IE2, 2006.	Prem. Eff., 2006.	Prem. Eff.: 10%; High Eff.: 32%; Std. Eff.: 58%.
New Zealand ^b	High Eff./IE2, 2006.	Prem. Eff., 2006.	n.a.
Brazil ^b	Std. Eff./IE1, 2002; High Eff./IE2, 2009.	n.a.	High Eff. (15%).
China ^{d,e}	Std. Eff./IE1, 2002; High Eff./IE2, 2007 ^d .	High Eff., 2002; Prem. Eff., 2010.	High Eff.: 10%; Std. Eff.: 90%. ^e
Korea ^b	IE2, 2008.	Std. Eff., 1996.	High Eff.: 10%; Std. Eff.: 90%.
Taiwan	IE1, 2002.	n.a.	n.a.

*Source: a) NEMA 2007, b) ICA 2005, c) CEMEP, d) SEEEM 2007, and e) ICA 2007.



Fig. 2.16. IM market in 2005: (a) USA; (b) USA vs. EU [2].

Since many of the motors sold, promoted by many utilities and industry associations, exceeded these minimum EPAct mandatory requirements/levels, and the industry continues to improve their products efficiency, NEMA felt a need to define a classification scheme for premium higher efficiency motors and, in June 2001, created a special label for IMs designated by “NEMA Premium”. The introduction of the NEMA Premium Label has resulted in a moderate market acceptance of these very efficient motors, particularly in large industrial consumers. However sales

of NEMA Premium motors appear to remain stable at around 20% for the last few years. As a result, the American Council for an Energy-Efficient Economy (ACEEE) and NEMA have agreed to propose a new set of energy efficiency standards for industrial electric motors that has been included in the Energy Independence and Security Act of 2007, approved by the US Congress in December 2007. The proposal sets higher minimum mandatory efficiency levels but also broadens the scope of existing standards, to be enforced three years after enactment, as follows. First, current minimum efficiency standards of general purpose IMs as defined in 1992's EPAct and covered by federal legislation should be raised to NEMA Premium levels (NEMA MG1 Table 12-12). Second, seven types of low-voltage, integral-horsepower IMs not currently covered under federal law should be subjected to minimum efficiency standards at the levels defined in NEMA MG1 (2006) Table 12-11. Third, general purpose IM with power ratings between 200 and 500 hp should also meet minimum efficiency levels as defined in NEMA MG1 (2006) Table 12-11 [4].

In Fig. 2.27, a comparison of efficiency levels for IE2/EPAct and IE3/NEMA Premium motors for TEFC²² motors is presented. For ODP²³ motors different efficiency levels are defined, and this type of enclosure is not used in Europe. IE3/NEMA Premium motors have about 15 to 20% lower losses than EPAct motors, which typically translate in an efficiency improvement of 1 to 4%, depending on the motor power level. The new Australian Energy Performance Program – MEPS or AS 1359.5:2004 – has efficiency levels similar to EFF 1/EPAct. This is a mandatory measure started in 2006 and applies to single-speed IMs with the characteristics shown in Table 2.10 [4].

In 1998, a voluntary agreement supported by European Committee of CEMEP and the European Commission was established and signed by 36 motor manufacturers, representing 80% of the European production of standard IMs. This agreement defined a target to promote more efficient IMs (TEFC-type). In this agreement it was decided to define the previously mentioned motor efficiency classification scheme (EFF 1, EFF 2, and EFF 3). The CEMEP/EU agreement was a very important first step to promote motor efficiency classification and labelling, together with a very effective market transformation. Based on the CEMEP/EU classification scheme there was a voluntary undertaking by motor manufacturers to reduce the sale of EFF 3 motors. The original EU target of CEMEP/EU agreement was to reduce joint sales of low efficiency EFF 3 motors by 50% after agreement period (2003). The aim was completely achieved, since EFF 3 motor sales of CEMEP members decreased from 68% in 1998 to 3% in 2006, as it can be seen in Fig. 2.17, essentially being removed from the EU IM market, which is a positive development and proved the effectiveness of the measure on market transformation. However, the penetration rate of IE2/EFF 1 high-efficiency motors was (and is) very modest and deserves to be improved. The main reason for this situation is due to the fact that original equipment manufacturers (OEMs) purchase 80% to

²² Totally Enclosed Fan-Cooled.

²³ Open Drip-Proof.

90% of the motor market sales²⁴. This large share of the market combined with the higher IE2/EFF 1 motor prices, which typically were 20 to 30% (now 15 to 25%) above IE1/EFF 2 motor prices, for both 50 Hz and 60 Hz leads to a low penetration of EFF 1 motors. Although the CEMEP/EU agreement was an important first step towards the reduction of less efficient motor sales, other countries have achieved better results by the implementation of mandatory agreements, which introduced higher minimum efficiency levels. These mandatory agreements have produced more relevant market transformations [4].

In 2007, IMs with efficiencies under IE2/EPAct (equivalent to Europe EFF 1) constituted a modest 25% of the USA motor market, while low and medium efficiency motors have a significant 91% market share in EU, as it can be seen in Fig. 2.16b. The penetration of high efficiency motors in the USA market is currently much higher than that of the EU. High efficiency and Premium motors now account for more than $\frac{3}{4}$ of motor sales in North America (USA, Canada and Mexico). Other countries around the world are taking similar initiatives [4].

This emphasizes the actual need to promote the market transformation in other countries. The 50-Hz and 60-Hz motor markets have the same key players and use the same design techniques and materials. Market transformation has been initiated mostly in 60-Hz markets and lessons learned may influence the 50-Hz markets. Moreover, whereas in North America NEMA Premium motors are easily available, in Europe IE3/Premium 50-Hz motors are not yet available for all power levels.

Actually, 4-pole 50 Hz IE3/Premium motors are now being introduced by some European manufacturers, covering the 7.5 to 75 kW power range. The typical average price premium of IE3/Premium motors in relation to IE2/EFF 1 motors is estimated to be around 15% and 10% for 50 Hz and 60 Hz, respectively, depending on individual motor. However, it should be emphasized that in the low power range (up to about 5.5 kW), some IE3 motors can require larger frame sizes than standardized in the EN50347 or IEC60072-1 standards, even considering the use of copper-cage rotor technology. In principle, in the medium-high power range the standard frame sizes can be kept, but for some sizes copper-cage rotors are required.

An IE4 super-premium class (up to 30 kW) is under consideration, both for line-fed motors and inverter plus motor units. However, feasibility limitations can exist. Some European manufacturers see no technical feasibility to reach IE4 levels with induction motor technology with the same frame sizes as IE1/IE2. Very high efficiency motors with permanent-magnet rotor technology are being introduced which allow reaching IE4 levels.

²⁴ In 1994, since electrical engineering sector market accounts for 60% of all copper used, German Copper Institute (DKI), decide to investigate the reasons for the relatively low penetration of HEMs in the market, since they were actually available since 1985. It was found that one of the main reasons for that is the fact that about 80% of all standard IMs and VSDs are sold to OEMs, who have no real incentive to buy the more expensive HEMs, as they manufacture but do not use the equipment into which the motors are built.

There are no motor efficiency voluntary agreements or minimum efficiency standards regulation regarding motors other than IMs. Single-phase induction motors are subject of voluntary labelling schemes in Brazil, India and Mexico.

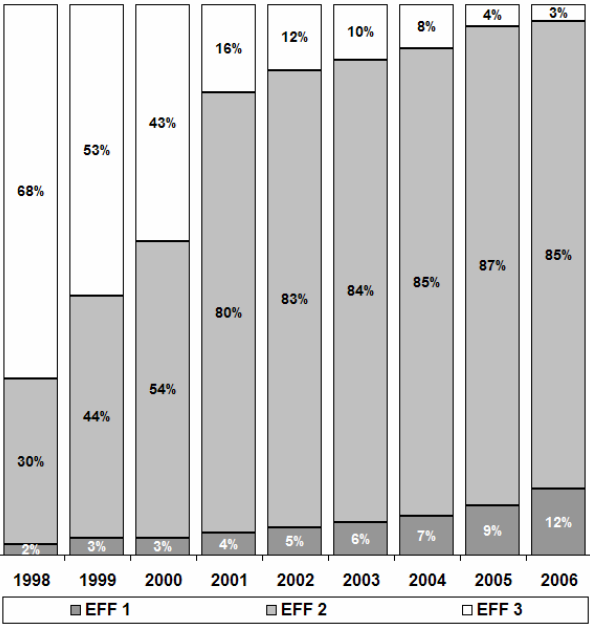


Fig. 2.17. Total motor sales of CEMEP members in the scope of the Voluntary Agreement of CEMEP-EU in the period 1998-2006 (CEMEP, 2008).

In order to compare efficiency requirements, it must be considered that different test methods are used in the assessment of the efficiency of the motor. These test methods can produce significantly different results and therefore the comparison of efficiency levels is not possible straightforwardly. Furthermore, measurement tolerances vary in the different test methods, and the impact of the supply frequency (50 Hz or 60 Hz) used during the test on the final test results complicates things further. The efficiency measurements using IEEE 112-B or the old IEC 60034-2 standards lead to different results, as evidenced previously.

Fig. 2.19 presents a comparative assessment of different efficiency levels associated with MEPS and voluntary agreement classification schemes, in which the 60-Hz motor data was converted to 50-Hz (Fig. 2.18) and adjustments were made when needed to take into account typical values for SLLs [14]. As it can be seen, current IE2/EFF 1 motors, under the CEMEP/EU agreement, are roughly on the same efficiency level as EPAct and Aus/NZ MEPS compliant motors. NEMA Premium and Australian/New Zealand high efficiency levels are equivalent to IE3.

As it is possible to see from the previous section, several different energy efficiency levels/classes are currently in use around the world, increasing potential confusion and creating market barriers. For the manufacturers this is a problem because they design motors for a global market. That is why IEC is proposing the IEC 60034-30 standard.

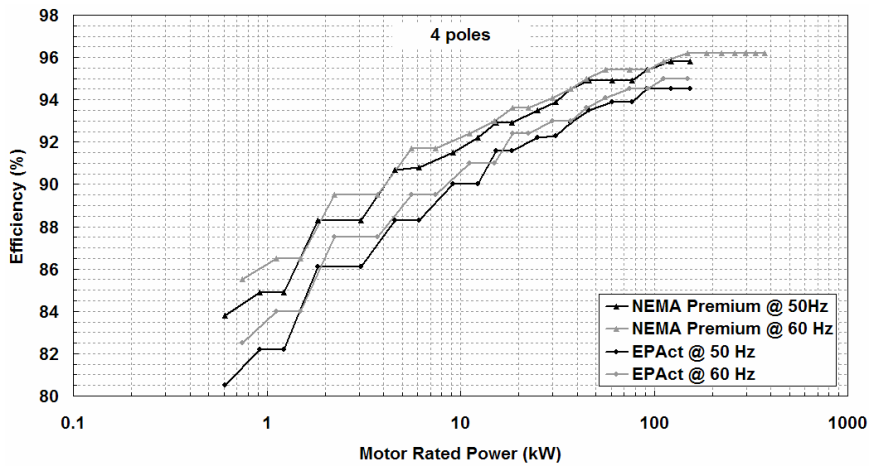


Fig. 2.18. NEMA and EPAAct minimum efficiency requirements for 60 & 50 Hz [2].

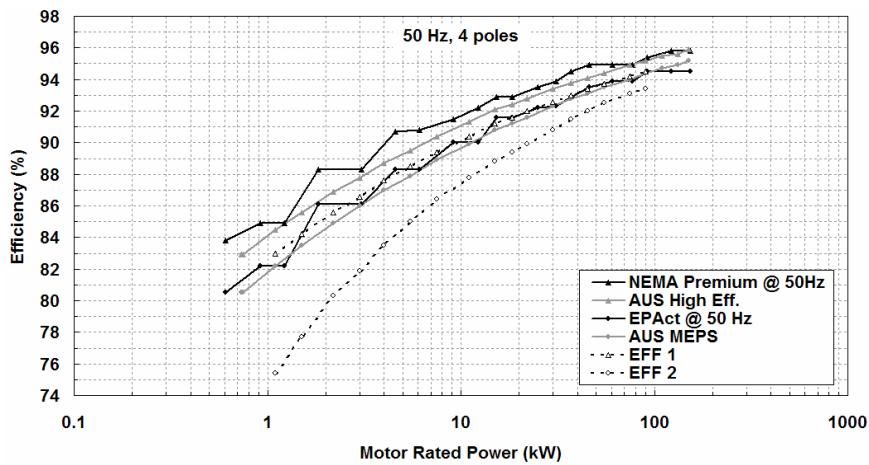


Fig. 2.19. Comparison of minimum efficiency requirements in different parts of the world [2].

2.3.3 Minimum Motor Efficiency Requirements Impact in the EU

Regarding the EU, a study on the introduction of MEPS, based on IEC 60034-30 classification scheme, was carried out. The compliance of MEPS for motors can be, at least in an initial period, based on self-verification by the manufacturers, using the new IEC standards for efficiency testing and classification, including the allowable tolerance levels. Mechanisms can be developed to discourage non-compliance.

Four scenarios for possible implementation of market regulatory measures in the period 1998-2020, defined in Table 2.8, were considered, and the resultant evolution of the motor stock for the industrial sector, shown in Fig. 2.20, was analyzed.

First, business as usual (BAU), based on the information collected and the evolution of the electricity consumption in the EU. The 1998 (base year) installed electric motor base is conservatively assumed to be divided by efficiency level according to the sales in that year. The motor stock in 1998 was based in previous studies and in the period 1998-2020 the evolution of motor sales in this scenario was made according to the evolution of the electricity consumption in the respective sectors. In the period 1998-2005 the sales by efficiency class were considered. After 2005 the sales by efficiency class are considered to remain stable. In Scenario I, IE3 class motors

are considered not to have an important market penetration (constant 2% of new motors sold). In all scenarios, a residual number of sales (15%) of motors under the IE1 class are maintained to take into account special purpose motors that fall out of the product definition.

Fig. 2.21, summarizes the results, which show that the implementation of minimum efficiency levels for motors sold in the EU from 2011 forward would result in a saving of 14 TWh/yr of electricity for Scenario I, of 17 TWh/yr for Scenario II and of 19 TWh/yr for Scenario III, in the year 2020. It should be emphasized that these figures do not show the total savings potential, since the full impact of MEPS with IE2 level would only be achieved in 2030, as the stock rotation initiated in 2011 will take 20 years to be completed. A similar reasoning can be applied to the potential impact of IE3 MEPS, which if initiated in 2015 would take an additional 20 years to be completed. If the current electricity production methods remain unchanged, this electricity savings would translate in the reduction of GWP emissions by 8.8 Mt/yr of CO_{2eq} in 2020. Larger savings are possible by promoting the replacement of old inefficient motors when they fail by IE2 or IE3 motors.

TABLE 2.8
IMPLEMENTING DATES FOR POSSIBLE MEPS FOR IMS MANUFACTURED IN OR IMPORTED INTO THE EU.

Motor Power Range: 0.75-200 kW	Efficiency level to be met or exceeded	
	Before/After Jan. 1, 2011	Before/After Jan. 1, 2015
Date of implementation	Before/After Jan. 1, 2011	Before/After Jan. 1, 2015
Business as Usual (BAU)	BAU/BAU	BAU/BAU
Scenario I	BAU/IE2	IE2/IE2
Scenario II	BAU/IE2	IE2/IE3 ($P_N \geq 7.5$ kW) ²⁵
Scenario III	BAU/IE2	IE2/IE3

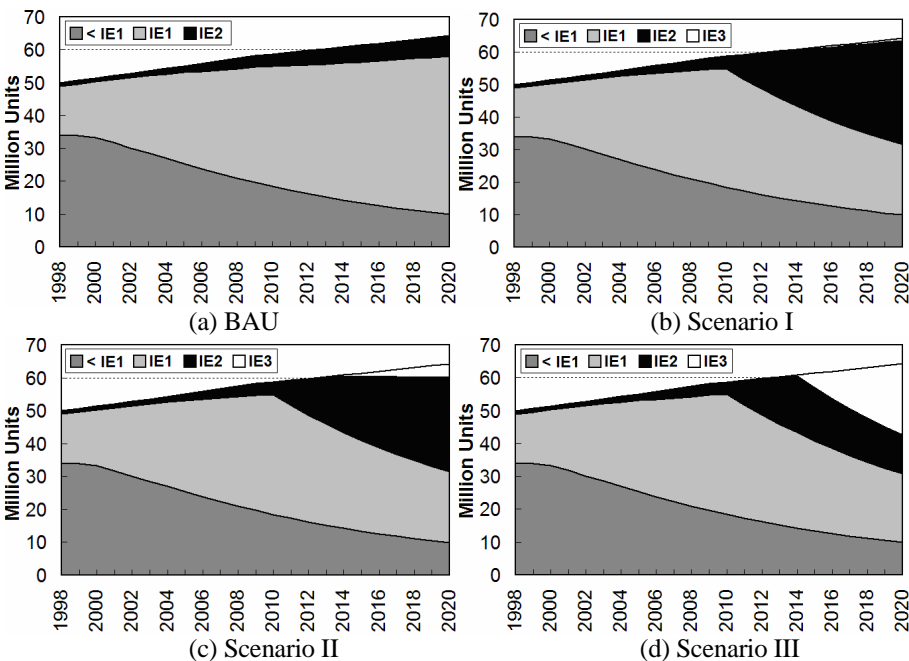


Fig. 2.20. Evolution of the motor installed base in Industry.

²⁵ According to a number of European manufacturers, IEC-frame sizes may not allow achieving IE3 efficiency levels for small IMs (e.g., below 7.5 kW), without increasing the frame size, even if using more expensive copper-cage rotor IMs.

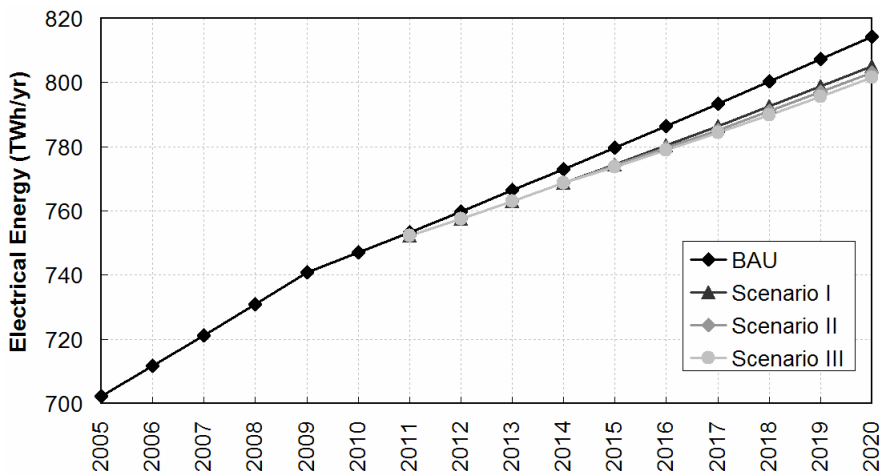


Fig. 2.21. Evolution of the annual electricity consumption in the Industry.

2.4 Study on Eco-Design of Electric Motors

The use-phase cost of most electric industrial motors, including the consumed energy and maintenance costs, dominates by far their overall life-cycle cost (LCC). As a consequence of the Energy-Using Products (EuP) Directive 2005/32/EC of the European Parliament and of the Council, a preparatory study to identify and recommend ways to improve the life-cycle environmental performance of electric motors at their design phase was carried out.

This study addresses several key issues in the EU, namely: a) Motor market characterisation; b) Relevant environmental aspects of the products and their technical/economical potential for improvement; c) Existing relevant legislation and self regulation by industry and standards; d) LCC assessment of average or base-case technology (BCT); e) Technical analysis of the best available technologies (BAT) and of the best next available technologies (BNAT); f) Scenario, policy, impact and sensitivity analysis.

A well-known analysis methodology (named MEEUP²⁶ [7]) for assessment of environmental impact and eco-design of energy using products was used, outlined in Fig. 2.22.

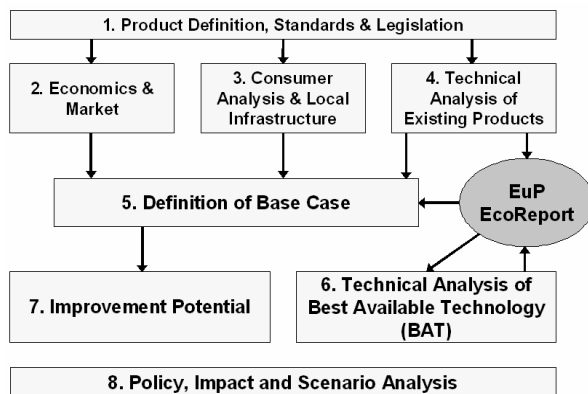


Fig. 2.22. Methodology for Eco-design of Energy-Using Products (EuP).

²⁶ MEEUP - Methodology for Eco-design of Energy-Using Products.

To apply this analysis methodology/tool, several preliminary assumptions were defined for the particular case of electric motors. This section focus is on the LCC assessment of BCT, which are considered to be IE1 (EFF 2 adjusted) motors, and of the BAT, which includes IE2 (EFF 1 adjusted) and IE3 (equivalent to NEMA Premium) motors.

2.4.1 Some Relevant Assumptions

On the basis of the foregoing information, in the presented analysis, only IMs are considered, since they represent, by far, the majority of the electric motors' market.

The study also addressed new motor technologies (e.g., permanent magnet motors, IM-VSD integrated units, etc.), which may have advantages in some applications, but those results are not presented here.

According to the MEEUP methodology, primary and secondary performance parameters were defined on the basis of the functional aspects of the product considered. The product "electric motor" is defined as a device that converts electric energy into mechanical energy. The assumed primary functional parameters are the output power (the provided mechanical/shaft power in kW) and the speed (or number of poles). The torque is also a key functional parameter but it is directly related to the above-mentioned quantities. The assumed main secondary functional parameter is the motor efficiency class/nominal efficiency.

IMs larger than 5 kW are normally repaired when they fail. For small motors it is in general not economical to repair them. An IM is normally repaired at least 2 times during its lifetime but, in some cases, it can be repaired up to 4 times [15]. Typically, the repair process includes rewinding and bearing replacement. A value of 2.5 repairs is assumed for IMs over 5 kW operating 8000 hour/year, but under 5 kW no repairs are considered. For the sake of simplicity, it is assumed that the number of repairs decreases linearly with the decrease of the operating time.

Regarding material recycling at end-of-life, it is considered that 5% is not recovered (landfill), 1% of the plastics are re-used (closed loop recycling), 9% of the plastics are recycled, 90% of the plastics are thermal recycled (non hazardous incineration optimized for energy recovery), and 95% of metals are recycled.

The study covered power range of 0.75 to 200 kW (1 to 275 hp) considering three base-case motors, corresponding to different output powers, 1.1 kW, 11 kW and 110 kW, all being IE1 motors, which corresponds to 85% of IMs sold by CEMEP members in Europe in 2006.

The considered motor efficiency values are presented in Table 2.9. Four scenarios are considered in terms of operating hours: 2000, 4000, 6000, and 8000 h/yr. The base scenario of 4000 h/yr is used for the presented eco-analysis. A 60% load factor is considered for all motors. 12, 15 and 20 years lifetime for the 1.1-, 11-, and 110-kW motors, respectively, are considered.

In terms of motor price distribution, the average list price of a motor ranged from typically 160 €²⁷ for a 0.75-kW, EFF 2-class IM, to 15000 € for a 200-kW, EFF 2-class IM [36]. In general the market is very competitive with large discounts offered to OEMs. At higher power ratings there are lesser pressure, as the degree of competition is not considered as fierce. For this study an average 40% discount below list price is assumed. The cost of an IE2/EFF 1 motor is estimated at around 20 to 30% higher cost than an EFF 2 motor, which accounts for the vast majority of sales in the market. Prices for IE3/Premium motors can be as much as 40 to 60% higher than the price of an EFF 2 motor. As the rated power grows the difference is attenuated. The average electricity price for a European industrial consumer 0.0754 €/kWh was considered.

The LCC and the total annual consumer expenditure in EU, for the three analyzed base-case models, were also computed. In all LCC calculations a discount rate (interest minus inflation [4]) of 2% is considered.

TABLE 2.9
MOTOR FULL-LOAD EFFICIENCY VALUES CONSIDERED IN THE STUDY.

Motor Efficiency Class	Motor Rated Power		
	1.1 kW	11 kW	110 kW
IE1	75.1%	87.6%	93.3%
IE2	82.7%	90.2%	94.5%
IE3	85.3%	91.7%	95.4%

2.4.2 Evaluation of Environmental Impact and Life-Cycle Costs

The study collected data from several sources, [14], [15], [36], considered relevant for the evaluation of the environmental impact and of the LCC both for individual products and for the EU stock. These models will provide the reference for the assessment of environmental and technical/economical improvements, to be established further on. To evaluate the base-case motors environmental impact, a reporting software tool named VHK EuP EcoReport is used [5].

Table 2.10 presents percentage of use-phase environmental impact of IE1 motors, considering a loss-based environmental impact analysis. It should be noted that the use phase clearly has the most impact, completely dominating the life-cycle impact of the product.

For analysis of the BAT, IE2 and IE3 motors are analyzed in order to evaluate the potential for improvement. IE2 motors are high efficiency products, whose sales have grown in recent years, as shown previously. In a way similar to NEMA Premium definition in USA, IE3 motors are estimated to achieve 15 to 20% lower losses compared to IE2 efficiency levels [33].

Table 2.11 presents the environmental impact associated with the replacement of IE1 (base-case) by BAT motors (IE2 & IE3 motors), considering only the use phase.

²⁷ 1 € (EURO) = 1.4705 \$ (USD), January 25, 2008.

It should be noted that in Tables 2.10 and 2.11 a loss-based environmental impact analysis is presented because electric motors are defined as “energy converters” and not as “end-use device”. Only the motor losses are really consumed inside the motor, with the remaining consumed energy being transmitted as mechanical power.

Fig. 2.23 shows the LCC as a function of motor rated power, considering different efficiency classes and number of operating hours. In all the presented LCC analysis, the total consumed energy is considered. Fig. 2.24 shows the LCC as a function of the operating time, considering different efficiency classes, motor rated powers and electricity prices.

TABLE 2.10
USE-PHASE IMPACT OF IE1-CLASS MOTORS CONSIDERING ONLY LOSSES [2], [3], [4].

4000 h/year scenario	Motor Rated Power		
	1.1 kW	11 kW	110 kW
Main Indicators			
Total Energy	99.08%	98.84%	98.59%
Of which, Electricity	99.87%	99.85%	99.83%
Water (process)	98.01%	97.77%	97.63%
Waste, non-hazardous/landfill	74.68%	62.26%	56.39%
Waste, hazardous/incinerated	87.63%	91.61%	93.64%
Emissions to the Air			
Greenhouse Gases in GWP100	98.55%	98.23%	97.83%
Acidification Agents	97.65%	96.01%	95.12%
Volatile Organic Compounds	94.50%	93.71%	91.09%
Persistent Organic Pollutants	72.25%	68.66%	65.78%
Heavy Metals	81.79%	77.04%	73.94%
Polycyclic Aromatic Hydrocarbons	82.98%	82.49%	74.57%
Particulate Matter, dust	69.98%	77.09%	60.31%
Emissions to the Water			
Heavy Metals	77.55%	74.57%	71.87%
Eutrophication	26.13%	26.78%	28.04%

TABLE 2.11
LOSS-BASED ENVIRONMENTAL IMPACT VARIATION (BAT vs. IE1) [2], [3], [4].

4000 h/year scenario	Motor Rated Power					
	1.1 kW		11 kW		110kW	
BAT Efficiency Class	IE2	IE3	IE2	IE3	IE2	IE3
Total Energy	-36%	-49%	-23%	-35%	-19%	-32%
Of which, Electricity	-37%	-50%	-23%	-36%	-19%	-33%
Water (process)	-36%	-49%	-23%	-35%	-18%	-32%
Waste, non-hazardous/landfill	-16%	-20%	-3%	8%	-11%	-2%
Waste, hazardous/incinerated	-32%	-44%	-21%	-33%	-18%	-31%
Emissions to the Air						
Greenhouse Gases in GWP100	-36%	-49%	-22%	-34%	-18%	-31%
Acidification Agents	-35%	-47%	-21%	-31%	-18%	-30%
Volatile Organic Compounds	-34%	-45%	-20%	-30%	-17%	-27%
Persistent Organic Pollutants	-17%	-22%	-8%	-7%	-7%	-5%
Heavy Metals	-26%	-35%	-14%	-18%	-13%	-17%
Polycyclic Aromatic Hydrocarbons	-27%	-36%	-15%	-19%	-28%	-35%
Particulate Matter, dust	-22%	-30%	-15%	-11%	-11%	-13%
Emissions to the Water						
Heavy Metals	-26%	-34%	-14%	-20%	-14%	-19%
Eutrophication	-5%	-6%	-1%	2%	-3%	3%

As it would be expected, the results show very significant reduction of the LCC for the low power motors, with savings reaching more moderate levels as the motor power increases. Most of the improvement occurs when the efficiency level moves from IE1 to IE2, but a noticeable improvement can still be seen when the efficiency level reaches the IE3 level. Moreover, the higher the motor rated power the lower the influence of the operating hours on the LCC reduction. Although the prices of IE2 and IE3 motors are considerably higher than those of IE1 motors, a reduction in LCC is achieved in all cases for a fairly reduced number of operating hours per year – around 2000 h/yr for the scenario of the lowest electricity prices. Moreover, as expected, the LCC as a function of the motor cost (or investment), tends to “saturate”, evidencing the decreasing of the economical benefits of high-efficient motors for high power ratings, as it can be seen in Figs. 2.25 and 2.26.

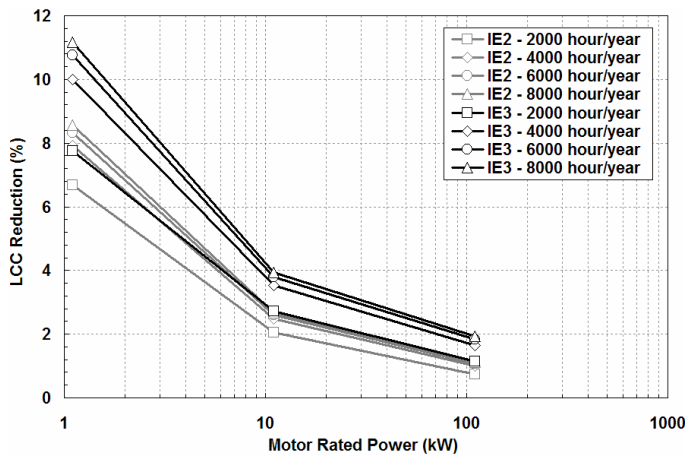


Fig. 2.23. LCC reduction as a function of motor rated power (BAT vs. IE1) [2], [3], [4].

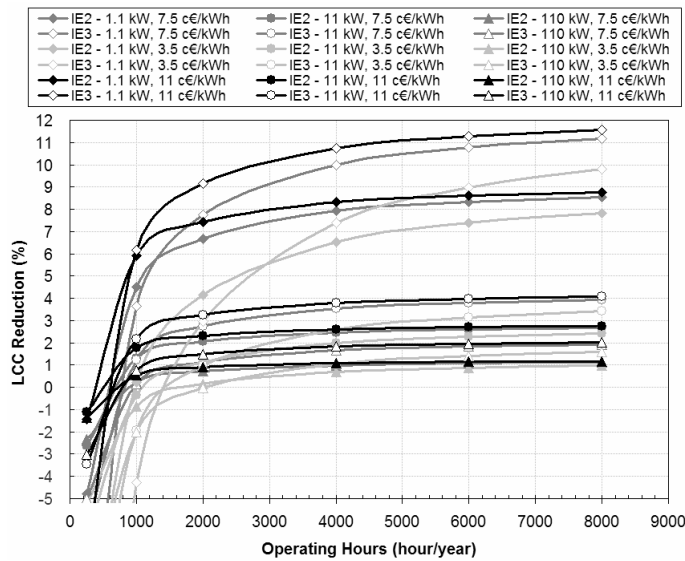


Fig. 2.24. LCC reduction as a function of operating hours (BAT vs. IE1) [2], [3], [4].

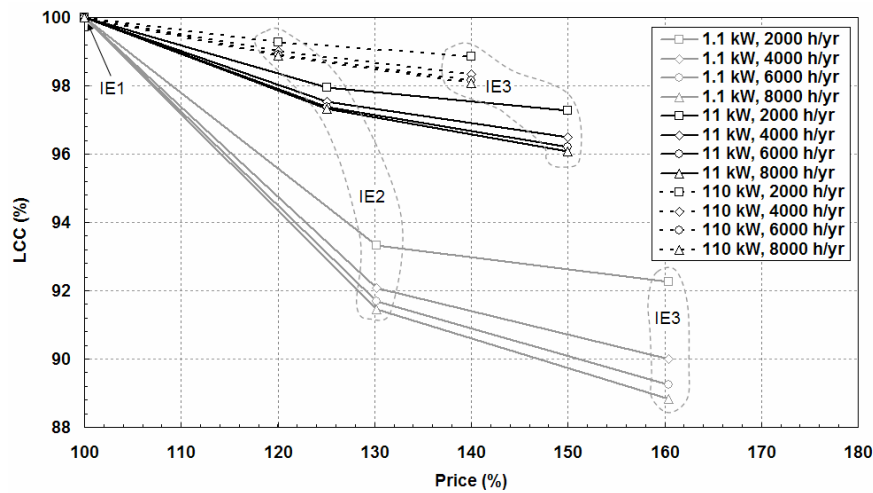


Fig. 2.25. Percentage LCC as a function of percentage motor price, for 7.5 c€/kWh.

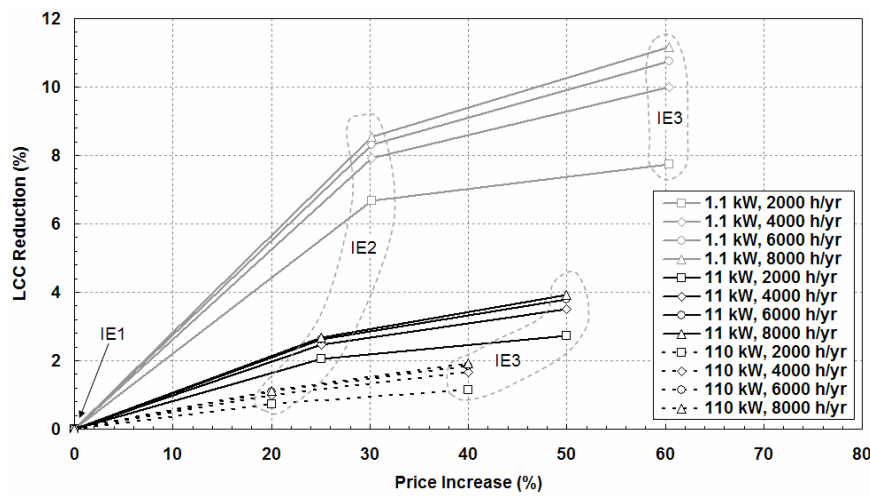


Fig. 2.26. LCC reduction as a function of motor price increase, for 7.5 c€/kWh.

2.5 Automatic Systems for Motor Efficiency Measurement

As previously discussed, direct methods are generally more accurate, but its use has not been widespread around the world due, in part, to the need to minimize the costs associated with setting up the testing laboratories. Therefore, on the scope of the efficiency measurement standards, it is important to develop accurate and quick motor testing systems to short the time, and thus the cost, spent by motor manufacturers on performance testing activities. In order to contribute to that aim a computer controlled high-precision full-automated electric motor testing facility was developed, providing a suitable framework for testing the behaviour of electric motors under different conditions, as well as it provides a good introduction to automatic testing stations. A brief description is given in this section, and additional information is provided in Appendix 6.

The developed motor testing facility is able to perform automatically or manually a quick and accurate no-load to full-load analysis of low-voltage electric motors (up to 5.5 kW) including the measurement of efficiency (direct and indirect methods), power factor, speed, torque, external and internal operating temperatures, currents, voltages, real power and reactive power, according to the

main motor testing standard. The efficiency according to IEEE 112-B, IEC 60034-2 (Ed. 2), and IEC 60034-2-1 standards can be determined automatically, fulfilling the instrumentation accuracy requirements. The system control is made by means of user-friendly software. The standards procedures automatic implementation is significant faster than the manual/visual implementation, which requires the reading of the measure devices and introduction of values in a calculation sheet. The execution period is about 4 minutes, after the motor thermal stabilization, significant lower than the 15 minutes typically required by manual implementation. Furthermore, one of the main arguments used by manufacturers to avoid direct method is the cost associated with direct methods when considering a huge amount of IMs being tested, but this barrier is potentially eliminated by the proposed system, which is an important advantage. Of course the capital investment for such test bench can be large for higher power ranges. Additionally, the possible human reading errors are eliminated. In the performed tests similar results were obtained with manual and automatic implementation of the tests. An important advantage is the user-friendly interface and the efficient graphical analysis of results generated by computer.

This system can be upgraded to allow electric motor system regeneration testing, by means of incorporating a high-inertia wheel, a DC motor or a VSD-fed IM, and a shaft torque sensor. This is very important to test multi-quadrant VSDs, e.g., used in lifts and electric vehicles.

2.6 Motor System Efficiency Improvement

The decision to buy a product in the global competition is increasingly being influenced by the follow-up cost arising from the LCC, including disposal of the product, and no longer only by the initial investment cost. Considerations on the LCC of ownership will become more and more important in particular for the drive engineering components of a machine or system. Compared to the overall investment in a system, the investment costs for electrical drives certainly only makes sense for a small percentage, as previously referred. But the chosen technology decisively influences the follow-up costs. This is why the choice of the motor has a great cost-saving potential. Factors such as functionality and efficiency during operation, service and maintenance cost, as well as follow-up cost resulting from scheduled and unscheduled downtimes, are often underestimated. The high-quality product solutions allow to significantly reduce system LCC, making a sustainable contribution to the reduction of CO₂ emissions and thus to actively protect our environment. High-reliability product solutions lead to higher system availability and less maintenance costs.

According to [8], the estimated savings potential for industrial electrical energy use is about 2-8% for high-efficiency motors and 5-20% for VSDs, and 30-60% for optimized systems,

evidencing the importance of the overall system optimization, instead of one part or module optimization.

Electric motor driven systems (EMODS) integrate several different modules or equipments, namely power supply, command and protection devices (minor impact on system efficiency, AC or DC electric motors, mechanical transmission units, and end-use devices or load. Optionally, EMODS can integrate electronic control devices (AC/AC or AC/DC converters). In Fig. 2.27, a diagram of an EMODS can be seen. Command and protection devices have minor impact on system efficiency, thus being neglected in the performance analysis. Nowadays, brushed DC motors and AC/DC converters are rare. AC/AC converters can be VSDs or voltage regulators (VRs). As shown in Chapter 5, a star/delta connection management device can also be considered, although not interfering directly in the power line, since they act at contactors level (command and protection devices), influencing only the motor efficiency and load, thus this solutions should be considered as an improved motor with a change in the efficiency curves as a function of load. The consumption of such control devices should also be taken into account.

The efficiency of a motor driven process depends upon several factors which may include motor efficiency, motor speed controls, power supply quality, system oversizing, distribution network, mechanical transmission, maintenance practices, load management and cycling and efficiency of the end-use device (e.g., fan, pump, etc.).

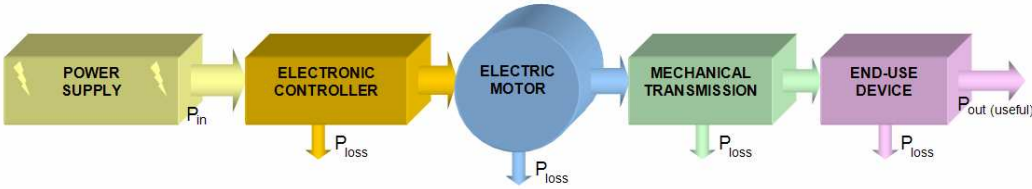


Fig. 2.27. Diagram of an electric motor driven system integrating an electronic controller, an electric motor, mechanical transmission, and an end-use device or load.

The overall efficiency of an EMODS is given by product of the individual system module efficiency. For a system with m components with efficiency η_i at load ζ_i , the overall efficiency is given by (2.4). Considering the efficiency dependency on load for each system module, as in (2.5), (2.6), and (2.7), it can be concluded that, if no changes are made in the equipment of a system its overall efficiency actually depends on the end-use device load, corresponding to a specific system operating point. The system speed at the mechanical side and the voltage frequency and amplitude are also variables that have to be taken into account since they have a strong impact on the load and efficiency of the modules. Additionally, the power quality can also influence significantly the electronic controller and the motor efficiency, being a very important aspect.

$$\eta_{\text{sys}} = \prod_{i=1}^m \eta_i(\zeta_i) \quad (2.4)$$

In Fig. 2.28, the plot of the efficiency for a system with two components A and B as a function of the components efficiency, showing that the highest efficiency is achieved when the efficiencies of both components are equal. For example, assuming a base case of $\eta_A = \eta_B = 0.5$, the increase of η_A to 1.0 (50 p.p. increase) gives a total efficiency $\eta_{\text{sys}} = 0.5$, but increasing η_A and η_B to 0.75 (25 p.p. increase in each module) gives $\eta_{\text{sys}} = 0.5625$. Assuming equipments with same cost per efficiency increase, the second scenario is the most advantageous.

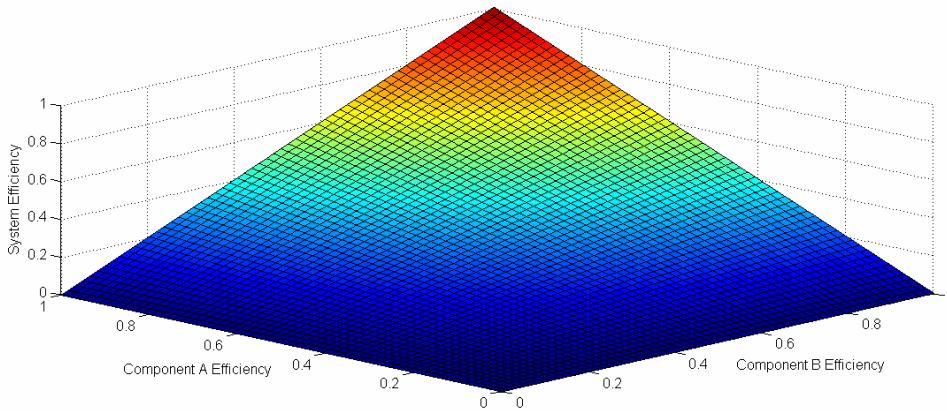


Fig. 2.28. Efficiency of a system with two components A and B as a function of the components efficiency.

$$\eta_{\text{sys}} = \eta_{ec}(\zeta_{ec}) \cdot \eta_{mtr}(\zeta_{mtr}) \cdot \eta_{trs}(\zeta_{trs}) \cdot \eta_{load}(\zeta_{load}) \quad (2.5)$$

$$\zeta_{trs} = f(\eta_{load}, \zeta_{load}) \quad \zeta_{mtr} = f(\eta_{trs}, \zeta_{trs}) \quad \zeta_{ec} = f(\eta_{mtr}, \zeta_{mtr}) \quad (2.6)$$

$$\eta_{\text{sys}} = f(\zeta_{load}) \quad (2.7)$$

Due to the dependency between efficiency and load of each module, the sizing and savings have to be calculated iteratively (if the efficiency curves are known) or using simulations (if the models are known). For example, if the end-use device efficiency increases for the same output after implementing a particular measure, the required mechanical power will be lower and, therefore, the motor will experience a change in its load, leading to a different efficiency level. The motor input power has to be recalculated on the basis of those changes, and, therefore, the VSD load inherently changes, leading to a change in its efficiency, and so on. Considering now that a standard motor is replaced by a high-efficiency motor, it is likely to occur a speed increase, which increases the power required by the end-use device. This will change the system operating point, thus changing its overall efficiency. Concluding, it is necessary to study the motor system as a whole and iteratively considering the interdependency of all variables including torque, speed,

load, frequency, voltages and currents. Although complex and perhaps impracticably in some systems, a more complete analysis actually integrate the power source size and cables losses and voltage drops and the impact of those phenomena on other sensible equipment. Power factor should also be quantified, since it has an associated cost. Possible reductions in the contracted power resulting from power reductions after motor system improvements should also be taken into account. Nevertheless, for the sake of simplicity of economical evaluations, those factors are typically not considered in the savings calculations.

In order to optimize the investment in a system, the share of investment in each module should be evaluated. For example, considering a system with two components A and B, with base efficiencies η_{A0} and η_{B0} , efficiency increase $\Delta_{\eta A}$ and $\Delta_{\eta B}$, and efficiency increase cost a and b (in €/p.p., assumed to be constant²⁸) the additional investment, Δ_{cost} , is given by (2.8). The efficiency increase cost, c_{η} , is calculated by (2.9).

In Fig. 2.29, the increase in the system efficiency, as a function of the efficiency increase of its components, on the basis of (2.9), can be seen, considering different values of a , b , η_{A0} , and η_{B0} , evidencing the most advantageous investment strategy.

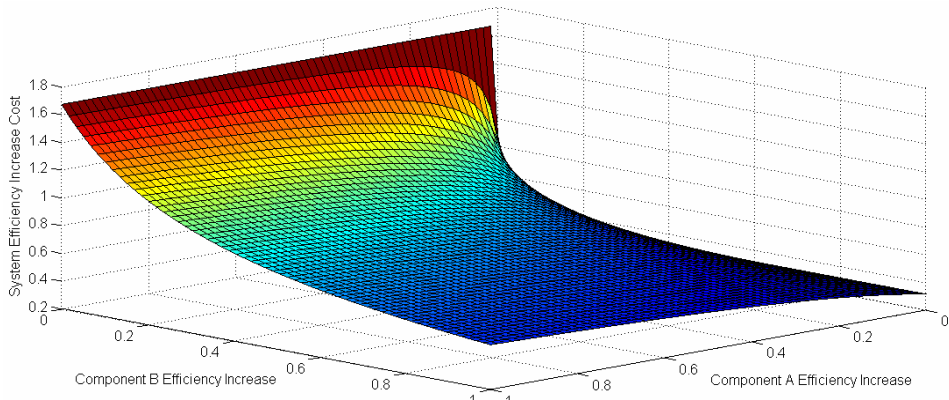
It can be concluded that the investment priorities should depend on the actual modules efficiency and on the efficiency increase cost of each module. For the same actual efficiency and efficiency increase cost, the investment should be equally shared, as it can be seen in Fig. 2.29d. Graphically, the optimum investment share corresponds to the easiest way (with less increase in system cost axis) from the point (0,0) to the point (1,1) of the horizontal plan axes.

$$\Delta_{cost} = \Delta_{costA} + \Delta_{costB} = a \cdot \Delta_{\eta A} + b \cdot \Delta_{\eta B} \quad (2.8)$$

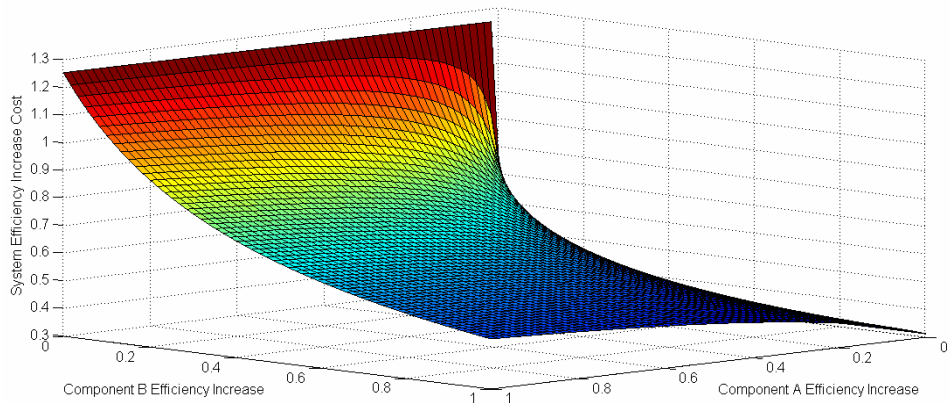
$$c_{\eta} = \frac{\Delta_{cost}}{\Delta_{\eta}} = \frac{a \cdot \Delta_{\eta A} + b \cdot \Delta_{\eta B}}{\Delta_{\eta A} \cdot \eta_{B0} + \Delta_{\eta B} \cdot \eta_{A0} + \Delta_{\eta B} \cdot \Delta_{\eta A}} \quad (2.9)$$

System integrated improvement is the most advantageous approach. In fact, it is more advantageous to invest in order to achieve a moderate efficiency increase in all modules instead of investing in a very high efficiency in only one module, remaining the other modules with a poor efficiency.

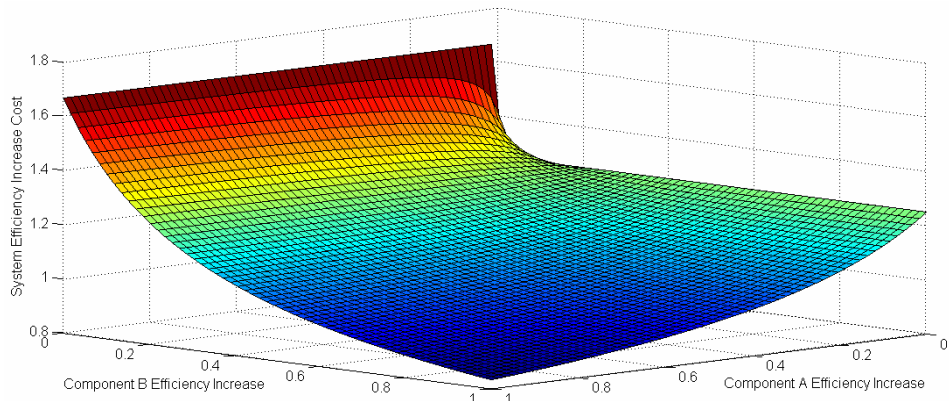
²⁸ In fact, for most systems, a and b are not constant, being a function of the rated power and efficiency level.



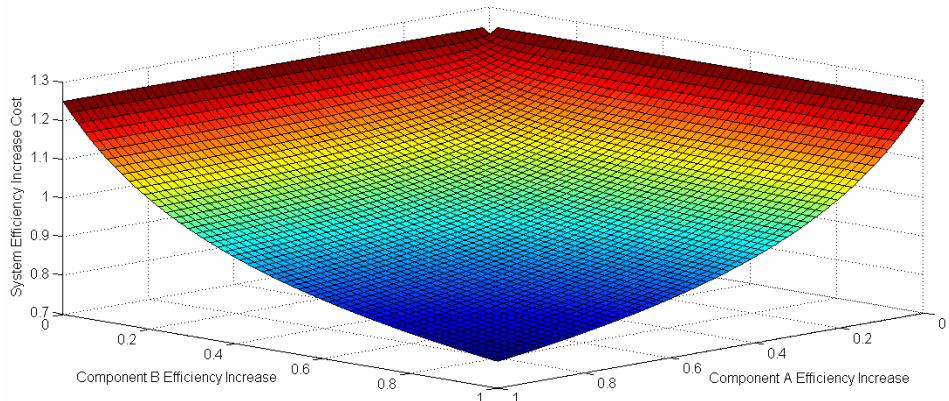
(a) $a = 1; b = 0.25; \eta_{A0} = 0.8; \eta_{B0} = 0.6$.



(b) $a = 1; b = 0.25; \eta_{A0} = 0.8; \eta_{B0} = 0.8$.



(c) $a = 1; b = 1; \eta_{A0} = 0.8; \eta_{B0} = 0.6$.



(d) $a = 1; b = 1; \eta_{A0} = 0.8; \eta_{B0} = 0.8$.

Fig. 2.29. System efficiency cost as a function of the efficiency increase of its components.

The available capital should be invested in the most advantageous way. For example, in a system with two modules, A and B, with 50% efficiency (resulting a 25% system efficiency), if the increase of the efficiency of each module is 100 €/per each additional 12.5 efficiency percentage points, the user can invest 200 € to increase either module B or module A efficiency to 75%, yielding a 37.5% system efficiency, or invest 100 € in each module simultaneously, yielding a 39.1% system efficiency. The last hypothesis is the most advantageous for the same investment, with a 1.6 percentage points gain. This can be demonstrated mathematically as follows.

Assuming that the overall system efficiency is given by (2.10), where $\Delta\eta_{\epsilon}$ is the percentage points increase in efficiency per € of additional investment (in p.p./€, assumed to be constant, for the sake of simplicity), and x is the additional investment.

$$\eta_{\text{sys}} = (\eta_{A0} + x_A \cdot \Delta\eta_{\epsilon A}) \cdot (\eta_{B0} + x_B \cdot \Delta\eta_{\epsilon B}) \quad (2.10)$$

The total additional investment, x_{total} , is given by (2.11).

$$x_{\text{total}} = x_A + x_B \quad (2.11)$$

Therefore, (2.10) can be written as a function of x_A and x_{total} , yielding (2.12).

$$\eta_{\text{sys}} = (\eta_{A0} + x_A \cdot \Delta\eta_{\epsilon A}) \cdot (\eta_{B0} + (x_{\text{total}} - x_A) \cdot \Delta\eta_{\epsilon B}) \quad (2.12)$$

The operating cost of the system, OC_{sys} , is given by (2.13), where K is a constant depending on the number of operating hours, electrical energy price and output power. In a simplified form, the LCC of the system can be given by (2.14), where X_0 is the base investment.

$$OC_{\text{sys}} = K \cdot \eta_{\text{sys}}^{-1} \quad (2.13)$$

$$LCC = X_0 + OC_{\text{sys}} + x_{\text{total}} \quad (2.14)$$

Considering fixed base and additional investment, the optimal investment share is that maximizing the total system overall efficiency, corresponding to the solution of (2.15).

$$\frac{d\eta_{\text{sys}}}{dx_A} = 0 \quad (2.15)$$

Solving (2.15), yields $x_A = \frac{1}{2} x_{\text{total}}$, with $\eta_{B0} \cdot \Delta\eta_{\epsilon A} = \eta_{A0} \cdot \Delta\eta_{\epsilon B}$, which is valid for $\eta_{A0} = \eta_{B0}$ and $\Delta\eta_{\epsilon A} = \Delta\eta_{\epsilon B}$. For example, the maximum system efficiency for $x_{\text{total}} = 200$ €, $\eta_{A0} = \eta_{B0} = 0.5$, and $\Delta\eta_{\epsilon A} = \Delta\eta_{\epsilon B} = 0.125$ p.p./€ is:

$$\eta_{\text{sys}} = \left(\eta_{A0} + \frac{x_{\text{total}}}{2} \cdot \Delta\eta_{\epsilon A} \right) \cdot \left(\eta_{B0} + \frac{x_{\text{total}}}{2} \cdot \Delta\eta_{\epsilon B} \right) = \left(0.5 + \frac{200}{2} \cdot 0.125 \right)^2 = 0.3906.$$

In Fig. 2.30, the system efficiency as a function of the investment in module A, for the given example, is shown.

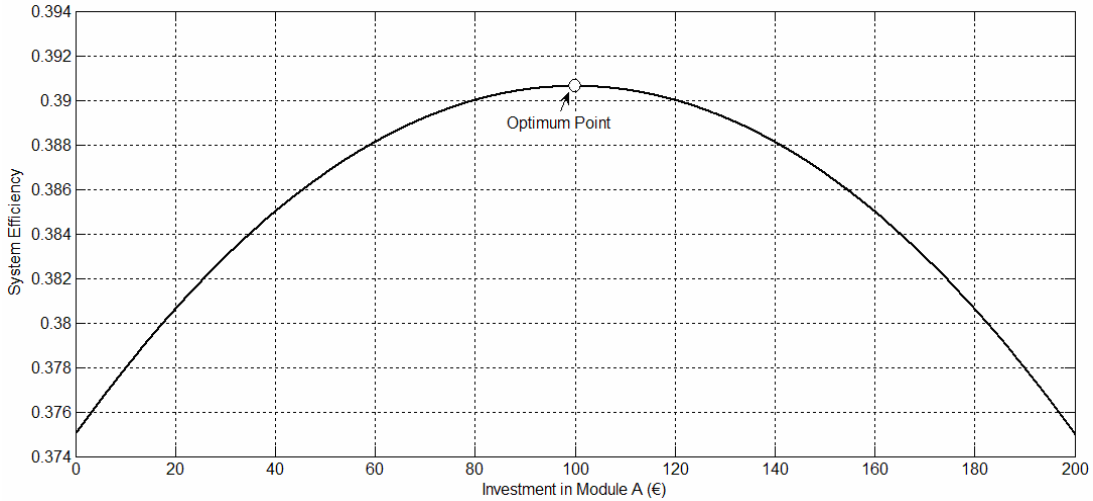


Fig. 2.30. Plot of the system efficiency as a function of the additional investment in Module A, assuming $x_{\text{total}} = 200$ €, $\eta_{A0} = \eta_{B0} = 0.5$, and $\Delta\eta_{\epsilon A} = \Delta\eta_{\epsilon B} = 0.125$ p.p./€.

The proposed strategy to optimize investment is useful to users when investment restriction exists, allowing an optimum investment strategy to be implemented in a particular system with several modules. For several (more than 2) modules, the system can be divided into 2 groups of modules for a first analysis, and, after that, each group can be divided into 2 sub-groups, and so on. This strategy makes more sense if the typical saturation of the efficiency-cost curve is taken into account.

Since an analytical approach is rather difficult to formalize and solve, a discrete approach can be applied, in which all combinations are analysed. For a system with two modules, one with n and the other with m discrete levels of investment and efficiency, the number of combinations is n times m . The most advantageous investment share is that minimizing the system efficiency increase cost. For example, considering a system with a motor and a belt-pulley transmission, both components with 3 different costs and efficiency levels in the market, the number of combinations

is 9, as it can be seen in Table 2.12. On the basis of the results presented in Table 2.12, if no maximum efficiency targets are established, the best choice is the solution 7. The solutions can be listed, from the lowest to the highest cost to improve efficiency ($\Delta\epsilon\Delta\eta$) as follows: solution 7, 2, 6, 5, 9, 8, 3, and 4. For 180 € \pm 2% of extra investment over base case, the user should invest in the solution 6 (better than solutions 4 and 9, requiring the same amount of investment).

Another example can be given. In a centrifugal fan or pump system requiring significant flux regulation, the decision of investing a limited capital in the replacement of a standard motor by a high-efficiency motor, maintaining throttling-based flux regulation or, instead, in a VSD for speed-based flux regulation (removing the throttle), maintaining the standard motor – the investment priority should be given to the VSD since the energy saving benefit or system efficiency increase per invested Euro is significantly higher. Of course, ideally, the user should invest in both the high-efficiency motor and VSD.

It should be noted that payback analysis is similar to the efficiency increase cost analysis, i.e., the lowest payback corresponds to the lowest cost to improve efficiency, and vice-versa. The presented decision principle can also be applied in investment decision in multiple systems, being in these cases necessary to take into account the different loads and operating hours associated to each system. With the proposed strategy, assuming limited economic resources, the user can maximize the energy saving benefit by investing in the most advantageous systems, modules and/or technologies.

TABLE 2.12
EXAMPLE OF INVESTMENT EVALUATION AS A FUNCTION OF SYSTEM EFFICIENCY INCREASE COST.

Solution	Motor Class	Belt Type	$\Delta\epsilon$	η_{sys}	$\Delta\epsilon\Delta\eta_{\text{sys}}$	Savings (€)	Payback (yr)
1	IE1	Smooth V	--	83.22%	--	--	--
2	IE2	Cogged V	93 €	87.49%	21.78 €/p.p	270.95 €	0.4
3	IE3	Synchron.	359 €	90.06%	52.49 €/p.p.	421.64 €	0.85
4	IE1	Synchron.	179 €	85.85%	68.11 €/p.p.	170.07 €	1.05
5	IE2	Smooth V	90 €	85.69%	36.44 €/p.p.	160.02 €	0.6
6	IE3	Cogged V	183 €	89.14%	30.91 €/p.p.	368.69 €	0.6
7	IE1	Cogged V	3 €	84.97%	1.71 €/p.p.	114.34 €	0.03
8	IE2	Synchron.	269 €	88.40%	51.93 €/p.p.	325.31 €	0.83
9	IE3	Smooth V	180 €	87.31%	44.01 €/p.p.	260.06 €	0.9

Notes:

Base case: IE1-class motor (11-kW, 4-pole, 50-Hz, IM) and smooth-V belt.

Motor Efficiencies: $\eta_{IE1} = 87.6\%$; $\eta_{IE2} = 90.2\%$; $\eta_{IE3} = 91.9\%$.

Motor Prices: $C_{IE1} = 360$ €; $C_{IE2} = 450$ €; $C_{IE3} = 540$ €.

Belt Efficiencies: $\eta_{\text{smoothV}} = 95\%$; $\eta_{\text{coggedV}} = 97\%$; $\eta_{\text{synchron}} = 98\%$.

Belt Prices: $C_{IE1} = 15$ €; $C_{IE2} = 18$ €; $C_{IE3} = 194$ €.

Scenario for savings and payback calculations: 100% load, 6000 h/yr, and 0.07 €/kWh.

Looking at the energy savings it is possible to analyse a system in order to maximize the savings. For a system with two components A and B, the equation (2.16) applies. Fig. 2.31 shows simulated results using (2.16).

$$S_{yr} = \frac{1}{\eta_{A0} \cdot \eta_{B0}} - \frac{1}{(\eta_{A0} + \Delta_{\eta A}) \cdot (\eta_{B0} + \Delta_{\eta B})} \quad (2.16)$$

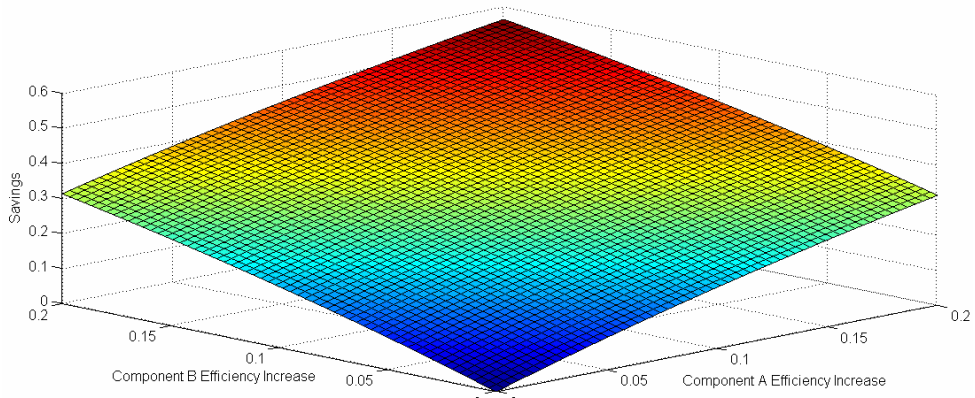
As previously discussed, the most relevant technologies for efficiency improvement of EMODS, excluding the end-use device or load itself, are the HEMs and VSDs. High-efficiency mechanical transmission, high-quality motor repair, readaptation and/or maintenance practices, and power quality have also a significant impact on the efficiency and reliability of EMODS.

End-use devices can also be improved according to the system requirements, but are not discussed in this thesis, since they fall out of its main scope. Nevertheless, information about end-use devices performance can be found in several sources, including a number of reports from European projects reports.

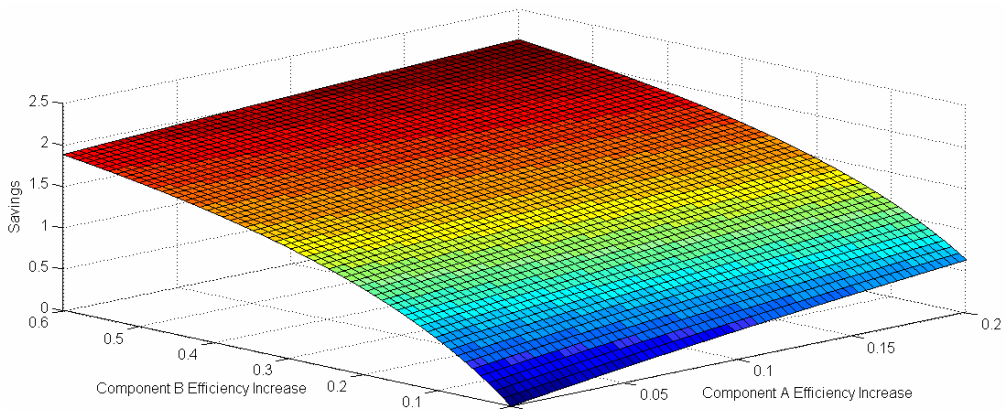
At this stage, it is important to emphasise that EMODS should be designed and optimized from the output to the input, since it is the only way for the correct (re)sizing of all the system components for the actual required output power. For example, for a specific output mechanical power, the increase of the mechanical transmission efficiency leads to a lower required input mechanical power and, therefore, a smaller motor can be chosen. If a HEM is chosen, a smaller VSD is required. Therefore, efficiency optimization can actually decrease the required rated power of each module, leading to a significant reduction in the initial system or module cost, and, of course, in the use-phase cost, as well as, if applicable, in the payback time. However, in new systems, or system upgrade investments, the priorities associated with the investment share over a period should be evaluated in order to maximize the efficiency or savings gain as a function of the amount to be spent in each module, requiring a careful study.

There are other aspects that can be also evaluated from the overall system perspective, as the feeding cables from the motor control and command centre to the motor. Here, the cable gauge upgrade possibility can also be evaluated if the ambient temperature is relatively high, the cable length is long (> 50 m), the power factor is poor, and/or the drawn current is high, since significant Joule losses and voltage drops can be involved. This is particularly interesting for new applications. In some cases, the extra cost to increase the cable gauge can be recovered in a short period considering the energy savings.

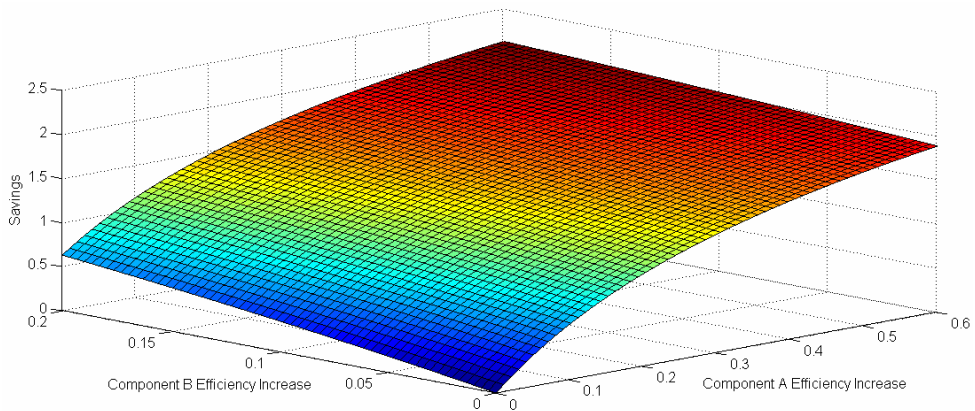
Additional notes and examples on specific EMODS overall optimization are presented in Appendix 6.



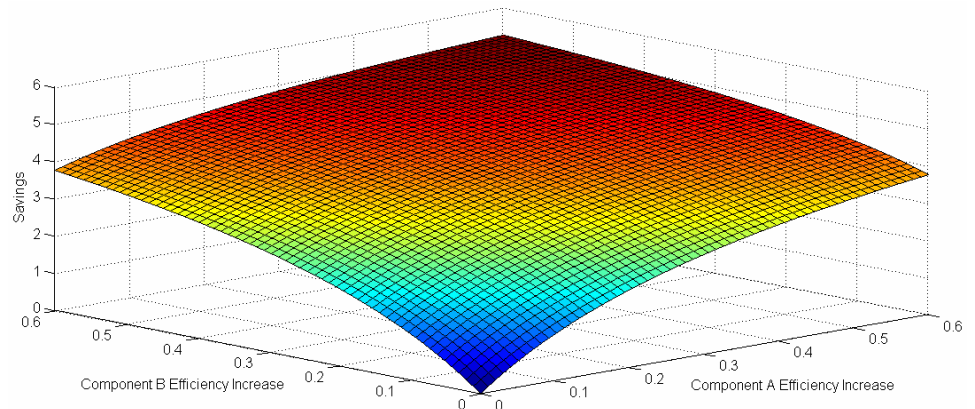
(a) $\eta_{A0} = 0.8; \eta_{B0} = 0.8.$



(b) $\eta_{A0} = 0.8; \eta_{B0} = 0.4.$



(c) $\eta_{A0} = 0.4; \eta_{B0} = 0.8.$



(a) $\eta_{A0} = 0.4; \eta_{B0} = 0.4.$

Fig. 2.31. System savings as a function of the efficiency increase of its components.

2.7 Conclusions

Regarding efficiency standards, the harmonization of the currently different requirements for IMs efficiency levels around the world, including efficiency testing and classification, seem essential to promote effectively a global motor market transformation, which will have a strong impact on the electrical energy consumption all over the world, particularly in fast developing countries [26]. The establishment of global energy performance classes, using the same or an equivalent international standard, allows fair global market trades for manufacturers and avoids errors on economic evaluations by the users. If, in the future, super-premium efficiency class is defined, it can be a positive step towards the promotion of other than IM technology in the low-medium power electric motor market, using for example PM technology.

Motor efficiency testing standards based on direct method, with or without loss segregation, which is actually the one that leads to the lowest uncertainty level, are prevailing over the old indirect method-based standards, and, at least to low-medium power motors, although the complexity of the required testing procedures, they can be implemented automatically, using systems similar to the one proposed, reducing application time, cost and error.

It was evidenced that mandatory minimum energy performance standards are a powerful tool to force motor market transformation, leading to significant energy savings around the world, as it was demonstrated in the USA.

It was found that use-phase cost of most electric industrial motors, namely the consumed energy, dominates by far their overall life-cycle cost and, if high-efficiency-class motors replace standard-efficiency-class motors, significant reductions in the environmental impact would happen.

Regarding motor manufacturers, the implementation of minimum efficiency levels for motors sold in the EU would result in a more regulated market where innovative manufacturers would profit from current and past R&D investments. The adoption of MEPS for IMs is not likely to cause a market shift towards another cheaper and/or less efficient technology since those technologies do not offer the same overall performance advantages as IMs. The previous adoption of MEPS in other countries proves this point since a market shift has not occurred there either. The adoption of IE2 efficiency level, in the short term, does not seem to pose particular problems to the EU industry since most EU manufacturers are already producing this type of motors for the whole power range under consideration. However, the adoption of IE3 efficiency levels in the medium term can pose problems to the EU industry for two main reasons. First, most EU manufacturers are not yet producing this type of premium efficiency motors. There is a need to invest in new designs and new manufacturing tools, which may represent a large amount of investment, particularly for small companies. Second, IEC-frame sizes may not allow achieving IE3 efficiency levels for small

IMs (e.g., below 7.5 kW), without increasing the frame size, even if using more expensive copper-cage rotor IMs. This issue deserves to be further investigated.

Regarding employment, the possible measures to implement do not seem to pose an adverse impact on employment. On the opposite, it is expected that by removing from the market imported low-performance IMs, the market share taken by the European manufacturers will increase. A gradual approach to increasing the minimum efficiency levels, allows motor manufacturers to adapt smoothly to more demanding market requirements. The increase in the use of VSDs, sold both as integrated units with the motors, as well as separated units, can lead to a substantial increase in additional business and can also lead to the creation of new jobs.

Growing environmental concerns and energy costs make more and more important to look at the LCC. Using the European eco-design methodology, on the basis of the previously presented results, it is possible to state that if IE3/IE2-class high-efficiency motors, replace IE1-class or sub-standard motors, significant reductions in the environmental impact will be achieved under most operating circumstances (motor operating time and load factor). However, the LCC reductions associated with IE2 to IE3 upgrade are not significant when correlated to the cost increase, particularly for high-power motors.

It should be emphasized that most electric motors used in industry are not ordered by the final user and are instead purchased by OEMs. OEMs do not have to pay running costs and want to minimize the first cost of equipment. Therefore MEPS seem essential to remove from the market inefficient motors and to promote energy-efficient models, which are very cost-effective on a life-cycle basis. The replacement of old inefficient motors when they fail, by efficient motors with proper sizing, can lead to further savings.

Although not presented in this thesis, important additional information on the foregoing issues can be consulted in [4], including eco-design analysis of PM motors and VSD-fed IMs.

2.8 References

- [1] de Almeida, A.; Ferreira, F.; Busch, J.; Angers, P.: “Comparative Analysis of IEEE 112-B and IEC 34-2 Efficiency Testing Standards Using Stray Load Losses in Low-Voltage Three-Phase, Cage Induction Motors”, IEEE Trans. on Industry Applications, Vol. 38, No. 2, pp. 608-614, Mar./Apr. 2002.
- [2] de Almeida, A.; Ferreira, F.; Fong, J.; Conrad, B.: “Electric Motor Standards, Ecodesign and Global Market Transformation”, IEEE Industrial and Commercial Power Systems Technical Conf., Conf. Proc., U.S.A., May 2008.
- [3] de Almeida, A.; Ferreira, F.; Fong, J.: “Ecodesign of Electric Motors”, 5th Inter. Conf. on Energy Efficiency in Motor Driven Systems (EEMODS’07), Conf. Proc., Vol. I, pp. 27-38, Beijing, 2007.
- [4] de Almeida, A.; Ferreira, F.; Fong, J.; Fonseca, P.: “Ecodesign Assessment of Energy-Using Products - EuP Lot 11 Motors”, Final Report for the European Commission, ISR-University of Coimbra, February 2008.
- [5] MEEUP, Methodology Study for Ecodesign of Energy-Using Products, VhK, 2005.
- [6] de Almeida, A.; Ferreira, F.: “User-Friendly High-Precision Electric Motor Testing System”, 4th Inter. Conf. on Energy Efficiency in Motor Driven Systems (EEMODS’05), Conf. Proc., Vol. I, pp. 149-157, Heidelberg, Germany, Sept. 2005.
- [7] Doppelbauer, M.: “Energy Efficient Electric Drives”, VEM Meeting 2007.
- [8] Doppelbauer, M.: “Saving Energy and Costs in Electrical Drive Systems”, SEW-Eurodrive, 2007.
- [9] Doppelbauer, M., SEW-Eurodrive, *Expert opinion*, 2006.
- [10] Fassbinder, S.: “Saving Energy with High-Efficiency Motors”, Briefing paper, Leonardo Energy, Sept. 2007, available on-line: www.leonardo-energy.org.

- [11] de Almeida, A.; Greenberg, S.: “*Technology assessment: energy-efficient belt transmissions*”, Energy and Buildings, No. 22, Elsevier Science, pp. 245-253, 1995.
- [12] Stoft, S.: “*The Economics of Conserved-Energy “Supply” Curves*”, University of California Energy Institute, Workable Energy Regulation (POWER), April 1995.
- [13] Balvanyos, T.; Lave, L.: “*Economical Analysis Methods*”, Carnegie Mellon University, Pittsburgh, Pennsylvania.
- [14] de Almeida, A.; Fonseca, P.; Ferreira, F.; Guisse, F.; Diop, A.; Previ, A.; Russo, S.; Falkner, H.; Reichert, J.; Malmose, K.: “*Improving the Penetration of Energy-Efficient Motors and Drives*”, Prepared for the European Commission, DGTE, SAVE II Programme, 2000;
- [15] de Almeida, A.; Ferreira, F.; Parasiliti, F.; Walters, D.: “*Barriers Against Energy-Efficient Electric Motor Repair*”, Prepared for the European Commission, DG XVII, SAVE II Programme, 1999;
- [16] IEEE 112 Std., 2004: “*Test Procedure for Polyphase Induction Motors and Generators*”.
- [17] IEC 60034-2, Ed. 2, 1996: “*Methods for determining losses and efficiency of rotating electrical machinery from tests - excluding machines for traction vehicles*”.
- [18] IEC 61972, 2002: “*Method for determining losses and efficiency of three-phase cage induction motors*”.
- [19] IEC 60034-2-1: “*Rotating electrical machines - Part 2-1: Standard methods for determining losses and efficiency from tests (excluding machines for traction vehicles)*”, Doc. IEC 2/1433/FDIS, 2007.
- [20] IEC 60034-2-3, 2008: “*Rotating Electrical Machines – Part 2-3: Specific test methods for determining losses and efficiency of converter-fed AC machines*”, First working document, TC2 WG 28/52/WD, January 2008.
- [21] CSA C390-98, 2005: “*Energy Efficiency Test Methods for Three-Phase Induction Motors*”.
- [22] AS Std. 1359.102.1, 1007: “*Rotating electrical machines – General requirements: Methods for determining losses and efficiency – General*”.
- [23] AS Std. 1359.102.2, 1997: “*Rotating electrical machines – General requirements: Methods for determining losses and efficiency—General*”.
- [24] AS/NZS Std. 1359.102.3, 2000: “*Rotating electrical machines – General requirements: Methods for determining losses and efficiency—Three-phase cage induction motors*”.
- [25] AS/NZS Std. 1359.3, 2004: “*Rotating electrical machines – General requirements: Three-phase cage induction motors - High efficiency and minimum energy performance standard requirements*”.
- [26] Brunner, C.; de Almeida, A.; Niederberger, A.; Keulenaer, H.: “*Standards for Efficient Electric Motor Systems SEEEM - Building a Worldwide community of Practice*”, Inter. Conf. on Energy-Efficiency in Motor Driven Systems (EEMODS’07), Conf. Proc., Beijing, June 2007.
- [27] Aoulkadi, M.; Binder, A.: “*The Eh-star Method for Determination of Stray Load Losses in Cage Induction Machines*”, 4th Inter. Conf. on Energy Efficiency in Motor Driven Systems (EEMODS’05), Conf. Proc., Vol. 1, pp. 130-1405, Heidelberg, Germany, Sept. 2005.
- [28] Gerada, C.; Bradley, K.; Arellano-Padilla, J.: “*An Investigation into the Suitability of Unbalanced Motor Operation, the Eh-Star-Circuit for Stray Load Loss Measurement*”, IEEE Industry Applications Conf., 2005.
- [29] Radgen, P.; Blaustein, E.: “*Compressed Air Systems in the European Union*”, Edited by Fraunhofer ISI, 2001.
- [30] Gröning, N., KSB Aktiengesellschaft, Fachvortrag VEM Fachtagung, Wernigerode, Juni 2003.
- [31] Witt, M., WiH & Sohn AG, Fachvortrag VEM Fachtagung, Juni 2003.
- [32] Aoulkadi, M.; Binder, A.: “*Comparison of Different Measurement Methods for Stray Load Losses in Cage Induction Machines: Input-Output Method, RRT-Method and Eh-Star-Method*”, 40th Inter. Universities Power Engineering Conf. (UPEC’05), Cork, Ireland, 7-8 Sept. 2005.
- [33] IEC 60034-30, Ed. 1: “*Rotating electrical machines - Part 30: Efficiency classes of single-speed, three-phase, cage-induction motors (IE-code)*”, Committee Draft for Vote (2/1464/CDV), August 31, 2007.
- [34] IEC 60034-1, Ed. 11, 2004: “*Rotating electrical machines - Part 1: Rating and performance*”.
- [35] Keulenaer, H.; Belmans, R.; Blaustein, E.; Chapman, D.; de Almeida, A.; Watcher, B.; Radgen, P.: “*Energy Efficient Motor Driven Systems*”, Motor Challenge Programme, European Copper Institute, 2004.
- [36] EURODEEM - The European Database of Efficient Electric Motors, European Commission, 2005.
- [37] EUROSTAT, Statistics in Focus, Environment and Energy, “*Electricity prices for EU households and industrial consumers on January 2006*”, <http://epp.eurostat.ec.europa.eu>, Nov. 2006.
- [38] SEW-Eurodrive, *Technical notes on mechanical transmission*, Portugal, 2006.
- [39] Muravlev, O.; Muravleva, O.; Vekhter, E.: “*Energetic Parameters of Induction Motors as the Basis of Energy Saving in a Variable Speed*”, IEEE 2005, pp. 1-4.
- [40] Petro, J.: “*Super High Efficiency Appliance Motors*”, 5th Inter. Conf. on Energy Efficiency in Motor Driven Systems (EEMODS’07), Conf. Proc., Beijing, 2007.
- [41] Rossi, T.: “*Permanent Magnet Synchronous Motors for Pump Applications*”, 5th Inter. Conf. on Energy Efficiency in Motor Driven Systems (EEMODS’07), Conf. Proc., Beijing, 2007.
- [42] Lo, C.: “*Motors in Household Appliances and HVAC: High Performance Motor Design for Hermetic DC Compressors*”, 5th Inter. Conf. on Energy Efficiency in Motor Driven Systems (EEMODS’07), Conf. Proc., Beijing, 2007.
- [43] Sofronis, I.: “*Tools for the Evaluation of Energy Efficient Motor Systems*”, 5th Inter. Conf. on Energy Efficiency in Motor Driven Systems (EEMODS’07), Conf. Proc., Beijing, 2007.
- [44] McCoy, G.: “*Latest Development of the IMSSA Software*”, 5th Inter. Conf. on Energy Efficiency in Motor Driven Systems (EEMODS’07), Conf. Proc., Beijing, 2007.
- [45] Dems, M.; Komez, K.; Wiak, S.; Stec, T.; Kikosicki, M.: “*Application of circuit and field-circuit methods in designing process of small induction motors with stator cores made from amorphous iron*”, The Inter. Journal for Computation and Mathematics in Electrical and Electronic Eng., Emerald Group Publishing Limited, 2006, Vol. 25 Issue 2, pp. 283-296, 2006.
- [46] Williamson, S.; Smith, S.; Barnes, M.; Apsley, J.: “*Efficiency Gains in Multi-Phase Induction Motor Drives*”, 5th Inter. Conf. on Energy Efficiency in Motor Driven Systems (EEMODS’07), Conf. Proc., Beijing, 2007.
- [47] Belmans, R.; Deprez, W.; Stevens, S.; Dexters, A.; Parasiliti, F.: “*The Combined Effect of Practical Operating and Material Choice on the Performance of Induction Machines*”, 5th Inter. Conf. on Energy Efficiency in Motor Driven Systems (EEMODS’07), Conf. Proc., Beijing, 2007.

- [48] Wang, S.; Zhao, Z.: “*The Influence of Different Materials on the Performance of Induction Motors*”, 5th Inter. Conf. on Energy Efficiency in Motor Driven Systems (EEMODS’07), Conf. Proc., Beijing, 2007.
- [49] Liang, D.: “*A Report on Analysis of the Performance and Cost of Energy Efficient and Super-Efficient Copper Rotor Based Motor*”, 5th Inter. Conf. on Energy Efficiency in Motor Driven Systems (EEMODS’07), Conf. Proc., Beijing, 2007.
- [50] Danish Technological Institute: “*Optimization of System in Motor Driven Systems*”, 5th Inter. Conf. on Energy Efficiency in Motor Driven Systems (EEMODS’07), Conf. Proc., Beijing, 2007.
- [51] Fuchsloch, J.; Noltman, J.; Peters, D.; Brush, E.; Cowie, J.: “*Systematic Design Approach for a New Series of Ultra-NEMA Premium Copper Rotor Motors*”, Inter. Conf. on Energy Efficiency in Motor Systems (EEMODS’07), Conf. Proc., Beijing, China, June 2007.
- [52] Ferreira, F.: “*Técnicas Avançadas de Manutenção Curativa e Reabilitação de Motores de Indução Trifásicos de Baixa Tensão/ Curative Maintenance and Rehabilitation Advanced Methods for Low-Voltage, Three-Phase, Induction Motors*”, Tese de Mestrado/Master Science Thesis (available in Portuguese only), Universidade de Coimbra/University of Coimbra, 2002.
- [53] Boldea, I.; Chris, L.; Wallace, A.: “*Load Testing of Induction Machines without Torque Measurements*”, IEEE Inter. Conf. on Electric Machines and Drives (IEMD’99), Conf. Proc., pp. 162-164, 1999.
- [54] Boglietti, A.; Cavagnino, A.; Lazzari, M.; Pastorelli, A.: “*Induction Motor Efficiency Measurements in Accordance to IEEE 112-B, IEC 34-2 and JEC 37 International Standards*”, IEEE Inter. Electric Machines and Drives Conf. (IEMDC’03), Conf. Proc., Vol. 3, pp. 1599-1605, 2003.
- [55] EASA/AEMT: “*The Effect of Repair/Rewinding on Motor Efficiency – EASA/AEMT Rewinding Study and Good Practice Guide to Maintain Motor Efficiency*”, U.K., 2003.

3 Motor Speed Adjustment

Overview – Motor torque, speed, and/or position control is of paramount importance in raising productivity and quality, as well as in reducing energy and equipment maintenance costs in most modern industries. Electric motor systems share most of industrial motion control applications. International markets for electric motor systems are rising approximately at 10% annual rate and represent a market worldwide of several thousands of million of Euro. Motor speed control/adjustment represents one of the largest opportunities for cost-effective electricity savings around the world. In the EU, VSDs were identified as the motor systems technology having the most significant electricity savings potential. However, only a small percentage of this potential is being used. In this chapter, aspects related to the thermal and mechanical limits of VSD-fed IMs are discussed. An extensive comparison between two-level and three-level voltage-source inverters is presented. The characterization of VSDs market is presented, including the average prices, the installation costs, and the total sales in each EU country, per power range. The key barriers to a wider application of VSDs are identified. As a complement to this chapter, in Appendix 6, a number of technical and economical considerations on VSDs are presented, including a short description of some VSD applications with a significant savings potential, as well as a discussion on the power quality, EMI and reliability problems associated with the use of VSDs. Additionally, in Appendix 6, a technology assessment on fixed-speed mechanical transmission systems is offered, considering cost, reliability and efficiency, and a methodology for proper selection of IMs for variable-speed applications is proposed. In the scope of this chapter, a number of publications were made, namely, [11], [13],[15], [20], [38] and [54].

3.1 Introduction

A major part of this section summarizes the results of a large European study¹ [54] about the technical and economical considerations in the large-scale application of VSDs for EMODS. A number of previous studies identified VSDs as the motor systems technology having the most significant energy savings potential. The loads in which the use of speed controls in electric drives can bring the largest energy savings are the fluid handling applications (e.g., pumps, fans and compressors) with variable flow requirements. Other applications that can benefit from the application of VSDs include conveyors, escalators, machine-tools, lifts, centrifuges, etc. The diffusion of speed controls for fluid circulation applications has been very slow. This is in striking contrast to process control applications for which speed and/or torque variation is necessary for industrial reasons (for instance in paper production lines or in steel mills), where the newest generation of electronic VSDs have become the standard technology [11], [54].

For practical purposes, IMs are constant-speed motors. However, a number of methods can be used to vary their speed, namely frequency/voltage control (using VSDs), stator poles changing, stator phase voltage regulation at fixed frequency (e.g., using electronic voltage regulators, autotransformers, or stator-winding connection mode change), rotor resistance variation, and injection of an EMF into the rotor circuit. The last two apply to wound-rotor IMs. In this thesis only the first three are discussed. Theoretical information can be found in most technical books and technical texts on electrical machines and power electronics (e.g., [10], [16]-[19], [25], [26], [43], [44], [45], [50] and [52]).

¹ This study includes Portugal, France, U.K., Germany, Denmark and Netherlands.

The presently dominant variable-speed motor technology – VSD-fed IMs – has practically replaced other technological solutions, such as mechanical, hydraulic, and electromagnetic, as well as DC-brushed motors and pole-amplitude modulation (PAM) or two-speed IMs. A summary of the main industrial applications and power range of electric drives is shown in Fig. 3.1. As described before, in IMs, the speed of the rotating magnetic field created by the stator windings, and, therefore the rotor speed, is directly linked with the frequency of the voltage supply. VSDs can produce variable frequency, variable voltage waveforms which can be used to control the motor speed, torque and/or shaft position. Fig. 3.2 shows examples of commercial separated and integrated VSD units.

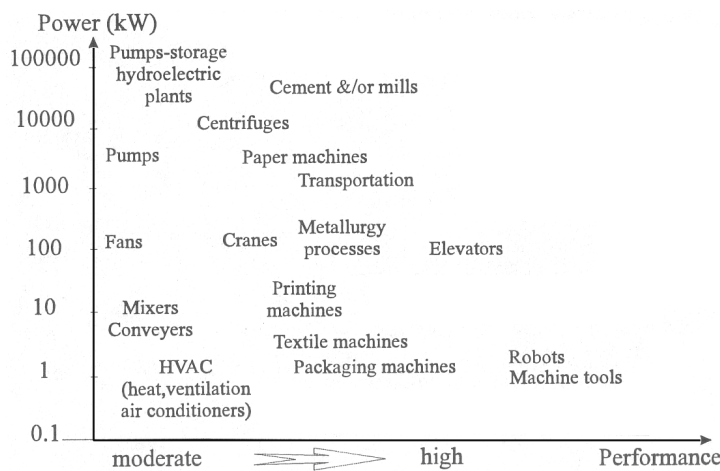


Fig. 3.1. Main industrial applications and power range of electric variable-speed drives [19].

There are several types of VSDs, but the vast majority incorporate voltage-source inverters (VSIs) using pulse-width modulation (PWM) technique, integrating three main modules (see Fig. 3.3): AC/DC converter (rectifier with or without input filter), DC bus or link with filter, and voltage-source inverter or DC/AC converter. The inverter stage converts the DC voltage into a three-phase voltage system with variable amplitude and frequency (typically varying between 0 and 150 Hz). The success of the VSI-PWM topology is related with their advantages over other possible topologies, as summarized in Table 3.1. VSDs can also incorporate a line-side AC filter designed to reduce the flow of harmonic currents into power network. In the DC bus, a DC-filter capacitor connected across the rectifier output to reduce voltage ripple and, in some cases, a DC-filter inductor connected in series with the output of the rectifier to reduce current ripple. Due to the relatively high impedance of the motor, although the output voltage PWM-shape waveform, the current waveform results practically sinusoidal. The rated voltage to rated frequency ratio, U/f , corresponds to the ratio that leads to rated air-gap flux, providing rated torque per ampere, otherwise motor torque and speed result different from rated values, as it can be seen in Fig. 3.4. In order to provide constant torque for frequencies lower than rated, the voltage amplitude has to be properly reduced with frequency. Typically, the control of the PWM pulses is made by a

microprocessor or a digital signal processor (DSP). The most simple control used in VSD, based on the fundamental voltage and frequency regulation, is called scalar control (U/f and current-slip frequency control, with or without slip compensation, and with or without motion sensors, but typically sensorless), and it is the most commonly used for VSDs, and, although losing momentum, have so far provided satisfactory speed adjustment in applications requiring low dynamics and low speed accuracy, such as fans, pumps, compressors, and conveyors, and other applications in which position and/or torque control is not necessary. Nowadays, most modern commercial general-purpose VSD units also integrate vector control² capability in the same unit [31], [41], [46]. In the VSDs using vector control, instantaneous speed and torque control by means of quasi-instantaneous and independent control of both flux- and torque-related currents is made [43].

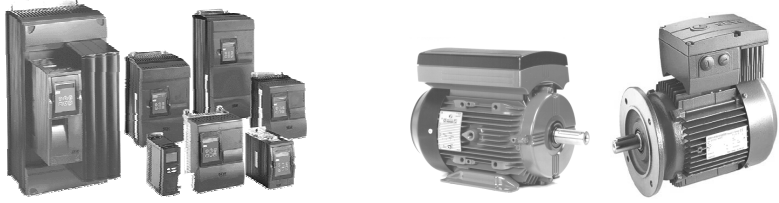


Fig. 3.2. Typical aspect of commercial VSDs: (left) separated units; (right) integrated units.

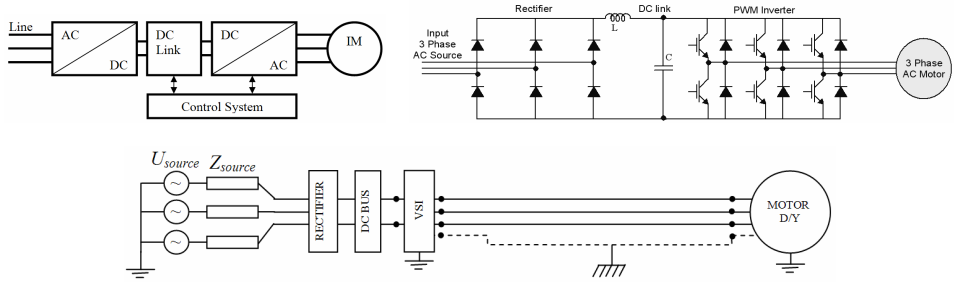


Fig. 3.3. Basic topology (top) of a VSD and (bottom) of an EMODS with power source plus VSD plus IM system.

However, since the aim of this thesis is the steady-state analysis of EMODS, from the efficiency and reliability perspective, the modern control techniques are not addressed, although briefly mentioned.

The maximum torque of an IM is approximately proportional to the square of the magnetizing flux, and therefore approximately proportional to the square of the U/f ratio, ignoring the voltage drop across the stator windings. In scalar control, the U/f relation (e.g., linear or quadratic)

² A number of advanced control techniques for IMs is offered in modern VSDs (e.g., vector current and voltage control, direct torque and flux control, and feedback linearization control, with or without motion sensors, [16], [17], [18] [19], [43], [44], [46] and [52]), which can be divided in three main groups – field oriented control (FOC), direct torque control (DTC), and direct self control (DSC). A number of papers have been published on this matter, e.g., [64]-[71], [96], [97]. In essence, vector control consists in decoupling the excitation current from the torque producing current, similar to a DC brushed motor drive where the field excitation current is separated from the armature current. Once this relationship has been established, further control becomes straight forward like DC drives. This is an over-simplification of the process, but gives a general idea of the complex computation that is going on continuously in a vector control system [44]. In fact, fast torque dynamics and speed control require closed-loop speed control and even torque closed-loop control. Linearizing the torque-speed characteristic, or the torque-current characteristic, as in DC brushed motors, is the essence of the modern control schemes, by intelligent manipulation of IM equations using space-phasors. The rapid development of powerful DSPs led to a kind of universal IM drive that, on a menu basis, may work in various modes. The main advantages are the precise control of speed, torque and power, even in constant voltage range, quick response to changes in load and speed or torque commands, rated torque at zero speed capability, smooth low speed operation, smooth forward/reverse and start/stop operation, and less mechanical stress (avoids jerks). Typical applications where vector control is used are cranes, hoists, winders/unwinders, paper machines, extruders, positive displacement pumps and compressors, loads where load torque and moment of inertia vary wildly, and any application where maximum probability of success is required [44].

should depend on the application or load torque-speed curve, in order to maximize motor efficiency. For $f \approx 0$ Hz the voltage is set to a value properly defined to compensate the voltage drop at the stator windings (voltage offset or boost). In most VSDs, it is not possible to increase the voltage magnitude above its nominal value. Further increase in speed leads to a fast drop in motor maximum torque.

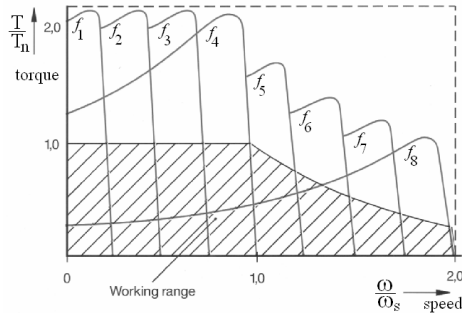


Fig. 3.4. IM torque-speed curves for different frequencies and linear U/f relation ($f_1 < f_2 < \dots < f_4 = f_N$) [45].

TABLE 3.1
COMPARISON OF THE MOST COMMON TYPES OF INVERTERS [16].

	VSI-PWM	VSI-Square Wave	CSI
Input Power Factor	+	-	--
Torque Pulsations	++	-	-
Multimotor Capability	+	+	-
Regeneration	-	-	++
Short-Circuit Protection	-	-	++
Open-Circuit Protection	+	+	-
Ability to Handle Undersized Motors	+	+	-
Ability to Handle Oversized Motors	-	-	-
Efficiency at Low Speeds	-	+	+
Size and Weight	+	+	--
Ride-Through Capability	+	-	-

Nowadays, in small-medium power ranges, the most used transistor is the insulated gate bipolar transistor (IGBT), since it allows to use a high switching frequency, f_s , with low switching losses. In most VSD units, f_s can be selected by the user within a 2-20 kHz range, for the IGBT-based inverters. IGBTs allow voltage rise times as short as 70-100 ns, leading to high voltage variation rates (du/dt), typically between 2.5 and 9 kV/ μ s, which, although reducing significantly the lower switching losses, can lead to accelerated ageing of the windings, as it is discussed in Appendix 5. IGBTs are still being improved in terms of efficiency and response [47]. Nevertheless, in general, IGBTs lead to a better performance, controllability, efficiency and reliability of the inverter. Typically, VSDs full-load efficiency is within 96-98%, decreasing slightly with the load decrease and switching frequency increase. The power factor of VSDs with three-phase, six-pulse, diode rectifiers is typically within 0.85-0.90 range, decreasing with load decrease (this is further analysed).

Due to their installation and control flexibility, high efficiency, fair power factor over all load range, high reliability, motor application range extension, decreasing prices and short payback in suitable applications (in Industry, typically less than 2 years, depending on application profile), VSDs penetration has increased significantly in the last decade in industrial and tertiary sectors, either as integrated or separated product. Over 2002, 1.2 million of VSDs were sold in the EU-15. Nowadays, in Germany³ about $\frac{1}{3}$ of the new motors is fitted with a VSD [106], [107]. In Portugal, this ratio is within $\frac{1}{8}$ - $\frac{1}{6}$. Presently, it is estimated that 5-15% of in-operation motors are fed by VSDs.

When fed by VSDs, IMs can be used in almost all sort of variable-speed applications or applications requiring motion control. Contrarily to the conventional IM speed regulation processes, requiring interposition of a mechanical (e.g., gears) or hydraulic device between motor and load, VSDs offer adaptation flexibility and are compact. In general, the speed control or adjustment is an excellent mean to improve the control process and product quality, increase the productivity, less wear in the mechanical equipment, less acoustic noise (considering reduced speed), and saving electrical energy in a wide range of applications. Significant energy savings associated with speed control are reported between 20% and 70%, and even more in VSDs with regeneration⁴. Regeneration is particularly advantageous in high-inertia and/or high-speed industrial loads (e.g., fly-wheel presses, large rotary saws, industrial centrifuges, etc.) with frequent starts/stops, or even in loads with extended braking periods (e.g., lifts, large hoists/cranes and escalators). For example, VSDs lead to substantial energy savings (even when the VSD and motor efficiency variation is taken into account [42]) when applied to the fluid/air flux control in centrifugal pumps and fans, in which the required power is approximately proportional to the speed cube. Significant savings can also be obtained in compressors, elevators, escalators, conveyors, etc. VSDs also offer several technical advantages, including soft starts/stops, which decrease significantly the starting current, rotor losses, and the mechanical wear of the driven equipments⁵, and several motor protection features⁵, which did not need to be acquired separately. Additional features are also important in the scope of energy savings such as

³ In 1996, 1 in 10 motors were sold with a VSD in Germany. Nowadays, 1 in 3 motors are sold with a VSD, being the number of motors and VSDs sold per year roughly 3 million (this number is stagnated for more than one decade) and 1 million, respectively. The number of VSDs used in motor speed control is rising at a 10% annual rate in Germany [106], [107]. In Portugal, in 2007, 21.3 thousand VSDs were sold. From 2005 to 2006 and from 2006 to 2007, a 2.8% and a 16.3% increase on the number of units sold per year occurred, respectively (see Appendix 6). This suggests that energy-wasting mechanical controls are increasingly being replaced by modern electronic controls in the existing plant base as well as in new plants.

⁴ Conventional VSDs rely on a braking resistor (resistor in series with an IGBT switch) connected to the DC bus, which is fed when the DC-bus voltage exceeds a pre-assigned value, dissipating the generated energy when the motor operates as a brake or generator (2nd or 4th quadrants), during deceleration periods. Regenerative VSDs (with an active front-end) reconvert the energy in the rotating load back to the main power supply. This increases significantly the overall energy efficiency of the process, increasing the energy savings. To achieve this there needs to be a complete reverse circuit, and so, regenerative VSDs are more expensive than standard types. In fact, the input stage is identical to the output stage, allowing power flow in the power line wise, i.e., 4-quadrant operation, as well as power factor control and improved THD, which is an additional advantage of this sort of VSDs [11], [54]. It should be referred that, in certain cases (e.g., automatic storage systems and multi-lift/elevator systems), it can be advantageous to use a common DC-bus feeding multiple inverters if some of them are supplying power into the DC-bus when the others are braking or regenerating, resulting in a significant increase in the overall efficiency [105]. Regeneration capability can lead to significant savings in, for example, lifts and cranes.

⁵ Motor protection against over/under voltage, overcurrent, overload, overtemperature, line transients, voltage unbalance, single-phasing, short-circuit, etc., as well as ride-through capabilities.

the standby operation capability (sleep function when not active), low-loss switches, adaptive switching frequency for additional loss reduction, low-loss passive components and speed-controlled fans, efficient control algorithms as a function of the process (influences the inverter, motor and process efficiency), and active front-end for low THD and/or high power factor. Other important aspect is, of course, the correct choice and sizing of motor and inverter and the use of high-efficiency motors.

Other important potential advantages associated with VSDs are motor efficiency maximization as a function of load by proper flux regulation (even if no significant frequency variations are made), line-side power factor improvement (particularly for low loads), possibility of communication/integration with other devices and/or sensors ride-through capability (in some cases, increasing system reliability), and easy installation, since no mechanical adaptation is required between motor and driven load. These additional capabilities should be taken into account in the technical and economical evaluation. For example, investing in a VSD avoids, in principle, the investment in soft-starting devices and/or part of the typically required protection devices. VSDs can also lead to the increase of the production and reliability of the systems, as well as to the maintenance reduction due to the absence of several mechanical systems used to vary the speed or pressure. In general, the adjustment of the motor speed through the use of VSDs can lead to the referred advantages but some potential drawbacks can also be referred such as conducted and radiated electromagnetic interference (EMI), harmonics injection into the power network and the possible reduction of efficiency and lifetime of motors due to the extra motor stress factors (insulation system and bearings), being necessary some special care with the choice, repair and/or maintenance of the IMs [1], [11], [14], [15], [42]. It should be noted that, by itself, a VSD, as an additional series module in the EMODS, decrease the overall theoretical system reliability⁶.

3.2 Technical Barriers to the Use of VSDs

3.2.1 Impact of VSDs on IMs

VSD-fed IMs may have to support three main additional motor stress factors that are shortly described next, namely, internal temperature increase, partial discharges and increased voltage stress of the stator windings insulation system (associated with voltage transients generated at the motor terminals), as well as bearing currents⁷. The last two issues can contribute significantly to motor lifetime shortening, and are addressed in Appendix 5. Moreover, the full-load average

⁶ However, in general, even considering that an additional component is being added to the system, the overall system reliability can improve, if proper measures are taken to mitigate the impact of VSDs in the IMs.

⁷ Since the IM parasitic or stray capacitances between the windings and frame, windings and rotor, rotor and frame, and inside the bearings, high frequency currents can circulate in the bearings of VSD-fed IMs. These currents can, therefore, significantly decrease the lubricant and bearing lifetime.

stator winding temperature of VSD-fed IMs increases typically 5-10°C, which is mainly due to the harmonics related motor iron and copper losses increase (motor overall losses can increase typically 10-30%, depending on load) [14], [27]. This temperature increase accelerates insulation system and lubricants degradation⁸ [11], [14]. Due to the temperature increase, partial discharges and increased voltage stress, the insulation system of older motors (in particular) with long cable runs may have a significant shortened lifetime when fed by VSDs. Besides increasing motor losses, 5th, 11th and 17th harmonics, although normally low, can become relevant in the overmodulation region, contributing to the motor starting torque reduction. Note that sophisticated control techniques have been developed in modern VSDs to minimize harmonics, particularly on the motor side [16], [17], [52]. In the case of self-cooled motors (e.g., TEFC or IP5x types), the temperature increase can be also due to the reduction of motor speed and, consequently, the reduction of cooling airflow-dependent equivalent thermal resistance between motor frame and ambient [11]. Therefore, it is important to properly size the motor for loads requiring speeds lower than nominal, as it can be seen in the Fig. 3.5.

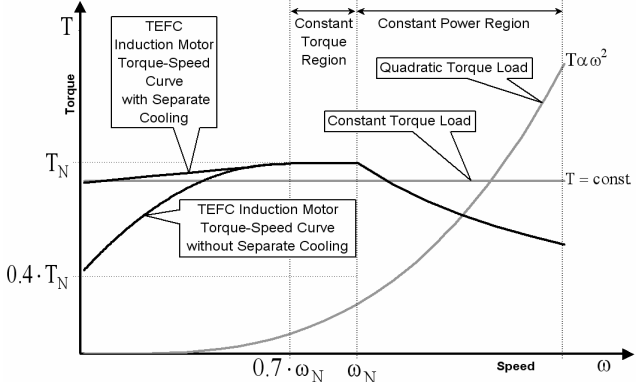


Fig. 3.5. Motor loadability (torque and power limitations) in TEFC VSD-fed IMs, assuming motor constant nominal operation temperature ($f_s > 5$ kHz, field weakening point at nominal frequency). Torque-speed curves for different load types [11], [26], [46].

For low speeds (below 70% of the nominal speed) an external ventilator may be required to avoid motor overheating. These issues are discussed further. Regarding constant power capability region, it should be referred that, with proper control, it is possible to increase slightly the corresponding torque limits.

3.2.2 Harmonics and Electromagnetic Interference Associated with VSDs

VSDs generate harmonis and conducted noise in line-to-inverter power cables and high-frequency airborne radiated EMI in the inverter-to-motor power cable. Harmonics and EMI can interfere significantly with nearby electrical equipments, causing, for example, malfunction and loss increase. An overview and a number of important considerations are presented in Appendix 6.

⁸ On the basis of the Arrhenius' law, every 10°C increase in the operating temperate leads to a 50% and 35% decrease in the insulations and lubricants lifetime, respectively [14], [53].

3.3 Comparison between Two-Level and Three-Level Voltage-Source Inverters

As already mentioned, a voltage-source inverters (VSIs) are by far the most common technology to control the speed and torque of IMs. Nowadays, different VSI-technologies are commercially available, having different impacts on the performance and reliability of IMs. When compared to the two-level VSIs, the three-level VSIs are typically seen as an expensive solution. However, in some applications, three-level VSIs can lead to significant improvements in the reliability and performance of the IMs, justifying the additional investment from a life-cycle cost perspective. In this section, the main conclusions of a comparative study of two different technologies of VSIs – two-level and three-level – applied to low-power, low-voltage IMs, is presented. This study is based on simulated and experimental results and focuses motor and inverter losses, inverter output voltage wave quality, motor vibrations, motor acoustic noise, motor electrical insulation stress, and high-frequency bearing currents, considering only steady-state operation. Considerations about the PWM parameters are also presented. Economical issues are discussed. The outcomes of the presented study are useful for motor users, helping them to decide technically and economically between both analyzed technologies. The main results presented in this section were published in [15].

3.3.1 Introduction on Two-Level and Three-Level Voltage-Source Inverters

Two-level voltage-source inverters (2L-VSIs) are a well-explored technology, being widely used in low-voltage applications. Three-level voltage-source inverters (3L-VSIs) are presented as a new technology for low-voltage and relatively low-power applications. Although commercially available, they are not commonly used, mainly due to its higher cost in relation to the 2L-VSIs (twice the number of power devices is needed in the output stage). Actually, there are topologies with a number of levels higher than 3, named multi-level inverters, which can have significant advantages, but the inherent cost increase makes them a forbidden technology from the economical perspective, being only used in high-power critical applications [94], [95]. The same applies to multi-phase inverters [93], feeding multi-phase motors (which can be more efficient). In Fig. 3.6, the typical topology of a 2L- and a 3L-VSI (diode-clamped or neutral point-clamped type, typically denoted as NPC [18], [32], [108]) is shown. Each arm of the 3L-VSI consists of four switching devices along with their anti-parallel diodes and two neutral clamping diodes. The well-known control strategies can be fully implemented in the 3L-VSIs.

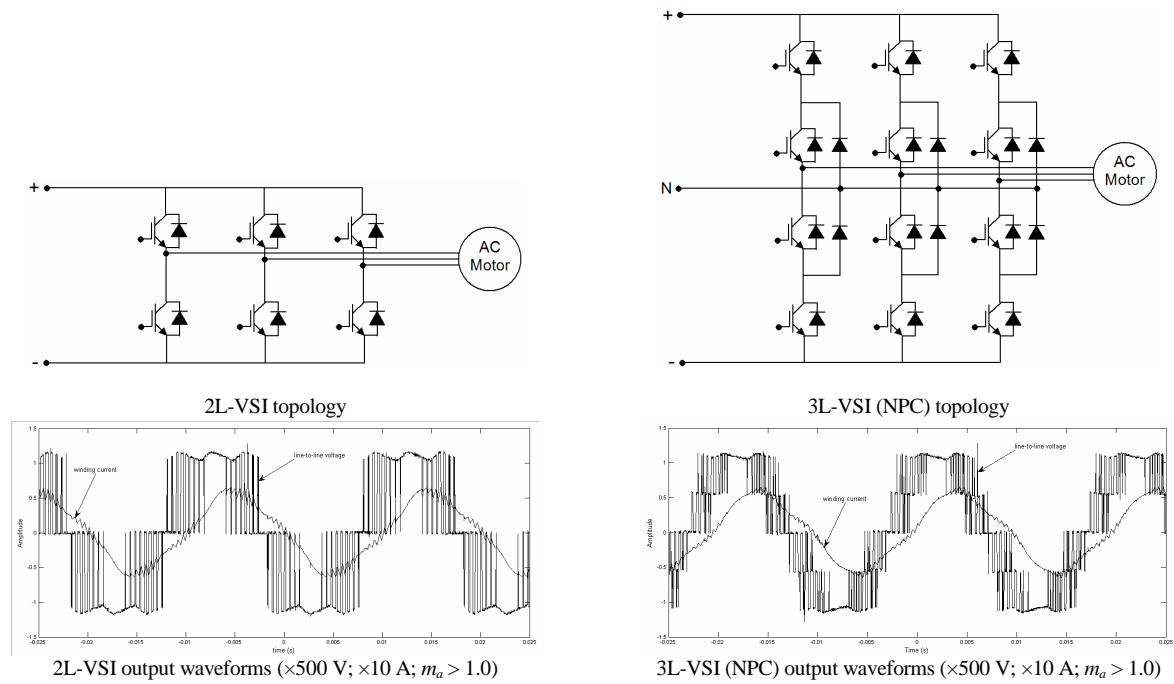


Fig. 3.6. Typical topology and experimental output waveforms for: (left) 2L-VSI; (right) 3L-VSI (NPC).

Different PWM techniques have been used to produce the output voltages, but the simplest method is based on the intersection between a sinusoidal wave and a triangular wave(s) (or carrier wave(s)), known as sinusoidal pulse-width modulation (SPWM), used to generate the transistor command pulses⁹. Nowadays, IGBTs are the most widely used transistors in low-voltage inverters [47]. In Fig. 3.6, the low frequency ripple in the PWM waveforms are due to the DC-bus voltage oscillation with a frequency 6 times the fundamental line-to-line voltage frequency ($6 \times 50 \text{ Hz} = 300 \text{ Hz}$) at the diode rectifier input (see Appendix 4).

3.3.2 Simulations and Experimental Tests Methodology

The results for the comparison of both technologies (2L-VSI and 3L-VSI) were obtained either by simulations and/or by experimental tests. The simulated results were generated/processed using the software MATLAB and SIMULINK [32]. The experimental results were processed using the software MATLAB and MICROSOFT EXCEL.

In the first set of simulations, a constant RL-series delta-connected three-phase load, a reference DC-bus voltage equal to 1 V, a fundamental frequency equal to 50 Hz, and ideal models (ideal switching) for both VSIs, were considered. The most important outputs of the first set of simulations are voltage and current waves, fundamental and total RMS values, full and partial total harmonic distortion, *THF* (according to [33], see Appendix 6), individual harmonics,

⁹ In fact, the SPWM technique is being replaced by the space vector PWM (SVPWM) technique. However, for wave quality comparative analysis purposes, they are, in practice, identical.

as a function of the amplitude modulation index¹⁰ (or ratio), m_a , and frequency modulation index¹¹ (or ratio), m_f . Examples of results obtained with the first set of simulations are presented in Figs. 3.7, 3.9, 3.10-3.20, 3.31, 3.32, 3.40-3.44.

In the second set of simulations, 2L-VSI and 3L-VSI accurate/realistic models and a 3-kW, 4-pole, 400-V, 50-Hz IM dynamic model, were used, both based on models available in MATLAB/SIMULINK “SimPowerSystems” Toolbox [5], as it can be seen in Appendix 2. The used IGBT and diode models simulate properly the conduction losses (taking into account forward voltages and internal on-state resistance). However, the IGBT switching losses are not simulated in the available models. Therefore, additional features were added to the inverter models to take into account the IGBT switching losses as a function of the number of ON-OFF and OFF-ON state transitions and of the IGBT collector current magnitude in each transition instant [16], [18], [100]. The IGBT and diode loss related model constants and functions were based on manufacturer datasheets and on experimental results (see Appendix 2). Different operating conditions were simulated, i.e., different fundamental frequency, fundamental voltage, motor load, and switching frequency. Part of the results obtained with the second set of simulations are presented in Fig. 3.27.

In the experimental results, two 3.7-kW, 400-V 2L- and 3L-VSIs (both commercially available) and a 3-kW, 4-pole, 400-V, 50-Hz IM, were used. The 3L-VSI is a NPC-type inverter. The three-phase, 6-pulse, diode rectifier is equal for both inverters. Since commercial inverters were used (in which the user is not able to access internal processing), the amplitude modulation ratio was estimated on the basis of the DC-bus voltage, U_{DC} , and of the output fundamental voltage, U_I , and, for the overmodulation, simulated correction curves were used (U_I/U_{DC} as a function of m_a).

The testing facility used to test the VSI plus IM system, fulfils the accuracy requirement of the main motor testing standards (see Chapter 2 and Appendix 6). Motor and inverter efficiencies were measured by means of the input-output method, in which the efficiency is equal to the quotient between the input power (DC power in the case of the inverter and AC power in case of the motor) and the output power (AC power in the case of the inverter and mechanical or shaft power in the case of the motor), being both DC and AC powers measured by digital integration. Examples of experimental results are presented in Figs. 3.6, 3.21-3.26, 3.28-3.30, 3.33-3.36, 3.38, 3.39, 3.45-3.47, 3.49-3.50, and 3.53.

¹⁰ The amplitude modulation index or ratio is defined by the quotient between the peak amplitude of the sinusoidal control/reference wave (or modulating wave) and the peak amplitude of the triangular signal or carrier wave (generally kept constant), used to generate the switching signals when compared to the control signal.

¹¹ The frequency modulation ratio, m_f , is defined by the quotient between the carrier or switching frequency (of the triangular wave) and the fundamental frequency (of the modulating wave).

3.3.3 Inverter Output Voltage and Current Waveforms

In this section, the quality of the output voltage and current waves for both inverters is analyzed, based on simulated and experimental results.

In Fig. 3.7, the simulated output line-to-line (or phase-to-phase) voltage and phase current waveforms (current amplitude divided by the peak value of the current fundamental component at $f_l = 50$ Hz & $m_a = 1.0$) for both VSIs, considering $m_f = 41$ and $f = 50$ Hz, are presented. It should be noted that, for the 3L-VSI, if $m_a < 0.5$ then the output line-to-line voltage has a similar waveform to that of the 2L-VSI, but with halved limits.

In Fig. 3.8 the theoretical U_l/U_{DC} ratio as a function of m_a for m_f values, is present [16]. In Figs. 3.9 and 3.10, the line-to-line fundamental voltage to average DC-bus voltage ratio, U_l/U_{DC} , as a function of m_a is presented for 2L-VSI inverters, showing that in some situations the relation between U_l and U_{DC} is not linear in the so called linear region ($m_a < 1.0$), particularly when the m_f is even. In fact, the m_f can influence significantly the U_l/U_{DC} curve. In the presented cases, it can be seen that the 5- or 10-kHz switching frequency is an improper choice for 50 Hz, since it results in $m_f = \{100, 200\}$. In the case of 3L-VSIs, the nonlinearity U_l/U_{DC} relation for $m_a < 1.0$ does not happen for the referred m_f values, as it can be seen in Fig. 3.9. Nevertheless, the critical m_f values can be avoided by slightly changing f_s or f_l , to force the m_f to be noninteger or odd¹². These curves are directly related with the *THF* curves. If odd m_f is adopted, as recommended in [16], the *THF* is slightly lower, particularly for the 2L-VSI. However, for medium-high switching frequencies, as those considered in Fig. 3.9, the impact is not relevant. In practice, the U_l/U_{DC} relation does not depend on the fundamental frequency, as it can be seen in Fig. 3.10.

In Figs. 3.11 and 3.12, the fundamental and RMS values for the voltage and current are presented. In Figs. 3.13 and 3.14, full¹³ and partial *THF* of the voltage and current, as a function of m_a and m_f , can be seen. In Figs. 3.15 and 3.16, the 5th and 7th order harmonics of the current and voltage, as a function of m_a and m_f , can be seen. In Figs. 3.17 and 3.18 show the simulated power factor and the real power, as a function of m_a and m_f . In Figs. 3.19 and 3.20, the current and voltage partial and full *THF* as a function of m_f is presented for $m_a = \{0.25, 0.5, 0.75, 1.0, 1.25, 1.5\}$, evidencing the *THF* variation and particular peaks for both phase current and line-to-line voltage. Therefore, proper selection of m_f is required for *THF* reduction.

¹² It should be referred that, for large values of $m_f (> 21)$, the amplitudes of subharmonics associated with the asynchronous PWM (fixed triangular-wave frequency and variable modulating-wave frequency) are small. Therefore, at large values of m_f , the asynchronous PWM can be used, resulting in noninteger values of m_f for most of the output frequency values. However, if the inverter is supplying an IM, the subharmonics at zero or close to zero frequency, though small in amplitude, can result in large currents that are highly undesirable. For low values of $m_f (\leq 21)$, to eliminate the even harmonics, a synchronized PWM should be used and m_f should be an odd integer and multiple of 3, being the latter condition necessary to an equal harmonic content in the three phase voltages and, therefore, to cancel out the most dominant harmonics in the output line-to-line voltages. During overmodulation ($m_a > 1.0$), regardless of the value of m_f , the conditions pertinent to a small m_f should be observed [16].

¹³ Full *THF* means that all the mathematically possible harmonics of the simulated spectrum range. Partial *THF* means that only harmonics up to 19th order are being considered.

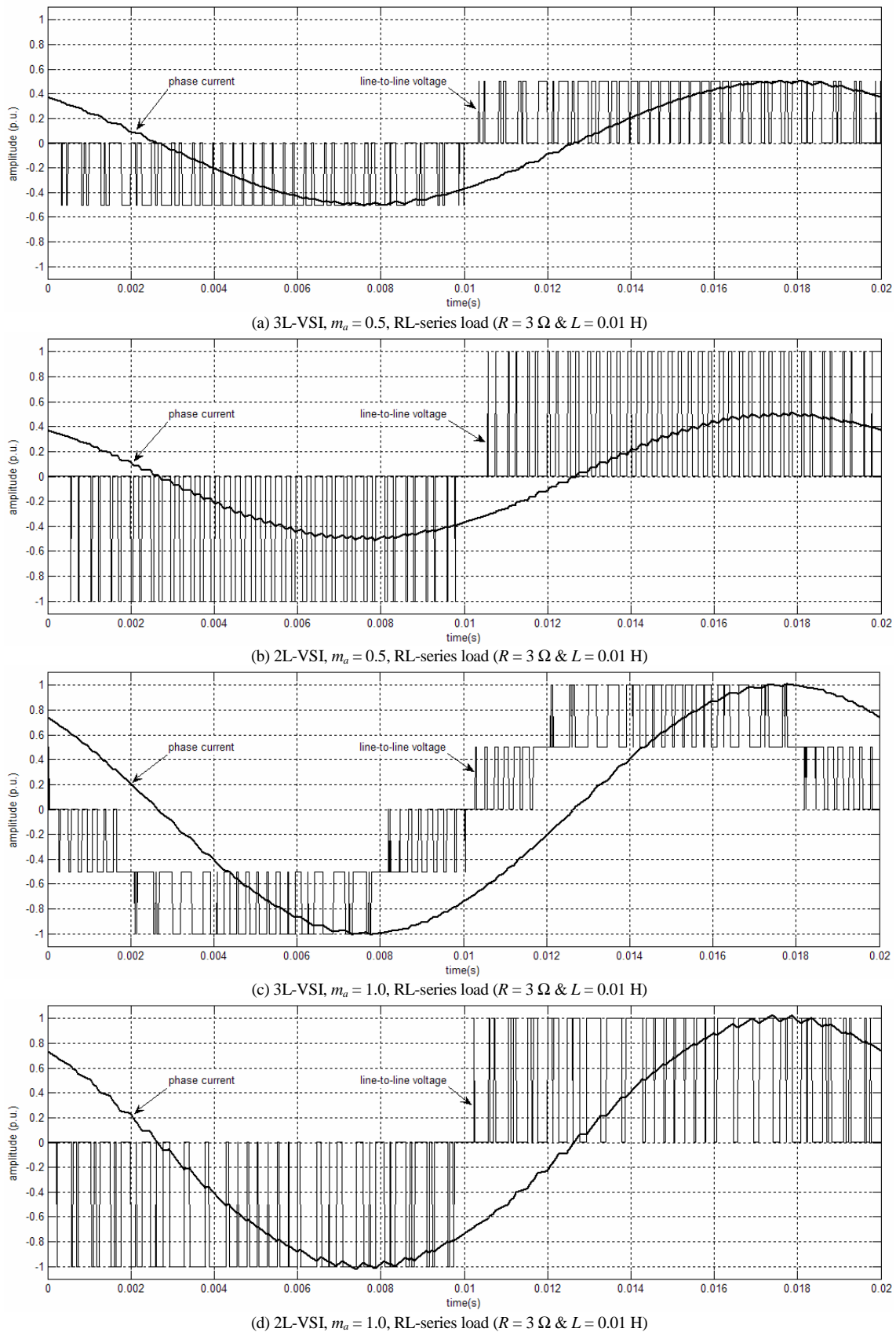


Fig. 3.7. Simulated phase current and line-to-line voltage waveforms.

On the basis of the first set of simulations, some remarks can be made [15]: (a) The 3L-VSI leads to a significant lower voltage and current full *THF*, particularly for $m_a < 1.0$; (b) Significant differences were found between the full and partial *THF*, having the first a more

regular variation; (c) For $m_f > 20$, its influence on the voltage wave quality is minor, regardless the m_a value, particularly when the full *THF* is considered; (d) The 2L-VSI produces higher low-frequency harmonics (which are represented by the partial *THF*); (e) In general, the low-frequency harmonics increase with m_a ; (f) The full *THF* decreases significantly with the increase of m_a , being this variation higher for the 3L-VSI; (g) The partial *THF* is, in general, minimized for $m_a = 1.0$; (h) Some specific m_a - m_f combinations lead to a significant increase of the voltage partial *THF* and of the current partial and full *THF*, and, therefore, they should be avoided; (i) A significant increase of the 5th and 7th voltage harmonics happen for m_a values in the range [1.0 2.0], in which it is included the typical m_a value for inverters generating fundamental line-to-line voltage equal or near to the rectifier input line-to-line voltage (typically 400 V); (j) The 2L-VSI has more m_a - m_f combinations with specific high amplitudes for the 5th and/or 7th harmonics; (l) The motors should be properly adapted to the inverters to avoid the operation in the overmodulation region; (m) In general, the m_f has no significant influence on the relation between the m_a and the fundamental component of the voltage, as expected; (n) For $m_f > 20$, the nature (even or odd) of m_f has minor influence on the *THF*; (o) For $m_f < 100$, the phase current full *THF* increases regularly with the decrease of the m_f . An important conclusion is that, in general, the m_a should be as near as possible to unity to minimize the voltage and current *THF*.

On the basis of steady-state results of the simulations with IM dynamic model and VSI realistic models (second set of simulations, Fig. 3.27), it is possible to conclude that, for the same fundamental voltage, m_a has to be slightly higher for the 3L-VSI due to its slightly higher voltage drop in the IGBT sets (in relation to the 2L-VSI), leading to a slight increase in low-order harmonics (particularly the 5th and 7th harmonics). Additionally, when compared with the 2L-VSI, the 3L-VSI produces a voltage *THF* significantly lower, regardless the m_f value, and for both inverters the current *THF* increases significantly with the decrease of m_f , as expected.

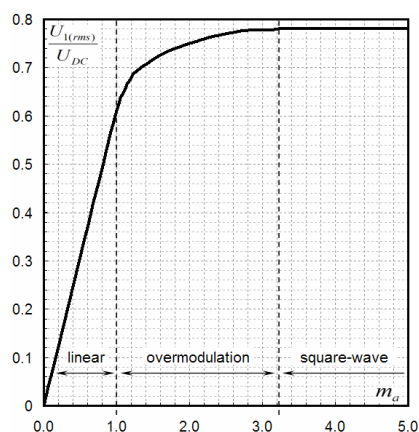


Fig. 3.8. Theoretical U_1/U_{DC} ratio as a function of m_a for 3-phase, 2-level, voltage-source inverters ($m_f = 15$). Square-wave operation for $m_a = 3.24$ [16], [17], [18], [52].

In Fig. 3.21, the experimental *THF* of the line-to-line voltage, can be seen, for a 7.5-kW motor. In Figs. 3.22 and 3.25, the experimental line-to-line voltage and phase current *THF* for different motor loads and the average values of the 5th, 7th and 11th voltage harmonics for a set of different motor load points, are presented, being the m_a values estimated. The experimental results confirm that the variation of the voltage *THF* as a function of m_f can be, in general, ignored, but it increases significantly with the decrease of m_a , as it was demonstrated in the simulated results. It is also evidenced that the lower voltage and current distortion for the 3L-VSI.

Fig. 3.24 shows that, for $m_a \leq 0.5-0.6$, the 3L-VSI leads, in general, to higher low-frequency harmonics. This can be explained, in part, as a consequence of the much higher equivalent m_a (calculated on the basis of half the DC voltage value), i.e., for an absolute $m_a \leq 0.5-0.6$ (calculated on the basis of DC-bus voltage and fundamental output voltage), the 3L-VSI has an equivalent m_a near 1.0 (see Fig. 3.7a,b). As expected, the low-order harmonics are much lower for $m_a < 1.0$. It is important to refer that, due to the high voltage drop in the 3L-VSI¹⁴, for the same U_l it is necessary a higher m_a , leading to higher low-order harmonics (e.g., 5th and 7th order). Full *THF* of the voltage produced by the 2L-VSI is significantly higher over all the m_f range. In general, the output current *THF* is higher for the 2L-VSI, but exceptions may occur in some particular m_f values. Fig. 3.23 also shows that voltage *THF* is, in practice, independent of the motor load.

Partial *THF* (which includes the 5th, 7th, 11th, 13th, 17th and 19th harmonics) of the voltage produced by the 2L-VSI is significantly higher for the lower m_f values, and, except for some specific m_f values, is in general equivalent to the *THF* of the 3L-VSIs for higher m_f values, as it can be seen in Fig. 3.20.

In Fig. 3.21, the voltage *THF* and *THD* difference can be seen, which is slight for low *THF* values, but for higher values it can be significant, thus being important to identify which standard is being considered for comparison or analysis purposes. There is no significant variation of the total voltage distortion with the inverter load, as expected.

In a VSI using SPWM technique, the m_a should be maintained as close as possible to 0.8-1.0 range, as explained before. There are two main types of PWM: synchronous (constant m_f , encouraged for $m_f \leq 21$, providing it is multiple of 3 and odd integer [16]) or asynchronous (constant switching frequency, encouraged for $m_f > 21$ [16]). The asynchronous PWM is a typical strategy in general-purpose commercial inverters. In the linear modulation ($m_a \leq 1.0$), the fundamental-frequency component in the output voltages varies linearly with the m_a except for the particular m_f values previously referred and sideband harmonics centered around the

¹⁴ There is always one IGBT of the 4 IGBT per leg in ON-state.

frequencies of harmonics of order m_f and its multiples are the most significant, and, although without significant impact on motor torque, are responsible for most harmonic core losses.

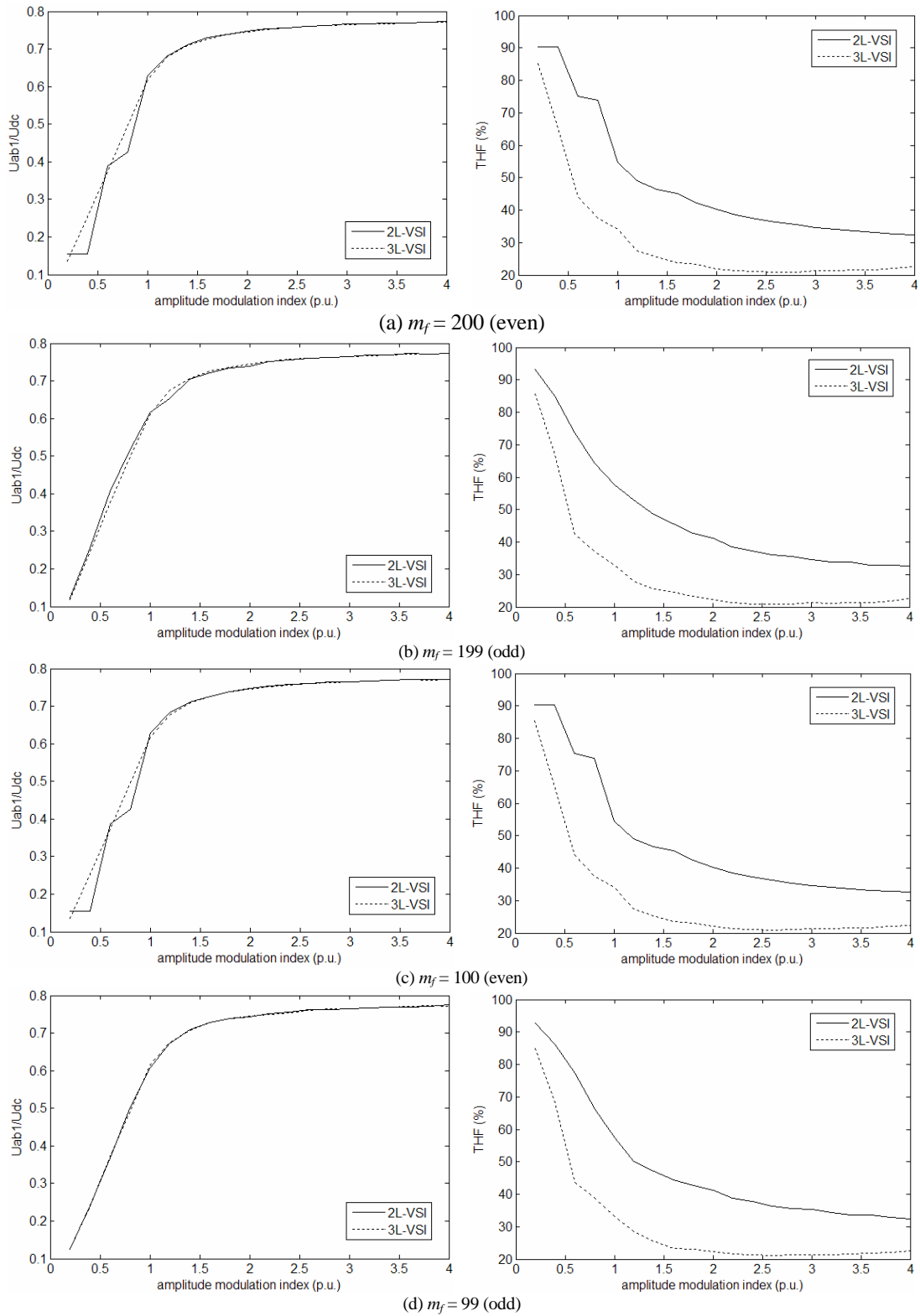


Fig. 3.9. Simulated U_j/U_{DC} and THF as a function of m_a for 2L- and 3L-VSIs, $f_l = 50$ Hz and $m_f = \{99, 100, 199, 200\}$.

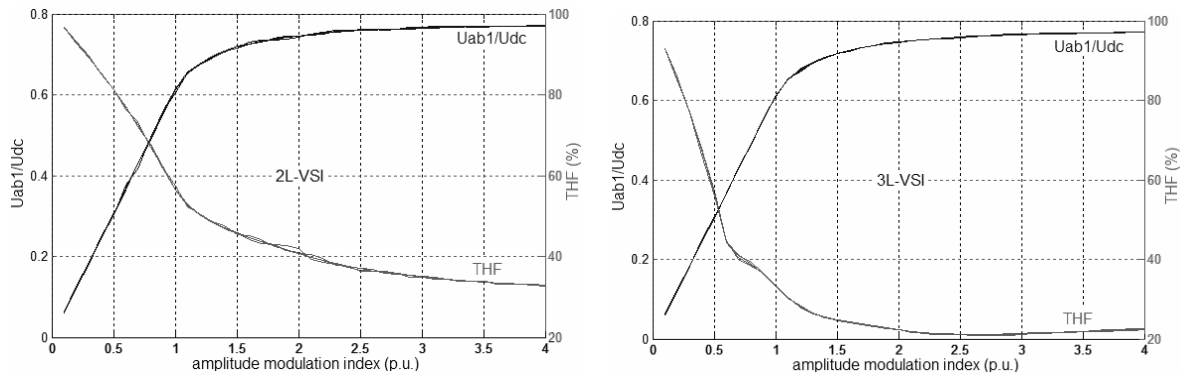


Fig. 3.10. Simulated U_j/U_{DC} and THF as a function of m_a for the 2L-VSI (left) and the 3L-VSI (right). Superposition of the curves for $m_f = \{81, 41, 27, 21\}$ and $f_1 = \{25, 50, 75, 100\}$ Hz,

In a 2L-VSI using SPWM operating in the linear region, the m_a is given by (3.1), where the hat “^” denotes the maximum or peak value [16], [17], [18]. In a three-phase, six-pulse, diode rectifier without output capacitor, the DC or average output voltage is given by (3.2) [16], [17], [18]. Substituting (3.2) into (3.1) yields (3.3), which is valid for the linear region. The 3L-VSI has, in practice, two modulation indexes - one related to the PWM waveform for voltages up to half the nominal voltage and another for voltage higher than half the nominal voltage (the SPWM strategy for the 3L-VSIs is described in Appendix 2). This aspect is the key for improved PWM waveform of the 3L-VSIs. The voltage THF difference for both 2L- and 3L-VSIs is particularly high for m_a near 0.5. For low fundamental frequencies and/or voltages, this difference is attenuated (Fig. 3.24).

$$m_a = \frac{\hat{U}_{control}}{\hat{U}_{carrier}} = \frac{2\sqrt{2} \cdot U_{ll-1}}{\sqrt{3} \cdot U_{DC}} = 1.634 \frac{U_{ll-1}}{U_{DC}} \quad (3.1)$$

$$U_{DC} = \frac{3}{\pi} \sqrt{2} \cdot U_{ll(grid)-1} = 1.35 \cdot U_{ll(grid)-1} \quad (3.2)$$

$$U_{ll-1} = \frac{3\sqrt{3}}{2\pi} \cdot m_a \cdot U_{ll(grid)-1} = 0.827 \cdot m_a \cdot U_{ll(grid)-1} \quad (3.3)$$

As it can be seen in Figs. 3.8-3.11, in the nonlinear or overmodulation¹⁵ ($1 < m_a < \approx 3.5$) and square-wave ($m_a > \approx 3.5$) regions, (3.1) and (3.2) are no longer valid. In the overmodulation region, the peak of the control voltages is allowed to exceed the peak of the triangular waveform. Unlike the linear region, in this mode of operation the fundamental-frequency voltage magnitude does not increase proportionally with m_a , thus, as referred before, the m_a has to be estimated based on the simulated curves if only the U_{ll-1} and U_{DC} are known.

¹⁵ There are techniques to extend the linear modulation region by means of injection of 3rd order harmonics in the reference/modulating waves.

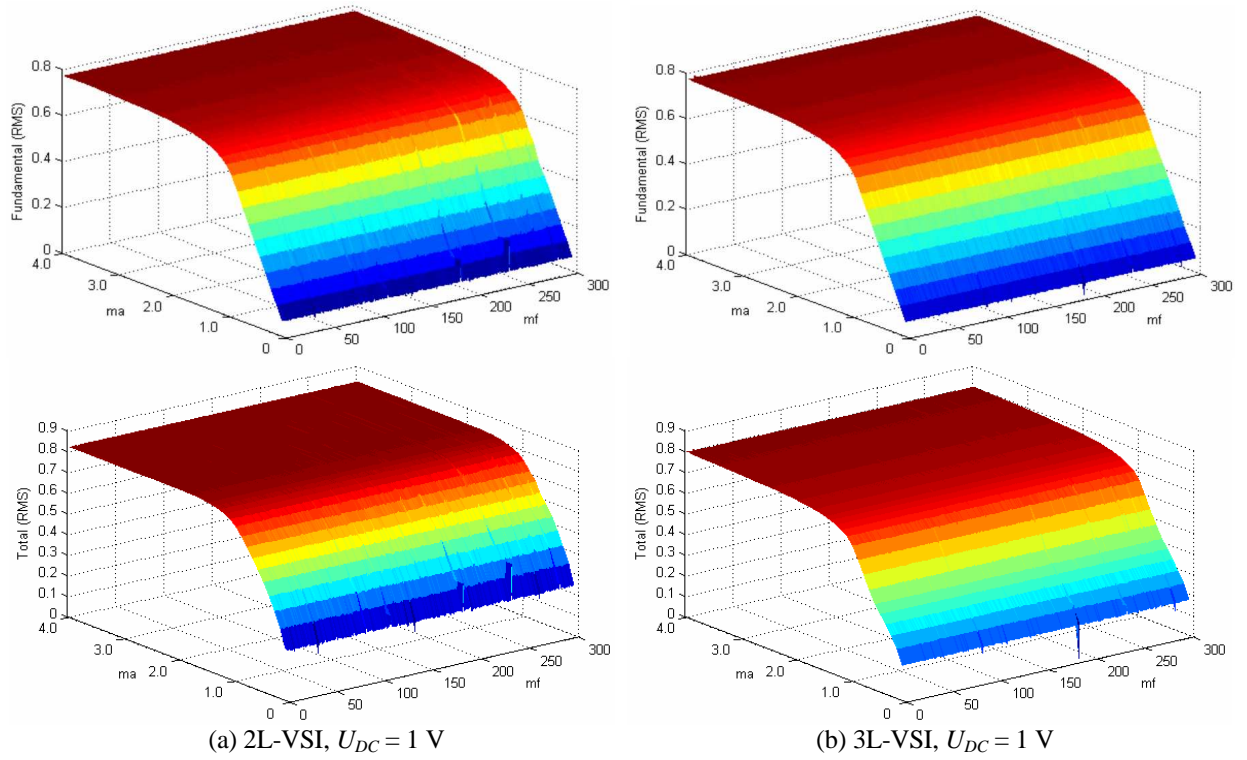


Fig. 3.11. Simulated fundamental and total RMS line-to-line voltage, as a function of m_a and m_f , for $f_j = 50$ Hz.

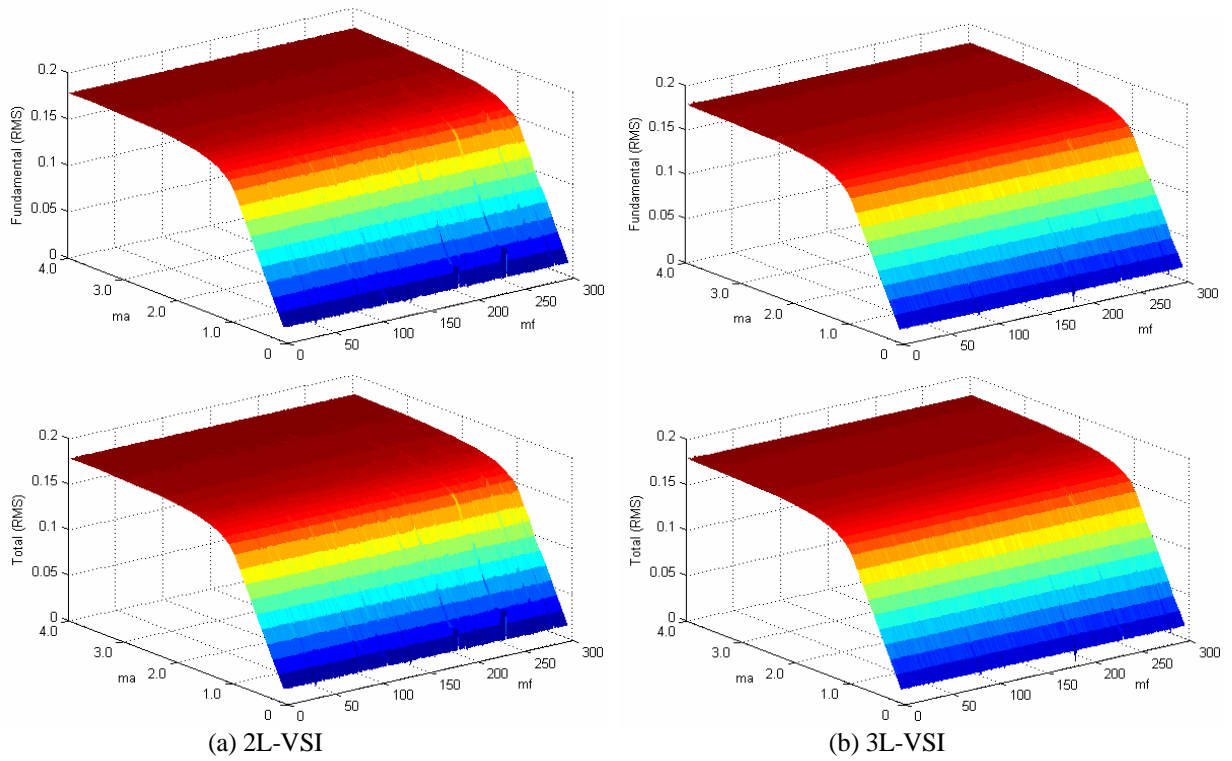
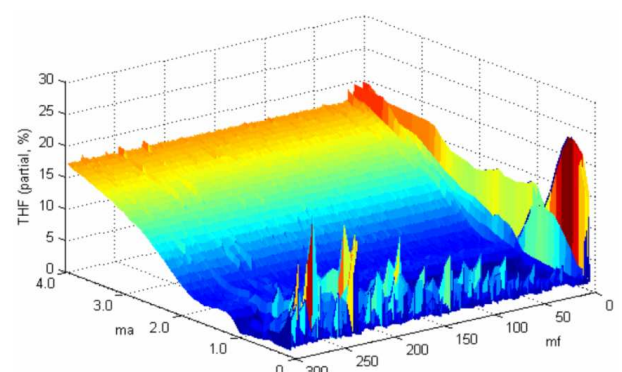
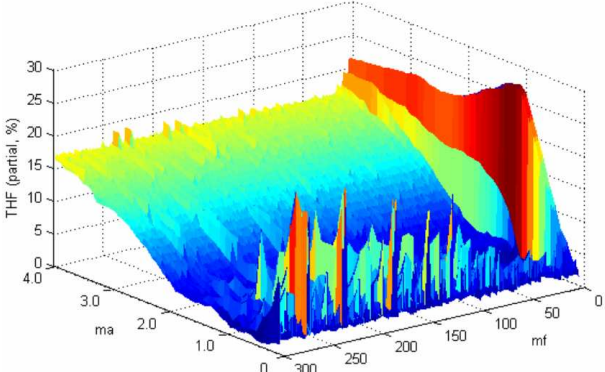
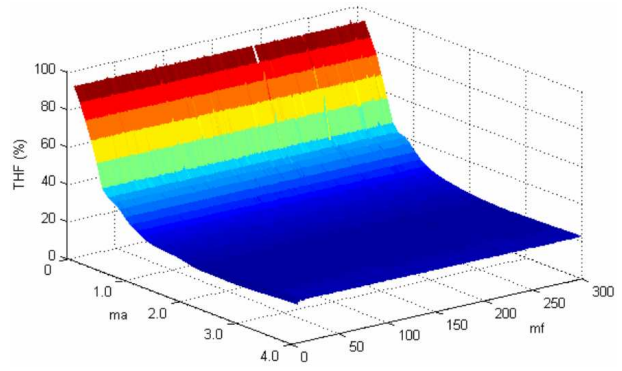
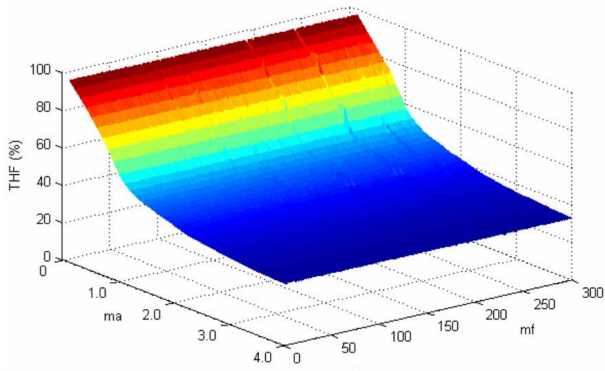


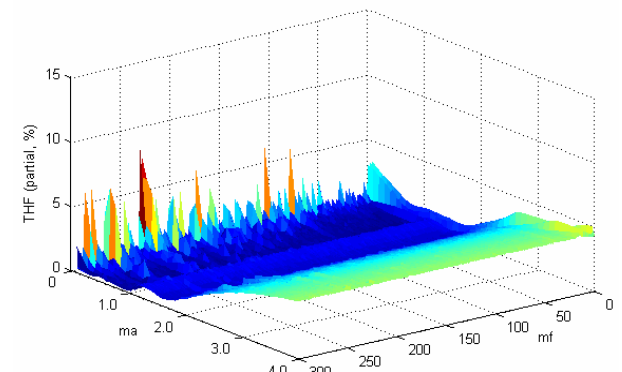
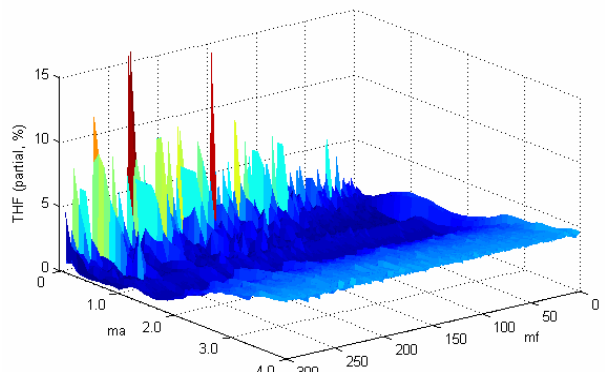
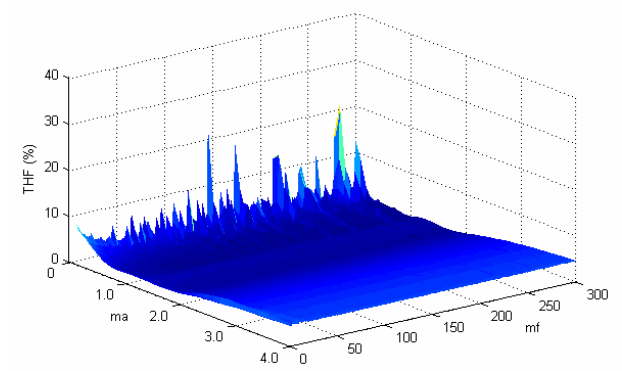
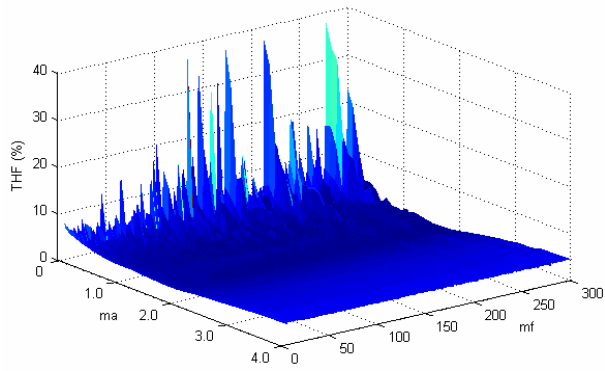
Fig. 3.12. Simulated fundamental and total RMS value of the phase current, as a function of m_a and m_f , for $f_j = 50$ Hz.



(a) 2L-VSI

(b) 3L-VSI

Fig. 3.13. Simulated line-to-line voltage *THF* (full and partial), as a function of m_a and m_f , for $f_j = 50$ Hz.



(a) 2L-VSI

(b) 3L-VSI

Fig. 3.14. Simulated phase current *THF* (full and partial), as a function of m_a and m_f , for $f_j = 50$ Hz.

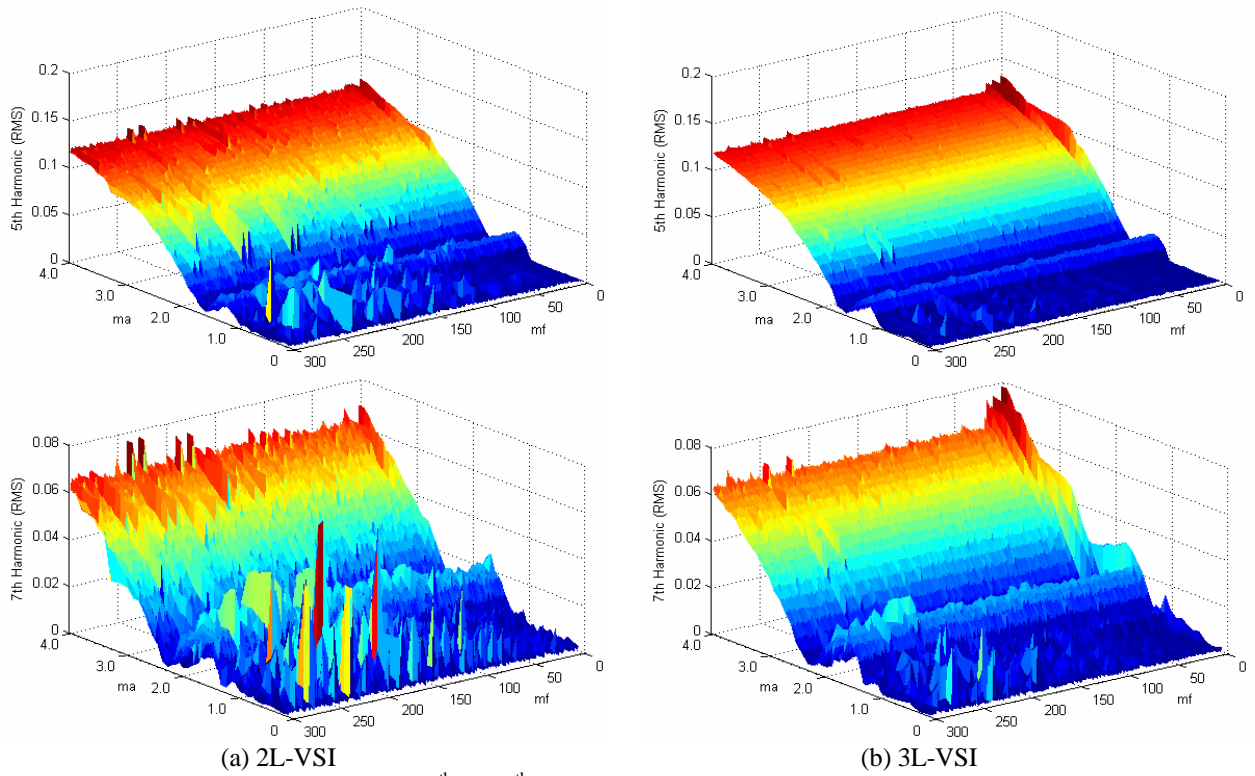


Fig. 3.15. Simulated line-to-line voltage 5th and 7th harmonic, as a function of m_a and m_f , for $f_i = 50$ Hz.

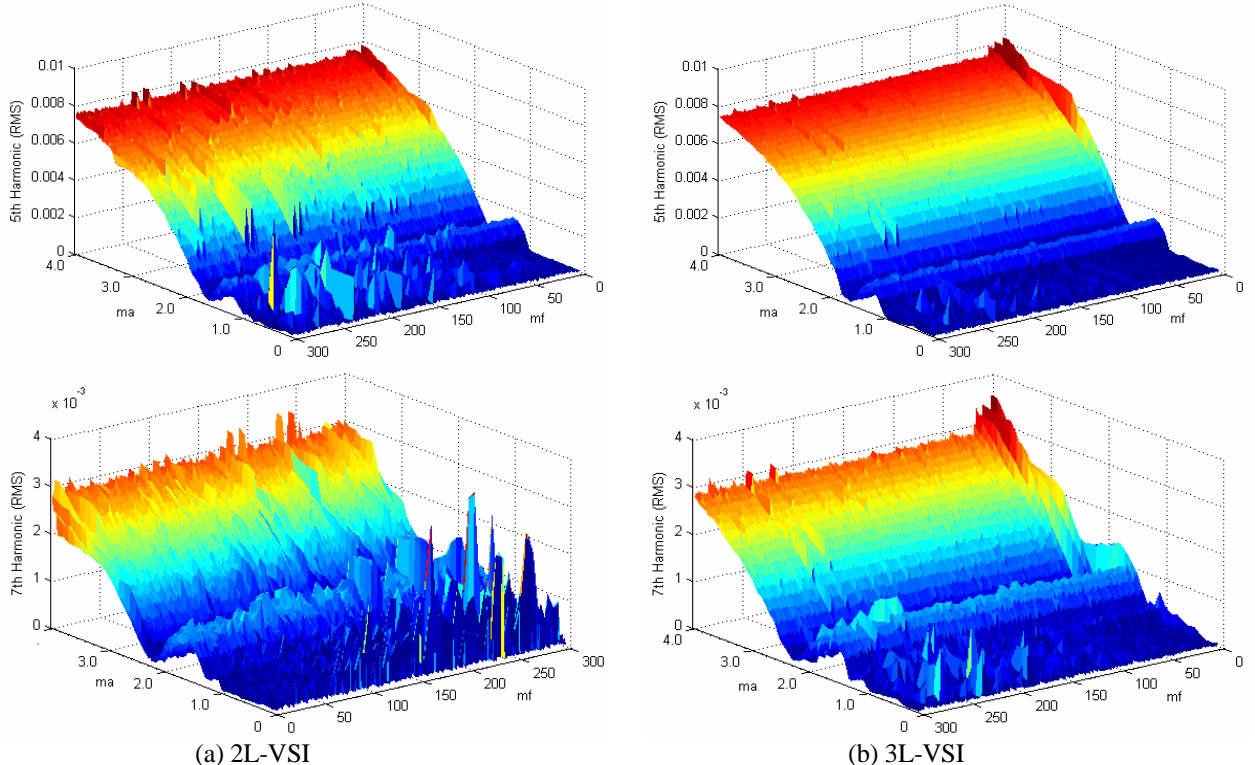


Fig. 3.16. Simulated phase current 5th and 7th harmonic, as a function of m_a and m_f , for $f_i = 50$ Hz.

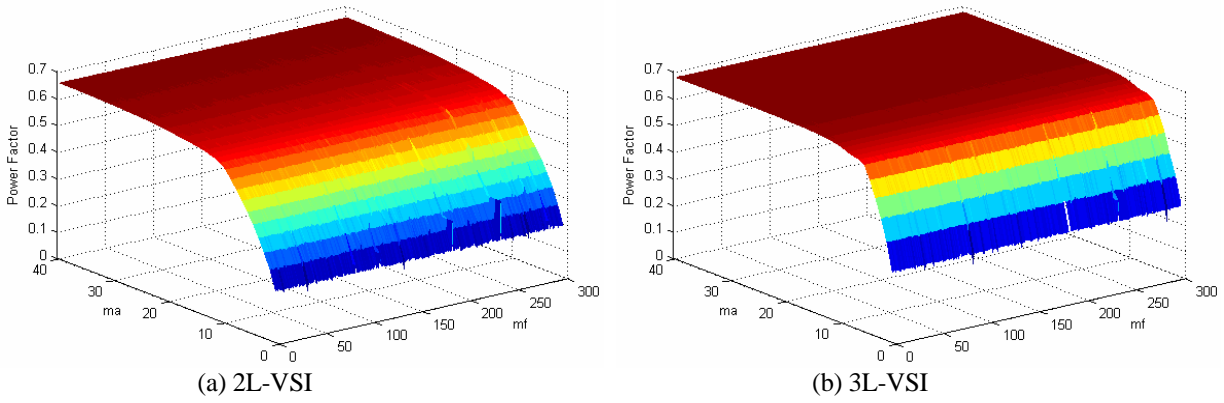


Fig. 3.17. Simulated power factor as a function of m_a and m_f , for $f_l = 50$ Hz.

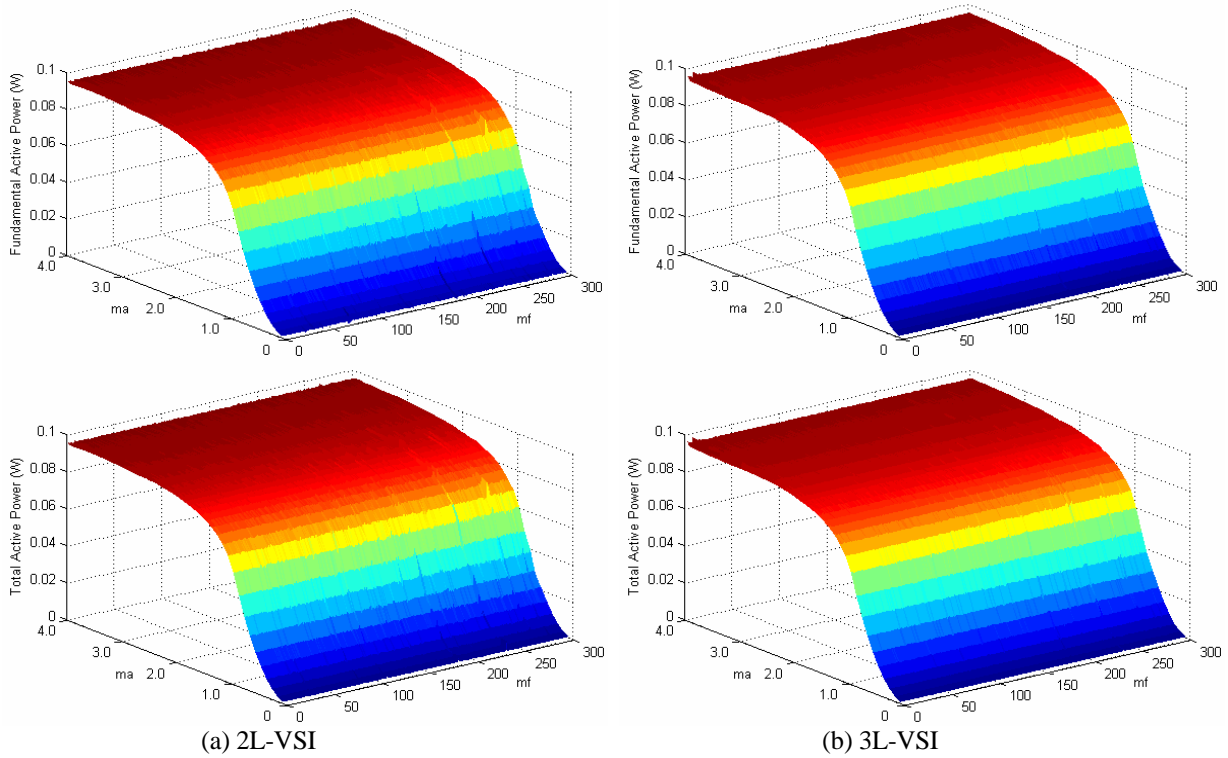


Fig. 3.18. Simulated fundamental and total active (or real) power as a function of m_a and m_f , for $f_l = 50$ Hz.

For sufficient large values of m_a , the PWM degenerates into a square-wave inverter waveform (square-wave mode operation), and the fundamental line-to-line voltage component in the output can be calculated by (3.4), resulting in a maximum value of $U_{ll,1}$ approximately equal to $0.78 \cdot U_{DC}$. In the square-wave mode of operation, the inverter itself cannot control the magnitude of the output AC voltages [16].

$$U_{ll,1} = \sqrt{\frac{3}{2}} \frac{4}{\pi} \frac{U_{DC}}{2} = \frac{\sqrt{6}}{\pi} U_{DC} \approx 0.78 \cdot U_{DC} \quad (3.4)$$

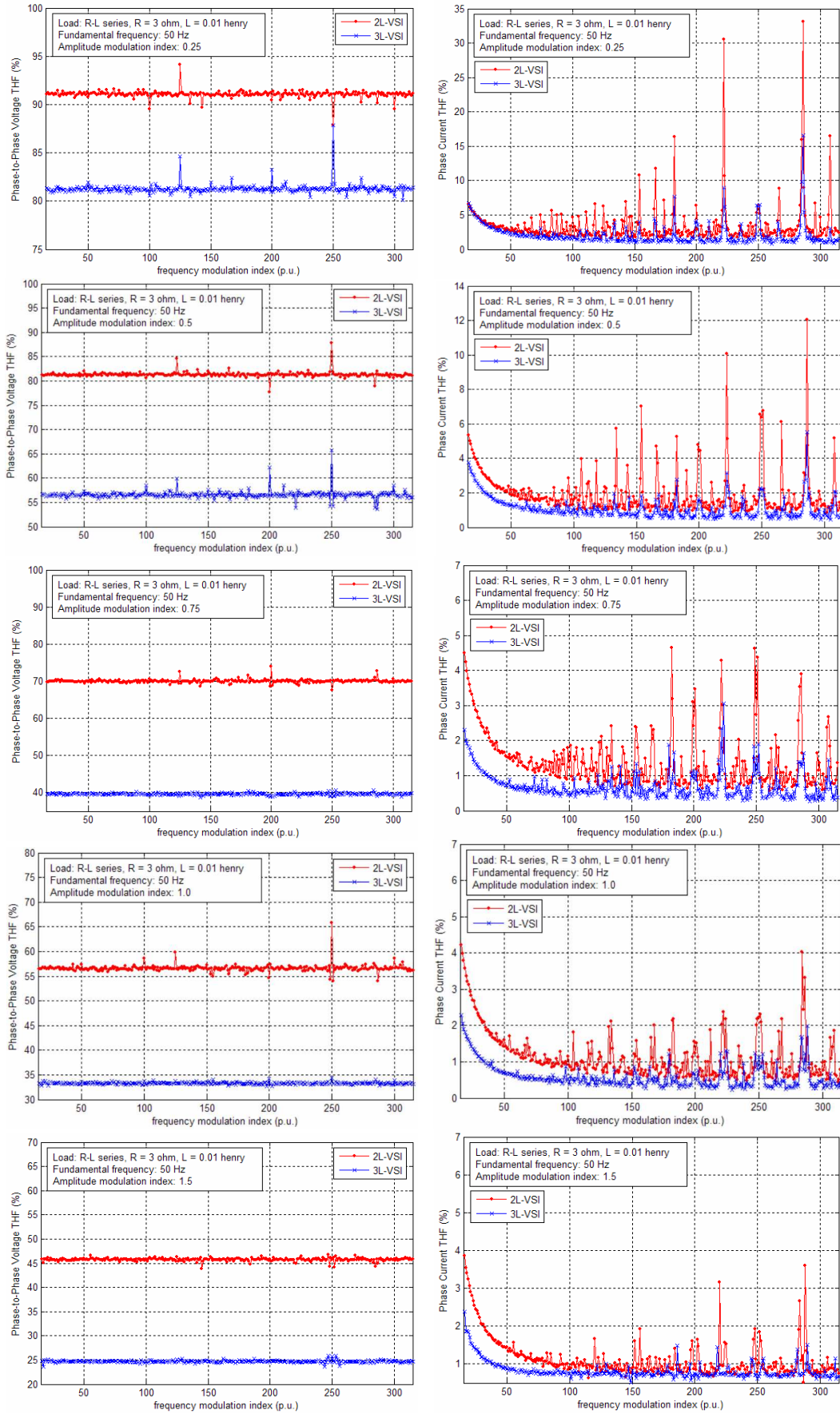


Fig. 3.19. Simulated current and voltage full THF as a function of m_f for different m_a .

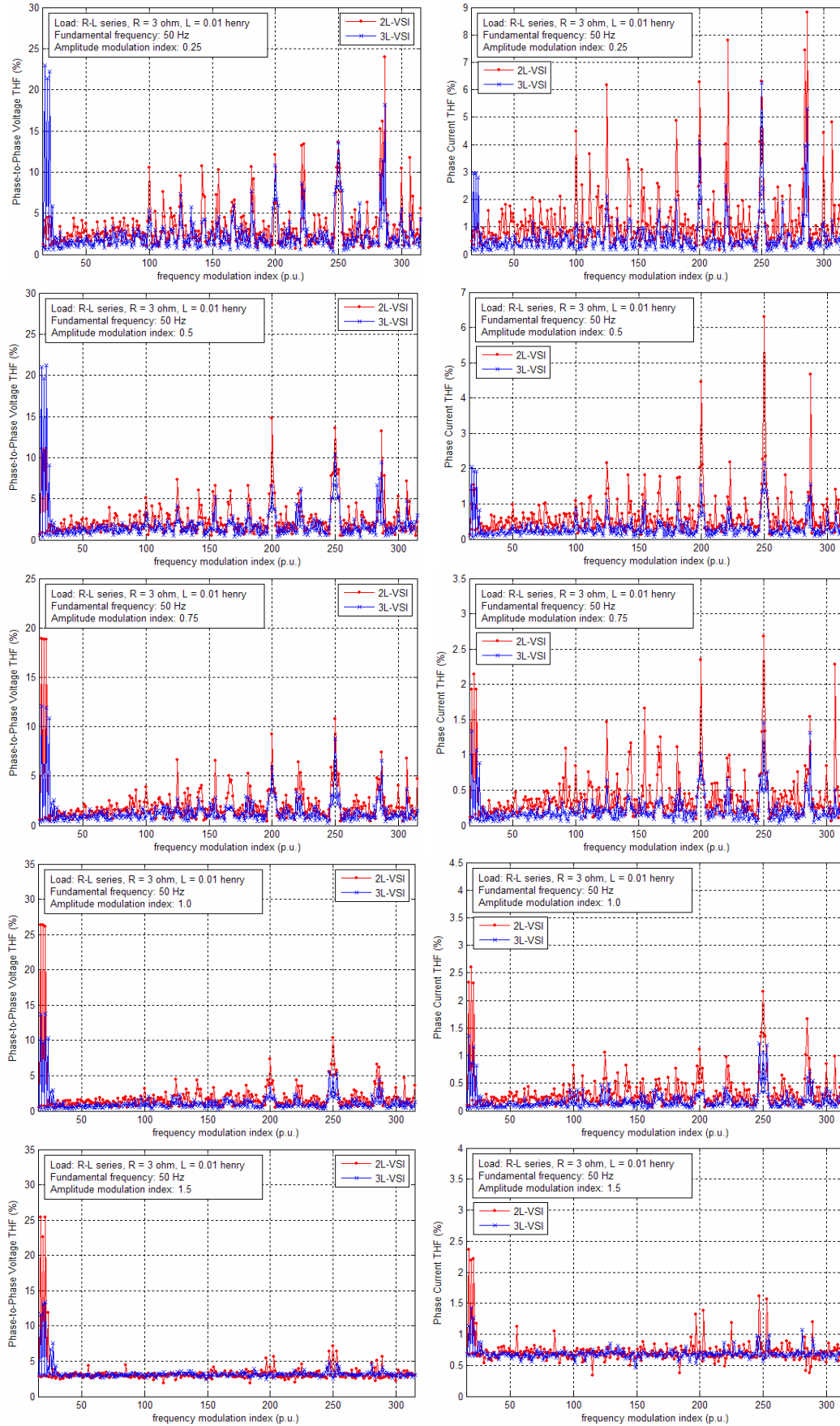


Fig. 3.20. Simulated current and voltage partial THF as a function of m_f for different m_a .

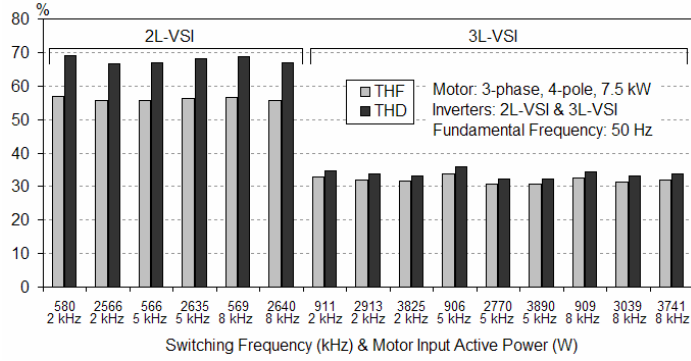


Fig. 3.21. Experimental *THD* and *THF* of line-to-line voltage, for a delta-connected, 4-pole, 7.5-kW, IM, fed by a 2L- and a 3L-VSI. Calculation with MATLAB [33].

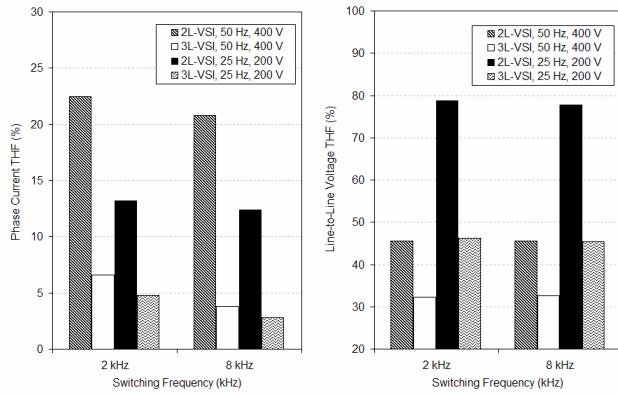
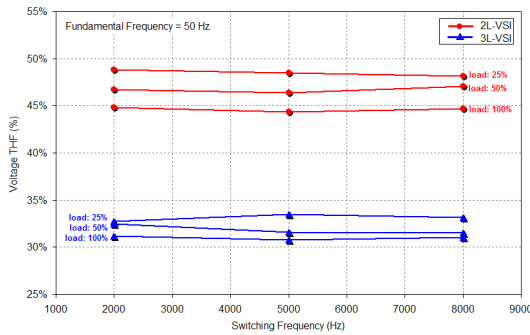
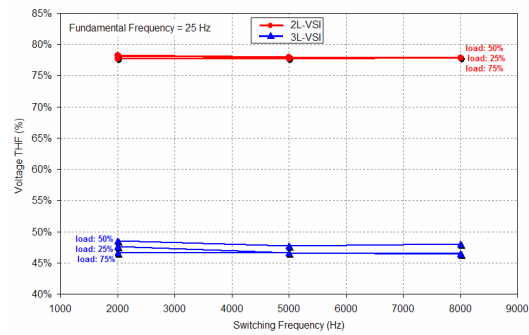


Fig. 3.22. Experimental line-to-line voltage and phase current *THF* for a delta-connected, 4-pole, 3-kW IM with 30% load. Calculation with MATLAB.



(a) $f_1 = 50$ Hz, $U_1 = 400$ V



(b) $f_1 = 25$ Hz, $U_1 = 200$ V

Fig. 3.23. Experimental line-to-line voltage *THF* for different motor loads, as a function of f_s , for a delta-connected 4-pole, 3-kW IM fed by a 2L- and a 3L-VSI.

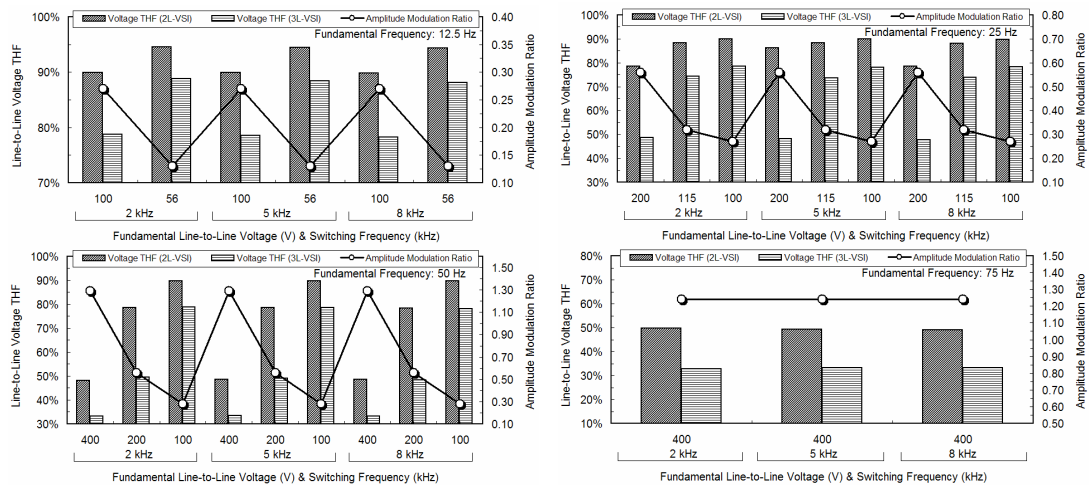


Fig. 3.24. Experimental line-to-line voltage *THF*, for no-load operation and different f_s , f_1 and U_1 (3-kW, 4-pole, delta-connected motor, *THF* calculated directly by the Power Analyser)

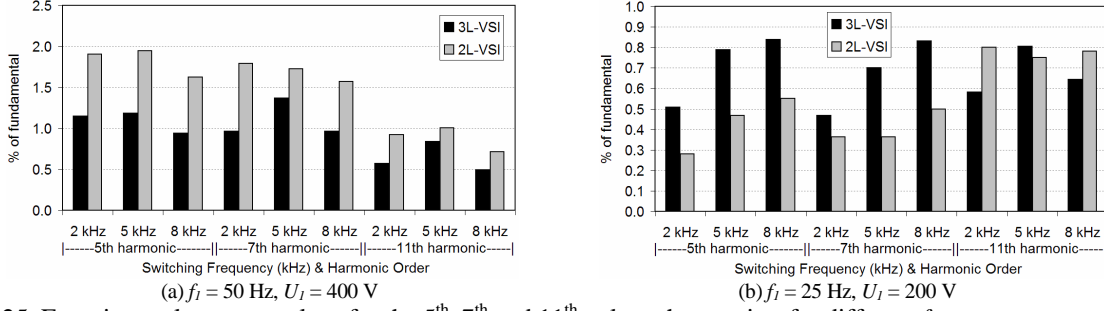


Fig. 3.25. Experimental average values for the 5th, 7th and 11th voltage harmonics, for different f_s .

Considering a grid with 400-V line-to-line voltage, the inverter input DC voltage is 540 V (without output capacitance), but can reach 566-585 V, being that value dependent on the DC-bus capacitance, on actual inverter load, and on the actual grid line-to-line voltage¹⁶. Therefore, for $m_a = 1.0$, the output line-to-line voltage fundamental component can vary within 331-358 V, forcing the inverter to operate in the overmodulation region to feed the motor at fundamental voltage equal to the VSD input voltage (400 V). Overmodulation can be used to push up the output voltage, but more sideband harmonics centered around the frequencies of harmonics of order m_f and its multiples, with relatively low amplitude [16], and higher low-order harmonics, will appear, as it can be seen in Fig. 3.13, potentially leading to extra motor losses. In the square-wave region, the maximum inverter output line-to-line voltage fundamental component can reach 421-456 V, depending on the referred factors, and contains significant low-order harmonics ($h = 6n \pm 1; n = 1, 2, 3, \dots$), whose amplitudes are proportional to the reciprocal of their harmonic order, according to (3.5), and are responsible for motor torque pulsations, torque-speed curve degradation, slip increase and extra losses. The most undesirable are particularly the negative-sequence harmonics (5th, 11th, etc.), as shown in Appendix 4.

$$U_n = \frac{0.78}{h} U_{DC} \quad (3.5)$$

Considering a 400-V grid connected VSD with 566-V DC-bus voltage, feeding a 400-V IM, for $m_a \approx 1.0$, at 50 Hz, the expected line-to-line fundamental voltage at the motor terminals is 346 V, and to rise up the fundamental voltage to 400 V the m_a has to be increased up to approximately 1.4 (overmodulation), creating significant low-order harmonics, inevitably. One way to avoid entering into overmodulation region is (re)designing the IM stator winding (e.g., if the motor needs to be rewound) to a rated voltage within 345-355 V, for example, following the methodology proposed in Appendix 3. Moreover, the proposed (re)matching strategy between IM and VSD, since there is a higher voltage percentage increase above motor

¹⁶ The line-to-line voltage can vary over the day, in part, due to the variation of the power network load.

rated voltage capability (say, from 345 V to 440 V fundamental voltage), the field weakening operation region (with higher motor slip, thus poor efficiency) will start at a frequency 27.5% higher than rated frequency, which can be an important advantage. Of course, if the VSD-fed IM is oversized at rated frequency, the lower voltage required to optimize magnetizing flux and, thus, motor efficiency, can be, in some cases, held by the VSD within linear region.

It should be also referred that the increase of the DC-bus voltage lead, in general, to the increase of the inverter switching losses (and, consequently, to the reduction of the inverter efficiency), due to the higher pulse amplitude handled by the power switches and to the higher number of switching instants per fundamental period (lower m_a).

In Fig. 3.26, the experimental power factor curves for a 3-kW motor as a function of load, when fed by the 2L-VSI and by the 3L-VSI, are shown. Since the distortion is lower for the 3L-VSI, the power factor at the motor input results slightly higher, as expected, leading to a slightly higher line current RMS value for the same real power, contributing to extra losses in the inverter.

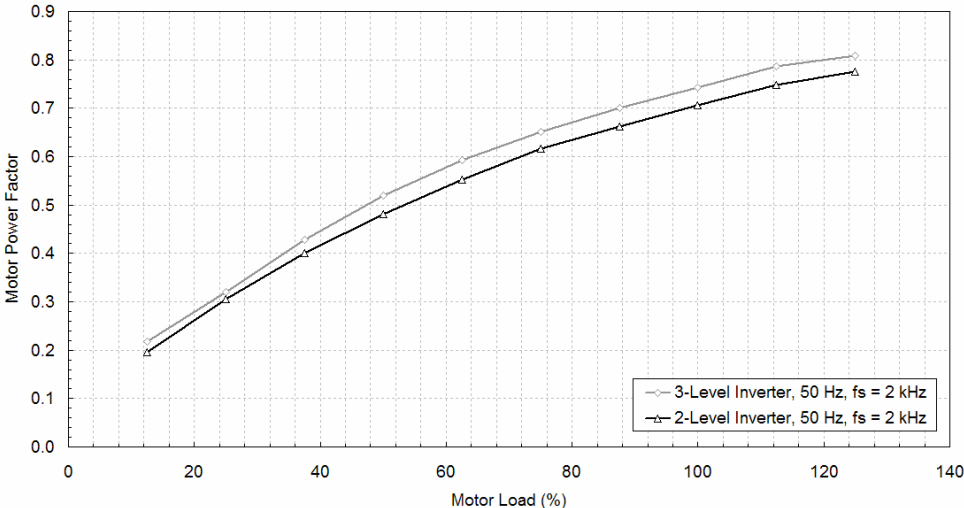


Fig. 3.26. Experimental motor power factor as a function of load, $U/f = 8$, for a 3-kW system.

3.3.4 Inverter Losses

In this section, the losses of both VSIs are analyzed based on simulated and experimental results. In Fig. 3.27, the simulated inverter losses and efficiency for both VSIs, as a function of switching frequency, for motor full-load, $f = 50$ Hz, $U_1 = 400$ V, are shown. In Figs. 3.28 and 3.29, the experimental inverter losses and efficiency for both VSIs, as a function of switching frequency and motor load, are shown. The matching between simulated and experimental results is fair. Fig. 3.30 shows the average of the experimental inverter losses for a set of different motor loads.

On the basis of Fig. 3.27, it is possible to conclude that, for a particular load point, the inverter efficiency is maximized for a specific switching frequency ($f_s = 2$ kHz for the presented results), which depends on the balance between switching and ON-state (or conduction) losses. Above that point, the inverter losses increase with m_f , as expected, as it was verified by both simulated and experimental results (Figs. 3.27 and 3.28). Therefore, it is possible to state that, for each inverter, there is an optimum switching frequency, which minimizes the inverter total losses (but not necessarily the overall system losses). The inverter efficiency also increases significantly with the load or output current, as expected (Fig. 3.28). For $f_s \leq 10$ -12 kHz and motor loads between 75% and 100% of full-load, the 3L-VSI has higher losses (being less efficient) than the 2L-VSI, but for higher switching frequencies and/or significant lower loads, this condition can be reversed. It was also verified that the 3L-VSI has a higher ON-state losses component, as expected, thus being more sensitive to the load or current variation. The 2L-VSI has higher switching losses component, being more sensitive to the switching frequency variation. However, as it can be seen in Fig. 3.29, the 3L-VSI is, in general, less efficient than the 2L-VSI.

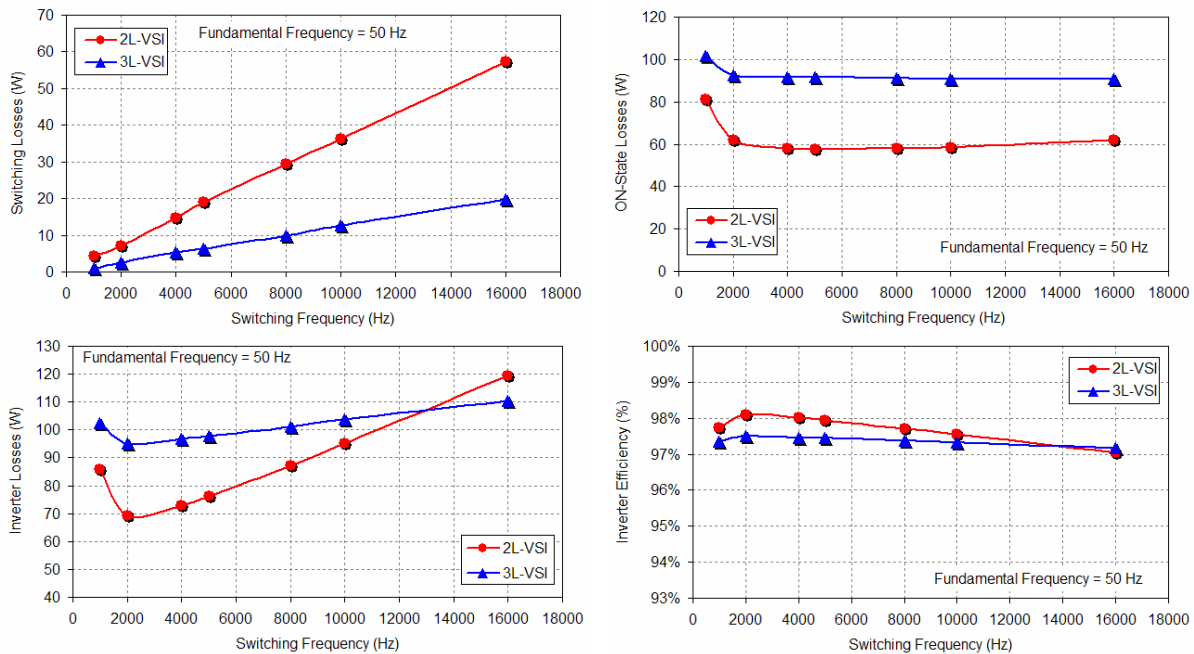
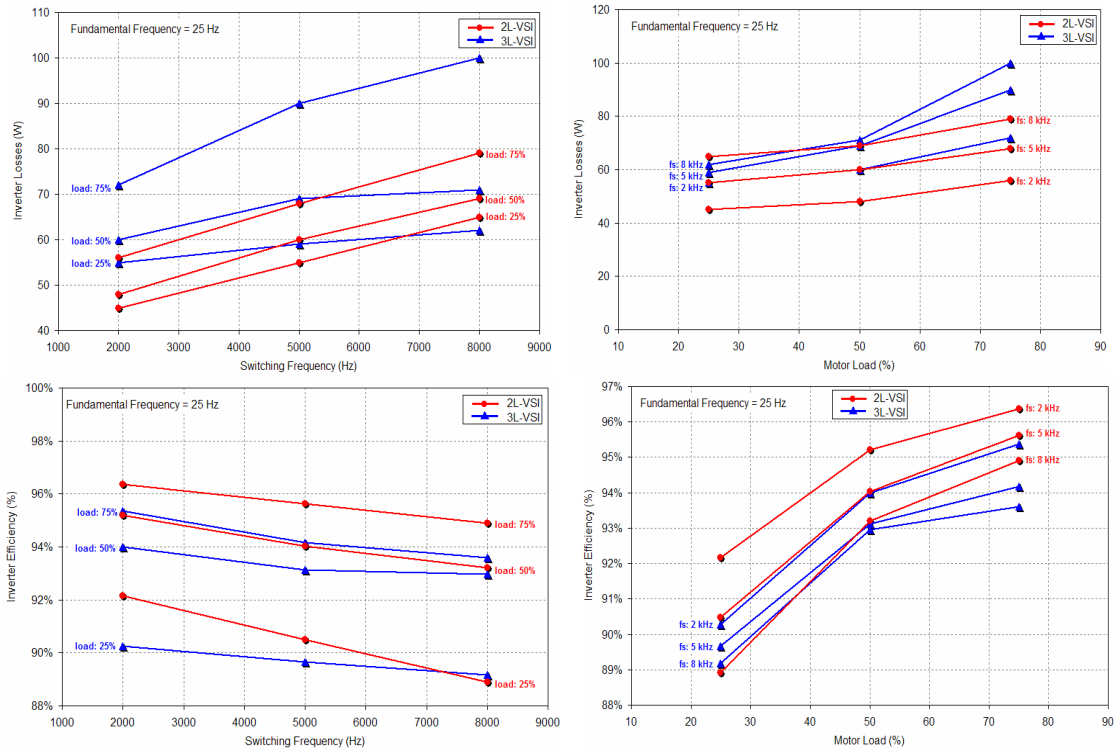
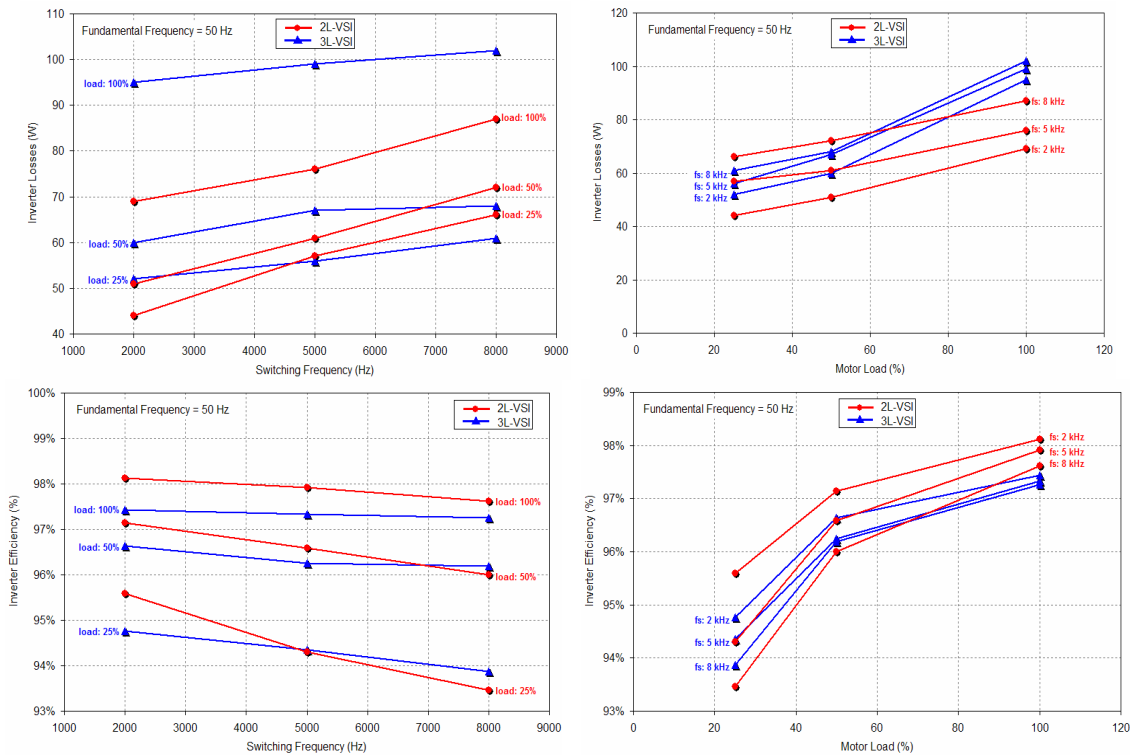


Fig. 3.27. Simulated inverter losses and efficiency, as a function of f_s ($U_I = 400$ V, full-load) [15].



(a) $f_i = 25$ Hz, $U_i = 200$ V



(b) $f_i = 50$ Hz, $U_i = 400$ V

Fig. 3.28. Experimental inverter losses and efficiency, as a function of f_s and motor load [15].

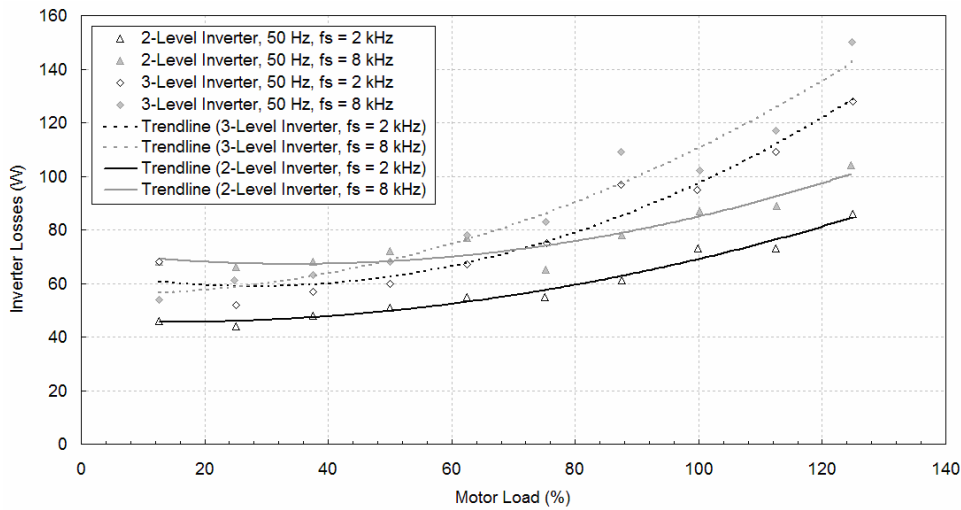


Fig. 3.29. Experimental inverter losses as a function of motor load for a 3-kW system, for constant magnetizing flux ($U_l = 400$ V, $f_l = 50$ Hz).

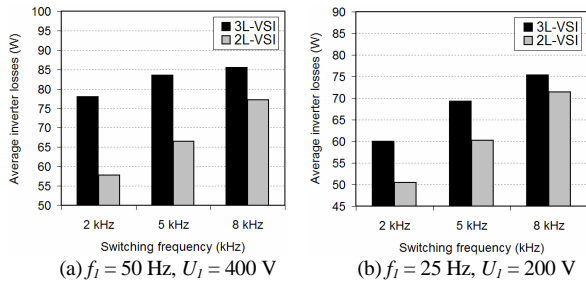


Fig. 3.30. Average of the experimental inverter losses for a set of different motor loads (equally spaced) [15]:

(a) 11 different motor loads ranging from no-load to 125% of rated power;

(b) 8 different motor loads ranging from no-load to 87.5% of rated power.

3.3.5 Impact of the Inverter on the Motor Performance and Reliability

Regarding motor losses, an important analysis is the current ripple generated by the PWM, which influences the motor harmonic core losses [11], [15]-[18], [27], [99]. The current ripple generates medium-high frequency magnetizing fluxes, and although they present low amplitude, the resultant losses can be significant due to their frequency range (the hysteresis losses and eddy current losses are approximately proportional to the frequency and to square of the frequency, respectively). The core losses increase in VSD-fed IMs is evidenced in [15], [27], and [99]. In Fig. 3.31, simulated phase current waves for both VSIs are shown, in which it can be seen that the ripple magnitude is significantly higher in the 2L-VSI. In Fig. 3.32, a comparison between the Fast-Fourier Transform (FFT) of the simulated waves presented in Fig. 3.31 is shown. In Fig. 3.33, the experimental no-load harmonic losses of the motor are shown, for different switching frequencies and different fundamental voltage values. The motor harmonic no-load losses decrease with the increase of the switching frequency, as expected.

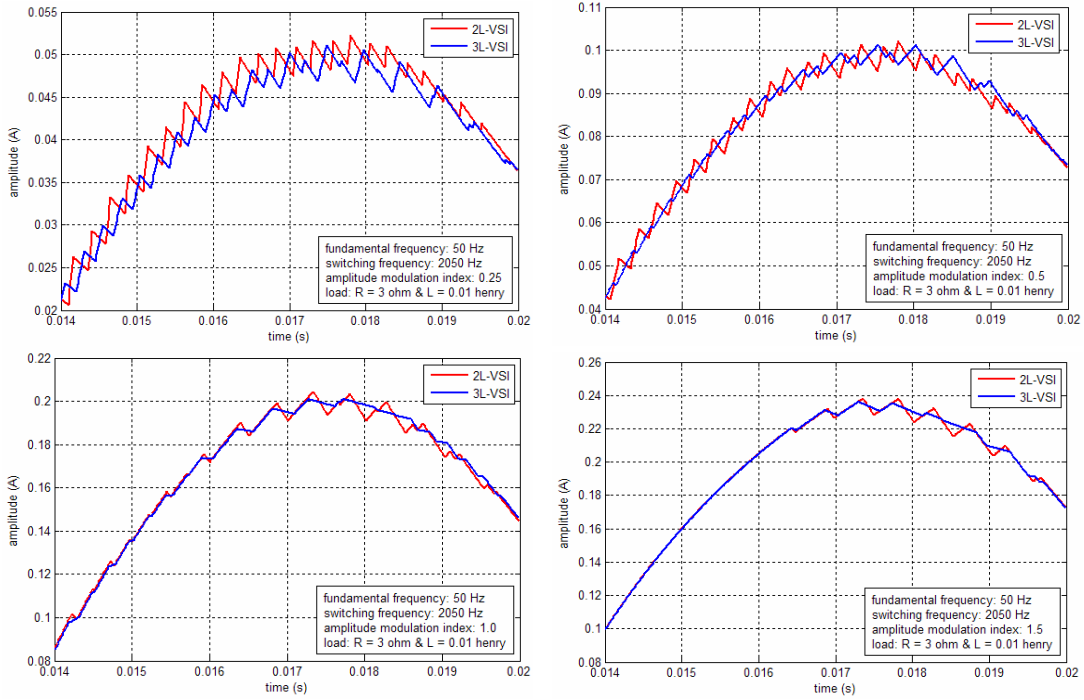


Fig. 3.31. Zoom of the simulated phase current wave (delta-connected load), for different values of m_a [15].

In absolute terms, for $m_a = 0.25$, the 5th and 7th harmonics are almost 3 times higher for the 2L-VSI.

It can be concluded that the 3L-VSI leads to lower inverter losses and also to lower high frequency magnetic losses (e.g., associated with minor hysteresis loops and extra Foucault currents losses), which mainly depend on the stator current ripple amplitude and frequency.

In fact, only the fundamental-frequency components of the phase voltage, u_{An1} , and current, i_{A1} , are responsible for the power conversion since the back-EMF, e_{An1} , is practically sinusoidal (rotor reacts mainly to the fundamental), with exception for low-order harmonics (corresponding to a frequency $f \leq 1$ kHz). That said, for a star-connected winding, the instantaneous phase voltage, u_{An} , can be described by (3.6), where e_l is the instantaneous fundamental phase back-EMF and i_A is the instantaneous phase current [43].

$$u_{An} \approx R_s \cdot i_A + L_s \cdot \frac{di_A}{dt} + e_{An1} \quad (3.6)$$

Using the principle of superposition, all the ripple in u_{An} , $u_{ripple} (= u_{An} - u_{An1})$, appears across the stator impedance, and the phase current ripple, $i_{ripple} (= i_{An} - i_{An1})$, is obtained by (3.7), where K is a constant and t is a variable of integration [16].

$$i_{ripple}(t) = R_s^{-1} \cdot u_{ripple} + L_s^{-1} \cdot \int_0^t u_{ripple}(t) dt + K \quad (3.7)$$

On the basis of the foregoing discussion, it can be said that high-order harmonic losses are concentrated in stator and the absolute current ripple is independent of the power transferred to the load, that is, the current ripple would be the same so long as, the ripple in the inverter output voltage remains constant in magnitude and frequency. However, the resulting current *THF* decreases with the load increase, due to the decrease of percentage ripple current value in relation to fundamental current. Therefore, regarding harmonic losses evaluation, the no-load test is adequated.

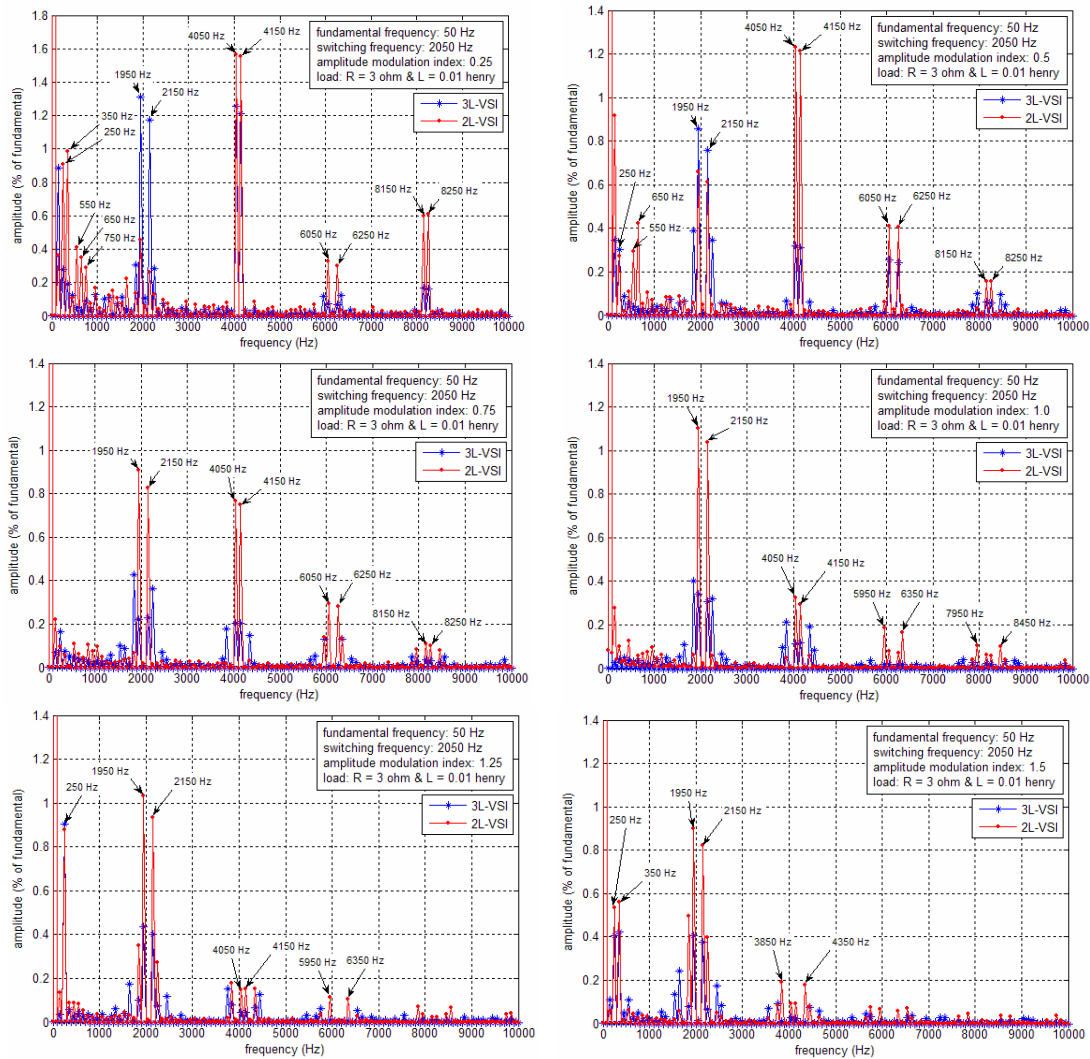


Fig. 3.32. FFT of the simulated phase current, for different values of m_a .

For large values of m_f , compared to the square-wave operation, the linear operation results in a substantially smaller peak ripple current (although characterized by higher frequencies).

This shows the advantage of pushing up the voltage harmonics of the inverter output to as high frequencies as feasible, thereby reducing the losses in the load by reducing the output current harmonics, particularly due to the reduction of the iron losses. However, for switching frequencies higher than a certain limit (typically 10 kHz), no major reduction in the *THF* and

harmonic core losses happens for both 2L- and 3L-VSIs. However, on the other side, using higher inverter switching frequencies, would result in more frequent switchings and hence higher switching losses in the inverter. Therefore, from the viewpoint of the overall system energy efficiency, a compromise must be made in selecting the inverter switching frequency, but above 15-16 kHz, in general, since no significant motor loss reduction occurs and relevant switching loss increase happens, the overall system efficiency is likely to decrease. Therefore, it is recommended switching frequencies between 2 and 10 kHz, inclusively, not only due to the efficiency improvement, but also due to the reduced EMI problems. In fact, a switching frequency as low as 2 kHz appears to be proper, if no major acoustic noise occurs. Additionally, problems associated with leakage currents in the power cables, voltage transients and bearing currents become more serious when high-switching frequencies are used (see Appendix 5).

The balance of the losses can be addressed in a simple way - when the inverter losses equal the harmonic losses in the motor, the system efficiency should be near the maximum value. This rule assumes that the inverter losses increase with the switching frequency and the harmonic losses in the motor decrease with the switching frequency.

In fact, for low switching frequencies (≤ 1 kHz) a significant increase on the motor core losses (either harmonic eddy current loss and harmonic minor-loop hysteresis loss components [99]) can occur with the decrease of m_a (for $f_l = 50$ Hz, in a 7.5-kW motor fed by a 2L-VSI, the increase of m_a from 0.50 to 0.86 leads to a decrease of more than 30% in the core losses), which is related with the increase of high-order harmonics amplitude, and, therefore, the *THD* or *THF*.

This can also be verified in Fig. 3.33, where the experimental motor no-load harmonic losses as a function of f_s and U_l are presented for a 3-kW and a 75-kW IM (delta ad star connection in the case of the 7.5-kW IM) evidencing the previously presented conclusions. This increase depends on the frequency, load, m_f and m_a . In general, the no-load harmonic losses have modest impact in overall losses. For example, considering 750 W of losses at full-load (80% efficiency), an increase of 10-28 W affects the efficiency in 0.2-0.6 p.p. (results in 79.8-79.4% efficiency). For motors operating with low loads and/or speeds and, consequently¹⁷, with low m_a , the difference between motor harmonic losses for the 2L- and 3L-VSIs can be more significant. This is related with the harmonic distortion of the inverter output voltage. For 2 kHz, it is 40%, 60%, and 12.5% higher for a m_a of 1.3, 0.55, and 0.3, respectively. Minor variations were found with the switching frequency. As expected, the *THF* increases with the decrease of the m_a for both inverters. It can be stated that, regarding the output voltage, the waveform quality depends mainly on the m_a (as widely known) and, for the same m_a , the 3L-VSI has significant lower *THF*. Of course this behavior is different for the current and input power, which vary with the

¹⁷ For low speeds, the m_a is inherently low. For low loads, the m_a is low if the inverter, by means of proper magnetizing flux regulation, performs motor efficiency optimization as a function of its actual load.

switching frequency. However, it is possible to observe that, when the *THF* difference is maximized (i.e., for the $m_a = 0.55$) the no-load harmonic losses are maximized too. This is also valid for the minimum values.

As it can be seen in Fig. 3.33, the maximum motor harmonic losses difference happens for $m_a = [0.5 \ 0.6]$, and, in general, they decrease with the increase of the switching frequency. For $m_a > 1$, the losses are very close for both inverters. For $m_a \approx 0.5$, the 3L-VSI-fed IM losses are minimized and the 2L-VSI-fed IM losses are maximized, therefore, the loss difference is maximized. For $m_a < 0.5$, the 3L-VSI-fed IM losses increase and the 2L-VSI-fed IM losses decrease. Nevertheless, in all cases, the 3L-VSI-fed IM harmonic losses are lower.

In Fig. 3.34, the average of the experimental motor total losses for a set of different motor loads is shown for different switching frequencies (no voltage compensation as a function of load), being the motor total losses lower for the 3L-VSI in the case of $f_i = 50$ Hz and $U_i = 400$ V. However, for $f_i = 25$ Hz and $U_i = 200$ V, the situation inverts mainly due to the presence of higher amplitude low-order harmonics, related to the voltage waveshape and extra voltage drop in the switching devices (see Fig. 3.25). Moreover, motor average losses decrease with the increase of the switching frequency, as expected.

Additionally, for the same magnetizing flux level, it was experimentally verified that, in relation to delta connection, the star connection leads to lower harmonic losses (this is also analysed in Appendix 3). Regarding the temperature rise, in Figs. 3.35 and 3.36, motor temperature rise as a function of motor load is shown for a 3-kW motor fed by the 2L- and 3L-VSIs. The 3L-VSI leads to a slight decrease in the motor stator windings temperature, being as high as the motor load is.

In Fig. 3.35, it can be seen that the motor loadability decreases to about 40% at 25 Hz (assuming constant magnetizing flux). After a specific value of switching frequency no motor efficiency improvements are obtained.

Regarding voltage transients, it is known that the steep voltage changes associated with PWM pulses generated by VSIs integrating IGBTs cause lifetime reduction of the IMs insulation system. In fact, as a result of the voltage reflection effect in the power cable between VSI and IM, voltage transients (i.e., short-duration overvoltages) appear at the IM terminals, even when relatively short cables (≈ 5 m) are used, accelerating the ageing process of the IM insulation system (turn-to-turn, phase-to-phase and/or phase-to-ground insulation), which may breakdown due to the time-accumulated damaging effects, particularly in those zones near the winding leads (first turns of the winding). In fact, as much as 85% of the voltage transients magnitude can be found across the first 2-3 turns of the first coil of the motor winding. In the worst cases, the voltage reflection effect causes the voltage doubling at the IM terminals. Therefore, it is very

likely that dielectric partial discharge occur in the ending region of the machine winding, accelerating the normal ageing process and, in the worst case, the partial discharge forms a fixed channel and eventually causes major insulation failure.

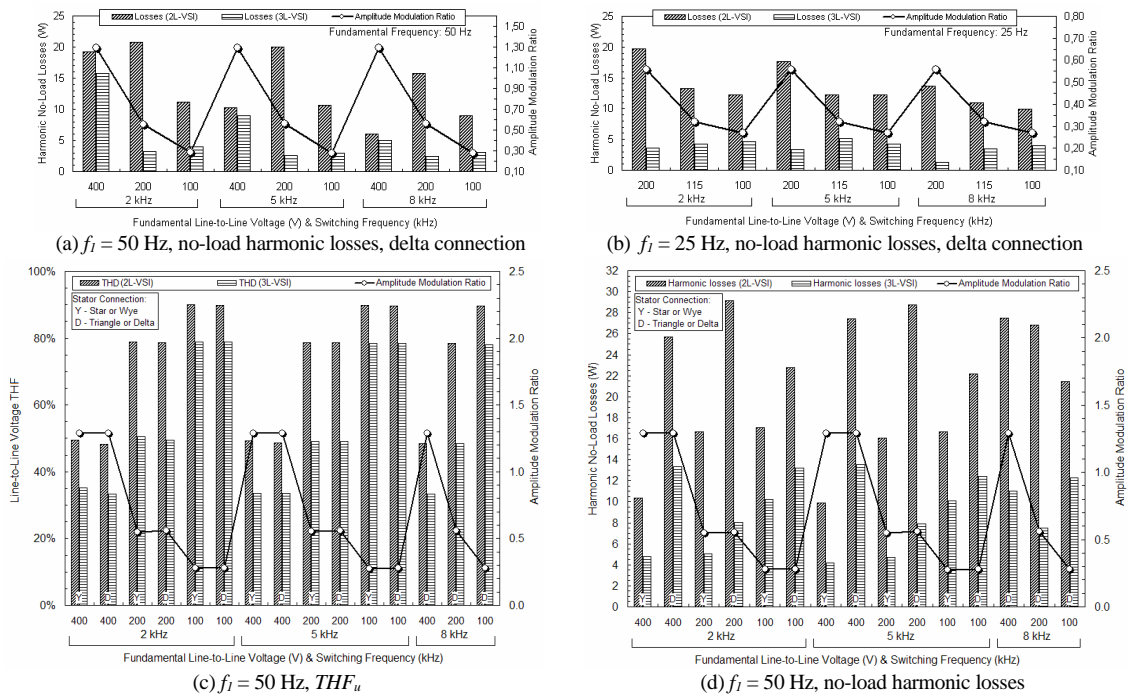


Fig. 3.33. Experimental no-load harmonic losses, m_a and THF_u , as a function of f_s and U_l , for 3-kW (a, b) and 7.5-kW (c, d) motors.

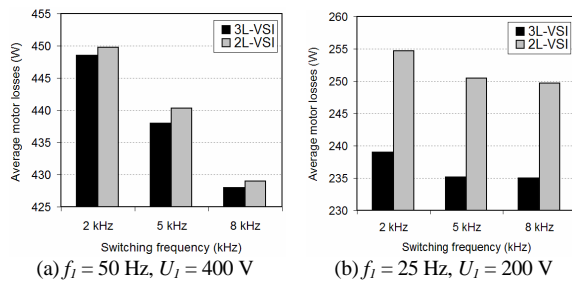


Fig. 3.34. Average of the experimental 3-kW, 4-pole motor total losses for a set of different motor loads (equally spaced):
 (a) 11 different motor loads ranging from no-load to 125% of rated power;
 (b) 8 different motor loads ranging from no-load to 87.5% of rated power.

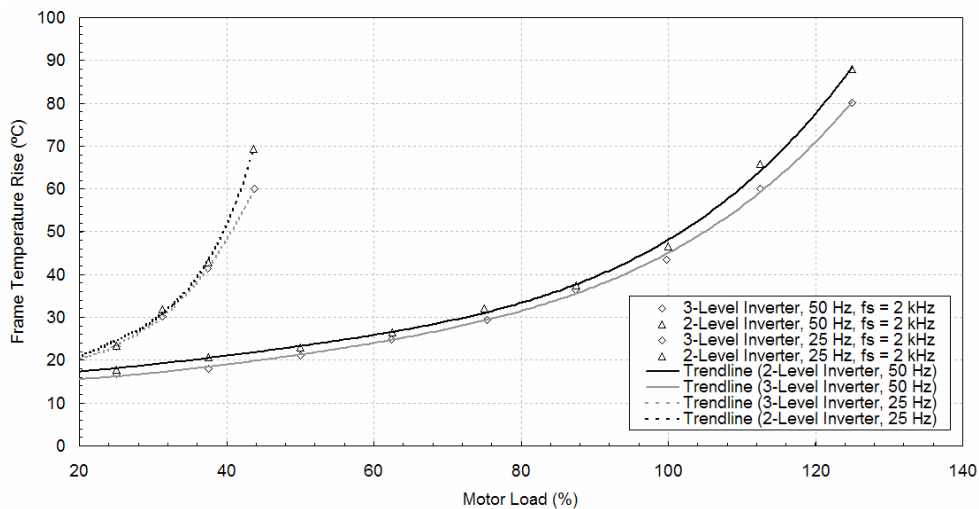


Fig. 3.35. Experimental frame temperature rise as a function of motor load, for a 3-kW system.

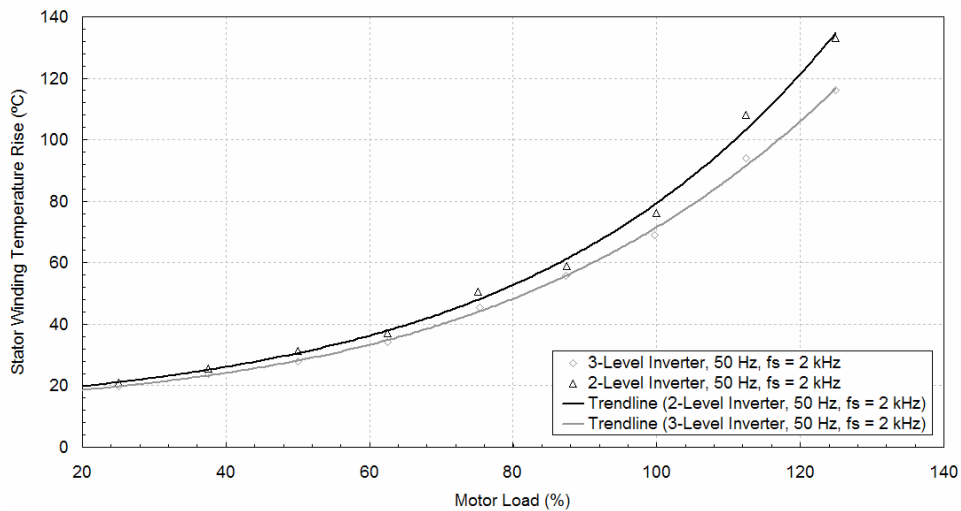


Fig. 3.36. Experimental stator winding distributed temperature rise as a function of motor load, for a 3-kW system.

The voltage reflection phenomenon is related to the mismatch between power cable and IM characteristic impedances. Typically, the IM characteristic impedance is 10 times larger than that of the cable. The magnitude and slope of the voltage transients depends mainly on the voltage change rate (du/dt) of the PWM pulses, cable length, cable conductors cross-section, cable type (shielded, unshielded, etc.), and IM rated power. In general, the magnitude of the voltage transients increases with the power cable length (until a certain length) and with the du/dt . It should be noted that, the higher the du/dt , the shorter the critical cable length (minimum cable length after which voltage doubling occurs). The occurrence rate of the voltage transients depends directly on the switching frequency. Typical solutions to mitigate the voltage transients impact on the motor include the use of inverter-rated/reinforced enamel-covered copper wire in the windings, improved impregnation, the reduction of the switching frequency, the reduction of the cable length¹⁸, the use of special cables (e.g., shielded-type and ferrite-type cables), and the installation of filters and/or reactors (to limit the du/dt and to mitigate harmonics). Further considerations are presented in Appendix 5.

The voltage reflection effect and the consequent voltage transients were experimentally studied¹⁹, for comparison purposes, using an unshielded, 4-conductor, 12-m power cable between the VSI and the 3-kW IM (Fig. 3.37). The voltages at the VSI and IM terminals were monitored and processed (one part of the results are presented in this section and the other part in Appendix 5).

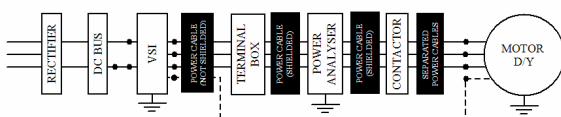


Fig. 3.37. Set-up for voltage reflection monitoring. All the cables used in the interconnections have the same characteristic impedance.

¹⁸ This is only possible if the inverter is mounted near the motor or embedded in it.

¹⁹ Theoretically, this phenomenon is studied using the theory of transmission lines.

Figs. 3.38 and 3.39 show the voltage peak values and the distribution of the voltage instantaneous values by voltage ranges, during the acquisition period, at the VSI and IM terminals, for phase-to-ground and phase-to-phase voltages (no-load operation). It is possible to conclude that, in general, when compared to the 2L-VSI, the 3L-VSI reduces both phase-to-ground and phase-to-phase voltage peak values at the IM terminals, leading to a lower voltage stress between winding turns, coils and phases and between winding and ground. Therefore, a higher lifetime is expected for the IMs fed by 3L-VSIs (important advantage). This is explained by the lower du/dt of the PWM pulses produced by the 3L-VSI (see waveshapes in Fig. 3.6 and Appendix 5).

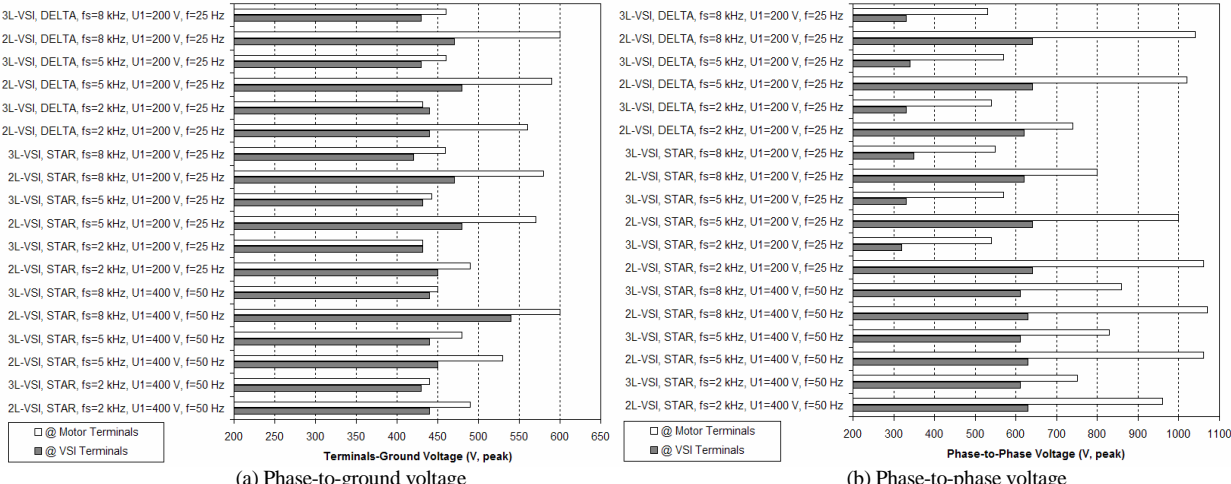


Fig. 3.38. Experimental voltage peak values.

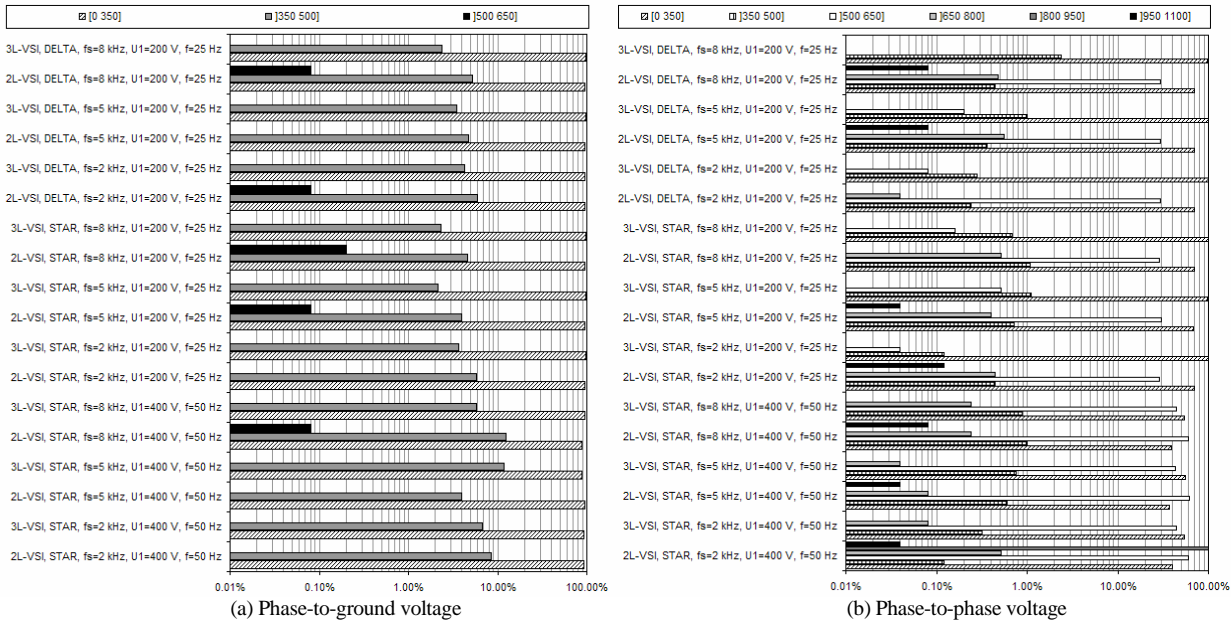


Fig. 3.39. Experimental instantaneous voltage distribution by voltage range.

The bearing and leakage currents are now addressed, but further considerations are presented in Appendix 5. The neutral-to-ground voltage in star-connected stator windings represents the common-mode voltage (CMV), which excite the parasitic capacitances in the IM and power cable, leading to the circulation of bearing and leakage currents [11], [35]. In Figs. 3.40-3.44 show, the simulated CMVs for different PWM generation techniques. It can be seen that the 2L-VSI produces CMVs with significantly higher amplitude and higher du/dt . Experimental waves can be found in Appendix 5. Moreover, hysteresis band technique (HBPWM) can also contribute to the reduction of amplitude of most relevant CMV frequencies (become less concentrated).

The origin of the CMVs, results from the instantaneous voltage unbalance. Considering a VSI supplying an IM, star connected (star neutral point denoted by n), and sinusoidal induced phase back-EMFs e_{An1} , e_{Bn1} , and e_{Cn1} , under balanced operating conditions, it is possible to express the inverter phase output voltages u_{AN} , u_{BN} , and u_{CN} , in terms of the inverter output voltages with respect to a reference ground point or DC-bus middle point (denoted by N). In a simplified form, each phase voltage can be expressed by (3.8) [43].

$$\begin{cases} u_{An} = u_{AN} - u_{nN} \approx R_s \cdot i_A + L_s \cdot \frac{di_A}{dt} + e_{An1} \\ u_{Bn} = u_{BN} - u_{nN} \approx R_s \cdot i_B + L_s \cdot \frac{di_B}{dt} + e_{Bn1} \\ u_{Cn} = u_{CN} - u_{nN} \approx R_s \cdot i_C + L_s \cdot \frac{di_C}{dt} + e_{Cn1} \end{cases} \quad (3.8)$$

In a 3-phase, 3-wire load, under balanced and ideal operating conditions, the 3 back-EMFs are a balanced 3-phase set of voltages, and therefore (3.9) is valid. From (3.8) and (3.9), one can write (3.10). Therefore, combining (3.8) and (3.10), the common-mode component, caused by the instantaneous unbalance of the inverter output voltages, is given by (3.11). Relations (3.12) and (3.13) are valid for star-connected windings and (3.13) for delta-connected windings. For star connection, a low-frequency CMV component exists in the neutral point for overmodulated operation. A high-frequency common-mode component also exists in the neutral point, but it will be mostly, concentrated in the frame and in the shaft, due to the parasitic or stray capacitances. If a leakage current, i_{lk} , circulate between windings and ground (closing the circuit by the ground path through the inverter and/or power source), (3.14) becomes valid [43].

$$\begin{cases} i_A + i_B + i_C = 0 \\ \frac{d}{dt}(i_A + i_B + i_C) = 0 \\ e_{An} + e_{Bn} + e_{Cn} = 0 \end{cases} \quad (3.9)$$

$$u_{An} + u_{Bn} + u_{Cn} = 0 \quad (3.10)$$

$$u_{nN} = \frac{1}{3}(u_{AN} + u_{BN} + u_{CN}) \quad (3.11)$$

$$\begin{cases} u_{An} = \frac{2}{3}u_{AN} - \frac{1}{3}(u_{BN} + u_{CN}) \\ u_{Bn} = \frac{2}{3}u_{BN} - \frac{1}{3}(u_{CN} + u_{AN}) \\ u_{Cn} = \frac{2}{3}u_{CN} - \frac{1}{3}(u_{AN} + u_{BN}) \end{cases} \quad (3.12)$$

$$\begin{cases} u_{AB} = u_{AN} - u_{BN} \\ u_{BC} = u_{BN} - u_{CN} \\ u_{CA} = u_{CN} - u_{AN} \end{cases} \quad (3.13)$$

$$i_A + i_B + i_C = i_{Rk} \quad (3.14)$$

For delta connection, the low-frequency CMV component cannot exist in ideal stator windings. However, due to the parasitic capacitances, the low- and high-frequency CMV components can actually exist between windings and both motor frame and rotor/shaft (denoted here by subscript R) and between rotor/shaft and frame, allowing common-mode currents to circulate.

Considering a balanced stray capacitance (C_{WR}) star whose neutral corresponds to the shaft, in turn connected to the motor ground by a stray capacitance (C_{RS}), for both star or delta connected winding, equations (3.15), (3.16), and (3.17), can be written, where $i_{RN} (= i_{AR} + i_{BR} + i_{CR})$ is the current flowing from rotor/shaft to ground, through C_{RS} .

$$\begin{cases} u_{AR} = u_{AN} - u_{RN} = C_{WR}^{-1} \cdot \int i_{AR} dt \\ u_{BR} = u_{BN} - u_{RN} = C_{WR}^{-1} \cdot \int i_{BR} dt \\ u_{CR} = u_{CN} - u_{RN} = C_{WR}^{-1} \cdot \int i_{CR} dt \end{cases} \quad (3.15)$$

$$u_{RN} = \frac{1}{3}(u_{AN} + u_{BN} + u_{CN}) \quad (3.16)$$

$$i_{RN} = i_{AR} + i_{BR} + i_{CR} = \frac{du_{RN}}{dt} C_{RS} \quad (3.17)$$

On the basis of the foregoing analysis, for:

- delta-connected IMs: the existence of low- and high-frequency CMVs at the shaft is possible and, therefore, bearing current circulation can occur;
- star-connected IMs: the existence of low-frequency CMV components at the neutral point (< 1 kHz) and high-frequency CMV components at the shaft (> 1 kHz) is possible.

In practice, in a SPWM three-phase bridge inverter, the phase-to-ground voltage wave is a 2-level wave, the phase-to-phase voltage is a 3-level wave, and, for the case of star-connected loads, the phase-to-neutral voltage is a 5-level wave, over the full cycle. This indicates an advantage of the star-connected windings.

Figs. 3.40-3.44 show the simulated CMVs for different PWM generation techniques. Figs. 3.45 and 3.46 show the experimental FFT, the instantaneous peak values, and the distribution of instantaneous values by voltage range, during the acquisition period, for the experimental no-load neutral-to-ground voltage (no-load, star-connected motor). In general, the neutral-to-ground voltage harmonics amplitude is significantly higher when the IM is fed by the 2L-VSI, particularly for the harmonics corresponding to the switching frequency and their multiples. As it was explained in [11], [15], [35], the shaft-to-ground voltages are directly related with the CMVs and, therefore, the activity of the resulting bearing currents and their impacts on the bearing lifetime will be lower for the 3L-VSI, in relation to the 2L-VSI. The 3L-VSI also leads to lower leakage currents (parasitic currents that circulate from the stator windings and power cables to the ground).

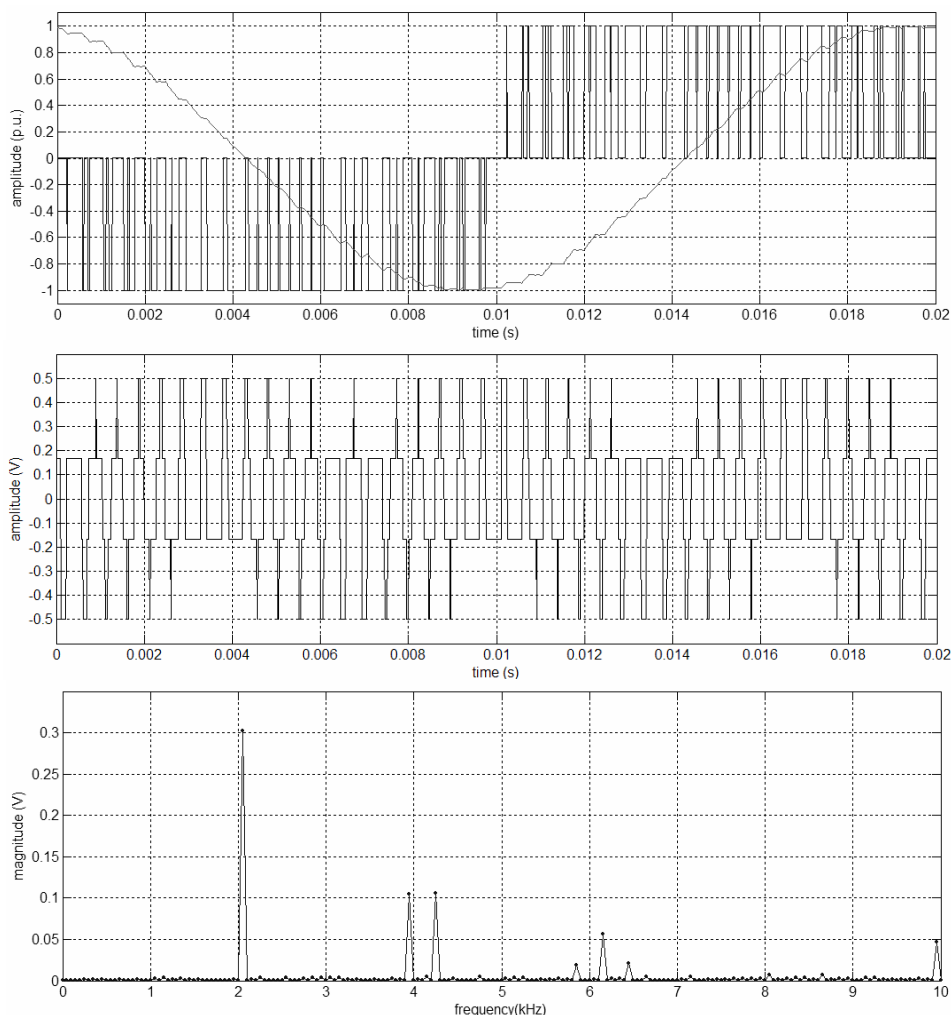


Fig. 3.40. Simulated U_{nN} (top), CMV wave (middle) and CMV FFT (bottom) for the 2L-VSI, $m_a = 1.0$, $U_{DC} = 1.0$ V, no-load, using sinusoidal PWM (SPWM) technique.

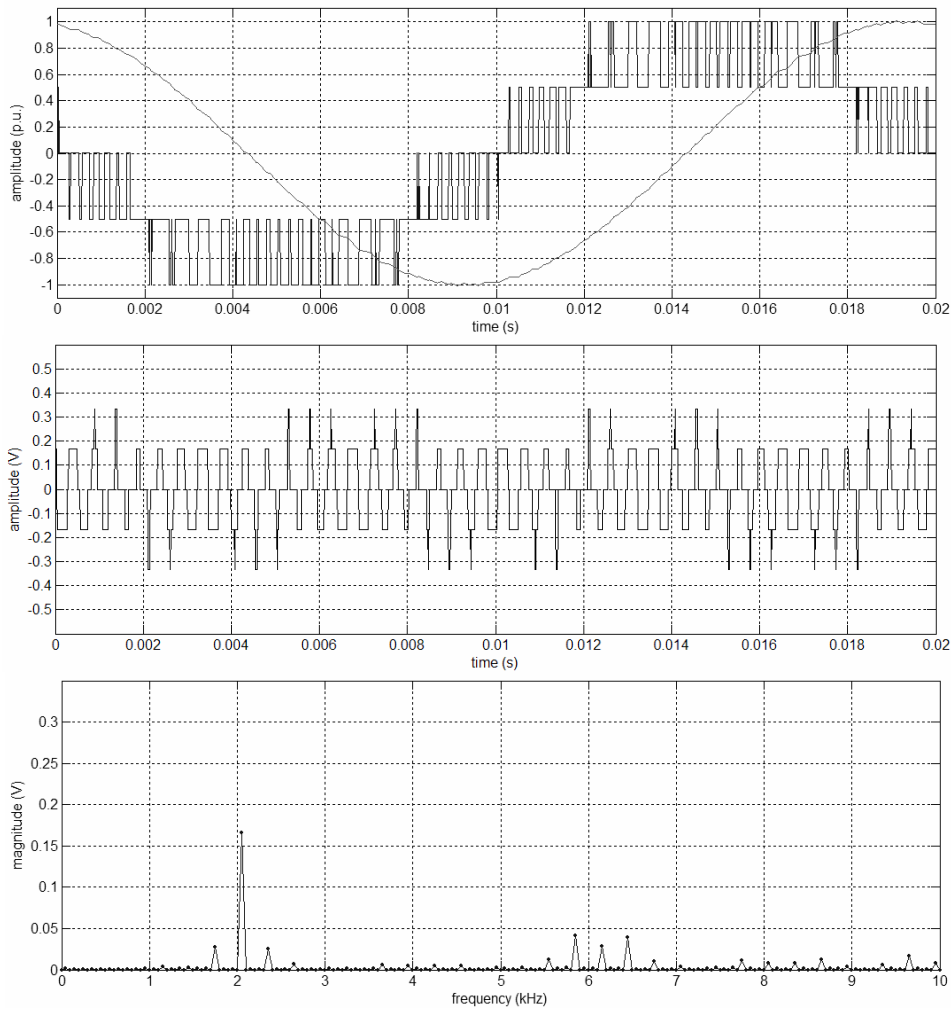


Fig. 3.41. Simulated U_{nN} (top), CMV wave (middle) and CMV FFT (bottom) for the 3L-VSI, $m_a = 1.0$, $U_{DC} = 1.0$ V, no-load, using sinusoidal PWM (SPWM) technique.

The voltage between the motor shaft and frame (connected to the inverter and/or power source ground) are shown in Fig. 3.47 for star connection, 50 Hz, no-load and for the 3-kW and 7.5-kW motors, confirming that the 3L-VSI leads to a lower voltage between the shaft and ground, in all the tested switching frequencies (but the switching frequency). This is valid for peak value, most relevant harmonic amplitudes and voltage distribution by voltage range. However, for certain circumstances, the shaft to ground can be higher for the 3L-VSI, e.g., if a low-frequency zero-sequence harmonic exists, which can actually occur in the overmodulation region.

Regarding vibration and acoustic noise, the aim of the following analysis is not to evaluate the absolute levels of the motor mechanical vibration and acoustic noise (or sound) but, instead, to compare their amplitudes for the 2L-VSI-fed and 3L-VSI-fed IM in steady-state operation. To measure the acoustic emission and the mechanical vibration of the motor, three different sensors were used: a standard PC microphone (frequencies up to 16 kHz), a standard sound level meter (dB output, 0.5-m distance from the motor) and a unidirectional accelerometer (for frequencies up to 15 kHz). The setup is shown in Fig. 3.48.

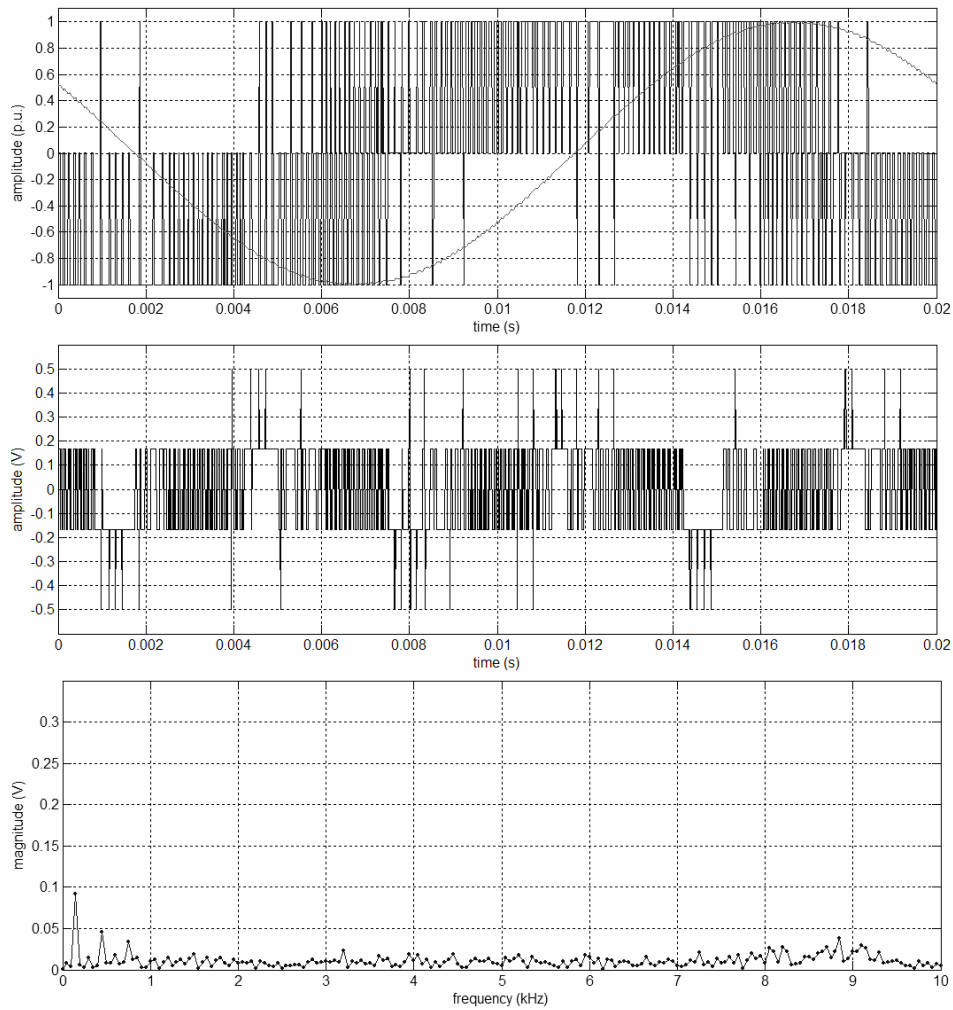


Fig. 3.42. Simulated U_{mN} (top), CMV wave (middle) and CMV FFT (bottom) for the 2L-VSI, $m_a = 1.0$, $U_{DC} = 1.0$ V, no-load, using hysteresis band PWM (HBPWM) technique (or hysteresis current control) with current HB = 0.0075.

In Figs. 3.49 and 3.51, the FFT and the level (dB) of the motor acoustic emission are presented, respectively. In Fig. 3.50, the FFT of the motor mechanical vibration is presented. When compared to the 2L-VSI, the 3L-VSI leads to significant lower amplitudes (almost halved) for the most significant frequency components of the motor mechanical vibration and emitted acoustic noise.

The switching frequency related vibrations and acoustic noise are significantly reduced with the 3L-VSI. In fact, the vibration spectrum is very similar when the motor is fed by the 3L-VSI at 8 kHz and directly by the line. As expected, the increase in the switching frequency leads to a significant decrease in the acoustic noise, particularly in the 2L-VSI. For the steady-state operation, no differences were found for different control strategies (scalar vs. vector control).

Furthermore, there is an obvious relation between harmonic content and vibrations - specific voltage harmonics lead to specific vibrations, which are, in part, converted to acoustic noise.

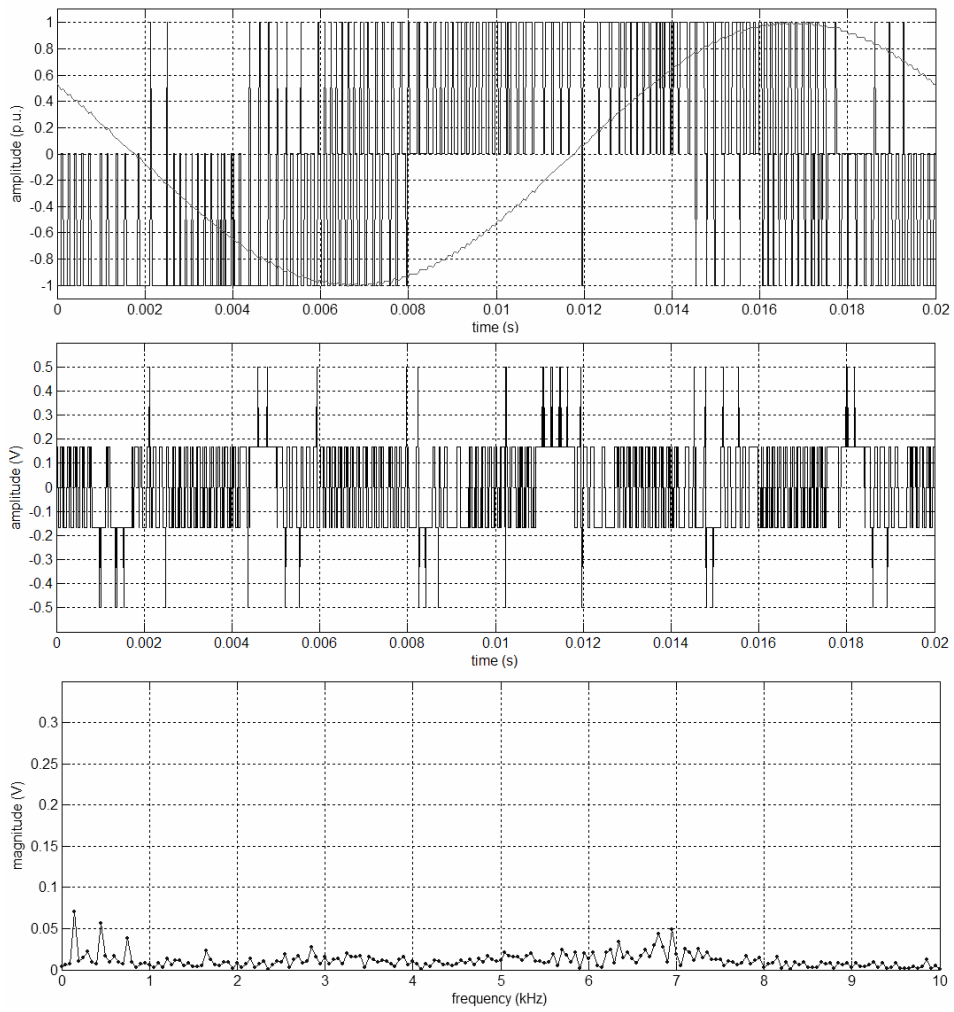


Fig. 3.43. Simulated U_{nN} (top), CMV wave (middle), and CMV FFT (bottom) for the 2L-VSI, $m_a = 1.0$, $U_{DC} = 1.0$ V, using hysteresis band PWM (HBPWM) technique (or hysteresis current control) with current HB = 0.01.

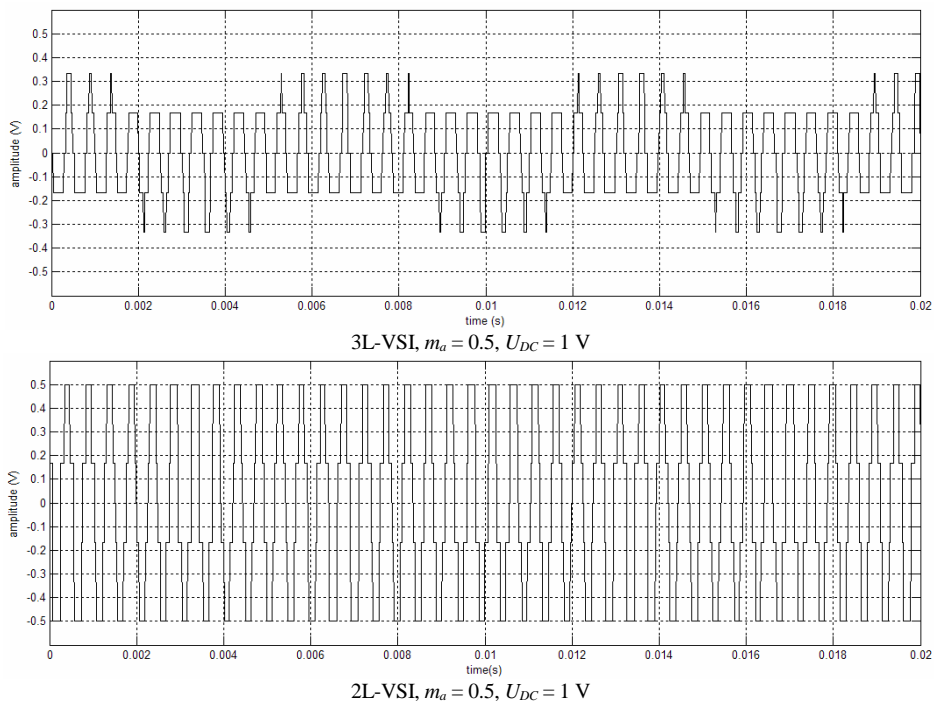


Fig. 3.44. Simulated CMV waves (same conditions considered in Fig. 3.7), $m_a = 0.5$.

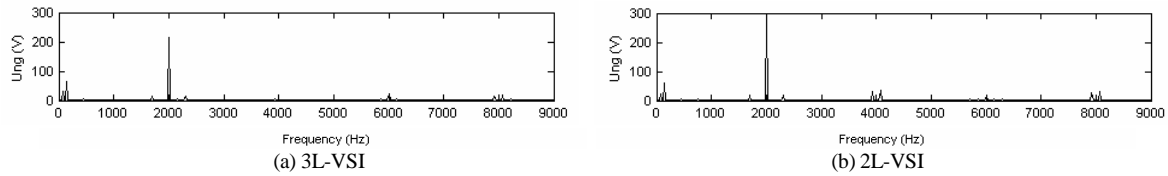


Fig. 3.45. FFT of the experimental star neutral-to-ground voltage wave (no-load).

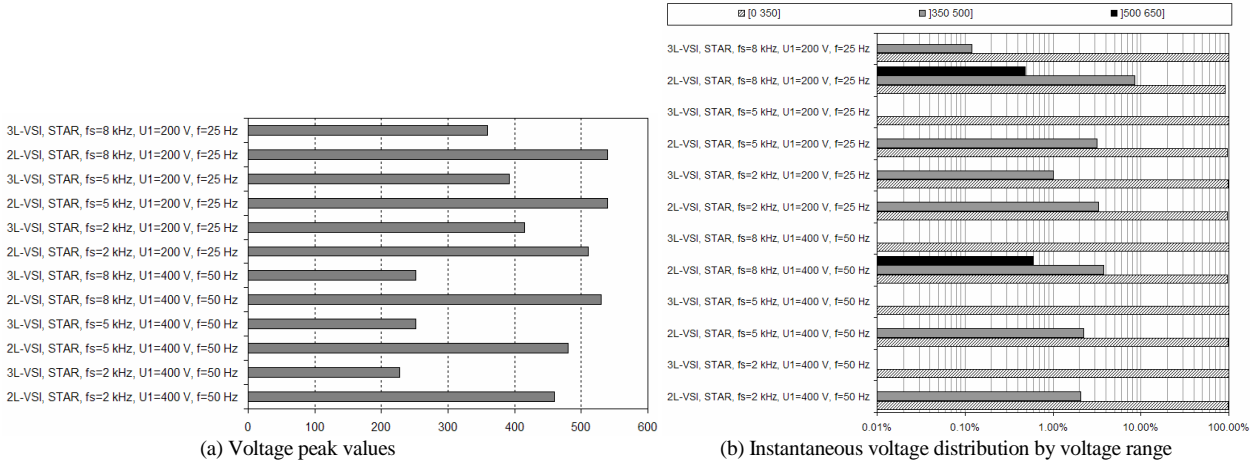


Fig. 3.46. Experimental star neutral-to-ground voltage (no-load).

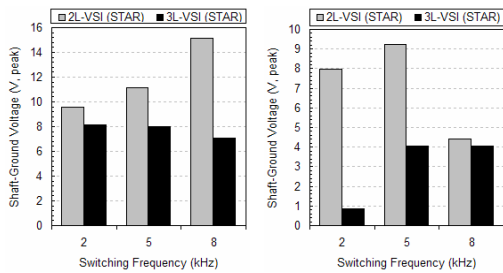


Fig. 3.47. Shaft-to-ground voltage peak value: (left) 7.5-kW motor; (right) 3-kW motor, no load.

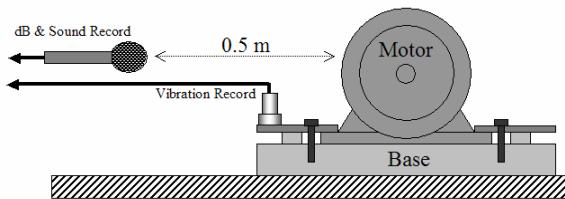


Fig. 3.48. Set-up for sound and vibration measurement.

According to the Fig. 3.51, the differences in the motor acoustic noise level are more significant for $f_s < 8$ kHz. For $f_s = 2$ kHz and $f_s = 5$ kHz, the motor acoustic noise level decreases approximately 2.5 dB and 5 dB, respectively, when the 3L-VSI is feeding the motor. As expected, the increase in the switching frequency leads to a significant decrease in the motor acoustic noise level, particularly in the 2L-VSI (a decrease of about 10 dB was obtained). When considering a huge amount of VSI-fed motors operating simultaneously, the reduction in the overall acoustic noise can be significant if 3L-VSIs are used instead of 2L-VSIs. For example, in HVAC systems, noise level plays a decisive role.

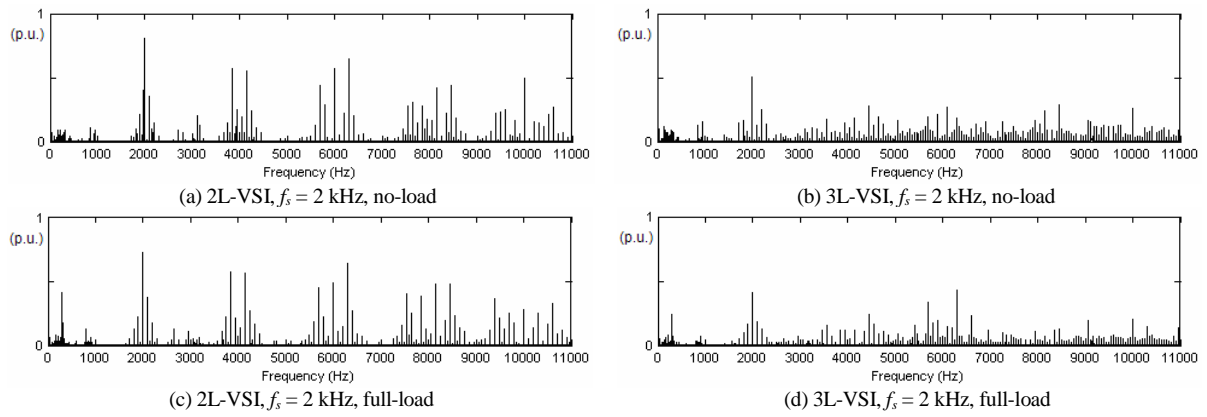


Fig. 3.49. FFT of the experimental acoustic emission (microphone output voltage, in p.u.) for a 4-pole, 3-kW IM ($f_l = 50$ Hz, $U_l = 400$ V).

In general, lower mechanical vibrations are expected in 3L-VSI-fed IMs, leading to lower acoustic emissions, as well as to lower mechanical wear of some motor parts (e.g. stator winding insulation system and bearings), thus reducing the VSI impact on motor lifetime. These are important advantages associated with the 3L-VSIs that should be also taken into account.

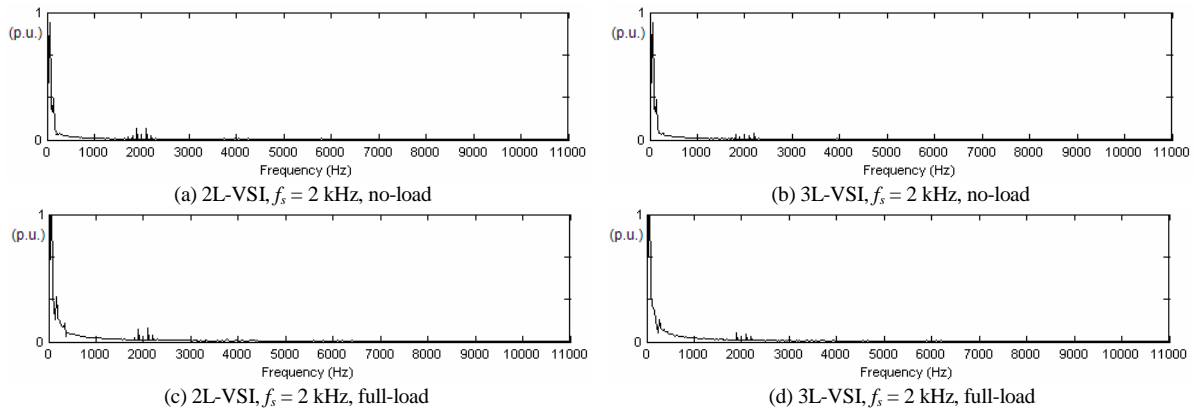


Fig. 3.50. FFT of the experimental mechanical vibration (accelerometer output voltage, in p.u.) for a 4-pole, 3-kW IM ($f_l = 50$ Hz, $U_l = 400$ V).

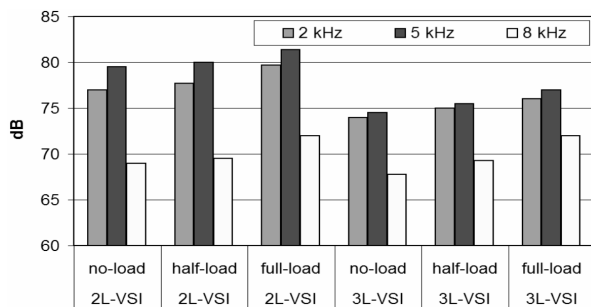


Fig. 3.51. Experimental motor acoustic noise/sound levels for different switching frequencies and motor loads, 4-pole, 3-kW IM, 0.5-m distance.

One of the typical argues to push-up the switching frequency is the reduction of the motor acoustic noise. However, as explained before, the higher the switching frequency, the faster the wear and ageing of the motor insulation system and bearings. The 3L-VSI has the advantage of producing lower acoustic noise with lower switching frequencies (e.g., the 3L-VSI at $f_s = 2$ kHz

produces less acoustic noise than the 2L-VSI at $f_s = 5$ kHz), allowing the switching frequencies to be pushed-down, which can lead to a significant increase of motor lifetime.

In vibration spectral analysis-based diagnostic methods, the identified differences between both technologies should be taken into account, in order to establish specific patterns for comparison purposes. Furthermore, there is an obvious relation between harmonic content and vibrations - specific voltage harmonics lead to specific vibration components, which are, in part, converted to acoustic noise.

3.3.6 Economical Considerations

As it can be seen in Fig. 3.52, below 22 kW, the 3L-VSIs cost 10-12% more than the 2L-VSIs, which is a modest difference if the user take into account the benefits of the 3L-VSIs, making them a good choice for these power ranges. Equal or above 22 kW, the difference in the price is significantly higher, reaching 40-50% more. In these cases, 3L-VSIs are only a cost-effective option for critical applications, in which motor reliability is an important factor or the distance between the motor and the inverter output is significantly long ($> 50-75$ m). Moreover, since the 3L-VSI avoids the use of output filters, the associated cost should be taken into account in the economic evaluation.

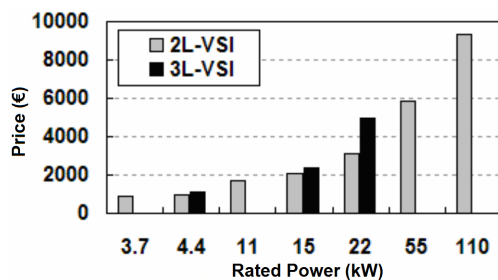


Fig. 3.52. VSDs reference prices [31].

In Fig. 3.53, the difference between the average overall system losses (motor and inverter losses for a set of different motor loads) for both 2L-VSI and 3L-VSI systems, is shown, evidenced that the system loss difference is, in general, not significant. However, in the 3L-VSI system, slightly higher losses are expected for loads near full-load, and slightly lower losses are expected for low loads. It can be concluded that the system efficiency and losses are not a major issue in the comparison of both 2L-VSI and 3L-VSI technologies.

Of course, the cost of the power switches is decreasing [47], and one can expect a decrease of the cost difference between both technologies in the next decade, as well as the increase of the 3L-VSIs efficiency due to the expectable decrease of the conduction loss component of the power switches.

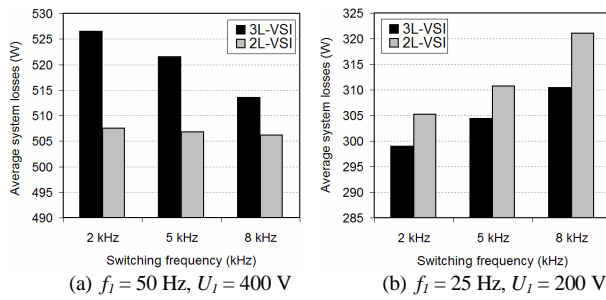


Fig. 3.53. Average of the experimental system losses (3-kW, 4-pole motor plus inverter) for a set of different motor loads (equally spaced):
 (a) 11 different motor loads ranging from no-load to 125% of rated power;
 (b) 8 different motor loads ranging from no-load to 87.5% of rated power.

3.4 Considerations on PWM Strategies

For the sake of completeness, a brief on the PWM strategies, from the steady-state perspective, is presented in this section, based on [16], [17], [18], and [43], as well as on simulations. Among all the PWM strategies, three can be underlined: sinusoidal PWM (SPWM), space vector²⁰ PWM (SVPWM), selected harmonic elimination PWM (SHEPWM), and the hysteresis band PWM²¹ (HBPWM).

The most common PWM technique used in Industry is the SPWM (also called triangulation or the subharmonic or suboscillation method), which as been explained before. In the SPWM, which is a carrier-based open loop (asynchronous or synchronous carrier) technique, the characteristic (or inverter voltage transfer characteristic) is linear up to $m_a = 1.0$ and $U_{III}/U_{DC} \approx 0.61$ (low range). The U_{III}/U_{DC} limit of the linear region can be increased (up to 0.707) by mixing third or triplen harmonics with modulating wave. The nonlinear transfer characteristic in overmodulation range is a disadvantage, but allows to increase the output voltage up the value corresponding to the square-wave operation. Of course, as explained before, fundamental frequency related low-order harmonics at the output appear in the overmodulation region, being difficult to filter. Moreover, the DC-link voltage ripple introduces additional output ripple. In fact, depending on the DC-bus capacitance and inverter load, input voltage unbalances can propagate through DC-bus to the output PWM voltage waves, reducing motor performance (this phenomenon is addressed in Appendix 4). In the case of high-power inverters using SPWM, the switching frequency is typically low because of the large switching losses, and, therefore, in these cases, to avoid subharmonics at low switching frequencies, the modulating wave requires synchronization with triangular wave.

The SVPWM technique is indirectly carrier-based open loop (asynchronous or synchronous carrier). It is indicated for isolated-neutral 3-phase output. It has large undermodulation range ($m_a \leq 0.707$). The linearization in overmodulation up to square-wave is relatively easy. The switching frequency-related ripple at overmodulation is large. The DC-link voltage ripple

²⁰ Also known as space vector modulation (SVM).

²¹ Also known as hysteresis current control.

introduces additional output ripple, as in SPWM technique. It requires complex and intensive computation, performed by a microcomputer, DSP and/or FPGA. Nowadays, the majority of manufacturers is implementing this technique²².

In the SHEPWM technique, no carrier base is used, being the switching frequency determined by the number of notches. It is difficult to apply at low fundamental frequency and the output may not be harmonically optimum. This technique is most useful when specific harmonic orders are harmful for the load (e.g., 5th order harmonic in the case of IMs). The linearization in whole modulation range is relatively easy. The DC-link voltage ripple introduces additional output ripple, as in the previous techniques. This technique can be implemented by means of a look-up table using a microcomputers or DSP.

The HBPWM technique is one of the simplest control PWM techniques. Basically, it is an instantaneous feedback current control method, in which the actual current continuously tracks the command current within a preassigned hysteresis band (HB). If the actual current exceeds the HB limits, the upper device of the half-bridge is turned OFF and the lower device is turned ON. As the current decays and crosses the lower band, the lower device is turned OFF and the upper device is turned ON. If the HB is narrowed, the harmonic quality of the wave will improve, but the switching frequency will increase, which will in turn cause higher switching losses. The HBPWM implementation is very simple, and the control is fast. The device current is directly limited. The main disadvantages are the harmonically nonoptimum waveform (harmonic ripple), the slight phase lag that increases with frequency, the need of close-loop current control, the variable switching frequency and the additional distortion in the isolated-neutral three-phase loads. However, the distance between the two limits of the HB can vary over the period to reduce or control harmonic generation. Different types of HB patterns (constant and non-constant band width) were proposed in [48] order to improve waveform quality, revealing promising results the some space for new research. A number of advantages can be referred as easy operation from zero frequency, the fast transient response, the DC-link ripple compensation, permitting the use of lower capacitances in the DC-link. Actually, this technique can partially isolate DC-link perturbations from motor, being a significant advantage if significant voltage supply anomalies are expected, e.g., voltage unbalances or magnitude deviations (this was verified with a number of simulations). HB can also reduce the shaft-ground voltage peaks (as previously shown in Figs. 3.40 and 3.44) and provides smooth transition from undermodulation to overmodulation. This technique is rarely used in commercial inverters.

²² Typically, the control tasks are performed by a DSP and the output PWM is generated by a FPGA.

3.5 Considerations on Steady-State Efficiency Improvement Strategies

For the sake of completeness, some steady-state efficiency improvement strategies are briefly discussed in this section.

IMs are typically designed for fixed voltage and frequency, being the maximum efficiency achieved within 60% and 100% of full load. However, for low loads, if the magnetizing flux is kept constant and equal to the rated value, the motor efficiency and power factor become poor. This is related, in part, to the fact that stator core losses still approximately constant for fixed voltage. For low loads, the rotor losses are relatively reduced and the magnetizing current contributes significantly to the stator winding losses. If the voltage decreases, the magnetizing flux, iron losses and stator winding losses also decrease, but the rotor losses increase slightly due to the slip increase. If the voltage decrease too much, the iron losses become small, but the rotor losses and stator winding losses increase significantly. For an accurate analysis, the friction and windage losses, which, in VSD-fed IMs, vary significantly, should be also taken into account. That said, it can be stated that, for all operating points (corresponding to a certain torque and speed), there is a magnetizing flux (or a phase voltage) minimizing the motor or system losses or, in other words, maximizing motor efficiency [3], [5], [85], [86], [87]. Analytical optimum slip or current can be easily estimated, providing that all motor parameters are known [81]. First developed strategies aimed the minimization of motor losses and not the converter losses, being this only reasonable for drives (motor plus VSD) up to 10 kW, since VSD losses are not relevant. For larger drives, the VSD losses have to be taken into account, particularly above 90 kW rated power. In fact, VSD efficiency varies from $\approx 95\%$ for 1 kW rated power to $\approx 98\%$ to 250 kW rated power VSDs [3], which evidences the relatively increasing importance of VSD losses in relation to motor losses (the efficiency level of VSDs and IMs approximate each other, with the rated power increase). It is important to optimize flux in an appropriate, simple, and cheap way, particularly in HVAC applications where stator current and DC-link voltage are measured by sensors. The frequent low-load operation and the low-dynamic response requirement make HVAC ideal for optimized efficiency control.

In Figs. 3.54-3.58 simulated results are shown for a 4-pole, 3-kW motor, evidenced the relation between efficiency and power factor with load, slip and voltage. In Fig. 3.54, for example, it is possible to see that, at 50 Hz, the optimum voltage level for 40% load is between 300 and 320 V. In Fig. 3.56, it is possible to conclude that, at 20% load, 25 Hz, the optimum voltage is roughly 160 V. In Fig. 3.59, the experimental relation between torque and speed for different efficiency values is shown for a 37-kW, 2-pole, 60-Hz IM [83]. In Fig. 3.60 experimental efficiency curves as a function of load and slip are shown for a 3-kW, 4-pole, 50-Hz IM, fed at 25 and 50 Hz ($U_1/f_1 = 8$). In [42], a number of experimental results showing the impact of the fundamental

frequency variation in the motor and system efficiency-load curves, in which it was concluded that the relative extra losses associated with the maximum efficiency drop (both due the fundamental losses balance change, the extra motor harmonic losses and VSD losses) are overshadowed by the savings provided by the load input power reduction (particularly fans and pumps), thus not interfering significantly with the cost-effectiveness of VSDs. Moreover, it also states that a by-pass in parallel with VSD can also be cost-effective in loads with large fundamental frequency operation periods, in which the VSD can be out of operation, avoiding extra motor harmonic losses and VSD losses. However, the contactor energy consumption to perform the by-pass, although typically low, has also to be take into account.

Therefore, it is important to establish methods for the adjustment of the motor magnetizing flux level in order to maximize the motor efficiency and improve power factor for each operating point, also leading to lower magnetizing current and lower inverter losses.

The higher the rated power, the lower the load has to be for large savings [3]. Moreover, the higher the speed is, the higher the savings potential associated with flux level optimization will be [5]. The higher the motor savings potential, the higher the VSD savings potential, particularly for medium-high power since VSD losses depend on motor input current (although motor losses dominate). In fact, for inverters with power up to 50 kW the losses are relatively low when compared with motor losses, being not critical to take into account the inverter losses in the system efficiency maximization. A number of papers where published on this issue. In principle, if the motor losses were minimized, the inverter losses will also be minimized. For systems with hundreds of kW, the motor and inverter losses are both relevant, and should be taken into account simultaneously for system efficiency maximization purposes.

The control strategy for efficiency maximization can be divided into three categories [3], [5]: simple state control, motor model-based control and search control.

In the simple state control it is assumed that, for a certain load point, the efficiency maximization is associated with a specific value of a certain electrical or mechanical quantity. One of the electrical quantities typically used is the power factor. The rated power factor is typically considered as reference, but, since most IMs maximize efficiency at 60-85% load, the corresponding power factor should be previously identified and used. Since the power factor is relatively easy to measure, the control strategy based on the maintenance of a certain power factor²³ is considered as a low-cost and the results are fair to good. In fact, in [3], it was shown (although not considering thermal variations and its influence on motor parameters) that, for any speed, the power factor-based control practically minimizes system losses. The motor slip (or rotor slip frequency) can also be used [3], which is approximately constant when the efficiency is

²³ The power factor is almost constant for maximum efficiency, but varies with speed.

maximized regardless the fundamental frequency, assuming that the motor is not excessively saturated (saturation higher than rated saturation level). However, to use this strategy, the rated and actual speed and load of the motor has to be known.

In the motor (loss) model-based control, the motor parameters have to be known, including the core loss and/or SLL resistances and inductance saturation, and more calculations are required in relation to other methods [3], [5], [7]. A number of papers were published on this scope [77], in which core losses are represented in the direct and quadrature equivalent circuits (motor dynamic d-q model), and the motor efficiency maximization is theoretically achieved (with invariable motor parameters) when the losses associated with the direct or field current equals the losses associated with the quadrature or torque current²⁴ [2], [3]. This sort of methods have a number of disadvantages. For example, besides the significant computational efforts, the fact that motor parameters actually depend on the motor actual temperature (particularly the rotor resistance [7]), saturation and skin effect, leading to inaccurate results (method detuning – there are some techniques to override this problem [7]), and, obviously, motor parameters have to be known, which is not a suitable solution for general purpose VSDs. Therefore, this sort of methods are not recommended for common industrial applications. Moreover, for different frequencies there are different friction and windage losses, which are not taken into account. However, for large drives, it can be a good solution and promising techniques were proposed in [3] and [5]. It provides a relatively smooth and fast adaptation (< 1 s) of the flux, being recommended for industrial drives. Actually, in most applications, the fast response is not critical due to the relatively high mechanical time constant of the overall system.

The main advantage of this method is that it can be easily combined with speed control using vector (or field vector) control techniques [3], since they already use d-q axes.

In order to force motor to converge to maximum efficiency, a classical proportional-integral (PI) or Fuzzy Logic²⁵ based controller can be used, considering the difference between both the direct and quadrature loss components as the input, and the flux as the output. The speed control can alternatively be made using Fuzzy-Logic (expert system), artificial neural networks (ANN) or Neuro-Fuzzy Networks based scalar speed control methods [19], [52].

In the search-based control the aim is, for a certain steady-state load point (constant shaft power), to iteratively find the motor flux level that minimizes the input real power. For such

²⁴ As shown in [5], for steady-state equivalent circuit, IM losses are minimized when the losses associated with rotor current equal the losses associated with air-gap flux (constant torque and speed). From another perspective, considering constant rotational losses (friction, windage, and core losses) and ignoring the magnetizing current, it can be easily demonstrated that the motor efficiency reaches the maximum value when $\dot{I}R$ losses equal rotational losses.

²⁵ Fuzzy logic is a mathematical system that analyzes analogue input values in terms of logical variables that take on continuous values between 0 and 1, in contrast to classical or digital logic, which operates on discrete values of either 0 and 1 (true and false). Fuzzy logic-based control has the advantage that the solution to the problem can be cast in terms that human operators can understand, so that their experience can be used in the design of the controller. In many cases, the mathematical model of the control process may not exist, or may require significant computer processing and memory, and a system based on empirical rules may be more effective. Furthermore, fuzzy logic is well suited to low-cost implementations based on cheap sensors, low-resolution analogue-to-digital converters, and 8-bit microcontroller chips. Such systems can be easily upgraded by adding new rules to improve performance or add new features [19], [59]–[62].

purpose, the flux is iteratively changed in small steps and the input power is measured, until its minimum is found. The mechanical power is normally maintained constant, since speed and torque are maintained constant. A number of search strategies are proposed in [6], [2], [17], [52], [91], [92].

Theoretically, this method offers the optimal solution without knowledge of the drive. However, some disadvantages appear in practice, such as continuous disturbances in the torque [5], slow adaptation [2], [3], oscillations around the optimal air-gap flux value²⁶ [5], difficulties in tuning the algorithm for a given application, and the need for precise load information [3]. For these reasons, this is not a good method for industrial drives, but since the processing efforts are quite lower, it has been used in most drives [5], which also use lookup tables (which require a number of costly and time consuming measurements for each motor).

It is proposed a simple voltage amplitude searching scheme for optimal voltage control for efficiency optimization purposes in scalar controlled inverters.

First, the acceleration is made maintaining the motor slip within a predefined range to avoid excessive starting currents and rotor losses, which can be significant to extended start-up period, leading to excessive internal temperatures. Additionally, for high starting currents, significant electromagnetic forces act on the coil heads and between conductors causing space shifts (or movements) and vibration, contributing to accelerated insulation system and copper wear, particularly in the coil heads base, which is the most critical spot in the stator windings [14]. This is a feature typically incorporated in most modern VSDs.

Second, the selection of the dominant load behaviour to establish a first U_1 - f_1 relation. It can be used the relation (3.18), which does not include the relation for constant power loads. A voltage boost or offset (mainly dependent on the stator-winding resistance value) should be also incorporated in (3.18). This relation allows for primary voltage regulation when changing fundamental frequency to reach a desirable speed.

$$U_1(f_1) = \begin{cases} U_1 = K_1 \cdot f_1, & T_{load} = const. \\ U_1 = K_2 \cdot f_1^{\frac{3}{2}}, & T_{load} \propto \omega_{load} \\ U_1 = K_3 \cdot f_1^2, & T_{load} \propto \omega_{load}^2 \end{cases} \quad (3.18)$$

Third, the slip should be regulated maintaining the desirable operating point (fixing torque and speed), requiring proper U and f variation. The operating point speed can be approximately estimated indirectly by means of proper processing of current instantaneous values²⁷. Alternatively, the torque can be assumed as proportional to the slip in the quasi-linear zone of the

²⁶ This is due to the smooth and flat curve around the minimum.

²⁷ For example, speed can be easily estimated by input current spectral analysis [70] or based on the motor input currents, line-to-line voltages and motor parameters [5], [63], [64], [65], [66], [67], [68], [69], or directly measured.

motor torque-speed curve, being necessary only to know the operating point speed. Using approximate relations between fundamental voltage, fundamental frequency, torque, slip and frequency, it is possible to define the relation $\Delta(v/f)$ (influencing the motor torque) and Δf (influencing the system synchronous speed) to maintain the load speed and torque when changing slip, by means of changing the slope of the quasi-linear part of the torque-speed curve, according to (3.19), where it is assumed that the torque-speed curve is approximately linear up to 2 times the nominal slip (therefore $2s_N$ was used as auxiliary slip value), and ω_{op} is the motor angular speed corresponding to the steady-state operating point.

Alternatively, a PI or Fuzzy Logic²⁸ controller can be used to simultaneously (parallel processing) maintain the speed, acting on the frequency, when the voltage is varied.

$$U_{t1} = U_{t0} \frac{f_{t1}}{f_{t0}} \sqrt{\frac{(2\pi \cdot p^{-1} \cdot f_{t0} - \omega_{op}) \cdot (2\pi \cdot p^{-1} \cdot (f_{t1} - f_{t0}) + 2s_N)}{(2\pi \cdot p^{-1} \cdot f_{t1} - \omega_{op}) \cdot 2s_N}} \quad (3.19)$$

After reaching the desirable load operating point, i.e., the mechanical steady state (which can be evaluated by means of P_{in} and f stabilization), it is proposed a simplified approach to maximize efficiency, as follows:

- 1) Slight increase of the fundamental frequency by $\Delta f_{ref} = a$ for $U = U_{t0}$, $f = f_{t0}$, and $P_{in} = P_{in_{t0}}$;
- 2) $f := f + \Delta f_{ref}$, $f_{t1} := f$ and compensate voltage according to (3.19);
- 3) Read P_{in} , compute $\Delta P_{in} = P_{in} - P_{in_{t0}}$, and $P_{in_{t0}} := P_{in}$;
- 4) $\Delta f_{ref} := -\Delta f_{ref} \cdot \text{sign}(\Delta P_{in}) \cdot \frac{1}{b} |\Delta P_{in}|$;
- 5) If $\Delta P_{in} \in [c \ d]$ ends the cycle, else go to step 2).

Constants a , b , c , and d should be properly adjusted (c and d define the tolerance window for stabilization²⁹), and P_{in} can be either the DC power input (rectifier losses not taken into account) to inverter, the AC real power input to motor (VSD losses not taken into account), and AC real power input to the VSD (all losses taken into account). This method is immune to temperature variations. The proposed strategy can also be implemented with Fuzzy Logic, considering ΔP_{in} and ΔU as inputs for two membership functions, and rules and defuzzification (e.g., rule outputs defuzzified using a discrete centroid computation) defined for the output ΔU , which allows to

²⁸ Speed reference as input, actual speed as feedback, and frequency as output. In the case of Fuzzy Logic controller, the inputs for membership function should be the actual speed and speed variation/step, and the rules and defuzzification have to be defined for an output frequency.

²⁹ The curve flattening near the optimum efficiency point allow considering wide window for fast stabilization.

compute the final U to be imposed to the motor. The rules for this strategy can be based on empirical methods, basically a methodical approach to trial-and-error.

In [3], it was shown that the difference in the obtained results (in terms of final flux level) for the VSD-input-power-based (or minimum system loss-based) and for motor-input power-based (or minimum motor loss-based) criteria, although increasing with the speed, is, in general, negligible. Moreover, due to the flat-bottom-shape of loss curves, even noticeable difference in air-gap flux produces no effect on the system loss. Therefore, in practice, the minimum motor criteria is just as good as the minimum system loss criteria, assuming moderate VSD losses.

The main advantage of the search methods is that the optimum point, or a point near it, is found regardless the motor and inverter parameters. Another advantage is that, in VSI-fed IMs, it is possible to easily measure DC input power at the inverter DC link. The major disadvantage is that speed has to be known, requiring its measurement or estimation (e.g., on the basis of motor input current). The converging period can be higher than 5 seconds, being in general slower than the other two [2]. Another disadvantage is the fact that, for very low loads, the flux can become extremely low and, if a steep disturbance or load increase occurs, the IM can be not able to drive the load, operating in the unstable region of the torque-speed curve, and decelerates significantly or stops. This problem is particularly critical for scalar control. Also, the step transient response (equal or near rated load) when the motor is operating in a low-load operating point becomes slow due to the reduced flux (required to maximize efficiency). However, to avoid that problem, the slip can be controlled and if it exceeds a certain limit, the control changes to transient mode, centred on the dynamic response of the motor.

A technical issue is associated with this efficiency maximization technique, which is the fact that the motor input real power variation as a function of magnetizing flux is very near the maximum efficiency point, requiring an accurate and without noise power measurement. This problem can be easily solved by means of the use of filters, and is not critical if the control input power is the inverter DC input power, which can be measured accurately.

In general, the efficiency optimization methods, have the advantage of compensating the voltage variation over the day in the power network, which can have a significant negative impact on output voltages and on motor efficiency. Another important aspect, not mentioned on the consulted references, is that, since most motors are oversized, and with such methods, a reduced fundamental voltage will be applied to the motor terminals, leading to a lower m_a (probably in the linear region), minimizing low-order voltage harmonics and increasing motor efficiency and lifetime.

To improve the dynamic performance of EMODS (on the response to load changes) the vector control should be used, in combination with efficiency optimization strategies, being necessary to measure or estimate the rotor speed. The vector control allows a faster flux change than the scalar control [2]. That is related to the fact that, in the vector control, it is possible to apply all the available voltage in the field axis (by means of increasing the field current) without changing the motor torque value. In the scalar control, the voltage increase applies to both axis, resulting in a lower field current rising rate. Scalar control associated with the search control with speed measurement or estimation has a good performance in terms of perturbation response [2]. Regarding the load perturbations, the speed drop is higher if the flux is low. However, as previously referred, the efficiency maximization control is to be used in steady-state and, if a significant load perturbation occurs it will be disabled and the vector control enabled.

For loads with frequent variations over duty cycle, the simple state and motor model control potentially leads to higher savings than search control. This is because search control is not fast enough to stabilize, losing part of time in which savings can be obtained.

The savings associated with efficiency maximization techniques can be significant for variable speed and/or variable load applications.

It is also important to underline that optimizing magnetizing flux level, the power factor will be much improved (see Figs. 3.54-3.57) reducing the motor line current (magnetizing current is reduced), and, therefore, the inverter losses are also reduced.

Due to the significant dependency of motor efficiency on fundamental frequency and voltage [42], [82], [83] (see Figs. 3.59 and 3.60), IEC is working on a standard for specific test methods for determining losses and efficiency of converter-fed AC machines [82].

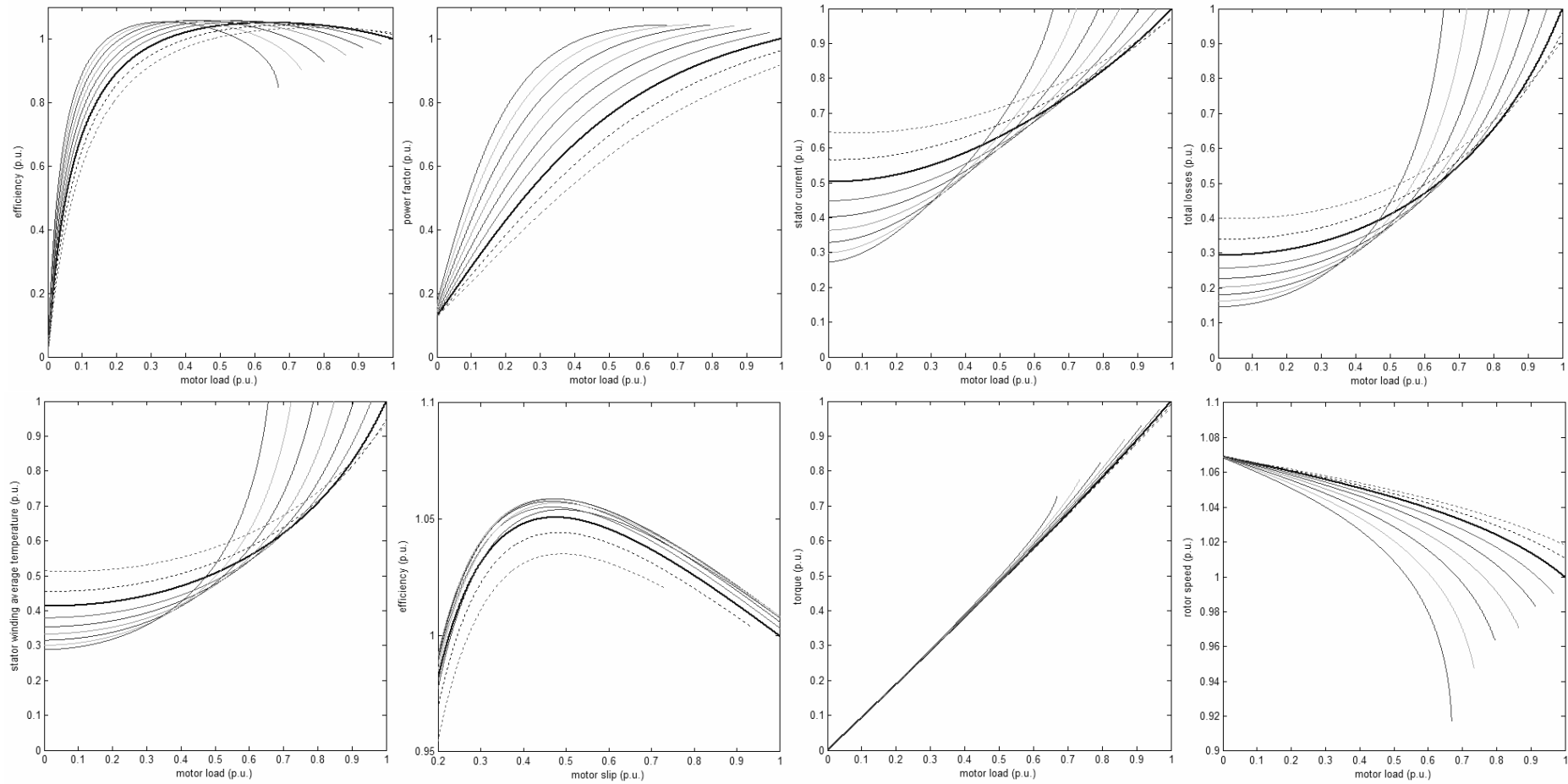


Fig. 3.54. Simulation of a 3-kW, 4-pole, 50-Hz IM at 50 Hz/400 V as a function of load considering different voltage levels (bold solid line: 200 V; solid lines: -5% steps, dashed lines: + 5% steps; p.u. values obtained in relation to nominal values at 50 Hz/400 V).

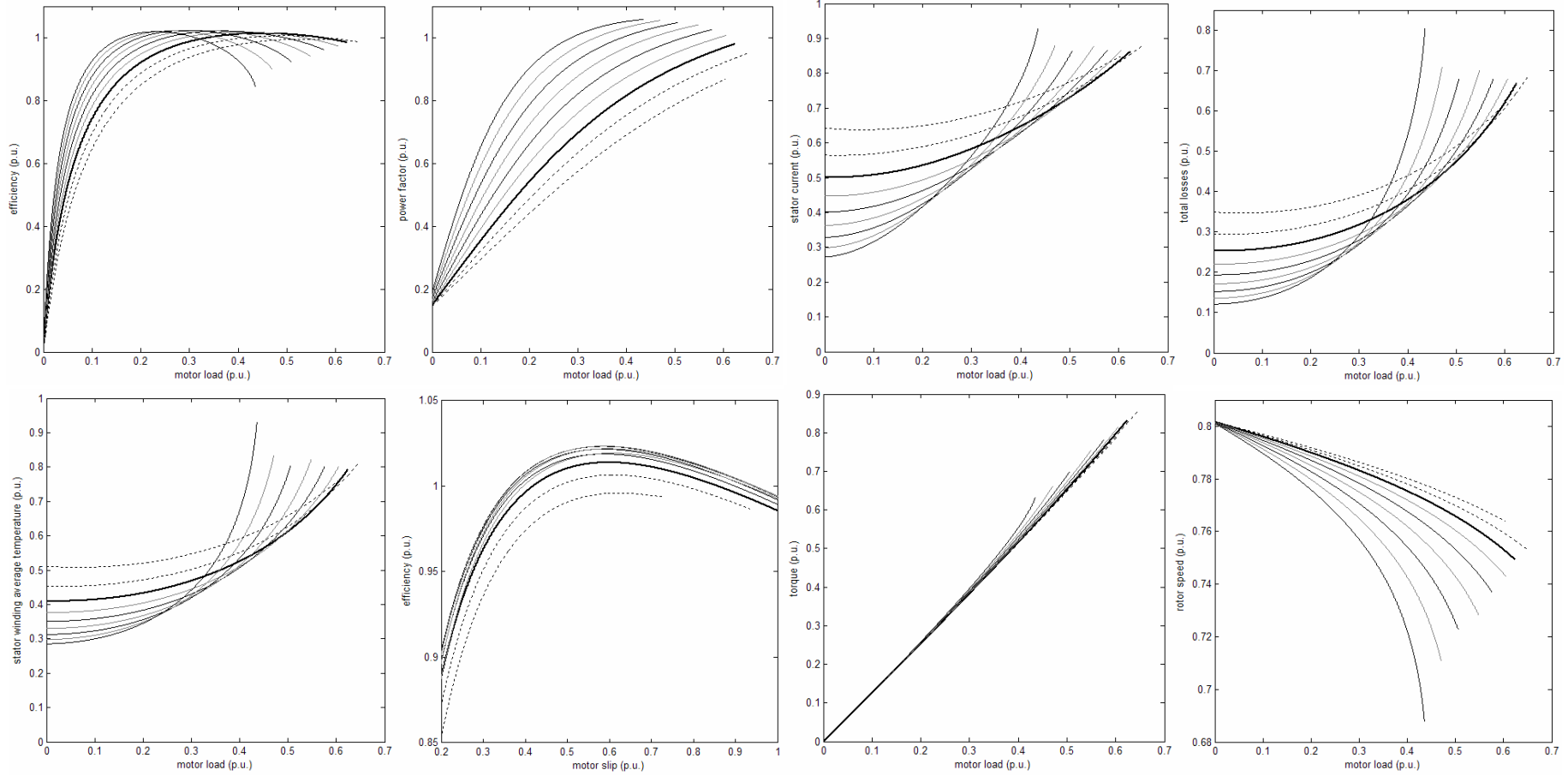


Fig. 3.55. Simulation of a 3-kW, 4-pole, 50-Hz IM at 37.5 Hz/300 V as a function of load considering different voltage levels (bold solid line: 200 V; solid lines: -5% steps, dashed lines: + 5% steps; p.u. values obtained in relation to nominal values at 50 Hz/400 V).

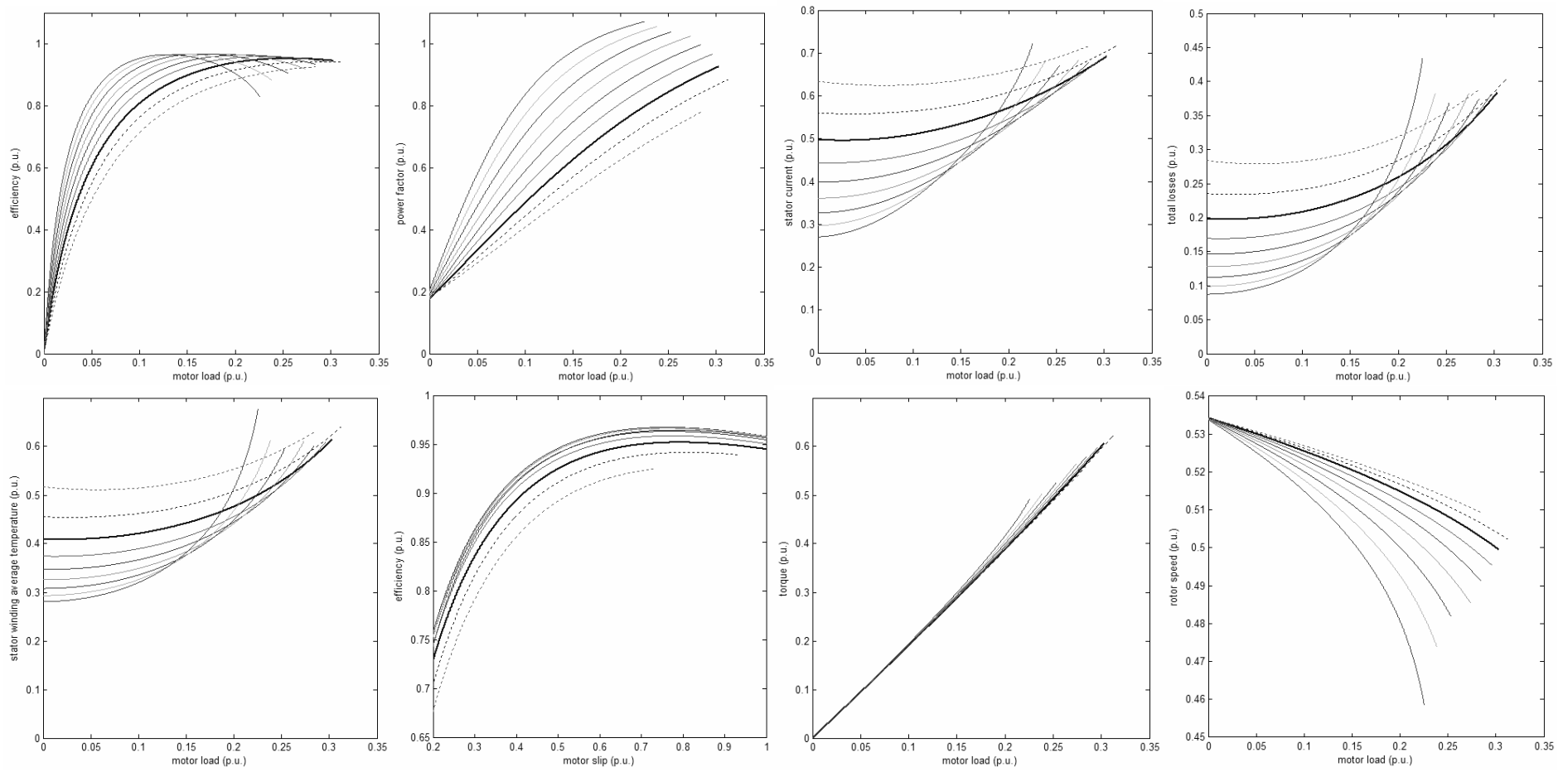


Fig. 3.56. Simulation of a 3-kW, 4-pole, 50-Hz IM at 25 Hz/200 V as a function of load considering different voltage levels (bold solid line: 200 V; solid lines: -5% steps, dashed lines: + 5% steps; p.u. values obtained in relation to nominal values at 50 Hz/400 V).

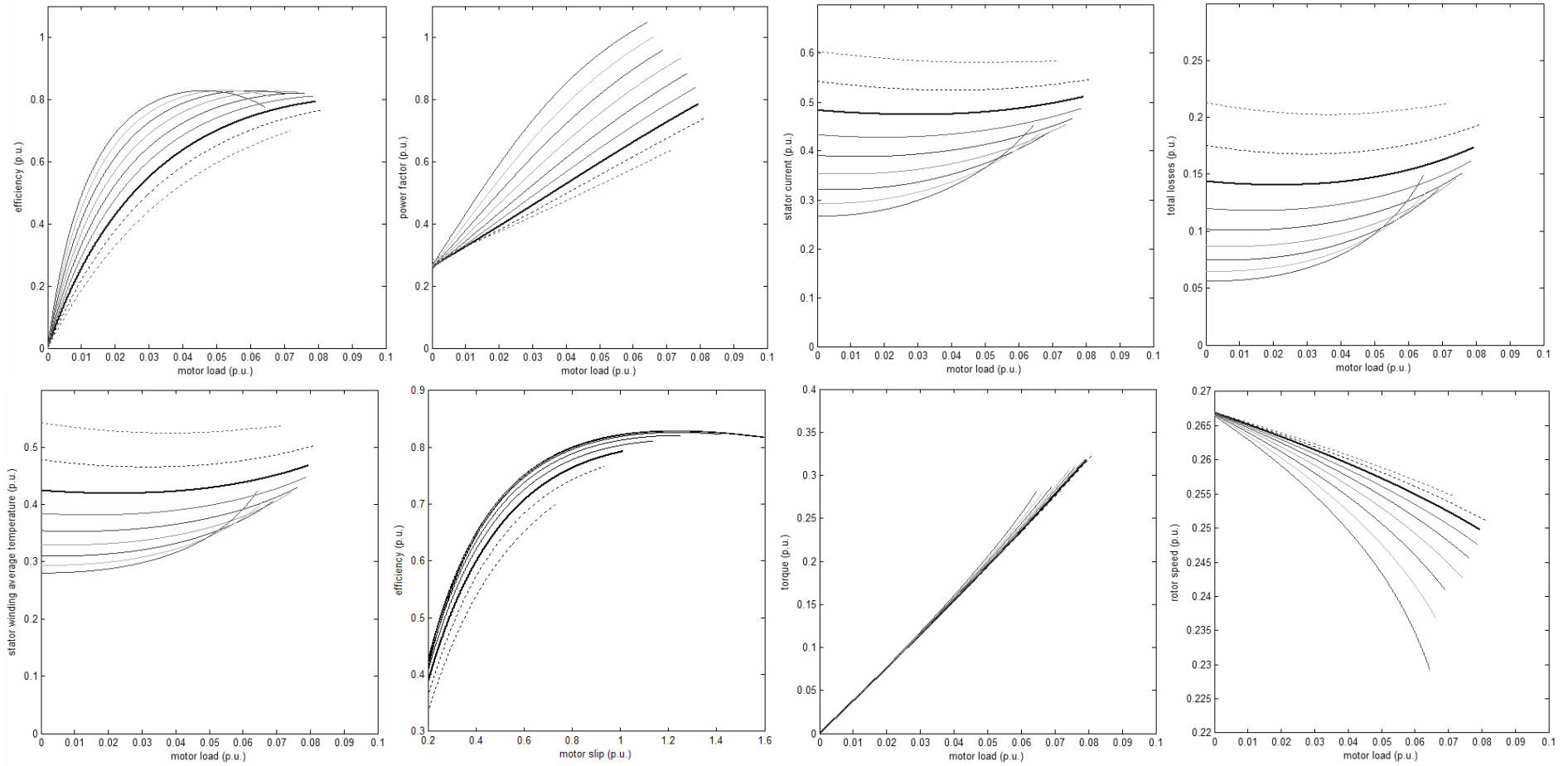


Fig. 3.57. Simulation of a 3-kW, 4-pole, 50-Hz IM at 12.5 Hz/100 V as a function of load considering different voltage levels (bold solid line: 200 V; solid lines: -5% steps, dashed lines: + 5% steps; p.u. values obtained in relation to nominal values at 50 Hz/400 V).

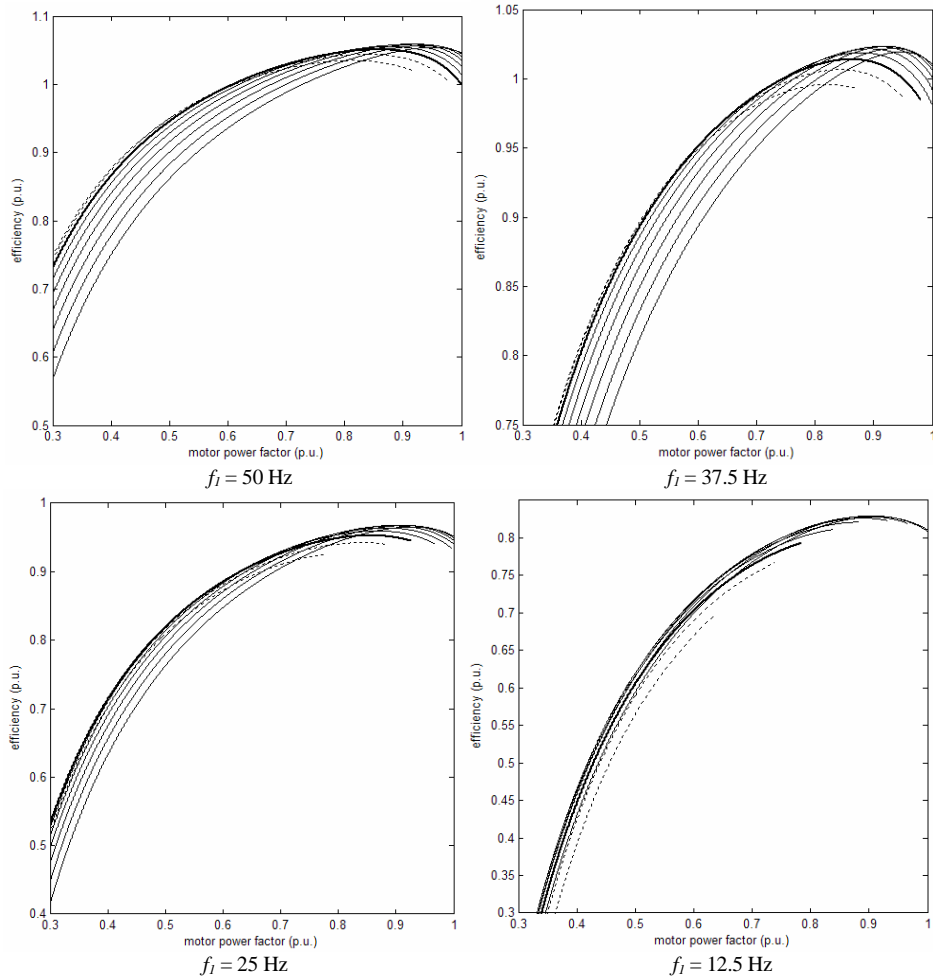


Fig. 3.58. Simulation efficiency as a function of power factor of a 3-kW, 50-Hz, 400-V, 4-pole, IM as a function of load considering different voltage levels (bold solid line: 200 V; solid lines: -5% steps, dashed lines: +5% steps; p.u. values obtained in relation to nominal values at 50 Hz/400 V).

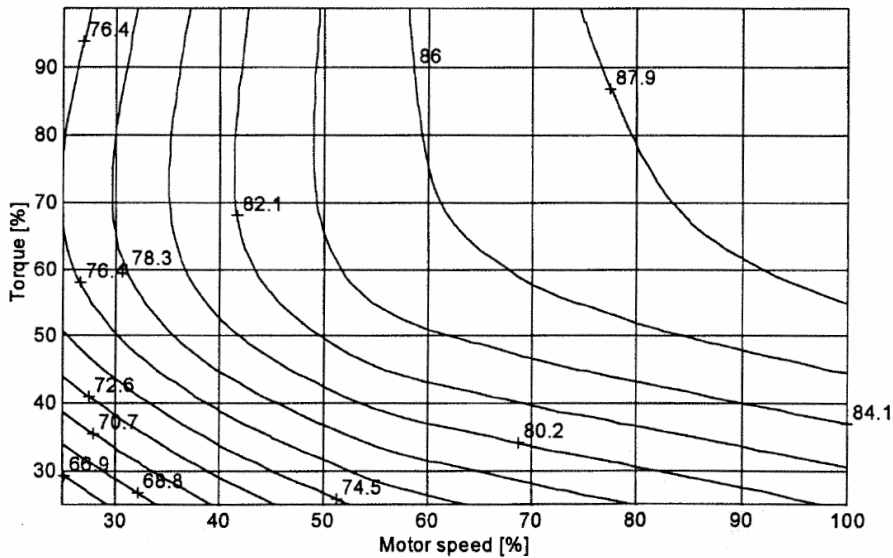


Fig. 3.59. Experimental results for a 37-kW, 2-pole, 60-Hz IM with 89% nominal efficiency [83].

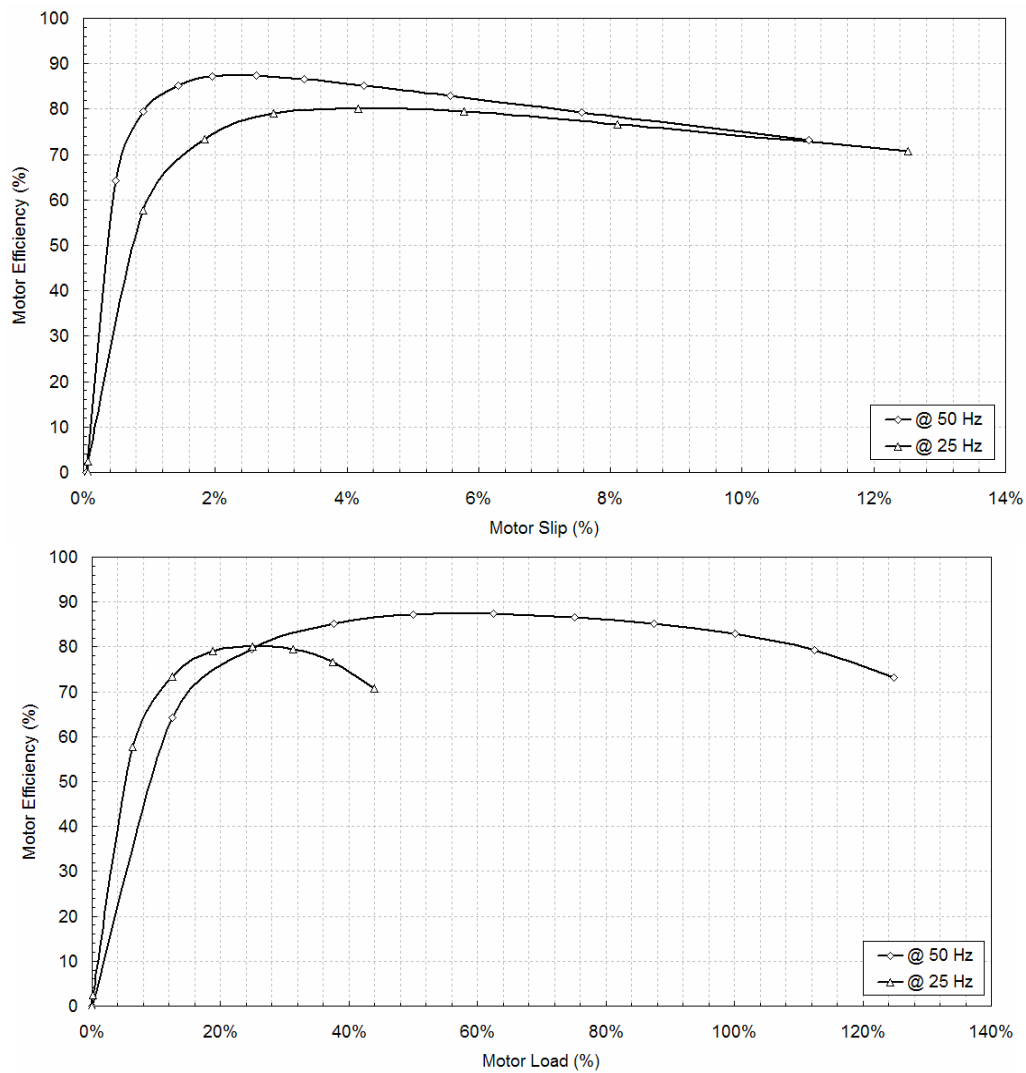


Fig. 3.60. Experimental results with a 3-kW, 4-pole IM ($U_1/f_1 = 8$).

3.6 Ride-Through Capability of VSDs

VSDs are often susceptible to voltage disturbances such as sags, swells, flickers, unbalances, distortion, transients and momentary interruptions (outages). Depending on the application, and the characteristics of the disturbance, the VSD controlled process may be momentarily interrupted or permanently tripped out. This can result in costly down time. The most demanding processes in the modern digital economy need electrical energy with very high reliability (nine “9s”) in order to provide peak performance. Between 1993 and 1999, Electrical Power Research Institute (EPRI) carried out a study in the USA. in order to characterize the power quality on low voltage distribution networks. This study concluded that 92% of disturbances in power quality were voltage sags with amplitude drops up to 50% and duration below 0.5 s. Fig. 3.61 shows the typical distribution of sags and micro-interruptions under 0.5 s [11].

The situation in Western Europe³⁰ is very similar to the one observed in the U.S.A. In industry and commercial sectors more than 90% of the disturbances are under 1 s. Therefore a ride-through capability with a duration of 1 s would decrease dramatically the downtime of VSD-based equipment [11], [101], [102].

In continuous process systems such as metal casters, paper machines, winders, extruders, etc., any interruption can halt the entire manufacturing flow, with very costly implications. Industries with critical production processes have reported losses ranging from 10 k\$ to 10 M\$ per disruption event [11].

VSD ride-through alternatives include the use of the system (motor plus load) inertia, topology modifications and energy storage technologies.

In the system inertia technique, the VSD software control must be modified such that when a power disturbance causes the DC-bus voltage to fall below a specified value the inverter will adjust to operate a frequency slightly below the motor frequency, causing the motor to act like a generator, maintaining the DC-bus at a specified level. There are no delays to start accelerating the motor as soon as the AC power line returns to normal, assuming the load can handle it. Commercial drives are available on the market with this feature with 2 s of ride-through capability for sags down to 80% of the nominal voltage. This solution is, of course, suitable for high-inertia loads [11].

The more advanced hardware modifications include boost converter ride-through capability and the active rectifier VSD front-end.

The boost converter ride-through is used to maintain the DC-bus voltage during a voltage sags and can be integrated between the rectifier and the DC-bus capacitors. This technology can provide ride-through for sags up to 50%. In the case of an outage, the boost converter will not be able to provide ride-through, and the drive will trip [11].

A VSD with active rectifier front have an active PWM rectifier. By this method, ride-through for sags up to 10% can be provided at full load. By derating the rectifier by a factor of 1.5, the ride-through capability can be extended to sags of up to 40% at full load [11]. This technology has several other advantages, namely, the VSD unity power factor, low distortion (compliance to Std. IEEE 519 distortion limits) and regenerative braking capability, as referred previously. The main disadvantages are the high cost and larger size of the VSD package.

Energy storage technologies which can provide full power VSD ride-through capability include battery back-up systems, capacitors, super-capacitors, motor-generator sets, flywheels, superconducting magnetic energy storage (SMES) and fuel cells.

³⁰ In Portugal, for 60 kV and 150 kV systems, according to [101], the vast majority of the voltage sags registered in 2006, presented a duration lower than 250 ms and a decrease of the RMS voltage value up to 30%. According to [102], only $\approx 1\%$ of the sags registered in 2006 in the medium-voltage power network had duration higher than 1 s, and $\approx 70\%$ had duration within 0 and 100 ms (with a 10 to 30% drop in the voltage amplitude). In 124 distribution low-voltage substations, 13137 sags were registered in 2006, 27.5% were within 0 and 100 ms, and 3.2% lasted more than 1 s.

By adding conventional capacitors to the DC-bus, additional energy needed for full power ride-through during a voltage sag can be provided to the motor. This technique is simple and rugged. However, it can only provide limited ride-through for minor disturbances, the cost is relatively high (but expected to decrease in the future) and a large cabinet space is needed.

Higher performance can be achieved by including in the circuit layout a booster supplied by an energy storage module (Fig. 3.62). The energy storage capacity is a function of the duration and of the voltage decrease of the maximum disturbance for which it is intended to provide ride-through capabilities.

For critical processes requiring full power (full speed and torque) ride-through of up to 5 s, supercapacitors (or ultracapacitors) are the most cost-effective approach for VSDs up to 100 kVA, whereas flywheel technologies are the most suitable for VSDs between 100 kVA and 10 MVA. Supercapacitors have experienced a significant increase in energy density and a decrease in price in the last decade. A VSD can be designed with integrated supercapacitors, or as an add-on module. The main advantages of supercapacitors are the ride-through capabilities for deep sags and full outages, long life cycle, fast recharge rates, easy state and charge monitoring and minimal maintenance needs. The main disadvantages are the additional hardware and space requirements, though much less than with standard capacitors. This technique is further addressed in Appendix 4.

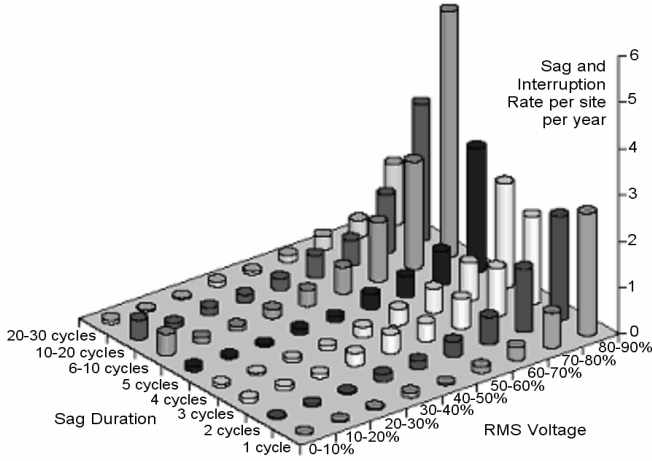


Fig. 3.61. Distribution of sag and micro-interruption in low voltage networks in USA [11].

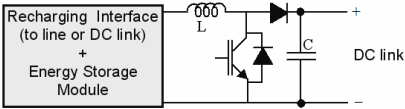


Fig. 3.62. Add-on energy storage module for VSD with ride-through capability [11].

3.7 Economical Advantages Associated with VSDs

Whether or not the VSD is a good investment depends in part on its cost-effectiveness. Whether energy conservation is being used as the sole or partial justification for installing the VSD, accurate savings values are required to ensure the rate of return of the additional capital

cost of the VSD installation is properly calculated. Several benefits are associated with VSDs as energy savings, smoother operation, acceleration/deceleration control, compensate for changing process variables, adjust the rate of production, allow accurate positioning, control torque or tension, just to name a few. The energy savings potential associated with VSD (and to speed control in general) in a number of important loads or systems is evidenced in Appendix 6, which includes a comparison of different variable-speed motor technologies.

3.8 Comparison of Motor Speed Adjustment by means of VSDs and Voltage Regulators

In this section, it is only shown part of the results of an experimental performance comparison of IM speed adjustment using voltage regulators (VRs) and VSDs. The experimental tests were carried out on two commercial axial fan systems, designed for a cooling systems. Part of the results are presented in Figs. 3.63-3.66, being the remaining results presented in Appendix 6.

Several conclusions can be pointed out. As expected, VR-based flow-regulation is less efficient, as clearly evidenced in Fig. 3.63. Only at rated voltage and speed the VR has better performance (due to the by-pass). Power factor is lower for the VR, except for $U \approx U_N$. The line current distortion is higher for the VSD. Voltage and current low-order harmonics at motor input are higher for the VR. Therefore, although VR is cheaper than VSD, it leads to higher distortion at the motor input, reducing its efficiency and lifetime (extra heating is produced). The power factor is, in general, much lower for the VR, except to loads close to rated, in which phase-cutting is minor. In fact, for rated voltage, the VR is automatically by-passed to avoid losses. Bypassing VSD can also be cost effective, as shown in [42]. Therefore, the extra price of VSD over VR, can be recovered quickly in applications operating a large number of hours per year. Of course, both VR- and VSD-based flow regulation are advantageous over throttle-based flow regulation, leading to significant energy savings.

An alternative solution to the VRs is the use of IMs with pole- and/or connection-change capability. In fact, if no continuous speed regulation is required, IMs with automatic stator-winding connection mode change, using two-connection or six-connection modes IMs, single-speed or two-speed type, can be an attractive solution. This solution is potentially cheap and avoid harmonic distortion into the power network and motor. Further information on this issue is presented in Chapter 5. Autotransformers are bulky and expensive, not being, in general, cost effective. Motor energy controller (MEC) can also be a fair solution [103].

It should be referred that for all IM voltage-based speed regulation techniques, the torque-speed curves should have a low-slope quasi-linear region and a high starting torque (e.g., NEMA C-class or D-class rotors [10]), to avoid starting problems and increase speed regulation range.

Therefore, in principle, and without considering double-cage or deep-bar rotors, high-efficiency IMs are not indicated for that purpose.

It should be noted that, as referred, in order to maximize IMs efficiency when performing speed regulation using a VSD, proper voltage regulation has to be made as a function of load. This applies to all load types.

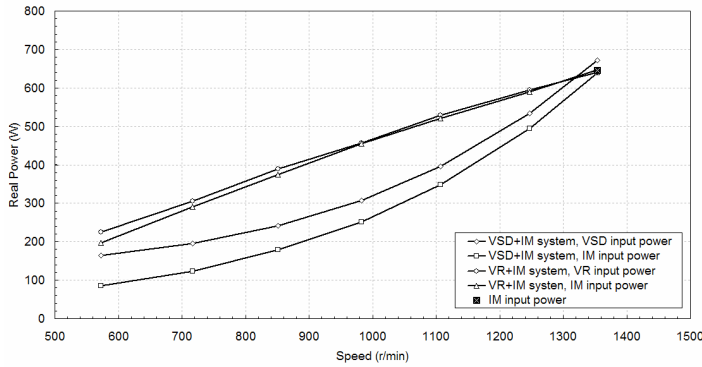


Fig. 3.63. Active input power for a 0.5-kW axial fan system, for different speed control techniques.

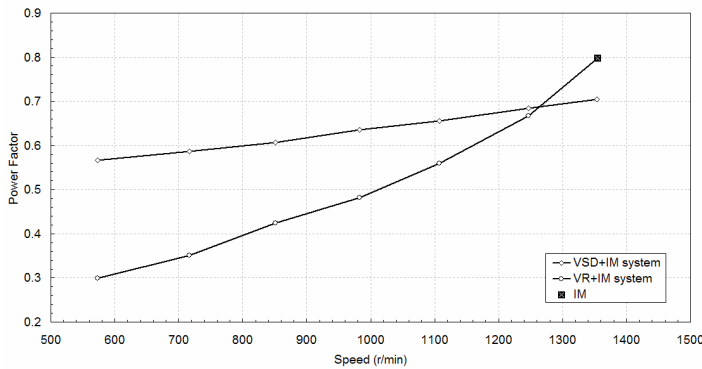


Fig. 3.64. Power factor for a 0.5-kW axial fan system, for different speed control techniques.

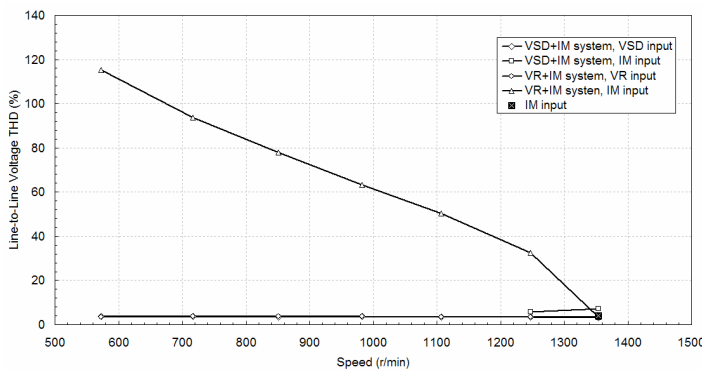


Fig. 3.65. Line-to-line voltage THD for a 0.5-kW axial fan system, for different speed control techniques.

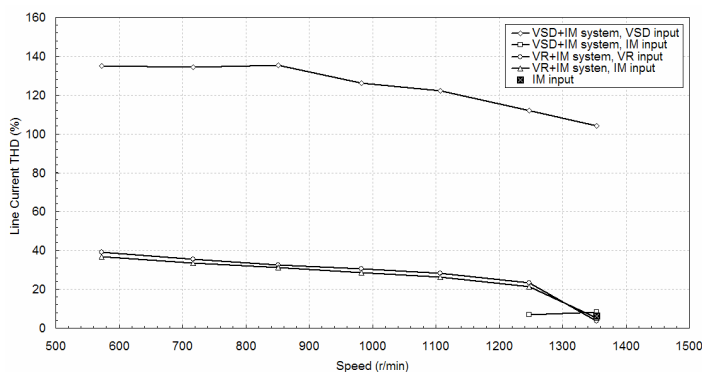


Fig. 3.66. Line current THD for a 0.5-kW axial fan system, for different speed control techniques.

3.9 Considerations on Mechanical Transmission

Mechanical transmission transfers the mechanical power from the motor to the load, and can also be used to adapt the speed and torque. The efficiency of these system components vary typically from 60% to 95%, having a significant impact on the overall EMODS efficiency, as well on the maximum output driving torque. Mechanical transmission also affects the system mechanical transient response. The choice of the transmission system should depend on several factors, e.g., load type, speed and torque required, surrounding ambient temperature and contamination degree, acoustic noise, reliability, mechanical response, etc. In industrial and commercial sectors, the majority of the mechanical transmission systems can be divided into four major groups, namely direct coupling, gears, belts and chains, which will be individually discussed in the following sections.

In general, the transmission ratio and efficiency for a transmission system is given by (3.20), where ω , η_{trs} , T and P are angular speed, efficiency, torque and power, respectively, and the subscripts *in* and *out* refer to the input and output of the transmission system.

$$i = \frac{\omega_{in}}{\omega_{out}} = \frac{P_{in} \cdot T_{out}}{P_{out} \cdot T_{in}} = \frac{T_{out}}{\eta_{trs} \cdot T_{in}} \quad (3.20)$$

For the sake of completeness, the most common mechanical transmission systems are described in Appendix 6, being made a number of technical and economical considerations.

Additionally, in Appendix 4 (Section A4.4.1), some considerations on elastic mechanical transmission are presented.

3.9.1 Combined Pole-Number Change and Transmission Ratio

Since, in general, the higher the number of poles is, the lower the motor efficiency (see Table 3.2 and Fig. 3.68) and the higher the motor price per kW (particular for small motors, Fig. 3.67) will be, when possible, it is desirable to minimize the number of poles. However, for an application requiring belts, chains or gears for motor position, speed adjustment and/or mechanical fuse purposes (in the case of belts), the balance between motor pole-number and transmission ratio has to be properly evaluated, in order determine the most economically and technically advantageous situation.

In order to clarify the proposed idea, an example is considered. Consider two different fixed-torque conveyors driven by means of an IM plus V belt system, one requiring to the motor ≈ 19 N.m at ≈ 1455 r/min (system A) and the other ≈ 38 N.m at ≈ 725 r/min (system B). Two solutions can be considered for each system, namely, adapted number of poles plus near-unitary

transmission ratio or minimum number of poles and adapted transmission ratio, being both following evaluated.

The characteristics of some motors commercially available are presented in Table 3.2, which evidences that, in most cases, the motor efficiency and power factor decreases significantly with the increase of pole pairs, either considering constant rated power or approximately constant rated torque, being in the last case more accentuated. The weight also increases significantly with the pole number increase for the same rated output (Fig. 3.68). In some cases, the frame sizes can be maintained for a different number of poles either considering constant rated power or constant torque. The inertia increases with the number of poles either for the constant rated power and approximately constant torque solutions (Fig. 3.68). In general, the higher the number of poles is, the lower the power-weight ratio and the higher the torque-weight ratio will be (Fig. 3.68).

On the basis of Table 3.3, which shows different possible solutions for required load torque and speed, it is possible to conclude that, for the system A with belt-pulley transmission system, solutions I and II have roughly the same efficiency and the same difference rated torque and required torque, thus the extra speed above rated is roughly the same. However, in solution I the rated speed is higher, thus the input power will be higher too. If fractional transmission ratio is admitted, for slight speed adjustments both solutions give similar performance. Direct coupling (solution II-direct) is the most efficient and cheapest solution, and requires less maintenance. It should be noted that, in the case of gear units, increasing input speed leads to higher friction losses and lubricant leakages, therefore the manufacturers recommend the use of IMs with a pole number equal or higher than 4. As expected, in terms of efficiency, solution I-gear leads is better than solution I-belt.

Regarding system B, with belt-pulley transmission, solution I-belt is the most advantageous, with extra 5.43 p.p. on efficiency over the solution III-belt. Here, decreasing the number of poles is advantageous, leading to higher efficiency, reduced cost and similar maintenance. This consideration are important if belts have to be used for motor positioning purposes, regardless the transmission ratio. Comparing the geared system, solution II-gear is better, since, in this case, the motor efficiency does not vary significantly from 4 to 2 poles, but a 1 p.p. drop in the gear efficiency is considered when doubling the transmission ratio. In this case, direct transmission system is not the most advantageous solution. Solution II-gear is the best option.

This analysis evidences the need for a combined pole-number & transmission ratio analysis for all systems, considering the resulting efficiency and load of each component, in order to identify the best solution.

TABLE 3.2
RATED CHARACTERISTICS OF SOME COMMERCIAL 400-V, 50-Hz, IEC TEFC IMs.

Branch & Year	P_N (kW)	Pole Pairs	ω_N (r/min)	T_N (N.m)	η_N (%)	λ_N	I_N (A)	Frame Size	Weight (kg)	J_{rr} (kg.m ²)
A – 2002	3	1	2920	9.9	87.6	0.86	5.9	100LB	25	0.005
A – 2002	3	2	1455	19.7	87.5	0.81	6.2	112MA	34	0.018
A – 2002	3	4	720	40	82.0	0.68	7.8	132M	53	0.045
A – 2002	30	1	2955	97	93.2	0.88	53	200MLA	175	0.15
A – 2002	30	2	1475	194	93.4	0.84	55	200MLB	205	0.34
A – 2002	30	4	735	390	92.8	0.79	59	250SMA	280	1.25
A – 2002	3	1	2900	10	83.8	0.88	5.95	100L	21	0.0041
A – 2002	1.5	2	1440	10	85.6	0.82	3.2	100LA	21	0.0069
A – 2002	0.75	4	700	10	72.0	0.59	2.55	100LA	20	0.0069
B – 1996	3	1	2895	9.8	83.0	0.86	6.1	100L	21	0.0038
B – 1996	3	2	1430	20.0	80.0	0.8	6.8	100L	24	0.0058
B – 1996	3	4	700	40.0	79.0	0.69	7.9	132M	46	0.019
B – 1996	30	1	2945	97.0	92.3	0.89	53	200L	165	0.14
B – 1996	30	2	1465	196.0	91.8	0.86	55	200L	170	0.24
B – 1996	30	4	730	392.0	91.6	0.82	58	250M	435	1.1
B – 1996	3	1	2895	9.8	83.0	0.86	6.1	100L	21	0.0038
B – 1996	1.5	2	1410	10.0	74.0	0.81	3.6	90L	15.6	0.0035
B – 1996	0.75	4	665	11.0	65.0	0.77	2.15	100L	18	0.0053
C – 1999	3	1	2875	10	83.0	0.86	6.3	100L42	20	0.0032
C – 1999	3	2	1400	20.5	80.0	0.8	7.1	100L44	21	0.0056
C – 1999	3	4	700	41	78.0	0.7	8	132M88	44	0.03
C – 1999	30	1	2935	98	91.5	0.9	55	200L62	150	0.115
C – 1999	30	2	1470	195	91.0	0.86	58	200L64	160	0.15
C – 1999	30	4	735	390	90.5	0.75	71	250M48	395	0.82
C – 1999	3	1	2875	10	83.0	0.86	6.3	100L42	20	0.0032
C – 1999	1.5	2	1380	10.4	74.0	0.78	3.9	90L44	13.5	0.0037
C – 1999	0.75	4	695	10.3	70.0	0.59	2.9	100L48	21	0.0056
D – 2003	3	1	2890	9.9	85.6	0.87	5.81	100L	31	0.00617
D – 2003	3	2	1420	20.2	84.7	0.86	5.94	100L	34	0.00995
D – 2003	3	4	710	40.4	83.5	0.72	7.2	132M	75	0.08531
D – 2003	30	1	2960	96.8	92.7	0.88	53.1	200L	239	0.2063
D – 2003	30	2	1475	194.0	93.0	0.85	54.8	200L	233	0.33096
D – 2003	30	4	730	393.0	91.8	0.83	56.7	250S/M	440	1.22377
D – 2003	3	1	2890	9.9	85.6	0.87	5.81	100L	31	0.00617
D – 2003	1.5	2	1420	10.1	81.7	0.83	3.19	90L	23	0.00673
D – 2003	0.75	4	700	10.2	69.0	0.59	2.66	100L	27	0.00953

TABLE 3.3
DIFFERENT SOLUTIONS FOR TWO CONSTANT TORQUE MOTOR
DRIVEN APPLICATIONS (19 N.m/≈1455 r/min AND 38 N.m/≈725 r/min).

System Ref.	System Solution	Motor Branch & Year	Motor Poles & Transmission Ratio	$T_{N(mtr)}$ (N.m)	ω_{syst} (r/min)	T_{mtr} (N.m)	η_{syst} (%)
A	I-gear / I-belt	A – 2002	$p = 1$ & $i = 2$	9.9	≈ 1460	9.7 / 9.8	85.85 / 84.97
	II-direct / II-belt	A – 2002	$p = 2$ & $i = 1$	19.7	≈ 1455	19.1 / 19.6	87.06 / 84.87
B	I-gear / I-belt	A – 2002	$p = 1$ & $i = 4$	9.9	≈ 730	9.8 / 9.8	84.97 / 84.97
	II-gear / II-belt	A – 2002	$p = 2$ & $i = 2$	19.7	≈ 728	19.4 / 19.6	85.75 / 84.88
	III-direct / III-belt	A – 2002	$p = 4$ & $i = 1$	40	≈ 720	38.2 / 38.2	81.59 / 79.54

Notes:

Gear Units: transmission ratio equal to 2 and 4, with 98% and 97% efficiency, respectively.

Belt-Pulley Units: transmission ratio equal 1, 2 or 4, with 97% efficiency in all cases.

Direct Coupling: 99.5% efficiency.

Motors: 3-kW, 400-V, 50-Hz, TEFC IMs. Motor load ≈ 100%.

In terms of mechanical transient periods, considering the equivalent inertia at the transmission input and that the torque to rotor inertia ratio increases significantly with the decrease of the number of poles (see Table 3.2 and Fig. 3.68), a better transient response is expected with the

pole decrease and transmission ratio decrease, even considering the inertia associated with transmission systems.

Moreover, when applicable, the lower the number of poles is, the higher the kW/kg ratio and the lower the N.m/kg ratio will be (see Fig. 3.68). This can be important for maximization of those ratios with different motor-gear or motor-belt unit, particularly if the motor is also moved with the load (e.g., industrial trolleys, trains or vehicles). Additionally, although motor production is in general optimized to minimize the 4-pole motors price (major part of the market), for most cases, the lower the number of poles, the lower the €/kW ratio (see Fig. 3.67), which is another benefit that should be taken into account.

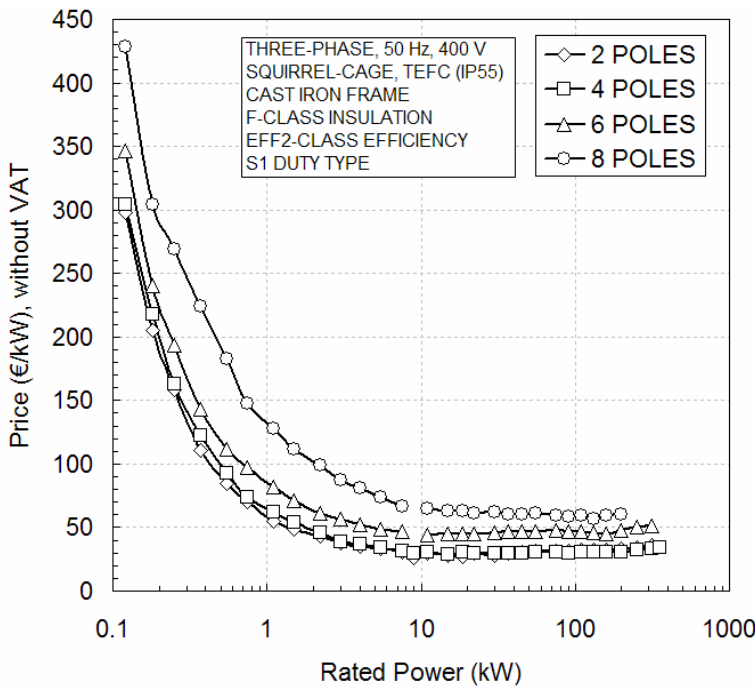


Fig. 3.67. Prices per kW (without VAT) for 50-Hz, 4-pole, cast iron frame IMs [88].

3.10 Motor Selection for Variable-Speed Applications

Selection or sizing of IMs for variable-speed applications is a very important issue. Although not presented in the main text of this thesis, for the sake of completeness, in Appendix 6, several issues related to the thermal and mechanical limitations of VSD-fed TEFC (equivalent to IP 55 protection degree) IMs are discussed and a methodology for proper IM selection for variable-speed EMODS is proposed, with the focus on steady-state operation.

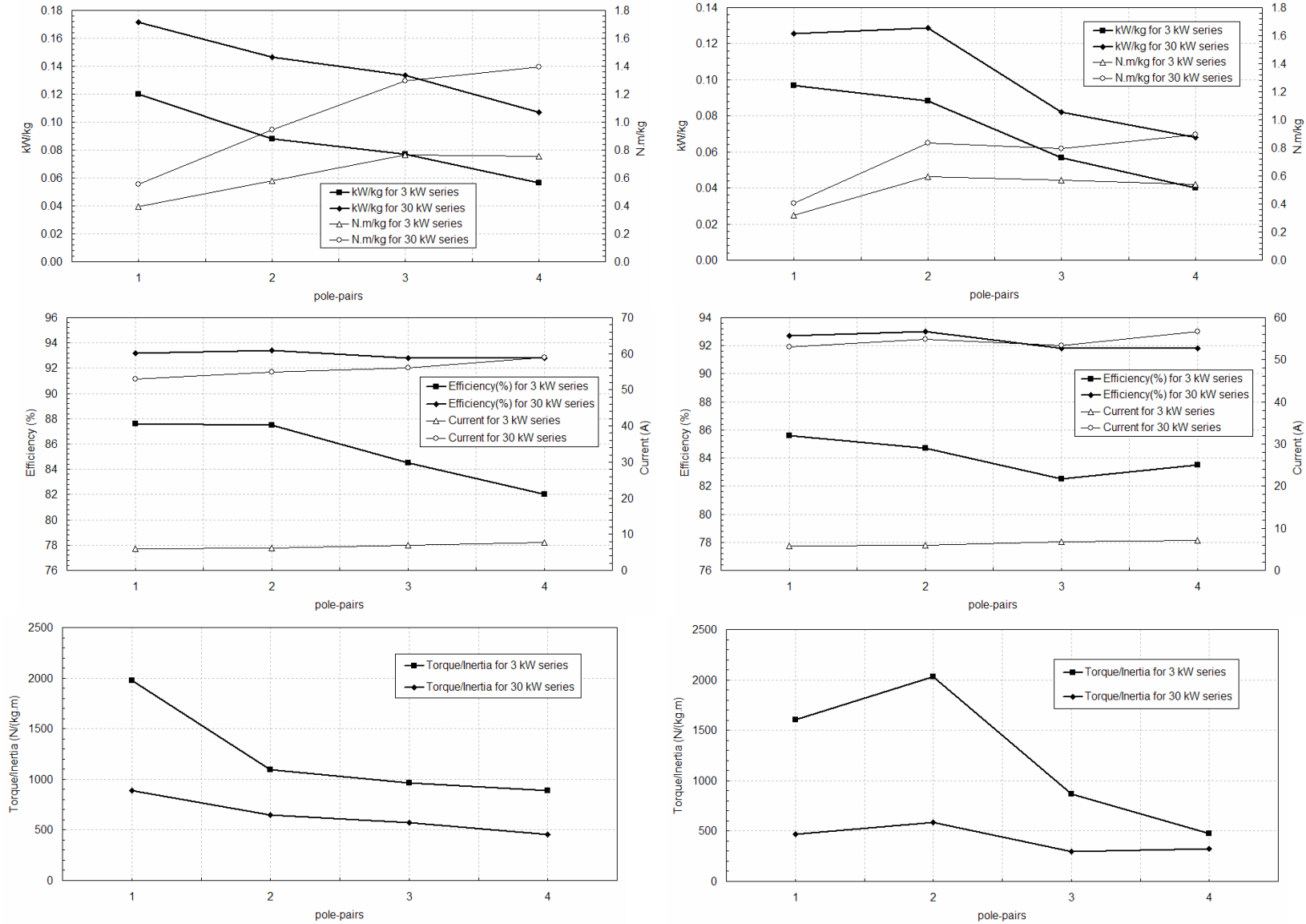


Fig. 3.68. Characteristics of motors with a different number of poles: (left) brand A; (right) brand E; (top) power/weight and torque/weight ratios; (middle) rated efficiency and current; (bottom) torque/rotor inertia ratio.

3.11 VSDs Market Characterization

The presented characterisation of the VSDs market in the EU includes the number of units sold in each country, the average retail prices and total cost of VSDs per kW and per power range. The information was collected, through several sources (questionnaires, trade associations, large manufacturers, etc.) in each country of the study (Denmark, U.K. and Ireland, France, Germany and Austria, Netherlands, Portugal³¹ and Spain) [11]. These EU countries represent around 70% of the total EU VSD market, and the estimated average values were then extrapolated to the EU, based on previous studies and EU statistics. The base year for the market characterisation was 2002. Fig. 3.69 shows the disaggregation of the VSDs market by country in the EU. Fig. 3.70 shows the number of VSD units sold in the EU per power range. This figure shows that the VSDs market, in 2002, was dominated by low power drives in the range of 0.75 to 4 kW, representing about 76% of the total units sold in the considered countries. The number of VSD units sold in the EU in 2002 was 1.8 million units, representing a total value of over 1 G€.

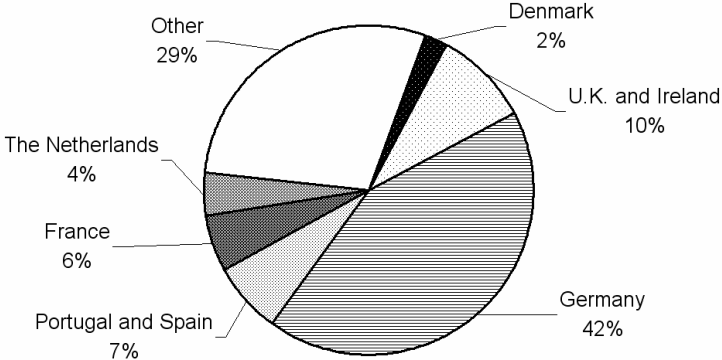


Fig. 3.69. Distribution of the VSD market in terms of the total number of units sold per each country, in 2002 [11].

IMs are by far the dominant type of motor used with VSDs, but, as already referred, other more advanced motor designs are entering the market (e.g., permanent magnet and reluctance AC motors), particularly in the low power range.

As it can be seen in Fig. 3.71, the prices per kW decrease with the increase of the power, since for higher power only the power stages are different, being the control circuits identical [11], but more sharply in the low-medium power ranges. In fact, the prices per kW decrease until the 30 to 70 kW range, then they stabilize in the higher power ranges. Fig. 3.71 also shows the total cost (unit cost plus installation) per kW. This curve is influenced by the fact that the higher the power is, the lower the installation costs per kW will be.

³¹ In Appendix 6, information concerning the VSDs and Soft-Starters Portuguese market, for the years 2005, 2006, and 2007, is presented.

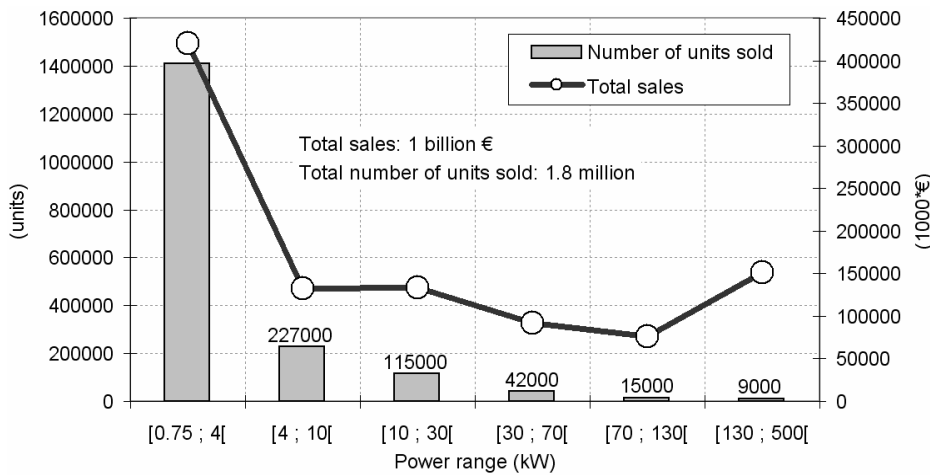


Fig. 3.70. Number of units sold in the EU and sales value per power range, in 2002 (1 billion = 1 G) [11].

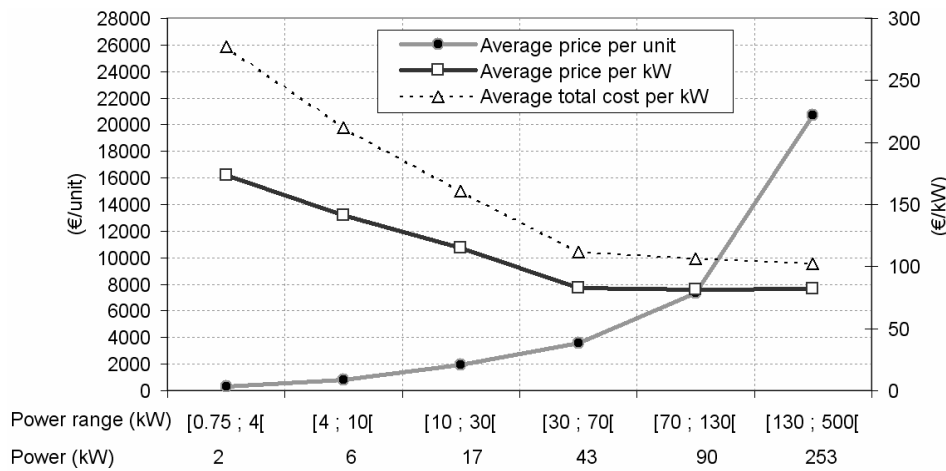


Fig. 3.71. Average unit costs and average per kW costs, for the different power ranges in the EU [11].

3.12 VSDs Savings Potential

The estimated motor electricity consumption in the EU by 2015 is 721 TWh in Industry and 224 TWh in the tertiary/commercial sector. For the assessment of electricity savings potential with the application of VSDs, three different scenarios have been considered: the technical savings potential, economic savings potential assuming constant VSD prices, and the economic savings potential assuming a VSD price decrease of 5% per year. In general, VSDs are not cost-effective in the lower power ranges. In the economic saving potential the cost-effectiveness constraints are considered. Only the power ranges with a CSE lower than the average price of kWh in the sector of application are considered. In the technical potential no economic restrictions are considered. Table 3.4 summarises the technical and economic savings potential in the industrial and in the tertiary sector with the application of VSDs.

The identified economic electricity savings potential (assuming VSD constant prices) with the application of VSDs, by 2015, would translate into 19 Mt of CO₂ savings, contributing to the goal of reducing the greenhouse gas emissions in the EU. Table 3.4 also shows the technical and

economic potential CO₂ and Euro savings in industrial and tertiary sectors, with the application of VSDs, by 2015.

In Table 3.5, the estimated savings potential associated with VSD integration in different applications in the EU, is shown.

Although roughly 25% of the new electric motor being equipped with VSDs, they represent a relevant growing market when integrated in variable speed motor driven systems they have a number of advantages evidenced previously. With the large-scale use of VSDs in a wide range of applications of different sectors, significant energy savings can be obtained and, consequently, avoided the associated CO₂ emissions. Depending on the application, VSDs can be a short-payback technology and, additionally, lead to acoustic noise reduction and to the improvement of process control, productivity increase, product quality improvement, and to the mechanical equipment/component wear reduction. VSDs can also be able to ride-through the most power disturbances being a valuable characteristic in continuous process systems, avoiding costly downtime [11].

TABLE 3.4
ESTIMATED SAVINGS POTENTIAL IN EU-15 BY 2015 [11].

	Technical Potential	Economical Potential	
		Constant Prices	5%/yr Price Decrease
Total Industry (TWh/yr)	62	39	43
Total Tertiary (TWh/yr)	22	8	11
Total (TWh/yr)	84	47	54
³² Savings (Mt/yr of CO ₂)	33	19	22
Savings (106 €/yr)	5600	2050	3500

TABLE 3.5
INTEGRATION OF VSDS IN DIFFERENT APPLICATIONS IN THE EU:
ESTIMATED SAVINGS POTENTIAL, APPLICABILITY AND APPLICATIONS ALREADY INTEGRATING VSDS [54].

Application	Savings Potential	Applicability	Applied
Fans	35%	60%	7%
Pumps	35%	60%	9%
Compressors	15%	30-40%	4-5%
Conveyors	15%	60%	8%

3.13 Actions to Promote VSDs

VSDs are typically considered as an extra component to “common” systems or machines. They are acquired either directly by the end-user from the VSD supplier or through intermediate parties such as OEMs and installers. A relatively small part of the potential end-users is willing to actively search for VSD related solutions. These typically are early market clients. VSDs have to move further to main market clients. Most of these will rely upon their traditional channels for

³² Considering an average emission of 0.4 kg of CO₂ per kWh generated, and average electricity prices of 0.05 and 0.1 €/kWh in industrial and tertiary sectors, respectively

EDMOS, such as system suppliers, OEMs and installers. For successful dissemination of VSDs these parties will become more crucial. They will have to play an important role in actions to promote VSDs. Though VSDs face strong growth, the general impression is that applications are driven mainly by process-related considerations (extra throughput, process control advantages, quality enhancements, etc.). The relative growth in the market segments “driven” by energy-efficiency advantages lag significantly behind in growth and maturity. The reasons are well known, e.g., low priority for energy efficiency, low visibility of benefits of VSDs in most energy-driven applications, and the market is dominated by lowest first cost decisions in competitive bidding procedures. The difference in market maturity between process-driven and energy-driven applications clearly indicates that most barriers are not technology related [11].

For many energy-relevant applications VSDs are not yet generally perceived as “good quality for money”. This is not caused by low payback times, but rather by the feeling that it takes too much time and effort to assess possibilities and to procure VSD systems. This time is rather given to the core business. Pragmatic or conservative users usually prefer: (a) Standard (off-the-shelf) solutions; (b) To be acquired and used without extra risks or effort; (c) Not too costly. If extra costs are involved, the extra benefits should be evident, clearly visible and competitive with core business investments; (d) Integrated solutions by familiar distribution channels, with preferably one single responsible supplier [11].

In short, more standardised and integrated VSD solutions are needed. For some applications increasingly standard-off-the-shelf systems become available. Examples are small VSD-pump and small VSD-motor combinations and medium size compressed-air systems with integrated speed controls. For other systems alternative methods have to be facilitated to achieve more standardised, transparent and comparable integrated VSD solutions. Most end-users do not consider VSD systems as their core business and will rely upon their common suppliers in improving systems and services. As a result it will be largely the business of OEMs, system suppliers etc. to achieve the easier and more accessible integrated VSD solutions. Actions are also needed to increase the awareness of economic benefits and process improvements by end-users, associated with the use of efficient VSD systems [11].

3.14 Conclusions

The efficiency improvement potential associated with speed adjustment in EMODS is large. VSDs are a very relevant growing market, although only 10-35% of new motors are equipped with VSDs. They allow to control with precision the speed and torque of IMs, increasing its application spectrum. When integrated in variable speed EMODS, they have significant economical and technical advantages. Huge energy savings, and the associated reduction in

environmental emissions, are possible through the large-scale application of VSDs in a wide variety of loads in the different sectors of the economy. However, there are several barriers, both technical and non-technical which prevent a larger scale adoption of VSDs. Due to the lack of knowledge of the VSDs economical and technical advantages in industrial and commercial sectors, actions to promote awareness of those advantages should be implemented. Additionally, VSDs may introduce problems related to the motor efficiency and reliability, power quality and EMI. For the majority of the referred problems, solutions are now available and new improved ones are in investigation, which can avoid or mitigate those problems. With proper installation and proper motor construction, VSDs can be a very cost effective technology that can lead to better process control, less wear in the mechanical equipment, less acoustic noise, and significant energy savings. More recently, with recent hardware advances, VSDs can also integrate the ride-through capability to overcome the majority of power disturbances, which is a valuable feature in continuous process systems such as metal casters, paper machines, winders, extruders, etc., avoiding very costly downtime.

A comparative experimental and simulated study focusing the main advantages/disadvantages in steady-state operation of low-voltage, low-power, two-level and three-level voltage-source inverters was carried out. In general, when compared to the 2L-VSI units, the 3L-VSI units lead to lower du/dt in the output voltage pulses, which attenuates the voltage reflection effect in the power cable between VSI and IM, reducing the magnitude of the voltage transients, potentially leading to a longer lifetime of the IM insulation system and, additionally, to less EMI problems. The 3L-VSI units also lead to lower distortion of the output voltage and current waves, reducing slightly the motor losses and operating temperature. When the 3L-VSI units are used, the bearing currents activity is expected to be lower due to the lower amplitude of the generated common-mode voltages, potentially leading to a longer lifetime of the IM bearings. Moreover, due to the lower mechanical vibration in the 3L-VSI-fed IMs, lower motor acoustic noise and lower mechanical wear of the motor bearings and insulation system are expected. The referred factors are important advantages of the 3L-VSI technology, and contribute all to a higher motor reliability. In short, commercially available 3L-VSI units have significant benefits over the equivalent 2L-VSI units, in terms of motor reliability and acoustic noise reduction (for $f_s < 8$ kHz), but no energy benefits should be expected – actually, a slight increase in the overall system consumption can happen for higher system loads. Although 3L-VSI units have higher price in relation to 2L-VSI units, in critical applications demanding high reliability levels, or using long power cables between the inverter and the motor, 3L-VSI units can be cost-effective if the motor degradation rate (including windings and bearings) and maintenance costs were

taken into account. Of course, in these cases, one can use a 2L-VSI unit and a special motor termination unit, which eliminates almost totally the voltage overshoots at the motor terminals.

EMODS initial and operation costs should be properly analysed, being the last related to the power factor (reactive power/energy), efficiency (real power/energy) and reliability (maintenance and downtime) of the system. An oversized EMODS has lower maintenance and downtime costs, but has higher operation costs. The relevance of each type of costs depends on the type of Industry. The minimization of the total costs associated with variable-speed EMODS require the correct sizing of the IM and of the VSD, i.e., the IM should be adequate to the load and the VSD should be adequate to the IM. System optimization or improvement of system modules (and the establishment of investment priorities) should be made starting on the load up to power supply. In a number of cases the potential motor useful lifetime gain cannot compensate the additional cost of an oversized motor. In the case of short-time violation of the IM thermal limits (significantly lower than the thermal time constant), and considering that in the majority of the operating time the IM operates within thermal limits, it is an acceptable solution. A practical methodology is proposed, allowing the proper selection of IMs for variable speed loads. The presented method can also be used for grid-fed IMs, for fixed speed loads (in this case the 10% reduction in the torque limit is not considered). A number of examples were presented, and for the same rated power and without affecting reliability, it is possible to choose an IM more adapted to the load by simply changing the number of poles, being this a solution clearly more economic than being a larger IM and VSD. Another admissible solution, although with an efficiency and reliability potentially lower, is the adaptation of the EMODS speed range by means of a proper mechanical transmission relation.

The improvement of the mechanical transmission between motor and load is essential to the overall motor system optimization in terms of efficiency and reliability, as well as in terms of mechanical response. A number of options are available with different price, performance, robustness, flexibility, speed, torque, etc. However, in economical and technical terms, for each application it is possible to choose the most suitable transmission type that fulfils the system particular requirements. For in-operation systems improvement, proper replacement of existing transmission (retrofit) can be made if cost-effective alternatives are commercially available. High-efficiency transmissions can lead to longer lifetime, lower energy losses and lower input power requirement, which can lead to a reduction of the motor rating required for the system. If a system is being optimized, and the motor is to be replaced by a high-efficiency motor, the motor rating reduction can lead to a significant capital investment in the motor. Therefore, for new systems, an integrated design is necessary to ensure overall optimization, including the

mechanical transient response, which is actually important in terms of process quality and system reliability.

3.15 References

- [1] Jouanne, A.; Zhang, H.; Wallace, A.: "An Evaluation of Mitigation Techniques for Bearing Currents, EMI and Overvoltages in ASD Applications", IEEE Trans. on Industry Applications, Vol. 34, No. 5, Sept./Oct. 1998, pp. 1113-1122.
- [2] Abrahamsen, F.; Blaabjerg, F.; Pedersen, J.K.; Grabowski, P.Z.; Thogersen, P.: "On the Energy Optimized Control of Standard and High-Efficiency Induction Motors in CT and HVAC Applications", IEEE Trans. on Industry Applications, Vol. 34, Issue 4, pp. 822-831, July/Aug. 1998.
- [3] Abrahamsen, F.; Blaabjerg, F.; Pedersen, J.; Thogersen, P.: "Efficiency-Optimized Control of Medium-Size Induction Motor Drives", IEEE Trans. on Industry Applications, Vol. 37, Issue 6, pp. 1761-1767, Nov./Dec. 2001.
- [4] Abrahamsen, F.; David, A.: "Adjustable Speed Drive with Active Filtering Capability for Harmonic Current Compensation", 26th Annual IEEE Power Electronics Specialists Conf. (PESC '95), Conf. Record, Vol. 2, pp. 1137-1143, 18-22 June 1995.
- [5] Kioskeridis, I.; Margaris, N.: "Loss Minimization in Induction Motor Adjustable-Speed Drives", IEEE Trans. on Industrial Electronics, Vol. 43, No. 1, pp. 226-231, February 1996.
- [6] Kioskeridis, I.; Margaris, N.: "Loss Minimization in Scalar-Controlled Induction Motor Drives with Search Controllers", IEEE Trans. on Power Electronics, Vol. 11, No. 2, pp. 213-220, March 1996.
- [7] Mastorocostas, C.; Kioskeridis, I.; Margaris, N.: "Thermal and Slip Effects on Rotor Time Constant in Vector Controlled Induction Motor Drives", IEEE Trans. on Power Electronics, Vol. 21, N.º 2, pp. 495-504, March 2006.
- [8] Carlson, R.: "The Correct Method of Calculating Energy Savings to Justify Adjustable-Frequency Drives on Pumps", IEEE Trans. on Industry Applications, Vol. 36, No. 6, pp.1725-1733, Nov./Dec. 2000.
- [9] Maxwell, J.: "How to Avoid Overestimating Variable Speed Drive Savings", IETC - Industrial Energy Technology Conference, <http://txspace.tamu.edu/handle/1969.1/5621>, 2005.
- [10] Guru, B.; Hiziroglu, H.: "Electric Machinery and Transformers", 2nd Edition, Oxford University Press, New York, 1995.
- [11] de Almeida, A., Ferreira, F., Both, D.: "Technical and Economical Considerations to Improve the Penetration of Variable Speed Drives for Electric Motor Systems", IEEE Trans. on Industry Applic., Vol. 41, No. 1, pp. 188-199, Jan./Feb. 2005.
- [12] Bertoldi, P.; de Almeida, A.; Falkner, H.: "Energy efficiency Improvements in Electric Motors and Drives", Springer-Verlag, Berlin, Heidelberg, 2000.
- [13] Ferreira, F.; Sá, C.: "Considerações sobre a Seleção de Motores de Indução Trifásicos para Accionamentos de Velocidade Variável", Revista Kéramica N.º 277, Março/Abril de 2006;
- [14] Ferreira, F.: "Técnicas Avançadas de Manutenção Curativa e Reabilitação de Motores de Indução Trifásicos de Baixa Tensão/ Curative Maintenance and Rehabilitation Advanced Methods for Low-Voltage, Three-Phase, Induction Motors", Tese de Mestrado/M.Sc. Thesis (available in Portuguese only), Universidade de Coimbra/University of Coimbra, 2002.
- [15] Ferreira, F.; de Almeida, A.; Baoming, G.: "Comparative Study on 2-Level and 3-Level Voltage-Source Inverters", 5th Inter. Conf. on Energy Efficiency in Motor Driven Systems (EEMODS'07), Conf. Proc., Vol. II, pp. 581-602, Beijing, China, 2007.
- [16] Mohan, N.; Undeland, T.; Robbins, W.: "Power Electronics - Converters, Applications, and Design", 2nd Ed., John Wiley & Sons, Inc., New York, 1998.
- [17] Mohan, N.: "Power Electronics, Circuits, Devices, and Applications", New Jersey, Prentice-Hall, Inc., 1996.
- [18] Bose, B.: "Power Electronics and Motor Drives – Advances and Trends", Elsevier, Academic Press, New York, 2006.
- [19] Boldea, I.; Nasar, S.: "Electric Drives", CRC Press, 2nd Edition, New York, 2006.
- [20] Trovão, J.; Ferreira, F.: "Distorção Harmónica no Sector Industrial - Causas, Efeitos e Soluções", Revista Manutenção, N.º 88, 2006;
- [21] IEEE Std. 519, 1992: "IEEE Recommended Practices and Requirements for Harmonic Control in Electric Power Systems";
- [22] Ziehl-Abegg: "Speed Control of Fans for Refrigeration and Air Conditioning – A Comparison of Different Systems for Speed Control", Motor Challenge, 2007.
- [23] Dugan, R.; McGranaghan, M.; Wayne, H.: "Electrical Power Systems Quality", McGraw-Hill, New York, USA, 1999.
- [24] Deflandre T.; Mauras, P.: "Les Harmoniques sur les Reseaux Electriques", Eyrolles, Paris, France, 1998.
- [25] Hughes, A.: "Electric Motors and Drives", 2nd Edition, Newnes, Oxford, 1995.
- [26] ABB Motors: "Basic Motor Technology", Finland, 1996.
- [27] Haring, T.: "Design of Motors for Inverter Operation", in "Energy Efficiency Improvements in Electric Motors and Drives", Springer-Verlag, Berlin, Heidelberg, 2000.
- [28] Swardt, H.: "Hazardous areas – "ex" Motors with VSDs", Drives & Switchgear, Vector, Nov/Dec 2003, pp. 23-24.
- [29] WEG: Catálogo W21 Line, 2003.
- [30] EFACEC: "Catálogo de Motores de Indução com Rotor em Curto-Circuito", 2001.
- [31] OMRON/YASKAWA: "F7 Drive and User Manual and G7 Drive Technical Manual", Technical & Commercial Departments and Technical Literature, 2006.
- [32] MATLAB Version 7.0.1 (R14), Help Information, The MathWorks, Inc., 2004.
- [33] IEC 61800-2, 1st Ed., 1998-03, Inter. Std.: "Adjustable speed electrical power drive systems – Part 2: General requirements – Rating specifications for low voltage adjustable frequency a.c. power drive systems".
- [34] de Almeida, A. and Ferreira, F.: "User-Friendly High-Precision Electric Motor Testing System", 4th Inter. Conf. on Energy Efficiency in Motor Driven Systems (EEMODS'05), Conf. Proc., Vol. I, pp. 149-157, Heidelberg, Germany, Sept. 2005.
- [35] Ferreira, F.; Pereirinha, P.; de Almeida, A.: "Study on the Bearing Currents Activity in Cage Induction Motors using Finite-Element Method", 17th Inter. Conf. on Electric Machinery (ICEM'06), Conf. Proc., Sept. 2006.

- [36] de Almeida, A.; Greenberg, S.: “*Technology assessment: energy-efficient belt transmissions*”, Energy and Buildings, No. 22, pp. 245-253, Elsevier Science, 1995.
- [37] Nadel, S.; Shepard, M.; Greenberg, S.; Katz, G.; de Almeida, A.: “*Energy-Efficient Motor Systems – A Handbook on Technology, Program, and Policy Opportunities*”, American Council for an Energy-Efficient Technology, Washington D.C., 2nd Ed., 2002.
- [38] de Almeida, A., et al.: “*Improving the Penetration of Energy-Efficient Motors and Drives*”, European Commission, DG TREN, SAVE II Programme, 2000.
- [39] Doppelbauer, M.: “*Energy Efficient Electric Drives*”, VEM Meeting 2007.
- [40] Doppelbauer, M.: “*Saving Energy and Costs in Electrical Drive Systems*”, SEW-Eurodrive, 2007.
- [41] SEW-Eurodrive, Experts opinion, Catalogues, and Technical Brochures, 2007.
- [42] Rooks, J.; Wallace, A.: “*Energy Efficiency of VSDs*”, IEEE Industry Applications Magazine, May/June 2004, pp. 57-61.
- [43] Leonhard, W.: “*Control of Electric Drives*”, 2nd Edition, Springer-Verlag, Berlin, 1997.
- [44] Phipps, C.: “*Variable Speed Drive Fundamentals*”, 3rd Edition, The Fairmont Press, Prentice Hall PTR, 1999.
- [45] VEM Catalogue: “*Three-Phase High-Voltage Asynchronous Motor – 140-8000 kW*”, 2007.
- [46] SEW-Eurodrive: “*Movdrive MDX60B/61B Drive Inverters – System Manual*”, Edition 06/2005, 11323728/EN.
- [47] Lorenz, L.: “*New development in power electronics components and their impact on energy efficiency*”, 5th Inter. Conf. on Energy Efficiency in Motor Driven Systems, Conf. Proc., Beijing, 2007.
- [48] Kadjudj, M.: “*Speed Sliding Control and Variable Bands Current Controllers of PMSM Drives*”, 5th Inter. Conf. on Energy Efficiency in Motor Driven Systems, Conf. Proc., Beijing, 2007.
- [49] Dems, M.; Komez, K.; Wiak, S.; Stec, T.; Kikosicki, M.: “*Application of circuit and field-circuit methods in designing process of small induction motors with stator cores made from amorphous iron*”, The Inter. Journal for Computation and Mathematics in Electrical and Electronic Eng., Emerald Group Publishing Limited, Vol. 25, Issue 2, pp. 283-296, 2006.
- [50] Palma, J.: “*Accionamentos Electromecânicos de Velocidade Variável*”, Fundação Calouste Gulbenkian, Lisboa, 1999.
- [51] “*A Gremlin Called Harmonic Distortion*”, Vector, Nov./Dec. 2003, pp. 25.
- [52] Bose, B.: “*Modern Power Electronics and AC Drives*”, Prentice Hall PTR, New Jersey, 2005.
- [53] Jackson, D.: “*Low Voltage Insulation System Endurance Against Electronic Waveform and Cable Length*”, IEE Colloquium on Effects of High Speed Switching on Motors and Drives, Ref. No. 1999/144, pp. 6/1-6/7, June 1999.
- [54] de Almeida, A., et al.: “*VSDs for Electric Motor Systems*”, European Commission, DG TREN, SAVE II Programme, 2001.
- [55] IEC 61800-3: “*Adjustable Speed Electrical Power Drive Systems - Part 3: EMC requirements and specific test methods*”.
- [56] “*Cycloidal Speed Reducers*”, Vector, Drives & Switchgear, pp. 32, Sept. 2003.
- [57] www.durali.com, December 2007.
- [58] www.michelin.com, December 2007.
- [59] J. Jang, J.; Sun, C.: “*Functional Equivalence Between Radial Basis Function Networks And Fuzzy Inference Systems*”, IEEE Trans. on Neural Networks, 4(1), pp. 156-159, 1993.
- [60] Gerla, G.: “*Fuzzy Logic Programming and fuzzy control*”, Studia Logica, No. 79, pp. 231-254, 2005.
- [61] Hájek, P.: “*Metamathematics of Fuzzy Logic*”, Kluwer Academic Publishers, Dordrecht, The Netherlands, 1998.
- [62] Mamdami, E. H.: “*Application of Fuzzy Algorithms for the Control of a Simple Dynamic Plant*”, Proc. IEEE, pp. 121-158, 1974.
- [63] J. Holtz, J.: “*Sensorless Control of Induction Machines - With or Without Signal Injection?*”, Trans. on Industrial Electronics, Vol. 53, No. 1, pp. 7- 30, Feb. 2006.
- [64] Depenbrock, M; Evers, C.: “*Model-Based Speed Identification for Induction Machines in the whole Operating Range*”, Trans. on Industrial Electronics, vol. 53, no. 1, pp. 31- 40, Feb. 2006.
- [65] Boussak, M.; Jarray, K.: “*A High-Performance Sensorless Indirect Stator Flux Orientation Control of Induction Motor Drive*”, Trans. on Industrial Electronics, Vol. 53, No. 1, pp. 41- 49, Feb. 2006.
- [66] Lascu, C.; Boldea, I.; Blaabjerg, F.: “*Comparative Study of Adaptive and Inherently Sensorless Observers for Variable-Speed Induction-Motor Drives*”, Trans. on Industrial Electronics, Vol. 53, No. 1, pp. 57- 65, Feb. 2006.
- [67] Lee, K.; Blaabjerg, F.: “*Reduced-Order Extended Luenberger Observer Based Sensorless Vector Control Driven by Matrix Converter with Nonlinearity Compensation*”, Trans. on Industrial Electro., Vol. 53, No. 1, pp. 66- 75, Feb. 2006.
- [68] Edelbahr, G.; Jezernik, K.; Urlep, E.: “*Low-Speed Sensorless Control of Induction Machine*”, Trans. on Industrial Electronics, Vol. 53, No. 1, pp. 120- 129, Feb. 2006.
- [69] K. Ide, K.; Ha, J.; Sawamura, M.: “*A Hybrid Speed Estimator of Flux Observer for Induction Motor Drives*”, Trans. on Industrial Electronics, vol. 53, no. 1, pp. 130- 137, Feb. 2006.
- [70] Comanescu, M.; Xu, L.: “*Sliding-Mode MRAS Speed Estimators for Sensorless Vector Control of Induction Machine*”, Trans. on Industrial Electronics, Vol. 53, no. 1, pp. 146- 153, Feb. 2006.
- [71] Duran, J.; Duran, J. L.; Perez, F.; Fernandez, J.: “*Induction-Motor Sensorless Vector Control with Online Parameter Estimation and Overcurrent Protection*”, Trans. on Industrial Electronics, Vol. 53, No. 1, pp. 154- 161, Feb. 2006.
- [72] Saejia, M.; Sangwongwanich, S.: “*Averaging Analysis Approach for Stability Analysis of Speed-Sensorless Induction Motor Drives with Stator Resistance Estimation*”, Trans. on Industrial Electro., Vol. 53, No. 1, pp. 162- 177, Feb. 2006.
- [73] Ohyama, K.; Asher, G.; Sumner, M.: “*Comparative Analysis of Experimental Performance and Stability of Sensorless Induction Motor Drives*”, Trans. on Industrial Electronics, Vol. 53, No. 1, pp. 178- 186, Feb. 2006.
- [74] Lopez, J.; Romeral, L.; Arias, A.; Aldabas, E.: “*Novel Fuzzy Adaptive Sensorless Induction Motor Drive*”, Trans. on Industrial Electronics, Vol. 53, No. 4, pp. 1170- 1178, Aug. 2006.
- [75] D. Alexa, A. Sirbu, A. Lazar, “*Three-Phase Rectifier With Near Sinusoidal Input Currents and Capacitors Connected on the AC Side*”, Trans. on Industrial Electronics, Vol. 53, No. 5, pp. 1612-1620, Oct. 2006.
- [76] C. M. G. Vega Gonzalez, J. R. Rodriguez Arribas, D. P. Ramirez Prieto, “*Optimal Regulation of Electric Drives With Constant Load Torque*”, Trans. on Industrial Electronics, Vol. 53, No. 6, pp. 1762-1769, Dec. 2006.
- [77] G. Dong, O. Ojo, “*Efficiency Optimizing Control of Induction Motor Using Natural Variables*”, Trans. on Industrial Electronics, Vol. 53, No. 6, pp. 1791-1798, Dec. 2006.
- [78] Mendes, A.; Cardoso, A.: “*Fault-Tolerant Operating Strategies Applied to Three-Phase Induction-Motor Drives*”, Trans. on Industrial Electronics, Vol. 53, No. 6, pp. 1807-1817, Dec. 2006.

- [79] L. Yacoubi, K. Al-Haddad, L.-A. Dessaint, F. Fnaiech: “*Linear and Nonlinear Control Techniques for a Three-Phase Three-Level NPC Boost Rectifier*”, Trans. on Industrial Electronics, Vol. 53, No. 6, pp. 1908-1918, Dec. 2006.
- [80] Sundareswaran, K.; Palani, S.: “*Design of High Gain Controller for Part-Load Performance Optimization of Variable Voltage Induction Motor Drive*”, IEEE Inter. Conf. on Power Electronics and Drive Systems (PEDS’99), Conf. Proc., pp. 273-275, Hong Kong, July 1999.
- [81] Jian, T.; Schmitz, N.; Novotny, D.: “*Characteristic Induction Motor Slip Values for Variable Voltage Part Load Performance Optimization*”, IEEE Trans. on Power Apparatus and Systems, Vol. PAS-102, No. 1, Jan. 1983, pp. 38-46.
- [82] IEC 60034-2-3, 2008: “*Rotating Electrical Machines – Part 2-3: Specific test methods for determining losses and efficiency of converter-fed AC machines*”, First working document, TC2 WG 28/52/WD, January 2008.
- [83] Angers, P.: “*Test Protocol For Determination Of Efficiency For Variable Frequency Drives (VFD)*”, CSA C838 Meeting, September 28, 2007.
- [84] “*Integrated motor-drive combinations*”, Control Engineering Europe, Feb. 2001.
- [85] “*Motor Energy Controller*”, Power Electronics Systems Ltd., www.pe-sys.com, 2007.
- [86] Ferreira, F.; de Almeida, A.: “*Method for In-Field Evaluation of the Stator Winding Connection of Three-Phase Induction Motors to Maximize Efficiency and Power Factor*”, IEEE Trans. on Energy Conversion, Vol. 21, No. 2, June 2006.
- [87] Ferreira, F.; de Almeida, A.: “*Novel Multi-Flux Level, Three-Phase, Squirrel-Cage Induction Motor for Efficiency and Power Factor Maximization*”, IEEE Trans. on Energy Conversion, Vol. 23, No. 1, pp.101-109, March 2008.
- [88] WEG-Euro Portugal, Maio de 2005.
- [89] Jezernik, K.: “*VSS Control of Unity Power Factor*”, IEEE Trans. on Industrial Electronics, Vol. 46, No. 2, pp. 325-332, April 1999.
- [90] Nola, F.: “*Power Factor Control System for AC Induction Motor*”, U.S. Patent 4052648, Oct. 1997.
- [91] Kusko, A.; Galler, D.: “*Control Means for Minimization of Losses in AC and DC Motor Drives*”, IEEE Trans. Industr. Applic. , Vol. IA-19, Jul./Aug. 1983, pp. 561-570.
- [92] Kirchen, D.; Novotny, D.; Lipo, T.: “*Optimal Efficiency Control of an Induction Motor Drive*”, EPE’97, Conf. Proc., pp. 3711-3716, 1997.
- [93] Kelly, J.; Strangas, E.; Miller, J.: “*Multiphase Space Vector Pulse Width Modulation*”, IEEE Trans. on Energy Conversion, Vol. 18, No. 2, pp. 259-264, June 2003.
- [94] Tolbert, L.; Chiasson, J.; McKenzie, K.; Du, Z.: “*Elimination of Harmonics in a Multilevel Converter with Nonequal DC Sources*”, IEEE Applied Power Electronics Conf., Conf. Proc., pp. 589-595, Miami, Florida, Feb. 2003.
- [95] Tolbert, L.; Chiasson, J.; McKenzie, K.; Du, Z.: “*Control of a Multilevel Converter Using Resultant Theory*”, IEEE Trans. on Control Systems Technology, Vol. 11, No. 3, pp. 345-354, May 2003.
- [96] Nava-Segura, A.; Hernández, C.; Mino-Aguilar, G.: “*Instantaneous Space Vector Model for Direct Flux and Torque Control of an Inverter Controlled Induction Motor*”, CIEP’2000, Conf. Proc., pp. 35-41, Mexico, Oct. 2000.
- [97] Peralta-Sánchez, E.; Hernández-Arámburo, C.: “*Prototype of an Induction Motor Direct Stator Flux and Torque Vector Control*”, IEEE-ISIE’2000, Conf. Proc., pp. 219-224, Mexico, 2000.
- [98] Seo, J.; Ahn, J.; Jung, H.: “*Parameters Calculation for Inverter Driven Induction Machine Including Field Weakening Operation*”, ICEM’04, Conf. Proc., 2004.
- [99] Zakrzewski, K.: “*Method of Calculation of Unit Power Losses in Magnetic Laminations Taking into Account Sinusoidal and PWM Supply Voltage*”, ICEM’04, Conf. Proc., 2004.
- [100] Mihalič, F.; Jezernik, K.; Krischam, K.; Rentmeister, M.: “*IGBT Spice Model*”, IEEE Trans. on Industrial Electronics, Vol. 42, No. 1, pp. 98-105, Feb. 1995.
- [101] “*Relatório de Qualidade de Serviço*”, REN – Rede Eléctrica Nacional, S.A., 2006.
- [102] “*Relatório de Qualidade de Serviço*”, EDP – Electricidade de Portugal, S.A., Distribuição, 2006.
- [103] “*MEC – Motor Energy Controller*”, Datasheet, Power Electronics Systems, 2008.
- [104] NP/EN 50160, 2ª Edição, Dez. 2001: “*Características da Tensão Fornecida Pelas Redes de Distribuição Pública de Energia Eléctrica*”, Inst. Português da Qualidade (IPQ), 2001.
- [105] Karlsson, P.: “*Small-Signal Modelling and Analysis of DC Distributed Power Systems*”, EPE Journal, No. 2, pp. 49-58, Jun. 2007.
- [106] Reinert, J.; Karlsson, P.: “*Improving performance and energy consumption of industrial processes by using variable speed drives*”, Emotron – Dedicated Drive, European Center for Power Electronics e.V. (ECPE) Seminar, “Towards Energy Gain and Savings – Emerging Drives and Generator Systems”, 15-16 April 2008, Warsaw, Poland.
- [107] “*Saving Energy with Electrical Drives*”, German Electrical and Electronic Manufacturers Association, Division Automation/Electric Drive Systems (ZVEI – Automation), Frankfurt, April 2006.
- [108] Walker, G.: “*Modulation and Control of Multilevel Converters*”, Ph. D. Thesis, Dep. of Computer Science and Electrical Engineering, University of Queensland, Nov. 16, 1999.

4 In-Field Motor Load Estimation

Overview – Due to poor motor system design or excessive safety factors, it is common to find oversized three-phase induction motors in the industrial and tertiary sectors, i.e., with a rated power higher than that actually necessary by the driven equipment. If the oversizing is significant, besides the unnecessary extra capital investment, motors will operate with efficiency and power factor levels significantly lower than the respective nominal levels, being an undesirable situation for the user. Additionally, poor dynamic performance and extra starting losses are expected due to the higher rotor inertia, in relation to a well-sized motor. Therefore, it is important to check the actual in-service motors load, in order to establish proper replacement and/or optimization schemes. In this chapter, different techniques for in-field motor load estimation are analysed, including their feasibility, accuracy and intrusion level. The presented analysis is based on existing technical texts, experimental tests, and simulations, being used information from independent laboratories, manufacturers, and public motor databases. An overview on well-known methods is presented, and improvements on the simplest low-cost methods are proposed to improve their accuracy. For the sake of completeness, some of the most complex methods are also briefly analysed. Part of the content of this chapter will be presented in [36].

4.1 Introduction

Several technical texts (e.g., reports, papers, brochures, etc.) on in-field motor efficiency estimation methods, requiring motor load estimation and input power measurement, are described and analyzed in [1]-[9]. The aim of this section is to discuss the motor load estimation only, regardless motor efficiency. This is justified by the fact that, for replacement versus repair decision purposes, the key factor is the motor load, which gives an idea of the efficiency and power factor improvement potential, as well as the expected investment associated with proper replacement or customized repair of the motor being evaluated. In [10], an average of approximately 60% load factor for motors in industrial and tertiary sectors was estimated for the EU. In [11], an average 75% load factor is estimated for industrial motors in the USA. Both data are more or less in accordance, if the inclusion of the tertiary sector (characterized by lower load factors) in the first referred estimation is taken into account. Therefore, it is common to find oversized motors in both industrial and tertiary sectors, i.e., with a rated power higher than that actually necessary by the driven equipment (average power over duty cycle or over some periods of duty cycle), justifying the efforts to assess the actual motor load, particularly if large-scale replacements of IE1-class motors by IE2-class or IE3-class motors, or even customized repairs (to optimize the motor stator winding to its actual load and/or terminal voltage, as it is discussed in Appendix 3), are being planned. Moreover, besides the extra capital invested in oversized motors, they operate with poor efficiency and power factor, starting, and stopping periods are extended due to the extra rotor inertia, leading to extra losses during starting period and poor dynamic performance. Additionally, oversized motors have extra friction and windage losses and produce extra acoustic noise due to the larger cooling fans¹.

¹ For example, in 400-V, 50-Hz, EFF2-class IMs [33], of 1.1, 2.2, 11, 22, 110 and 200 kW, the acoustic noise (sound pressure level, LP dB(A), 1 m) is 47, 51, 62, 64, 77, 79 dB(A).

If the user waits until a motor fails, the primary concern will be the quick replacement, and its optimization becomes less relevant. To avoid that, all motors in a facility should be evaluated in order to determine if it is cost effective to save energy and increase reliability by replacing them by properly-sized IE2- or IE3-class IMs. The development of a replacement and/or proper repair scheme for all critical motors is very important, defining which motors should be replaced by high-efficiency and/or smaller size models after failure and/or should be properly changed during repair process.

The adequacy of the motor rated power to the average power required by the driven load, is one of the most important factors influencing the motor efficiency and power factor. If motors are significantly oversized, besides the unnecessary additional capital and maintenance investment, they can operate with efficiency and power factor levels significantly lower than the respective nominal levels. Most motors reach peak efficiency between 65% and 100% load (depending on size and type), therefore, in some cases, a slight oversizing, under electrical rated conditions, can actually maximize motor efficiency (but the power factor results lower). Moreover, since the voltage at the motor terminals is typically slightly below the rated value, the peak efficiency load point is slightly shifted to the left (lower load direction), therefore improving the efficiency of moderately oversized motors.

Continuous operation or S1-duty type² IMs³ fed by a power system with distortion and unbalanced levels within the limits established in [1], and a terminal voltage equal or very near the rated voltage, can be considered significantly oversized when its load is lower than 50-60% of rated power, and significantly undersized if its load is higher than 105-110% of rated power⁴. The motor undersizing should be avoided due to the consequent motor efficiency decrease and overtemperature, shortening dramatically motor lifetime. The motor undersizing effects can be aggravated by a number of factors such as voltage lower than the rated voltage, dissipation capacity affected by altitude, and/or ambient temperature higher than a specified value (typically 40°C). However, in the case of variable-load IMs (e.g., S10-duty type motors), the motor can operate at or near full load in some periods and at very low loads in other periods, or even, for short-duration periods (shorter than thermal time constant), with a load slightly higher than full load. In these cases, the motor load cannot be classified directly, being typically used the load factor definition over the operating cycle. However, it is possible to classify motors as oversized if the highest value of the required shaft power in steady state is lower than the rated power. The estimation of IMs load, particularly of those of S1-duty type, allows the user to make technical and

² Note that the load duty type is different from motor service factor [26].

³ TEFC (enclosure IP55, and cooling system IC411, meaning self-ventilated or self-cooled), three-phase, squirrel-cage induction motors.

⁴ Assuming 1.0 service factor motors. Motors with 1.15 service factor, withstand 115% overload without significant impact on its lifetime.

economical decisions about motor replacement and repair, as well as to establish programmes or schemes to optimize EMODS, as referred before.

A significant advantage of in-service motor load estimation methods is that the motor does not have to be removed from service and the manufacturing process is not interrupted, avoiding downtime costs. In general, electrical measurements can be taken quickly with voltage probes and clamp-on current probes⁵ (which can be inserted directly around the power conductors or around the current transformers (CTs) output conductors). Typically, these measurements are taken at the motor control center (MCC) or switchgear, but they may be taken into the motor if higher accuracy for voltage, frame and/or temperature measurement is needed. Often in-field testing is the only practical method for motor load testing because the user permits neither removal of the motor nor operational downtime. Additionally, as discussed in Appendix 4, voltage magnitude deviation, unbalance and harmonic distortion can have a severe effect on motor performance and lifetime. Those power quality parameters can be measured easily with a handheld power analyser when voltage, current and power measurements are being taken. These measurements can then be used to evaluate whether motor derating is necessary.

The fundamental disadvantage associated with in-field testing is that motor output torque is not directly measured. Instead, measured current, voltage, power factor, real power, speed and temperature are used in conjunction with nameplate, catalogue and/or database data to estimate the motor output power and, if necessary, its efficiency.

The most common motor load in-field estimation methods are generally divided into three groups: those based on motor speed, current or input power, those based on the motor equivalent circuit and those based on air-gap torque. The in-field estimation methods can also be classified by intrusion level – low, medium and high – depending upon the data acquisition processes necessary to implement the method. Each method has an inherent level of accuracy that is related to the assumptions and simplifications used in it. Methods based on current, slip, input power, power factor, temperature, and equivalent circuit, in their simplest form, are considered as low intrusion methods. In general, the higher the intrusion level is, the higher the accuracy of the method will be. Examples of medium intrusion methods are the Stanford Wilke Method (or Empirical Method) and the Ontario Hydro Modified (OHM) Method. The air-gap torque-based methods are considered as high-intrusion level methods, because they normally require a no-load test (implying mechanical decoupling) [1]. Further information on those methods can be found in Appendix 6.

Since the aim of this chapter is to evaluate and, in some cases, improve simplest low-cost methods to indirectly estimate the motor load, the relatively complex and/or time consuming

⁵ Integrating Hall-effect current sensors.

methods (e.g., equivalent circuit-based and air-gap torque-based methods⁶) are only briefly discussed for the sake of completeness, being the focus of this chapter on methods based upon the current, voltage, power factor, real power, speed (or slip), and temperature, which require a few simple in-field measurements with relatively low-cost equipment and information from the nameplate, manufacturers, catalogues, and/or public databases, having a fair accuracy if applied to specific motors and load ranges. These methods can be applied quickly, easily and economically in the field. The analysed methods are only applicable in constant load periods with duration long enough to achieve the motor thermal equilibrium. Some improvements and combined solutions are proposed to the referred methods.

In the case of repaired motors, the IEC60034-1 Std. [12] states that an additional nameplate has to be fixed to the motor frame with the changes made during repair (if any). However, in practice this rarely happens. Nevertheless, in this chapter it is assumed that repairs are done well (according to “best practice”), and no significant changes occur in the original characteristics of the motor.

4.2 Motor Load and Motor Load Factor

The motor load, ζ , is given by the quotient between the motor output shaft power (or useful power), P_{mech} , and its rated power, P_N , according to (4.1).

$$\zeta = \frac{P_{mech}}{P_N} \quad (4.1)$$

The motor rated power is given in the nameplate, but to calculate the actual shaft power it is necessary to know the motor shaft (or electromechanic) torque, T , and the angular speed, ω , being the shaft power equal to the product of both (if the T and ω are expressed in N.m and rad/s, respectively). The motor angular speed is $\omega = \omega_{sync} \cdot (1 - s)$, being s the slip and ω_{sync} the synchronous speed.

The motor load factor, ζ_{avg} , is given by the quotient between the average output power over a period Δt and the motor rated power, which can be divided into n periods approximately constant load, according to (4.2). This value represents the average motor load.

$$\zeta_{avg} = \frac{1}{P_N} \cdot \frac{1}{\Delta t} \int_t^{t+\Delta t} P_{mech}(t) dt = \frac{\sum_{i=1}^n \Delta t_i \cdot \zeta_i}{\sum_{i=1}^n \Delta t_i} \quad (4.2)$$

⁶ These methods are particularly recommended when the aim is to estimate the motor efficiency with a fair accuracy.

The major problem to obtain the motor shaft power in the field is the measurement of the torque, which is, in most cases, impossible, except when a torque sensor is installed between the motor and the driven equipment, which is an extremely rare situation. The speed is easily obtained by a stroboscopic or optical tachometer. Therefore, in the field, only an indirect estimation of motor load is feasible or practical in the vast majority of the cases, justifying the development and improvement of motor load estimation methods not requiring torque measurement.

4.3 Data Available from Manufacturers

The data available from manufacturers can be divided into four different sources: motor nameplate, catalogues, databases and non-published internal technical information. In the motor nameplate, the main rated values are written, e.g., voltage, current, power factor, speed, frequency, shaft power, efficiency class, thermal class, etc., according to standards. In the catalogues, the information available is wider, and, besides the nameplate rated values, include not only but also the rated torque, the part-load power factor and the efficiency (e.g., at 25%, 50%, 75% and 100% load). In public motor databases as EURODEEM [20] and MOTORMASTER [21], besides the nameplate and catalogues data, the motor no-load current and power factor can also be available.

It should be noted that, according to standard IEC 60034-1, Section 9.1 (routine tests), manufacturers have to measure and record periodically, by means of motor routine tests, in each motor series being manufactured, the resistance of stator winding (cold state), the no-load motor input power and current, the direction of rotation, and the results of voltage withstand or high potential test. Knowing the no-load input power and no-load current at rated voltage, the no-load power factor can be calculated.

Depending on the motor rated power, the manufacturers internal technical information, can include much more information for the motor prototype corresponding to each series, e.g., motor current, power factor and efficiency as a function of load, as well as locked-rotor and no-load tests data, torque versus speed curves, equivalent circuit parameters, thermal variations, etc.

For relatively recent motors, all the referred data can be obtained from manufacturers, but, for old motors, the nameplate data is often the only available motor data.

It should be noted that the motor efficiency value from manufacturer depends upon the used standard and method, existing significant differences between direct or input-output methods and indirect or loss summation methods, as explained in Chapter 2. Although existing now the new standard IEC 60034-2-1 (Ed. 1, 2007), which includes the direct method, the European manufacturers still apply the standard IEC 60034-2 (Ed. 2, 1996), which is based on the indirect method, and the vast majority of the motors operating in the EU were tested and classified on the basis of that standard.

4.4 Useful Accuracy, Tolerances and Instrumentation Accuracy

An important aspect that should be taken into account in the evaluation of motor load estimation methods (whose main goal is to identify oversized motors which can be, eventually, replaced by properly sized motors) is the minimum accuracy that those methods should have. This minimum accuracy should be enough for the user to decide if the motor should or should not be replaced by another one, and what should be the rated power of the new motor. This accuracy is denominated in this chapter by “useful accuracy”, and ensures that, if the user decides to replace an in-service or damaged motor by another one with a different rated power, the latter would not be excessively undersized (load higher than 102.5%) or oversized (load lower than 75%), providing that starting torque is adequate for the driven load. Motor starting issues are not address in this chapter. In the case of motor load evaluation for customized repair (by proper stator winding change, which is addressed in Chapter 5), the definition “useful accuracy” is not applicable.

To define the useful accuracy, the commercial available rated power levels for IMs must be known, which can be extracted from the motor databases EURODEEM and/or MOTORMASTER. On the basis of that information, it is possible to compute the power variation between a specific commercially available rated power and the adjacent rated powers (immediately higher or lower), as it can be seen in Fig. 4.1. Fig. 4.2 shows the general variation between the commercially available power ratings in relation to the lower power rating, in which it is possible to see that, in a number of situations, particularly for small motors, it is not possible to choose a motor to operate between 75% and 100% load, since the required rated power value is not available in the conventional motor market. For example, in Fig. 4.2, those situations happen when the yellow trace, whose limits are bounded by a bold, orange trace, is lower than -25% (i.e. the obtained values are within the variation range between -25% and -50%). If a 1.1-kW motor operates at fixed 72% load (load lower than the recommended minimum of 75%) and a 0.75-kW motor is chosen to replace it, a 5.6% overload (undersizing) is expected in the new motor, which is an undesirable situation due to the resulting accelerated thermal ageing of its electrical insulation system (assuming a 1.0 service factor). However, in general, a continuous 2.5% overload, although undesirable, is admissible for most motors, without major effects on their lifetime (a 2.5-3% increase in winding rated temperature is expected). Nevertheless, a slight oversizing is preferable over a slight undersizing in most cases and, for the example given, it would be preferable to maintain the 1.1-kW motor operating at 72% load. On the basis of Fig. 4.2, it is possible to conclude that, for motors with a rated power equal or higher than 7.5 kW, the commercially available power levels allow to guarantee a motor load within 75% and 100%. The lower limit of this motor load range can actually be increased to roughly 90% for motors larger than 200 kW. For large motors, a load as low as 40-50% does not have significant influence on the efficiency level

(the efficiency-load curves are flatter), but denotes excessive non-profitable capital and maintenance investment, being desirable to install a proper sized motor and, if possible, move the oversized motor to other suitable application. Moreover, even for large motors, the power factor starts to decrease significantly for loads below 60-70%.

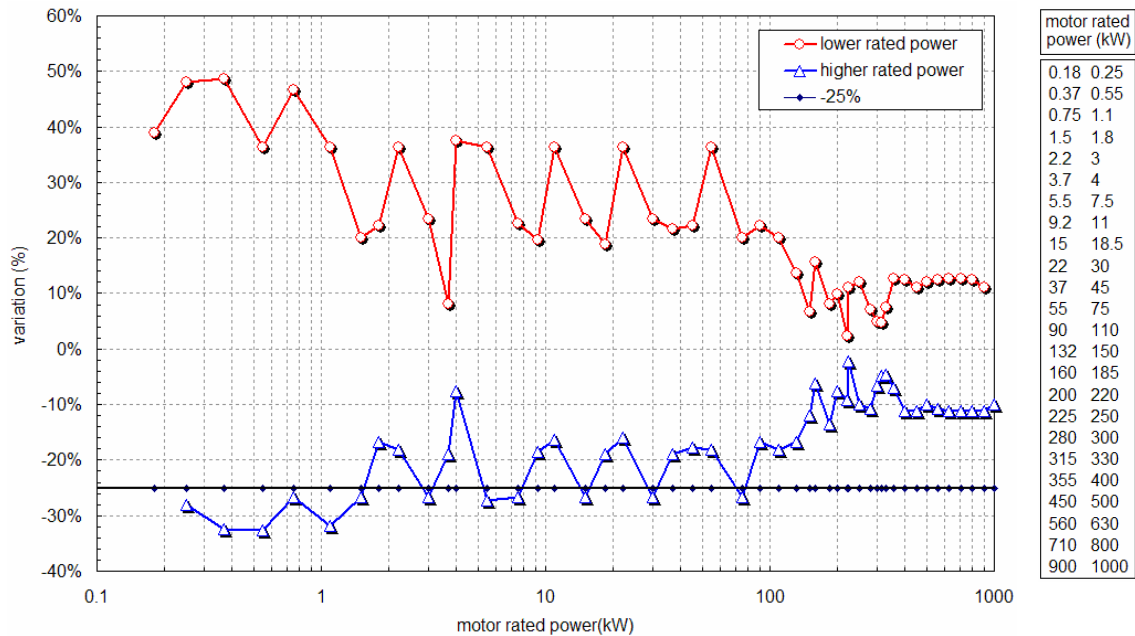


Fig. 4.1. Variation between adjacent commercially available rated powers for 4-pole motors: (blue trace with triangles) in relation to the immediately lower rated power, considering higher rated power as reference; (red trace with circles) in relation to the immediately higher rated power, considering lower rated power as reference.

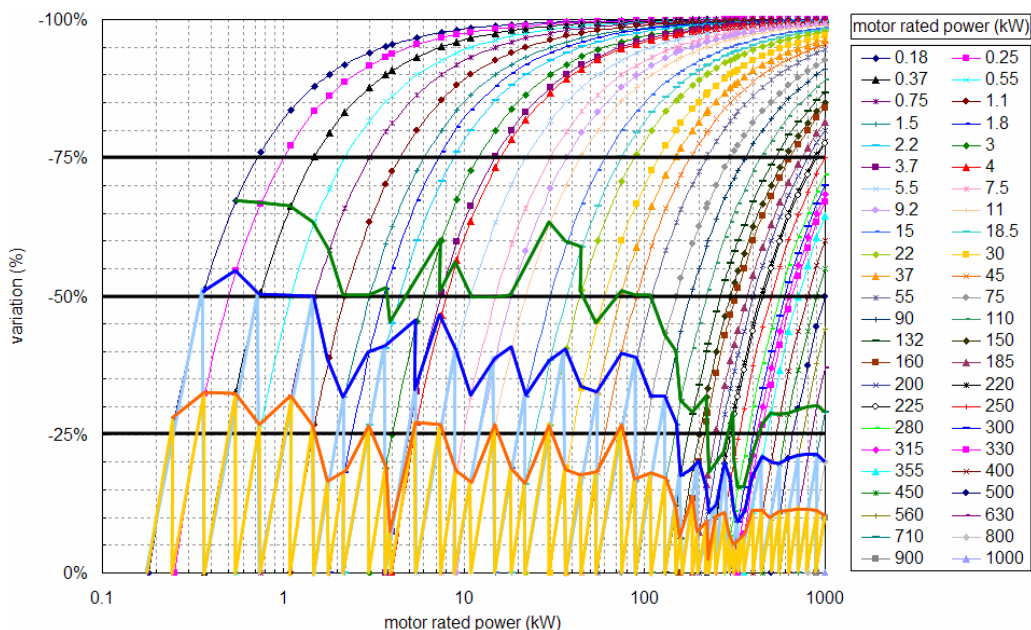


Fig. 4.2. General variation between adjacent commercially available rated powers in relation to a lower rated power (higher power as reference), for 4-pole motors: (orange bold trace) one rated power level below; (blue bold trace) two rated power levels below; (green bold trace) three rated power levels below.

The information presented in Figs. 4.1 and 4.2 allows the defect and excess errors to be established, corresponding to the useful accuracy to each nominal power. For example, ignoring

the slight speed change⁷, for a 1.1-kW motor and a specific load, when the motor rated power is changed, the power level immediately lower corresponds to a variation of -32% (0.75-kW motor) and the power level immediately higher corresponds to a variation of +36% (1.5-kW motor). In this case, only makes sense to replace the 1.1-kW motor by another one with a different power if its load is equal or lower than 70% (leading to 102.5% load for the 0.75-kW motor), or higher than 102.5% (leading to a 75% load for the 1.5-kW motor), otherwise, the original rated power should be maintained. If, in relation to actual motor load, it is estimated full load, and the maximum error by defect is -32 percentage points (p.p.), means that the motor should not be replaced by the immediately lower rated power motor, and if the maximum error by excess is +2.5 p.p., means that the motor should not be replaced by the immediately higher power motor. However, if the error by defect is higher than -32 p.p. or the error by excess is higher than 2.5 p.p., the estimation error falls over an ambiguous range, and it would be impossible to decide properly or with a fair certainty level if the motor should or should not be replaced.

Considering now that the estimated motor load is 75% (0.825 kW), and the error by defect is -6.8 p.p. (which means that the actual load level is between 75% and 68.2%), the motor should not be replaced by the immediately lower power motor. If the error by defect is higher than 6.8 p.p., the estimation error falls again over an ambiguous range, and it would be impossible to decide properly if the motor should or should not be replaced. In this case, the admissible excess error can be 27.5 p.p., since the motor should not be replaced by the immediately larger, even if the actual load is 102.5%.

For an estimated load of 50% (0.55 kW), it is necessary to consider in the analysis a power two rated levels lower, which corresponds to a 0.55-kW motor. In this case, the admissible error (which avoids falling in ambiguous ranges), by defect, is 25 p.p. The admissible error, by excess, is 2.5 p.p.

On the basis of the foregoing principles, it is possible to construct the curve presented in Fig. 4.3 for a 1.1-kW motor, representing the admissible error (by defect and by excess) for each rated power. It should be noted that an overload level of 2.5% and an underload level of 25% are being admitted. It is also assumed that is always preferable to crossover the underload level than the overload level, thus an extension in the admissible error by defect is considered. The sum of the vertical segments corresponding to the height of the represented steps leads to a motor load scale, equivalent to a mechanical power scale, which is continuous due to the introduction of the defect error extension, translated into load level for the reference 1.1-kW motor, in the vertical axis (ordinates axis) scale. It is possible to understand that, when the motor load level is varied to

⁷ The speed decrease leads to a decrease of the mechanical power required by the driven equipment (except for constant power loads), slightly reducing the motor load.

values different than those corresponding to the nominal values of each commercial rated power, the admissible errors (both by defect and by excess) also vary. For example, for a power 2.5% higher than 1.1 kW, the defect error increases 2.5 p.p. and the excess error becomes null. For a power 25% lower than 1.1 kW, the admissible error by excess increases 25 p.p. (becomes 27.5%) and the admissible error by defect is equal to the extension of the error by defect.

Considering the previously discussed principles, it is possible to generalize the analysis to all motor rated power levels (commercially available). For that purpose, and on the basis of the previously considered assumptions, the admissible errors were computed and presented in Figs. 4.4 and 4.5.

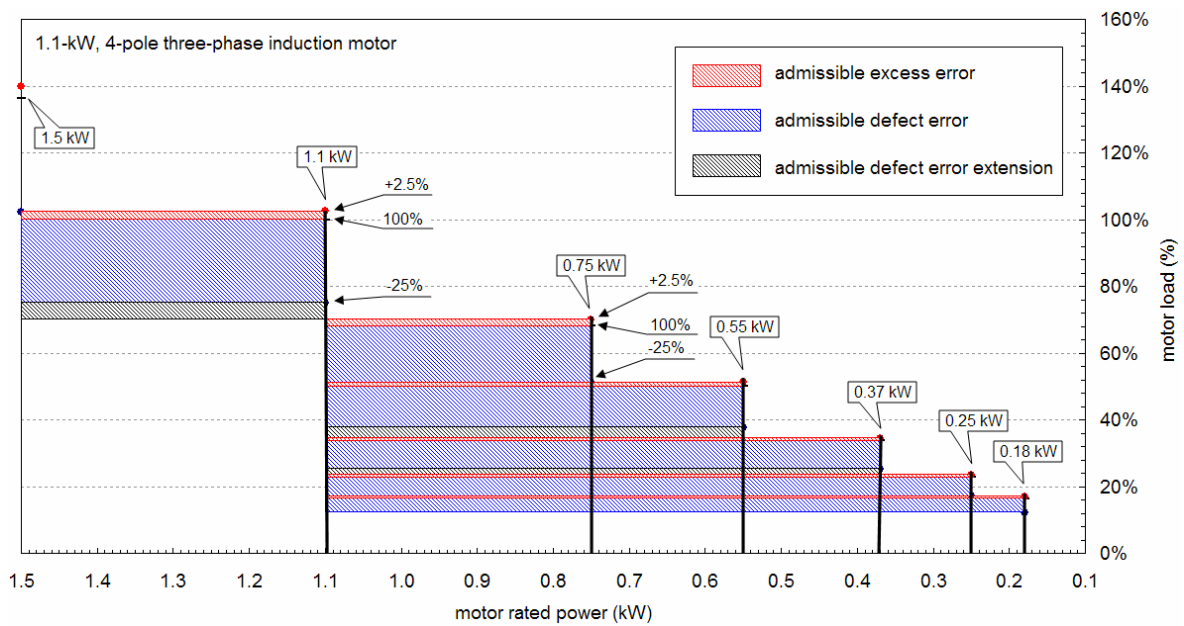


Fig. 4.3. Admissible error variation for a 1.1-kW, 4-pole three-phase squirrel-cage induction motor.

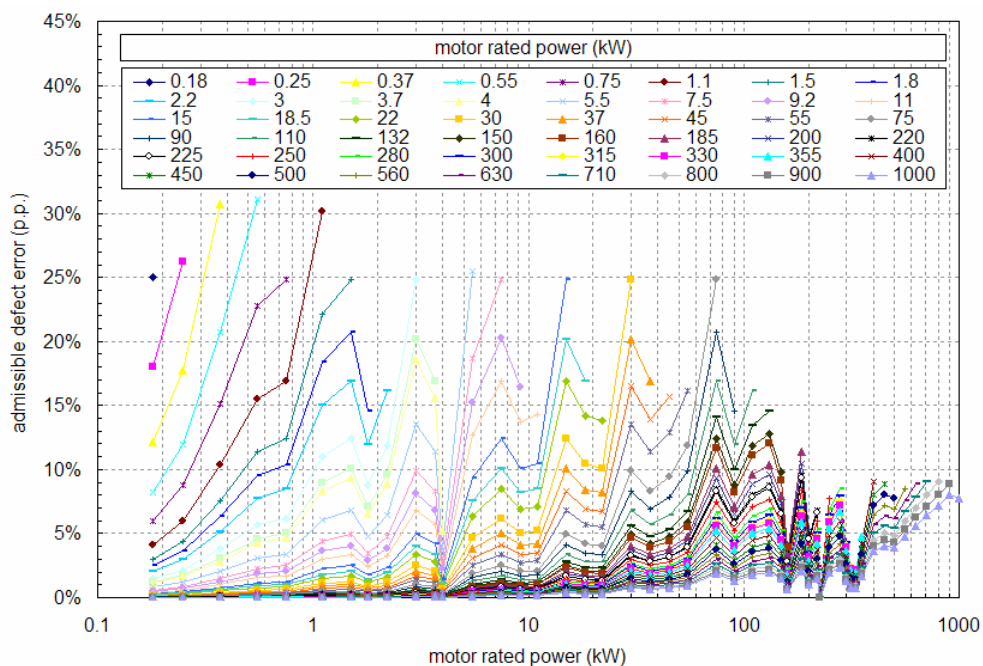


Fig. 4.4. Admissible error by defect for all commercially available 4-pole squirrel-cage induction motors.

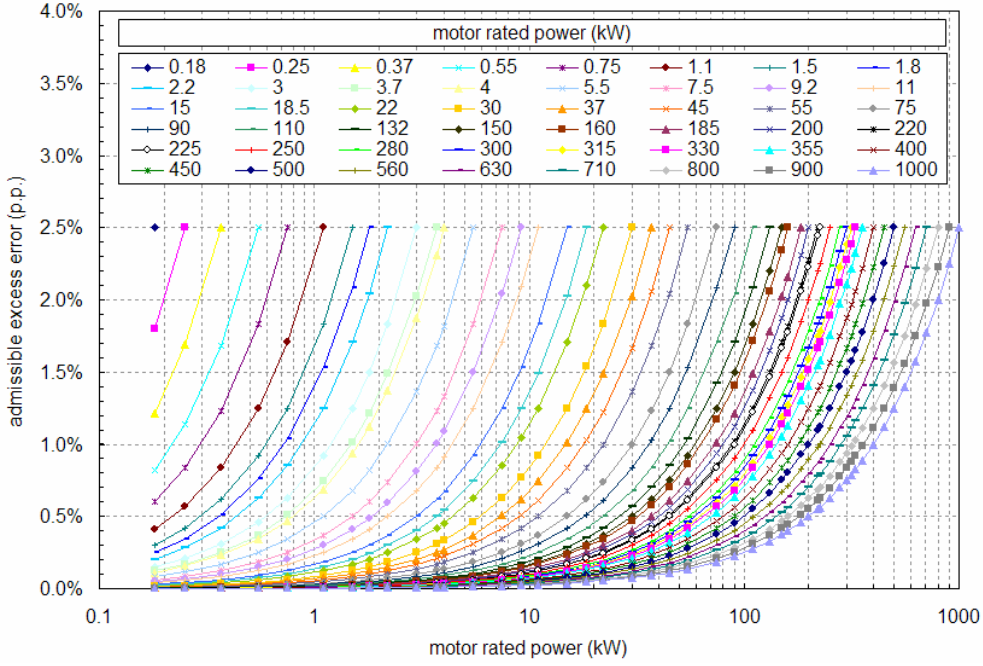


Fig. 4.5. Admissible error by excess for all commercially available 4-pole squirrel-cage induction motors.

In order to allow a clear comparison and analysis of the admissible error or useful accuracy, some equations are defined, being the admissible error (i.e., the admissible deviation) given in percentage points, for the estimated motor load. Equations (4.3) and (4.5) define the admissible excess and defect errors (denoted by the subscripts \uparrow and \downarrow , respectively), as a function of motor load, for the points a , b and c , represented in Fig. 4.6, as well as the straight lines between them, which are expressed by (4.4) and (4.6), respectively. Fig. 4.6 shows the resulting admissible error as a function of motor load for 1.1-kW, 11-kW, 110-kW, and 300-kW motors. For the considered admissible load range, it can be concluded that, the larger the motor, the narrower the admissible error band. In the load points corresponding to the rated powers, the admissible defect error is minimized.

$$\left\{ \begin{array}{l} \text{point a: } \delta_{\uparrow a,i} = 0 \text{ with } \zeta = 1.025 \cdot \frac{P_{N,i}}{P_{N,ref}} \\ \text{point b: } \delta_{\uparrow b,i} = 0.025 \cdot \frac{P_{N,i}}{P_{N,ref}} \text{ with } \zeta = \frac{P_{N,i}}{P_{N,ref}} \\ \text{point c: } \delta_{\uparrow c,i} = \frac{1.025}{P_{N,ref}} \cdot (P_{N,i} - P_{N,(i-1)}) \text{ with } \zeta = 1.025 \cdot \frac{P_{N,(i-1)}}{P_{N,ref}} \end{array} \right. \quad (4.3)$$

$$\left\{ \begin{array}{l} \text{line a - b: } \delta_{\uparrow ab} = \frac{\delta_{\uparrow a} - \delta_{\uparrow b}}{\zeta_a - \zeta_b} (\zeta - \zeta_b) + \delta_{\uparrow b} \\ \text{line b - c: } \delta_{\uparrow bc} = \frac{\delta_{\uparrow b} - \delta_{\uparrow c}}{\zeta_b - \zeta_c} (\zeta - \zeta_c) + \delta_{\uparrow c} \end{array} \right. \quad (4.4)$$

$$\left\{ \begin{array}{l} \text{point a: } \delta_{\downarrow a,i} = -\frac{1.025}{P_{N,ref}} \cdot (P_{N,i} - P_{N,(i-1)}) \text{ with } \zeta = 1.025 \cdot \frac{P_{N,i}}{P_{N,ref}} \\ \text{point b: } \delta_{\downarrow b,i} = -\frac{1}{P_{N,ref}} \cdot (P_{N,i} - 1.025 \cdot P_{N,(i-1)}) \text{ with } \zeta = \frac{P_{N,i}}{P_{N,ref}} \\ \text{point c: } \delta_{\downarrow c,i} = 0 \text{ with } \zeta = 1.025 \cdot \frac{P_{N,(i-1)}}{P_{N,ref}} \end{array} \right. \quad (4.5)$$

$$\left\{ \begin{array}{l} \text{line a - b: } \delta_{\downarrow ab} = \frac{\delta_{\downarrow a} - \delta_{\downarrow b}}{\zeta_a - \zeta_b} (\zeta - \zeta_b) + \delta_{\downarrow b} \\ \text{line b - c: } \delta_{\downarrow bc} = \frac{\delta_{\downarrow b} - \delta_{\downarrow c}}{\zeta_b - \zeta_c} (\zeta - \zeta_c) + \delta_{\downarrow c} \end{array} \right. \quad (4.6)$$

A 2.5-p.p. minimum defect error can be considered in (4.3)-(4.6), because otherwise it would be impracticable, and, when deciding between two adjacent rated power motors, the higher power motor should be chosen if there is uncertainty related to the overload degree that can result from the choice of the lower power motor. The previous equations allow the useful accuracy for any motor rated power and load level to be established.

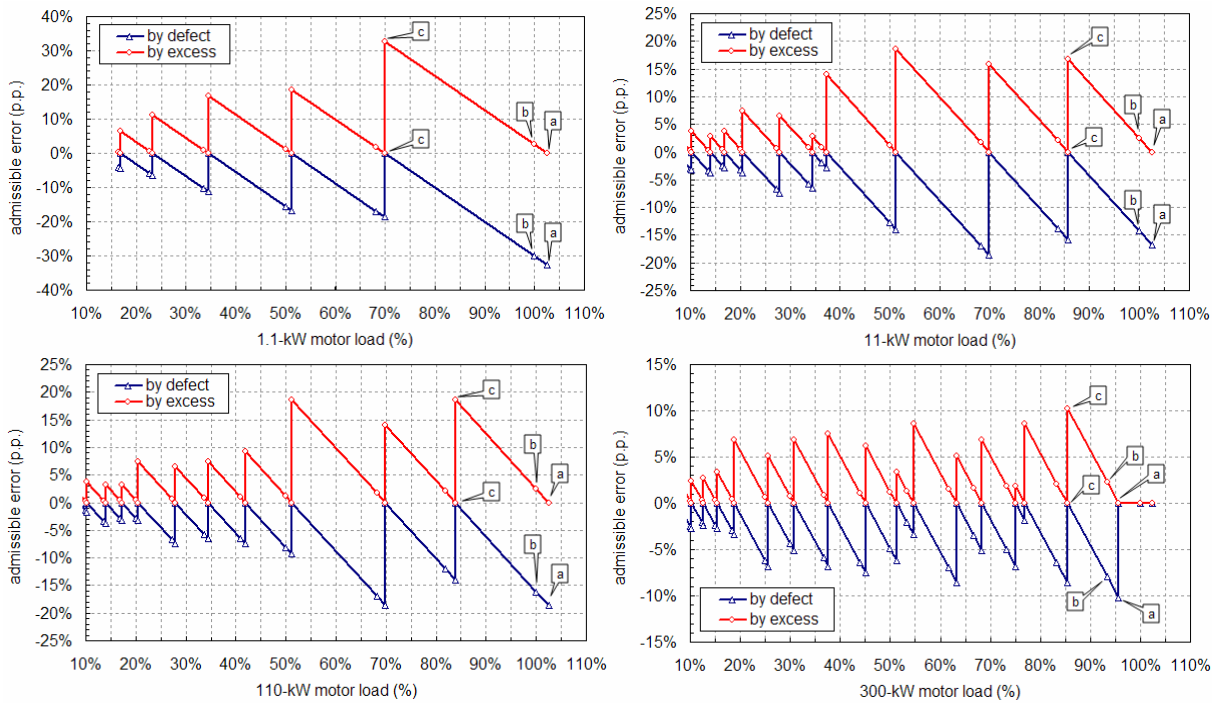


Fig. 4.6. Admissible error (in percentage points) for 1.1-kW, 11-kW, 110-kW and 300-kW motors.

The admissible error, corresponding to the useful accuracy, defined in this section, is used to evaluate the effectiveness or adequacy of the motor load estimation methods. This is a new evaluation criteria introduced by the author.

Besides the measurement accuracy levels, the standards also impose maximum allowable tolerances⁸ for the nameplate values. The tolerances are defined because of the slight variation that can occur during the manufacturing process (dimensions, material characteristics, etc.).

According to [12], which is the reference standard of this analysis, there are the absolute tolerances for the following quantities:

- Power factor, λ : $-(1-\lambda)/6$, with absolute minimum of 0.02 and maximum of 0.07.
- Efficiency, η : -15% of $(1-\eta)$, in the machines with power up to 150 kW (inclusive), and -10% of $(1-\eta)$ for the machines with power exceeding 150 kW.
- Total losses: $+10\%$ of total losses, for the machines with power exceeding 150 kW.
- Slip, s (at full load and thermal equilibrium⁹): $\pm 30\%$ of slip, for motors with rated power lower than 1 kW, and $\pm 20\%$ of slip, for motors with rated power equal or higher than 1 kW. NEMA Std. [25] states a tolerance of $\pm 20\%$ of rated slip, when measured at rated voltage, frequency, and load, and with an ambient temperature of 25°C [1], [4].
- Locked rotor or starting current, I_s : $+20\%$ of I_s .

Tolerances for locked rotor, pull-up and breakdown torque are also specified in [12].

In most cases, manufacturers respect those limits. That was verified by the author by means of an analysis of a set of motor data provided by one of the major motor manufacturers, corresponding to 885 motors with powers of 1.1, 3, 18.5, 37, 55, 75, and 90 kW, including high-efficiency and standard type motors. On the basis of that analysis, it is possible to conclude that about 70% of the motors have slip errors (difference between measured full-load slip and rated slip divided by rated slip) in the range $\pm 10\%$ of rated slip, and the $\pm 20\%$ deviation tolerance of rated slip, imposed by [12], is not exceeded for the analysed universe (or population). Therefore, for practical purposes, a deviation of $\pm 10\%$ can be considered. The slip tolerance allows manufacturers to round numerically the real motor speed at full load to multiples of 5 r/min, resulting an error of ± 2.5 r/min, for motors with a slip equal or higher than 12.5 r/min considering $\pm 20\%$ tolerance and for motors with a slip equal or higher than 8.3 r/min considering $\pm 30\%$ tolerance. However, although being a minority, motors with a slip as low as 7 r/min (e.g., 110-kW, 8-pole motors) can be found, and, in those cases, the manufacturers cannot round the speed to 5 r/min multiples but, instead, they have to use a resolution of 1 r/min for the nameplate speed.

In the presented methods only the voltage compensation is considered. Yet, if the voltage limits defined in [12] are exceeded, the estimations become more uncertain. The same is valid if the frequency deviation exceeds $\pm 0.3\%$ of the rated frequency. A maximum deviation of $\pm 5\%$ for voltage and $\pm 2\%$ for frequency is stated in [12].

⁸ The tolerance is the permitted deviation between the declared value and the measured value of a certain quantity [12].

⁹ The full load thermal equilibrium is determined by performing a load test in which, even not knowing the actual motor torque, the input current is increased up to the rated value, and the winding distributed/average temperature is measured according to the IEC 60034-1, Ed. 11, Section 8-6 [12].

In [12], no tolerance for nameplate current values is defined but, according to [25], when operated at rated voltage, rated frequency, and rated power, the input current shall not vary from the nameplate value by more than 10%. This is a source of error for the methods that use the nameplate current [4].

Regarding the imposed accuracies in the measurement devices for electrical and mechanical quantities, in [13] it is defined that, to measure electrical quantities, the instruments should have an accuracy class of 0.2 (meaning 0.2% of full scale), according to the IEC 60051 Standard. Additionally, once the instruments accuracy is in general expressed as a percentage of the full scale, the scale maximum value should be as lower as possible. For the routine tests described in [12], an accuracy class of 0.5 is enough.

Moreover, according to [13], the line current and line-to-line voltage values are the arithmetic average of the three phase values, except if something else is specified. The instrument transformers shall have a precision according to IEC 60044-1 Std., such that the errors associated with them are limited to $\pm 0.5\%$ for generic tests and $\pm 0.3\%$ for induction machines, loss summation method with stray load losses determined according to the Section 8.2.2.5.1 of [13].

In the frequency measurement, the equipments should have an accuracy of $\pm 0.1\%$ of full scale. For electrical resistance measurement, the error should be limited to $\pm 0.5\%$ [13].

To measure the torque, the instruments should have an accuracy of $\pm 0.2\%$ of full scale, and for the speed, the accuracy should be of ± 1 r/min. The instrumentation used to measure the winding temperature should have an accuracy of $\pm 1^\circ\text{C}$ [12], [13].

According to IEC 60034-2, IEC 60034-2-1, and IEEE 112-B standards, the reference ambient temperature for motor efficiency calculation is 25°C . IEC 60034-1 standard states that a maximum ambient (or room) temperature of 40°C should be tolerated by the motor without derating it. Regarding instrumentation accuracy, see also Table 2.2 in Chapter 2 for information associated to the old 60034-2 (Ed. 2) and IEEE 112-B.

The foregoing information allows one to conclude that the tolerances for the slip, power factor, and efficiency are relatively high, when compared to the imposed minimum accuracies for the electrical quantities measurement, being one of the major source of error in the motor load estimation methods. Therefore, for the evaluation of the error associated with nameplate speed and input power only the tolerances referred in [12] are considered, as well as the error associated to the speed measurement by handheld optical or stroboscopic tachometer, because of its significant impact on the slip measurement. The efficiency tolerance is only important if the efficiency value is used to calculate the part-load and/or full-load current and input power. Nevertheless, the error introduced by the slip and power factor tolerances is the most relevant. No tolerances are considered for nameplate current and voltage. Obviously, the difference between the reference

ambient temperature and the local ambient temperature also introduces a significant error (rated slip and rated current). However, it is not considered in the following analysis.

The typical errors for the handheld measurement devices required for the discussed methods are ± 0.5 r/min for the stroboscopic tachometer (depends on the user experience), being the percentage error higher for lower speed, about ± 0.2 - 0.5% for clamp-on current probe ammeter, if no significant magnetic interference occurs from the motor or power cables (depends on the user experience), about ± 0.05 - 0.25% for modern digital voltmeters, about ± 0.2 - 0.5% for modern digital wattmeters (depends on the clamp-on current probe accuracy) [23]. Only clamp-on-type current probes are considered because only in-service methods (not requiring the motor to be disconnected) are being considered. Portable monitoring instruments typically consist of clamp-on current transformers or hall-effect pickups and some means of voltage transduction. Some clamp-on style probes are available with manufacturer-specified accuracies approaching 0.5% , but, even for these high accuracy clamp-on probes, there are practical considerations that can considerably reduce actual accuracies. The practical accuracy, for power monitoring purposes, is dependent upon both phase angle and amplitude. The phase-angle shift is not provided but the associated error can be significantly greater than associated to the amplitude. For example, a phase-angle shift of 1.5° , which is typical for high-accuracy clamp-on transformers (although some can have larger shifts [4]), results in a power indication error of about 2.7% at an actual power factor of 0.7 , if compensation for phase shift is not made. Since phase-angle shift is a function of amplitude, it is a difficult proposition to provide full bandwidth compensation. This also applies to instrument transformers, but, in some cases, the referred errors can be properly compensated [31]. Two other factors can greatly influence clamp-on accuracies are proper jaw closure and conductor centering. Hall-effect probes are typically more affected by centering considerations, and both Hall-effect probes and transformers are significantly affected by proper jaw closure and alignment factors. The exact magnitude of both amplitude and phase-angle effects can vary considerably, but errors for non-centered conductors (particularly for Hall-effect probes) can easily exceed 1% for amplitude, and phase-angle shifts larger than 5° [4].

In [13] and [14], the specified maximum errors for electrical quantities include both amplitude and phase-angle effects.

For field measurements, instrument accuracy is obviously an important issue. When portable instruments or permanently installed instruments, that are not intended for precision metering, are used, the accuracies specified in [13] and [14] can be extremely difficult to achieve, but the referred typical accuracies are enough for simplest load methods and, except for the speed measurement case, can be ignored in relation to the nameplate values tolerance.

In the scope of intrusion level it is important to refer that there are commercially available voltage probes that can be connected even if there are no conducting terminals available, because they have conducting thick needle-type leads, which can penetrate in conductors insulation, with negligible damage. These probes facilitate significantly the voltage measurement, allowing the methods requiring voltage measurement to be classified as low-intrusion methods. However, in practice, most motors have no access to the individual power cables, unless the terminal box is opened, increasing significantly the time and efforts to apply the voltage-requiring methods. If the voltage is measured at the MCC, the user cannot assess the actual terminal voltage, unless the cable voltage drop is estimated on the basis of the length, cross-section, and actual current of the cable conductors. However, this process gives only an estimation of the terminal voltage. To avoid much additional efforts, in preliminary evaluations the user can actually neglect the cables voltage drop, even knowing the consequent reduction in the method accuracy. Nevertheless, it is assumed that voltage measurement is, in principle, an easy task.

The voltage unbalance also affects the accuracy of the load estimation methods. However, this issue is not addressed, being assumed a voltage unbalance not exceeding 0.5% (therefore, without significant effects on the motor performance), and that the arithmetic average of the currents and voltages is used. These assumptions are actually valid for the experimental results presented.

Regarding the measurement duration, particularly in the field, it is important to recognise that the load of many machines can actually fluctuate significantly, over the long term (e.g., from change of the plant or process conditions), medium term (e.g., voltage fluctuations over the day related to the power network load), and/or short term (e.g., load fluctuations from belt drives). In order to ensure that data accurately reflect the true average load, it is convenient to collect either several samples and develop a statistically valid measure in the case of handheld, digital, fixed sample period devices, or to acquire a relatively long duration means a period that sample of data (here, long can range from a few seconds to minutes, depending on the nature of the load) in the case of digital full-programmable measurement equipments. In belt-driven applications, relatively large load fluctuations (as much as 10% or more) can occur (as shown in Chapter 3). Thus, a single short-duration sample (for example, acquisition over a few cycles in duration) may grossly misrepresent the actual average load condition.

The importance of a particular error is entirely dependent upon what is done with the measurement result. If an error of ± 1 r/min in the measure speed is made in a field measurement, the consequences can be significant for the load estimation in low slip motors, but can be minor if motor efficiency, not actual shaft power, is the subject of interest and efficiency is estimated from either vendor efficiency-load curves or from motor models, as long as the actual motor operation is between half load and full load. This is simply an inherent result of the typically flat efficiency-

load curve for motors operated in that zone (particularly for large motors). For lightly load conditions (less than 25% load), percentage errors from all sources tend to be magnified.

4.5 Motor Experimental Data and Public Databases

In laboratorial experimental tests for motors up to 7.5 kW, the instrumentation accuracy, voltage distortion and unbalance limits defined in IEEE 112 in the new IEC 60034-2-1 standards, were respected (see Chapter 2). The ambient temperature was controlled in the range 22-25°C, and in all motors, the motor thermal equilibrium was reached ($\Delta\theta < 2$ K/h). Additional experimental data is used for larger motors (11 kW to 55 kW), provided by an independent laboratory [22]. Part of the motor manufacturers' information was extracted from the EURODEEM [20] and MOTORMASTER [21] public databases.

4.6 Slip-Based Motor Load Estimation Method

In the slip-based or speed-based motor load estimation method, the motor output power is estimated using the actual slip to rated slip ratio times the motor rated power. The nameplate data may be corrected by the square of the ratio of the actual terminal voltage to the rated terminal voltage. It is a low-intrusion method, but relatively inaccurate because of the motor rated speed tolerances and speed measurement errors, as well as to the actual nonlinearity of the torque slip curve. This method is in common use today and it is quite attractive due to its simplicity, being the motor slip or speed easily obtained using a stroboscopic tachometer, which does not require any painted marks or reflective straps on the motor shaft or mechanical coupling, having a typical accuracy of ± 0.5 r/min. When voltage compensation is not used, this method is the simplest since, in most IMs, the shaft or the cooling fan (in the case of TEFC motors) is visually accessible to the tachometer light. However, since the slip is a function of motor actual voltage, the voltage should also be measured for compensation purposes, in order to reduce the error associated with this method, increasing the intrusion level. The potential error associated with the voltage measurement is by far negligible in relation to the error associated with nameplate speed tolerance and speed measurement. The motor temperature also influences the slip-load relation, which, therefore, should be also taken into account, if possible. For fixed ambient temperature and line-to-line voltage, the slip depends on motor rated power, number of poles and efficiency class, as it can be seen in Figs. 4.7 and 4.8. In Fig. 4.7, it should be noted that, although the percentage slip increases with number of poles, the absolute slip value in r/min decreases with the number of poles.

In [2], (4.7) and (4.8) are used to estimate the motor load using the motor speed or slip with and without voltage compensation, respectively. The voltage compensation is needed because actual motor voltage can be significantly different from the rated voltage and, for a certain slip, the torque

is approximately proportional to the squared magnetizing flux and, assuming fixed frequency, to the squared voltage. That effect can be compensated as in (4.8).

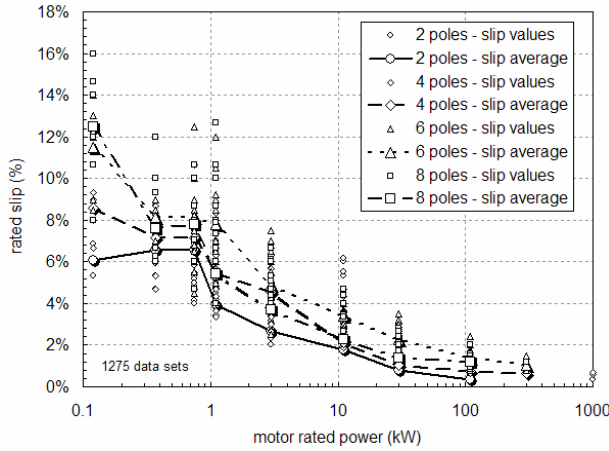


Fig. 4.7. Average slip for a universe of 1275 motors, of 2 poles (364 data sets), 4 poles (389 data sets), 6 poles (281 data sets), and 8 poles (241 data sets). Data extracted from [20].

$$\zeta_{\omega} \approx \frac{\omega_{\text{sync}} - \omega_{\text{mea}}}{\omega_{\text{sync}} - \omega_N} = \frac{s_{\text{mea}}}{s_N} \quad (4.7)$$

$$\zeta_{\omega} \approx \frac{\omega_{\text{sync}} - \omega_{\text{mea}}}{\omega_{\text{sync}} - \omega_N} \cdot \frac{U_{\text{mea}}^2}{U_N^2} \quad (4.8)$$

Equation (4.8) is proposed in most published technical texts (e.g., [1], [2], [4]), being considered in this section as the reference for comparison purposes. It has several error sources, namely associated with the approximation of the equation itself (this also applies to (4.7)), the measured quantities, and the nameplate values and motor temperature variation, as explained before. Taking into account only the slip-load relation approximation error, Fig. 4.9 (top) shows the resulting experimental error or deviation between real slip-load curve and proportional or linear slip-load curve, for a set of 11-kW/4-pole, 55-kW/6-pole and 75-kW/4-pole motors, reaching a maximum error of 4.2%, 5.8% and 6.4%, respectively. Fig. 4.9 (top) proves that (4.8) has significant errors, being its application only acceptable for motors with a rated power lower than 11 kW and a number of poles of 2 or 4. Instead of (4.8), it is proposed the use of (4.9), in order to reduce slightly the approximation errors. Fig. 4.9 (bottom) shows the resulting experimental error or deviation between real (slip-slip²)-load curve and proportional or linear (slip-slip²)-load curve, associated with (4.9), for a set of 11-kW/4-poles, 55-kW/6-poles and 75-kW/4-poles motors, reaching a maximum error of 3.6%, 5.2% and 6.2%, respectively. When compared to (4.8), equation (4.9) leads to a slight reduction in the defect error (estimated value lower than the actual value), without increasing the method complexity, being an advantageous alternative. In Fig. 4.10, the error associated with the torque-slip proportionality assumption is shown, demonstrating that there is always an inevitable error associated with the analysed method.

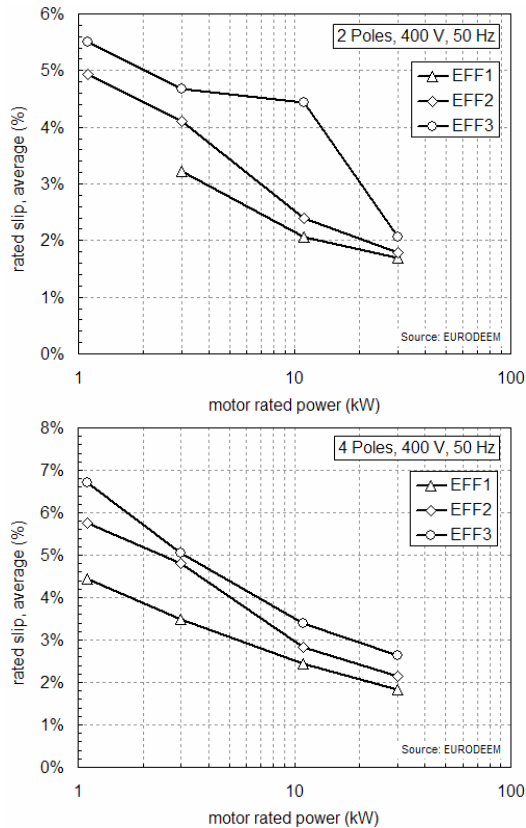


Fig. 4.8. Average slip for a universe of 17 motors of 2 poles (364 data sets) and 4 poles (389 data sets). Data extracted from [20].

In Fig. 4.11, the experimental resulting average error of estimated motor load is shown for both (4.8) and (4.9) equations, showing the slight error reduction when (4.9) is used, particularly for motor loads lower than full load, as it can be seen in Fig. 4.12, which shows the difference or error between both equations, considering (4.8) as reference ((4.8)-based load minus (4.9)-based load, divided by (4.8)-based load). In Fig. 4.13, the average percentage difference between methods is shown for 25% and 75% loads.

On the basis of the foregoing discussion, it is possible to state that, the lower the load and the rated power and the higher the number of poles are, the higher the decrease in error will be if (4.9) is used instead of (4.8). The estimated load by (4.9) results higher than that estimated by (4.8), leading to the error (by defect) reduction because the estimated motor load using the slip-based method is lower than the actual load. The presented arguments prove that (4.9) is better than (4.8), reducing the error slightly, without increasing the method complexity or intrusion level. It should be referred that the temperature also influences the motor slip (due to the rotor resistance dependency on temperature).

However, as for (4.8), (4.9) is also an approximate form to estimate the motor load due the actual non-proportionality between torque and slip, as previously discussed. Yet, in all slip-based methods, it is assumed torque-slip proportionality in the range between rated load (or a load slightly higher) and no-load slips. In fact, those considerations can be made without introducing

significant errors for loads higher than 25%, as shown previously, and as it can be seen in Figs. 4.14 and 4.15, which show experimental and simulated separated results (non-averaged) for a number of motors, respectively. As it can be seen in Fig. 4.14 and 4.15, for loads lower than a specific value (around 15-25% for large motors and 40-50% for small motors), the error introduced by torque-slip proportionality assumption is significantly high in absolute value and inverts its value (i.e., the torque-slip curve crosses the linear or proportionality curve), particularly for low power motors, due to the increase of the relevance of the friction and windage losses, or of the no-load slip (which, in general, decreases with the motor rated power). In fact, in the crossover points, the error is zero.

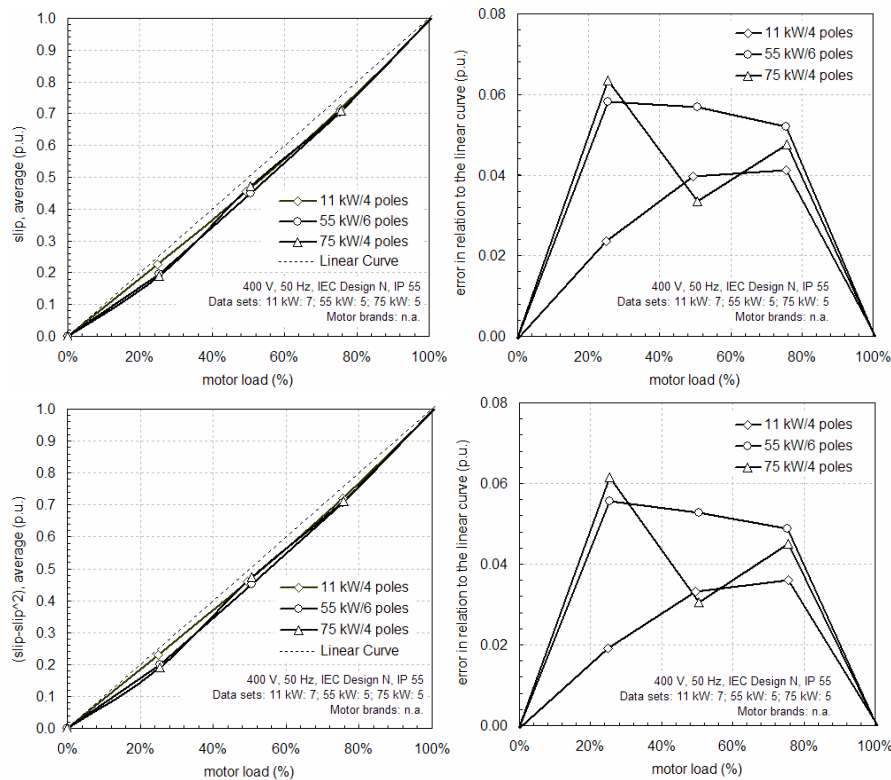


Fig. 4.9. Experimental average slip-load curve (top) and $(\text{slip}-\text{slip}^2)$ -load curve (bottom), and associated errors in relation to the proportional curve, for 11-kW/4-pole, 55-kW/6-pole and 75-kW/4-pole motors (data extracted from [22]), assuming zero slip at zero load.

$$\zeta_{\omega} = \frac{P_{mech}}{P_N} = \frac{\omega \cdot T}{\omega_N \cdot T_N} \approx \frac{\omega_{sync} \cdot (1 - s_{mea}) \cdot K \cdot s_{mea}}{\omega_{sync} \cdot (1 - s_N) \cdot K \cdot s_N} \cdot \frac{U_{mea}^2}{U_N^2} = \frac{s_{mea} - s_{mea}^2}{s_N - s_N^2} \cdot \frac{U_{mea}^2}{U_N^2} \quad (4.9)$$

Regarding errors resulting from the nameplate speed, Fig. 4.16 presents the error considering the use of (4.9).

In Fig. 4.16, only the errors associated with the stroboscopic tachometer (± 0.5 r/min) and to motor nameplate speed (± 2.5 r/min tolerance, except when this tolerance exceeds the one stated in [12], which can occur for large motors) are considered, since voltage can be measured with

insignificant or negligible errors in relation to the mentioned errors. On average, the maximum error (by defect and by excess) at full load is expected not to exceed 20% for motors with power up to 3 kW, but can be significantly higher for larger motors. In general, the higher the number of poles is, the higher the error will be. The error also increases with the decrease of motor load due to the consequent reduction in slip.

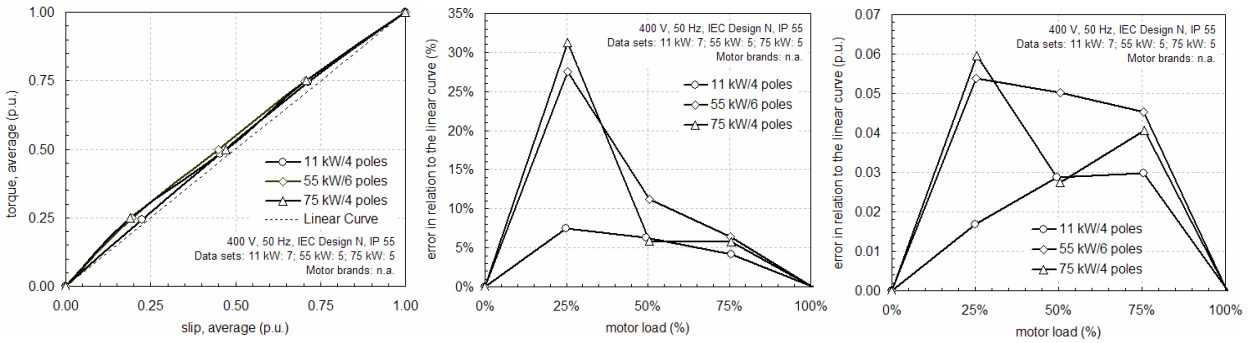


Fig. 4.10. (left) Experimental average torque vs. slip and (middle and right) the error associated with torque-slip proportionality assumption in percentage and p.u., for 11-kW/4-pole, 55-kW/6-pole and 75-kW/4-pole motors (data extracted from [22]), assuming zero slip at zero load.

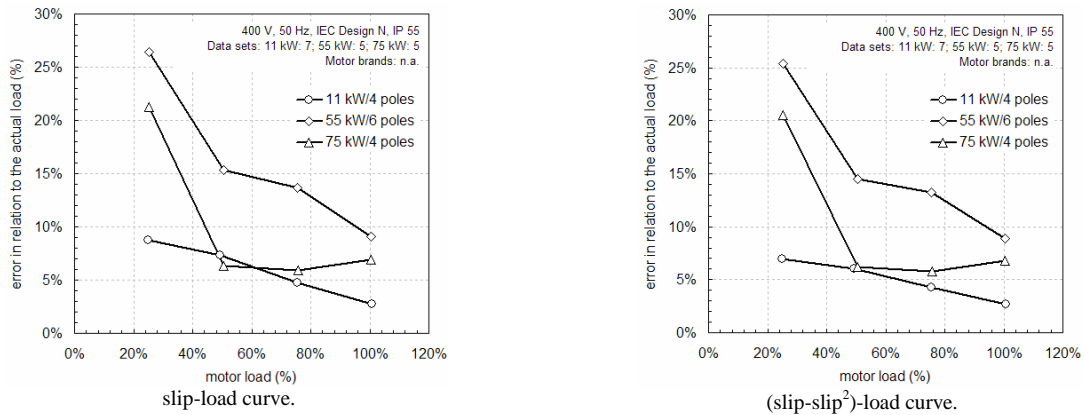


Fig. 4.11. Experimental average error (by defect) in relation to actual load (left) for (4.8)-based method, and (right) for (4.9)-based method, for 11-kW/4-pole, 55-kW/6-pole and 75-kW/4-pole motors (data extracted from [22]).

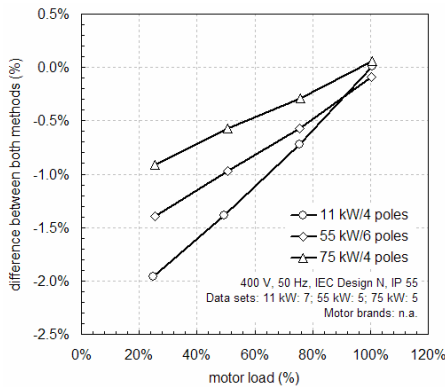


Fig. 4.12. Experimental average difference between the estimated motor load for both (4.8)- and (4.9)-based slip methods, considering (4.8) as reference, for 11-kW/4-pole, 55-kW/6-pole and 75-kW/4-pole motors (data extracted from [22]).

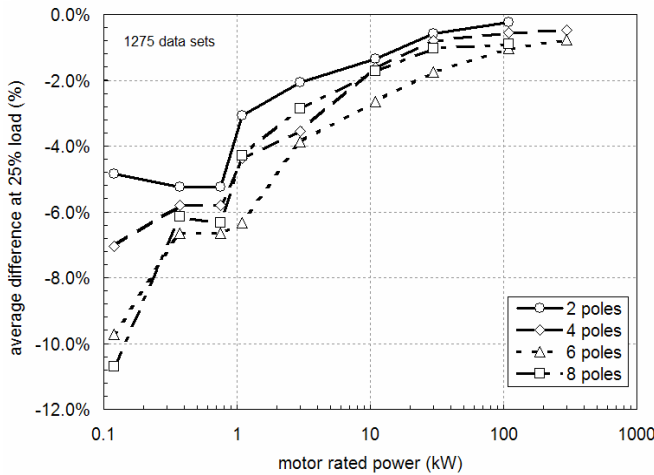
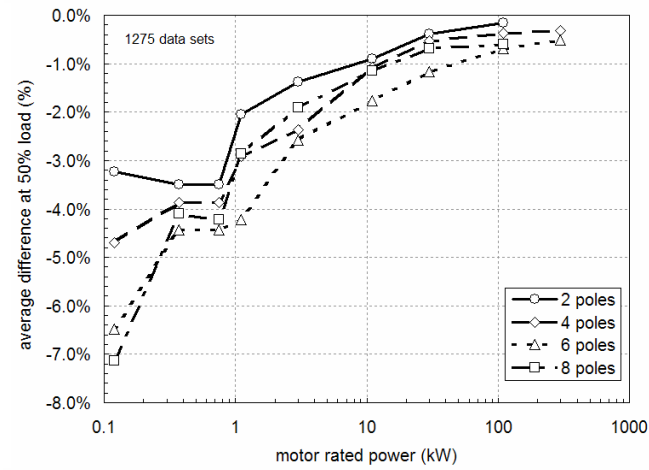
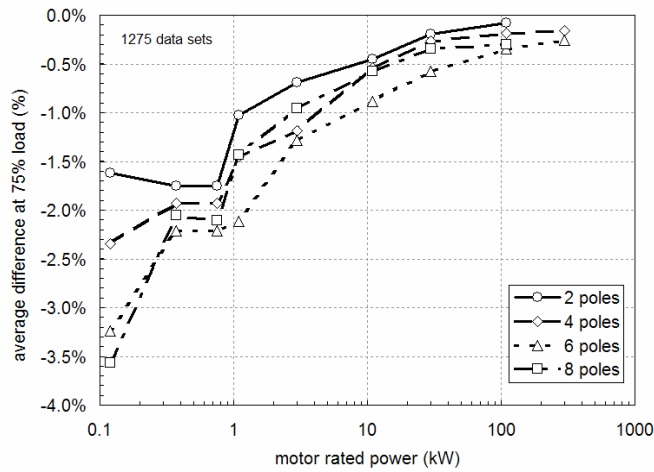


Fig. 4.13. Average percentage difference between (4.8)-based and (4.9)-based estimated load, assuming the first as reference, for 25% and 75% load. Data extracted from [20].

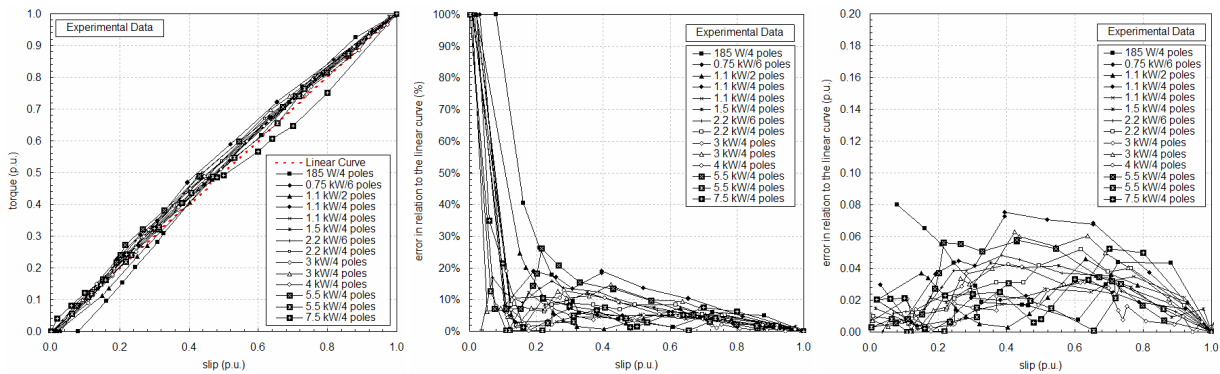


Fig. 4.14. Experimental torque-slip curves and absolute value of the torque error resulting from the torque-slip proportionality assumption, for a number of motors with rated power up to 7.5 kW.

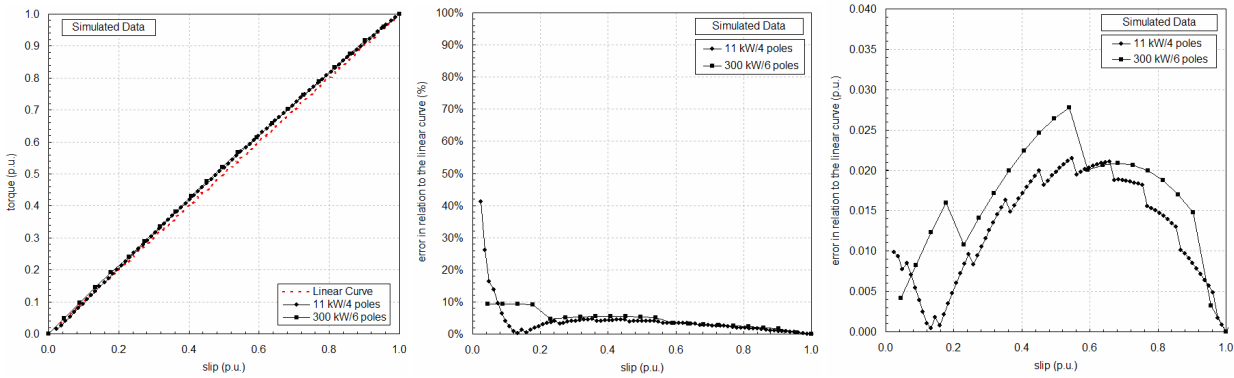


Fig. 4.15. Simulated torque-slip curves and torque absolute value of the error resulting from the torque-slip proportionality assumption, for 11-kW/6-pole and 300-kW/6-pole motors.

On the basis of the presented information, the slip-based method should be avoided for motors with a number of poles higher than 4 (due to the reduced slip in r/min) and rated power higher than, say, 30-50 kW. Should also be avoided for loads lower than 25%.

Note that the non-regular behaviour (stepped behaviour) of the error curves in Fig. 4.15 is related to the resolution used in simulations and rounding processes after simulations. These errors have no relevance when compared to those associated with the measured and nameplate speed.

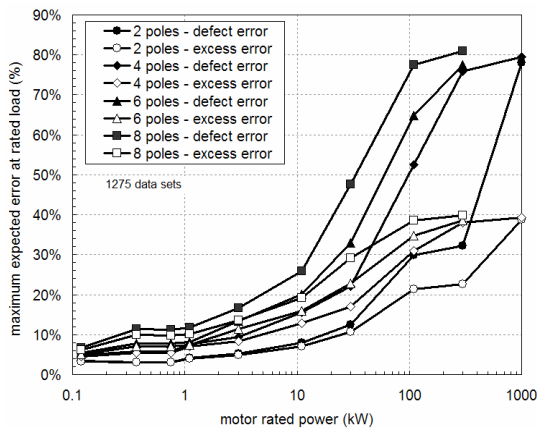


Fig. 4.16. Average of the maximum error expected at full load for (4.9), assuming an error of ± 2.5 r/min in the nameplate and an error of ± 0.5 r/min in the stroboscopic tachometer. Data extracted from [20]

As it can be seen in Fig. 4.8, the slip of the high-efficiency motors (e.g., IE2/EFF1 or IE3/NEMA Premium) is typically lower, resulting in a higher error, particularly for low power motors (≤ 30 -50 kW). Therefore, care must be taken when applying the slip-based method to this sort of motors (a lower curvature helps minimizing the error, but a lower nominal slip increases it). Even for the recommended ranges, this method is considerably inaccurate, particularly if all the significant error sources were taken into account, namely those associated with the rated values, measured values and non-proportionality between torque and speed.

The error is dependent, in one hand, on the curvature of the torque-slip curve in the zone between no-load and rated load, and, on the other hand, on the rated and measured slip. Therefore,

the motor rotor type (e.g., normal- or high-starting torque), also influence the error mode, which is higher for low-resistance rotors (e.g., copper rotors).

These results are important because allows to define the acceptable application domain in terms of motor type, rated power, rated speed, and load range.

In general, the applicability of this method should be defined as a function of the rated slip. Assuming an admissible maximum error of within 8-10% at estimated full load, theoretically, on the basis of the errors associated with the rated and measured speeds, the slip-based method should not be applied to motors with a rated slip lower than 35 r/min, since the error by defect exceeds that limit, as it can be seen in Fig. 4.17.

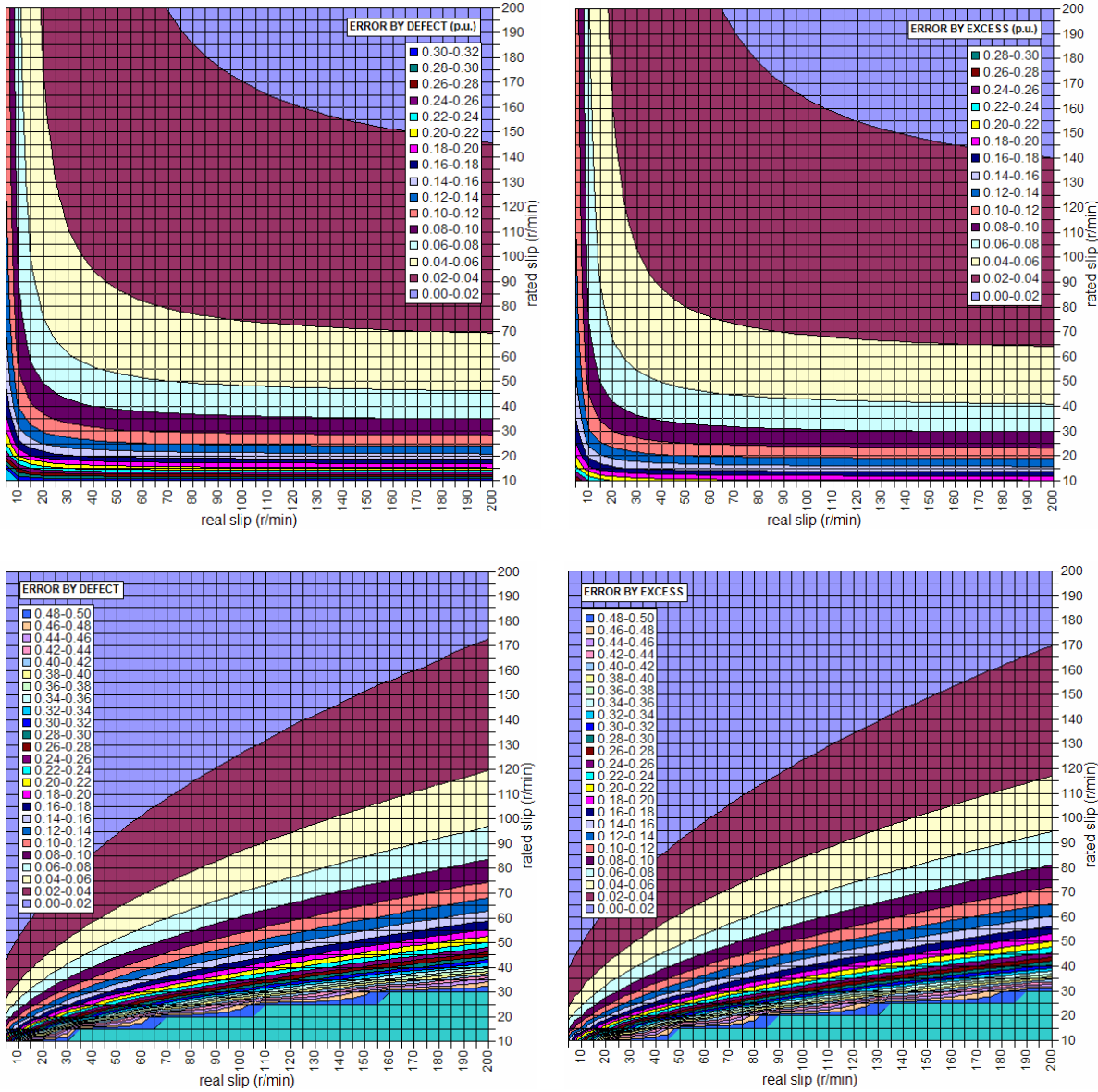


Fig. 4.17. Load estimation error resulting from the measured and rated speed values, as a function of the rated and actual slip, considering the equation (4.7), and an error of ± 2.5 r/min in the nameplate and of ± 0.5 r/min in the stroboscopic tachometer: (top) error in percentage divided by 100 or p.u. (estimated load minus real load, divided by estimated load); (bottom) error in percentual points divided by 100 (estimated load minus real load).

An average correction factor can be applied in order to attenuate the torque-slip non-proportionality, based on experimental and simulated results, as presented in Fig. 4.18.

Fig. 4.19 shows the estimated motor load and the inherent error for 14 motors (ranging from 185 W to 7.5 kW) experimentally tested and for 2 simulated motors. Fig. 4.20 shows the actual and the estimated motor load and the inherent error for motors ranging from 11 W to 75 kW at 3 different load levels, experimentally tested. The higher error for the 11 kW motor is related to the higher curvature of the quasi-linear torque-slip curve.

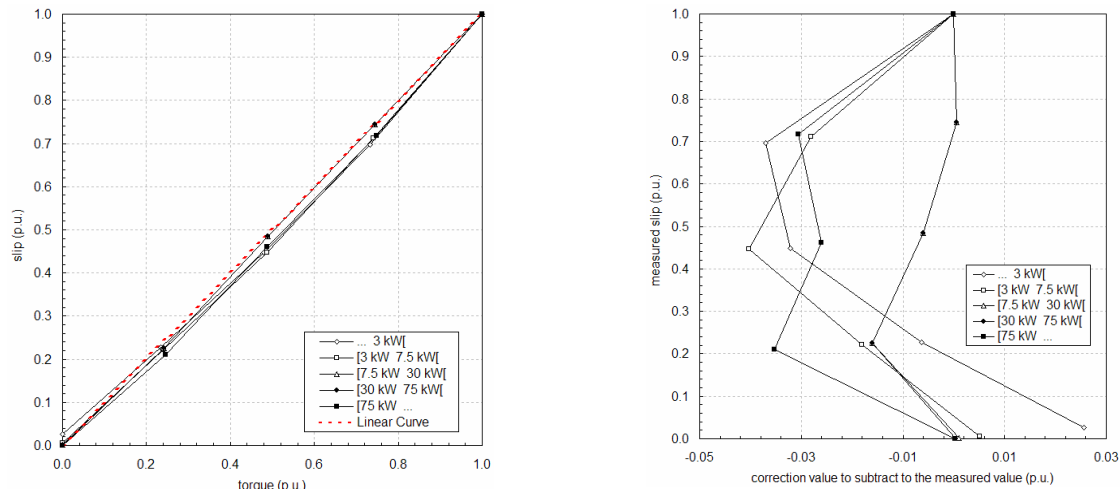


Fig. 4.18. Average torque-slip relation and correction factor for slip, by power range (based on experimental and simulated results for a set of motors with different number of poles).

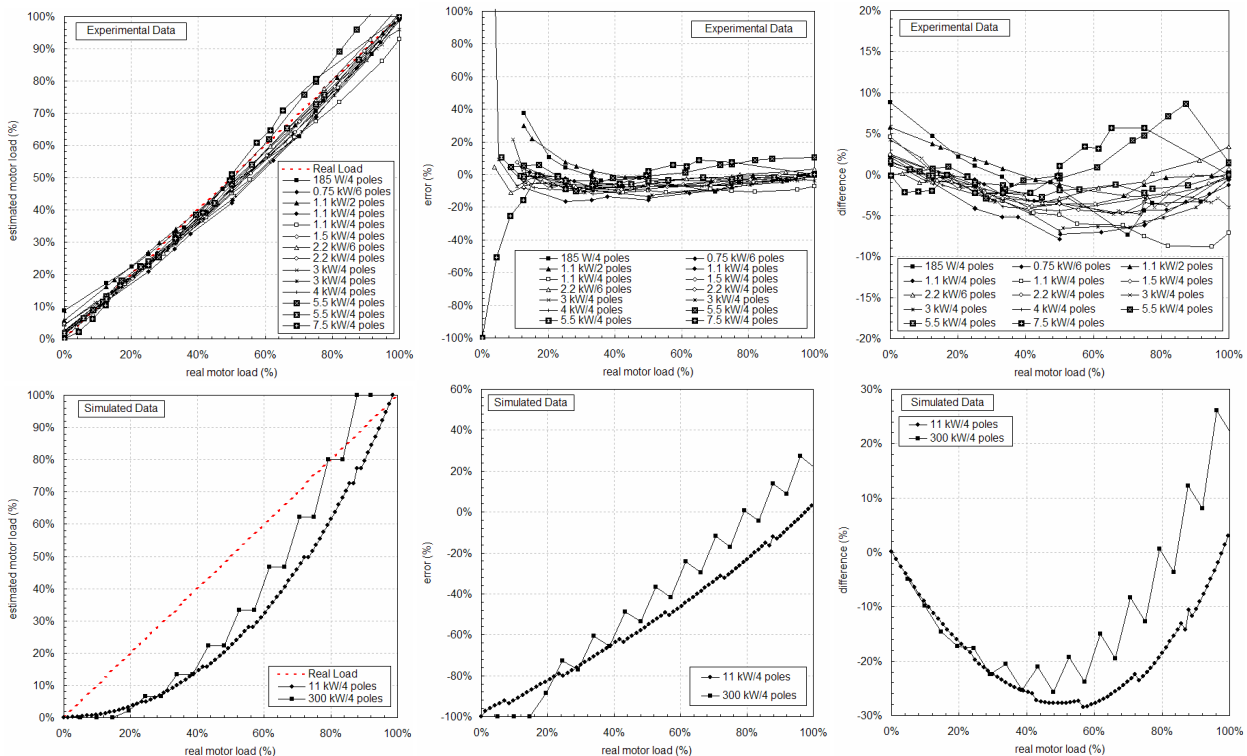


Fig. 4.19. Slip-based method: actual and estimated motor load and the respective error (in %) and difference (in p.p.) for different motors.

¹⁰ Error (in %) = (estimated load – actual load)/actual load.

¹¹ Difference (in p.p.) = estimated load (in %) – actual load (in %).

In order to illustrate the final error resulting from the application of the slip-based method, experimental examples are presented in Fig. 4.21, in which the difference between the rated and measured speed at full load (for thermal equilibrium, ambient temperature between 22°C and 25°C) is the main source of error. In Fig. 4.22, the average error of the data presented in Fig. 4.21 is presented. It can be concluded that, for the considered universe, between 25% and 75% load, the absolute error is acceptable (maximum 0.06 or 6 p.p.), allowing the user to estimate, at least, a motor load range. For example, a motor with an estimated load equal to 20% has a strong possibility of being operating, actually, below 25% load. Fig. 4.22 shows that the error oscillates between 8% and -47% (average equal to 11.2% at 25% load). This method is quite inaccurate, but can be used to identify the motor load range. For example, the average defect error does not exceed 3.5 p.p., as it can be seen in Fig. 4.23, which shows the comparison between the slip based method error (in p.p.), and the useful accuracy for 3 different motors. It shows that only for small motors the slip-based method allows useful load estimation for proper replacement. Moreover, using this method it would be difficult to estimate the load with accuracy enough to decide the rated power for proper replacement.

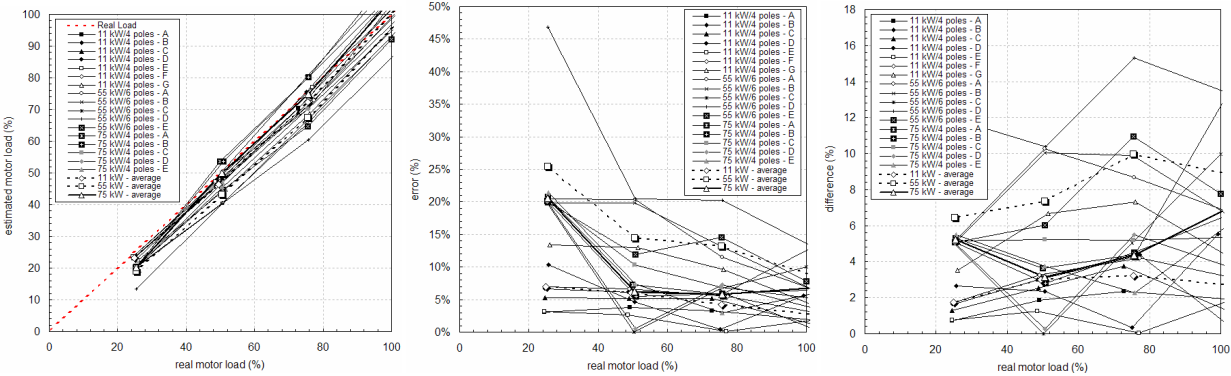


Fig. 4.20. Slip-based method: experimental actual and estimated motor load and the absolute value (or modulus) of the respective error (in %) and difference (in p.p.), for 11-kW/4-pole, 55-kW/6-pole and 75-kW/4-pole motors (data extracted from [22]).

The influence of the motor temperature variation before stability and motor steady-state temperature is also very important because of its impact on rotor resistance. For example, a variation of 25 r/min between the post-start instant (cold operation) speed and steady-state operation (operation with thermal equilibrium) speed for a 3-kW 4-pole motor can occur (experimentally verified). For motors with an operating cycle characterized by periods with a duration shorter than the motor thermal constant, or motors operating in locals with an ambient temperature higher than 40°C and/or altitudes higher than 1000 m, the rated speed is no long valid, mainly due to the change of the rotor bars resistance value, which influences significantly the motor torque-speed curve. Therefore, besides the thermal equilibrium condition, it is desirable to

compensate the slip as a function of the temperature difference, taking into account the reference temperature defined by the standard associated with the nameplate.

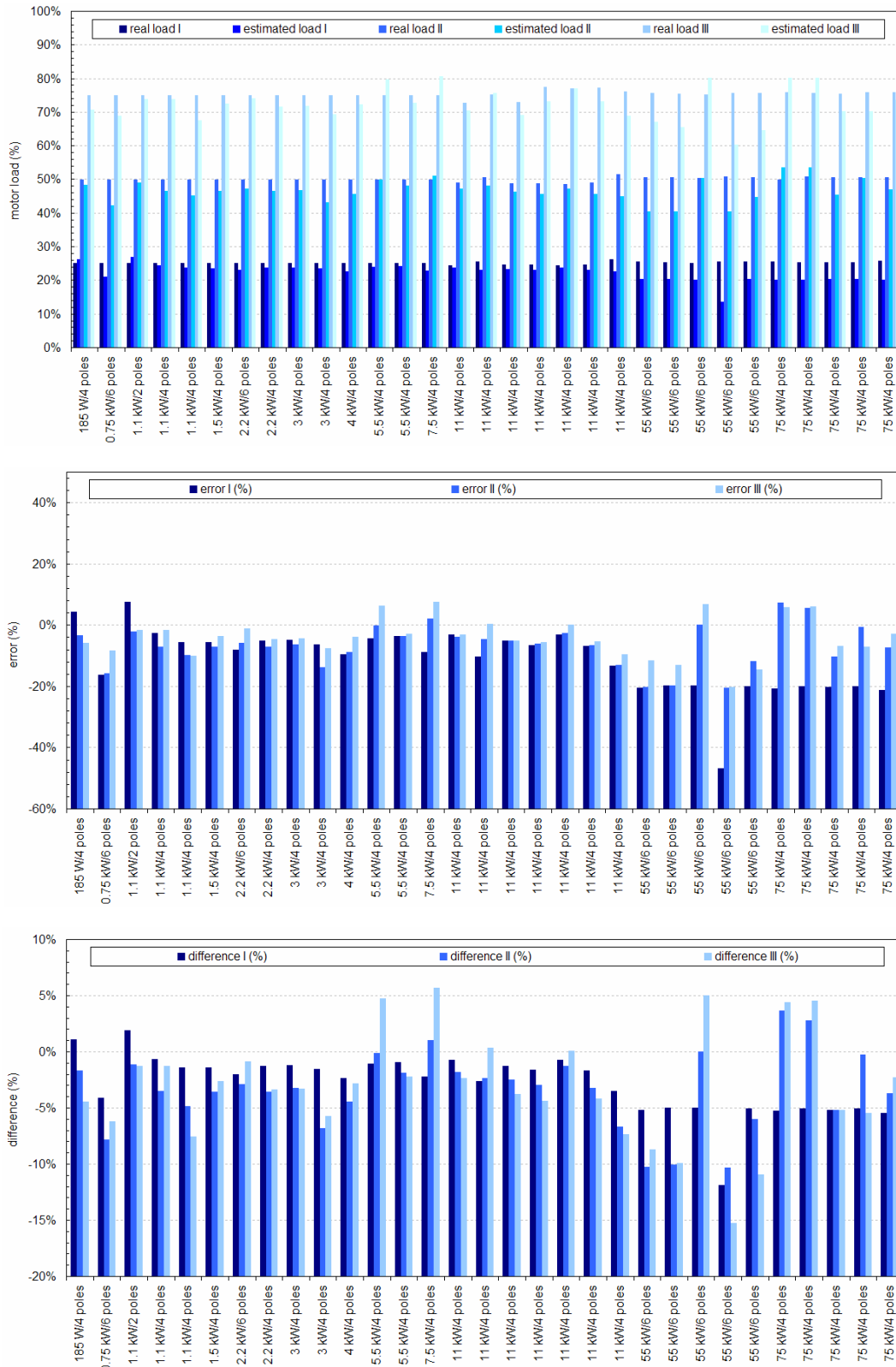


Fig. 4.21. Slip-based method: experimental actual and estimated motor load and the respective error (in %) and difference (in p.p.) for different motors and three load levels ($\approx 25\%$, $\approx 50\%$ and $\approx 75\%$).

The principle for the slip thermal compensation is described in the IEEE 112 and IEC 60034-2-1 standards [14]. Note that, a known increase in the stator and rotor temperature leads to a known increase of their circuit resistance, and the rotor resistance increase leads to a decrease of the torque roughly the same magnitude order, for a given slip. This relation can be taken into account in (4.9). This temperature dependency is a significant disadvantage and source of error associated with the slip-based method.

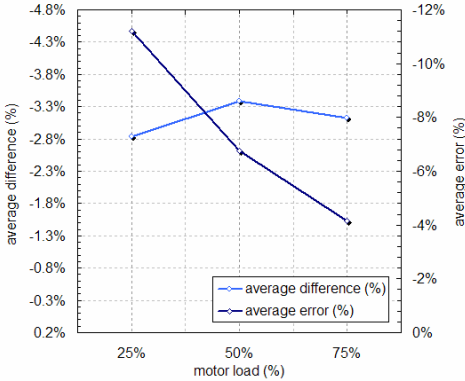


Fig. 4.22. Average difference (in p.p.) and error (in %) for the data presented in Fig. 4.21.

As an alternative, to reduce the uncertainty level for low loads, it is proposed testing the motor in star connection (if the delta is the rated connection) and comparing the obtained slip with the delta-connected motor slip. This allows the motor load range to be determined regardless the ambient temperature and nameplate speed associated error. It should be noted that, it is not always necessary to identify the exact motor load, but, instead, a load zone, enough to classify the motor in terms of load, e.g., strongly oversized or undersized, regardless the exact load level. This method is particularly attractive for motors with a start-delta starting system, being the level of intrusion maintained low in those cases. Concretely, if the quotient between the slip for star connection and the slip for delta connection is approximately equal or lower than 3, the motor load is expected to be lower than $\frac{1}{3} \pm 10\%$, else if that quotient is higher than 3 the motor load is expected to be higher than $\frac{1}{3} \pm 10\%$. Those limits were verified experimentally for motors between 185 kW and 7.5 kW, and by simulation for an 11-kW and a 300-kW motor. Obviously, a slip near zero for star connection indicates a near no-load operation. This procedure also allows the user to evaluate if it is advantageous to connect the motor permanently in star mode, as it is shown in Chapter 5.

As a final evaluation, the errors (in p.p.) resulting from the application of this method are now superposed with the useful accuracy defined previously, being the resulting curves presented in Fig. 4.23.

It should be noted that a smaller error would be expected for the 11-kW motor, but the considered motor (simulation parameters extracted from [28]) is characterized by a strong curvature in the quasi-linear zone of the torque-speed curve. Actually, looking at Fig. 4.19, it is

possible to conclude that the experimental error/difference in percentage point is within $\pm 10\%$. On the basis of the previous figures, it is possible to conclude that this method is only acceptable for low-power 2- and 4-pole motors (say, smaller than 11 kW), for loads higher than 20-25%, if the user goal is to decide the new replacing motor rated power, taking into account that, considering the expected error, it is always preferable an oversized motor than an overloaded motor. In general, low-slip motors are not suitable to be evaluated by this method, as referred before. Therefore, for low-loaded low-power motors, high-power motors, medium-high power high-efficiency motors and/or motors with a pole number higher than 4 this method should be avoided. Most of these recommendations for the universe of application can be ignored (e.g., application of the method to 2- and 4-pole motors up to 30-50 kW) if the goal is a first load evaluation in which the star connection use can be helpful.

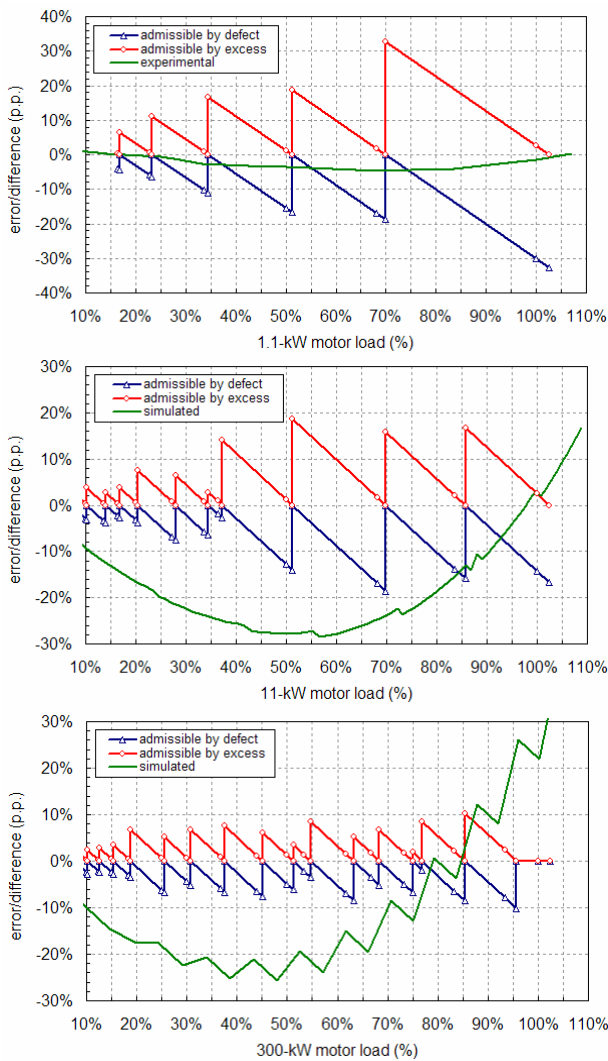


Fig. 4.23. Superposition of the error or difference (in p.p.) associated with slip-based method (using (4.9), taking into account the nameplate and measured speed errors) and the useful accuracy, for 1.1-kW (experimental), 11-kW (simulated), and 300-kW (simulated) motors.

4.7 Current-Based Motor Load Estimation Method

In the line current-based motor load estimation method, it is assumed that the motor load is closely proportional to the measured line current to rated current ratio, in percentage. Several published works address this method such as [1], [2], and [4]. Although commonly used on its simplest form in Industry, its accuracy is expected to be poor, unless the current-load curve is fully provided by the manufacturer, which typically is only possible for medium/large motors. In this method, the motor load is estimated comparing the line current with the rated current (nameplate current), according to (4.10), which includes voltage compensation. In fact, (4.10) relates the actual apparent (or complex power modulus) power with the nominal apparent power.

$$\zeta_i \approx \frac{I_{\text{mea}} \cdot U_{\text{mea}}}{I_N \cdot U_N} \quad (4.10)$$

Nevertheless, the current is not proportional to the motor load, as it can be seen in Figs. 4.24 and 4.25. In Fig. 4.26, the average error in relation to the actual load is shown for the data presented in Fig. 4.25. In fact, the current is almost proportional for loads higher than 50%. For loads lower than 25-50%, due to the magnetizing current (reactive component), the current-load curve becomes unstraight or nonlinear and (4.10) is inherently significantly inaccurate for those load levels. The current-load curve can be represented approximately by a set of straight lines. In the current-load curve, there is a positive no-load offset. The higher the motor power and the lower the number of poles are, the lower the load corresponding to the lower limit below of which the current as a function of load is practically constant until no-load will be, as it can be seen in Fig. 4.24. Equation (4.10) is an approximation of (4.11), being the power factor ignored.

$$\zeta_i \approx \frac{P_{\text{ele_mea}}}{P_{\text{ele_N}}} = \frac{I_{\text{mea}} \cdot U_{\text{mea}} \cdot \lambda_{\text{mea}}}{I_N \cdot U_N \cdot \lambda_N} \quad (4.11)$$

The approximation inherent to (4.10) is gross, due to the significant power factor variation as a function of motor load, as it can be seen in Fig. 4.50. This variation decreases with the motor rated power and increases with the number of poles. As a result of the current-load disproportionality and of ignoring the power factor, (4.10) results considerably inaccurate, for loads lower than nominal.

One way to improve this method is to use empirical correction factors calculated on the basis of specific values for particular motor or average values by power range and by number of poles, obtained for example from motor manufacturers, catalogues and/or databases. The use of average

values is a quick and simple approach and the associated error is reduced, due to the relative low standard deviation. In the previously referred major public motor databases ([20], [21], available in the Internet), it is possible, in most cases, to find the necessary motor data.

Another way to improve the accuracy of (4.10), proposed in several published technical documents (e.g., [1], [2], and [4]), is the application of a linear interpolation between the full-load value and the half-load value for loads higher than 50%, according to (4.12), recommended only for motors with rated power higher than 7.5 kW.

$$\zeta_i \approx 0.5 + 0.5 \cdot \frac{(I_{mea} \cdot U_{mea} \cdot U_N^{-1}) - I_{50\%}}{I_N - I_{50\%}} \quad (4.12)$$

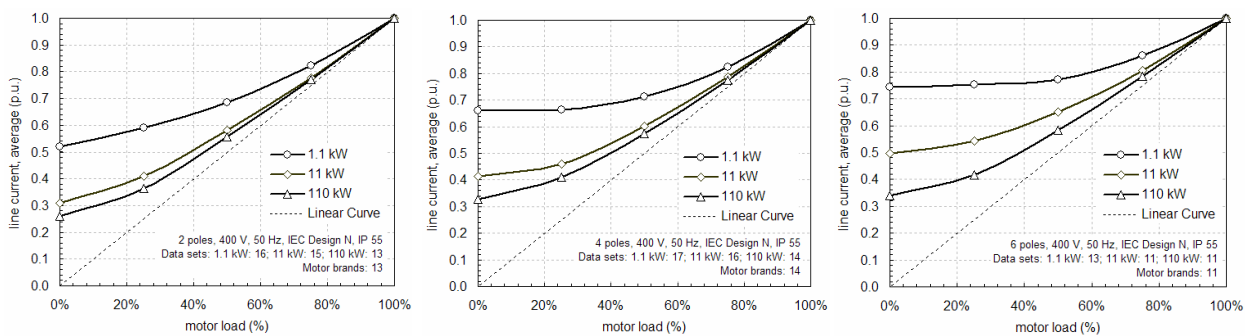


Fig. 4.24. Average current value as a function of load for 1.1-kW, 11-kW and 110-kW motors, with 2, 4 and 6 poles (data extracted from [20]).

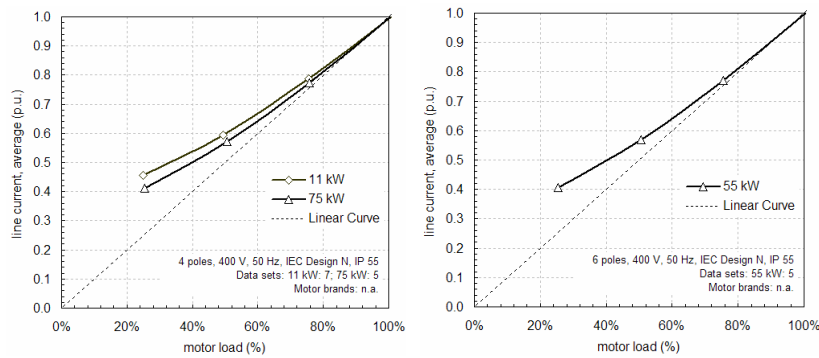


Fig. 4.25. Experimental average line current as a function of motor load (data extracted from [22]).

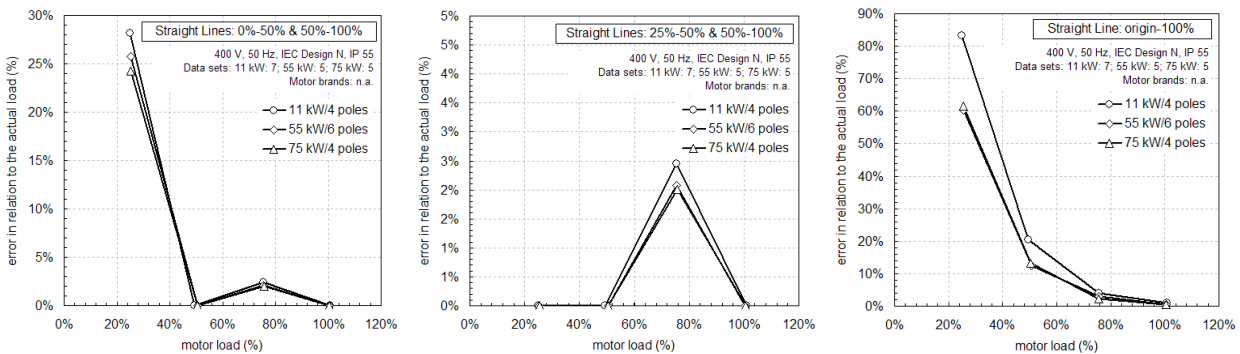


Fig. 4.26. Current-based method: experimental average error in relation to the actual motor load, for 11-kW/4-pole, 55-kW/6-pole and 75-kW/4-pole motors (data extracted from [22]), considering different approximations of the line current curve as a function of load.

The half-load current value is not normally included in the motor catalogues and databases. One hypothesis to know that value is to ask manufacturer for it, which is typically time consuming. Another hypothesis is to use empirical average values, as it is shown in Fig. 4.27.

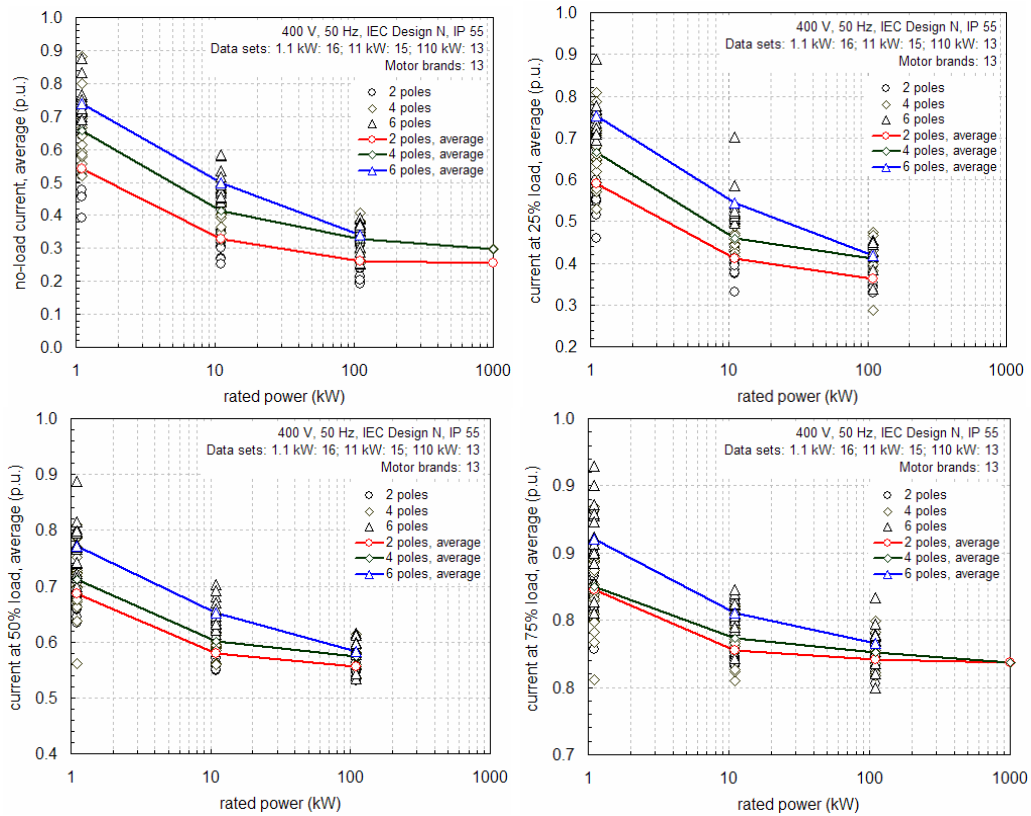


Fig. 4.27. Line current average values at 0%, 25%, 50% and 75% load for IMs with different rated powers and number of poles (data extracted from [20]).

Yet, it is proposed that the estimation of the part-load current, for nominal voltage, on the basis of motor part-load efficiency and power factor values, typically available in the catalogues and databases for 50%, 75% and 100% load, and in some cases for 25% load, using (4.13).

$$I_{\zeta} = \frac{P_N \cdot \zeta}{\sqrt{3} \cdot \eta_{\zeta} \cdot U_N \cdot \lambda_{\zeta}} \quad \eta_{\zeta} = \frac{P_N \cdot \zeta}{\sqrt{3} \cdot U_N \cdot I_{\zeta} \cdot \lambda_{\zeta}} \quad (4.13)$$

However, although the significant improvement of the method using the part-load current, (4.12) is limited to loads higher than the lower load limit considered for part-load current estimation (typically 50%). Therefore, it is also proposed the inclusion of the no-load current value, which, nowadays, is typically available for most of the motors in the referred databases. If not, the user can always ask manufacturers for that value ([12] obligates the manufacturer to register that value periodically), use empirical average values, or, alternatively, to carry out the no-load test, which is

relatively simple, but requires the mechanical uncoupling of the motor, which is a hard task. The measurement of no-load current is typically required in old motors because it is usually not found on their nameplate, and it is unreasonable to ask manufacturers for that value. Of course, the motor no-load test only makes sense for medium-large motors operating a large number of operating hours per year. In [1] it is proposed that, when the no-load current is not available, it can be quickly but grossly estimated by multiplying the rated current by 0.3. However, looking at Fig. 4.27, that assumption is not reasonable, due to the dependence upon the motor rated power and number of poles.

Just as for the slip-based method, after the motor load estimation, to obtain motor efficiency one will have to either use typical interpolated efficiency-versus-load curves or use the measured input power [4]. Motor current measured by a clamp-on current probe corresponds to a relatively low level of intrusiveness. According to [4], the measurement of the input power has a high degree of intrusion, but, if special voltage probes are used (insulation penetration capability), the intrusiveness level can be considered as low/medium.

Knowing the maximum number of part-load and no-load current values as possible, which, in the best cases, can include the current at 0%, 25%, 50%, 75% and 100% load, the user can apply (4.14) for each possible current-load \overline{ab} straight-line segment between load points a - b (e.g., 0%-25%, 25%-50%, 50%-75%, and 75%-100% load straight segments). The higher the number of part-load points is, the lower the interpoint error will be, as it can be seen in Figs. 4.28-4.37. Additionally, the lower the motor power and the higher the number of poles are, the higher the number of intermediate points that should be considered. It should be emphasized that using straight-line between intermediate points, the load becomes underestimated (error by defect), although the absolute error is significantly reduced in relation to the simplest situation considering only the origin and full-load points, which result in overestimated load.

$$\zeta_i \approx \zeta_a + (\zeta_b - \zeta_a) \cdot \frac{(I_{\text{mea}} \cdot U_{\text{mea}} \cdot U_N^{-1}) - I_a}{I_b - I_a} \quad (4.14)$$

It is interesting to note that, considering the origin-100% segment, the motor load results overestimated, considering no-load-100% segment, the motor load results underestimated, over all load range.

The results of interpolation can be much more improved if, for example, instead of linear interpolation, a 2nd order polynomial interpolation, of the type $I_l = A \cdot \zeta^2 + B \cdot \zeta + C$, is used. For this approach, due to the 3 constants, at least 3 points are needed, preferable including the no-load, an intermediate-load and the full-load points. This leads to a significant error reduction between

points, but requires more calculations. The user can either solve a 3-equation, 3-variable system or use mathematical software tools (e.g., MICROSOFT EXCEL or MATLAB) to draw automatically fitting lines of the referred form and to generate the respective mathematical equations.

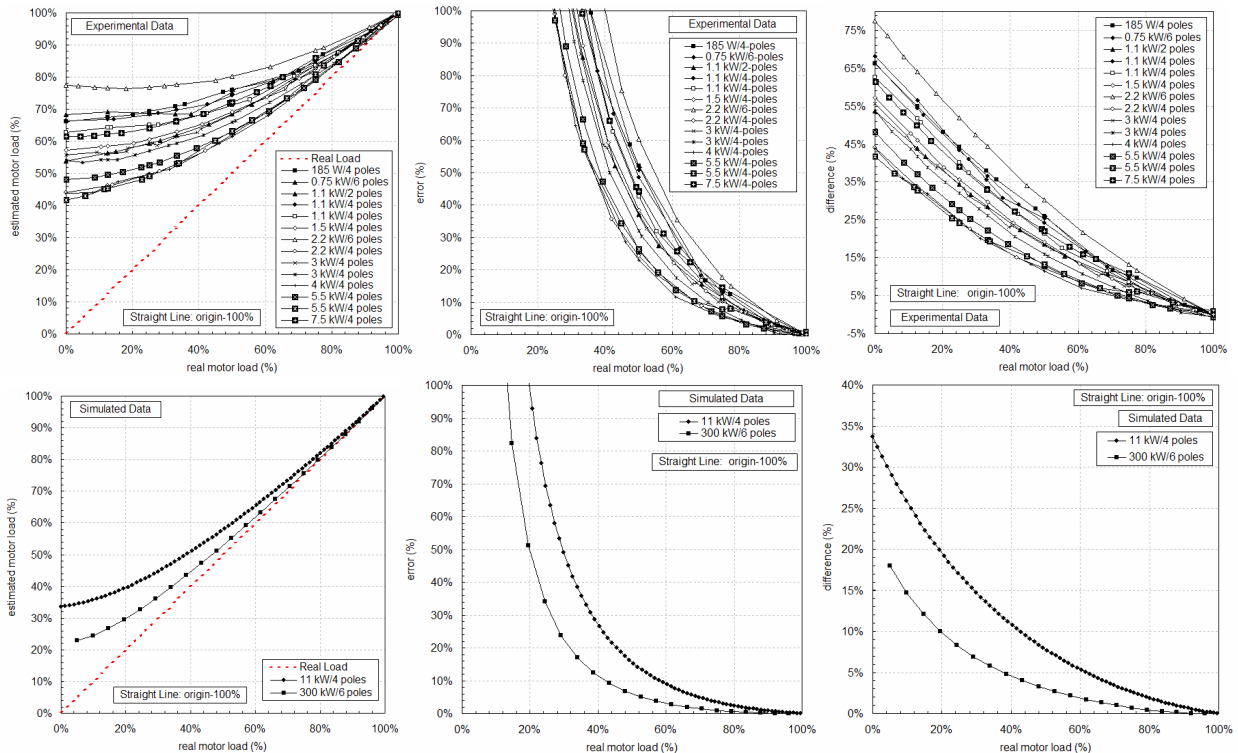


Fig. 4.28. Current-based method: actual and estimated motor load and the respective error (in %) and difference (in p.p.) for different motors, approximating the current curve as a function of load by one segment - origin (zero load, zero current) and full-load points segment.

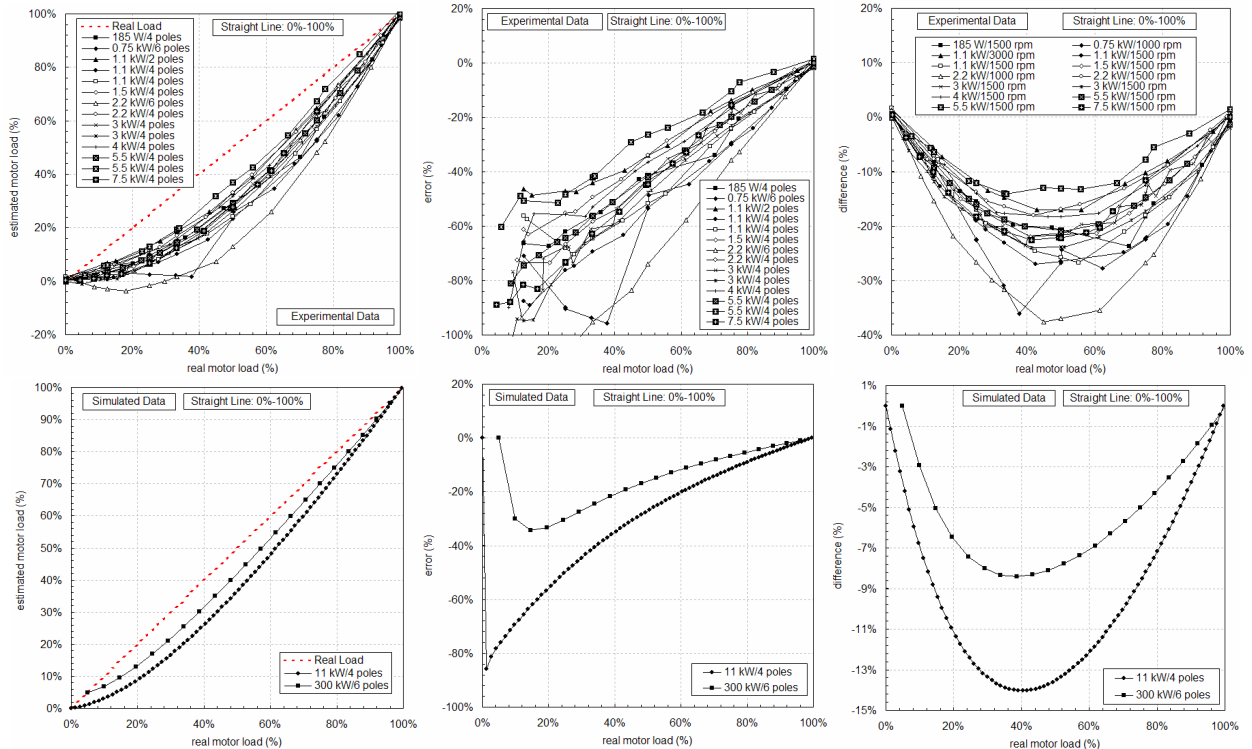


Fig. 4.29. Current-based method: actual and estimated motor load and the respective error (in %) and difference (in p.p.) for different motors, approximating the current curve as a function of load by one segment - no-load (zero load, no-load current) and full-load points segment.

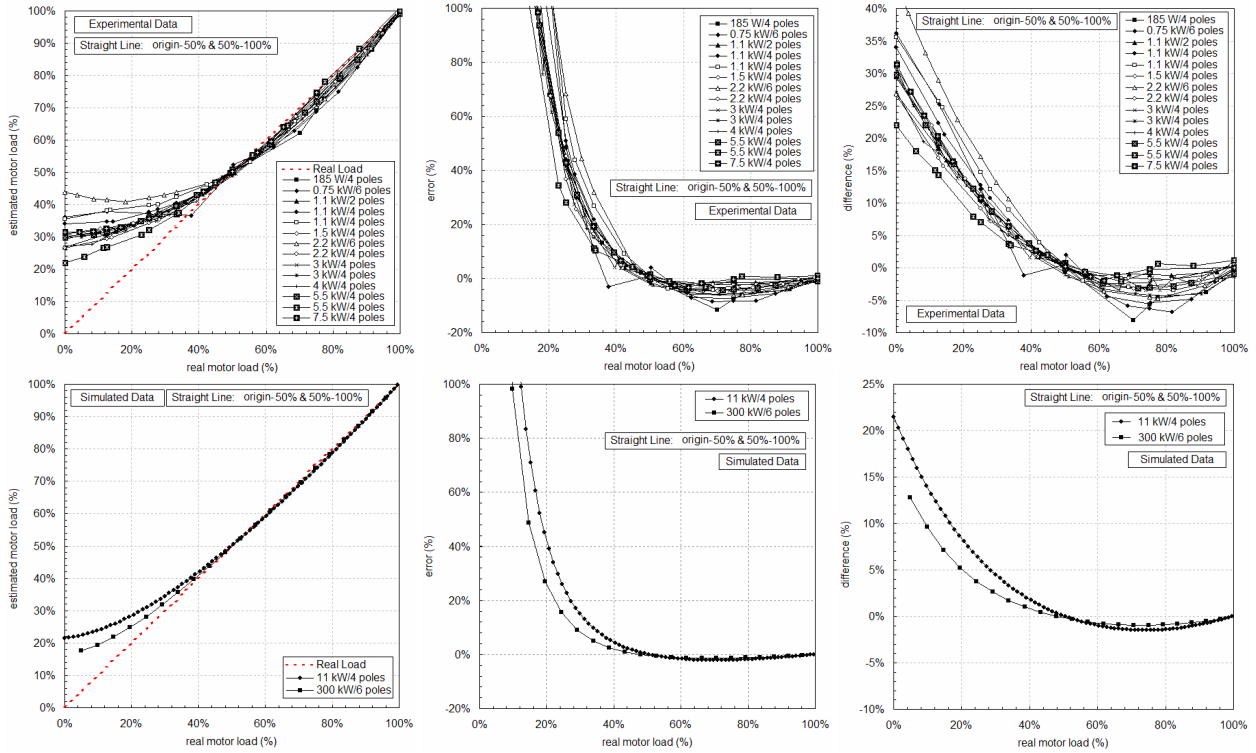


Fig. 4.30. Current-based method: actual and estimated motor load and the respective error (in %) and difference (in p.p.) for different motors, approximating the current curve as a function of load by two segments - origin-50% and 50%-100% load points segments.

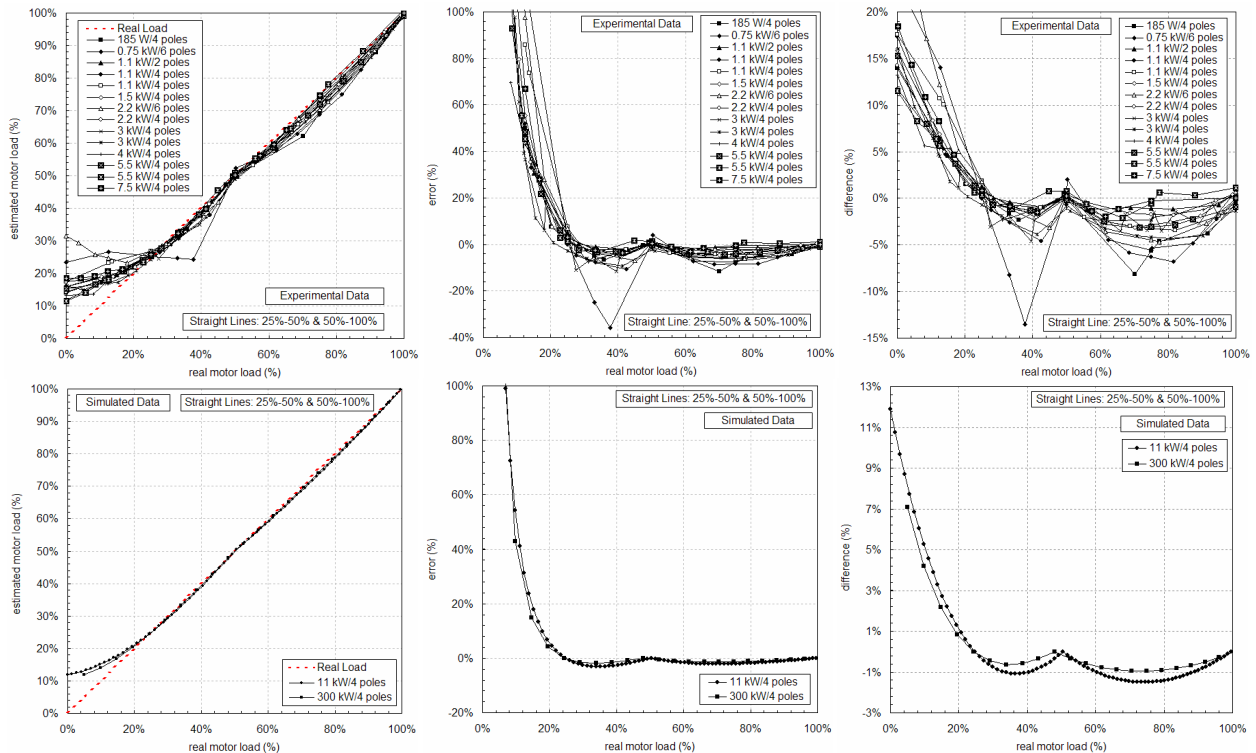


Fig. 4.31. Current-based method: actual and estimated motor load and the respective error (in %) and difference (in p.p.) for different motors, approximating the current curve as a function of load by two segments - 25%-50% and 50%-100% load points segments.

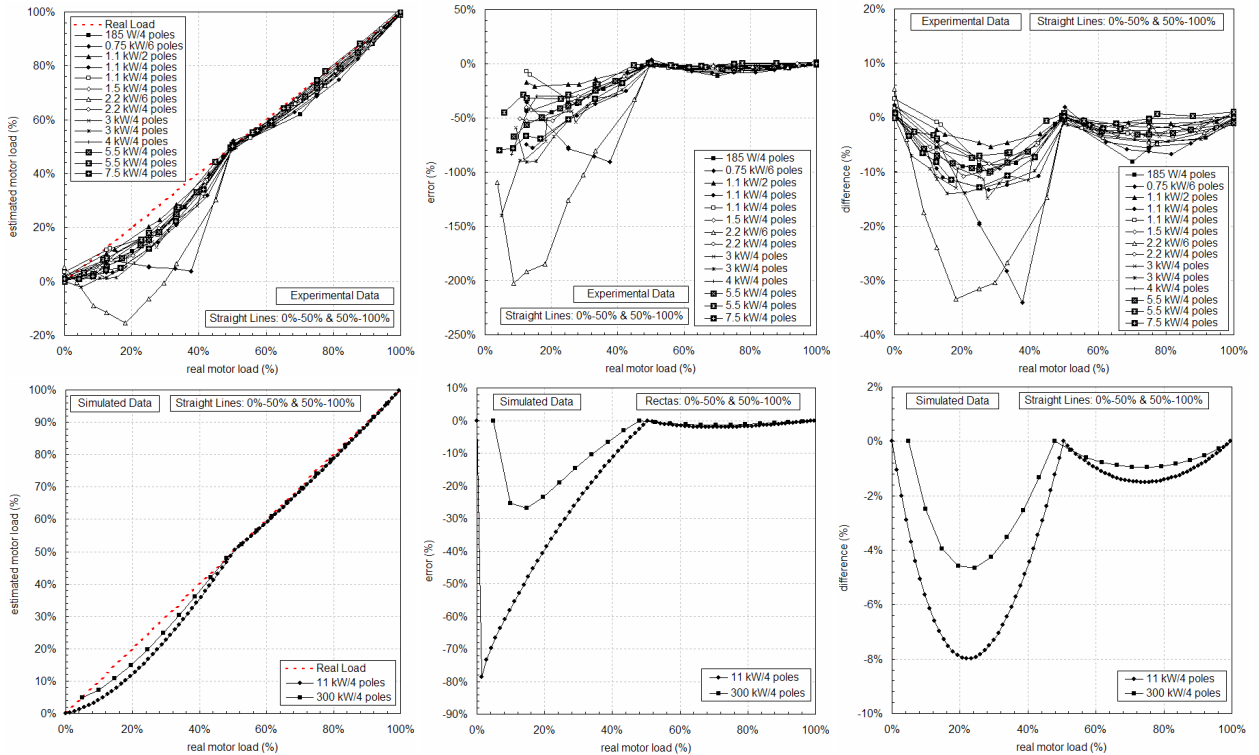


Fig. 4.32. Current-based method: actual and estimated motor load and the respective error (in %) and difference (in p.p.) for different motors, approximating the current curve as a function of load by two segments - 0%-50% and 50%-100% load points segments.

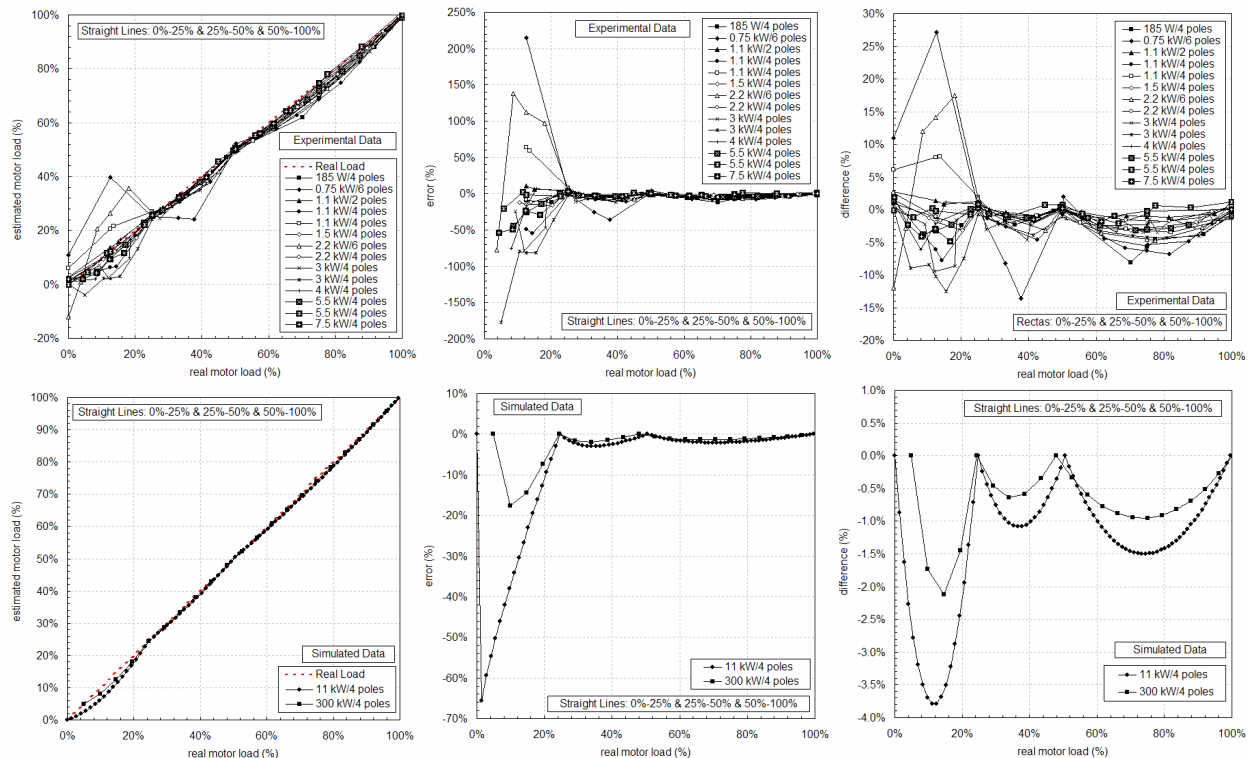


Fig. 4.33. Current-based method: actual and estimated motor load and the respective error (in %) and difference (in p.p.) for different motors, approximating the current curve as a function of load by three segments - 0%-25%, 25%-50% and 50%-100% load points segments.

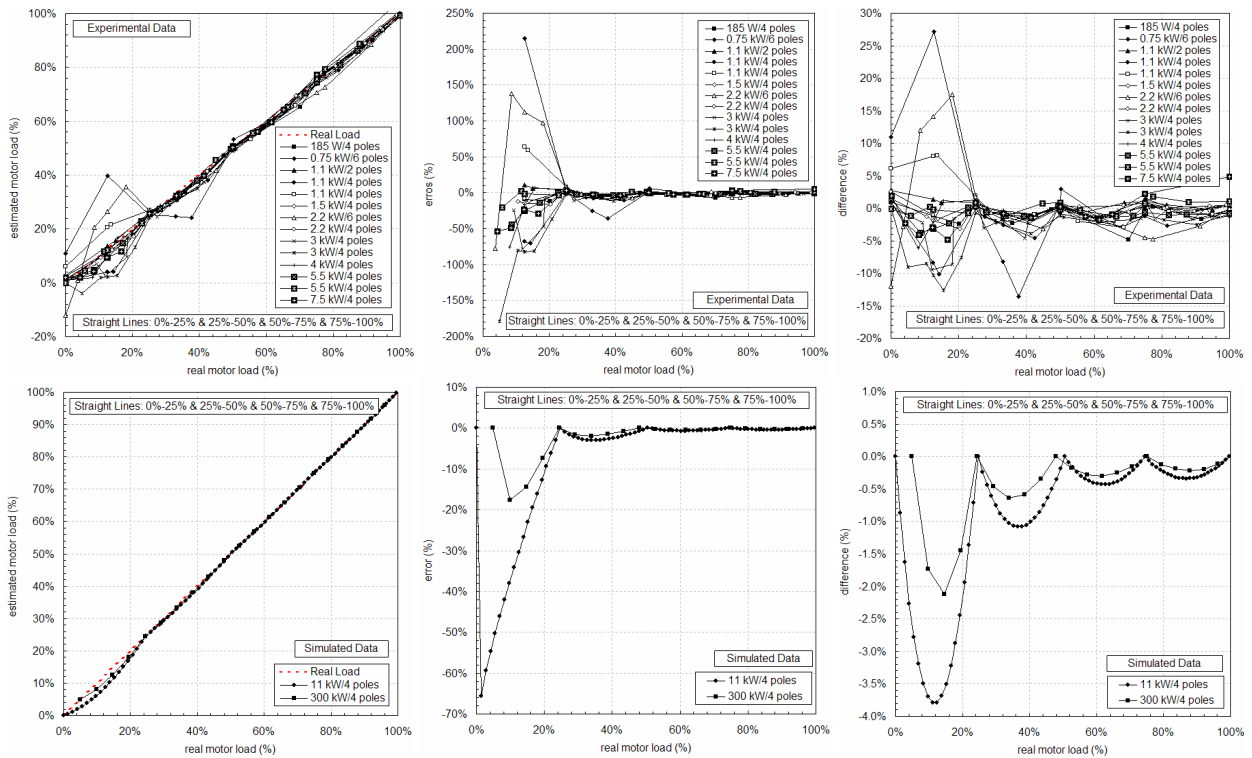


Fig. 4.34. Current-based method: actual and estimated motor load and the respective error (in %) and difference (in p.p.) for different motors, approximating the current curve as a function of load by four segments - 0%-25%, 25%-50%, 50%-75% and 75%-100% load points segments.

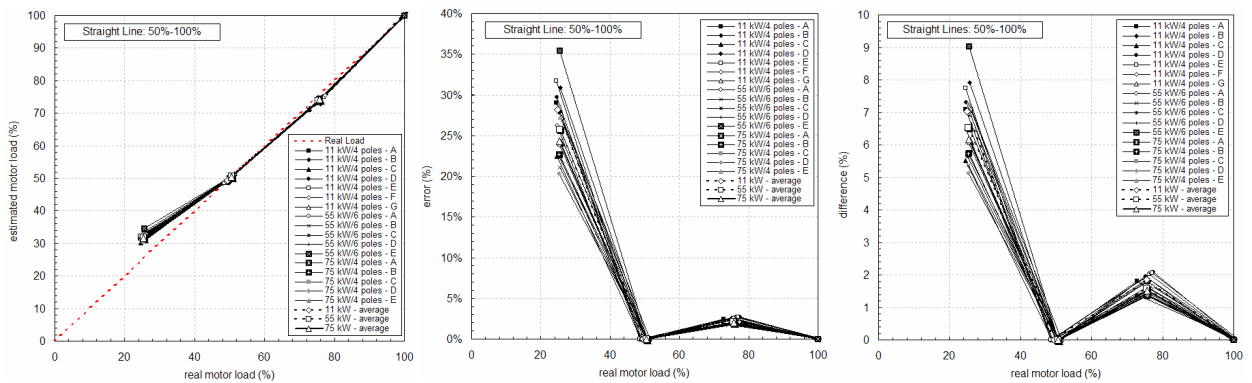


Fig. 4.35. Current-based method: experimental actual and estimated motor load and the respective absolute error (in %) and difference (in p.p.) for 11-kW/4-pole, 55-kW/6-pole and 75-kW/4-pole motors (data extracted from [22]), approximating the current curve as a function of load by one segment - half-load to full-load points segment.

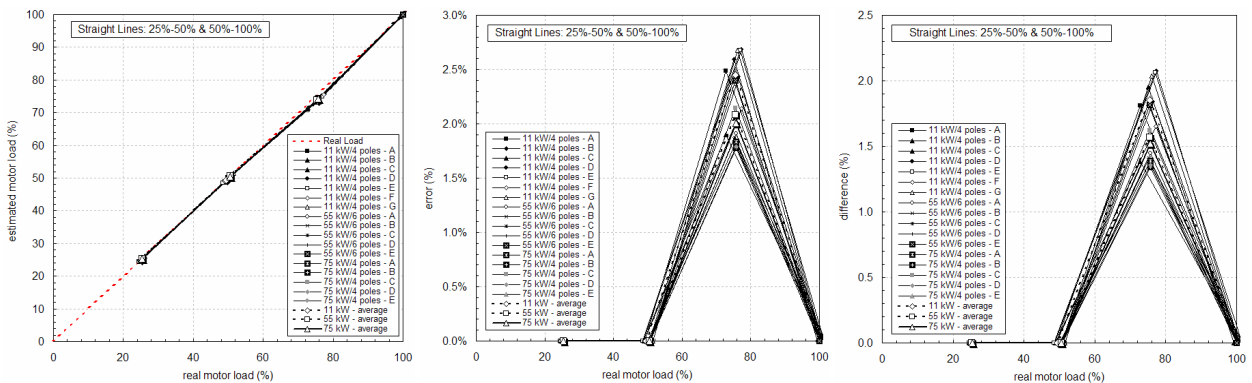


Fig. 4.36. Current-based method: experimental actual and estimated motor load and the respective absolute error (in %) and difference (in p.p.) for 11-kW/4-pole, 55-kW/6-pole and 75-kW/4-pole motors (data extracted from [22]), approximating the current curve as a function of load by two segments - 25%-50% and 50%-100% load points segments.

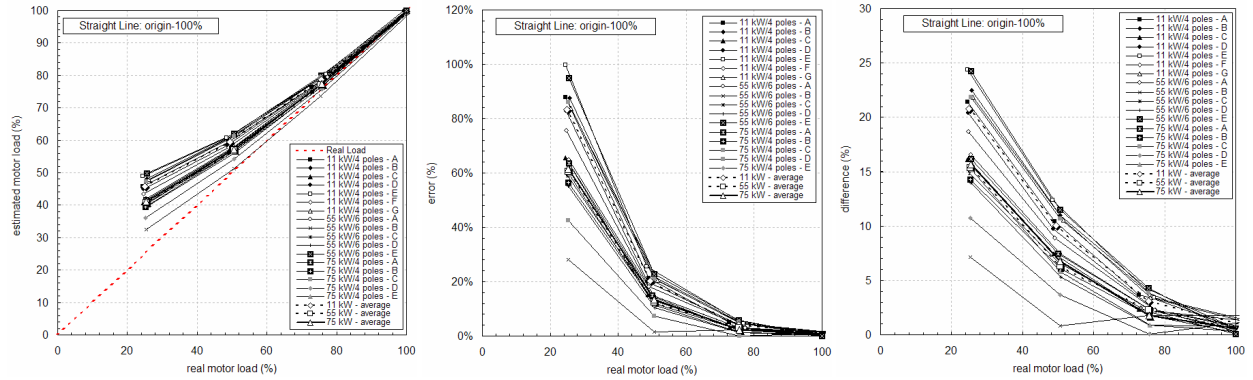


Fig. 4.37. Current-based method: experimental actual and estimated motor load and the respective absolute error (in %) and difference (in p.p.) for 11-kW/4-pole, 55-kW/6-pole and 75-kW/4-pole motors (data extracted from [22]), approximating the current curve as a function of load by one segment - origin to full-load points segment.

An experimental example of this is presented in Fig. 4.39, in which the delta- and star-connection line currents are described and represented by a 2nd order polynomial curve, presenting an excellent matching with the experimental points over all load range.

The comparison between the current-based methods expectable errors and the useful accuracy is shown in Fig. 4.38, being possible to conclude that each method scheme as its own load range for a fair accuracy.

In Figs. 4.45 and 4.47 experimental results and the average difference and error as a function of the motor load for the presented experimental data are shown.

In general, the current-based method is indicated for medium/large motors (power higher than 30 kW) and a pole number up to 4, with a fair accuracy even for loads as low as 20-25%. Of course, that depends on the number of intermediate points considered. Table 4.1 presents a summary of the proposed current-based method application strategy, taken into account the foregoing discussion.

It is now proposed the use of the star connection, when applicable, to improve the current-based method. The theoretical relation between the no-load current for the star and delta connections, ignoring saturation, is approximately 0.33, but, on the basis of experimental data (inherently with saturation effects), the average is about 0.26, depending on motor characteristics (e.g., the motor presented in Fig. 4.39 has a relation of 0.24). Therefore, using the average for the analysed universe, the star no-load line current is considered to be equal to the delta no-load approximate line current value divided by 3.85 (if possible a quick no-load test in star can also be made). It is proposed the use of an exponential curve between 0% and 33% load for star connection, and the respective line current at 33% load obtained dividing the delta connection line current at 33% load by $\sqrt{3}$ (or the full-load delta connection current by 3). Once more, saturation effect is ignored. Of course, more accurate values can be used, for example, interpolated from the curves in Fig. 4.23 and 4.27. The 33% load current value for delta connection can be estimated by interpolation using

the straight lines $a-b$ for 25-50% or 0-50% load points, according to (4.15), or by extrapolation using the straight lines 0-25%, 50-75%, or 50-100% load.

$$I_{33\%} = \frac{(\zeta_{33\%} - \zeta_a) \cdot (I_b - I_a)}{\zeta_b - \zeta_a} + I_a \quad (4.15)$$

It is also important to underline that, after connection change, the new motor load also changes as a function of the load torque-speed curve. Therefore, different load types (e.g., constant, linear, and quadratic torque loads) lead to different new loads, being this phenomenon a source of error, although, in practice, for the purposes being considered, it can be ignored.

TABLE 4.1
APPLICATION STRATEGY FOR CURRENT-BASED MOTOR LOAD ESTIMATION METHOD.

poles	power range	motor load	recommended interpolation segments	
			recommended	at least
6 & 8	≤ 5 kW	≥ 50%	50-75% & 75-100%	50%-100%
6 & 8	[7.5 kW 75 kW]	≥ 33%	0-25% & 25-50% & 50-75% & 50-100%	0-25% & 25-50% & 50-100%
6 & 8	[75 kW 550 kW]	≥ 0%	0-25% & 25-50% & 50-100%	0-100%
6 & 8	> 550 kW	≥ 0%	0-100%	0-100%
4	≤ 5 kW	≥ 33-50%	50-75% & 75-100%	50-100%
4	[7.5 kW 75 kW]	≥ 33%	0-25% & 25-50% & 50-75% & 50-100%	0-25% & 25-50% & 50-100%
4	[75 kW 550 kW]	≥ 0%	0-25% & 25-50% & 50-100%	0-100%
4	> 550 kW	≥ 0%	0-100%	0-100%
2	≤ 5 kW	≥ 0%	50-75% & 75-100%	50-100%
2	[7.5 kW 75 kW]	≥ 0%	0-25% & 25-100%	0-25% & 25-50% & 50-100%
2	[75 kW 550 kW]	≥ 0%	0-25% & 25-50% & 50-100%	0-100%
2	> 550 kW	≥ 0%	0-100%	0-100%

After the calculation or estimation of no-load and 33% load currents for star-connection mode, the respective current-load curve can be approximately described by an exponential curve, according to (4.16).

$$I_{Y(0-33\%)} = A \cdot e^{B \cdot \zeta} \quad (4.16)$$

Note that a solution of the form $I = A \cdot \zeta^2 + B \cdot \zeta + C$ (2nd order polynomial curve) is slightly more accurate for the purpose being discussed, but requires 3 equations to find the constants A , B , and C . Using (4.16) only 2 equations are needed. Solving (4.16) in order to the motor load, results (4.17).

$$\zeta = \frac{1}{B} \ln \left(\frac{I_{Y(0-33\%)}}{A} \right) \quad (4.17)$$

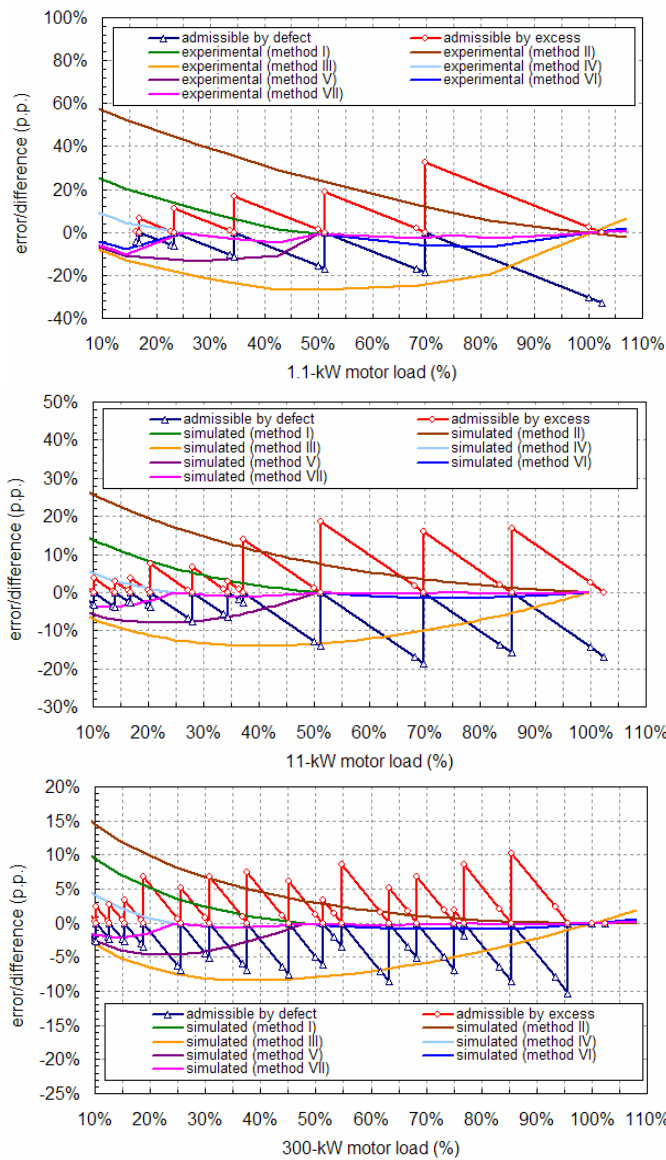


Fig. 4.38. Superposition of the error or difference (in p.p.) associated with current-based methods and the useful accuracy (in p.p.), for 1.1-kW (experimental), 11-kW (simulated), and 300-kW (simulated) motors. Method I: origin-50% & 50%-100% load points segments; Method II: origin-100% load points segment; Method III: no-load-100% load points segment; 25%-50% & 50%-100% load points segments; Method IV: 0-50% & 50%-100% load points segments; Method V: 0-50% & 50%-100% load points segments; Method VI: 0-25% & 25-50% & 50-100% load points segments; Method VII: 0-25% & 25-50% & 50-75% & 75%-100% load points segments.

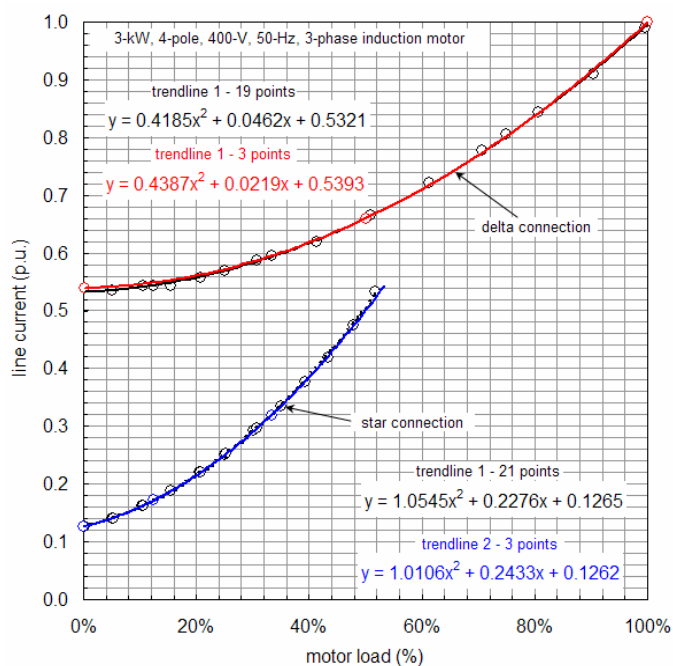


Fig. 4.39. Mathematical description of the line current for a 3 kW, 4-pole IM operating in star and delta connection modes.

The constants A and B are calculated on the basis of the two current values, according to (4.18).

$$\begin{cases} I_{0\%} = A \cdot e^{B \cdot 0.00} \\ I_{33\%} = A \cdot e^{B \cdot 0.33} \end{cases} \Leftrightarrow \begin{cases} A = I_{0\%} \\ B = 3 \cdot \ln\left(\frac{I_{33\%}}{I_{0\%}}\right) \end{cases} \quad (4.18)$$

In Fig. 4.49, an experimental example of application of the exponential and polynomial curves for star connection is presented, evidencing that both results are very similar.

In the case of the 0%-33% load points straight line for star connection, it should be used (4.19).

$$\zeta_i \approx 0.33 \cdot \frac{(I_{\text{mea}_Y} \cdot U_{\text{mea}} \cdot U_N^{-1}) - I_{0\%_Y}}{I_{33\%_Y} - I_{0\%_Y}} \quad (4.19)$$

Similarly, in the case of the origin-33% load points straight line for star connection, it should be used (4.20).

$$\zeta_i \approx 0.33 \cdot I_{\text{mea}_Y} \cdot U_{\text{mea}} \cdot U_N^{-1} \cdot I_{33\%_Y}^{-1} \quad (4.20)$$

In the case of the origin-100% points load straight line for delta connection, if the load is lower than 33%, it can be directly related to the relation between the star current and the rated current, according to (4.21), being the error at low load significantly reduced in relation to the method using only delta connection, as it can be seen in Figs. 4.39 and 4.44.

$$\zeta_i \approx I_{\text{mea}_Y} \cdot U_{\text{mea}} \cdot U_N^{-1} \cdot I_N^{-1} \quad (4.21)$$

In fact, the last proposed method is quite simple and leads to fair results for motors with a power equal or higher than 11 kW.

By means of the proposed schemes, it is possible to reduce the errors associated to the current-based method for loads lower than 33%, which is the load range in which the method is more inaccurate or even impossible to apply due to the very reduced slope or derivative of the curve. For 2- and 4-pole motors larger than 30-55 kW, this method can be applied in its simplest form (without star connection use) without significant errors for loads higher than 20-25%.

If the known points are not sufficient, average values can be used, as a function of the motor power range and its number of poles, as presented in Fig. 4.27. In general, it is also necessary to limit the use of the method for situations in which the current does not vary significantly with the

load, which happens, for example, for loads lower than 20-25% in the case of motors with a number of poles higher than 2, being, in these cases, impossible (using only rated connection) to estimate the load through the current. In these cases, only an operation range can be defined, i.e., if the motor load is lower than a certain value. It should be noted that the change from delta to star connection mode can solve this issue, because increases the current variation as a function of load for low loads.

The use of the star connection can be justified by the importance of the motor, and the connection change is a simple and quick task if the motor has already a star-delta starting system¹².

In these cases, if a load lower than 30-50% is identified, the connection mode can be changed to star, decreasing the line current, allowing the application of (4.21). In the delta connection, the no-load, 50% load and full-load points were considered. In the star connection, the no-load, 12.5% load and 33% load points were considered.

But the major advantage of this strategy is the increase of the current variation as a function of motor load for loads between 16.7% and 33.3%, particularly for motors up to 30-50 kW, independently of the number of poles. In fact, without introducing significant errors, it is also possible to represent approximately the current-load curve by a straight line between 16.7% and 33.3% load, corresponding the star connection line current at 16.7% load to roughly $\frac{1}{3}$ of the delta line current at 50% load.

In Figs. 4.40-4.48, experimental and simulated results are presented on estimated motor load and error associated with delta/star-connection current-based methods. In Figs. 4.46 and 4.48, the average difference and error as a function of the motor load are shown for the data presented in Figs. 4.45 and 4.47, respectively.

This novel methodology allows extending the application range or increase the accuracy of the method for low power motors and/or with a pole number higher than 2, but it can be applied to all motors with a load lower than 50% as a complementary method. Besides that, allows the most advantageous connection to be identified, as a function of the motor load, as discussed in Chapter 5. Obviously, as previously referred, due to the fact that the delta-star change leads to a reshape of the torque-speed curve, it is necessary to take into account the reduction of the required power by the load as a result of the slip increase (except for constant power loads). However, if the type of load is known, the load can be easily compensated using the classical mathematical descriptions.

¹² Nowadays, in fixed-speed motors (fed by fixed-frequency supply, without speed control), the Y/D starting method is being replaced by the use of electronic soft-starters or voltage regulators.

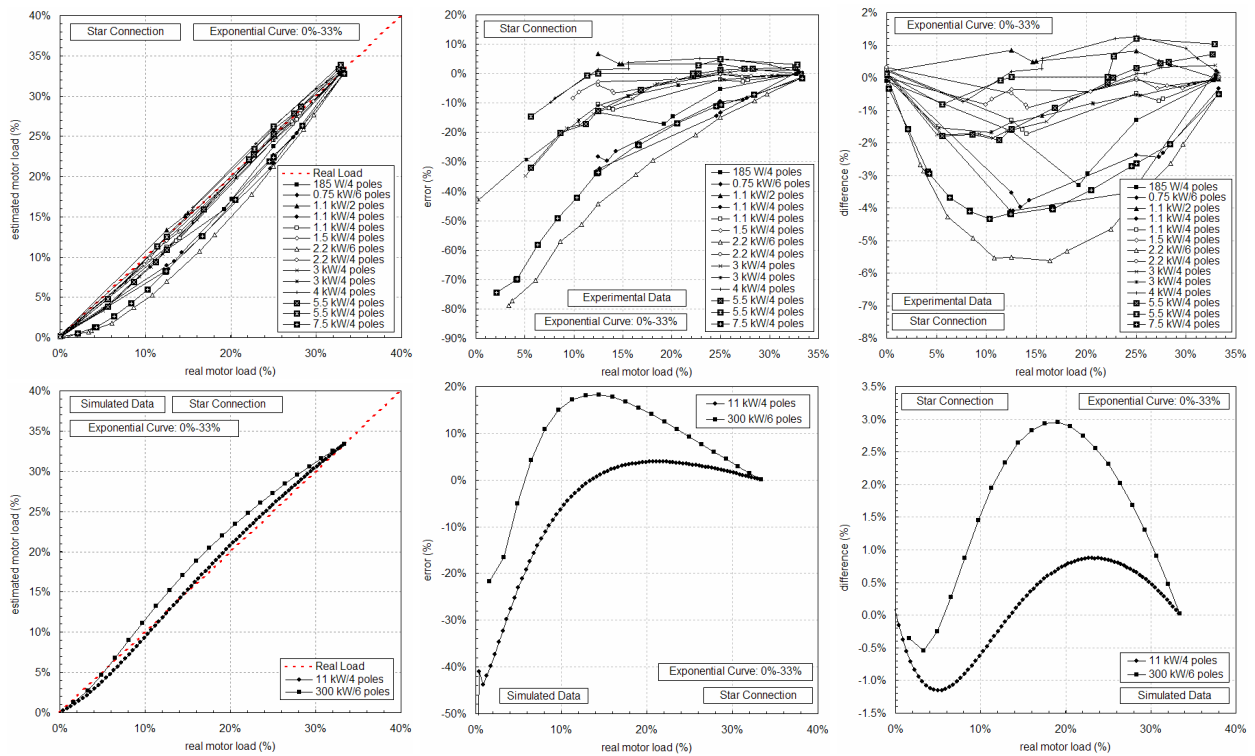


Fig. 4.40. Current-based method: actual and estimated motor load and the respective error (in %) and difference (in p.p.) for different motors, approximating the current curve as a function of load by an exponential curve from 0% to 33% load (star connection), according to (4.16).

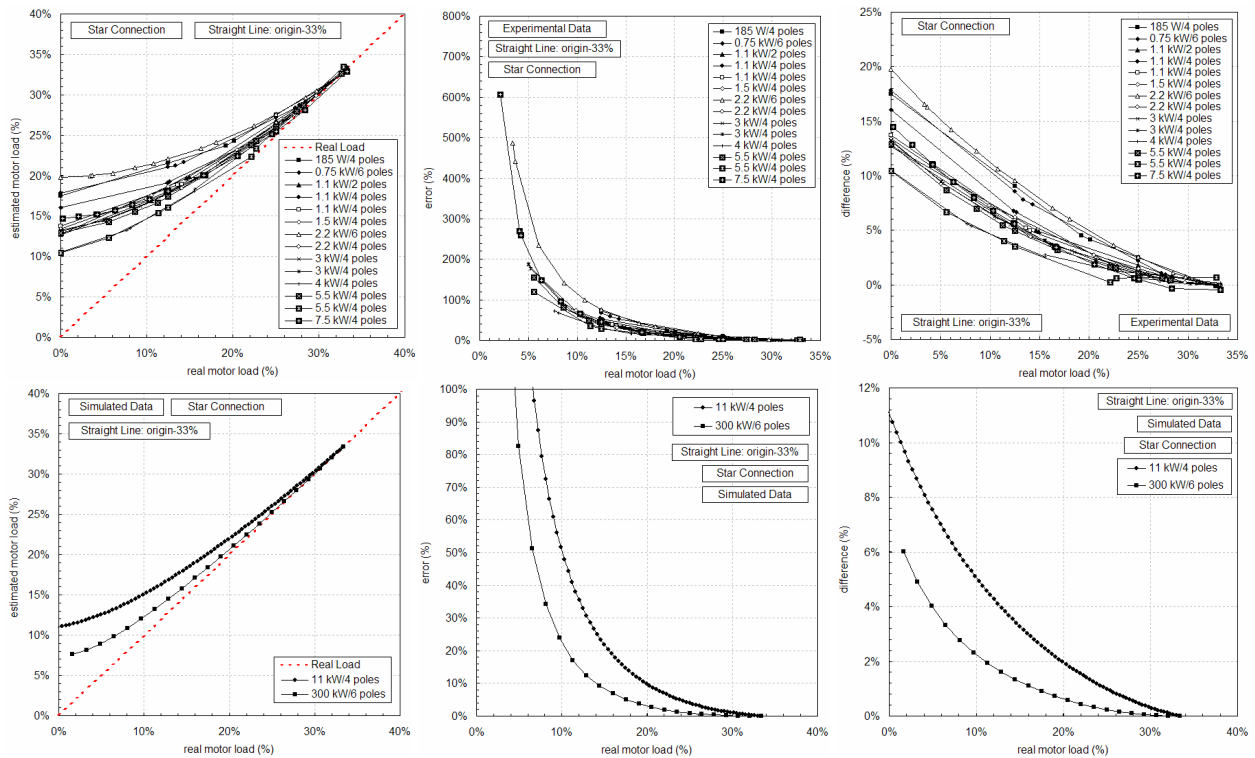


Fig. 4.41. Current-based method: experimental actual and estimated motor load and the respective error (in %) and difference (in p.p.) for different motors, approximating the current curve as a function of load by one segment - origin and 33% load points segment. Motor connected in star mode.

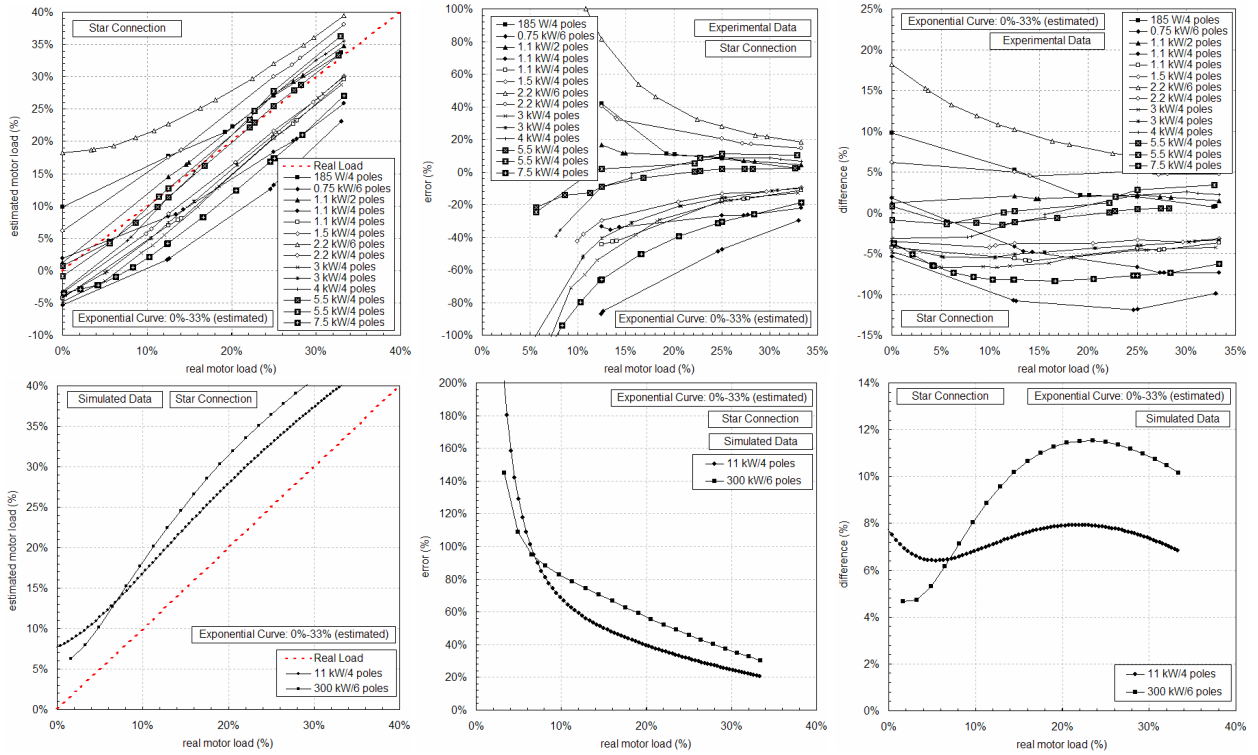


Fig. 4.42. Current-based method: experimental actual and estimated motor load and the respective error (in %) and difference (in p.p.) for different motors, approximating the current curve as a function of load by an exponential curve from 0% to 33% load, according to (4.16). Current at 33% load estimated. Motor connected in star mode.

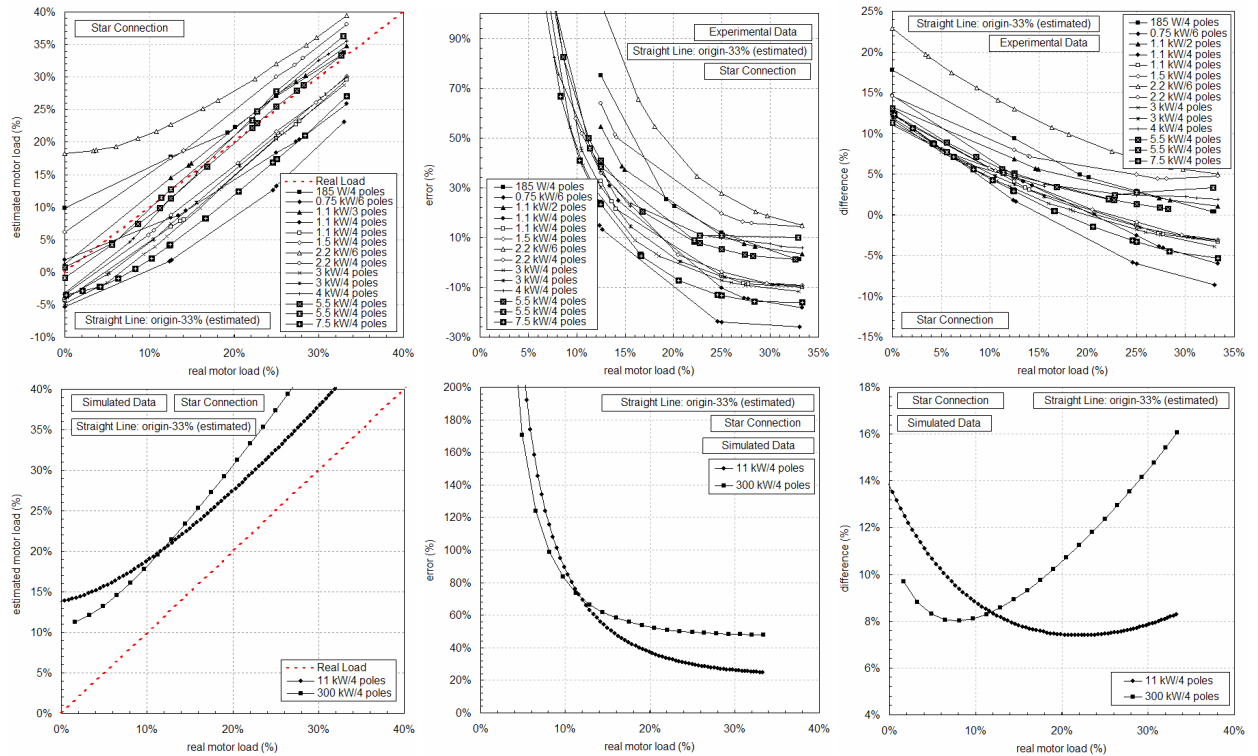


Fig. 4.43. Current-based method: experimental actual and estimated motor load and the respective error (in %) and difference (in p.p.) for different motors, approximating the current curve as a function of load by one segment - origin and 33% load points segment. Current at 33% load estimated. Motor connected in star mode.

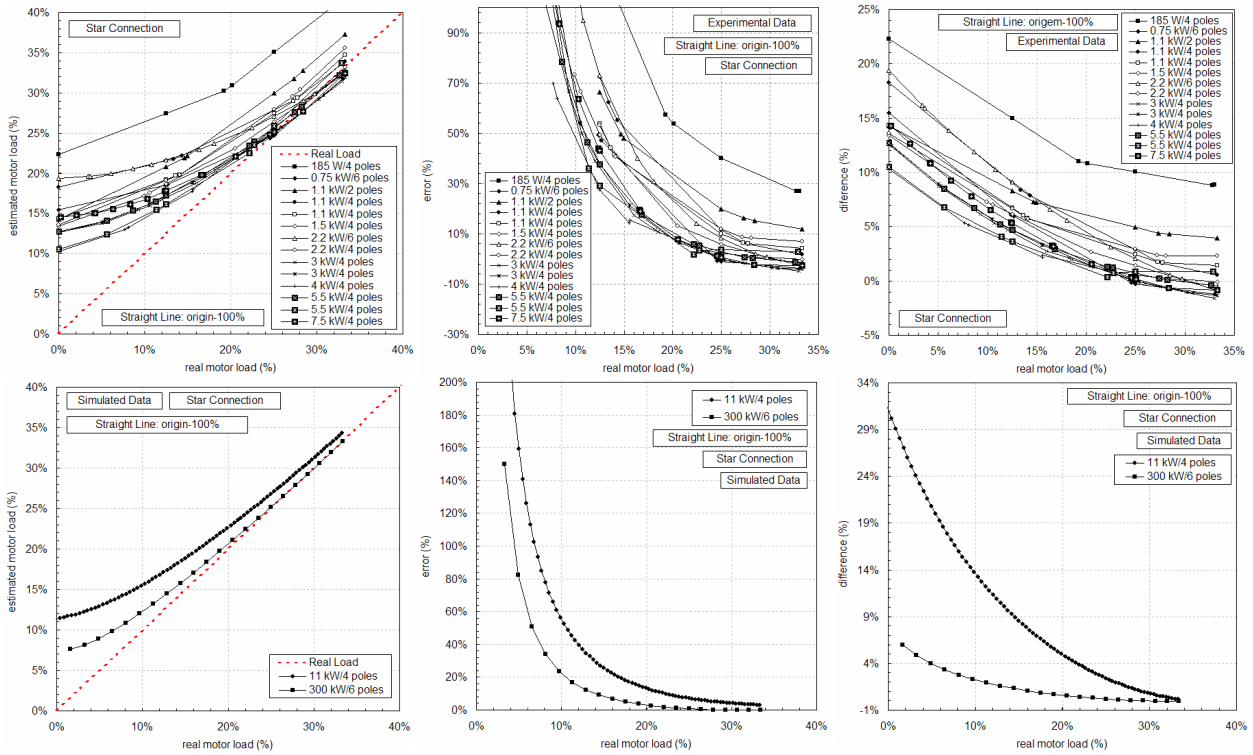


Fig. 4.44. Current-based method: experimental actual and estimated motor load and the respective error (in %) and difference (in p.p.) for different motors, approximating the current curve as a function of load by one segment - origin and 100% load points segment. Motor connected in star mode.

On the basis of the foregoing discussion, for the star connection the segment between 16.7 and 33% load points can be defined by (4.22). The line current in star connection at 16.7% load is approximately one sixth of the nominal line current in delta connection. The line current in star connection at 33% load is approximately one third of the nominal line current in delta connection.

$$\zeta_{i_y} \approx 0.167 + (0.33 - 0.167) \cdot \frac{(I_{mea_Y} \cdot U_{mea} \cdot U_N^{-1}) - I_{Y(16.7\%)}}{I_{Y(33\%)} - I_{Y(16.7\%)}} \quad (4.22)$$

As a way to resume the described concept, a set of relations useful for decision is presented in Table 4.2. Note that, if the connection change load limit is increased to 50%, the error between 33% and 50% load is considerably reduced, as it can be seen in Fig. 4.39. The star/delta values relation can also be used to estimate or confirm the estimated load.

In order to clarify the understanding of the proposed concept, it is presented in Fig. 4.49 the star and delta current for a 3-kW, 4-pole motor, as well as the considered approximations. Between 33% and 50% load, the star connection current is quasi-linear. If the 50% load limit is used, there is no dangerous for the motor since the resultant winding current is lower than the rated winding current. For star connection, two straight segments can be used (0-16.7% & 16.7-30/50% load points), and for delta connection, one or two straight segments can be used (30/50-100% or 50-75% & 75-100%).

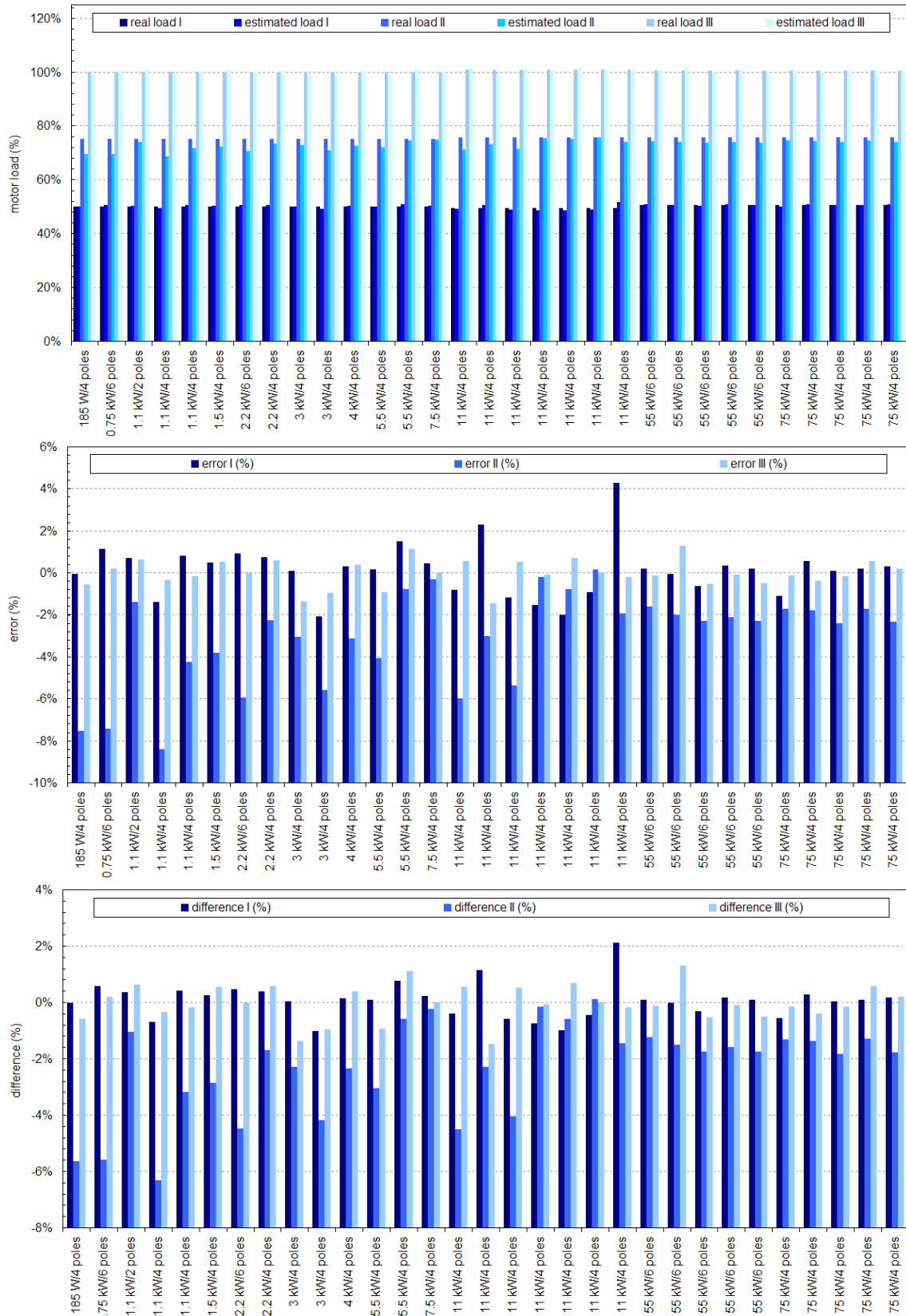


Fig. 4.45. Current-based method: experimental actual and estimated motor load and the respective error (in %) and difference (in p.p.) for different delta-connected motors and three load levels ($\approx 25\%$, $\approx 50\%$ and $\approx 75\%$), approximating the current curve as a function of load by two segments - 25%-50% and 50%-100% load points segments.

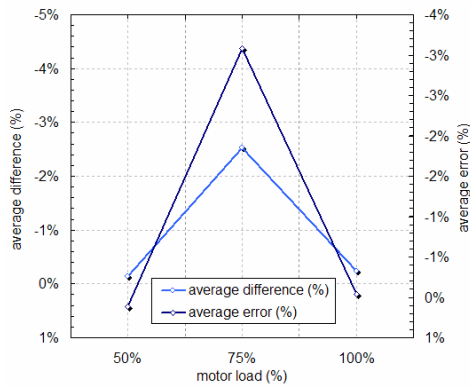


Fig. 4.46. Average difference (in p.p.) and error (in %) for the data presented in Fig. 4.45.

TABLE 4.2
LINE CURRENT-BASED METHOD WITH STATOR-WINDING CONNECTION CHANGE.

IF	OR	THEN	ACTION
$I_{\sqrt{3}}/I_d \approx 1/\sqrt{3}$	$I_{\sqrt{3}}/I_{dN} \approx 1/3$	$\zeta \approx 33\%$	Confirmed.
$I_{\sqrt{3}}/I_d \approx 1/\sqrt{2}$	$I_{\sqrt{3}}/I_{dN} \approx 1/2$	$\zeta \approx 50\%$	Confirmed.
$I_{\sqrt{3}}/I_d < 1/\sqrt{3}$	$I_{\sqrt{3}}/I_{dN} < 1/3$	$\zeta < 33\%$	Use star connection.
$1/\sqrt{3} < I_{\sqrt{3}}/I_d < 1/\sqrt{2}$	$1/3 < I_{\sqrt{3}}/I_{dN} < 1/2$	$33\% < \zeta < 50\%$	Use star connection.
$I_{\sqrt{3}}/I_d > 1/\sqrt{2}$	$I_{\sqrt{3}}/I_{dN} > 1/2$	$\zeta > 50\%$	Use delta connection.
$I_{\sqrt{3}}/I_d \approx 1/3$	$I_{\sqrt{3}}/I_{dN} \approx 1/9$	$\zeta < 10\%$	Confirmed.

Therefore, for load estimation purposes, the motor connection can be changed to star during a short time period (significantly lower than motor thermal time constant). If possible, compensation as a function of the load type should be made.

In this method there is an error associated with the rated voltage and current values, but since it is typically relatively low in relation to other error sources, it can be ignored.

4.8 Power Factor-Based Motor Load Estimation Method

When the motor power factor is known, it can be used to estimate the motor load, if some part-load values are known. Typically, in the manufacturers catalogues the power factor can be found for 100%, 75% and 50% load, being common to find in motor databases the values for 25% load. The no-load power factor can be estimated by no-load test, and, if not possible, it can be assumed as 10% of rated value (typical value). Although not being proposed by the main references, it can be effectively used for the motor load estimation. In relation to the current-based method, the power-factor-based method can be used for low loads because, contrarily to the current, the power factor vary significantly with motor load, even for very low loads. Fig. 4.50 shows the average values of the motor power factor as a function of load. In Fig. 4.51, the rated power factor as a function of motor rated power can be seen. In Fig. 4.52, the average values for the rated power factor as a function of motor rated power are shown. As referred before, the standard IEC 60034-1 states a specific tolerance for power factor¹³.

¹³ For example, for a rated power factor of 0.8, the tolerance is $\pm 0.2/6$ giving ± 0.0333 , i.e., the actual power factor can vary until $0.8 - 0.0333 = 0.7667$, being the maximum error admissible 4% for the considered value.

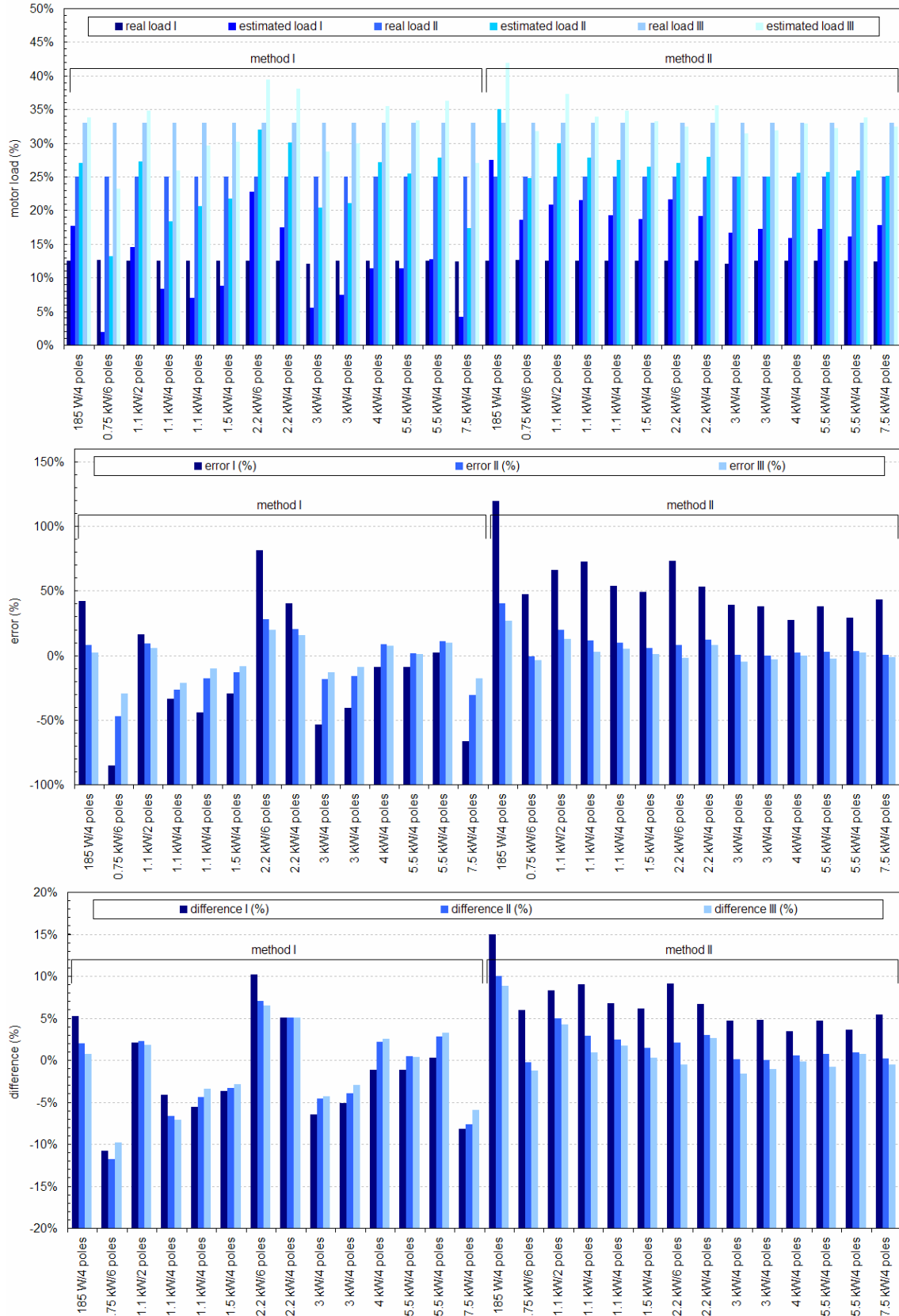


Fig. 4.47. Two different current-based methods: experimental actual and estimated motor load and the respective error (in %) and difference (in p.p.) for different star-connected motors and three load levels ($\approx 25\%$, $\approx 50\%$ and $\approx 75\%$), approximating the current curve as a function of load by an exponential curve from 0% to 33% load, with the 33% load current estimated (method I) and by one segment from origin to 100% load (method II).

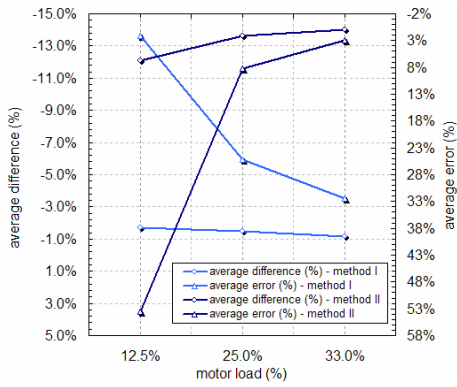


Fig. 4.48. Average difference (in p.p.) and error (in %) for the data presented in Fig. 4.47.

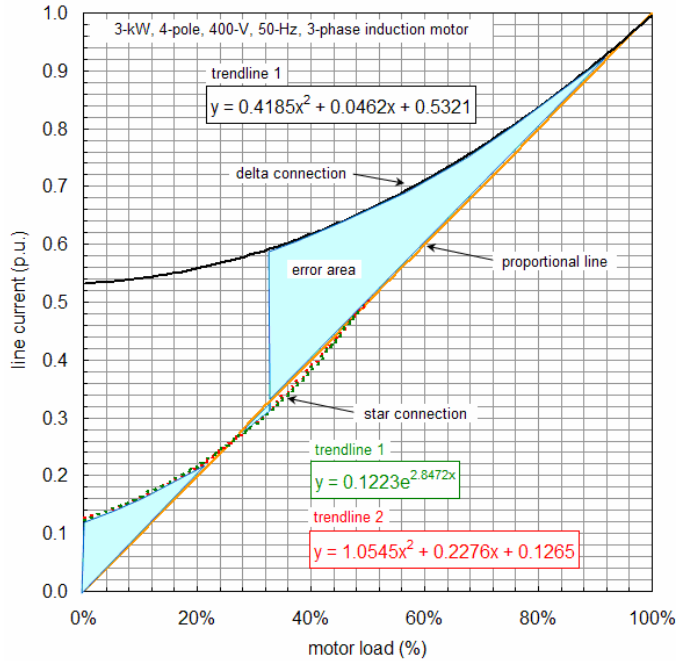


Fig. 4.49. Mathematical representation of the line current for star and delta connections for a 3-kW, 4-pole motor, and the resulting error area when using both connections to estimate motor load considering only one straightline from origin to full load.

Note that the power factor is not directly measured, but rather is computed from the current and voltage signals (either by analogue or digital means). There are fundamentally two means for making the calculation: a) by the ratio of real to apparent power, and b) by a zero-crossing detector. The first method provides a “true” measure of the effective power factor over the full cycle and, in practice, can be applied using a digital wattmeter. The second method is normally employed by digital phase angle meters, which compare the time between the instant of zero crossing for two signal waveforms (voltage and current), not taking into account the harmonic distortion. The power factor can be easily obtained with a handheld oscilloscope (in the absence of significant current and voltage distortion and/or unbalance values), or with a digital wattmeter. For standard induction motors running directly from the line, the two methods will normally closely agree, unless there is considerable harmonic or other spectral content in the voltage and/or current.

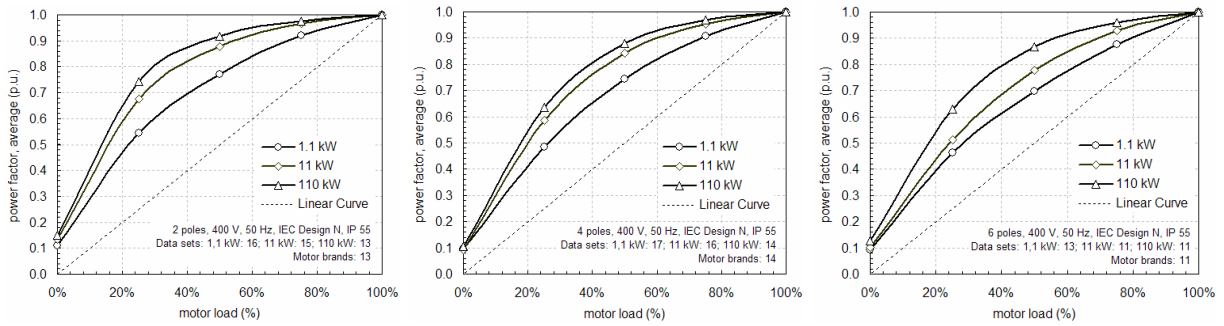


Fig. 4.50. Average power factor as a function of load for 1.1-kW, 11-kW and 110-kW motors, with 2, 4, and 6 poles.

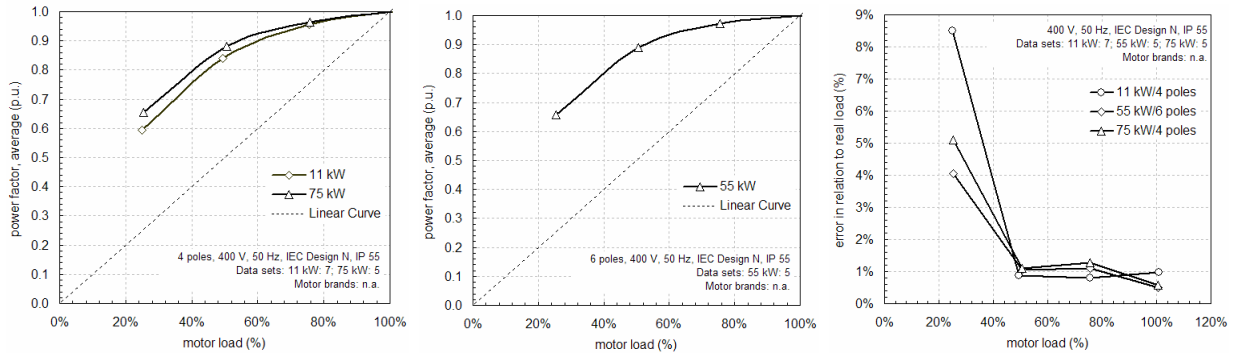


Fig. 4.51. Average power factor as a function of load for 11-kW/4-pole, 55-kW/6-pole and 75-kW/4-pole motors.

Then, it is possible to estimate the motor load comparing the measured power factor and an interpolation-based power factor (using 5 points: 0%, 25%, 50%, 75%, and 100% load points), according to (4.23), which includes a correction as a function of the voltage level (which is not exact, but reduces the error), and subscripts a and b correspond to the lower and higher load levels of each segment considered in the interpolation (4 straight segments), respectively.

$$\zeta_{\lambda} \approx \zeta_a + (\zeta_b - \zeta_a) \cdot \frac{(\lambda_{mea} \cdot U_{mea} \cdot U_N^{-1}) - \lambda_a}{\lambda_b - \lambda_a} \quad (4.23)$$

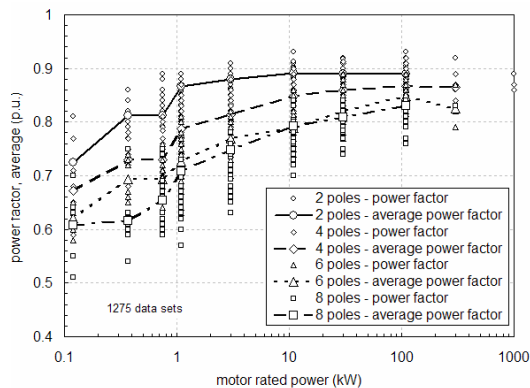


Fig. 4.52. Average values for the rated power factor as a function of motor rated power. Data extracted from [20].

This method can be time consuming and, in some cases, it is not possible to apply, but it can be applied over all load range, rated powers and number of poles. If the no-load test cannot be carried out, the no-load power factor can be asked to the manufacturer. Otherwise, it is possible to limit the

application of the method to the range corresponding to the available power factor values. At least, the full-load and half-load power factors are available in the vast majority of motor catalogues and/or databases. Alternatively, empirical average values can be used.

With the recent vulgarization of the digital handheld wattmeters, it is possible to determine the power factor quickly, accurately and economically (being the error negligible). The main error source is the rated value tolerance allowable by the standards. However, since the equipment necessary to apply this method is identical to that required for the real power-based method, it is preferable to apply the latter, since it is much more accurate, and does not require necessarily part-load points, as it is explained in the next section.

4.9 Input Power-Based Motor Load Estimation Method

The motor input real (or active) power can also be used to estimate its load. The input power-based motor load estimation method is proposed in some technical texts [4], but no accuracy analysis was carried out. In this method, the input power is compared to the nameplate-based rated input power, according to (4.24). For that purpose a three-phase wattmeter, two single-phase wattmeters (as in [13]) or, in the absence of unbalances, one single-phase wattmeter can be used. For example, the Metrix PX 120 handheld single-phase wattmeter has an accuracy of 1% for the real power, 3% for the power factor, and 0.5% for the voltage and current measurement [22]. The single-phase wattmeters are considerably cheaper than three-phase wattmeters. Some manufacturers provide adapters for easy application of the two-wattmeter method using one single-wattmeter [22]. In such devices, since the current is measured by means of a clamp-on current probe or an internal current transducer plus current transformer (if necessary), which is to be used in conjunction with the measured voltage (by means of a sensor/probe), there is a phase error (typically $\approx 1.5^\circ$, leading) that can affect the real power and power factor calculation, as explained before. Generally, the higher the power factor is, the lower the error will be. Note that, if the current is being used for its own measurement only, the phase error is of no consequence.

$$\zeta_p \approx \frac{P_{in(meas)}}{P_N} \cdot \eta_N = \frac{P_{in(meas)}}{P_{in_N}} = \frac{P_{in(meas)}}{U_N \cdot I_N \cdot \lambda_N \cdot \sqrt{3}} \quad (4.24)$$

The error associated with (4.24) is mainly due to the slight non-proportionality between the load and the real power, as it can be seen in Figs. 4.53 and 4.54, being the nameplate-associated errors negligible for the purpose under consideration. However, it should be noted that the referred non-proportionality is less accentuated than that of the power factor and of line current, which, in fact, compensate each other, explaining why the real power is almost proportional to the load.

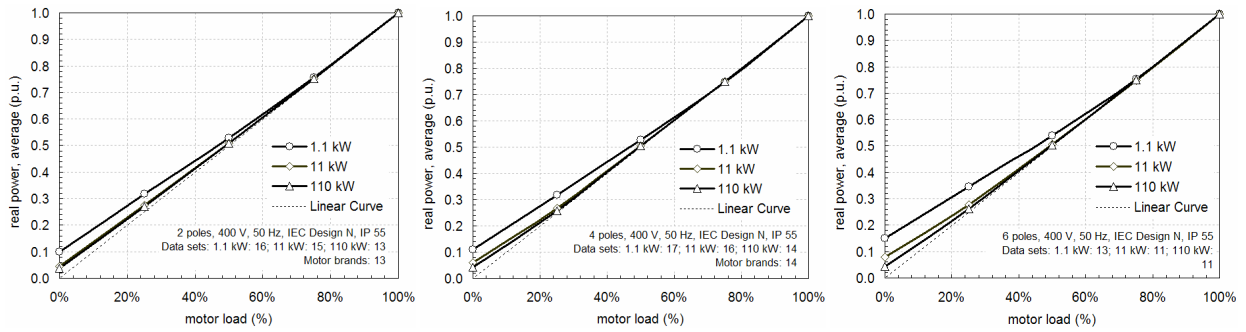


Fig. 4.53. Average input real power as a function of the motor load, for 1.1-, 11- and 110-kW motors, with 2, 4 and 6 poles.

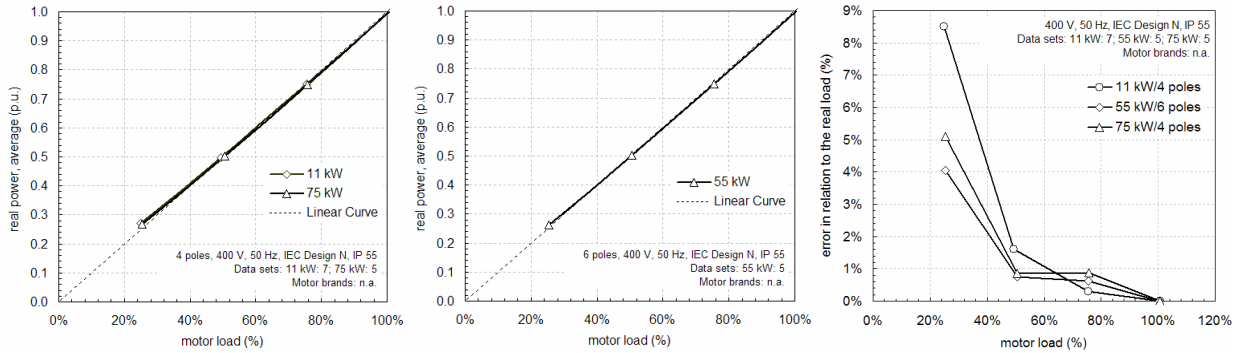


Fig. 4.54. Average input power and error (absolute value) in relation to the actual load of the input power-based method, as a function of the motor load, for 11-kW/4-pole, 55-kW/6-pole and 75-kW/4-pole motors.

If only 2 reference points are considered, no-load and full-load input power, the larger errors occur at low loads, depending on the relevance of no-load losses (no-load stator Joule losses, core losses, and friction and windage losses). Consequently, the error (by excess, i.e., the estimated value is higher than the actual value) decreases with the number of poles, particularly for small motors, in which no-load are more relevant. Therefore, the lower the motor rated power is, the higher the error will be.

Nevertheless, in order to improve this method, in one hand, it is possible to change the connection to star mode as a way to reduce the error for loads lower than 33.3% (similarly to the strategy proposed in the current-based method), and, on the other hand, to settle the reference values taking into account the data available in the manufacturers' catalogues and/or databases. Known the efficiency values for 100%, 75%, 50% and 25% load points (which are available for most motors in the referred motor databases), as well as the no-load real power (the no-load power can be measured during no-load test, or estimated on the basis of no-load power factor and current values, which, in the motor databases, are available for most motors), it is possible to estimate approximately (with an error associated with the efficiency values, as explained in Chapter 2), the real power for the referred 5 load points. It should be noted that the full-load efficiency determined by indirect method according to old IEC 60034-2 (Ed. 2) standard can lead to significant efficiency errors (see Chapter 2), but for motor load estimation purposes, the error has a relatively minor

impact. Moreover, the new IEC 60034-2-1 and the IEEE 112-B leads to accurate efficiency values for all loads.

It is also possible to consider average efficiency curves as a function of the number of poles and rated power, and motor efficiency class, which, at least, allow the reduction of the estimation error, particularly for low loads. Note that the standard deviation for the average efficiency curves presented in Figs. 4.53 and 4.54 is low.

The real input power can also be estimated as a function of motor load by interpolation on the basis of the power factor and current values for 0%, 25%, 50%, 75%, and 100% load, which are more difficult to obtain. Alternatively, average values can be used, or values of a similar motor (same power, number of poles, type, efficiency class, etc.), whose data is available in catalogues and/or databases. In [1], it is recommended that, if no-load power is not available, 8.2% of rated input power (average value) should be used. In [4], a value of 3.5% of input rated power (average value), corresponding to the combined windage, friction and core losses, is recommended. As shown in the experimental results, this percentage strongly depends on the motor rated power and number of poles.

Assuming that part-load input powers are not available, and only the input power is measured, the major error happens within the load zone up to 40-50% load, as it can be seen in Figs. 4.54, and 4.55.

As previously referred, the error in that zone can be significantly reduced by means of changing the motor connection from delta to star, which allows the accuracy of the method to be increased because of the significant reduction of the no-load losses (particularly the core losses), which is a major error source when considering an interpolation between origin and full load. The star-connected motor input power curve (0% to 33-40% load) combined with the delta-connected input power curve (33-40% to 100% load), become practically proportional to the motor load, as it can be seen in Fig. 4.61. As a general rule, the star connection can be adopted for loads lower than 40%. The connection change is a simple and quick operation if the motor has a star-delta starting system, otherwise, it could be a time consuming task. This concept was tested experimentally for motors in the range 0.75 kW to 7.5 kW and tested by simulation¹⁴ for the 11-kW and 300-kW motors, being the results presented in the Figs. 4.56 and 4.57. In Fig. 4.57, the input power-load curve, for motor loads up to 33%, is presented in detail.

On the basis of Fig. 4.55, for delta connection, it is possible to observe that the percentage difference between the estimated load and the actual load is considerably reduced for loads higher than 60% ($\pm 5\%$), corresponding to a maximum error of $\pm 10\%$. As expected, the error decreases with the increase of the motor rated power. For example, for the simulated 300-kW motor, the

¹⁴ Using the exact per-phase equivalent circuit (steady-state model).

percentage difference does not exceed 2 p.p., corresponding to a maximum error of 4% for loads between 5 and 100%. For motors with rated power higher than 7.5 kW an error lower than 10% (corresponding to a percentage difference of 2.5 p.p.) is expected, for loads higher than 25%.

As it can be observed in Fig. 4.56, the use of the star connection for loads up to 33% and the use of the delta connection for loads higher than 33%, leads to a significant reduction of the error, limiting the percentage difference between +3% and -2% for motors larger than 7.5 kW, which can be considered a very low difference for the purpose of the method. For example, if 20% load is estimated, for an actual motor load of 17.3%, the error has minor importance, because it is identified that the in-service motor should be replaced by a motor 5 times smaller, which, if chosen according to the estimated load, would operate at 82.5% load (neglecting the expected variation in the speed due to the expected slip increase), being a recommended motor load. For motors up to 7.5 kW, the percentage difference varies between -2% and +13%, being the higher limit significantly lower than that obtained with the delta connection-based method (+22%). It should be noted that, for the experimental data, there is a small error for full load, demonstrating the disparity between the rated input power (calculated from the nameplate data) and the measured input power at full load.

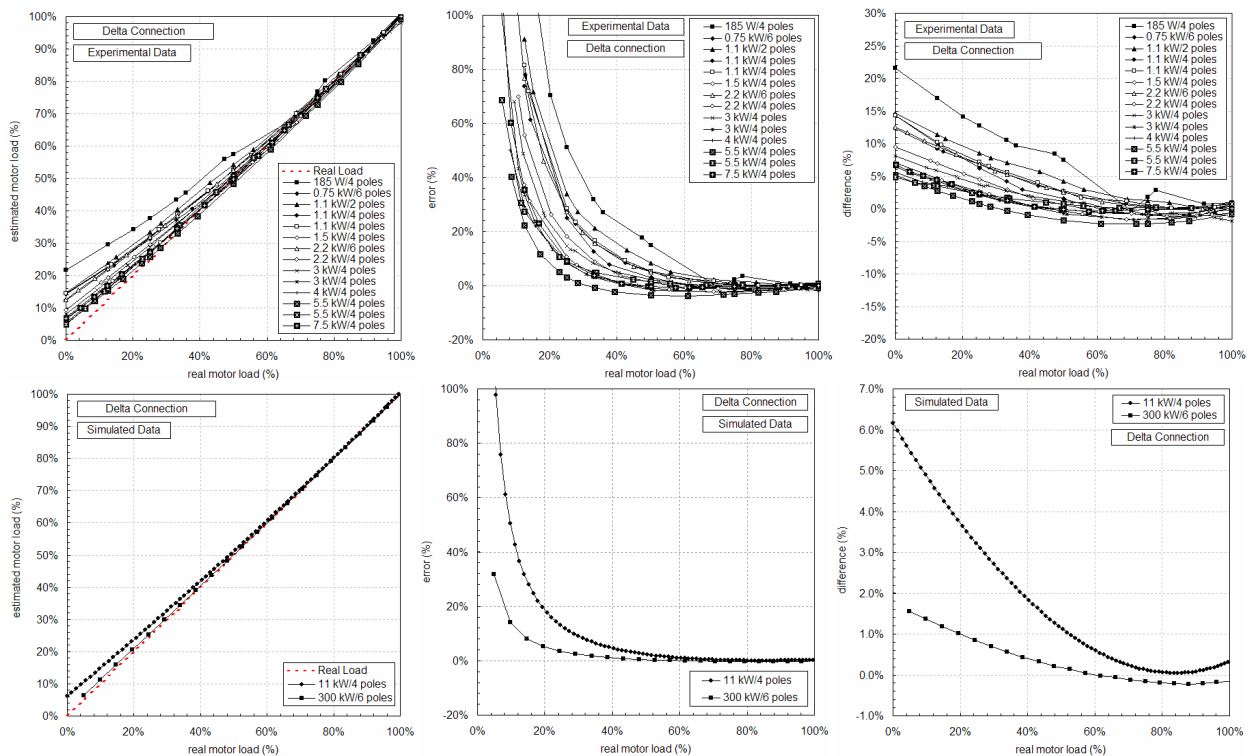


Fig. 4.55. Power-based method: actual and estimated motor load and the respective error (in %) and difference (in p.p.) for different delta-connected motors, approximating the input power curve as a function of load by one segment - origin and full-load points segment.

The foregoing discussion evidences the advantage of the novel star/delta-based method, being recommended for all motors, over the entire load range, if the importance of the motor justifies delta to star change and/or it has already installed a star-delta starting system. This novel method is particularly indicated for medium power motors¹⁵. However, for motors with power lower than 7.5 kW, this method should be used only for loads higher than 10%. One way to reduce the error is the use of an empirical correction factor for motors up to 7.5 kW.

Regarding the error associated with the nameplate values, it is assumed, as reference, the tolerance and measurement accuracy stated in [12] and [13]. The power factor tolerance lead to an admissible error of -7% for $\lambda = 0.7$ and of -4% for $\lambda = 0.8$, being fair the assumption of an average error of $0/-5\%$, taking into account the typical values for the power factor. The error of the input real power is related to the error of the electrical quantities, but the major source of error is by far the power factor tolerance.

For example, considering an accuracy of $\pm 0.2\%$ for the voltage and current values, the expectable error can be considered roughly between $\approx +0.4\%$ and $\approx -5.4\%$, which is the highest error to be considered for the rated input real power. Considering now that the torque sensors can have an error of $\pm 0.2\%$ at full scale and that the speed can have an error of ± 0.5 r/min ($\pm 0.033\%$ for 1500 r/min, $\pm 0.025\%$ for 1000 r/min and $\pm 0.067\%$ for 750 r/min) the motor rated power can have an error of about $\pm 0.23\%$ for 4-pole motors, which can be neglected in the motor load estimation scope.

For example, considering the input power error ($+0.4\%/-5.4\%$), if the estimated load is 100%, the actual load could be either 99.6% (error by excess) or 105.4% (error by defect). This variation explains the errors associated with full load input power obtained in the experimental tests.

It is important to refer that all nameplate values strongly depend on the motor operating temperature (which depends on the ambient temperature), and the part-load values in catalogues and databases are obtained according to the main standards, which adjust those part-load quantities for the rated temperature. The actual values of those quantities are in most cases slightly different.

Thus, it is important to ensure that, at least, the motor temperature is stabilized (thermal equilibrium), which is easy to verify by measuring the frame temperature in half-hour intervals.

In Figs. 3.59-3.60 and 3.62-3.63, experimental results for motors between 185W and 75 kW are presented. Figs. 4.62 and 4.63, show clearly the reduction in the error when the star/delta-based method is used over the delta-based method.

¹⁵ In most high-power motors, only 3 terminals are accessible at the terminal box, and the stator winding is typically connected in delta (D).

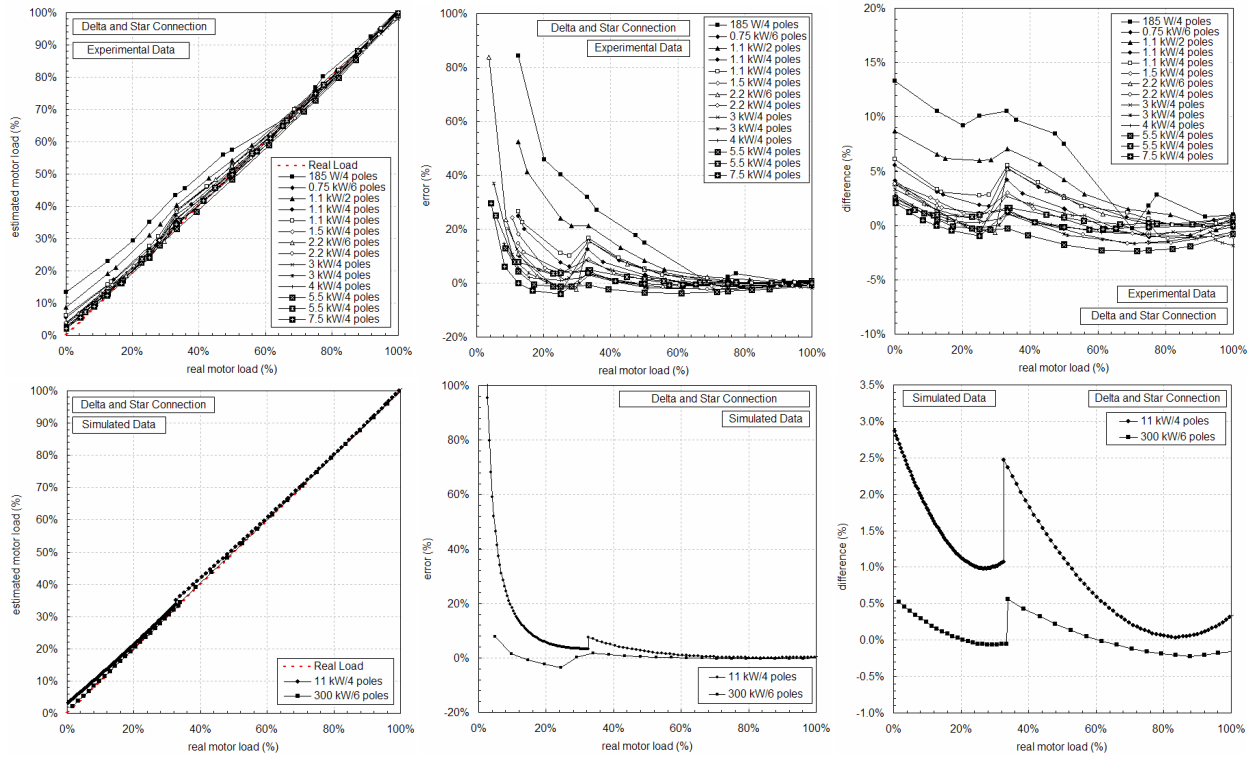


Fig. 4.56. Power-based method: experimental actual and estimated motor load and the respective error (in %) and difference (in p.p.) for different motors connected in star and delta modes (star connection for load equal or lower than 33%), approximating the input power curve as a function of load by one segment - origin and full-load points segment.

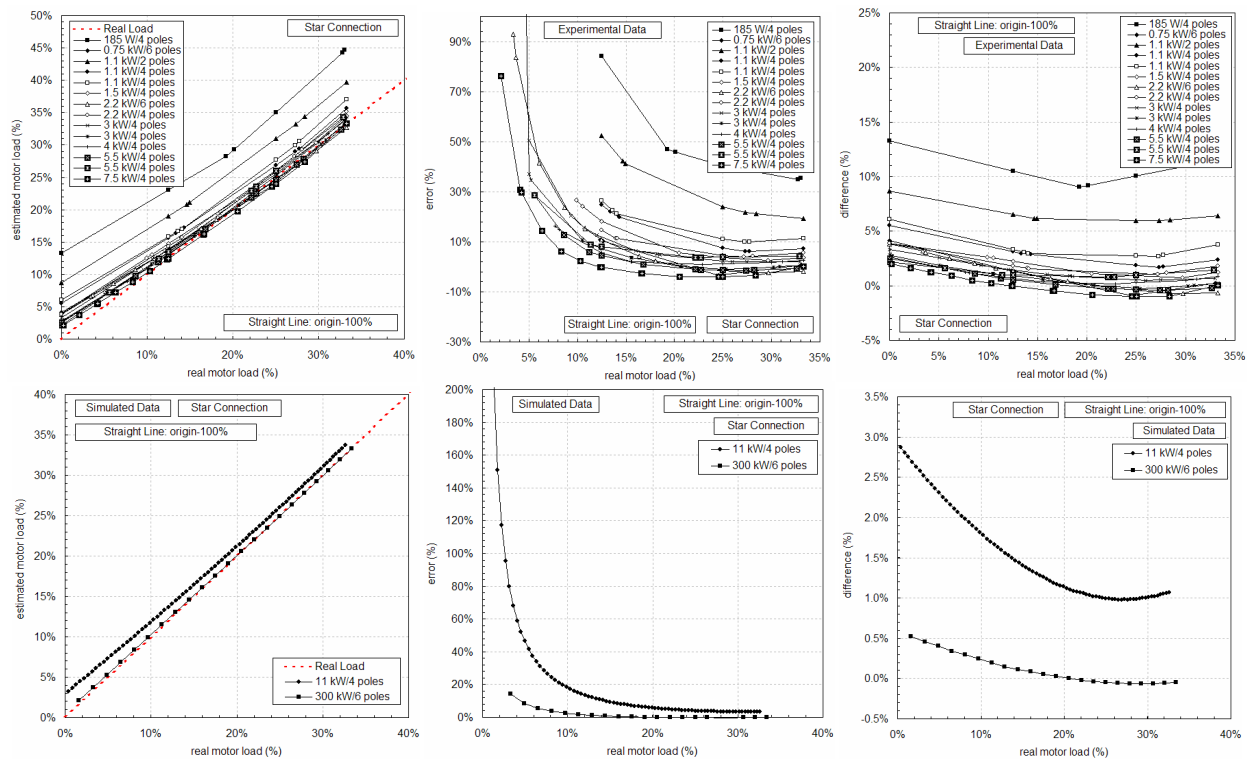


Fig. 4.57. Power-based method: experimental actual and estimated motor load and the respective error (in %) and difference (in p.p.) for different star-connected motors (motor load up to 33%), approximating the input power curve as a function of load by one segment - origin and full-load points segment.

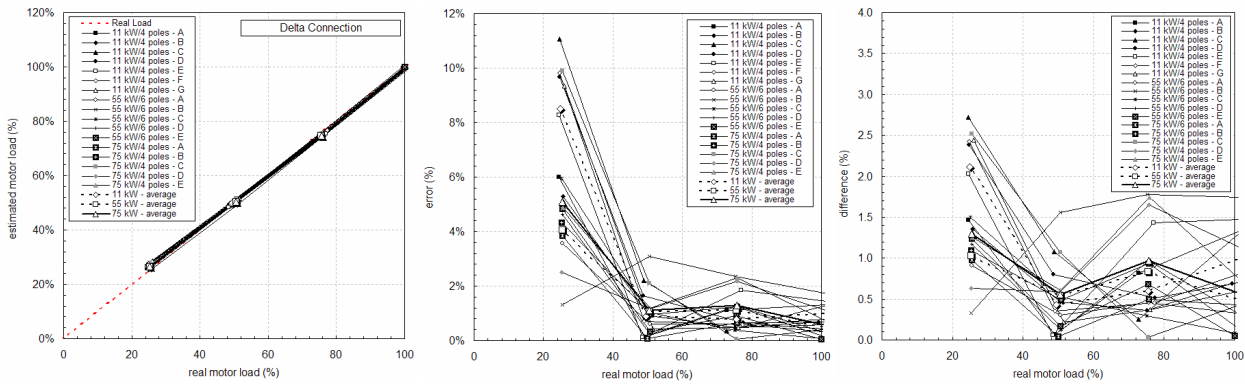


Fig. 4.58. Power-based method: experimental actual and estimated motor load and the respective absolute error (in %) and difference (in p.p.) for 11-kW/4-pole, 55-kW/6-pole and 75-kW/4-pole delta-connected motors (data extracted from [22]), approximating the input power curve as a function of load by one segment - origin to full-load points segment.

If the useful accuracy is taken into account, it is possible to verify that the maximum errors by excess and by defect, associated with input-power based method are fairly low when compared to the calculated admissible errors or useful accuracy, particularly in the neighbouring of the full load. Fig. 4.65 shows the superposition of the resultant error or difference, in percentage points, for the star/delta- and delta-based methods and the useful accuracy, evidencing the advantages of the first technique.

Regarding no-load, the corresponding errors, which influence the low-load error, are significant in relation to the useful accuracy for the delta-based method (Method I), but almost negligible when the star/delta-based method (Method II) is used, as it can be seen in Fig. 4.65, being recommended the use of the star/delta-based method for loads up to 33-40%.

The accuracy of the star/delta-based method is excellent over the entire load range, particularly for medium/large motors. The method is by far more accurate than those previously analysed, being recommended its application after preliminary load range identification with the other methods (slip-based or current based). The delta-based method only leads to excellent results for loads higher than 33-40%.

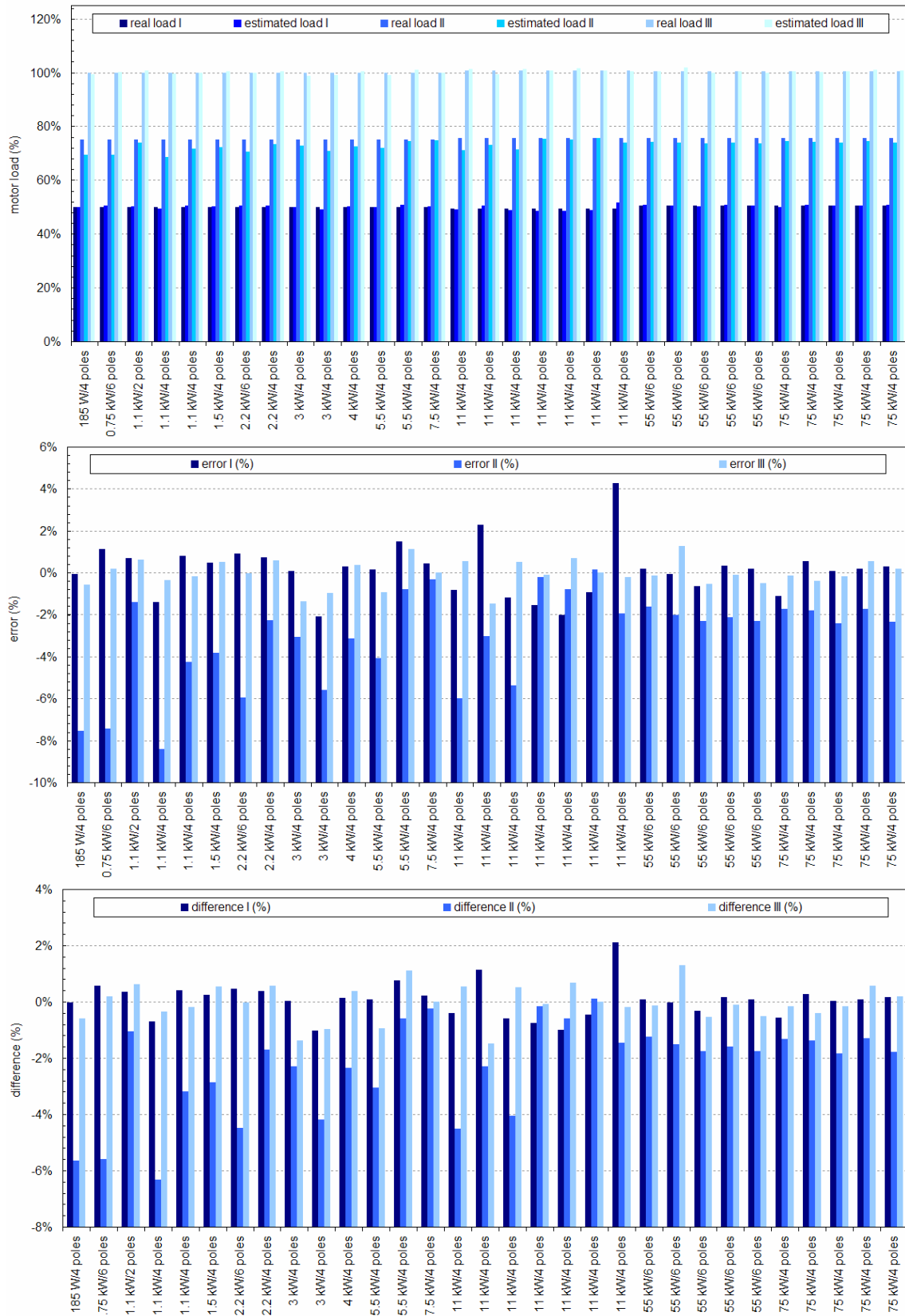


Fig. 4.59. Power-based method: experimental actual and estimated motor load and the respective error (in %) and difference (in p.p.) for different delta-connected motors and three load levels ($\approx 25\%$, $\approx 50\%$ and $\approx 75\%$).

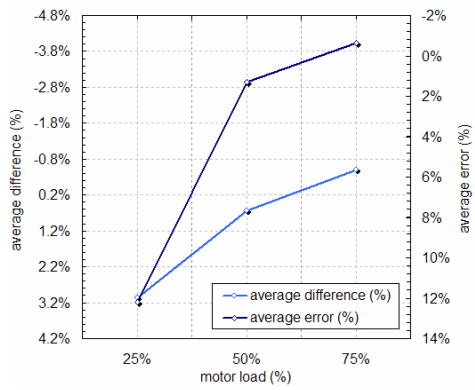


Fig. 4.60. Average difference (in p.p.) and error (in %) for the data presented in Fig. 4.59.

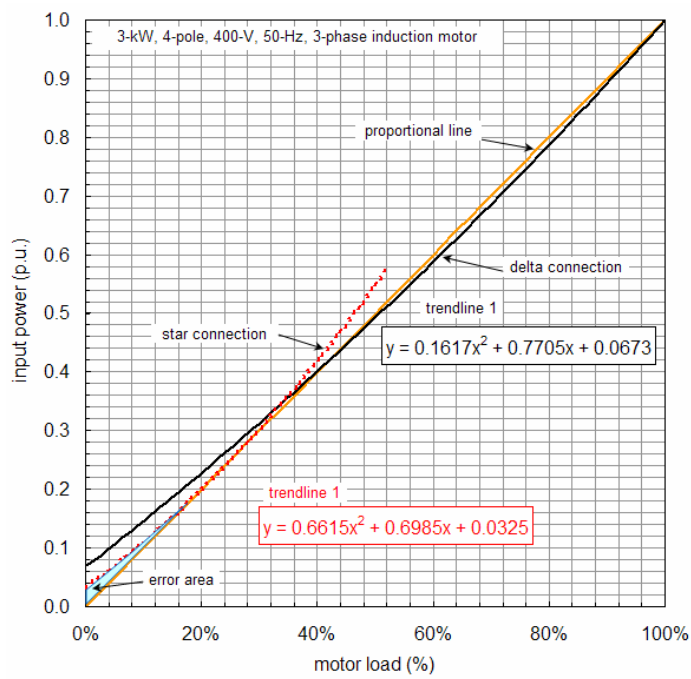


Fig. 4.61. Input real power for the delta and star connection of a 3-kW, 4-pole motor.

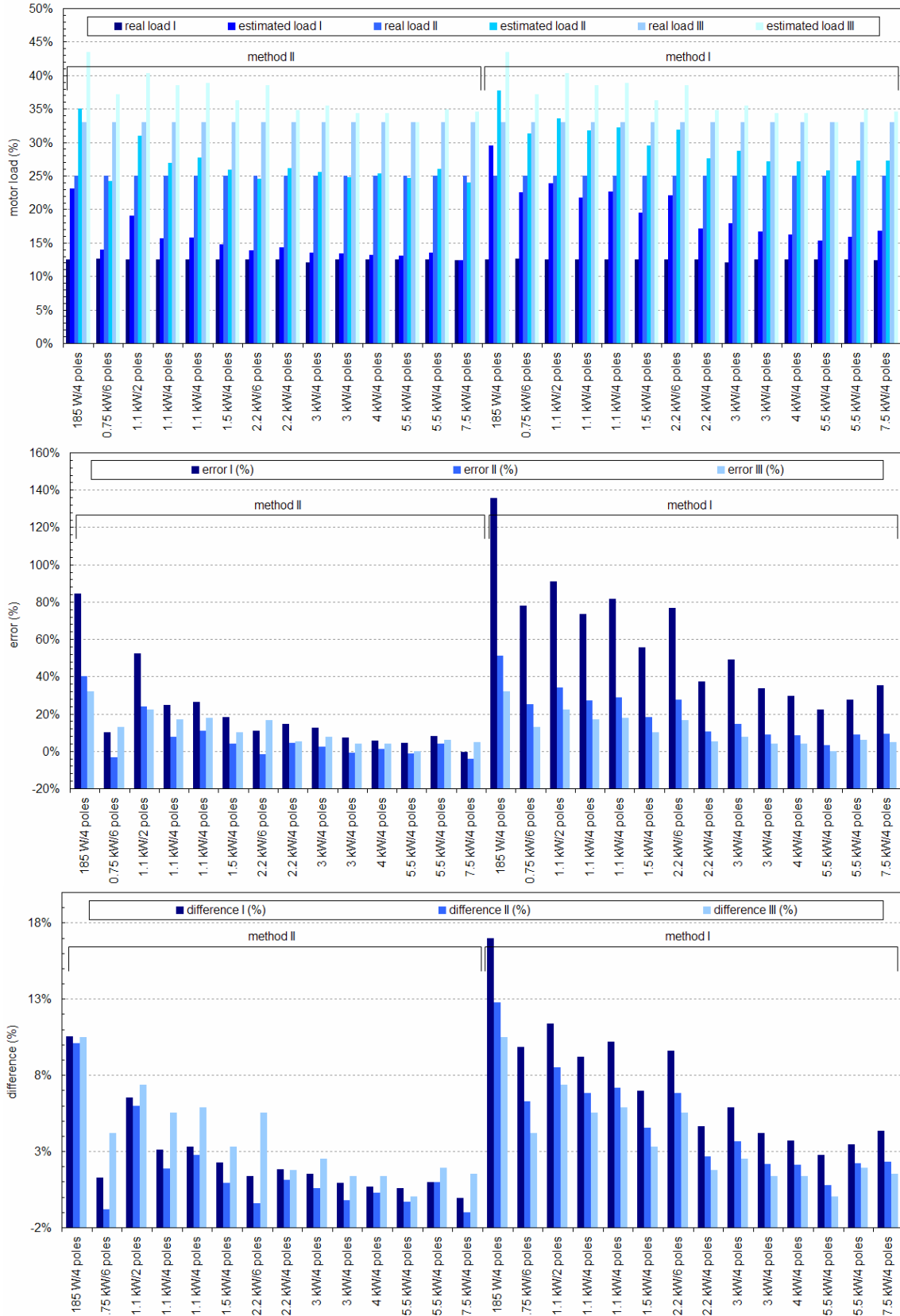


Fig. 4.62. Power-based method: experimental actual and estimated motor load and the respective error (in %) and difference (in p.p.) for different motors connected in star mode (method II) and delta mode (method I), and three different load levels up to 33%.

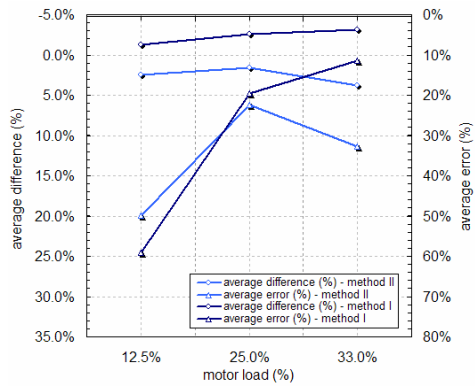


Fig. 4.63. Average difference (in p.p.) and error (in %) for the data presented in Fig. 4.62.

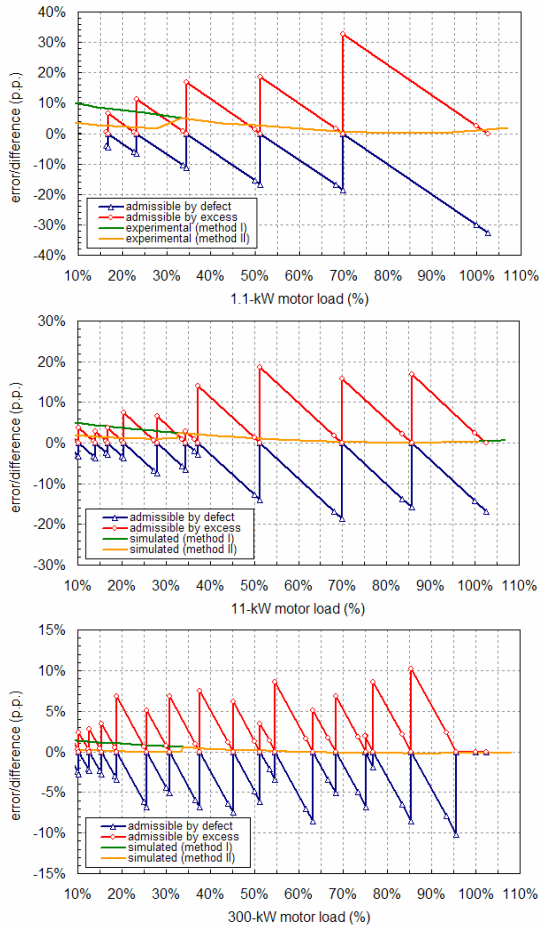


Fig. 4.64. Superposition of the error or difference (in p.p.) associated with input power-method and the useful accuracy (in p.p.), for 1.1-kW (experimental), 11-kW (simulated) and 300-kW (simulated) motors. Method I: delta connection. Method II: star/delta connection.

4.10 Temperature-Based Motor Load Estimation Method

The IEC 60034-1 standard defines and obligates the motor thermal classes to be included in the motor nameplate information, as well as the temperature or the temperature rise admissible (if lower than the thermal class), and, if necessary, the measurement method, being the reference temperature for the thermal tests 40°C [12]. However, for efficiency estimation purposes, the reference ambient temperature is 25°C [13], [14]. For example, for the thermal class F, corresponding to an absolute admissible temperature of 155°C, the IMs with rated power between

600 W and 200 kW, admit a temperature rise of 105°C (measured by means of winding resistance method [12]), being 10°C associated with hotspots.

In the temperature-based method, to estimate the motor temperature rise, under thermal equilibrium, it is possible to measure the winding resistance at the motor terminals with an ohmmeter either by disconnecting (turning-OFF) the motor (which can not be possible in some situations), or by using the superposition method (defined in the IEC 60279), which does not require the motor to be disconnected, and compare measured value with that at ambient temperature. In the last method, a DC current is superimposed to the AC current, corresponding the ratio between the resulting DC voltage component and the DC current to the DC line-to-line winding resistance. This method has the advantage of being immune to voltage distortion, voltage unbalance, and magnitude deviation, giving directly the thermal load (see Appendix 4). Manufacturers can provide the cold resistance value for a certain ambient temperature, or it can be measured by the user during off-operation periods, requiring only a handheld ohmmeter and a handheld thermometer (e.g., infrared-type thermometer). The estimated temperature rise allows to estimate if the motor is near or not the rated load.

Obviously that this method, as proposed, is only valid if there are no significant power abnormalities as voltage dips/sags, voltage unbalance and voltage distortion, or this parameters are within the limits defined in the IEC 60034-1 standard.

Additionally, since the total losses are not proportional to the motor load (see, for example, Fig. 3.54 in Chapter 3), and it is rather difficult to provide part-load temperatures (for different ambient temperatures, the frame and winding temperatures are easily compensated), the motor load cannot be estimated for part-load points, being only possible to estimate if the motor is operating below, near or above full-load.

If a reference (rated load) value for a specific point/spot in the frame at a specific ambient temperature exists (some manufacturers can provide such data), using an infrared thermometer, this method is quick and easy to apply, by simply comparing the reference and the measured temperatures. However, dirt in the frame and cooling system due to poor cleaning can introduce significant changes in the frame temperature as a function of load.

However, due to the foregoing reasons, it is not a recommended method to identify if the motor needs or not to be replaced by another motor of different rated power.

This method can be used as a first approach to identify potential oversized or undersized motors, being necessary to use other accurate methods to estimate the motor load and define the proper motor power for the system under evaluation.

Of course that, if motor full-load, part-load and/or no-load steady-state temperature values were known in a specific motor part (and for a specific ambient temperature), this method can be

potentially accurate, similarly to the current method, depending on the number of points for interpolation. Note that the temperature variation in the motor winding and frame as a function of motor load as a similar shape to the current-load curves (see, for example, Fig. 3.54 in Chapter 3). If, for example, the manufacturer is able to provide those values for a specific motor frame spot or point (for a reference ambient temperature), the user can estimate very easily the motor load. In fact, it is likely that manufacturers have this sort of data for the prototype corresponding to specific motor series.

4.11 Air-Gap Torque-Based Motor Load Estimation Method

The Air-Gap Torque Method can have several variants, but, in short, is based on the torque and power transferred across the motor air-gap by means of voltage and current waveforms acquisition and the measurement of phase resistance, speed and no-load power (see Appendix 6) [1], [34]. If a no-load test is made to find the core loss and friction and windage loss, this method can be highly accurate (yielding efficiency estimative with an accuracy that could be within ± 1 p.p. error from actual values). Since the harmonic components can be obtained from the waveforms, the loss associated with the power supply distortion can also be assessed. According to [1], this is a high intrusion level method.

The most sophisticated devices calculate the speed from the current spectrum. However, although the theoretical medium/high accuracy, there are several error sources associated with this method (which are inherent to the commercial devices using it) such as the lack of accurate information or non-consideration of SLLs, friction and windage losses, temperature variation impact on the stator and rotor resistance values, skin effect on rotor resistance, saturation (which depend on the voltage level), negative-sequence winding spatial components, and iron losses increase due to poor repair, just to enumerate a few. In the equipment applying this method, if the stator resistance is not introduced by the user, it is estimated by the equipment on the basis of average values (which lead to significant errors due to the high dispersion level, particularly to low-power motors).

For three-phase four-lead motors, two line voltages and three line current need to be measured for air-gap torque calculations. For three-phase three-lead motors (which are the majority), waveforms of two line voltages and two line currents are required, for air-gap torque calculations. Additional information on this method can be found in [1], [3]-[9], [16], [32], [35].

A comparative study on the most relevant commercially available non-intrusive motor efficiency or in-service motor performance estimation devices is made in [9], including the EXPLORER (from BAKER Co.) and the MCE-Max (from PdMA Co.). They include voltage and current acquisition, storage and processing system. The processing is made by means of an embedded PC,

using proper software developed using LABVIEW and/or MATLAB. They measure only operational parameters at the electrical terminals accessible in a motor starter or MCC cabinet (basic requirement of non-intrusion). This sort of equipments is expensive (> 10000 €) and requires the connection of 2 or 3 current clamps and 2 or 3 voltage probes. It should be noted that the equipment calculates the shaft power by the product between the torque and speed. The torque is estimated using the motor $d-q$ axes equations (see Appendix 2) and the speed is obtained by current spectral analysis [16]. The advantage of such devices is that, besides the motor performance evaluation, they also allow carrying out motor condition diagnosis. Typically, they allow to estimate/measure the motor speed, torque, efficiency, load, power factor, voltages and currents, etc., and can be used in line-fed or inverter-fed motors. However, besides the motor nameplate information, it is necessary to introduce, at least, previously the stator winding resistance of the motor being analysed. According to [9], the accuracy of the estimations is very good for loads above 50%. If the motor load appears to be below 50%, the efficiency and load estimations need to be considered more carefully. However, in [9], it is evidenced that the EXPLORER and MCE-Max devices provide performance data that, in general, are in good agreement with laboratory measurements, even for low loads, particularly for medium/large motors. In fact, the air-gap torque method is more accurate for large motors due to the reduced absolute friction and windage losses (although in % of losses they increase).

In order to test the performance of such devices for small motor load estimation, laboratorial tests were carried out at the same time for the EXPLORER II, using a 4-pole, 400-V, 50-Hz, 3-kW IM. The reference measures were obtained by direct method, using a high-accuracy testing system integrating a dynamometer (with speed and torque sensors) and a power analyser (YOKOGAWA 1030M), as described in Chapter 2. For the sake of simplicity, only the results of one of the tests performed are presented in Table 4.3, for line-fed situation. More results can be found in [15] and [16]. It should be noted that, typically, the air-gap torque method overestimates the torque value, unless the assumed average values for the friction and windage losses are high than the actual values, which seems to be the case. Therefore, the obtained torque overestimation is a problem inherent to the equipment settings and not to the method itself.

TABLE 4.3
EXPERIMENTAL COMPARISON BETWEEN
EXPLORER AND YOKOGAWA DEVICES FOR STEADY-STATE MOTOR LOAD AND EFFICIENCY MEASUREMENT.

Device	U_n	I_n	λ	P_n	ω	T	P_{out}	η	ζ	$\Delta\zeta$
Yokogawa	400.4 V	7.13 A	0.8101	4.01 kW	1404 r/min	20.8 N.m	3.06 kW	76.2%	102%	--
Explorer	400.0 V	7.2 A	0.81	4.1 kW	1404 r/min	16.5 N.m	2.4 kW	59.7%	80%	22 p.p.

Notes: 400-V, 4-pole, 50-Hz, 3-kW, Delta-Connected, Three-Phase, Squirrel-Cage Induction Motor. Motor frame temperature at full-load after thermal equilibrium: $\approx 70^\circ\text{C}$. Room temperature: $\approx 18^\circ\text{C}$.

Significant differences between the values estimated by the EXPLORER device and the values measured by YOKOGAWA, namely the torque and consequently the output power and efficiency, were found. In the motor load, a 22 p.p. difference was found. For lower loads, this difference can increase significantly. In some conditions, inaccuracies in the speed estimation were also found. The error is, in part, related to the operating temperature of the motor. In fact, in the beginning of the test (motor approximately at room temperature), the errors were significantly higher. This is due to the fact that the motor rated values are only reached after thermal equilibrium at full-load and the measured room temperature winding resistance (introduced in the device software) is significantly different at full-load. Additionally, significant differences can be found between the actual full-load speed and the rated or nameplate speed, which is typical, due to the slip tolerances allowed by standards. As expected, the electrical measurements are accurate.

The EXPLORER also requires the motor rated values for voltage and current, for compensation/correction purposes (e.g., the speed estimation can be corrected on the basis of the relation between the rated and measured voltage).

In PWM environment (inverter-fed motors), the electrical quantities measurement and processing effectiveness depends strongly on the considered analysis spectrum band or range, being quite difficult for the user to adjust the equipment properly to each application (particularly if they have not deep technical skills). The consequent errors can influence significantly the estimated speed and torque.

It should be noted that the voltage and current values can be firstly acquired with a data acquisition system and processed subsequently, at a later date.

It can be concluded that, although the higher cost and time consuming procedures, this sort of sophisticated equipments cannot estimate the motor load with the desirable accuracy, particularly for small motors (rated power equal or lower than 30-50 kW).

An important advantage of using instantaneous voltage and current, combined with nameplate data, is that it is possible to implement wireless meshes over the industrial plant and estimate massively the motor load and efficiency over the entire duty cycle, as proposed in [34].

4.12 Other Relevant Motor Load Estimation Methods

The Nameplate Equivalent Circuit Method is a modified version of IEEE standard 112 F method. An additional resistance is added in series with rotor branch to account for SLLs. The information needed to construct the equivalent circuit is taken from the motor nameplate. Only the measurement of motor speed is required to estimate the motor load and efficiency (the circuit can be easily simulated using MATLAB or SIMULINK). The accuracy of the method depends upon the accuracy of the equivalent circuit model, which in turn depends upon the accuracy of the

nameplate data. This method can yield reasonably accurate results for efficiency estimation purposes (error lower or equal than ± 5 p.p.). This method, as well as the current and slip methods, is considered a low intrusion level method [1]. The estimation of the per-phase equivalent circuit parameters using motor nameplate data and data from databases or standards, is described in [1] (see Appendix 6). However, saturation, thermal compensation, skin effect are not considered, introducing significant errors in the method, particularly for low loads. Moreover, the equivalent circuit method is not, in general, easy to apply in the European motors, due to the commonly available data, but can be properly adapted.

The empirical method, also named Stanford Wilke, was developed at Stanford University, to be applied to 7.5-37.5 kW range IMs. Some of the empirical assumptions are taken from IEEE 112, while others arose from authors' experience. This method can yield reasonably results for efficiency estimation purposes (error equal or lower to ± 4 p.p.) [1]. This is a medium intrusion level method.

The Ontario Hydro Modified (OHM) Method is a modification of the Ontario Hydro version of IEEE 112 E Segregated Loss Method (see Appendix 6) [1]. In the general method an empirical value of 3.5% is used to find the no-load losses (in lieu of performing a no-load test). Thus, the no-load loss is estimated as 0.035 of the nameplate full load power. The modified version uses a value based on motor size, and the SLLs approximation described in IEEE Standard 112 (empirical factor for finding SLLs based on motor size). The full-load real power is estimated using the nameplate current and voltage and a power factor of 0.8. The anticipated accuracy is on the order of that expected for the Stanford Wilke Method. According to [1], this is a medium intrusion level method.

For motor efficiency (and load) estimation purposes, in [1] the following methods are recommended:

- Low-intrusion level: Nameplate Equivalent Circuit Method;
- Medium-intrusion level: Ontario Hydro Modified Method;
- High-intrusion level: Air-Gap Torque Method.

Some manufacturers provide per-phase equivalent circuit parameters determined according to standards (IEC or IEEE Stds.) for medium/high power motors, although with a number of simplifications. For example, IEC-based per-phase equivalent circuits assume friction and windage losses integrated into the iron losses resistance. Regarding equivalent circuits, the SLLs are not considered by the standards. Moreover, no thermal compensation is considered due to the inherent complexity.

Therefore, besides the potentially fair accuracy of equivalent circuit-based method, due to the inherent in-field impracticability for the vast majority of low/medium power motors, being only justified for a few critical medium/high power motors.

4.13 Multiparametric Motor Load Estimation Methods

In order to increase the certainty level for an estimated motor load level or range, or to manage properly the efforts to motor load assessment for a wide motor population, the user can apply the discussed methods in a certain sequence (starting on the most simple to apply) and combine their individual results.

Being the temperature-based and the slip-based method the quickest and easiest methods, they can be applied in a first stage for a preliminary evaluation. For example, the slip-based method results, in most cases, in an underestimation of the load, allowing the user to conclude that the load is above the estimated level. In the case of the temperature-based method, its resolution on load estimation depends on the number of load points for which the frame or windings temperature is known considered for interpolation. In this stage, if a quasi-rated load is identified in a motor, it can be excluded from a second more accurate evaluation, otherwise a more careful load analysis should be carried out.

After that, in the motors justifying a confirmation of the load, the current-based method and, if justified, the power-based method, or even other methods such as equivalent circuit or air-gap torque methods, should be applied. For medium/large motors, which are the most important, only the power-based is recommended for accurate load assessment.

Crossing-data analysis can be made taking into account the underestimation and overestimation levels of each applied method, in order to increase the certainty degree. On the basis of that principle, it is proposed the fusion of the current-based and slip-based methods.

In Fig. 4.65, an example of slip-based and current-based methods (using only rated current value and the delta/star connection) combination is given. In order to clarify the idea, let the actual load of the considered motor be 60%. The corresponding actual slip and line current values are 0.54 and 0.71 p.u. (points *a* and *b* in the Fig. 4.65), respectively. Therefore, if those values were measured, the resulting estimated load would be 53% and 71% (points *c* and *e*), respectively, assuming that origin-100% load straight line is used. As it is known, in those conditions, the slip method leads to an error by defect over the most the major part of the load range¹⁶, and the current method leads to an error by excess¹⁷, being possible to define a high-certainty load range, which, in this particular case is [53% 71%] load. The lower the actual load, the wider the high certainty load interval. This

¹⁶ In fact, the slip-based method underestimates the load within a load range, whose lower limit varies with power and number of poles.

¹⁷ Assuming that one straight line from origin to 100% load is used. The load overestimation in the current-based method is no longer valid when introducing intermediate points in current-based method.

example shows how much this approach can be useful. If the no-load current and/or intermediate load points are included to establish a set of segments for interpolation in the current-based method, this approach can no longer be applied.

The combination of the slip and current values can also be made by means of constructing a circle diagram (Ossanna circle [26], [28], Appendix 6) of the motor being analysed. For example, as it can be seen in Fig. 4.66, knowing the no-load and rated current and power factor, the circle diagram can be defined. Note that only one half circle is possible for the referred two currents, since its centre has to be the horizontal line crossing point A . In fact, the circle centre can be defined by drawing a straight-line perpendicular and crossing the centre of the segment \overline{AB} , whose intersection with the horizontal line crossing point A is the circle centre. If the no-load power factor is not known (neither an average nor a particular value), it can be assumed as 0.08-0.1, without introducing major errors. The starting current can then be positioned into the circle taking into account its magnitude. Only one position is possible for the starting current¹⁸, denoted by point C . After that, the segment \overline{AC} can be drawn. The vertical distance between that segment and the top of the circle corresponds to the output power, which is used to calculate the motor load. At this stage, the circle diagram can be used to calculate the motor output power based on the input current value. To combine the current values with the slip values, the rated slip can be taken into account to establish the segment \overline{XZ} . Note that the slope of this segment, or the $\overline{XX'}$ length, must be properly defined, considering Z as a fixed point. Usually, the relation between the stator and rotor resistance are used for that purpose. However, in the absence of those values, which is the case, the \overline{XZ} segment can be iteratively adjusted until the relation between \overline{XY} and \overline{XZ} lengths match the rated slip. After that, either the slip or current can be both used to estimate the motor output power, which, after divided by the rated power gives the motor load. The rated power segment, P_N , is used to define the power scale of the diagram, allowing output power computation in watt or kilowatt. The user can directly calculate the motor load by dividing the length of the output power segment for a given current and/or slip by the length of the rated power segment. This approach is indicated to medium/large machines, since they have relatively low stator impedance, and therefore can be fairly represented by the approximate per-phase equivalent circuit (exact per-phase equivalent circuit circle diagram is more complex). If the output power corresponding to the current- and slip-based estimation match (or \overline{AY} and \overline{AB} segments match), there is a high degree of certainty. If not, the degree of uncertainty associated with the mismatching degree (e.g., proportional to the angle between \overline{AY} and \overline{AB} segments), and the average of both

¹⁸ When estimating the starting current from locked-rotor test, since the short-circuit reactance is considered constant and the applied voltage is significant lower than the rated voltage, the actual saturation level is not taken into account, resulting in an underestimated starting current for rated voltage condition, which introduces additional errors in the circle diagram. However, since, in general, the starting current provided by motor manufacturers takes into account the actual saturation level (measured at the rated voltage), if that value is used in the circle diagram, the associated errors are strongly reduced.

output power values should be considered. Other data fusion strategies can be investigated. Moreover, actual voltage and power factor values can also be taken into account in the diagram circle. Mathematical equations can be derived from the circle diagram or from the per-phase approximate equivalent circuit (which is the basis for the circle diagram construction, and its main impedance branches can be easily known on the basis of the referred voltage, currents, power factor and slip values) to allow analytical application of the proposed method.

Some manufacturers provide with large motors a set of technical information, which can include load curves, exact equivalent circuit parameters (including start, nominal and maximum power rotor resistance and leakage values), rated per-phase information, etc. This information can be directly used in a model or to draw the circle diagram to estimate motor load. If available, the current-load curve can be directly used to estimate load. Alternatively, if the exact equivalent circuit parameters are known, a simulation using MATLAB or SIMULINK can be made with more accurate results than those obtained with circle diagram (although not considering thermal compensation).

It should be noted that, besides it is based on the approximate equivalent circuit [28], the classical circle diagram as several simplifications, not taking into account the SLLs, temperature effect on the resistive parameters of the per-phase equivalent circuit, and the no-load losses slight variation with load, just to name a few.

The greater efforts on the application of most accurate methods can be justified particularly for medium/large critical motors, particularly if the load assessment is the key factor to decide their replacement, representing a large investment.

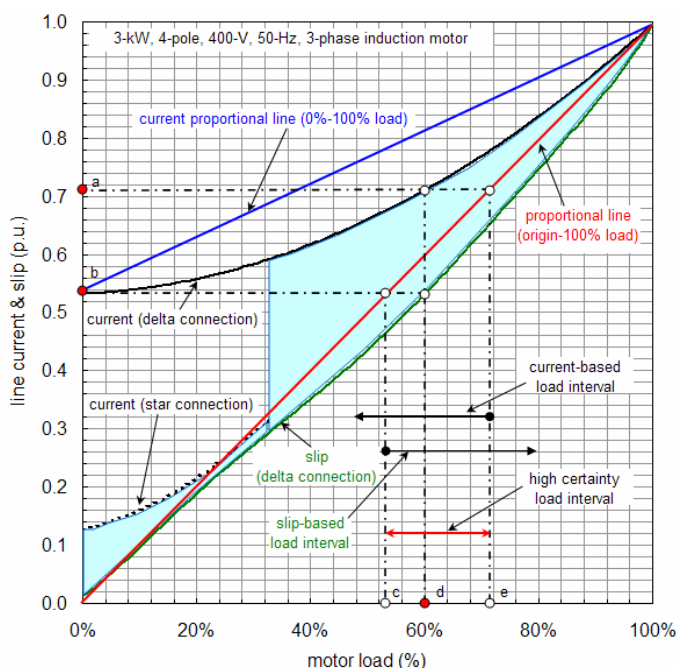


Fig. 4.65. Combination of the results of both slip-based and current-based methods to find a high-certainty load level range.

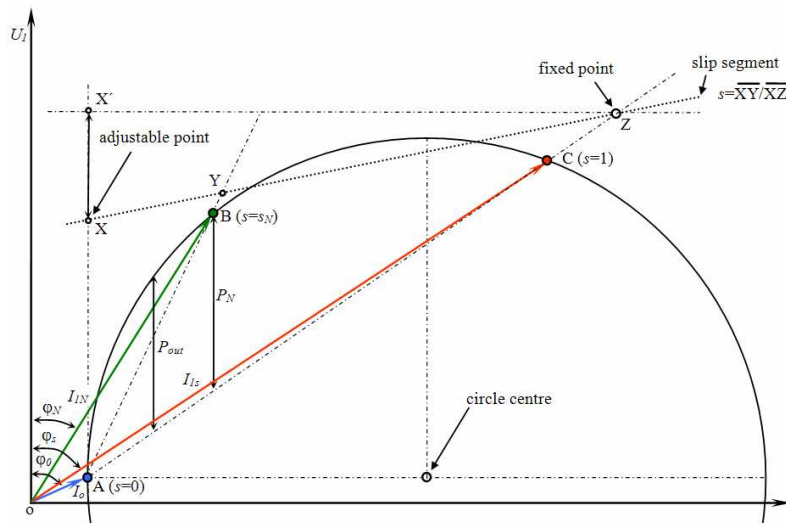


Fig. 4.66. Circle diagram of an IM, based on the approximate per-phase equivalent circuit (impressed voltage $U_i = E_1$).

4.14 Considerations on Motor Oversizing

The replacement of an oversized IM is recommended when the smaller IM commercially available fits the load with resulting 75-100% load. Besides the obvious starting current peak values reduction, the savings of energy and the improvement of the motor power factor, as well as the reduction of the acoustic noise (see Table 4.4), there is also the advantage of reducing the rotor inertia, therefore reducing the starting period and the associated rotor losses. It should be noted that short-circuit impedance of IMs decreases with the rated power, as it can be seen in Table 4.5. Therefore, for smaller IMs, the starting current is lower, and the rotor losses are inherently lower. This is an advantage normally not referred when motor sizing is discussed. Therefore, the dynamic response of the system can improve significantly, if motor oversizing is avoided.

TABLE 4.4
ACOUSTIC NOISE FOR 400-V, 50-Hz, 4-POLE, EFF2 IMs [33].

Power, kW	1.1	2.2	11	22	110	200
Noise, dB(A)*	47	51	62	64	77	79

*Sound Pressure Level, LP dB(A) @ 1-m distance.

TABLE 4.5
EXAMPLES OF PER-PHASE EQUIVALENT CIRCUIT PARAMETERS FOR 400-v, 50-Hz, 4-POLE IMs [29].

Rated Power (kW)	R_s (Ω)	L_s (H)	R_r (Ω)	L_r (H)	L_m (H)	J ($\text{kg}\cdot\text{m}^2$)	B (N.m.s/rad)	ω (r/min)	T_N (N.m)
4	1.405	0.005839	1.395	0.005839	0.1722	0.0131	0.002985	1430	26.7
7.5	0.7384	0.003045	0.7402	0.003045	0.1241	0.0343	0.000503	1440	49.7
15	0.2147	0.00099	0.2205	0.00099	0.06419	0.102	0.009541	1460	98.1
37	0.08233	0.000724	0.0503	0.000724	0.02711	0.37	0.02791	1480	238.7
75	0.03552	0.000335	0.02092	0.000335	0.0151	1.25	0.03914	1484	482.6
110	0.02155	0.000226	0.01231	0.000226	0.01038	2.3	0.05421	1487	706.4
160	0.01379	0.000152	0.007728	0.000152	0.00769	2.9	0.05658	1487	1027.5

Note: R_{fe} increases with rated power.

There is a number of applications where the rotor inertia reduction and the rotor resistance increase can lead to significant savings, such as, for example, in compressors with ON/OFF control

and intensive cycling. In order to demonstrate the potential savings a simulation was carried out for a 7.5-kW, 4-pole IM and for a 4-kW, 4-pole IM, driving a friction-type load (representing a compressor-type or conveyor-type load) and a fan-type load. The 7.5-kW IM is oversized for the considered loads (53.6% coulomb friction; 55.8% fan-type load), being the 4-kW perfectly sized with roughly 100% load (99.5% load for both load types). The results are presented in Figs. 4.67 and 4.68, confirming the higher currents and energy consumption during starting period. It is possible to conclude that, for an IM without speed control, with an intensive ON/OFF cycling, the oversizing is clearly undesirable, due to the poor dynamic performance and, thus, to the extra losses and internal temperature rise. Even if the user thinks that a higher power motor starts quickly, due to the higher starting torque, it actually does not happen due to the considerably higher rotor inertia. Additionally, smaller motors are less sensitive to voltage unbalance (see Appendix 4).

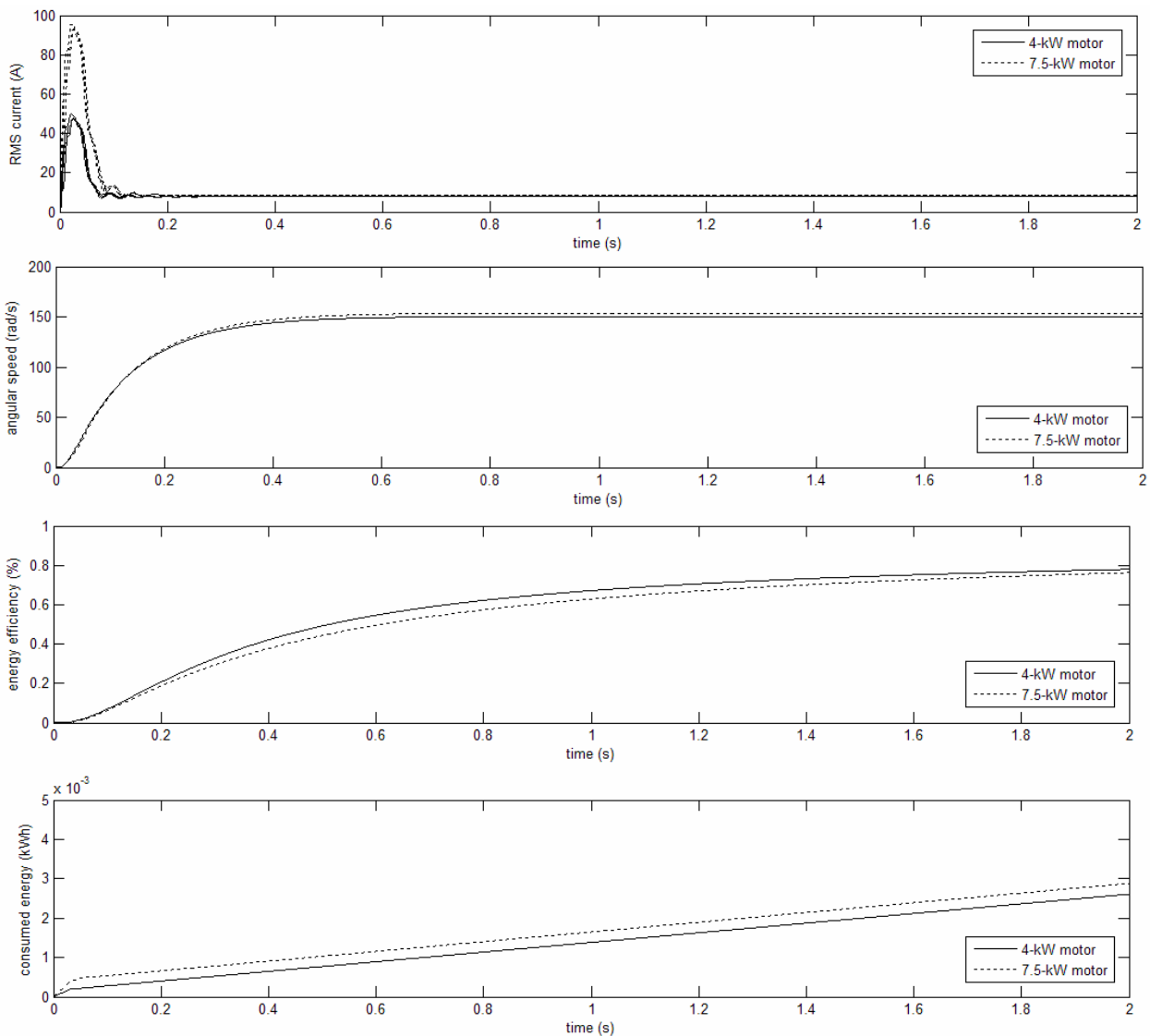


Fig. 4.67. Simulated starting period for 4-kW and 7.5-kW motors driving a load with combined static and viscous friction ($T_{load} = 24.5 + 0.01 \cdot \omega$).

In applications requiring high dynamic response, where incorporating speed control is out of the possible solutions package, at least a well sized, copper-cage rotor motor (with the same rotor resistance by smaller size) should be used to minimize the rotor inertia and losses, during starting or acceleration periods.

The foregoing discussion demonstrates that the motor oversizing has more disadvantages than those typically identified in most technical texts.

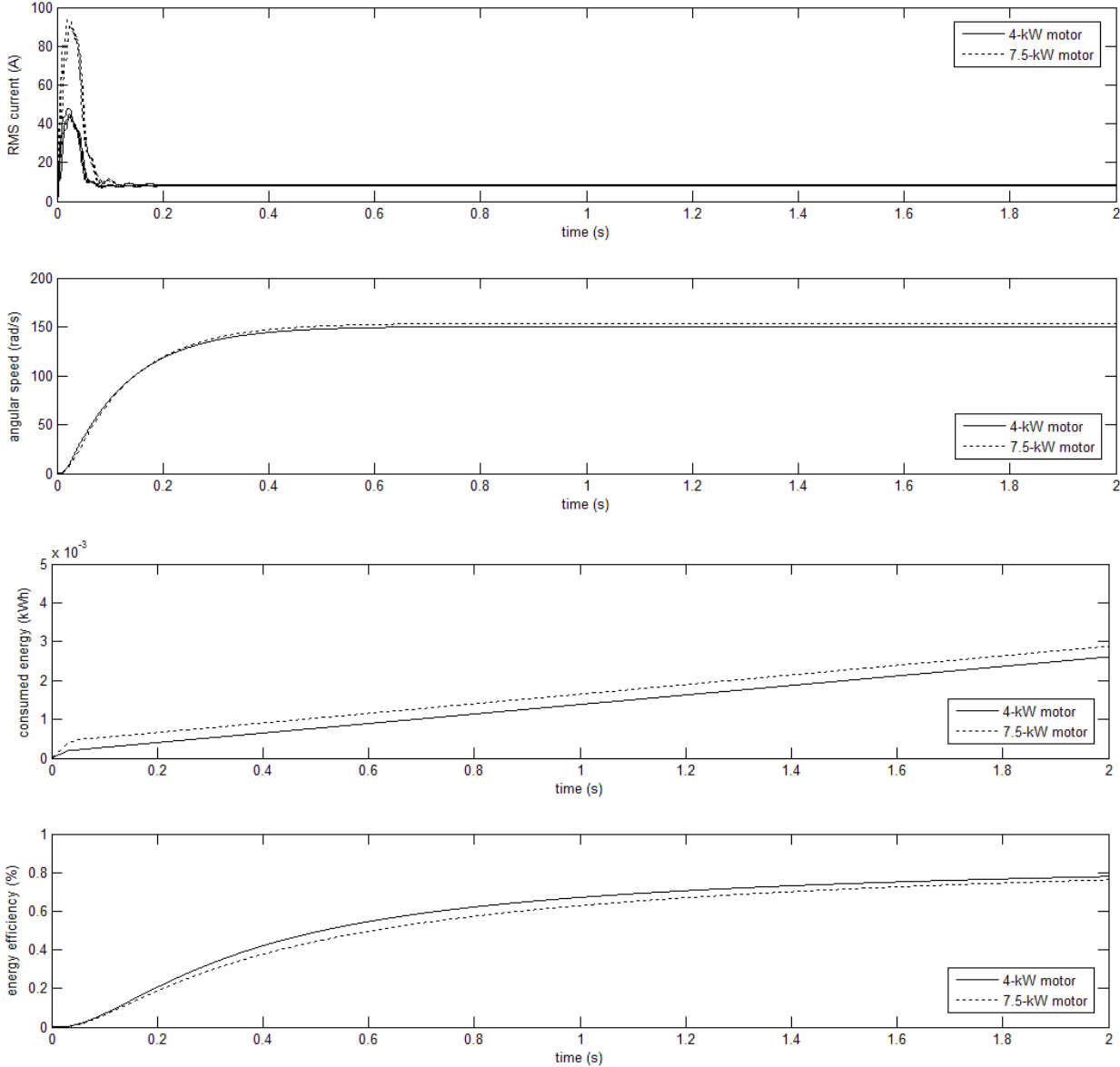


Fig. 4.68. Simulated starting period for 4-kW and 7.5-kW motors driving a fan-type load with a slight static friction component ($T_{load} = 0.00115 \cdot \omega + 0.0001$).

4.15 Conclusions

It is possible to conclude that, among the low complexity, low intrusion methods, the input power-based method is the most accurate for the vast majority of the cases. It presents a relatively

reduced error, regardless the motor power, number of poles and load level, although a significant error can occur for very low loads, particularly for small motors. For loads higher than 50-60%, the maximum error that may be expected is 8%, which is mainly associated with the motor efficiency variation with load. The delta/star connection-mode change improves significantly the method accuracy at low loads, particularly for low power motors. However, this method requires relatively expensive equipment (digital wattmeter), and it can be applied only if the power conductors/cables to the motor are accessible, which sometimes does not happen. The power factor-based method is not recommended due to the fact that requires the same equipment as the real power-based method, and it is preferable to apply the latter method, since it is much more accurate.

The slip-based method can lead to significant errors for all load levels, even for low-power motors, being, however, a fair method for a first approach or large-scale evaluation, in order to identify a minimum guaranteed load level.

The current-based method can have several variants. If a fair number of part-load points, including the no-load point, and/or the delta/star connection mode change were considered, the accuracy can be quite good, and can be used either for a first approach in its simplest form, or for an accurate load evaluation in its improved forms.

The proposed improvements in the slip, current and power methods lead to a significant reduction in the respective error, particularly for small/medium motors with low loads.

A significant improvement of the results is expected if combined approaches are used, for example, combining slip and current values. This can be done either using the estimated maximum and minimum load levels in a slip- and current-load combined curve or using the circle diagram.

More sophisticated methods, such as the equivalent circuit or air-gap torque methods, lead, in general, to more accurate results, but, besides being impossible or impracticable to apply in some cases, are time consuming and/or require expensive equipment, and, in some cases, can actually lead to significant errors, as it was demonstrated. In particular, the equivalent circuit method is not, in general, easy to apply in the European motors, due to the commonly available data, but can be properly adapted.

The proposed new evaluation criteria for load estimation methods, based on the useful accuracy, is an important tool to evaluate if a certain method is or not adequate for a certain rated power and number of poles, if the aim of the motor load evaluation is to define properly the rated power of a new replacing motor. On the basis of this new approach, the analysed methods were requalified.

It should be emphasized that the motor derating assessment as a function of the PQ is also very important to take into account on the load estimation (see Appendix 4).

Lastly, as an overview, Table 4.6 presents a summary of the simplest low-cost in-field motor load estimation methods and the respective recommended application domain.

TABLE 4.6
SUMMARY TABLE ON THE SIMPLEST LOW-COST IN-FIELD LOAD ESTIMATION METHODS.

Method	Principle & Equipment Required	Recommended General Application		
		Rated Power	No. of Poles	Load Range
Slip-Based Method	Relates actual and rated slips. Requires speed and voltage measurement. Good for a first survey.	< 30-50 kW	≤ 4	25-100%
Current-Based Method (Simple)	Relates actual and rated line currents. Requires current measurement. Good for a first survey.	≥ 30-55 kW	≤ 4	50-100% See Table 4.1.
Current-Based Method (With Interpolations)	Uses empirical and/or statistical part-load current values for interpolation. Good for a second/accurate survey.	≥ 11 kW	≤ 4	25-100% See Table 4.1.
Current-Based Method (With Delta/Star Change)	Uses empirical and/or statistical part-load current values for interpolation and star connection. Good for a second/accurate survey.	All	2-8	0-50% See Table 4.2.
Power Factor-Based Method (With Interpolations)	Uses empirical and/or statistical part-load power factor values for interpolation. Good for a second/accurate survey.	All	2-8	0-100%
Real Power-Based Method (Simple)	Relates actual and rated input real power values. Requires real power measurement. Good for a second/accurate survey.	≥ 5.5 kW	2-8	25-100%
Real Power-Based Method (With Delta/Star Modes)	Uses delta and star connection. Good for a second/accurate survey.	≥ 1.5 kW	2-8	5-100%
Slip and Current-Based Combined Method	Combines the slip-load and current-load curves. Good for a first survey to identify a load range.	≥ 30-55 kW	≤ 4	25-100%
Circle Diagram-Based Combined Method	Combines the slip and current values by means of circle diagram. Good for a second/accurate survey.	≥ 30-55 kW	≤ 4	25-100%
Temperature-Based Method	Relates the actual and rated frame or winding temperatures, taking into account the ambient temperature. Good for a first survey, to identify motors potentially oversized.	All	2-8	> 75%

4.16 References

- [1] Kueck, J.; Olszewski, M.; Casada, D.; Hsu, J.; Otaduy, P.; Tolbert, L.: "Assessment of Methods for Estimating Motor Efficiency and Load Under Field Conditions", Prepared by Oak Ridge National Laboratory, Managed by Lockheed Martin Energy Research Corp., for U.S. Department of Energy, under contract DE-AC05-96OR22464, January 1996.
- [2] "Determining Electric Motor Load and Efficiency", United States of America Department of Energy, Fact Sheet, Motor Challenge, 1997.
- [3] A. K. Wallace et al.: "A Laboratory Assessment of In-Service Motor Efficiency Testing Methods", IEEE Inter. Conf. on Electric Machines and Drives (EMDC'97), Conf. Rec., WC1/7.1-WC1/7.3, 18-21 May 1997.
- [4] Hsu, J.; Kueck, J.; Olszewski, M.; Casad, d.; Otaduy, P.; Tolbert, L.: "Comparison of Induction Motor Field Efficiency Evaluation Methods", IEEE Trans. on Industry Applications, Vol. 34, No. 1, pp. 117-125, Jan./Feb. 1998.
- [5] Wallace, A.; Wiendenbürg, E.: "Motor Efficiency Determination: From Testing Laboratory to Plant Installation", IEEE Pulp and Paper Technical Conf., Conf. Rec., pp. 190-195, 21-25 June 1999.
- [6] Wiendenbürg, E.; Wallace, A.: "In-service testing of Three-Phase Induction Motors", IEEE Inter. Symposium on Diagnostics for Electric Machines, Power Electronics and Drives (SDEMPED'99), Conf. Proc., pp. 210-224, Gijon, Spain, 1999.
- [7] Wiendenbürg, E. et al.: "Modern On-line Testing of Induction Motors for Predictive Maintenance and Monitoring", IEEE Pulp and Paper Industry Technical Conf., Conf. Record, pp.163-168, 18-22 June 2001.
- [8] Hsu, J.; Scoggins, B.: "Field test of motor efficiency and load changes through air-gap torque", IEEE Trans. Energy Conversion, Vol. 10, pp. 471-477, Sept. 1995.
- [9] Agamloh, E.; Wallace, A.; Jouanne, A.; Anderson, K.; Rooks, J.: "Assessment of Nonintrusive Motor Efficiency Estimators", IEEE Trans. on Industry Applic., Vol. 41, No. 1, pp. 127-133, Jan./Feb. 2005.
- [10] de Almeida, A., et al.: "Improving the Penetration of Energy-Efficient Motors and Drives", European Commission, DG TREN, SAVE II Prog. 2000, Edited by ISR-University of Coimbra, 2000.
- [11] "Understanding AC motor efficiency", Electrical Apparatus Service Association, St. Louis, MO.
- [12] IEC 60034-1, Ed. 11, 2004: "Rotating electrical machines - Part 1: Rating and performance".
- [13] IEC 60034-2-1, Ed. 1, 2007: "Methods for determining losses and efficiency of rotating electrical machinery from tests - excluding machines for traction vehicles", Final Draft International Standard, 2/1443/FDIS.
- [14] IEEE 112 Std., 2004: "Test Procedure for Polyphase Induction Motors and Generators".
- [15] Ferreira, F.: "Comparative Study of Two Different Power Analyzers - Baker Explorer & Yokogawa WT1030M (with speed and torque sensors)", 1st and 2nd technical reports for academic discussion, confidential – only for academic purposes, ISR-University of Coimbra, Nov. & Dec. 2005.

- [16] E. J. Wiendenbürg: “Voltage measurements of Explorer II”, Technical Report, Confidential – only for academic purposes, Reply to [15], Jan. 2006.
- [17] de Almeida, A.; Ferreira, F.; Angers, P.; Busch, J.: “Comparative Analysis of IEEE 112-B and IEC 34-2 Efficiency Testing Standards using Stray Load Losses in Low Voltage Three-Phase, Cage Induction Motors”, IEEE Trans. on Industry Applic., Vol. 38, No. 2, pp. 608-614, Mar./Apr. 2002.
- [18] Sen P., “Principles of Electric Machines and Power Electronics”, John Wiley & Sons.
- [19] Doebelin, E.: “Measurement Systems - Application and Design”, 4th Ed., McGraw-Hill, Inc., New York, 1990.
- [20] EuroDEEM, The European Database of Efficient Electric Motors Motor Database, <http://sunbird.jrc.it>, 2007.
- [21] MotorMaster, An energy-efficient motor selection and management tool (motor database), <http://www1.eere.energy.gov>, 2007.
- [22] Dep. Electrical Engineering, Katholieke Universiteit Leuven, Heverlee, Belgium, 2000.
- [23] Chauvin Arnoux/Metrix Test & Measurement Catalogue, www.chauvin-arnoux.com, 2004.
- [24] “Optimizing your motor-driven system”, Motor Challenge, Fact Sheet, www.motor.doe.gov.
- [25] NEMA MG-1, 1998: “Motors and Generators”.
- [26] Köfler, H.: “Can Solid State Voltage Regulation Devices Save Energy in Induction Machines? An Experimental Proof with Some Theoretical Explanations”, 16th Inter. Conf. on Electrical Machines (ICEM’04), Conf. Proc., Krakow, Poland, 2004.
- [27] Technical Information about ABB motors (200 kW/4 poles; 200kW/2 poles; 400 kW/4 poles; 400 kW/2 poles).
- [28] Alger, P.: “Induction Machines – Their Behavior and Uses”, Gordon and Breach Publishers, 3rd Edition, 1995.
- [29] MATLAB/SIMULINK Version 7.0.1 (R14), Default values for 3-phase cage induction motors, The MathWorks, Inc., 2004.
- [30] Ferreira, F.; de Almeida, A.; Almeida, J.: “Estimação do Factor de Carga em Campo para Motores de Indução Trifásicos com Rotor em Gaiola de Esquilo”, Revista Kéramica, Ano XXIX, N.º 265, Março/Abril de 2004.
- [31] Eren, L.; Devaney, M.: “Instrument Transformer Error Compensation in Fourier Based Power Metering”, IEEE Instrumentation and Measurement Technology Conf., Conf. Proc. Anchorage, AK, USE, 21-23 May, 2002, pp. 1467-1470.
- [32] Boldea, I.; Chris, L.; Wallace, A.: “Load Testing of Induction Machines without Torque Measurements”, IEEE Inter. Conf. Electric Machines and Drives (IEMD’99), Conf. Proc., pp. 162-164, 9-12 May 1999.
- [33] WEG: “Cast Iron Motors – W21 Line”, Catalogue, 2006.
- [34] Lu, B.; Habetler, T.; Harley, R.; Gutiérrez, J.; Durocher, D.: “Applying Wireless Sensor Networks in Industrial Plant Energy Evaluation and Planning Systems”, IEEE Industry Applications Magazine, pp. 17-23, Mar./Apr. 2007.
- [35] Hsu, J.; Sorenson, P.: “Field Assessment of Induction Motor Efficiency through Air-Gap Torque”, IEEE Trans. on Energy Conversion, Vol. 11, No. 3, pp. 489-494, Sept. 1996.
- [36] Ferreira, F.; de Almeida, A.: “Considerations on In-Field Induction Motor Load Estimation Methods”, 18th Inter. Conf. on Electrical Machines (ICEM’08), Conf. Proc., Vilamoura, Portugal, Sept. 2008.

5. Stator Winding Connection Change

Overview – Most oversized IMs operate with relatively low efficiency and power factor, which is by far the most important cause of poor power factor in industrial installations. In low-load operating periods, motor performance can be improved in terms of efficiency and power factor if the magnetizing flux is properly regulated. This can be made by means of proper stator winding connection-mode change as a function of the motor actual load. In this section, stator winding connection-mode management strategies (basic principles) to improve the performance (in terms of efficiency and power factor) of variable-load or permanently oversized IMs with conventional six-terminal windings (connected in delta or star mode) or special twelve-terminal windings (with two sets of turns, sharing the same positions in the stator slots, connected either in series or in parallel, having more than six connection modes) are discussed. In the latter case, among all the possible stator winding connections, six modes were selected and analysed. Several considerations regarding the simulation of multi-connection IMs by means of changing the per-phase equivalent circuit parameters are presented. A novel practical method to quickly and easily evaluate which stator winding connection is more appropriate for the actual motor load profile is proposed, being suitable for in-field evaluation, because it requires only the use of inexpensive equipment and has enough accuracy to allow a proper decision to be made. The automatic change of the stator winding connection, as a function of the motor line current, is also analysed. An electronic device for automatic winding connection mode change is proposed, as well as a contactor concept for the multi-connection motor. Most of the material presented in this chapter was published in [8], [10], [12], [16] and [17], and a small part of it will be presented in [48]. Further research is being carried out on IMs with multi-connection stator windings (see Appendix 6) and part of the respective results will be presented in [41] and [44].

5.1 Introduction

As it was referred in Chapter 2, in Industry, the vast majority of the electrical motors are IMs. In the EU, the average load factor for IMs, in both industrial and tertiary sectors, is less than 60% (Fig. 5.1). However, the average load factor per power range in some sectors can be as low as 25% [1], [2]. Individual motors in those ranges have even lower load factors. Since the motor load factor is an average of the motor load during a defined period (e.g., motor duty-cycle period), the motor load can alternate between values which are lower and higher than the motor load factor. As previously referred, motor oversizing is mainly due to poor motor system design or due to the gross overestimation of the mechanical power required by the load [1]. Additionally, motor oversizing is a widespread practice due to the motor market structure, which is largely dominated by OEMs. Therefore, motors with a wide load variation, alternating between very low load (e.g. less than 30% of full load) and near full load (e.g., more than 75% of full load) during their duty cycle, can also be found. In these cases, the motor is sized to provide the load peak power, but it can operate during long periods with a very low load. These situations may lead to a significant reduction of both efficiency and power factor of motors. In fact, in variable-load applications (e.g., conveyors, escalators, lifts, mixers, fans, pumps, high-inertia saws and presses, etc.), motors can have low-load operating periods, in which its efficiency and power factor can be significantly low [10]. However, if the stator winding voltage is properly regulated, efficiency and power factor of motors can be both improved significantly in the low-load operating periods. In general, voltage regulation (continuous or discrete) in IMs has an associated savings potential up to 10% [26]. In

the following sections, the benefits associated with the connection management in conventional single-voltage IMs and in multi-connection or multi-flux level IMs (MFLIM) are analysed.

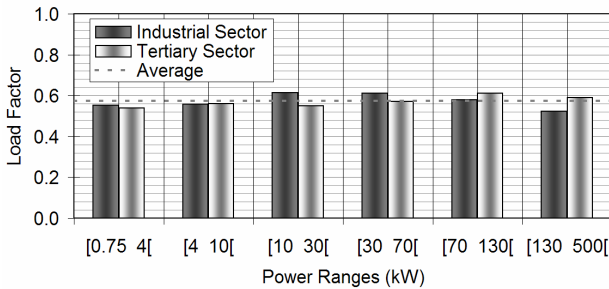


Fig. 5.1. Average load factor by power range for motors, in the industrial and tertiary sectors, in the European Union, 2000 [1].

5.2 Star-Delta Connection Management

For specific conditions, the stator winding connection change from delta (or triangle, hereafter denoted by D) to star (or wye, hereafter denoted by Y) can significantly improve both motor efficiency and power factor. This possibility is only available for motors designed to operate at the nominal power with D connection and with access to the 6 winding terminals (Fig. 5.2), which are the vast majority. This represents an innovation in relation to the traditional application of D and Y connections, which is mainly for motor starting and for two-voltage capability (in this case, if the higher voltage connection is used, the Y/D starting is not possible).

In this section, an in-field evaluation method to access the most appropriate motor stator-winding connection is proposed and analysed, in the perspective of motor efficiency and power factor. The automatic change of the motor stator-winding connection, as a function of the motor line current, is also analysed. In [22], this principle was briefly analysed based on simulations using simple motor equivalent circuit (with no thermal compensation). For both methods, technical and economical considerations associated with motor stator-winding connection are presented. The importance of this work is highlighted by the recent concerns on electric motor systems optimization in the industrial and tertiary sectors, as discussed in Chapter 1.

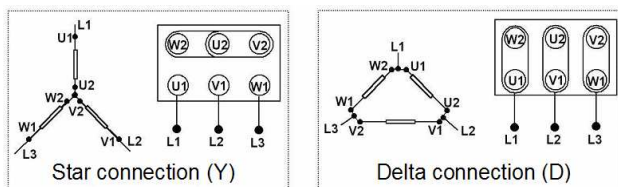


Fig. 5.2. Motor stator-winding connections (on the left: star or wye connection; on the right: delta or triangle connection).

5.2.1 Theoretical Principle

A well-designed IM usually meets most of the following guidelines: (a) The stator winding resistance is kept small in order to reduce the stator copper loss; (b) The stator winding leakage

reactance is minimized by reducing the mean-turn length of each coil; (c) Thin laminations of low-loss steel are used to cut down the core loss; Thus, the equivalent core-loss resistance is usually high; (d) The permeability of steel selected for laminations is high, and the operating flux density in the motor is kept below the knee of the magnetization curve. Thus, the magnetization reactance is usually high.

Provided such conditions, the inaccuracy of the per-phase approximate equivalent circuit¹ (AEC), which is shown in Fig. 5.3, is negligible for a well designed motor [3]. Additionally it simplifies the mathematical motor analysis.

Ignoring the saturation and space-harmonics effects, for a fixed line-to-line voltage, the change of the stator connection from delta to star leads to the reduction of the winding voltage by a factor of $\sqrt{3}$, which is applied to the per-phase equivalent circuit voltage, or to the increase of the equivalent circuit parameters 3 times, being these relations demonstrated as follows. The following equations are based on the AEC [3]-[7].

The torque developed by an IM, T_{em} , can be computed using (5.1). Finding the zero of the first derivative of T_{em} with respect to s , the breakdown or maximum torque slip, s_{brk} , is given by (5.2). Therefore, the expression for the maximum torque developed, $T_{em(max)}$, is given by (5.3). Considering phase voltage regulation provided by delta to star change, and ignoring saturation and space-harmonics effects, the relation between the respective maximum torques is given by (5.4). Actually, the saturation affects mainly the L_m parameter, but L_2 parameter is also affected, which can have a significant impact on $T_{em(max)}$. Assuming fixed U_1 , the previous change is similar to increase 3 times the equivalent circuit parameters, as it can be seen in (5.5).

$$T_{em} = \frac{\frac{3U_1^2 R_2}{s}}{\left[(R_1 + R_2)^2 + (X_1 + X_2)^2 + \left[\frac{R_2(1-s)}{s} \right]^2 + \frac{2(R_1 + R_2)R_2(1-s)}{s} \right] \omega_{sync}} \quad (5.1)$$

$$s_{brk} = \frac{R_2}{\sqrt{R_1^2 + (X_1 + X_2)^2}} \quad (5.2)$$

$$T_{em(max)} = \frac{3U_1^2}{2\omega_{sync}} \left[\frac{1}{R_1 + \sqrt{R_1^2 + (X_1 + X_2)^2}} \right] \quad (5.3)$$

$$T_{em(max)_Y} = \frac{3 \left(\frac{U_1}{\sqrt{3}} \right)^2}{2\omega_{sync}} \left[\frac{1}{R_1 + \sqrt{R_1^2 + (X_1 + X_2)^2}} \right] = \frac{1}{3} T_{em(max)_D} \quad (5.4)$$

¹ In the per-phase approximate equivalent circuit, the R_1 - R_2 - X_1 - X_2 series branch is in parallel with the R_2 - L_m parallel branch.

$$T_{em(max)_Y} = \frac{3U_1^2}{2\omega_{sync}} \left[\frac{1}{3R_1 + \sqrt{9R_1^2 + 9(X_1 + X_2)^2}} \right] = \frac{U_1^2}{2\omega_{sync}} \left[\frac{1}{R_1 + \sqrt{R_1^2 + (X_1 + X_2)^2}} \right] = \frac{1}{3} T_{em(max)_D} \quad (5.5)$$

This analysis can be easily extended to the other operating points, but, for that, saturation effects have to be taken into account to improve the model accuracy. Nevertheless, for a first approach, ignoring saturation, the D/Y change simulation can be made either considering a voltage decrease of $\sqrt{3}$ times maintaining the same equivalent circuit parameters² or, assuming a constant line-to-line voltage, by increasing 3 times the equivalent circuit parameters. The saturation effect can be included, at least, on L_m value, providing a proper dependency on magnetizing current I_m . This procedure is implemented in a special per-phase exact equivalent circuit (EEC), described in Appendix 2. The equivalent circuit transformation by changing its parameters value is discussed further in Section 5.3.

Since the torque is roughly proportional to the squared voltage (neglecting the stator leakage reactance and resistance), it is reduced 3 times after a delta to star change. For a given slip (actually, due to the torque-slip curve reshape, the slip increases for the Y connection), the motor output power is thus reduced 3 times. The result is a single-voltage two-power motor. After D to Y change, since core losses and stator Joule losses³ will decrease but the friction and windage losses remain approximately constant (assuming minor slip changes), the efficiency-load curve for the low-power operating mode (Y connection) can present a peak efficiency different (lower or higher) from that corresponding to the high-power operating mode depending on the share of those losses and its relation with the motor output. Since windage and friction losses, as a percentage of the output power, are more relevant for very low-power motors⁴ (< 7.5 kW), in those cases, the peak efficiency is likely to be slightly lower for the Y-connected operating mode. For larger motors, an increase in the Y-mode peak efficiency is expected, particularly for motors with a number of poles equal or higher than 4. However, it is clear that, if the load of a motor with D as rated connection is low enough to operate it with Y connection, due to the core and stator Joule losses reduction, significant improvements can be obtained in the motor efficiency, power factor and reliability (the motor can actually run cooler). Basically the winding voltage is regulated within two states as a function of the motor load to improve motor efficiency and power factor.

² In this case, for the delta connection, the motor input line current is obtained by multiplying the phase (or the equivalent circuit) current by $\sqrt{3}$.

³ After D to Y change, the saturation level decrease, and, therefore, the magnetizing current will decrease more than if linearity or fixed magnetizing inductance were assumed when reducing phase voltage, leading to lower Joule (or ohmic) losses in the stator windings. Additionally, since the iron losses are also reduced, the average stator winding and rotor temperature decrease, lowering the respective Joule losses. The only losses that remain approximately constant are those associated with windage and friction.

⁴ In the case of 2-pole motors, since the friction and windage losses, in percentage of total losses, are higher, the peak efficiency decrease in Y-mode is expected to be higher. Moreover, since, in general, the core and stator Joule losses, in percentage of total losses, increase with the number of poles, and those losses are reduced after the connection change to Y-mode, the peak efficiency in that mode is expected to be higher for motors with a number of poles equal or higher than 4.

5.2.2 Simulated Results

The efficiency-load curves for 3 motors were simulated in the MATLAB/SIMULINK software tool, using the exact motor per-phase equivalent circuit (EEC, Fig. 5.3) [3]-[7]. However, no thermal compensation and saturation effects were taken into account. For the Y connection, a voltage $\sqrt{3}$ times lower than the voltage considered in the D connection was considered in the simulation. For the 3-kW motor (Brand A) the per-phase equivalent circuit parameters were experimentally obtained [10]. For the 11-kW and 300-kW motors the per-phase equivalent circuit parameters were obtained from book data in [5] and [7]. The mechanical losses, as a function of motor speed, were also considered in the simulations. In Fig. 5.4, the simulated motor efficiency-load curves for both D and Y connections, for the three motors can be seen, as well as the motor parameters. Further simulations were carried out for the 3-kW motor considering thermal compensation and saturation, being the results presented in Fig. 5.24-5.28.

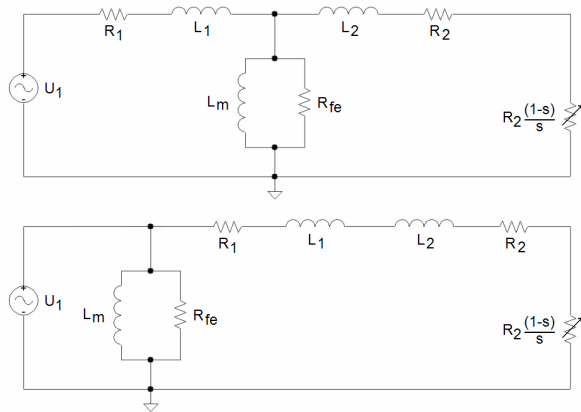


Fig. 5.3. Per-phase equivalent circuit (referred to the stator): (top) exact (EEC), used in the simulations; (bottom) approximate (AEC), used as a basis for some theoretical demonstrations.

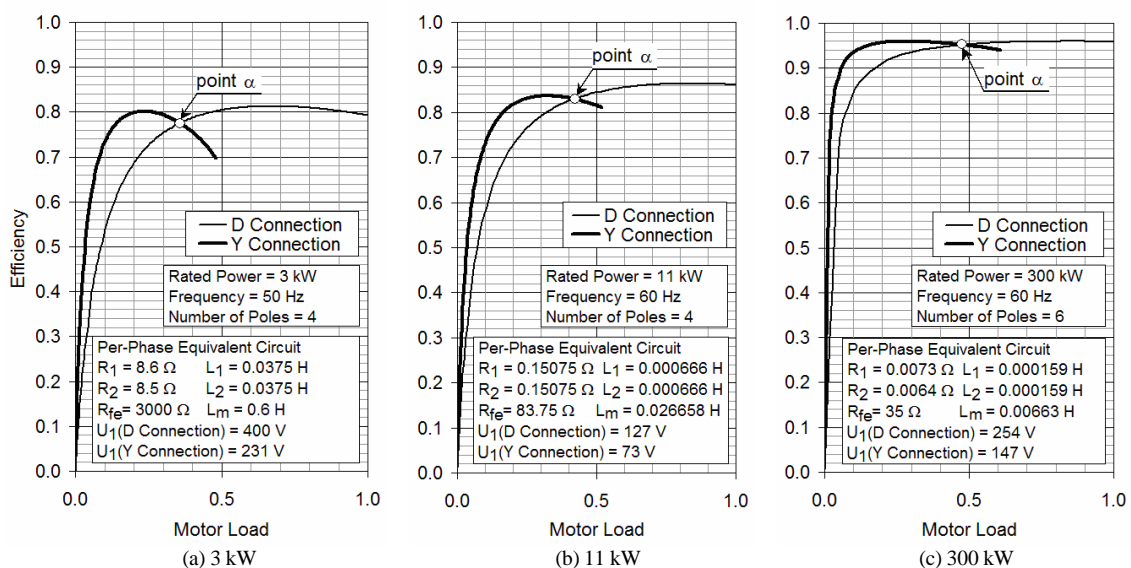


Fig. 5.4. Simulated motor efficiency, as a function of the load, for motors with different power ratings: (a) 3 kW, (b) 11 kW, and (c) 300 kW [10].

The intersection point between the efficiency-load curves, hereafter denominated by point α , for the efficiency-load simulated curves for the D and Y connections corresponds to a motor load of 0.36, 0.42 and 0.47, for the 3-kW, 11-kW and 300-kW motors, respectively.

Note that, according to the Fig. 5.4, the load corresponding to the crossover point α increases with the motor nominal power, because the efficiency curves become flatter (due to the relative lower core losses), which can be observed in Fig. 1.8 of Chapter 1.

Regarding the transient behaviour, simulations were carried out for a 37-kW, 4-pole motor, driving a fan-type load, being the results presented in Section 5.3.3.

5.2.3 Experimental Results

The motor test facility used in the experimental tests fulfils the main motor testing standards, as described in Chapter 2. To measure the electrical and mechanical variables a high accuracy power analyzer is used. A dynamometer is used as a variable load, which includes an encoder to measure speed, and a load cell to measure the torque. The power analyzer acquires the values of both sensors and directly measures the motor efficiency.

Thirteen totally enclosed fan-cooled IMs of five different brands (denominated in this section by A, B, C, D and E), with nominal powers between 185 W and 7.5 kW, were tested. In Table 5.1, the nameplate values of these motors, considering the D connection, can be seen. Eleven motors have 4 poles, one has 2 poles and the remaining one has 6 poles.

In all the tests, the motor thermal equilibrium was guaranteed, for the same room temperature. The temperature correction of the motor parameters was not considered, in order to allow a real evaluation of the motor performance for both D and Y connections and different load points.

A summary of the experimental results is presented in Table 5.1. In Fig. 5.5, the motor efficiency, power factor, speed and line current, as a function of the load (denoted by ζ), for Y and D connections, for the 3-kW (Brand A) and 5-kW (Brand B) motors, both 4-pole motors, are presented. For a motor load lower than point α , the motor efficiency and power factor for the Y connection are higher than for the D connection (Fig. 5.5a and Fig. 5.5b). For any motor load, the D to Y change also leads to a speed decrease (Fig. 5.5c). For the tested motors (which are all in a very narrow low power range), the point α has no regular relation with brand, nominal power, number of poles, and it is between $\zeta = 0.27$ and $\zeta = 0.43$ (average $\zeta = 0.36$, see Table 5.1). However, as it can be seen in previous section, for motors with significant higher power, the point α moves to a higher load.

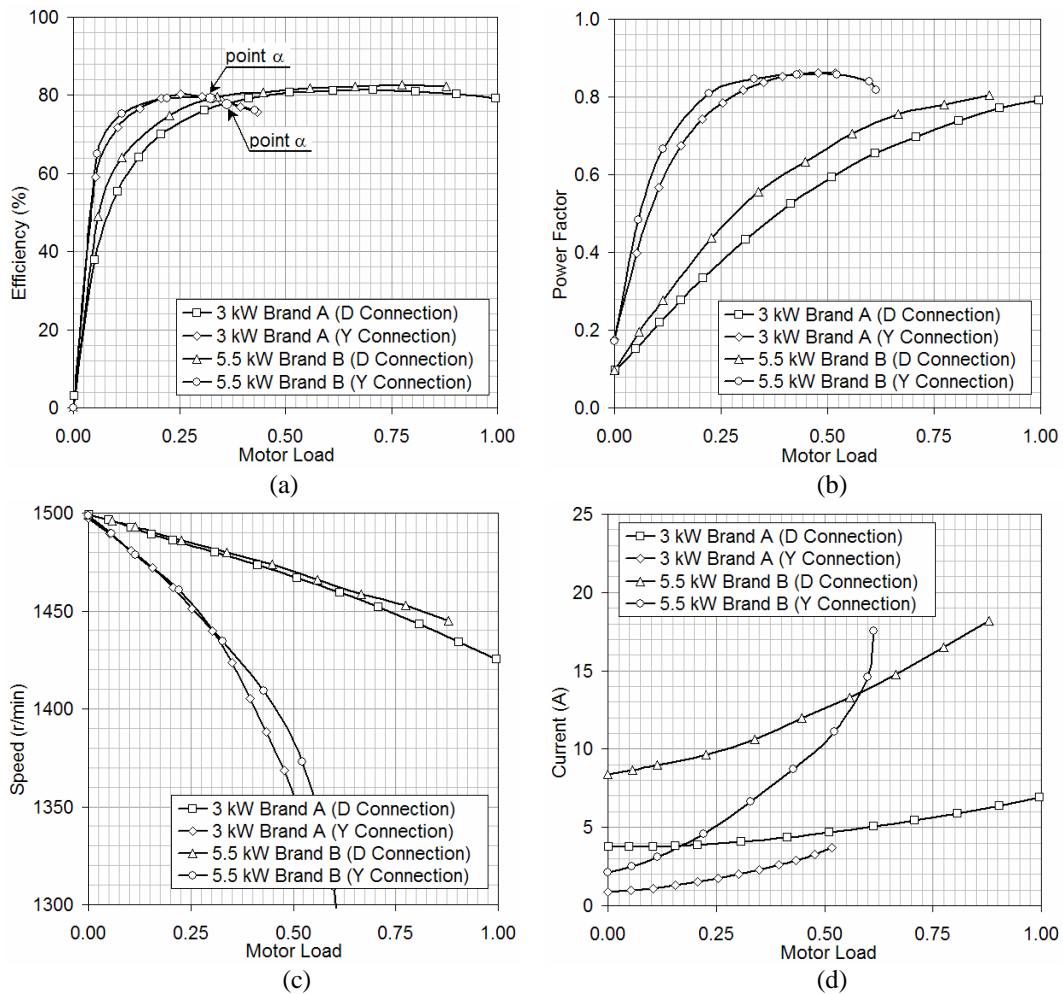


Fig. 5.5. Experimental results for the 3 kW, 4-pole motor (Brand A) and for the 5.5 kW, 4-pole motor (Brand B): (a) motor efficiency, (b) motor power factor, (c) motor speed, and (d) motor line current, as a function of the load [10].

The experimental and simulated point α for the 3-kW motor (Brand A), are approximately in accordance. Note that the actual difference in the motor operating temperature and saturation for both D and Y connections in the different load points is not considered in the simulation.

From Fig. 5.5, it can be concluded that the user should evaluate several factors before changing the motor stator-winding connection. The most important factor should be the motor efficiency. For a specific load below point α , the increase in the power factor and in the slip after the D to Y connection change is well known.

5.2.4 Methods for Different Load Profiles

The motor stator-winding connection change can be made either by a manual method (permanent change) or by an automatic method (dynamic change). Each method should be chosen according to the motor load profile. If the load profile is similar to the load shape of the Figs. 5.6a or 5.6b, the stator-winding should be permanently connected, after starting, in Y or D, respectively. In both cases, if the motor load slightly crosses the point α load level, during short periods, the respective connection can still be used (this issue is addressed in Section 5.2.5). If the load profile

is similar to the load shape of the Fig. 5.6c, the stator-winding connection should be automatically managed by a suitable control device.

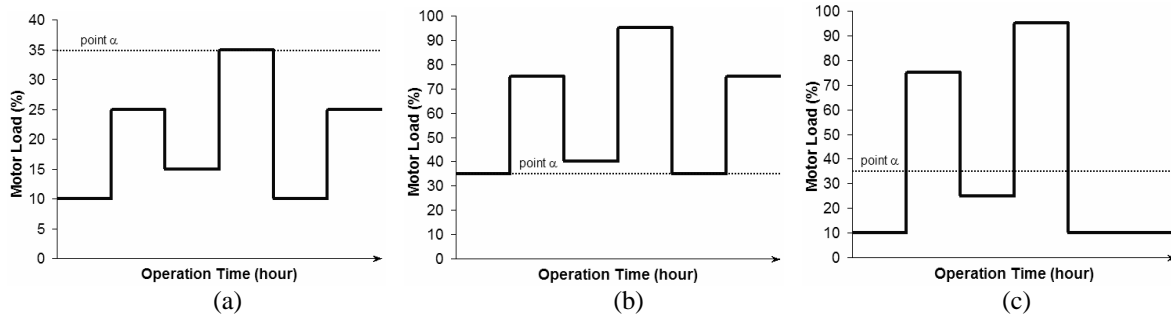


Fig. 5.6. Motor load profiles for: (a) permanent Y connection, (b) permanent D connection, and (c) automatic management of the connection [10].

5.2.4.1 Permanent Change of the Winding Connection

When the stator-winding connection is changed from D to Y, the winding voltage decreases $\sqrt{3}$ times. In point α , the efficiency, the mechanical power and the active electrical power values, for both D and Y connections, are equal. Therefore, in point α , and assuming a balanced system, the relation (5.6) is true, where I_l is the line current and λ is the power factor [10], [12].

$$\frac{I_{l(D)}^\alpha}{I_{l(Y)}^\alpha} = \frac{\lambda_Y^\alpha}{\lambda_D^\alpha} \quad (5.6)$$

In order to identify point α , four indicators based on the motor in-field measurements and motor nameplate values (nominal values), are analysed, namely, two line current based indicators, K_{I1} and K_{I2} , and two slip based indicators, K_{s1} and K_{s2} .

The proposed indicators are based on values easily obtained in the field, using common measurement devices (voltmeter, clamp ammeter and stroboscopic tachometer), namely, the RMS line-to-line voltage, the RMS line current, and the motor speed. The measurement of the power factor is avoided because it requires the use of a power factor measurement device, a wattmeter or a power analyzer, which, to have sufficient accuracy, are expensive devices.

The indicators K_{I1} , K_{I2} , K_{s1} and K_{s2} are defined by (5.7), (5.8), (5.9) and (5.10), where I_N is the motor rated line current, U_N the motor rated line-to-line voltage, U_{meas} is the actual motor line-to-line voltage, s_N is the motor nominal slip and s_{meas} is the actual motor slip.

$$K_{I1} = \frac{I_{l(D)}}{I_N} \quad (5.7)$$

$$K_{I2} = \frac{I_{I(D)}}{I_{I(Y)}} \quad (5.8)$$

$$K_{s1} = \left(\frac{\omega_{\text{sync}} - \omega_{\text{meas}(D)}}{\omega_{\text{sync}} - \omega_N} \right) \cdot \left(\frac{U_N}{U_{\text{meas}}} \right)^2 = \frac{s_{\text{meas}(D)} \cdot U_N^2}{s_N \cdot U_{\text{meas}}^2} \quad (5.9)$$

$$K_{s2} = \frac{s_{\text{meas}(D)}}{s_{\text{meas}(Y)}} \quad (5.10)$$

The indicators K_{II} and K_{sI} are obtained without disconnecting the motor, and the indicators K_{I2} and K_{s2} require the motor stator-winding connection change.

In Table 5.1, a summary of the indicator values, their average values, standard deviation and variation with load, in relation to the point α , for the tested motors, is presented. In Table 5.2, a summary of the obtained indicator values, in relation to the point α , for the simulated motors, is presented.

The standard deviation, σ , of a generic variable, x , is given by (5.11), where n is the number of samples or population size.

$$\sigma = \frac{1}{n} \sqrt{n \sum_{i=1}^n x_i^2 - \left(\sum_{i=1}^n x_i \right)^2} \quad (5.11)$$

It is also important to evaluate the variation of each indicator, when the motor load is moving away from the point α . In Table 5.1, the average variation of the indicators in the neighbourhood of point α ($\pm 10\%$ variation), is presented.

The indicator K_{sI} is easy to obtain (it requires a stroboscopic tachometer and a voltmeter) but has errors related to the speed measurement device errors (typically ± 1 r/min) and to the nameplate speed errors due to the numerical rounding process (the speed is rounded to 5 r/min multiples) [10]. The indicator K_{sI} includes a voltage correction related to the fact that, for a constant torque, the motor slip is approximately inversely proportional to the squared voltage. Therefore, if there is a difference between the motor actual voltage and its nominal voltage, it is necessary to compensate the slip, considering the relation between both voltages. The variation between K_{sI} for the tested motors, in the point α , is reduced ($\sigma = 0.04$ for an average equal to 0.29). It can be concluded that if a motor has a $K_{sI} \leq 0.25$ there is a fair possibility (93% of the tested motors and 100% of the simulated motors verify that condition) of being operating in the zone where energy consumption reduction can be obtained after the stator-winding connection change from D to Y. In the simulated data, it can be concluded that K_{sI} can slightly increase with the motor rated power.

The indicator K_{s2} is also easy to obtain (it also requires a stroboscopic tachometer and a voltmeter) and it is more reliable than K_{s1} , but requires the motor stator-winding to be changed. The variation between K_{s2} for the tested motors, in the point α , is reduced ($\sigma = 0.03$ for an average equal to 0.27). It can be concluded that, if a motor has a $K_{s2} \geq 0.30$, there is a high possibility (100% of the tested and simulated motors verify that condition) of being operating in the zone where energy consumption reduction can be obtained after the stator-winding connection change from D to Y.

The K_{II} is not a good indicator because, when the motor load is moving away from point α , for the tested motors, it has a very low average variation ($\pm 2\%$), tending to 0% for motors with $P_N \leq 1$ kW.

The K_{I2} average is 1.67 ($\sigma = 0.11$), which is also equal to the ratio between the Y and D power factors, in point α , as it was demonstrated in (5.6).

On the basis of previous conclusions, a simple in-field method to evaluate which connection is more appropriated for the motor stator-winding, as a function of the motor slip, can be defined, based only on the K_{s1} and K_{s2} indicators (see Fig. 5.7). In this evaluation, the higher loads of the motors during their duty-cycle should be considered. Firstly, the possibility of motor efficiency improvement after the stator-winding connection change from D to Y should be determined based on the nameplate and actual motor speed and voltage, using K_{s1} . The D to Y change should only be made if $K_{s1} \leq 0.25$, with a fair possibility of efficiency improvement. After the D to Y change, a slip based re-evaluation should be made using K_{s2} . If $K_{s2} \geq 0.30$ the Y connection should be maintained, otherwise the winding should be re-connected to D.

Note that, even if there are no significant efficiency improvements due to the proximity between the motor load and the point α , the power factor still significantly improves.

Although the proposed method was only experimentally validated for the 185 W-7.5 kW motor power range, in principle, it can be applied to all the motors, because K_{s2} has a very low dependency on the motor rated power and K_{s1} can slightly increase with the motor rated power, as it was demonstrated by the simulated results (see Table 5.2).

The permanent stator-winding connection should be re-evaluated periodically if the load characteristics change. The proposed method is suitable for grossly oversized motors and/or motors driving loads with low duty-cycles and high inertia (e.g., fly-wheel press machines⁵ and high-inertia rotary saws⁶). Since it requires only low-cost and easy-to-use equipment (a

⁵ A low duty-cycle in a flywheel press machine means a low pressing rate, i.e., the pressing period duration is significantly shorter than the non-pressing period duration.

⁶ In these load types, if the motor stator winding is Y connected, and the time between the maximum load periods is sufficient to allow the acceleration and speed stabilization of the inertia wheel, there are no operating problems. For high inertia loads D connection starting can be used, in order to reduce the starting period.

stroboscopic tachometer and a voltmeter), the proposed method can be integrated into the category of low-cost measures with a significant energy savings potential.

TABLE 5.1
EXPERIMENTAL VALUES FOR THE INDICATORS IN THE POINT α [10].

Nominal values of the tested motors (D connection)	Rounded values in the point α				
	ζ	K_{I1}	K_{I2}	K_{s1}	K_{s2}
185 W / 1375 r/min / Brand A 50 Hz / 230 V / 1.02 A / $\lambda = 0.75$	0.31	0.69	1.75	0.25	0.21
0.75 kW / 900 r/min / Brand D 50 Hz / 220 V / 3.7 A / $\lambda = 0.75$	0.41	0.73	1.69	0.34	0.24
1.1 kW / 1380 r/min / Brand A 50 Hz / 230 V / 5 A / $\lambda = 0.79$	0.43	0.70	1.75	0.29	0.25
1.1 kW / 1400 r/min / Brand B 50 Hz / 230 V / 5 A / $\lambda = 0.77$	0.39	0.64	1.68	0.32	0.24
1.1 kW / 2800 r/min / Brand C 50 Hz / 220 V / 5.8 A / $\lambda = 0.86$	0.37	0.60	1.57	0.31	0.28
1.5 kW / 1410 r/min / Brand B 50 Hz / 230 V / 6.4 A / $\lambda = 0.78$	0.41	0.63	1.60	0.33	0.26
2.2 kW / 1410 r/min / Brand B 50 Hz / 230 V / 8.5 A / $\lambda = 0.83$	0.33	0.52	1.52	0.29	0.30
3 kW / 1400 r/min / Brand A 50 Hz / 400 V / 7.1 A / $\lambda = 0.8$	0.36	0.59	1.75	0.23	0.28
3 kW / 1430 r/min / Brand E 50 Hz / 400 V / 6.8 A / $\lambda = 0.82$	0.42	0.65	1.63	0.40	0.27
4 kW / 1420 r/min / Brand B 50 Hz / 230 V / 15.2 A / $\lambda = 0.84$	0.36	0.53	1.53	0.28	0.28
5.5 kW / 1435 r/min / Brand A 50 Hz / 400 V / 12.8 A / $\lambda = 0.78$	0.27	0.49	1.85	0.25	0.30
5.5 kW / 1430 r/min / Brand B 50 Hz / 400 V / 19.1 A / $\lambda = 0.85$	0.32	0.55	1.57	0.27	0.30
7.5 kW / 1435 r/min / Brand A 50 Hz / 400 V / 16.5 A / $\lambda = 0.81$	0.37	0.67	1.82	0.26	0.25
Average	0.36	0.61	1.67	0.29	0.27
Standard Deviation	0.05	0.07	0.11	0.04	0.03
Average Variation for $1.1 \cdot \zeta_{\text{point } \alpha}$	+10%	+2%	-9%	+11%	-8%
Average Variation for $0.9 \cdot \zeta_{\text{point } \alpha}$	-10%	-2%	+10%	-10%	+6%

TABLE 5.2
SIMULATED VALUES FOR THE INDICATORS IN THE POINT α [10].

Nominal values of the simulated motors	Rounded values in the point α				
	ζ	K_{I1}	K_{I2}	K_{s1}	K_{s2}
3 kW / 4 poles / 50 Hz	0.36	0.58	1.59	0.30	0.27
11 kW / 4 poles / 60 Hz	0.42	0.52	1.21	0.39	0.27
300 kW / 6 poles / 60 Hz	0.47	0.51	1.05	0.45	0.30

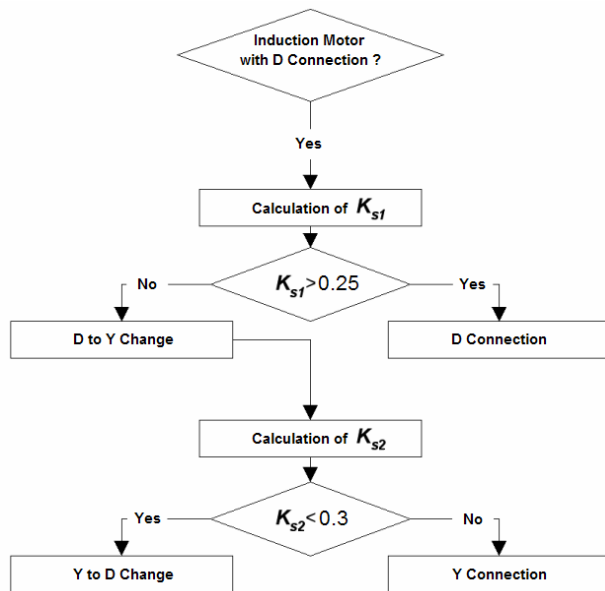


Fig. 5.7. Flowchart of the in-field method to evaluate the motor stator-winding connection [10].

5.2.4.2 Automatic Change of the Winding Connection

The automatic change of the stator-winding connection is particularly suitable for motors with significant load variation during their duty-cycle, including relatively long, low load (below point α) periods. The automatic connection change in such motors can lead to significant energy savings and improvement of the motor power factor in the low-load operating periods, largely compensating the additional modest investment.

The experimental results, using a microcontroller based electronic device, for the automatic change of the motor stator-winding connection, as a function of the motor line current, named “Smart-Switch” or “Smart-Relay” [8], [10], are presented. Fig. 5.8 shows a basic and an advanced topologies of such device. Fig. 5.9 shows a simplified flowchart of the decision algorithm (program) implemented in the microcontroller. The device controls the D/Y and the line contactors. The connection mode management is based on the current measurement because it is the most suitable variable to be acquired and processed by an electronic device for industrial purposes. Assuming fixed line-to-line voltage, the choice of the stator winding connection is based on both the actual motor line current and the actual connection mode⁷. For the presented experiments a low cost Hall-effect current sensors was used (internal sensor). Alternatively, an external current sensor (e.g., a clamp type current sensor) can be used. Internal sensor is designed to acquire the current from an instrumentation current transformer, which have a typical output in the 0-5 A range. With this approach, the device can control large motors. The gain and offset of the amplification circuit of the output voltage of the current sensor are adjustable. In order to avoid the use of too many analogue inputs, a voltage comparator based setpoint crossover detection module

⁷ If long line-to-line voltage variations/fluctuations are expected, the actual voltage should also be taken into account in the automatic connection management process.

providing digital outputs (e.g., 8-bit digital word) to one digital input port can be implemented outside the microcontroller. To improve the device performance, external ADC can be used. Alternatively, the setpoints can be programmed directly in the microcontroller by means of a proper user interface (e.g., LCD or USB-based communication with a computer, using proper software). The system can be initiated or stopped using the RUN and RESET push buttons, respectively. The line contactor interrupts the power if the RESET push-button is pressed. One digital output of the microcontroller is used to control the Y connection contactor. The Y connection contactor has an additional normally closed contact for the D connection contactor control. Therefore, when Y connection contactor is ON, D connection contactor is OFF, and vice-versa. With proper timings, it is assured that the state change of the Y/D contactors is made during the OFF state period of the line contactor.

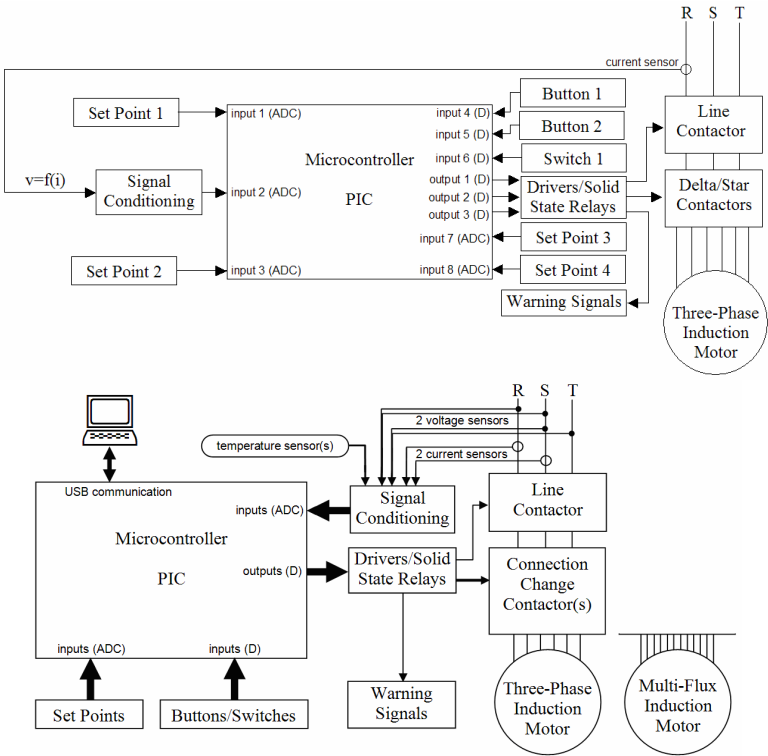


Fig. 5.8. (top) Basic topology (or lowest cost, using only one current sensor) and (bottom) advanced topology of an electronic device for the automatic change/management of the motor stator-winding connection (for two- or multi-connection motors) [8], [10].

As it can be seen in the Fig. 5.8, two different setpoints were considered in the device because, for the motor load that corresponds to the intersection point between the efficiency-load curves for the D and Y connections (point α), the motor line current is different for the D and Y connections. Therefore, it is necessary to set two different line current setpoints/thresholds (setpoints 1 and 2) for each connection change load point (corresponding to the intersection between the efficiency-load curves), leading to a hysteric behaviour in the transition zones (see Appendix 6). This applies also to more than two connections, as addressed in Section 5.3. The stator-winding

connection change has to be dependent on the actual connection mode and on the current thresholds crossover.

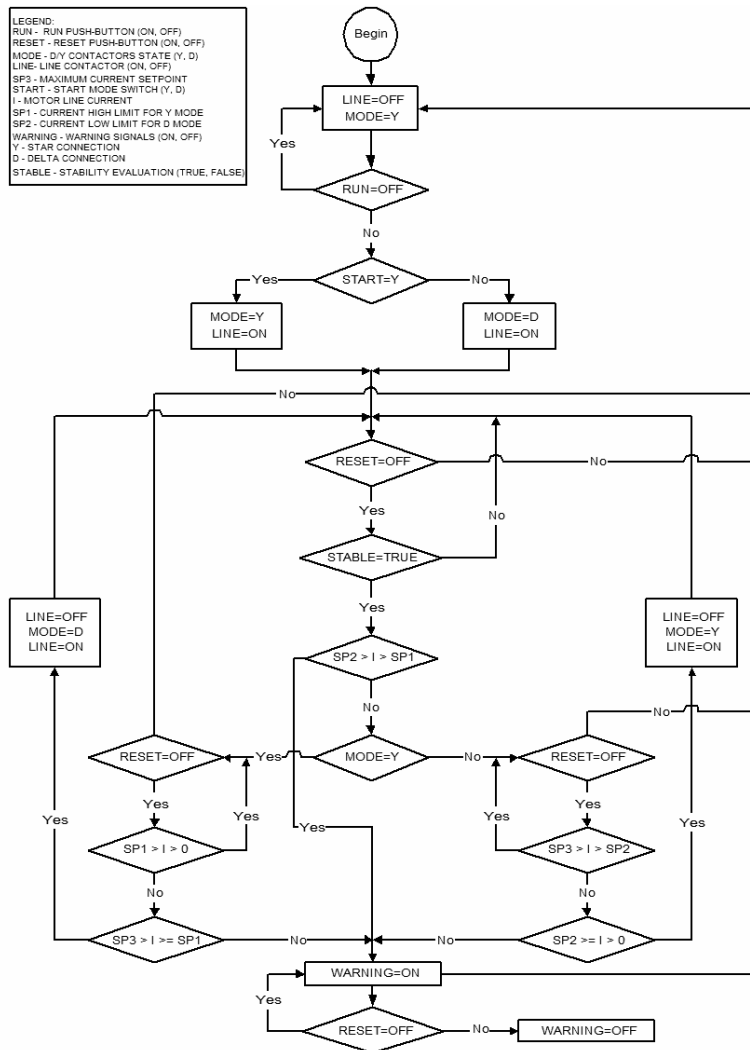


Fig. 5.9. Simplified flowchart of the decision algorithm of the basic version of the Smart-Switch, assuming constant line-to-line voltage [8].

For those load points, the motor line current is different for each connection due either to the change of the connection mode and/or to the change of the slip value (due to the torque-speed curve change). A third setpoint (setpoint 3) to set overcurrent limit was provided. If the motor line current exceeds the preset limit, the line contactor breaks the power and the warning signals are activated (provided by an intermittent LED and a small loudspeaker). To turn OFF the warning signals the RESET push button should be pressed. To restart the system, the RUN push button should be pressed. Motor thermal protection can also be implemented using a temperature sensor.

The starting mode (Y or D) can also be defined using a panel switch (Y/D start switch). After the motor start-up period (i.e., when the motor line current becomes stable), the device begins the automatic management cycle, as a function of the motor line current. The current is considered stable if the standard deviation of a defined number of consecutive samples is lower than a defined limit. The current sampling rate is adjusted by a fourth setpoint (setpoint 4). The longer the

mechanical time constant of the motor-load system is, the lower the current sampling rate for stability evaluation should be. The stability of the system was also verified. If the first stable current value after the stator-winding connection change falls into the interval between setpoints 1 and 2, the line contactor breaks the power and the warning signals are activated. In principle, with proper adjustment of setpoints 1 and 2, after the Y to D change, the current will increase to a value higher than setpoint 2. Similarly, after the D to Y change, the current will decrease to a value lower than setpoint 1. Additionally, if a high number of winding connection changes is detected in a short time period, the line contactor breaks the power and the warning signals are activated. If the current sensor signal, due to some reason, becomes zero during the motor operation, the device will consider this as a system failure situation and the line contactor breaks the power, and the warning signals are activated. The adjustment of setpoints 1 and 2 (or more) should be based on experimental results, i.e., the direct measurement of the motor efficiency or, alternatively, it can be based only on the measurement of the motor input real power or line current, for both D and Y connections (iterative process) for each load point. To facilitate the in-field adjustment process, the user can ask the motor manufacturer to provide the necessary values.

The duration of each different operating period of the motor duty-cycle should be long enough to avoid an excessive number of stator-winding connection changes, in order to avoid a significant decrease of the contactors⁸ and motor lifetime. Actually, the number of D→Y commutation can be limited to a maximum number per period, but the Y→D commutations cannot be limited since the motor can experience problems in driving the load.

In Fig. 5.10a, the motor efficiency, power factor, current ratios and speed ratios, are shown for the 3-kW, 4-pole motor (Brand A), as a function of the load, for both Y and D connections. After proper calibration of the setpoints 1 and 2 (see Fig. 5.10b), which correspond to the two levels of the motor line current in the point α for the D and Y connections, the stator-winding connection is automatically and properly changed, as a function of the motor line current, leading to an improvement of the motor efficiency and power factor, for loads lower than point α .

A more sophisticated device with extended protection related features is now under development⁹ (Fig. 5.8, bottom) by the author of this thesis (prototype finished), and incorporates two current and two voltage sensors (the current sensors can be used with instrumentation current transformers for large motors). The microcontroller acquires the instantaneous values over a period, and calculates the current and voltage RMS values, as well as the real power, the apparent power and the power factor. Additionally, allows the user to measure the energy consumed over a predefined period, in order to evaluate the energy benefits of the connection change in relation to

⁸ Regarding contactors, in this type of application, it is important to select properly the class (AC3, AC4, etc.) and rating, to ensure a high number of manoeuvres for the expected duty-cycle, in order to achieve a long lifetime.

⁹ The company supporting the development expects to put the device into the market until the end of 2009.

the fixed-connection operation mode. This real power measurement allows to implement checking routines to evaluate if the input real power decreases after connection change, and force the system back to the previous connection if that is not verified. Moreover, the device can incorporate a learning scheme to iteratively carry out auto-setting routines for proper setpoint evaluation (e.g., if after a D-to-Y change the motor input real power increases and the line current is admissible, the related setpoint current value should be properly lowered). The setpoints (or thresholds) are all programmed via USB port using a portable computer with dedicated software. The device has only some LEDs for alarm and operation mode signalling purposes. This last generation of the device can be used for improved motor protection (based on current and voltage values, e.g., single-phasing or excessive supply unbalance) and performance, and as a power monitoring system for energy benefit and power quality assessment. Features such as load estimation based on the air-gap torque estimation, and protection based on unbalance current, negative sequence current and/or voltage, overload, overcurrent and/or overtemperature, can be fully implemented, and are being studied. Actually, the last version of the device incorporates an external sensor input that can be used for temperature protection by means of a temperature sensor in the motor, or for ON/OFF and Y/D or MFLIM control purposes as a function of an external variable, extending the range of application of such device (e.g., can be used to control motor-driven fans as a function of a temperature, in refrigerating/cooling or HVAC systems). Moreover, if three current sensors were used (increasing the device cost), current leakages to ground can be quantified/monitored over time and used for motor insulation system diagnosis purposes. The user can define the Y-D switching time as a function of the load type and inertia, which is critical in terms of motor deceleration. If the motor deceleration during the connection mode transition is excessive, the system inertia can be slightly increased, if practical.

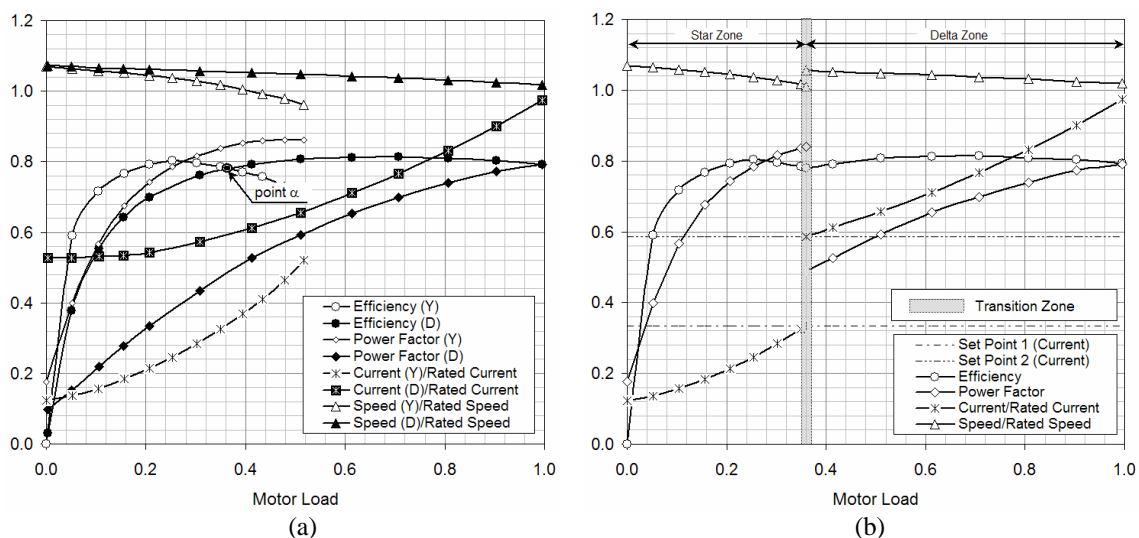


Fig. 5.10. Experimental motor efficiency, power factor, current (p.u.) and speed (p.u.) as a function of the load, for the 3 kW, 4-pole motor (Brand A): (a) without automatic change, and (b) with automatic change.

The device has several digital outputs for conventional contactor control purposes, and also a digital output generating a variable-duty-cycle PWM, that allows controlling the shaft position of a small servo-motor (a small stepper motor can also be used, requiring a different control scheme) to drive a special multi-position rotary contactor (shown in Fig. 5.52), which is proposed to facilitate the change of the connection mode in the multi-connection motor.

Additional restrictions can be used for protection and adjustment purposes. For example, if the line current exceeds a predefined maximum value (overcurrent situation), or, due to some reason, becomes zero during the motor operation (the device can consider this a system failure situation), proper action can take place, e.g. the line contactor can break the power and/or activate warning signals. The same applies for the motor protection features as single-phasing or excessive unbalance detection.

An important advantage associated with the latest version of the proposed device is the energy consumption and power quality monitoring, which are very useful features in modern industries.

The same principle can also be applied to YY/D connection change (possible in dual-voltage motors, YY as nominal connection¹⁰) if the load variation range is between 65% and 100% of full-load, still being a two-connection decision.

In Figs. 5.11 and 5.12 the last prototype of the Smart-Switch AUTOCAD drawing (with the outer case dimensions) and inner and outer aspect photographs. The software developed to upload and download information (measured data, setting, etc.) from the device, as well as for motor database purposes, is shown in Fig. 5.13.

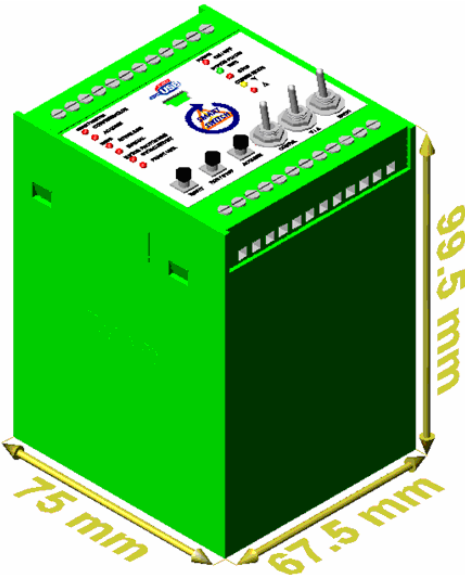


Fig. 5.11. Dimensions of the last version of the Smart-Switch (AUTOCAD drawing).

¹⁰ In this case, the D (series) connection leads to a magnetizing flux 25% lower than that for the YY (parallel) connection.

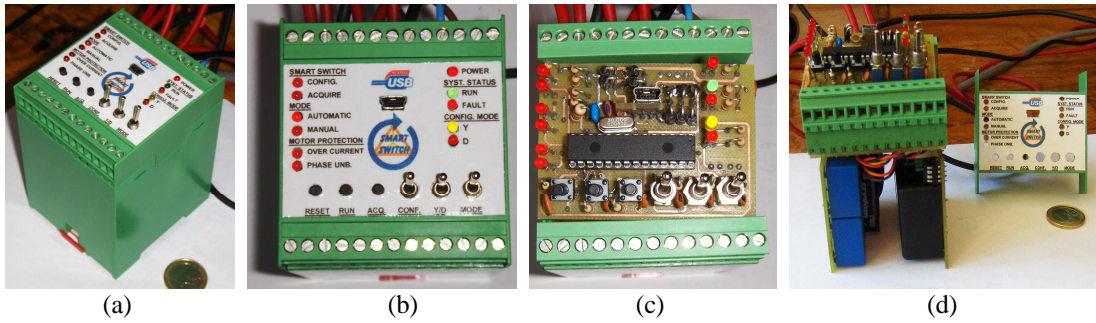


Fig. 5.12. Last version of the Smart-Switch prototype photos: (a) standard package outside; (b) front panel; (c) microcontroller (PIC18F2550, Microchip Technology) and front panel PCB; (d) microcontroller PCB (top part), sensors PCB (down, left part), and power source PCB (down, right part).

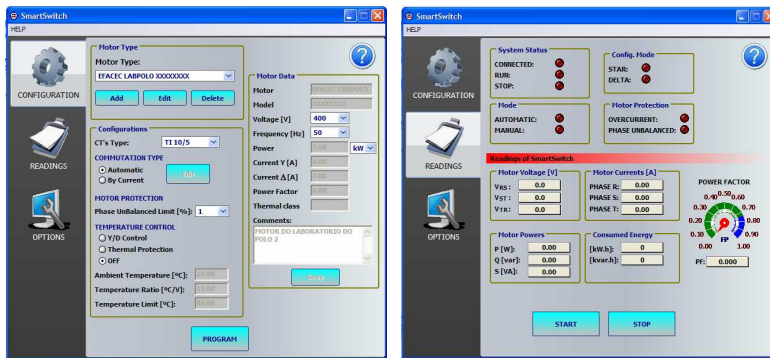


Fig. 5.13. Software developed to upload and download information from the Smart-Switch and for motor database purposes.

Examples of loads in which the automatic change method can be potentially applied with possible energy savings are given in Section 5.2.6.

5.2.5 Technical Considerations

5.2.5.1 Motor Load and Speed

The motor speed and load variation after the stator-winding connection change also deserve to be analysed. After the stator-winding connection change from D to Y, the motor line current significantly decreases and the motor speed slightly decreases (in the point α , the motor slip increases 3-4 times). After the Y to D change, the motor line current significantly increases and the motor speed slightly increases. The decrease of the motor speed after the D to Y change is related to the stator-winding voltage decrease (decreases $\sqrt{3}$ times) and the consequent reshape of the motor torque-speed curve¹¹. The slight increase or decrease of the motor speed after the stator-winding connection change, generally leads to an increase or decrease of the motor load, respectively. This fact can lead to significant power reductions in constant, linear¹² or quadratic torque loads, particularly for the last ones (e.g., centrifugal pumps and fans). For a speed variation of $\Delta\omega = (\omega_D - \omega_Y)/\omega_D$ several outcomes are possible depending on the type of load, namely:

- loads with constant horsepower, $\zeta_Y \approx \zeta_D$,
- loads with constant torque, $\zeta_Y \approx \zeta_D(1 - \Delta\omega)$,

¹¹ Assuming fixed frequency, the torque is approximately proportional to the squared voltage.

¹² Linear torque loads are those with a dominant viscous friction.

- loads with linear torque, $\zeta_Y \approx \zeta_D(1 - \Delta\omega)^2$, and
- loads with quadratic torque, $\zeta_Y \approx \zeta_D(1 - \Delta\omega)^3$.

Care must be taken to ensure that the motor speed at steady-state after stator-winding change from D to Y is still appropriate to the driven load operation. For example, in a centrifugal pump, it is necessary to ensure that the speed reduction does not lead to insufficient fluid flow (the pump flow is proportional to the speed) and lifting incapacity¹³ (the pump head is proportional to the square of the speed), as it can be seen in Fig. 5.14.

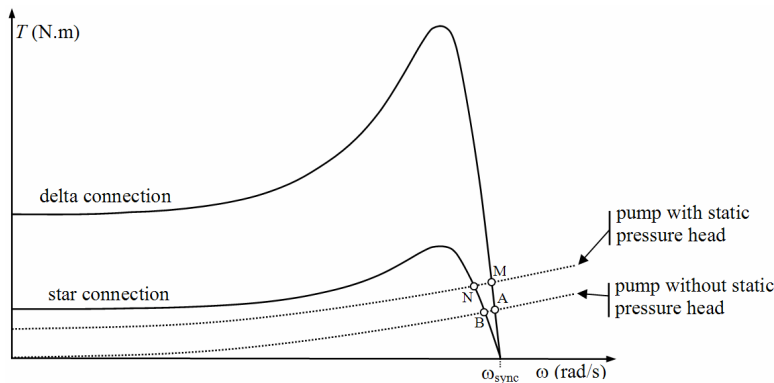


Fig. 5.14. Torque-speed curves for an IM with star-connected and delta-connected stator windings, and torque-speed curves for a centrifugal pump with and without static pressure head.

However, the lower the motor load is, and the higher the motor rated power is, the lower the motor speed variation will be, after stator-winding connection change. Moreover, if the D to Y change is made near the point α , in most cases, the motor slip will never exceed the nominal slip.

5.2.5.2 Motor Start-Up Precautions

Manufacturers define the highest permitted number of starts and reversings per hour at no load, which with the inertia of motor and load, number of starts and reversings per hour and motor rated output of motor in continuous duty, allow to compute the permitted output power [13]. When a motor experiences frequent startings, it cannot be loaded at its rated output due to the thermal starting losses in the windings. The limit imposed by mechanical stresses may be lower than that imposed by thermal factors [13]. From the temperature rise point of view, the starting time must not exceed the time specified by manufacturers (e.g., starting from normal operating temperature, motor size 112, 4 poles: DOL-starting 15 s; Y/D starting 45 s). The values can be doubled if starting from cold [13].

When the motor stator-winding is connected in the Y mode, or if a star or star/delta start-up scheme is adopted over a direct on-line delta starting, the starting torque is reduced approximately to $\frac{1}{3}$ of the nominal value (for D connection), as it can be seen in Fig. 5.15, which can lead to a

¹³ If there is a system head associated with providing a lift to the fluid in a pumping system, the pump must overcome the corresponding static pressure.

significant increase of the starting period or even to the lack of starting capabilities, requiring a verification to assess if it still is appropriate for the application. If the Y starting mode is adopted, the user should evaluate the increase of the starting timeframe and the increase of the temperature that can result from such situation, potentially shortning motor lifetime. Therefore, the user has to evaluate if the motor torque is able to accelerate the motor in a suitable timeframe, particularly for high inertia loads and/or loads with high demanding torque requirements (e.g., constant horsepower or constant torque loads).

At the starting instant, the winding current in Y mode is $\sqrt{3}$ times lower than for the D mode. Therefore, the Joules losses for the starting period in Y mode are, approximately, $\frac{1}{3}$ of those for the D mode. Thus, the motor starting timeframe can increase approximately 3 times without increasing the motor thermal stress. If this time is exceeded, D starting has to be used (or alternatively, if applicable, a soft-starter or VSD).

Stall conditions (Y-D change at very low speed) can also occur when starting the motor in Y mode. In these cases, the protection can trip or may have to be disabled, and since the stator current jumps rapidly for the D connection, which can result in severe damages in the switchgear and motor (e.g., due to flashovers), the advantages of Y-D become null¹⁴ [27].

Moreover, when considering frequent starts/stops it should be taken into account the influence of the motor internal temperature increase after first operating period on torque-speed curves, since the starting torque increases with temperature due to the rotor resistance increase (e.g., for a 200 kW, 4-pole motor, if a cold start lasts for 36 seconds, a hot start can last for 20 seconds, almost half).

5.2.5.3 Motor Losses and Temperature

Considering the steady state, when the motor operates in Y mode with a load below point α , the overall losses are lower than those for the D mode, leading to a lower motor operating temperature and longer motor lifetime. For a motor load below point α , the stator winding connection change from D to Y leads to a decrease of the core losses, and can lead to the decrease of the stator winding current for low power motors (Fig. 5.15), but may not lead to a stator winding current decrease for medium/high power motors (Fig. 5.16). This is related to the balance between core (or magnetic) and Joule effect (or I^2R) losses.

Note that, for the Y connection, the stator winding current and the line current are equal, but for the D connection, the stator-winding current is $\sqrt{3}$ times lower than the line current.

¹⁴ It should be noted that starting current determines to a large extent the size of the cable used, circuit breakers, fuses and transformers, having significant implications on cost saving. Therefore, cost reductions will only result when a new installation is done. If the transformers, switchgear, cables and protection were initially selected for the high starting currents, then would not be a significant cost saving by installing Y-D starting or a soft-starter [27].

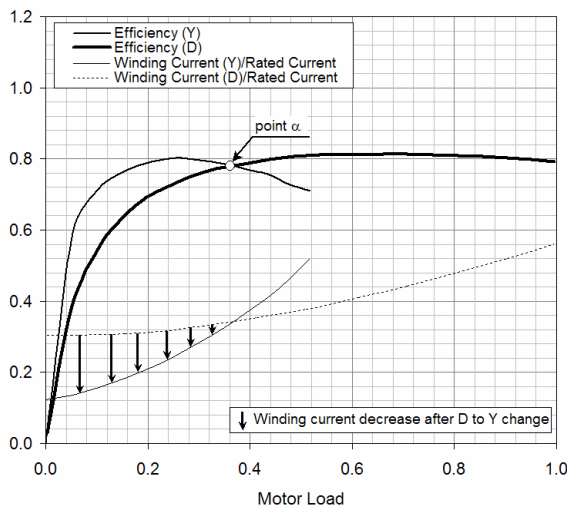


Fig. 5.15. Motor efficiency (p.u., 100% as reference), winding current (p.u., I_N as reference) and line current (p.u., 100% as reference) as a function of the load for the 3 kW, 4-pole motor (Brand A).

For motors operating with a load below point α (as well as for loads higher than point α), the D to Y change leads to an increase of the motor rotor losses (as a result of the increase of the rotor current), as it can be seen in the Fig. 5.17 (for a 3 kW motor), which depends on the motor parameters and load.

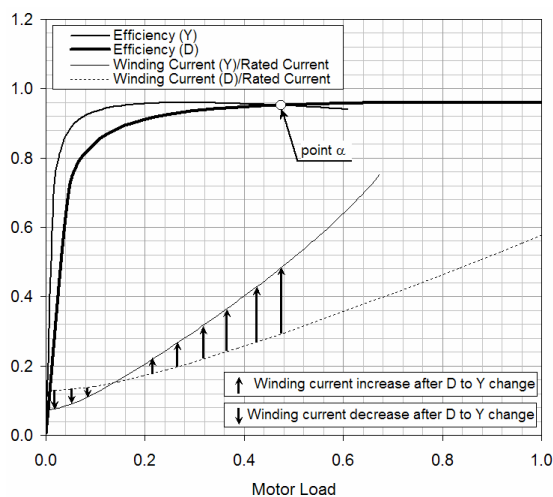


Fig. 5.16. Simulated motor efficiency (p.u., 100% as reference), winding current (p.u., I_N as reference) and line current (p.u., I_N as reference) as a function of the load for a 300 kW, 6-pole motor.

For the motors operating with a load below point α , after the D to Y change, the motor stator-winding and rotor currents are lower than the nominal values, for steady state. Below point α , the motor operating temperature is lower in the Y connection due to lower overall losses¹⁵.

A potential benefit of the Y connection is that it eliminates the circulating currents, which can exist in the D connected windings, and are related, for example, to electromagnetic unbalance in the motor and to the current triplen-harmonics due to magnetic saturation. The circulating currents are responsible for additional winding losses.

¹⁵ The peak efficiency for Y connection, below point α load, can be lower than that for the D connection, if the reduction in core losses (due to the phase voltage decrease) and copper losses (due to the temperature decrease) does not compensate the increase of the percentage share of friction and windage losses in the overall losses.

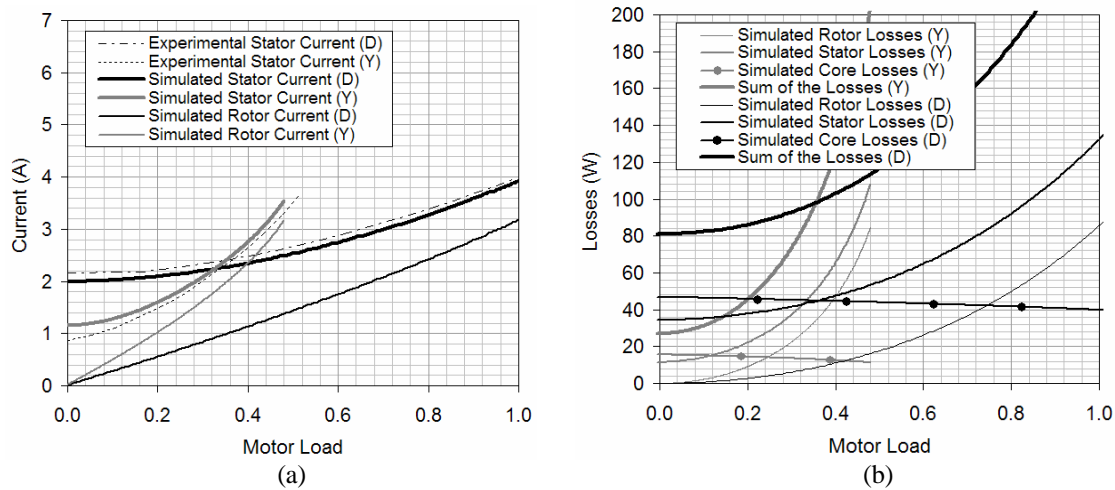


Fig. 5.17. (a) Motor stator-winding and rotor currents, and (b) motor per-phase losses, as a function of the load, for the 3 kW, 4-pole motor (Brand A).

5.2.6 Economical Considerations

The increase of the motor efficiency and power factor leads to a reduction in motor operating costs. Oversized motors are by far the most important cause of poor power factor in power systems networks, additionally leading to large voltage fluctuations. This problem is particularly serious in developing countries, which already face an undercapacity problem. In practical terms the power factor increase leads to a decrease of reactive energy bill, and to a better exploitation of the electric installations, including lower network losses, as well as lower power factor capacitance requirements. The efficiency improvement has a direct impact on the electricity bill.

Considering the D to Y change in the operating periods with loads under point α , the value of the annual savings, S (€/yr), is given by (5.12), where i is the motor operating period with a duration h^i (h/yr), in which the shaft output power is P_{mech}^i (kW) and an electrical energy cost C^i (€/kWh).

Except for constant power loads, after the D to Y change, the motor input active power decreases not only due to the motor efficiency increase, but also due to the slight decrease of the motor speed, which leads to a decrease of the output mechanical power.

$$S = \sum_i \left[\left(\frac{P_{mech}^i(D)}{\eta_D^i} - \frac{P_{mech}^i(Y)}{\eta_Y^i} \right) \cdot h^i \cdot C^i \right] \quad (5.12)$$

For the automatic change, the longer the motor operating periods with a load below the point α are, the higher the energy savings potential is. The improved motor protection provided by the latest version of the proposed electronic device, as well as the starting current reduction (improved starting), should be also taken into account, since the investment in dedicated equipment (e.g.,

thermal relays and soft-starters) is avoided. The motor lifetime is also extended due to the lower operating temperature. Moreover, it is a distortion-less device. Its inherent low cost, associated with the significant energy savings potential, can lead to a short-time payback.

5.2.6.1 Permanent Winding Connection Change

For the economical analysis of the stator-winding permanent change only one example is considered. Assuming that the 7.5 kW motor (Brand A) with D connected windings drives a centrifugal fan at 25% of full-load ($P_{mech} = 1871$ W), the efficiency is 74%, the power factor is 0.35, the speed is 1489 r/min, and the torque is 12 N·m. The D to Y change results in the speed reduction to 1463 r/min, the torque reduction to 11.6 N·m and, consequently, the motor load reduction to 24% ($P_{mech} = 1777$ W), with an efficiency of 82% and a power factor of 0.76. Since the Y connection speed is 1.7% lower (–26 r/min) than D speed, there is a 5% reduction in the required fan power. Considering 8000 hours/year and 0.05 €/kWh, the D to Y change leads to annual savings of 144 €/year. Additionally, there is a power factor increase of approximately 0.41 (from 0.35 to 0.76).

5.2.6.2 Automatic Winding Connection Change

For the economical analysis of the automatic change, some examples are considered. In order to simplify the estimation of the energy savings, the impact of the slight variation of the motor speed after stator-winding connection change is not considered. Two types of loads are considered in the following economical analysis – elevating/inclined conveyors¹⁶ (which, from the load perspective, are equivalent to escalators) and mixers. It is also considered that the described loads operate 16 hours per day and 360 days per year, and that the average electrical energy cost is 0.05 €/kWh. It is considered that the elevating conveyor (Fig. 5.18) operates 12 hours/day at 25% of full load, 4 hours/day at 95% of full-load. The industrial mixer (Fig. 5.19) operates 7 hours/day at 25% of full-load, 5 hours/day at 15% of full-load and 4 hours/day at 95% of full-load. The estimated commercial cost for the electronic device presented is 50-75 €, which can be considered low [8]. Obviously, the task performed by the proposed device can be performed by a commercial programmable logic controller (PLC), but it would be much more expensive, and a poor application for the available capabilities of such devices. Moreover, the proposed device can perform calculations on acquired instantaneous values, which is typically not feasible with PLCs.

Considering the 3-kW motor (Brand A) with the automatic change, the energy savings are 419 kWh/yr and 444 kWh/yr for the conveyor and mixer, respectively. This can be translated into 21 €/yr and 22 €/yr, respectively. For both cases the simple payback time for the automatic change

¹⁶ In such applications, assuming that the motor is operating with Y connection at low load, the proposed electronic device can anticipate a significant load increase by means of an external presence or weight sensor positioned slightly before or in the very beginning of the inclined conveyor-belt input and, as a function of that, switch to D connection (if the predicted load justifies that connection change) shortly before a significant increase in load actually occurs. This strategy can avoid an excessive motor speed decrease during the connection change instants and reduce the magnitude of the inherent high current transients during the power supply reconnection.

device can be less than 2.4-3.6 years. For motors with the same operating conditions and a rated power 3.5 times higher than the previously considered, the energy savings can increase about 2.7 times, reducing the simple payback time to less than 10 months. The average daily power factor of the 3-kW motor improves 0.31 points (increases from 0.47 to 0.78) and 0.31 points (increases from 0.44 to 0.75), for the conveyor and mixer, respectively. The motor power factor improvement for 25% and 15% of full load is 0.41 points (from 0.37 to 0.78) and 0.39 points (from 0.28 to 0.67), respectively [8], [10].

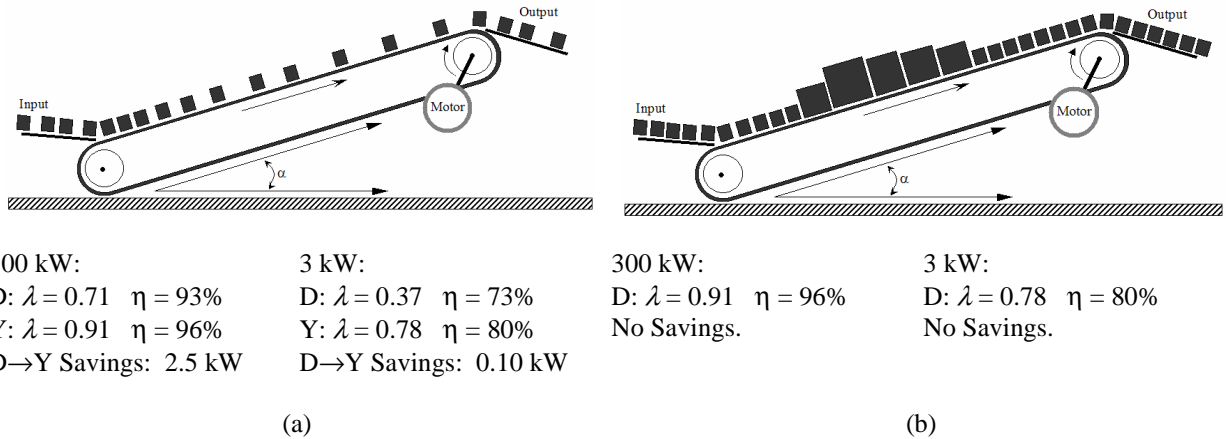


Fig. 5.18. Elevating conveyor with different load levels.

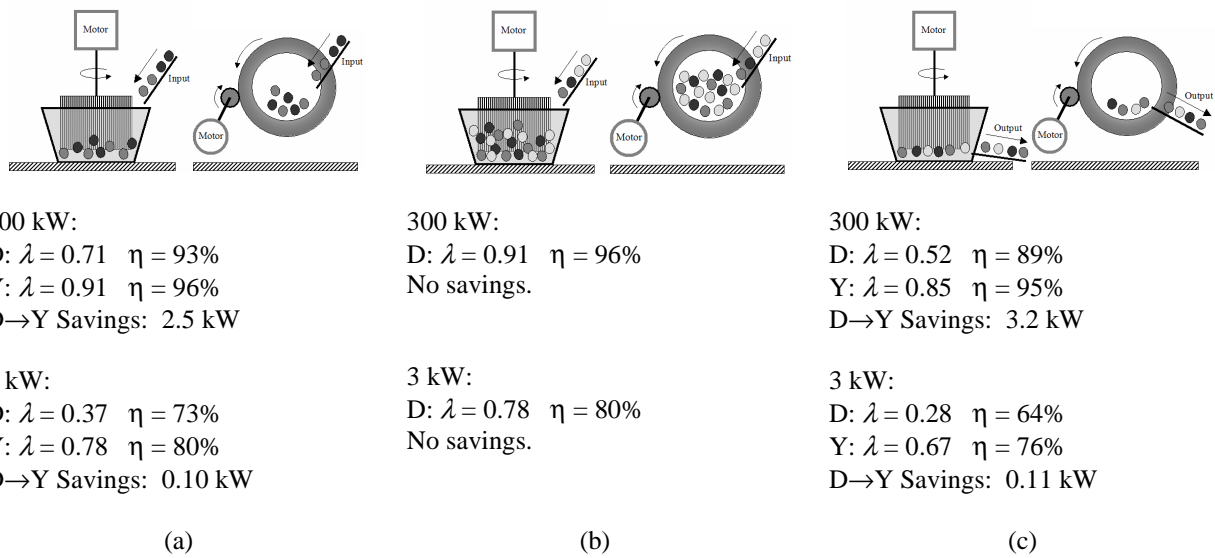


Fig. 5.19. Industrial mixer (horizontal or vertical) with different load levels.

Considering the simulated 300-kW motor with automatic change, the energy savings are 10887 kWh/yr and 12099 kWh/yr for the conveyor and mixer, respectively. This can be translated into 544 €/yr and 605 €/yr, respectively. For this case, the simple payback time for the automatic change device can be 1-2 months. The daily average of the 300-kW motor power factor improves 0.15 (from 0.76 to 0.91) and 0.19 (from 0.70 to 0.89) for the conveyor and mixer, respectively. The

motor power factor improvement for 25% and 15% of full load is 0.20 points (from 0.71 to 0.91) and 0.33 points (from 0.52 to 0.85), respectively [8], [10].

This concept can also lead to significant energy savings in high-inertia (or fly-wheel) presses, saws (sheet or rotary disk), grinders, lathes, crushers, as a function of the actual duty-cycle of such loads, since the main energy transfer is provided by the energy stored in the rotating high inertia wheel. Industrial centrifuges can also benefit from connection change after acceleration period. Large cranes are also an application where the proposed concept can be applied, since they can actually operate in the majority of the situations with an actual load significantly lower than the maximum allowable load, being advantageous to change the connection to star. As referred before, inclined conveyors, escalators and industrial mixers are also examples of applications in which the automatic connection management should be also considered.

The speed regulation of fans, pumps, and/or compressors, can also be performed as a function of a temperature (of the zone or fluid). For example, in chillers of cooling systems, as a function of the differential between the external and chiller temperature. Three states are possible using the proposed electronic system, OFF (stopped), Star (low speed) and Delta (high speed), or five states if a 2-speed motor is used. Although star speed regulation is inefficient, the efficiency drop is not significant when compared to the savings of power required by the load. For speed regulation purposes, high-resistance, deep-bar or double-cage rotors are preferable (NEMA Design C & D or IEC Design H, see Appendix 6), since the voltage regulation band is extended, but in that choice the load curve should obviously be taken into account, as it can be seen in Fig. 5.20. The same principle can be applied simultaneously or independently in fans (axial or centrifugal), pumps and compressors, integrated condenser units in refrigeration systems, walk-in freezers¹⁷, HVAC systems, air-treatment units, or roof-top chillers, as it can be seen in Fig. 5.21. In this sort of applications (including general pumps, fans, and compressors speed and/or flux regulation), the 2-speed motors with automatic connection management can increase significantly the savings potential.

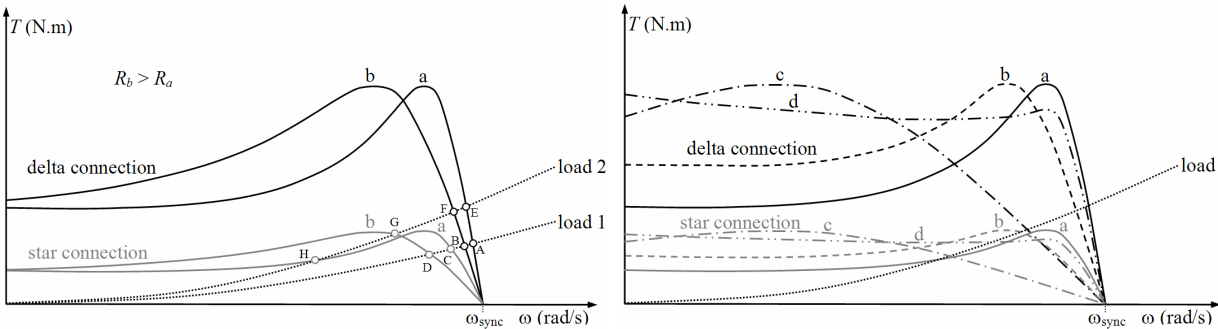


Fig. 5.20. Operating points for different torque-speed curve shapes.

¹⁷ In industrial walk-in freezers or open freezers in supermarkets, to reduce the ON/OFF cycling, as a function of the inner temperature, it can be used the “e-cube” technology, which, after coupled with the temperature sensor, simulates the food (meat, fish, vegetables, etc.) thermal inertia, leading to 10-30% energy savings.

For example, as presented in Chapter 3 for the VSDs case, in a roof top chiller system (Fig. 5.21), the automatic connection mode change can be applied to manage 3 different states (stopped, low speed, and high speed) for the pump speed, based on zone temperature control, and/or for the fan speed, based on the coolant return temperature. The result, compared with an ON/OFF cycling control, is a more stable temperature in the controlled space and more efficient operation, leading to significant energy savings and, in principle, to a short payback time. In this sort of applications, the automatic management of multi-connection (up to six) single- or two-speed IMs as a function of temperature can also be applied, although at a higher cost, potentially not being a competitive solution over electronic VRs or VSDs.

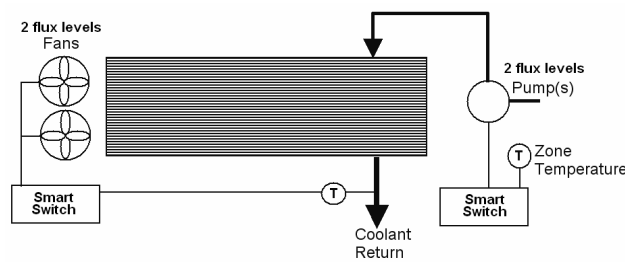


Fig. 5.21. Application of the automatic winding connection management concept in a roof-top chiller.

5.2.8 Another Potential Application

If the Y-D automatic change is incorporated between an inverter and the motor, and the motor rated connection is Y, if the mains voltage decreases significantly, leading to a DC-bus voltage decrease, the Y-D connection change can be performed simultaneously with an amplitude modulation index adjustment, allowing the motor windings voltage to be maintained at nominal values, extending the ride-through capacity of the system when, for example, long, moderate undervoltages (down to 70-80%) occur in the power network. Basically, the inverter have to detect a lowering in the DC-bus voltage, turn OFF the output, change connection mode, turn ON the output with adjusted amplitude modulation index. The power switches have to be designed to withstand $\sqrt{3}$ times the normal current, since the line current of a delta connected motor is $\sqrt{3}$ times higher for the same power. This solution increases significantly the system cost, and it can only be justified for critical applications, and there are other solutions, probably more suitable for that purpose. Moreover, it requires further studies.

5.3 Multi-Connection Motor

In this section, a novel (not from the construction perspective but from the utilization perspective) multi-flux level motor (hereafter denoted by MFLIM) is proposed, with different possible stator winding connections, which, for fixed line-to-line voltage, allow the magnetizing

flux to be chosen among up to six different levels [16], [17]. Alternatively, for fixed magnetizing flux, the MFLIM can operate with up to six different voltage levels. This novel concept can improve significantly both the efficiency and the power factor of the motor in a wide load and/or voltage range. Similar ideas are proposed in [21], [23], [24], and [25]. In [21], two per-phase winding parts with different number of turns either connected in start-delta (YD) or delta-star (DY) are introduced, but no performance analysis is presented, and there are no major advantages associated with the concept. In [23], a three-mode connection winding is proposed (star-series, delta-series and YD connections) and a switching device (analogue technology based), but efficiency, power factor, currents, operating temperatures and connection management analysis is very weak. In [24], four connection modes for the windings of a double-stator, double-rotor motor and a switching scheme are proposed, claiming starting and operating characteristics improvement, but no accurate analysis is actually presented. In [25], a theoretical analysis is made for a winding with four parts per phase, applied to a synchronous generator, to allow multiple line-to-line voltages, using YD principle. No motor considerations are made. Additional work is being developed on multi-step YD (including full Y and full D), considering spatially displaced winding groups, and a preliminary discussion is presented in Appendix 6.

In Section 5.2, an in-field evaluation method to assess the most appropriate permanent stator winding connection (delta or star) for grossly oversized motors and a low-cost electronic device for automatic change of the stator winding connection (delta or star) in variable-load motors are proposed, which can be both extended to the MFLIM concept. In section, besides the detailed analysis of the MFLIM, a special multi-position rotary contactor (or relay) is proposed for the purpose of stator winding connection change. Some technical and economical considerations related to the application of the MFLIM are also discussed.

5.3.1 Preliminary Theoretical Analysis

Typically, in the conventional IMs, with 6 terminal leads of the stator winding accessible, only two connections are possible - delta and star. Considering a stator winding with two sets of turns (or groups, which can be connected either in series or in parallel) sharing the same positions in the stator slots, several connection combinations are possible. A preliminary analytical study was carried out and the main results are presented in Table 5.3, showing the voltage vector diagram (assuming nominal magnetizing flux level) and the maximum line current. The nominal (or reference) connection is assumed to be the delta connection with the two sets of turns connected in parallel (denoted by DP). In Table 5.3, the sets of turns (or groups) are represented by grey rectangles (the arrows inside them represent the flux direction), U_w denotes the voltage between the terminals of each set of turns, U_{ll} denotes line-to-line voltage, I_w denotes per-group winding current, and I_l denotes line current, all being RMS values. The six first connections in Table 5.3,

namely Delta-Parallel (DP), Star-Parallel (YP), Delta-Series Type I (DS1), Star-Delta (YD), Star-Series Type II (YS2) and Star-Series Type I (YS1), are different in terms of the resultant line-to-line voltage, and were selected for the following analysis. The other connections presented in Table 5.3 (there are even more possible connections) can be considered redundant or alternative connections, with a resultant line-to-line voltage equal to that of one of the previous six connections. The YD and YS2 connections are proposed and analysed for the first time from the IMs' efficiency perspective.

The voltages between the terminals of each set of turns (or group) of the same phase have the same phase angle, because they share the same flux path in the stator core. In the line-to-line voltage estimation for each connection mode, it was assumed nominal magnetizing flux and winding symmetry (same number of turns for all groups). In Table 5.4, the calculation of the resultant line-to-line voltage for the six selected connections is shown.

Assuming a symmetrical, undistorted voltage supply system with constant frequency, and ignoring the stator leakage inductance and resistance and the MMF space harmonics, the average fundamental magnetizing flux per pole and phase, ϕ , of an induction motor under no-load operation is approximately given by (5.13).

$$\phi \approx U_w \cdot (4.44 \cdot K_{wl} \cdot f \cdot N)^{-1} \Rightarrow \phi \propto U_w \quad (5.13)$$

Considering nominal line-to-line voltage, U_N , the approximate resultant magnetizing flux can be calculated using (5.13) and the previously estimated relation between the line-to-line voltage and the voltage between the terminals of each set of turns. The output shaft power, P_{out} , that maximizes the motor efficiency in each stator winding connection mode, can be estimated as a function of the motor nominal power, P_N , assuming that the motor torque is approximately proportional to the square of the magnetizing flux and the motor speed is maintained approximately constant. Therefore, based on (5.13) and Table 5.4, one can present Table 5.5, in which Δ_ϕ is the magnetizing flux variation in relation to the nearest connection with higher magnetizing flux level.

Considering a per-group winding current limit, $I_{w \max}$, which leads to nominal stator Joule losses, the line current limit, $I_{l \max}$, can be established, which is presented in Table 5.3. The line current limits, as well as the expected higher stator Joule losses for the same per-phase current, are the main reasons to reject the use of the considered redundant or alternative connections.

TABLE 5.3
STATOR WINDING CONNECTIONS CONSIDERING TWO SETS OF TURNS PER PHASE.

Name	Winding Diagram	Voltages Vector Diagram (assuming nominal magnetizing flux)
Delta-Parallel (DP)		Reference or nominal power connection mode. $U_{ll} = U_w = U_N$ $I_{l\max} = 3.46 \cdot I_{w\max}$
Star-Parallel (YP)		$U_{ll} = 1.73 \cdot U_w$ $I_{l\max} = 2 \cdot I_{w\max}$
Delta-Series Type I (DS1)		$U_{ll} = 2 \cdot U_w$ $I_{l\max} = 1.73 \cdot I_{w\max}$
Star-Delta (YD)		$U_{ll} = 2.65 \cdot U_w$ $I_{l\max} = I_{w\max}$
Star-Series Type II (YS2)		$U_{ll} = 3 \cdot U_w$ $I_{l\max} = I_{w\max}$
Star-Series Type I (YS1)		$U_{ll} = 3.46 \cdot U_w$ $I_{l\max} = I_{w\max}$
Star-Series Type III (YS3)		$U_{ll} = 1.73 \cdot U_w$ $I_{l\max} = I_{w\max}$
Delta-Series Type II (DS2)		$U_{ll} = U_w$ $I_{l\max} = 1.73 \cdot I_{w\max}$
Delta-Series Type III (DS3)		$U_{ll} = 1.73 \cdot U_w$ $I_{l\max} = 1.73 \cdot I_{w\max}$
Delta-Series Type IV (DS4)		$U_{ll} = 1.73 \cdot U_w$ $I_{l\max} = 1.73 \cdot I_{w\max}$

TABLE 5.4
ESTIMATED LINE-TO-LINE VOLTAGE FOR
THE SIX SELECTED CONNECTIONS (DP AS NOMINAL CONNECTION).

Connection	Line-to-Line Voltage
DP	$U_{ll} = U_N$ (<i>reference</i>)
YP	$U_{ll} = U_w \angle 0^\circ - U_w \angle 120^\circ = \sqrt{3} \cdot U_w$
DS1	$U_{ll} = U_w \angle 0^\circ + U_w \angle 0^\circ = 2 \cdot U_w$
YD	$U_{ll} = U_w \angle 0^\circ + U_w \angle 0^\circ - U_w \angle 120^\circ = \sqrt{7} \cdot U_w$
YS2	$U_{ll} = \sqrt{3} \cdot U_w \angle 30^\circ - \sqrt{3} \cdot U_w \angle 150^\circ = 3 \cdot U_w$
YS1	$U_{ll} = 2 \cdot U_w \angle 0^\circ - 2 \cdot U_w \angle -120^\circ = 2\sqrt{3} \cdot U_w$

TABLE 5.5
ESTIMATED OUTPUT POWER AND MAGNETIZING FLUX FOR THE 6 SELECTED CONNECTIONS (DP AS NOMINAL CONNECTION).

Connection	Output Power	Magnetizing Flux
DP	$P_{out} = P_N$	$\phi = \phi_N$ (<i>reference</i>)
YP	$P_{out} \approx \frac{1}{3} P_N$	$\phi \approx 0.58 \cdot \phi_N$ ($\Delta_\phi = -42\%$)
DS1	$P_{out} \approx \frac{1}{4} P_N$	$\phi \approx 0.50 \cdot \phi_N$ ($\Delta_\phi = -14\%$)
YD	$P_{out} \approx \frac{1}{7} P_N$	$\phi \approx 0.38 \cdot \phi_N$ ($\Delta_\phi = -23\%$)
YS2	$P_{out} \approx \frac{1}{9} P_N$	$\phi \approx 0.33 \cdot \phi_N$ ($\Delta_\phi = -14\%$)
YS1	$P_{out} \approx \frac{1}{12} P_N$	$\phi \approx 0.29 \cdot \phi_N$ ($\Delta_\phi = -11\%$)

TABLE 5.6
ESTIMATED OUTPUT POWER AND MAGNETIZING FLUX FOR THE 6 SELECTED CONNECTIONS (YP AS NOMINAL CONNECTION).

Connection	Output Power	Magnetizing Flux
DP	$P_{out} \approx 3P_N$	$\phi \approx 1.73 \cdot \phi_N$ ($\Delta_\phi = +73\%$)
YP	$P_{out} = P_N$	$\phi = \phi_N$ (<i>reference</i>)
DS1	$P_{out} \approx \frac{3}{4} P_N$	$\phi \approx 0.86 \cdot \phi_N$ ($\Delta_\phi = -14\%$)
YD	$P_{out} \approx \frac{3}{7} P_N$	$\phi \approx 0.66 \cdot \phi_N$ ($\Delta_\phi = -23\%$)
YS2	$P_{out} \approx \frac{1}{3} P_N$	$\phi \approx 0.57 \cdot \phi_N$ ($\Delta_\phi = -14\%$)
YS1	$P_{out} \approx \frac{1}{4} P_N$	$\phi \approx 0.50 \cdot \phi_N$ ($\Delta_\phi = -11\%$)

For example, for nominal line-to-line voltage, the DS2 connection produces the same magnetizing flux as the DP connection, but the line current limit is twice lower, and the per-phase resistance is four times higher, leading to higher stator Joule losses (considering the same per-phase current). Similar analysis justifies the rejection of the DS3, DS4 and YS3 connections, in relation to the YP connection.

Among all the six selected connections, and depending on the motor load profile, some connections can be neglected due to their proximity in terms of flux level to the nearest connection modes. For example, the YS2 connection can be neglected due to its proximity to the YD and YS1 connections, leading to a practical five-flux level motor.

Analysing Table 5.5, different flux steps after proper connection change (assuming that a connection is changed to one of the two with the nearest flux level) are found. The highest step happens in the DP→YP connection change ($\Delta\phi = -42\%$).

A wide load range between those two points has no regulation. In order to harmonise the flux steps, the winding can be designed to operate at full load in the YP connection (the turns per phase have to be properly reduced), which becomes the reference connection.

This would lead to a better balance between the flux steps, as it can be seen in Table 5.6, and the DP connection can be used as a boost connection for high transient peak loads (with poor efficiency).

This concept can be adjusted to specific applications, according to the predicted or actual motor load diagram or duty cycle. For example, excluding the connections DP, DS1 and YS2 from Table 5.6, no major changes occur in the efficiency-load curve (this is demonstrated in the following sections), being used only three different connections, simplifying the connection change process. However, the use of all connections is always advantageous in terms of power factor improvement.

In fact, to simplify the connection management system and reduce the number of switchings over the duty cycle, two properly selected connections may be enough to achieve significant energy savings in most applications. For example, choosing YP and DS1 (YP as reference) can be enough for a number of applications, as proposed in [40]. In this cases, a management scheme similar to that used in the Y/D connection change can be used.

5.3.2 Steady-State Simulation

In order to simulate the steady-state performance of the MFLIM, the EEC has to be properly changed, in relation to the reference circuit, for a given fixed fundamental frequency. In the following analysis, it is assumed that the magnetizing flux and frequency are maintained constant and, consequently, the iron losses¹⁸, P_{fe} , are assumed constant for parallel- and series-connected windings. The thermodynamic behaviour of the motor, temperature effect on the resistive parameters, the saturation effect on magnetizing inductance and iron loss resistance (this can actually be a considerable source of error if fluxes with a value higher than nominal are considered), and the rotor parameters (both leakage inductance and resistance) dependency on rotor current frequency or motor slip (e.g., in part due to the skin effect), are not considered.

¹⁸ Besides hysteresis losses and eddy current losses, a third (but minor) component can be considered, named excess losses [20]. According to [20], the balance between hysteresis and eddy components can vary from 90%/10% for 10 Hz to 35%/65% for 150 Hz, considering a 0.65-mm thickness sheet and $B = 1$ T. Iron losses can be described as $P_{fe} = K_A f^2 \cdot B^2 + K_B f B^a$, being K_A , K_B and a assumed as constants. For the sake of simplicity, a (Steinmetz coefficient or index) is considered equal to 2. However, it can vary between 1.5 and 2.5 (most common values in the 1.7-2.0 range), depending on the material and on the induction value (higher induction values lead to higher a values) [5], [20], [36], [42]. As a consequence, R_{fe} parameter can actually depend slightly on the saturation level [36]. For fixed E , $P_{fe} = K_C + K_D f^{1-a}$, being K_C and K_D constants. Considering $a = 2$, $P_{fe} = K_C + K_D f^{-1}$. Manufacturers of ferromagnetic materials express this losses as $P_{kg} = a \cdot f^b \cdot B^c$ (W/kg). For example, for the ARMCO Silicon Steel M14 and M11, $a = 0.557 \times 10^{-3}$; $b = 1.68$; $c = 1.86$ and $a = 0.438 \times 10^{-3}$; $b = 1.67$; $c = 1.87$, respectively.

5.3.2.1 Partial Windings Connection in Series and in Parallel

The EEC parameters for fixed frequency and magnetizing flux for the parallel- and series-connected partial windings (denoted by subscripts srs and prl) can be defined by (5.14) and (5.15), being υ the transformation ratio between stator and rotor ($\upsilon = E_1 \cdot E_2^{-1} = N_1 \cdot N_2^{-1}$), and parameter subscripts r , s , m , and fe denote rotor, stator, magnetizing, and iron core, respectively.

To analyse the effect of the changes presented in (5.14) and (5.15) over the EEC, a simplified analysis for $s = 0$ and $s = 1$ is made (for $s = 1$, the rotor parameters dependency on motor slip is ignored).

For the parallel connection, the total impedance of the EEC for $s = 0$ and $s = 1$ is given by (5.16) and (5.17), respectively.

$$\left\{ \begin{array}{l} L_{s,prl} = N_{s,prl}^2 \cdot \mathfrak{R}_s^{-1} \\ R_{s,prl} = \rho \cdot l_{s,prl} \cdot S_{s,prl}^{-1} \\ L_{m,prl} = N_{s,prl}^2 \cdot \mathfrak{R}_m^{-1} \\ E_{prl} = k \cdot N_{s,prl} \cdot \phi_{mag} \\ P_{fe,prl} = R_{fe,prl}^{-1} \cdot E_{prl}^2 \\ R_{fe,prl} = P_{fe,prl}^{-1} \cdot E_{prl}^2 \\ L_{r,prl} = \upsilon^2 \cdot L_{r,real} \\ R_{r,prl} = \upsilon^2 \cdot R_{r,real} \end{array} \right. \quad (5.14)$$

$$\left\{ \begin{array}{l} L_{s,srs} = (2N_{s,prl})^2 \cdot \mathfrak{R}_s^{-1} = 4L_{s,prl} \\ R_{s,srs} = \rho \cdot 2l_{s,prl} \cdot (2^{-1}S_{s,prl})^{-1} = 4R_{s,prl} \\ L_{m,srs} = (2N_{s,prl})^2 \cdot \mathfrak{R}_m^{-1} = 4L_{m,prl} \\ E_{srs} = k \cdot 2N_{s,prl} \cdot \phi_{mag} = 2E_{prl} \\ P_{fe,srs} = R_{fe,srs}^{-1} \cdot E_{srs}^2 = P_{fe,prl} \\ R_{fe,srs} = 4R_{fe,prl} \\ L_{r,srs} = (2\upsilon)^2 \cdot L_{r,real} = 4L_{r,prl} \\ R_{r,srs} = (2\upsilon)^2 \cdot R_{r,real} = 4R_{r,prl} \end{array} \right. \quad (5.15)$$

$$Z_{prl,s=0} = R_{s,prl} + j\omega L_{s,prl} + \frac{R_{fe,prl} \cdot j\omega L_{m,prl}}{R_{fe,prl} + j\omega L_{m,prl}} \quad (5.16)$$

$$Z_{prl,s=1} = R_{s,prl} + j\omega L_{s,prl} + R_{r,prl} + j\omega L_{r,prl} \quad (5.17)$$

For the series connection, the EEC total impedance for $s = 0$ and $s = 1$, described as a function of the parallel connection parameters, is given by (5.18) and (5.19), respectively. Therefore, comparing both connection modes for partial windings, one can obtain (5.20).

$$Z_{ref,srs,s=0} = 4R_{s,prl} + j\omega 4L_{s,prl} + \frac{4R_{fe,prl} \cdot j\omega 4L_{m,prl}}{4R_{fe,prl} + j\omega 4L_{m,prl}} \quad (5.18)$$

$$Z_{srs,s=1} = 4R_{s,prl} + j\omega 4L_{s,prl} + 4R_{r,prl} + j\omega 4L_{r,prl} \quad (5.19)$$

$$\frac{Z_{srs}}{Z_{prl}} = 4 \quad (5.20)$$

Ignoring saturation effect (influencing mainly L_m parameter) and considering fixed slip, frequency and voltage applied to the EEC (which simulates the fixed line-to-line voltage in real systems), if the connection mode change from parallel to series simulation is made by means of parameters change, the motor phase currents result four times lower, as demonstrated in (5.21). Regarding the Joule effect losses in the stator windings, P_{joule} , on the basis of (5.21), they can be described by (5.22).

$$\begin{cases} U_{ph} = I_{srs} \cdot 4Z_{prl} \\ U_{ph} = I_{prl} \cdot Z_{prl} \\ I_{srs} = 4^{-1} \cdot I_{prl} \end{cases} \quad (5.21)$$

$$P_{joule,srs} = 4R_{s,prl} \cdot (4^{-1} \cdot I_{prl})^2 = 1/4 P_{joule,prl} \quad (5.22)$$

For the same conditions, the voltage drop across the stator windings (due to resistance and leakage inductance), U_{drop} , is given by (5.23), demonstrating that it is the same for both connections, as expected. The developed mechanical power, P_{mec} , for the same slip (which roughly corresponds to the same relative position in the efficiency-load curve), is given by (5.24). Since the same slip is being considered, the electromagnetic torque, T_{em} , can be described by (5.25). Note that the shaft mechanical power is equal to the developed mechanical power minus friction and windage losses.

$$U_{drop,srs} = 4Z_{s,prl} \cdot 4^{-1} \cdot I_{prl} = U_{drop,prl} \quad (5.23)$$

$$P_{mec,srs} = 4R_{r,prl} \cdot (s^{-1} - 1) \cdot (4^{-1} \cdot I_{r,prl})^2 = 1/4 P_{mec,prl} \quad (5.24)$$

$$T_{em,srs} = 1/4 T_{em,prl} \quad (5.25)$$

On the basis of foregoing discussion, it is demonstrated that, in order to adapt the EEC parameters for motor performance analysis with two partial windings connected in series or in parallel (maintaining the same amount of active copper), the parameters should be multiplied by 4. This deduction is valid for star and delta connections.

5.3.2.2 Star, Delta and Star-Delta (Hybrid) Connections

EEC parameters obtained with delta-based tests can be converted to delta-equivalent star-based EEC parameters, requiring the line-to-line voltage to be divided by $\sqrt{3}$ and parameters divided by 3. Using the same principles described in Section 5.2, to simulate the delta to star connection

change, maintaining the phase voltage applied to a delta-based EEC, the parameters should be multiplied by 3. However, when considering the EEC for a delta connection, the obtained current is the phase current, being necessary to multiply that value by $\sqrt{3}$ to obtain line current, but the used phase voltage corresponds to the actual line-to-line voltage. In the EEC for star connection, the current obtained is the line current, but the line-to-line voltage is $\sqrt{3}$ times higher than phase voltage. Considering fixed phase voltage and slip applied to the EEC, if the star-connected winding impedance is 3 times higher than the delta-connected winding impedance, one can write (5.26), which describes well known relations. The Joule losses in the stator winding are given by (5.27). For the same conditions, the stator winding voltage drop is given by (5.28). The stator winding voltage drop is equal in both connections. The developed mechanical power, for the same slip, is given by (5.29). Since fixed slip is being considered, the electromagnetic torque relation is given by (5.30).

$$\begin{cases} U_{ph} = I_Y \cdot 3Z_D \\ U_{ph} = I_D \cdot Z_D \\ I_Y = 3^{-1} \cdot I_D \end{cases} \quad (5.26)$$

$$P_{joule,Y} = 3R_{s,D} \cdot (3^{-1} \cdot I_D)^2 = \frac{1}{3} P_{joule,D} \quad (5.27)$$

$$U_{drop,Y} = 3Z_{s,D} \cdot 3^{-1} \cdot I_D = U_{drop,D} \quad (5.28)$$

$$P_{mec,Y} = 3R_{r,D} \cdot (s^{-1} - 1) \cdot (3^{-1} \cdot I_{r,D})^2 = \frac{1}{3} P_{mec,D} \quad (5.29)$$

$$T_{em,Y} = \frac{1}{3} T_{em,D} \quad (5.30)$$

Considering now a star-delta or hybrid connection mode, connecting correctly the partial windings, in relation to delta-parallel connection (see Table 5.3), considering fixed magnetizing flux, the relation between these line-to-line voltages is $\sqrt{7}$. Applying the same principles, the delta-parallel winding impedances have to be multiplied by 7 to convert the considered connection to start-delta connection. If the star-connected winding impedance is 7 times higher, thus, for fixed slip, the approximate relations in (5.31) can be written. Actually, (5.31) has a slight error due to the fact that the resistance does not obey to the “7 times” rule.

$$\begin{cases} U_{ph} \approx I_{YD} \cdot 7Z_{DP} \\ U_{ph} \approx I_{DP} \cdot Z_{DP} \\ I_{YD} \approx \frac{1}{7} I_{DP} \end{cases} \quad (5.31)$$

In relation to $R_{s,YD}$, since the phase current in the outer phase partial winding (e.g. I_{RA} in Table 5.3) is $\sqrt{3}$ times higher (and has a 30° time lead displacement) than the inner triangle phase partial winding (e.g. I_{AC} in Table 5.3), the losses in relation to the YS1 connection considering the same current are given by (5.32). Therefore, to embed this relation into the EEC, the relation between the stator resistances is given by (5.33). Since $R_{s,YS1} = 12R_{s,DP}$, thus the equivalent stator resistance for the YD connection can be given by (5.34). The Joule losses of the stator winding are given by (5.35). The stator winding voltage drop is given approximately by (5.36). The developed mechanical power, for a given slip, is given by (5.37), similarly to the previous demonstrations.

$$\frac{P_{joule,YD}}{P_{joule,YS1}} = \frac{R_w \cdot I_w^2 + R_w \cdot \frac{1}{3} I_w^2}{2R_w \cdot I_w^2} = \frac{\frac{4}{3} R_w \cdot I_w^2}{2R_w \cdot I_w^2} = \frac{2}{3} \quad (5.32)$$

$$\frac{R_{s,DY}}{R_{s,YS1}} = \frac{2}{3} \quad (5.33)$$

$$\frac{R_{s,DY}}{R_{s,YS1}} R_{s,DY} = \frac{2}{3} 12R_{s,DP} = 8R_{s,DP} \quad (5.34)$$

$$P_{joule,YD} = 8R_{s,DP} \cdot \left(\frac{1}{\sqrt{8}} I_{DP}\right)^2 = \frac{1}{8} R_{s,DP} \cdot I_{DP}^2 = \frac{1}{8} P_{joule,DP} \quad (5.35)$$

$$U_{drop,YD} \approx \sqrt{(8R_{s,DP})^2 + (7X_{s,DP})^2} \cdot \frac{1}{\sqrt{8}} I_{DP} \approx U_{drop,DP} \quad (5.36)$$

$$P_{mec,YD} \approx 7R_{r,DP} \cdot (s^{-1} - 1) \cdot \left(\frac{1}{\sqrt{7}} I_{r,DP}\right)^2 = \frac{1}{7} R_{r,DP} \cdot (s^{-1} - 1) \cdot I_{r,DP}^2 = \frac{1}{7} P_{mec,DP} \quad (5.37)$$

Therefore, to adapt the delta-parallel based EEC parameters in order to represent the star-delta connection, maintaining fixed phase voltage, all the parameters should be multiplied by 7, except stator resistance which should be multiplied by 8.

5.3.2.3 Displacement between Per-Phase Partial Voltages

In order to introduce the displacement effect between partial voltages in the same phase, it is proposed the introduction of an effective number of turns, defined by (5.38), where θ_1 and θ_2 are the phase angles of the partial voltages. The amplitude of both partial voltages (assuming partial windings with the same number of turns) is assumed to be the same.

$$N_{effective} = N_{real} \cdot (0.5\angle\theta_1 + 0.5\angle\theta_2) \quad (5.38)$$

This affects all the EEC turns-dependent or flux-dependent parameters, which should be multiplied by $N_{effective} \cdot N_{real}^{-1}$. The only parameter that is not affected by this change is the stator resistance, because there is no actual change of the series turns. For example, if the partial voltages were in phase opposition (180° time displacement between both), the effective turns and the magnetizing flux would be null, and the EEC would be just composed by a resistance (assuming that leakage fluxes are also in opposite direction and also cancel each other, which, in reality, does not fully happen). On the basis of the foregoing discussion, it is possible to adapt the EEC parameters to the connection modes with displacements between partial voltages, e.g., the YS2 connection, in which (5.39) is valid. For the YS1 connection, (5.40) is valid.

$$N_{effective,YS2} = N_{real,YS2} \cdot (0.5\angle 0^\circ + 0.5\angle 60^\circ) = 2^{-1} \cdot \sqrt{3} \cdot N_{real,YS2} \quad (5.39)$$

$$N_{effective,YS1} = N_{real,YS1} \cdot (0.5\angle 0^\circ + 0.5\angle 0^\circ) = N_{real,YS1} \quad (5.40)$$

Equation (5.39) means that all the turns and flux dependent parameters for the YS1 connection have to be multiplied by $(2^{-1}\sqrt{3})^2$. In this case, the stator resistance is equal for both YS1 and YS2 connections, being the YS1 connection more efficient. In general, the introduction of a phase shift between partial voltages leads to a less efficient operation. Moreover, in the extreme case, in which the fluxes are in anti-phase (or opposite phase), the winding efficiency is null, because no flux is produced (demagnetizing effect), but Joule effect losses occur.

5.3.2.4 Summary of the Rules for EEC Parameters Change as a Function of Connection Mode

In general, in the absence of partial phase flux displacements, the EEC parameters should be multiplied by the square of the quotient between the expected line-to-line voltage (for the same magnetizing flux) for the new connection and the line-to-line voltage for the reference connection, which is used to set-up the known initial or reference EEC parameters values. This rule is valid for connection changes, with or without parallel conductors, assuming that no variation in the amount of copper occurs in the stator windings (e.g., turns increase have to be accomplished by an equal equivalent copper cross-section decrease).

Known the EEC parameters for one of the mentioned connection modes, it is possible to define the changes to be made in the parameters to simulate other connection modes, maintaining the same voltage applied to the EEC, reflecting the motor performance change, at least theoretically, considering the simplifications made in the beginning of this section.

Obviously, for an accurate steady-state analysis, thermal compensation has to be made, taking into account the motor thermal behaviour and the differences in all losses (including the friction

and windage losses), as well as the saturation effect and the slip dependency of rotor parameters¹⁹ (related to the rotor current frequency). Actually, the variation in losses is rather easy to estimate on the basis of the proposed rules.

Considering the EEC parameters for the DP connection as reference, the EEC parameters to simulate the other 6 connection modes are presented in Table 5.7.

TABLE 5.7
MULTIPLYING FACTORS TO CONVERT EQUIVALENT CIRCUIT PARAMETERS FOR DIFFERENT CONNECTION MODES.

EEC Parameter	Multiplying Factors (DP Connection as Reference)					
	DP	YP	DS1	YS1	YD	YS2
R_s	1	3	4	12	8	12
L_s	1	3	4	12	7	9
R_r	1	3	4	12	7	9
L_r	1	3	4	12	7	9
R_{fe}	1	3	4	12	7	9
L_m^*	1	3	4	12	7	9

* The value of the parameter L_m requires proper correction in order to take into account the saturation effect.

Regarding the saturation effect on EEC parameters, which is important to consider for steady-state performance analysis, particularly for slip values lower than nominal slip, some considerations can be made. If the phase voltage is changing, the magnetizing flux will be different and the saturation level will be modified. No saturation level or magnetizing current dependency is necessary neither in the stator and rotor resistances, nor in the leakage reactances²⁰, at least in a first attempt of approximation. For fixed frequency, the core losses resistance in the vertical parallel branch of the EEC will be constant if it is assumed that core losses are proportional to E^2 (which is close to the phase voltage for medium/large motors), as in (5.41), where P_{fe} is the core losses for a given E .

$$R_{fe} \approx \frac{3 \cdot E^2}{P_{fe}} \approx \frac{3 \cdot E^2}{K_1 \cdot E^2} = K_2 \quad (5.41)$$

The case of magnetizing inductance is different. A saturation factor, k_s , can be defined in dependence with air-gap magnetomotive force, MMF_{ag} , and tooth and yokes magnetomotive force, MMF_{fe} , or in dependence of no-load current, I_0 , at nominal phase voltage, U_{Nph} , for both saturated and unsaturated core (see Fig. 5.22), according to (5.42) [30], [33], [34], which, for

¹⁹ In the IEC 60034-28 standard [47], the dependency of both L_m and L_s inductances on magnetizing current (or saturation level), at zero-slip operation, is evidenced and considered, but, since the L_s value is relatively low, the impact of its variation on motor no-load impedance is minor.

²⁰ In fact, there is an influence of the saturation on the leakage inductances and some technical books give methods of calculation. This influence is particularly important for starting transient operation when the 4-6 times larger current in the slots saturates the tooth tips leading to a decrease (in the order of 20-30%) of the leakage inductance part associated with the slots, or a change in current distribution occurs, particularly in deep-bar or double-cage rotors, changing the leakage inductance and resistance (these values become higher during starting period). However, even considering the slight variation of the rotor leakage inductance as a function of motor load (and, hence, of motor slip), since that variation is quite lower than that of the rotor resistance, and it is being considered only the phase voltage variation for motor operation in the quasi-linear region of the torque-speed curve, this effect is not relevant, and can be ignored without introducing significant errors, particularly for motor efficiency-centered analysis.

typical motors is in the range 1.3-1.7 (e.g., for a 380-V, 50-Hz, 11-kW, 4-pole IM, the $k_s \approx 1.3$ for nominal voltage), and rapidly increases with magnetizing flux, meaning it is strongly influenced by the phase voltage.

$$k_s = 1 + \frac{MMF_{fe}}{MMF_{ag}} \approx \frac{I_0}{I_{0(uns)}} \quad (5.42)$$

A certain degree of saturation is necessary for economical use of the materials²¹, being typically considered in most motor designs. But, for example, in underloaded motors, designed for a certain level of saturation for delta connection, if the connection is changed to star, the saturation factor will become almost 1 (e.g., $\phi_Y \approx 0.577 \cdot \phi_D$ and $B_{teeth,D} = 1.6$ T at $H_{teeth,D} = 30$ A/cm becomes $B_{teeth,Y} = 0.92$ T at $H_{teeth,Y} < 3$ A/cm).

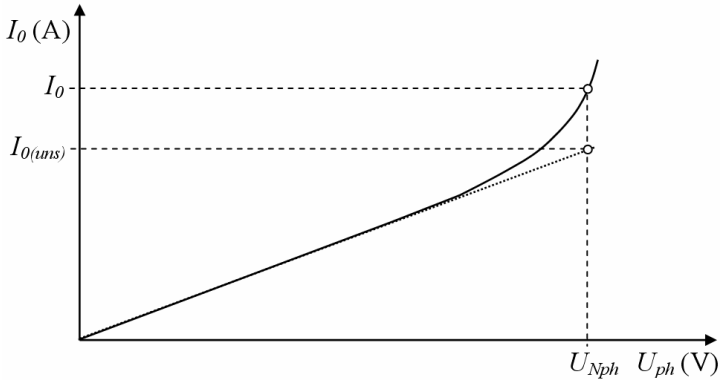


Fig. 5.22. No-load current as a function of phase voltage for saturated (real situation) and unsaturated core.

Magnetizing inductance increases almost in the ratio of the old/new saturation factor. The no-load magnetizing current and the EMF versus air-gap flux density are given by (5.43) and (5.44), where δ is the air-gap radial length, and α is the flattening factor. The magnetizing inductance can be given by (5.45), where τ_p is the pole pitch, k_C is the Carter factor²² (or coefficient) and l the effective core length. The subscript “peak” denotes maximum or peak value [34].

$$E = \sqrt{2} \cdot \pi \cdot f \cdot N \cdot K_w \cdot \alpha \cdot \tau_p \cdot L \cdot B_{ag(peak)} \quad (5.43)$$

$$I_{0\mu} = \frac{\pi}{3\sqrt{2}} \cdot \frac{p}{N \cdot K_w} \cdot \frac{B_{ag(peak)} \cdot \delta \cdot k_C \cdot k_s}{\mu_0} \quad (5.44)$$

$$L_m = \frac{E}{2\pi \cdot f \cdot I_{0\mu}} = \frac{3 \cdot \mu_0 \cdot f \cdot N^2 \cdot K_w^2 \cdot \alpha \cdot \tau_p \cdot l}{\pi \cdot f \cdot p \cdot \delta \cdot k_C \cdot k_s} \quad (5.45)$$

²¹ This is even more critical taking into account the recent increase in raw materials cost.

²² The Carter factor allows taking into account the slot opening effect on the air-gap permeance.

Flattening factor is the ratio of average to maximum (or peak) value of B_{ag} defined on a pole pitch (or half pole pitch, considering symmetry), according to (5.46). This factor is considered in a number of technical books as equal to $\frac{2}{\pi}$, but that assumption is only valid to motors without saturation. Depending on the degree of saturation of the tooth or yokes, these coefficients depend on the so called saturation harmonics (not space harmonics). In Fig. 5.23, the flattening factor dependence on the tooth saturation, $k_{s(teeth)} = MMF_{teeth}/MMF_{ag}$, assuming negligible yoke saturation factor ($k_{s(yoke)} = MMF_{yoke}/MMF_{ag} \approx 0$), is shown. It should be noted that saturation factor is given by $k_s = 1 + k_{s(teeth)} + k_{s(yoke)}$. In many motors, it can be verified that when yokes are saturated, $k_{s(yoke)}/k_{s(teeth)} \approx 5/3$, it is possible to keep flattening factor close to $\frac{2}{\pi}$ [34]. A form factor can also be introduced in (5.43), also depending on tooth k_s , varying between 1.11 (or $\pi \cdot (2 \cdot \sqrt{2})^{-1}$, which is value for unsaturated motors) and 1.07.

$$\alpha = B_{ag(avg)} \cdot B_{ag(peak)}^{-1} = \phi \cdot \tau_p^{-1} \cdot l^{-1} \cdot B_{ag(peak)}^{-1} \quad (5.46)$$

If yokes are saturated, there is other kind of influence of saturation on the air-gap flux density. In fact, even when the teeth are saturated, α has a low value because the yokes have a degree of saturation too. Increasing yoke saturation leads to the flattening factor decrease [33]. In [33], a simple programme to calculate air-gap flux density shape, neglecting yoke curvature, is proposed. In fact, if yokes are saturated the curves for flattening factor defined in [30] are no longer valid and should be calculated from case to case taking into account the interdependence between the MMF of tooth and yokes and the wave shape of air-gap flux density [31], [32].

Changing the level of saturation, the flattening factor of the air-gap flux density changes, but not as strongly as k_s changes. For example, from delta to star connection, k_s can vary from 1.3-1.5 to almost 1, affecting directly L_m .

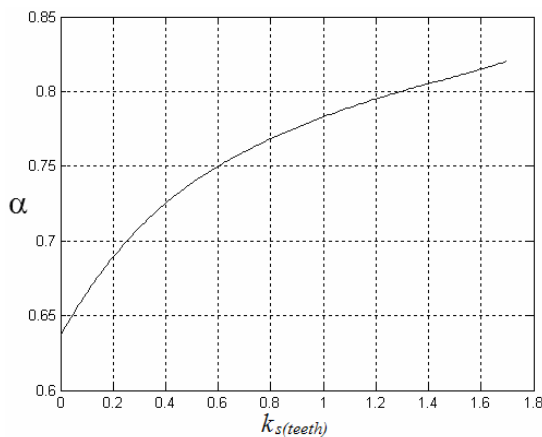


Fig. 5.23. Typical relation between flattening factor and $k_{s(teeth)}$ (ratio of the rotor plus stator tooth MMF to air-gap MMF), valid for negligible yoke saturation [30], [34].

In Table 5.7, it is assumed that if the applied voltage on the ECM is constant and the values of the parameters are modified, it is possible to simulate stator winding connection or phase voltage changing. However, on the basis of the foregoing discussion, it is possible to conclude that saturation level influences the magnetizing inductance L_m , which will have a different multiplying factor in relation to the parameters. Comparing L_m in star (low voltage) and delta (full rated voltage), yields (5.47).

$$\frac{L_{mY}}{L_{mD}} = \frac{\alpha_Y}{\alpha_D} \cdot \frac{k_{sD}}{k_{sY}} = r_\alpha \cdot r_k \quad (5.47)$$

The first ratio r_α is smaller than 1, since the flattening factor will decrease. The second ratio r_k is almost k_{sD} because k_{sY} is very close to 1, because phase voltage decreases $\sqrt{3}$ times becoming over the linear portion of the no-load current-phase voltage curve (see Fig. 5.23). For a 11-kW, 4-pole IM, with $\alpha_Y = 0.69$, $\alpha_D = 0.72$, $k_{sY} = 1.0$, and $k_{sD} = 1.308$, the magnetizing inductance is increased in the ratio

$$\frac{L_{mY}}{L_{mD}} = \frac{0.69}{0.72} \cdot \frac{1.308}{1} = 1.25.$$

In this case, considering delta (or DP) to star (or YP) connection change, the corrected multiplying factor for L_m would be 1.25 times 3, yielding 3.75. When k_s increases for a given nominal phase voltage, the L_m increase with the phase voltage decrease will be more pronounced. This can be applied to the L_m multiplying factor for the other connections. Therefore, a correction for the L_m multiplying factor can be performed at least taking into account the saturation factor, which can be easily estimated by means of a variable-voltage no-load test.

Nevertheless, since the L_m variation as a function of I_m was implemented in the EEC used for the steady-state simulations (see Appendix 2), the saturation effect is properly taken into account. In fact, when experimentally defining $L_m = f(I_m)$ for the delta connection (no-load test), since k_s and α depend on I_m ($\approx I_0$), the effect of those parameters is already included, but I_m has to be multiplied by the square root of 3 to reflect the actual I_m value in star connection (e.g., for the delta to star change case, $I_{mY} = I_{mD} \cdot \sqrt{3}$). Therefore, assuming that saturation effect is properly estimated on the basis of I_m and L_m interdependency, the values in Table 5.7 can be used. In practice, only for the change between DP and other connections (or between D and Y connections, in the case of conventional motors), significant variation on saturation occurs, requiring the discussed

compensations. For the connection change between the other connection modes (other than DP), since the saturation is very low (quasi-linear zone of operation), no adjustments in L_m are necessary. Of course, if other reference connections are considered, different flux step would result, requiring a proper saturation effect analysis.

5.3.2.5 Steady-State Simulations of the Different Stator Winding Connections

To illustrate the presented concepts, a simulation was carried out for a 3-kW, 4-pole motor, using a model with thermal compensation (see Appendix 2), obtained from experimental tests. The main results are presented in Figs. 5.24-5.26, considering the 6 selected connections. In Figs. 5.24 and 5.25, it is assumed DP connection (with imaginary parallel conductors) as reference connection, and rated and half rated friction and windage losses, respectively. The windage and friction losses have a significant impact on the efficiency peak values for the low power connections, as it can be observed by comparing Figs. 5.24 and 5.25. In Fig. 5.26, it is assumed that the YP connection is the reference connection, and rated friction and windage losses.

The YS2 connection, although improving the power factor for the corresponding load range, leads to no improvements in the resultant upper limit of efficiency-load curve (considering efficiency-load curves for all the considered connections). This still happen when the YP connection is considered as nominal connection, as it can be seen in Fig. 5.26. Therefore, YS2 is a candidate to be excluded from the useful or practical connections. As previously mentioned, in order to simplify the connection change process and reduce the connection change frequency over duty cycle, other connection modes combinations (in terms of reference connection and number of additional connections) can be considered as a function of the application (e.g., YP, as reference, and DS1 connections).

Fig. 5.27 shows the torque and current as a function of slip, considering the 6 possible connections (DP as nominal connection), nominal friction and windage losses and thermal compensation. Fig. 5.28 shows the torque as a function of slip considering fixed 25°C temperature in all motor parts.

The presented results are the expected ones, proving the validity of the proposed strategy as a way to improve motor efficiency and power factor for load lower than rated load. It can be anticipated that the simulated results are in accordance with experimental results. Additionally, it can be noted that the advantage of continuous voltage regulation (e.g., using electronic voltage regulators) is minor in terms of efficiency for loads higher than 15%, particularly taking into account the typical discrete behaviour of most loads (2-5 different load levels).

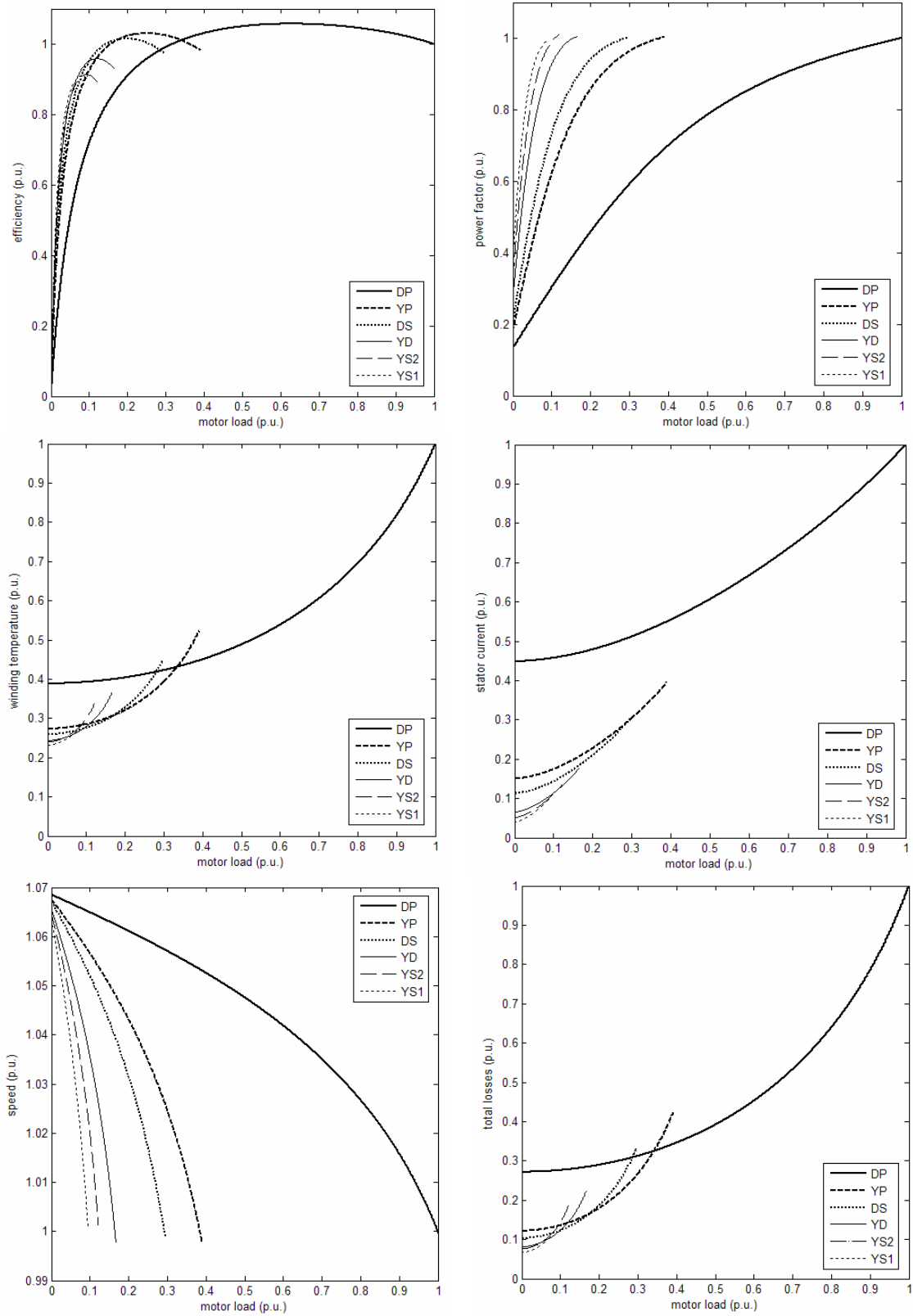


Fig. 5.24. Simulated efficiency, power factor, phase current, winding temperature, speed and losses, as a function of motor load, for a 3-kW, 4-pole motor, considering 6 different connections (DP as nominal connection), nominal friction and windage losses, and thermal compensation.

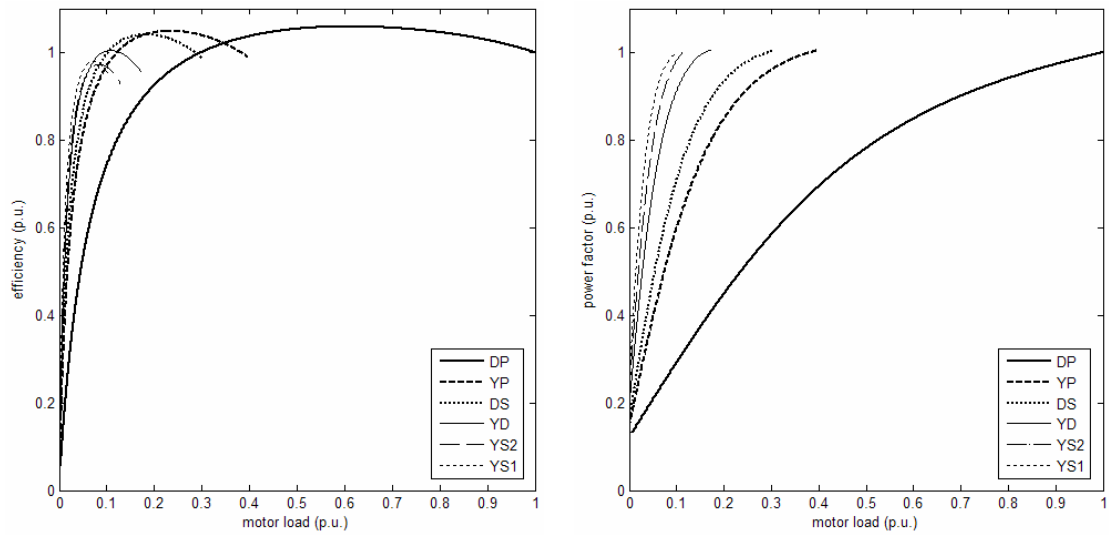


Fig. 5.25. Simulated efficiency and power factor, as a function of motor load, for a 3-kW, 4-pole motor, considering 6 different connections (DP as nominal connection), half the nominal friction and windage losses, and thermal compensation.

From Figs. 5.27 and 5.28 it is possible to conclude that properly managing all the available connections, soft starts and speed control (although limited and with poor efficiency) can be made. Although some connections can be considered redundant in terms of efficiency, from the speed regulation perspective, all connections can actually be used to provide more intermediate torque-speed curves. Here, motors with a low-slope quasi-linear torque-speed curve part are recommended for wider speed variation range.

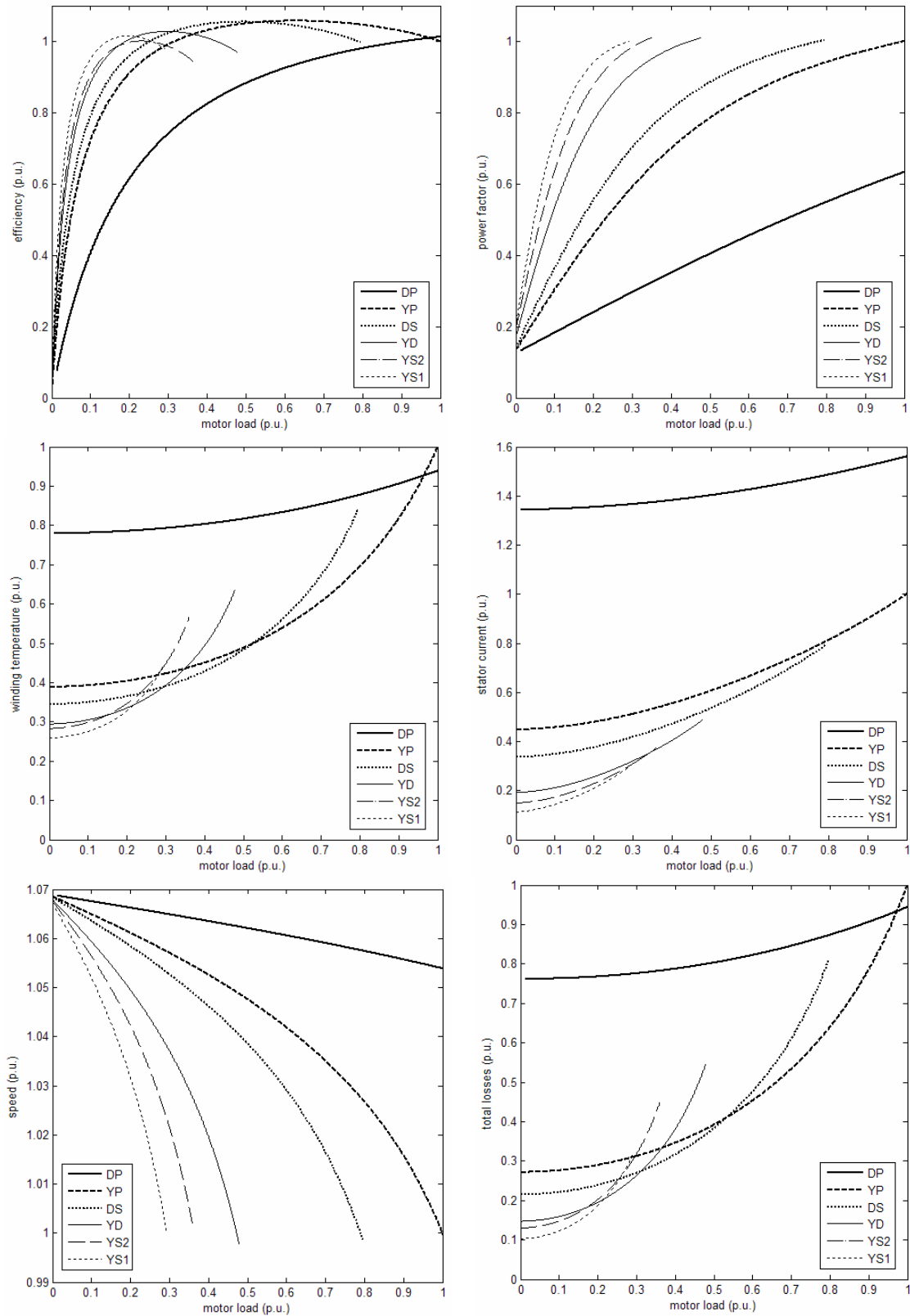


Fig. 5.26. Simulated efficiency, power factor, phase current, winding temperature, speed and losses, as a function of motor load, for a 3-kW, 4-pole motor, considering 6 different connections (YP as nominal connection), nominal friction and windage losses, and thermal compensation.

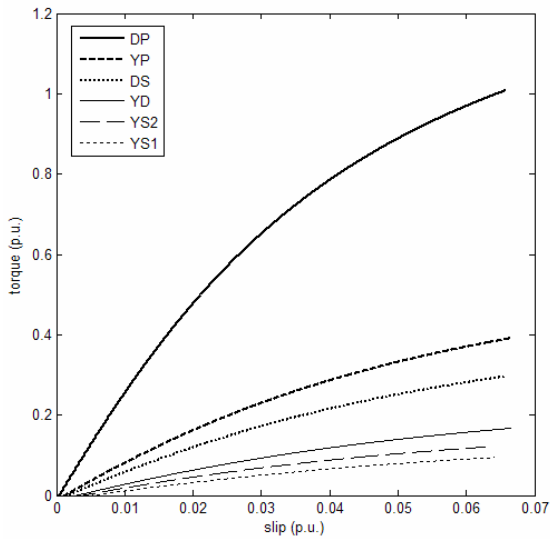


Fig. 5.27. Simulated torque as a function of slip for a 3-kW, 4-pole motor, considering 6 different connections (DP as nominal connection), nominal friction and windage losses, and thermal compensation.

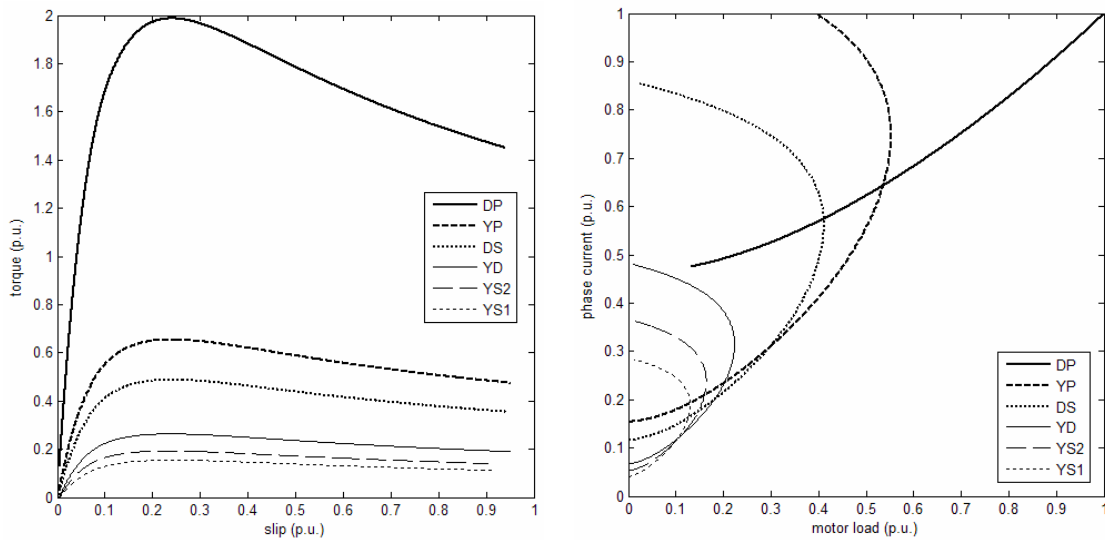


Fig. 5.28. Simulated torque as a function of slip and phase current as a function of motor load, for a 3-kW, 4-pole motor, considering 6 different connections (DP as nominal connection), nominal friction and windage losses, and fixed 25°C temperature in all motor parts.

5.3.3 Connection Change Transient Analysis

Regarding the connection change transient analysis resulting from the mains/line ON→OFF (power interruption) and OFF→ON (power reconnection) switching instants, two different switching strategies are analysed in this section, namely, using a conventional contactor and a using thyristor-based electronic circuit. Using SIMULINK software tool, several simulations were performed for a 37-kW, 4-pole motor, driving a fan-type load, considering a motor dynamic model (described in Appendix 2) and a power supply with impedance. The considered motor model has an inherent star connection.

5.3.3.1 Contactor-Based Switching

For the case of contactor-based switching, which is the most common motor line ON-OFF strategy, when the disconnection of the three phases is made simultaneously, inevitably, at any instant in time, at least two currents not crossing zero point. Since the motor is basically an inductive-resistive load, when the disconnection occurs (ON→OFF) at non-zero current instants, a voltage transient occurs at the motor terminals because of its inductive nature ($u_L = Ldi/dt$). These voltage transients can reach very high values, potentially producing an arc over the contactor terminals, hence reducing its lifetime. Additionally, line-to-ground voltage transients can happen, stressing the motor insulation system. In fact, the very high-magnitude short-duration voltage peaks occurring in the power disconnection instants can originate partial discharges near the motor terminals. In Fig. 5.29, a very-low capacitance (10^{-9} F) RC-series snubber circuit is considered, which can roughly represent the stray capacitance associated with the contactor contacts. In Fig. 5.30, a significant RC-series snubber circuit with a 10^{-6} F capacitor is considered. The introduction of snubber circuits in parallel with the contactor contacts can reduce the voltage transient magnitude, as it can be concluded by the observation of Figs. 5.29 and 5.30. The transient voltages across the contactor terminals and between the motor terminals and the ground, over the ON→OFF transition, can be considerably reduced when the snubber capacitance increases. Therefore, appropriate snubber circuits are recommended when a high number of winding connection changes is expected during a short period, if automatic connection-mode management is used.

During power reconnection (OFF→ON), significant short-duration current peaks can occur, being the duration dependent upon the actual motor speed after deceleration and the peak value dependent upon the displacement between the mains voltages and the motor terminals voltage. The current peaks over OFF→ON transition practically do not depend on the snubber circuit.

5.3.3.2 Thyristor-Based Switching

In the case of thyristor-based line switching, using a circuit similar to those used in the thyristor-based soft-starters (requiring 6 back-to-back connected thyristors; schematic shown in Appendix 6), the disconnection is made naturally at the zero-current points, without complex firing control [11]. This strategy reduces dramatically the voltage transients when ON→OFF transitions occur, even with negligible RC-series snubber circuit, as it can be seen in Figs. 5.31 and 5.32. In this case the snubber circuit has no major effect on the voltage transients. However, the current transients during OFF→ON transitions can still reach very high values. With a proper per-phase control circuit taking into account the actual voltage across the thyristors, it is possible to minimize those transients by firing the thyristors at the most suitable instant to reconnect the motor to the power

grid, avoiding for example the reconnection during motor-grid voltage phase opposition instants. This strategy can be justified if the expected number of connection changes during motor duty cycle is high. Of course, during ON-state thyristor operation there are losses associated with the current flowing (from anode to cathode) and forward voltage drop, being desirable the use of a bypass contactor to eliminate the conduction losses associated with thyristors.

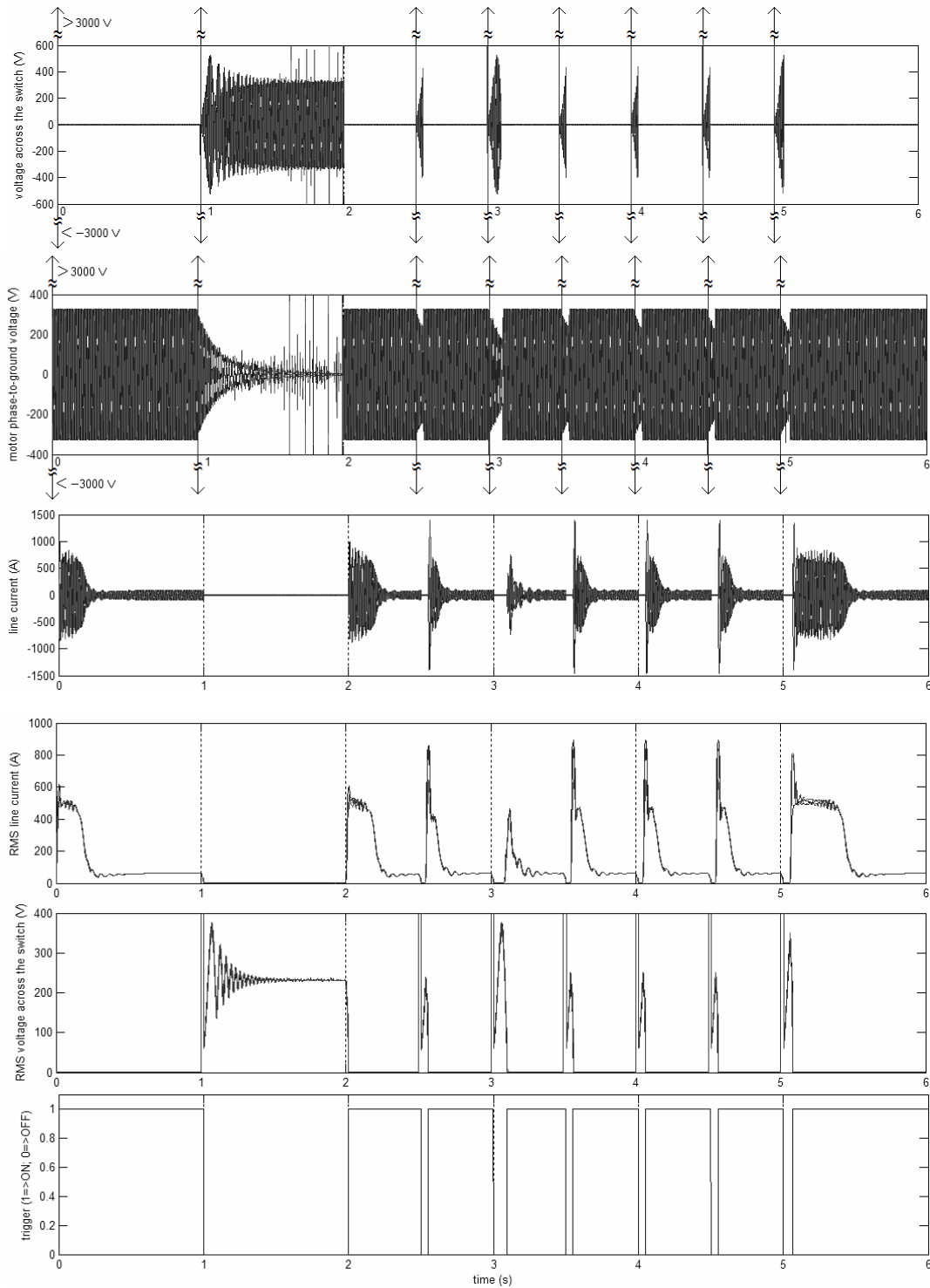


Fig. 5.29. Simulated instantaneous currents and voltages at the motor terminals and at the contactor terminals during transition instants, for contactor-based switching with negligible snubber circuit ($R_{snubber} = 10 \Omega$, $C_{snubber} = 10^{-9} \text{ F}$, $R_{on} = 0.001 \Omega$, $R_s = 0.08233 \Omega$, $L_s = 0.000724 \text{ H}$, $L_m = 0.02711 \text{ H}$, $R_r = 0.0503 \Omega$, $L_r = 0.000724 \text{ H}$, $B = 0.02791 \text{ N.m.s/rad}$, $p = 2$, $f = 50 \text{ Hz}$, $N = 1480 \text{ r/min}$, $P_N = 37 \text{ kW}$, $J = 0.37 \text{ kg.m}^2$, $T_{load} = 1025 \cdot 10^{-5} \cdot \omega^2$).

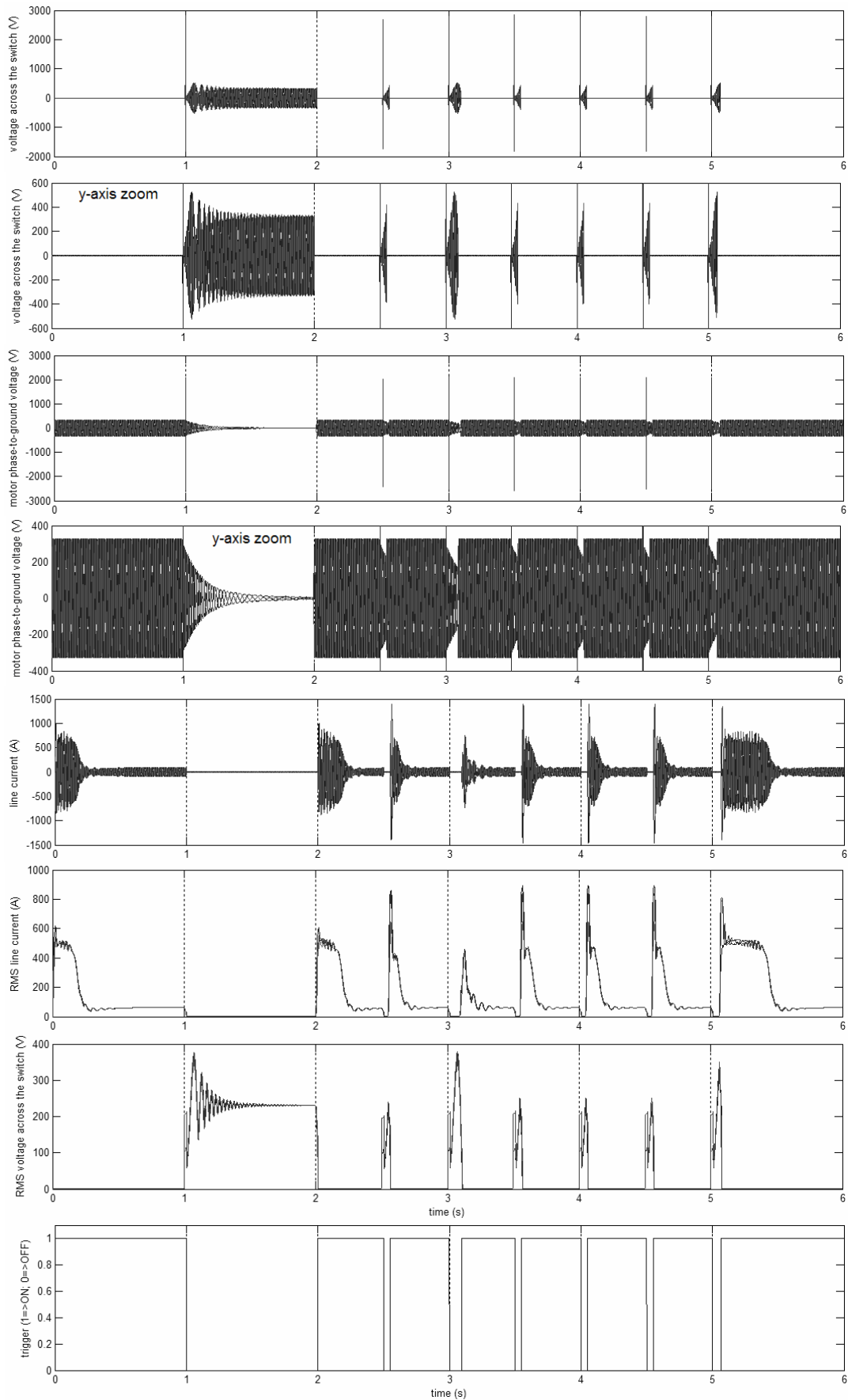


Fig. 5.30. Simulated instantaneous currents and voltages at the motor terminals and at the contactor terminals during transition instants, for contactor-based switching with significant snubber circuit ($R_{snubber} = 10 \Omega$, $C_{snubber} = 10^{-6} \text{ F}$, $R_{on} = 0.001 \Omega$, $R_s = 0.08233 \Omega$, $L_s = 0.000724 \text{ H}$, $L_m = 0.02711 \text{ H}$, $R_r = 0.0503 \Omega$, $L_r = 0.000724 \text{ H}$, $B = 0.02791 \text{ N.m.s/rad}$, $p = 2$, $f = 50 \text{ Hz}$, $N = 1480 \text{ r/min}$, $P_N = 37 \text{ kW}$, $J = 0.37 \text{ kg.m}^2$, $T_{load} = 1025 \cdot 10^{-5} \cdot \omega^2$).

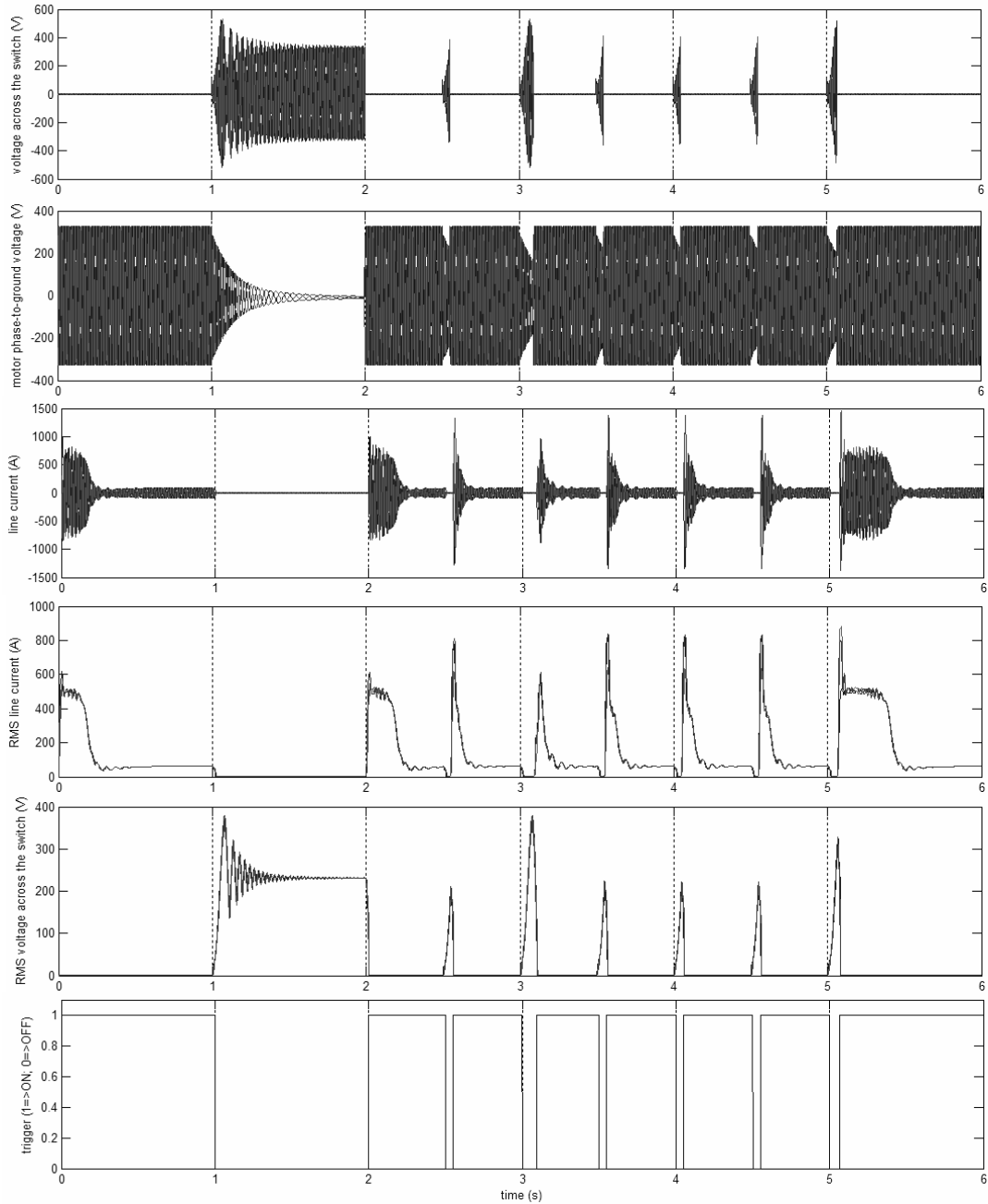


Fig. 5.31. Simulated instantaneous currents and voltages at the motor terminals and at the thyristor terminals during transition instants, for thyristor-based switching with negligible snubber circuit ($R_{snubber} = 10 \Omega$, $C_{snubber} = 10^{-9} \text{ F}$, $R_{on} = 0.001 \Omega$, $R_s = 0.08233 \Omega$, $L_s = 0.000724 \text{ H}$, $L_m = 0.02711 \text{ H}$, $R_r = 0.0503 \Omega$, $L_r = 0.000724 \text{ H}$, $B = 0.02791 \text{ N.m.s/rad}$, $p = 2$, $f = 50 \text{ Hz}$, $N = 1480 \text{ r/min}$, $P_N = 37 \text{ kW}$, $J = 0.37 \text{ kg.m}^2$, $T_{load} = 1025 \cdot 10^{-5} \cdot \omega^2$).

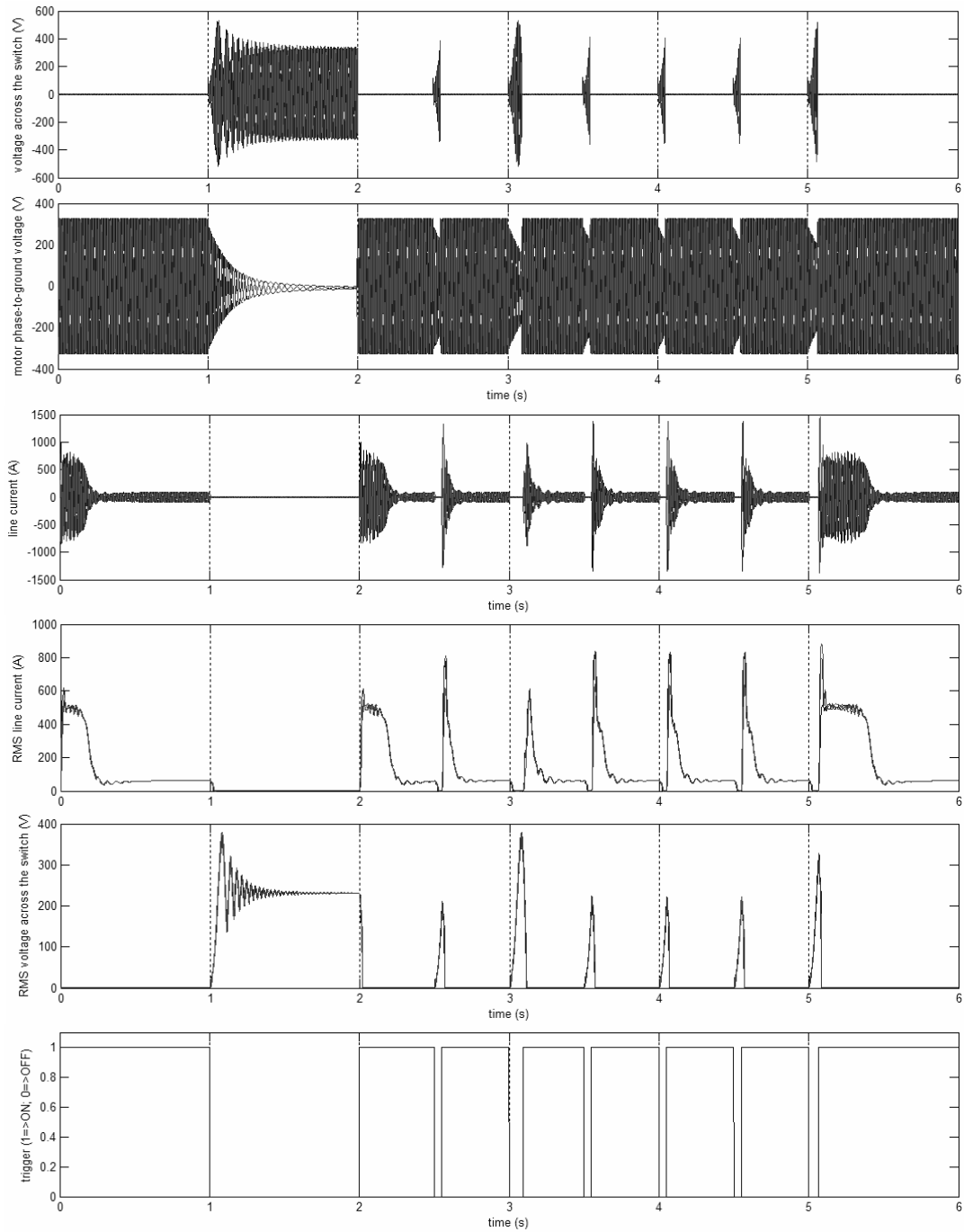


Fig. 5.32. Simulated instantaneous currents and voltages at the motor terminals and at the thyristor terminals during transition instants, for thyristor-based switching with significant snubber circuit ($R_{snubber} = 10 \Omega$, $C_{snubber} = 10^{-6} \text{ F}$, $R_{on} = 0.001 \Omega$, $R_s = 0.08233 \Omega$, $L_s = 0.000724 \text{ H}$, $L_m = 0.02711 \text{ H}$, $R_r = 0.0503 \Omega$, $L_r = 0.000724 \text{ H}$, $B = 0.02791 \text{ N.m.s/rad}$, $p = 2$, $f = 50 \text{ Hz}$, $N = 1480 \text{ r/min}$, $P_N = 37 \text{ kW}$, $J = 0.37 \text{ kg.m}^2$, $T_{load} = 1025 \cdot 10^{-5} \cdot \omega^2$).

5.3.3.3 System Inertia Influence

One of the most important factors in the admissible connection change frequency is the inertia of the system (motor rotor plus load inertia). A 37-kW, 4-pole motor was simulated with different system inertias (0.5, 1.0 and 1.5 p.u.), being the results presented in Figs. 5.33 and 5.34.

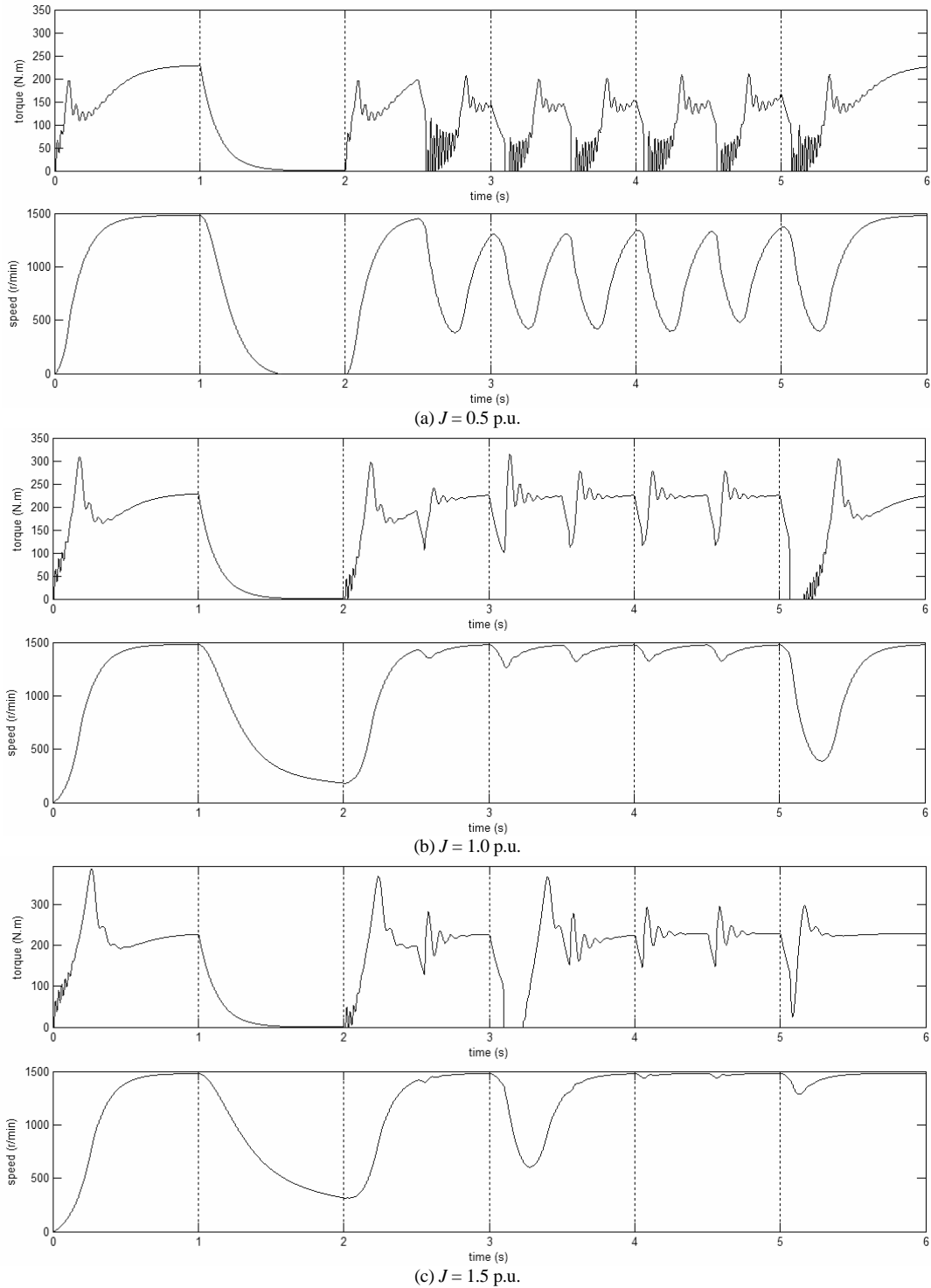


Fig. 5.33. Simulated motor speed and torque considering different system inertias (original motor inertia equivalent to 1 p.u.).

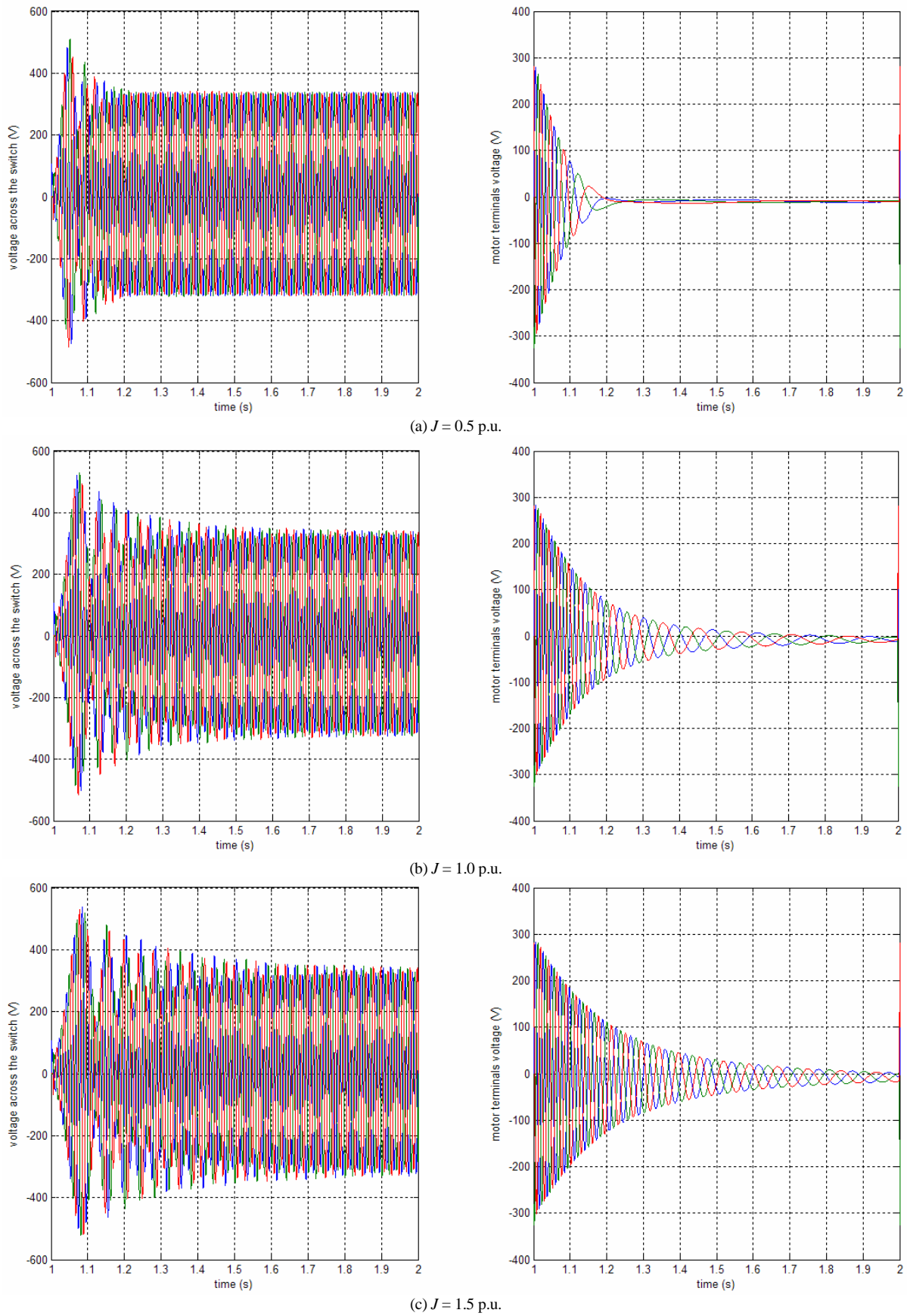


Fig. 5.34. Simulated voltage across the switches and at the motor terminals after reaching steady-state followed by a ON→OFF command to thyristors ([1 2] s period), considering different system inertias.

In Fig. 5.34, a 1-2 s period time zooming of voltages across the thyristors and the voltage between the motor and ground is presented, showing that, after the motor disconnection, a significant voltage amplitude at their terminals is generated, decreasing in amplitude and frequency with time. On the basis of the simulated results, as expected, it is possible to conclude that, the higher the system inertia is, the longer the time period for voltage to reach zero will be and, even for low inertia systems, if the commutation duration period is shorter than 0.1 s, the deceleration is not significant. Therefore, the reconnection can be made in a wider time window without significant motor speed loss, but the possibility of a large electrical potential difference between mains and motor terminals voltage is also higher. In fact, if voltages are in opposite phase during reconnection instants, significant currents can actually occur in the subsequent instants, as shown in previous section.

5.3.4 Experimental Results

5.3.4.1 Preliminary Tests with a Three-Phase Transformer

In a first stage, several experimental tests were conducted using a three-phase three-limb transformer with multiple windings (4 identical windings per magnetic column), in order to confirm the resulting magnetic flux. In each phase, two windings were considered as primary (representing the motor stator windings) and one open winding as secondary (representing the magnetizing flux). The magnetizing flux magnitude variation produced by the different connections was measured by means of induced voltage in a third winding. In Table 5.8, a summary of the experimental results is presented, allowing one to conclude that the previous considerations are correct. These results were also confirmed by simulations (using the three-phase transformer models in SIMULINK).

TABLE 5.8
EXPERIMENTAL TRANSFORMATION RATIO IN A THREE-PHASE TRANSFORMER FOR DIFFERENT CONNECTIONS.

Connection	Transformation ratio (p.u.)
Delta-Parallel (reference) *	1.0 (DP)
Delta-Series *	2.0 (DS1)
Delta-Series Direct Zigue-Zague 1	1.0
Delta-Series Direct Zigue-Zague 2 **	Inf.
Delta-Series Inverse Zigue-Zague 2	1.0
Delta-Series Direct Zigue-Zague 1	1.0
Star-Parallel *	$\sqrt{3}$ (YP)
Star-Series *	$2\sqrt{3}$ (YS1)
Star-Series, Direct, Zigue-Zague 1	$\sqrt{3}$
Star-Series, Direct, Zigue-Zague 2	$\sqrt{3}$
Star-Series, Inverse, Zigue-Zague 1 *	3.0 (YS2)
Star-Series, Inverse, Zigue-Zague 2	3.0
Star-Delta, Direct *	$\sqrt{7}$ (YD)
Star-Delta, Inverse	1.0
Star-Delta, Inverse, Zigue-Zague 1	$\sqrt{7}$
Star-Delta, Direct, Zigue-Zague 1	1.0
Star-Delta, Direct, Zigue-Zague 2	2.0
Star-Delta, Inverse, Zigue-Zague 2	2.0

* Selected connections.
** Meaning extremely high in experimental results and infinity in simulations.

5.3.4.2 Experimental Tests with a Multi-Connection Induction Motor

For the experimental analysis, a 7.5-kW, three-phase, four-pole, squirrel-cage induction motor (400 V, 50 Hz, TEFC) was properly rewound (hereafter denoted by MFLIM_E). The stator winding was designed using the software BOBISOFT (see Appendix 3). The original 36-slot concentric winding was replaced by an optimised short-pitched (7-slot span), eccentric (or lap) winding, as it can be seen in Fig. 5.35, with 2 sets of turns per phase (DP connection as nominal) and the 12 lead-terminals available.

The facility used to test the MFLIM_E, fulfils the motor testing standard requirements (see Chapter 2). To measure the electrical and mechanical variables, a high accuracy power analyzer was used. A hysteresis dynamometer was used as a variable load (constant torque load), which includes an encoder to measure speed and a load cell to measure the torque. The power analyzer acquires the values of both sensors. In Fig. 5.36, the MFLIM_E and the dynamometer are shown.

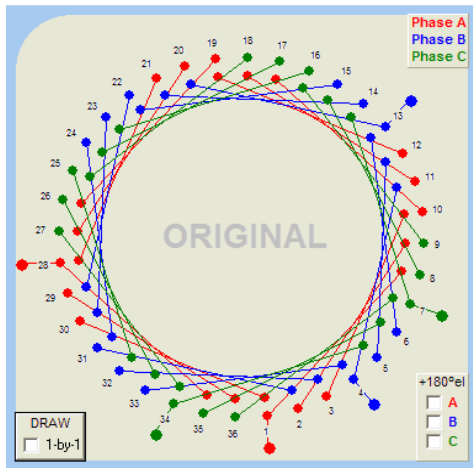


Fig. 5.35. Circumferential stator winding scheme of one of the two parallel groups of the MFLIM_E (36 slots, eccentric double-layer winding, coil pitch 7/9), produced by BOBISOFT.

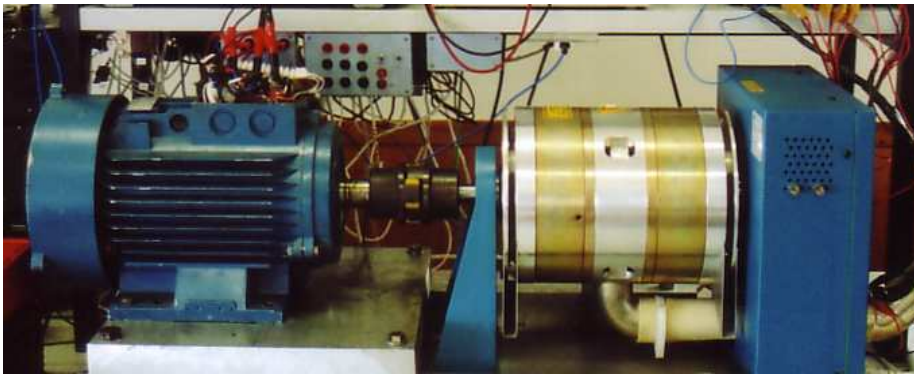


Fig. 5.36. Photograph of the MFLIM_E coupled with the dynamometer.

In Figs. 5.37-5.45, the motor efficiency, power factor, line current, speed and stator winding temperature, as a function of motor output power, as well as the torque-slip curves, for the considered stator winding connection modes, are shown (the core losses are shown in Appendix 6). The intersection points (named point α in Section 5.2, [15], [10]) can be easily identified (signalled by vertical lines). Five practical zones between the intersection points were established, denoted by A, B, C, D and E, and for each one there is a proper connection mode. The YS2 connection was not considered in those zones because it does not contribute to the improvement of the resultant motor efficiency curve, although it can contribute to a slight improvement of the resultant power factor curve, as it can be seen in Fig. 5.39. This is in accordance with the simulated results presented in Fig. 5.24 for a 3-kW, 4-pole motor.

From Fig. 5.44, it is possible to conclude that if the defined setpoints are respected (see Fig. 5.41), the stator winding average temperature never exceeds the nominal temperature, therefore not affecting the lifetime of the motor. In fact, when comparing to the DP connection, the use of the other connections can lead to a significant temperature decrease, increasing the motor lifetime. This fact can be considered another important advantage.

In Fig. 5.45, the MFLIM_E total impedance value, obtained dividing the voltage by the current, as a function of the slip is shown. The results presented in Fig. 5.45 are according to those anticipated in previous sections in relation to the EEC parameters value adaptation for the different

connections. The relation between the impedances is roughly maintained for the presented slip values, being the differences justified mainly by the saturation effect on EEC inductances (particularly on L_m , as discussed previously) and, in less extent, by motor steady-state temperature differences on EEC resistances, when operating with different connections, which are factors neglected in the theoretical analysis (but considered in the simulations), for the sake of simplicity. It is interesting to note that, as predicted, the saturation effect is only relevant for the L_m multiplying factor corresponding to the change from DP to one of the other connections, as it can be seen in Fig. 5.46. However, the experimental relation between the multiplying factors associated with the other connections (YP included) is fairly according to the saturation-less theoretical values presented in Table 5.7, as expected, due to the low saturation values.

If the YP connection is adopted as nominal connection mode, one should expect the estimated efficiency curves presented in Fig. 5.47 (not taking into account the exact saturation level for each connection mode and the actual fan cooling power contribution at each load point). Comparing the curves in Figs. 5.47 and 5.26, it can be concluded that, adopting the YP as the nominal connection mode, the efficiency transitions become smoother, but at very low loads the efficiency becomes worse. This aspect can be attenuated if the actual saturation and the actual fan cooling power contribution at each load point (in the case of self-cooled motors) are both taken into account, leading to an increase in the efficiency levels for the lower flux connections. This was verified in the simulated results presented in Figs. 5.24 and 5.26, which include the effect of the temperature and friction and windage losses on efficiency-load curves. Smoother power factor and current transitions are also expected. In Fig. 5.47, the YS2 and DP connections were excluded, but the four considered connections lead to a quite good result in terms of efficiency.

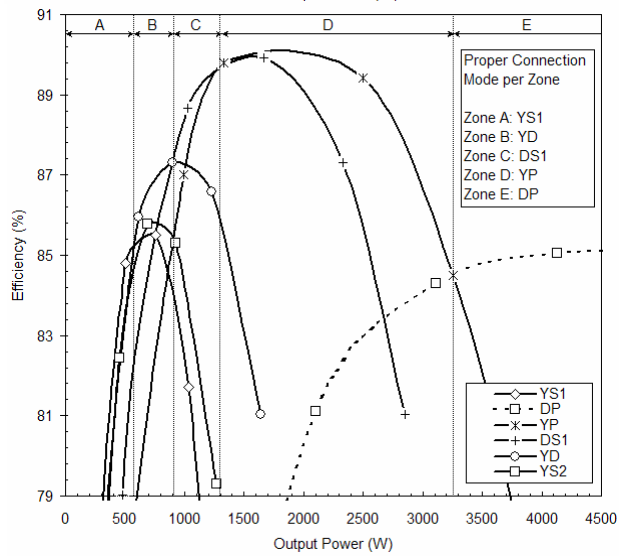
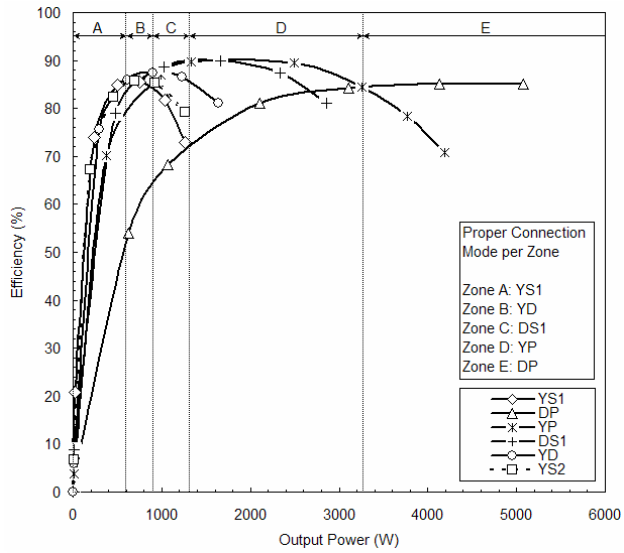


Fig. 5.37. Efficiency as a function of output power, for the MFLIM_E: (top) overview; (bottom) close-up.

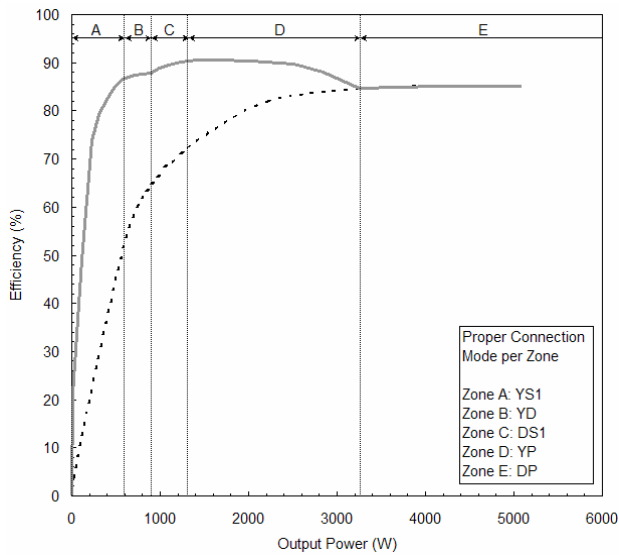


Fig. 5.38. Maximum efficiency curve with proper connection mode change (grey solid line) and efficiency curve for DP connection (black dashed line) as a function of output power, for the MFLIM_E.

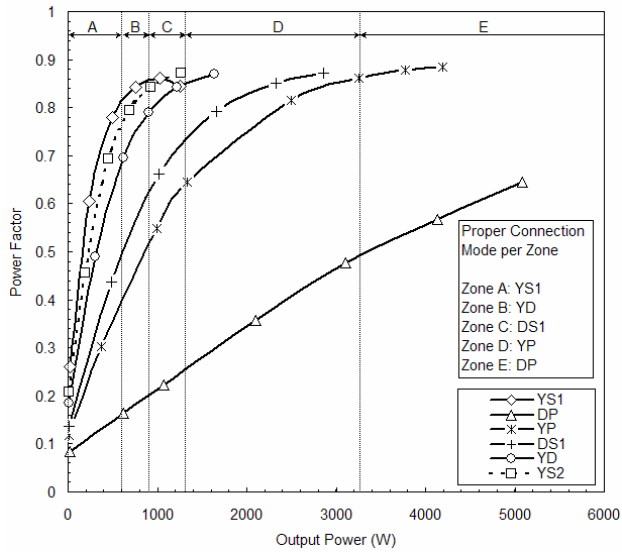


Fig. 5.39. Power factor as a function of output power, for the MFLIM_E.

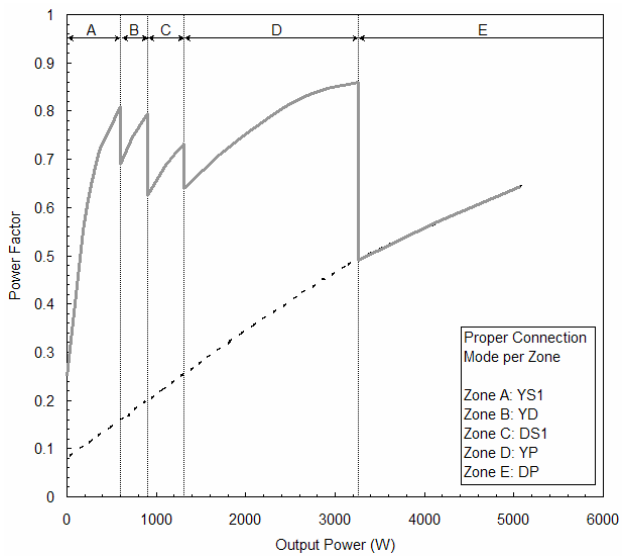


Fig. 5.40. Resultant power factor curve with proper connection mode change (grey solid line) and power factor curve for DP connection (black dashed line) as a function of output power, for the MFLIM_E.

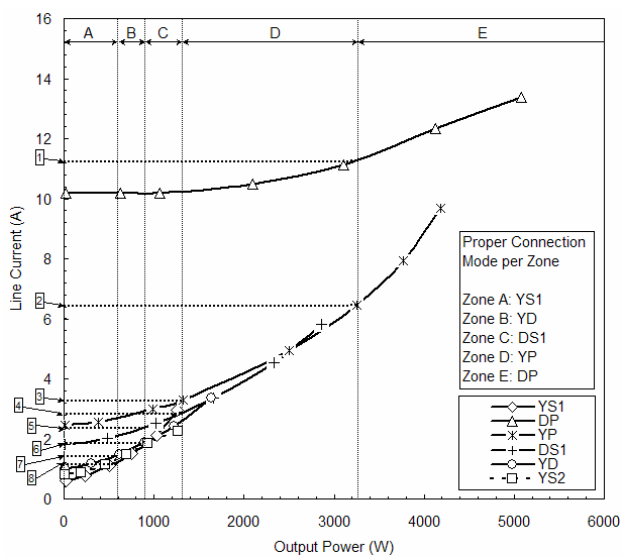


Fig. 5.41. Line current as a function of output power, for the MFLIM_E.

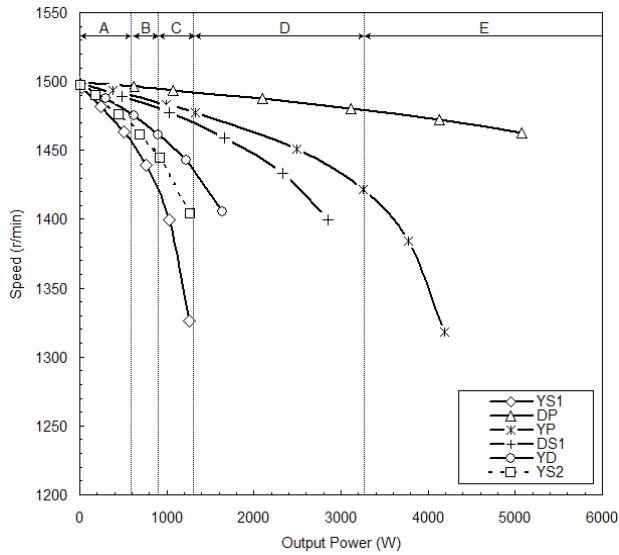


Fig. 5.42. Speed as function of output power, for the MFLIM_E.

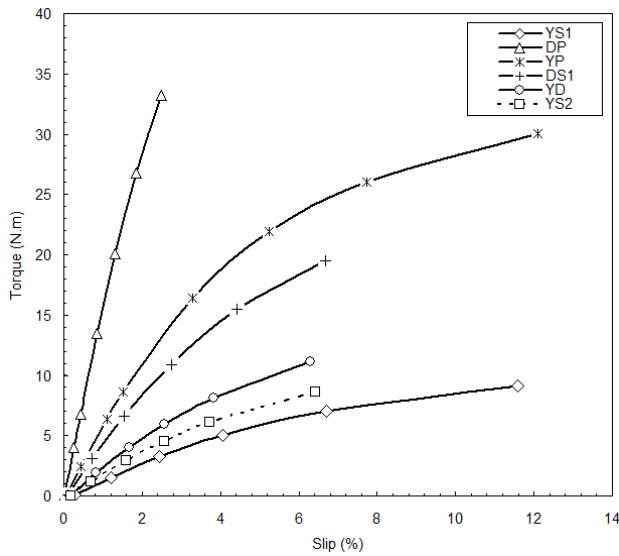


Fig. 5.43. Torque as a function of slip, for the MFLIM_E.

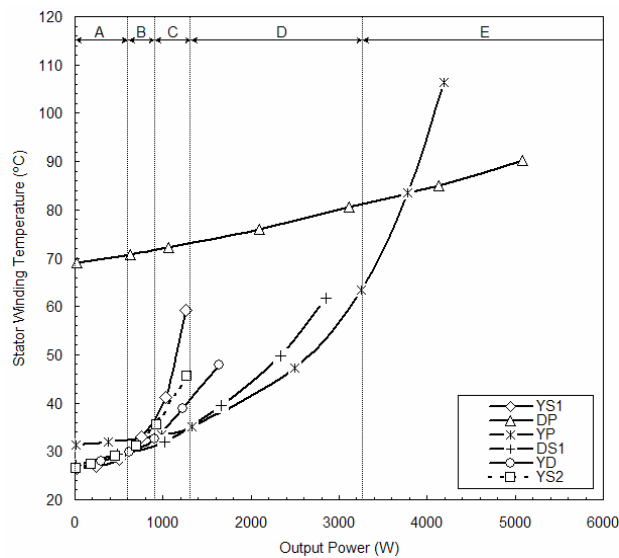


Fig. 5.44. Stator winding average temperature (measured by means of the stator winding resistance) as a function of output power, for the MFLIM_E.

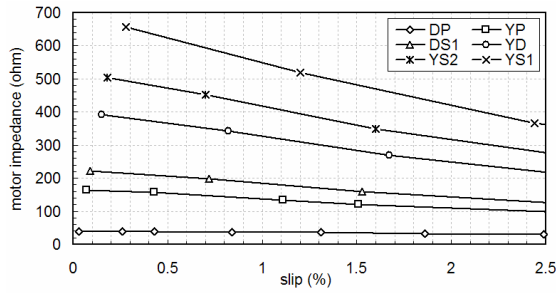


Fig. 5.45. Total impedance value (voltage divided by the current) for the MFLIM_E, as a function of the slip.

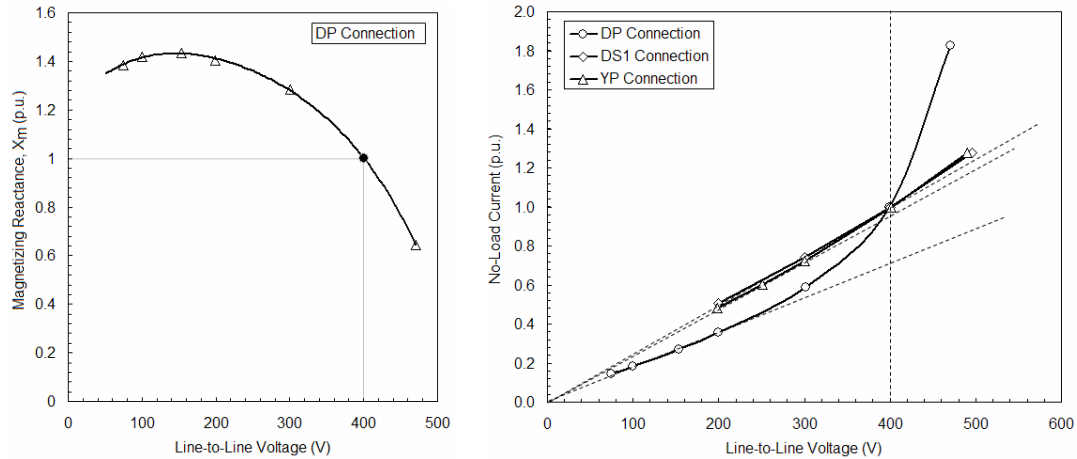


Fig. 5.46. Additional experimental tests on MFLIM_E: (left) X_m variation as a function of line-to-line voltage for the DP connection. (right) no-load current as a function of line-to-line voltage for the DP, DS1 and YP connections, evidencing the saturation effect in the DP connection.

The presented concept can also be associated to the method of consequent poles, commonly known as *Dahlander*, in which, for an even number of pole-pairs equal to or higher than 2, the number of poles can easily be changed by a factor of 2:1 with only simple changes in coil connections (polarity inversion of half of the coil-groups), being typically used 3 different connection types: constant torque (D/YY)²³, constant power (D/D) and quadratic torque or fan drive (Y/YY) [4], [16], [18]. Considering this pole change principle, the fusion of both concepts leads to a two-speed MFLIM, with 24 lead-terminals. This kind of motor becomes even more flexible, with different levels of flux, voltage, power, speed and torque, allowing efficiency and power factor maximization, as a function of load. Further considerations on this solution are presented in Section 5.3.6.

For two-speed applications, the comparison should be made between VSDs, two-speed motors (with or without voltage regulation by either electronic device of connection mode change), or simple voltage regulation. The last solution is only admissible for quadratic torque load, due to the slip and torque limitations. For the same power range, two-speed motors have, however, a similar efficiency in both low-speed and high-speed operating modes (see Fig. 5.48). The torque-speed relation has to be properly chosen according to the load type to avoid low load at reduced speed.

²³ “YY” is the standard notation for the YP connection.

However, the typical poor efficiency of two-speed motors can be largely compensated by the inherent power savings in some loads associated with the speed decrease.

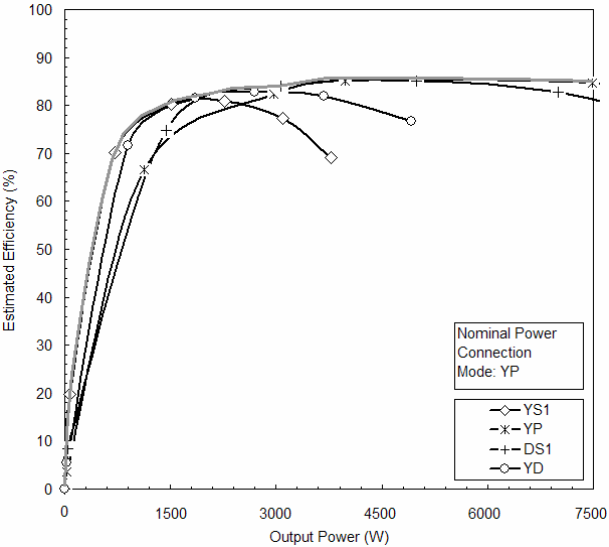


Fig. 5.47. Estimated maximum efficiency curve (grey solid line) as a function of output power, assuming the YP connection as nominal.

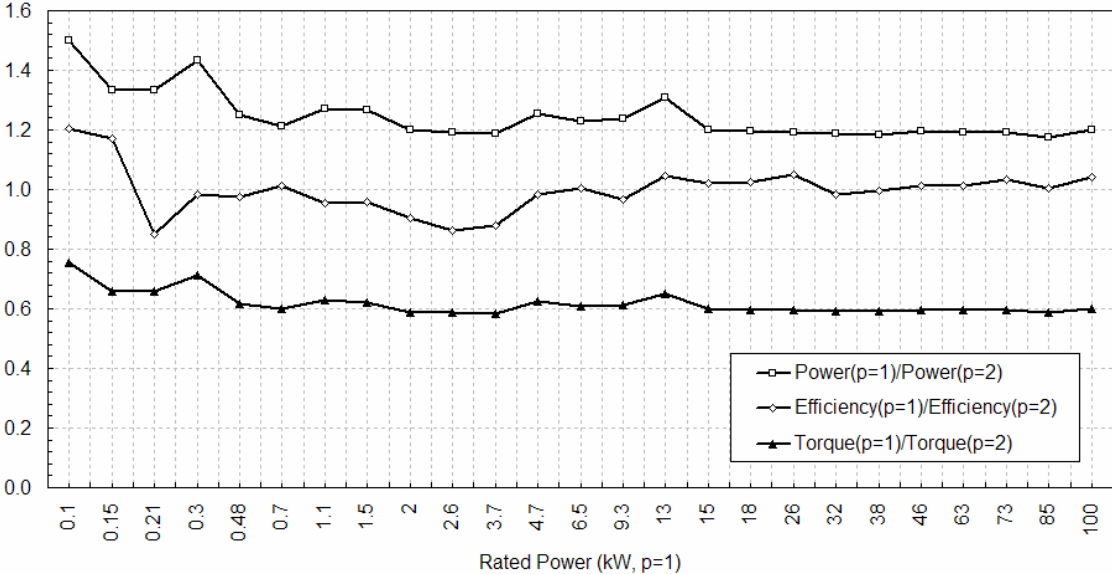


Fig. 5.48. Relation between the operation for 1 and 2 pole-pairs in the two-speed motors of one of the major motor manufacturers (1996).

On average, when changing from 2-pole to 4-pole mode, the available power decreases 19%, the efficiency is maintained approximately equal, and the rated torque increases 62%.

Of course, for particular customized speeds, the only feasible solution is using VSDs and/or gearboxes or belts.

5.3.5 Connection-Mode Change

The connection mode decision has to take into account both the line-to-line voltage at the motor terminals and the motor load, and should be based on the intersection points between efficiency curves. These issues were analysed in [8], [10], [12], [15], [16], and [17]. For the sake of

simplicity, only the load aspect is addressed in the following analysis, considering the voltage fixed at the rated value.

The connections for the single- or two-speed motor can be made directly in a 12- or 24-terminal block (Fig. 5.49), respectively, similarly to the delta/star connections in the conventional 6-terminal blocks. If the connections were made using unfixed 12 lead-terminals, a 7-terminal block would be enough, either for the single- or two-speed motor.

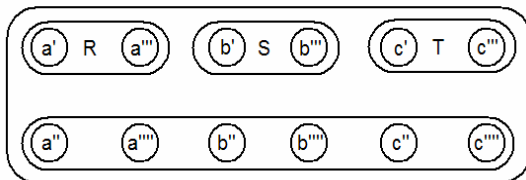


Fig. 5.49. Example of an YP connection in a 12-terminal block (nomenclature according to Table 5.3).

The user can identify the best winding configuration based on the motor slip or speed (e.g. measured using a stroboscopic tachometer, with proper voltage correction) or on the line current (e.g., measured using a clamp ammeter), as described in Section 5.2 and [10], [15].

From the perspective of automatic change, a solution similar to the one described in Section 5.2 and [10] can be used, in which the line-current is used to establish the connection change setpoints. In fact, the current is easier to acquire and process by an electronic device than the speed. For a simple delta/star decision, two main setpoints are needed for line-current based decision. For the proposed system, considering five different connections, eight main setpoints (signalled in Fig. 5.41 by horizontal dashed lines and numbers in rectangular boxes) are needed for line-current based decision, but a few more can be used for protection and adjustment purposes [15], [10]. A possible logic table for the line-current based connection change, considering only five connections, is presented in the Table 5.9 (SP denotes setpoint), which can be adapted for particular load profiles (e.g., some connection modes can be neglected), as previously referred.

A device for automatic connection change is proposed in Fig. 5.51, considering only one current sensor (a more sophisticated device is presented in Figs. 5.8, 5.11, and 5.12). The principles discussed in Section 5.2 for automatic and manual connection change apply here. A proper decision algorithm has to be implemented in the microcontroller, based on Table 5.9. The motor start-up can be optimized, using the different available connections, potentially leading to a strong reduction of the starting current, particularly when series connections are used. In fact, the optimal current points to make the transition of the stator winding connection during motor start-up (if the magnitude of the load justifies that transition) can be detected. After the motor start-up period (i.e., when the motor line current becomes stable), the device begins the automatic management cycle, as a function of the motor line current. The duration of each different operating period of the motor

should be long enough to avoid an excessive number of stator winding connection change, in order to avoid a significant decrease of the contactors and motor lifetime.

TABLE 5.9
BASIC LOGIC TABLE FOR PROPER CONNECTION MODE SELECTION.

IF	OR	THEN
$I_l \geq SP1 \ \& \ DP$	$I_l > SP2 \ \& \ YP$	DP (E-Zone)
$I_l < SP1 \ \& \ DP$	$I_l \leq SP2 \ \& \ YP$	YP (D-Zone)
$I_l \geq SP3 \ \& \ YP$	$I_l > SP4 \ \& \ DS1$	YP (D-Zone)
$I_l < SP3 \ \& \ YP$	$I_l \leq SP4 \ \& \ DS1$	DS1 (C-Zone)
$I_l \geq SP5 \ \& \ DS1$	$I_l > SP6 \ \& \ YD$	DS1 (C-Zone)
$I_l < SP5 \ \& \ DS1$	$I_l \leq SP6 \ \& \ YD$	YD (B-Zone)
$I_l \geq SP7 \ \& \ YD$	$I_l > SP8 \ \& \ YS1$	YD (B-Zone)
$I_l < SP7 \ \& \ YD$	$I_l \leq SP8 \ \& \ YS1$	YS1 (A-Zone)

In order to facilitate the change of the connection mode, a special multi-position rotary contactor is proposed, which can be seen in Fig. 5.50.

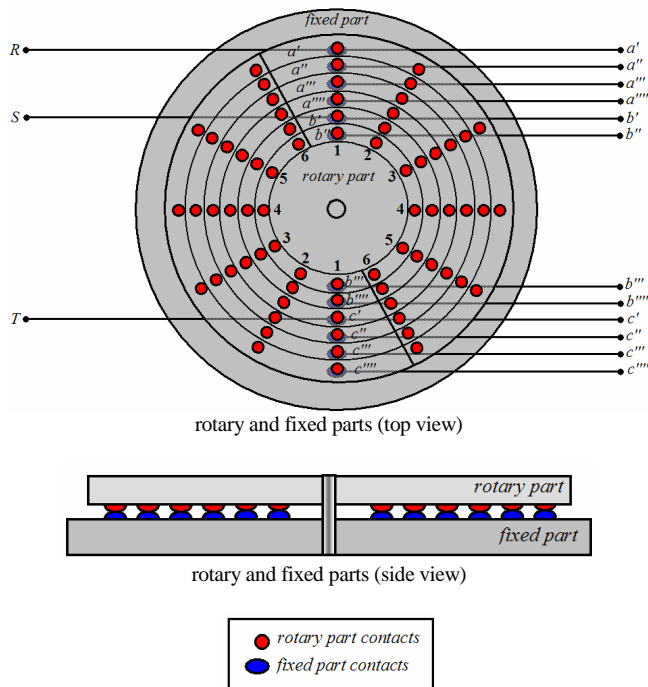


Fig. 5.50. Top and side view of the proposed 6-position rotary contactor.

For the single- and two-speed MFLIM a 6- and 12-position contactor is needed, respectively (to each position corresponds a connection mode). The movement of the rotary part to the correct positions can be either made manually or automatically driven by a motor system, which can be controlled by the microcontroller-based device presented in Fig. 5.51, which has several digital outputs for contactor control purposes, including a digital output generating a variable duty-cycle PWM (e.g., if a small stepper motor is used, its shaft position can be controlled by 4 digital outputs; if a servo-motor is used, its shaft position can be controlled via programmable duty-cycle

PWM output). The rotary part contact points can be properly connected to each other in the upper side. The connection change is, of course, made off-line, using a line contactor.

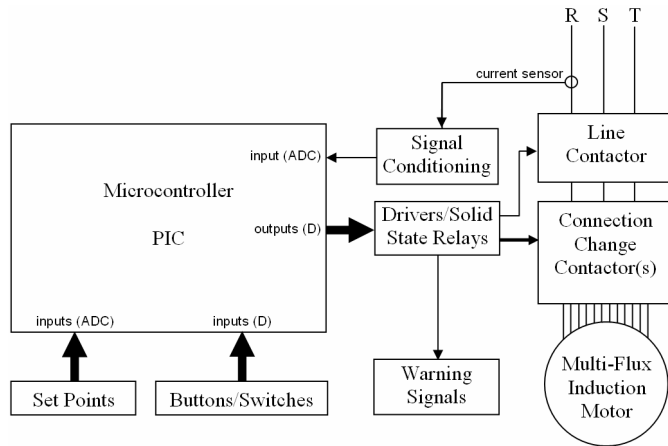


Fig. 5.51. Basic topology of a device for automatic connection mode change, using only one current sensor.

A device for winding connection change within 3 modes is proposed in [24]. A connection mode scheme for 4 modes is proposed in [23].

5.3.6 Technical and Economical Considerations

After the stator winding connection change from a low to a high flux connection mode, the motor line current increases significantly and the motor speed increases slightly (due to the reshape of the motor torque slip curve, as it can be seen in Fig. 5.52), and vice-versa. The slight increase or decrease of the motor speed after the stator winding connection change leads to an increase or decrease of the motor load, respectively, which is responsible for the hysteretic behaviour of the motor line current, power factor and speed, as a function of motor load. The slight decrease of the motor speed can lead to significant power reductions in constant, linear or quadratic torque loads.

The torque-speed curve shape change can be used as a simple discrete slip-based speed regulator (although in a limited range, and with reduced efficiency) to control for example airflow in fans, instead of using throttle control. If a two-speed motor is applicable, a better speed regulation can be provided.

Care must be taken to ensure that the motor speed reduction after the stator winding change is still appropriate to the driven load operation. However, the lower the motor load and the higher the motor power are, the lower the motor speed variation will be after stator winding connection change.

In order to avoid starting problems and increase the speed regulation range for the different connections, motors with low-slope quasi-linear part of the torque-speed curve (type IMs with high slip and high startig torque, e.g., NEMA Design C or D), should be used if slip-based speed regulation is to be done. This also applies to two-speed motors.

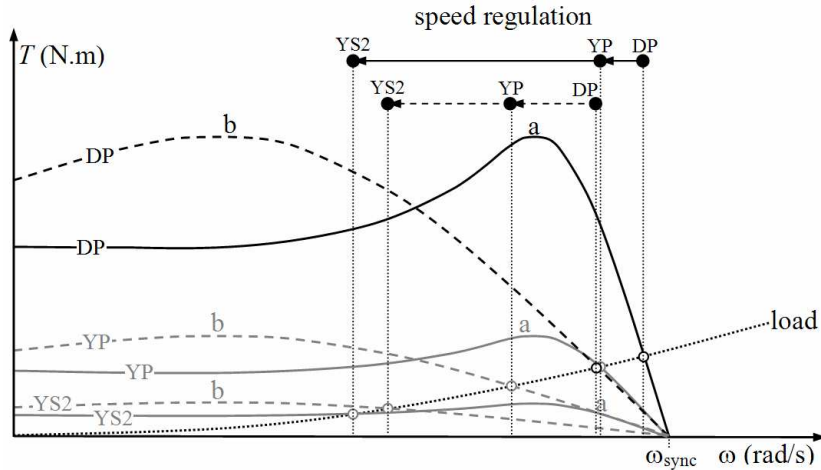


Fig. 5.52. Speed regulation for different torque-speed curve shapes and winding connection mode: curve “a” is for a low-resistance rotor and curve “b” is for a high-resistance rotor.

As it was experimentally shown, if the connection change is properly made, the overall losses are lower than those for the DP connection mode, leading to a lower motor operating temperature and longer motor lifetime, due essentially to the lower core losses. In the MFLIM_E, the no-load losses minus stator Joule losses decrease from 522 W (for the DP connection) to 85 W (for the YS1 connection). The stator winding and rotor current issues were analysed in Section 5.2. If the setpoints are properly adjusted, the motor slip after the connection change never exceeds the nominal motor slip.

If a low flux starting mode is adopted, the user should evaluate the increase of the starting time and the increase of the temperature that can result from such situation (due to the high slip), potentially leading to a decrease in the motor lifetime.

Besides the described energy benefits of the Y type connections when properly used, they also eliminate the circulating currents, which can exist in the D type connections. The circulating currents are responsible for additional winding losses.

From the perspective of motor reliability, a potential benefit of the low-flux winding connections is that they lead to the reduction of the inter-turn and inter-coil insulation voltage stress, and therefore to a longer motor lifetime. Moreover, since parallel partial windings are available, if a failure occurs in one partial winding, the motor can continue to operate if properly rearranged, until the most opportune moment to send it for repair, avoiding catastrophic failure, which can be cost expensive in some Industries.

As it was previously referred, a technical advantage of the use of an electronic device for automatic change is that it can provide optimal motor start-up, as well as motor overcurrent, overtemperature and excessive unbalance detection, which can be used for overload, locked rotor and excessive unbalance protection.

Additionally, another major advantage of automatic voltage regulation is to properly adapt the motor winding to the typical voltage fluctuation over the day (typically within $\pm 5\%$ [43]).

Since the connections between motor and contactors require 12-conductor cables in the case of single-speed MFLIM (instead of the typical 3-conductor cables), the device and the contactors should be mounted as near as possible to the motor.

An important conclusion of this study is that the single-speed MFLIM, for the low power operation modes, can have a performance similar to the high-efficiency motors because the core and Joule losses, as well as the operating temperature, are significantly lower. The only drawback, in the case of self-cooled motors, is the approximately constant fan cooling power, which is excessive for the low loads, contributing to the reduction of the peak efficiency, but in principle, for 4-pole motors with rated power equal or higher than 7.5 kW, it is still higher than the peak efficiency for the nominal connection.

From the perspective of multi-voltage stator winding, if, for example, a motor with the YP connection as nominal is operating at full load with actual line-to-line voltage between 76% and 93% of the nominal value, the most advantageous connection in terms of efficiency and power factor is the DS1.

The presented concept is particularly suitable for motors with significant load variation during their duty-cycle, including relatively long, low load periods and some near full-load periods, in which significant energy savings and motor power factor improvements in the low-load operating periods can be obtained, leading to the reduction of the motor operating costs. Except for constant power loads, after connection change to a lower flux connection, the motor input active power decreases mainly due to the motor efficiency increase, but also due to the slight decrease of the motor speed, which leads to a slight decrease of the required mechanical power. Examples of loads where the MFLIM can be applied with technical and economical benefits are industrial mixers, conveyors, escalators, lifts, fans, pumps, high-inertia saws and presses, cranes, etc., as previously mentioned for the Y/D connection change.

According to the opinion of some motor repairers/rewinders, the cost of a winding with two sets of turns per phase is equivalent to the cost of the conventional windings, but an additional cost with the 12-terminal block is inevitable. It should be noted that there are commercially available dual-voltage motors, with 12 or 9 terminal leads [17], [29]. The 12-terminal leads dual-voltage motors can be used to apply the previously presented concept, being this an advantage, since standardized motors can be used. Moreover, the price of such motors is in general similar to the single-voltage motors. For the automatic connection change, although the cost of a control device is in principle low, the cost of a special contactor or several conventional contactors can be significant.

For the economical analysis of the proposed system an example is considered. In order to simplify the estimation of the energy savings, the slight variation of the motor speed after stator winding connection change is not considered. In Fig. 5.53, a hypothetical daily motor load profile can be seen, which is considered in the following economical analysis. It is also considered that the described load operates 16 hours per day and 360 days per year. For the sake of simplicity, an average price of 0.07 €/kWh is considered. Considering that the connection modes of the 7.5-kW MFLIME are properly changed as a function of load (instead of using only the DP connection), the annual energy savings are 2.1 MWh/yr, as it can be seen in the Fig. 5.54, which also shows the efficiency variation. This can be translated into 149 €/yr. The energy savings, for this particular case, are 15%. If the duration of the low load periods increase, the savings can be even more. The energy savings potential increases with the increase of the motor power and of the electrical energy cost. The daily average power factor of the 7.5-kW MFLIM_E improves from 0.28 to 0.67, as it can be seen in Fig. 5.55. As a consequence, less power factor correction capacitance is needed, and lower electrical network losses are expected. Since the motor runs at a low temperature, extended lifetime is also expected.

Some examples of variable load applications where the application of MFLIM can be advantageous are presented in Figs. 5.56-5.61. Note that in relation to horizontal conveyors, elevating/inclined conveyors have higher steady-state torque (considering the same handled material mass) since the gravity component²⁴ of the material handled is present. Therefore, if the amount of material handled varies, the load torque also varies. Industrial mixers torque is mainly characterized by a viscous friction component, being roughly proportional to the speed. In this kind of load the flux regulation can lead to a significant improvement of the motor efficiency and power factor. In cranes and elevators, the connection change can be made as a function of the actual load, which is likely to vary significantly in such loads, and underloading is a common situation.

In the case of the two-speed MFLIM concept, significant savings can be achieved in some applications, when applicable, particularly in the centrifugal pumps and fans (when used to regulate the flux, combined with throttle control or instead). For example, in many pumping applications several pumps are used in parallel to produce the required flow. Operating all pumps at reduced speed rather than cycling the pumps ON/OFF according to the demand, significant energy savings can be obtained. Using two two-speed MFLIM to drive a low-static head, two-pump system, with independent piping circuits, providing in some periods 50% of the maximum flow, it is possible to operate both pumps at 50% of the rated flow, requiring approximately 25% of the power required for a single pump operating at 100% of the rated flow (Fig. 5.55). Simultaneously, the motor efficiency and power factor can be maximized with proper flux level

²⁴ Constant torque component in steady state.

regulation. Other advantages are that motors stay warm (no condensation in the windings) and the seals of the pumps stay wet and alive. Also it is possible to control the “water-hammer” effect, which degrades the pipes, by controlling acceleration and deceleration through optimised management of the motor speed and flux. The two-speed concept, also leads to loss reduction during start-up, although lower losses are achieved with the use of variable-speed drives.

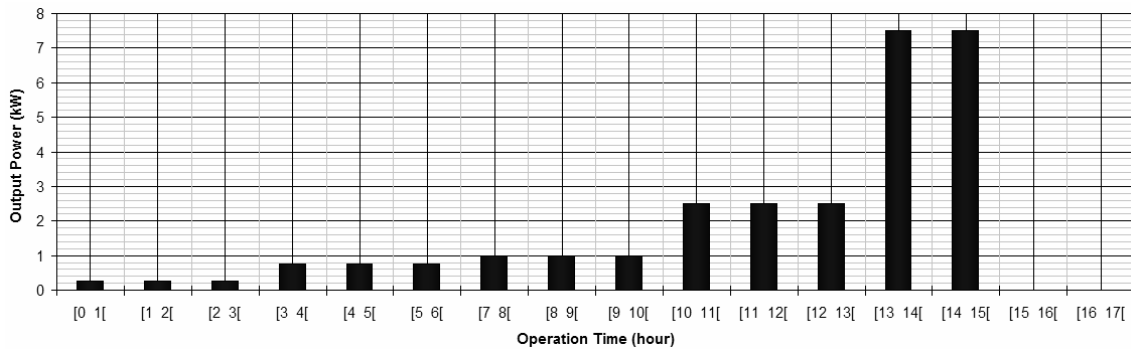


Fig. 5.53. Considered daily motor load diagram.

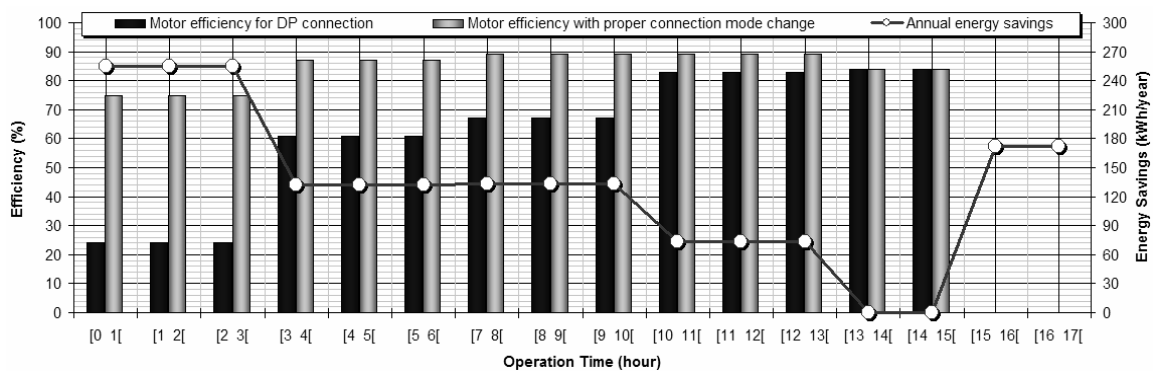


Fig. 5.54. Motor efficiency and energy savings (considering the MFLIM_E).

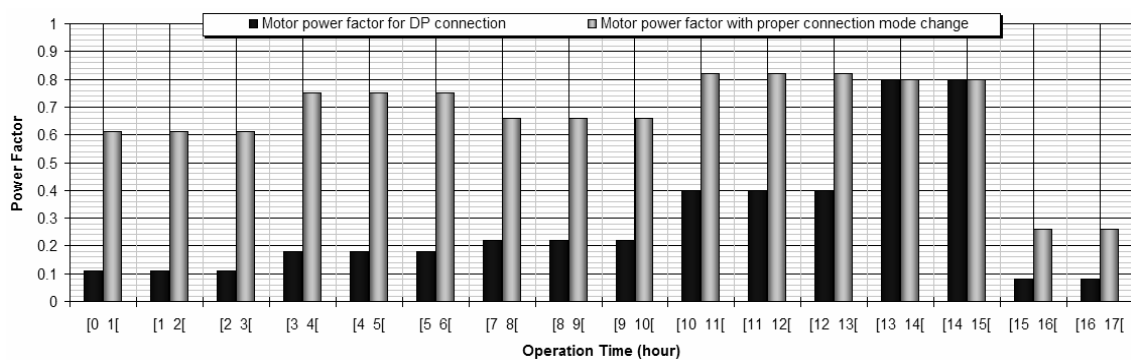


Fig. 5.55. Motor power factor (considering the MFLIM_E).

In horizontal conveyors (constant torque device), the required torque is approximately independent of the transported load and speed (it is only friction dependent). Typically, the materials handling output of a conveyor is controlled through the regulation of input quantity, and the torque and speed are roughly constant. But, if the materials input to the conveyor is increased, and the materials output is to be maintained, the speed can be reduced and significant energy

savings will be obtained, proportional to the speed reduction. Assuming that the materials output has to vary between 100% and 50% according to the process demand, instead of varying the materials input to the conveyor between 100% and 50%, and keeping the speed and the required power constant, the two-speed MFLIM can be used to change the speed between 100% and 50%, and, consequently, the required power will be 100% and 50%, respectively, leading to significant savings in the low demand operating periods. Simultaneously, the motor efficiency and power factor can be maximized by proper flux level regulation.

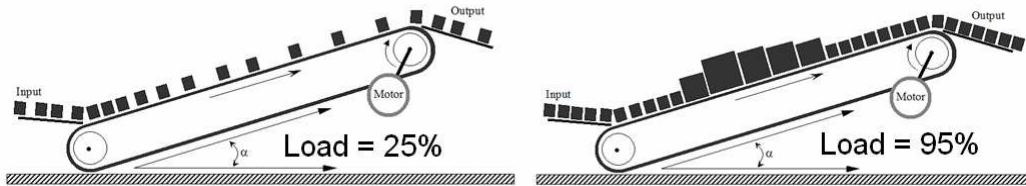


Fig. 5.56. Elevating conveyor operating with different load levels.

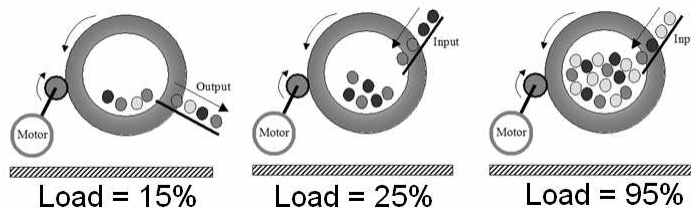


Fig. 5.57. Industrial mixer operating with different load levels.

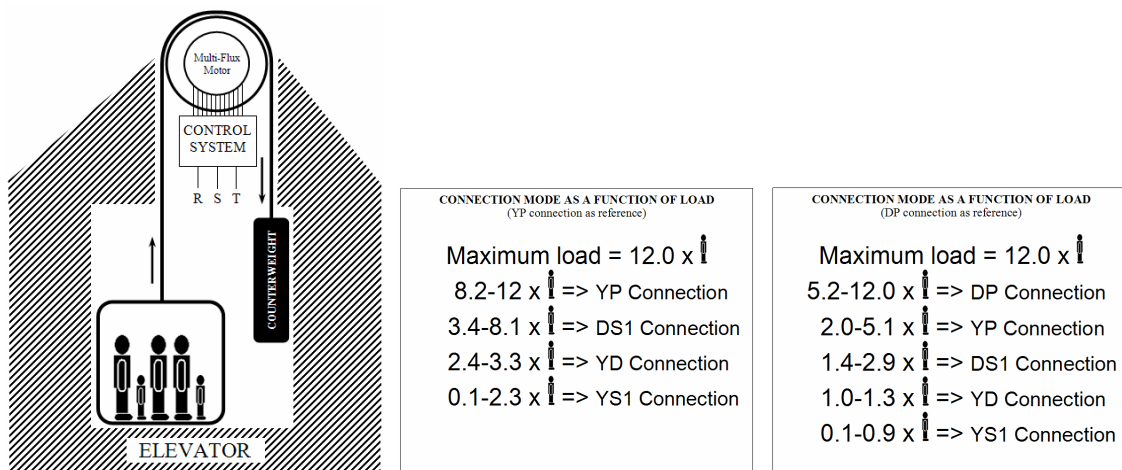


Fig. 5.58. Elevator or lift: MFLIM connection management as a function of load.

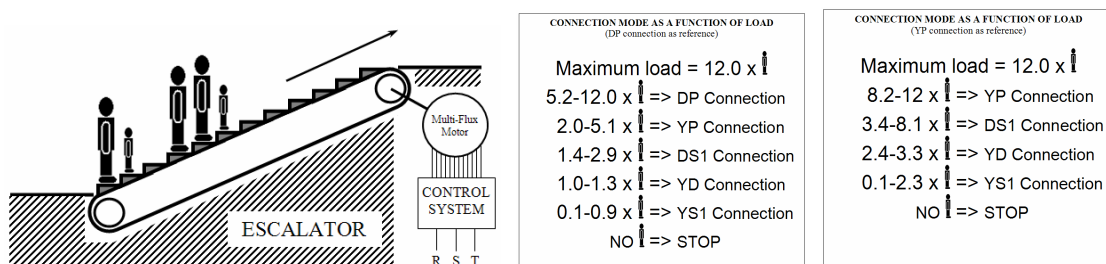


Fig. 5.59. Escalator: MFLIM connection management as a function of load.

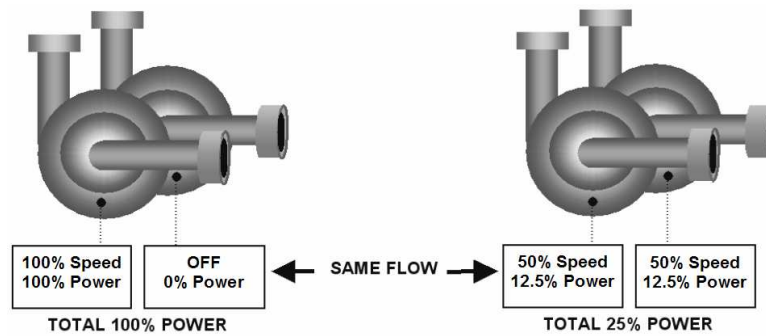


Fig. 5.60. Pumping system: useful relation to consider in independent closed-loop piping systems, where static head is not a major factor.

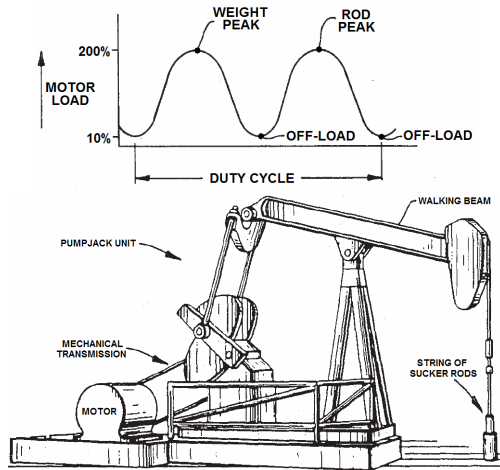


Fig. 5.61. Pumpjack unit: oil well pumping. The motor drives a gear box which in turn rocks the walking beam so that a string of sucker rods reciprocates a downhole pump (not shown) located downhole in a borehole [24].

In the production of hydrocarbon from wellbores, it is common to employ a pumpjack²⁵ unit for actuating a string of sucker rods which reciprocates a bottomhole pump. Each cycle of the pumpjack unit imposes varying loads on the pump and rodstring and accordingly, the load on the motor continually varies in a cyclic manner each reciprocation of the pumpjack, as shown in Fig. 5.61. One complete reciprocation of a rod string of a pumpjack unit, with a upstroke and a downstroke of the pumpjack unit. The motor load varies from 10-20% up to 180-200% of rated load. Each cycle of operation or stroke has a rod peak, a weight peak, and two off-peaks. The frequency of the cycle or stroke depends on the strokes per minute that the pump is reciprocating and is, generally, in the range of 4-10 s in duration. Most oilwell pumping motors driving pumpjack units are low-voltage IMs, ranging from 7.5 kW to one 90 kW. Here, the connection mode change can be applied but requires special study/design due to the high frequent of connection switchings or short downtime duty cycle.

Another advantage associated to the use of the low flux winding connections, when convenient, is the reduction of the inter-turn insulation voltage stress, which can lead to the increase of the

²⁵ A pump-jack, nodding donkey, pumping unit, or horse-head pump, is the over ground drive for a reciprocating piston or pump installed in a borehole. It is commonly powered by IMs, and it is used to mechanically lift liquid out of the well if there is not enough bottom pressure for the liquid to flow all the way to the surface. Depending on the size of the pump, it generally produces 5 to 40 litres of a crude oil-water mixture (called emulsion) at each stroke.

motor lifetime. Additionally, the automatic pole change and/or simultaneously with flux regulation, can also be used to reduce significantly the rotor losses during starting period.

Additional considerations on the application and benefits of the proposed strategies are presented in Appendix 6, including the combined use of VSD and connection change, energy recovery strategy in 2-speed in line-fed IMs during stopping or deceleration periods [44], etc. However, further discussion on the principles presented in Appendix 6 is necessary, being the objective to provide academic ideas that could be developed in the future.

5.4 Proposed Device versus Other Voltage Regulation Techniques

Regarding magnetizing flux or phase-voltage regulation (either statically or dynamically) in IMs, it has a large saving potential in most applications, either to maximize efficiency²⁶ and power factor in oversized and/or variable-load motors, as well as to regulate motor speed. Commercial and industrial applications that can benefit with this technique are HVAC, escalators, conveyors, mixers, grinders, fans, pumps, cranes, etc., as previously enumerated. It should be noted that improving efficiency and power factor reduces motors losses and overall installation losses (power network losses). The power factor compensation requirements are also reduced. It is estimated that the voltage regulation in oversized motors can lead to 20 to 50% line current reduction, up to 20% real power reduction (depending on load), 30% to 70% reduction on installation plus transformer losses, 15 to 60% of power factor improvement, 15 to 50% of apparent power reduction, and 15 to 50% of reactive power reduction. The power factor reduction also reduces the energy bill. The cost savings associated with reduction of the capacitors size for power factor correction are also an economical benefit [39]. A general comparison of different voltage regulation technologies for fixed-speed oversized or variable-load IMs is presented in Table 5.10. All of the technologies allow improved starting and energy savings.

Some case studies regarding the voltage regulation are reported in [39]. For example, in a commercial building HVAC system (400 V, 68 A), whose IMs were operating at 56% load, the voltage regulation led to a reduction of 14%, 15%, 28%, and 20% for real power, current and apparent power, network losses, and reactive power, respectively. In an industrial inclined crushed-rock conveyor, with a 15-kW IM with a variable load within 18% to 56% led to a reduction of 18%, 48%, 73%, and 58% for real power, current and apparent power, network losses, and reactive power, respectively. The power factor was improved 0.25 points, and starting current was limited to 1.76 times the rated current. Since the conveyor was operating 6000 h/yr, savings of 5340 kWh/yr (or 534 €/yr, for 10 c€/kWh) were obtained. A network loss reduction of 1676 kWh/yr (or 168 €/yr, for 10 c€/kWh) was achieved. The paybacktime was of 2.2 yr. There were also additional savings related to the power factor improvement, increased reliability and reduced

²⁶ Reduced losses (core and copper losses) and operating temperature.

maintenance costs. In an air-treatment fan system, driven by 45-kW IMs, with an average loading of 49%, a reduction of 15%, 40%, 64%, and 58% for real power, current and apparent power, network losses, and reactive power, respectively. The power factor was improved by 0.23, and starting current was limited to 1.8-2.2 times the rated current. In an escalator, driven by a 11-kW IM, with a load varying between 27% (no passengers) and 100%, a reduction of 18%, 58%, 83%, and 65% for real power, current and apparent power, network losses, and reactive power, respectively. The power factor was improved by 0.31.

The automatic connection change device (Smart-Switch) proposed in previous sections, can compete directly with the commercial solid-state voltage regulators based on AC full-wave phase-control devices, incorporating back-to-back connected thyristors [11], [14]. Although these devices allow to regulate continuously the voltage RMS value by increasing the firing phase angle, they distort voltage and current significantly for lower voltage levels [9]. At full voltage they typically have a by-pass, thus not distorting the input and output voltages and currents. Therefore, for full load voltage, i.e., D-connection rated voltage, they are equivalent to the proposed solution. However, at low voltages, due to the inherent voltage and current distortion, relatively low power factor (due to distortion), and significant internal conduction losses, as well as the additional harmonic losses in the motor [9], they are not recommended for continuous operation [9], being only used for starting purposes (in this particular case they are called soft-starters). However, such devices are also commercialised for speed regulation purposes (in this case called voltage regulators) or voltage regulation for motor efficiency improvement (in this case called energy savers), operating continuously, with the referred associated disadvantages.

On the basis of the foregoing discussion, and considering that a load vary within at least two load levels (S3 or S4 duty type²⁷), one of which up to 40% of full load and a relatively long duration, the proposed device, acting on the motor contactors, can perform an optimized Y/D²⁸ start (although worse than that performed by the soft-starter), and regulate the voltage (within two levels) as a function of motor load, acting as an energy saver but without voltage and current distortion and high motor efficiency and power factor levels.

Despite all the advantages of the proposed device, the contactor cycling impact on its lifetime and on the motor lifetime should also be taken into account, although difficult to estimate, but if proper measures are implemented (e.g., snubber circuits), that impact can become negligible. It should be also referred the technology Motor Energy Savers (MEC) [39], which is based in a special autotransforming scheme (see description in Appendix 6), allowing to regulate dynamically the voltage at the motor terminals within 2 discrete values (100% and 75% rated voltage), as a

²⁷ The duty types are indicated by the symbols S1 ... S9 according to IEC 60034-1 and VDE 0530 Part 1. The outputs given in the catalogues are based on continuous running duty, S1, with rated output [13].

²⁸ In the case of multi-connection motors, more connections can be used during starting.

function of the actual motor load. However, such devices are bulky and relatively expensive in relation to the proposed device for automatic connection change management.

TABLE 5.10
GENERAL COMPARISON BETWEEN DIFFERENT VOLTAGE REGULATION TECHNIQUES FOR FIXED-SPEED VARIABLE-LOAD IMs [39], [40].

Feature	Technology							
	Direct On-line (D.O.L.)	Auto-Transformers	Automatic Y/D Change in Conventional Motors (Smart-Switch)	Automatic YY/D Change in Dual-Voltage Motors (Smart-Switch)	Automatic Multi-Connection Change in Dual-Voltage Motors (Smart-Switch)	Motor Energy Controller (MEC), see Appendix 6	Soft-Starters and/or Phase Controllers (VR)	VSDs
I_{start}/I_N	4-8	1.7-4	1.3-2.7	1.5-2.7	1.0-2.7	1.5-2	3-5	1.5-2
Harmonic Distortion	Pure Sinusoidal	Pure Sinusoidal	Pure Sinusoidal	Pure Sinusoidal	Pure Sinusoidal	Pure Sinusoidal	Generates Harmonics	Generates Harmonics
Power Factor	--	Improvement	Improvement	Improvement	Improvement	Improvement	Worsening	Improvement
Device Losses	None	4-6%	< 0.1%	< 0.1%	< 0.1%	< 0.5%	< 0.5%	4-6%
Relative Size	--	700%	25-50%	25-50%	60-70%	100%	50%	100%
Motor Additional Losses	--	No	No	No	No	No	Yes	Yes
High-Frequency Motor Bearing Currents	--	No	No	No	No	No	No	Yes
Voltage Transients at Motor Terminals	--	No	Negligible	Low/Medium	Low/Medium	Low/Medium	Low	High
Motor Operating Temperature	--	Decreases	Decreases	Decreases	Decreases	Decreases	Increases	Increases
Motor Lifetime	--	Extended	No significant influence	No significant influence	No significant influence	No significant influence	Shortened	Shortened
Radiated EMI	--	No	No	No	No	No	Yes (Low)	Yes (High)
Extra Motor Torque Pulsation	--	No	No	No	No	No	Significant	Low (with proper control)
Rotor Losses During Starting	High	Medium	Medium	Medium/High	Medium	Medium/High	Medium	Low
Recommended Motor Load Variation Range	75-100%	0-100%	20-100%	65-100%	10-100%	50-100%	0-100%	0-100%
Price	--	High	Low	Low	Low/Medium	High	Medium/High	High

It can also be used to regulate the speed in a fan within two levels, acting as a voltage regulator, but without the disadvantages referred above, and with high efficiency and power factor levels. It should be noted that the power factor improvement also leads to the decrease of the cable losses, thus reducing its temperature and extending their lifetime. Additionally, it leads to the reduction of the voltage drop in motor cables, installation, and transformers, improving the voltage at other motors terminals and at other voltage-sensible equipment.

5.5 Conclusions

Grossly oversized line-fed IMs operate with lower efficiency and power factor, which is by far the most important cause of poor power factor in industrial installations. The replacement of an oversized standard efficiency motor, by a properly sized high-efficiency motor is, in most cases, the most economical advantageous option, but requires additional investment. In some situations, motor performance can be improved both in terms of efficiency and power factor through stator winding connection change from delta to star (assuming that delta is the rated connection). However, for variable-load, line-fed IMs, one fixed connection is not an acceptable solution, and if the duty-cycle of such motors includes near full-load operating periods, a smaller motor cannot be used.

A novel multi-connection motor was introduced, which can be valuable in Industry due to its flexibility, particularly for variable-load applications in which significant energy savings can be obtained, and can also be used as new or rewound general-purpose spare motor, since, in practice, it has up to six different levels of voltage (for fixed flux and power) or of magnetizing flux (for fixed voltage, variable power). In the latter case, the magnetizing flux regulation as a function of the actual motor load can lead to significant energy savings and power factor improvements. In fact, it can operate as a high-efficiency motor for the lower power levels (the efficiency is equivalent to that of a high-efficiency motor with a rated power equivalent to the output power at the lower load levels). If necessary, at rated frequency, for the nominal power, it can be used as a multi-voltage motor, and be fed with different line-to-line voltage levels without efficiency and power factor decrease. Theoretical considerations for EEC-based simulations of multi-connection motors were also presented. Proper selection of the nominal (or reference) connection mode can improve the motor suitability for particular load profiles.

The basic principles for proper stator winding connection-mode selection in both conventional two-connection and special multi-connection motors were provided, including an in-field technique/method, based on simple measurements, which can be used to select the most appropriate operating mode.

For variable-load, line-fed motors, with long, low-load operating periods and some near full-load operating periods during their duty-cycle, an automatic stator-winding management device can be implemented in both conventional two-connection and special multi-connection motors, but it is particularly indicated for conventional motors already started by star-delta method. A prototype of such device was developed and tested successfully, being the inherent investment estimated to be moderate.

Regarding the connection change transient analysis resulting from the mains/line power interruption and power reconnection switching instants, it was shown that, even for low inertia systems, if the commutation duration period is shorter than 0.1 s, the deceleration is not significant. However, during power reconnection, significant short-duration current peaks can occur, being the duration dependent upon the actual motor speed after deceleration and the peak value dependent upon the displacement between the mains voltages and the motor terminals voltage. Very high-magnitude short-duration voltage peaks occur in the power disconnection instants. These voltage transients can originate partial discharges near the motor terminals. If the star-delta automatic management system is to be applied, it can be advantageous to reinforce slightly the inertia of the system to reduce the deceleration level during the connection change (but starting period is inherently extended). Simulation results considering an improved thyristor-based power interruption, using an AC full-wave phase controller, being the power interruption inherently improved for a firing angle equal to zero degrees. With this approach it is possible to reduce significantly the disconnection voltage transients. It can be concluded that using a thyristor based power control device, current and voltage transients can be significantly reduced. Snubber circuits can be properly designed to minimize those transients. After state change, such device can be bypassed by means of a contactor. If the application justifies, the reconnection can be made using individual control of the firing signals for the instant of minimum voltage across the thyristors, in order to reduce significantly the voltage transients magnitude. Moreover, as it is discussed in Appendix 4, the motor deceleration is quite lower for linear or quadratic torque loads, but can be significant for constant torque loads, considering fixed inertia. Therefore, in some cases, moderate to high system inertia applications are more suitable for stator winding connection changes.

If the user applies the proposed methods/strategies to IMs meeting the criteria described, the active and reactive electrical energy bill can significantly be reduced, since they can lead to the improvement of the efficiency and power factor of permanently oversized motors, motors with a load variation between low-load and near full-load during their duty-cycle, and/or motors driving medium/high-inertia, low-duty-cycle loads. The proposed methods are particularly suitable for industrial plants, where, typically many electric motor systems are oversized and/or can have a wide load variation. In general, the presented work can contribute significantly to the loss

reduction in EMODS. Additionally, if the motor average efficiency increases, the motor overall losses decrease and, therefore, the motor lifetime is extended. However, for large motors, the author recommends the users to first consult the motor manufacturer before changing the motor stator-winding connection.

Airflow regulation in ventilation/fan systems, for example, is possible by changing the flux level, which is another potential application of the described concepts, but more effective regulation is achieved if the two-speed, multi-flux motor concept is used.

When compared to the savings potential in suitable loads, the additional cost of the proposed solutions is modest (if a faulty motor is properly rewound for that purpose), even considering the cost of the equipment for the automatic connection change (electronic control device and contactors).

Further research is being carried out on other types of multi-connection stator windings [41], being the preliminary results presented in Appendix 6. Moreover, the concept addressed in [41], can be combined with the presented multi-flux concept to introduce more magnetizing flux levels between 57.7% and 100%.

In some cases, the proposed solutions can compete directly with continuous voltage regulation commercial electronic devices, and for some special cases, with variable-speed drives. It should be noted that, contrarily to the referred technologies, the proposed low-consumption, low-cost electronic device for automatic connection change is distortion-free and EMI/RFI-free (sinusoidal operation) and, besides the energy savings and power factor improvement, it also extends motor lifetime due to the reduced motor temperature at low load, and to the avoidance of high frequency voltage transients and bearing currents, which is a critical issue in VSD-fed IMs. All the referred factors can contribute to the reduction of the motor LCC.

5.6 References

- [1] de Almeida, A., *et al.*: “*Improving the Penetration of Energy-Efficient Motors and Drives*”, European Commission, DG TREN, SAVE II Programme, 2000.
- [2] de Almeida, A., *et al.*: “*VSDs for Electric Motor Systems*”, European Commission, DG TREN, SAVE II Programme, 2001.
- [3] Guru, B.; Hiziroğlu, H.: “*Electric Machinery and Transformers*”, 3rd Edition, Oxford University Press, New York, 2000.
- [4] Chapman, S.: “*Electric Machinery Fundamentals*”, 4th Edition, McGraw-Hill, New York, 2004.
- [5] Alger, P.: “*Induction Machines – Their Behavior and Uses*”, Gordon and Breach Publishers, 3rd Edition, New York, 1995.
- [6] Fitzgerald, A.; Kingsley, C.; Umans, S.: “*Electric Machinery*”, 6th Edition, McGraw-Hill Higher Education, New York, 2003.
- [7] Beaty, H.; J. Kirtley: “*Electric Motor Handbook*”, McGraw-Hill, New York, 1998.
- [8] F. Ferreira, *et al.*: “*Automatic Change of the Stator-Winding Connection of Variable-Load Three-Phase Induction Motors to Improve the Efficiency and Power Factor*”, IEEE Inter. Conf. on Industrial Technology (ICIT’05), Conf. Proc., Hong Kong, 14-17 December 2005.
- [9] Köfler, H.: “*Can Solid State Voltage Regulation Devices Save Energy in Induction Machines? An Experimental Proof with Some Theoretical Explanations*”, XVI Inter. Conf. on Electrical Machines (ICEM’04), Conf. Proc., 2004.
- [10] Ferreira, F.; de Almeida, A.: “*Method for In-Field Evaluation of the Stator Winding Connection of Three-Phase Induction Motors to Maximize Efficiency and Power Factor*”, IEEE Trans. on Energy Conversion, Vol. 21, No. 2, pp. 370-379, June 2006.
- [11] Bose, B.: “*Power Electronics and Motor Drives – Advances and Trends*”, Academic Press, Elsevier, 2006.
- [12] Ferreira, F., *et al.*: “*Avaliação do Rendimento e do Factor de Potência dos Motores de Indução Trifásicos em Função da Carga e da Ligação dos Enrolamentos*”, Conf. Científica e Tecnológica em Eng., Inst. Superior de Eng. de Lisboa, 2002.
- [13] “*Basic Motor Technology*”, Catalogue BA/Basic GB95-06, ABB Motors.

- [14] Mohan, N.; Undeland, T.; Robbins, W.: “*Power Electronics - Converters, Applications, and Design*”, 2nd Edition, John Wiley & Sons, Inc., New York, 1995.
- [15] Ferreira, F.; de Almeida, A.: “*Three-Phase Induction Motor Stator Winding Connection Type Field Evaluation Method for Efficiency Maximization*”, 4th Inter. Conf. on Energy Efficiency in Motor Driven Systems (EEMODS’05), Conf. Proc., Heidelberg, Germany, September 2005.
- [16] Ferreira, F.; de Almeida, A.: “*Novel Multiflux Level, Three-Phase, Squirrel-Cage Induction Motor for Efficiency and Power Factor Maximization*”, Inter. Conf. on Industrial Technology (ICIT’06), Conf. Proc., Mumbai, India, Dec. 2006.
- [17] Ferreira, F.; de Almeida, A.: “*Novel Multiflux Level, Three-Phase, Squirrel-Cage Induction Motor for Efficiency and Power Factor Maximization*”, IEEE Trans. on Energy Conversion, Vol. 23, No. 1, pp. 101-109, March 2008.
- [18] “*Information Guide for General Purpose Industrial AC Small Medium Squirrel-Cage Induction Motor Standards*”, National Electrical Manufacturers Assoc. (NEMA), Standards Publication, USA, 2002.
- [19] Boglietti, A.; Ferraris, P.; Lazzari, M.; Profumo, F.: “*Effects of Different Modulation Index on the Iron Losses in Soft Magnetic Materials Supplied by PWM Inverter*”, IEEE Trans. on Magnetics, Vol. 29, No. 6, pp. 3234-3236, Nov. 1993.
- [20] Boglietti, A.; Cavagnino, A.; Lazzari, M.: “*Predicting Iron Losses in Soft Magnetic Materials with Arbitrary Voltage Supply: An Engineering Approach*”, IEEE Trans. on Magnetics, Vol. 39, No. 2, pp. 981-989, March 2003.
- [21] Korthals-Altes, W.: “*Motor-Winding*”, US Patent No. 1267232, 1918.
- [22] Silva, F.; Saraiva, E.; Abreu, A.: “*Economias de Energia em Motores de Indução – I’*, Lisboa, Endiel 83, 1983.
- [23] Satake, S., *at al.*: “*Driving Means Formed by Induction Motor and Method for Starting the Same*”, US Patent No. 6154003, 2000.
- [24] Taylor, N.; Taylor, P.: “*Automatic Load Seeking Control for a Motor*”, US Patent No. 4691155, 1987.
- [25] Fogarty, J.: “*Combined Delta-Wye Armature Winding for Synchronous Generators and Method*”, US Patent No. 6704993 B2, 2005.
- [26] Doppelbauer, M., *Expert Opinion*, SEW-Eurodrive, 2007.
- [27] Swardt, H.: “*Star-Delta Starting*”, Vector, Oct. 2003, pp. 25.
- [28] Swardt, H.: “*Dual Voltage Motors*”, Vector, Nov./Dec. 2003, pp. 28.
- [29] Spescam Measuregraph: “*Three-Phase Motors*”, Vector, Drives & Switchgear, Oct. 2003, pp. 21.
- [30] Liwshitz, M.: “*Calcul des machines electriques*”, Tome I, Spe Lausane-Dunod, Paris, 1967.
- [31] Weh, H.: “*Ueber die Berechnung magnetischer Spannungen in hochgesattigten Jochen von Drehstrmmaschinen*”, AfE, H2, pp.77-95, 1957.
- [32] Weh, H.: “*Analitische Behandlung des magnetischen Kreises von Asynchronmaschinen*”, AfE, H1, 1961, pp.27-40.
- [33] Cistelean, M.; Onica, P.: “*New improvements in the computation of the polyphase induction motor magnetic circuit*”, Proc. IEE, No. 123, pp. 335-341, 1976.
- [34] Cistelean, M., *Technical Notes*, unpublished.
- [35] Rajaraman, K.: “*Theory and design of part winding starting*”, IEEE Trans. on Energy Conversion, Vol. 14, No.1, pp. 31-36, March 1999.
- [36] Jian, T.; Schmitz, N.; Novotny, D.: “*Characteristic Induction Motor Slip Values for Variable Voltage Part Load Performance Optimization*”, IEEE Trans. on Power Apparatus and Systems, Vol. PAS-102, No. 1, pp. 38-46, Jan. 1983.
- [37] Ong, C.: “*Dynamic Simulation of Electric Machinery Using MATLAB/SIMULINK*”, Prentice Hall PTR, New Jersey, 2006.
- [38] Belmans, R.; Deprez, W.; Bastiaensen, C.; Dexters, A.: “*Induction Machine Efficiency in Motor and Generator Mode*”, 5th Inter. Conf. on Energy Efficiency in Motor Driven Systems (EEMODS’07), Conf. Proc., Beijing, 2007.
- [39] “*Motor Energy Controller*”, Power Electronics Systems Ltd., www.pe-sys.com, 2007.
- [40] Kostić, M.; Janda, Ž.; Radaković, J.; Miskolci, L.: “*Induction Motors with YY/ Δ Connection Change for Efficiency and Power Factor Increasing at Loads up to 75-85%*”, XVI Inter. Conf. on Electrical Machines (ICEM’04), Conf. Proc., 2004.
- [41] Cistelean, M.; Ferreira, F.; Cosan, B.: “*Generalized MMF Space Harmonics and Performance Analysis of Combined Multiple-Step, Star-Delta, Three-Phase Windings Applied on Induction Motors*”, 18th Inter. Conf. on Electrical Machines (ICEM’08), Vilamoura, Portugal, Sept. 2008.
- [42] Mastorocostas, C.; Kioskeridis, I.; Margaris, N.: “*Thermal and Slip Effects on Rotor Time Constant in Vector Controlled Induction Motor Drives*”, IEEE Trans. on Power Electronics, Vol. 21, Issue 2, March 2006, pp. 495-504.
- [43] EDP Corporation, Web QReport, 2008.
- [44] Ferreira, F.; Cistelean, M.; Baoming, G.: “*Simple Strategy to Recovery Energy During Stopping Period in Large High-Inertia Line-Fed Induction Motor Driven Systems*”, 18th Inter. Conf. on Electrical Machines (ICEM’08), Vilamoura, Portugal, Sept. 2008.
- [45] Ionel, D.; Cistelean, M.; Miller, T.; McGlipe, M.: “*A New Analytical Method for the Computation of Air-Gap Reactances in 3-Phase Induction Motors*”, 31th Industry Applications Conference, Conf. Proc., Vol. 1, pp. 65-72, 12-15 Oct. 1998.
- [46] Chen, Y.; Chen, Z.: “*Investigation of a New AC Electrical Machine Winding*”, IEE Proc. – Electr. Power Appl., U.K., Vol. 145, No. 2, pp. 125-132, March 1998.
- [47] IEC 60034-28 Standard, Ed.1, 2005: “*Electrical rotating machines – Part 28: Test methods for determining quantities of equivalent circuit diagrams for three-phase cage induction motors*”.
- [48] Ferreira, F.; Cistelean, M.: “*Simulating Multi-Connection, Three-Phase, Squirrel-Cage, Induction Motors by means of Changing Per-Phase Equivalent Circuit Parameters*”, 18th Inter. Conf. on Electrical Machines (ICEM’08), Vilamoura, Portugal, Sept. 2008.

6. Main Conclusions and Recommendations for Future Work

6.1 Main Conclusions

A number of strategies, methods and technologies to improve efficiency and reliability of EMODS were proposed or identified and their technical and economical advantages/disadvantages evidenced. In particular, the following main original contributions and conclusions can be found in this thesis:

- Use-phase cost of most electric industrial motors, namely the consumed energy, dominates by far their overall life-cycle cost and, if high-efficiency-class motors replace standard-efficiency-class motors, significant reductions in the environmental impact would happen. The adoption of MEPS for IMs is not likely to cause a market shift towards another cheaper and/or less efficient technology since those technologies do not offer the same overall performance advantages as IMs. In fact, MEPS seem essential to remove from the market inefficient motors and to promote energy-efficient models, which are very cost-effective on a life-cycle basis. The replacement of old inefficient motors when they fail, by efficient motors with proper sizing, can lead to further savings [4], [7], [8].
- The adoption of IE2 efficiency level, in the short term, does not seem to pose particular problems to the EU industry since most EU manufacturers are already producing this type of motors for the whole power range considered. The adoption of IE3 efficiency levels in the medium term can pose problems to the EU industry [4], [7], [8].
- If IE3/IE2-class high-efficiency motors, replace IE1-class or sub-standard motors, significant reductions in the environmental impact will be achieved under most operating circumstances. LCC reductions associated with IE2 to IE3 upgrade are not significant when correlated with the cost increase, particularly for high-power motors [4], [7], [8].
- The replacement of standard by high-efficiency IMs is clearly recommended, leading to significant energy, financial and environmental benefits, but a careful system analysis, including protection and command devices, system steady-state speed and motor start-up period, is required. In general, motor repair services are still not controlled by the motor users and, due to the poor-quality services typically offered by most of the repair shops, the post-repair motor efficiency can drop significantly. A high-quality repair is required to maintain the motor efficiency levels close to the original, particularly in the case of high-efficiency motors. To maintain the benefits of the high-efficiency motors over their entire lifetime, users should be able to pay more for a high-quality repair service in order to protect the respective investment [1], [2], [5], [16], [23].

- The motor efficiency measurement on the basis of the direct input-output method is the most appropriate way to quantify accurately the motor efficiency for its classification as a function of that value. Indirect loss-based method should be clearly avoided. It is possible to implement automatically the direct-method-based motor efficiency testing standards, using systems similar to the one proposed, reducing application time, cost and error [19], [25].
- The savings potential associated with motor speed adjustment is significant and the cost-effectiveness of VSDs for a large number of applications is very attractive. Due to the technical and economical benefits associated with VSDs in a large number of applications, when applicable, they are a recommended technology, even considering the negative impact on the grid (e.g., production of harmonics), on the surrounding environment (e.g., extra acoustic noise and EMI), and on the motor losses and reliability (e.g., additional losses, production of voltage transients at the motor terminals, and generation of bearing currents), since most of such negative effects can be mitigated by means of proper passive or active measures. Ride-through capability is also an important aspect to be taken into account in VSDs, particularly when downtime costs are high. This aspect can be significantly improved by directly adding extra capacitance to the DC bus of the VSD. The implementation of magnetizing flux (or voltage) and slip optimization strategies (e.g., using searching algorithms instead of predefined voltage-frequency curves) during steady-state operation is a very important aspect in VSDs, since it allows improving significantly the motor efficiency. VSDs integrating 3-level inverters can only be justified (or are only cost-effective) from the reliability perspective in particular/critical applications, where the reliability of the system is of extreme importance, since, in general, energy benefits are not expected [3], [6], [9], [15], [22], [29].
- Proper line- and VSD-fed motor sizing is clearly an important aspect in the scope of the motor performance improvement and, using adequate methodologies, it can be a relatively easy task to do. The simplest, low-cost methods for in-field motor load estimation were analysed/evaluated, and a number of improvements proposed, including combined methods. With the proposed improvements, a significant reduction in the load estimation error can be obtained, particularly for low loads. A novel evaluation methodology based on a “useful accuracy” was introduced [30].
- The proposed stator winding connection mode management strategy, either manual or automatic, can have a significant energy saving potential for variable-load or strongly oversized motors. It can be used either in conventional motors or in the proposed multi-connection motor. The proposed electronic device, Smart-Switch/Relay, is potentially cost-

effective in a number of applications, and can provide a number of other useful capabilities, such as motor commissioning and protection. Optimized starting and slip- and/or pole-change-based speed adjustment is another potential benefit associated with the proposed automatic connection change technique. The multi-flux/multi-connection motor concept seems to be an excellent solution for variable-load motors, if automatic connection change is provided, and for spare motors, since they can operate with high efficiency and power factor levels at different voltage and/or loads. Still in the scope of the stator connection change, the proposed pole-changing-based energy recovery strategy for line-fed motors is also quite promising [11], [12], [17], [18], [20], [28], [27].

- Power quality is a critical issue in EMODS, since it can have a significant influence on their efficiency and reliability, being the most critical factors the voltage magnitude deviation and unbalance. In the opinion of the author, the power derating curves for voltage unbalance and distortion presented in the standards should be revised [10].
- Mechanical transmission is an important part of the motor systems, and should be properly chosen and optimized for each particular application. Moreover, it can be used to allow the user to decrease the number of motor poles, potentially resulting in some efficiency gains.
- The proposed optimized stator winding (re)design to adjust motor voltage to the actual motor terminal voltage and load (or load profile) can be an excellent strategy for most industrial plants. In fact, in a large number of cases, it is possible to convert a low-efficiency motor in a high-efficiency motor of lower rated power (downsizing) during rewinding service (if the stator core has no major damages), leading to a high-efficiency low-cost motor, not requiring any mechanical adaptation. Large-scale motor downsizing schemes can be an alternative low-cost solution to the investment in high-efficiency motors, and can lead to the increase of the EMODS efficiency, and to the extension of the motors life-cycle, which has ecological benefits. For that purpose, the user-friendly stator winding design software developed by the author can be used [5], [13], [21].

The original contributions of this thesis are extensive, and a major part of them were published in international conferences and/or journals. Some subjects were even published in Portuguese technical magazines, due to its importance and direct application in Industry. In the opinion of the author, a large part of the information contained in this thesis has a significant value for the industrial and tertiary sectors, as a package of strategies, methods/techniques, technologies, tools, and guidelines to improve the efficiency and reliability of EDMOS.

6.2 Recommendations for Future Work

The proposed and discussed ideas are valid for the present technological scenario. As new motor technologies are emerging, new targets have to be defined. For example, it is expected that line-start and/or electronically controlled/commutated permanent magnet synchronous motors penetration starts to increase in the next decades, being necessary to analyse their performance and cost-effectiveness from the systems perspective.

Part of the research results and conclusions presented should be intended as a starting point on the respective subjects, requiring further investigation, improvement and/or experimental validation. In particular, the following issues can be pointed out for future researching and/or validation work:

- Multi-flux/multi-connection motor concept – More magnetizing flux regulation techniques by means of stator connection change in multi-connection motors should be investigated and experimentally tested [26].
- Stator winding connection mode management – The manual/permanent connection change should be tested in the field in a large number of motors within a wide power range. The automatic connection change, by means of the proposed electronic device, should be also tested extensively in a large number of motors. Further experimental analysis is required on the voltage transients during the power connection/disconnection instants and on the techniques to mitigate their effects. An assessment of the contactors and motor lifetime in such operating conditions is also required. The proposed rotary contactor can be constructed and implemented. Full solid-state-based circuits can be studied as an alternative, high-reliability solution to conventional electromechanical contactors. Optimized starting and slip- and/or pole-change-based speed adjustment also require further investigation. The closed-loop connection management using an external sensor (temperature, weight, force, etc.) can also be exploited in some particular applications.
- Smart-Switch/Relay – New advanced features can be incorporated in the proposed electronic device, originally developed for automatic stator winding connection change, such as improved motor protection schemes, motor diagnosis algorithms, and motor starting/stopping and speed adjustment schemes. The proposed prototype can also be improved in terms of size, consumption, and cost.
- Motor equivalent circuit-matrix simulation models with thermal, saturation and skin effects compensation – Simple and systematic electric and thermal parameters determination methods can be defined and experimentally validated [14].
- Assessment of the power quality impact on IMs and the related power derating curves – The experimental validation of the simulations-based conclusions is required. It is recommended further investigation on the motor power derating curves definition and

presentation, taking into account all the points referred, such as the combined effects and motor characteristics. A careful revision of the voltage unbalance and distortion quantification for derating purposes is also recommended, as topic for future research.

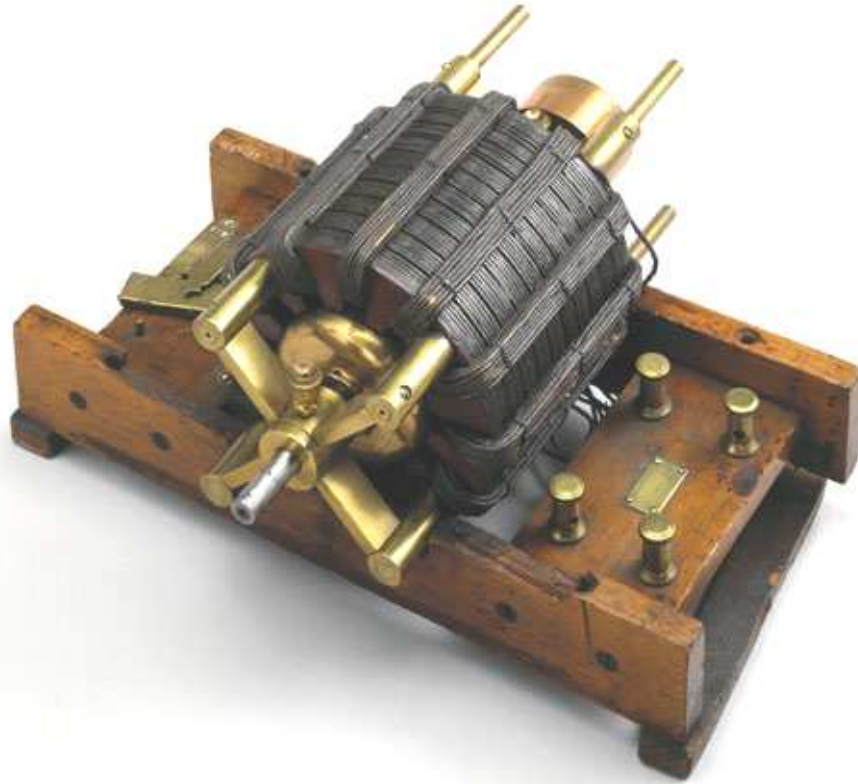
- Optimum voltage level searching method for VSDs – The proposed algorithm should be experimentally tested.
- Motor load estimation methods – The simplest methods were well analysed, but the improved and combined methods require further research, particularly concerning feasibility and accuracy [30].
- Stator-winding optimization software – The developed software, which is already being used by a number of motor manufacturers/repairers, can be improved in several aspects, such as the inclusion of a fast winding optimization module as a function of the motor actual operating conditions, in which the user introduce the actual and rated values of the motor slip and voltage and the software computes the most advantageous number of phase turns. Additional databases with motor reference technical data can also be implemented.
- Large-scale motor downsizing schemes – The large-scale adaptation of motors to their actual operating conditions can be implemented as a pilot project, requiring keeping an updated database with the motor load and terminal voltage profile, in order to allow a proper stator winding redesign during motor repair/maintenance.
- VSD ride-through capability improvement – It is proposed the improvement of this characteristic by means of significantly increasing the DC-bus capacitance of the VSD (without using DC-DC converters) and, from an academic perspective, by proper stator winding connection management. Both solutions require experimental evaluation.
- Energy recovery in line-fed motors by means of pole changing – This innovative solution, although based on a right principle, experimental validation is required. Voltage and current transients during power connection/disconnection should be analysed in detail. A careful cost-benefit analysis has to be carried out. The application of a device identical to Smart-Switch/Relay for this purpose should be also analysed [27].
- Bearing Currents Mitigation Techniques – Experimental comparison between inner and outer insulation in insulated bearings in term of bearing currents mitigation effectiveness is required, as well as the experimental validation of the proposed in-slot partial electrostatic shield [15].
- Motor condition diagnosis by means of correlating leakage/ground currents and shaft-ground voltage – the principle behind the proposed method is valid, but experimental validation is required [29].

Although a significant research work has been developed on the scope of this thesis, based on the foregoing information, it is evident that most of the topics addressed require further investigation in order to improve, clarify, and/or validate the presented ideas.

6.3 References

- [1] de Almeida, A.; Ferreira, F.; Walters, D.; Parasiliti, F.: “Barriers Against Energy-Efficient Electric Motor Repair”, European Commission, SAVE Project, 1999.
- [2] de Almeida, A.; Fonseca, P.; Ferreira, F.; Guisse, F.; Diop, A.; Previ, A.; Russo, S.; Falkner, H.; Reichert, J.; Malmose, K.: “Improving the Penetration of Energy-Efficient Motors and Drives”, European Comm., DG TREN, SAVE II Prog., 2000.
- [3] de Almeida, A.; Ferreira, F.; Fonseca, P.; Chretien, B.; Falkner, H.; Reichert, J.; West, M.; Nielsen, S.; Both, D.: “VSDs for Electric Motor Systems”, European Commission, DG TREN, SAVE II Programme, 2001.
- [4] de Almeida, A.; Ferreira, F.; Fong, J.; Fonseca, P.: “Ecodesign Assessment of Energy Using Products - EuP Lot 11 Motors”, Final Report for the European Commission, Institute of Systems and Robotics, University of Coimbra, February 2008.
- [5] Ferreira, F.: “Técnicas Avançadas de Manutenção Curativa e Reabilitação de Motores de Indução Trifásicos de Baixa Tensão/ Curative Maintenance and Rehabilitation Advanced Methods for Low-Voltage, Three-Phase, Induction Motors”, Tese de Mestrado/Master Science Thesis (available in Portuguese only), Universidade de Coimbra/University of Coimbra, 2002.
- [6] de Almeida, A.; Ferreira, F.; Both, D.: “Technical and Economical Considerations to Improve the Penetration of Variable-Speed Drives for Electric Motor Systems”, IEEE Trans. on Industry Applications, Vol. 41, No. 1, pp. 188-199, Jan./Feb. 2005.
- [7] de Almeida, A.; Ferreira, F.; Fong, J.: “Ecodesign of Electric Motors”, 5th Inter. Conf. on Energy Efficiency in Motor Driven Systems (EEMODS’07), Conf. Proc., Vol. I, pp. 27-38, Beijing, 2007.
- [8] de Almeida, A.; Ferreira, F.; Fong, J.; Conrad, B.: “Electric Motor Ecodesign and Global Market Transformation”, IEEE Industrial & Commercial Power Systems Conf., Conf. Proc., Florida, USA, May 4-8, 2008.
- [9] Ferreira, F.; de Almeida, A.; Baoming, G.: “Comparative Study on 2-Level and 3-Level Voltage-Source Inverters”, 5th Inter. Conf. on Energy Efficiency in Motor Driven Systems (EEMODS’07), Conf. Proc., Vol. II, pp. 581-602, Beijing, China, 2007.
- [10] Ferreira, F.; de Almeida, A.; Deprez, W.; Belmans, R.; Baoming, G.: “Impact of Steady-State Voltage Supply Anomalies on Three-Phase Squirrel-Cage Induction Motors”, Inter. Aegean Conf. on Electric Machines and Power Electronics (ACEMP’07) and Electromotion Joint Conf., Conf. Proc., pp. 607-615, Bodrum, Turkey, 10-12 Set. 2007.
- [11] Ferreira, F.; de Almeida, A.: “Novel Multi-Flux Level, Three-Phase, Squirrel-Cage Induction Motor for Efficiency and Power Factor Maximization”, IEEE Trans. on Energy Conversion, Vol. 23, No. 1, pp. 101-109, March 2008.
- [12] Ferreira, F.; de Almeida, A.: “Novel Multi-Flux Level, Three-Phase, Squirrel-Cage Induction Motor for Efficiency and Power Factor Maximization”, IEEE Inter. Conf. on Industrial Technology (ICIT’06), Conf. Proc., Mumbai, India, December 2006, paper selected for oral presentation and invited for publication in a special issue of IEEE Trans. on Industrial Electronics.
- [13] Ferreira, F.; de Almeida, A.: “Considerations on the Custom Design of the Stator Winding of Low-Voltage, Three-Phase, Cage Induction Motors to Improve their Efficiency and Reliability”, 17th Inter. Conf. on Electric Machinery (ICEM’06), Sept. 2006.
- [14] Ferreira, F.; de Almeida, A.; Baoming, G.: “Three-Phase Induction Motor Simulation Model Based on a Multifrequency Per-Phase Equivalent Circuit Considering Stator Winding MMF Spatial Harmonics and Thermal Parameters”, XVII Inter. Conf. on Electric Machinery (ICEM’06), September 2006.
- [15] Ferreira, F.; Pereirinha, P.; de Almeida, A.: “Study on the Bearing Currents Activity in Cage Induction Motors using Finite-Element Method”, 17th Inter. Conf. on Electric Machinery (ICEM’06), Sept. 2006.
- [16] de Almeida, A.; Ferreira, F.: “Advanced motors, VSDs, transmissions, and systems design”, Improvement potentials and barriers, Industrial Electric Motor Systems Workshop, Paris, France, May 2006.
- [17] Ferreira, F.; de Almeida, A.: “Method for In-Field Evaluation of the Stator Winding Connection of Three-Phase Induction Motors to Maximize Efficiency and Power Factor”, IEEE Trans. on Energy Conversion, Vol. 21, No. 2, pp. 370-370, June 2006.
- [18] Ferreira, F.; de Almeida, A.; Baoming, G.; Faria, S.; Marques, J.: “Automatic Change of the Stator-Windings Connection of Variable-Load Three-Phase Induction Motors to Improve the Efficiency and Power Factor”, IEEE Inter. Conf. on Industrial Technology (ICIT’05), Conf. Proc., Hong Kong, 2005.
- [19] de Almeida, A.; Ferreira, F.: “User-Friendly High-Precision Electric Motor Testing System”, 4th Inter. Conf. on Energy Efficiency in Motor Driven Systems (EEMODS’05), Conf. Proc., Vol. I, pp. 149-157, Heidelberg, Germany, Sept. 2005.
- [20] Ferreira, F.; de Almeida, A.: “Three-Phase Induction Motor Stator Winding Connection Type In-Field Evaluation Method for Efficiency Maximization”, 4th Inter. Conf. on Energy Efficiency in Motor Driven Systems (EEMODS’05), Conf. Proc., Vol. II, pp. 128-137, Heidelberg, Germany, Sept. 2005.
- [21] Ferreira, F.; de Almeida, A.: “Electric Machinery Winding Design Software for Teaching and Rewinding”, Proceedings, XVI Inter. Conf. on Electric Machinery (ICEM’04), September 2004;
- [22] de Almeida, A.; Ferreira, F.: “Actions to Promote VSDs”, in *Energy Efficiency in Motor Driven Systems*, ISBN 3540006664, Springer-Verlag, 2003.
- [23] de Almeida, A.; Ferreira, F.: “Actions to Promote Energy-Efficient Electric Motor Repair”, Inter. Journal of Energy Technology and Policy, Vol. 1, No. 3, pp. 302-314, 2003.
- [24] de Almeida, A.; Fonseca, P.; Ferreira, F.: “Carbon savings of energy-efficient motor technologies in Central and Eastern Europe”, Inter. Journal of Energy Technology and Policy, Vol. 1, No. 3, 2003;
- [25] de Almeida, A.; Ferreira, F.; Busch, J.; Angers, P.: “Comparative Analysis of IEEE 112-B and IEC 34-2 Efficiency Testing Standards Using Stray Load Losses in Low-Voltage Three-Phase, Cage Induction Motors”, IEEE Trans. on Industry Applications, Vol. 38, No. 2, March/April 2002 (2001 Committee Prize Paper Award of the Energy Systems Committee, IEEE).

- [26] Cistelecan, M; Ferreira, F.; Cosan, B.: “*Generalized MMF Space Harmonics and Performance Analysis of Combined Multiple-Step, Star-Delta, Three-Phase Windings Applied on Induction Motors*”, 18th Inter. Conf. on Electrical Machines (ICEM’08), Conf. Proc., Vilamoura, Portugal, Sept. 2008.
- [27] Ferreira, F.; Cistelecan, M; de Almeida, A; Baoming, G.: “*Simple Strategy to Recovery Energy During Stopping Period in Large High-Inertia Line-Fed Induction Motor Driven Systems*”, 18th Inter. Conf. on Electrical Machines (ICEM’08), Conf. Proc., Vilamoura, Portugal, Sept. 2008.
- [28] Ferreira, F.; Cistelecan, M.: “*Simulating Multi-Connection, Three-Phase, Squirrel-Cage, Induction Motors By Means of Changing Per-Phase Equivalent Circuit Parameters*”, 18th Inter. Conf. on Electrical Machines (ICEM’08), Conf. Proc., Vilamoura, Portugal, Sept. 2008.
- [29] Ferreira, F.; Trovão, J.; de Almeida, A.: “*Motor Bearings and Insulation System Condition Diagnosis by Means of Common-Mode Currents and Shaft-Ground Voltage Correlation*”, 18th Inter. Conf. on Electrical Machines (ICEM’08), Conf. Proc., Vilamoura, Portugal, Sept. 2008.
- [30] Ferreira, F.; de Almeida, A.: “*Considerations on In-Field Induction Motor Load Estimation Methods*”, 18th Inter. Conf. on Electrical Machines (ICEM’08), Conf. Proc., Vilamoura, Portugal, Sept. 2008.



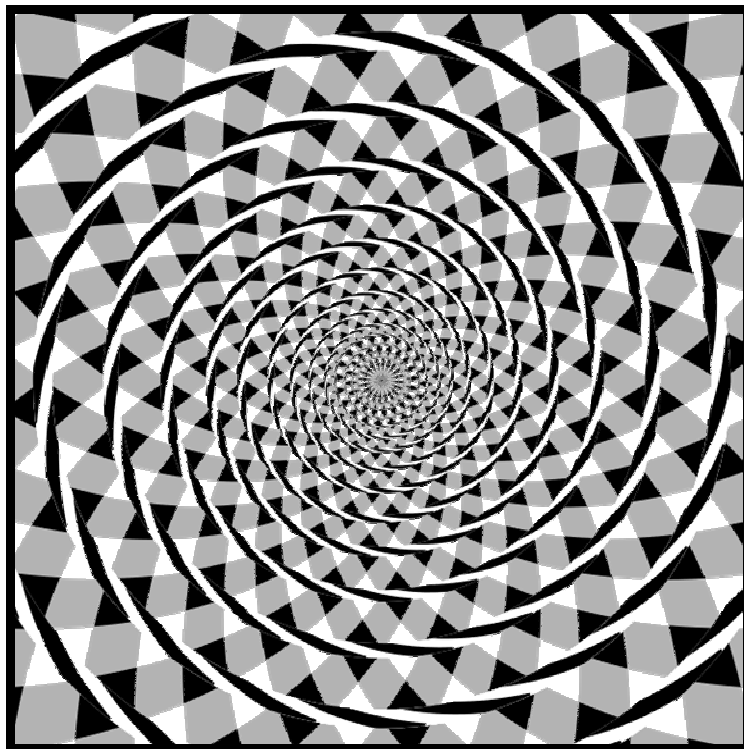
Original Tesla induction motor, 1887-1888. Nikola Tesla (1856-1943), who was born in Croatia but worked in America, made the first practical induction motors. He made this working model motor to illustrate the claims in his patents. Later, Tesla gave it to William Edward Ayton (1847-1908), of the City and Guilds College (now part of Imperial College of Science Technology and Medicine). It is a two-phase machine (that is, it uses two alternating currents to produce the rotating magnetic field that makes the rotor turn).

Source: www.sciencemuseum.org.uk



Department of Electrical and Computer Engineering
University of Coimbra

STRATEGIES TO IMPROVE THE PERFORMANCE OF THREE-PHASE INDUCTION MOTOR DRIVEN SYSTEMS



Fernando José Teixeira Estêvão Ferreira

VOLUME II

Coimbra
2008

Picture in the cover: Fraser spiral illusion – Optical illusion that was first described by the British psychologist James Fraser in 1908. The illusion is also known as the false spiral, or by its original name, the twisted cord illusion. The overlapping black arc segments appear to form a spiral. However, the arcs are a series of concentric circles. The visual distortion is produced by combining a regular line pattern (the circles) with misaligned parts (the differently coloured strands). The illusion is augmented by the spiral components in the chequered background.

Fernando
J. T. E.
Ferreira

STRATEGIES TO IMPROVE THE PERFORMANCE OF
THREE-PHASE INDUCTION MOTOR DRIVEN SYSTEMS

VOLUME II

Ph. D. Thesis



Coimbra
2008

Appendix 1 – Symbols, Acronyms and Constants

A1.1 List of the Main Symbols, Acronyms and Subscripts

Symbol/Acronym	Meaning	Unit
W	energy	W.s, J
P or p	power, active (or real) power, pressure, number of pole pairs	W, W, Pa or N/m^2 , --
Q	reactive power or fluid flux	var or m^3/s
S	apparent or complex power, savings	VA, €
λ	power factor, failure rate	--
E	electric field	V/m
EMF, E or e	electromotive force	V
U, u	voltage RMS, voltage instantaneous value	V
I, i	current RMS, current instantaneous value	A
J	current density, moment of inertia	A/m^2 , $kg.m^2$
R	ohmic resistance, thermal resistance	Ω , $^{\circ}C/W$
L	inductance	H
C	capacitance, thermal or heat capacity, cost	F, $J/^{\circ}C$, €
Z	impedance, number of stator slots	Ω , --
H	magnetic field intensity, head	A/m, m
B	magnetic induction (flux density), viscous friction coefficient	Wb/m^2 or T, N.m.s/rad
ϕ	magnetic flux	Wb
ψ	flux linkage	Wb.turn
MMF	magnetomotive force	A.turn
\mathfrak{R}	magnetic reluctance	A/Wb or 1/H
σ	electric conductivity	$1/(\Omega.m)$ or S/m
ρ	electric resistivity	$\Omega.m$
μ	magnetic permeability	H/m
ϵ	electric permittivity	F/m
T	torque	N.m
F	force	N
ω	angular frequency, angular speed	rad/s or r/min
v	linear velocity or speed	m/s
α	angular acceleration	rad/s^2
a	linear acceleration	m/s^2
f	frequency	Hz
δ	skin depth	m
θ	temperature, angular displacement	$^{\circ}C$, rad
k	thermal conductivity	W /m. $^{\circ}C$
c	specific heat capacity	J/(g. $^{\circ}C$)
q	heat transfer rate or thermal flux	J/s or W
ζ_{avg}	load factor	--
ζ	motor load	--
η	efficiency	--
N	number of turns	--
K_w	winding factor	--
K_d	distribution factor	--
K_p	pitch factor	--
τ_p	polar pitch	rad, slots or m
α_e	effective coil pitch	rad, slots or m
α_{avg}	average coil pitch	rad, slots or m
s	slip, space harmonic order	--
h	time harmonic order	--
i	transmission relation or ratio	--
r	radius of a circumference, ohmic resistance	m
d	distance, circumference diameter	m
\otimes	in-paper wise	--
\odot	out-paper wise	--
l	length	m

<i>K</i>	constant	--
. or ,	decimal separator	--
×	cross product of two vectors or multiplication of two scalars	--
•	dot or inner product of two vectors	--
.	multiplication of two quantities	--
p.p.	percentage points	--
pu or p.u.	per unit	--
sign	signal of a quantity	--
sqrt	square root of a quantity	--
m_a	amplitude modulation ratio (or index)	--
m_f	frequency modulation ratio (or index)	--

Subscript	Meaning
0	homopolar, DC component
1	relative to stator, fundamental component
2	relative to rotor, 2 nd order harmonic
<i>ag</i>	relative to air-gap
<i>air</i>	relative to air
<i>al</i>	aluminium
<i>arsn</i>	anti-resonance
<i>AVG</i> or <i>avg</i>	average or mean value
<i>brg</i>	relative to bearings
<i>brk</i>	brake
<i>c</i>	relative to capacitance or carrier/switching frequency
<i>circ</i>	relative to circulating currents
<i>cond</i>	relative to the conductors
<i>const</i>	constant
<i>conv</i>	convection
<i>cu</i>	copper
<i>DC</i> or <i>dc</i>	average or continuous component of a quantity
<i>DC_bus</i>	relative to the DC bus/link of the VSD
<i>disch</i>	relative to electric discharge
<i>disr</i>	relative to disruption
<i>dvc</i>	device
<i>e</i>	relative to eddy (or Foucault) currents
<i>eem</i>	relative to energy-efficient or high-efficiency motors
<i>ela</i>	elastic or elasticity
<i>elec</i>	electrical or electric
<i>em</i>	electromagnetic
<i>epoxy</i>	relative to the epoxy resin
<i>eq</i>	equivalent
<i>fe</i>	relative to iron core
<i>g</i>	ground
<i>h</i>	relative to time harmonic order, hysteresis or hours
<i>hydr</i>	hydraulic
<i>IM</i>	relative to induction motors
<i>in</i>	input, consumed or absorbed
<i>ind</i>	induced
<i>insu</i>	insulation
<i>je</i>	Joule effect
<i>kWh</i>	electrical energy or electricity (kilowatt-hour)
<i>lf</i>	lifetime
<i>lg</i>	line-to-ground or phase-to-ground
<i>line</i>	line, grid, or mains
<i>lk</i>	leakage
<i>ll</i>	line-to-line or phase-to-phase
<i>ln</i>	line-to-neutral or phase-to-neutral
<i>load</i>	relative to the motor-driven load
<i>loss</i>	relative to losses
<i>m</i> or <i>mag</i>	relative to magnetization
<i>max</i>	maximum or peak value
<i>mea</i>	measured

<i>mech</i>	mechanical
<i>min</i>	minimum value
<i>mtr</i>	motor
<i>N or R</i>	rated or nominal value
<i>opt</i>	optimum value
<i>out</i>	output or provided
<i>peak</i>	peak or maximum value
<i>ph</i>	phase
<i>r</i>	relative to ohmic resistance or rotor
<i>rep</i>	repair or repaired
<i>rms</i>	root mean square value
<i>rotor or rtr</i>	relative to rotor
<i>RS</i>	between rotor and stator
<i>rsn</i>	resonance
<i>s</i>	relative to space harmonic order, stator or switching frequency
<i>sg</i>	shaft-to-ground
<i>si</i>	relative to the silicon
<i>slot</i>	relative to slots
<i>src</i>	power source/supply
<i>ss</i>	steady state
<i>stator or str</i>	relative to stator
<i>std</i>	relative to standard motors
<i>sync</i>	synchronous
<i>sync</i>	synchronous or synchronism
<i>trs</i>	transmission
<i>ts</i>	transient state
<i>vent</i>	ventilation
<i>wdg</i>	relative to the stator winding
<i>WR</i>	between windings and rotor
<i>WS</i>	between windings and stator
<i>yr</i>	year

Acronym	Meaning
AC	Alternate Current of a Quantity
AEC	Approximate Per-Phase Equivalent Circuit
AEMT	Association of Electrical and Mechanical Trades
ANSI	American National Standard Institute
AS	Australian Standard
ASD	Adjustable Speed Drive
ATD	Ambient Temperature Deviation
AVG	Average or Mean Value of a Quantity
BS	British Standards
CC	Circulating Current
CEMEP	Comité Européen de Constructeurs de Machines Electriques et d'Electronique de Puissance/European Committee of Manufacturers of Electrical Machines and Power Electronics
CENELEC	Comité Européen de Normalisation Electrotechnique/European Committee for Electrotechnical Standardization
CMC	Common-Mode Current
CMV	Common-Mode Voltage
COPANT	Comissão Pan-Americana de Normas Técnicas/Pan-American Commission for Technical Standards
CSA	Canadian Standards Association
CSE	Cost of the Saved Energy
D	Dee or Delta Connection
DC	Direct Current or AVG/Continuous Component of a Quantity
DoE	Department of Energy (USA)
DS	Dielectric Strength
DSM	Demand Side Management
DV	Disruptive Voltage
EASA	Electrical Apparatus Service Association
EC	European Commission or Per-Phase Equivalent Circuit
EC (Motor)	Electronically Commutated/Controlled (Motor)

ED	Electric Discharge
EDM	Electric Discharge Machining
EEC	Exact Per-Phase Equivalent Circuit
EEM	Energy-Efficient Motor
EHD	Even Harmonic Distortion Coefficient
EIS	Electric Insulation System
EMC	Electromagnetic Compatibility
EMI	Electromagnetic Interference
EMODS	Electric Motor-Driven System
EN	European Standards
EPAct	Energy Policy Act
EPRI	Electrical Power Research Institute
EU	European Union
EU-15	Austria, Belgium, Denmark, Finland, France, Germany, Greece, Ireland, Italy, Luxemburg, Netherlands, Portugal, Spain, Sweden, UK.
EU-25	EU-15 plus Poland, Czech Republic, Slovakia, Hungary, Slovenia, Estonia, Latvia, Lithuania, Malta and Cyprus.
EuP	Energy-Using Product
FEM	Finite-Element Method
FEA	Finite-Element Analysis
FFT	Fast-Fourier Transform
FV	Forced or separated ventilation or cooling
GB	China (or Guobiao, GB) National Standard ¹
GER	Gross Energy Requirement
GHG	Greenhouse Gases
GWP	Global Warming Potential
HEM	High-Efficiency Motor
HVAC	Heat, Ventilation, and Air-Conditioning
HVF	Harmonic Voltage Factor
IEA	International Energy Agency
IEC or CEI	International Electrotechnical Commission
IEEE	Institute of Electrical and Electronic Engineers
IEL	Industrial Electrotechnology Laboratory
IFIM	Inverter-fed induction motor
IGBT	Insulated Gate Bipolar Transistor
ITIC	Information Technology Industry Council (of USA)
IM	Three-Phase, Squirrel-Cage, Induction Motor
INV	Investment or Additional Investment
ISO	International Standard Organization
JEC	Japanese Electrotechnical Committee
JIS	Japanese Industrial Standard
JISC	Japanese Industrial Standards Committee
LBD	Loss-Based Derating
LCC	Life Cycle Cost
LMT	Length Mean Turn
MEEUP	Methodology Study for Ecodesign of Energy-Using Products
MEPS	Minimum Energy Performance Standards
MLT	Mean Length of Turn
MTBF	Mean Time Between Failures
MTTF	Mean Time to Failure
NEMA	National Electrical Manufacturers Association
NPV	Net Present Value
NZS	New Zealand Standard
ODP	Open Drip Proof
OEM	Original Equipment Manufacturer
PB	Payback Period
PD	Electric Partial Discharge
PRODCOM	Production Communautaire
PWM	Pulse-Width Modulation
PHD	Partial Harmonic Distortion Coefficient
RMS	Root Mean Square of a Quantity

¹ Set of mandatory and recommended standards regulated by SAC.

REMA	Rotating Electrical Machines Association
ROR	Rate of Return
S	Electric Switch
SAC	Standardization Administration of China
SEEEM	Standards for Energy Efficiency of Electric Motor Systems
SPB	Simple Payback Period
STD	Standard Motor
SV	Self-Ventilated or Self-Cooled
SVGS	Savings
SS	Steady State
TBD	Temperature-Based Derating
TEAO	Totally-Enclosed, Air Over
TEBC	Totally-Enclosed, Blower Cooled
TEFC	Totally-Enclosed, Fan-Cooled
TENV	Totally-Enclosed, Non-Ventilated
THD	Total Harmonic Distortion
THF	Total Harmonic Factor
TSC	Torque-speed curve (steady state)
TTL	Torque thermal limit curve (steady state)
USA or US	United States of America
UK	United Kingdom
VFD	Variable-Frequency Drive
VD	Voltage Distortion
VMD	Voltage Magnitude Deviation
VR	Voltage Regulator
VSD	Variable-Speed Drive
VSI	Voltage-Source Inverter
VT	Voltage transient
VVR	Voltage variation rate
Y	Wye or star connection

A1.2 List of the Main Constants and Unit Conversions

Symbol	Meaning	Unit	Value ²
ϵ_0	vacuum permittivity	F/m	8.854×10^{-12}
ϵ_{air}	air relative permittivity (or dielectric constant)	F/m	1.0005
ϵ_{epoxy}	epoxy resin/varnish relative permittivity (or dielectric constant)	F/m	3.5-5.0
ϵ_{teflon}	Teflon® relative permittivity (or dielectric constant)	F/m	≈ 2
ϵ_{oil}	mineral oil relative permittivity (or dielectric constant)	F/m	2.2-2.5
μ_0	vacuum permeability	F/m	$4\pi \times 10^{-7}$
$\mu_{r_{fe_cast}}$	cast iron relative permeability	--	60
$\mu_{r_{fe}}$	iron (pure) relative permeability	--	4000
$\mu_{r_{steel}}$	machine steel relative permeability	--	300
$\mu_{r_{air}}$	air relative permeability	--	1
$\mu_{r_{epoxy}}$	epoxy resin/varnish relative permeability	--	1
$\mu_{r_{al}}$	aluminium relative permeability	--	1
$\mu_{r_{sheet}}$	Armco oriented M-6 steel sheets relative permeability	--	2000
E_{dis_air}	air disruption electric field (1 bar)	V/m	3.2×10^6
E_{dis_epoxy}	epoxy resin/varnish disruption electric field	V/m	4.0×10^7
σ_{air}	sweet water electrical conductivity (20°C)	1/(Ω .m)	1×10^{-3}
σ_{epoxy}	epoxy resin/varnish electrical conductivity (20°C)	1/(Ω .m)	$< 10^{-9}$
σ_{fe}	iron electric conductivity (20°C)	1/(Ω .m)	$0.8-1.0 \times 10^7$
σ_{cu}	copper electric conductivity (20°C)	1/(Ω .m)	$5.7-5.8 \times 10^7$
σ_{al}	aluminium electric conductivity (20°C)	1/(Ω .m)	3.6×10^7
σ_{steel}	stainless steel electric conductivity (20°C)	1/(Ω .m)	1.0×10^6
σ_{sheet}	Armco oriented M-6 steel sheets electric conductivity	1/(Ω .m)	2.8×10^6
k_{air}	air thermal conductivity (27°C)	W/(m.K)	0.03

² The presented values were extracted from [1]–[10] and, in some cases, due to slightly discrepancies, the arithmetic average of two or more different values is presented.

k_{epoxy}	epoxy resin/varnish thermal conductivity (27°C)	W/(m.K)	2.02
k_{fe}	iron thermal conductivity (27°C)	W/(m.K)	80.2
k_{cu}	copper thermal conductivity (27°C)	W/(m.K)	396
k_{al}	aluminium thermal conductivity (27°C)	W/(m.K)	237
k_{steel}	steel sheets thermal conductivity (27°C, Mn < 1%, Si < 0.6%)	W/(m.K)	52
k_{insul}	electric wire enamel thermal conductivity, typical value	W/(m.K)	0.4
k_{insul_slot}	slot insulation thermal conductivity, typical value	W/(m.K)	0.22
c_{cu}	copper heat capacity	J/(g.K)	0.385
c_{air}	air heat capacity	J/(g.K)	≈1.01
c_{iron}	iron heat capacity	J/(g.K)	0.450
c_{al}	aluminium heat capacity	J/(g.K)	0.897

Quantity/Unit

Equal or equivalent to

1 horsepower (hp)	0.746 kilowatt (kW)
1 euro (€ or EUR)	1.4705 US dollar (US\$ or USD), January 25 th , 2008
1 foot (ft), International	0.3048 meter (m)
1 pound (lb)	0.4535924 kilogram (kg)
1 tonne (t)	1000 kilogram (kg)
1 year (yr)	8760 hour (h), for a 365-day year
1 kelvin (K)	-273 degree Celsius (°C), $\theta(^{\circ}\text{C}) = \theta(\text{K}) - 273$

A1.3 References

- [1] Chatelain, J.: “*Machine Électrique*”, Tome I, DUNOD, 1983.
- [2] Hayt, W.: “*Engineering Electromagnetics*”, 5th Ed., McGraw-Hill, 1989.
- [3] Metaxas, A.: “*Foundations of Electroheat - A Unified Approach*”, John Wiley & Sons, New York, 1996.
- [4] Çencel, Y.: “*Heat Transfer - A Practical Approach*”, WCB/McGraw-Hill, 1998.
- [5] “*Handbook of Industrial Materials*”, 2nd Edition, Elsevier Science Publishers Ltd, Elsevier Advanced Technology Oxford, U.K, 1992.
- [6] Farth, E. P. Wohl: “*Ferromagnetic Materials - A handbook on the properties of magnetically ordered substances*”, Vol. 1, North-Holland Publishing Company, Amsterdam, 1980.
- [7] Saenger: “Formulario”, Junio 1978.
- [8] Almeida, G.: “*Sistema Internacional de Unidades (SI) - Grandezas e Unidades Físicas*”, 2^a Edição, Plátano Editora S.A., Lisboa, 1997.
- [9] EngNet Tools, EngNet, Engineerig Network, Version 1.4 (1.4.2.0, Comax), 2002-2003.
- [10] Gieck, R.: “*Manual de Fórmulas Técnicas*”, 4^a Edição Revista Ampliada, Dinalivro, Hemus, 1996.

Appendix 2 – Simulation Models

A2.1 Insulated Gate Bipolar Transistors

The switches used in the three-phase inverters are *Insulated Gate Bipolar Transistors* (IGBTs). The simulation models available in MATLAB/SIMULINK software packages were used. Each IGBT model block has the equivalent circuit and operation mode represented in Figs. A2.1 and A2.2, respectively. IGBTs are devices controlled by a gate signal, being simulated as a series combination of one internal resistance R_{ON} , internal inductance L_{ON} , and one DC-voltage source or forward voltage, U_f , in series with a switch controlled by a logic signal, g , as it can be seen in Fig. A2.1. R_{ON} , L_{ON} , and U_f have to be specified. IGBTs commutate to ON state (or conduction state) when the collector-emitter voltage, is positive and higher than U_f , and a positive signal is applied to the gate ($g > 0$). It commutates to OFF state (non-conduction state) when $g = 0$. The IGBT is in OFF state when U_{CE} is negative. In IGBT models have anti-parallel diodes (free-wheeling diodes), and RC snubber parallel circuits. The IGBT turn-OFF characteristic can be represented approximately by two segments (Fig. A2.2). When the gate signal falls to 0, the collector current decrease from 100% to 10% of I_{max} , over the falling time, t_f , and from 10% to 0% of I_{max} during tail time, t_t . It is also possible to specify an initial current value for the IGBT, normally set to 0 to start the simulation with the device in OFF state. There are some assumptions and limitations associated with the IGBT block. For example, the IGBT block does not take into account the device geometry or the physical complex process [30], being modulated as a current source. It cannot be connected in series with an inductive load, a current source, or an open-circuit, unless a snubber circuit is used.

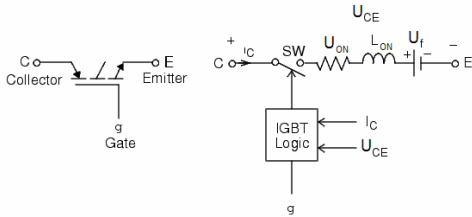


Fig. A2.1. IGBT simulation model: equivalent circuit [30].

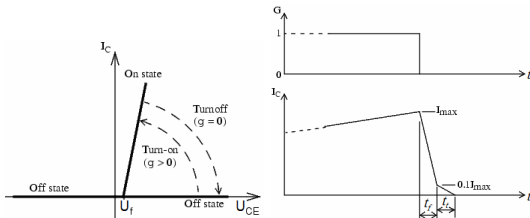


Fig. A2.2. IGBT simulation model: characteristic curves [30].

Considering the most common situation, the current flowing through a switch also must flow through series inductances. When the switch is ON, the entire current to be handled, I_C , flows through the switch. When the switch is turned OFF, the current flows through a free-wheeling (or anti-parallel) diode and a voltage equal to the input

voltage U_{DC} appears across the switch, assuming a zero voltage drop across the considered diode (ideal device).

The foregoing described model is used to simulate the waveforms and efficiency for different operating conditions taken into account only the ON and OFF state losses, on the basis of the handled current I_C flowing through the switch and on parameter U_f and R_{ON} . Since the OFF state losses due to leakage current are typically lower than 1% of the ON-state losses [30], they can be ignored. The U_f , R_{ON} , and L_{ON} , are typically given by manufacturers datasheets¹. However, it is too heavy or time consuming to simulate a circuit during several fundamental periods with a resolution short enough to analyse the transient/switching periods ($t_r = 50-200$ ns, $t_f = 25-45$ ns). To study the inverter efficiency, the described model is not fully adequate because it does not simulate the rise and fall times and, therefore, does not take into account the corresponding switching losses. Therefore, a complementary model to compensate for the switching losses was implemented, based on the real characteristics of the IGBTs. Regarding IGBTs and the respective free-wheeling diodes, a relation between the dissipated energy during rise time, $W_{OFF \rightarrow ON}$, and during fall time, $W_{ON \rightarrow OFF}$, as a function of the current circulating between emitter and collector can be, in practical terms, mathematically fitted by (A2.1). For a better fitting, the curves can be described separately by two fitting curves for different current ranges.

$$\begin{cases} W_{OFF \rightarrow ON} = f_r(I_C) \approx A + B \cdot |I_{CE}^a| \\ W_{ON \rightarrow OFF} = f_f(I_C) \approx C + D \cdot |I_{CE}^b| \end{cases} \quad (\text{A2.1})$$

The constants, A , B , C , D , a , and b (typically, $a \approx b \approx 2$) are defined on the basis of the characteristic curves (extracted from datasheets) and experimental tests carried out with a three-phase IGBT-based inverter with full access to the IGBT points (shown in Fig. A2.4), connected to an acquisition board and controlled by software developed in LABVIEW. The losses estimated by such approach include the turn-OFF losses of the free-wheeling diodes. Further information on IGBT losses can be found in [40]. In SIMULINK environment, the loss energy can be easily defined by a fitting curve (e.g., using A2.1), or a lookup table, on the basis of datasheet curves (Fig. A2.3) and experimental results. Additional information on U_{CE} and I_C curves (turn-ON and turn-OFF) for a half-bridge module 2 IGBTs and free-wheeling diodes feeding a resistive-inductive load is presented in [36].

Based on the foregoing assumptions, the switching energy losses are obtained by summing the energy associated with the logic state change in all IGBTs over a fundamental period, the power switching losses are then computed by dividing the energy losses by the fundamental period $P_{loss(OFF \rightarrow ON)} = W_{(OFF \rightarrow ON)} / f_1$. In each

¹ For low-voltage components, the R_{ON} both for IGBTs and diodes varies within 0.01-0.03 Ω , and the U_f within 0.8 and 1.0 V.

transition instant, the entire current handled by the IGBT (current after turn-ON for turn-ON losses estimation and current before turn-OFF for turn-OFF losses estimation) is used to estimate the losses in each transition. This switching losses estimation strategy is integrated into the gate pulse generation system. Ignoring the IGBT OFF-state losses and ON→OFF diode switching losses, the average power losses (during a fundamental period), P_{loss} , in each IGBT plus anti-parallel diode unit and in each diode are given by (A2.2), (A2.3), and (A2.4), where T is the averaging period (assumed as $1/f_i$), i is the i^{th} ON-state during T , j is the j^{th} OFF→ON transition during T , and k is the k^{th} ON→OFF transition during T .

$$P_{loss(IGBT+diode)} = P_{loss(IGBT)} + P_{loss(diode)} \quad (A2.2)$$

$$\begin{cases} P_{loss(IGBT)} = P_{loss(OFF \rightarrow ON)} + P_{loss(ON \rightarrow OFF)} + P_{loss(ON-state)} \\ P_{loss(diode)} = P_{loss(ON-state)} \end{cases} \quad (A2.3)$$

$$\begin{cases} P_{loss(IGBT)} = \frac{1}{T} \left(\sum_i W_{ON_i} + \sum_j W_{s(ON)_j} + \sum_k W_{s(OFF)_k} \right) \\ P_{loss(diode)} = \frac{1}{T} \left(\sum_i W_{ON_i} \right) \end{cases} \quad (A2.4)$$

Both IGBT and diode ON-state losses are inherently calculated in the used models. In all instants, the value of the current and voltage handled by each device should be known. Equation (3.4) has to be applied to all switches in the inverter.

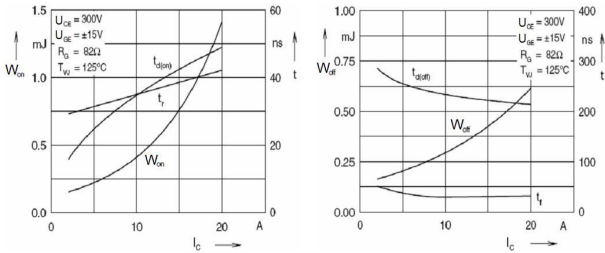


Fig. A2.3. Example of datasheet characteristic curves related to switching losses (6 IGBT+Diode Module, IXYS - MUBW 10-06 A7): (left) OFF-ON transition; (right) ON-OFF transition.

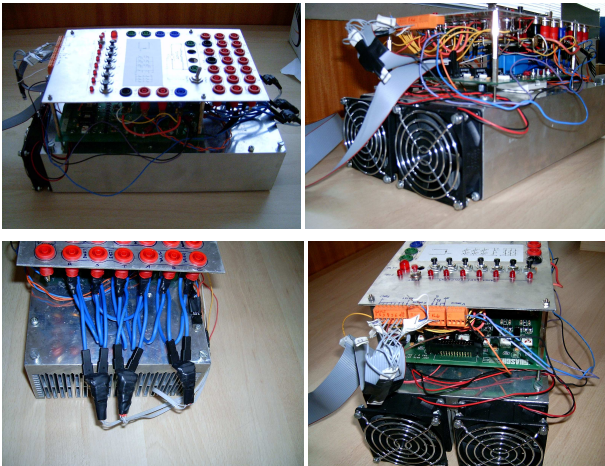


Fig. A2.4. 5-kW 3-phase low-voltage inverter (testing setup) to measure the switching losses associated with the IGBT/Diode sets. Also used for other purposes.

Moreover, the values extracted from datasheets have to be adjusted for the voltage handled by each switch (multiplied by the quotient between the actual voltage and

the data sheet reference voltage). For an inverter, since the ON and OFF state losses inherently calculated for diodes and IGBTs, the total loss calculation requires only adding the switching losses associated with the IGBT+diode units, yielding (A2.5), which was the process used to calculate the inverter efficiency.

$$P_{inverter} = P_{in} - P_{out} + P_{switching(ON \rightarrow OFF)} + P_{switching(OFF \rightarrow ON)} = \frac{1}{T} (W_{in} - W_{out} + W_{s(ON \rightarrow OFF)} + W_{s(OFF \rightarrow ON)}) \quad (A2.5)$$

Additionally, appropriate values for the snubber circuit components were properly defined. For that purposes, equations (A2.6) and (A2.7) can be used, where P_N is the inverter nominal power (VA), U_N the rated line-to-line voltage (RMS), f is the output fundamental frequency (Hz), and T_s is the sampling period (or the fixed step of the simulation) [30].

$$C_s < \frac{P_N}{1000 \cdot 2\pi \cdot f \cdot U_N^2} \quad (A2.6)$$

$$R_s > 2 \frac{T_s}{C_s} \quad (A2.7)$$

For example, considering a 3000-VA inverter generating 400-V, 50-Hz output, and a 2-kHz sampling rate, the snubber capacitance $C_s = 60$ nF and the snubber resistance $R_s = 16.8$ kΩ. The leakage current at fundamental frequency should be lower than 0.1% the nominal current during OFF state, and the time constant of the RC-series snubber circuit should be twice higher than the sampling period T_s [30].

The fall and tail times are not defined in the “Three-Level Bridge Block” of SIMULINK. However, for both IGBTs and diodes, it is possible to define the ON-state equivalent resistance, R_{ON} , and the forward voltages, U_f and U_{fd} . For the forced-switching devices (GTO, IGBT or MOSFET), the inverter block operates fairly with a purely resistive snubber [30].

Since the nonlinear elements (such as IGBTs) in the “SimPowerSystems” blocks are modulated as current sources, it is necessary to guarantee a parallel path to them, in order to allow its connection to an inductive circuit such as an IM. A high resistance value does not affect the circuit performance.

A2.2 Three-Phase Voltage-Source Inverters

In the studies carried out using voltage-source inverters, two types of inverters were considered, the 2-level and the 3-level voltage-source inverters.

In part of the simulations, MATLAB scripts defining simplified models for both types of inverters and for the respective load (RL-series fixed load) were used, in order to reduce simulation efforts. Due to their extension, the MATLAB scripts are not presented.

More accurate simulations were made using SIMULINK-based models. For the 2-level inverter, specific switching control blocks or modules were developed, with 3 inputs, namely, the fundamental frequency, f_1 , the amplitude modulation index, m_a , and the switching or carrier frequency, f_s , as it can be seen in Fig. A2.5. The typical topology is presented in Fig. A2.6. For

a 3-arm bridge, 6 gate pulses are generated, as shown in Fig A2.7.

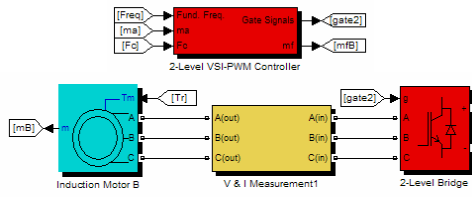


Fig. A2.5. Modules used in the SIMULINK for 2-level inverters simulation.

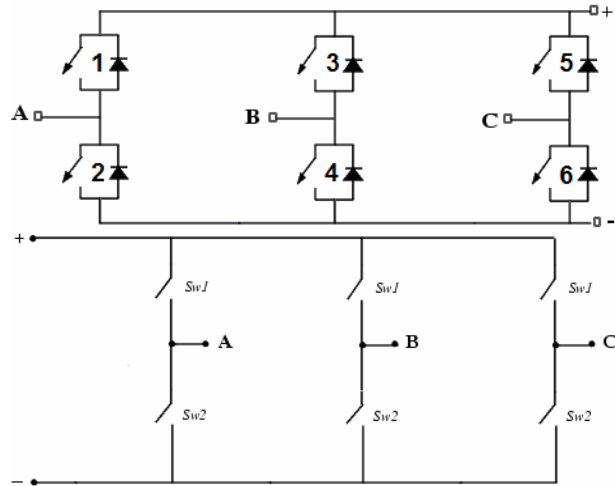


Fig. A2.6. Two-level inverter: (top) topology with switches and diodes; (bottom) simplified topology.

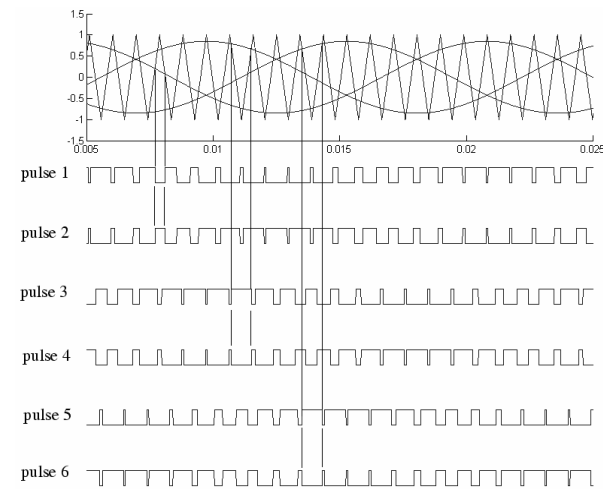


Fig. A2.7. Triangular and reference sinusoidal/modulating waves and the resulting gate pulses for 2-level inverters.

Firstly, a triangular wave, c , is generated using (A2.8), where $\omega_s t = 2\pi \cdot f_s \cdot t$. The control or reference sinusoidal waves, $u_{A,B,C}$, are given by (A2.9).

$$c = \frac{1}{\pi} \sin^{-1}(\sin(\omega_s t)) \quad (A2.8)$$

$$\begin{cases} u_A = A \cdot \sin(\omega t) \\ u_B = A \cdot \sin(\omega t - \frac{2}{3} \pi) \\ u_C = A \cdot \sin(\omega t + \frac{2}{3} \pi) \end{cases} \quad (A2.9)$$

Comparing (or intersecting) the triangular with sinusoidal waveforms, the gate pulses are established, according to (A2.10).

$$\begin{cases} \text{if } u_A(t) \geq C \text{ then } output_1 = 1 \text{ else } output_1 = 0 \\ \text{if } u_B(t) \geq C \text{ then } output_2 = 1 \text{ else } output_2 = 0 \\ \text{if } u_C(t) \geq C \text{ then } output_3 = 1 \text{ else } output_3 = 0 \end{cases} \quad (A2.10)$$

The control of the IGBT gate pulses in each inverter-arm is defined in Table A2.1.

TABLE A2.1
TWO-LEVEL INVERTER GATE PULSES.

Firing Pulses		
output _{1,2,3}	IGBT 1, 3, 5	IGBT 2, 4, 6
1	1	0
0	0	1

Although several existing different PWM techniques (SVPWM, SHE, and HB), the one presented is easier to implement and the results in steady-state are very similar to the ones expected for the SVPWM, and is enough for the steady-state performance analysis. All the described processes were fully implemented in MATLAB and SIMULINK. In MATLAB, the hysteresis-band (HB) technique was also implemented for common-mode voltage evaluation purposes. In Fig. A2.8, the triangular/carrier, the reference/modulating and the output PWM voltage waves are shown for one phase.

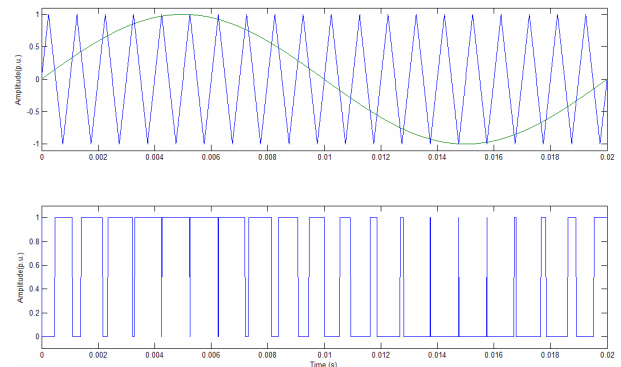


Fig. A2.8. Triangular/carrier and reference/modulating sinusoidal waves and the resulting gate pulses for a 2-level inverter.

Regarding 3-level inverters, in Figs. A2.9 and A2.10, the SIMULINK model and the typical topology are shown, respectively.

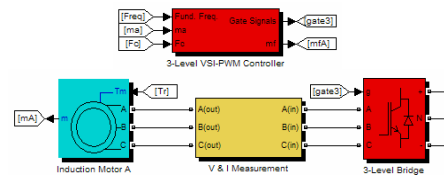


Fig. A2.9. SIMULINK model for the 3-level inverter.

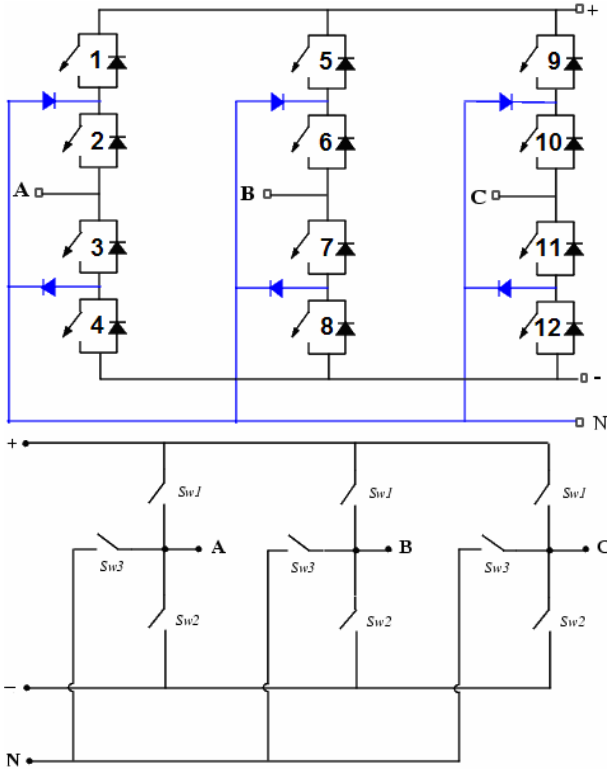


Fig. A2.10. Three-level inverter: (top) topology with switches and diodes; (bottom) simplified topology [30].

The sinusoidal and triangular waves for the gate pulse generation in the 3-level inverters are similar to those described for the 2-level inverter. However, two triangular waves are now necessary, waves c^+ and c^- , generated according to (A2.11), which oscillate between 0 and 1 and between -1 and 0, respectively.

$$\begin{cases} c^+ = \frac{1}{\pi} \sin^{-1}(\sin(\omega_s t)) + 0.5 \\ c^- = \frac{1}{\pi} \sin^{-1}(\sin(\omega_s t)) - 0.5 \end{cases} \quad (\text{A2.11})$$

The IGBT control pulses are generated by means of comparison (intersection) between triangular and reference/modulating sinusoidal waves, according to (A2.12) and (A2.13), to each arm of the inverter.

$$\begin{cases} \text{if } u_A(t) \geq c^+ \text{ then } signal_1 = 1 \text{ else } signal_1 = 0 \\ \text{if } u_A(t) \leq c^- \text{ then } signal_2 = 1 \text{ else } signal_2 = 0 \\ \text{if } u_B(t) \geq c^+ \text{ then } signal_3 = 1 \text{ else } signal_3 = 0 \\ \text{if } u_B(t) \leq c^- \text{ then } signal_4 = 1 \text{ else } signal_4 = 0 \\ \text{if } u_C(t) \geq c^+ \text{ then } signal_5 = 1 \text{ else } signal_5 = 0 \\ \text{if } u_C(t) \leq c^- \text{ then } signal_6 = 1 \text{ else } signal_6 = 0 \end{cases} \quad (\text{A2.12})$$

$$\begin{cases} output_1 = signal_1 - signal_2 \\ output_2 = signal_3 - signal_4 \\ output_3 = signal_5 - signal_6 \end{cases} \quad (\text{A2.13})$$

The control of the IGBT gate pulses in each inverter-arm is defined in Table A2.2. In Fig. A2.11, the triangular, the reference/modulating and the PWM voltage waves are shown for one phase. For the other arms it is only necessary to introduce the proper displacement.

TABLE A2.2
THREE-LEVEL INVERTER GATE PULSES.

State	Gate pulses			
output ₁	IGBT 1	IGBT 2	IGBT 3	IGBT 4
1	1	1	0	0
0	0	1	1	0
-1	0	0	1	1

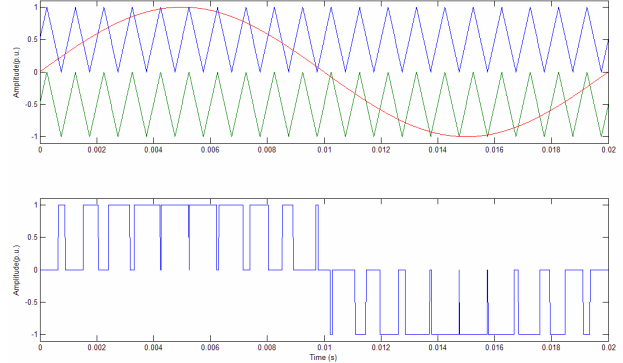


Fig. A2.11. Triangular and reference sinusoidal waves and the resulting gate pulses for a 3-level inverter.

A2.3 Diode Rectifiers and DC Bus

To simulate the three-phase six-pulse diode rectifiers (or non-controlled six-pulse rectifier, Fig. A2.12), the bridges available in the SIMULINK were used, which allow to define the main parameters related with (including the diode U_f and R_{ON}). It should be noted that the most significant characteristics for efficiency estimation purposes were considered, which are the diode forward voltage drop and the diode turn-OFF losses (turn-ON losses ignored), as referred in [39].

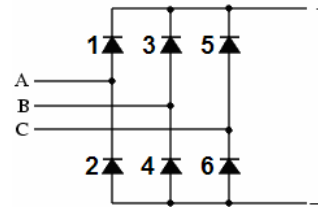


Fig. A2.12. Three-phase diode rectifier topology.

In relation to the DC-bus model feeding the inverters, for the 2-level inverter, it can have or not have an intermediate level, acting as a floating ground, being typically provided by means of two large series-connected capacitors (or capacitor sets), which constitute the main DC-bus capacitance. For the 3-level inverter, this intermediate DC-bus level is necessary. In the commercial 2- and 3-level inverters that intermediate DC-bus point, or floating ground, is not connected to the mains ground (not externally accessible). The accessible ground point of the VSDs is usually the intermediate point of two series-connected small capacitors and two large resistances in the DC bus, as it can be seen in Fig. A2.13.

Regarding the differences between the 2- and 3-level inverters, major differences were found in relation to the total DC-bus capacitance value.

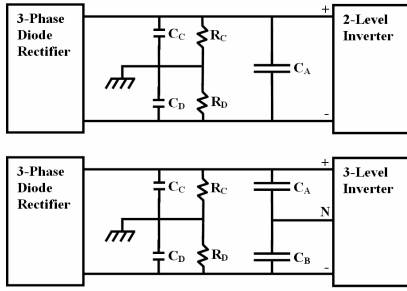


Fig. A2.13. DC-Bus capacitances in Inverter commercial VSD units: (top) 2-level inverter ($C_A \approx 250 \mu\text{F}$; $C_C = C_D \approx 0.7 \mu\text{F}$; $R_C = R_D \approx 5 \text{M}\Omega$); (bottom) 3-level inverter ($C_A \approx 225 \mu\text{F}$; $C_B \approx 225 \mu\text{F}$ $C_C = C_D \approx 0.7 \mu\text{F}$; $R_C = R_D \approx 5 \text{M}\Omega$).

A2.4 Three-Phase Cage Induction Motors

A2.4.1 Dynamic Model

To simulate three-phase, squirrel-cage, induction motors (IMs), the models available in the SIMULINK were used, named “*Asynchronous Machine Block*”. The asynchronous machine block operates in either generator or motor mode. The sign of the electromechanical torque, T_{em} , dictates the mode of operation. If $T_{em} > 0$, the machine acts as a motor, if $T_{em} < 0$, the machine acts as a generator.

The electrical part of the machine is represented by a fourth-order state-space model and the mechanical part by a second-order system [30], [31], [49]. Regarding electrical part, all electrical variables and parameters are referred to the stator in the equivalent circuits. All stator and rotor quantities are in the arbitrary two-axis reference frame (d - q frame, q -axis lagging), as it can be seen in Fig. A2.14. Subscripts d , q , r , s , l , and m , denote d axis quantity, q axis quantity, rotor quantity, stator quantity leakage inductance, and magnetizing inductance. The equations for the circuits presented in Fig. A2.14 are (A2.14)-(A2.16), where φ is the linkage flux, ω_{rr} is the rotor angular speed, ω_r is the rotor electrical angular speed ($\omega_{rr} \cdot p$), θ_{rr} is the rotor angular position, p the number of pole pairs, ω is the d - q axes angular speed, T_{em} the electromagnetic torque. The mechanical system is described by (A2.17), where T_{load} is the shaft mechanical torque, B is the combined rotor and load viscous friction coefficient (in N.m.s/rad; therefore the viscous friction torque is given by $T_{friction} = B \cdot \omega_{rr}$), and J_{syst} is the system inertia (including rotor inertia) [30], [31]. In (A2.14), for IMs, $u_{qr} = u_{dr} = 0$. The rotor quantities are referred to

stator (here, the superscript mark “ r ”, typically used to denote the quantities referred to the stator, is omitted).

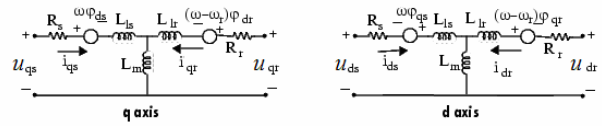


Fig. A2.14. Three-phase induction motor d - q electrical system [30].

$$\begin{cases} u_{qs} = R_s \cdot i_{qs} + \frac{d\varphi_{qs}}{dt} + \omega \cdot \varphi_{ds} \\ u_{ds} = R_s \cdot i_{ds} + \frac{d\varphi_{ds}}{dt} - \omega \cdot \varphi_{qs} \\ u_{qr} = R_r \cdot i_{qr} + \frac{d\varphi_{qr}}{dt} + (\omega - \omega_r) \cdot \varphi_{dr} \\ u_{dr} = R_r \cdot i_{dr} + \frac{d\varphi_{dr}}{dt} - (\omega - \omega_r) \cdot \varphi_{qr} \end{cases} \quad (\text{A2.14})$$

$$\begin{cases} \varphi_{qs} = L_s \cdot i_{qs} + L_m \cdot i_{qr} \\ \varphi_{ds} = L_s \cdot i_{ds} + L_m \cdot i_{dr} \\ \varphi_{qr} = L_r \cdot i_{qr} + L_m \cdot i_{qs} \\ \varphi_{dr} = L_r \cdot i_{dr} + L_m \cdot i_{ds} \\ L_s = L_{ls} + L_m \\ L_r = L_{lr} + L_m \end{cases} \quad (\text{A2.15})$$

$$T_{em} = \frac{2}{3} p (\varphi_{ds} \cdot i_{qs} - \varphi_{qs} \cdot i_{ds}) \quad (\text{A2.16})$$

$$\frac{d\omega_{rr}}{dt} = \frac{d^2\theta_{rr}}{dt^2} = \frac{1}{J_{syst}} (T_{em} - B \cdot \omega_{rr} - T_{load}) \quad (\text{A2.17})$$

SIMULINK provides a set of predetermined electrical and mechanical parameters for a number of IM ratings of power, voltage, frequency and speed.

Regarding reference frame that is used to convert input voltages (a - b - c reference frame) to the d - q reference frame, and output currents (d - q reference frame) to the a - b - c reference frame, three options are available, namely the rotor (Park transformation), stationary (Clarke or α - β transformation), and synchronous [30], [49].

The relation between the a - b - c and d - q reference frames for line-to-line voltages and phase current is described by (A2.18)-(A2.21), where θ_f is the electrical angular position of the reference frame and θ_r is the rotor electrical angular position [30]. The rotor quantities are referred to stator.

The two line-to-line input voltages are used instead of the three line-to-neutral voltages. Therefore, phase C currents are given by (A2.22).

$$\begin{bmatrix} u_{qs} \\ u_{ds} \end{bmatrix} = \frac{1}{3} \begin{bmatrix} 2 \cos \theta_f & \cos \theta_f + \sqrt{3} \sin \theta_f \\ 2 \sin \theta_f & \sin \theta_f - \sqrt{3} \cos \theta_f \end{bmatrix} \begin{bmatrix} u_{ab-s} \\ u_{cb-s} \end{bmatrix} \quad (\text{A2.18})$$

$$\begin{bmatrix} u_{qr} \\ u_{dr} \end{bmatrix} = \frac{1}{3} \begin{bmatrix} 2 \cos(\theta_f - \theta_r) & \cos(\theta_f - \theta_r) + \sqrt{3} \sin(\theta_f - \theta_r) \\ 2 \sin(\theta_f - \theta_r) & \sin(\theta_f - \theta_r) - \sqrt{3} \cos(\theta_f - \theta_r) \end{bmatrix} \begin{bmatrix} u_{ab-r} \\ u_{cb-r} \end{bmatrix} \quad (\text{A2.19})$$

$$\begin{bmatrix} i_{as} \\ i_{bs} \end{bmatrix} = \begin{bmatrix} \cos \theta_f & \sin \theta_f \\ \frac{1}{2}(-\cos \theta_f + \sqrt{3} \sin \theta_f) & \frac{1}{2}(-\sin \theta_f - \sqrt{3} \cos \theta_f) \end{bmatrix} \begin{bmatrix} i_{qs} \\ i_{ds} \end{bmatrix} \quad (\text{A2.20})$$

$$\begin{bmatrix} i_{ar} \\ i_{br} \end{bmatrix} = \begin{bmatrix} \cos(\theta_f - \theta_r) & \sin(\theta_f - \theta_r) \\ \frac{1}{2}(-\cos(\theta_f - \theta_r) + \sqrt{3} \sin(\theta_f - \theta_r)) & \frac{1}{2}(-\sin(\theta_f - \theta_r) - \sqrt{3} \cos(\theta_f - \theta_r)) \end{bmatrix} \begin{bmatrix} i_{qr} \\ i_{dr} \end{bmatrix} \quad (\text{A2.21})$$

Since it is considered that the stator-windings are connected in Y mode without neutral connection, there is no homopolar component for currents.

$$\begin{cases} i_{cs} = -i_{as} - i_{bs} \\ i_{cr} = -i_{ar} - i_{br} \end{cases} \quad (\text{A2.22})$$

The choice of reference frame affects the waveforms of all d - q variables. It also affects the simulation speed and, in certain cases, the results. Since the use of a stationary frame is recommended if unbalances or discontinuities exist in stator voltages (and the rotor voltages are balanced or null) [30], it was the selected reference for the simulations and, therefore, $\theta_f = 0$. In the available models, some initial conditions can also be defined, namely, slip, electrical angle, stator current magnitude and phase angle.

Regarding the limitations, the model described does not include representation of iron losses and saturation. Moreover, neither skin effect influence on the rotor resistance and inductance nor thermal compensation are included.

A2.4.2 Equivalent Circuit-Based Model with Thermal Compensation

When IMs are fed by distorted power sources, e.g., voltage-source PWM inverters or installations with poor PQ, their performance can be significantly affected. The time and space harmonics, which mainly depend on the stator winding features, influence the motor performance. IMs performance is also affected by the internal temperature, which also affects their lifetime. The core saturation and the skin effect also affect the IM behaviour, forcing its mathematical representation to be nonlinear. Therefore, when simulating IMs, the time and space harmonics, the core saturation, the skin effect, and the temperature variation should be taken into account, particularly for motors driving variable speed loads.

Several steady-state or dynamic IM models (e.g., d - q models), based on modified or extended per-phase equivalent circuit models (ECMs) were proposed in previous works [1]-[5], [37], [49]. A dynamic model including SLLs and core losses, and with a simple thermal compensation is proposed in [37], to improve rotor time constant estimation and vector control. Since they are based in only one ECM, the proposed models have a common drawback - the skin effect cannot be properly embedded in only one circuit, because it has a different impact for each harmonic frequency, unless the resistance is defined as a function of current time variation instead of current frequency, which is a complex task. Moreover, these models require complex FEM-based analysis and the thermal compensation is in most cases not considered. In fact, the estimation of the motor internal temperatures is important for accurate motor performance estimation and compensation of the motor parameters used in the modern control strategies implemented in the VSDs, e.g., avoiding detuning when vector control strategies are used and allowing optimum efficiency control of IMs. In [6] tuned filters at the input of the ECM were proposed in order to improve the accuracy (or the response) of the waveforms, when PWM supply is considered. Of the several possible ECM descriptions in form of a two-port

network (e.g., Γ and T), the T-model (or the exact equivalent circuit) is prominent because it reflects best the motor physical properties [5]. In [7]-[10] some thermal considerations in the ECM were proposed.

In this section, a motor simulation matrix model based on a multi-frequency, T-model, nonlinear ECM, considering stator-winding MMF space harmonics and thermal compensation, is proposed [26], being used in a number of simulations presented in this thesis. The proposed model is meant for steady-state analysis, but the principles discussed can also be applied to dynamic models.

Moreover, it allows taking into account the stator winding characteristics, skin effect, core saturation and the motor thermal behaviour, and can be used to estimate the motor torque-speed capability curves and the change of the motor performance along the operation periods, particularly for the motors driving variable speed and/or variable torque loads. The proposed model can be also used to study the impact of space and time harmonics on the motor performance.

A2.4.2.1 Per-Phase Equivalent Circuit Matrix Model

In order to define a more accurate, easy-to-obtain steady-state equivalent circuit for each voltage time harmonic, one of the aims of this work is to use experimental-based estimated lumped-parameters, obtained by typical motor standard test procedures, and assuming some well known motor behaviours related to temperature (affecting resistive parameters), frequency (affecting the resistive and inductive parameters) and saturation of the main flux paths² (affecting magnetizing inductance), rendering the representation nonlinear.

The proposed multi-frequency lumped-parameter ECM is important for the study of the behaviour of cage induction motors fed by non-sinusoidal voltage sources (i.e., sources with a significant harmonic distortion), as those fed by PWM voltage-source inverters. In all the following considerations a balanced three-phase system is assumed.

For a given frequency, the IM parameters in the proposed lumped-parameter ECM (Fig. A2.15) are, in part, derived and measured from no-load and impedance tests data, according to IEEE 112-B Std. [11], for different voltages and frequencies. Rotor voltage, current, resistance, and reactance values are all referred to the stator and are not absolute rotor values.

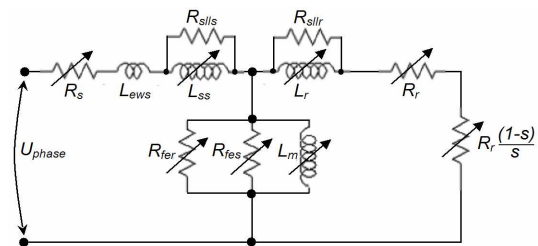


Fig. A2.15. Proposed lumped-parameter modified per-phase equivalent circuit for squirrel-cage three-phase induction motors [26].

² Leakage flux paths and, therefore, leakage inductances, are also affected by saturation but in a lower extent. In fact, for moderated levels of saturation, negligible variation occurs in relation to magnetizing inductance variation, as a function of the saturation or magnetizing current.

The stator resistance, R_s , is defined as a function of temperature and frequency, the in-slot stator leakage inductance, L_{ss} , and the stator end-windings leakage, L_{sew} , are defined as a function of frequency. The stray-load losses (SLLs) resistances, R_{slls} and R_{sllr} , are considered constant³, the rotor resistance, R_r , is defined as a function of temperature and rotor current fundamental frequency, the rotor leakage inductance, L_r , is defined as a function of temperature, frequency and saturation, the stator core losses resistance, R_{fes} , is defined as a function of temperature and frequency, the rotor core losses resistance, R_{fer} , is defined as a function of the rotor frequency and temperature. In Fig. A2.16, the temperature effect on core losses is shown.

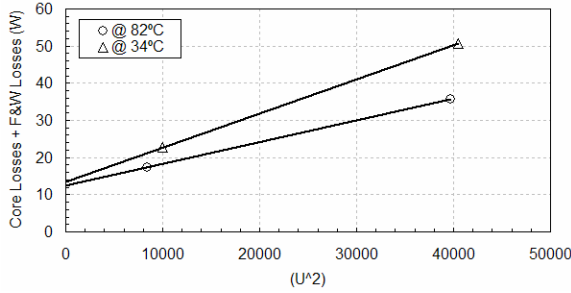


Fig. A2.16. Core losses plus friction & windage losses as a function of the squared voltage for a 3-kW, 4-pole IM, considering two different temperatures.

In order to estimate the parameters of the circuit considered in Fig. A2.15, including their dependency on frequency, temperature and/or saturation, no-load and impedance tests were performed for different frequencies in the range 5-100 Hz (including constant U/f and constant- f variable- U tests, and the IEEE 112 Method 2 test procedure), combined with classical mathematical approaches (which can be found in [2], [4], [5], [7], [8], [12], [14]-[16], [20]-[22], and [50]) and some new calculation/estimation procedures. The parameters can be considered valid for frequencies up to 2 kHz, and the effect of the parasitic (or stray) capacitances (between windings and stator core, windings and rotor, and stator core and rotor) in the motor are not considered, which, for the frequency range considered and for the purpose of the model, can be ignored.

The stator leakage inductance was separated into end-windings and in-slot leakage inductances, L_{ews} and L_{ss} (the total stator leakage is $L_s = L_{ews} + L_{ss}$).

The stator core losses were estimated on the basis of the IEEE 112-B Std. procedures, for different frequencies, which allow the calculation of the constants used in the classical equations that describe the eddy current and hysteresis losses as a function of frequency. Classical formulations for thermal compensation and skin effect impact on eddy current loss component were used.

The rotor core losses are represented by the parameter R_{fer} , which is in parallel with stator core losses resistance, R_{fes} . In [37] and [38], it is assumed that the stator and rotor cores have the same quantity of active iron producing

core losses, which is not true for most cases. The approximate relation between stator and rotor core losses is obtained from the relationship between stator and rotor core volume or mass. In fact, the rotor core losses can be significant when compared to stator core losses, particularly in heavy load operation, and if harmonic core losses were considered [20], [21]. Based on that, R_{fer} is estimated according to the relation between the stator and rotor core mass, m , according to (A2.23), for unitary slip. The R_{fer} value depends on frequency, slip, and temperature. For null slip, the P_{fer} is approximately zero.

$$R_{fer} = R_{fes} \frac{m_s}{m_r} \quad (\text{A2.23})$$

Ignoring skin effect on core sheets, iron losses can be described approximately by (A2.24). The maximum induction or flux density B_{max} is proportional to the air-gap voltage E . Assuming that B_{max} is uniform over the cross-section area, A , of the core, B_{max} is given by (A2.25), where K_{mtr} is a machine constant, E is the air-gap voltage, K_h hysteresis core losses coefficient, K_e eddy current core losses coefficient, n is Steinmetz coefficient (n can have values within 1.5-2.5, but a 2.0 average value is assumed, for the sake of simplicity [37]) and f is the frequency. The per-phase iron losses can be written as in (A2.26).

$$P_{fe} \approx K_h \cdot f \cdot B_{max}^n + K_e \cdot f^2 \cdot B_{max}^2 \quad (\text{A2.24})$$

$$B_{max} = K_{mtr} \cdot E \cdot f^{-1} \quad (\text{A2.25})$$

$$P_{fe} \approx (K_h \cdot f^{-1} + K_e) \cdot E^2 \cdot K_{mtr}^2 \quad (\text{A2.26})$$

The per-phase representation of the iron losses by means of a resistance in parallel with the magnetizing inductance is given by (A2.27).

$$R_{fe} = \frac{E^2}{P_{fe}} = K_{mtr}^{-2} \cdot (K_h \cdot f^{-1} + K_e)^{-1} \quad (\text{A2.27})$$

Therefore, considering two different frequencies f' and f'' , (A2.28) can be written.

$$\frac{R_{fe}''}{R_{fe}'} = \frac{f''(K_h + f' \cdot K_e)}{f'(K_h + f'' \cdot K_e)} \quad (\text{A2.28})$$

Considering f' the base frequency, it is then possible to compute the R_{fe} for different frequencies, considering as inputs the base and actual frequency, base resistance, hysteresis loss component constant, and eddy currents loss component constant. For moderate frequencies and low eddy current loss coefficient, it is expected that $K_h \gg f \cdot K_e$, and, for those cases, (A2.28) can be simplified to (A2.29).

$$\frac{R_{fe}''}{R_{fe}'} = \frac{f''}{f'} \quad (\text{A2.29})$$

³ The SLLs can be represented by a series resistance in the rotor branch of the ECM (i.e., SLLs proportional to the squared rotor current). In fact, for small motors, the SLLs are actually concentrated in the rotor.

The eddy currents loss coefficient is also thermal compensated using (A2.30), where the iron conductivity depends on the temperature, which is estimated by the thermal model. However, this compensation has minor impact on iron loss estimation for normal operating temperature and low eddy-current coefficients.

$$\frac{K_e''}{K_e'} = \frac{\sigma_{fe}''}{\sigma_{fe}'} \quad (\text{A2.30})$$

SLLs are mainly related to the iron losses associated with stator and rotor leakage flux paths (which depends on several phenomena, e.g., non-symmetry of the machine, such as eccentricity and anisotropy), slotting effects, eddy currents induced on the in-slot conductors crossed by stray fluxes (particularly relevant for high frequency excitations, e.g., related to harmonics, and/or high loads), and rotor slot inter-bar currents. The additional losses in the stator and rotor teeth due to slot leakage flux, which depends on induction level (e.g., the increase with the induction level of the rotor losses induced by the passing of the stator teeth facing it). From the no-load test, it can be seen that the rotor Joule losses, which are negligible with the nominal voltage, increase as soon as the induction level increases, which reveals that the stator teeth induce high-frequency currents in the rotor cage [23]. There are also losses due the eddy currents on the conductors crossed by stray time-varying fields. The no-load and impedance (or locked rotor) tests are insufficient to estimate the SLLs. However, it is possible to obtain the SLLs from the IEEE 112-B or, alternatively, from the Eh-Star Method (considered as medium-high uncertainty method) in the new standard IEC60034-2-1, which have a significant impact in the motor efficiency as it was demonstrated in [24] and [25]. To represent SLLs, additional parameters were introduced in the ECM additional resistances were considered, R_{slls} and R_{sllr} , namely, in parallel with L_{ss} and L_r leakage inductances, respectively [1], [2]. These parameters are hard to estimate by analytical methods or by FEM [2]. However, they can be approximately estimated using the SLLs value, P_{sll} , and the stator currents for a specific load point. Considering R_{slls} and R_{sllr} equal for the base frequency (equal distribution of SLL over rotor and stator), their estimation for a specific load point is proposed as in (A2.31). However, since the rotor SLL component is higher than the stator component for small-medium motors⁴, $\frac{1}{4}$ and $\frac{3}{4}$ of SLLs are imputed to stator and rotor, respectively, requiring a slight change in (A2.31).

$$R_{slls} = 24 \frac{(\pi \cdot f_s \cdot L_{ss} \cdot I_s)^2}{P_{sll}} \quad (\text{A2.31})$$

The importance of SLLs on the overall motor losses increases with the rating increase, as it can be seen in Fig. A2.17. In [37] and [38], since it is considered that SLLs are approximately proportional to the square of the rotor current, a resistance is used in the rotor branch of the

⁴ In IEEE 112-B Std., SLLs are set to zero at no-load. Therefore, on that basis, SLLs can be represented by a resistance in the rotor branch (i.e., it is assumed that SLLs are only located in the rotor).

equivalent circuit, which is also an alternative way to represent SLLs in low/medium IMs.

One of the critical parameters is the magnetizing inductance, L_m , which strongly depends on saturation [43], [44]. The effect of saturation on leakage inductances can be ignored [38]. From no-load tests, the magnetizing inductance variation with the magnetizing current can be estimated from experimental tests (Fig. A2.18).

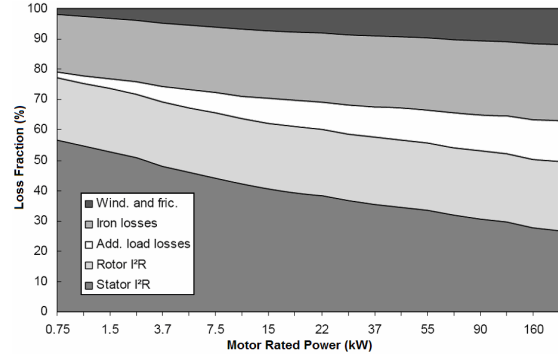


Fig. A2.17. Fraction of full-load losses for 4-pole IMs (Add. load losses = SLLs) [48].

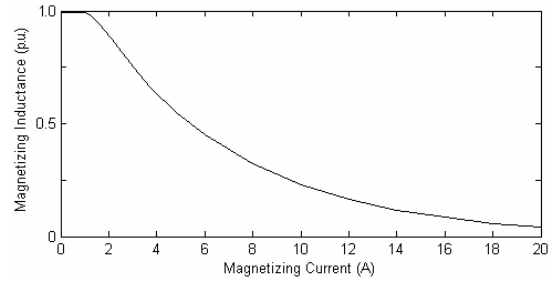


Fig. A2.18. Magnetizing inductance as a function of magnetizing current curve for a 3-kW, 4-pole IM. Curve obtained on the basis of experimental results.

When saturation occurs in an IM, the relation between electrical quantities becomes nonlinear⁵. This can be handled by considering the equivalent circuit linear in a per period basis, being the impedances adapted as a function of the saturation level, slip and temperature. The saturation is introduced by means of a variable magnetizing inductance as a function of the magnetizing current, which in turn depends on the magnetizing inductance⁶. Therefore, after a number of iterations a stable point is reached for both variables. The same apply

⁵ This is an important approximation to allow the application of the superposition principle. The superposition principle, applied to linear systems, establishes that the response produced by the simultaneous application of two or more different excitations is equal to the sum of the individual responses. Consequently, for linear systems the response to a number of inputs can be calculated considering only one input at a time and adding the results. This principle allows the construction of complicated solutions for linear differential equations from simple solutions. There are time-invariant and time-variant linear systems. A differential equation is linear if the coefficients are constant or a function of (and only) the independent variable. In practice, all real systems have some non-linear relations between variables, in some ranges. However, in some ranges, they can be approximated to linear systems. The normal operation of a system can be around an equilibrium point, and the signals can be considered small around that point. In these cases, it is possible to approximate a nonlinear system to a linear system, for a limited operation range.

⁶ This technique is similar to that used in [38] to deal with saturation, but it uses experimental results.

to temperature since the parameters of the circuit influence the losses and thus the temperature of the motor, which in turn influences the value of the parameters.

In delta-connected windings, due, in part, to the core saturation, delta-circulating currents (e.g., 3rd order harmonic currents) are produced⁷, which contribute to additional losses in the windings. However, the losses associated with the circulating currents are not considered in the proposed model.

Since the proposed model is a per-period linearized model, for the sake of simplicity, the saturation for the time harmonics, represented by the magnetizing inductance variation, is a function of the degree of deviation between the magnetizing inductance nominal and actual values for fundamental frequency.

Regarding the rotor parameters (R_r and L_r) representation for different rotor types (e.g., deep-bar, double-cage, etc.), since they are inherently estimated as a function of rotor frequency or slip by means of the locked rotor test, and that dependency is directly implemented in the ECM, it is avoided, for example, the use of two parallel impedance branches to describe a double-cage rotor, as it can be seen in Fig. A2.19 (similarly to the method used by some manufacturers to describe the motor impedance for key operating points, according to the IEC standard, e.g., for a 2-pole, 200-kW LV IM: $R_{r(start)} = 26 \text{ m}\Omega$; $R_{r(rated_slip)} = 4.8 \text{ m}\Omega$; $L_{r(start)} = 0.1337 \text{ mH}$; $L_{r(rated_slip)} = 0.5730 \text{ mH}$. Curiously, in these cases, the friction and windage losses are embedded in the core loss resistance.

A2.4.2.2 Time and Spatial Harmonics

The harmonic content of the rotating air-gap MMF waveform results from the interaction between the excitation time harmonics and the MMF space harmonics. The resulting torque-speed curve (Fig. A2.20) depends on the MMF waveform. In the following analysis, although relevant, the slot effects and related spatial harmonics are ignored. Neglecting the even and triplen harmonics, besides the fundamental, there are two groups of time and space harmonics to be considered, interacting all each other, namely, $6n+1$, or positive sequence, which produce positive rotating field, and $6n-1$, or negative sequence, which produce negative rotating field, being n a positive integer [26].

Time Harmonics - In the absence of spatial harmonics, the excitation time harmonics, of h^{th} order, will produce, each one, harmonic rotating MMFs with different amplitude, angular speed and direction. The negative-sequence harmonic rotating MMFs rotate in opposite (or backward) direction to the fundamental MMF, producing opposite torque. The positive-sequence order harmonic rotating MMFs rotate in the same (or forward) direction as fundamental MMF, producing an adding torque. For example, for a 4-pole motor, the 5th time harmonic component of the winding excitation produces a rotating MMF in the opposite direction, with angular speed 5 times higher than fundamental. In the proposed model, the

user defines the voltage time harmonics amplitude. The effects of time harmonics on torque-speed curves are represented in Fig. A2.20b.

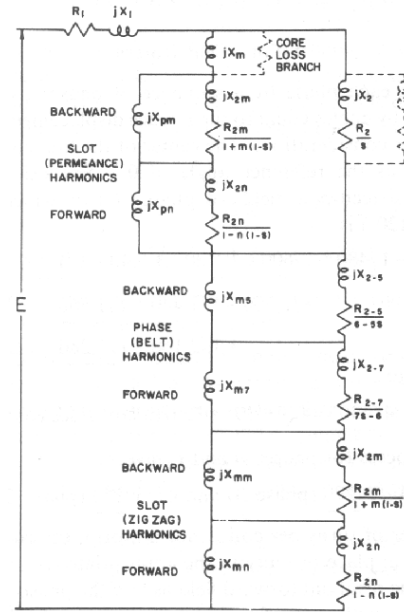


Fig. A2.19. General equivalent circuit for a three-phase induction motor (classical approach) [28], [32].

It should be noted that the harmonic currents calculation using the ECM assumes that the distorted voltages are periodic, thus can be decomposed in Fourier series and analyzed using the superposition principle. Assuming three symmetric voltages and a balanced motor, only one phase and odd nontriplen harmonics are required for motor performance analyses.

Space harmonics - Assuming now that the excitation is purely sinusoidal, the space harmonics, of s^{th} order, will produce, each one, harmonic rotating MMFs with different amplitude, angular speed and direction. The negative-sequence space harmonic rotating MMFs rotate in opposite direction to the fundamental MMF, producing opposite torque. The positive-sequence space harmonic rotating MMFs rotate in the same direction as fundamental MMF, but with lower angular speed, affecting negatively the torque in the steady-state operation. The space harmonics can be interpreted as coexisting multiple pole-pairs, also called “shaft machines”. For example, for a 4-pole motor, the 5th space harmonic, for a purely sinusoidal excitation, is similar to an additional winding with 10 pole-pairs, which produces a rotating MMF in opposite direction with angular speed 5 times lower than fundamental. The effects of space harmonics on torque-speed curves are represented in Fig. A2.20a.

Typically, spatial harmonics are represented by the extended ECM shown in Fig. A2.19, whose parameters can be, in principle, calculated, but it is likely to be a very complex and time-consuming task [28], [32], [33]. With the proposed approach, the representation results rather simple since the fundamental-frequency circuit parameters are used to simulate the spatial harmonics, although, in principle, less accurate.

⁷ For electromagnetic balanced motors, fluxes produced by the per-phase 3rd order current harmonics cancel each other, but the currents can still circulate.

Space harmonics depend mainly on the stator winding factors, which depend on the number of stator and rotor slots, poles, winding type, number of coil sides per slot and coil pitch, according to well-known formulas or computing algorithms [13]. For a specific winding configuration, one can use the respective winding factor to estimate the voltage to be applied on a specific spatial harmonic ECM, ignoring the stator impedance ($Z_s = R_s + jX_s$) voltage drop and the rotor field interaction.

Space and Time Harmonics Interaction - When both space and time harmonics coexist, the resultant MMFs can be estimated. For example, considering the previous examples, the effect of the 5th time harmonic ($h = 5$) winding excitation component on the 5th space harmonic

($s = 5$) is the production of a rotating MMF with the same speed and direction of the fundamental MMF, but with lower amplitude. The final voltage to be applied to the harmonic pair s - h ECM (s – space harmonic order; h – time harmonic order), $U_{ph(s-h)}$, is defined by (A2.32), which reflects the amplitude of the MMF produced in the air-gap by the stator winding, when it is sinusoidally excited, where m is the maximum nontriplen, odd space harmonics order to be considered and K_w the stator winding factor [26].

$$U_{ph(s-h)} = U_{ph(h)} \cdot \frac{K_{ws} \cdot s^{-1}}{\sqrt{\sum_{n=1}^m (K_{wn} \cdot n^{-1})^2}} \quad (\text{A2.32})$$

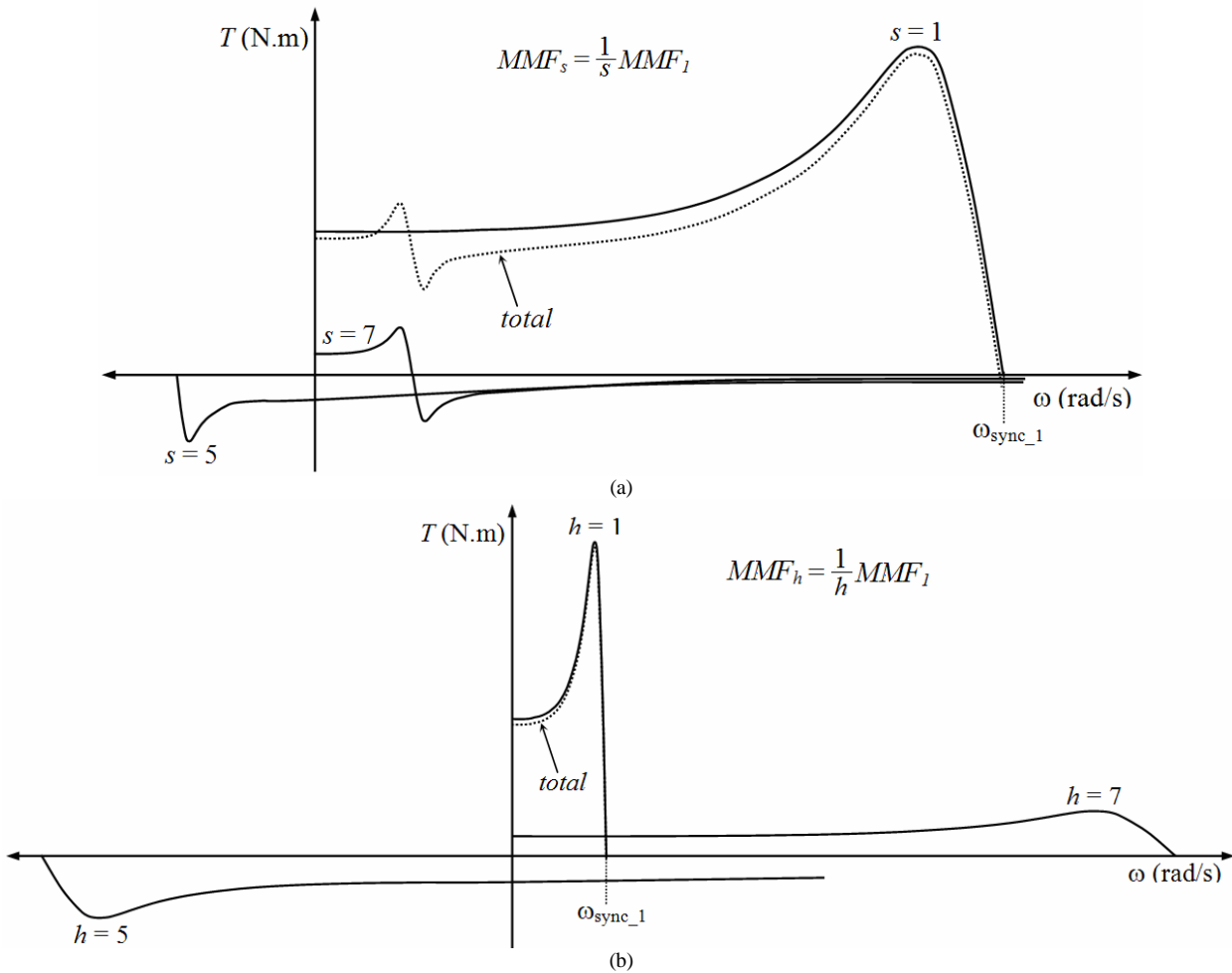


Fig. A2.20. Approximate representation of the independent effect of time and spatial harmonics on the torque-speed curve of IMs, considering: (a) 5th and 7th order spatial harmonics; (b) 5th and 7th order time harmonics.

The number of “shaft machine” pole-pairs is s and the excitation frequency is $f_h = h \cdot f_1$, being f_1 the fundamental frequency. The slip associated with each ECM is trivially given by $s_{(s-h)} = (\omega_{sync(s-h)} - \omega_{rr}) / \omega_{sync(s-h)}$. The torque sign has to be properly defined. A matrix of ECMs with $s \times h$ size is needed to implement the h time and s space harmonics to be considered. For example, besides the fundamental, if the 5th, 7th, 11th and 13th space and the 5th, 7th, 11th, 13th, 17th and 19th time harmonics were considered, a 5×7 matrix is needed. Each element of the matrix has an independent ECM, with appropriate

parameter values and pole-pairs. When spatial and time harmonics with same direction rotating MMF (either positive or negative speed) interact, a positive torque results, otherwise, a negative torque results. In (A2.33), the matrix of pairs s - h is shown.

In (A2.34), the resultant synchronous speeds matrix to each of the pairs in (A2.33) is shown, including the rotation direction in superscript (“+” signal denotes the fundamental forward direction, and “-” signal the opposite backward direction).

$$(s-h) = \begin{bmatrix} 1-1 & 1-5 & 1-7 & 1-11 & 1-13 & 1-17 & 1-19 \\ 5-1 & 5-5 & 5-7 & 5-11 & 5-13 & 5-17 & 5-19 \\ 7-1 & 7-5 & 7-7 & 7-11 & 7-13 & 7-17 & 7-19 \\ 11-1 & 11-5 & 11-7 & 11-11 & 11-13 & 11-17 & 11-19 \\ 13-1 & 13-5 & 13-7 & 13-11 & 13-13 & 13-17 & 13-19 \end{bmatrix} \quad (\text{A2.33})$$

$$\frac{\omega_{\text{sync}(s-h)}}{\omega_{\text{sync}(1-1)}} = \begin{bmatrix} 1.00^+ & 5.00^- & 7.00^+ & 11.0^- & 13.0^+ & 17.0^- & 19.0^+ \\ 0.20^- & 1.00^+ & 1.40^- & 2.20^+ & 2.60^- & 3.40^+ & 3.80^- \\ 0.14^+ & 0.71^- & 1.00^+ & 1.57^- & 1.86^+ & 2.43^- & 2.71^+ \\ 0.09^- & 0.45^+ & 0.64^- & 1.00^+ & 1.18^- & 1.55^+ & 1.73^- \\ 0.08^+ & 0.38^- & 0.54^+ & 0.85^- & 1.00^+ & 1.31^- & 1.46^+ \end{bmatrix} \quad (\text{A2.34})$$

The negative speeds create negative torque and speeds below fundamental create dragging torque, both contributing to reduce the resultant torque, and to create dips in the starting zone of the torque-speed curve. The speed equal or higher than fundamental, create useful torque, both adding to the resultant torque. Typically, the mean torque contribution due to the harmonics is small. Therefore, the harmonic input power is almost all converted into losses [4]. From (A2.32), (A2.33), and (A2.34), 35 outputs can be computed, e.g., produced torque, loss components, input power, output power, etc. Only the fundamental space-time ECM has the friction and windage loss parameters. Based on the superposition principle, the overall motor outputs are obtained by means of proper summation of the individual components of each ECM. The summation of all the losses is particularly important not only for efficiency estimation but also for temperature estimation, which is an input of the thermal model, presented next. Note that the slip has to be properly determined for each ECM, based on the rotor speed that results of the imposed load, in which the motor rotor inertia has to be included. If a slip-based steady-state analysis is to be made, the speed of the fundamental ECM is used to calculate the slip for the harmonic ECMs. The efficiency is considered to be equal to the quotient between total output power and total input power. For the balanced operation, the power factor is given by the ratio of the total input real (or active) power and apparent power (calculated on the basis of total current and voltage RMS values), including all harmonics. Additional considerations on power factor are given in Section A2.4.2.6.

Air-gap torque pulsations (that result in vibration and acoustical noise) result from the interaction between rotor MMFs and stator magnetizing MMFs (e.g. interaction between fundamental rotor flux and excitation 5th and 7th harmonics) and, although important, are not considered in the presented model. However, the impact of harmonics in the electromagnetic torque and vibration can be analyzed as follows. Using complex or phasor notation, (A2.35) can be written (rotor quantities referred to stator), where ω is the angular frequency of the stator quantities (orthogonal d - q axes moving at angular speed ω) and ω_{rr} is the rotor angular speed. Here, single rotor cage is considered and core losses are ignored. On the basis of A2.35, the electromagnetic torque is given by (A2.36).

Assuming rotor fluxes essentially sinusoidal (rotor reacts mainly to the fundamental), one pair of poles ($p = 1$), and null initial instant flux angle, (A2.37) can be

written, where ω is the stator excitation frequency. Considering only the 5th and 7th time harmonics, the stator currents can be described by (A2.38) and the electromagnetic torque yields (A2.39). Considering $\gamma_{s5} = \gamma_{s7} = 0$, the electromagnetic torque yields as in (A2.40).

$$\begin{cases} \bar{u}_s = u_{ds} + j \cdot u_{qs} \\ \bar{u}_r = u_{dr} + j \cdot u_{qr} \\ \bar{\phi}_s = \phi_{ds} + j \cdot \phi_{qs} \\ \bar{\phi}_r = \phi_{dr} + j \cdot \phi_{qr} \\ \bar{i}_s = i_{ds} + j \cdot i_{qs} \\ \bar{i}_r = i_{dr} + j \cdot i_{qr} \\ \bar{u}_s = R_s \cdot \bar{i}_s + \frac{d\bar{\phi}_s}{dt} + j \cdot \omega \cdot \bar{\phi}_s \\ 0 = R_r \cdot \bar{i}_r + \frac{d\bar{\phi}_r}{dt} + j(\omega - p \cdot \omega_{rr})\bar{\phi}_r \end{cases} \quad (\text{A2.35})$$

$$\begin{aligned} T_{em} &= \frac{3}{2} p \cdot L_m (\bar{i}_{qs} \cdot i_{dr} - i_{ds} \cdot \bar{i}_{qr}) = \\ &= \frac{3}{2} p \cdot \frac{L_m}{L_r} (\phi_{dr} \cdot i_{qs} - \phi_{qr} \cdot i_{ds}) = \frac{3}{2} p \cdot \frac{L_m}{L_r} \text{Re}\{j\bar{\phi}_r \bar{i}_s^*\} \end{aligned} \quad (\text{A2.36})$$

$$\bar{\phi}_r = \phi_r e^{j\alpha} \quad (\text{A2.37})$$

$$\begin{aligned} \bar{i}_s &= I_{s1} e^{j(\omega t + \gamma_{s1})} + \\ &+ I_{s5} e^{j(-5\omega t + \gamma_{s5})} + \\ &+ I_{s7} e^{j(7\omega t + \gamma_{s7})} \end{aligned} \quad (\text{A2.38})$$

$$T_{em} = \frac{3}{2} \frac{L_m}{L_r} \phi_r \text{Re} \left\{ \begin{aligned} &j I_{s1} e^{j(-\gamma_{s1})} + \\ &+ j I_{s5} e^{j(6\omega t - \gamma_{s5})} + \\ &+ j I_{s7} e^{j(-6\omega t - \gamma_{s7})} \end{aligned} \right\} \quad (\text{A2.39})$$

$$T_{em} = \frac{3}{2} \frac{L_m}{L_r} \phi_r \left[I_{s1} \sin(\gamma_{s1}) + (I_{s7} - I_{s5}) \sin(6\omega_s t) \right] \quad (\text{A2.40})$$

These results can be easily generalized. Therefore, the 5th and 7th current harmonics interacting with rotor flux, lead to the production of a pulsating or oscillating torque component (6th order torque harmonic), which results in motor vibration.

A2.4.2.3 Thermal Model with Lumped Parameters

For the thermal compensation of the resistive ECM parameters, the average temperature of the spot that they represent in the motor has to be known, which in turn depends on the ambient temperature, motor losses and

motor equivalent thermal capacity and resistance. The proposed motor thermal model (TM) is based on well-known simplified lumped-parameter thermal steady-state circuit models, but incorporates also an estimated per-node thermal capacity to allow the study of the motor thermal transient behaviour, which is very important for the variable-load, variable-speed motors, providing useful information to estimate the internal temperature variation as a function of the motor operating point, including the estimated total losses, rotor speed and the speed and temperature of the external cooling air.

According to [23], in the case of TEFC low-power motors, it is possible to conclude that the main part of the heat transfer is governed by conduction in the stator. The contribution of the convection in the thermal exchanges of stator end-windings is not negligible. The radiation heat transfer mode has a minor contribution in the stator and rotor and, therefore, can be ignored. Based on that, for average temperature estimation purposes in the TEFC low-power IMs, the TM shown in Fig. A2.21 is proposed. The presented TM is significantly simplified when compared to other previously proposed nets [9], [10]. Since its aim is the estimation of the average temperature in key points for the thermal compensation of ECM resistive parameters, seven points were considered, namely: stator windings, stator core, rotor, bearings, frame, shaft, and stator core teeth.

The equivalent thermal resistances used in the TM circuit, were obtained and calibrated from experimental data and well-known analytical equations. The equivalent thermal capacitances for the considered points were computed using analytical equations, which take into account the mass and calorific capacitance of the different materials. The controlled current sources represent the loss sources in each node, and are equal to the estimated loss power. The frame-ambient equivalent thermal resistance, R_{fa} , depends on the linear speed of the air flux along the external surface of the frame (which, in fact, varies along the frame length). The thermal resistance representing the convection between the stator end-windings and the frame, R_{wf} , also depends on the rotor speed.

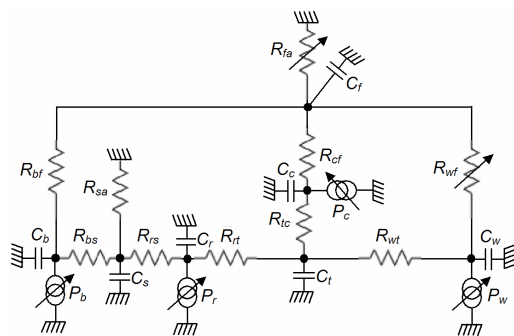


Fig. A2.21. Proposed nonlinear simplified lumped-parameter thermal equivalent circuit for a totally enclosed cage induction motor (Thermal resistances: R_{fa} - frame-ambient, R_{cf} - core-frame, R_{tc} - teeth-core, R_{wf} - winding-teeth, R_{wf} - end winding-frame, R_{rt} - rotor-teeth, R_{rs} - rotor-shaft, R_{sa} - shaft-ambient, R_{bs} - bearings-shaft, R_{bf} - bearings-frame; Thermal or heat capacities: C_f - frame, C_c - core, C_t - teeth, C_w - stator windings, C_r - rotor, C_s - shaft, C_b - bearings; Sources: P_c - core losses, P_w - stator winding losses, P_r - rotor losses, P_b - bearing friction losses).

Thermal resistances were calculated from a number of experimental tests, including DC- and AC-current tests and tests at different speeds. Confirmation/adjustment of the simulation model by means of external and stator winding temperatures was made. Rotor temperature was also measured for verification purposes by means of a fast blocked rotor test.

A2.4.2.4 Matrix Model with Thermal Compensation

The proposed hybrid model includes both the ECMs matrix and the TM, and was developed using SIMULINK/MATLAB language. Since the thermal time constant is significantly higher than the electrical time constant (and, typically, higher than the mechanical time constant), the motor transient TM was directly combined with the steady-state ECM matrix, as shown in Fig. A2.22. In order to test the proposed hybrid model, the electrical, mechanical and thermal parameters for a 3-kW, low-voltage, three-phase, TEFC, squirrel-cage induction motor, were estimated experimentally.

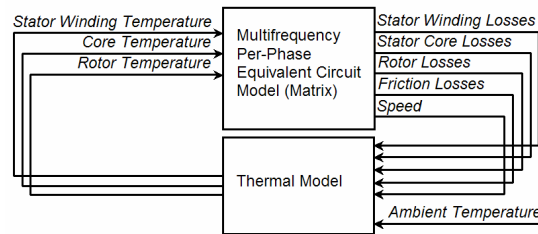


Fig. A2.22. Multifrequency per-phase nonlinear equivalent circuit matrix model with thermal compensation for IMs.

A2.4.2.5 Change of the ECM Parameters as a Function of Stator Winding Connection and Motor Active Materials

Using the software BOBISOFT (described in Appendix 3 and Appendix 6) it is possible to simulate the impact of the different stator winding types in the resistance and leakage reactance associated with the end-windings, from a relative perspective. Assuming a fixed rotating MMF fundamental value and impedance symmetry, these variations can be used to change the respective values in the equivalent circuits. Therefore, it is possible to estimate the improvement in the motor efficiency reached by the winding type change. For example, a leakage inductance depends on the squared number of turns and on the end-windings length, and the stator resistance depends on the end-windings length and on the number of turns. These values are automatically computed by BOBISOFT, assuming that end-winding shape is maintained. The number of turns change can be studied in a similar form, being necessary to change properly the values of all ECM parameters, including the rotor parameters (referred to stator), except the iron loss resistance, which actually depends on the resultant magnetizing flux and frequency.

The stator-winding connection change can be simulated by either changing the phase voltage applied to the ECM or changing the parameters value (see Chapter 5). However, it should be noted that the star connection (without neutral connection) blocks the phase homopolar currents (e.g., odd, triplen harmonics) and therefore, these

components should not be considered, even if they exist in the power supply. In the delta connection, there are no homopolar voltages between the winding terminals, but circulating currents can exist, which can be considered if additional homopolar circuits are used in the ECM matrix, in order to take into account the associated losses. However, if the motor is tested in delta connection, the computed parameters already include the additional losses associated with the eventual circulating currents. When the circulating currents are significant, the delta-based computed parameters are inadequate for the star simulation, using the conversion scheme presented in Chapter 5.

Therefore, it is recommended the motor to be tested in delta and star considering the same phase fundamental voltage, followed by a comparison of the results in order to estimate the relevance of the circulating-current losses.

In short, neglecting the delta circulating-current losses, and assuming that the aspects related to the saturation are properly addressed, the star to delta change and vice-versa, requires only the proper change of either the voltage level or the parameters value for each specific time harmonic.

The active materials and/or core length change can also be studied by properly changing the per-phase equivalent circuit parameters, either using analytical calculations, design software, or experimental tests of prototypes. In Table A2.3, the main characteristics and parameters of seven 4-pole, 7.5-kW IMs (with identical frame size), are shown.

TABLE I
CHARACTERISTICS OF THE TESTED
AND SIMULATED IMs (7.5 kW, 4 POLES, TEFC, 231/400V) [47].

	SSAL	SSCU	PSCU	LSSCU	LPSCU	C-CU	C-AL
Steel Type	SS	SS	PS	SS	PS	N/A	SPS
Cage Material	Al	Cu	Cu	Cu	Cu	Cu	Al
Stator Slots	36	36	36	36	36	36	48
Rotor Slots	46	46	46	46	46	N/A	40
l_{stack} (mm)	160	160	160	180	180	N/A	170
L_r (H)	0.0062	0.0053	0.0055	0.0024	0.0024	0.0058	0.0033
L_m (H)	0.0848	0.0887	0.0908	0.0812	0.0928	0.1212	0.1174
R_r (Ω)	0.2672	0.141	0.1659	0.1938	0.1883	0.2103	0.2982
R_s (Ω)	0.503	0.5242	0.505	0.4128	0.4169	0.4769	0.5052
L_s (H)	0.0092	0.0079	0.0082	0.0036	0.0036	0.0083	0.0043

Five motors have an identical stator and rotor cross-sectional geometry. The first IM has a standard magnetic steel (SS) core and an aluminium-cage rotor. The second IM (denoted by SSCV) has a core equal to that of the SSAL, but a copper-cage rotor. The third IM (denoted by PSCU) has premium magnetic steel (PS) and a copper-cage rotor. The fourth and fifth IMs (denoted by LSSCU and LPSCU, respectively), are longer stack length versions of SSCU and PSCU designs. The last two motors are commercial EFF 1-class IMs, one with copper-cage rotor (denoted by C-CU) and one with aluminium-cage rotor (denoted by C-AL). The relative permeability and specific loss at 50 Hz and 1.5 T of the SS, PS and SPS are 1700, 1550 and 2470 and 5.5, 3.5 and 3.7 W/kg, respectively.

A2.4.2.6 Operation with Unbalanced Supply

The simulation of the voltage unbalance impact in the motor performance is also important. The proposed model

allows, with a number of minor changes, to study this issue effectively.

According to the Fortescue theorem, an unbalanced three-phase system can be decomposed in three balanced or symmetrical systems (three phasors with the same magnitude): direct system (or positive sequence), \mathbf{U}^+ , inverse system (or negative sequence), \mathbf{U}^- , and homopolar system (or zero sequence), \mathbf{U}^0 . The relation between the unbalanced system phases and the system symmetrical components is given by (A2.41) and (A2.42), where $a = 1 \angle 120^\circ = e^{j120^\circ}$.

$$\begin{bmatrix} \bar{U}_A \\ \bar{U}_B \\ \bar{U}_C \end{bmatrix} = \begin{bmatrix} 1 & 1 & 1 \\ 1 & a^2 & a \\ 1 & a & a^2 \end{bmatrix} \cdot \begin{bmatrix} \bar{U}_A^0 \\ \bar{U}_A^+ \\ \bar{U}_A^- \end{bmatrix} = \mathbf{A} \begin{bmatrix} \bar{U}_A^0 \\ \bar{U}_A^+ \\ \bar{U}_A^- \end{bmatrix}, \quad (\text{A2.41})$$

$$\begin{bmatrix} \bar{U}_A^0 \\ \bar{U}_A^+ \\ \bar{U}_A^- \end{bmatrix} = \frac{1}{3} \begin{bmatrix} 1 & 1 & 1 \\ 1 & a & a^2 \\ 1 & a^2 & a \end{bmatrix} \cdot \begin{bmatrix} \bar{U}_A \\ \bar{U}_B \\ \bar{U}_C \end{bmatrix} = \mathbf{A}^{-1} \begin{bmatrix} \bar{U}_A \\ \bar{U}_B \\ \bar{U}_C \end{bmatrix} \quad (\text{A2.42})$$

Although described by line-to-neutral voltages, equations (A2.41) and (A2.42) are also valid to line-to-line voltages, as well as for the currents in a three-phase system.

According to (A2.42), if the vector summation of the voltages \bar{U}_A , \bar{U}_B and \bar{U}_C is null, there is no homopolar component. It can be concluded that, when the line-to-neutral voltages are replaced by line-to-line voltages, the homopolar component is null, since the voltages sum is zero. Therefore, the homopolar component never exists when the line-to-line voltages are being considered, independently on the unbalance level. However, the line-to-neutral voltages can contain homopolar components.

For a delta-connected load, (A2.43) can be written. The line currents absorbed by a delta-connected load have no homopolar components, since (A2.44) is valid.

$$\begin{cases} \bar{I}_A = \bar{I}_{AB} - \bar{I}_{CA} \\ \bar{I}_B = \bar{I}_{BC} - \bar{I}_{AB} \\ \bar{I}_C = \bar{I}_{AB} - \bar{I}_{BC} \end{cases} \quad (\text{A2.43})$$

$$\bar{I}_A^0 = \frac{1}{3}(\bar{I}_A + \bar{I}_B + \bar{I}_C) = 0 \quad (\text{A2.44})$$

If circulating currents, \bar{I}_{AB}^0 , exist in the triangle, they cannot be computed using the line currents. The current direct and inverse components are given by (A2.45).

$$\begin{aligned} \bar{I}_A^+ + \bar{I}_A^- &= (\bar{I}_{AB}^+ - \bar{I}_{CA}^+) + (\bar{I}_{AB}^- - \bar{I}_{CA}^-) = \\ &= (1-a)\bar{I}_{AB}^+ + (1-a^2)\bar{I}_{AB}^- \end{aligned} \quad (\text{A2.45})$$

Regarding the symmetric delta-connected load, the equation (A2.46) is valid.

$$\begin{cases} \bar{U}_{AB} = \bar{Z}_D \cdot \bar{I}_{AB} \\ \bar{U}_{BC} = \bar{Z}_D \cdot \bar{I}_{BC} \\ \bar{U}_{CA} = \bar{Z}_D \cdot \bar{I}_{CA} \end{cases} \quad (\text{A2.46})$$

Therefore, since the line-to-line voltages sum is null, (A2.47) can be written.

$$\bar{U}_{AB} + \bar{U}_{BC} + \bar{U}_{CA} = 3\bar{U}_{AB}^0 = 3\bar{Z}_0 \bar{I}_{AB}^0 = 0 \quad (\text{A2.47})$$

It can be concluded that, in a delta-connected circuit with impedances only, without sources of mutual couplings, it is not possible to exist circulating currents. However, for specific circumstances, circulating currents can be produced in delta circuits of transformers, generators, and motors, due to the induction and to the homopolar voltages generated. Regarding IMs, the circulating currents are common due, for example, to the presence of electromagnetic asymmetries and saturation effects. Furthermore, even when homopolar currents are generated in the delta phases, no homopolar voltages can exist between the triangle terminals.

Therefore, in the case of IMs, the star connection is, from the analysed perspective, more advantageous.

In short, for IMs with only 3 wires, without neutral, if the stator were connected in star there is no homopolar circulating currents, if the stator were connected in delta mode, homopolar circulating currents can exist, which, if

known in magnitude, can be introduced in a homopolar equivalent circuit fed by a proper voltage source. This procedure can be extended to all homopolar harmonic components, and the impact is only at losses level. However, it is difficult to predict the values of such currents to different frequencies.

Regarding the electromagnetic torque development, only the direct and inverse systems are needed. The following analysis is valid to any frequency or harmonic but, for the sake of simplicity, is confined to fundamental frequencies. The direct system originates a rotating MMF, which produces a forward or positive torque. The indirect system originates a turning MMF, which produces a backward or indirect torque [35]. Therefore, besides reducing the produced forward torque in the motor shaft, leads to additional losses, reducing the motor efficiency and increasing the operating temperature.

Assuming that only the fundamental system is unbalanced, (A2.48) and (A2.49) can be written, in which a new column was introduced.

$$(s-h) = \begin{bmatrix} 1-1^+ & 1-1^- & 1-5 & 1-7 & 1-11 & 1-13 & 1-17 & 1-19 \\ 5-1^+ & 5-1^- & 5-5 & 5-7 & 5-11 & 5-13 & 5-17 & 5-19 \\ 7-1^+ & 7-1^- & 7-5 & 7-7 & 7-11 & 7-13 & 7-17 & 7-19 \\ 11-1^+ & 11-1^- & 11-5 & 11-7 & 11-11 & 11-13 & 11-17 & 11-19 \\ 13-1^+ & 13-1^- & 13-5 & 13-7 & 13-11 & 13-13 & 13-17 & 13-19 \end{bmatrix} \quad (\text{A2.48})$$

$$\frac{\omega_{\text{sync}(s-h)}}{\omega_{\text{sync}(1-1)}} = \begin{bmatrix} 1.00^+ & 1.00^- & 5.00^- & 7.00^+ & 11.0^- & 13.0^+ & 17.0^- & 19.0^+ \\ 0.20^- & 0.20^+ & 1.00^+ & 1.40^- & 2.20^+ & 2.60^- & 3.40^+ & 3.80^- \\ 0.14^+ & 0.14^- & 0.71^- & 1.00^+ & 1.57^- & 1.86^+ & 2.43^- & 2.71^+ \\ 0.09^- & 0.09^+ & 0.45^+ & 0.64^- & 1.00^+ & 1.18^- & 1.55^+ & 1.73^- \\ 0.08^+ & 0.08^- & 0.38^- & 0.54^+ & 0.85^- & 1.00^+ & 1.31^- & 1.46^+ \end{bmatrix} \quad (\text{A2.49})$$

The amplitude to be considered in the ECM voltages representing the direct and inverse systems has to be computed using the previously presented equations.

The application of a positive- and a negative-sequence equivalent circuit was proposed previously, being emphasized the importance of considering the skin effect impact on the effective rotor resistance and rotor leakage inductance.

Regarding internal impedance unbalance due, for example, to a different number of turns in the stator windings, such situation can be addressed by changing properly the ECM parameters values in each phase, in order to allow the identification of the currents in each phase and establish a voltage similar which produces the same current. A per-phase voltage level reflecting the impedance unbalance per phase has to be found. For a more accurate simulation, the referred changes should be considered in a dynamic model.

In an unbalanced distorted system, the total power factor can be calculated by (A2.50), where P_{p1} and P_{n1} are the positive- and negative-sequence three-phase fundamental powers, respectively, and S_1 is the three-phase fundamental complex power, defined by (A2.51) [27]. In a distorted, balanced system, the power factor can be given by (A2.52).

$$\lambda_{\text{total}} = \lambda_{\text{unb1}} \cdot \lambda_{\text{THD}} = \frac{P_{p1} + P_{n1}}{|S_1|} \cdot \lambda_{\text{THD}} \quad (\text{A2.50})$$

$$\begin{aligned} \lambda_{\text{total}} &= \frac{P_{\text{total}}}{U_{\text{rms}} \cdot I_{\text{rms}}} = \\ &= \lambda_1 \cdot \lambda_{\text{THD}} = \frac{P_1}{U_1 \cdot I_1} \cdot \lambda_{\text{THD}} = \\ &= \frac{P_1 + \sum_{h>1} P_h}{\sqrt{U_1^2 + \sum_{h>1} U_h^2} \cdot \sqrt{I_1^2 + \sum_{h>1} I_h^2}} \end{aligned} \quad (\text{A2.51})$$

$$\begin{aligned} \bar{S}_1 &= P_{AB} + P_{BC} + P_{CA} + j(Q_{AB} + Q_{BC} + Q_{CA}) = \\ &= \bar{U}_{AB} \bar{I}_{AB}^* + \bar{U}_{BC} \bar{I}_{BC}^* + \bar{U}_{CA} \bar{I}_{CA}^* = \\ &= 3(\bar{U}_p \bar{I}_p^* + \bar{U}_n \bar{I}_n^*) = \\ &= 3(P_1 + jQ_1) = \\ &= 3[P_p + P_n + j(Q_p + Q_n)] = \\ &= 3[\text{Re}\{\bar{S}_1\} + j(\text{Im}\{\bar{S}_1\})] \end{aligned} \quad (\text{A2.52})$$

Since three-phase line-connected motors are almost exclusively connected in delta or in ungrounded-star, the zero-sequence component is trivially zero, and zero-sequence line power does not exist.

A2.4.2.7 Examples, Validation and Conclusions

To test and validate the proposed hybrid model, the electrical, mechanical and thermal parameters for a TEFC, low-voltage 3-kW IM (Fig. A2.23), were

estimated experimentally and analytically. The winding parameters were obtained using the software BOBISOFT, using the data presented in Table A2.4. In Fig. A2.24, the winding scheme is presented.

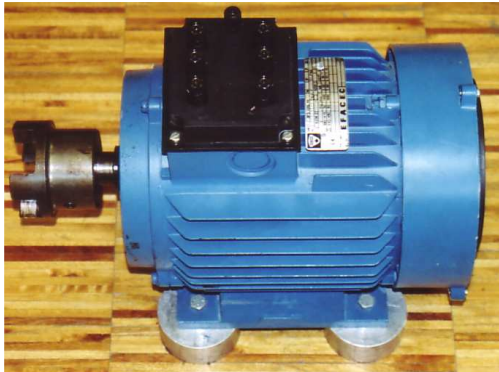


Fig. A2.23. Photograph of the 3-kW, 4-pole, TEFC IM used to validate the proposed model.

TABLE A2.4
CHARACTERISTICS OF THE 3-kW IM USED IN THE EXPERIMENTAL TESTS.

Slots	36
Inner Stator Diameter	95 mm
Outer Stator Diameter	160 mm
Outer Rotor Diameter	94 mm
Core Length	100 mm
Shaft Diameter	28 mm
Rotor Volume	= 48.6% of Stator Volume
Air-Gap Thickness	0.5 mm
Power	3 kW
Voltage	400 V (380-415 V)
Frequency	50 Hz
Current	7.1 A
Rated Torque	20.5 N.m
Rated Power Factor	0.8
Rated Speed	1400 r/min
Poles	4
Winding Connection	Delta
Frequency	50 Hz
Winding Type	Double-Layer Concentric
Phase Turns	372
End-Windings Additional Length	70%
Wire Section (2 parallel cond.)	0.246301 mm ² + 0.246301 mm ²

Some of the possible simulated outcomes, considering different operating conditions and harmonics, are now presented.

The simulated results presented in Fig. A2.25 were compared with key experimental points (initial and final instants of each different operating period), and an error of less than $\pm 3^{\circ}\text{C}$ was obtained⁸. It can be concluded that the model has a good matching for losses and temperatures.

In Figs. A2.26-A2.27, the simulated curves for motor efficiency, power factor and average stator winding temperature as a function of slip, for different fundamental frequencies (increasing in 4-Hz steps), considering only space harmonics, are shown. It should be noted that, for the maximum efficiency, the slip, in r/min,

⁸ The rotor temperature for particular steady-state load points was also verified by means of a fast locked-rotor test, in which the stator windings resistance was also measured, allowing the calculation of the rotor resistance variation, and, therefore, the temperature variation.

is maintained approximately constant but, in %, it increases with speed or frequency decrease.

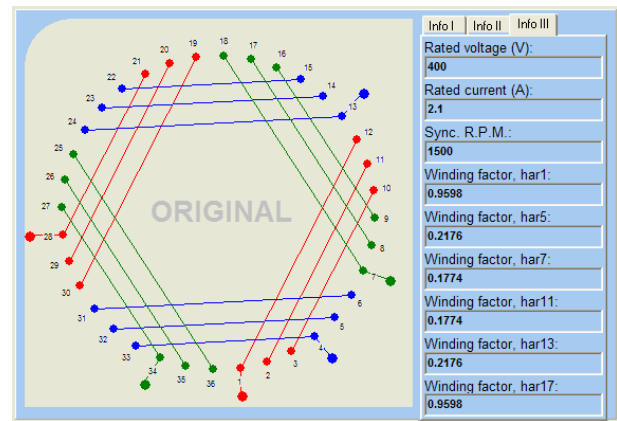


Fig. A2.24. Stator winding scheme for a 3-kW, 4-pole IM.

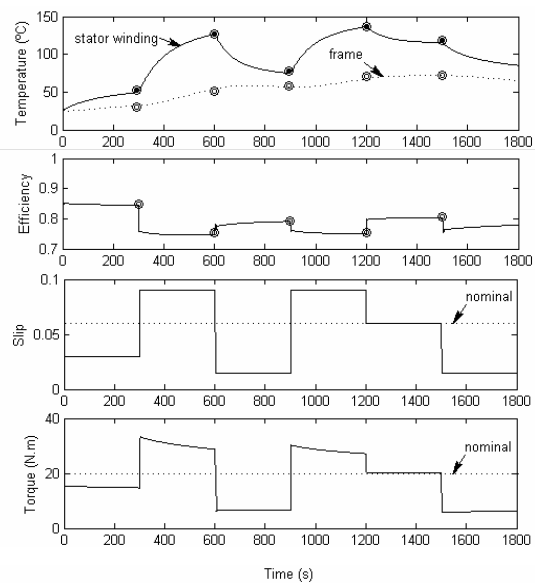


Fig. A2.25. Simulated motor slip, torque, efficiency, and temperature, as a function of time, considering only the space harmonics, $U_1 = 400$ V, $f_1 = 50$ Hz, and an ambient temperature of 25°C . Discrete experimental results identified with circles.

In Fig. A2.28, the simulated torque-speed and torque-frequency capability curves are shown, including the field-weakening or constant power region, considering continuous operation. The same curves can also be estimated for short-time operation. This curve is very important to predict the temperature and torque limits of the motor.

In fact, after the proper adjustment of all electric, mechanical and thermal parameters, the suitability of a given motor for a particular demanding variable load (e.g. electric vehicle) can be evaluated accurately, according to the expected load profile and ambient temperature.

In Fig. A2.29, the impact of the space harmonics on the torque-slip curve can be seen, being of small relevance. The influence of the time harmonics on the torque-slip curve was also analysed but, due to their negligible impact, the resulting curves are not presented.

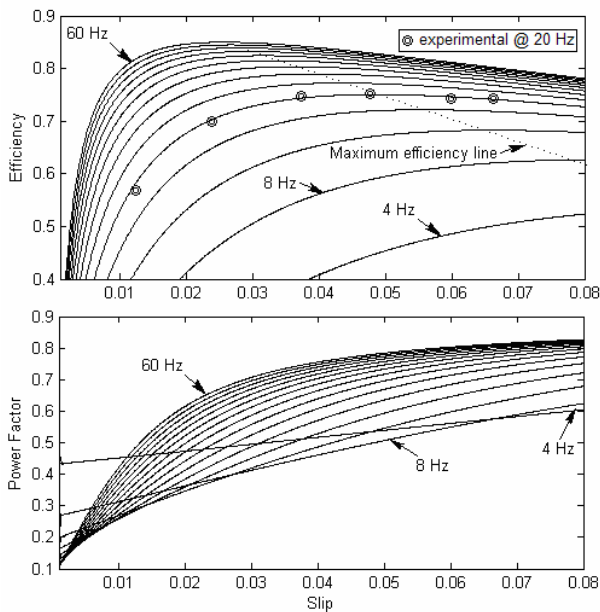


Fig. A2.26. Motor efficiency and power factor as a function of slip, for different fundamental frequencies (4-Hz steps), $U_1/f_1 = 8$, and without considering space and time harmonics.

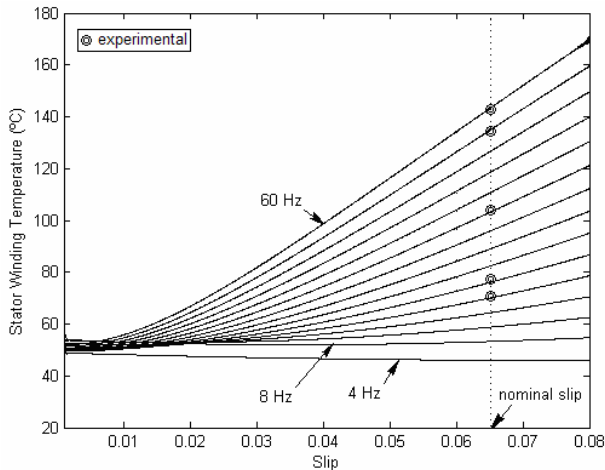


Fig. A2.27. Motor stator winding average temperature as a function of slip, for different fundamental frequencies (4-Hz steps), $U_1/f_1 = 8$, and without considering space and time harmonics.

With the proposed model, it is possible to analyze the motor torque-speed capability curves and the space and time harmonics impact in the motor performance, including the internal temperature variation. Optimal control strategies based on the voltage and frequency variation can be studied. It is also possible to estimate if the load peaks magnitude and duration can be critical to the motor. Starting problems can also be identified using the estimated torque-speed curves. The heat related effects on the lifetime of the bearing and stator winding insulation system can be estimated, considering the well-known Arrhenius' law. A major advantage of the proposed approach is the modular concept, allowing the user to consider any harmonic number and order, according to the motor power source and stator winding features.

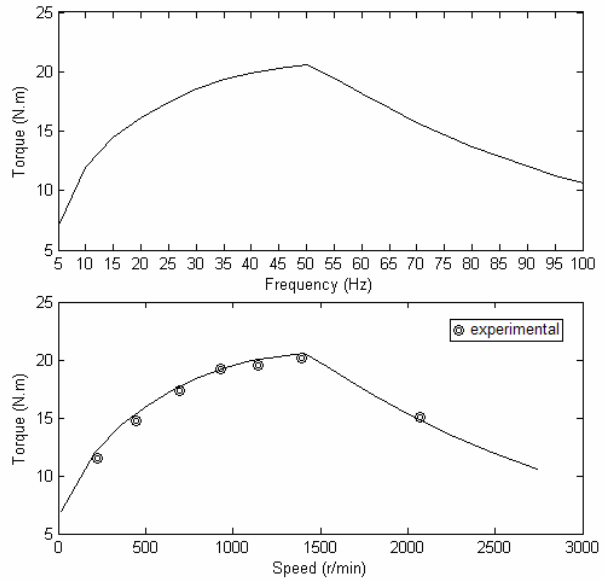


Fig. A2.28. Torque-speed and torque frequency capability curves including field-weakening zone, considering $U_1/f_1 = 8$ for $f_1 \leq 50$ Hz, and $U_1 = 400$ V for $f_1 > 50$ Hz. Ambient temperature equal to 25°C and a constant winding temperature equal to 120°C. No space and time harmonics were considered. Discrete experimental results identified with circles.

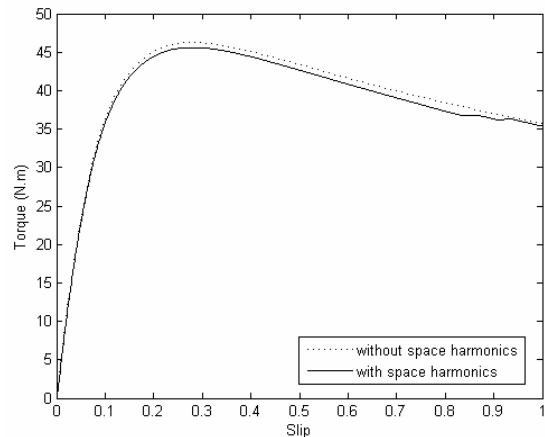


Fig. A2.29. Torque-slip curve with and without space harmonics ($K_{w1} = 0.9598$; $K_{w5} = 0.2176$; $K_{w7} = 0.1774$; $K_{w11} = 0.1774$; $K_{w13} = 0.2176$), considering constant, homogeneous temperature equal to 25°C, $U_1 = 400$ V, and $f_1 = 50$ Hz.

A2.5 References

- [1] Vamvakari, A. et al.: "High Fidelity Equivalent Circuit Representation of Induction Motor Determined by Finite Elements for Electrical Vehicle Drive Applications", IEEE Trans. on Magnetics, Vol. 35, No. 3, pp. 1857-1860, May 1999.
- [2] Papazacharopoulos, Z., et al.: "Dynamic Model for Harmonic Induction Motor Analysis Determined by Finite Elements", IEEE Trans. on Energy Conversion, Vol. 19, No. 1, pp. 102-108, 2004.
- [3] Tatis, K.; Kladas, A.; Tegopoulos, J.: "Harmonic Iron Loss Determination in Laminated Iron Cores by Using a Particular 3-D Finite-Element Model", IEEE Trans. on Magnetics, Vol. 40, No. 2, pp. 860-863, March 2004.
- [4] Kinnares, V. et al.: "Effect of Motor Parameter Changes on Harmonic Power Loss in PWM Fed Induction Machines", IEEE Inter. Conf. on Power Electronics and Drive Systems (PEDS'99), Conf. Proc., pp. 1061-1066, Hong Kong, 1999.
- [5] Stiebler, M.: "Determining Induction Machine Parameters Using Equivalent Circuit Models", 16th Inter. Conf. on Electrical Machines (ICEM'04), Conf. Proc., Krakow, Poland, 2004.
- [6] Smith, K.; Ran, L.: "A Time Domain Equivalent Circuit for the Inverter-Fed Induction Motor", 9th IEE Inter. Conf. on Electrical Machines and Drives, Conf. Publication No. 468, pp. 1-5, 1999.

- [7] Mukhopadhyay, S. C.; Pal, S. K.; Roy, D.; Bose, S.: "Software Aided Derating and Performance Prediction of Cage-Rotor Induction Motors under Distorted Supply Conditions", Inter. Conf. on Power Electronics, Drives and Energy Systems for Industrial Growth, Conf. Proc., Vol. 1, pp. 452-457, Jan. 1996.
- [8] Roy, D.; Mukhopadhyay, S. C.; Pal, S. K.; Bose, S.: "Novel Thermal Model Aided Motor Derating Under Waveform Distortion", 1997 Inter. Conf. on Power Electronics and Drive Systems, Conf. Proc., Vol. 2, pp. 829-833, May 1997.
- [9] Boglietti, A. et al.: "A simplified thermal model for variable-speed self-cooled industrial induction motor", IEEE Trans. on Industry Applications, Vol. 39, No. 4, pp. 945-952, 2003.
- [10] Boglietti, A., Cavagnino, A., Staton, D.: "TEFC induction motors thermal models: a parameter sensitivity analysis", IEEE Trans. on Industry Applic., Vol. 41, No. 3, pp. 756-763, 2005.
- [11] IEEE Std. 112, 2004: "Standard Test Procedure for Polyphase Induction Motors and Generators".
- [12] Kandianis, T., et al.: "Electrical Vehicle Drive Control based on Finite Element Induction Motor Model", IEEE Trans. on Magnetics, Vol. 33, No. 2, pp. 2109-2112, March 1997.
- [13] Ferreira, F., de Almeida, A.: "Electric Machinery Winding Design Software for Teaching and Rewinding", 16th Inter. Conf. on Electrical Machines (ICEM'04), Conf. Proc., Krakow, 2004.
- [14] Lee, J., et al.: "Loss Distribution of Three-Phase Induction Motor Fed by Pulsewidth-Modulated Inverter", IEEE Trans. on Magnetics, Vol. 40, No. 2, pp. 762-765, March 2004.
- [15] Boglietti, A., et al.: "Predicting Iron Losses in Soft Magnetic Materials with Arbitrary Voltage Supply: An Engineering Approach", IEEE Trans. on Magnetics, Vol. 39, No. 2, pp. 981-989, March 2003.
- [16] Gerlando, D.; Perini, R.: "Evaluation of the Effects of the Voltage Harmonics on the Extra Iron Losses in the Inverter Fed Electromagnetic Devices", IEEE Trans. on Energy Conversion, Vol. 14, No. 1, pp. 57-65, March 1999.
- [17] Boglietti, A., et al.: "Loss Separation Analysis in Ferromagnetic Sheets under PWM Inverter Supply", IEEE Trans. on Magnetics, Vol. 34, No. 4, pp. 1240-1242, July 1998.
- [18] Boglietti, A., et al.: "Change of the Iron Losses with the Switching Supply Frequency in Soft Magnetic Materials Supplied by PWM Inverter", IEEE Trans. on Magnetics, Vol. 31, No. 6, pp. 4250-4252, Nov. 1995.
- [19] Loddick, S.: "Modelling Frequency Dependency of Induction Machine Equivalent Circuit Parameters", IEE Conf. Power Electronics and Variable Speed Drives, Conf. Publication, No. 429, pp. 30-35, Sept. 1996.
- [20] Green, T.; Hernández-Arámburo, C.; Smith, A.: "Losses in Grid and Inverter Supplied Induction Machine Drives", IEE Proc.-Electr. Power Appl., Vol. 150, No. 6, pp. 712-724, 2003.
- [21] Hernández-Arámburo, C., Green, T.; Smith, S.: "Assessment of Power Losses of an Inverter-Driven Induction Machine With Its Experimental Validation", IEEE Trans. on Industry Applications, Vol. 39, No. 4, pp. 994-1004, Jul./Aug. 2003.
- [22] Boglietti, A.; Cavagnino, A.; Lazzari, M.: "A Recursive Algorithm to Resolve the Skin Effect in Rotor Bars of Squirrel Cage Induction Motors", XVI Inter. Conf. on Electrical Machines (ICEM'04), Conf. Proc., Krakow, Poland, 2004.
- [23] Trigeol, J., et al.: "Estimation of the Heat Losses in an Electrical Machine Using an Inverse Method", XVI Inter. Conf. on Electrical Machines (ICEM'04), Conf. Proc., Krakow, 2004.
- [24] de Almeida, A.; Ferreira, F.; Busch, J.; Angers, P.: "Comparative Analysis of IEEE 112-B and IEC 34-2 Efficiency Testing Standards Using Stray Load Losses in Low Three-Phase, Cage Induction Motors", IEEE Trans. on Industry Applications, Vol. 38, No. 2, pp. 608-614, March/April 2002.
- [25] Boglietti, A., et al.: "International Standards of the Induction Motor Efficiency Evaluation: A Critical Analysis of the Stray-Load Loss Determination", IEEE Trans. on Industry Appl., Vol. 40, No. 5, pp. 1294-1301, Sept./Oct. 2004.
- [26] Ferreira, F., de Almeida, A., Baoming, G.: "Three-Phase Induction Motor Simulation Model Based on a Multifrequency Per-Phase Equivalent Circuit Considering Stator Winding MMF Spatial Harmonics and Thermal Parameters", 17th Inter. Conf. on Electrical Machines (ICEM'06), Conf. Proc., Crete, Greece, 2006.
- [27] Grainger, J.; Stevenson, W.: "Power System Analysis", McGraw-Hill Inter. Editions, Electrical Eng. Series, New York, 1994.
- [28] Beatty, H.; Kirtley, J.: "Electric Motor Handbook", McGraw-Hill Handbooks, New York, 1998.
- [29] Mohan, N.; Undeland, T.; Robbins, W.: "Power Electronics: Converters, Applications, and Design", John Wiley & Sons, Inc., New York, 1995.
- [30] MATLAB/SIMULINK Version 7.0.1 (R14), Help Information, The MathWorks, Inc., 2004.
- [31] Ong, C.: "Dynamic Simulation of Electric Machinery Using MATLAB/SIMULINK", Prentice Hall PTR, New Jersey, 2006.
- [32] Alger, P.: "Induction Machines – Their Behavior and Uses", Gordon and Breach Publishers, 3rd Edition, 1995.
- [33] Williamson, S.; Smith, S.; Barnes, M.; Apsley, J.: "Efficiency Gains in Multi-Phase Induction Motor Drives", 5th Inter. Conf. on Energy Efficiency in Motor Driven Systems (EEMODS'07), Conf. Proc., Beijing, 2007.
- [34] Mastorocostas, C.; Kioskeridis, I.; Margaris, N.: "Thermal and Slip Effects on Rotor Time Constant in Vector Controlled Induction Motor Drives", IEEE Trans. on Power Electronics, Vol. 21, Issue 2, pp. 495-504, March 2006.
- [35] Cummings, P., Dunki-Jacobs, J., Kerr, R.: "Protection of Induction Motors Against Unbalanced Voltage Operation", IEEE Trans. on Ind. Applic., Vol. IA-21, No. 4, pp. 778-792, May/June 1985.
- [36] Mihalič, F.; Jezernik, K.; Krischan, K.; Rentmeister, M.: "IGBT Spice Model", IEEE Trans. on Industrial Electronics, Vol. 42, No. 1, pp. 98-105, Feb. 1995.
- [37] Mastorocostas, C.; Kioskeridis, I.; Margaris, N.: "Thermal and Slip Effects on Rotor Time Constant in Vector Controlled Induction Motor Drives", IEEE Trans. on Power Electronics, Vol. 21, No. 2, pp. 495-504, March 2006.
- [38] Kioskeridis, I.; Margaris, N.: "Loss Minimization in Induction Motor Adjustable-Speed Drives", IEEE Trans. on Industrial Electronics, Vol. 43, No. 1, pp. 226-231, Feb. 1996.
- [39] Abrahamson, F.: "Efficiency-Optimized Control of Medium-Size Induction Motor Drives", IEEE Trans. on Industrial Applications, Vol. 37, No. 6, pp. 1761-1767, Nov./Dec. 2001.
- [40] Blaabjerg, F.; Jaeger, U.; Munk-Nielsen, S.: "Power Losses in PWM-VSI Inverter using NPT or PT IGBT Devices", IEEE Trans. Power Electronics, Vol. 10, No. 3, pp. 358-367, May 1995.
- [41] McCleer, P. et al.: "Nonlinear Model and Momentary Performance Capability of a Cage Rotor Induction Machine Used as an Automotive Combined Starter-Alternator", IEEE Trans. on Industry Applic., Vol. 37, No. 3, pp. 840-846, May/June 2001.
- [42] Seo, J.; Ahn, J.; Jung, H.: "Parameters Calculation for Inverter Driven Induction Machine Including Field Weakening Operation", 16th Inter. Conf. on Electrical Machines (ICEM'04), Conf. Proc., Krakow, 2004.
- [43] Erdogan, N.; Henao, H.; Grisel, R.: "A General Comparison Between Conventional and Improved Induction Machine Models", 16th Inter. Conf. on Electrical Machines (ICEM'04), Conf. Proc., Krakow, 2004.
- [44] Pugsley, G.; Chillet, C.; Fonseca, A.: "Cost-Performance-Size Optimization for Automotive Induction Machines. A Fast and Accurate FEM, Analytical Model and Optimization Mixed Procedure", 16th Inter. Conf. on Electrical Machines (ICEM'04), Conf. Proc., Krakow, 2004.
- [45] Zakrgewski, K.: "Method of Calculation of Unit Power Losses in Magnetic Laminations Taking into account Sinusoidal and PWM Supply Voltage", 16th Inter. Conf. on Electrical Machines (ICEM'04), Conf. Proc., Krakow, 2004.
- [46] Nuscheler, R.; Meyer, W.; Schmid, M.: "Efficiency-Optimized Simulation of Asynchronous Machines Combined with PWM Converters", 16th Inter. Conf. on Electrical Machines (ICEM'04), Conf. Proc., Krakow, 2004.
- [47] Ferreira, F.; Deprez, W.; Parasility, F.; de Almeida, A.: "Simulated and Experimental Evaluation of Steady-State Voltage Unbalance Impact on the Performance of Different Induction Motor Types", 18th Inter. Conf. on Electrical Machines (ICEM'08), Conf. Proc., Vilamoura, Portugal, Sept. 2008.
- [48] de Almeida, A.; Ferreira, F.; Fong, J.; Conrad, B.: "Electric Motor Standards, Ecodesign and Global Market Transformation", IEEE Industrial and Commercial Power Systems Technical Conf., Conf. Proc., U.S.A., May 2008.
- [49] Leonhard, W.: "Control of Electric Drives", 2nd Completely Revised and Enlarged Edition, Springer-Verlag, Berlin, 1997.
- [50] Cummings, P.: "Estimating Effect of System Harmonics on Losses and Temperature Rise of Squirrel-Cage Motors", IEEE Trans. on Industry Applications, Vol. IA-22, No. 6, pp. 1121-1126, Nov./Dec. 1986.

Appendix 3 – Stator Winding Improvement and Motor Repair

Overview – Typically, IMs are typically submitted to curative maintenance operations 2 to 4 times over their overall lifetime of around 12 to 20 years. More than ¼ of their failures are related to the stator windings. When IMs have to be rewound, the original stator winding can be properly changed or customized, according to the actual motor operating conditions, potentially leading to the improvement of the motor efficiency and reliability. This appendix presents an overview on energy, electromagnetic, endurance and economical aspects associated with the design of low-voltage, three-phase stator windings. A general methodology for evaluation and identification of the most advantageous characteristics of stator windings is presented. Several rewinding techniques are also briefly addressed. A scheme for efficiency improvement of oversized motors is proposed, which can lead to significant energy savings. A user-friendly software tool for three-phase winding (re)design is also proposed, which can help rewinders and manufacturers to easily optimize windings, not requiring extensive technical background. The proposed software can also be used for academical purposes. Since it only makes sense to spend additional time and better quality materials during repair if the motor can actually be improved, stator core losses and rotor condition evaluation techniques are also addressed, being proposed a current and vibration spectral analysis-based software tool that uses artificial neural networks to combine the input data. Several publications were made in the scope of this appendix, namely, [2]–[5], [19] and [26].

A3.1 Introduction

IMs are the most important electric motors in the industrial and tertiary sectors, being used in 80 to 90% of the EMODS, as shown in Chapter 1. Statistically, depending on the operating conditions, the IMs are typically repaired/rewound 2 to 4 times over their lifetime of around 12 to 20 years [5], [19]. Roughly ¼ of their failures are related to stator windings (see Appendix 5). In applications where speed, torque and/or position control is required, IMs are typically fed by VSDs, commonly integrating voltage-source inverters with pulse-width modulation (see Chapter 3). Although the well-known technical and economical advantages of VSDs, they can reduce the efficiency and reliability of motors, particularly when they are old or improperly (re)designed/(re)wound¹ [3], [26], [36]. With proper winding (re)design, IMs can be customized, in order to be (re)matched to the actual operating conditions, if they are different from rated, improving their performance and extending their lifetime, either if they are line- or inverter-fed motors (e.g., line-fed designed motors can be converted to inverter-rate motors). In particular, during motor rewinding and/or rehabilitation, the motor can be customized, yielding an excellent opportunity to maximize the motor efficiency, power factor and reliability, as a function of the actual motor load, voltage, frequency and/or power supply type (line or inverter), with modest additional costs. In general, for low-medium ratings, this is not possible when users buy new standardized off-the-shelf motors.

This is important because most motors in industry are oversized and often operate with voltages different from the rated. The motor load can be estimated in the field with a fair accuracy by means of a number of simple and easy-to-apply methods, as described in Chapter 4.

¹ Complete information on motor repair or curative maintenance, including motor rewinding, can be found in [26].

Most low-voltage IMs are in the power range below 100 kW, which, typically, have random-wound stator windings², unlike the medium/high-voltage motors, which are generally built with form-wound stator windings³. Typically, for low-voltage motors, the manufacturers use a few different stator winding types, taking into account the limitations of the mass-production industrial equipment for automatic winding, which also have limitations related to the slot-filling factor and to the end-windings (or coil-heads) length. Fewer limitations exist when stator windings are implemented manually. In fact, manual techniques have not the technical constraints of automated windings, being possible to introduce a number of improvements. Furthermore, the rewinders can make a customized stator winding design considering the actual motor operation conditions. Therefore, in some cases, the rewinders can replace the original winding by a new improved one, with lower copper losses, improved air-gap magnetomotive force waveform, and, if necessary, adapted to the actual motor load and/or power supply voltage. This is important because, as previously referred, most motors in Industry are oversized and sometimes operate with a voltage lower than rated voltage or are fed by inverters. In these cases, the motor can actually be (re)matched simultaneously to the load (or load cycle) and to the power supply during rewinding.

In the past, little consideration has been given to the impact of rewinding methods on motor efficiency. In developed countries it is generally accepted that it is cheaper to repair damaged electric motors above 3-5.5 kW than to replace them⁴. In developing countries, with much lower labour costs, basically all electric motors are repaired. In the EU, it is known that, in terms of units, the electric motor repair market represents more than 2-3 times the new electric motor market [5], [19]. This is why the improvement of the repair market is so important in order to avoid the increasing of the motor operating costs.

When a motor fails, the main concern of most motor users and rewinders is to get it back into service as quickly and inexpensively as possible. This situation sometimes leads to the use of inadequate repair processes, which can significantly reduce the efficiency and reliability of the motor. However, the increasing awareness of the huge amount of electricity consumed by electric motors, together with the increasing focus on energy-efficiency issues and on the increasing penetration of HEMs (see Chapter 2), has highlighted the effects that motor repair can have on their performance. Several laboratory testing studies confirm that the practices commonly applied in motor repair/rewinding (Fig. A3.1) lead to a reduction of motor efficiency typically 0.5 to 1 p.p. in motor efficiency and, sometimes, in worst cases, this reduction can achieve 4 p.p., as well as to

² Random-wound stator windings have random-wound coils, where the wire cross-section is round and the arrangement between the turns is not definite.

³ Form-wound stator windings have form-wound coils, where the wire cross-section is square or rectangular and the turns are systematically arranged.

⁴ According to the service and repair department manager of one large European motor manufacturer, nowadays, motors of all sizes are being repaired after stator winding failure [68]. According to a large number of repair shops over the countryside in Germany, only in large automotive plants motors below 3 kW are replaced. Most of the other German users repair (and not replace) even smaller motors (including fractional horsepower), independently of their brand [68].

the decrease of the motor reliability and reshape of the motor torque-speed curve [19], [26]. These are numbers measured in the USA and in the EU, but the decrease in efficiency in developing countries is likely to be even worse due to the lack of technically qualified human resources and adequate equipment. This is because the rewinding processes are, in general, not as well controlled as the original design and production of the motors. Together, these factors degrade significantly the performance of the motor and, consequently, of the EMODS [3], [5], [19], [34], [35]. Additionally, some rewinding shops do not have the equipment or the information necessary to repair every type of motor to the manufacturers' specifications. Furthermore, most users ignore or do not know what happens during the repair process, nor they do not worry about the possible motor efficiency drop after the repair. They are usually unaware of the energy bill increase due to the reduction of the efficiency levels of electric motors after repair.

The deterioration of the motor characteristics after repair are mainly due to inadequate stator winding stripping-out and stator core cleaning processes, improper/incorrect replacement of the winding (in terms of specification or change, mainly related to the lack of technical expertise) poor quality of materials used, poor winding impregnation, improper bearing replacement (including extraction/insertion methods and bearing quality/type⁵ adequacy), rotor core outer-surface machining, and improper fan replacement. The two main causes of increased motor losses following a repair are the damage of the stator core (leading to core loss increase) during stator winding stripping-out process and the increase of the resistance of the new winding (smaller wire gauge and longer end-windings, leading to higher copper losses). However, there are many other factors contributing to the poor-quality repair service that can be found in [3], [5], [19], [34], and [35]. For example, the inappropriate change of winding turns and configuration, which lead to the reshape of the motor efficiency-load and torque-speed curves, have a strong negative impact in motors performance, including possible starting problems.

The increase of the motor losses leads to the increase of the motor operating temperature and, therefore, to the reduction of the insulation system and bearing lubricant useful lifetime. In general, as referred previously, every 10°C increase in the operating temperature of the insulation system leads to a reduction of 50% in its lifetime (Arrhenius' law) [5], [26], [71]. It is estimated that a reduction of 1% in the efficiency of totally enclosed fan-cooled motors of 4, 45 and 132 kW, results in a useful lifetime decrease of 22, 30 and 31%, respectively [19]. Although less significant, the bearing lubricant also suffers approximately a 50% lifetime decrease per every 15°C temperature increase (for mineral lubricants, which are the most commonly used) [5], [26], [71]. Therefore, besides the additional motor consumption, its mean time to failure (MTTF) is strongly

⁵ The replacement of an open or shielded bearing by a sealed bearing in motors where extra protection level is not actually necessary, leads to increased friction.

reduced, potentially increasing maintenance costs. This is one important factor that should be taken into account when deciding if the motor should be repaired or replaced.

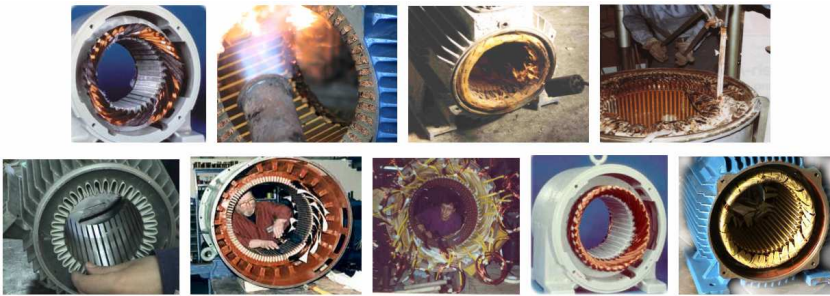


Fig. A3.1. Examples of processes associated with repair/rewinding of IMs.

From the LCC perspective, since motor running costs are by far dominant in relation to purchase and repair costs, in the vast majority of cases, it is economically advantageous to spend more money in high-quality repair services, providing that they can ensure an efficiency and reliability equal or higher than the original [5]. For example, on the basis of Fig. A3.2, a 12.5% increase in the repair service cost to avoid a 1 p.p. efficiency decrease in a 45-kW induction motor, operating 7500 h/yr at full load, leads to a simple payback of half year. Although the additional cost of the repair service, a reduction in the motor LCC is obtained, as well as, in principle, an extension of its useful lifetime. For the example given, the user can save 242 €/yr.

To be possible the motor performance improvement, the rotor and stator in particular cannot have extensive damages, being critical the evaluation of those motor parts before deciding to repair the motor. The extension of the actual damages should also be a factor to take into account when evaluating the possibility of a high-quality repair service, since it can only lead to cost-effective results if the motor parts other than stator winding and bearings are fairly healthy.

With the increasing penetration of HEMs in the market, the motor efficiency must be even more a priority concern during the repair process, and there is a need to promote a large-scale effort to promote the market transformation of motor repair. In the future, it will be very important that repair service companies/shops can provide high-quality services and ensure that the original efficiency is maintained, perhaps by means of creating a standard quality label, which could be applied to motors repaired in accordance with a prescribed “best practice”. This mark/label could be the quality image of repair shops in the future, helping users to easily identify which repair shops after high-quality services. To achieve these goals in the EU, some relevant demand-side management (DSM) programs/actions should be created concerning the transformation of the motor repair market, as discussed and proposed in [5], [19], and [26].

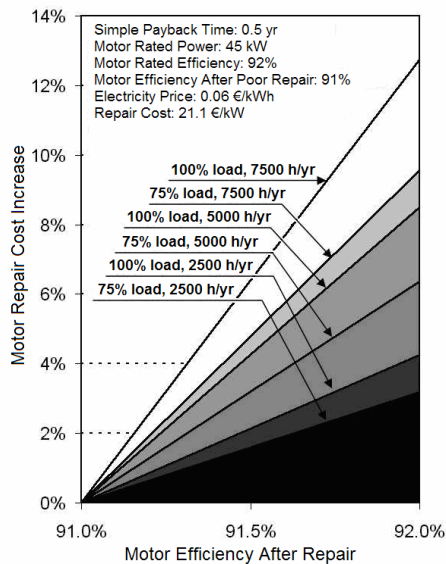


Fig. A3.2. Relation between the repair service cost increase and the resulting post-repair rated efficiency, for a 45-kW IM, considering a simple payback time equal to ½ yr and different loads and number of operating hours per year. It is also assumed that the 75%-load efficiency is equal to the rated efficiency (flat efficiency-load curve).

The demand for quick repairs by motor users coupled with the lack of understanding of many repairers on the impact of repair processes in the motor performance, are primary reasons for poor-quality repair services. For example, repairers may install a winding with overhangs longer than the original (thus increasing copper loss and quantity) because it is quicker and easier to insert it in the stator core slots. As referred before, lower efficiency implies higher operating costs and, possibly, more frequent maintenance and repair interventions.

With the application of “best practice or high-quality motor repair services” the reduction in motor efficiency is estimated to be less than 0.25 p.p. (assuming original winding copy, and replacement of damaged fan and bearings by original ones). If the motor has an initial efficiency of 90%, and if it drops 1 p.p. after a standard practice repair (poor repair), the losses increase 10%. After the first poor repair, there is an increment in the annual motor running costs of 1.1%. If best-practice repair is applied, the expected increment in running costs is up to 0.2%. The difference seems low, but if the total population of motors in a factory is considered, the overall increase in the energy bill can be significant. Due to the motor losses increase, the resulting higher operating temperature can significantly shorten the motor lifetime, as it can be seen in Fig. A3.3. When a motor is damaged, the users have two obvious options: repair or replace the motor. The first could be a good option if repair shops assure the original efficiency (even if the repair price increases, as explained before), but, unfortunately, it may not happen in most cases, requiring a careful technical and economical evaluation, considering the expected post-repair motor efficiency, the repair price, and the motor efficiency class⁶. The second option, specially recommended in the case of old and

⁶ In general, if the motor is of standard efficiency class (old EFF3 class), the repair cost is less than 50-65% of the cost of an EEM (old EFF2 class) or of a HEM (old EFF1 class), and the repair shop offers a quality assurance program, it should be repaired, otherwise, it should be replaced by an EEM or HEM. In the case of EEMs or HEMs, they should be repaired only if the repair shop offers quality assurance program [26]. When a standard old motor fails, its replacement by an EEM or HEM leads, in most cases, to paybacks no longer than 2 years, depending on the motor operating time, motor load, and electricity cost. Typically, replacing a standard damaged motor by a new equal motor can lead to paybacks no longer than 5 years. Standard oversized motors can also be replaced by well-sized HEMs.

badly damaged motors with a large number of operating hours per year, is to replace the damaged motor by a HEM.

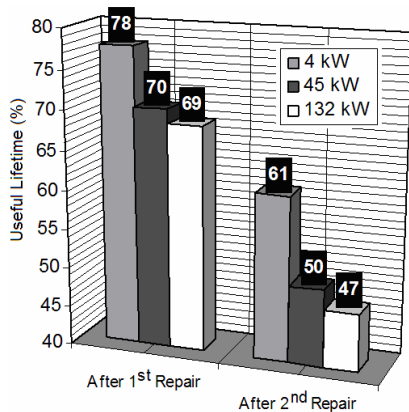


Fig. A3.3. Expected evolution of motor useful lifetime after repair. Assumptions: 1 p.p. drop on full-load efficiency after repair (poor repair), and average efficiency values of 83%, 92%, and 94%, for 4-, 45- and 132-kW motors, respectively [5].

It is important to note that rewinding option is less competitive on smaller machines (particularly with rated power below 3-5.5 kW).

In the EU, it is estimated that poor repair will lead, in 2015, to electricity losses of 5.6 TWh/yr (380 M€/yr), representing 2.8 Mt/yr of CO_{2eq} emissions (Fig. A3.4). Assuming that electric motors consume about ½ of the total electricity consumed in the world [19], [20], [23], and ⅓ of electric motors were repaired at least once, and suffered an 1 p.p. efficiency drop (poor repair), it is estimated that worldwide poor repair, for industrial and tertiary sectors, will lead, in 2015, to extra electrical energy losses of approximately 60 TWh/yr, representing an extra emission of 30 Mt/yr of CO_{2eq}. These 2015-year figures represent losses that worth 380 M€/yr and around 4 G€/yr for the EU and the World, respectively [5].

The replacement of poorly repaired motors, in applications with a large number of operating hours, by HEMs would lead to even larger electricity savings, as evidenced in Chapter 1.

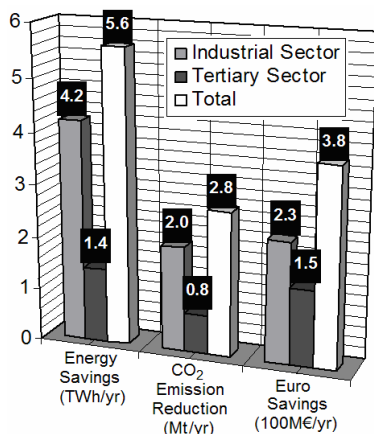


Fig. A3.4. Estimated annual savings potential for the EU, in 2015, and the corresponding CO_{2eq} emission reduction. Assumptions: 1-p.p. full-load efficiency drop after repair (poor repair); EU average values for motor energy consumptions, average electrical energy prices (0.055 €/kWh and 0.1 €/kWh for industrial and tertiary sectors, respectively), and CO_{2eq} emission per kWh of electricity produced (0.5 kg/kWh); ⅓ of the in-operation motors repaired at least once [5].

As a conclusion, energy-efficient motor repair practices can save a substantial amount of electrical energy and, at the same time, they can lead to productivity improvements due to reduced

motor driven equipment downtime. This figures evidenced the need to provide education, training and technology transfer to motor repairers. There is also the need to increase the awareness of motor users about the possible options that they have when a motor fails. In the case of old inefficient oversized motors, operating a large number of hours per year, the most cost-effective choice is the replacement of the damaged or faulty motor by an energy-efficient or high-efficiency motor. Several motor market transformation mechanisms have successfully been used around the world. If the motor user chooses to repair the damaged motor, certification schemes should be enforced to ensure that motor repair is carried without degrading the motor performance. Extensive analysis and recommendations on motor repair can be found in [26], being the stator winding (re)design related issues addressed in the next section.

A3.2 Considerations on Stator Windings

Complete theoretical information on stator windings can be found in several books and papers, such as [1], [28], [29], [31], [34], [35], and [42]-[46].

Assuming unsaturated core, the RMS value for the winding per-phase electromotive force (EMF), E_w , considering space harmonics of s^{th} order can be given by (A3.1), where ϕ is the per-phase, per-pole, air-gap magnetizing flux, B is the induction⁷, f is the frequency, N is the per-phase number of turns, and K_w is the winding factor [1].

$$E_w = \sqrt{\sum_{s=1}^{\infty} \left(4.44 \cdot N \cdot f \cdot \phi_1 \cdot \frac{B_s}{B_1} \cdot K_{ws} \right)^2} \quad (\text{A3.1})$$

Moreover, the even order harmonics do not exist due to pole symmetry, considering three-phase symmetry (absence of electrical and/or magnetic asymmetries). The triplen order harmonics are not considered because they do not contribute to the line-to-line voltage. The typical three-phase windings only react significantly to the fundamental component of the air-gap flux. The harmonics of the EMF resulting from the space harmonics associated to the magnetizing flux distribution over the air-gap are mitigated/cancelled by the three-phase connection (star or delta) and/or by the winding distribution, which typically leads to $K_{ws} \cdot s^{-1} \ll K_{w1}$. Thus, in practice, the EMF calculation requires only the fundamental harmonic ($s = 1$). Assuming the no-load test, for an IM, the per-phase stator winding rated voltage, U_w , can be calculated by (A3.2), where R_s is the per-phase stator winding resistance, X_s is the stator winding leakage reactance, and I_m is the magnetization current [1].

⁷ The maximum induction is limited by the saturation and magnetic loss limits.

$$\bar{U}_w = \bar{I}_m(R_s + jX_s) + \bar{E}_w = \bar{I}_m \cdot \bar{Z}_s + \bar{E}_w \quad (\text{A3.2})$$

The voltage-drop $I_m \cdot Z_s$ is typically lower than 5% of U_w (for well designed motors [42]), which, for $s = 1$, allows the practical approximation $U_w \approx E_w$ [1]. The per-pole air-gap flux harmonics, assuming sinusoidal spatial distribution for the air-gap reduction, are given by (A3.3), where $B_{s(\max)}$ is the induction maximum, τ_p is the pole pitch, and l_u is the stator core useful length.

$$\phi_s = \frac{2 \cdot B_{s(\max)} \cdot \tau_p \cdot l_u}{\pi \cdot s} = \phi_1 \cdot \frac{B_{s(\max)}}{s \cdot B_1} \quad (\text{A3.3})$$

The stator core useful length, l_u , is given by (A3.4), where l_t is the total core length, c_v is the length associated with the ventilation ducts, and K_{pck} is the packaging factor, defined by the quotient between the sum of the individual steel sheets thickness of the stator core stack (without including the interlaminar insulation) and the total stator core length (including interlaminar insulation).

$$l_u = (l_t - c_v) \cdot K_{pck} \quad (\text{A3.4})$$

The winding factor is the product between the pitch factor, K_p , and the distribution factor, K_d . For the s^{th} harmonic, the winding factor is defined by (A3.5).

$$K_{ws} = K_{ds} \cdot K_{ps} \quad (\text{A3.5})$$

Winding factors have direct impact on the produced EMFs (in the case of generators) and on the produced magnetomotive forces (MMFs, in the case of motors). For the s^{th} harmonic, the distribution and pitch factors for three-phase symmetric windings, are defined by (A3.6) and (A3.7), where γ_e is the coil effective pitch⁸ (in slots), p the number of pole pairs, and Z the number of stator slots. There are general algorithms to calculate (A3.6) and (A3.7) taking into account the position and number of turns of each coil (see Section A3.3.1) [1].

$$K_{ds} = \left| \frac{\sin\left(\frac{s \cdot \pi}{6}\right)}{\frac{Z}{6 \cdot p} \cdot \sin\left(\frac{s \cdot p \cdot \pi}{Z}\right)} \right| \quad (\text{A3.6})$$

⁸ Lower distance between the first slots of two adjacent coil-side groups or belts (with opposite current direction) of the same coil group.

$$K_{ps} = \left| \sin \left(\frac{s \cdot \gamma_e \cdot p \cdot \pi}{Z} \right) \right| \quad (\text{A3.7})$$

The pole pitch, τ_p , is defined by in slots (A3.8), and it gives the distance between two consequent poles which, by definition, is $\pi \text{ rad}_{\text{ele}}$.

$$\tau_p = \frac{Z}{2 \cdot p} \quad (\text{A3.8})$$

Multiplying (A3.8) by $\pi D / Z$ gives the pole pitch in meters (measured along or over stator inner periphery), where D is the stator core internal diameter (in meters). For a symmetrical (unbalanced) and sinusoidally (without distortion) excited three-phase stator winding, three pulsating MMFs are generated, resulting in a rotating MMF, defined by (A3.9), where K is a constant, p is the number of pole-pairs, s is the space harmonic order, and θ_{ele} is the stator inner surface angular position (in electrical degrees). For the reasons previously referred, triplen and even space harmonics can be excluded from (A3.9). For a certain p , the Z increase leads to the reduction of the K_w associated to harmonics higher than fundamental, improving the flux distribution in the air-gap. The term ωt in (A3.9) is preceded by a minus signal ($-$) for the $s = 6 \cdot n + 1$ order harmonics (positive-sequence space harmonics, with the same forward direction as the fundamental), and by a plus signal ($+$) for the $s = 6 \cdot n - 1$ order harmonics (negative-sequence space harmonics, with opposite or backward direction to the fundamental), being n a positive integer.

$$MMF(\theta_{\text{ele}}, t) = K \cdot \frac{N \cdot I}{p} \cdot \sum_{s=1}^{\infty} \left(\frac{K_{ws}}{s} \cdot \cos(s\theta_{\text{ele}} \mp \omega \cdot t) \right) \quad (\text{A3.9})$$

The synchronous speed of the rotating MMF is given by $\omega_{\text{sync}} = 2\pi \cdot f \cdot p^{-1}$. The motor slip is given by $s = (\omega_{\text{sync}} - \omega_{\text{rr}}) \cdot \omega_{\text{sync}}^{-1}$, where ω_{rr} is the rotor angular speed. In general, excitation time harmonics corresponding to $6 \cdot n \pm 1$ order produce MMFs potentially problematic to IMs, thus should be avoided [29], [31].

A3.2.1 Stator Winding Evaluation Factors

Regarding stator winding evaluation factors, a number of considerations can be made.

Only coil-sides embedded in the slot (useful copper) contribute to the mechanical power production or electromagnetic torque generation. The coil-heads or out-slot copper (useless⁹ copper), which shunt the in-slot coil sides (Fig. A3.5), do not contribute to generate electromagnetic torque, and contribute significantly to the copper losses and to the stator leakage inductance (accounts for about ¼ to ⅓ of the total stator leakage inductance). The ratio or balance between the useless and the useful copper or head/slot copper ratio, *BAL*, is defined by the quotient between coil-heads and in-slot copper, according to (A3.10).

$$BAL = \frac{\gamma_{avg}}{l_t} \quad (A3.10)$$

The lower the *BAL* is, the higher the motor efficiency will be, and, in principle, the higher the motor reliability [2]. The minimization of the *BAL* is also important to improve the overall thermal dissipation of the heat produced in the stator windings, because it leads to the reduction of the amount of copper in a higher thermal resistance mean (air) and increases the amount of copper in a lower thermal resistance mean (core and electrical insulation materials). If the motor runs cooler, the copper losses will be lower, which in turn contributes to the decrease of the temperature.

The coil-heads can have different shapes (e.g., diamond or round, as in Fig. A3.5). The mean length of turns (MLT) can be defined as the total length, including useful and useless copper, of the conductor of an average coil turn. The volume of copper, V_{cu} , which depends on MLT, phase-turns, and conduction section, can be easily calculated, and it is also important factor to take into account in the evaluation of the stator winding. The actual coil-head conductor average length is longer than the corresponding average coil-pitch, γ_{avg} .

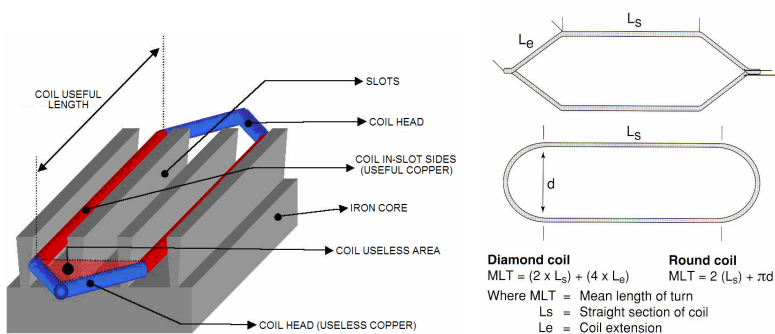


Fig. A3.5. Useful and useless copper in the coils and the mean length of turn (MLT) [35].

The quality of the produced rotating air-gap MMF waveform can be evaluated by the total space harmonic distortion, *TSHD*, considering, for example, only the four or six most relevant space harmonics, according to (A3.11).

⁹ From the torque production perspective.

$$TSHD = K_{wl}^{-1} \cdot \sqrt{\sum_s \left(\frac{K_{ws}}{s} \right)^2} \cdot 100\% \quad (\text{A3.11})$$

To improve the MMF distribution, it is convenient to maximize the space fundamental component ($s = 1$) and minimize the space harmonic components ($s > 1$), particularly those generating rotating MMFs in opposite direction in relation to the fundamental rotating MMF (5th, 11th, 13th order harmonics). The other space harmonics also contribute to drag the rotor because they generate rotating MMFs with an angular speed lower than fundamental rotating MMF. The contribution of such waves to the torque is negative, and they are responsible for additional vibrations and rotor losses in the motor. They can be seen as parasitic “shaft machines” with $s \cdot p$ pole-pairs [1], [3], [28], [29], [31], [39]. The slot effect perturbs the considered harmonics, introducing new components in each pole number, depending on the slot number. Therefore, space harmonics can distort the torque-speed curve, particularly in the starting zone (see Appendix 6), which, in some cases, can lead to starting problems. The combination of space and time harmonics results in a wide range of rotating harmonic MMFs. However, in this section, this issue is not addressed, being considered non-distorted winding excitation. A winding design focused on the mitigation of the excitation time harmonic effects with proper space harmonic variation (properly choosing the coil-pitch¹⁰), has minor impact on the motor performance. In fact, in terms of torque-speed curve, the effect of the time-space harmonic pairs is negligible when compared to the time or space harmonic effect separately. For example, although the combination of 5th order space and time harmonics produce a rotating MMF with speed and direction equal to fundamental, the amplitude is equal to the product of the amplitude of both waves, which is actually very low, thus having minor effects on the motor torque-speed curve, when compared to the effect of individual space or time harmonics. Yet, particular space harmonics attenuation (as well as proper slot skewing) can be considered to minimize the torque pulsations¹¹ and motor vibrations, which are related to the interaction between the fundamental and harmonic stator and rotor fluxes, as well as to the slotting effects. For example, the 5th and 7th space harmonics can be combined to produce a torque that pulsates at a frequency corresponding to the 6/5th (equal to 1.2 times the fundamental

¹⁰ Further considerations on pitch shortening are discussed in Section A3.2.11. The coil-pitch shortening is often used in double-layer windings in order to reduce or suppress some MMF space harmonics. Double-layer means 2 coil-sides per slot (considering 2 slot zones – upper zone and lower zone). Single-layer means 1 coil-side per slot.

¹¹ Pulsating torques are cyclic fluctuations of the steady-state motor torque, measured as a peak-to-peak variation, caused by interaction between harmonic currents and the fundamental frequency magnetic field. In fact, in the torque pulsations caused by interaction between MMF components with same pole number but different speeds, the pulsating magnitudes depend upon the magnitude of the interacting MMFs and speed difference. For example, if a three-phase winding sinusoidally excited at fundamental frequency produces a rotating forward MMF at fundamental synchronous speed, and a 5th excitation current harmonic exists in the winding, producing a backward MMF with a speed 5 times higher than the fundamental synchronous speed, the interaction between the stator 5th harmonic MMF and the rotor fundamental MMF results in a pulsating torque with a frequency equal to $1 + 5 = 6$ times the fundamental frequency. The 5th and 7th time harmonics produce each one a pulsating torque with a frequency equal to $1 + 5 = 6$ and $-1 + 7 = 6$ times the fundamental frequency, respectively.

frequency) and $6/7^{\text{th}}$ (equal to 0.857 times the fundamental frequency) order excitation harmonics (which are actually inter- and sub-harmonics), being potentially worse than that pulsating at a frequency corresponding to the 6^{th} (6 times the fundamental frequency) order excitation harmonic frequency produced by homonymous excitation time harmonics, due to the fact that the effect of torque ripple in the rotor speed ripple is inversely proportional to the torque ripple frequency and to the system inertia, assuming that no resonance occurs. Actually, in the case of 5^{th} and 7^{th} excitation time harmonics, if the system inertia is significant, the torque ripple effect may result in negligible speed ripple [37]. Independently on the harmonic sequence of the $6 \cdot n \pm 1$ order time harmonics, the torque pulsating frequency is $\omega_{pulsation} = 6 \cdot n \cdot \omega_1$, where ω_1 is the excitation fundamental angular frequency and n is a positive integer [31].

Typically, in the case of inverter-fed IMs, the switching frequency is defined in order to minimize the excitation time harmonics of lower order, and, in most IMs, the windings have a pitch that reduces the space harmonics. Consequently, the most significant torque pulsations found in line-fed or inverter-fed IMs are those resulting from the interaction between 1 or 2 harmonic magnetic fields and the fundamental field, with $2p$ poles and frequency ω_{sync} .

It is also important to evaluate the amount of copper used as a function of the MLT and/or number of turns per phase.

For δ parallel conductors, the conduction section, S_{cond} (in m^2) is given by (A3.12).

$$S_{cond} = \sum_{i=1}^{\delta} S_i = \frac{\pi}{4} \cdot \sum_{i=1}^{\delta} d_i^2 \quad (\text{A3.12})$$

The copper volume, VOL (m^3), is approximately given by (A3.13), where the average coil-pitch, γ_{avg} (m), is given by (A3.14), where h is the slot depth (m), and D the stator core inner diameter (m).

$$VOL \approx 2 \cdot (l_t + \gamma_{avg}) \cdot N \cdot S_{cond} \quad (\text{A3.13})$$

$$\gamma_{avg} = \frac{\pi(D+h)}{Z^2} \cdot 6 \cdot p \cdot \sum_{c=1}^{Z/6p} \gamma_c \quad (\text{A3.14})$$

The average coil-pitch, in slots, is obtained by multiplying (A3.14) by $Z/(\pi(D+h))$. The actual coil-head conductor average length is about 30%-70% longer than γ_{avg} , depending on the coil-head shape and position, which, in the case of round coils, have a curvature radius and a distance from

stator core. For the sake of simplicity, this aspect is ignored in the following comparative analysis, i.e., it is assumed that the coil-head shape remains unchanged.

The per-phase copper winding resistance at temperature θ is given by (A3.15), where σ_{cu} is the copper conductivity and x the equivalent total copper length (in meters), given by (A3.16) [26].

$$R_w^\theta \approx \frac{x}{\sigma_{cu}^{20^\circ C} \cdot S_{cond}} \cdot (0.9214 + 0.00393 \cdot \theta) \quad (A3.15)$$

$$x \approx \frac{VOL}{S_{cond}} \quad (A3.16)$$

The slot-filling factor, SFF , is defined by (A3.17), where S_{cu} is the total conduction (or copper) section in the slot (or useful cross-sectional conduction area), given by (A3.18), and S_{slot} is the slot total useful section, according to Fig. A3.6. There are mathematical methods to determine the S_{slot} precisely for a given slot geometry [2], [26]. However, in this section, for the sake of simplicity, the approximate value of S_{slot} is calculated by the product between the slot average width and the slot depth. The difference between S_{slot} and S_{cu} gives the useless cross-section area, from the electromechanical power production perspective

$$SLL = \frac{S_{cu}}{S_{slot}} \quad (A3.17)$$

$$S_{cu} = S_{cond} \cdot \frac{6 \cdot N}{Z} \quad (A3.18)$$

The TSHD, resistance, copper balance and slot-filling factor variation is given by (A3.19)-(A3.22), respectively.

$$\Delta_{TSHD} = \left(\frac{TSHD''}{TSHD'} - 1 \right) \cdot 100\% \quad (A3.19)$$

$$\Delta_{R_w} = \left(\frac{R_w''}{R_w'} - 1 \right) \cdot 100\% \quad (A3.20)$$

$$\Delta_{BAL} = \left(\frac{\gamma_{avg}''}{\gamma_{avg}'} - 1 \right) \cdot 100\% \quad (A3.21)$$

$$\Delta_{SFF} = \left(\frac{SFF''}{SFF'} - 1 \right) \cdot 100\% \quad (A3.22)$$

Assuming that the winding resistance and the air-gap flux are maintained unchanged, the *SFF* and *VOL* variation can be given in percentage by (A3.23) and (A3.24), where one- and two-line superscripts denote original (base case) and new values, respectively. *VOL* allows the evaluation of the amount of copper savings.

$$\Delta_{SFF} = \left(\frac{(l_t + \gamma_{avg}^{\prime\prime}) \cdot (K_{w1}^{\prime\prime})}{(l_t + \gamma_{avg}^{\prime}) \cdot (K_{w1}^{\prime})} - 1 \right) \cdot 100\% \quad (\text{A3.23})$$

$$\Delta_{VOL} = \left(\frac{(l_t + \gamma_{avg}^{\prime\prime}) \cdot (U_w^{\prime\prime} \cdot f^{\prime} \cdot K_{w1}^{\prime})^2}{(l_t + \gamma_{avg}^{\prime}) \cdot (U_w^{\prime} \cdot f^{\prime\prime} \cdot K_{w1}^{\prime\prime})^2} - 1 \right) \cdot 100\% \quad (\text{A3.24})$$

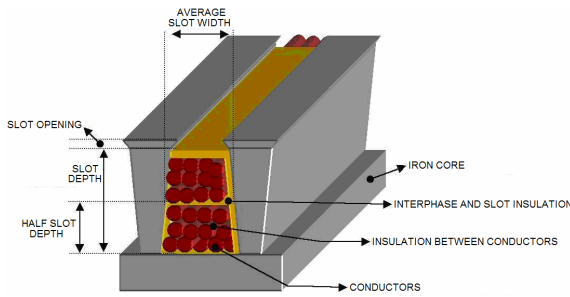


Fig. A3.6. Conductors and insulation system for a semi-closed, double-layer slot.

The goal of the optimization is to minimize R_w and *TSHD*, assuming fixed number of poles, fundamental flux per pole and phase, voltage and frequency.

The *VOL* minimization by means of *BAL* minimization, after *SFF* maximization, is important to minimize R_w , but also the amount of copper used and the associated cost. The optimization can be made by decreasing the coil pitch (slot-by-slot) and, at the same time, properly compensating the N to maintain the original or a proper per-pole magnetizing flux, until the most advantageous solution is found, i.e., *TSHD* and R_w minimized (if not minimized at the same pitch, R_w should have priority over *TSHD* if the aim is to maximize motor efficiency). In general, the pole-pitch should not be lower than $\frac{2}{3}$ of the polar-pitch. It is also necessary to ensure that the current density is equal or lower than the original or a proper value, and that the new slot filling-factor is feasible.

A3.2.2 Number of Turns

The redesign of the stator winding should take into account all the main variables related to the operating condition of the motor, namely, the voltage, load and frequency. A proper redesign maximizes the motor efficiency, power factor, and reliability. Regarding the number of turns, in particular, if the original winding factor, frequency and/or voltage is to be changed, maintaining the original fundamental component of the per-pole, per-phase magnetizing flux (providing that the recommended core maximum induction is not exceeded, particularly in the core teeth), and, therefore, the electromechanical characteristic of the motor, the phase-turns should be properly

changed, according to (A3.25), where one- and two-line superscripts denote original and new values.

$$N'' = N' \cdot \frac{U_w''}{U_w'} \cdot \frac{K_{w1}'}{K_{w1}''} \cdot \frac{f'}{f''} \quad (\text{A3.25})$$

The phase-turns increase can be physically impossible due to the slot space limits. The improper change of the air-gap flux, due to the improper and/or lack of change/compensation of phase-turns leads to the motor efficiency-load, power factor-load and torque-speed curves reshape, which has impact on the starting torque, maximum torque and rated torque (for the quasi-linear part of the torque-speed curve, the torque is approximately proportional to the squared flux), detuning the motor rated power and the corresponding performance (motor efficiency and power factor). However, the number of turns change can be used to rematch oversized motors to the actual load, with significant benefits in terms of motor efficiency and power factor. Figs. A3.7-A3.10 show the simulated results for a 3-kW, 4-pole motor, considering thermal compensation¹² and varying phase turns, without stator resistance compensation by means of conductors diameter variation. In Fig. A3.11, an example of the flux variation effect in a 15-kW motor is shown, extracted from [34]. It is possible to conclude that, the higher the motor power, the lower the efficiency gains due to the flatter efficiency load curves.

However, in some cases, with a careful study, including the motor load profile over time (e.g., using current- or slip-based in-field motor load estimation methods, see Chapter 4) and actual terminal voltage profile¹³, the readaptation or rematching of the motor to specific operating conditions can lead to the improvement of its efficiency and power factor. The proposed idea is to reduce properly the rated power of oversized motors by redesigning the stator windings and, if possible, reducing the cooling fan power (which also reduces the acoustic noise¹⁴) and replacing standard bearings by low-friction bearings. This approach allows converting standard motors (old EFF3 class), which represent the vast majority of in-operation motors stock, in energy-efficient (EFF2 or IE1 class) or high-efficiency (EFF1 or IE2 class) motor, if there are no major damages in stator core and rotor. Additionally, the proposed strategy only makes sense if the motor start/stop

¹² The motor temperature varies with the ambient temperature, load and efficiency, and has an impact in the motor parameters. The operating temperature also influences the length and slope of the quasi-linear part of the torque-speed curve, because of the rotor resistance variation as a function of the temperature. Therefore, the slip is directly related to the rotor resistance. The stator resistance and copper losses also depend on temperature. Therefore, thermal dependency and compensation of the motor parameters is very important to consider in simulations.

¹³ According to IEC 60034-1, IMs should be able to operate continuously at full load with long term voltage deviation of voltage of $\pm 5\%$ (in this situation the motor temperature can increase up to 10°C) for rated frequency, being acceptable voltage deviations of $\pm 10\%$ over short periods. According to NEMA, for full-load continuous operation a $\pm 10\%$ voltage deviation is admissible. In Portugal, the voltage drop from voltage supply to motor should not exceed 5% (for continuous operation) and 10% during starting period. However, this voltage drop can be combined to network voltage fluctuations (e.g., peak and off-peak periods) potentially leading to higher variations. For redesign purposes only constant components should be considered.

¹⁴ The acoustic noise can be given in pressure ($L_p = 20 \cdot \log_{10}(P/P_{ref})$) or in power ($L_w = 20 \cdot \log_{10}(W/W_{ref})$), and increases with the frame size and rated speed (depending on the number of poles) [26].

rate and/or required dynamic response are low, since decreasing the motor rated power maintaining the same rotor inertia, increases significantly the relative mechanical time constant of the motor.

It should be noted that the typical low motor load factor (on average, 50-60%) is an important factor behind the mismatch between actual and rated motor efficiency, which is a common situation, even considering the allowed voltage-drop in power cables (which should also be considered in the redesign), as well as the fact that a large part of the motors operating in industrial plants with more than 10-15 yr are rated to 380 V and are actually being supplied at 400 V (+5.3%), pushing the efficiency-load curve peak to higher loads.

Regarding voltage, the fluctuations depending on external, changeable, non-controlled factors should also be taken into account. For example, for a 7.5-kW, 4-pole, TEFC motor, assuming that there are no starting problems, if the motor load is 50%, an increase of 5% in the phase turns, with proper increase of conductors diameter to maintain the same winding resistance, results into an efficiency increase of approximately 2%, and a power factor increase of 0.08 (from 0.56 to 0.64).

Phase-turns can be properly matched to the actual motor load profile taking into account the actual voltage at its terminals, during the most demanding period (or maximum steady-state load) of the operating cycle.

If the phase-turns change takes place, to ensure that the winding resistance does not increase, it is necessary to change the wire conduction section accordingly, as in (A3.26), where N is the number of turns per phase.

Additionally, to overcome the standard gauges limitation, combination of parallel conductors can be used.

$$S_{cond}'' \geq S_{cond}' \cdot \frac{(l_t + \gamma_{avg}'') \cdot N''}{(l_t + \gamma_{avg}') \cdot N'} \quad (\text{A3.26})$$

For motors operating with loads lower or equal than nominal, if the winding factor, frequency and/or voltage are to be changed (in relation to original values), a simple criteria/method to adapt the phase-turns to the actual motor operating conditions (by properly changing the fundamental per pole magnetizing flux level) can be used which is defined by (A3.27), where one- and two-line superscripts denote original (or base case) and new values, respectively. Equation (A3.27) does not take into account the speed variations as a function of load type.

$$N'' \approx N' \cdot \frac{U_w'' \cdot K_w' \cdot f'}{U_w' \cdot K_w'' \cdot f''} \cdot \frac{1}{\sqrt{\zeta}} \quad (\text{A3.27})$$

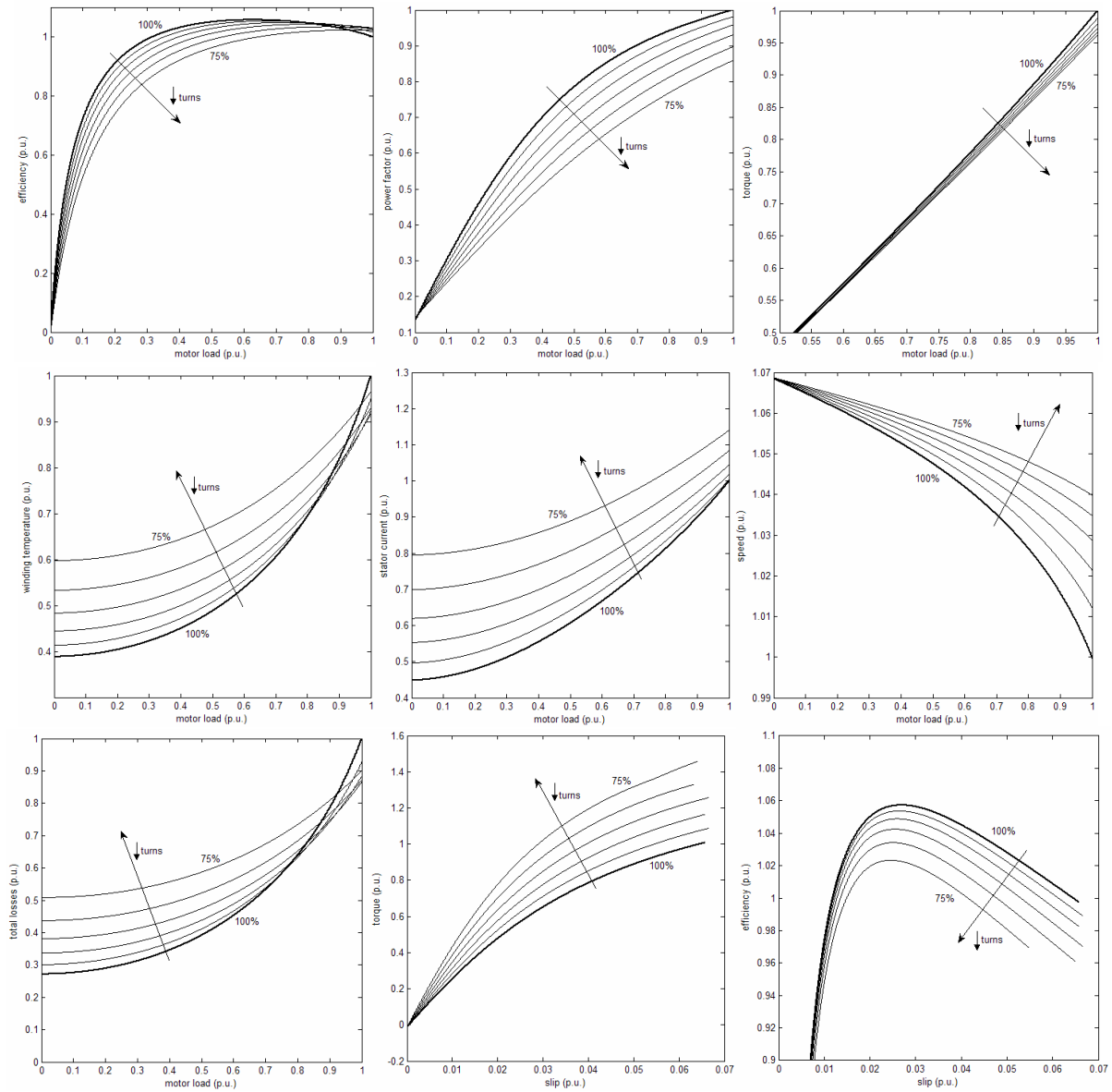


Fig. A3.7. Simulated efficiency, power factor, torque, winding temperature, stator current, speed, and total losses for a 3-kW, 4-pole motor, decreasing motor turns in 5% steps (25°C ambient temperature).

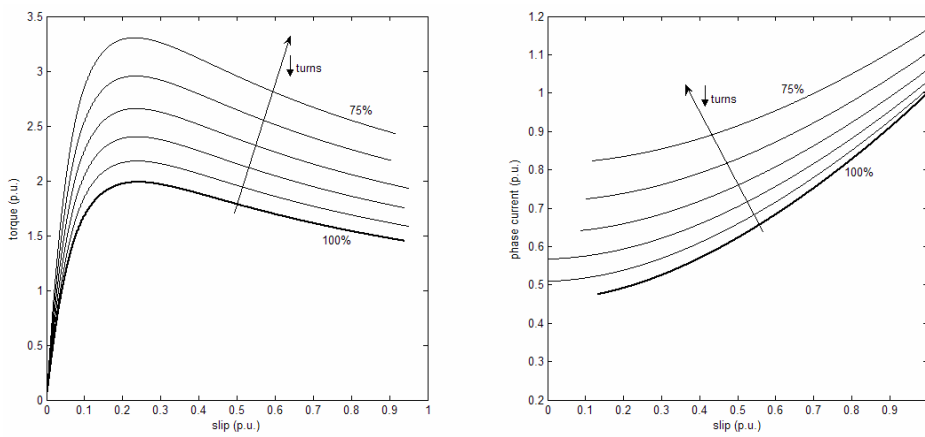


Fig. A3.8. Simulated torque and phase current for a 3-kW, 4-pole motor, decreasing motor turns in 5% steps and considering 25°C constant temperature in all motor parts homogenous temperature.

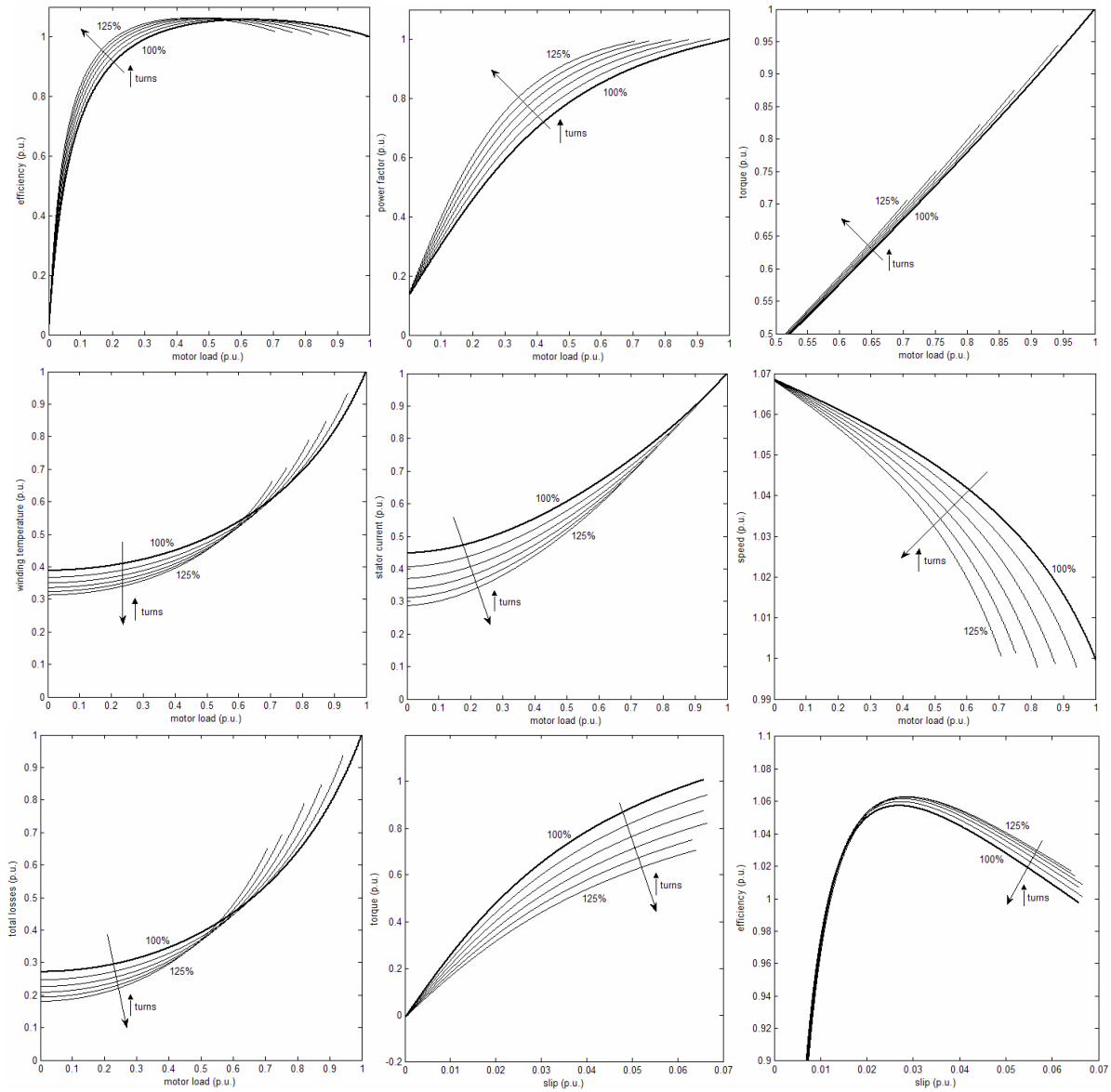


Fig. A3.9. Simulated efficiency, power factor, torque, winding temperature, stator current, speed, and total losses for a 3-kW, 4-pole motor, increasing motor turns in 5% steps (25°C ambient temperature).

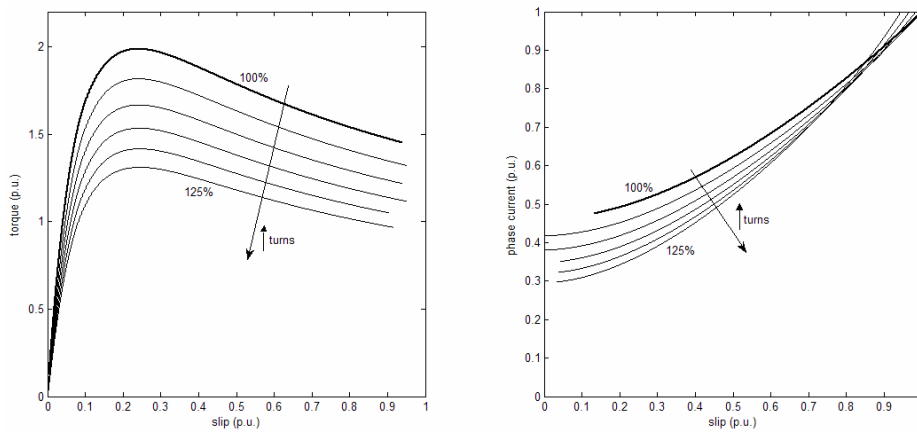


Fig. A3.10. Simulated torque and phase current for a 3-kW, 4-pole motor, increasing motor turns in 5% steps and considering 25°C constant temperature in all motor parts.

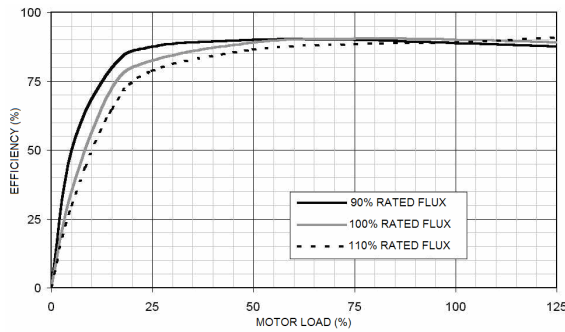


Fig. A3.11. Effect of the magnetic flux variation in the efficiency curves for a 15-kW three-phase induction motor (assuming unsaturated core) [34].

A more accurate method is presented in Table A3.1, in which the motor load type and terminal voltage profile should be known. The most used load point should be selected for motor optimization, providing that it is still able to drive the load in the highest demand situations, without overheating (derating of overload conditions shorter than motor thermal constant). For the same voltage, knowing the optimum slip or efficiency-peak corresponding slip (typically between 60% and 100% of the nominal slip) and the actual slip, the winding can be redesigned in order to ensure that the new slip is close to the optimum slip. Of course, to apply the described method, the nominal and actual slips before motor failure have to be known. The motor slip has to be recorded/monitored for the highest motor load level, as well as the actual voltage and frequency at the motor terminals for the same conditions, in order to check if they match the rated values (nameplate information). It should be noted that, when the motor is operating in the quasi-linear part of the torque-speed curve, the motor load is approximately proportional to the slip. Ignoring the internal temperature variation and considering $y = s''/s'$ (s'' should be the optimum slip) and $T \propto \phi^2$ (which is an approximate relation for the quasi-linear part of the torque-speed curve), in order to maintain motor operating close to the maximum efficiency, the flux can be changed (reduced) as a function of the type of load according to the rules presented in Table A3.1, assuming fixed pole-pairs and winding connection, small turn increase ($\leq 10\%$) and/or frequency changes ($\leq \pm 10\%$), proper conduction section compensation and $U_w \approx E_l$. No voltage compensation is made on slip because, as it can be seen in Fig. 3.65 (Chapter 3), the variation of the optimum slip with the voltage is very reduced (practically inexistent). If the previous equations are respected, the efficiency will be maintained close to its maximum, for a motor load, voltage, frequency and/or winding factor different from the original, as a function of the load type.

If the motor load is equal or close to full load (rated power), improper reduction of phase-turns leads to the increase of the flux (until full saturation is reached), iron losses, torque (starting, maximum and rated) and no-load current, as well as to a reduction in the power factor (see Fig. A3.8). For overloaded motors, the only acceptable solution is their replacement by properly sized

motors¹⁵. When an oversized motor is redesigned for a lower power, with lower flux, and the fan is shortened properly (in the case of TEFC motors), it will run efficiently and the peak efficiency will increase, because the steady-state internal temperature, current, copper losses and the core losses will decrease significantly (this was experimentally confirmed). This approach is encouraged if there is no major damage in the core (e.g., due to winding burnout process during rewinding) and proper bearings are used. Moreover, the phase-turns can also be more accurately optimized using simulations with equivalent circuits with thermal compensation, although this process is extremely time consuming if the motor parameters have to be experimentally estimated.

In the case of VSD-fed motors, in order to avoid the operation in the overmodulation zone (which produces 5th and 7th time harmonics) and/or the operation with a large slip (poor efficiency), the winding rated voltage can also be properly reduced to match the fundamental inverter output voltage for unity amplitude modulation index at the rated operation frequency, improving motor performance. It should be noted that typical VSDs operate in the overmodulation region when producing a fundamental output voltage equal to the input fundamental line voltage. Additionally, if the user wants to avoid the field-weakening zone for frequencies higher than rated, the number of turns can be properly reduced in order to reduce the voltage at rated frequency for rated flux (this is equivalent to maintain rated voltage and increase rated frequency). Of course, this reduction has to be accomplished by conduction section increase, in order to maintain a proper current density value in the conductors. The VSD must also be able to handle the extra current. Under steady state, considering constant torque, a motor with rated power corresponding to the highest required power has to be used.

For example, in order to avoid overmodulation, or, instead of that, linear modulation with high slip operation (poor efficiency), for a 400-V line-to-line voltage system the winding rated voltage can be properly reduced to 330-340 V, potentially leading to an improvement in the motor performance.

The number of turns can be adapted to the actual operating voltage at motor terminals, in order to match the stator winding voltage to the supply voltage. This can be useful when, for example, there is significant voltage reduction due to the power cable voltage drop. However, those changes should be made taking into account the actual motor maximum load in steady state.

If the motor is oversized, an increase in the number of turns, N , and the consequent reduction of the flux, can lead to improvements in the motor efficiency and power factor.

Sometimes, to reduce the execution time and/or the used amount of copper, the rewinders reduce the N , which leads to the increase of the flux. In these circumstances, if the motor load is equal or

¹⁵ In overloaded motors a decrease in the N can lead to an increase of the motor efficiency and mechanical overload limits, as well as to a significant increase of the starting torque if the saturation level is still acceptable, which is not likely to happen in practice, but the thermal limits of the motor will be exceeded, shortening its lifetime.

close to full-load (rated power), an increase in the iron losses, start, maximum and rated torque and no-load current will occur, as well as a reduction in the power factor.

The described approaches can be used by motor rewinders and designers for optimization of the motor operation, and contributes to the rehabilitation of oversized motors, bringing their efficiency up to higher levels, particularly in Industry, where most motors are oversized.

If there is no damage in the core during rewinding and proper bearings and fans are used, the oversized motor will run efficiently for lower levels of flux (this was experimentally confirmed). When the new load is considerable lower than the original, the motor efficiency improves significantly if a smaller fan is used.

When the number of phase-turns results fractional, it should be rounded to the nearest integer. However, when coil-turns result fractional, the resulting extra turns have to be ignored (resulting in a slight flux increase) or increased (resulting in a slight flux decrease) in eccentric windings to avoid asymmetries, but can be properly distributed by the coils in concentric windings, allowing to maintain the flux very close to the specified air-gap flux level, following the optimum distribution (see Appendix 6). This will result in a better flux distribution for concentric windings, with less spatial harmonic distortion. For example, if one turn has to be introduced in each group of coils per pole, it should be added to the coil with higher number of turns for the optimum distribution. It is very important to guarantee symmetrical flux distribution. Phase-turns unbalance, similarly to voltage unbalance, has a negative impact in the efficiency and reliability of the motor, because it will run hotter and with decreased efficiency. These situations have to be avoided, and can be easily identified using an ammeter and/or a surge test (Fig. A3.12).

TABLE A3.1
MOTOR MAGNETIZING FLUX AND PHASE-TURNS AS A FUNCTION OF LOAD TYPE AND SLIP FOR EFFICIENCY MAXIMIZATION.

Load Type	Magnetizing Flux	Number of Turns per Phase
Constant Torque (e.g., lifts, conveyors, and piston compressors)	$\phi'' \approx \phi' \cdot \frac{1}{\sqrt{y}}$	$N'' \approx N' \cdot \sqrt{y} \cdot \frac{U_w'' \cdot f' \cdot K_w'}{U_w' \cdot f'' \cdot K_w''}$
Linear Torque (e.g., industrial mixers)	$\phi'' \approx \phi' \cdot \frac{1}{\sqrt{y}} \cdot \sqrt{\frac{1-y \cdot s'}{1-s'}}$	$N'' \approx N' \cdot \sqrt{y} \cdot \frac{U_w'' \cdot f' \cdot K_w'}{U_w' \cdot f'' \cdot K_w''} \cdot \sqrt{\frac{1-s'}{1-y \cdot s'}}$
Quadratic Torque (e.g., centrifugal fans and pumps)	$\phi'' \approx \phi' \cdot \frac{1}{\sqrt{y}} \cdot \frac{1-s'}{1-y \cdot s'}$	$N'' \approx N' \cdot \sqrt{y} \cdot \frac{U_w'' \cdot f' \cdot K_w'}{U_w' \cdot f'' \cdot K_w''} \cdot \frac{1-y \cdot s'}{1-s'}$

Note: $y = \frac{s''}{s'}$

If N and/or K_w are used to regulate the magnetizing flux, there is also a change in the motor parameters (particularly stator leakage and magnetizing inductances), leading to a different slip for the maximum efficiency [54]. However, for small N and/or K_w variations, no significant changes will occur in the optimum slip, as it can be seen in Figs. A3.7 and A3.9.

The inappropriate change of N and/or K_{wl} can lead to an undesirable motor efficiency-load curve deformation, as it can be seen in the Figs. A3.7, A3.9 and A3.11. Other motor characteristics are also changed, such as the torque and starting current [47]. In fact, the flux per pole value defines the torque-speed curve and, consequently, the starting torque, maximum torque and rated torque, as it can be seen in Figs. A3.8 and A3.10. If the objective is to preserve the original electromechanical characteristic of the motor, the N should be properly adjusted to compensate the change of K_{wl} , $E_I \approx U_w$, and/or f , according to (A3.27), considering 100% load. As a result of inappropriate increase of N , the IM operates out of rated characteristics (for which it has been designed), which can lead to a decrease of the motor efficiency for a particular load point. Additionally, the increase of N and the reduction of the coil-pitch can also aggravate the negative effects that the VSDs have on the IMs because of the increase of the stator winding leakage impedance, which can lead to an increase of the reflection phenomena in the cables (see Appendix 5).

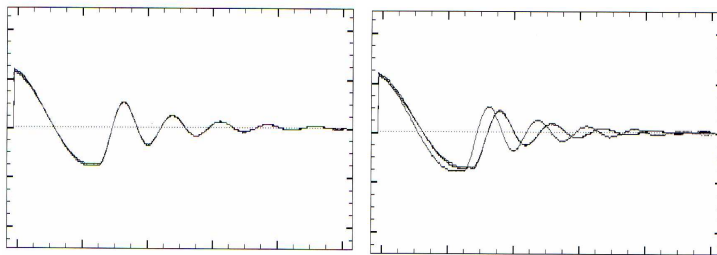


Fig. A3.12. Experimental surge test traces: (left) trace indicating satisfactory winding; (right) trace indicating faulty winding [56].

A3.2.3 Winding Connection

Regarding winding connection, the rated connection, star or delta, can also be properly chosen. Star and delta as rated connections require the same amount of copper, but the star connection requires $\sqrt{3}$ times less turns and $\sqrt{3}$ higher conduction section, for the same performance. On one hand, the rated star connection can be a better choice for the inverter-fed motors or motor started by soft-starters (for such motors, the direct starting problems do not exist), leading to a number of advantages such as delta circulating currents (due to combined effects associated with, for example, saturation¹⁶ and electromagnetic asymmetries) elimination, which produce additional losses, phase turn-to-turn voltage distribution improvement, phase-to-ground voltage stress reduction¹⁷ (as it can be seen Figs. A3.13 and A3.14), bearing current attenuation, phase-voltage waveform improvement, and possibility of extended operation above rated frequency using the delta connection (without entering in the overmodulation and/or in the field weakening operation

¹⁶ Considering the rotor as a short-circuited delta or star (with neutral connected to the short circuited terminals), if the stator is connected in delta, homopolar phase current components can actually circulate in the delta circuit, as well as in the rotor. This 3rd order saturation-related homopolar component grows with the increase of the saturation level (experimentally verified).

¹⁷ This is valid both for voltage peaks in inverter-fed motors (or voltage transients tolerance of line-fed motors) and for fundamental voltage amplitude in the case of line-fed and inverter-fed motors.

zone, in which the motor efficiency is poor), or for short-duration high-torque demand situations, in which the efficiency is not a priority. On the other hand, in a VSD-fed motor rated to delta connection, if the motor operates always below $(\sqrt{3})^{-1}$ of the rated frequency, the winding can be changed for star connection, allowing the amplitude modulation ratio to be kept nearer to unity, in which the harmonic core losses are generally lower (due to the lower THD, for fixed switching frequency), as explained in Chapter 3. However, for line-fed motors, rated delta connection allows to implement a star/delta energy saving management scheme (manual or automatic) as a function of motor load and voltage, as explained in Chapter 5.

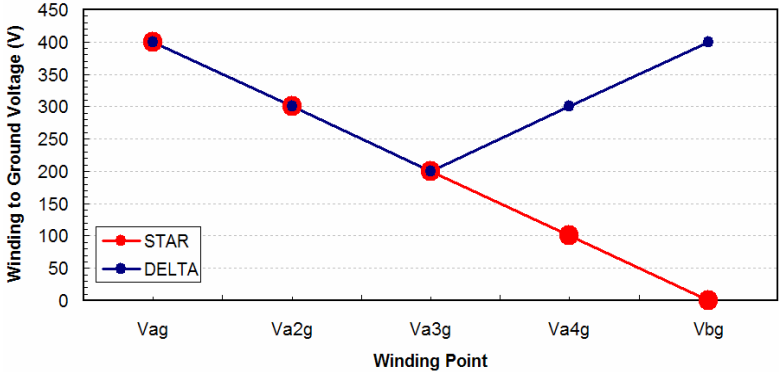


Fig. A3.13. Theoretical, winding to ground voltage for different intermediate winding points and connection modes.

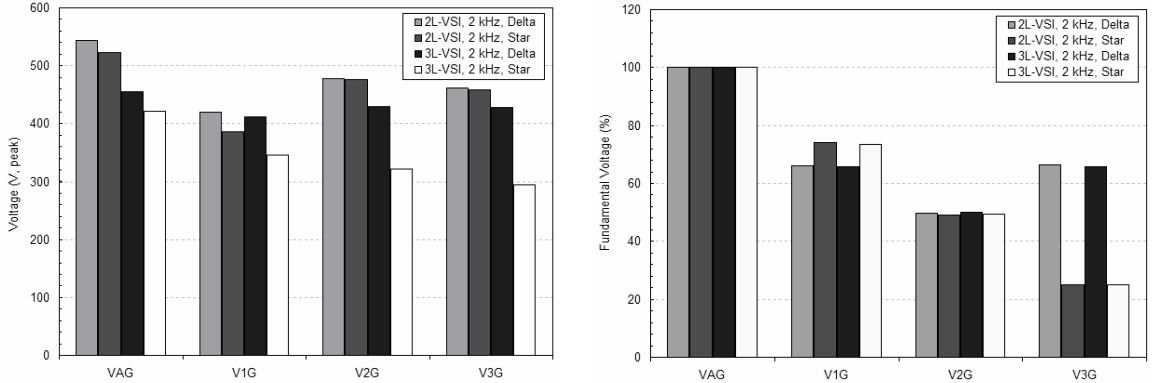


Fig. A3.14. Experimental peak voltage and fundamental voltage between winding phase intermediate points and ground for a 7.5-kW, 4-pole motor fed by a 2-level and by a 3-level inverter (VAG – terminal lead; V1G – first intermediate point; V2G – second intermediate point; V3G – third intermediate point).

A3.2.4 Parallel Conductors

The use of parallel conductors has a number of advantages, namely, easier coil-insertion in core (coils become more flexible), varnish-retaining improvement during impregnation¹⁸ (due to the contact area extension, as it can be seen in Fig. A3.15), slot-filling factor increase (due to the improved conductor distribution in slots, as it can be seen in Fig. A3.16), better heat dissipation,

¹⁸ This is a critical aspect of the impregnation process, since even when high-quality impregnation processes such as vacuum-pressure impregnation (VPI) are used, if the varnish/resin retention degree is poor (mainly related to impregnant viscosity), it will leakout from windings during curing or drying process increasing air-cavities (this can be avoided by rotating curing process).

copper loss reduction, winding temperature decrease, electrical and mechanical robustness increase, and harmonic stator Joule loss reduction [26].

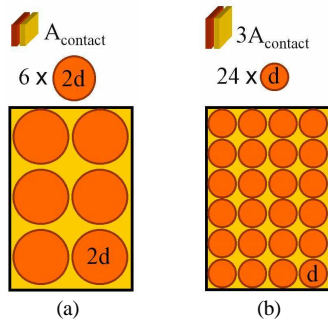


Fig. A3.15. Effect of number and gauge of conductors in the impregnant reduction during curing process. Contact area between conductors and resin or varnish: (a) 6 conductors with diameter $2d$; (b) 24 conductors with diameter d .

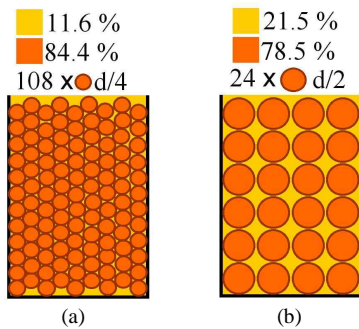


Fig. A3.16. Influence of the conductors gauge and number on the slot-filling factor: (a) 108 conductors with diameter $d/4$, $SLL = 84.4\%$; (b) 24 conductors with diameter $d/2$, $SLL = 78.5\%$.

Considering the same rated current, the total conduction section of the parallel conductors has to be equal or higher than the total original conduction section, in order to not exceed the maximum current density values in the conductors or increase the Joule effect losses, as explained before. If δ parallel conductors with section S_δ are used, condition (A3.28) has to be fulfilled. The new conductor diameter is given by (A3.29). If δ parallel conductors with different sections S_i are to be used, (A3.30) has to be fulfilled. Of course, the available standard or normalized gauges have to be taken into account in (A3.28)-(A3.30), and the calculated or the immediately higher gauge should be chosen. The number of parallel conductors and the respective gauge should be chosen in order to maximize SLL . However, the increase of the conduction cross-section is some times impossible in terms of available slot space.

$$S_\delta'' \geq S_\delta' \cdot \frac{\delta'}{\delta''} \quad (\text{A3.28})$$

$$d_\delta'' \geq \frac{2}{\sqrt{\pi}} \cdot \sqrt{S_\delta' \cdot \frac{\delta'}{\delta''}} \quad (\text{A3.29})$$

$$\sum_{i=1}^{\delta''} S_i'' \geq \sum_{i=1}^{\delta'} S_i' \quad (\text{A3.30})$$

A winding with parallel conductors or construction of coils with parallel conductors can be made with individual coils wound with parallel conductors (parallel conductors wound simultaneously - adequate process), or with parallel-connected, one-conductor, separated coils (coils wound separately and after connecting them in parallel). In the latter process, the physical contact between the last turns of one coil and the first turns of other parallel-connected coil should be avoided (by optimized coil winding), because it results in a significant voltage between them, potentially decreasing the winding reliability or electrical robustness. In general, the first and last conductors of coils should be avoided and, when possible, first turns of a coil should be located at the inside/central part of the coil cross-section, reducing the partial discharge occurrence possibility (see Appendix 5).

Assuming that the enamelled wire insulation thickness is significantly lower than its section radius, the use of parallel conductors leads to a slight increase of the space associated to the wire insulation but the cross-sectional conduction area gain due to the conductor conditioning improvement in the slot, makes that increase negligible. In a 37-kW, 4-pole motor, an increase of the total conduction section was achieved by replacing a 2.16-mm² wire by two 1.18-mm² wires in parallel (total of 2.36-mm² section), leading to a reduction of 8.5% in the stator copper losses [3], [26].

For the rewinders, the use of conductors in parallel can also be a good solution when the stock of the needed wire gauge(s) ends, because a proper combination of different conductors in parallel can be found. It should be referred that, due to several reasons, such as cost reduction, lack of electric wire with the proper gauge, or facilitation of the introduction of the coils in the slots, in some cases, the repairer uses conductors with a section lower than the original, which leads to the SLLs decrease and to the stator copper losses increase.

In the case of inverter-fed motors, the use of parallel conductors (with reduced cross section) can reduce the high-frequency harmonic (or additional) Joule losses in stator, which are, in part, related to the skin effect¹⁹ (Fig. A3.17) and eddy currents induced in the stator conductors (Fig. A3.18) by flux harmonics (they can also be induced by fundamental frequency leakage fluxes), providing that conductors have an individual radius equal or lower than the predicted skin depth (when the skin depth becomes lower than the conductor radius its effective resistance increases) [26].

As it can be easily seen in some published finite-element method (FEM) analysis (Fig. A3.18a), the higher the motor load or slip is, the higher the flux crossing the stator and rotor slots (this phenomenon is potentially intensified for high-frequency harmonics, found in non-sinusoidal voltages waves produced by inverters), which inevitably induces eddy (or Foucault) currents in the stator winding and rotor cage conductors (crossed by those fluxes), increasing harmonic losses and,

¹⁹ During skin effect, harmonic current circulates in conductors without being affected in amplitude, but concentrates at the outer limits, increasing the current density in those parts. The result is an increased effective resistance of the conductor, leading to high Joule losses.

in a small extent, the fundamental losses. When the conductors are crossed by low-amplitude high-frequency magnetic fluxes, currents are induced, increasing Joule effect losses, as it can be seen in Figs. A3.18b and A3.18c. In general, for frequencies lower than 2 kHz, the additional losses are approximately proportional to the conductor conductivity and to the square of the frequency, induction, and conductor diameter [26].

Using parallel conductors with reduced cross section, this loss component can be reduced, since the exposed conductive area, which depends on conductors' diameter, is reduced. Of course, to avoid extra Joule losses and ensure proper current density value, the total conduction section has to be equal or higher than the minimum required section. The skin effect reduction also reduces the high-frequency impedance of the motor, decreasing voltage reflection effect.

Additionally, the parasitic closed-loop eddy currents that can circulate in the paths formed by the electrically connected parallel conductors can be blocked (or strongly reduced) if the parallel conductors were slightly twisted, as it can be seen in Fig. A3.19 [37].

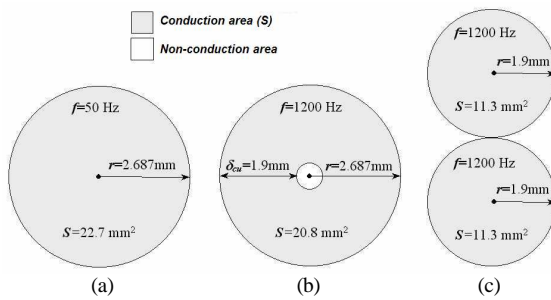


Fig. A3.17. Influence of conductor section/gauge in the conduction area, considering skin effect.

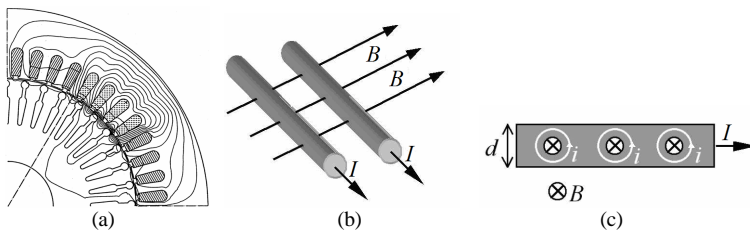


Fig. A3.18. High-frequency additional copper losses production: (a) Typical distribution of high-frequency magnetic fluxes; (b) Conductors crossed by the magnetic flux; (c) Eddy currents in the conductors ($B = B_{max} \text{ sen } \omega t$).

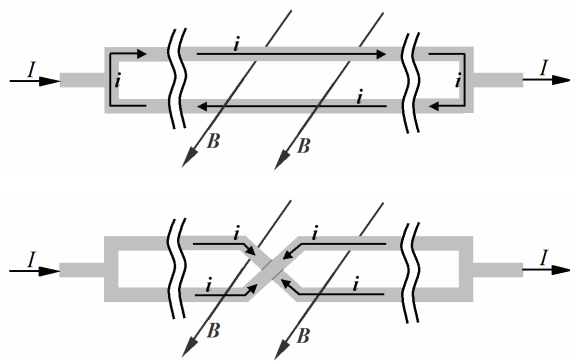


Fig. A3.19. Induced or eddy currents in parallel conductors crossed by a time-varying magnetic flux (induction, $B = B_{max} \text{ sen } \omega t$): (top) regular parallel conductors; (bottom) twisted parallel conductors.

As previously referred, the use of parallel conductors can also improve the impregnation process and the slot-filling factor, contributing to the improvement of the thermal dissipation capacity, to

the stator copper losses reduction and, consequently, to the reduction of the winding temperature. The IM will benefit of improved efficiency and reliability.

Based on the foregoing discussion, the use of parallel conductors in either line- or inverter-fed motors is recommended, particularly for the latter case.

A3.2.5 Parallel Groups

The use of parallel-groups allows the increase of phase-turns, and the decrease of conductor gauge, with the benefits referred in the previous section. Additionally, if the lead-terminals for each parallel group were accessible, flux change (or regulation) using different connection combinations is possible (star and delta combined with parallel and series connection modes). For two per-pole pair parallel-groups, four different useful combinations are possible. If per-phase parallel-groups (made from parallel conductors) are used, more combinations are possible (as explained in Chapter 5). However, the possibility of partial discharge occurrence in the initial part of the winding increases, and the common-mode leakage currents from winding to ground (for the case of inverter-fed motors) are also likely to increase.

A3.2.6 End-Windings

Shorter end-windings lead to: (a) shorter MLT, (b) higher coil-heads mechanical and electrical robustness, (c) reduction of the coil-heads movement/vibration, (d) lower stator copper losses, (e) lower stator leakage reactance²⁰, and (f) lower useless and total amount of copper, and lower amount of copper in a high-thermal-resistance mean (air), increasing the overall dissipation capability of the heat produced in the stator windings. If the motor runs cooler²¹, the copper losses will be lower, contributing to the decrease of the temperature itself. All these effects, lead to the improvement of the motor efficiency and reliability. Since the reduction of the head length leads to the increase of the mechanical robustness of the winding, an increased reliability is expected, particularly for motors with frequent starts and/or driving high-inertia loads. The reduction of end-windings movement/vibration (particularly during motor starting [26]) and local temperature by means of coil-heads length reduction is important because it contributes to the reduction of the probability of insulation breaking in the base of the coils (which is the most critical zone), particularly in the motors with frequent starts. However, if the end-windings are too close to the core, the air does not circulate between them, thus, the heat flow from the end-windings to the frame by internal convection will be potentially worse. Nevertheless, the impact of that is minor,

²⁰ The leakage reactance is related to the leakage flux and includes mainly the flux that closes around the coil heads and the flux that crosses the stator slots without crossing the rotor squirrel-cage conductors. Note that, if the IM is fed by a VSI-PWM, it is convenient to reduce the leakage reactance associated with the coil heads in order to reduce the voltage reflection coefficient in the power cables between the inverter and the motor and, consequently, the amplitude of the voltage transients (peaks) at the motor terminals. However, the increase of the stator leakage inductance can contribute to the harmonic and loss reduction. If the IM is fed directly by the line, it is advantageous to reduce the leakage reactance associated to the coil heads since it will contribute to the motor power factor improvement.

²¹ Due to the lower local heating, there is a lower thermal degradation of the insulating system. The insulation properties (dielectric constant and strength) depend on the frequency and temperature.

because the heat produced by stator windings flows mainly by conduction in the slots. Moreover, there are always small spaces between the coil-heads and the core.

In general, it is convenient to maximize the amount of copper in the slots, since the heat dissipation by conduction is more effective than by convection, ultimately leading to a decrease in the average motor temperature.

Therefore, the end-windings can and should be minimized, by means of reducing the average coil-pitch and the distance between end-windings and the core stack ends. In this process, the rewinder has the handwork advantage, and, therefore, a more efficient winding can be obtained when compared to those obtained with the mass-production industrial equipment for automatic winding, which generally leads to a higher end-winding length. Due to the described benefits, the end-windings minimization is recommended for all motors, but particularly for those with frequent and/or long starts.

Regarding inverter-fed IMs, the impact of end-winding length on the stator leakage inductance, L_s , and, therefore, on current harmonics, deserves some additional considerations. As referred before, the motor slip will be different to each time harmonic associated to the inverter output PWM or 6-step voltage wave. Since the non-fundamental slips are approximately equal to the unity, and the reactances becomes significantly larger than resistances, for the sake of simplicity, it can be assumed that the resultant motor equivalent circuit for the harmonics is only composed by a short-circuit inductance directly connected to an equivalent harmonic voltage source. Harmonic currents magnitude practically does not depend on the motor load. On the basis of the foregoing information, and considering a 6-step inverter, in which $U_h = U_1 \cdot h^{-1}$, the motor approximate harmonic current is given by (A3.31), where $L_{cc} = L_r + L_s \approx 2 \cdot L_s$, and ω is the fundamental frequency.

$$I_h \approx \frac{U_h}{h \cdot \omega \cdot L_{cc}} = \frac{U_1}{h^2 \cdot \omega \cdot L_{cc}} \quad (\text{A3.31})$$

It can be concluded that, if the attenuation of harmonic currents and losses in the motor is important, it can be advantageous to design special machines and stator windings with a large L_s (e.g., by means of implementing larger end-windings), since it will act as a low-pass filter for those currents, without interfering significantly with the fundamental current. However, the L_s increase aggravates the voltage reflection effect in the power cables (voltage reflection coefficient increases), which is an important drawback to be taken into account.

A3.2.7 Slot-Filling Factor

For a given phase-turns number, the higher the *SFF* is (typically it varies between 30% and 65%), the lower stator copper losses (assuming fixed number of turns), the higher the thermal dissipation of the heat generated by the coils, the lower the movement possibility of in-slot conductors, lead all these factors to the motor efficiency and reliability increase. Therefore, for a given phase-turns number, the *SFF* should be maximized.

During coil construction and insertion in the slots, the coil conductors should be properly packed/conditioned in the slot in order to minimize the space between conductors, as it can be seen in the Fig. A3.20a. When the conductors are packed according to the Fig. A3.20b the relation between the useful area (conduction cross-sectional area) and the area delimited by the external boundary of a set of conductors is 79%. When the conductors are packed according to the Fig. 9.20a, this relation increases to 91%. Slots with a low and a high *SFF* are shown in the left and right photos of Fig. A3.21a, respectively. In Fig. A3.21b, the effect of slot filling factor on average (or equivalent) thermal conductivity can be seen. The average thermal resistance²² of the motor is inversely proportional to the thermal conductivity.

The *SFF* also depends on the thickness of the slot and inter-phase insulation and on the rewinder skills. Generally, the handwork, particularly during coil insertion in the slots, due to its flexibility, can lead to *SFFs* higher than those achieved by the mass-production industrial equipment for automatic winding used by manufacturers.

To avoid crossed turns, the better conditioning of the coil turns can be achieved by constructing coils with adequate machines (semi-automatic or automatic), including adequate tensioners and de-reelers.

For the same dielectric strength, the high-quality insulation materials have typically a smaller thickness and higher thermal conductivity, allowing the increase of the *SFF* and, consequently, of the improvement of thermal dissipation between the windings and the core, as it can be seen in Fig. A3.21b [40].

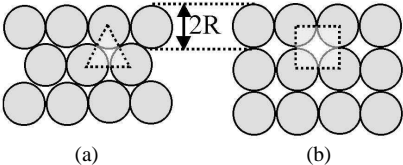


Fig. A3.20. Conductor packing in the slots: (a) Recommended; (b) Unrecommended.

²² The average thermal resistance can be calculated roughly dividing the difference between the distributed winding temperature and ambient temperature, by the motor overall losses.

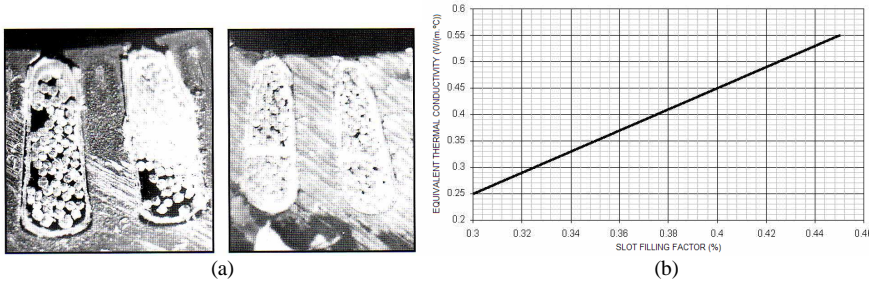


Fig. A3.21. (a) Example of low (left) and high (right) slot-filling factors [35]. (b) Influence of the slot-filling factor on the average thermal conductivity [26].

A3.2.8 Insulation System

Insulation between end-windings and coil-sides of different phases should be used, which is particularly important for inverter-fed motors. Furthermore, the coil-ends of different phases should be insulated, fixed and properly impregnated.

The stator windings of inverter-fed motors, depending on the difference between the cable and motor characteristic impedances and on the voltage variation rate (du/dt) of the inverter output voltages, can experience voltage transients (or peaks) with amplitudes up to 2 times the normal values, which occur with high frequency (depending on PWM switching frequency) and, associated to the high voltage variation rates, lead to the accelerated degradation of the insulation system due, for example, to partial discharges (see Appendix 5). In that way, a premature disruption of the insulation system can occur, leading to shorter motor lifetime. Therefore, in these cases, an insulation system with high electrical robustness should be provided, which can be achieved by combining single-layer windings, high-quality slot and inter-phase insulation materials, reinforced or inverter-rated enamelled wire (different types are commercially available under several different names [26]), and high-quality impregnation (in terms of varnish or resin type, impregnation methods and curing methods²³) [26], [40]. Significant progress has been made in the development of insulation materials able to withstand higher temperatures (F-class and H-class insulation materials). Due to the expected temperature increase in the inverter-fed motors, insulation of F or H classes should be used (and B class should be avoided), which are already the most used insulation classes, particularly the F class, as it can be seen in Fig. A3.22, which shows the market evolution of motor insulation classes in Europe [40].

The increase of the thermal insulation class can be cost-effective in critical systems with high downtime (planned or unplanned) cost, such as continuous process industries. For example, on the basis of Arrhenius' law (see also graphs presented in Appendix 6), expressed by (A3.32), where B is equal to -0.0693 and -0.0431 for insulations and mineral lubricants, respectively, according to Table A3.2, increasing the thermal class from B to F (25°C increase) and from F to H (20°C

²³ For example, vacuum pressure impregnation (VPI) using H-class solventless resin plus rotary curing process can lead to excellent results, minimizing the cavities or air-spaces, reducing hot spots and winding conductors movement during starting, and increasing resistance to moisture ingress [50]. Further information on these issues can be found in [26].

increase), leads to a lifetime 5.7 times higher and 4.0 times higher, to a B-class and F-class temperature rise motor, respectively.

$$t''_{lf} = t'_{lf} \cdot e^{B(\theta^* - \theta')} \tag{A3.32}$$

On average, insulations and lubricants lifetime decreases 50% and 35%, respectively, per each 10°C increase in temperature, as previously referred.

In fact, there are some manufacturers that are incorporating insulation systems with thermal classes higher than the actual temperature rise of the motors at full load in order to extend their lifetime and increase overload capability (e.g., E or B class temperature rise and F or H class insulation system) [50], [70]. Since end-windings opposite to the fan side the highest temperature in the windings of the TEFC IMs, the reinforcement of the insulation system (particularly between phases) in those parts is recommended, including the use of high-temperature grade materials and improved or duplicated impregnation.

It should be noted that the average winding operating temperature depends on and affects the motor efficiency. For a given fixed stator current, stator copper losses increase by approximately 3% when the temperature increases 10°C [26]. Due to their lower losses, energy-efficient or high-efficiency motors can operate at lower temperature, leading to a longer lifetime.

TABLE A3.2
THERMAL CLASSES FOR INSULATION SYSTEMS (ACCORDING TO THE STANDARD IEC 60085) [26].

Thermal classes for insulation systems	A	E	B	F	H
Absolute maximum operation temperature (°C)	105	120	130	155	180

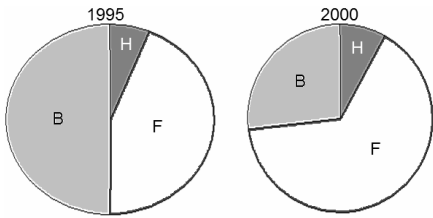


Fig. A3.22. Market evolution of motor insulation classes (B, F and H) in Europe [40].

A3.2.9 Impregnation

A good impregnation is essential to ensure a high electrical, mechanical and chemical robustness, as well as a good thermal dissipation, leading to a longer motor lifetime and, in a smaller extent, to a higher efficiency. Particularly, to improve the coil-heads robustness²⁴, they should be properly fixed and impregnated. As previously referred, reinforced or duplicated impregnation is recommended in the coil-heads opposite to the fan side. For inverter-fed motors, the minimization of the impregnation heterogeneity is critical (e.g., in order to minimize the

²⁴ The base of the coil-head is one of the most critical parts of the insulation system since most failures occur in there.

presence of air-cavities and/or moisture between conductors or between conductors and slot walls), potentially reducing the partial-discharge activity, which accelerates the degradation of the insulation system. The resin or varnish should be chosen properly according to the insulation class and power waveform. A high-quality impregnation is characterized by a proper combination of impregnation, resin or varnish type, and curing methods, in order to ensure a high homogeneity. In general, the recommended processes are the vacuum pressure impregnation, automatic rotary trickle impregnation and manual trickle impregnation repeated twice (see also Appendix 6). Further information on impregnation can be found in [26], [34], [35], and [40].

A3.2.10 Winding Type

Based on a recently developed stator winding design software [2] and on a number of recently published studies, a comparative analysis of the most popular three-phase stator winding types for three-phase cage induction motors is presented in this section.

In the case of low-voltage motors with random-wound stator windings, manufacturers use a few different optimized stator winding types, taking into account the limitations of the mass-production industrial equipment for automatic winding. However, in some situations, the proper winding (re)design, considering the less-limited handwork, can lead to the improvement of the motor performance, as previously referred. Note that, when the motor winding fails and the skills of the rewinder are poor, the exact copy of the original winding is recommended [26].

In this section, the two most popular groups of windings are analyzed, namely, the concentric windings, used by most manufacturers, and the eccentric (also known as lap) windings, used by most rewinders. There are also wave windings but they are not typically used in IMs.

As previously referred, the windings can be classified as a function of the number of coil sides per slot – double-layer if two coil sides per slot are used and single-layer if one coil side per slot is used. In the double-layer windings, each coil has one side in the bottom of one slot and other side in the top of other slot, being possible to change the coil pitch. Neither the fractional windings nor windings with different number of turns per coil are addressed in this section. In the two winding groups referred, there are several types, and the most used are the single- and double-layer eccentric windings, single layer concentric with 2-tier and 3-tier and double-layer concentric winding [26], [34], [35].

Several winding types are thus considered: single-layer eccentric (SLE), double-layer eccentric full- and shortened-pitch (DLEF/S), single-layer concentric 2- and 3-tier (SLC2T, SLC3T), double-layer concentric full- and shortened-pitch (DLCF/S), and a new one, named by the author as double-layer concentric 3-tier full- and shortened-pitch (DLC3TF/S). It is also possible to implement a single layer skip-slot lap (for a 36-slot, 4-pole winding, the coil-spans are 1-10, 3-12, and 5-14) [35], but the *TSHD* is significantly worse than the considered full-pitch windings (the 5th

and 7th harmonics are significantly higher), and, therefore, it is not addressed. Table A3.3 shows the main advantages and disadvantages of the different stator winding types typically used in IMs (additional winding schemes are shown in Appendix 6).

Regarding the Table A3.3, in the DLCS (concentric coils with 5-, 7-, 9-slot pitches, double layer, shortened pitch), the coil-turns can be distributed as follows (related to the total number of turns corresponding to a pole pair): 15.27% on the larger coil (9-slot pitch); 22.67% on the average coil (7-slot pitch) and 12.06% on the smallest coil (5-slot pitch). A fundamental winding factor of about 0.916 is obtained, and all the space non-triplen harmonics up to the order $Z/p \pm 1$ (slotting harmonics) are cancelled (the proposed method²⁵ for this calculation is presented in Appendix 6). This results in non-uniform *SFFs* (there are two types of slots, one type with the two larger coil sides with 30.54% of the phase turns, and a second type with one medium coil and one small coil sides with 34.73% of phase turns. However, non-uniform *SFFs* are complex to design (and may require unequal slot sizes in the stator core) and, although the possible winding improvement in a number of cases, they are not practical for rewinders. Moreover, this kind of optimization is only performed for concentric windings. Nevertheless, for concentric windings, the method described in Appendix 6 can be used to decide in which coil is more advantageous to add the extra turns when non-integer turns per coil result after the total number of turns calculations for a given fundamental flux, winding factor and required electromotive force, assuming that the primary objective is to have all coils with the same number of turns.

SLC2T and SLC3T windings are also named as “by consequent poles” and “by poles”, respectively (Fig. A3.23). The winding in Fig. A3.23a has an average pitch of $((11+9+7)/3) = 9$, and the winding in Fig.A3.23b has an average pitch of $((9+7+7)/3) = 7.7$. In the last case, there is a reduction of the coil-heads copper. SLC2Ts are typically used by manufacturers on IMs with frame sizes smaller than 132, $p = 2$ and $Z = 36$ [26], [34], [35].

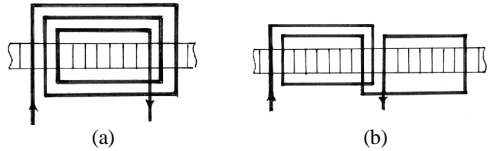


Fig. A3.23. Concentric 4-pole windings for a 36-slot stator: (a) by consequent poles or with 2 tiers ($Z = 36$, $p = 2$, $\gamma_e/\tau_p = 9/9$, $\gamma_{avg}/\tau_p = 9/9$); (b) by poles or with 3 tiers ($Z = 36$, $p = 2$, $\gamma_e/\tau_p = 9/9$, $\gamma_{avg}/\tau_p = 7.7/9$).

DLCS windings became popular in large DL motors (frame size within 225-355) because they can be implemented by a winding machine developed in the 80’s [34], [35].

In general, when compared to the double-layer, short-pitch windings, the single-layer or full-pitch windings have higher electrical robustness, due to the fact that the slots accommodate

²⁵ Optimization processes are based on the Fourier series analysis of the windings, being computed the coil-turns that lead to the mitigation of certain spatial harmonics.

coil sides of the same phase, and, since there is no need for additional insulation between coil sides in the slot, the *SFF* is potentially higher and the rewinding process time is shorter.

Independently of the average coil pitch, double-layer windings, when compared to the single-layer windings, have two times more coils (with half number of turns), making the rewinding process longer, but have better thermal dissipation in the coil-ends²⁶. This aspect is particularly important because the insulation system disrupts mainly in the coil base (near the core stack, particularly in the side opposite to the cooling fan side) and the reduction of the local temperature helps to increase the reliability of the winding. All the winding types need additional insulation between coil-ends of different phases, which is particularly important to the VSD-fed IMs.

The windings of VSD-fed IMs, depending on the power cable length and on the PWM switching frequency and du/dt , can be exposed to a high number of voltage transients over fundamental period, which can lead to the accelerated degradation of the insulation system due, for example, to the partial discharges occurrence. Therefore, all VSD-fed IMs should have reinforced electrical robustness, which can be achieved by the use of single-layer windings, high-quality slot and inter-phase insulation, use of reinforced enamelled wire, and high-quality impregnation with proper varnish or resin.

As previously referred, when applicable, the coil pitch should be properly optimized, being this issues addressed in the next section.

In general, the concentric windings, in relation to the eccentric windings, require more coil forms of different sizes (except for the case of $Z = 6$). In the concentric windings, the SLC3T windings require fewer coil-form sizes than the SLC2T windings, being easily implemented.

Since the SLE windings are electrically robust and easy to implement are recommended for VSD-fed IMs. DLEF windings are also electrically robust and have a good thermal dissipation in the coil-ends, and, although the longer rewinding process duration (in relation to SLE windings, require twice of the coils), are also recommended for VSD-fed IMs. SLC3T windings have simultaneously high electrical robustness, low TSHD and shorter average coil pitch (lower than that for the SLC2T, SLE and DLEF winding) and, although the longer rewinding process duration in relation to that for the SLE windings (requires coils with different pitches, although fewer than those required by the SLC2T winding), are also recommended for VSD-fed IMs.

For IMs fed by VSDs the SLE, DLEF and SLC3T windings are a good alternative for the SLC2T windings. The SLC3T windings are the most advantageous. The SLC2T windings can be replaced by the SLE or DLEF windings, without motor efficiency decrease, and by the SLC3T windings, with a strong possibility of motor efficiency improvement.

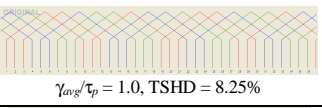
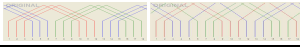
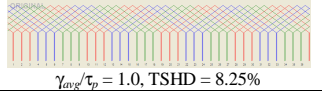
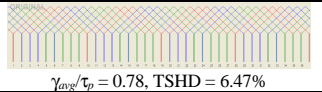
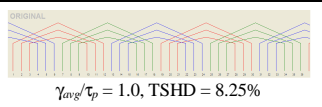
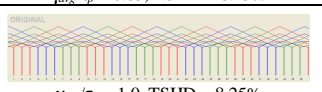
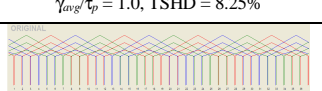
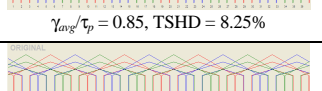
²⁶ The better thermal dissipation is a consequence of the increase (in principle) of the exposed or external area of the coil-ends of the double-layer windings, in relation to the single layer winding, which have twice the number of conductors.

For the line-fed IMs, the DLES windings are the best choice due to the advantages associated with the short pitch and with the double layer. For example, in [35], it was shown that, for an IM with $Z = 36$ and $p = 2$, the replacement of a SLC2T by a DLES with $\gamma_s/\tau_p = 8/9$ leads to an increase of 0.5 p.p. in the motor efficiency. For $\gamma_s/\tau_p = 9/9$ (full pitch) the changes were slight. Alternatively, the SLC3T windings are also a good option when compared to the SLC2T, DLCS, SLE and DLEF windings.

The SLC3T windings should only be replaced by the DLES windings, but the average coil pitch of the latter has to be equal or lower than that of the former. In the replacement of a DLCS by a DLES winding, each of the DLES-winding coils should have a pitch equal or lower than the effective coil pitch of the DLCS winding and, if the coil pitch of the DLES winding does not exceed the average coil pitch of each concentric group of the DLCS winding, in principle, the motor efficiency will not be changed. The SLC2T windings can be replaced by SLE or DLEF windings without motor efficiency reduction, and by DLES or SLC3T windings with a strong possibility of motor efficiency improvement.

TABLE A3.3

ADVANTAGES AND DRAWBACKS OF THE MAIN STATOR WINDING TYPES USED IN IMS [3].

Winding Type	Planar Scheme (for 36 slots and 4 poles)	Advantages (♣) & Drawbacks (♣)	Alternative Windings and their Potential Benefits (♣) & Notes (⚡)
Eccentric or Lap Windings	Single-layer (SLE)  $\gamma_{avg}/\tau_p = 1.0$, TSHD = 8.25%	♣ one coil-form size; ↑ electrical robustness; ♣ insulation material; easy and quick to implement; good for inverter-fed motors. ♣ ↑ losses; ↑ TSHD; poor end-windings distribution.	♣ DLES: ↓ losses, ↓ THSD, ↓ amount of copper, and better end-windings distribution; ♣ SLC3T: ↓ losses, ↓ amount of copper, and ↑ reliability); ♣ DLEF: better end-windings distribution. ⚡ Other possible configurations (with poor end-windings distribution): 
	Double-layer, full-pitch (DLEF)  $\gamma_{avg}/\tau_p = 1.0$, TSHD = 8.25%	♣ one coil-form size; ↑ electrical robustness; ♣ insulation material; good end-windings distribution; good thermal dissipation, good for inverter-fed motors. ♣ long implementation time; ↑ losses; ↑ TSHD.	♣ DLES: ↓ losses, ↓ THSD, and ↓ amount of copper; ♣ SLE: ↓ implementation time, and ↑ reliability; ♣ SLC3T: ↓ losses, ↓ amount of copper, and ↓ implementation time.
	Double-layer, shortened-pitch (DLES)  $\gamma_{avg}/\tau_p = 0.78$, TSHD = 6.47%	♣ one coil-form size; good end-windings distribution; ↓ losses; ↓ TSHD. ♣ ↑ implementation time; ↑ insulation material.	♣ SLC3T: ↑ reliability, ↓ implementation time, ↓ insulation material. ⚡ Reduced average coil-pitch.
Concentric Windings	Single-layer, 2-tier (SLC2T)  $\gamma_{avg}/\tau_p = 1.0$, TSHD = 8.25%	♣ several coil-form sizes; ↑ losses; ↑ TSHD; poor end-windings distribution. ♣ ↑ electrical robustness; ↓ insulation material; easy and quick to implement.	♣ DLES: ↓ losses, ↓ THSD, ↓ amount of copper, and better end-windings distribution; ♣ SLC3T: ↓ losses, ↓ amount of copper, and better end-windings distribution; ♣ SLE: ↓ implementation time, and better end-windings distribution; ♣ DLEF: better end-windings distribution. ⚡ Also known as “by consequent poles”; Typically used by manufacturers on motors with frame sizes up to 132.
	Single-layer, 3-tier (SLC3T)  $\gamma_{avg}/\tau_p = 0.85$, TSHD = 8.25%	♣ several coil-form sizes; poor end-windings distribution; ↑ TSHD. ♣ ↑ electrical robustness; ↓ insulation material; easy and quick to implement; ↓ losses; good for inverter-fed motors.	♣ DLES: ↓ TSHD, and better end-windings distribution; ⚡ Also known as “by poles”. ⚡ Reduced average coil-pitch. ⚡ Require fewer coil-form sizes forms than the SLC2T winding.
	Double-layer, full-pitch (DLCF)  $\gamma_{avg}/\tau_p = 1.0$, TSHD = 8.25%	♣ several coil-form sizes; ↑ losses; ↑ TSHD; ♣ ↑ implementation time. ♣ ↑ electrical robustness; ↓ insulation material; good end-windings distribution; good thermal dissipation; good for inverter-fed motors.	♣ DLES: ↓ losses, ↓ THSD, ↓ amount of copper, and better end-windings distribution; ♣ SLC3T ↓ losses, ↓ amount of copper, ↓ implementation time, and ↑ reliability. ⚡ In the 80’s, became popular in large motors (frame sizes within 225-355). ⚡ Reduced average coil-pitch.
	Double-layer, shortened-pitch (DLCS)  $\gamma_{avg}/\tau_p = 0.78$, TSHD = 6.47%	♣ several coil-form sizes; ↑ insulation material; ♣ ↑ implementation time. ♣ good end-windings distribution; ↓ losses; ♣ ↓ TSHD.	♣ DLES: ↓ implementation time, and better end-windings distribution; ♣ SLC3T: ↓ implementation time, ↑ reliability, and ↓ insulation material. ⚡ Reduced average coil-pitch.
	Double-layer, 3-tier, full-pitch (DLC3TF)  $\gamma_{avg}/\tau_p = 0.85$, TSHD = 8.25%	♣ ↑ electrical robustness; ↓ insulation material; ♣ ↓ losses; good end-windings distribution; good thermal dissipation; good for inverter-fed motors. ♣ several coil-form sizes; ↑ implementation time; ↑ TSHD.	♣ DLES: ↓ TSHD, and better end-windings distribution; ♣ SLE: ↓ implementation time; ♣ SLC3T: ↓ implementation time. ⚡ Reduced average coil-pitch.
	Double-layer, 3-tier, shortened-pitch (DLC3TS)  $\gamma_{avg}/\tau_p = 0.93$, TSHD = 6.47%	♣ several coil-form sizes; ↑ insulation material; ♣ ↑ implementation time. ♣ good end-windings distribution; ↓ TSHD.	♣ SLC3T: ↓ losses, ↓ amount of copper, ↑ reliability, ↓ implementation time, and ↓ insulation material; ♣ DLES: better end-windings distribution, and ↓ implementation time.
	General Notes	<p>⚡ The time of implementation depends on the coil-sides insulation and on the number of coils to insert in the stator. Therefore, double-layer windings take more time to implement, particularly for shortened-pitch.</p> <p>⚡ The thermal dissipation is related, in part, to the amount in-slot insulation and the end-windings distribution.</p> <p>⚡ Concentric windings, in relation to the eccentric winding, require more coil forms of different sizes (except for the case of 6-slot stators).</p> <p>⚡ Double-layer windings, in relation to the single-layer windings, have twice the coils (with half turns) making the rewinding process longer, but have better thermal dissipation in the end-windings zone, due to the increase of the end-windings air-exposed surface, reducing the winding temperature and extending insulation system lifetime. Only in the double-layer windings it is possible the coil-pitch change.</p> <p>⚡ In general, when compared to the double-layer shortened-pitch windings, the single-layer or full-pitch windings have higher electrical robustness, due to the fact that the slots accommodate coil-sides of the same phase, and, since there is no need for additional insulation between coil sides in the slot, the slot-filling factor is potentially higher and the rewinding process time is shorter.</p> <p>⚡ TSHD includes harmonics up to 17th order.</p>	

A3.2.11 Coil-Pitch

In general, shortening the coil-pitch leads to: (a) shorter end-windings (leading to the advantages described in the previous sections), (b) reduced TSHD (better distribution of MMF wave), and (c) reduced per-phase EMF, which has to be properly compensated by means of increasing in the phase-turns and wire-gauge, which can compromise the winding feasibility in terms of slot space. The optimum coil pitch, for each particular case, can be identified using mathematical tools or by an iterative process, using the computed values for each coil-pitch. Starting with full-pitch (equal to pole-pitch, τ_p), the coil-pitch can be decreased slot-by-slot, until the most proper solution is found, which, for specific flux and current values, flux density values equal or lower than the original, and feasible *SFF*, minimizes the TSHD and/or specific space harmonics (electromagnetic benefit), as well as the winding resistance (and, therefore, the stator copper losses - energy benefit). Typically, due to the slot-space limitation, the coil-pitch has to be equal or higher than $\frac{2}{3}$ of pole-pitch. If the winding becomes not feasible due to the excessive *SFF*, the coil pitch should be increased slot-by-slot until feasibility is achieved. Note that, for pitches immediately longer than optimum, the *SFF* variation is slightly negative, meaning that the wire gauge can potentially be slightly increased until *SFF* becomes equal or slightly higher than the original value, reducing the stator copper losses or, alternatively, without resistance variation, the amount of copper used. If the energy aspect is critical, the winding resistance minimization should prevail over TSHD minimization. Figs. A3.24-A3.26, the stator winding performance for different pitches and number of slots is theoretically compared, considering four poles ($p = 2$), core length twice the pole-pitch ($l_t = 2\tau_p$, this relation affects copper volume and *SFF* variation), proper phase-turns and conduction section compensation, for constant current density, fundamental flux and winding resistance, disregarding fractional phase-turns and standard wire gauges. According to Figs. A3.24-A3.26, for 72-, 48- and 36-slot stator, the optimal pitch is 15/18, 10/12 and 7-8/9, respectively. It should be noted that, for the SLC3T winding, the average coil-pitch is naturally reduced (e.g., 72-slot: 15/18; 36-slot: 7.67/9). In some cases, copper savings are possible, without increasing winding resistance. In Table A3.4, an optimization example is presented considering integer and equal number of turns for all coils. The optimum pitch was found to be 7, which minimizes the TSHD and the winding resistance, and, with proper compensation of the number of turns, maintains the original flux. Theoretical and experimental examples of stator winding optimization are presented in Section A3.3.1.

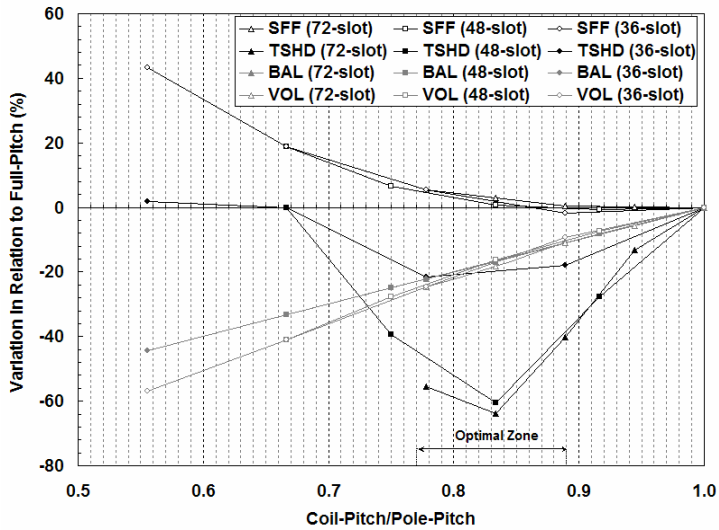


Fig. A3.24. Theoretical analysis of coil-pitch and number of slots influence in the stator winding performance ($p = 2$ and $l_t = 2\tau_p$): SFF, TSHD, BAL, and VOL variation in relation to full-pitch situation [3].

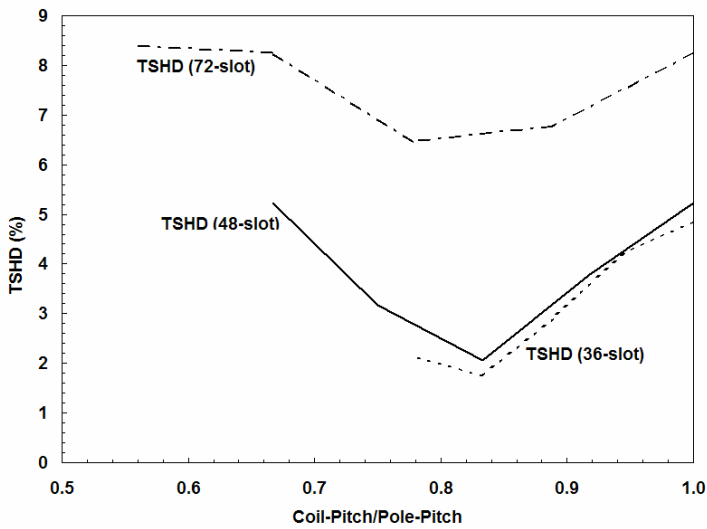


Fig. A3.25. Theoretical analysis of coil-pitch and number of slots influence in the stator winding performance ($p = 2$ and $l_t = 2\tau_p$): TSHD [3].

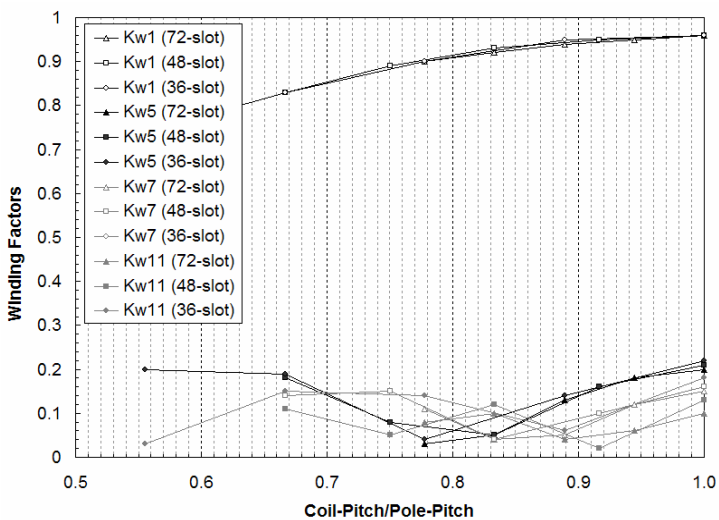
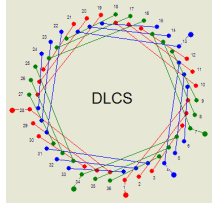
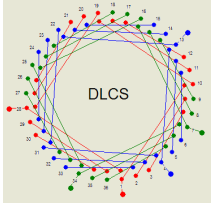
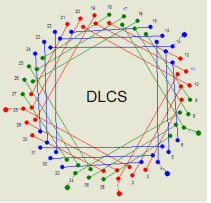
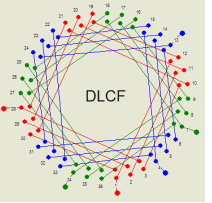
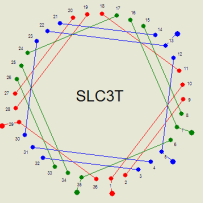


Fig. A3.26. Theoretical analysis of coil-pitch and number of slots influence in the stator winding performance ($p = 2$ and $l_t = 2\tau_p$): winding factors (K_{w1} , K_{w5} , K_{w7} , and K_{w11}) [3].

TABLE A3.4
EVALUATION OF DIFFERENT STATOR WINDING TYPES FOR A 7.5-kW, 4-POLE MOTOR [3].

DLES, DLCS			SLE, DLEF, SLC2T, DLCSF	SLC3T, DLC3TF
				
coil-pitch = 6 slots	coil-pitch = 7 slots	coil-pitch = 8 slots	coil-pitch = 9 slots	coil-pitch = 9 slots
$TSHD = 8.25\%$	$TSHD = 6.47\%$	$TSHD = 6.77\%$	$TSHD = 8.25\%$	$TSHD = 8.25\%$
$R_w = 2.1 \Omega @ 75^\circ\text{C}$	$R_w = 2.0 \Omega @ 75^\circ\text{C}$	$R_w = 2.1 \Omega @ 75^\circ\text{C}$	$R_w = 2.2 \Omega @ 75^\circ\text{C}$	$R_w = 2.0 \Omega @ 75^\circ\text{C}$
$SFF = 78.3\%$	$SFF = 71.2\%$	$SFF = 67.6\%$	$SFF = 67.6\%$	$SFF = 67.6\%$
$BAL = 63.7\%$	$BAL = 74.3\%$	$BAL = 85.0\%$	$BAL = 95.6\%$	$BAL = 81.4\%$
$B_{ag(\text{peak})} = 0.934 \text{ T}$	$B_{ag(\text{peak})} = 0.911 \text{ T}$	$B_{ag(\text{peak})} = 0.959 \text{ T}$	$B_{ag(\text{peak})} = 0.937 \text{ T}$	$B_{ag(\text{peak})} = 0.937 \text{ T}$
Flux = 0.008 Wb	Flux = 0.008 Wb	Flux = 0.008 Wb	Flux = 0.008 Wb	Flux = 0.008 Wb

Notes: 7.5-kW, 4-pole, 36-slot motor; Inner stator core diameter: 110 mm; Outer stator core diameter: 182 mm; Stator core length: 167 mm; Additional coil-heads length: 60%; Copper Conductivity: 59 MS/m. Calculations performed by the winding design software BOBISOFT [2].

A3.3 Winding Design Software Tool

As previously referred in Section A3.1, the improvement of the motor repair market is very important, in order to avoid the increase of the motor operating costs and failure rate over its lifetime. When a motor fails, the main concern of most motor users and rewinders is to get it back into service as quickly and inexpensively as possible. This situation sometimes leads to the use of inadequate repair processes, which can significantly reduce the efficiency and reliability of the motor, as previously explained.

Some users ask repair shops to change some motor characteristics (e.g., number of poles and/or turns), but the winding modification cannot be done correctly without detailed technical expertise, as evidenced in previous sections. In some cases, due to previous incorrect winding change or redesign (poor rewinding), the damaged winding is not the most adequate to the motor and the repair shop is not able to identify the motor manufacturers' specifications. In these cases the repair shop has to fully recalculate the damaged winding. Moreover, motor winding (re)design topics are often neglected or only slightly addressed in most Universities and technical schools and few technical motor rewinding/repair courses are normally available, leading to unprepared technicians/engineers with poor expertise in this field.

In this section, a software tool (named BOBISOFT) is described, which allows the calculations of several important parameters related to the three-phase winding design, with guiding comments, accompanied by numerical data and graphical representations, e.g., circumferential, planar and numerical coil connections drawings, as well as the air-gap MMF curves. With this software it is possible to compare simultaneously 2 different types of windings and, iteratively, change the characteristics until the most appropriate solution is found. Several electromagnetic and energy performance evaluation factors are available, allowing a quick comparison. Additionally, it

provides a display panel to perform core loss test calculations for assessing or control the stator core damage level. This feature is particularly important for motor rewinders. This software tool is appropriate for training, teaching and technical purposes.

Although there are sophisticated software packages for the design of electrical machines, as far as the author know, this was the first WINDOWS environment based software, that allows comparing automatically different types of windings, with different characteristics, providing optimization procedures.

It should be referred that novel general algorithms were developed for programming purposes, with mathematical systematization of the different types of the most common three-phase stator windings.

Nowadays, three motor maintenance companies and one motor manufacturer are being using BOBISOFT, providing feedback for further improvements.

An important advantage of the proposed software tool is the establishment of a methodology of motor specifications registration and the possibility of technical information exchange between users easily, accurately, and electronically (e.g., by e-mail), promoting the technical knowledge transfer in the motor repairers and academical communities.

A3.3.1 General Description

BOBISOFT was programmed in DELPHI language, being a WINDOWS-based software tool with a user-friendly interface, providing to the user a quick understanding of its running mechanism. It was specially developed for the design and comparative analysis of low-voltage, three-phase, squirrel-cage, induction motor stator windings, allowing simultaneous comparison between two different projects - the original winding project, or base case, and the new or modified winding project. One important feature of BOBISOFT is the possibility to assist the core loss test for stator core damage control after the winding stripping process. BOBISOFT supports up to 96 slots, 20 poles and 20 parallel coil-groups, although the implemented algorithms can handle any number slots, poles and parallel groups, providing that it is a feasible winding. At this stage, neither fractional windings nor coils with different number of turns are supported, but this capability can be easily developed in the future. The same applies to the core saturation, which is not considered yet in the calculations (but can be easily incorporated using look-up tables, previously inserted by the user). For MMFs calculation purposes, the in-slot coil representation is assumed to be concentrated in a point, being a common (particularly for semi-closed slots with narrow openings) but, obviously, introduces a small error. BOBISOFT is programmed to alert the user when the inserted data is outside the typical values range, or is physically impossible, being this feature useful for repairers, since it avoids gross mistakes. The input data panel, in which the motor mechanical and electrical data can be introduced, is shown in Fig. A3.24. There is required

and facultative data. The required data is used in the calculations and must be introduced. The facultative data is only for informative or database purposes. All data is saved in a specific file (*.bob). The required data can be divided into common and project (original and new) specific data. The common data include mainly the motor physical dimensions. However, fan, bearings and rotor information of both the original and new projects, is saved separately, because those parts of the motor can actually be change during the motor repair or maintenance. The stator slots information includes the shape (8 different shapes available) and the respective dimensions. It is possible to define some generic variables, namely, wire copper density, wire copper conductivity, motor internal operating temperature, core stacking factor, and additional coil-heads length. Up-to-date, this software has 8 different three-phase winding types available, namely, single-layer eccentric (or lap) winding (three different subtypes available), double-layer eccentric winding, double-layer concentric winding, single-layer 2-tier concentric winding, single-layer 3-tier concentric winding, and double-layer 3-tier concentric winding. The double-layer winding types are the only that allow changes in the coil pitch. This software also allows defining up to 20 parallel conductors with equal or different gauges (a database with the standard gauges used in the USA and in the EU is provided) [2], [48].

After the original and/or new data input process, the software calculates the winding factors up to a predefined order (typically, harmonics up to 17th order are enough to evaluate the winding performance), the air-gap magnetic flux per pole, the air-gap induction (or magnetic flux density) peak value, the wire current density, the wire length per phase, the winding resistance per phase, the copper losses per phase, the slot-filling factor, the heads/slots copper ratio, and the copper total weight. The magnetic values can be optionally calculated considering the slot opening effect. The lower the TSHD is, the higher the quality of the MMF curves will be, i.e., the spatial curve shape approximates to a sinusoid (ideal curve).

Winding factors of s^{th} harmonic order are calculated by means of an algorithm according to (A3.33), where C is the per-phase number of coils, c is the c^{th} coil, N_c is the number of turns of c^{th} coil, γ_c is the coil pitch (in electrical degrees), and β_c is the coil axis displacement from an arbitrary reference [1], [48]. Auxiliary tables are generated from the winding drawing algorithms (which are not described due to their complexity and extension), with all the data required for the winding factors calculation [48]. It should be emphasized that, at this stage, the software only simulates symmetrical poles, i.e., poles with equal width and distance between them. Therefore, the winding even order harmonics are null. Moreover, although the per-phase pulsating MMF spatial curves contain triplen harmonics, the resulting rotating MMF curves (instantaneous spatial sum of the pulsating MMFs of each phase) have no triplen harmonics, since it is considered a

balanced voltage or excitation three-phase supply system and a perfectly symmetric motor electromagnetic system [1], [48].

$$K_{ws} = \sqrt{\left(\sum_{c=1}^c N_c \cdot \sin\left(\frac{s \cdot \gamma_c}{2}\right) \cdot \sin(s \cdot \beta_c)\right)^2 + \left(\sum_{c=1}^c N_c \cdot \sin\left(\frac{s \cdot \gamma_c}{2}\right) \cdot \cos(s \cdot \beta_c)\right)^2} \cdot \left(\sum_{c=1}^c N_c\right)^{-1} \quad (\text{A3.33})$$

Of course, since the in-slot copper cross-sectional area and slot opening are considered concentrated in a point, for calculation purposes, after a certain harmonic order there are no gains in terms of accuracy in the winding factors-based representation of the MMF waveform.

To allow a quick evaluation of the introduced changes impact on the winding performance, a general benefit index is also provided, which is a parameter related to the TSHD and per-phase winding resistance. The higher the general benefit index, the better the motor performance [2].

In the calculations of the new winding, the air-gap induction peak value (related to the motor magnetic saturation [27]) and either the winding current density²⁷ (related to the motor thermal limitation [27]) or the winding resistance, as default, are forced to be equal or lower than the original values. Optionally, the air-gap magnetic flux per pole (related to the maximum efficiency load point) is forced to be approximately equal to the original value. However, the user is free to change the proposed values. Combining these data with other input data (e.g., voltage, current, etc.) the software calculates the number of turns per phase, the number of coils per phase, the number of turns per coil and the theoretical wire section to maintain the same current density or, alternatively, the same winding copper losses. As it was mentioned before, in this software, it is assumed equal number of turns in all the coils. However, for concentric windings it is possible to have coils with different number of turns without violating the symmetry principle [27]. In fact, new features are being developed for optimization purposes, including the possibility to introduce a different number of turns per coil, as well as a module for per-coil turns optimization in concentric windings (see Appendix 6), and turns (re)calculation (automatic optimization of the new winding) as a function of motor actual load (which can be easily measured by motor users), according to the principles discussed in Section A3.2.2, and a module for estimation of core losses variation.

The graphical and numerical output panel (Figs. A3.25) allows a comparative global analysis between the original and the new winding design final results. In this panel, the original and new design air-gap MMF curves are simultaneously or individually presented. It is possible to visualize the MMF pulsating and harmonic curves. Mainly for teaching purposes, it is possible to change the

²⁷ In fact, a database with typical values (provided by a motor manufacturer) of maximum allowable air-gap induction peak values and admissible current densities is used for a continuous comparison of the resultant values, alerting the user when the reference values are exceeded.

time value of the waveforms to analyze the time evolution of MMF curves, to invert per-phase excitation polarity (increasing time phase 180°) in each phase, and to switch excitation of two phases. The MMF peak value and the magnetizing current are also estimated, using classical formulations [1], [28].

In the graphical and numerical output panel, the user can also visualize the circumferential (Fig. A3.26), planar (Fig. A3.27) and numerical (Fig. A3.28) schemes of the winding coils and the respective connections. The circumferential and numerical schemes allow a quick and simple interpretation of the stator coil position and of the connections between them. This is particularly important to the rewinders. In this panel, the most relevant output data of original and new winding designs is simultaneously presented for an easier comparative analysis.

Generally, in the circumferential diagram, the higher the internal area without the lines representing the coil-heads, the lower the copper losses. It is also possible to visualize the step-by-step virtual winding construction and the introduction of a spatial displacement of 180 electrical degrees in each phase winding, which is useful to optimize the relative three-phase coil-heads position.

Since the winding stripping-out process can have a significant impact in the motor efficiency, it is important to control the losses before and after that motor repair phase. This can be done by means of the EASA²⁸ core loss test (defined in the EASA Tech. Note No. 17 [34], [35]), which is based on the core temperature and losses variation, measured before and after stripping-out the windings [26]. Therefore, the software has also a module to assist the needed stator core losses calculations (see Appendix 6).

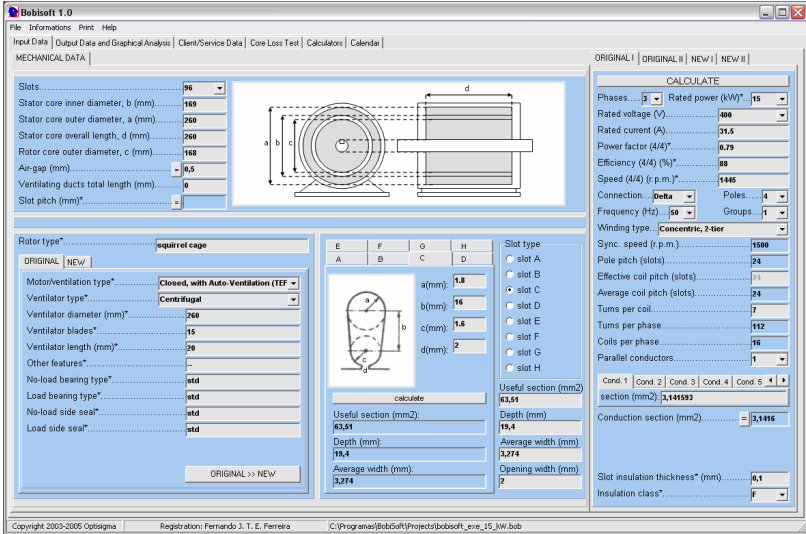


Fig. A3.24. BOBISOFT interface: mechanical and electrical input data panel [2], [48].

²⁸ Electrical Apparatus Service Association.

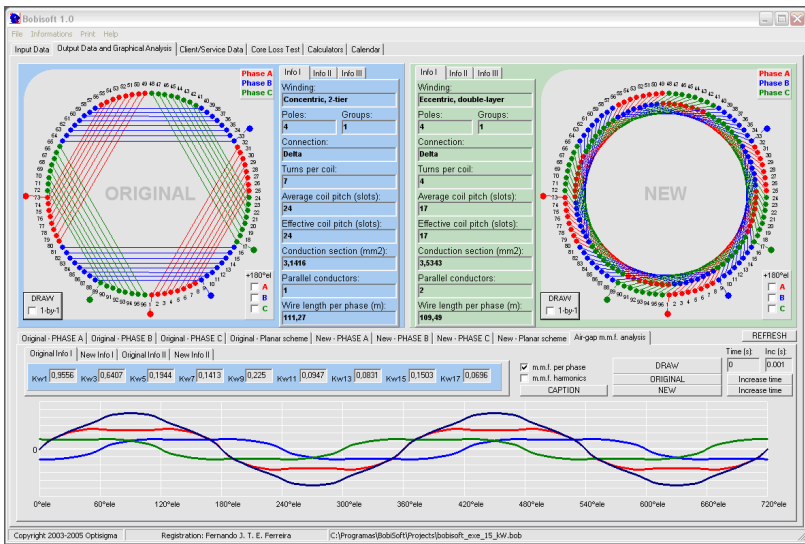


Fig. A3.25. BOBISOFT interface: output data and graphical analysis panel (considering only space harmonics up to 17th order) [2], [48].

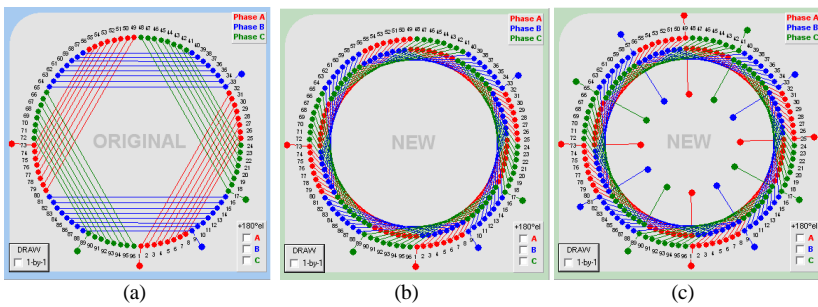


Fig. A3.26. BOBISOFT interface: winding circumferential schemes: (a) original (base case); (b) new; (c) new with parallel groups.

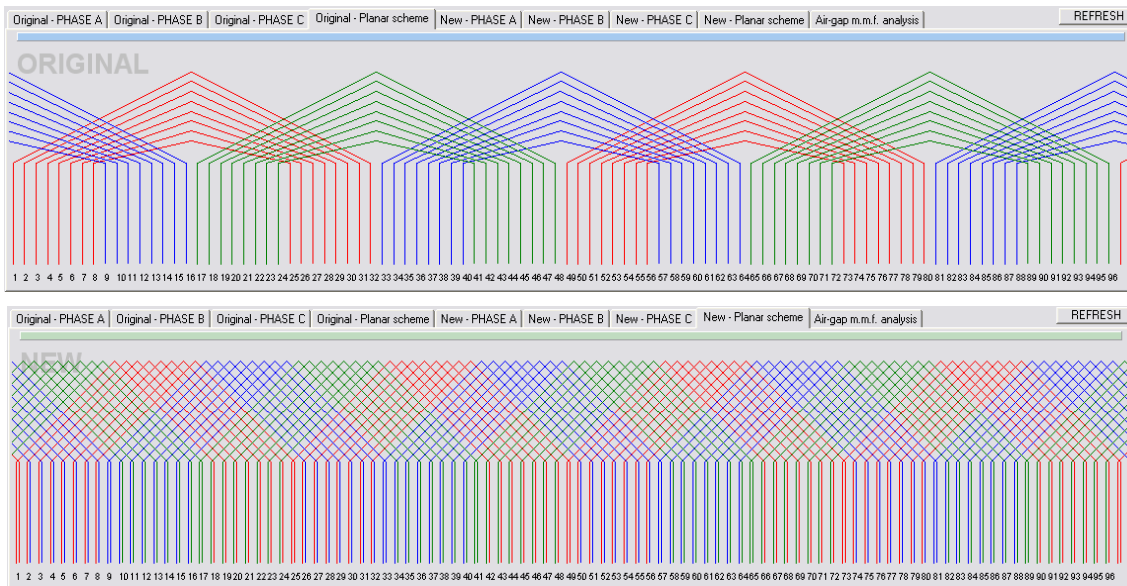


Fig. A3.27. BOBISOFT interface: winding planar scheme: (top) original (base case); (bottom) new.

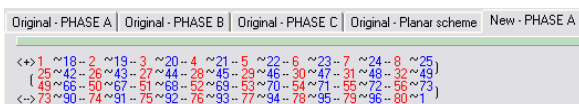


Fig. A3.28. BOBISOFT interface: new winding numerical scheme.

Moreover, the software automatically generates reports with the design data, numerical schemes, circumferential schemes, MMF curves, core loss test data and the service/client data.

It should be referred that there are several software packages for electric motor design (such as the one used in [49]), which perform very accurate FEM-based analyses, but, besides the reduced number of available winding types (in some cases, the per-slot number of conductors is required, instead of being computed automatically), are relatively complex and time consuming to use, requiring deep knowledge and skills on electric motor design theory.

In short, the major benefit of BOBISOFT is the automatic overall winding construction, with minimum information required, and the instantaneous results on windings being compared, as well as the information exchange between rewindings in an electronic format. Additional useful features will be added in the future, such as the optimized winding redesign as a function of the motor actual operating conditions, allowing the repairers to offer a new service to their customers.

It is also important to integrate in the software a more complete database with manufacturers' information related to the typical values of wire current density, air-gap induction and air-gap magnetic flux per pole as a function of motor class/type, power and number of poles. This information can help the user to identify previous incorrect rewindings.

A3.3.2 Application Examples

A3.3.2.1 Simulated Example

In this section the replacement of a concentric 2-tier winding (Fig.A3.26a) by a shortened-pitch (79%) double-layer eccentric winding (Fig.A3.26b) for a hypothetical IM is analyzed using BOBISOFT. Table A3.5 shows the main results. Theoretically, the new winding leads to: (a) reduction of 62% in the *TSHD*, potentially leading to a reduction of the motor acoustic noise and SLLs; (b) reduction of 93.5% in the 5th air-gap spatial MMF harmonic (negative sequence), potentially leading to a reduction of the rotor losses, an increase of the torque and a decrease of the starting current; (c) increase of 7.9% in the amount of copper used, slightly increasing the winding cost; (d) reduction of 8.5% in the copper losses, leading to the increase of motor efficiency [1]; (e) increase of 24.1% in the *SFF*, potentially leading to a better heating dissipation and, therefore, to a longer motor lifetime; (f) reduction of 26.3% in the head/slot copper ratio, potentially leading to the increase of the coil heads mechanical robustness and to the decrease of the motor internal temperature, due to the reduction of the amount of copper surrounded by air (high thermal conductivity mean).

Compared to the original winding (which is commonly used by most manufacturers), the new winding, in theoretical terms, leads to the increase of motor efficiency and reliability. Assuming that the motor had originally a full-load efficiency of 88% and copper losses representing 36.2% of total losses, the reduction of the copper losses in the new winding leads to an increase of 0.3 p.p. in the full-load efficiency. In principle, due to the 8.2% decrease in the per-pole air-gap flux, the core

losses also decrease and the maximum efficiency load point is slightly shifted to a lower load point. Since the torque-speed curve suffers an overall decrease, in this case, the user should take into account the actual load profile to evaluate if that torque decrease is admissible.

TABLE A3.5
WINDING CHARACTERISTICS FOR THE SIMULATED EXAMPLE.

Nominal power: 15 kW	Winding connection: Delta	
Nominal voltage: 400 V	Air-gap: 0.5 mm	
Nominal current: 32 A	Stator core length: 226 mm	
Number of slots: 96	Stator core inner diameter: 169 mm	
Number of poles: 4	Stator core outer diameter: 338 mm	
Winding	Original (Base Case)	New
Winding type	Concentric, 2-tier	Eccentric, double-layer
Average coil pitch	24 slots	19 slots (short-pitch)
Turns per phase	112 turns	128 turns
Air-gap induction peak value	0.92 T	0.82 T
Air-gap flux per pole	0.017 Wb	0.016 Wb
Wire current density	6.5 A/mm ²	6.0 A/mm ²
Wire(s) conduction cross section	2.835 mm ²	3.079 mm ²
Slot-filling factor (<i>SFF</i>)	24.1%	29.9%
Electrical resistance per phase	0.72 Ω @75°C	0.66 Ω @75°C
Copper losses per phase	247 W	226 W
Total space harmonic distortion (<i>TSHD</i>)	4.7%	1.8%
Copper weight per phase	7.6 kg	8.4 kg
Head/slot copper ratio (<i>BAL</i>)	98.95%	72.93%
Assumptions:		
Copper density @20°C: 8950 kg/m ³ ;		
Copper conductivity @20°C: 59 MS/m;		
Additional coil heads length for original winding: 45%;		
Additional coil heads length for new winding: 35%;		
Core stacking factor: 98%; Operating temperature: 75°C.		

A3.3.2.2 Experimental Example

In this section, a real replacement of a three-phase concentric 2-tier winding by a shortened-pitch (78%) double-layer eccentric winding in a 1.1-kW, 4-pole, TEFC IM, is analyzed. Table A3.6 shows the main results obtained with BOBISOFT. Theoretically, the new winding leads to: (a) reduction of 22% in the TSHD; (b) reduction of 83% in the 5th air-gap spatial MMF harmonic; (c) decrease of 8.7% in the amount of copper used; (e) reduction of 9.2% in the copper losses; (f) increase of 4.7% in the *SFF*; (g) reduction of 24.8% in the head/slot copper ratio.

In the new optimized winding the repair shop was able to increase significantly the *SFF* and to decrease slightly the distance between the coil heads and the core, which led to a lower coil-heads length. Additionally, the original winding stripping-out process was made without applying excessive heat to the stator core and the bearings were not replaced.

The motor efficiency and power factor of the IM with original and new windings were measured with a high-precision test bench (see Chapter 2), and are shown in Fig. A3.29. At full load, the

efficiency of the motor with the new winding is 1 p.p. higher and the power factor is 0.02 points higher, maintaining the same amount of copper, as it can be seen in Table A3.7. Due to the very small decrease (0.33%) of the per-pole air-gap flux, the maximum efficiency load point is approximately the same. However, that flux change led to a slight increase of the motor power factor.

TABLE A3.6
WINDING CHARACTERISTICS FOR THE EXPERIMENTAL EXAMPLE.

Nominal power: 1.1 kW	Winding connection: Star
Nominal voltage: 400 V	Air-gap: 0.5 mm
Nominal current: 2.9 A	Stator core length: 95 mm
Number of slots: 36	Stator core inner diameter: 91 mm
Number of poles: 4	Stator core outer diameter: 145 mm

Winding	Original (Base Case)	New
Winding type	Concentric, 2-tier	Eccentric, double-layer
Average coil pitch	9 slots	7 slots (short-pitch)
Turns per phase	366 turns	384 turns
Air-gap induction peak value	0.7538 T	0.73312 T
Air-gap flux per pole	0.00302 Wb	0.00303 Wb
Wire current density	9.3 A/mm ²	9.3 A/mm ²
Wire(s) conduction cross-section	0.3117 mm ²	0.3117 mm ²
Slot-filling factor (<i>SFF</i>)	46.6%	48.8%
Electrical resistance per phase	9.97 Ω @75°C	9.06 Ω @75°C
Copper losses per phase	83.88 W	76.15 W
Total space harmonic distortion (<i>TSHD</i>)	8.3%	6.5%
Copper weight per phase	1.26 kg	1.15 kg
Head/slot copper ratio (<i>BAL</i>)	117%	88%

Assumptions:
 Copper density @20°C: 8950 kg/m³;
 Copper conductivity @20°C: 59 MS/m;
 Additional coil-heads length for original winding: 40%;
 Additional coil-heads length for new winding: 35%;
 Core stacking factor: 98%; Operating temperature: 75°C.

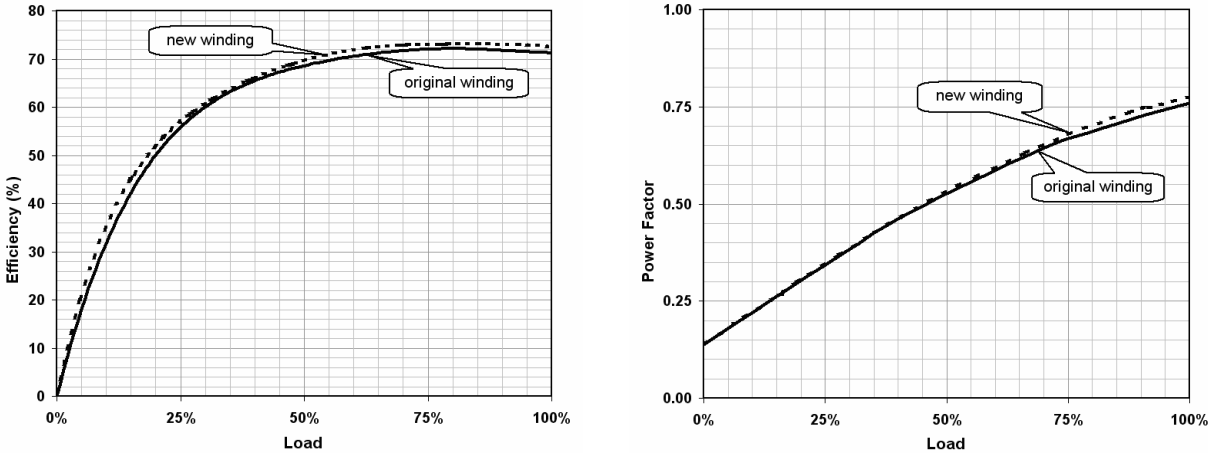


Fig. A3.29. Efficiency (left) and power factor (right) as a function of load, for a 1.1 kW, 4-pole TEFC IM with original (2-tier concentric winding) and new windings (double-layer eccentric winding, short-pitched to 78%).

TABLE A3.7
COMPARISON OF MOTOR NOMINAL EFFICIENCY AND POWER FACTOR.

Winding	Original (Base Case)	New
Full-load efficiency	72%	73%
Full-load power factor	0.76	0.78

More examples implemented by the repairers using BOBISOFT can be found in Appendix 6.

A3.4 Replacement of Faulty Windings

Since the winding improvement during repair only justifies the additional efforts if no major damages are inflicted in the stator core, it is briefly addressed in this section the processes associated with the replacement of faulty windings, as well as a number of recommended best practices.

Basically, the typical motor repair process integrates the following steps phases: (a) Disassembly of the covers (or end-shields) and rotor from the motor; (b) Visual inspection of the motor; (c) Stripping-out the old windings (including burning-out of the windings with a torch or an oven for varnish/resin weakening), cutting-off the winding heads in one side, and pulling-out the winding in the opposite, non-cut side (see also Appendix 6); (d) Cleaning the slots; (e) Introduction of the new insulation in the slots; (f) Coil forming; (g) Insertion of the windings; (h) Application of the end-straps in the coil heads; (i) Welding of the conductors in junctions; (j) Impregnation of the windings with varnish/resin; (l) Winding tests; (m) Replacement of the bearings²⁹; (n) Assemblage of all motor parts; (o) General inspection, insulation integrity tests, and basic operation of the motor; (p) External painting. The recommended post-repair tests to evaluate motor insulation system, rotor integrity and motor efficiency are described in [26].

In order to reduce to the minimum the downtime of the productive process, motor users first concern, when sending a motor for repair, is the quickness repair, no matter what happens to the motor efficiency. Moreover, the technical expertise of motor repairers is, in general, poor. Those facts are by far the most important barriers for a high-quality motor repair service. However, it is possible to maintain the efficiency of the motor during repair without increasing significantly the repair time, if an appropriate quality assurance programme is followed. With the increasing competitiveness in the industrial sector in the global market and the motor market share growth of energy-efficient (IE1 class) and high-efficiency (IE2 class) motors, the repair shops will have to consider efficiency issues if they want to offer a cost-effective service. Another important barrier for high-quality motor repair is the lack of adequate equipment both for the repair process and for motor testing after repair.

²⁹ Sealed bearings should only replace open or shielded bearings if the user wants to increase the motor protection level. The replacement of an open or shielded bearing by a sealed bearing, can lead to an increase of 35% in the friction losses, increasing the bearing temperature and reducing the motor efficiency. Improper bearing replacement is one of the most important factors contributing to the efficiency after repair [26].

There are several factors that can increase the motor losses. For example, as previously referred, excessive radial or axial pressure, excessive heating during winding burning-out process, mechanical damage of the core (e.g., rotor-stator surfaces contact), flux or induction increase due to phase-turns decrease, and mechanical or thermal damages directly inflicted in stator core (e.g., twisted teeth and short-circuited sheets due to interlaminar insulation damage), can all increase significantly the stator core losses. Increased MLT, reduced conductor section, some changes in the winding configuration, can all contribute to stator copper losses increase. Reduced air-gap flux (e.g., resulting from increased stator winding turns), rotor cage end-ring cross-section changing (e.g., resulting from end-ring machining or drilling), rotor conductors/winding changing/damaging, rotor skimming, and rotor-stator core contact, can all contribute to rotor losses increase. Improper replacement³⁰ or maintenance of bearings and seals (e.g., poor lubrication) and oversize fan, can all contribute to friction and windage losses increase. Damage to air-gap surfaces, skimming rotor with blunt tool, and rotor eccentricity, can all contribute to the SLLs increase. Detailed information on these issues can be found in [26].

Core (or iron) losses are associated with the flux time variation, and can be divided in Foucault (or eddy) currents (Joule effect losses in the steel sheets caused by the circulation of induced currents) and hysteresis losses (associated with the magnetizing cycles, i.e., the energy spent to invert the magnetic flux direction). In the sinusoidal domain, at the line frequency, are both approximately proportional to the squared induction, being the first proportional to the squared frequency and the second proportional to the frequency. Typically, its value varies between 15% and 27% of full-load total losses, depending on motor rated power, number of poles and efficiency class. Interlaminar insulation damage/destruction caused, for example, by the application of excessive heat to the stator core during winding stripping-out process, also leads to the core losses increase, since the higher the area crossed by a time-varying magnetic flux, the higher the Foucault currents and associated losses will be (Fig. A3.30) [5], [19], [26], [34], [35], [55].

In fact, assuming the volumes in Fig. A3.31, with a height h significantly longer than the width (or thickness) t , the core losses component associated with Foucault currents can be given by (A3.34), where K is a proportionality constant, d is the depth, ρ is the iron material resistivity, f is the frequency, and B the magnetic induction [26].

$$P_{fe_Foucault} \approx K \cdot \left(\frac{h \cdot d \cdot t^3}{\rho} \right) \cdot f^2 \cdot B_{peak}^2 \quad (\text{A3.34})$$

³⁰ Improper replacement includes the extraction/insertion bearings (in the shaft and end-shields) process and the type of bearing replacing the old one. For example, during insertion, the bearings should be properly heated using, for example, a bearing induction heater and, during extraction, manual or hydraulic extractors should be used. The use of a hammer to force bearing extraction/insertion should be avoided [26].

Assuming that depth and height are maintained, the relation between the Foucault current losses for one sheet with thickness t (Fig. A3.34a) and two sheets with thickness $t/2$ (Fig. A3.34b) is:

$$\frac{P_{fe_Foucault(t)}}{2 \cdot P_{fe_Foucault(t/2)}} = \frac{t^3}{2 \cdot (t/2)^3} = 4.$$

Therefore, dividing a sheet in half with an insulating film reduces 4 times the Foucault currents losses.

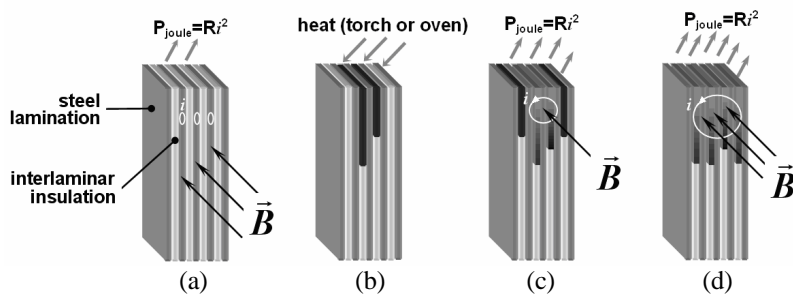


Fig. A3.30. Interlaminar insulation destruction linked process.

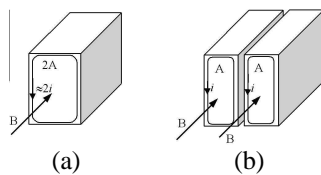


Fig. A3.31. Foucault currents in core steel sheets.

It should be noted that, if Foucault currents increase 2 times, the effect of the overheating caused increases 4 times.

Therefore, if the interlaminar insulation is destroyed in a particular zone, localized losses can increase significantly, causing hotspots, which, in turn, can damage the adjacent interlaminar insulation, extending the damage, as represented in Fig. A3.30, ultimately leading to a significant increase of the motor losses and operating temperature.

Typically, a severe overheating can be identified by a discoloration of rotor and/or stator surfaces. The winding stripping-out process has a minor impact on the hysteresis losses.

The condition of the core can also be affected by other factors, e.g., motor failure cause/process, interlaminar insulation and steel sheets quality, winding stripping-out mechanical process and core cleaning process (e.g., polishing and filling).

Therefore, before starting the insertion of the new winding, the condition of the stator core should be evaluated, including the identification of mechanical damages and overheating spots. For example, the rotor-stator surfaces contact (e.g., due to the failure of a bearing or excessive radial force) causes core scratching and short-circuits between core sheets, leading to the increase of Foucault currents-related losses (circulating in the closed circuit between the damaged spot and the

motor frame). If this type of damages is severe, the motor repair can become non cost-effective, unless reinsulation of core sheets is made. When sheets fusion occurs, e.g., due to short-circuits inside slots, the iron core is, in principle, irreparable [26]. A localized core overheating can actually occur during motor operation (e.g., extended starting period or high-slip steady-state operation), with enough intensity to cause interlaminar insulation destruction. In these cases, the motor load, voltage supply and cooling system should be analysed.

Due to the demand for quick repairs, repair shops normally perform the winding stripping-out process with too high temperatures in order to reduce the burning-out process time. Typically, the stripping-out process used is the winding burning/heating with a torch (see Appendix 6) followed by its cutting and pulling-out. The aim of the stator burning/heating process is to weak the impregnating varnish/resin, in order to allow an easier winding and slot insulation straps extraction from the core. If the interlaminar insulation is damaged, the core losses will increase, which actually happen in most cases. Consequently, the motor efficiency will be reduced and the operating temperature will rise, shortening the motor lifetime.

In fact, if the burning-out process is performed with temperatures above 350-360°C, the core losses increase significantly. Figs. A3.32-A3.34 show the experimental core losses variation as a function of the applied temperature to the core³¹, evidencing the different susceptibility to the temperature of varnish-³² and oxide-based interlaminar insulations.

The higher the temperature supported by the interlaminar insulation, the higher the reparability of the motors (some manufacturers consider that the application of 400°C during 8 hours is an indicator of high reparability [50]).

On the basis of the experimental results, it can be concluded that stators for frame sizes up to 180 (corresponding to 22-kW, 4-pole motors) the core losses increase is not significant for temperatures up to 350°C during 5 hours, independently on the interlaminar insulation. The application of 350°C during 5 hours is enough for an effective winding stripping-out process, but the necessary number of hours can be less for smaller motors.

It can also be concluded that excessive temperatures have not significant effect on the losses of cores with heat-resistant-varnish-based interlaminar insulation (e.g., L3-type), but the stator core and/or frame can become mechanically deformed (which can introduce or aggravate the motor eccentricities, ultimately increasing motor losses and vibration). The experimental results also show that previously repaired motors are more vulnerable to a second repair in terms of core losses increase, assuming excessive heat application.

³¹ The core losses of the tested motors were previously estimated by the motors' manufacturer. After that, motors were dismantled and stators sent to a large repair company, which carried out the winding impregnating varnish/resin carbonization/weakening process in an oven with temperature control. The cores were heated with controlled temperature applied during identical time cycles (5-hour duration), and, after the heating process, the windings were removed. Some stators were reheated to simulate the effect of a second repair. In the end, stators were rewound by the motor manufacturer, according to the original specifications, and the core losses were estimated again [19].

³² Organic/inorganic insulation.

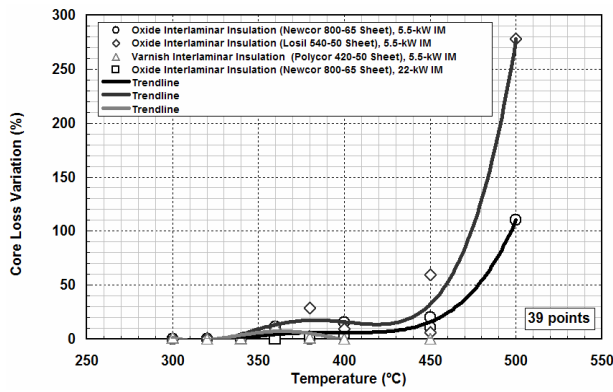


Fig. A3.32. Experimental core losses variation as a function of the applied temperature to the stator, for different types of interlaminar insulation and ferromagnetic sheet [19], [26].

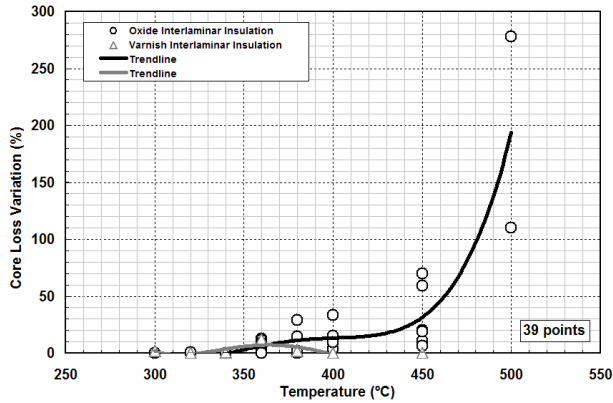


Fig. A3.33. Experimental core losses variation as a function of the applied temperature to the stator, for different types of interlaminar insulation [19], [26].

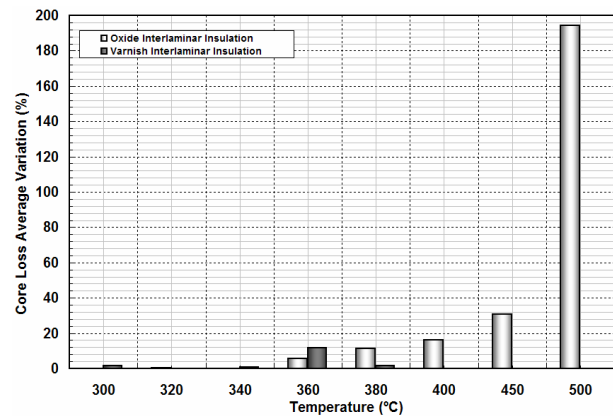


Fig. A3.34. Average variation of experimental core losses as a function of the applied temperature to the stator (or oven temperature), for different types of interlaminar insulation and ferromagnetic sheet [19], [26].

The winding stripping-out after submitting the stator to too low temperatures (lower than 350°C), i.e., temperatures which are unable to provide enough varnish/resin weakening, requires the application of higher traction forces to remove windings, which can mechanically damage the core, including its deformation. In general, the application of temperatures above 400°C can destroy significantly the interlaminar insulation, increasing motor core losses. The recommended temperature is 350-360°C, measured in the stator core teeth. The ideal temperature depends mainly on the interlaminar insulation. The processes to correctly extract the faulty windings and clean the core slots are well described in [26] and briefly described in Appendix 6 (e.g., the *Thumm* technique and the combined use of an oven with temperature control and an hydraulic winding pulling-out system).

A3.5 Motor Condition Diagnosis

It is important to the user evaluate the actual motor state before³³ decide if it is cost-effective to improve or repair the stator winding. At least, two motor main parts should be evaluated, namely, the rotor (in terms of cage end-rings and bars integrity, core surface, and dynamic balance³⁴) and the stator core (in terms of losses and surface). In most cases, if one of those parts is considerably damaged, the efforts to repair or optimize the motor cannot be economically justified. Although those parts can be repaired, in the majority of the cases, it is not practicable or cost-effective, being justified only for very special motors, not found in the market. The typical core quality/condition evaluation processes are well described in [5], [26], [34], and [35], and a more advanced method is described in [55]. Rotor bars integrity can be evaluated using a “growler test” although it is unable to identify fractured bars. Although sophisticated and highly effective and accurate techniques to detect rotor cage and stator winding anomalies have been proposed (such as those proposed in [62]-[66]) and, some of those techniques are actually being used, they are relatively complex to implement and use, particularly by users without deep skills or expertise on motor theory. In this section, a low-cost user-friendly on-line (or in-service) motor condition evaluation system is proposed³⁵, which can be used before motor failure and/or after motor repair.

It is well known that IMs are critical components in most industrial processes. The early failures of this type of motors are mainly associated with defects inherent to the motor itself and to inappropriate operating conditions. In some industries, the consequent unplanned motor downtime can be very costly. Due to the need of high reliability levels and minimization of production losses associated with motor failures in most industries, condition monitoring of motors has received considerable attention in recent years. Condition monitoring and early diagnosis of motor operation anomalies and faulty parts allow scheduling maintenance operations and, in most cases, avoid the occurrence of unexpected motor failures and further severe damages, extending motor lifetime. Additionally, the costs associated with spare parts inventories and non-planned maintenance are greatly reduced [6].

There are many ways to detect mechanical and electrical problems in IMs, either directly or indirectly, such as using vibration spectrum analysis [7], [52], motor current spectrum analysis [8]-[10], Park vector analysis, electromagnetic field monitoring, chemical analysis, temperature (either using temperature sensors or infrared cameras), acoustic noise analysis, and partial discharge

³³ Obviously, it is also important to evaluate the motor condition after repair or the repair service quality, particularly the insulation system integrity by means of the high-potential test and/or insulation resistance test (“megger test”). The efficiency control is also very important, but, for most repair shops, unpractical. If the fan is replaced, the noise level should be also evaluated.

³⁴ For example, an unbalanced rotor leads to extra vibrations, shortening the life of the motor insulation and fixing parts. The motor vibration should be evaluated to demonstrate the absence of eccentricities and/or asymmetries between the rotor and the stator and the appropriate dynamic balance of the rotor. Some manufacturers are designing motors to comply with IEEE grade R level, which means a 35% improvement to grade N level vibration limits, typically accepted by the market [50].

³⁵ This work was co-proposed and co-supervised by the author, being part of the graduation final report of an electrical engineering student, and presented in [51].

monitoring. Among the referred methods, vibration and current analysis are the most popular due to their easy application and relatively high reliability [6], [62]-[66]. Most currently available techniques require the user to have some degree of expertise in order to distinguish an abnormal operating condition. This is because the monitored spectral components (either vibration or current) can result from a number of sources, other than motor related faults/anomalies (e.g., load-produced vibrations, power network harmonics, etc.) [8]. Nowadays, artificial intelligence-based methods are being used to in-service condition monitoring, improving data interpretation. Examples of such methods are expert systems, artificial neural networks (ANN), support vector machines and fuzzy logic, being the results promising [6].

It is now proposed a condition evaluation or fault diagnosis system for IMs based on the line currents and mechanical vibrations spectral analysis correlation. Two line-current signals and one radial frame vibration signal are acquired³⁶, being the inputs of the system. The analysis of the measured signals is made using ANNs that, when properly trained, return the diagnostic results for the motor under evaluation. When the neural network indicates an anomalous situation, the system estimates the severity of the anomaly by evaluating relative amplitude of characteristic frequencies.

The system was designed to detect ten types of motor operation anomalies: single-phasing, phase unbalance, coils and turns short circuits, rotor resistance unbalance, broken rotor bars, rotor dynamic unbalance, eccentricities and bearing damages. The structure of this system is divided into two main modules: data acquisition and recording module (hardware and software) and data analysis module (software). The latter includes four submodules, namely, pre-processor, data selection, ANN algorithm and post-processor. In Fig. A3.35, a simplified diagram of the proposed motor condition evaluation system is presented. See Appendix 6, for complementary notes on this topic.

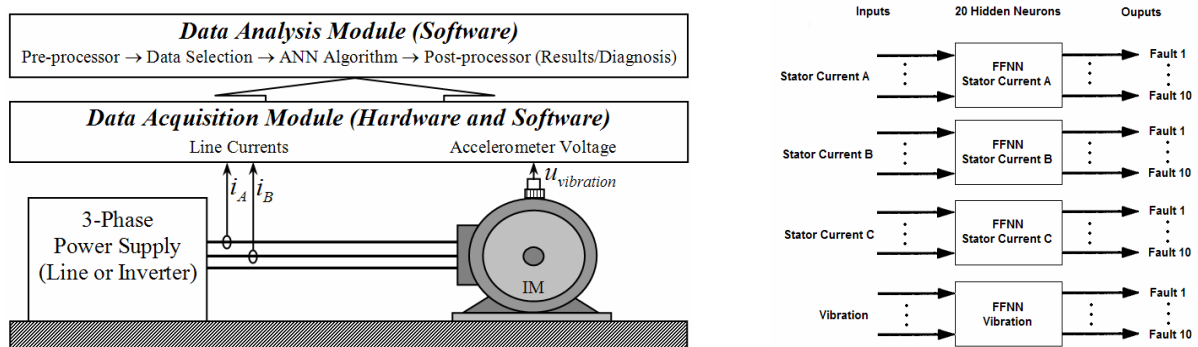


Fig. A3.35. (left) Diagram of the proposed motor condition evaluation system; (right) Feedforward ANN architecture [51].

³⁶ By means of a data acquisition card (connected to a PCI slot of a computer) and some hardware probes (Hall-effect current clamp-on current probes and accelerometer). The data acquisition interface software was developed in LABVIEW language.

The user interface of the proposed system was implemented with LABVIEW³⁷ [11] and the ANN algorithm was implemented with MATLAB³⁸ [15].

The postprocessor user-friendly interface, shown in Fig. A3.36, provides basic motor condition information. Additionally, the user can also visualize and compare the time and spectral graphs of the signals.

The four ANNs become fully functional after the training process is complete. Since the ANNs are not 100% effective, it is used a simple combination method to improve the faulty condition diagnosis. The results of the four ANNs were divided into two groups: the group of the stator currents and the group of the vibration data. In the group of the stator currents there must be at least two of them with same diagnostic to validate the group result. If the results of the two groups (currents and vibration) are identical, the system accepts the diagnostic. If they have different results, the system classifies the faulty situation as “possible”, instead of “detected”. After diagnosis, it is calculated the severity of the anomaly/fault (if exists), by comparing the magnitude of the characteristic frequencies associated with a specific type of anomaly/fault with the magnitude of the fundamental component. The severity degree of the anomaly/fault is presented in the motor condition report.

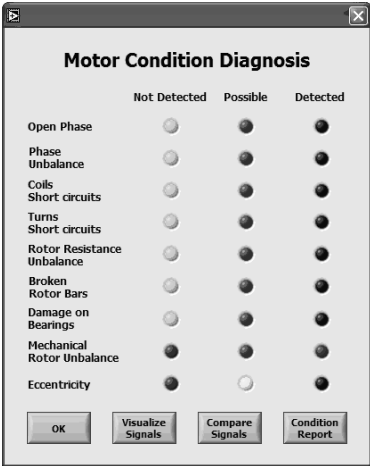


Fig. A3.36. Main window of the post-processor, for the case of a motor with a mechanical rotor unbalance [51].

The experimental tests were carried out using four 0.75-kW, 220/380-V, 3.34/1.93-A, 50-Hz, 4-pole, delta-connected, TEFC IMs, with 22-bar rotors, being the results presented in Appendix 6. Experimental data sets corresponding to each of the considered cases, collected over a 10-second window for each case were used, for the ANNs training process. Ten percent of these data sets were used for post-learning testing. The ANNs were configured as described previously and were successfully trained with the above-mentioned data. When submitted to other experimental data

³⁷ LABVIEW offers an easy-to-use graphical programming environment, which covers data acquisition, data analysis, and data visualization [12].
³⁸ MATLAB is a high-level programming language used widely in the scientific and engineering communities for research and development whose basic data type is a matrix that does not require dimensioning. In MATLAB all computations are done in complex valued double-precision arithmetic to guarantee high accuracy [13], [14].

sets corresponding to cases of healthy and faulty condition motors (other than those used for the training process) an accuracy of more than 95% was achieved.

In order to implement the described system in a portable unit, a LABVIEW's USB-acquisition module and a laptop computer, as well as suitable current and vibration transducers/probes for industrial purposes, will be used in the Future.

Moreover the shaft to ground voltage will be also incorporated (research is being now carried out), as well as the sum of instantaneous values of the line currents to provide common-mode information³⁹. The combination of these two waveforms allows to evaluate separately the motor insulation system condition (leakage current and partial discharge occurrence) and bearing condition (current activity and damages), as well as rotor-stator eccentricities and power supply unbalance, requiring the use of only one clamp-on current probe around the three line conductors and a voltage probe with a special lead for contact with the motor rotating shaft, as explained in [59], which is a novel diagnosis strategy proposed by the author (see also Appendix 6).

A3.6 Large-Scale Motor Customizing Scheme

System energy-efficiency improvement is one of the main strategies to achieve an energy sustainable development, since it leads to significant energy consumption reduction in a relatively short period at moderate costs, as referred in Chapter 1, and, in terms of electrical energy consumption, IMs are, by far, the most important load worldwide. Recent studies confirm that, in Europe, the motor load factor is, on average, less than 60% (in Portugal, is estimated to be lower), meaning that most motors are likely to be significantly oversized. Depending on a number of factors, including the motor efficiency, the operating (or running) cost dominates by far the LCC of IMs, reaching 50 to 200 times its purchase price. Therefore, small increments in motor efficiency can lead to significant reduction in the motors LCC, as evidenced in Chapter 2. The motor repair market represents, in terms of units, about 2-3 times the new motor market. Typically, the motor repair cost is 40-50% of motor initial cost, depending on rated power. In general, when a standard motor (EFF3 or IE1 class) fails, it is recommended its replacement by an energy-efficient (EFF2 or IE1 class) or a high-efficiency motor (EFF1 or IE2 class), requiring a significant extra investment, although in a many cases with a payback time up to 2-3 years, depending on motor rated power, annual operating hours, efficiency, load factor (or oversizing degree), and overall condition, as well as on the electricity price and on the motor repair service quality.

³⁹ Since the number and intensity of the electrical full- or partial-discharges in bearings and between winding and ground/frame are indicators of the respective level of degradation, they can effectively be used for the condition evaluation of those parts. Besides the frequency spectrum, the correlation should use the most significant time derivative values (d/dt) and relevant magnitude peaks of the acquired signals (shaft voltage and leakage current), and the respective instants of occurrence, allowing separating the leakage currents and bearing currents (full- or partial-discharges). This correlation and the associated event (e.g., electric full- or partial-discharges in bearings and insulation system) are similarly detected by proper learning. It should be noted that the leakage currents continuous components also reflects the insulation condition. Separating the leakage currents and the bearing currents (electric full- or partial-discharges).

In this section, a motor customization scheme or strategy is proposed, involving a set of low-cost technologies to readapt, reuse and optimize the operation of oversized motors, reducing significantly their LCC. Together, the proposed technologies integrate a novel EMODS maintenance concept (namely “smart service”), shortly described in Table A3.8.

The large-scale application or integration of the proposed technologies/solution in large EMODS optimization schemes/plans, can lead to significant energy savings and, additionally, to the improvement of the IMs power factor, which is also an important aspect to be taken into account, since the typical poor power factor of IMs is one of the major factors responsible for the low power factor in electrical power networks. The key-concept behind all the proposed solutions is the change of the motor efficiency-load curve. The motor load can be evaluated using the techniques described in Chapter 4 or using a wireless-based system such as that described in [67].

The first technology/solution (named “smart redesign”), consist in readapting the stator winding of damaged oversized motors to their operating conditions (load, voltage, etc.), improving significantly their efficiency and power factor, as well as extending their lifetime due to the lower operating temperature (as previously explained). Basically, it is proposed a large-scale motor downsizing. This concept can also be applied to off-use motors, as a way to rehabilitate them. The proposed solution is novel in relation to the commonly offered motor repair/maintenance services, which consist in the rewinding of the damaged motor according to the original (or close to original) design and/or replacement of the motor bearings. However, it can only be applied to motors with a low start/stop cycling rate and/or not requiring high dynamic performance (due to the reasons described in Chapter 5). Basically, it is proposed the conversion of the damaged (but without significant damages in the core and rotor) oversized EFF 3-class motors to well sized EFF 1- or EFF 2-class motors with a lower rated power matched to the actual load, at very low cost. If justified, this process can also include proper cooling fan resizing and, eventually, standard bearing replacement (e.g., by low friction bearings), particularly in the case of low-power motors.

Actually, the proposed solution has other advantages such as the possibility of conversion of an oversized motor to any lower power level, without the restrictions associated with the standardized power levels, and the avoidance of mechanical readaptation, typically required when a new well-sized smaller motor replaces a damaged oversized motor.

Additionally, the large-scale downsizing also can lead to a significant peak power reduction. Eventually, oversized damaged EFF 1-class or EFF 2-class motors can also be properly converted. In general, the rated power of oversized motors can be reduced with significant gains in efficiency and power factor. For example, even without considering stator winding optimization, fan downsizing and/or replacement of standard by low-friction bearings, the conversion of a 7.5-kW motor operating at 27% load into a 2-kW motor with a 100% load can lead to an efficiency

improvement from 80% to 90% () and an increase of the power factor from 0.35 to 0.75. If necessary, during rewinding, the insulation can also be properly upgraded for the power supply type. For an appropriate conversion, the described methods and recommendations (including the use of the BOBISOFT software tool) regarding stator winding redesign should be applied. In relation to the replacement of the damaged motors by EFF 2/EFF 1-class motors with a lower rated power, the proposed conversion/downsizing scheme during rewinding can be a very attractive, cheap and ecological solution⁴⁰, since it extends motor lifecycle and rely on the recycling/re-use principle. Although the well-known advantages associated with EFF 1-class motors (see Chapter 2), they are expensive and, when replacing significantly oversized motors (with a larger frame size), require changes in the mechanical transmission and fixation system, becoming less attractive than the proposed solution. In fact, for inverter-fed IMs, the stator windings can be properly redesigned for optimized operation over all the motor duty-cycle (in terms of torque and speed), taking into account the inverter operation limitations.

The second technology/solution (named “multiflux”) is the conversion of out-of-use or damaged motors to multi-flux motors (see Chapter 5) with multiple connections (up to 6), that can be used as spare motors to replace other damaged motors, being able to operate with a wide range of voltages and/or loads combinations⁴¹ with high efficiency and power factor levels. If combined with the Smart-Switch/Relay (electronic device) to allow automatic stator winding connection change, significant energy savings in fixed-speed, variable-load applications can be obtained, and smooth starting can be provided, at a low/moderate additional cost, as it is explained in Chapter 5. Slip-based stepped speed regulation is also possible in some applications, such as centrifugal and axial fans.

The third technology/solution consists in the automatic and manual winding connection mode (star or delta) management (named “Smart-Switch/Relay” and “Smart Change”), of in order to optimize the motor operation as a function of its load. For variable-load, fixed-speed motors, the automatic connection management is required, which, as previously referred, has a low/modest cost and also allows speed regulation within two levels by means of slip increase. For constant-load, fixed-speed motors a manual management based on a simple in-field evaluation methodology (requiring only the motor speed and voltage measurement), whose cost is estimated to be, in general, very low, depending on the situations. These solutions can lead to a significant increase of the motor efficiency and power factor of motors strongly oversized driving variable loads. For the

⁴⁰ Moreover, the price of the energy and of the raw materials is increasing. For example, regarding the average cost of the raw materials increase 65-75% since 2003 [59]. The cost of the copper has increased more than that average. The copper price has quintupled from the 60-year low in 1999, rising from US\$ 1.32/kg in June 1999 to US\$ 8.27/kg in May 2006, where it dropped to US\$5.29/kg in February 2007 then rebounded to US\$7.71/kg = €5.00/kg, in April 2007 [60]. This clearly justifies the efforts for recycling (e.g., windings copper) and re-use (e.g., frame, core and rotor) as much as possible the material in old motors.

⁴¹ This type of motor can operate with different voltages for fixed rated power or, alternatively, with different rated powers for fixed voltage. Optimum connection for combined voltage/load (or rated power) can also be properly selected (see Chapter 5).

case of the stator winding automatic connection management by means of the Smart-Switch/Relay, the improved motor starting and protection are also important advantages to be taken into account. Both the delta/star connection or multiconnection automatic management can, in some cases, compete directly with electronic soft starters, electronic voltage regulators, and, when considering small speed variations, with VSDs. Further information on the 2nd and 3rd technologies/solutions can be found in Chapter 5.

A3.7 Conclusions

An overview on the optimization of line- and VSD-fed IMs stator windings, in terms of efficiency and reliability, was presented, considering the actual motor operating conditions (e.g., motor load profile), which can be significantly different from the rated conditions. Several motor redesign strategies/techniques to properly readapt the motor to their actual operating conditions are proposed, potentially increasing its efficiency up to higher levels. The information offered is useful for motor designers/manufacturers (e.g., for specific OEM orders) and rewinders. However, it is necessary to know deeply all the effects associated with those changes in order to ensure that, depending on the motor application and operating conditions, efficiency and reliability benefits are actually obtained. Although manufacturers optimize the stator winding design taking into account the technological limitations associated with mass production, and, in the majority of the well-sized cases, a rigorous copy of the original winding is recommended when the motor winding fails. Nevertheless, in a number of cases, such as oversized motors or inverter-retrofitted motors, a correct stator winding redesign, presupposing manual rewinding techniques, inherently less limited than those for mass production processes, can lead to a significant improvement of the motor performance. When considering the motor life-cycle cost, the increase of motor efficiency and reliability can, in some cases, compensate the potential increase in the (re)winding or (re)designing cost, due to the eventual use of better quality and larger quantity of material and to the longer overall design and implementation time. In a short-term, the potential additional cost of high-quality repair services can be compensated by the motor efficiency decrease avoidance (in some cases the motor efficiency can actually be improved) and extended motor useful lifetime or MTTF. Motor users have an important role to play in the motor repair services quality improvement, because the quality offered by those services depends mainly on the demand requirements. Repair shops do not invest in quality unless it becomes a relevant decision factor for the clients. Motor users must be aware of the technical and economical benefits associated to high-quality repair services, and should change the typical requirements “low cost and fast service” to “fast service, with quality, even if more expensive”. Today, the industrial companies’ success key factors depend upon the high reliability and efficiency of the production processes. Therefore the repairers should






update their technical knowledge, invest in modern equipment, and achieve tight quality control criteria. If there is an effort from motor manufacturers to improve motor efficiency, the repair services have to follow the market trend, offering high-quality services, otherwise their utility and cost effectiveness can result strongly diminished.

In this scope, the developed winding design software tool allows the quick redesign of the windings. Winding (re)design calculations that typically take several hours can be done in a few minutes, even if the user has not deep technical knowledge. Additionally, it simplifies the core loss test application. For technical education purposes, the proposed software can be used as a virtual laboratory for the design and comparison between the different three-phase windings, including the rotating magnetic fields theory demonstration. In the future, the software can include more quality control modules (e.g., efficiency quantification according to the IEC/IEEE testing standards, high-potential insulation test, etc.), a module for winding optimized redesign as a function of motor load, voltage and frequency, and provide other winding types, namely single-phase, bi-phase, fractional and direct current machines armature windings. User-friendly software tools like the one developed, allow the modernization of repair shops not only in an education and training perspective, but also in the improvement of (re)design process of electric motor windings during repair/redesign services. The optimization of the stator winding of a damaged motor can compensate the possible increase of mechanical and/or core losses after repair. If the mechanical and core losses were maintained, a significant motor efficiency increase could be achieved with the optimization of the stator winding, particularly if it is taken into account the actual motor operating conditions, significantly promoting the repair/redesign services. Some of the proposed winding optimization methods/techniques, besides leading to the motor performance maintenance or improvement, can actually reduce the time associated with the (re)winding process. They can also be used to convert damaged/faulty oversized or out-of-use standard motors into well-sized energy-efficient motors with lower rated power (large-scale motor downsizing) and/or properly adapted to the power supply profile, which can be an interesting option, assuming that no major damages occur in the core during rewinding (or occurred in previous rewindings) and the rotor is healthy. In that perspective, a system for on-line condition evaluation of IMs is proposed, based on current and vibration spectra analysis, correlated each other. The motor operation anomaly-related patterns recognition is made by means of ANNs, which, after proper training, are able to distinguish “healthy” and “faulty” motor condition. The proposed strategy was experimentally tested on a set of 0.75-kW IMs under different types of motor anomalies, reaching a level of accuracy higher than 95% on the operating anomaly-type identification, which can be considered a quite good result. The system was also successfully tested in industrial environment with two practical cases (two low-voltage IMs driving a pump and a fan) [69]. Therefore, the approach discussed is satisfactory

and promising for post-repair and pre-failure on-line motor condition evaluation. Further experiments are required for larger motors and/or considering real industrial environment, in which EMI problems can actually occur.

TABLE A3.8

THREE-PHASE INDUCTION MOTOR MAINTENANCE SMART SERVICE CONCEPT.

Measure	Description	Target	Main Advantages
	Integrated motor repair program or scheme with 4 different solutions: smart redesign, multi-flux, smart switch/relay, and smart change.	All motors should be evaluated.	- Overall improvement of motor driven system at low cost.
	Stator winding redesign as a function of motor actual operating conditions. Insulation improvement according to power supply.	Oversized, damaged, and/or off-use motors.	<ul style="list-style-type: none"> - Very low additional investment; - Re-use of old motors; - Re-adaptation of damaged motors to the actual operating conditions; - Increase of the motor power factor and efficiency; - Possibility of conversion of standard motors to energy-efficient or high-efficiency motors; - Extension of the motor lifecycle; - Electrical energy consumption reduction.
	Conversion of standard motors in multi-flux motors with multiple voltage and power levels.	Damaged and/or off-use motors.	<ul style="list-style-type: none"> - Very low additional investment; - Re-use of old motors; - Flexibility of the converted motors to different voltages and/or loads, indicated for spare motor purposes; - Increase of the motor efficiency and power factor; - Extension of the motor life-cycle; - Electrical energy consumption reduction.
	Automatic change of stator winding connection mode as a function of motor load.	Variable-load motors.	<ul style="list-style-type: none"> - Modest additional investment; - Increase of the average value of the motor efficiency and power factor over the motor duty cycle; - Electrical energy consumption reduction; - Improved motor starting and protection; - Possibility of speed regulation in fans and pumps within two levels as a function of a sensor input.
	Manual change of stator winding connection mode as a function of motor load.	Constant-load oversized motors.	<ul style="list-style-type: none"> - Very low or absence of additional investment; - Increase of the average value of the motor efficiency and power factor; - Electrical energy consumption reduction.

Notes: A motor monitoring or diagnosis service can also be included in the smart service to evaluate the motor core and rotor condition and in-field operating conditions (e.g., motor load, power quality, etc.).

A3.8 References

- [1] Chalmers, B.; Williamson, A.: “*A.C. Machines – Electromagnetics and Design*”, John Wiley & Sons Inc., New York, USA, 1991.
- [2] Ferreira, F., de Almeida, A.: “*Electric Machinery Winding Design Software for Teaching and Rewinding*”, 16th Inter. Conf. Elect. Mach. (ICEM’04), Conf. Proc., Krakow, Poland, Sept. 2004.
- [3] Ferreira, F.; de Almeida, A.: “*Considerations on the Custom Design of the Stator Winding of Low-Voltage, Three-Phase, Cage Induction Motors to Improve their Efficiency and Reliability*”, 17th Inter. Conf. on Electric Machinery (ICEM’06), Conf. Proc., Crete, Greece, Sept. 2006.
- [4] Ferreira, F.; Carvalho, J.: “*Metodologia para Especificação dos Enrolamentos Estatóricos na Rebobinagem dos Motores de Indução Trifásicos de Baixa Tensão*”, Revista K eramica, Ano XXIX, N.º 264, Janeiro/Fevereiro de 2004.
- [5] de Almeida, A.; Ferreira, F.: “*Actions to Promote Energy-Efficient Electric Motor Repair*”, Inter. Journal of Energy Technology and Policy, Vol. 1, No. 3, pp. 302-314, 2003.
- [6] Han, T.; Yang, B.; Jong, L.: “*A New Condition Monitoring and Fault Diagnosis System of Induction Motors using Artificial Intelligence Algorithms*”, IEEE Inter. Conf. on Electric Machines and Drives, Conf. Proc., pp. 1967 – 1974, 15-18 May 2005.
- [7] Finley, W.; Hodowanec, M.; Holter, W.: “*An Analytical Approach to Solving Motor Vibration Problems*”, IEEE Trans. on Industry Applications, Vol. 36, No. 5, pp. 1467-1480, 2000.
- [8] Benbouzid, M.: “*A Review of Induction Motors Signature Analysis as a Medium for Faults Detection*”, IEEE Trans. on Industrial Electronics, Vol. 47, No. 5, pp. 984-993, Oct. 2000.
- [9] Cusido, J., et al.: “*New Fault Detection Techniques for Induction Motors*”, Electrical Power Quality and Utilisation, Magazine, Vol. II, No. 1, pp. 39-46, 2006.
- [10] Thomson, W.; Fenger, M.: “*Current signature analysis to detect induction motor faults*”, IEEE Trans. on Industry Applications, Vol. 7, pp. 26-34, 2001.
- [11] National Instruments: “*LabVIEW User Manual*”, April 2003.
- [12] Gani, A.; Salami, M.: “*A LabVIEW Based Data Acquisition System for Vibration Monitoring and Analysis*”, Student Conf. on Research and Development, Conf. Proc., Malaysia, pp. 62-65, 2002.
- [13] Nehrbass, J., et al.: “*Interfacing PC-based MATLAB Directly to HPC Resources*”, HPCMP Users Group Conf. (HPCMP-UGC’06), 2006.
- [14] Attia, J.: “*Teaching Electronics with MATLAB*”, FIE ’96, Conf. Proc., 1996.
- [15] Demuth, H.; Beale, M.; Hagan, M.: “*Neural Network Toolbox 5 User’s Guide for MATLAB*”, Mathworks, 2006.
- [16] Nejjari, H.; Benbouzid, M., “*Monitoring and Diagnosis of Induction Motors Electrical Faults using a Current Park’s Vector Pattern Learning Approach*”, Electric Machines and Drives Inter. Conf. (IEMD’99), 9-12 May 1999, pp. 275 - 277, 1999.
- [17] Chow, M.; Sharpe, R.; Hung, J.: “*On the Application and Design of Artificial Neural Networks for Motor Fault Detection*”, IEEE Trans. on Ind. Electronics, Vol. 40, No. 2, pp. 181-188, April 1993.
- [18] Alguindigue, I.; Loskiewicz-Buczak, A.; Uhrig, R.: “*Monitoring and Diagnosis of Rolling Element Bearings Using Artificial Neural Networks*”, IEEE Trans. on Ind. Electronics, Vol. 40, No. 2, pp. 209-217, April 1993.
- [19] de Almeida, A.; Ferreira, F.; Parasiliti, F.; Walters, D.: “*Barriers Against Energy-Efficient Electric Motor Repair*”, Report prepared for the European Commission, DGXVII, Edited by ISR-University of Coimbra, October 1999.
- [20] “*Actions to Promote Energy-Efficient Electric Motors*”, Report prepared for the European Commission, DGXVII, Motors Study Group, Edited by ISR-University of Coimbra, October 1996.
- [21] “*Improving the Penetration of Energy-Efficient Motors and Drives*”, Report prepared for the European Commission, DG TREN, SAVE II Programme, Edited by ISR-University of Coimbra, 2000.
- [22] “*Study on Technical/Economic and Cost/Benefit Analyses of Energy Efficient Improvements in Industrial Three-Phase Induction Motors*”, European Commission, DGXII, Energy, October 1999.
- [23] “*European Energy to 2020 - A Scenario Approach*”, European Commission, DGXVII, Spring 1996.
- [24] de Almeida, A.; Bertoldi, P.; Leonhard, W.: “*Energy Efficiency Improvements in Electric Motors and Drives*”, Springer-Verlag Berlin, 1997;
- [25] de Almeida, A.; Bertoldi, P.; Falkner, H.: “*Energy Efficient Improvements in Electric Motors and Drives*”, Springer-Verlag, Berlin, 2000;
- [26] Ferreira, F.: “*T ecnicas Avan adas de Manuten o Curativa e Reabilita o de Motores de Indu o Trif sicos de Baixa Tens o/Curative Maintenance and Rehabilitation Advanced Methods for Low-Voltage, Three-Phase, Induction Motors*”, Tese de Mestrado/Master Science Thesis (available in Portuguese only), Universidade de Coimbra/University of Coimbra, 2002.
- [27] Cistelec an, M.; Demeter, E.: “*Induction Motors with Low Copper Windings and Improved Performances*”, IEEE, 1996.
- [28] Beaty, H.; Kirtley, J.: “*Electric Motor Handbook*”, McGraw-Hill, New York, USA, 1998;
- [29] Williamson, S.; Laithwaite, E.: “*Generalised harmonic analysis for the steady-state performance of sinusoidally-excited cage induction motors*”, IEE Proc., Vol. 132, Pt. B, No. 3, May 1985;
- [30] Williamson, S.: “*Power-factor improvement in cage-rotor induction motors*”, IEE Proc., Vol. 130, Pt. B, No. 2, March 1983;
- [31] Williamson, S.; Smith, S.: “*Pulsating Torque and Losses in Multiphase Induction Machines*”, IEEE Trans. on Industry Applications, Vol. 39, No. 4, July/August 2003.
- [32] Indarack, P.; Douangsyala, S.; Joochim, C.; Kunakorn, A.; Kando, M.; Kinnares, V.: “*A Harmonic Loss Calculation of PWM-Fed Induction Motors Using Loss Factor Characteristics*”, IEEE 2004.
- [33] Lee, J., et al.: “*Loss Distribution of Three-Phase Induction Motor Fed by Pulsewidth-Modulated Inverter*”, IEEE Trans. on Magnetics, Vol. 40, No. 2, March 2004, pp. 762-765;
- [34] “*The Repair of Induction Motors - Best Practices to Maintenance Energy Efficiency*”, AEMT, U.K., 1997, and Department of the Environment, Transport and the Regions, U.S.A., 1998.
- [35] “*The Effect of Repair/Rewinding on Motor Efficiency – EASA/AEMT Rewinding Study and Good Practice Guide to Maintain Motor Efficiency*”, EASA/AEMT, U.K., 2003.

- [36] de Almeida, A., Ferreira, F., Both, D., “*Technical and Economical Considerations to Improve the Penetration of Variable-Speed Drives for Electric Motor Systems*”, IEEE Trans. on Industry Applic., Vol. 41, No. 1, pp. 188-199, Jan./Feb. 2005.
- [37] Mohan, N.; Undeland, T.; Robbins, W.: “*Power Electronics - Converters, Applications, and Design*”, 2nd Edition, John Wiley & Sons, Inc., New York, 1995.
- [38] Ferreira, F.; de Almeida, A.: “*Enquadramento da Manutenção Curativa no Custo do Ciclo de Vida dos Motores de Indução Trifásicos*”, Revista “Kerâmica”, Ano XXIX, N.º 261, Setembro/Outubro de 2003.
- [39] Ferreira, F., de Almeida, A., G. Baoming, G.: “*Three-Phase Induction Motor Simulation Model Based on a Multifrequency Per-Phase Equivalent Circuit Considering Stator Winding MMF Spatial Harmonics and Thermal Parameters*” 17th Inter. Conf. on Electric Machinery (ICEM’06), Conf. Proc., Crete, Greece, Sept. 2006.
- [40] Teinser Technical Personnel, *Experts opinion*, 2006.
- [41] Jung, J.; Lee, J.; Kwon, B.: “*Online Diagnosis of Induction Motors Using MCSA*”, Trans. on Industrial Electronics, Vol. 53, No. 6, pp. 1842-1852, Dec. 2006.
- [42] Alger, P.: “*Induction Machines – Their Behavior and Uses*”, Gordon and Breach Publishers, 3rd Edition, New York, 1995.
- [43] Chalmers, B.: “*Waveshape of flux density in polyphase induction motors under unsaturated conditions*”, IEEE Trans., 1971, PAS-90, pp. 564-569.
- [44] Chen, Y.: “*Investigation of a new AC electrical machine winding*”, IEE Proc.-Electr. Power Appl., Vol. 145, No. 2, March 1998, pp. 125-132.
- [45] Cidambaram, P.; Subbiah, M.; Krishnamurthy, M.: “*Generalized theory for the performance of three phase induction motor with star-delta winding*”, Electric Machines and Power Systems, 12, 1987, pp. 383-396.
- [46] Cistelec, M.; Bălă, C.: “*Infasurari combinate stea-triunghi pentru masini de c.a. trifazate*”, EEA – Electrotechnica, Vol. 47, nr. 3-4, 1999, pp. 1-9.
- [47] VEM Technical Reference Book, 2007.
- [48] Marinho, J.: “*Optimização de Enrolamentos de Motores de Indução Trifásicos/Optimization of Three-Phase Induction Motor Windings*”, Relatório Final de Projecto de Licenciatura/Graduation Project Final Report (available in Portuguese only), supervised by Aníbal T. de Almeida and Fernando J. T. E. Ferreira, Coimbra, Setembro de 2005.
- [49] Boglietti, A.; Cavagnino, A.; Staton, D.: “*Thermal Analysis of TEFC Induction Motors*”, 38th IEEE IAS Annual Meeting, Industry Applications Conf., Conf. Proc., Vol. 2, pp. 849-856, 12-16 Oct. 2003.
- [50] Alstom – Electrical Machines, “*High Specification Cast Iron LV Motors*”, Vector, Sept. 2003.
- [51] Santos, F.; Trovão, J.; Ferreira, F.; Coelho, D.: “*Three-Phase Induction Motor Condition Evaluation by means of Combined Current and Vibration analysis Using Artificial Neural Networks*”, 2nd Inter. Conf. on Electrical Engineering (CEE’07), Conf. Proc., Nov. 2007.
- [52] “*DUV10A diagnostic unit*”, Vibration-Based Diagnostic Unit, SEW-Eurodrive, www.sew-eurodrive.com, 2008.
- [53] Rajaraman K.: “*Theory and design of part winding starting*”, IEEE Trans. on Energy Conversion, Vol. 14, No.1, pp. 31-36, March 1999.
- [54] Jian, T.; Schmitz, N.; Novotny, D.: “*Characteristic Induction Motor Slip Values for Variable Voltage Part Load Performance Optimization*”, IEEE Trans. on Power Apparatus and Systems, Vol. PAS-102, No. 1, pp. 38-46, Jan. 1983.
- [55] Kliman, G., et al.: “*A New Method for Synchronous Generator Core Quality Evaluation*”, IEEE Trans. on Energy Conversion, Vol. 19, No. 3, pp. 576-582, Sept. 2004.
- [56] “*Winding Dielectric Test Instruments*” and “*MTA for Windows*”, Technical Datasheets, Baker Instrument Company, U.S.A.
- [57] Yong, T.: “*To Repair or Replace Industrial Electric Motors when they Fail*”, 5th Inter. Conf. on Energy Efficiency in Motor Driven Systems (EEMODS’07), Conf. Proc., Beijing, 2007.
- [58] COMAX – *Engineered Wires*, www.comax.uk.com, 2008.
- [59] “*O Índice de Preços de Matérias-Primas*”, Revista da Associação Portuguesa de Empresas do Sector Eléctrico e Electrónico (ANIMEE), N.º 294, pp. 64, Março/Abril de 2008.
- [60] Copper Trends: Live Metal Spot Prices, MetalSpotPrice.com.
- [61] Ferreira, F.; Trovão, J.; de Almeida, A.: “*Motor Bearings and Insulation System Condition Diagnosis by Means of Common-Mode Current and Shaft-Ground Voltage Correlation*”, 18th Inter. Conf. on Electrical Machines (ICEM’08), Conf. Proc., Vilamoura, Portugal, Sept. 2008.
- [62] Cruz, S.; Cardoso, A.: “*Rotor Cage Fault Diagnosis in Three-Induction Motors by Extended Vector Approach*”, Electric Machines and Power Systems, Taylor & Francis, 28:289–299, 2000.
- [63] Cruz, S.; Cardoso, A.; Toliyat, H.: “*New Developments in the Diagnosis of Faults in Line-Connected and Direct Torque Controlled Induction Motors*”, IECON’03, Invited Paper, Conf. Proc., pp. 1361-1368, 2003.
- [64] Cruz, S.; Cardoso, A.: “*Diagnosis of Stator Inter-Turn Short Circuits in DTC Induction Motor Drives*”, IEEE Trans. on Industry Applications, Vol. 40, No. 5, Sept./Oct. 2004.
- [65] Cruz, S.; Cardoso, A.: “*DSP Implementation of the Multiple Reference Frames Theory for the Diagnosis of Stator Faults in a DTC Induction Motor Drive*”, IEEE Trans. Energy Conversion, Vol. 20, No. 2, Jun. 2005, pp. 329-335.
- [66] Cruz, S.; Cardoso, A.: “*Multiple Reference Frames Theory: A New Method for the Diagnosis of Stator Faults in Three-Phase Induction Motors*”, IEEE Trans. Energy Conversion, Vol. 20, No. 3, Sept. 2005, pp. 611-619.
- [67] Lu, B.; Habetler, T.; Harley, R.; Gutiérrez, J.; Durocher, D.: “*Applying Wireless Sensor Networks in Industrial Plant Energy Evaluation and Planning Systems*”, IEEE Industry Applications Magazine, Mar./Apr. 2007, pp. 17-23.
- [68] Doppelbauer, M., *Expert opinion*, SEW-Eurodrive, 2007.
- [69] Santos, F.; Trovão, J.; Ferreira, F.: “*Avaliação do Estado de Funcionamento de Motores de Indução Trifásicos Através da Análise Combinada de Correntes e Vibrações Utilizando Redes Neurais*”, 9^o Congresso Nacional de Manutenção, INETI-CEGEF, 2007.
- [70] WEG: “*Cast Iron Motors – W21 line, IP 55 Multivoltage Motors*”, Motor Catalogue, 2004.
- [71] Jackson, D.: “*Low Voltage Insulation System Endurance Against Electronic Waveform and Cable Length*”, IEE Colloquium on Effects of High Speed Switching on Motors and Drives, Ref. No. 1999/144, pp. 6/1-6/7, June 1999.

Appendix 4 – Power Quality Impact on Motor-Driven Systems

Overview – In this appendix, a study on the impact of voltage distortion, voltage unbalance, and/or under/overvoltages in the performance of IMs is presented, including considerations on individual and combined effects of those power supply abnormalities on motor efficiency, reliability, and power derating curves. The impact of voltage unbalance and additional DC-bus capacitance in the output voltages of VSDs integrating three-phase, six-pulse, diode rectifiers and voltage-source inverters, is also investigated. Ride-through capability of VSDs to voltage sags is also addressed. Further research on voltage unbalance impact on IMs is being carried out, and will be presented in coming conferences.

A4.1 Introduction

It is important to design and install electrical systems that meet safety codes, minimize downtime, and reduce electrical losses.

Since the beginning of the second half of the 20th century, the effects of poor power quality (PQ) on IMs have been widely discussed (e.g., [22], [24], [25], [27], [37], [42]-[44]), including voltage unbalance and/or magnitude deviation, and, more recently, voltage distortion. In fact, a number of studies confirm that unbalance, distortion, and/or under/overvoltages long-term abnormalities lead to a significant increase of IM losses and, in the absence of derating actions, to the shortening of the motor lifetime. However, the combined effects of these supply voltage anomalies on IMs require further discussion. The main standards on IMs and PQ define limits for voltage magnitude deviation, unbalance and distortion, and, some of them, establish power derating curves for IMs, as a function of these parameters. Motor derating curves define output power limits under non-ideal power supply conditions to prevent motor early failure due to overheating. Derating curves or equations proposed in standards are based on average data, computed from theoretical analysis, simulations and/or experimental tests. As far as the author knows, combined effects are not covered by those derating curves or equations.

The most common PQ problems on power supply voltage are sags (or dips), very-short interruptions, long interruptions, spikes, swells, flickers, fluctuations (magnitude deviations), harmonic distortion, high-frequency noise and unbalance. All of them can occur in one, two, or three phases.

In this appendix, the impact of medium/long-deviation or steady-state power supply anomalies or disturbances on the performance (e.g., efficiency and slip) and lifetime of low-voltage IMs is addressed, focusing the voltage magnitude deviation (VMD), voltage unbalance (VU), and voltage distortion (VD). The influence of ambient temperature deviation (ATD) and motor characteristics on the required motor derating is also analysed. Knowing the effects that VU produces in the IMs, it is also important to discuss the VU propagation possibility from the input to the output of VSDs. Little references are found on this issue, but an overview and some remarks are presented in this

appendix, assuming only VSDs integrating three-phase six-pulse diode rectifiers and voltage-source inverters. Ride-through capability in the sequence of voltage sags is also analysed.

A4.2 Motor Derating Analysis

In the context of this appendix, data obtained from experiments, simulations and related reports, papers and documents, was processed, interpreted and summarized. Most of the consulted material is listed in the references. The motor simulations were carried out using per-phase exact equivalent circuit based models (ECMs). Three large and two small, low-voltage, TEFC, IMs (400 kW/4 poles; 200 kW/2 & 4 poles; 7.5 kW/4 poles; 3 kW/4 poles) were simulated. For the large IMs and the 7.5 kW IM, the typical IEC-defined ECM¹ was used, whose parameters were provided by one of the largest motor manufacturers, in the first case, and experimentally estimated by the author, in the latter case. For the 3-kW IM, an ECM-based model with thermal compensation (by means of a lumped parameter motor thermal model) was used, described in Appendix 2 and [41]. The skin effect impact on rotor effective leakage inductance and effective resistance [22], [25], [41], as well as the frequency dependent core loss resistance variation, are included in all models, using convenient adaptation. Magnetizing inductance variation as a function of magnetizing current (saturation effect) and SLLs are included only in the 3-kW IM model. Moreover, to simulate different types of rotor bars, six different rotor resistance cases (frequency dependent) are considered in the 3-kW IM model², shown in Fig. A4.1 and Table A4.1.

TABLE A4.1
ROTOR-BAR TYPES CONSIDERED ON THE SIMULATIONS OF THE 3-kW, 4-POLE IM [48].

Rotor #	Bar Material	Bar Section	Bar Depth	Bar DC Resistance
Rotor I	Al	Original	Original	Original
Rotor II	Cu	Original	Original	Lower
Rotor III	Al	Original	Higher	Original
Rotor IV	Al	Original	Lower	Original
Rotor V	Al	Higher	Original	Lower
Rotor VI	Al	Lower	Original	Higher

According to the standard IEC 60034-1 standard [8], depending on the value and duration (assuming that it is significantly longer than motor thermal time constant) of the different load levels within motor duty-cycle, the relative lifetime expectancy, t_{lf} , of a S1-duty type motor based on the thermal ageing of the insulation system can be calculated by (A4.1), where $\Delta\theta$ is the difference between the temperature rise of the winding at each of the various loads within motor duty-cycle and the temperature rise corresponding to S1-duty operation at rated load, Δt is the p.u. duration of a constant-load period within the load duty-cycle, k is the temperature increase ($^{\circ}\text{C}$ or

¹ ECM parameters determined according to the IEC 60034-28 standard. In order to take into account skin effect, variable rotor parameters, as a function of the rotor current frequency, were considered.

² In Appendix 2, the per-phase equivalent circuit parameters for 7.5-kW, 4-pole IMs with identical cross-sectional but different active materials (aluminium- and copper-cage rotors and standard and premium magnetic steel) and core lengths, are shown.

K) that leads to a shortening of the thermal lifetime expectancy of the insulation system by 50%, n is the number of different load values with the motor duty-cycle. Using (A4.1) it is possible to predict the impact that the motor internal operating temperature increase has on its insulation system lifetime.

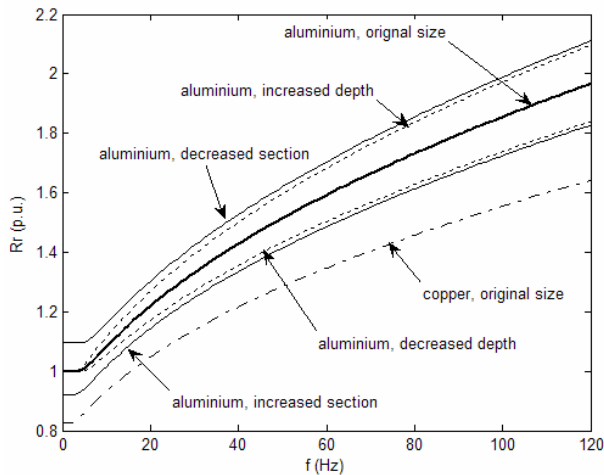


Fig. A4.1. Rotor effective resistance as a function of frequency, for different rotor-bar types [48].

$$\frac{1}{t_{lf}} = \sum_{i=1}^n \Delta t_i \cdot 2^{\frac{\Delta \theta_i}{k}} \quad (\text{A4.1})$$

Equation (A4.1) reflects approximately the reaction rate equation known as the Arrhenius' law, which is considered as a common rule-of-thumb [14], [26], [57]. The value of the quantity t_{lf} can be determined only when, in addition to information concerning the load cycle, parameter k for the insulation system is known. The parameter k has to be determined by experiments in conformity with IEC 60034-18 standard for the operating temperatures corresponding to each of the load levels of the duty cycle. However, for the sake of simplicity, k can be assumed as equal to 10, corresponding to the well-known rule of 50% lifetime decrease every 10 K increase in temperature (see also Appendix 6). For a given temperature, each insulation thermal class has a different lifetime. For the lubricants, a different value for k should be considered as a function of the type of lubricant (mineral, semi-synthetic, synthetic). Lifetime can be stated approximately as a relative value only. This value can be used by approximation to assess the real change in the motor thermal lifetime expectancy in relation to the S1 duty operation at rated output, because it may be assumed that, in consideration of the varying loads existing within the duty cycle, the remaining influences over the lifetime of the motor (e.g., dielectric stress, environmental influences, etc.) are approximately the same as in the case of S1 duty operation at rated output power [8]. The manufacturer of the machine is responsible for the correct compilation of the various parameters for determining the value of t_{lf} [8].

A more rigorous analysis on motor lifetime should also consider the temperature increase in the bearings to take into account the lubricant ageing acceleration.

The motors should be kept as cool as possible to extend their lifetime. Typical best practice actions are making certain motors shaded from the sun, located in well ventilated areas, and kept clean, since dirt acts as a thermal insulator [9].

Since the motors internal temperature (e.g., windings temperature) depends on ambient temperature and on the equivalent thermal resistance (as shown in Chapter 3), the motor derating curves establish the output power or loadability limits for a motor under non-ideal steady-state feeding conditions in order to ensure the expected original lifetime under ideal or within established supply conditions limits, meaning that the allowable motor output power cannot lead to a stator winding temperature higher than the rated temperature, corresponding to a temperature lower or equal than the admissible winding temperature corresponding to the motor thermal class.

A4.2.1 Voltage Distortion

Voltage distortion (VD) means that voltage and, consequently, current waveforms have a non-sinusoidal shape. The distorted periodic waveform corresponds to the sum of different sine waves with different magnitudes and phases, having frequencies that are multiples of the fundamental component of the supply system, commonly known as harmonics. The causes and consequences of this PQ problem are well known and described in several publications (e.g., [14], [17], [24], [25], [40], [44]) and standards (e.g., IEEE Std. 519). One of the main consequences of VD, under the scope of this thesis, is its detrimental effect on efficiency of electric machines (particularly motors).

Nonlinear loads change the sinusoidal nature of the current wave and, consequently, when the current flow through the grid impedance leads to harmonic voltage drops, which adds to the original voltage, originating its distortion. There are different types of distortion (harmonics, interharmonics, subharmonics, notching, noise, and DC component [1]), but only the harmonics (typically, symmetrical for the three phases) are considered in this section for discussion. The kVA rating of the non-linear loads on a voltage bus with respect to the voltage bus stiffness is a major factor influencing the VD level.

The extent to which harmonics can be tolerated is determined by the susceptibility of the load (or power supply) to them. The least susceptible type of equipments is that in which the main function is heating, such as ovens and furnaces. In this case, the harmonic energy is generally used and hence is completely tolerable. The most susceptible type of equipment is that whose design or operation assumes a (nearly) perfect sinusoidal fundamental input. This sort of equipment is frequently in the categories of communication or data processing equipment (e.g., metering and instrumentation devices). A type of load that normally falls within these two extreme cases of

susceptibility is the electric motor. Most motors are relatively tolerant to harmonics. Nevertheless, even in the case of the least susceptible equipment, harmonics can be harmful. In the case of an oven, for example, harmonics can cause dielectric thermal or voltage stresses, which cause premature ageing of electrical insulation. In fact, a major effect of harmonic voltages and currents in rotating machinery is the increased heating due to the additional losses at the harmonic frequencies. As a consequence of that, the harmonic components affect the machine efficiency and can also affect the developed torque. Harmonic currents in a motor can give rise to a higher audible noise emission as compared with sinusoidal excitation. Harmonics also produce a resultant flux distribution in the air gap, which can cause or enhance the well-known phenomena called cogging or crawling in IMs. Harmonic pairs, such as the 5th and 7th harmonics, have the potential for creating mechanical oscillations or vibrations (associated with pulsating torques, as explained in Appendix 3) in IMs. The mechanical oscillations result when the pulsating torques excite a mechanical resonant frequency, which can lead to the development of high-stress mechanical forces [5].

Table A4.2 defines the characteristic harmonic orders derived from a six-pulse converter when applied to the terminals of a rotating machine. Each odd non-triplen harmonic voltage originates a corresponding harmonic current in the stator of the machine. Each current harmonic constitutes a positive- or a negative-sequence component of the total current. These currents will produce additional heating in the motor and directly in the stator windings, which adds to the temperature rise caused by the fundamental current [5].

Another generally greater concern is the flow of harmonic currents in the rotor. The flow of each current in the stator will produce an air-gap rotating MMF that will induce currents in the rotor of the machine. Thus, from a rotor-heating standpoint, the 5th and the 7th order current harmonics in the stator combine to produce a $\approx 6^{\text{th}}$ order current harmonic in the rotor³. The 11th and the 13th order harmonics act in the same manner to produce the $\approx 12^{\text{th}}$ order harmonic current in the rotor, and so on with higher order harmonic. There are two major concerns with these rotor harmonics, in one hand, the resultant extra rotor heating, and, on the other hand, the torque pulsation. The amount of rotor heating that can be tolerated, as well as the amount that is incurred in a given case, depends on the type of rotor involved. Wound-rotor motors are more likely to be more seriously affected than squirrel-cage rotor motors, and deep-bar or double-cage squirrel-cage rotors are more affected than ordinary squirrel-cage rotors. Winding losses generally are of more concern than core losses. The combined effect of the harmonics is a reduction of the motor efficiency and life. The extra heating associated with harmonics typically reduces motor efficiency to 90-95% of the value

³ Actually, in this case, since the motor fundamental slip is not zero, it is produced a rotor current inter-harmonic corresponding to $5+(1-s)$ or $7-(1-s)$ times the fundamental stator current frequency. However, since the fundamental slip, in steady state, is typically significantly lower than 1 ($s \ll 1$), it can be assumed that 5th and 7th order stator current harmonics produce a $\approx 6^{\text{th}}$ order current harmonic in the rotor.

expected for pure fundamental sine waves. Pulsating torques can affect product quality where motor driven loads are sensitive to such variations, e.g., in some synthetic fiber spinning or some metal working applications, and, in some cases, as previously referred, can excite a mechanical resonance, and the resulting extra mechanical oscillations can cause accelerated ageing or fatigue of the shaft and of the connected mechanical parts.

TABLE A4.2

STATOR AND ROTOR CURRENT HARMONICS FOR A SIX-PULSE CONVERTER-FED INDUCTION MOTOR ASSUMING ZERO SLIP [5], [25].

Stator Current Harmonic Order	Frequency (Hz)	Sequence Network	MMF Rotation	Harmonic Slip	Rotor Current Harmonic Order
1 (fund.)	50	+	Forward	--	--
5	250	-	Backward	6/5	6
7	350	+	Forward	6/7	6
11	550	-	Backward	12/11	12
13	650	+	Forward	12/13	12
17	850	-	Backward	18/17	18

The factors that define the quality of electrical energy supply service include harmonic distortion in addition to more familiar factors such as safety of service (e.g., surge protection), service continuity, voltage regulation, and flickers. The distortion limits recommended in the main PQ related standards (such as [5]) establish the maximum voltage distortion at the point of common coupling (PCC) with each consumer. The recommended distortion limits should be used as system design values for the “worst case” under normal operation (conditions lasting longer than one hour). For shorter periods, during starting periods or unusual conditions, the limits may be exceeded by 50% [5]. Additional information on this topic is provided in Appendix 6.

Regarding power cables, they may be subjected to voltage stress and corona, which can lead to dielectric (insulation) failure, and, additionally, they are prone to heating [5]. Typical capacity derating curves have been plotted for a number of cable sizes, as shown in Fig. A4.2, for a six-pulse harmonic distribution. Typically, the effect of harmonic heating in cables is not a matter of great concern, as it can be seen in Fig. A4.2. Prudent design should, however, provide the required derating [5].

Not only can the harmonic magnitudes and predominant harmonic orders vary, but relative phase angles can also vary. Two waveforms with the same characteristic harmonic magnitudes can differ substantially if their harmonics have different phase angles relative to the fundamental. A relay, for example, can respond differently to each waveform shape even though each contains the same harmonic magnitudes.

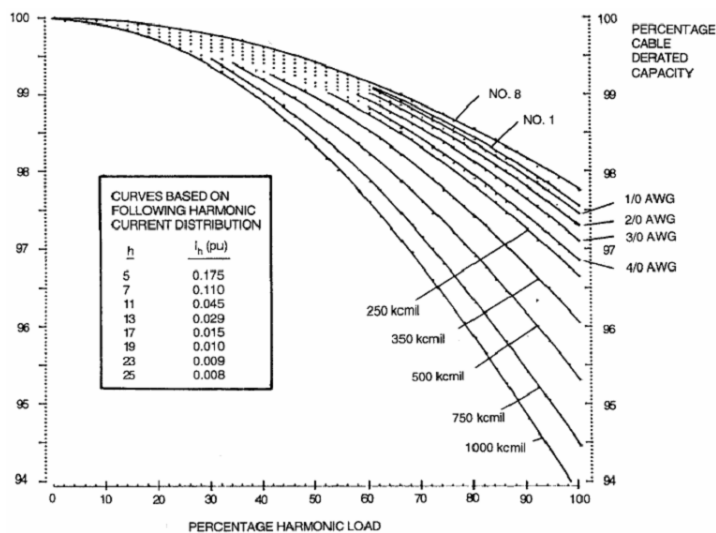


Fig. A4.2. Cable derating with 6-pulse converter harmonic current distribution [5].

Regarding IMs, when the supply voltage is significantly non-sinusoidal, the RMS values of the total and of the fundamental waveforms are both relevant in determining their performance [8].

NEMA MG-1 standard [38] defines a derating graph to account for the additional heat generated by the harmonic currents in the motor. For example, an experimental test was carried out on a 5-hp motor running at 80% load and fed by a programmable power supply generating 5th and 7th order harmonics, which reflect the largest components typically found in the field [7], [38], being observed that a “safe” load of only 80% can be still suffice to thermally stress a motor subjected to extremely poor power conditions [38]. Obviously, much lesser levels of distortion will be needed to trespass the service factor threshold of 1.0 for higher load levels [38].

Comparing the NEMA MG-1 standards derating curve⁴ as a function of harmonic voltage factor, *HVF*, presented in Fig. A4.4 with the results presented in [17] and [48], it can be concluded that, apparently, excessive derating is being recommended by NEMA, even considering the loss-based derating. Perhaps, the idea behind NEMA derating curve is to take into account the worst distortion situation for the most sensitive motor type. However, it can be anticipated that, since the derating curves depend on a number of factors such as motor rated power and type, and harmonics pattern, a unique derating curve makes no sense, as it will be shown further.

Although the extensive published work on this issue, considerations on motor rated power and type (number of poles, efficiency class, torque-speed curve, and frame type) are not well explored. For example, in [17], it is shown that the higher the pole number, the higher the derating as a function of *HVF*. One can also expect that the higher the motor efficiency the lower the derating, and the higher the starting to rated torque ratio, the higher the derating. Therefore, it is important to define general derating curves for different motor rating and types. It is also important to take into

⁴ The rated horsepower of the motor should be multiplied by the derating factor in order to ensure that the stator windings operating temperature does not exceed the nominal value, avoiding the motor lifetime shortening. This curve is developed under the assumption that only odd, non-triplen harmonics (except those divisible by three) of the fundamental frequency are considered. It is assumed that voltage unbalance or even harmonics, or both, if any, are negligible [38].

account the voltage waveform spectrum or harmonics pattern, for a given value of total harmonic distortion, *THD*.

In this section, a review of a number of published works is made and new considerations on motor derating are presented, mainly based on simulations.

Among all VD patterns or spectra found in the field, the most common is defined by (A4.2), where U_h is the h^{th} odd, non-triplen order harmonic voltage amplitude, U_1 is the fundamental voltage amplitude, and d is a constant depending on the VD level (according to (A4.2)). Of course, the balance between actual values of each harmonic can be significantly different from those defined by (A4.2).

$$U_h = d \cdot \frac{U_1}{h} \quad (\text{A4.2})$$

Regarding IMs, the odd, non-triplen excitation time harmonics can be divided into positive-sequence harmonics (order $h = 7, 13, 19, \dots$) and negative-sequence harmonics (order $h = 5, 11, 17, \dots$), which produce forward (direct) and backward (inverse) rotating MMF waves in the air-gap, respectively. Time harmonics under consideration can affect motor torque-speed curve (steady-state harmonic torques), increase motor vibration and acoustic noise, and produce additional losses heating, as referred in Appendix 3.

A rigorous analysis of the impact of time harmonics should include their interaction with the MMF space harmonics produced by the stator winding [41]. However, to reduce the computational efforts, those harmonics were not considered in the simulations performed. Additionally, it should be noted that, although their impact on IM performance, even harmonics, and particularly the 2nd harmonic (negative-sequence harmonic) [16], are not considered since they are not commonly found in practice.

For the same VD level, several combinations of harmonics can be found, with different impacts on IM performance. To quantify VD, different definitions exist, namely total harmonic distortion, *THD*, total harmonic factor, *THF*, distortion factor, *DF*, and harmonic voltage factor, *HVF*. In the following analysis the *HVF* is used, which, according to the IEC 60034-1 and NEMA MG-1 standards, is defined by (A4.3), where u_h is the ratio of the harmonic voltage U_h to the rated voltage U_R , h is the order of non-triplen order harmonic, and m is the maximum considered harmonic order, typically considered as 13th order ($m = 13$) [8], [38]. According to the IEC 60034-1, EN 50160, EN 61000-2-2 and IEC 61800-2 standards, the *THD* is defined by (A4.4), where U_1 is the fundamental voltage RMS value, and considering harmonics up to the m^{th} order (for the IEC 61800-2 standard $m = 40$). The IEC 61800-2 standard defines the *THF* as in (A4.5), where U_{total} is the total voltage RMS. The relation between *THF* and *HVF*, for the VD pattern defined by

(A4.2), is shown in Fig. A4.3. According to the IEEE 519 standard, DF is defined by (A4.6), being identical to the THD definition given by (A4.4) [43]. Variations of such definitions can also be found if only a specific group of harmonics in terms of order or nature (even or odd) is considered (e.g., partial harmonic factor, PHF , according to the IEC 61800-2 standard, see also Appendix 6).

The North American standard IEEE 519 limits the DF for industrial power systems to 5%. However, no limit is specified with regard to the individual harmonic content. The EN 50160 and EN 61000-2-2 standards, used in Europe, specify an 8% limit for THD and percent limits for specific harmonics (e.g., 6% for the 5th harmonic and 5% for the 7th harmonic), including triplen and even harmonics [53].

$$HVF = \sqrt{\sum_{h=2}^m \frac{U_h^2}{h}} = \frac{1}{U_R} \cdot \sqrt{\sum_{h=2}^m \frac{U_h^2}{h}} \quad (\text{A4.3})$$

$$THD = \frac{1}{U_1} \cdot \sqrt{\sum_{h=2}^m U_h^2} \quad (\text{A4.4})$$

$$THF = \frac{\sqrt{\sum_{h=2}^m U_h^2}}{U_{total}} = \frac{\sqrt{\sum_{h=2}^m U_h^2}}{\sqrt{\sum_{h=1}^m U_h^2}} \quad (\text{A4.5})$$

$$DF = \frac{1}{U_1} \cdot \sqrt{\sum_{h=2}^m U_h^2} \quad (\text{A4.6})$$

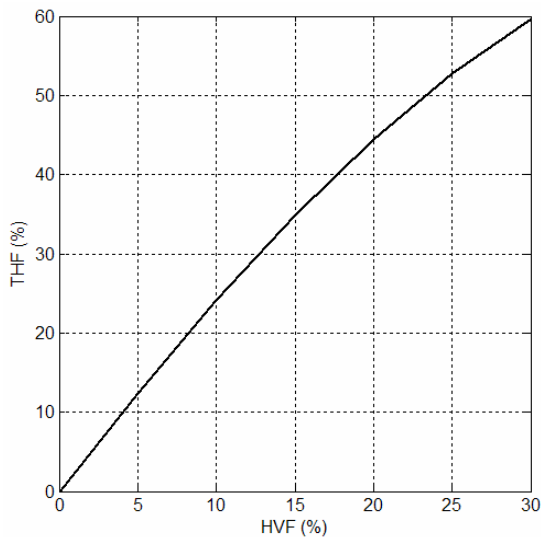


Fig. A4.3. Relation between the HVF and THF , considering the $U_R = U_1$, and VD pattern defined by (A4.2).

According to [8], which defines the electrical operating conditions for IMs, IMs for use on fixed-frequency power supplies shall be suitable for operation on a supply voltage having a HVF not exceeding 0.03 (3%) if of IEC design N and 0.02 (2%) otherwise, but IMs supplied from static

converters have to tolerate higher harmonic contents (refer to IEC 60034-17 standard for the case of cage motors within the scope of IEC 60034-12 standard). However, in the IEC 60034-1 and NEMA MG-1 standards, no limit is specified regarding the individual harmonic content.

For the simulations, *HVFs* of 0, 5, 10, 15, 20, and 25% are considered, and $U_I = U_R$, such that the h^{th} harmonic voltage is defined according to (A4.2). For the sake of simplicity, it is assumed that harmonics are balanced and, therefore, their representation in symmetrical components is not necessary. Even and triplen (divisible by three) harmonics are not considered.

There are two ways to calculate the motor power derating. In one hand, the derating can be calculated on the basis of stator winding temperature, which is obviously more correct approach, and, on the other hand, it can be calculated on the basis of motor total losses, which is useful if the motor thermal model is not known. Therefore, based on the motor temperature and losses variation, power derating curves were computed, i.e., the curves of admissible output shaft power maintaining the nominal stator windings temperature or nominal total losses. In the following simulations, both approaches are applied to a 3-kW, 4-pole motor, and the latter approach is applied to the other larger motors (due to the fact that the respective thermal model is unknown).

In Fig. A4.5, the main motor characteristics as a function of load for the 3-kW, 4-pole IM are presented. Figs. A4.4 and A4.6 show the simulated motor temperature-based power derating (TBD), loss-based power derating (LBD) curves, and the NEMA derating curves, as a function of *HVF*. Fig. A4.7 shows the TBD and LBD simulated curves for the 3-kW IM, considering different rotor-bar types.

In [14], [17], and [44], several experimental and/or simulated results for different IMs are presented. The presented results suggest an overderating associated with NEMA curves for small motors. LBD curves are more pronounced than TBD curves, leading to a safety error margin (overderating). Therefore, LBD can be used if the motor thermal model is not known. Of course, the motor overderating leads to an oversizing situation, in which the motor operates with poor efficiency and power factor. It should be noted that, errors are also obtained in the ECM-related outputs when thermal compensation of the resistive parameters is not made. Additionally, the higher the motor rated power the more pronounced the LBD, which is an expected result due to the higher rotor bar depth and section. However, in [16] it is shown that TBD is likely to decrease with the motor rated power increase because the loss percentage decreases with motor size and loss variation has less impact on motor temperature. Therefore, care must be taken when *HVF* loss-based derating is applied to medium/large motors.

Rotor-bar type also influences the motor derating, being the motor with “rotor III” (higher bar depth), which represents a high-starting torque motor, the most vulnerable to *HVF*, as expected.

On the basis of Fig. A4.6, the lower the number of poles is, the higher the derating will be.

In [16], it was also found that open drip-proof (ODP) motors are found to be less affected by harmonic distortion than the totally enclosed fan-cooled (TEFC) motors. Moreover, efficiency plays a very important role in the degree of derating. Less efficient machines would require a higher derating.

It should be noted that a simplified expression for estimating the effect of VD on the temperature rise of squirrel-cage motors is proposed in [25], in which the harmonic losses, P_{loss_H} , can be estimated by (A4.7), where P_{loss_N} is the nominal or rated electrical loss at rated current and voltage, U_N the RMS rated voltage, U_h the RMS value of the voltage harmonic of order h , and $K = 35$ (for normal slip motors).

$$\frac{P_{loss_H}}{P_{loss_N}} \approx K \cdot \sum_{h=5,7,11,\dots} \left(\frac{U_h}{\sqrt{h} \cdot U_N} \right)^2 = K \cdot HVF^2 \quad (\text{A4.7})$$

Equation (A4.7) predicts the losses with a reasonable error⁵. The main source of error is the coefficient K , which can vary with the motor geometry and fundamental frequency [25].

In [24] more results on the impact of the effects of VD on the temperature rise of squirrel-cage motors is presented, based on a very simplified motor thermal model, without thermal feedback or compensation of the resistive parameters.

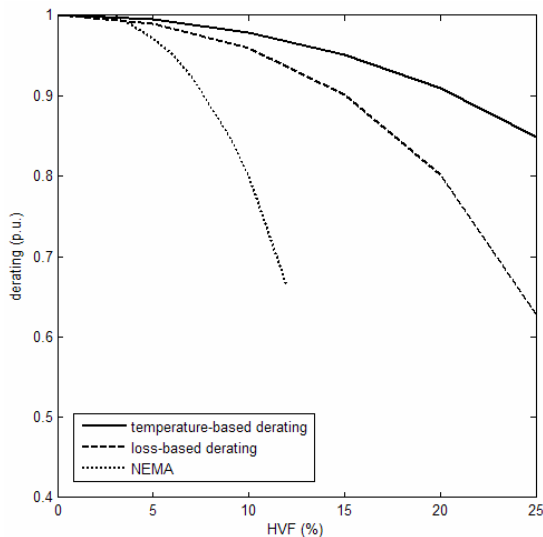


Fig. A4.4. 3-kW/4-pole IM: simulated motor power derating curves as a function of HVF [48].

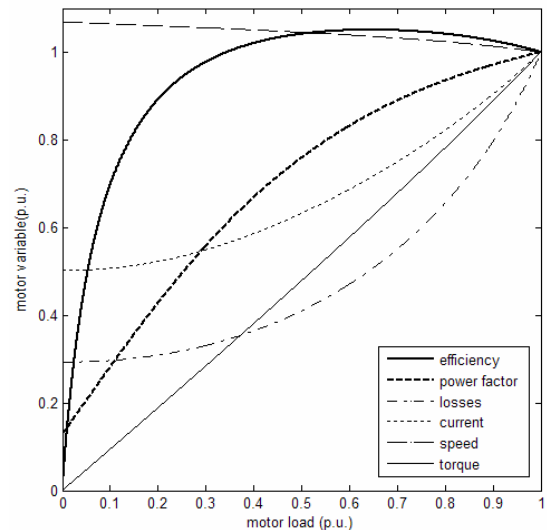


Fig. A4.5. 3-kW/4-pole IM: simulated motor main characteristics as a function of load, under ideal power conditions (ambient temperature of 25°C, 400 V, 50 Hz) [48].

⁵ For low/medium power motors an error up to $\pm 12\%$ can be expected [25].

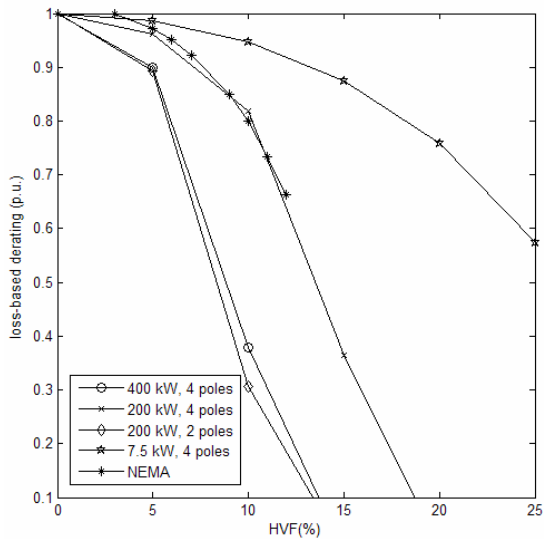


Fig. A4.6. 400-kW/4-pole, 200-kW/2&4-pole and 7.5-kW/4-pole IMs: simulated motor loss-based power derating curves as a function of *HVF* [48].

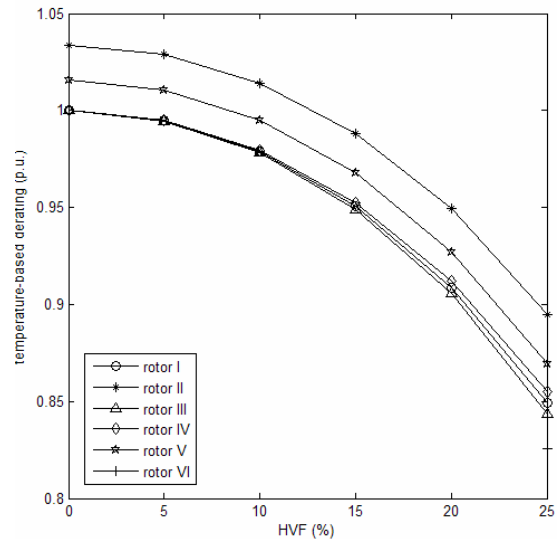


Fig. A4.7. 3-kW/4-pole IM: simulated motor temperature-based power derating curves as a function of *HVF*, considering different rotor-bar types [48].

In order to assess the impact that different *HVF* patterns have on the IMs, three different situations are compared on the basis of simulations. Considering $U_R = U_I$, and harmonic orders up to 13, three different harmonic content patterns, defining the order and magnitude of voltage harmonics, are now considered – pattern 1, pattern 2, and pattern 3 – being the respective harmonic voltages defined by (A4.8), (A4.9) and (A4.10), respectively (mathematical demonstration of such equations shown in Appendix 6), being the last the most severe operating condition for a reference *HVF*. Equation (A4.8) represents the pattern defined by (A4.2), used in the previously presented results. *HVFs* of 0, 5, 10, 15, 20, 25 and 30% are considered. The pattern defined by (A4.8) is more likely to be found in industrial installations [7], as previously referred.

Fig. A4.8 shows the simulated temperature-based derating for the different *HVF* patterns. Based on those results, it can be stated that the distortion pattern can have a significant influence on the *HVF* impact on motor performance and, therefore, should take into account in the motor derating.

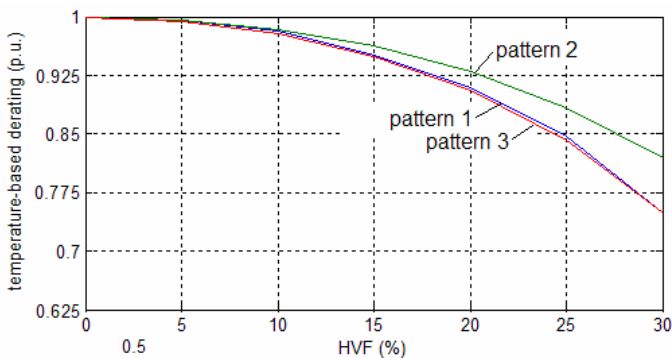
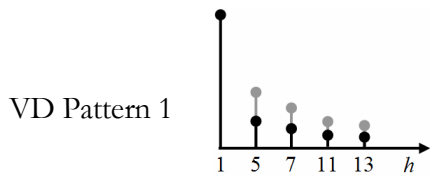


Fig. A4.8. 3-kW temperature-based derating curves, for different VD patterns: pattern 1 defined by (A4.8); pattern 2 defined by (A4.9); pattern 3 defined by (A4.10).

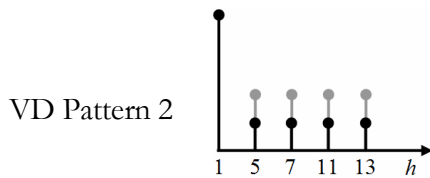
However, for the same *HVF* values, minor differences were obtained between the impact on IM performance of the patterns defined by (A4.8) and (A4.10), evidencing the importance of the 5th

order harmonic over the other harmonic orders. The pattern defined by (A4.9) led the lower derating.

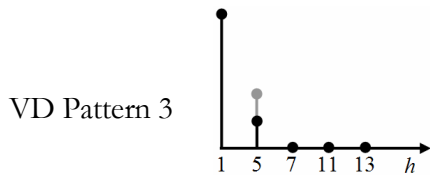
On the basis of the foregoing analysis, it can be concluded that the derating curves should be defined as a function of power ranges and of motor type, in terms of number of poles, efficiency class, frame type, and rotor type (bar shape and material). The distortion pattern is also an important factor to be taken into account. Moreover, based on the presented results, the commonly used pre-assigned curves are likely to lead, in general, to an overderating for most low power motors. For large motors, it seems to be appropriate.



$$U_h = \frac{U_1}{h} \cdot \frac{HVF}{\sqrt{\frac{1}{5^3} + \frac{1}{7^3} + \frac{1}{11^3} + \frac{1}{13^3}}} \quad (\text{A4.8})$$



$$U_h = \frac{U_1}{5} \cdot \frac{HVF}{\sqrt{\frac{1}{5^2 \cdot 5} + \frac{1}{5^2 \cdot 7} + \frac{1}{5^2 \cdot 11} + \frac{1}{5^2 \cdot 13}}} \quad (\text{A4.9})$$



$$U_5 = \frac{U_1}{5} \cdot \frac{HVF}{\sqrt{\frac{1}{5^2 \cdot 5}}} \wedge U_{7,11,13} = 0 \quad (\text{A4.10})$$

Therefore, at least, the harmonics up to 13th order should be measured and the distortion pattern defined. It is also important to refer that major differences between temperature-based and loss-based derating curves were observed. An overderating is obtained if loss-based analysis is made.

A4.2.2 Voltage Unbalance

Voltage Unbalance (VU) is another commonly known PQ phenomenon and its causes and adverse effects on IMs performance are fairly discussed in many publications over the past decades [10], [11], [12], [13], [22], [26], [27], [40], [43].

A three-phase voltage system is considered balanced or symmetric if the voltages and currents of the three phases have the same amplitude and the same displacement between them. If one of these two conditions is not verified, the system becomes unbalanced or asymmetrical. In other words, according to [53], VU is a condition where the RMS value of the phase voltages and/or the phase angles between consecutive phases in a 3-phase system are not equal. In most practical cases, the

load asymmetry in the system is the major cause for VU. Load asymmetry is associated with unbalanced loads as large single-phase or two-phase loads (e.g., induction furnaces, arc furnaces, traction loads, etc., mostly in HV and MV systems), incorrect distribution of all single-phase loads by the three phases of the system, phase-earth, phase-phase, and out-of-phase⁶ faults, different per-phase conductor gauges, faulty circuits, etc. [1]. In general, the use of large single-phase loads is identified as the main cause for VU. Other causes are the incomplete transposition of transmission lines [26], blown fuses on three-phase capacitor banks, etc. [11]. In fact, the impedance of the per-phase elements of electrical power network is not exactly the same as a consequence of the geometric configuration of the aerial lines, asymmetrical in relation to the earth, leading to a significant difference in the electrical parameters of the line. Normally, those differences are slight and the resulting effects can be ignored when proper precautions are adopted (e.g., lines transposition). In LV systems, the loads in the residential and tertiary sectors are generally single-phase, e.g., computers, lighting systems, household appliances, etc., and in the electric installation or grid design the load should be, when possible, properly divided by the three phases to ensure a fair balance in terms of installed power. However, the actual load balance in the power transformer fluctuates due to the different duty cycles of each load. These issues are aggravated by the fact that the presence of a small unbalance in the line voltages will cause an unproportional unbalance in the line currents in IMs. The main consequences are the existence of a negative-sequence fundamental component that can be harmful to some three-phase loads. An unbalanced system increases power network losses and reduces motor efficiency. Usually, the level of unbalance is small enough so as not to affect the operation of IMs adversely. Yet, occasions arise when the level of unbalance must be taken into account in terms of impact on IMs operation and protection devices. Among the different types of protection devices, the most common are the overload or overcurrent relays, overtemperature relays, negative-sequence voltage relays, negative-sequence current relays, and current unbalanced relays, whose effectiveness was analysed in [26]. For voltage unbalance situations, temperature sensors-based protection strategies are clearly the most effective.

Once the voltage is unbalanced, the effects on IMs will cause enormous impacts on power supply companies and consumers. In fact, studies concerning IMs operation under VU conditions can be found since the year 1950, demonstrating that IMs operating with unbalanced voltage experience a reduction in the efficiency and an increase in the operating temperature, which is likely to shorten its lifetime significantly [11]. In the last decade, researches in this field were mostly focused on the protection strategies. However, several important issues were not considered

⁶ Commonly known as single-phasing. Can be caused, for example, by a fuse blow. It is an extreme condition of unbalance voltage. Depending on load, the motor can be able to run in steady-state operation, but it will be not able to start (negative-sequence current equals the positive-sequence current, producing same starting torque but in opposite direction) [26].

in previous studies, as the effects of VU on the power consumption of IMs - unbalanced voltages lead to significant changes in the motor thermal and electromechanical behaviour and, consequently, in the real and reactive power consumption. In the past, most of the related research was focused on VU caused by under-voltage, but the over-voltage situations can also occur in several countries, particularly during off-peak period (e.g., during off-peak or national holidays).

In the presence of VU, the entire envelope of the torque-speed curve is reduced, by the presence of a negative-sequence torque (see Appendix 2). Thus an important implication is that the motor will take longer to run up in those conditions. This increases the thermal stress in the machine and will lead to loss in life or early failure. This is due, firstly, to a reduction in the magnitude of the positive-sequence voltage when compared to the balanced supply voltage and, secondly, to the presence of a negative-sequence current which creates a negative-sequence torque, which subtracts from the positive-sequence torque to yield a net torque that is even smaller. If full load is still demanded to the motor, then it will be forced to operate at a higher slip, thus increasing the rotor losses and heat generated. Premature failure can only be prevented by derating the motor in order to allow it to operate within its thermal limits (rated temperature). The reduction in the peak torque also reduces the ability of the motor to ride through dips and sags, thus affecting the stability of the entire system.

According to the EPRI, a VU above 3% is found in only 2% of distribution systems. However, the amount of VU within an industrial plant is typically higher. A 4% VU is a condition encountered with a fair frequency in the field, particularly in LV systems [26]. A 10% VU is a condition of extreme severity rarely found in the field.

As referred before, the simplest protection for VU is to derate the motor, i.e., to reduce its output power so it can tolerate the extra losses and heating imposed by the unbalanced supply.

An unbalanced three-phase system, without neutral connection⁷, can be described by means of two symmetrical components, namely, voltage and current positive-sequence components, U_p and I_p , and voltage and current negative-sequence components, U_n and I_n . I_n produces a backward rotating MMF wave in the motor air-gap, having a similar effect to that associated with negative-sequence excitation time harmonics, described before. Typically, in IMs subjected to VU there is one or more phases, which show a strong increase of current level beyond the average, causing localized additional Joule losses and overheating in one phase which accelerates the motor insulation ageing [7]. This aspect of localization has to be taken into account in simulations based on the per-phase motor equivalent circuit, in order to properly estimate the maximum per-phase stator winding losses and temperature. As shown in [26], the rotor losses will increase much more as a function of VU, in relation to the stator losses. However, squirrel-cage rotors are essentially

⁷ In delta- or ungrounded star-connected IMs, which account for the vast majority of the cases, the zero-sequence power does not exist.

uninsulated and not subject to insulation thermal ageing. Therefore, the rotor temperature increase is not a major factor to be taken into account regarding motor derating.

Three definitions or quantification methods of VU have been used, depending on the standards (IEC, IEEE, or NEMA) [10], [11], [12], [13], [43]. According to NEMA and IEC, the VU is defined and quantified by the line-to-line VU rate, *LVUR*, given by (A4.11), being U_{AB} , U_{BC} and U_{CA} the RMS values of the line-to-line voltages [1], [11], [13]. Percentage value is obtained multiplying (A4.11) by 100%.

$$LVUR = U_{avg}^{-1} \cdot \max\{U_{AB} - U_{avg}, U_{BC} - U_{avg}, U_{CA} - U_{avg}\} \quad U_{avg} = \frac{1}{3}(U_{AB} + U_{BC} + U_{CA}) \quad (A4.11)$$

Industry and utilities generally like to adopt the *LVUR* to define the degree of VU. However, the *LVUR* cannot offer enough information for a proper definition of the strategy to overcome the problem.

Most of the regulations about VU only specify the percentage of voltage unbalance factor, *VUF*, without indicating the VU conditions or pattern. For example, the British standard BS-4999⁸ states that IMs should deliver their rated power when fed continuously from a power supply having a $VUF \leq 2\%$. According to the Section 7.2.1.1 of the international standard IEC 60034-1 [8], IMs shall be suitable for operation with $VUF \leq 1\%$ over a long period or $VUF \leq 1.5\%$ over a short period, not exceeding a few minutes. The American standard NEMA MG-1 [38] specifies a line-to-line VU ratio, *LVUR*, instead of the *VUF* and recommends derating curves (represented either by a figure/plot or an equation) as a function of the *LVUR* (Fig. A4.9). NEMA MG-1 standard also states that IMs can operate without derating for a $LVUR \leq 1\%$, but should not operate with a $LVUR > 5\%$, due to the resultant excessive operating temperature, as previously referred [26].

The International and European standards EN 50160 and IEC 1000-3-x, $LVUR < 2\%$ as a limit for LV and MV systems, and $LVUR < 1\%$ as a limit for HV systems, measured on the basis of 10 minute average values, with a instantaneous maximum of 4% are defined.

Moreover, for a given value of *LVUR* or *PVUR* there are several possible values for the *VUF* [11], [13]. In other words, for a given *VUF* value, the *LVUR* and *PVUR* can vary within a range of values [12]. For example, a 5% *LVUR* corresponds to a *VUF* in the range 5% to 5.8% [12]. In principle, for a $LVUR \leq 5\%$ or a $VUF \leq 5\%$, the resulting differences in the motor derating are not significant, being the *LVUF* almost directly proportional to the *VUF* [26].

In [1] a system is considered unbalanced if the steady-state *LVUR* is within the 0.5%-2% interval.

⁸ Standard BS-4999: "General Requirements for Rotating Electrical Machines".

According to the IEEE 141 standard, the VU is defined and quantified as a phase voltage unbalance ratio, $PVUR$, given by (A4.11), but the RMS values of the line-to-line voltages $U_{AB,BC,CA}$ are replaced by line-to-neutral voltages $U_{AN,BN,CN}$ [11], [13].

$LVUR$ and $PVUR$ are commonly used because of its simplicity, since they only consider the voltage magnitude, but they cannot reflect fully the system VU regarding, for example, the phase angle unbalance [11].

The VUF is defined as the quotient between the line-to-line negative-sequence voltage component, U_n , and the line-to-line positive-sequence voltage component⁹, U_p , given by (A4.12) [11], [13], which is used in some IEC standards for VU limits definition and derating purposes (e.g., IEC 60034-1, Section 7.2).

$$VUF = \frac{U_n}{U_p} \quad (A4.12)$$

In fact, there are many possible VU patterns corresponding to the same VUF or $LVUR$. If only VUF (non-complex) or $LVUR$ are mentioned, then neither the exact VU situation can be estimated (ambiguous definition) nor can the impacts on the power system be properly evaluated.

Some examples of different VU patterns are presented in Table A4.3. To each of those patterns, the same value of $LVUR$, $PVUR$, or VUF , can be found, if those definitions are used alone.

TABLE A4.3
EXAMPLES OF DIFFERENT VOLTAGE UNBALANCE SITUATIONS/PATTERNS [11], [13].

Situation	Common Designation	Voltages	Causes
a)	Single-phase, under-voltage unbalance	$U_A - \Delta U_A; U_B; U_C$	This type of situation arises when there is a large single-phase load in the system and it does not have enough compensation. In this situation the voltage in that particular phase will be lower than the other two phases.
b)	Two-phase, under-voltage unbalance	$U_A - \Delta U_A; U_B - \Delta U_B; U_C$	This type of situation arises when two of the three phases have heavy load and do not have enough compensation. In this situation those two phases will have higher voltage drop than the third phase.
c)	Three-phase, under-voltage unbalance	$U_A - \Delta U_A; U_B - \Delta U_B; U_C - \Delta U_C$	This type of situation arises when the loads of three phases are all too heavy and not balanced.
d)	Single-phase, over-voltage unbalance	$U_A + \Delta U_A; U_B; U_C$	Capacitors are normally used to compensate system reactive power. If one of the three phase voltages has been over-compensated, the voltage of this phase will be higher than the rated value.
e)	Two-phase, over-voltage unbalance	$U_A + \Delta U_A; U_B + \Delta U_B; U_C$	If two of the three phases have been over compensated, the voltages of these two phases will be higher than the rated value.
f)	Three-phase, over-voltage unbalance	$U_A + \Delta U_A; U_B + \Delta U_B; U_C + \Delta U_C$	If the three-phase voltages are over-compensated to different degrees, then all these three phases voltages will be higher than the rated value and not equal. This type of situation usually occurs at the line when a factory is shut down but capacitors are still connected to the system.
g)	Unequal single-phase angle displacement	--	If the three phase voltages are balanced, the angle displacement between them should be equal to 120°. For a given reference phase, if the angle of one of the other two phases is deflected, unequal single-phase angle displacement occurs.
h)	Unequal two-phase angle displacement	--	For a given reference phase, if the angles of the other two phases are both deflected, unequal two-phase angle displacement occurs.

⁹ It is possible to study the voltage unbalance using decomposition in three symmetrical components – direct or positive-sequence system, U_p , inverse negative-sequence system, U_n , and homopolar or zero-sequence system, U_0 [10]. However, in a line-to-line voltage system, homopolar component is always zero [10]. Knowing the magnitudes and displacements of the voltage three-phase system it is possible to calculate the symmetrical components and vice-versa [10].

Each VU pattern has a different impact on the motor performance (e.g., different degree of extra temperature rise), as it was experimentally demonstrated in [11], considering different VUF values (4 and 6%) at full-load operation. Overall speaking, each unbalanced case would lead to a different degree of extra temperature rise. Actually, for a given VUF , the relative impact of the referred possible VU conditions on efficiency and temperature rise in an IM operating at full load are, starting from the worst, (c), (b), (a), (h), (g), (d), (e), and (f). However, the study presented in [11] is for small motors (1.5 kW and 2 kW) at rated load, and the findings cannot be considered valid for different motor load conditions¹⁰ and/or larger motors.

In [13], a simulated study was carried out considering different voltage unbalance patterns and VUF values (4, 8 and 12%) at full-load operation (3.7 kW, 7.5 kW, and 22.5 kW), but the core losses and motor parameters temperature dependency were not taken into account. Nevertheless, it was found that, for the same VUF , a higher U_p leads to lower copper losses, as expected.

In [14], a more sophisticated model was used, taking into account the temperature impact on the stator and rotor conductors and the core losses. Per-phase evaluation was made. However, the purposed model is time-consuming if an evaluation as a function of motor load is to be made. Moreover, the VU and VD levels were only defined as a percentage, missing the type of VU considered or the definition behind. Nevertheless, in [14], for the same percentage, it was found that VU leads to a higher increase of the stator winding highest temperature point than the VD, as expected.

In [10], the relation between VUF and $LVUR$ is explained in detail. The complex VUF can be defined for line-to-line voltages and currents by (A4.13) and (A4.14), respectively, and for line-to-neutral voltages by the product between (A4.13) and $e^{j\pi/3}$, being the modules the same. The same definition can be applied to the currents, yielding the current unbalance factor, IUF , given by (A4.14).

$$\overline{VUF} = VUF \cdot e^{j\alpha_u} = \frac{\overline{U}_n}{\overline{U}_p} \quad (\text{A4.13})$$

$$\overline{IUF} = IUF \cdot e^{j\alpha_i} = \frac{\overline{I}_n}{\overline{I}_p} \quad (\text{A4.14})$$

The complex definition of VUF requires manipulation of complex phasors, and this may cause a difficulty in estimating VUF as the phase angle of voltages are usually not readily available unless specialized equipments are provided. In [10], it is proposed an alternative expression to calculate VUF , which avoids the use of complex algebra in symmetrical components. The phasors of the

¹⁰ A strongly oversized IM can actually experience an improvement in its efficiency and power factor when subjected to under-voltage unbalance.

line-to-line voltages form a closed triangle, being possible to represent the VUF in terms of magnitude of line-to-line voltages. In fact, it is possible to demonstrate that the module of VUF is given by (A4.15), where K_e , K , and ε are defined by (A4.16), (A4.17), and (A4.18), respectively. The angle between positive and negative-sequences, α_u , is given by (A4.19), where the so-called “equivalent three-phase RMS voltage”, U_e , is given by (A4.20). For a particular VUF , angle α_u has a significant effect on the current unbalance relation, $LIUR$, and, consequently, on the derating curves (if they take into account the asymmetry of currents in the three phases) and on the motor power factor (λ). It is also possible to use approximate expressions to calculate VUF . According to [10], the best approximation is given by (A4.21). The error associated with (A4.21) is up to 5% in relation to the exact VUF for $VUF \leq 35\%$. For example, when $VUF = 35\%$, the approximate VUF , $AVUF$, yields a value greater than 33.25% (95% of the exact VUF). Previous equations demonstrate that, even with only the line-to-line voltage magnitudes, it is possible to calculate VUF magnitude and angle.

$$VUF = \sqrt{\frac{K_e - K}{K_e + K}} \quad (\text{A4.15})$$

$$K_e = \frac{U_{AB}^2 + U_{BC}^2 + U_{CA}^2}{4\sqrt{3}} \quad (\text{A4.16})$$

$$K = \sqrt{\varepsilon(\varepsilon - U_{AB})(\varepsilon - U_{BC})(\varepsilon - U_{CA})} \quad (\text{A4.17})$$

$$\varepsilon = \frac{U_{AB} + U_{BC} + U_{CA}}{2} \quad (\text{A4.18})$$

$$\alpha_u = \tan^{-1} \left(\frac{U_{BC}^2 - U_{CA}^2}{\sqrt{3}(U_{AB}^2 + U_e^2)} \right) \quad (\text{A4.19})$$

$$U_e^2 = \frac{U_{AB}^2 + U_{BC}^2 + U_{CA}^2}{3} \quad (\text{A4.20})$$

$$AVUF = \frac{1}{\sqrt{6}} \cdot \frac{\sqrt{(U_{AB}^2 - U_{avg}^2)^2 + (U_{BC}^2 - U_{avg}^2)^2 + (U_{CA}^2 - U_{avg}^2)^2}}{U_{avg}^2} \quad (\text{A4.21})$$

$$U_{avg} = \frac{U_{AB} + U_{BC} + U_{CA}}{3}$$

Based on the foregoing discussion, it can be stated that, for motor performance impact purposes, the VUF associated with U_p (or U_n) or alternatively the U_n associated with U_p , should be used simultaneously to define unequivocally the VU condition, since the angles α_u and α_i are not of

major importance for motor efficiency evaluation purposes [11], [13]. However, angles α_u and α_i are important to compute motor power factor and to extract the per-phase voltages and currents (which is important to evaluate the losses and temperature asymmetries).

In the subsequent analysis, VUF and IUF factors are used, both defined in their complex form by (A4.13) and (A4.14), since they reflect the true impact of VU on motor.

There are several ways to develop a motor derating curve as function of VU. One of them, which is based on many tests of a variety of motors, for balanced voltages, suggests that (A4.22) can be applied, where $\Delta\theta_{wdg}$ is the increase in winding temperature rise and DER is the motor derating (allowed motor shaft output power as a percentage of the rated power) [12]. Moreover, information developed by NEMA and various researchers, indicates that, when voltages are unbalanced, the percent increase in temperature rise equals about twice the squared percent VU [12]. This can be defined by (A4.23). In Fig. A4.9, equation (A4.23) is represented graphically.

$$DER = (1 + \Delta\theta_{wdg})^{-0.5882} \quad (A4.22)$$

$$DER = (1 + 200 \cdot LVUF^2)^{-0.5882} \quad (A4.23)$$

In [26], it is suggested that the main difference between the normal starting torque motors (IEC design N, equivalent to NEMA designs A/B) and the high starting torque (IEC design H, equivalent to NEMA design C/D) is in the X_m , $X_r(f_r)$, and $R_r(f_r)$, as in Table A4.4, reinforcing the idea that the motor impedance unbalance in the presence of VU depends on the rated power and rotor type. High starting torque motors are more susceptible to the unbalance effects due to the higher backward torques produced by negative-sequence components.

TABLE A4.4
SUMMARY OF LOW-VOLTAGE INDUCTION MOTOR PER-PHASE EQUIVALENT CIRCUIT AVERAGE DATA [26].

HP	Poles	Type	R_s	X_s	X_m	Positive Sequence		Negative Sequence	
						X_r^+	R_r^+	X_r^-	R_r^-
≤ 200	2, 4	NT	0.0256	0.0898	3.3948	0.1580	0.0121	0.0984	0.0536
201-500	2, 4, 6	NT	0.0180	0.0939	3.8030	0.1399	0.0117	0.0942	0.0571
≤ 200	4	HT	0.0256	0.0898	2.8000	0.1580	0.0121	0.0984	0.0800
201-500	4, 6	HT	0.0180	0.0939	3.0000	0.1399	0.0117	0.0942	0.0800

All data in per-unit, in relation to the motor input kVA base.

NT – Normal starting torque.

HT – High starting torque.

The application of unbalanced voltage conditions can be mathematically expressed by adding a negative-sequence excitation component, which produces a backward torque that attempts to turn the rotor in opposite rotational direction. In practice, relatively small voltage unbalances lead to significant current unbalances and can generate very substantial additional heat in the motor [26].

IMs can be represented by a positive- and by a negative-sequence per-phase equivalent circuit [26], [41]. In the presence of a negative-sequence component, the required forward torque has to be developed by means of a slip increase, causing motor to draw a higher stator current. Higher stator currents lead to greater voltage drops in the cables and transformer impedances. The reduced motor terminal voltages reduce the forward torque, imposing again an additional slip to the motor. The high frequency (approx. twice the line frequency) in the rotor causes the current to concentrate on the top of the rotor conductors, thus increasing the effective rotor resistance and decreasing the effective rotor leakage reactance. The increase of the rotor effective resistance leads to a significant increase in rotor losses for a given value of rotor current [26]. Due to the roughly doubling of the corresponding motor slip, the negative-sequence impedance is much lower than the positive-sequence impedance (see Fig. A4.13). Therefore, IMs operating at higher fundamental frequencies suffer more with voltage unbalance.

The varied ratios of negative-sequence voltages to currents indicate that the negative-sequence impedance is not a constant, decreasing with the increase of the negative-sequence current. This is mainly caused by saturation effects at the tips of the rotor teeth, leading to a rotor leakage inductance decrease [6]. In [6], the experimental results clearly show that the no-load negative-sequence current can be 3 times lower than the negative-sequence current at full-load. Therefore, the no-load losses do not cover most of the negative-sequence losses that actually occur when the motor is loaded.

Moreover, since the power supply has impedance, the motor terminal voltage change as load varies. Under unbalanced voltage supply, when the load goes up and further upsets the VU, the negative-sequence voltage increases.

These aspects should be taken into account during VU impact experimental analysis.

For the simulations carried out, load independent *VUFs* of 0%, 1.5%, 3%, 4.5%, 6%, 7.5% and 9%, $\alpha_u = 0^\circ$, and U_p equal to the rated line-to-line voltage (U_R), are considered. Doing so, it is possible to isolate the unbalance effect from the voltage magnitude deviation effect (see next section). Some of the results are presented in Fig. A4.9. The angle α_u is necessary for per-phase unbalanced phase current estimation, used for the asymmetry correction factor calculation. Therefore, if difference angles were considered, different results can be obtained. The curves are presented as a function of *VUF*. Note that, a compensation of the unbalanced temperature distribution is considered, based on the per-phase current estimation. In fact, when an unbalanced voltage is applied to an IM, the effect is equivalent to the superposition (assuming linearity) of the negative-sequence voltage on the positive-sequence voltage as explained in Appendix 2 and [11]. This principle is enough to simulate the torque-speed and efficiency of the motor, considering the average temperature and losses. However, at full-load operation, the temperature rise in the stator

windings could differ by as much as 10°C due to the non-uniformity of the three phase currents, being necessary to include this asymmetry in the stator windings losses and temperature [11], [26]. Therefore, in order to take into account the resulting current and temperature asymmetry when performing per-phase equivalent circuit-base analysis, an asymmetry correction factor, K_{asy} , defined as a function of the square of the maximum phase current deviation to the phase currents average, according to (A4.24), is considered to estimate the derating curves either based on temperature or on losses, which adjusts the simulated average losses and temperature, resulting in more realistic derating curves (identified as “adapted” in the presented figures). The final stator winding losses and average temperature for derating purposes are corrected as a function of the estimated maximum per-phase stator winding losses using (A4.25), where P_{wdg_loss} is the stator winding power loss.

$$K_{asy} = \left(1 + I_{avg}^{-1} \cdot \max\{I_A - I_{avg}, I_B - I_{avg}, I_C - I_{avg}\}\right)^2 \quad I_{avg} = \frac{1}{3}(I_A + I_B + I_C) \quad (\text{A4.24})$$

$$P_{wdg_loss(asy)} = P_{wdg_loss} \cdot K_{asy} \quad \theta_{wdg(asy)} = \theta_{wdg(avg)} \cdot (P_{wdg_loss(asy)} - P_{wdg_loss(avg)} + P_{loss(avg)}) \cdot P_{loss(avg)}^{-1} \quad (\text{A4.25})$$

It is clear that this is only an approximation and errors can result, particularly due to the fact that a thermal lumped model is being considered for the three-phase system, and no thermal interaction between phases is included [41]. In Fig. A4.10, the difference between the simulated losses and stator winding temperature with and without considering the asymmetry correction factor can be seen for a 3-kW, 4-pole motor. In the graph showing the adapted maximum per-phase winding temperature (distributed temperature), some experimental values¹¹ are also shown, validating (A4.25), which, for the analysed case, led to an error less than 3°C. In Figs. A4.12-A4.14 and A4.63 additional experimental results are presented, evidencing the impact of VU on IMs performance. In [26], simulations were carried out on VU based on the steady-state motor per-phase equivalent circuit, but although the variations on rotor effective resistance and leakage inductance were partially considered, the thermal compensation of the parameters was not implemented. This aspect is important because it will increase even more the rotor resistance in the presence of unbalance, leading to lower negative-sequence currents, and therefore, to a slightly lower steady-state rotor temperature. Additionally, in [26], only one type of unbalance was considered (one phase voltage decrease). For the sake of simplicity, the system impedance effect was not considered in the presented study. It was found that, when defined as a function of the

¹¹ During the experimental tests, an autotransformer was used to regulate the U_p and an automatic voltage regulator (AVR) was used to unbalance the voltage and, therefore, to regulate the U_n value. The voltage unbalance was achieved by lowering the line-to-ground voltage of one of the phases. After reaching the thermal equilibrium (assessed using an infrared thermometer in the motor frame), the winding distributed temperature was measured by means of the per-phase winding resistance, and the highest temperature value among the three-phases was selected.

VUF, “adapted” temperature-based derating curves (TBD curves) are slightly more pronounced than “adapted” losses-based derating curves (LBD curves), contrarily to the results obtained for the *HVF*. Therefore, it can be concluded that they can be used, since the derating results only slightly underestimated. Moreover, NEMA derating curve as a function of *LVUR* ($\approx VUF$ for low *LVUR* levels) seems to be properly defined for medium/large motors, matching fairly with the “adapted” TBD curves, but for small motors it results in an overderating. However, if “average” TBD or LBD curves (which practically match) are used, a significant under-derating is obtained. The motor with “rotor II” has the most pronounced derating curve and motor with “rotor VI” has the least pronounced derating curve, as expected. Therefore, on the basis of the presented results, IMs incorporating copper-cage rotors can be more affected by *VUF*.

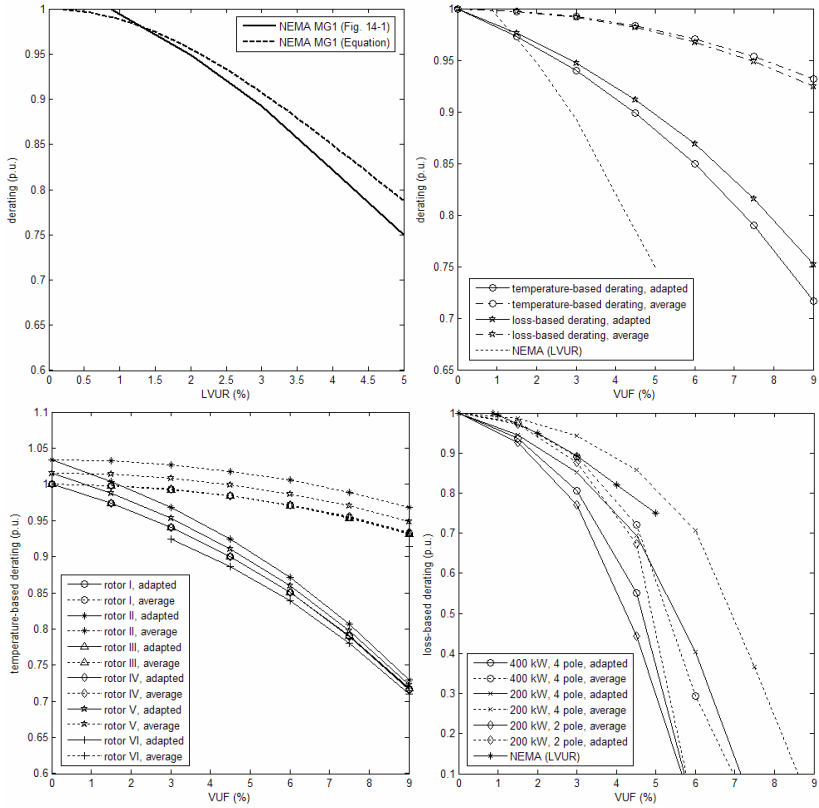


Fig. A4.9. (top left) NEMA MG1 motor steady-state derating curves as a function of *LVUR*, defined by means of a figure (solid line) or an equation (dashed line); (top right); 3-kW IM simulated derating curves as a function of *VUF*; (bottom left) 3-kW IM simulated derating curves as a function of *VUF*, considering different rotor-bar types; (bottom right) 400-kW, and 200-kW IMs simulated derating curves as a function of *VUF* [48].

The influence of the angle between the positive- and negative-sequence components is evidenced in the Fig. A4.11, for fixed $VUF = 3\%$ and $U_p = 400$ V. In terms of derating, the angle impact is not significant, being the considered angle $\alpha_u = 0^\circ$ one of the most severe of the analysed angles (the intermediate angles were not evaluated), except for loads lower than approximately 10%. It can be concluded that the angle is not important for the derating but, if possible, should be included on the unbalance specification to increase the derating accuracy. Furthermore, it is possible to conclude that there is a variation between 0° and 120° , but for angles higher than 120° the patterns will be identical in terms of unbalance.

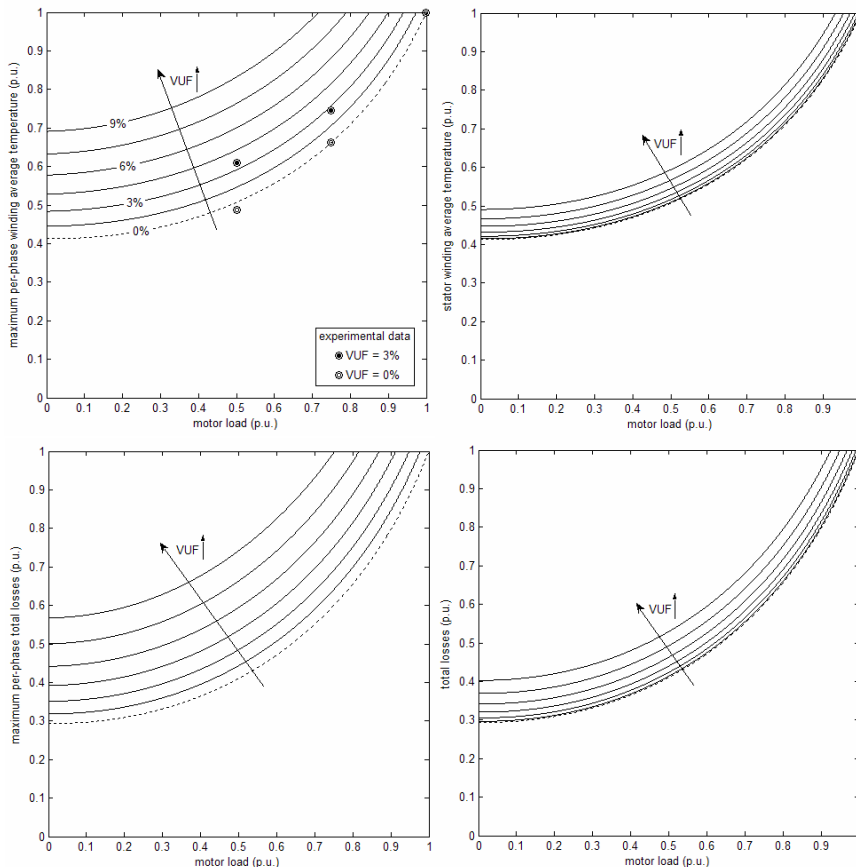


Fig. A4.10. Simulated total losses and stator winding temperatures curves, as a function of motor load for different values of VUF (increased 1.5% steps), considering the angle $\alpha_u = 0^\circ$, with and without asymmetry compensation factor, for a 3-kW, 4-pole motor.

According to [11], under the same VUF percent, the lower positive-sequence voltage, the higher the IM power factor, which is an expected result. The power factor of an IM fed by unbalanced voltages may be greater than that in the balanced case due to the extra losses, especially in the under-voltage cases in which the magnetizing current is lower.

It is worth mentioning that customers usually use capacitors to improve the power factor. The appearance of VU may result in over compensation of power factor and cause an over-voltage problem. In addition, unbalanced voltages will lead to a change in the load characteristics of IMs, and the real and reactive power consumption will differ from the balanced case. Since the major loads in a power system are typically IMs, which consume most of the electrical energy, these changes will deteriorate the voltage stability margin.

From the above analysis, it can be seen that using only the percentage of VUF to judge the severity of VU is not enough being recommended the combined specification of VUF , U_p , and α_u , for an effective system evaluation.

Regarding current unbalance, after performing a number of simulations whose results are presented in Table A4.5, A4.6, and A4.7, it was found that, in general, the higher the motor power, the higher the resulting current unbalance, and, therefore, the thermal asymmetry.

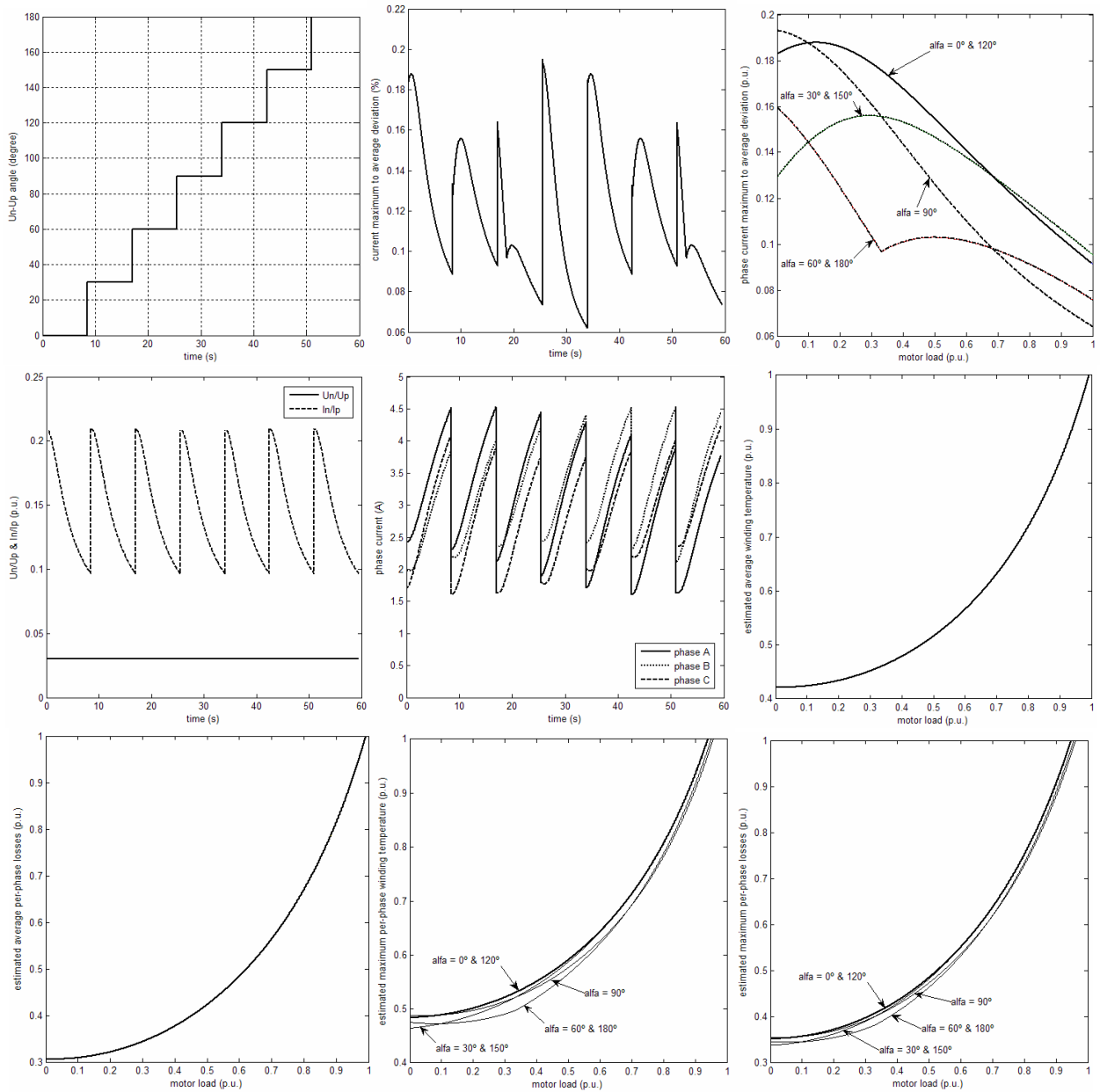


Fig. A4.11. Simulated influence of angle α between the positive- and negative-sequence voltage components on maximum current to average current ratio, negative-sequence current to positive-sequence ratio, phase current, phase current unbalance (maximum deviation from average to average ratio), maximum and average winding temperatures, and maximum and average per-phase losses, for a 3-kW, 4-pole IM, considering fixed $VUF = 3\%$ and $U_p = 400$ V.

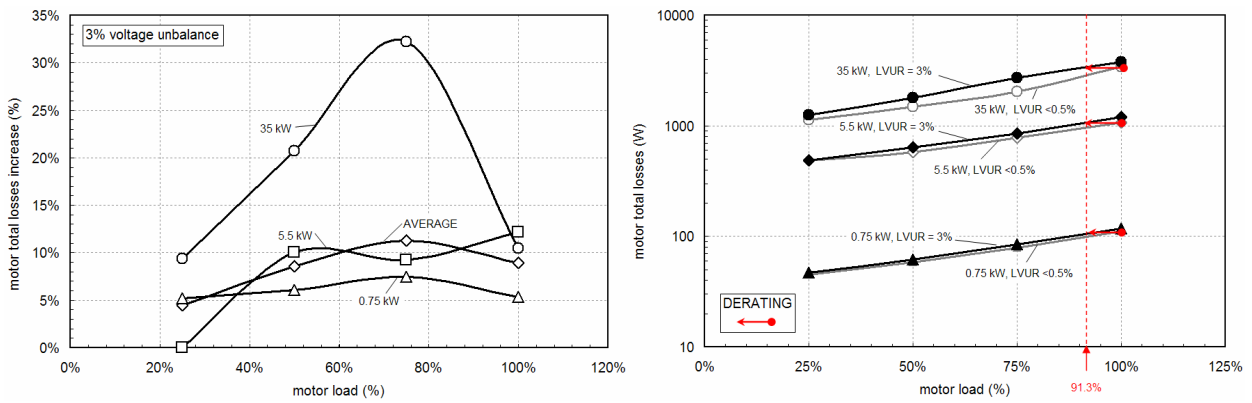


Fig. A4.12. Experimental motor total losses increase under unbalanced supply ($LVUR = 5\%$) in relation to the balanced supply situation ($LVUR < 0.5\%$), for 3 different 4-pole IMs.

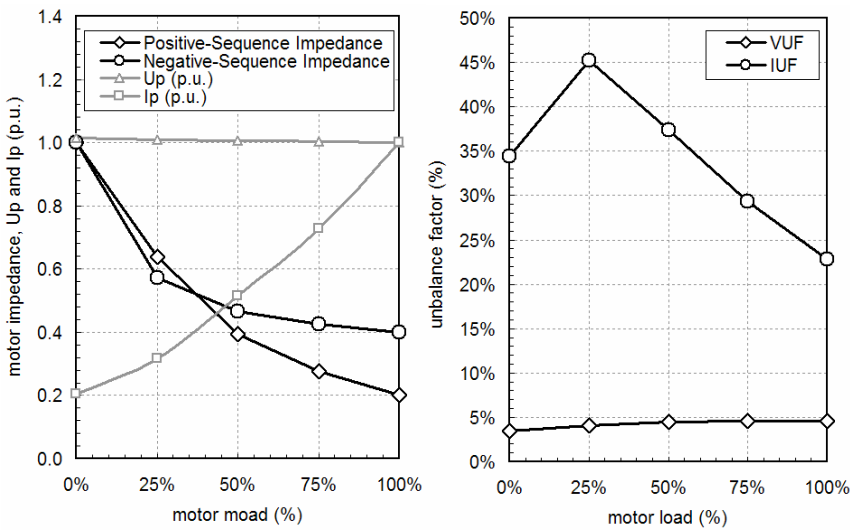


Fig. A4.13. Experimental motor impedance, U_p , I_p , VUF , and IUF , for a 50-hp IM [55].

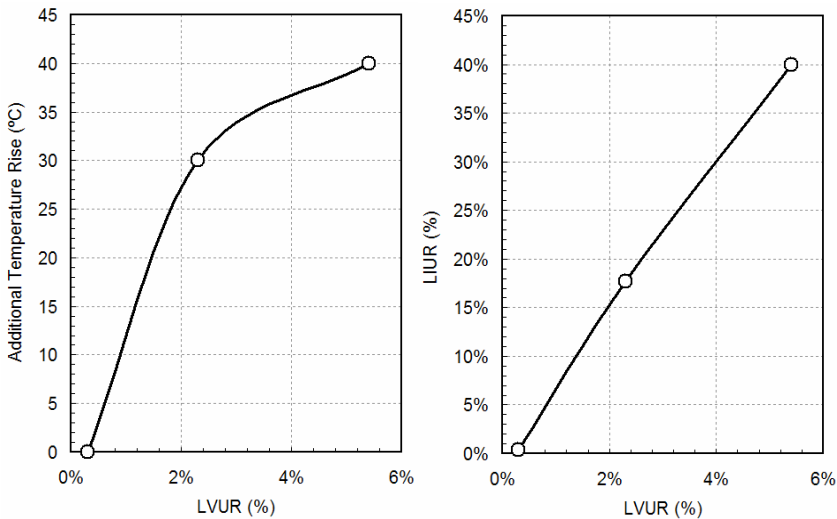


Fig. A4.14. Experimental additional temperature rise and the $LIUR$ - $LVUR$ relation, for a 5-hp, 1725-r/min, 230-V, 60-Hz IM [21].

Moreover, the higher the motor load, the lower the resulting currents unbalance. Additionally, it was found that the higher the rotor resistance, the higher the resulting current unbalance.

VSD-fed IMs can also suffer a derating associated with VU at the VSD input¹², being these issues following addressed.

In order to evaluate the propagation of the unbalanced condition through VSDs, several simulations were made considering a 4-kW, 4-pole motor driving a fan-type load and fed by a VSD integrating a two-level inverter, a DC bus, a three-phase 6-pulse diode rectifier, fed by a 400-V, 50-Hz power supply. In the simulations different capacitance in the DC bus, C_{DC-bus} , and two different output fundamental frequencies ($f_{1(mtr)} = 40$ Hz and $f_{1(mtr)} = 50$ Hz) associated with two different amplitude modulation indexes ($m_a = 0.95$ and $m_a = 1.8$), were considered. The motor and inverter simulation models are described in Appendix 2. The power supply voltages applied during the simulation are shown in Table A4.8 and Fig. A4.15. The main results are presented in Figs. A4.16-A4.57, but extra results (motor torque and common-mode voltage) are also provided in Appendix 6.

TABLE A4.5
CURRENT UNBALANCE FOR FIXED VOLTAGE UNBALANCE AND DIFFERENT MOTOR SIZES.

P_N (kW)	T_N (N.m)	ω_N (r/min)	PVUR (%)	LIUR (%)	ω_{avg} (r/min)
7.5	49.7	1438	6.897	10.17	1433
37	235	1480	6.897	13.15	1479
75	478	1484	6.897	13.33	1482
160	1024	1487	6.897	14.05	1486

Voltages: $U_{BN} = U_{CN} = 231$ V; $U_{AN} = 208$ V (10% decrease); Full-load; Y connection.

TABLE A4.6
CURRENT UNBALANCE FOR FIXED VOLTAGE UNBALANCE AND DIFFERENT MOTOR LOADS.

Motor Load (%)	T_{avg} (N.m)	P_{out} (W)	PVUR (%)	LIUR (%)
25.3	55	9250	6.763	80.01
48.8	115	18500	6.806	37.24
75.0	175	27750	7.500	29.78
100.0	235	36930	7.600	23.81

Voltages: $U_{BN} = U_{CN} = 231$ V; $U_{AN} = 208$ V (10% decrease); 37-kW Motor; Y connection. Highest current in phase B.

TABLE A4.7
CURRENT UNBALANCE FOR FIXED VOLTAGE UNBALANCE AND DIFFERENT ROTOR RESISTANCES.

Rotor Resistance (p.u.)	T_{avg} (N.m)	PVUR (%)	LIUR (%)
0.5	233	6.389	22.84
1.0 (0.0503 Ω)	235	7.600	23.81
1.5	236	7.600	23.07
2.0	239	6.239	22.60
2.5	241	6.680	22.31

Voltages: $U_{BN} = U_{CN} = 231$ V; $U_{AN} = 208$ V; 37-kW Motor; Approximately full-load.

The oscillations in the motor torque are related to the oscillations in the DC-bus voltage and the consequent additional distortion and/or unbalance of VSD output voltages. The distortion is mainly related to the $6 \times f_{1(line)}$ ripple component, under normal balanced operation. Under unbalanced

¹² Assuming that no compensation of output waveforms as a function of the DC-bus voltage variation is made by the VSD.

operation, the DC-bus voltage experiences a $2 \times f_{1(line)}$ ripple component, producing output unbalances and a pulsating torque with a frequency $\omega_{pulsating} = 2\omega_1$. Both $6 \times f_{1(line)}$ (and, in a minor extent, a $12 \times f_{1(line)}$ component) and $2 \times f_{1(line)}$ ripple components can exist at the same time in the DC-bus, as it can be seen in Fig. A4.18, A4.19, A4.25, A4.26, A4.32, A4.33, A4.39, A4.40, A4.46, A4.47, A4.53, and A4.54. The torque pulsation depends on those DC-bus ripple components and on the pulsating effects associated with negative-sequence component $\omega_{pulsating(neg. seq.)} = 2\omega_{1(mtr)}$. Therefore, for $f_{1(mtr)} = f_{1(line)}$ the torque oscillations can be amplified due to the superposition (with the same frequency) of the referred effects. The torque pulsation leads to speed oscillations. Moreover, the increase of the capacitance¹³ in the DC bus can lead to a slight amplification of the common-mode voltages (CMVs) under unbalance conditions.

TABLE A4.8
STAR-CONNECTED SUPPLY PHASE-TO-NEUTRAL VOLTAGES DURING SIMULATION.

Period (s)	Phase A (V, RMS)	Phase B (V, RMS)	Phase C (V, RMS)
0.0-0.2	230.94	230.94	230.94
0.2-0.4	80% of 230.94	230.94	230.94
0.4-0.6	230.94	230.94	230.94
0.6-0.8	1% of 230.94	230.94	230.94
0.8-1.0	230.94	230.94	230.94
1.0-1.2	80% of 230.94	80% of 230.94	230.94
1.2-1.4	230.94	230.94	230.94
1.4-1.6	80% of 230.94	80% of 230.94	80% of 230.94
1.6-1.8	230.94	230.94	230.94

Notes: Fan-type load equation: $T = \text{sign}(\omega) \cdot (0.00115 \cdot \omega^2 + 0.0001)$. Motor: $R_s = 1.405 \Omega$; $L_s = 0.005839 \text{ H}$; $R_r = 1.395 \Omega$; $L_r = 5.839 \text{ mH}$; $L_m = 0.1722 \text{ H}$; $J = 0.0131 \text{ kg.m}^2$; $B = 0.002985 \text{ N.m.s/rad}$; $\omega_N = 1430 \text{ r/min}$; $U_N = 400 \text{ V}$; $f_N = 50 \text{ Hz}$; $P_N = 4 \text{ kW}$; Reference Frame: Stationary. VSD: 6-pulse diode rectifier; 2-level VSI; $f_s = 2 \text{ kHz}$.

Regarding VU propagation through VSDs, for the cases studied, the positive-sequence voltage decrease is slightly attenuated, but the negative-sequence voltage component is reduced to roughly to half. Therefore, VSDs have the advantage of attenuating the VU effects on IMs. Looking at CMVs, it is possible to observe that in the presence of a relatively high VU, the 50-Hz fundamental zero-sequence component becomes dominant in relation to the 150-Hz zero-sequence harmonic. As expected, the attenuation of the VU propagation through VSDs is more effective if the DC-bus capacitance is increased, as it can be concluded by comparing Figs. A4.21, A4.28, A4.35, A4.42, A4.49, and A4.56.

It can be concluded that increasing DC-bus capacitance, the short-duration voltage unbalances (voltage sags/dips associated with power network switching or manoeuvres mainly related to protection equipments) VSD ride-through capability is increased significantly, particularly on the

¹³ Since nowadays there are commercially available super-capacitors at moderate prices, in the presented analysis, makes sense to consider DC-bus capacitance values significantly higher than those typically found in conventional VSDs. On that basis, a DC-bus capacitance up to 25 mF was considered in the simulations.

cases of one-phase undervoltage dips. Moreover, since VUF is significantly reduced, the impact on motor performance, including speed loss, is strongly reduced. The consequent asymmetries in the currents drawn by the IM, can lead to extra heating of power switches of the leg providing the highest current value, potentially increasing the possibility of damage.

For $f_{I(mtr)} < f_{I(line)}$, CMVs reach higher values, potentially increasing the shaft-ground voltage and the bearing currents activity.

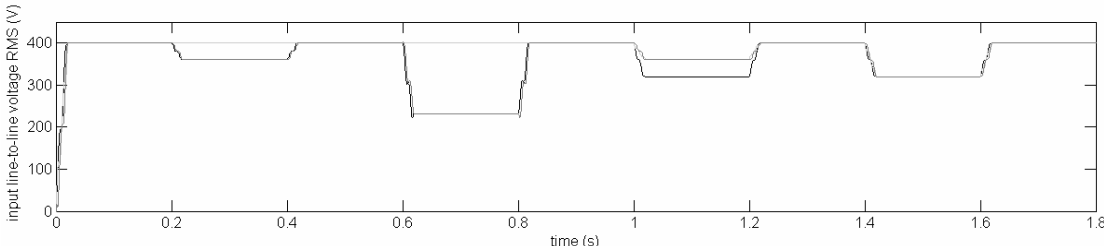


Fig. A4.15. Input line-to-line voltages, in relation to Table A4.4.

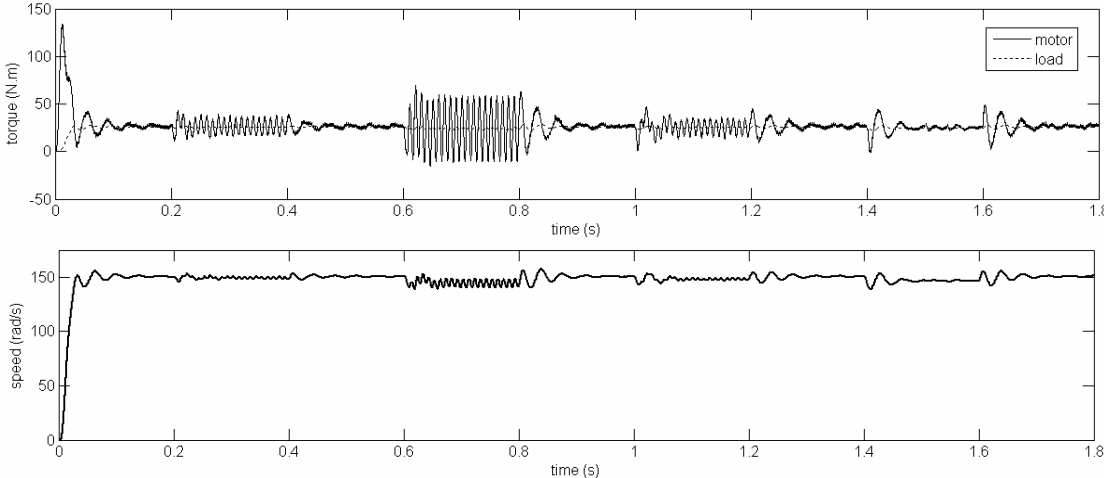


Fig. A4.16. Torque and speed for the motor and load ($C_{DC-bus} = 250 \mu F, f_{I(mtr)} = 50 \text{ Hz}, m_a = 1.8$).

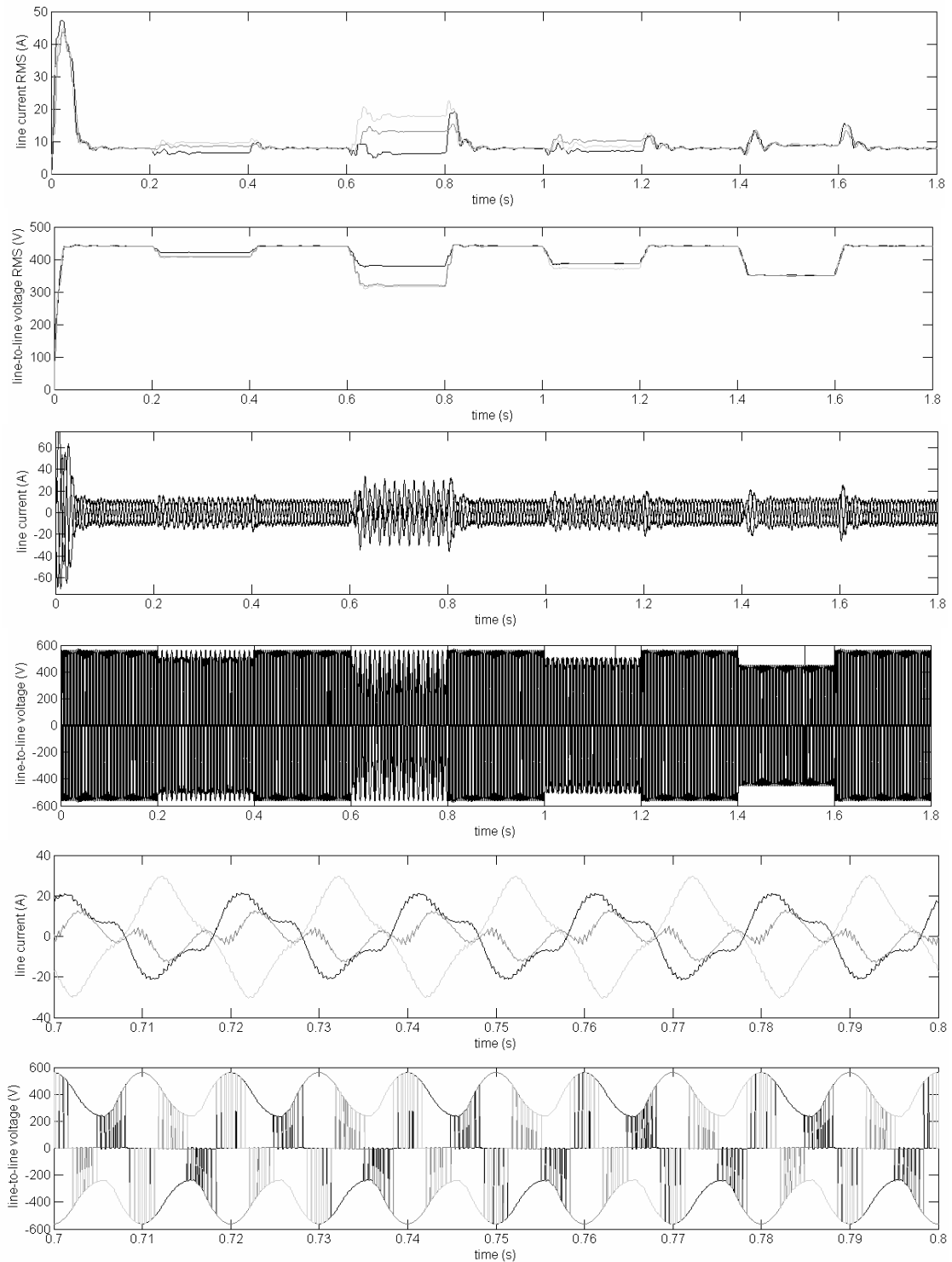


Fig. A4.17. Instantaneous and RMS values of the output phase-to-phase voltages and currents ($C_{DC-bus} = 250 \mu\text{F}$; $f_{1(mr)} = 50 \text{ Hz}$; $m_a = 1.8$).

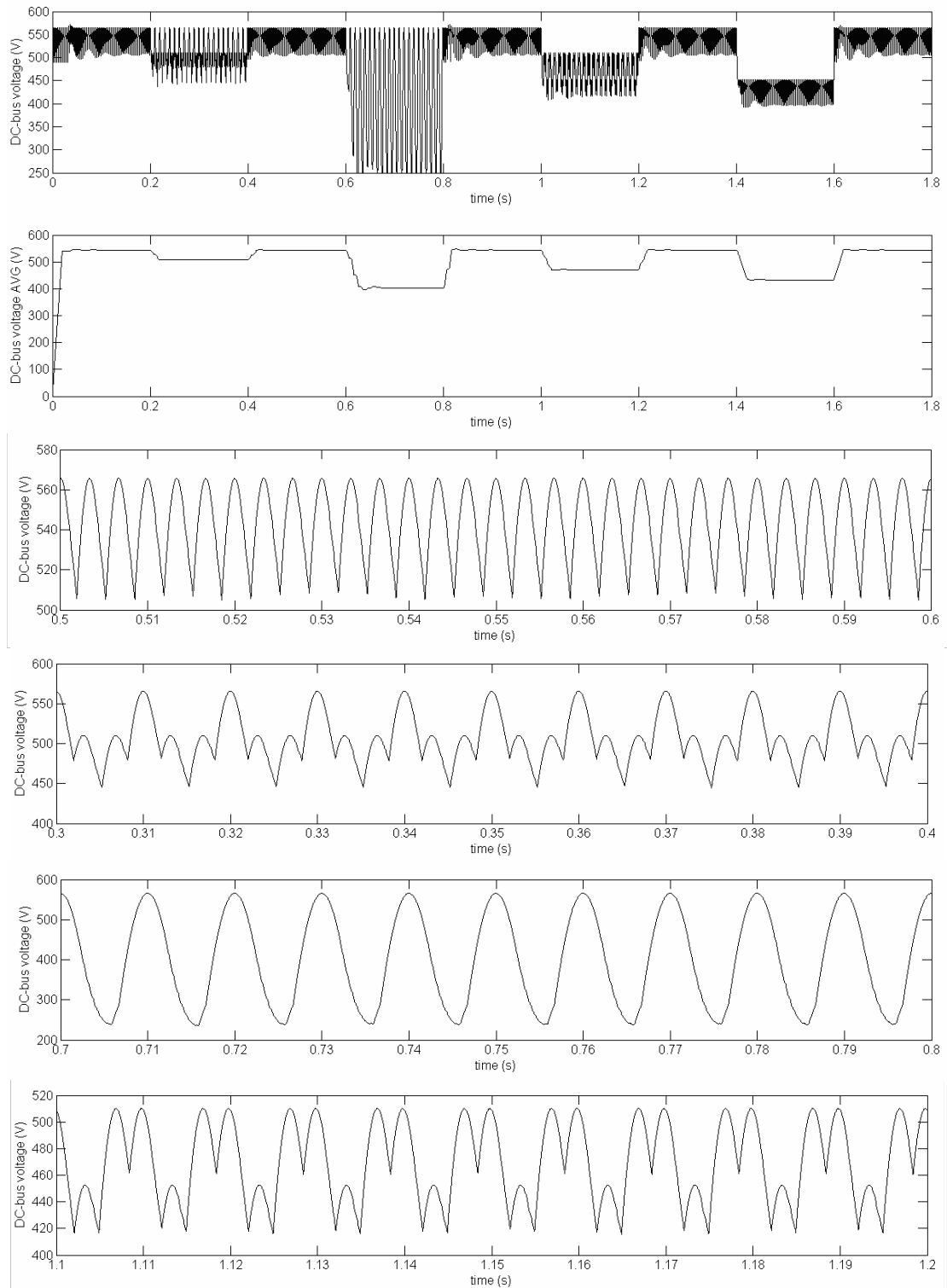


Fig. A4.18. Average value (or DC equivalent value) and instantaneous values of the DC-bus voltage ($C_{DC-bus} = 250 \mu\text{F}$; $f_{I(mtr)} = 50 \text{ Hz}$; $m_a = 1.8$).

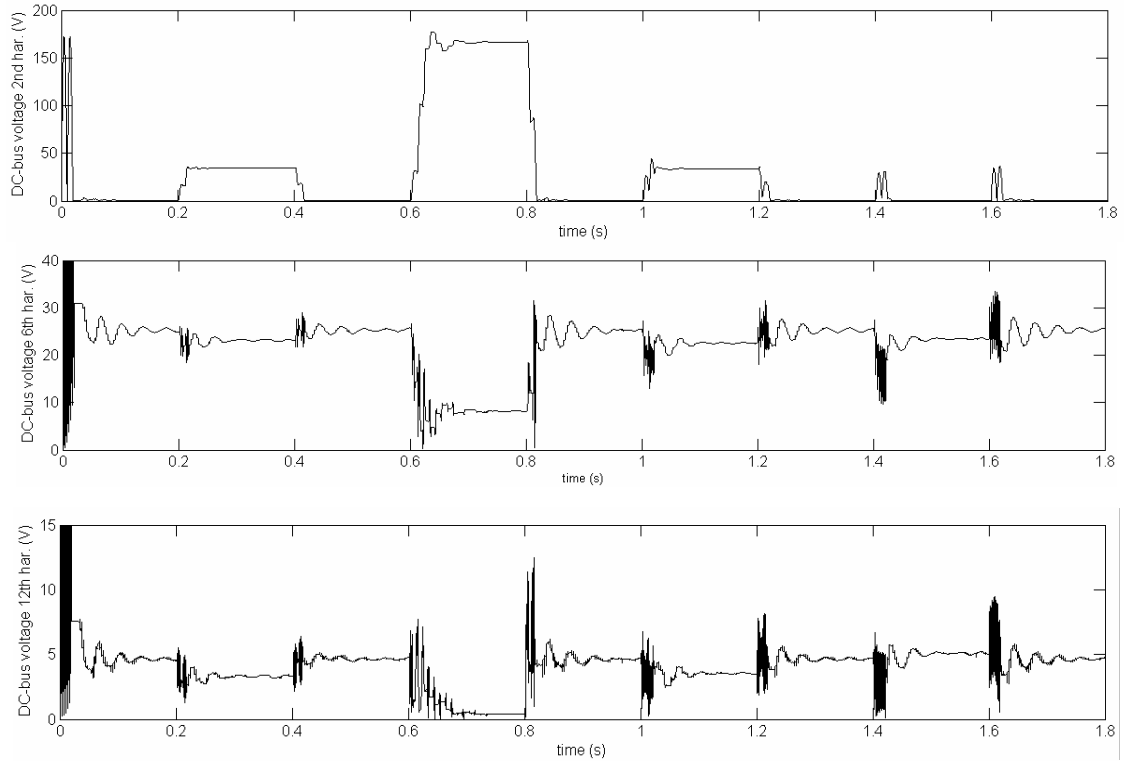


Fig. A4.19. DC-bus voltage 2nd, 6th, and 12th harmonic components (50 Hz base frequency), ($C_{DC-bus} = 250 \mu\text{F}$; $f_{I(mr)} = 50 \text{ Hz}$; $m_a = 1.8$).

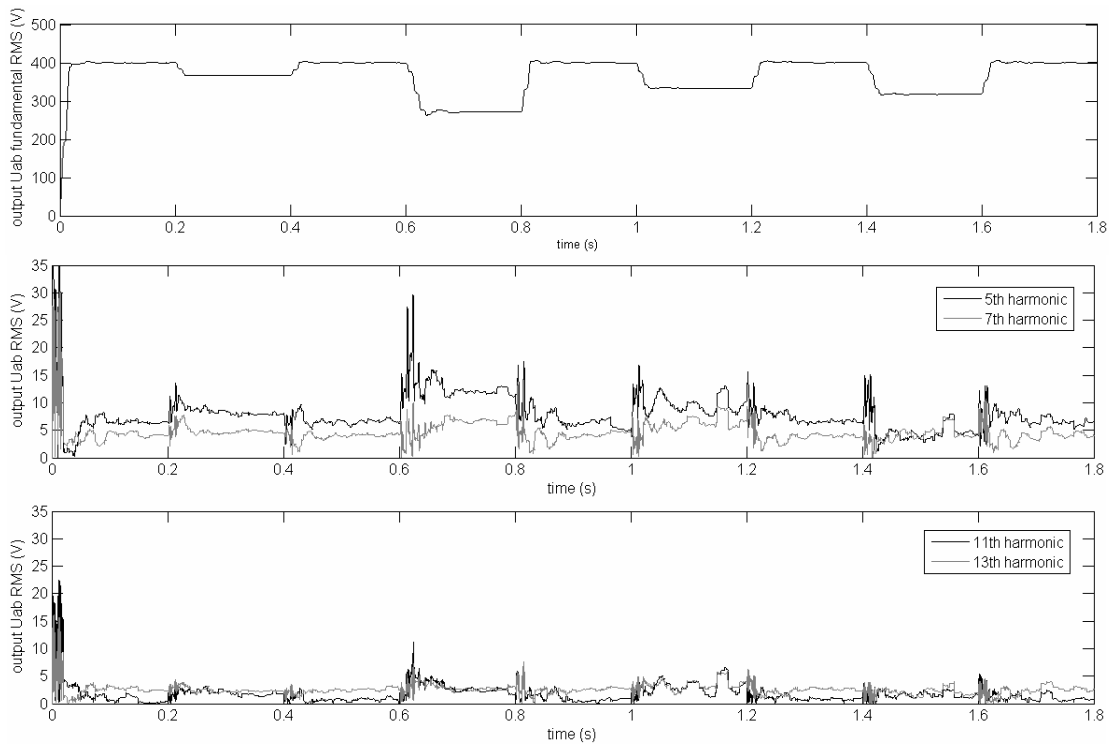


Fig. A4.20. VSD-output line-to-line voltage 2nd, 6th, and 12th harmonic components (50 Hz base frequency), ($C_{DC-bus} = 250 \mu\text{F}$; $f_{I(mr)} = 50 \text{ Hz}$; $m_a = 1.8$).

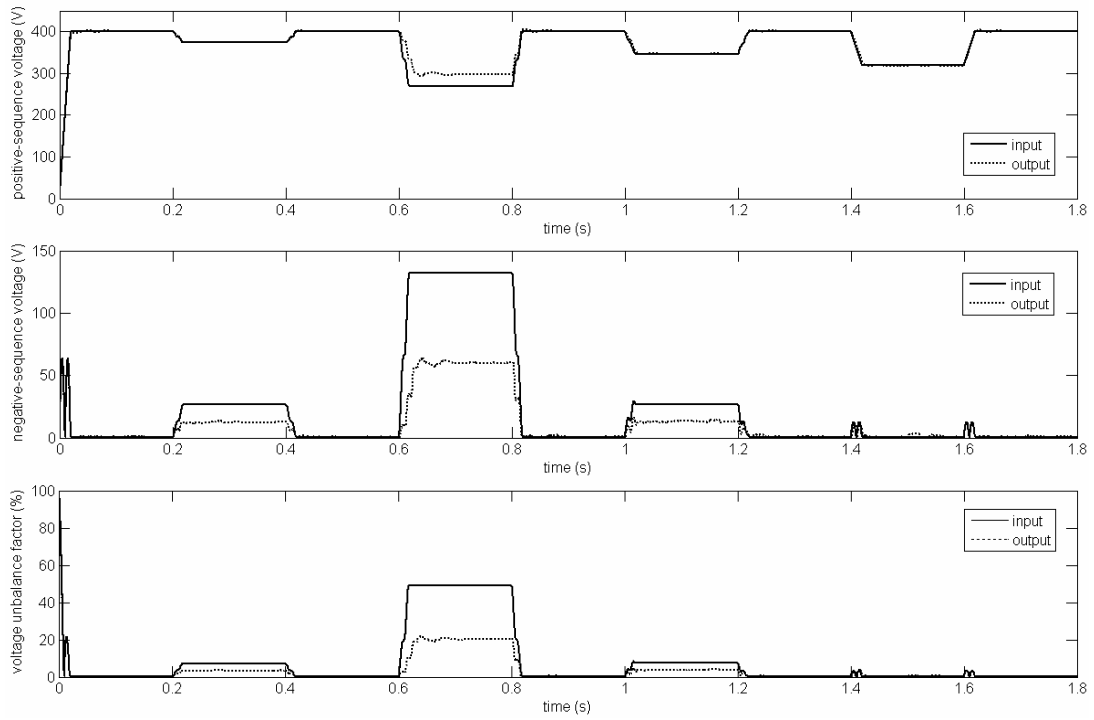


Fig. A4.21. Positive-sequence voltage, negative-sequence voltage, and voltage unbalance factor, ($C_{DC-bus} = 250 \mu\text{F}$; $f_{l(mtr)} = 50 \text{ Hz}$; $m_a = 1.8$).

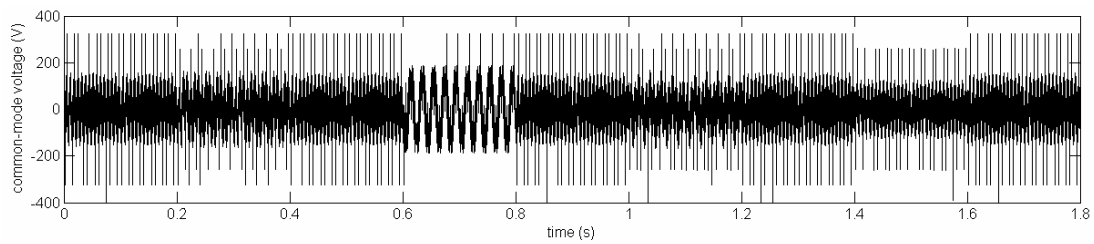


Fig. A4.22. Common-mode voltage (summation of phase-to-ground voltages divided by 3), ($C_{DC-bus} = 250 \mu\text{F}$; $f_{l(mtr)} = 50 \text{ Hz}$; $m_a = 1.8$).

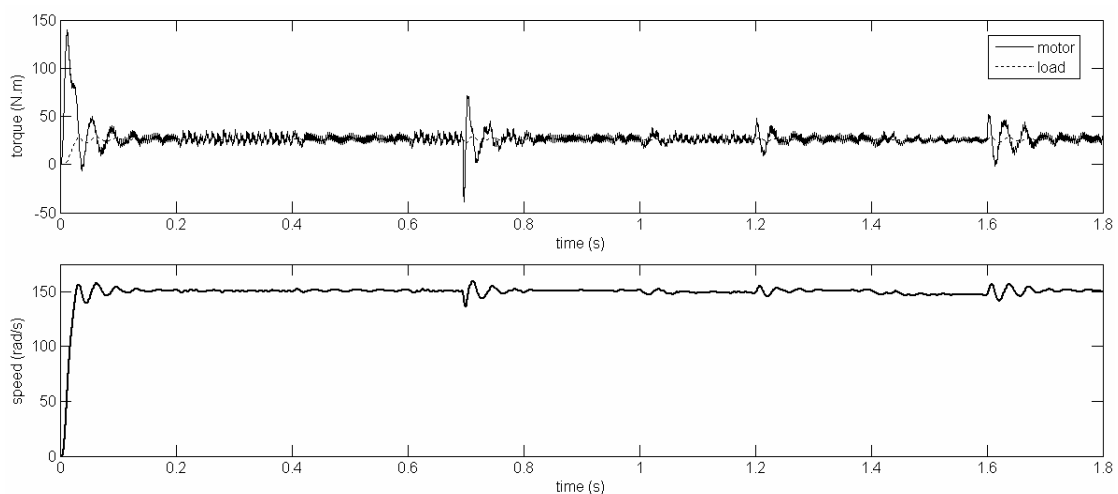


Fig. A4.23. Torque and speed curves for the motor and load ($C_{DC-bus} = 2500 \mu\text{F}$; $f_{l(mtr)} = 50 \text{ Hz}$; $m_a = 1.8$).

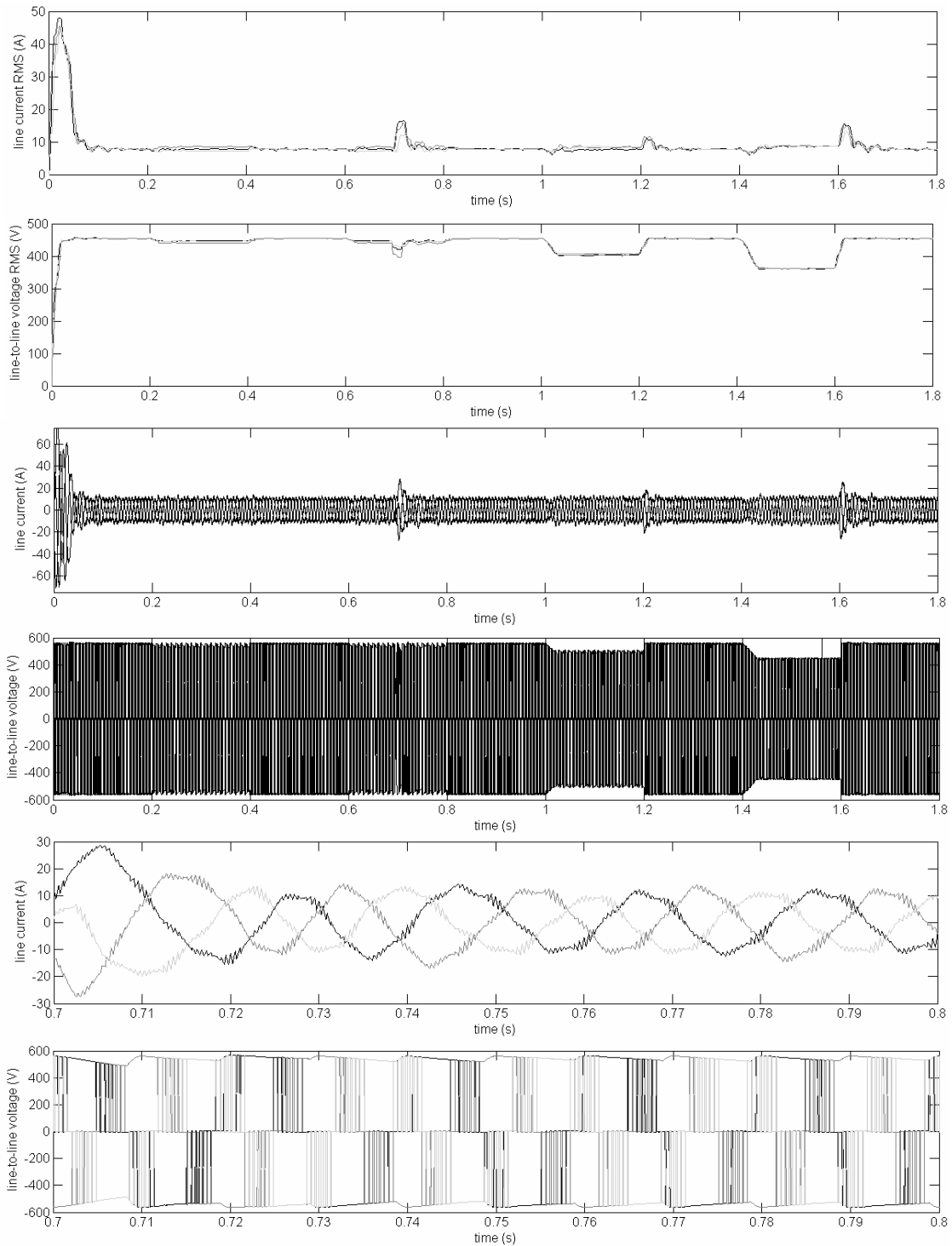


Fig. A4.24. Instantaneous and RMS values of the output phase-to-phase voltages and currents ($C_{DC-bus} = 2500 \mu\text{F}$; $f_1 = 50 \text{ Hz}$; $m_a = 1.8$).

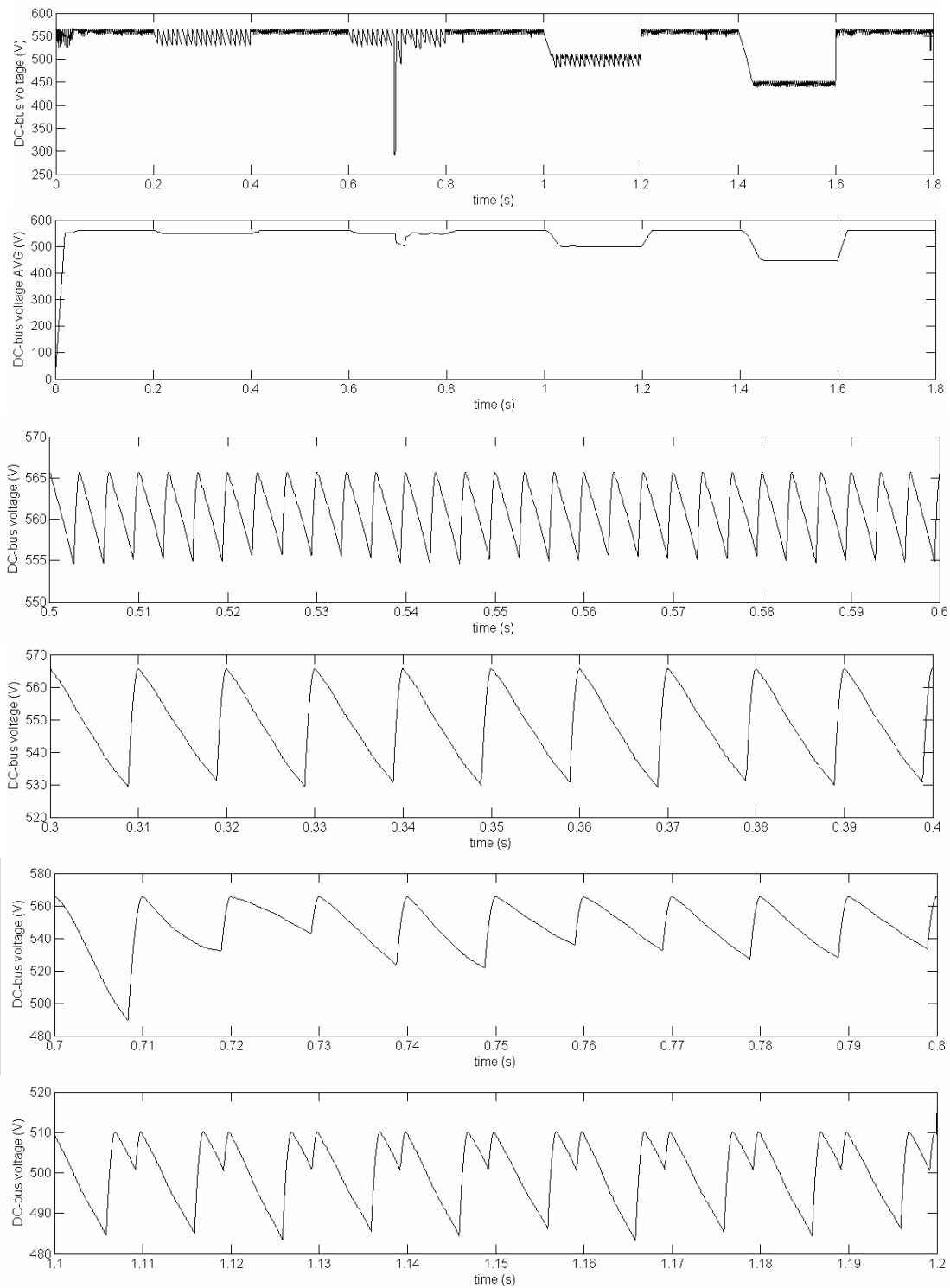


Fig. A4.25. Average value (or DC equivalent value) and instantaneous values of the DC-bus voltage ($C_{DC-bus} = 2500 \mu\text{F}$; $f_l = 50 \text{ Hz}$; $m_a = 1.8$).

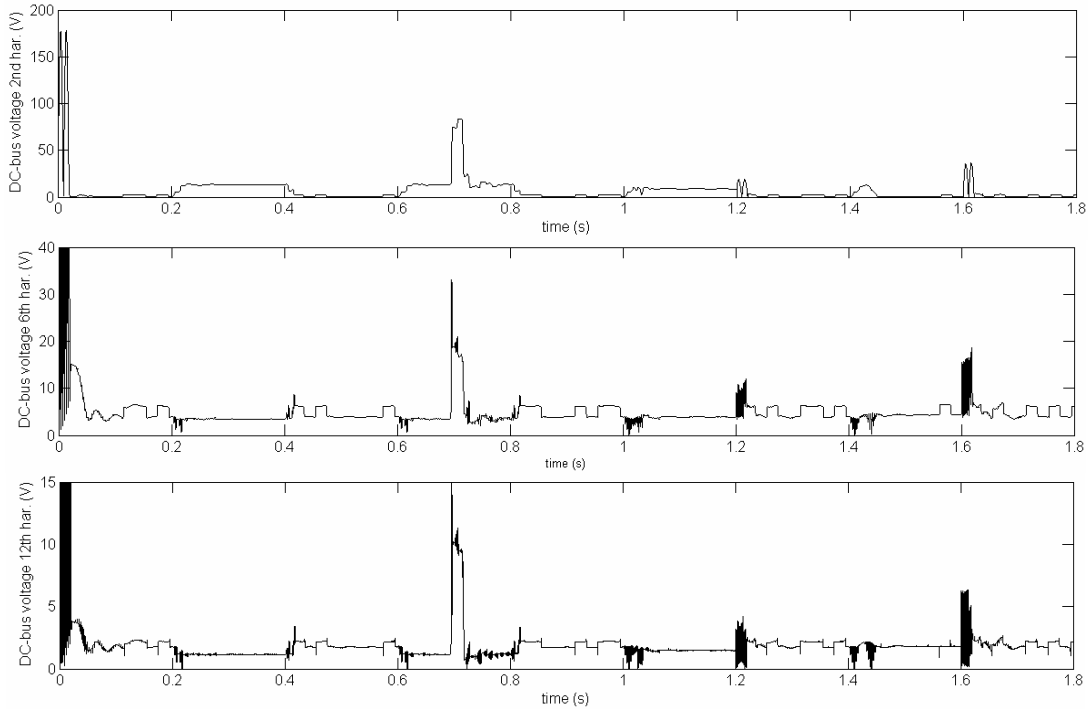


Fig. A4.26. DC-bus voltage 2nd, 6th and 12th harmonic components (50 Hz base frequency), ($C_{DC-bus} = 2500 \mu\text{F}$; $f_l = 50 \text{ Hz}$; $m_a = 1.8$).

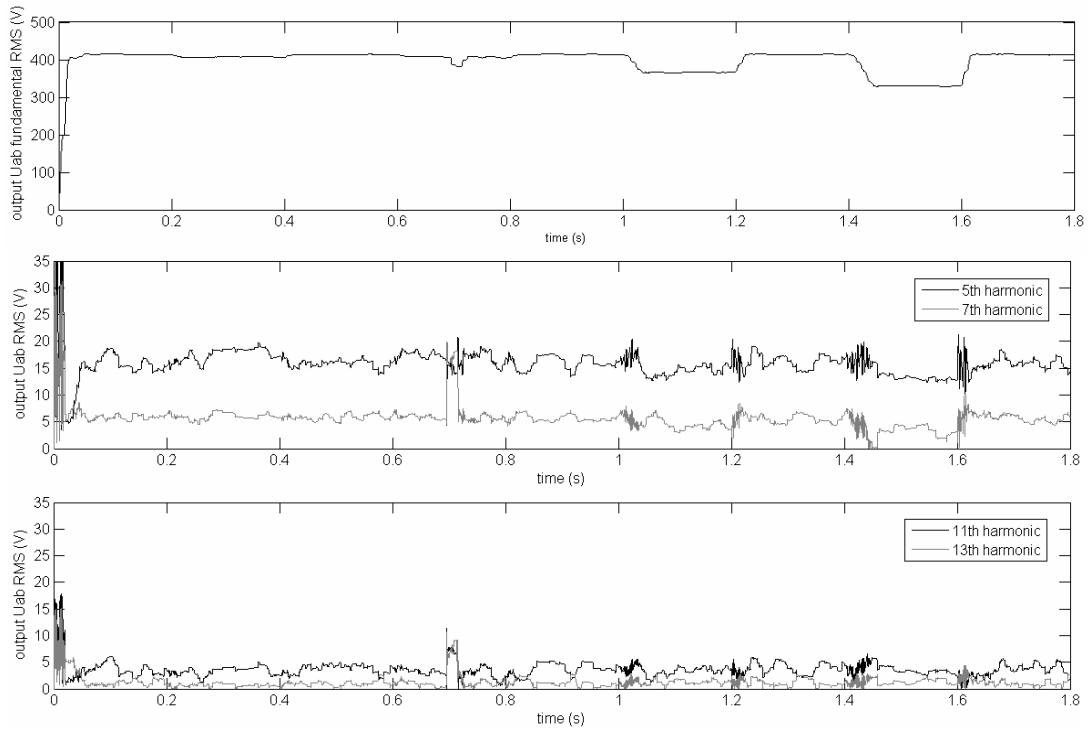


Fig. A4.27. DC-bus voltage 2nd, 6th, and 12th harmonic components (50 Hz base frequency), ($C_{DC-bus} = 2500 \mu\text{F}$; $f_l = 50 \text{ Hz}$; $m_a = 1.8$).

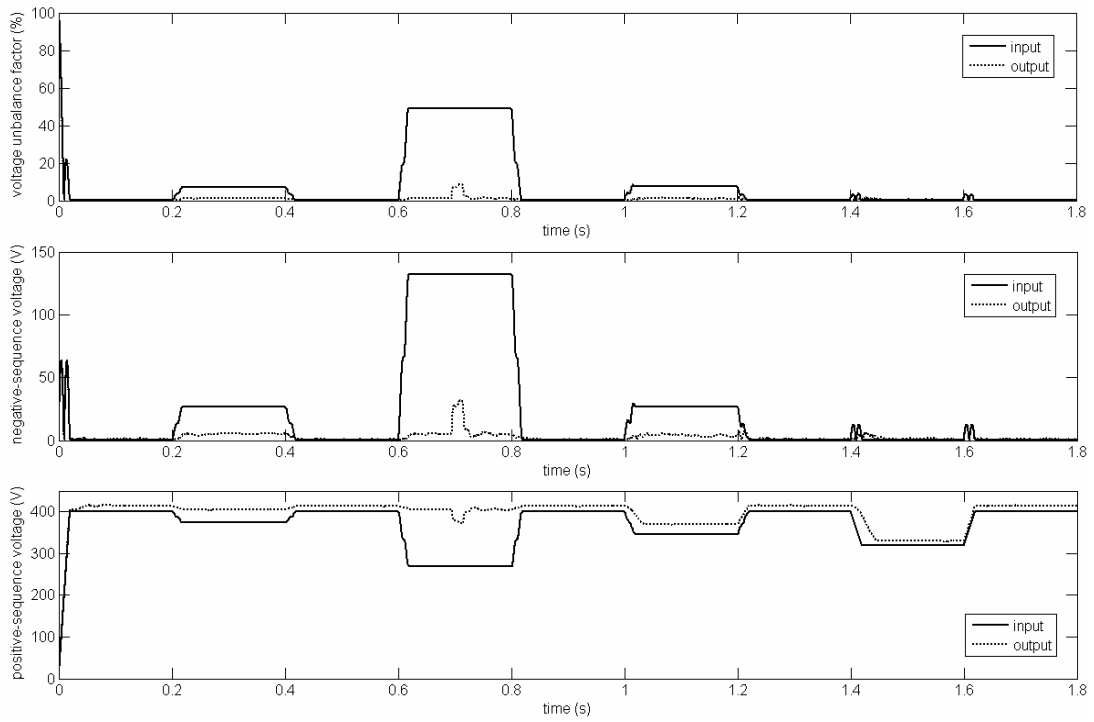


Fig. A4.28. Positive-sequence voltage, negative-sequence voltage, and voltage unbalance factor, ($C_{DC-bus} = 2500 \mu\text{F}$; $f_l = 50 \text{ Hz}$; $m_a = 1.8$).

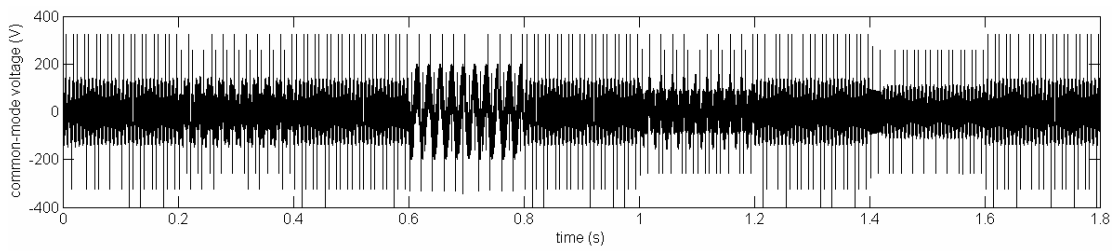


Fig. A4.29. Common-mode voltage (summation of phase-to-ground voltages divided by 3), ($C_{DC-bus} = 2500 \mu\text{F}$; $f_{l(mr)} = 50 \text{ Hz}$; $m_a = 1.8$).

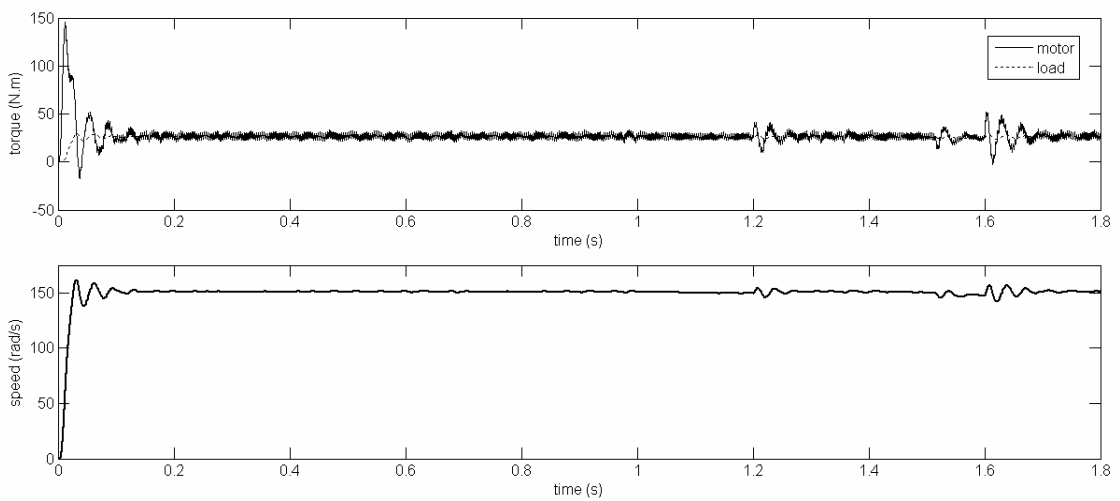


Fig. A4.30. Torque and speed for the motor and load ($C_{DC-bus} = 25000 \mu\text{F}$; $f_l = 50 \text{ Hz}$; $m_a = 1.8$).

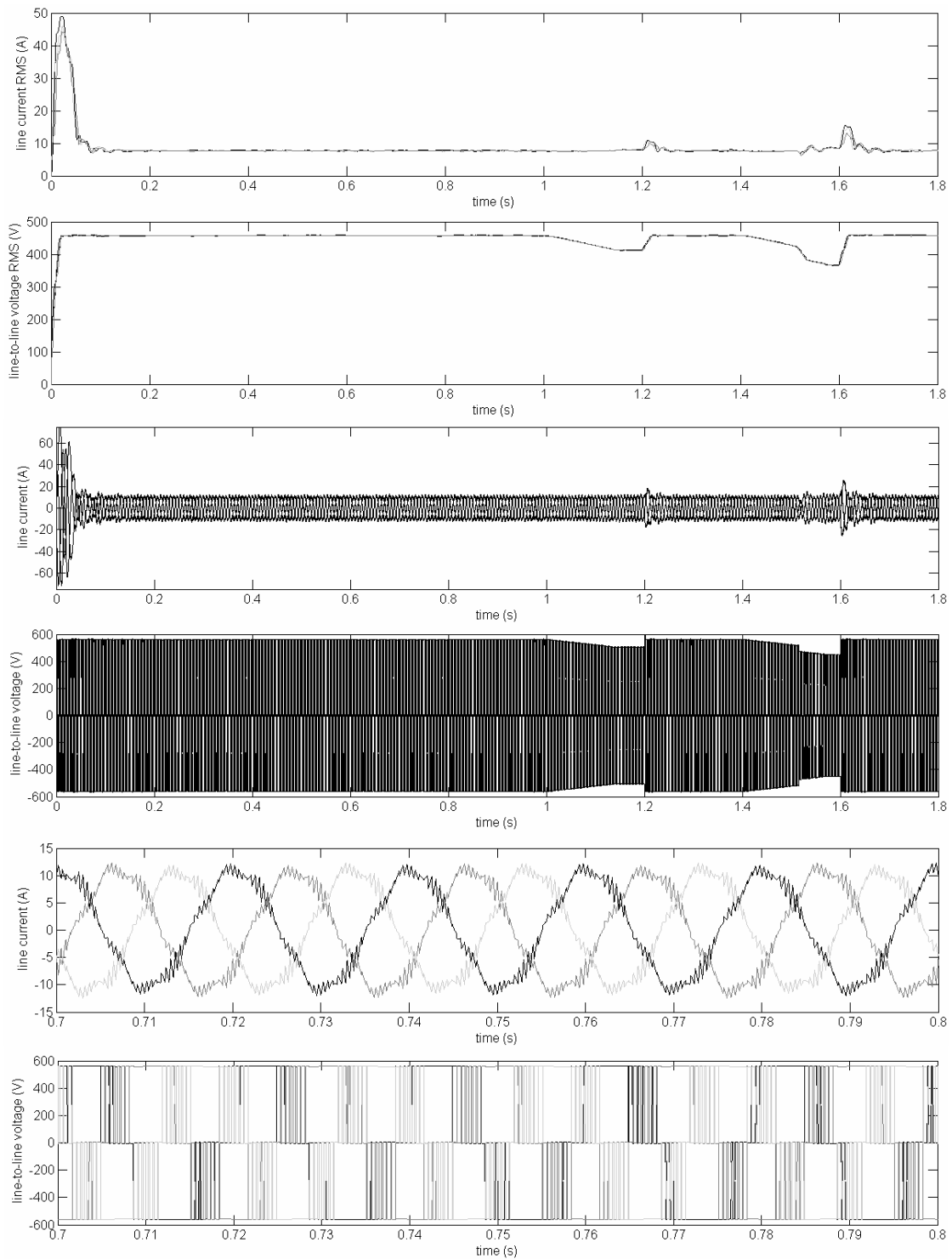


Fig. A4.31. Instantaneous and RMS values of the output phase-to-phase voltages and currents, ($C_{DC-bus} = 25000 \mu\text{F}$; $f_l = 50 \text{ Hz}$; $m_a = 1.8$).

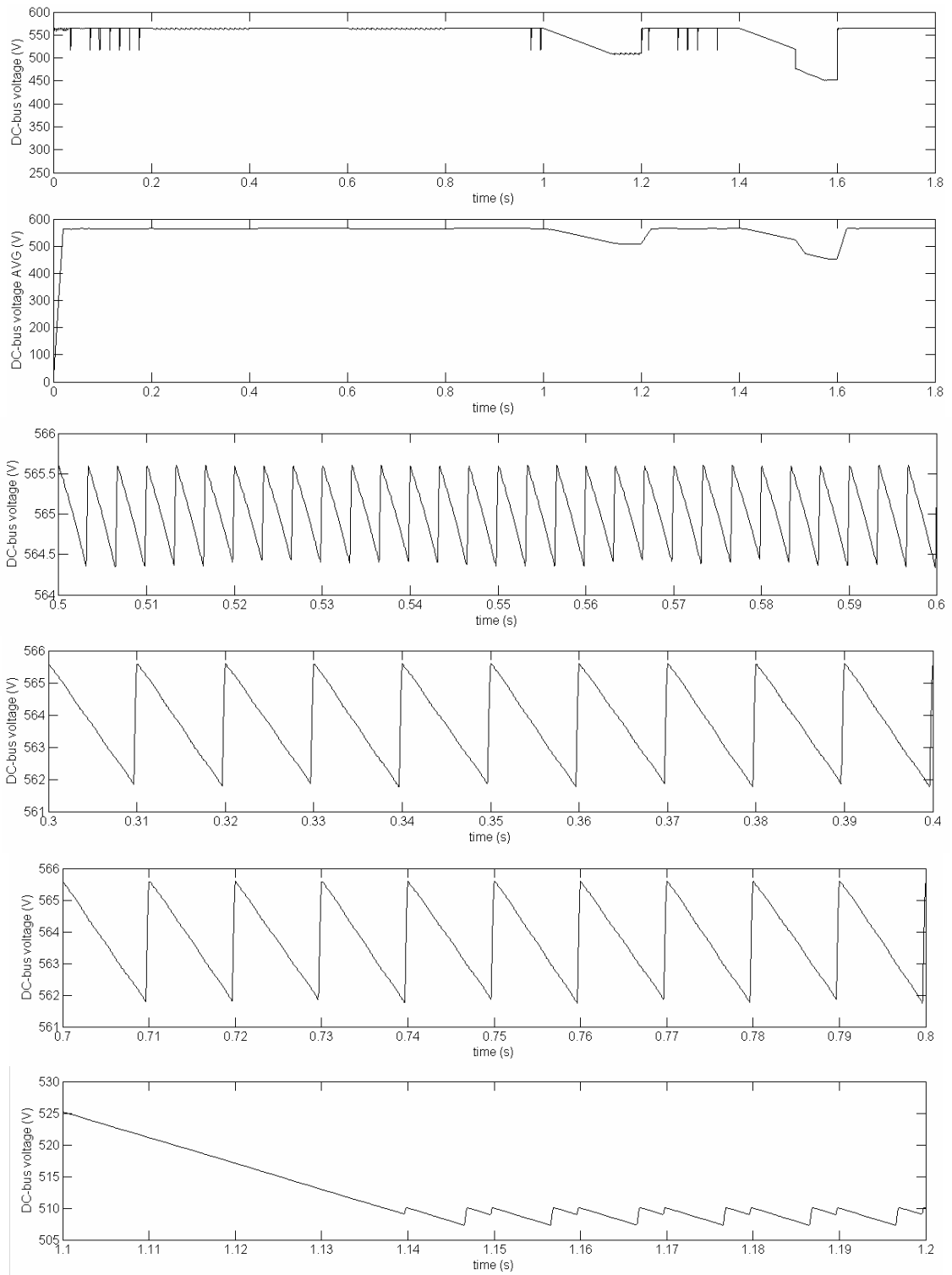


Fig. A4.32. Average value (or DC equivalent value) and instantaneous values of the DC-bus voltage, ($C_{DC-bus} = 25000 \mu\text{F}$; $f_j = 50 \text{ Hz}$; $m_a = 1.8$).

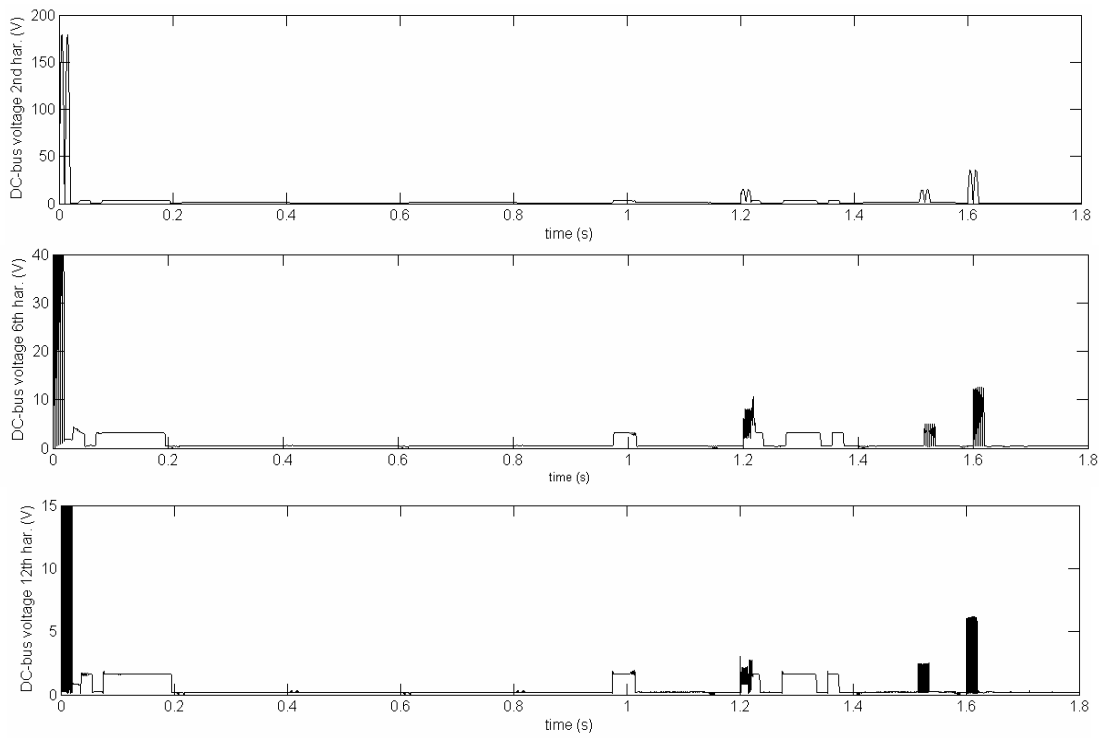


Fig. A4.33. DC-bus voltage 2nd, 6th, and 12th harmonic components (50 Hz base frequency), ($C_{DC-bus} = 25000 \mu\text{F}$; $f_{l(mr)} = 50 \text{ Hz}$; $m_a = 1.8$).

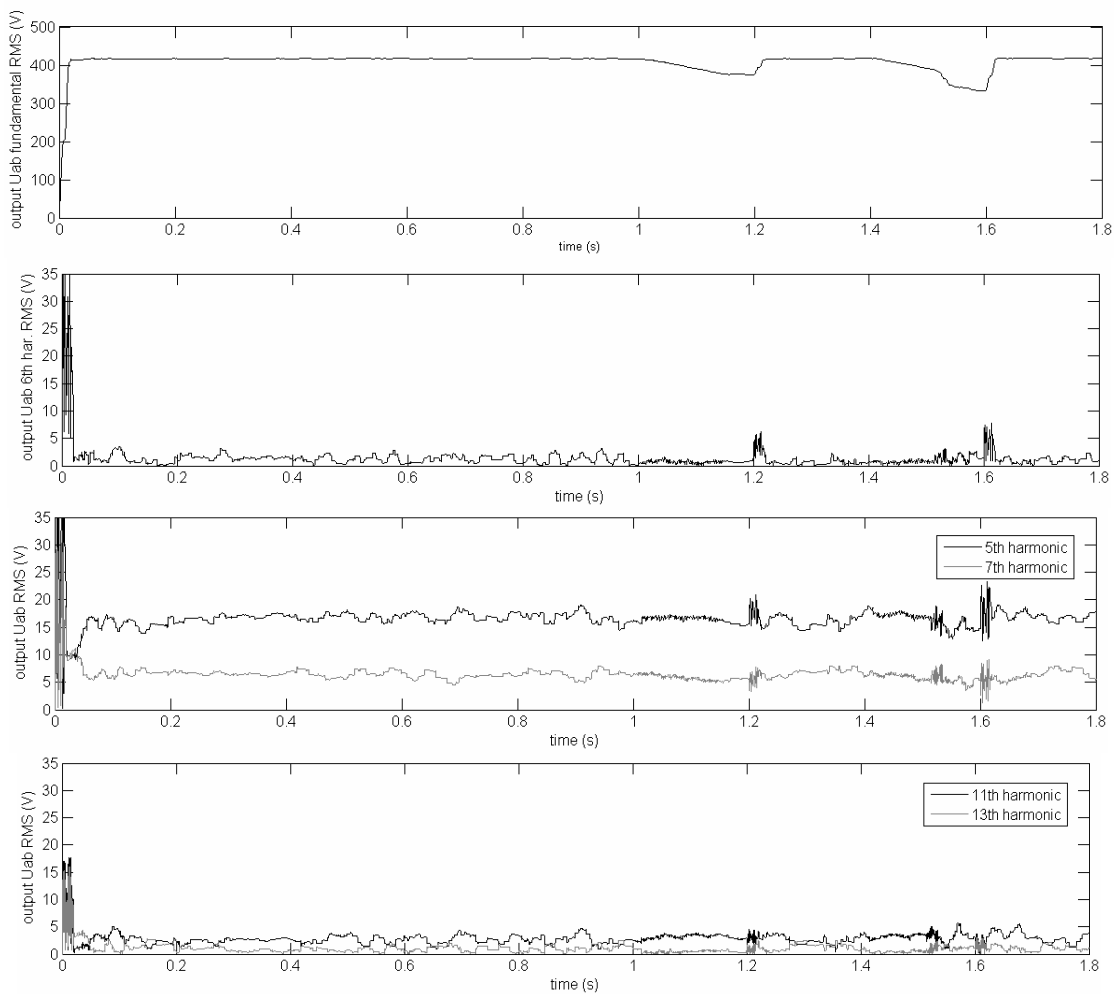


Fig. A4.34. Output line-to-line voltage fundamental, 5th, 6th, 7th, 11th, and 13th harmonic components (50 Hz base frequency), ($C_{DC-bus} = 25000 \mu\text{F}$; $f_{l(mr)} = 50 \text{ Hz}$; $m_a = 1.8$).

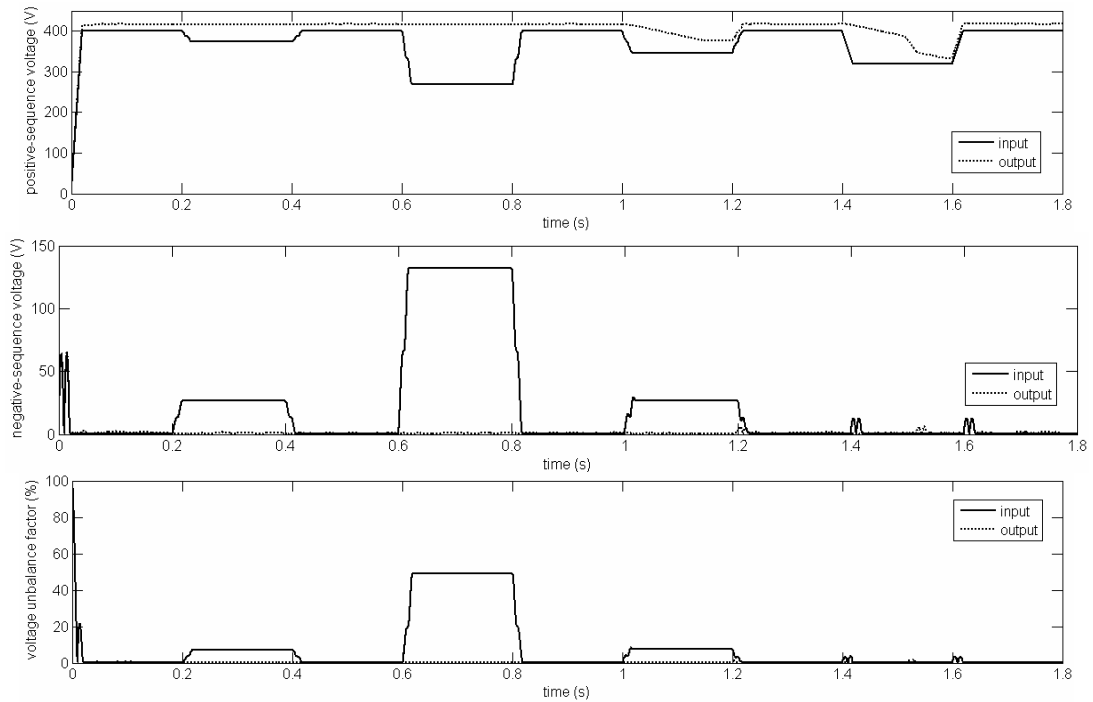


Fig. A4.35. Positive-sequence voltage, negative-sequence voltage, and voltage unbalance factor ($C_{DC-bus} = 25000 \mu\text{F}$; $f_{I(mr)} = 50 \text{ Hz}$; $m_a = 1.8$).

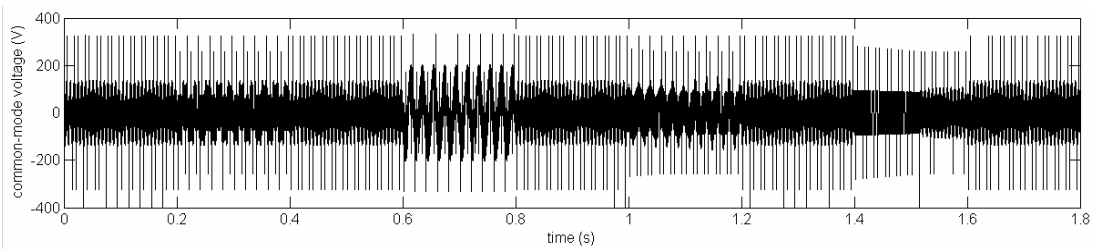


Fig. A4.36. Common-mode voltage (summation of phase-to-ground voltages divided by 3), ($C_{DC-bus} = 25000 \mu\text{F}$; $f_{I(mr)} = 50 \text{ Hz}$; $m_a = 1.8$).

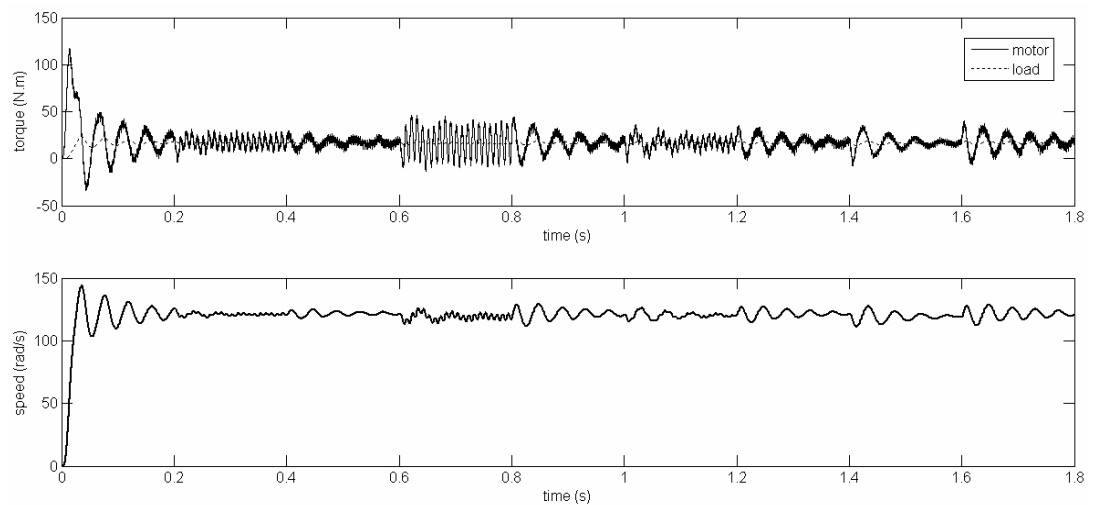


Fig. A4.37. Torque and speed for the motor and load, ($C_{DC-bus} = 250 \mu\text{F}$; $f_{I(mr)} = 40 \text{ Hz}$; $m_a = 0.95$).

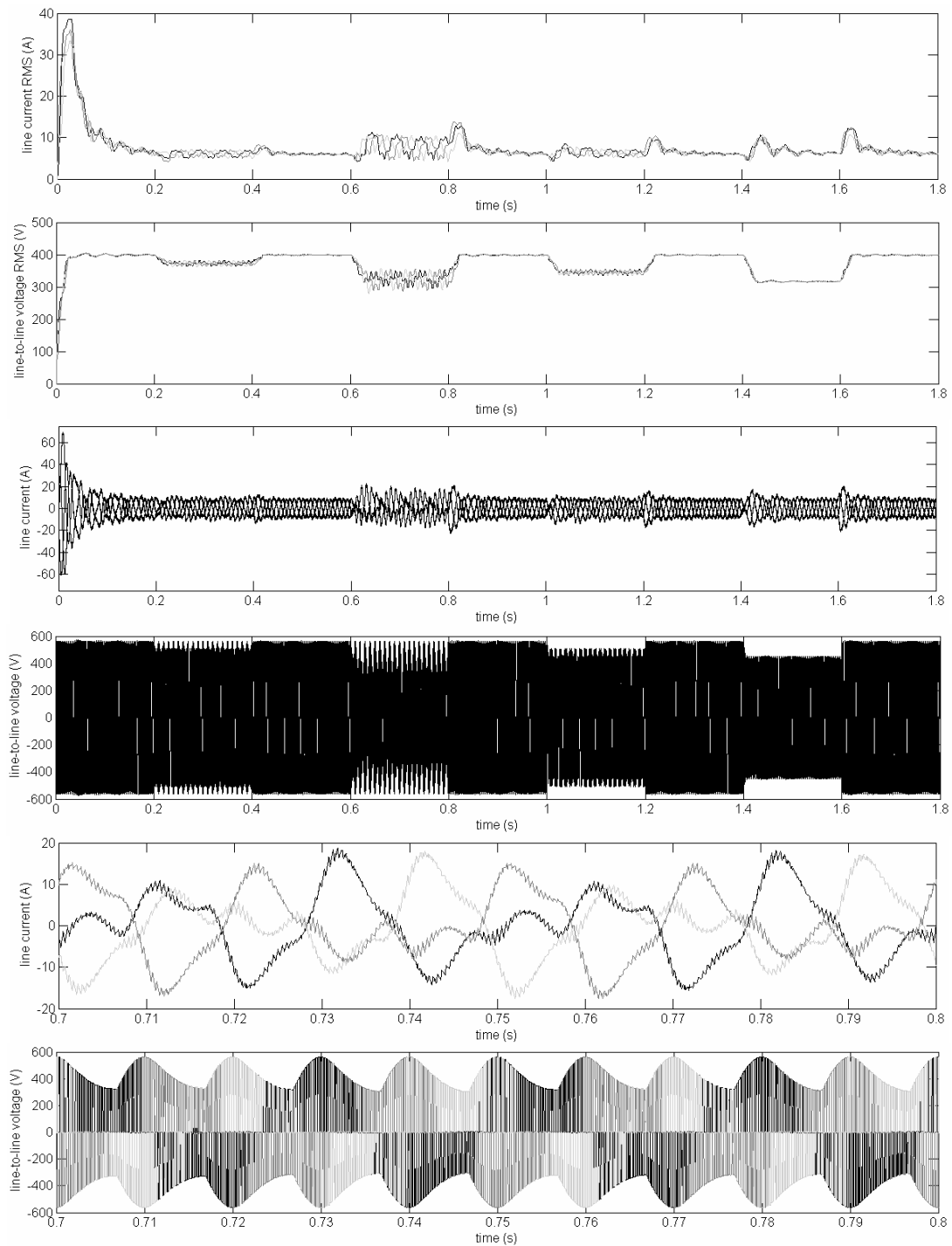


Fig. A4.38. Instantaneous and RMS values of the output phase-to-phase voltages and currents ($C_{DC-bus} = 250 \mu\text{F}$; $f_{I(mtr)} = 40 \text{ Hz}$; $m_a = 0.95$).

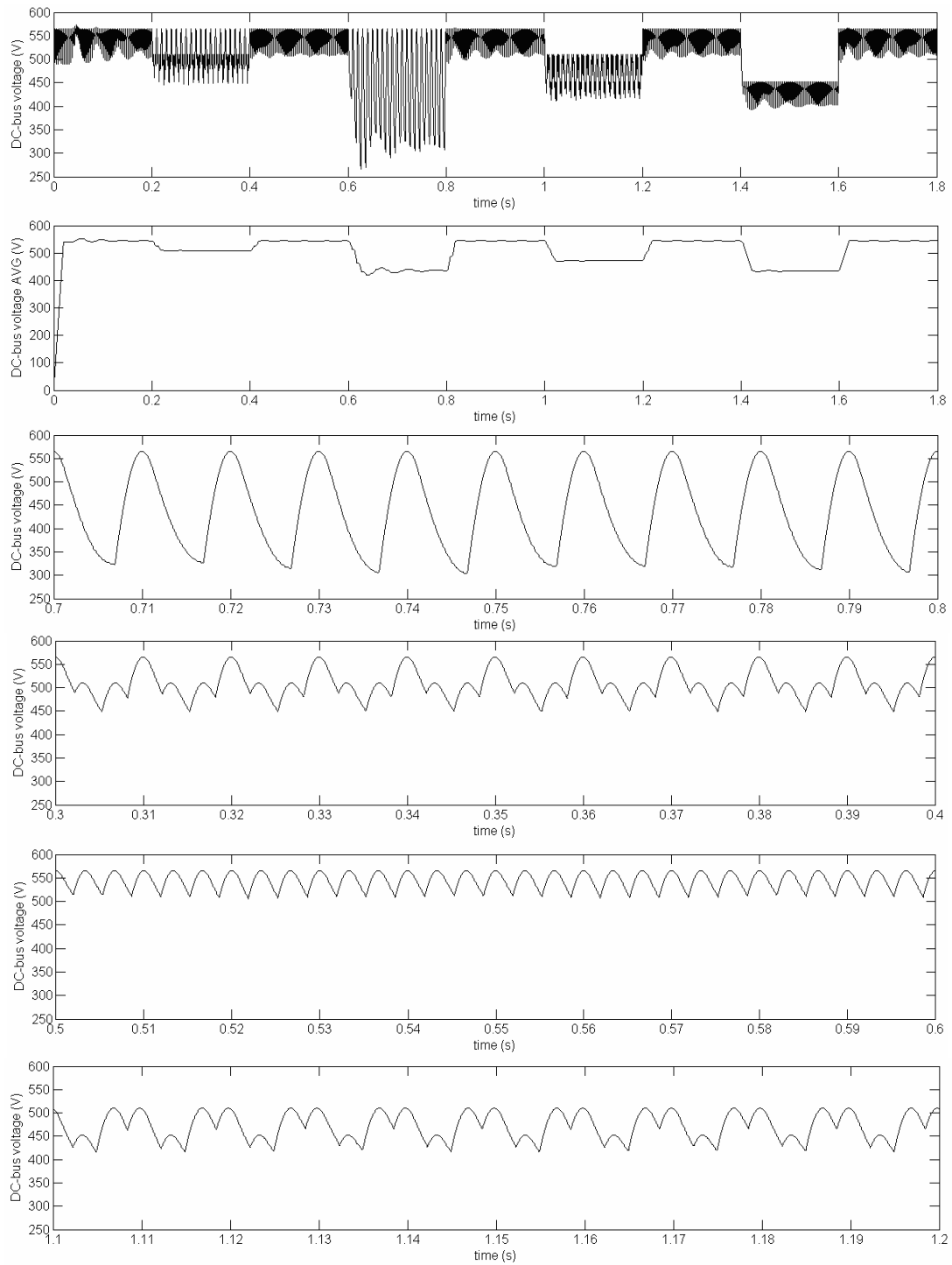


Fig. A4.39. Average value (or DC equivalent value) and instantaneous values of the DC-bus voltage, ($C_{DC-bus} = 250 \mu\text{F}$; $f_{l(mv)} = 40 \text{ Hz}$; $m_a = 0.95$).

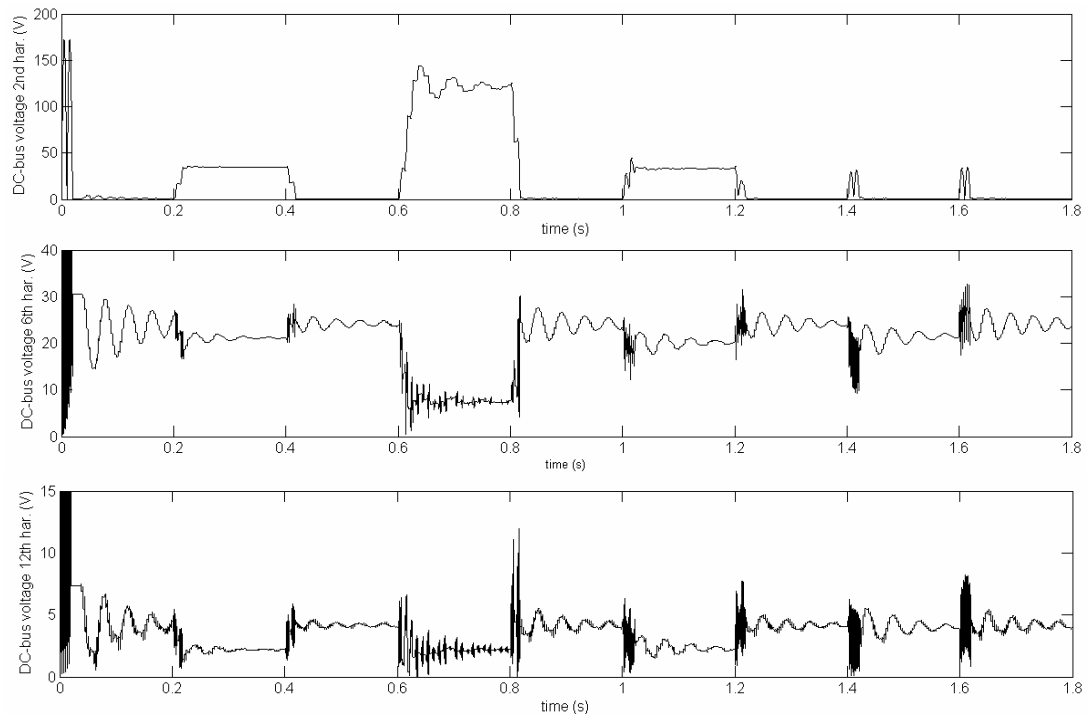


Fig. A4.40. DC-bus voltage 2nd, 6th, and 12th harmonic components (50 Hz base frequency), ($C_{DC-bus} = 250 \mu\text{F}$; $f_{l(mtr)} = 40 \text{ Hz}$; $m_a = 0.95$).

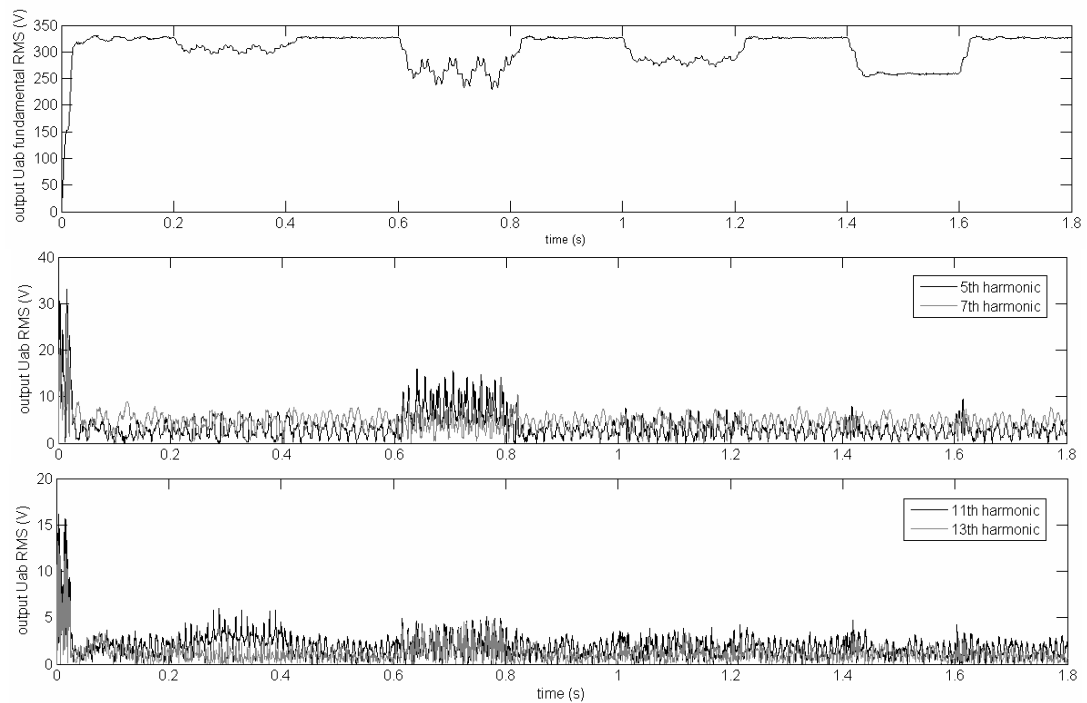


Fig. A4.41. Output line-to-line voltage fundamental, 5th, 6th, 7th, 11th, and 13th harmonic components (50 Hz base frequency), ($C_{DC-bus} = 250 \mu\text{F}$; $f_{l(mtr)} = 40 \text{ Hz}$; $m_a = 0.95$).

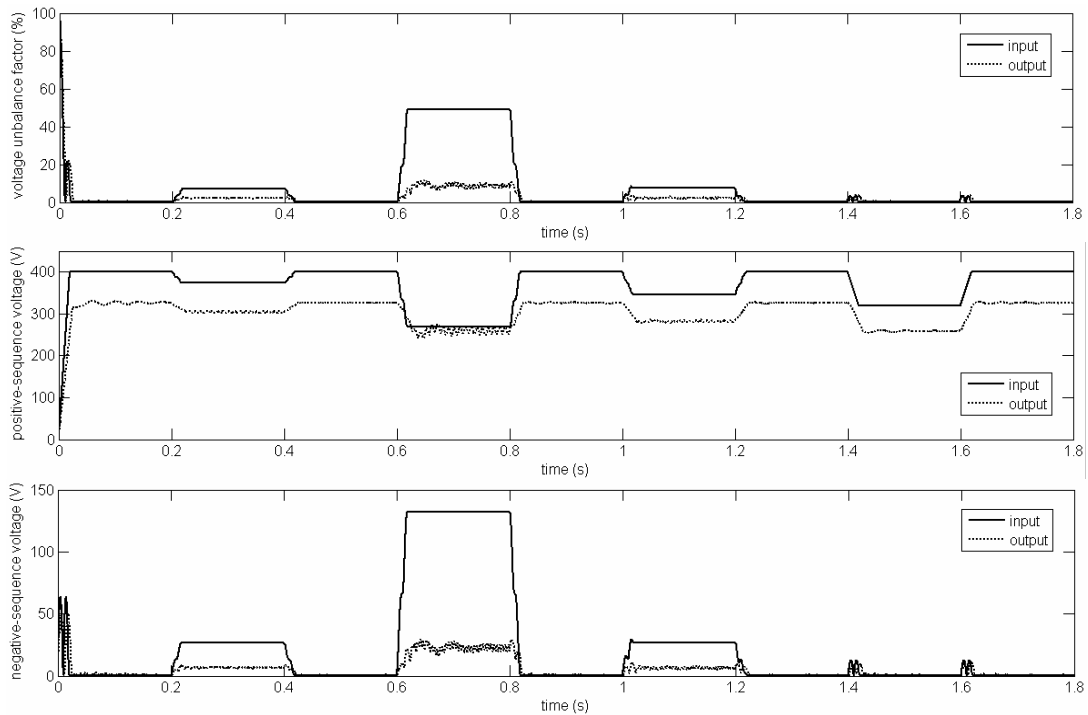


Fig. A4.42. Positive-sequence voltage, negative-sequence voltage, and voltage unbalance factor, ($C_{DC-bus} = 250 \mu\text{F}$; $f_{1(mtr)} = 40 \text{ Hz}$; $m_a = 0.95$).

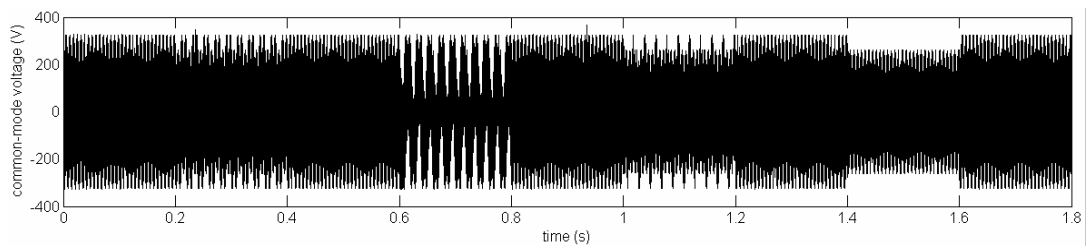


Fig. A4.43. Common-mode voltage (summation of phase-to-neutral voltages divided by 3), ($C_{DC-bus} = 250 \mu\text{F}$, $f_{1(mtr)} = 40 \text{ Hz}$, $m_a = 0.95$).

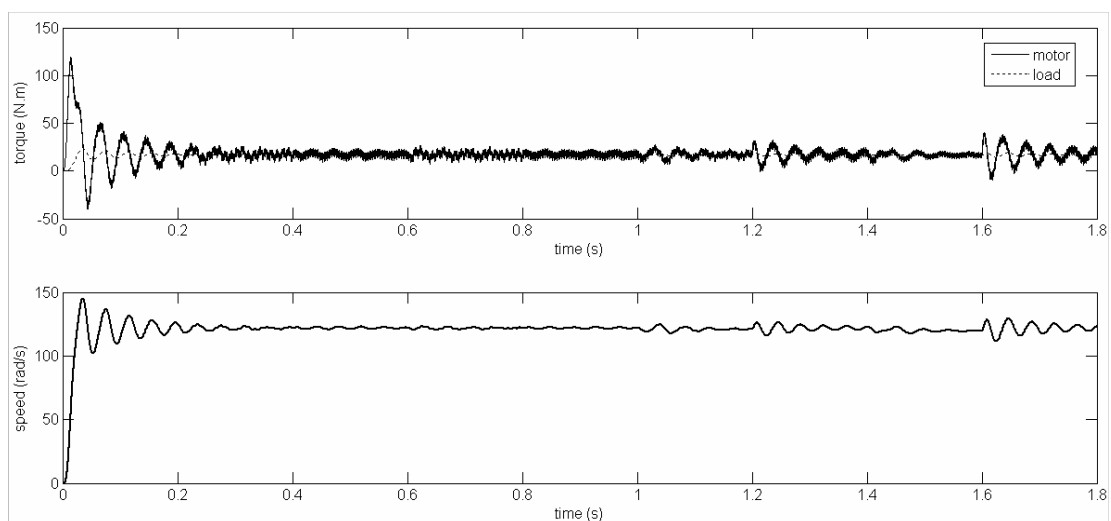


Fig. A4.44. Torque and speed for the motor and load ($C_{DC-bus} = 2500 \mu\text{F}$; $f_{1(mtr)} = 40 \text{ Hz}$; $m_a = 0.95$).

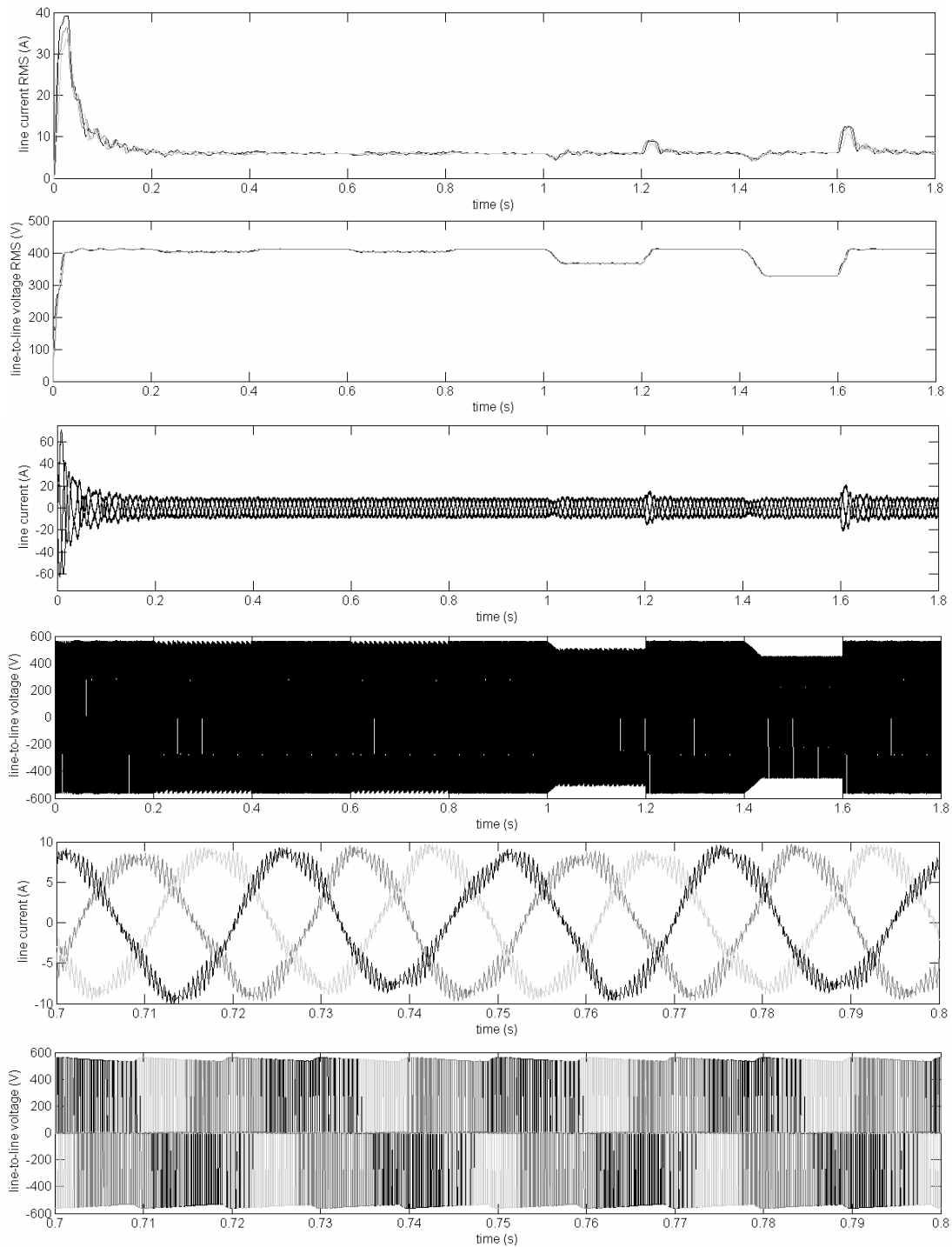


Fig. A4.45. Instantaneous and RMS values of the output phase-to-phase voltages and currents, ($C_{DC-bus} = 2500 \mu\text{F}$; $f_{1(mtr)} = 40 \text{ Hz}$; $m_a = 0.95$).

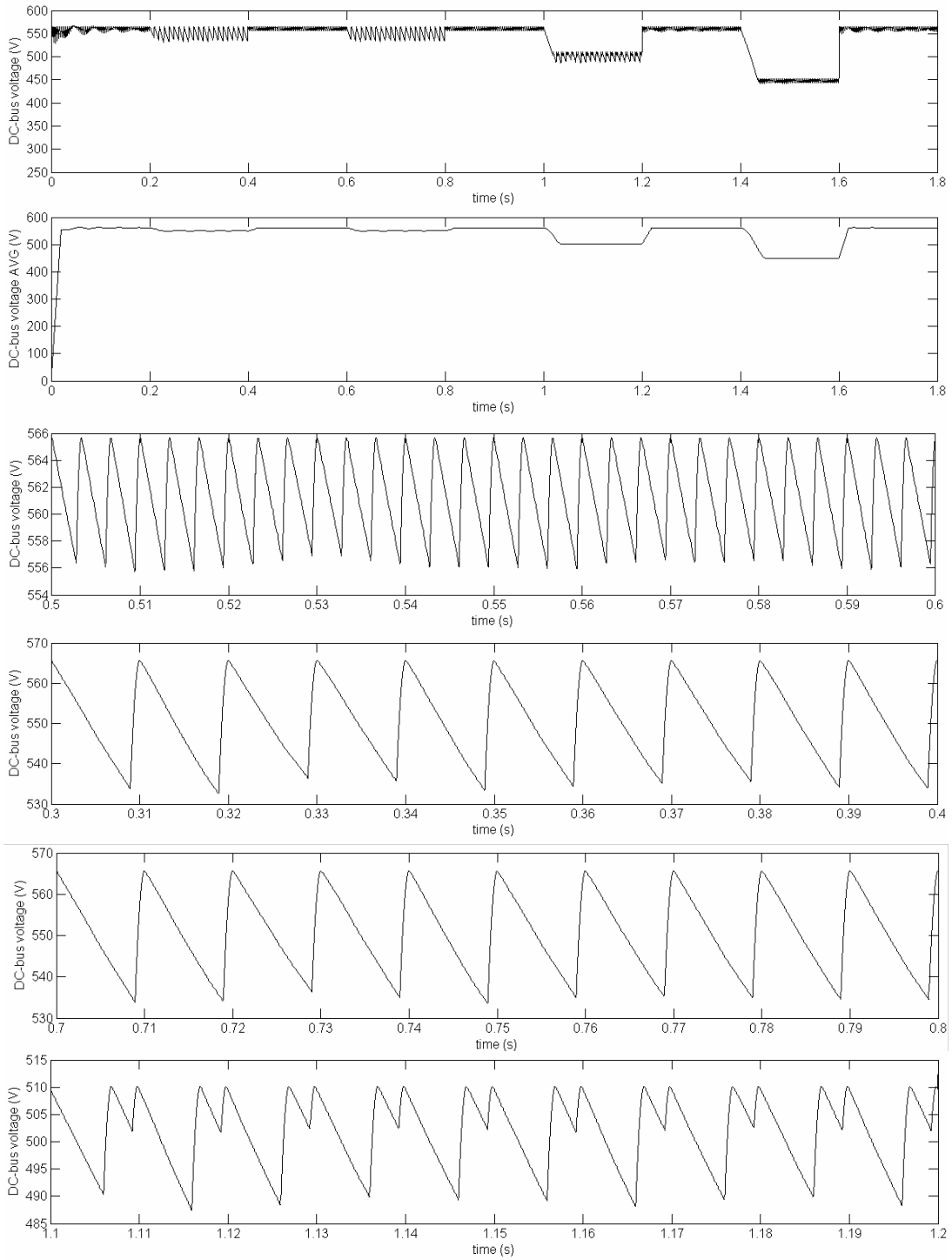


Fig. A4.46. Average value (or DC equivalent value) and instantaneous values of the DC-bus voltage, ($C_{DC-bus} = 2500 \mu\text{F}$; $f_{I(mtr)} = 40 \text{ Hz}$; $m_a = 0.95$).

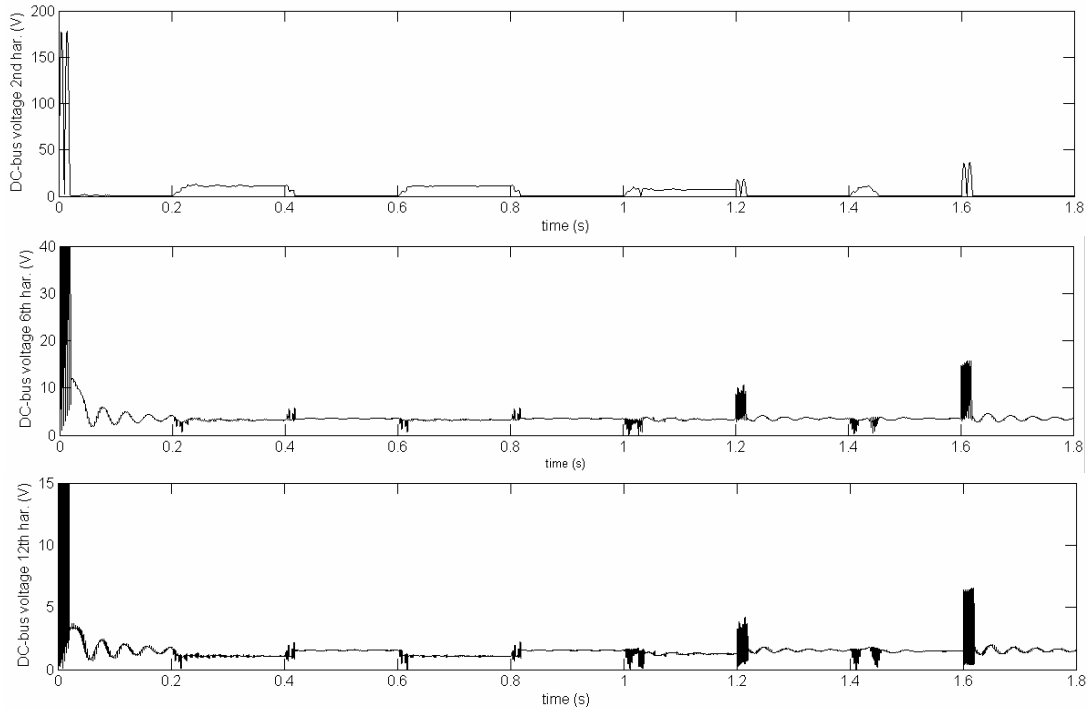


Fig. A4.47. DC-bus voltage 2nd, 6th, and 12th harmonic components (50 Hz base frequency), ($C_{DC-bus} = 2500 \mu\text{F}$; $f_{I(mtr)} = 40 \text{ Hz}$; $m_a = 0.95$).

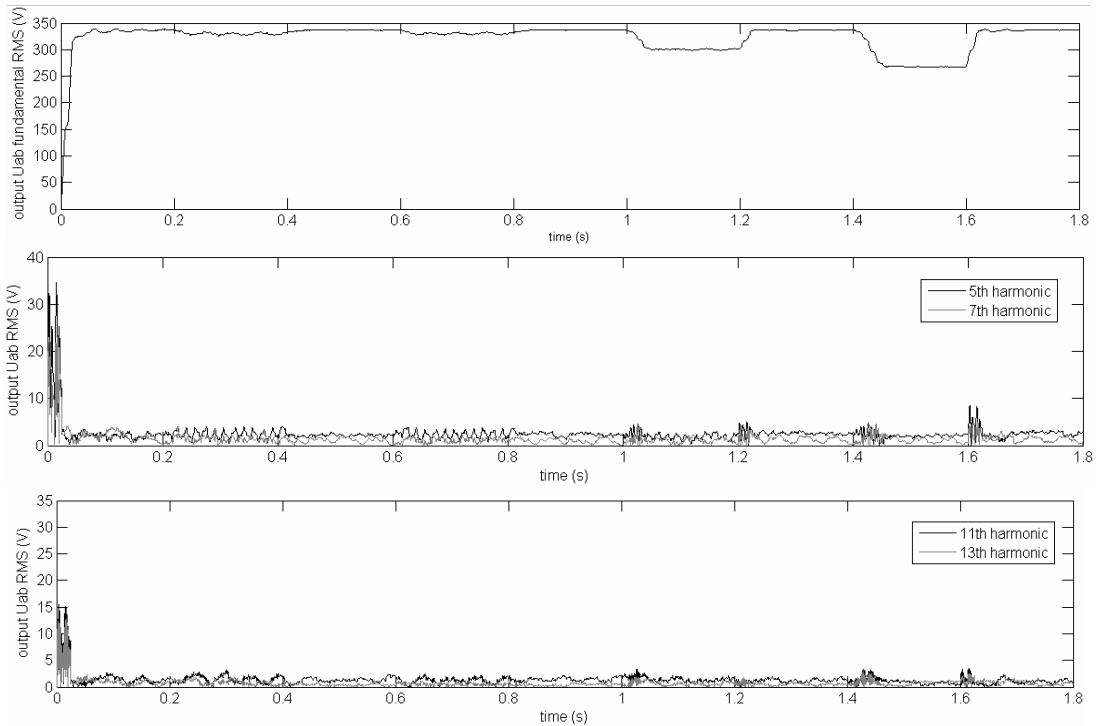


Fig. A4.48. Output line-to-line voltage fundamental, 5th, 6th, 7th, 11th, and 13th harmonic components (50 Hz base frequency), ($C_{DC-bus} = 2500 \mu\text{F}$; $f_{I(mtr)} = 40 \text{ Hz}$; $m_a = 0.95$).

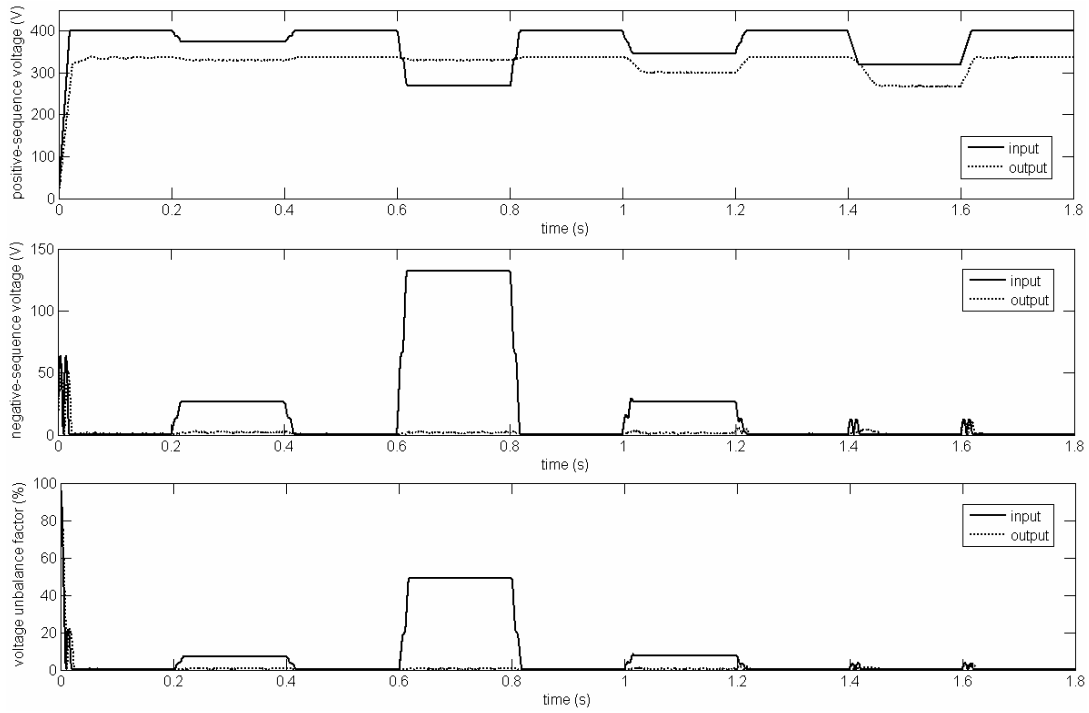


Fig. A4.49. Positive-sequence voltage, negative-sequence voltage, and voltage unbalance factor, ($C_{DC-bus} = 2500 \mu\text{F}$; $f_{l(mtr)} = 40 \text{ Hz}$; $m_a = 0.95$).

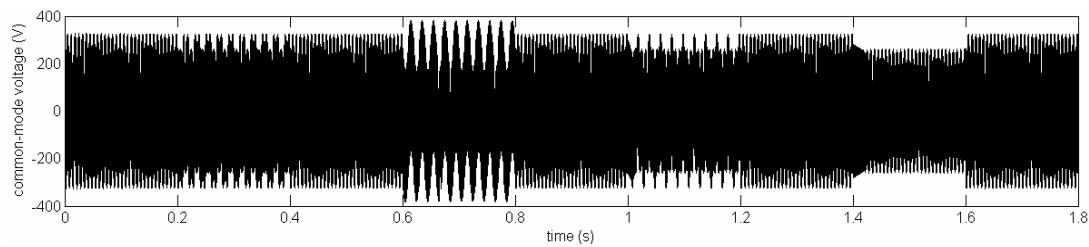


Fig. A4.50. Common-mode voltage (summation of phase-to-ground voltages divided by 3), ($C_{DC-bus} = 2500 \mu\text{F}$; $f_{l(mtr)} = 40 \text{ Hz}$; $m_a = 0.95$).

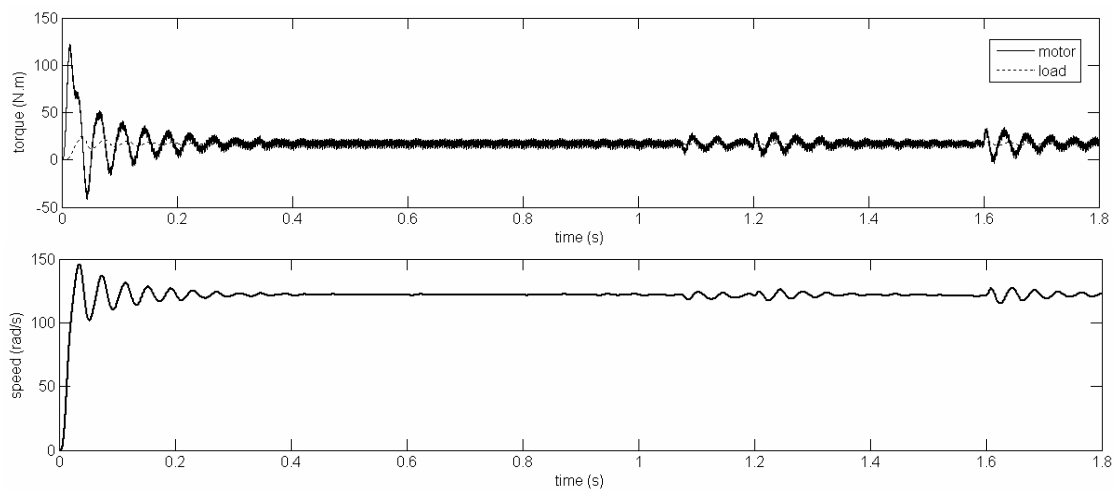


Fig. A4.51. Torque and speed curves for the motor and load, ($C_{DC-bus} = 25000 \mu\text{F}$; $f_{l(mtr)} = 40 \text{ Hz}$; $m_a = 0.95$).

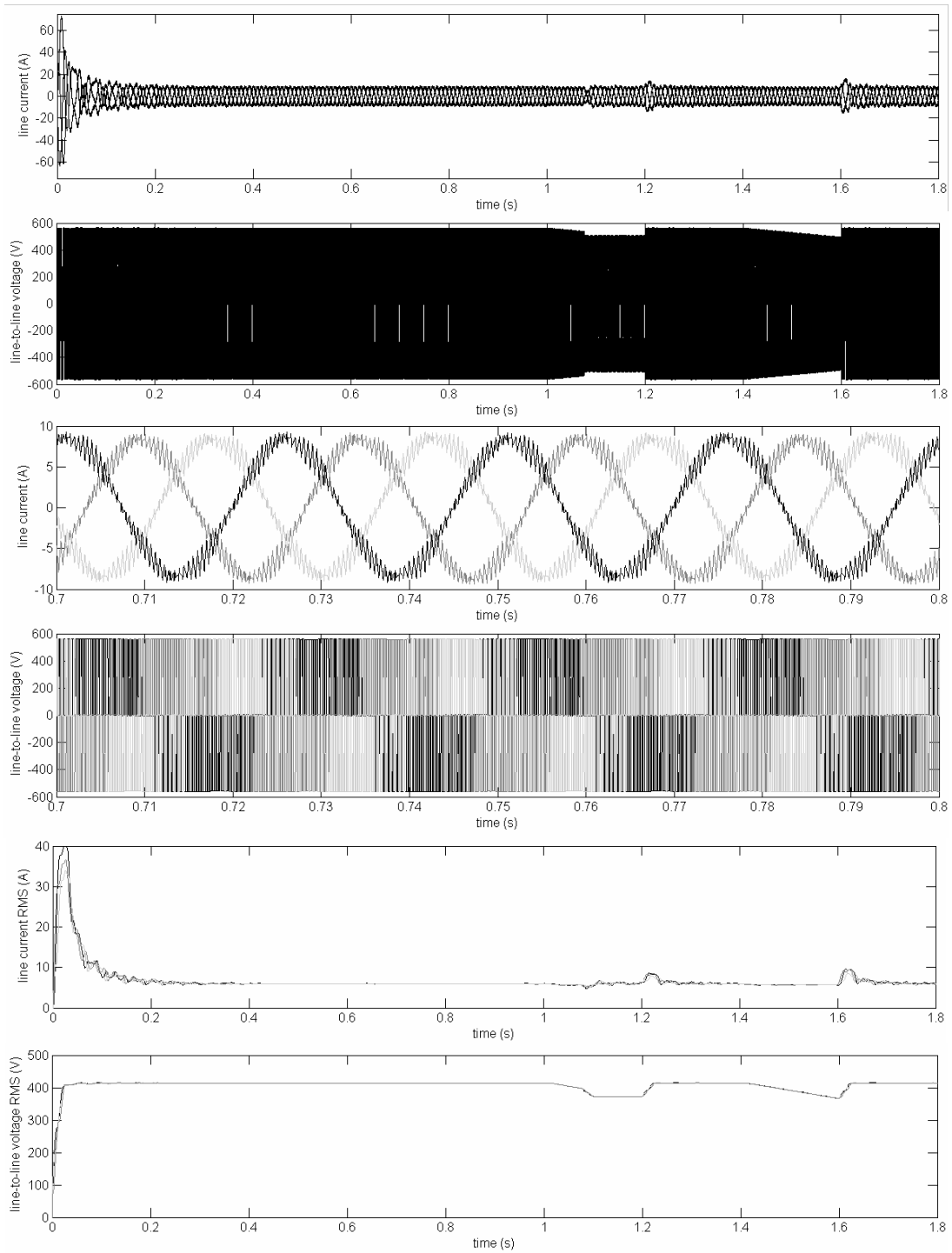


Fig. A4.52. Instantaneous and RMS values of the output phase-to-phase voltages and currents, ($C_{DC-bus} = 25000 \mu\text{F}$; $f_{I(mtr)} = 40 \text{ Hz}$; $m_a = 0.95$).

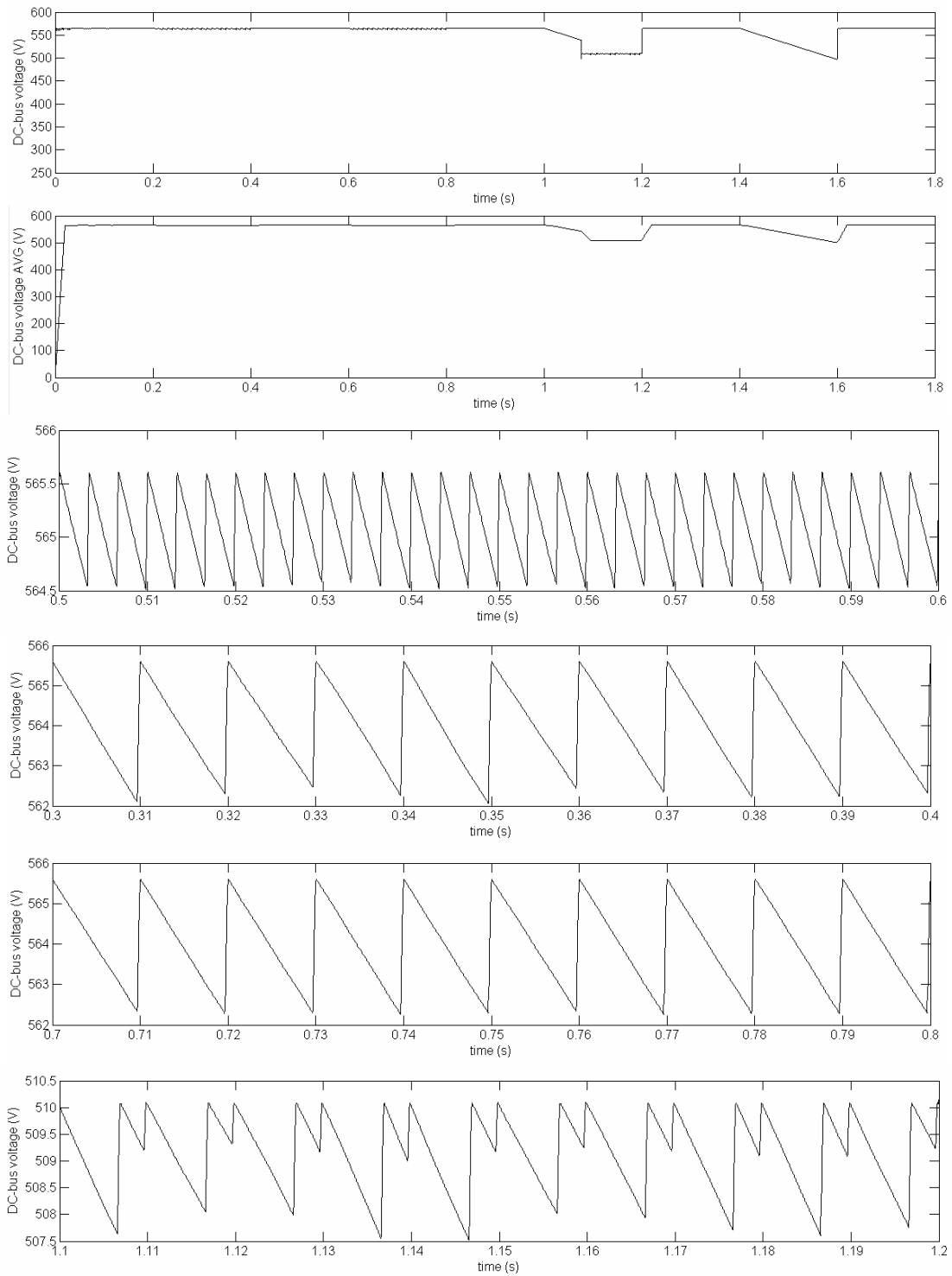


Fig. A4.53. Average value (or DC equivalent value) and instantaneous values of the DC-bus voltage, ($C_{DC-bus} = 25000 \mu\text{F}$; $f_{1(mtr)} = 40 \text{ Hz}$; $m_a = 0.95$).

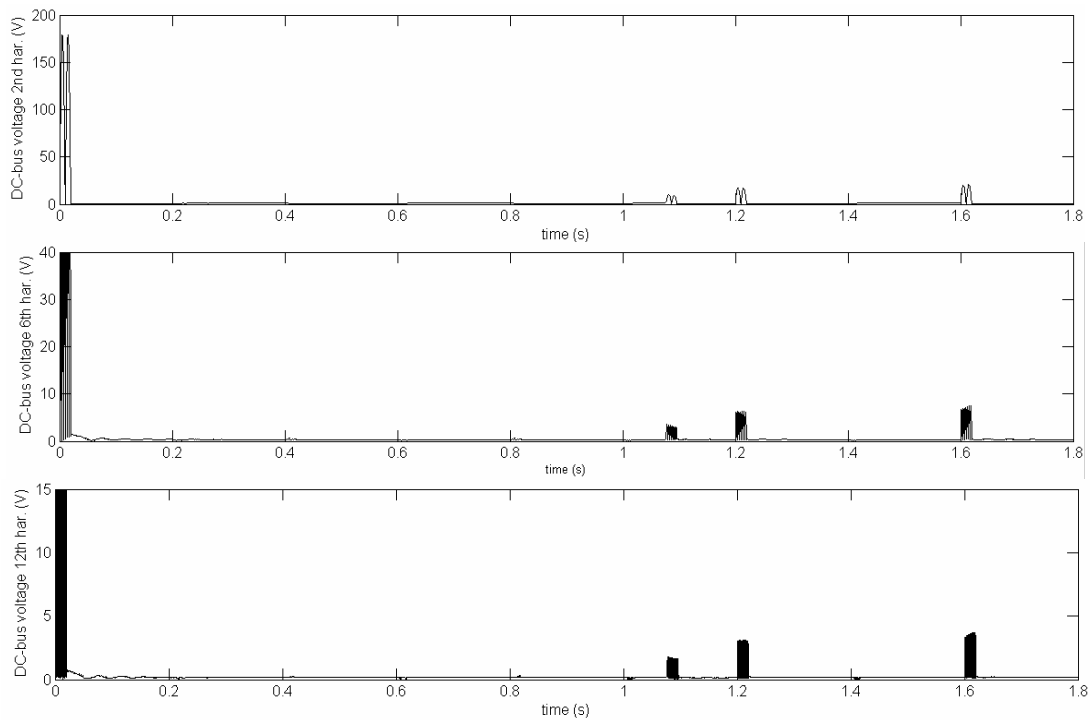


Fig. A4.54. DC-bus voltage 2nd, 6th, and 12th harmonic components (50 Hz base frequency), ($C_{DC-bus} = 25000 \mu\text{F}$; $f_{l(mr)} = 40 \text{ Hz}$; $m_a = 0.95$).

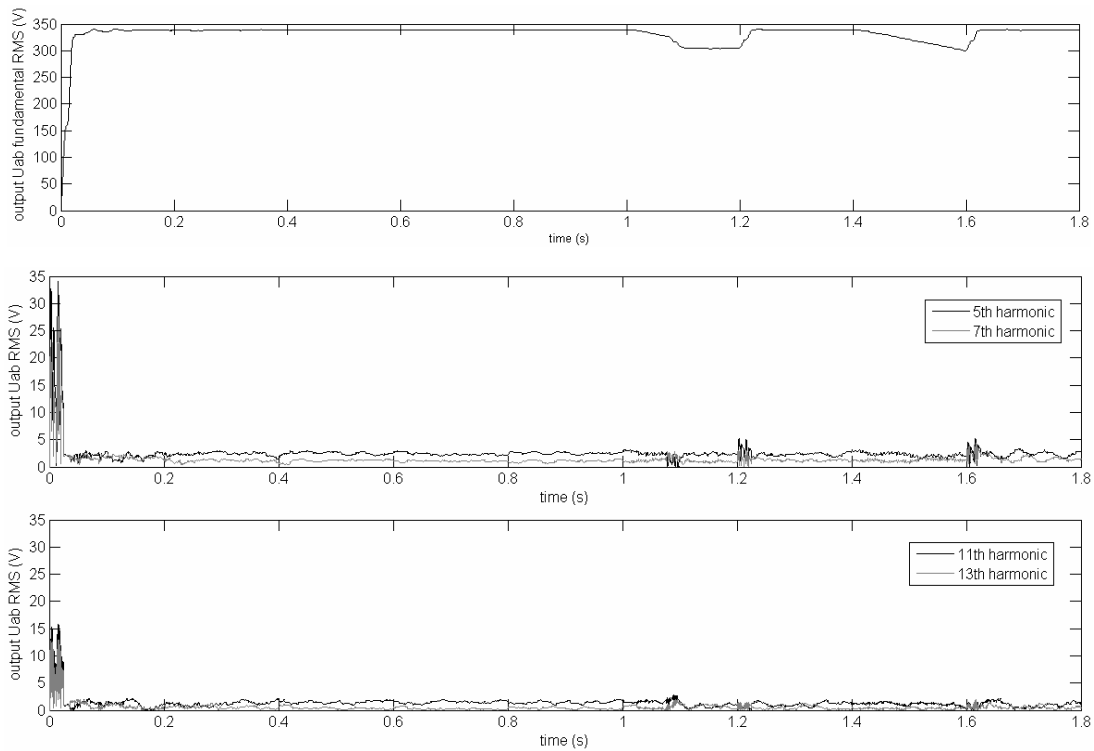


Fig. A4.55. Output line-to-line voltage fundamental, 5th, 6th, 7th, 11th, and 13th harmonic components (50 Hz base frequency), ($C_{DC-bus} = 25000 \mu\text{F}$; $f_{l(mr)} = 40 \text{ Hz}$; $m_a = 0.95$).

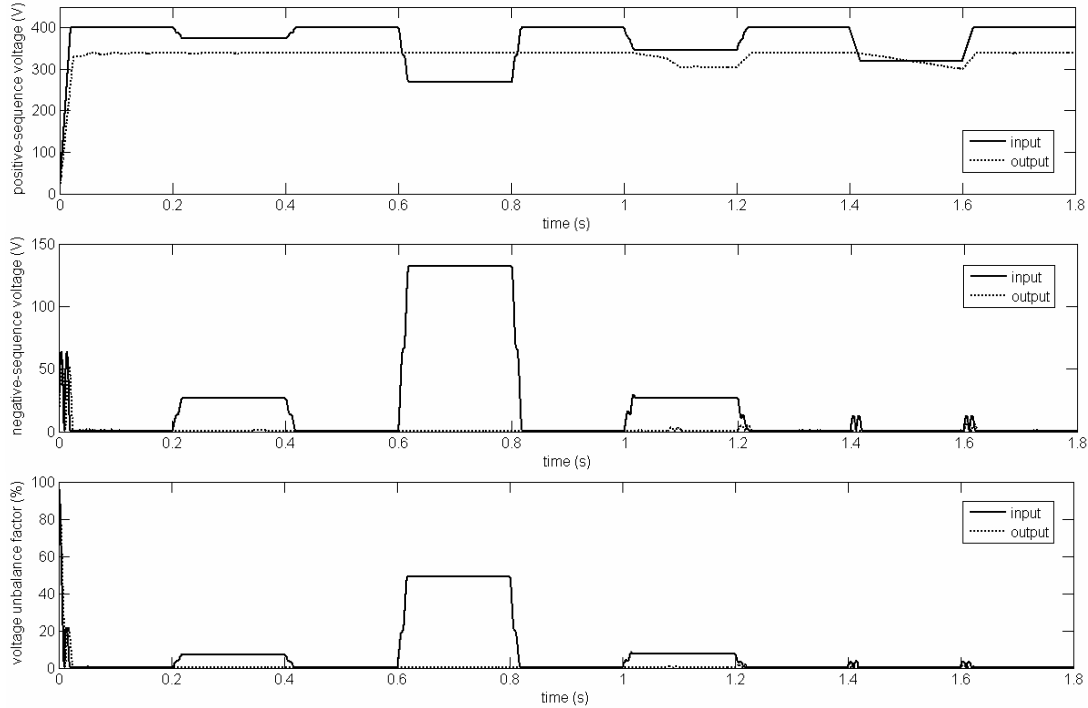


Fig. A4.56. Positive-sequence voltage, negative-sequence voltage, and voltage unbalance factor, ($C_{DC-bus} = 25000 \mu\text{F}$; $f_{I(mtr)} = 40 \text{ Hz}$; $m_a = 0.95$).

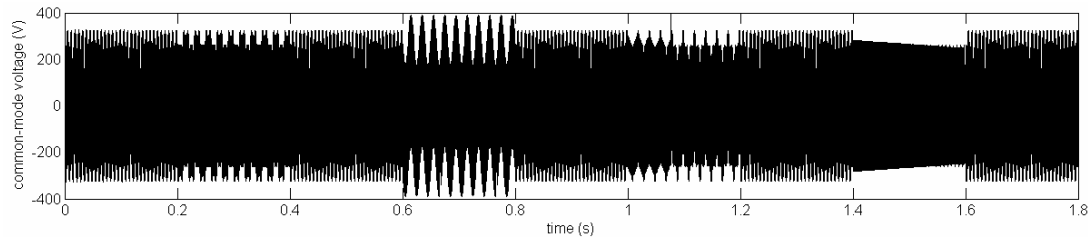


Fig. A4.57. Common-mode voltage ($C_{DC-bus} = 25000 \mu\text{F}$; $f_{I(mtr)} = 40 \text{ Hz}$; $m_a = 0.95$).

A4.2.3 Voltage Magnitude Deviation

Voltage magnitude deviation (*VMD*), i.e., under or overvoltage, at the IM terminals can be related to voltage sags/dips¹⁴, swells¹⁵, flickers¹⁶, voltage drops in cables, fluctuations, etc. [1], [22], [27]. In this case, the negative-sequence and zero-sequence components are null, and the positive-sequence magnitude can be different than the motor rated voltage. Depending on the duration and magnitude, *VMD* can significantly affect IMs performance and lifetime due to its impact on motor efficiency, power factor, torque, slip, current, and internal temperature. For example, a constant 10% decrease in the voltage at an IM operation at full-load can lead to a 23% increase in internal temperature due to the motor efficiency reduction [50]. Of course, the referred impacts depend on the actual IM load and, in some circumstances, can actually improve motor

¹⁴ Caused by operation manoeuvres, large motors starting, faulty currents circulation, atmospheric discharges, etc.

¹⁵ Caused by disconnection of large loads from power network.

¹⁶ Caused by high current consuming loads, such as arc furnaces and large motors.

performance [26], [45], [46]. IEC 60034-1 standard defines two zones of combinations of voltage and frequency steady-state or long-term deviations for line-fed IMs. For each zone, minimal requirements for performance and temperature behaviour are described. Additional notes on *VMD* are presented in Appendix 6. According to [53], the voltage deviation of LV and MV systems should not exceed $\pm 10\%$ over 95% of the time. The ITIC¹⁷ curves define the voltage deviations (in duration and magnitude) the electric equipment should be able to withstand without failing. *VMD* is typically defined by the deviation of the average voltage, U_{avg} , to the motor rated voltage. U_{avg} definition assumes the possibility of a slight unbalance existence. In order to avoid ambiguities, and to isolate the impact of *VMD* on motor operation, it is used in this section the U_p instead of the U_{avg} , according to (A4.26).

$$VMD = \frac{U_p}{U_R} - 1 \quad (\text{A4.26})$$

In the simulations, a constant, rated frequency and *VMD*s of -30, -25, -20, -15, -10, -5, 0, 5 & 10% are considered. Some of the results are presented in Figs. A4.58 and A4.59. More simulated results are presented in Fig. 3.54 of Chapter 3.

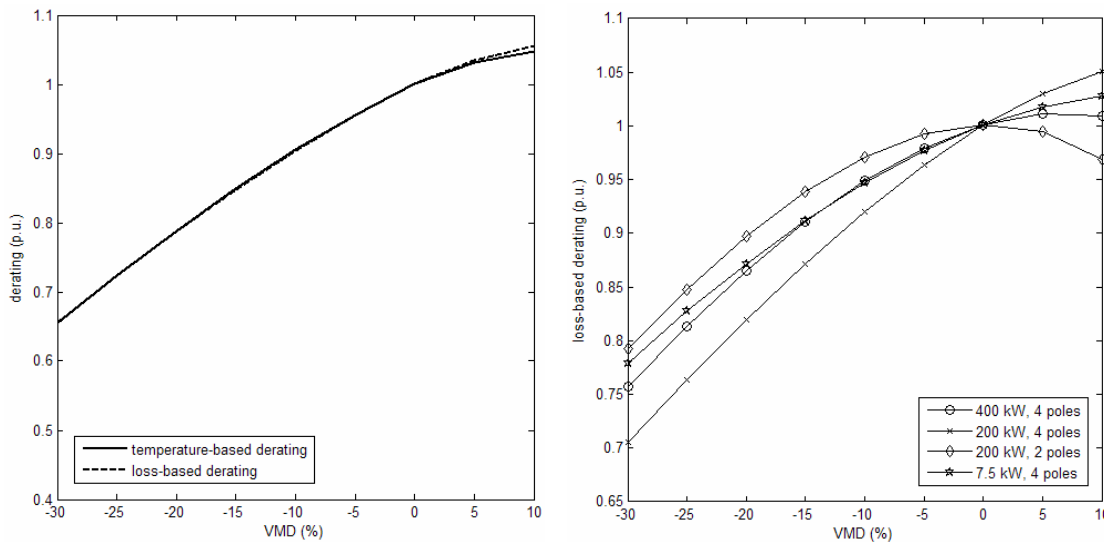


Fig. A4.58 (top) 3-kW IM: simulated derating curves as a function of *VMD*. (bottom) 400-kW, 200-kW and 7.5-kW IMs: simulated derating curves as a function of *VMD*.

Negligible differences were obtained between LBD and TBD curves. Therefore, both approaches are suitable for the *VMD* derating analyses. The higher the pole-number, the more pronounced the

¹⁷ The ITIC curves define that electrical equipment should be able to withstand the following voltage deviations: $0.8 \cdot U_N$ during 1 s; $(1 \pm 0.1) \cdot U_N$ during > 10 s (steady-state or permanent operation); $0.7 \cdot U_N$ during 400 ms; zero voltage during < 20 ms; $2 \cdot U_N$ during ≤ 3 ms. The ITIC curve was derived by a working group of Information Technology Industry Council (ITIC), and reflects the performance of typical single-phase 60-Hz computers and their peripherals, and other information technology items like faxing machines and point-of-sales terminals. The ITIC curve is generally applicable to other equipment containing solid-state devices.

derating curve as a function of negative VMD is (the situation is inverted for the positive VMD). Regarding the rotor type, “rotor II” leads to the most pronounced motor derating curve.

Experimental results presented in [7], [46], and [47] underline the findings obtained by the simulations. In general, the impact of balanced VMD on the motor torque, slip, efficiency and temperature is well known, and is also analysed in Chapter 5.

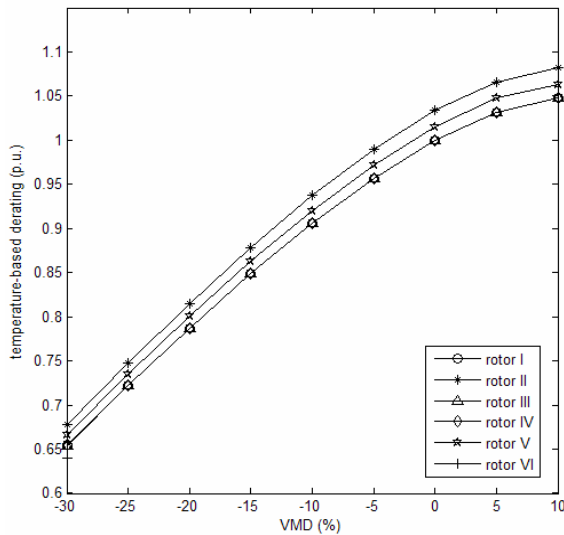


Fig. A4.59. 3-kW, 4-pole IM: simulated motor derating curves as a function of VUF , considering different rotor-bar types.

The 3-kW motor simulation model takes into account the saturation effect during overvoltage. The 200-kW motor model does not take into account the saturation effect, being considered only a negative VMD . But, actually, significant overvoltages are quite rare in the field.

The shift of the efficiency peak load as a function of the voltage variation is roughly given by $\Delta\zeta_{\eta_{\max(p.p.)}} \approx \Delta U(\%)$, i.e., reducing the voltage 30%, leads to a 30-p.p. shift of the peak efficiency load to a lower value.

On the basis of the curves presented in Fig. 3.54 of Chapter 3, it is possible to conclude that, even within the limits established by the standard IEC 60034-1 [8] for negative VMD (-5% , Zone A, see Appendix 6), a slight derating action is needed. For a positive VMD within Zone A, no derating is necessary. Outside the recommended limits (Zone B), a significant derating should be applied for negative VMD (about 10% for a VMD of -10%). For positive VMD within Zone B, no derating is needed. In general, up to 5-10%, no derating is needed, but for higher deviations, the motor operation is likely to be impracticable due to the saturation level and the consequent increase in the motor losses and temperature. It can be also said that the derating for negative VMD can be estimated either based on winding temperature or motor losses. For negative VMD , which are the vast majority of the cases, the derating can be considered as approximately equal to one minus the absolute value of the negative VMD .

The efficiency degradation depends upon the motor load. For the considered motor, the efficiency degradation is significant at full load for negative *VMD*, but can actually improve for low loads. At full load, the efficiency improves slightly for the considered values of positive *VMD*. Motor power factor has a regular behaviour, improving when the voltage is reduced and vice versa, regardless the motor load.

It can be concluded that it is very important to measure the actual motor voltage in order to establish the proper derating in order to ensure original lifetime and performance.

A4.2.4 Combined Effects

In this section, the combined effects of previously considered power supply voltage steady-state abnormalities are analysed, in order to study how the effects of one abnormality can amplify the effect of another. In [8], it is stated that, if the limits of the *HVF* and of the negative-sequence and zero-sequence voltage components are simultaneously reached (not crossed) in service, at the rated load, this shall not lead to any harmful temperature in the motor, and it is recommended that the resulting excess temperature rise related to the limits specified should be not more than approximately 10 K.

As shown in previous sections, the performance of the motor can be related with the U_p and U_n components, which allow to calculate the *VUF* and the *VMD* separately. Therefore, the following analysis assesses the combined effect of *HVF*, *VUF* and *VMD*. Due to its obvious impact, the ambient temperature deviation, *ATD*, is also considered. For the sake of simplicity, only the pattern 1 for the *HVF* is considered.

In unbalance systems, voltage harmonics are likely to be also unbalanced, and each harmonic has its own positive, negative, and zero-sequence component. These conditions would include unbalanced harmonic sources on the system, e.g., single-phase sources, single-phase capacitor banks, or unbalanced system loading. In some cases, even the unbalance introduced by untransposed transmission lines can be important, requiring a three-phase system representation for a proper analysis. However, for the sake of simplicity, it is assumed balanced harmonics.

Regarding previously published works, in [3], [12], and [14], simulations on combined effects are presented. In [11], [12], [21], and [26], experimental results can be found on combined effects. However, in the referred simulations, some important aspects were not taken into account. In [3], for example, the temperature effect on motor simulation model parameters is not considered. Moreover, no separation is made regarding *VMD* and *VUF*.

In [12] the combined effect of *VU* and *VMD* was studied, although the model used for simulations does not consider the influence of temperature on stator and rotor temperature. The core losses were determined experimentally, shown in Fig. A4.60, evidencing that the core loss increases with the voltage unbalance and, at same time, with the voltage magnitude.

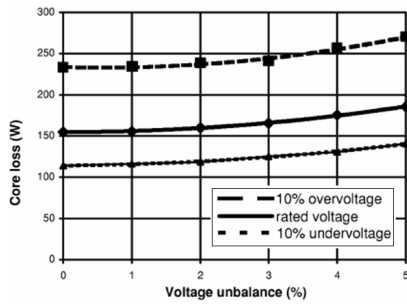


Fig. A4.60. Motor core loss variation with voltage supply unbalance, in combination with over- or undervoltages [12].

Fig. A4.61 shows the main simulated results for the 3-kW, 4-pole IM, considering different combinations of *HVF*, *VUF*, *VMD* and *ATD*. It is interesting to note that, for example, for *VUF* = 8%, the derating for *VMD* = -10% and *VMD* = 0% have a similar value. As it was concluded in other previously published works, in relation to the positive *VMD*, the negative *VMD* leads to a higher derating when combined *VUF* (for low *VUF*s), but the undervoltage reduces the “slope” of the *VUF* derating curves. Of course, these combined effects strongly depend on the motor actual load.

HVF and *VUF* combined can lead to higher motor temperatures, as discussed previously, but also to higher vibrations (both supply voltage anomalies can produce significant pulsating torques). The latter effect-related degradation adds to the thermal degradation, shortening significantly insulation lifetime. However, in this section, only the thermal ageing resulting from combined impact of *HVF*, *VUF*, *VMD* and *ATD*, considering 25°C as reference ambient temperature, is analysed. Manufacturers often provide derating curves for *ATD*. Fig. A4.62 shows typically *ATD* derating curves defined by manufacturers and estimated derating curves (once more, the typical derating curves given by manufacturers seem to lead to an overderating, at least for low power motors). Especially in Industry, the motors are in most cases placed inside some equipment or closed spaces, which, in some cases, have not good ventilation and/or contains other devices producing heat, thus the indoor/inside ambient temperature and, therefore, the motor internal temperature, may be higher for a given VU level than that expected for normal ambient temperature. However, only motor derating curves to normal ambient temperatures is provided in most of the related documentation and standards.

Experiments on combined *VUF-VMD* effects on a 7.5-kW (4 pole, TEFC) IM were carried out and the main results were presented in [43], but extra results are now presented in Fig. A4.63, which shows the *VUF*, U_p , and stator winding temperature, for 4 different situations. In Fig. A4.63, it is possible to observe, for example, for 8% *PVUR* and $U_p \approx 96\%$ of U_N the derating should be 72-73%. Although U_p is slightly lower than U_N , this result also demonstrates the overderating associated with NEMA curves.

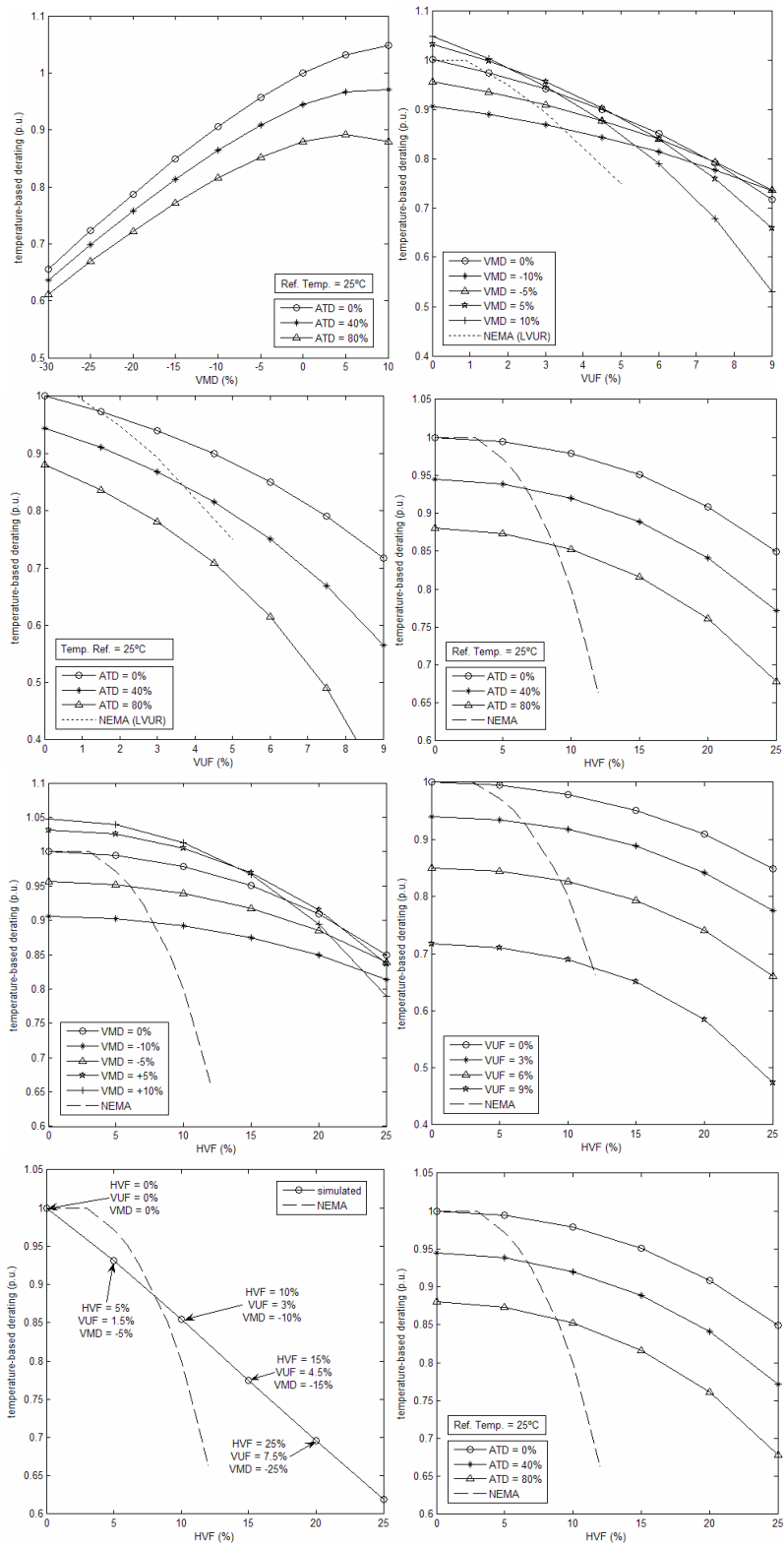


Fig. A4.61. Simulated power derating curves for a 3-kW, 4-pole IM, considering combined effect of *VUF*, *HVF*, *VMD*, and *ATD*.

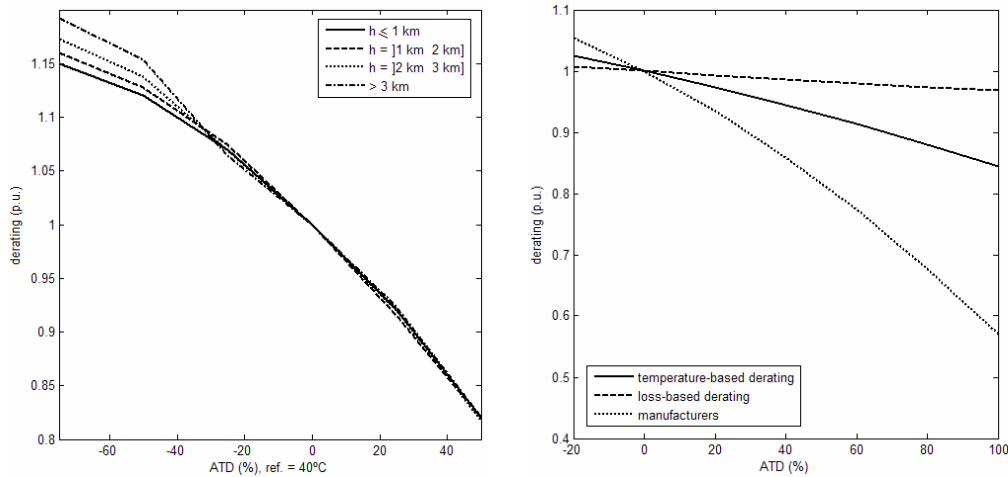


Fig. A4.62. Motor derating as a function of *ATD*: (left) For different altitudes, *h*, according to motor manufacturers, considering 40°C reference ambient temperature; (right) Simulated for a 3-kW, 4-pole IM, considering 25°C reference ambient temperature.

It can be concluded that all the considered parameters influence each other in terms of derating, and they should be considered all simultaneously, since, in practice, they rarely act alone. *ATD* has a significant impact on motor derating, particularly when combined to other PQ parameters, and should also be considered in the derating curves. Since the motor derating varies almost linearly with the percentage temperature variation, its combined influence can be evaluated by simply multiplying the *ATD*-based derating by the derating associated with the other PQ parameters, as it can be seen in Fig. A4.61.

According to the simulated results, *VUF-HVF* and *VUF-ATD* are the most critical combinations. It can be concluded, that, under combined effects, NEMA MG1 derating curves should not be used. Moreover, it is desirable to establish derating curves or functions considering combined effects.

A4.2.5 Pole-Number Effect on Motor Derating

On the basis of the foregoing discussion, more pronounced *HVF* and *VUF* derating curves are expected for 2-pole IMs, in relation to 4- and 6-pole IMs. Since the rotor-bars section and shape varies with the number of poles, the derating curves should also depend on this motor parameter.

A4.2.6 Rotor-Bar Type Effect on Motor Derating

As it is evidenced in [26], the skin effect on rotor bars is more accentuated for high-starting torque IMs (IEC design H or NEMA design C/D), when compared to normal-starting torque IMs (IEC design N or NEMA design A/B). Moreover, this principle is inherent to the *HVF* limits established by standard IEC 60034-1, which depend on motor design/type. In general, as it was previously shown, the higher the rotor-bar section and/or depth, the higher the impact of *VUF* and *HVF*, potentially leading to a higher motor derating.

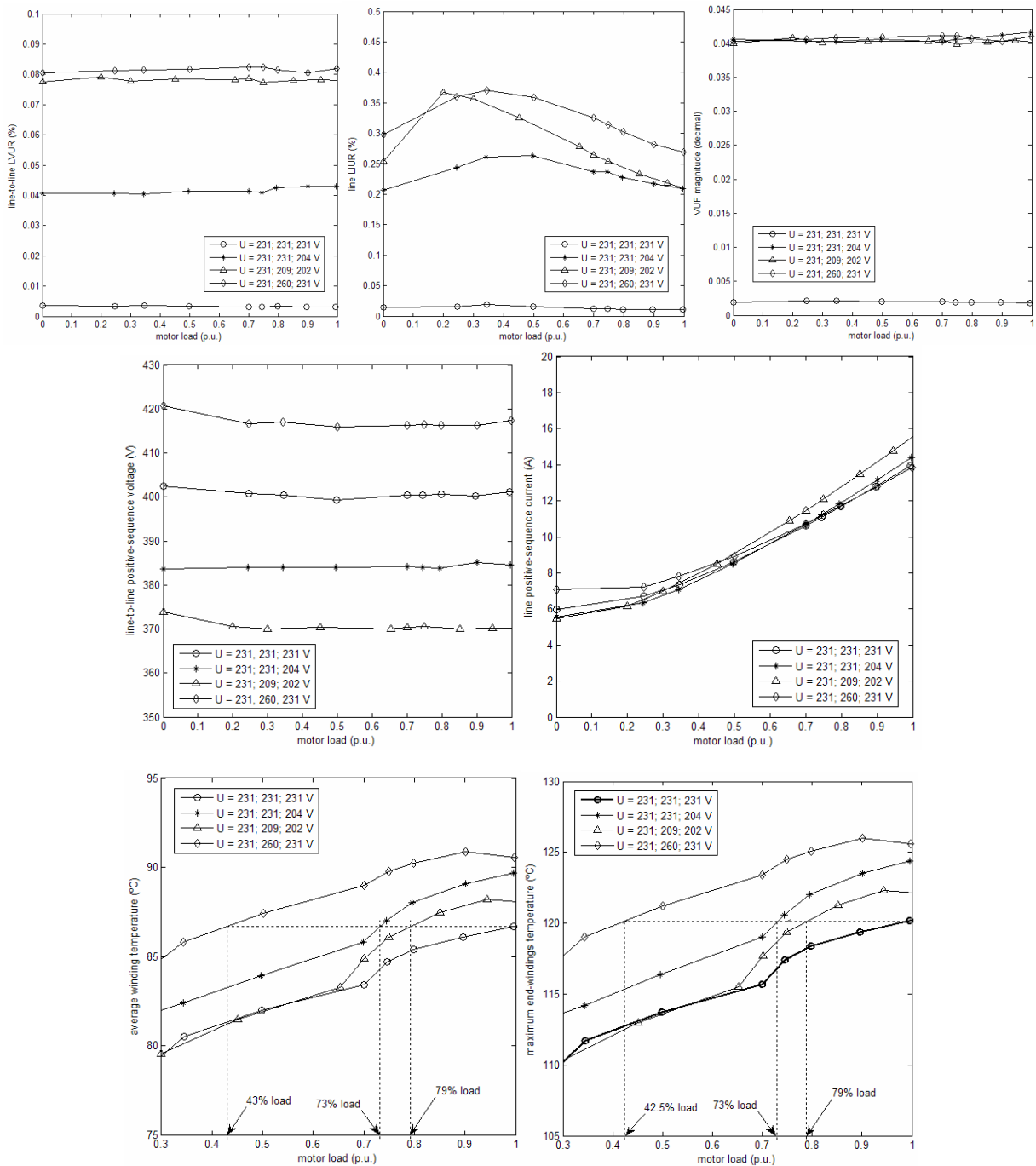


Fig. A4.63. 7.5-kW IM: experimental U_p , VUF , average windings temperature (measured by means of winding resistance), and maximum end-windings temperature (measured by means of a temperature sensor), considering different unbalance patterns (or combined VMD and VUF effects).

A4.2.7 Frame-Type Effect on Motor Derating

In steady-state operation, motor temperature is approximately proportional to motor losses. That relation depends on motor overall equivalent thermal resistance. Regarding the motor frame type, the overall thermal resistance of ODP motors is smaller than that of TEFC motors. Moreover, the stator-windings hottest points are typically at the driving-end side coil-heads (end-windings) for

TEFC motors and in the in-slot conductors for ODP [57]. Based on this and on the results presented in [16], it can be concluded that ODP motors are likely to be less affected by loss increase due to steady-state power supply voltage anomalies. Therefore, derating curves should be different for both frame types. Additionally, due to the lower temperature, a lower increase in slip is expected in ODP motors, thus reducing the negative impact on motor efficiency.

A4.2.8 Rated Power Effect on Motor Derating

Regardless the frame type, the higher the rated power, the lower the motor overall thermal resistance per kW and, consequently, the lower the impact of losses increase on motor temperature. In contrast with the higher rotor depth and the consequent accentuated skin effect, in general, for larger motors the resulting temperature increase is likely to be lower for moderate levels of *VUF* and *HVF*. Therefore, derating should be defined per power range or take into account the motor rated power.

A4.2.9 Efficiency Class Effect on Motor Derating

Efficiency plays an important role on derating. Lower starting torque, rated losses and operating temperature are features associated with high-efficiency IMs, which reduce the susceptibility of the motor to *HVF* and *VUF*. However, that susceptibility also depends on the design choices made to obtain the increased efficiency. As it was explained above, increasing rotor conductor section or decreasing the resistivity of the conducting material both lead to higher efficiency, but to different susceptibility.

A4.3 Mathematical Representation of Motor Derating

In this section, the mathematical representation of single-input and multiple-input motor derating functions is discussed.

A4.3.1 Fitting Curve-Based Single-Input Derating Functions

On the basis of the previous results, mathematical functions are proposed to each individual power supply voltage anomaly, similarly to the mathematical equation for motor derating as a function of unbalance proposed by NEMA MG1 [12]. The individual derating functions, *DER*, can be generally described by (A4.27), where *m* is a positive integer, *K_m* is a constant and *x* is the parameter under evaluation (e.g., *VUF*, *HVF*, *VMD*, and *ATD*) [48].

$$DER \approx 1 + \sum_m^n K_m \cdot x^m \quad (\text{A4.27})$$

Equation (A4.29) represents a polynomial fitting curve of order n (or n^{th} degree), which can be applied to the simulated curves for the 3-kW, 4-pole IM, yielding the constants presented in Table A4.9, generated by MATLAB on the basis of the presented TBD curves. This approach results well if only one input variable, one output variable function is considered. It is also possible to represent a function with 2 inputs and 1 output as a surface in a 3-dimension plot, which can be used, for example, to represent derating curves as a function of U_p and U_n or, alternatively, as a function of VMD and VUF .

TABLE A4.9
DERATING POLYNOMIAL FITTING CURVES PARAMETERS FOR THE 3-kW IM [48].

X	n	K_1	K_2	K_3	K_4	K_5
HVF	4	+1.5e-4	-2.5e-4	+3.0e-6	-1.2e-7	--
VUF	5	-1.6e-2	-1.3e-3	-2.7e-5	-2.8e-6	-2.1e-8
VMD	4	+7.6e-3	-2.3e-4	-5e-6	-5.8e-8	--
ATD	2	-1.3e-3	-2.6e-6	--	--	--

However, as was already evidenced, there are many parameters, such as IM power, number of poles, type, etc., interacting and influencing motor derating. This, added to the fact that combined effects should be considered simultaneously in the motor derating, makes this approach complex or impracticable. Therefore, for multi-input derating estimation, a different technique is proposed, described in next section.

A4.3.2 Neural Network-Based Multi-Input Derating Estimation

The studied power supply voltage anomalies are found simultaneously in most cases. Therefore, it is desirable to establish a generalized multi-input derating function. Artificial neural networks (ANNs) can be used for a fair and quick representation of multi-variable function, which inherently relate the interdependency between the considered variables. An ANN can be trained to perform a particular function by adjusting the values of the connections (weights) between elements. Commonly, ANNs are adjusted, or trained, so that a particular input leads to a specific target output. Typically many of such input/target pairs are used to train an ANN. To describe the motor derating as a function of multiple inputs, it is proposed a feed-forward back-propagation ANN, implemented using MATLAB. It is assumed that output is actually a function of all inputs. The preliminary tests led to fair results, considering an ANN with 3 inputs, 4 hidden layers (20-16-12-8-neuron structure), 1 output layer (1-neuron), and tangent-sigmoid (also called hyperbolic tangent) transfer or activate functions. The training process used the gradient descent with momentum and adaptive learning rate back-propagation training function, which updates weight and bias values according to gradient descent momentum and an adaptive learning rate. For the sake of simplicity, the proposed ANN was only tested for the 3-kW motor simulated results,

considering *HVF*, *VUF*, and *VMD* as inputs. It is easy to extend the study to other inputs (e.g. variables related to the motor itself). The training was made considering 25 input-output data sets, and was checked with new 5 input-output simulated results, with a maximum deviation of 1%, proving the suitability of the proposed solution. Of course, the learning process can be made using experimental data instead of simulated data. Further testing and improvements on this solution will be made in the future. Note that, the higher the number of training data sets the reliable the results. Moreover, open training possibility is a great advantage of the proposed solution, being possible to collect experimental data sets all over the world, in order to improve continuously the ANN. After proper training with a wide number of data sets, the final multi-input derating ANN can be released, helping the users to define adequate derating levels for their motors.

A4.4 Motor Efficiency, Torque, Speed and Lifetime Derating

A4.4.1 Torque-Speed Curves, Starting Time and Pulsating Torque

The influence of *HVF*, *VUF* and *VMD* on IM torque-slip curves is presented in Fig. A4.64 for the 3-kW, 4-pole IM and constant temperature (equal to 25°C). From these simulated cases it can be concluded that, *HVF* and *VUF* have negligible impact on motor torque-speed curve, therefore not affecting significantly the starting time (for direct on-line starting). The very slightly reduction is not perceptible in Fig. A4.64. However, it is well known that if *VUF* exceeds 10%-15%, the negative-sequence backward torque can significantly reduce the starting, peak and full-load rated torque, leading to extended starting time, reduced ability to ride through sags, and motor operating at a larger slip [12].

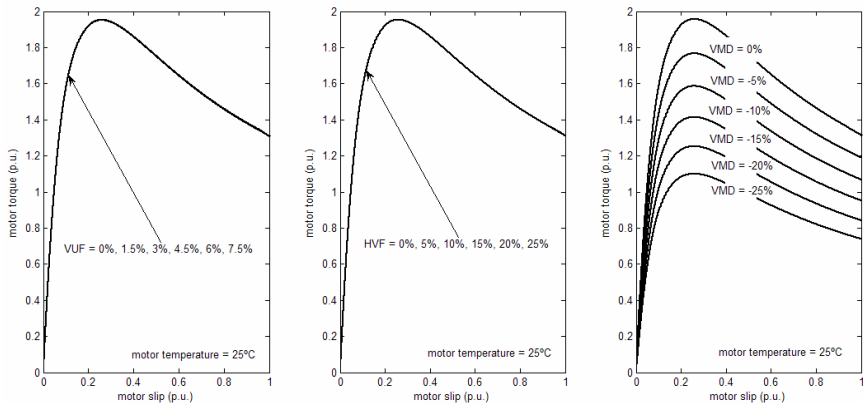


Fig. A4.64. 3-kW, 4-pole IM: influence of *VUF*, *HVF* and *VMD* on average torque-slip curves, considering constant homogenous temperature equal to 25°C.

In contrast, *VMD* has a significant impact, as expected. According to the results, *VMD* is, by far, the most critical parameter during starting, particularly for loads with a significant constant torque component. The shape of the torque-speed curves can also be modified if the rotor temperature changes significantly in the very beginning of the starting period (due to *ATD* and/or internal

temperature increase resulting from previous starts/operation¹⁸) and/or over the starting period up to the thermal equilibrium period (due to *HVF*, *VUF*, and/or *VMD*). These aspects were not taken into account in the presented curves yet, but further investigations are planned.

Regarding pulsating torques, similarly to those resulting from the interaction between time harmonic and fundamental fields, the negative-sequence field interacts with the positive-sequence field producing torque with frequency $\omega_{pulsating} = 2\omega_1$, as previously referred.

It is also important to analyse the effect of VU in the torque ripple since it can reduce the motor and driven equipment (transmission and end-use devices) lifetime, and can affect seriously the process quality.

In Fig. A4.65, the results of a simulation with a 4-kW, 4-pole motor driving a fan-type load are presented. On the basis of Fig. A4.65, it can be concluded that even a *PVUR* as low as 5% leads to a significant increase in the torque ripple magnitude in relation to the normal situation. The negative-sequence voltage causes a torque ripple and a large negative-sequence current [27].

Therefore, for critical process, requiring fixed speed and low oscillations, the power supply voltage balance has to be ensured. If cost-effective, one solution is to feed the IM with a VSD, since oscillations can be strongly reduced. However, a motor efficiency decrease should be expected due to harmonic distortion, as explained in Chapter 3. Another solution is to increase the system inertia, if applicable.

Torque ripple can be particularly dangerous/undesirable if elastic mechanical transmission is used and the resonant frequency of the system is reached. If that does not happen, the elastic transmission can actually damp the torque vibrations, as evidenced next.

The mechanical coupling between the motor and load (or end-use device) can lead to stability problems resulting from the dynamic behaviour of the system. In the case of direct (unitary transmission ratio) rigid transmission or coupling, the Newton equation applies normally, as in (A4.28), where J_{mtr} is the motor inertia, J_{load} is the load inertia, ω_{mtr} is the motor angular speed (in this case, equal to the load angular speed, ω_{load}), T_{em} is the motor electromagnetic torque, T_{load} is the load torque, and the mechanical losses of the motor (friction and windage losses) are ignored [56].

$$(J_{mtr} + J_{load}) \frac{d\omega_{mtr}}{dt} = T_{em} - T_{load} \quad (\text{A4.28})$$

¹⁸ The allowable starting time at cold temperature (ambient temperature) can be up to 2 times longer than the starting time at nominal internal temperature. The allowable starting time with Y/D connection change can be 3 times longer than the direct on-line D-connection starting time.

For an elastic transmission (Fig. A4.66), a difference between the motor speed and end-use device speed occurs.

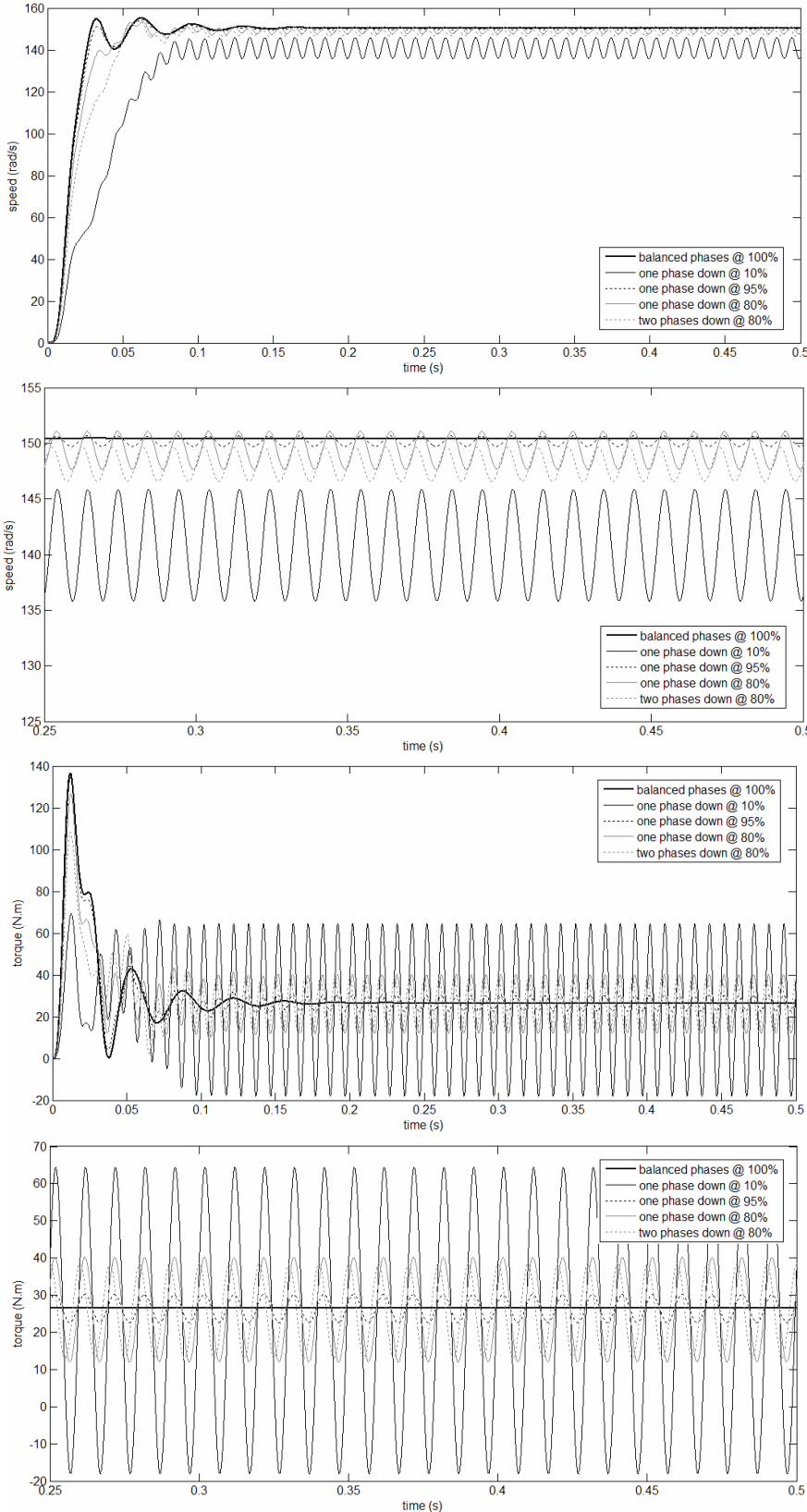


Fig. A4.65. Simulated speed and torque in a 4-kW, 4-pole IM driving a fan-type load ($T_{load} = 0.00115 \cdot \omega^2 + 0.0001$).

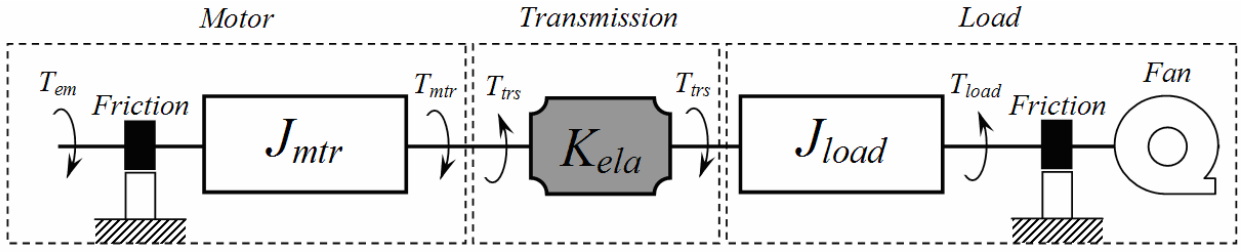


Fig. A4.66. Motor driving system with elastic transmission.

The torsion torque is given by (A4.29), K_{ela} is the elasticity coefficient or constant (the harder the material, the higher the elasticity coefficient), θ_{mtr} the motor shaft angular position, and θ_{load} the load shaft angular position [56]. Ignoring the mechanical losses in the motor, the system model can be described by (A4.30), where T_{mtr} is the motor output torque, T_{trs} is the transmission torque, and the other variables were previously identified [56]. The transfer function relating the speeds and the inertias is given by (A4.31). The transfer function between motor torque and speed is given by (A4.32), where the anti-resonance frequency ω_{arsn} and the resonance frequency ω_{rsn} are defined by (A4.33) and (A4.34).

$$T_{trs} = K_{ela} (\theta_{mtr} - \theta_{load}) \quad (A4.29)$$

$$\frac{d}{dt} \begin{bmatrix} \omega_{mtr} \\ T_{trs} \\ \omega_{load} \end{bmatrix} = \begin{bmatrix} 0 & -J_{mtr}^{-1} & 0 \\ K_{ela} & 0 & -K_{ela} \\ 0 & J_{load}^{-1} & 0 \end{bmatrix} \begin{bmatrix} \omega_{mtr} \\ T_{trs} \\ \omega_{load} \end{bmatrix} + \begin{bmatrix} J_{mtr}^{-1} & 0 \\ 0 & 0 \\ 0 & -J_{load}^{-1} \end{bmatrix} \begin{bmatrix} T_{em} \\ T_{load} \end{bmatrix} \quad (A4.30)$$

$$\omega_{mtr}(s) - \omega_{load}(s) = \frac{s}{s^2 + \omega_{rsn}^2} \left(\frac{T_{em}(s)}{J_{mtr}} + \frac{T_{load}(s)}{J_{load}} \right) \quad (A4.31)$$

$$\frac{\omega_{mtr}(s)}{T_{em}(s)} = \frac{s^2 + \omega_{arsn}^2}{J_{mtr} \cdot s \cdot (s^2 + \omega_{rsn}^2)} \quad (A4.32)$$

$$\omega_{rsn} = \sqrt{K_{ela} \cdot (J_{mtr} + J_{load}) \cdot J_{mtr}^{-1} \cdot J_{load}^{-1}} \quad (A4.33)$$

$$\omega_{arsn} = \sqrt{K_{ela} \cdot J_{load}^{-1}} \quad (A4.34)$$

In order to present the influence of the elasticity coefficient factor and the motor and system inertia on the behaviour of the electric drive, simulations were carried out using a 37-kW, 4-pole, 400-V, 50-Hz IM ($\omega_N = 1480$ r/min, $T_N = 239$ N.m, $J_{mtr} = 0.37$ kg.m², $R_s = 82.33$ m Ω , $R_r = 50.3$ m Ω , $L_s = 0.724$ mH, $L_r = 0.724$ mH, $L_m = 0.02711$ H, $B = 0.02791$ N.m.s/rad), driving a load, considering different inertias ($J_{load} = \{0.5 \cdot J_{mtr}, 2 \cdot J_{mtr}\}$ kg.m²) and elasticity coefficients ($K_{ela} =$

{250, 500, 1000} N.m/rad). The steady-state load torque is defined by $T_{load} = \text{sign}(\omega_{load}) \cdot (0.1 \cdot |\omega_{load}| + 100)$. The simulated motor and load speeds are presented in Figs. A4.67 and A4.68.

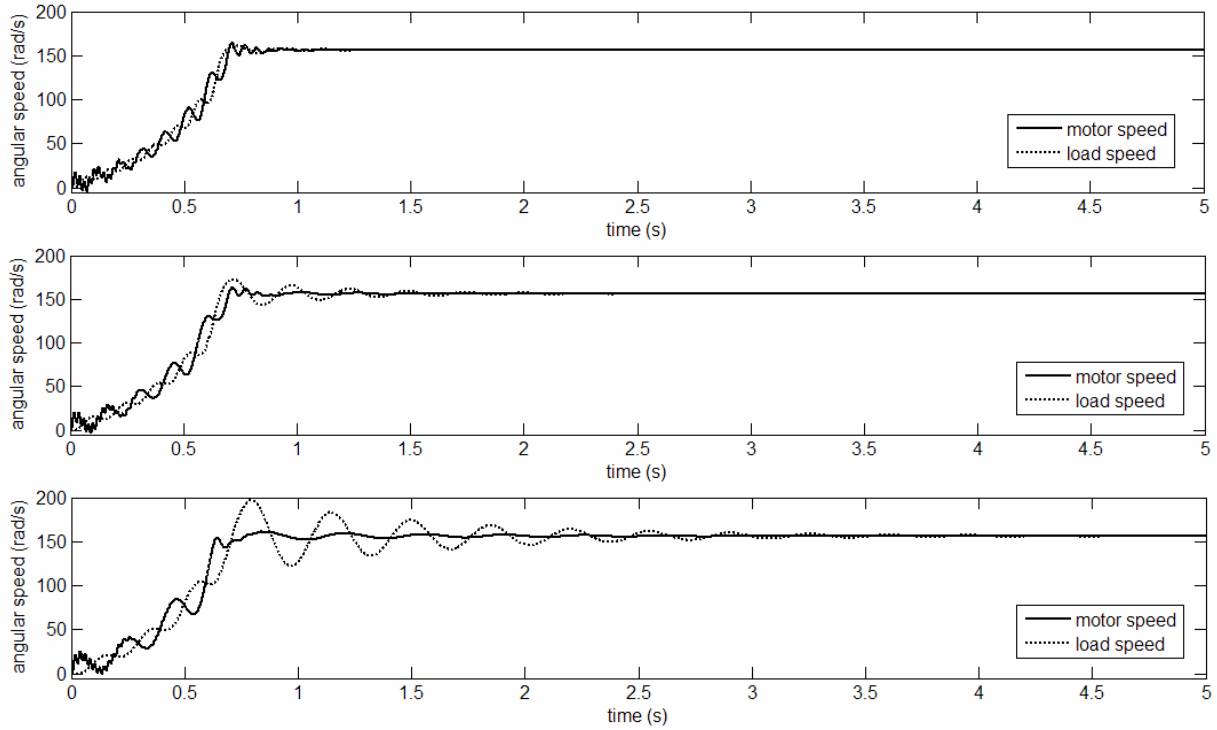


Fig. A4.67. Transient response of an elastic transmission, considering $J_{load} = J_{mtr}/2$ and $T_{load} = \text{sign}(\omega_{load}) \cdot (0.1|\omega_{load}| + 100)$: (top) $K_{ela} = 1000$ N.m/rad; (centre) $K_{ela} = 500$ N.m/rad; and (bottom) $K_{ela} = 250$ N.m/rad.

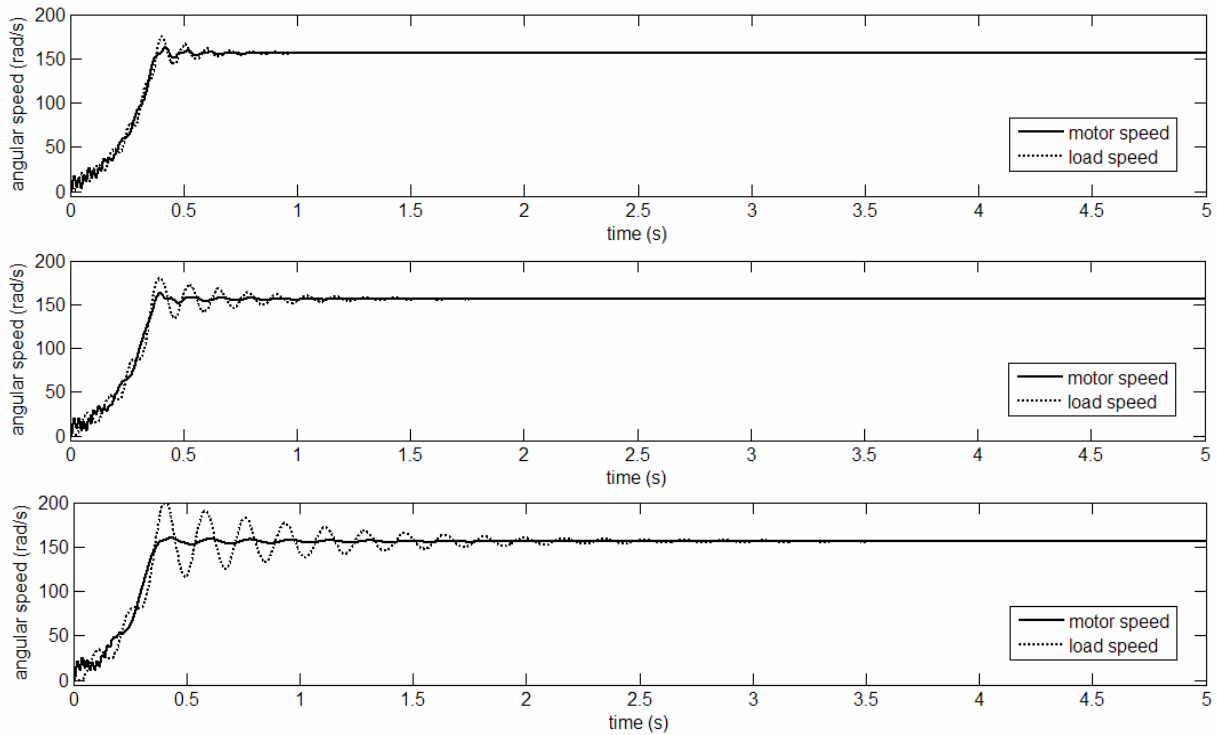


Fig. A4.68. Transient response of an elastic transmission, considering $J_{load} = 2 \cdot J_{mtr}$ and $T_{load} = \text{sign}(\omega_{load}) \cdot (0.1|\omega_{load}| + 100)$: (top) $K_{ela} = 1000$ N.m/rad; (centre) $K_{ela} = 500$ N.m/rad; and (bottom) $K_{ela} = 250$ N.m/rad.

It can be concluded that, for high-inertia loads a proper elasticity constant should be properly chosen to minimize oscillations during starting. High oscillation situation can actually happen, leading to extra mechanical wear of the load, motor and transmission itself, as well as to significant oscillations in the motor current and voltage. Therefore, for duty cycles with a high start/stop cycling rate and using belts or flexible direct coupling, a careful study on the mechanical transits should be done, in order to reduce mechanical wear of both load and motor shafts and bearings, as well as to avoid tripping of motor protection devices.

Another important issue is the behaviour of motor-load systems with elastic transmission when the motor is being fed by an unbalance voltage supply system. Figs. A4.69-A4.75 show the simulated results considering a balanced supply system scenario and a 20% decrease in one phase-to-ground voltage scenario, for different K_{ela} . It should be noted that, in those figures, the presented motor torque is the electromagnetic torque. More results are presented in Appendix 6. It is possible to observe the extended starting period, in the presence of voltage unbalance.

It can be concluded that, the elastic transmission can act as a low-pass filter, filtering the undesirable torque oscillations, which is an advantage, particularly in the presence of voltage unbalance since a higher torque ripple oscillation occurs in the motor.

However, speed oscillations during starting can be amplified in the motor side and the transient period extended, which can significantly increase the mechanical stress in the belt (for example) and in the motor. This is particular critical in the presence of voltage unbalance, which, even resulting of a small decrease of the voltage in one phase, can amplify the oscillations and, in some critical cases, extend significantly the starting period.

The low-pass filter behaviour of elastic transmission can be also an advantage in blocking the propagation of vibrations from the load to the motor. In the case of the belts, tension can actually influence the dynamic response of the system since the elastic constant is dependent upon that parameter.

Therefore, it is important to use a mechanical transmission system with the proper elasticity coefficient, particularly if voltage unbalance is likely to occur in the power network.

In Figs. A4.70, A4.73, and A4.75, it is possible to observe the current unbalance resulting from the voltage unbalance, leading to thermal asymmetries and loss increase in the motor.

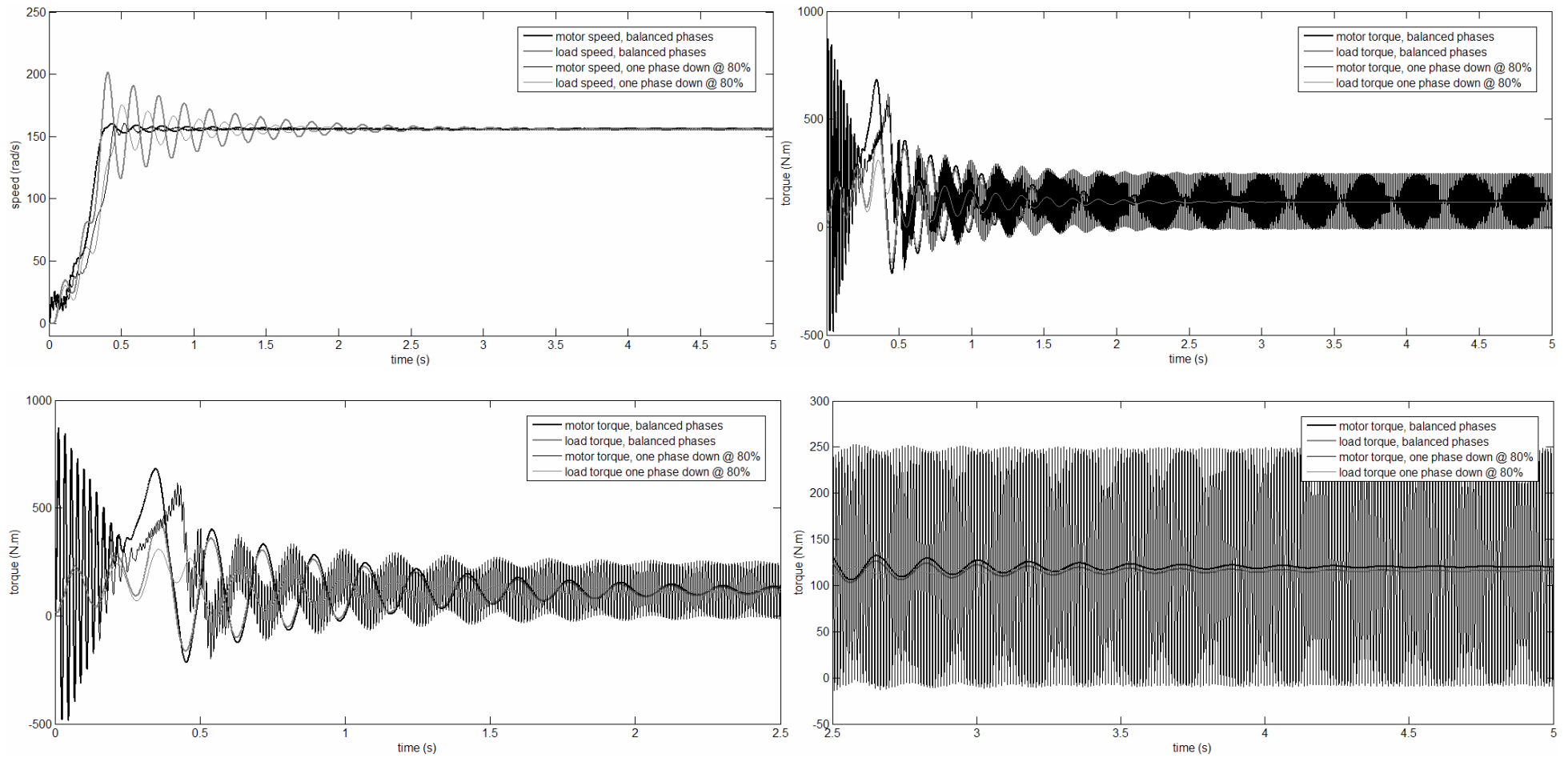


Fig. A4.69. Transient response (speed and torque) of an elastic transmission, considering $J_{load} = 0.5 \cdot J_{mr}$, $K_{ela} = 250$ N.m/rad, and $T_{load} = \text{sign}(\omega_{load}) \cdot (0.1|\omega_{load}| + 100)$ N.m (bottom figures show a zoom of the top-right figure).

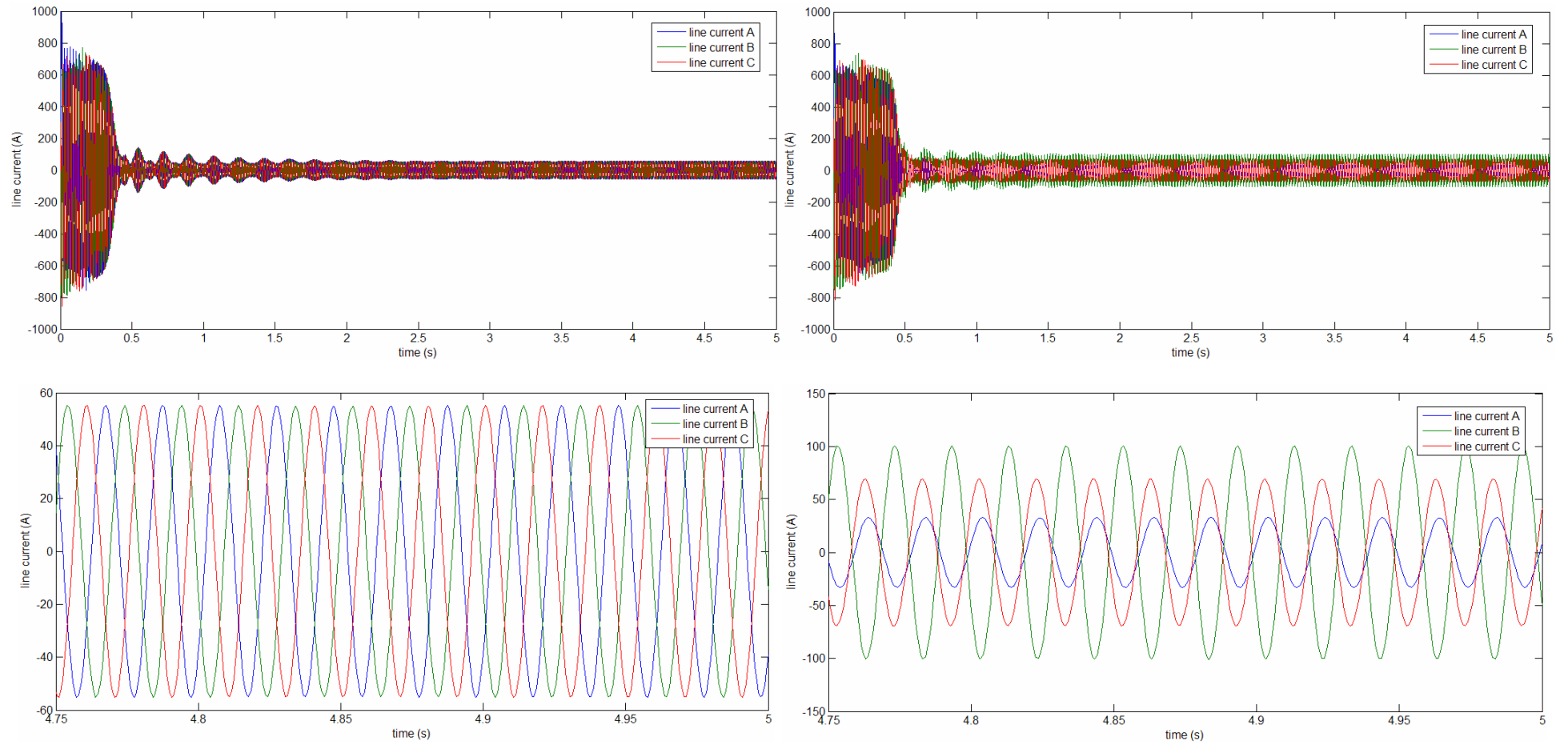


Fig. A4.70. Line currents during transient response of an elastic transmission, considering $J_{load} = 0.5 \cdot J_{mtr}$, $K_{ela} = 250$ N.m/rad, and $T_{load} = \text{sign}(\omega_{load}) \cdot (0.1|\omega_{load}| + 100)$ N.m: (top left) balanced phases; (top right) unbalanced phases; (bottom left) zoom for balanced phases; (bottom right) zoom for unbalanced phases.

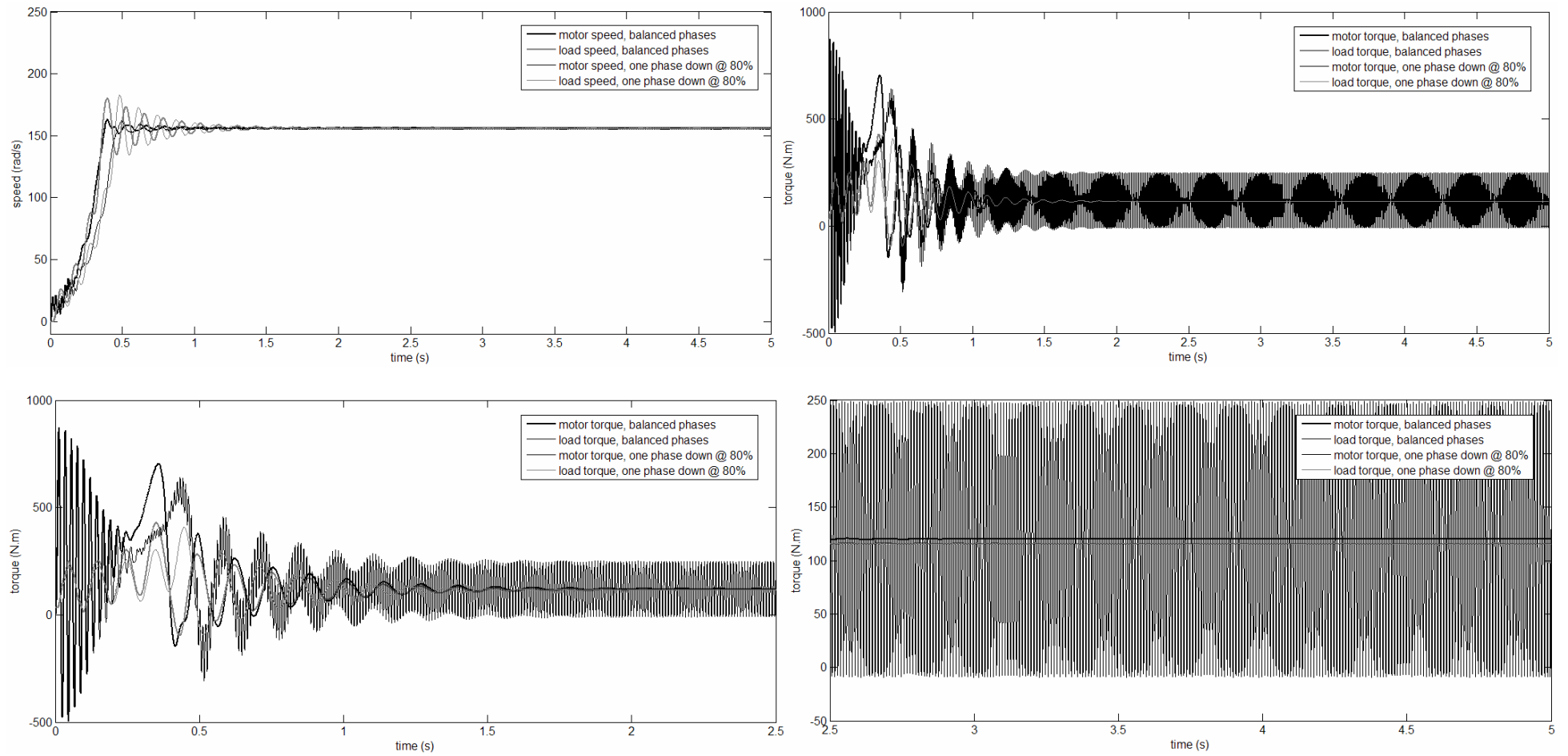


Fig. A4.71. Transient response (speed and torque) of an elastic transmission, considering $J_{load} = 0.5 \cdot J_{mvr}$, $K_{ela} = 500$ N.m/rad, and $T_{load} = \text{sign}(\omega_{load}) \cdot (0.1|\omega_{load}| + 100)$ N.m (bottom figures show a zoom of the top-right figure).

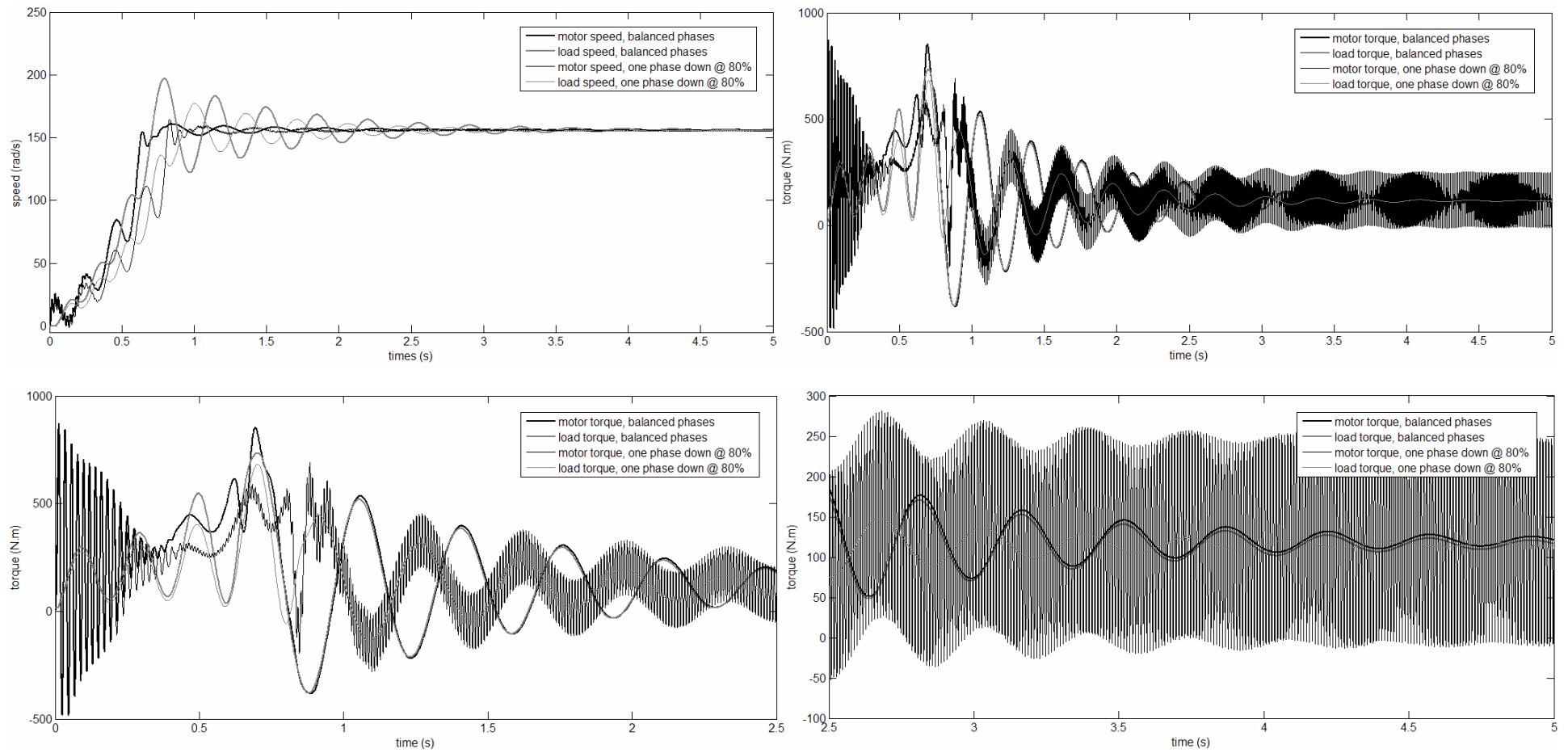


Fig. A4.72. Transient response (speed and torque) of an elastic transmission, considering $J_{load} = 2 \cdot J_{mtr}$, $K_{ela} = 250$ N.m/rad, and $T_{load} = \text{sign}(\omega_{load}) \cdot (0.1|\omega_{load}| + 100)$ N.m (bottom figures show a zoom of the top-right figure).

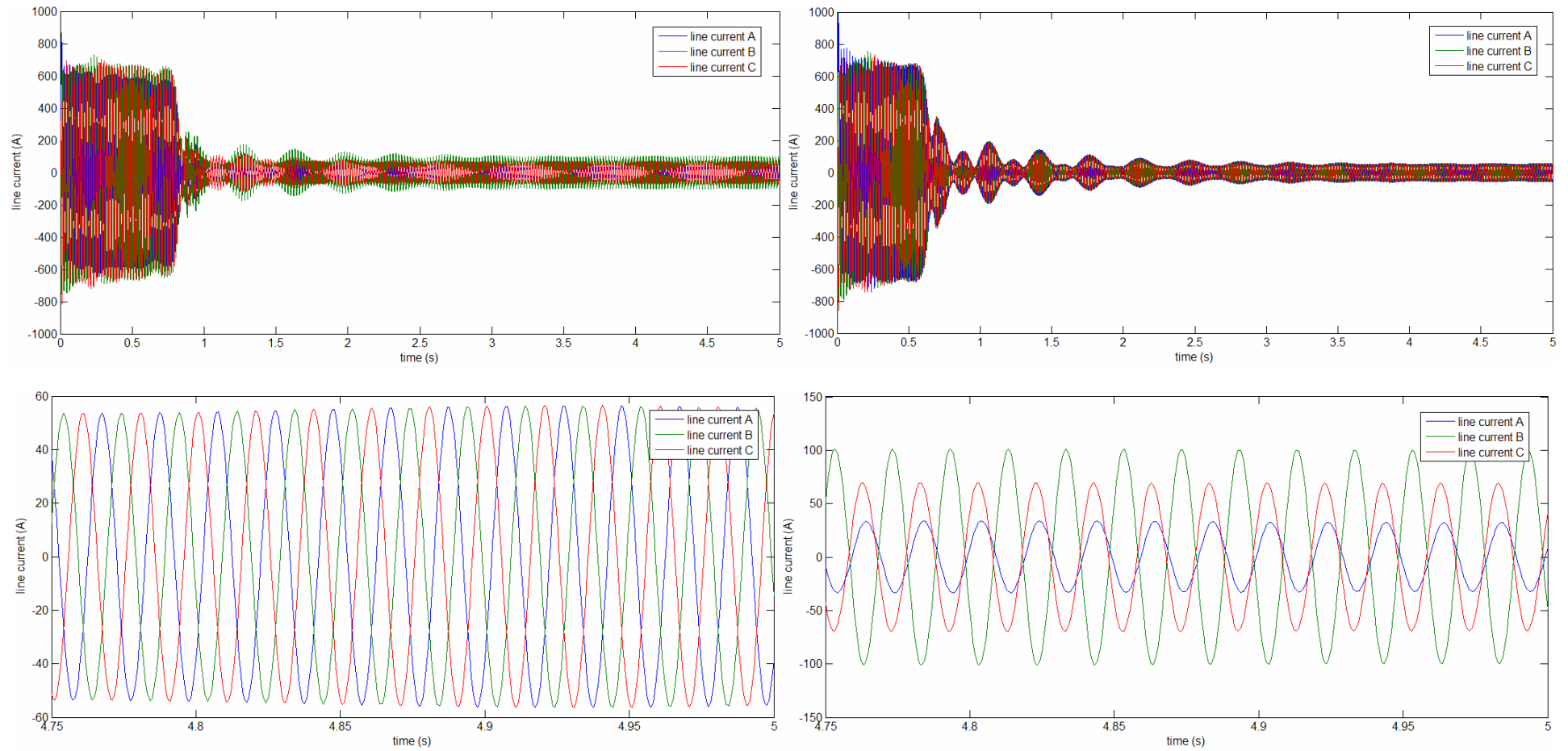


Fig. A4.73. Line currents during transient response of an elastic transmission, considering $J_{load} = 2 \cdot J_{mtr}$, $K_{ela} = 250$ N.m/rad, and $T_{load} = \text{sign}(\omega_{load}) \cdot (0.1|\omega_{load}| + 100)$ N.m: (top left) balanced phases; (top right) unbalanced phases; (bottom left) zoom for balanced phases; (bottom right) zoom for unbalanced phases.

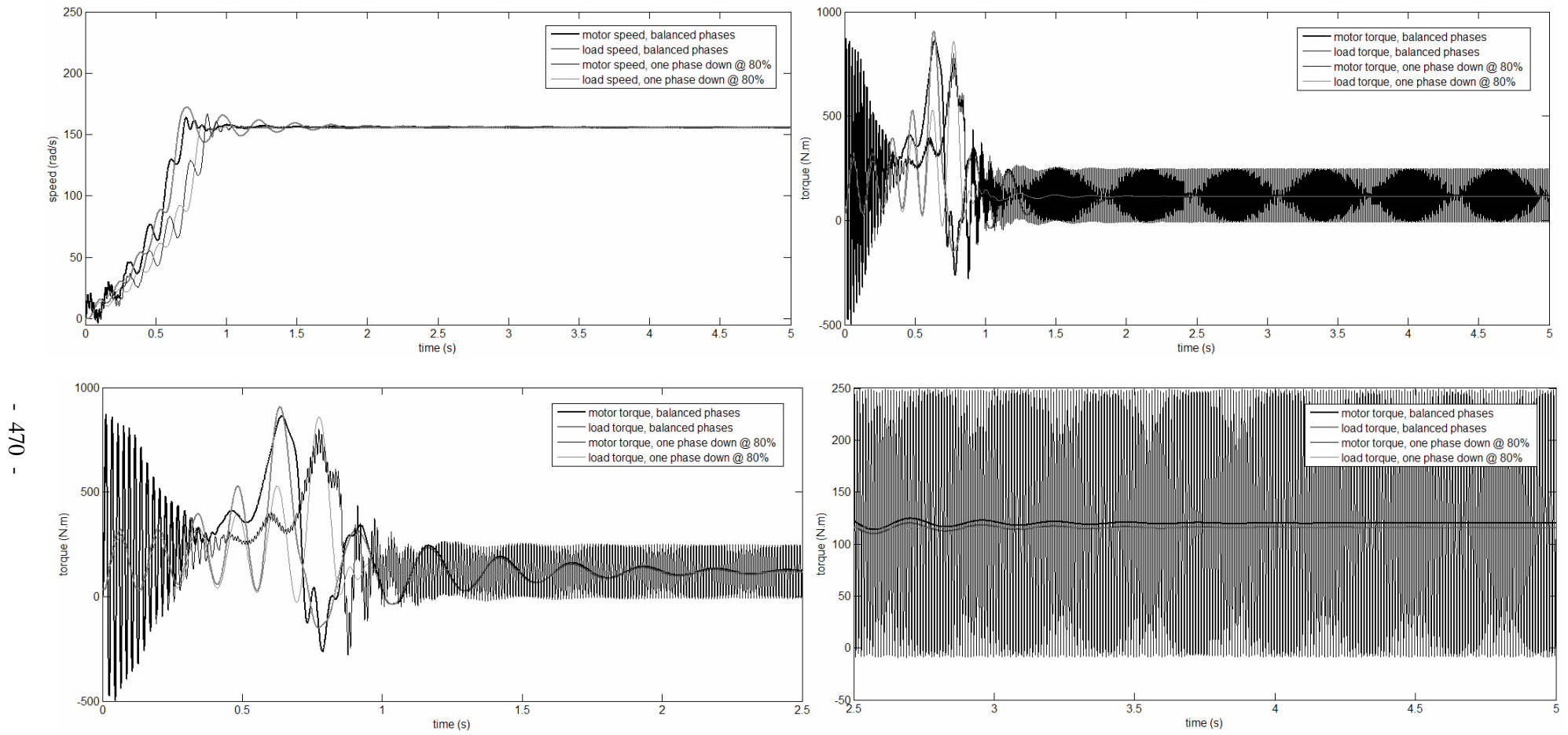


Fig. A4.74. Transient response (speed and torque) of an elastic transmission, considering $J_{load} = 2 \cdot J_{mtr}$, $K_{ela} = 500$ N.m/rad, and $T_{load} = \text{sign}(\omega_{load}) \cdot (0.1|\omega_{load}| + 100)$ N.m (bottom figures show a zoom of the top-right figure).

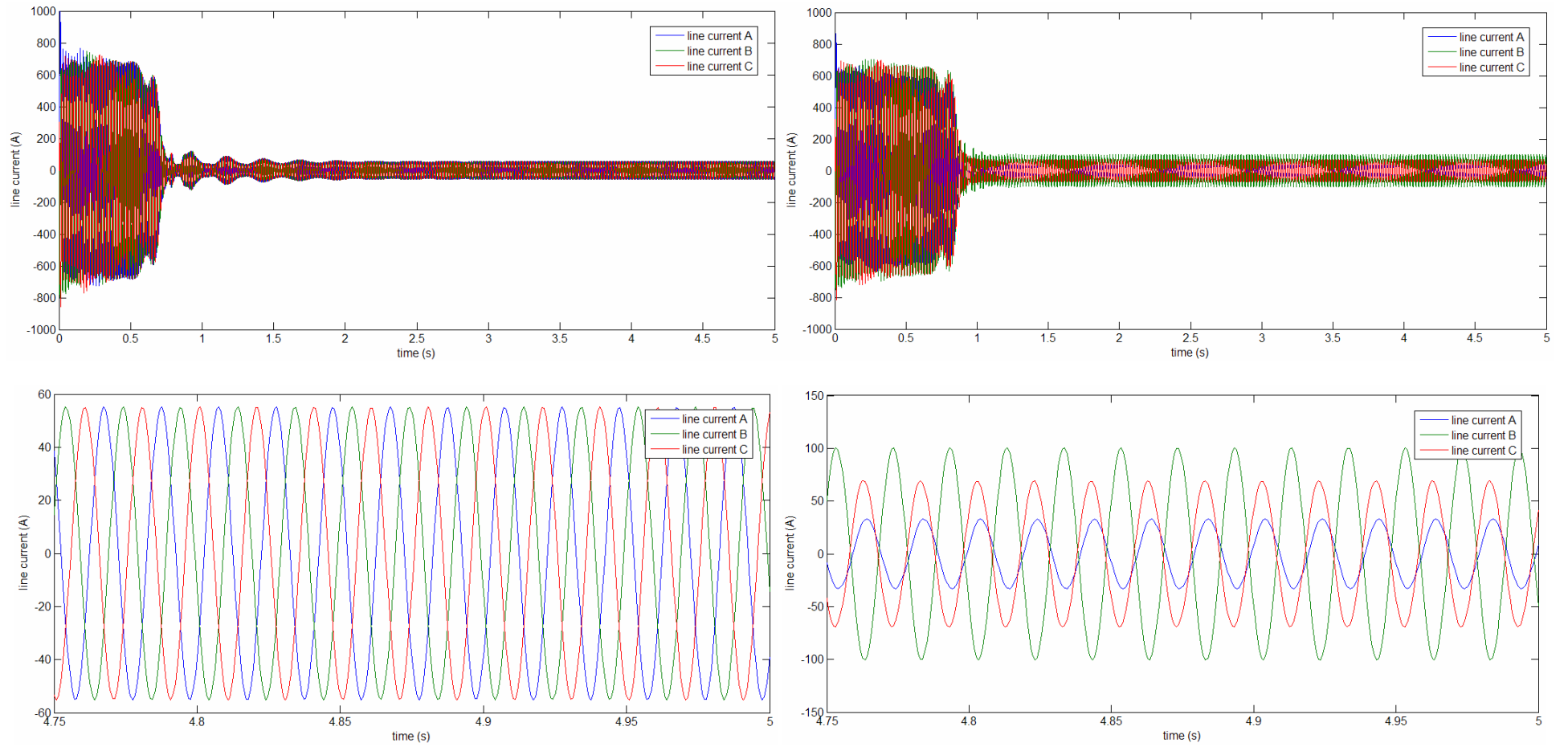


Fig. A4.75. Line currents during transient response of an elastic transmission, considering $J_{load} = 2 \cdot J_{mtr}$, $K_{ela} = 500$ N.m/rad, and $T_{load} = \text{sign}(\omega_{load}) \cdot (0.1|\omega_{load}| + 100)$ N.m: (top left) balanced phases; (top right) unbalanced phases; (bottom left) zoom for balanced phases; (bottom right) zoom for unbalanced phases.

A4.4.2 Motor Efficiency and Speed Derating

Part of the simulated results on motor speed and efficiency derating is presented in Figs. A4.76 and A4.77. Simulations demonstrate that, for example, motor speed derating is practically negligible as a function of *HVF*, *VUF* and *ATD* (considering typical values found in industrial plants).

As expected, the *ATD* has a significant impact on motor efficiency, particularly for motor operating near full load (Fig. A4.76).

However, the effect of *VMD* is considerable (see Fig. A4.76), showing its importance in the motor operating point. The type of rotor influences significantly the effects of *VMD*, *HVF* and *VUF* on motor operating point. On the basis of Fig. A4.76, it is possible to conclude that low-resistance copper-bar rotors lead to higher immunity to *HVF*, *VUF*, and *VMD*, in terms of power and speed derating. Moreover, the lower the number of poles and the higher the rated power, the higher the immunity to negative *VMD*.

Regarding motor efficiency derating, it is possible to conclude that the lower the number of poles and the higher the power rating, the lower the immunity to *HVF*, and the higher the immunity to *VUF*. Motor efficiency derating as a function of *VMD* depends strongly on the motor efficiency-load curve shape and load. The experimental results shown in Fig. A4.78 evidence that motor power efficiency and speed derating, as well as power factor increase with the U_p decrease, as expected. Moreover, comparing Figs. A4.78 and A4.63, it is possible to confirm that loss-based derating actually underestimates the actual derating.

From Fig. A4.79 and (A4.1), the lifetime expectancy as a function of *VUF* and *HVF* can be estimated for the 3-kW IM. For example, a $VUF = 3\%$ leads to a temperature increase of $\approx 10\%$, which can be translated into a lifetime reduction of about 50% (considering 100°C as the nominal stator winding temperature). The lifetime reduction is similar for $HVF = 15\%$. In [3], similar estimations were made, but significant discrepancies exist for both results. Nevertheless, both results allow to conclude that *VUF* affects severely motor lifetime if proper power derating is not made.

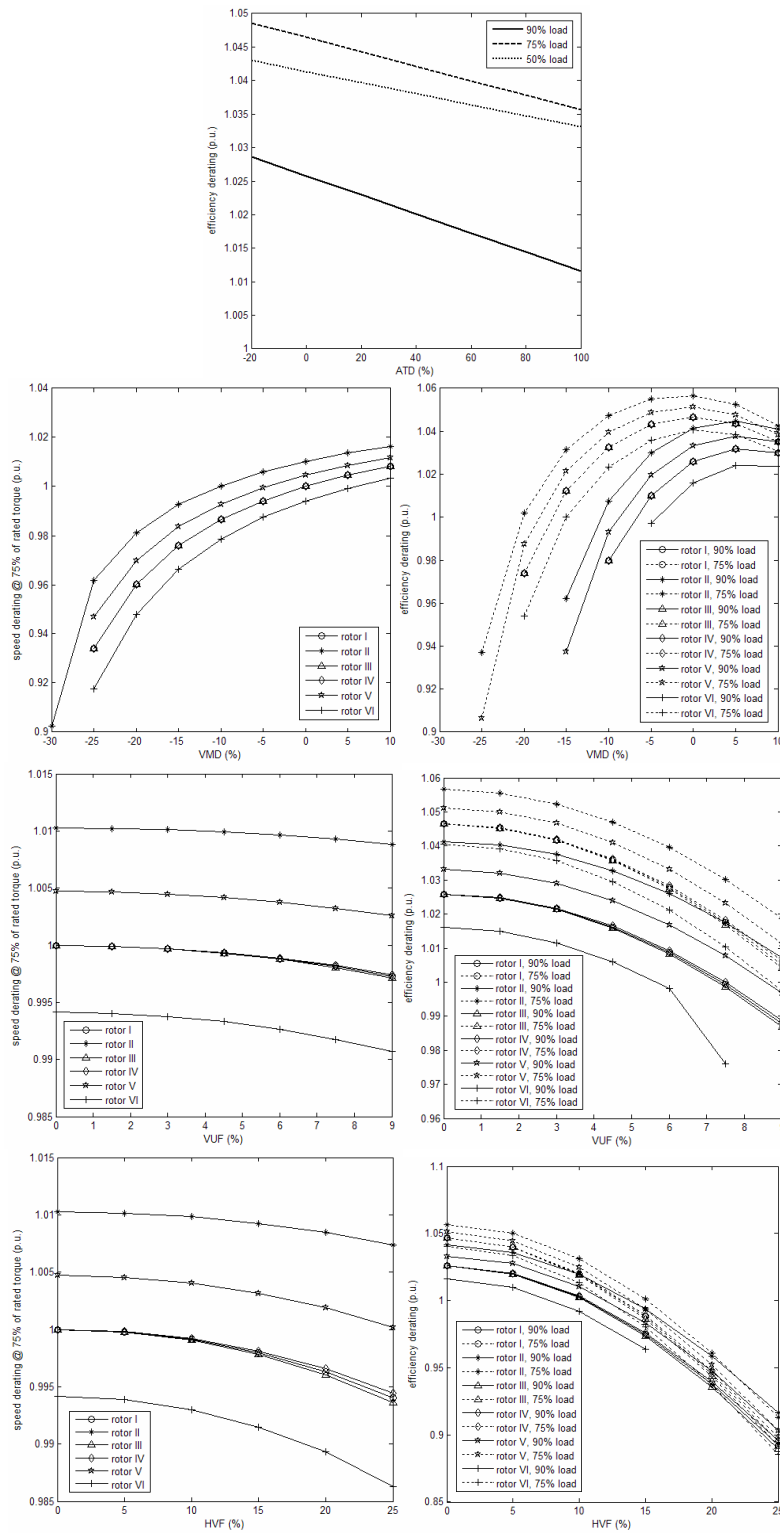


Fig. A4.76. 3-kW, 4-pole IM: simulated efficiency and speed derating as a function of *VMD*, *VUF*, *HVF*, and *ATD*, considering different rotor types.

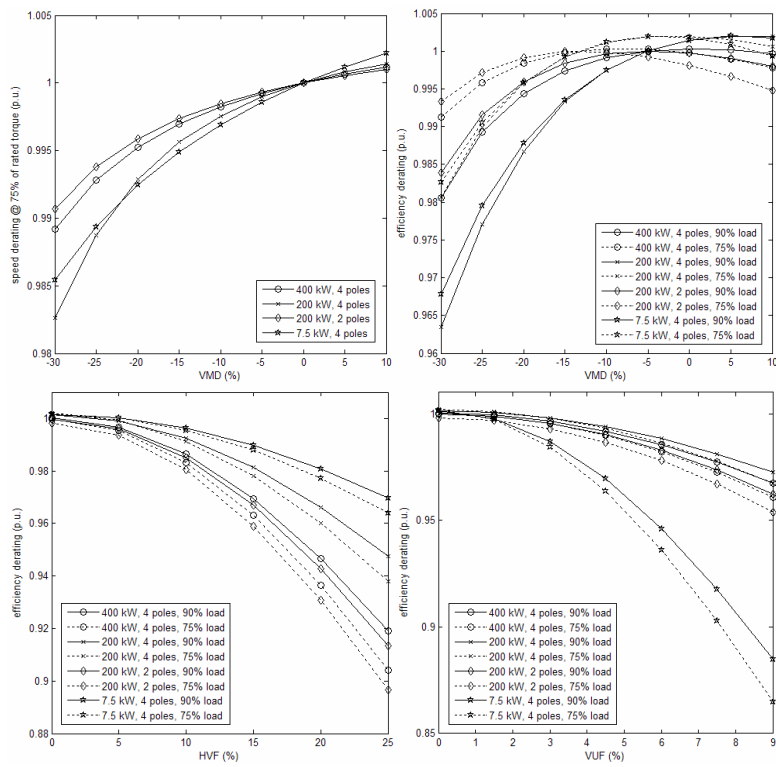


Fig. A4.77. 400-kW, 200-kW, 7.5-kW IMs: simulated speed and efficiency derating as a function of VMD, VUF and HVF, considering different rotor types.

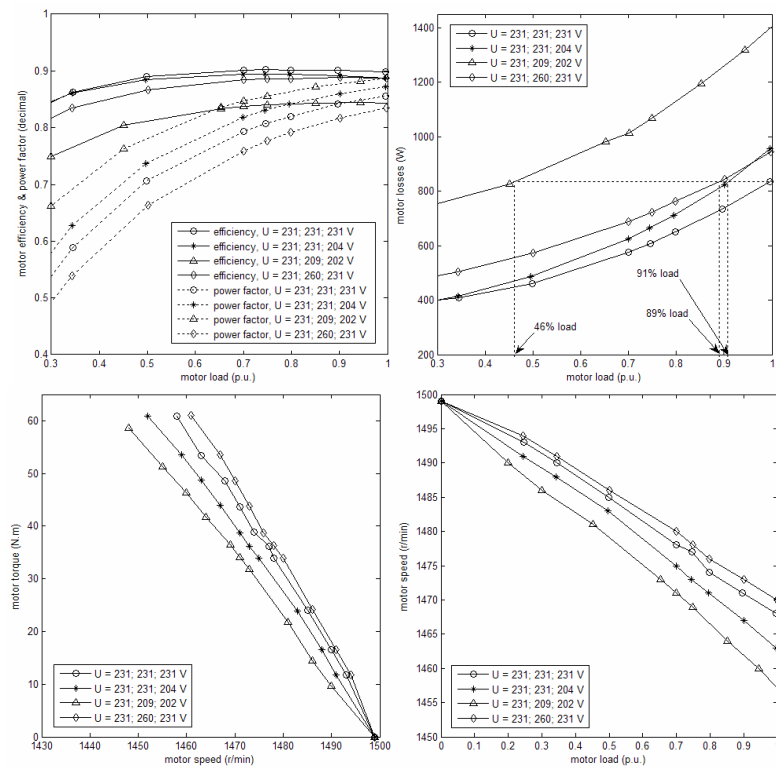


Fig. A4.78. 7.5-kW, 4-pole IM: experimental steady-state motor efficiency, power factor, losses, torque, and speed, under voltage unbalance conditions.

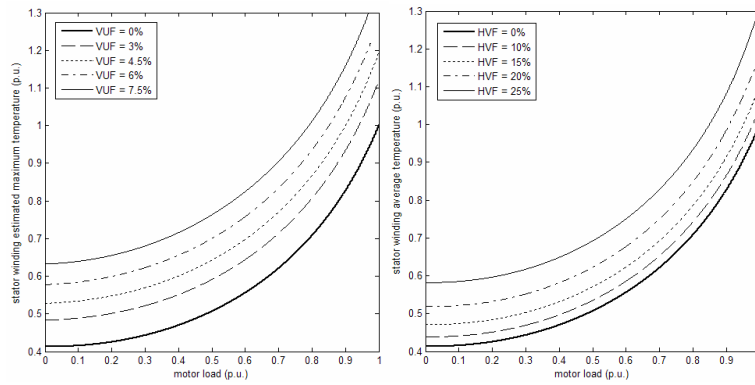


Fig. A4.79. 3-kW IM: simulated stator winding temperature as a function of motor load, considering different values of *VUF* and *HVF*.

A4.5 Effective or Thermal Motor Load

The foregoing relations can be used to find the approximate actual percentage motor load under various unbalanced conditions. In other words, the power derating necessary to hold the motor rated temperature rise can be approximately determined (this is an important issue in the scope of the Chapter 4). NEMA has also addressed this problem empirically by conducting tests on a number of motors, resulting the derating curve given in Fig. A4.9. For example, at 5% *LVUR*, the motor should not operate at more than 75-77% of its rated output, which becomes the equivalent or effective motor full load for the given power supply conditions. On the basis of the derating value, effective motor load, ζ_{eff} , can be defined as in (A4.35), where ζ is the actual motor load (determined on the basis of mechanical and/or electrical quantities¹⁹, as described in Chapter 4) and a 1.0 service factor is assumed.

$$\zeta_{eff} = \zeta \cdot DER^{-1} \quad (A4.35)$$

This is a very effective measure of the thermal loading of the motor subjected to power supply voltage anomalies. An ζ_{eff} larger than one identifies a motor that is running beyond its thermal limit, granted that ambient temperature and cooling conditions are normal.

A4.6 Impact of Sags on IMs

Despite the growing use of VSDs, the majority of IMs are still directly fed, i.e., the motor terminals are connected to a fixed-frequency, constant-voltage, power supply. Directly line-fed IMs are rather insensitive to short-duration voltage sags, although problems could occur when too many motors are fed from the same bus. The drop in terminal voltage will cause a drop in motor torque. Due to this drop in torque the motor will slow down until it reaches a new operating point. If the terminal voltage drops too much over a significant period, the load torque will be higher than

¹⁹ If the motor load is estimated on the basis of the average stator winding or frame temperatures (comparison between actual and rated conditions), the obtained value is the effective motor load, with the derating factor included.

the pull-out torque and the motor will continue to slow down. An IM is typically operated at half of its pull-out torque, which is approximately proportional to the square of the voltage (assuming fixed frequency, and a balanced three-phase system). A voltage drop to 70% or less leads only to a slight change in the stable operating point of the IM. The drop in speed is seldom a serious concern for directly fed IMs. Most line-fed IMs are used in processes that are not very sensitive to speed variations, and the speed variation is seldom more than 10%. Although IMs are normally rather insensitive to voltage sags, there are a few phenomena that could lead to process interruption due to a sag.

Deep sags lead to severe torque oscillations at sag commencement and when the voltage recovers. These could lead to damage to the motor and to process interruptions. The recovery torque becomes more severe when the internal flux is out of phase with supply voltage, thus when the sag is associated with a phase-angle jump [27].

Regarding IM influence on voltage three-phase drops in magnitude, the magnetic flux in the air-gap is no longer in balance with stator voltage. The magnetizing flux decays with a time constant of up to several cycles. During this decay the IM contributes to the fault and somewhat keeps up the voltage at the motor terminals. The decay in voltage causes a drop in electromagnetic torque. The result is that the IM slows down, taking a larger current (to the larger slip). This could bring down the voltage even more [27]. For small voltage drops, a new steady state could be reached at a lower speed, depending on the speed-torque behaviour of the mechanical load. For deep sags the motor will continue to slow down until it reached standstill, or until the voltage recovers, whichever comes first. The mechanical time constant of electrical motors is of the order of one second or more. Therefore the motor will normally not have reached zero speed yet upon voltage recovery. The moment the voltage recovers the opposite phenomena occur. The flux in the air-gap will build up again (electrical inrush). This causes a large inrush current, which slows down the voltage recovery. After that, the motor will re-accelerate until it reaches its pre-event speed (mechanical inrush). During the re-acceleration, the motor again takes a larger current with a smaller power factor, which can cause a post-fault voltage sag sometimes lasting for one to several seconds [27]. This can lead to tripping of undervoltage and overcurrent relays. This problem is more severe for a weak supply, and can become a problem when the motor load increases. The per-phase contribution of the IM load to the fault can be modelled as a voltage source behind reactance (ignoring the resistance). The voltage source has a value of about 1 p.u. at fault initiation and decays with the subtransient time-constant (between 0.5 and 2 cycles). The reactance is the leakage reactance of the motor, which is between 10% and 20% on the motor base. Note this is not the leakage reactance, which determines the starting current, but the leakage reactance at nominal speed. For double-cage rotor IMs these two can be significantly different.

The mechanical time constant of an IM plus load is typically in the range of 1 to 10 seconds [27]. With dead times of several seconds, the motor has not yet come to a standstill but is likely to have slowed down significantly. This reduction in the speed of the motors might disrupt the industrial process so much that the process control trips it. The motor can reaccelerate hence the voltage comes back, if the system is strong enough. For public distribution systems re-acceleration is seldom a problem. Also, the setting of the undervoltage protection should be such that it does not trip before the voltage comes back. This calls for coordination between the undervoltage setting of the motor protection and the reclose interval setting on the utility feeder. IMs fed via contactors are disconnected automatically as the contactor drops out. Without countermeasures this would always lead to loss of the load. In some industrial processes IMs are automatically reconnected when the voltage comes back: either instantaneously or staged (the most important motors first, the rest later).

Regarding IM under unbalance faults (e.g., single phase-to-ground fault), it can be said that, during the first one or two cycles after fault initiation the IM fields into the fault [27], raising the U_p value. In practice, negative-sequence voltage is not influenced. The IM slows down, causing a decrease in positive-sequence impedance (due to the slip increase). This decrease in impedance causes an increase in the drawn I_p and, therefore, a drop in the U_p . The negative-sequence impedance of the motor is low, typically 10-20% of the nominal positive-sequence impedance, and approximately independent of the slip. The U_p value due to the fault will thus be significantly damped at the motor terminals, and remain approximately constant during the event. When voltage recovers, the air-gap field has to be built up again. In weaker systems this can last up to 100 ms, during which the motor continues to slow down. This could be a problem in systems where the IMs are the dominant load or the motor load has grown over the years. In the last case, if in the past a voltage sag would not be a problem, the process can suddenly no longer withstand the rotor speed drop due to a sag. Fortunately, as referred, deep sags are rare.

In [51] and [52], the voltage dips/sags during 8 months were monitored in some facilities. Approximately 93% of them last less than 500 ms, and 87% last less than 250 ms. In general, the vast majority was concentrated around 100-ms duration. Regarding the voltage level, 89.18% reach an extreme value of 80% of rated voltage, but the vast majority is concentrated around 80%. A mix of situations was found, namely, one-, two-, or three-phase undervoltages or dips.

A4.7 Impact of Voltage Sags and Continuous Unbalance on VSDs

In general, most VSDs are very sensitive to short interruptions and to voltage sags. They normally trip well within 1 second, sometimes even within one cycle. Therefore, even the shortest interruption will cause a loss of the load.

VSD tripping can occur due to several factors, namely, when VSD controller or protection detect a change in operation conditions and trip the drive to prevent damage to the power electronic components, when DC-bus voltage drop resulting from the sag causes maloperation or tripping of the drive controller, when the increased AC currents during the sag or the post-sag overcurrents charging the DC-bus capacitor will cause an overcurrent trip or blowing of fuses protecting the power electronics components, and when the process driven by the motor will not be able to tolerate the drop in speed or the torque variations due to the sag.

After a trip, some modern VSDs restart automatically immediately the moment the voltage comes back, or after a certain delay time. Others require a manual restart. The various automatic restart options are only relevant when the process tolerates a certain level of speed and torque variations.

In fact, being disconnected from the supply for several seconds will often disrupt the process behind the drive so much that reconnection does not make much sense anymore.

Caution has to be taken when changing minimum tolerated DC-bus voltage since, when the voltage back to normal values, the overcurrents charging the DC-bus capacitor can be high enough to damage the rectifier diodes. In these situations can be preferable to stop the VSD and restart it with a current limiting resistor in the DC link. Additionally it is preferable to use fast response fuses rather than protection circuit breakers, since the latter devices have, in general, a slower time response, not fast enough to avoid diode damage.

Voltage tolerance in most VSDs can be as sensitive as 80-85% of rated voltage for less than six cycles. However it is possible that a large fraction of the VSDs are not sensitive to sags at all. In general, the lower the rated power, the higher the tolerance to a sag.

In Table A4.10, a summary of a number of experimental data reported in [28] and [29] can be seen. It is possible to conclude that very short interruptions (0% of the input line-to-line voltage during up to 33 ms) can be handled by almost all 2.2-kW VSDs and by a large part of the 15-kW VSDs. However, VSDs can have severe difficulties with sags during 100 ms or more, especially if a slightly decrease in the motor speed means a serious disruption of sensitive mechanical processes.

In fact, VSDs trip if the DC-bus voltage crosses a preset lower limit. The trip or malfunction can be due to the inverter controller not operating properly when the voltage gets too low, but it can also be due to the intervention of undervoltage equipment protection connected to the DC bus. Most likely, the protection will intervene before any equipment malfunction occurs. The DC-bus capacitance has only limited energy content (relative to the power consumption of the motor) and will not be able to supply the load much longer than a few cycles. An improved voltage tolerance of VSDs can be achieved by lowering the setting of the undervoltage protection of DC bus.

However the protection should trip before any malfunctions occur and before components are damaged. Not only the undervoltage is a potential source of damage itself, but also the consequent overcurrent when the AC voltage recovers, being the undervoltage protection critical in these situations to avoid damages in the power electronic devices.

TABLE A4.10
RESULTS OF EXPERIMENTAL VOLTAGE-TOLERANCE TESTING OF VSDs FEEDING VSDs [28], [29].

Applied Balanced Sag			Motor Speed Behaviour for a VSD due to a Voltage Sag		
Voltage Value (%)	Duration (ms)	No. of VSDs tested	Type I – Slight Drop in Speed Motor maintains or decreases slightly the speed, followed by a recovery	Type II – Automatic Restart Motor stops, followed by an automatic restart, back to nominal speed	Type III – Manual Restart Motor stops and the drive is unable to restart the motor.
0	33	23 ^{a)}	4×15 kW & 12×2.2 kW, 69.6%	1×15 kW, 8.7%	5×15 kW, 21.7%
50	100	40 ^{b)}	3×2.2 kW & 3×(?) kW, 15%	4×15 kW & 5×2.2 kW & 9×(?) kW, 45%	7×15 kW & 4×2.2 kW & 5×(?) kW, 40%
70	170	17 ^{c)}	12, 70.6%	5, 29.4%	0, 0%
70	1000	23 ^{a)}	1×2.2 kW, 4.3%	5×15 kW & 7×2.2 kW, 52.2%	6×15 kW & 4×2.2 kW, 43.5%

Notes: ^{a)} 11×15-kW & 12×2.2-kW VSDs; ^{b)} 11×15-kW & 12×2.2-kW VSDs & 17 VSDs with unreported power; ^{c)} 17×VSDs with unreported power.

The DC-bus voltage for VSDs during a three-phase sag behaves as follows. Considering a VSD providing a power $P_{vsd(out)}$, to a motor, a nominal DC-bus voltage U_{DC0} ²⁰, and capacitance C_{DC} connected to the DC-bus, we can use (A4.36) to calculate the initial decay of the DC-bus voltage during the sag [27], assuming DC-bus voltage at sag initiation equal the nominal voltage, as well as constant power load (thus, the energy $W_{vsd(out)} = P_{vsd(out)} \cdot t$), which is only an approximation, since in reality it does not occur. However, for a first approach, it can be assumed that constant power load, i.e., the motor does not notice anything from the sag. Therefore, the $P_{vsd(out)}$ is assumed to be independent of the U_{DC} .

$$u_{DC}(t) = \sqrt{U_{DC0}^2 - \frac{2P_{vsd(out)}}{C_{DC}}t} \quad (A4.36)$$

If the increase in inverter loss (related to the higher currents) due to the reduction of the DC-bus voltage is also neglected, a constant power condition is assumed, corresponding to an ideal inverter (no voltage drops in the inverter and no increase in losses during the sag). Therefore, the higher the load is, the lower the duration of the tolerance period will be.

VSDs trip either due to an active intervention by the undervoltage protection (which is the most common situation), or by a malfunction of the inverter controller. In both cases the trip occurs when the DC-bus voltage reaches a certain value $U_{DC(min)}$. As long as the AC voltage does not drop below this value, the drive will not trip. For sags below this value, (A4.37) can be used to calculate

²⁰ DC-bus voltage actually depends on a number of factors, e.g., input voltage level, load level, and DC-bus capacitance.

the time it takes for the DC-bus voltage to reach the value $U_{DC(\min)}$, being directly proportional to the DC-bus capacity.

$$t_{trip} = \frac{C_{DC}}{2P_{vsd(out)}} (U_{DC0}^2 - U_{DC(\min)}^2) \quad (\text{A4.37})$$

For example, considering the commercial VSDs tested in Chapter 3, feeding a 3-kW motor at full load, the VSD output power is about 3.6 kW. The overall capacitance of the DC-bus for the 2-level inverter is 253 μF and for the 3-level inverter is 450 μF . Assuming that the tripping voltage is 85% of U_{DC0} , ($U_{DC(\min)} \approx 480 \text{ V}$) the tolerated duration of a sag capable of dropping U_{DC} to such levels is 3.1 ms and 5.5 ms for the 2-level and 3-level inverters, respectively. Supposing that it is possible to reduce the setting of the DC-bus undervoltage protection to 70%, the duration would be 5.7 ms and 10.1 ms, respectively. This is by far ineffective for common sags, lasting 100-150 ms. The amount of capacitance connected to the DC-bus of modern VSDs in the 2-5 kW range is typically between 125 μF and 450 μF . Therefore, the voltage tolerance can be increased significantly by simultaneously increasing the C_{DC} (e.g., using super- or ultra-capacitors) and by reducing $U_{DC(\min)}$.

However, in most applications, the system has a significant inertia (load plus motor inertia), leading to a reduction in the $P_{vsd(out)}$, being most of the mechanical energy required by the system over the sag period provided by the kinetic energy stored in the system. Therefore, the inverter can block the output to avoid DC-bus voltage decrease or maintain zero slip by reducing progressively the frequency as the motor decelerates.

Moreover, the PWM pulses amplitude will be affected by the DC-bus voltage, roughly leading to a direct decrease of the RMS value for the same m_a , considering PWM generation without any compensation as a function of the output RMS voltage. This leads to the increase of the motor slip, and to a decrease of the motor output power, which actually can extend the duration of the tolerated period, in a quantity depending on the load type and level.

Based on the foregoing discussion, it is obvious that the amount of capacitance connected to the DC bus is not enough to offer any serious immunity against the most common voltage sags. The amount of DC-bus capacitance needed to obtain a voltage tolerance of $U_{DC(\min)}$, during t_{max} (i.e., the VSD trips when the voltage drops below $U_{DC(\min)}$ for longer than t_{max}), is given by (A4.38).

$$C_{DC} = \frac{2 \cdot P_{vsd(out)} \cdot t_{max}}{U_{DC0}^2 - U_{DC(\min)}^2} \quad (\text{A4.38})$$

Considering the previous example, if a ride-through capability over 2 and 5 s is needed, the necessary capacitance for the VSDs is of 162.6 mF and 406.4 mF, respectively.

This can be achieved by using a set of 210 series-connected, 2.7-V, 100-F super-capacitors, with an overall a capacitance of 476.2 mF. The associated cost is roughly 630-840 €, without considering the voltage balancing circuit. The cost can be justified in critical applications. Moreover, most sags last less than 500 ms. Therefore, considering cheaper capacitors with ten times lower capacitance would be enough for most situations.

In normal operation, the DC-bus voltage is smoothened by the capacitance, and the larger the C_{DC} , the smaller the voltage ripple.

In a three-phase diode six-pulse rectifier, the capacitor is charged six times every cycle. For a three-phase unbalance sag having different phases with different voltage drops (some phases can show a jump in phase angle), the behaviour of the DC-bus voltage and, therefore, of the VSD, is completely different than that for balanced voltage sags.

In general, considering two phases below nominal value, even considering small DC-bus capacitance values (DC-bus voltage with an initial rate of decay of 75%), the DC-bus voltage does not drop below 70%. For a larger capacitance (DC-bus voltage with an initial rate of decay of 10%), the DC-bus voltage hardly deviates from its normal operating value [27]. In the last case, the VSD will never trip during such sag, no matter how low the characteristic magnitude of the sag. As one phase remains at its pre-event value, the three-phase rectifier simply operates as a single-phase rectifier during the voltage sag. The drop in DC-bus voltage is only moderate, but the voltage ripple increases significantly.

Considering a significant voltage drop of one phase and a moderate voltage drop in the other two, the effect of such disturbances in the DC-bus voltage is that it becomes slightly below the peak value of the voltage in the two phases with the moderate drop. Again, the effect of the sag on the DC-bus voltage, and thus on the motor speed and torque, is much less than for a balanced sag. In a VSD with a large capacitor, it is the highest voltage peak that determines the DC bus voltage. In a VSD without capacitance, the minimum DC-bus voltage is determined by the lowest AC-side voltage, and the effect of the phase-angle jump is that the minimum DC-bus voltage gets lower [27].

On the basis of the foregoing discussion, it is obvious that large capacitances in DC bus lead to lower voltage ripple and lower average voltage drop in the DC bus, for a disturbance in one or two phases.

The size of the DC-bus capacitance as a function of the required voltage decay rate and of the DC-bus voltage at sag initiation is given by (A4.39).

$$C_{DC} = \frac{P_{vsd(out)}}{U_{DC0} \frac{du_{DC}(t)}{dt}} \quad (\text{A4.39})$$

In older VSDs, the control electronics for the PWM inverters were powered from the supply, leading to a high sensibility to disturbances in the supply. In modern VSDs, the control electronics are powered from the DC-bus voltage, which is more stable, although significant disturbances can occur, as discussed above. The controller requires a small amount of stored energy to ride-through sags. Moreover, the VSD cooling fan can also be disconnected during sags. The design of the control unit power supply should be such that the controller stays active at least as long as the power electronics of the inverter do not require a permanent trip. It should not be that the controller becomes the weak part of the VSD. The capacitance connected to the DC bus between the rectifier and the inverter is normally not big enough to supply the motor load and the controller during a balanced sag longer than a few cycles, as demonstrated before. The power supply to the controller can be guaranteed in a number of ways. First, by inhibiting firing of the inverter so that the motor no longer discharges the DC-bus capacitance. The power taken by the controller is so much smaller than the motor load, that the DC-bus capacitors can easily power the controller, even for long voltage sags. Moreover, the cooling fan can simultaneously be disconnected. When the supply voltage recovers, the controller can automatically restart the load. Second, additional capacitance can be installed on low-voltage side of the DC-DC switched-mode power supply between the DC bus and the control unit. As this capacitance only needs to power the controller, a relatively small amount of capacitance is needed. This is probably the simplest solution. Alternatively, a battery block can be used. Third, some drives use the kinetic energy stored in the system inertia to power the controllers during a voltage sag or short interruptions (motor operating as a generator). This causes small additional drop in motor speed, small enough to be negligible if the process does not depend on exact motor speed. A special control technique for the inverter is needed, as well as a method to detect the sag. Another solution is to increase system inertia, although the starting or recovery periods are likely to increase significantly.

Regarding the impact of input voltage unbalances in the output voltage, let the required motor instantaneous voltages be given by (A4.40).

$$\begin{cases} u_a = U_{mtr} \cdot \cos(2 \cdot \pi \cdot f_{mtr} \cdot t) \\ u_b = U_{mtr} \cdot \cos(2 \cdot \pi \cdot f_{mtr} \cdot t - \frac{2}{3} \pi) \\ u_c = U_{mtr} \cdot \cos(2 \cdot \pi \cdot f_{mtr} \cdot t + \frac{2}{3} \pi) \end{cases} \quad (\text{A4.40})$$

For the sake of simplicity, it is assumed that the inverter output high-frequency harmonics due to the PWM switching are all removed by a low-pass filter, but the variation in the DC-bus voltage is not removed. The motor voltages for a per unit DC-bus instantaneous voltage u_{DC} is given by (A4.41).

$$\begin{cases} u_a = u_{DC} \cdot U_{mtr} \cdot \cos(2 \cdot \pi \cdot f_{mtr} \cdot t) \\ u_b = u_{DC} \cdot U_{mtr} \cdot \cos(2 \cdot \pi \cdot f_{mtr} \cdot t - \frac{2}{3} \pi) \\ u_c = u_{DC} \cdot U_{mtr} \cdot \cos(2 \cdot \pi \cdot f_{mtr} \cdot t + \frac{2}{3} \pi) \end{cases} \quad (\text{A4.41})$$

The motor frequency can be (and it is in most situations) different from the grid/line frequency. Therefore, the voltage ripple in the DC-bus voltage is not synchronized with the motor voltages. This may lead to unbalances and inter-harmonics to the motor voltages. The output fundamental voltages are modulated or distorted by the DC-bus voltage. As discussed before, it is obvious that unbalances at the VSD input lead to unbalances at the VSD output, particularly if the DC-bus capacitance is small.

If the motor frequency is no longer an integer fraction of the main DC-bus voltage ripple frequency, inter-harmonics will appear. For example, if the DC-bus voltage ripple has a 300-Hz frequency (typical for balanced, 50-Hz line voltage) and the motor is operating at 27 Hz, the output voltages have inter-harmonics with frequency 10.111 times 27 Hz and 12.111 times 27 Hz (10.111 and 12.111 order inter-harmonics, respectively), as it is demonstrated by (A4.42) and (A4.43), where A and B are constants defining the amplitude relation between voltage ripple amplitude and DC-bus average voltage²¹. The frequency of the output harmonics associated with the most relevant ripple component of the DC-bus voltage is therefore given by (A4.44). The resultant harmonic order depends on the fundamental reference frequency (grid/line frequency, f_{line} , or VSD output frequency, f_{mtr}). Equations (A4.42), (A4.43), and (A4.44) can be applied to other typical ripple frequencies (such as 100 Hz, typical for unbalanced 50-Hz line voltage).

In fact, several simulations were made considering a 50-Hz, star-connected, balanced power supply (two situations considered, 0.1 Ω and 5 M Ω neutral-to-ground impedance), and a VSD ($C_{DC} = 250 \mu\text{F}$) feeding a motor at 27 Hz (two situations considered: $m_a = 1.0$ and $m_a = 1.5$), being part of the results presented in Table A4.11, which confirm the referred relations. For an unbalanced power supply a $2 \times f_{1(line)}$ frequency harmonic appears.

For isolated neutral, the 3rd and 9th line-related harmonics are mitigated. The higher the Z_{ng} , the lower the triplen harmonics (related to the reduction of the impedance of the Ground-Source-VSD-IM-Ground closed circuit). The 6th order line-related harmonic in the DC-bus does not propagate

²¹ By definition, for a continuous voltage, the voltage ripple is given by the difference between maximum and minimum values, divided by twice the average value.

itself to the output voltages. The 3rd and 9th order line-related harmonics can propagate to other voltages in relation to ground. Eliminating 6th DC-link harmonic, mitigates the 5th and 7th order line related harmonics are mitigated, if $f_{I(out)} = 50$ Hz. According to (A4.44), the 6th harmonic translates into $300 \text{ Hz} \pm f_{I(out)}$ harmonic frequency at the inverter output. The harmonics produced by overmodulation can amplify or reduce harmonics related to 6th order harmonics in the DC bus.

In the case at unbalanced power supply, a 100-Hz ripple occurs in the DC-bus voltage (see Figs. A4.18, A4.25, and A4.32), producing harmonics (or inter-harmonics) with frequency $100 \text{ Hz} \pm f_{I(out)}$ at the inverter output.

TABLE A4.11
MOST RELEVANT HARMONICS IN A VSD-IM SYSTEM FED BY A BALANCED POWER SUPPLY.

Set-up	$U_{ng(mtr)}$	$U_{ab(mtr)}$	$U_{ag(mtr)}$	$U_{sg(mtr)}$	U_{g-DC+} & U_{g-DC-}	$U_{DC(+/-)}$
$Z_{ng} = 0.1 \Omega$ $m_a = 1.5$	$h_{out} = 3,$ $h_{in} = 3, 9.$	$h_{out} = 5, 7, 10, 11, 11,$ 12.111.	$h_{out} = 3,$ $h_{in} = 3, 9.$	$h_{out} = 3,$ $h_{in} = 3, 9.$	$h_{in} = 3, 6, 9.$	$h_{in} = 6, 12.$
$Z_{ng} = 0.1 \Omega$ $m_a = 1.0$	$h_{in} = 3, 9.$	$h_{out} = 10, 11, 12, 11.$	$h_{out} = 10, 11, 12, 11.$ $h_{in} = 3, 9.$	$h_{in} = 3, 9.$	$h_{in} = 3, 6, 9.$	$h_{in} = 6, 12.$
$Z_{ng} = 5 \text{ M}\Omega$ $m_a = 1.0$	$h_{in} = 3, 9.$ 3 rd harm. very low.	$h_{out} = 10, 11, 12, 11.$	$h_{out} = 10, 11, 12, 11.$ $h_{in} = 3$ (very low).	$h_{in} = 3$ (very low).	$h_{in} = 3, 6.$ 3 rd harm. very low.	$h_{in} = 6, 12.$

Notes:
 h_{out} and h_{in} are the line fundamental frequency and the VSD output fundamental frequency related harmonic orders, respectively.
VSD inverter with SPWM technique.
Line frequency equal to 50 Hz ($f_{l(in)} = 50$ Hz).
VSD output frequency equal to 27 Hz ($f_{l(out)} = 27$ Hz).

$$\begin{cases} u_a = U_{DC} \cdot (A \cdot \sin(6 \cdot 2\pi \cdot f_{line} \cdot t) + B) \cdot U_{mtr} \cdot \cos(2\pi \cdot f_{mtr} \cdot t) \\ u_b = U_{DC} \cdot (A \cdot \sin(6 \cdot 2\pi \cdot f_{line} \cdot t) + B) \cdot U_{mtr} \cdot \cos(2\pi \cdot f_{mtr} \cdot t - \frac{2}{3}\pi) \\ u_c = U_{DC} \cdot (A \cdot \sin(6 \cdot 2\pi \cdot f_{line} \cdot t) + B) \cdot U_{mtr} \cdot \cos(2\pi \cdot f_{mtr} \cdot t + \frac{2}{3}\pi) \end{cases} \quad (\text{A4.42})$$

$$\begin{cases} u_a = U_{DC} \cdot U_{mtr} \cdot \left(\frac{A}{2} \cdot [\sin(2\pi \cdot t \cdot (6f_{line} + f_{mtr})) + \sin(2\pi \cdot t \cdot (6f_{line} - f_{mtr}))] + B \cdot \cos(2\pi \cdot f_m \cdot t) \right) \\ u_b = U_{DC} \cdot U_{mtr} \cdot \left(\frac{A}{2} \cdot [\sin(2\pi \cdot t \cdot (6f_{line} + f_{mtr}) - \frac{2}{3}\pi) + \sin(2\pi \cdot t \cdot (6f_{line} - f_{mtr}) + \frac{2}{3}\pi)] + B \cdot \cos(2\pi \cdot f_m \cdot t - \frac{2}{3}\pi) \right) \\ u_c = U_{DC} \cdot U_{mtr} \cdot \left(\frac{A}{2} \cdot [\sin(2\pi \cdot t \cdot (6f_{line} + f_{mtr}) + \frac{2}{3}\pi) + \sin(2\pi \cdot t \cdot (6f_{line} - f_{mtr}) - \frac{2}{3}\pi)] + B \cdot \cos(2\pi \cdot f_m \cdot t + \frac{2}{3}\pi) \right) \end{cases} \quad (\text{A4.43})$$

$$f_{ripple(mtr)} = f_{ripple(DCbus)} \pm f_{mtr} \quad (\text{A4.44})$$

Considering a voltage unbalance with two phases with lower amplitude, it is possible to simulate the resulting positive and negative sequence in the output voltages, as a function of output frequency. Some results are presented in Table A4.12. According to [27], the negative-sequence (thus the unbalance) is maximized when the VSD output frequency equals the mains frequency. For lower frequencies the unbalance is lower. Even for a small DC-bus capacitor, the unbalance at the motor terminals is significantly lower than at the supply terminals.

It can be concluded that, operating the VSD-fed motor at a slight lower frequency can lead to an improvement of its performance during voltage unbalance situations, and the increase of the capacitance contributes to the attenuation of the unbalance impact on motor.

TABLE A4.12
MOTOR TERMINALS AND DC-BUS VOLTAGES FOR VSDS DUE TO A 50% TWO-PHASE SAG [27].

	Positive-Sequence Voltage		Negative-Sequence Voltage	DC-Bus Voltage	
	MAX	MIN	MAX	AVG	RMS
Small Capacitance	88.88%	83.44%	5.56%	87.38%	87.80%
Large Capacitance	98.25%	96.91%	0.81%	97.83%	97.84%

Note: Supply voltage with 75% positive sequence and 25% negative sequence.

The ride-through capability over voltage sags depends on both DC-bus voltage decrease rate after the sag and on the minimum value reached in long-term sag. The DC-bus capacitance increase can increase significantly the VSDs ride-through capacity.

In order to evaluate the DC-bus capacitance value influence on the VSD ride-through capability, several simulations were performed considering a fixed RL-series load, being the results presented in Table A4.13 and Fig. A4.80 (more figures can be found in Appendix 6).

One important conclusion is that the steady-state DC-bus voltage average (SS-AVG) value decreases slightly when the capacitance is increased, requiring a higher amplitude modulation index for the same fundamental voltage amplitude. Moreover, except for the three-phase sags, increasing the capacitance four times can avoid VSD tripping during 220-ms duration sags. For three-phase sags, this only triplicates the time to achieve the minimum DC-bus voltage level considered.

It should be noted that, as previously referred in Chapter 3, in order to use all the energy stored in the capacitors, a DC-DC converter can be used, extending significantly the ride-through capability. Of course this solution is more complex and costly.

Unbalance of AC voltages not only causes an increased ripple in the DC voltage but also a large unbalance in AC currents. The current unbalance depends on the type of sag. Whereas in normal operation the capacitor is charged six times per cycle, if the number of charges per cycle is lower than six, those reduced pulses have to carry the same amount of charge as the original six pulses, leading to the increase of the peak value of those pulses. For example, if one of the voltages is lower than the other two, this results in four pulses per cycle, and the current of each pulse is 50% higher. If the magnitude of one phase is higher than the other two, this results in two pulses per cycle, and the magnitude of each current pulse is 200% higher.

In order to evaluate those input current issues, several simulations were carried out. In Fig. A4.81, the simulated currents for $C_{DC} = 250 \mu\text{F}$, $f_{I(out)} = 40 \text{ Hz}$, and fixed RL-series load (approximately corresponding to a constant slip motor) are presented. It can be concluded that single-phasing is the most critical situation in terms of line current increase, since the current in the other phases can reach 2.5 times the normal value for the balanced situation. Two single phases down is also a considerable dangerous situation. The extra currents can lead to the fuses blow or, in

the absence of that, to the diodes failure. This is another problem caused by poor PQ, which should be taken into account in technical and economical evaluation of unbalance correction.

TABLE A4.13
DC-BUS CAPACITANCE INFLUENCE ON THE RIDE-THROUGH CAPABILITY OF VSDs USING SPWM TECHNIQUE.

Fault Type	Input Line-to-Neutral Voltage					Output Line-to-Line Voltage					DC-Bus Voltage		
	DC-Bus Cap. (mF)	Fund. Ph. A (V, max)	Fund. Ph. B (V, max)	Fund. Ph. C (V, max)	PVUR Unb. (%)	Fund. Ph. AB (V, max)	Fund. Ph. BC (V, max)	Fund. Ph. CA (V, max)	LVUR Unb. (%)	Steady-State (SS) Avg. (V)	(%)	Approx. Time to achieve 85% of SS-AVG (ms)	Min. DC Voltage in the [0-220] ms interval (V)
Normal Operation	0.125	327	327	327	0.0	443	443	442	0.2	557.5	101.4	--	558
	0.250	327	327	327	0.0	438	437	435	0.4	549.8	100	--	550
	0.450	327	327	327	0.0	432	434	434	0.3	546.1	99.3	--	546
	0.500	327	327	327	0.0	434	434	432	0.3	545.7	99.3	--	546
	1.000	327	327	327	0.0	431	432	432	0.2	543.8	98.9	--	544
	4.750	327	327	327	0.0	432	431	429	0.4	542.4	98.7	--	542
	5.012	327	327	327	0.0	431	431	430	0.2	542.4	98.7	--	542
	476.2	327	327	327	0.0	430	431	431	0.2	542.0	98.6	--	542
1 Phase @ 80%	0.125	261	327	327	14.4	408	436	402	5.0	522.9	95.1	5	437
	0.250	261	327	327	14.4	442	435	404	5.4	537.5	97.8	5	448
	0.450	261	327	327	14.4	450	432	424	3.4	547.8	99.6	--	482
	0.500	261	327	327	14.4	448	431	423	3.2	546.2	99.4	--	486
	1.000	261	327	327	14.4	433	424	424	1.4	537.4	97.7	--	501
	4.750	261	327	327	14.4	422	420	419	0.4	528.9	96.2	--	525
	5.012	261	327	327	14.4	422	420	419	0.4	528.7	96.2	--	530
	476.2	261	327	327	14.4	420	421	420	0.2	528.0	96.0	--	540
2 Phases @ 80%	0.125	261	261	327	15.5	367	398	391	4.8	485.1	88.2	2.5	408
	0.250	261	261	327	15.5	371	417	396	6.0	496.1	90.2	5	415
	0.450	261	261	327	15.5	384	407	387	3.7	493.9	89.8	12.5	441
	0.500	261	261	327	15.5	385	404	385	3.2	492.5	89.6	15	449
	1.000	261	261	327	15.5	386	393	383	1.5	487.6	88.7	--	468
	4.750	261	261	327	15.5	387	388	385	0.4	486.9	88.6	--	484
	5.012	261	261	327	15.5	387	388	386	0.3	486.9	88.6	--	484
	476.2	261	261	327	15.5	387	386	385	0.3	485.8	88.4	--	539
3 Phases @ 80%	0.125	261	261	261	0.0	354	354	354	0.0	445.7	81.1	2.5	397
	0.250	261	261	261	0.0	349	348	349	0.2	439.6	80.0	5	424
	0.450	261	261	261	0.0	347	347	347	0.0	436.7	79.4	7.5	426
	0.500	261	261	261	0.0	347	346	346	0.2	436.3	79.4	7.5	422
	1.000	261	261	261	0.0	345	346	345	0.2	434.8	79.1	15	431
	4.750	261	261	261	0.0	344	345	344	0.2	433.7	78.9	70	433
	5.012	261	261	261	0.0	346	345	344	0.3	433.6	78.9	75	433
	476.2	261	261	261	0.0	344	345	345	0.2	433.4	78.8	> 2200	539
Single Phasing	0.125	0.1	327	327	100.0	369	422	327	13.2	466.9	84.9	2.5	307
	0.250	0.1	327	327	100.0	431	449	413	4.2	541.2	98.4	5	406
	0.450	0.1	327	327	100.0	450	432	424	3.4	547.7	99.6	7.5	458
	0.500	0.1	327	327	100.0	448	431	422	3.3	546.1	99.3	--	465
	1.000	0.1	327	327	100.0	432	424	422	1.4	537.4	97.7	--	465
	4.750	0.1	327	327	100.0	422	420	418	0.5	528.9	96.2	--	525
	5.012	0.1	327	327	100.0	421	420	418	0.4	528.4	96.1	--	525
	476.2	0.1	327	327	100.0	417	419	420	0.4	527.1	95.9	--	540

Notes:

Star-connected source: $U_{AN} = U_{BN} = U_{CN} = 231$ V, $f = 50$ Hz, $R_{N-GND} = 5$ M Ω .

Star-connected RL-series load: $L = 52.28$ mH & $R = 21.89$ Ω .

Inverter: $f_s = 2$ kHz, $m_a = 1$.

Diode Rectifier: $L_{series} = 1$ mH.

Initial condition of the DC-bus capacitor: steady-state average (SS-AVG) value.

Steady-state average computed during a 20-ms period.

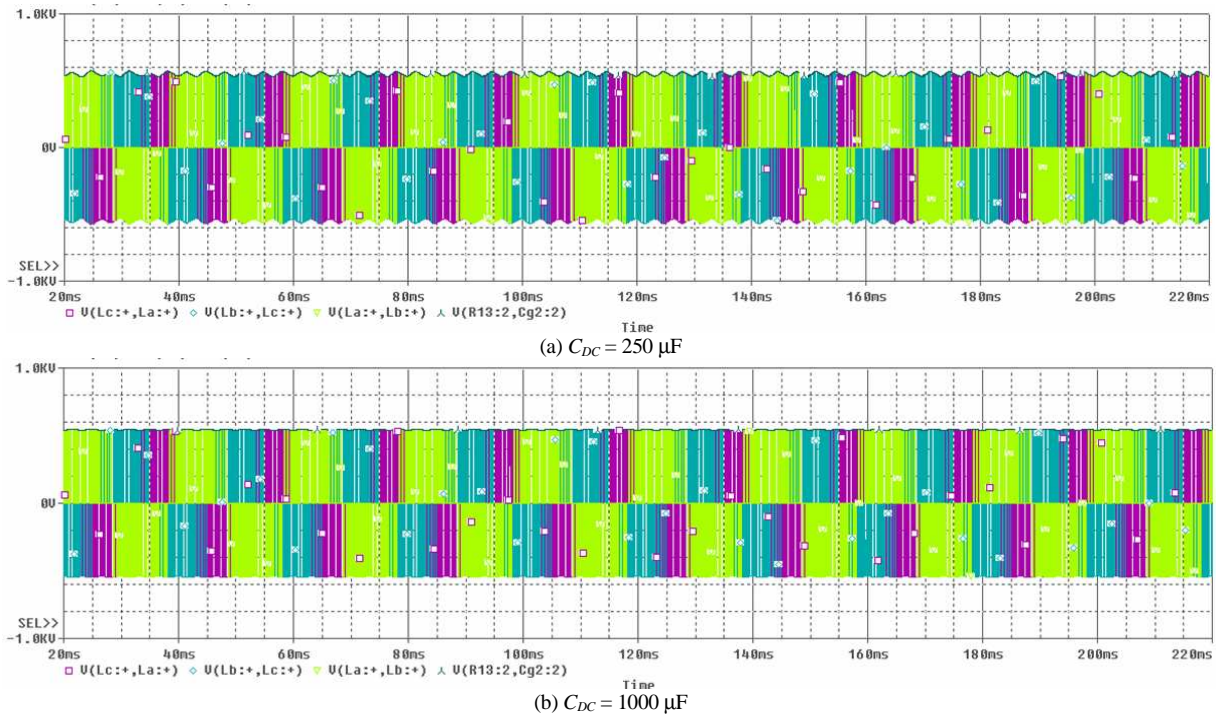
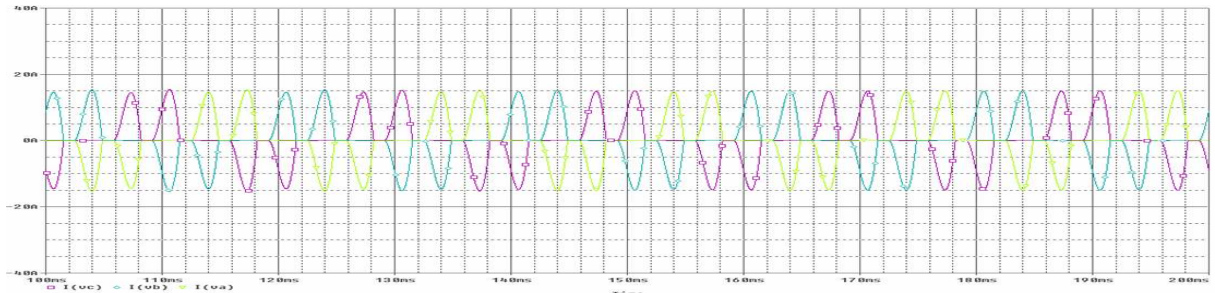


Fig. A4.80. Simulated DC-bus and inverter output line-to-line voltages for different DC-bus capacitance values.

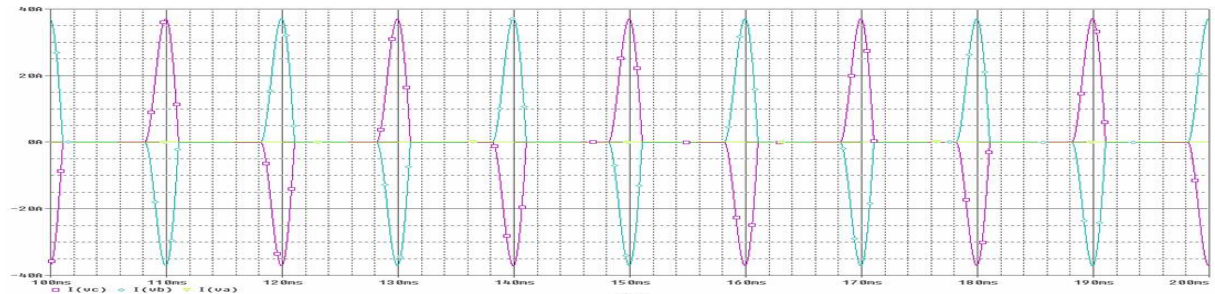
A4.8 DC-Bus Capacitance Influence on the Input Current Distortion of VSDs

Another important issue is the influence of the additional capacitance added to the DC bus of VSDs on the diode rectifier input current distortion, which influences directly the current harmonic distortion and, therefore, the power factor. To evaluate that influence, simulations were carried out using PSPICE software package, considering a fixed RL-series load approximately equivalent to the full-load impedance of a typical 3-kW, 4-pole IM fed by a VSD, considering balanced input power supply. Fig. A4.82 shows the input current and the DC-bus voltage waves (more figures can be found in Appendix 6). In Table A4.14, a summary of the simulated results is presented.

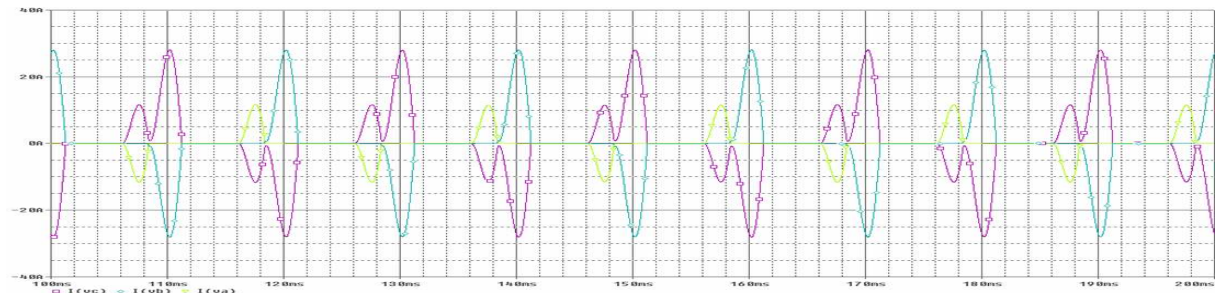
On the basis of the obtained results, it can be concluded that adding extra capacitance to the DC bus of a VSD with three-phase 6-pulse diode rectifier, the DC-bus voltage average value decreases slightly but the voltage ripple, which, for balanced voltages, is mainly characterized by a 6th and a 12th order harmonic (with respect to the mains frequency) decreases significantly, being an advantage, since output voltage waveforms improve. Moreover, the increase of the capacitance in the DC bus leads to a significant decrease of the input current harmonic distortion, thus improving significantly the VSD power factor. It should be noted that the current distortion decrease is slightly attenuated by the fundamental current component decrease for higher capacitances, due to the slight DC-bus average voltage decrease. Therefore, the investment in additional capacitance can be a way of improving input and output waveforms power quality in VSD units, as well as the ride-through capability.



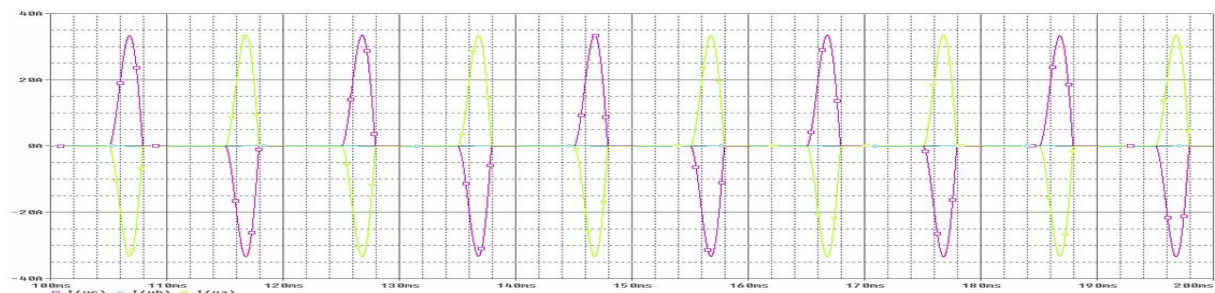
(a) Balanced Voltages



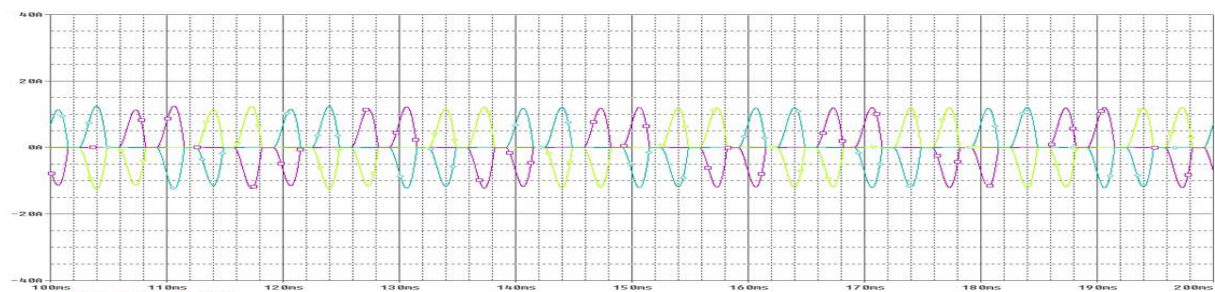
(b) Single-Phasing (One Phase at 0.1%)



(c) One Phase at 80%



(d) Two Phases at 80%



(e) Three Phases at 80%

Fig. A4.81. Simulated input currents of a VSD (6-pulse diode rectifier, $C_{DC} = 250 \mu\text{F}$, $L_{series} = 1 \text{ mH}$, fixed RL-series load), during different sags (according to Table A4.12).

TABLE A4.14
DC-BUS CAPACITANCE INFLUENCE ON THE INPUT CURRENT AND DC-BUS VOLTAGE OF VSDs.

DC Bus Capacitance	Diode Rectifier Input Line Current						DC Bus Voltage		
	Fund. (A)	5 th Har. (p.u.)	7 th Har. (p.u.)	11 th Har. (p.u.)	13 th Har. (p.u.)	THD (%)	Average (V)	Ripple	
								6 th Har. (V)	12 th Har. (V)
125 μF	7.013	0.8027	0.6364	0.2893	0.1527	107.97	557.52	37.87	5.60
250 μF	6.894	0.7588	0.5644	0.2004	0.0923	97.71	549.82	16.94	1.74
450 μF	6.845	0.7340	0.5266	0.1635	0.0823	92.75	546.12	8.88	0.775
500 μF	6.816	0.7306	0.5225	0.1595	0.0824	92.18	545.70	7.91	0.677
1000 μF	6.808	0.7157	0.4989	0.1424	0.0833	89.37	543.76	3.82	0.315
4750 μF	6.784	0.7033	0.4805	0.1313	0.0860	87.17	542.37	0.78	0.063
5012 μF	6.782	0.7031	0.4803	0.1311	0.0862	87.14	542.36	0.74	0.060
476.2 mF	6.780	0.6697	0.4753	0.1287	0.0872	86.56	542.03	< 0.01	< 0.001

Notes:

Star-connected source: $U_{AN} = U_{BN} = U_{CN} = 231$ V (balanced voltages), $f_l = 50$ Hz, $R_{N-GND} = 5$ M Ω .

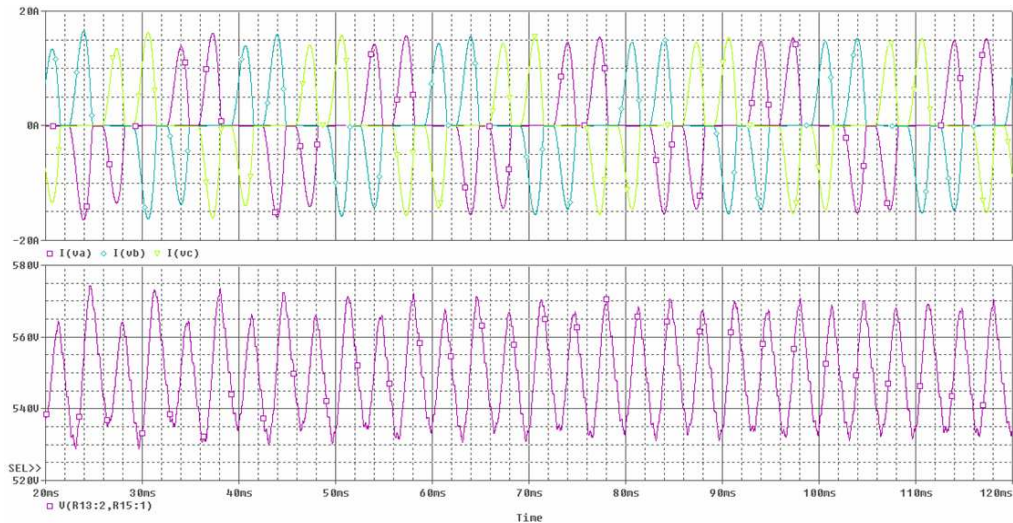
Star-connected RL-Series Load: $L = 52.28$ mH & $R = 21.89$ Ω .

Inverter: $f_s = 2$ kHz, $m_a = 1$, $f_{l(out)} = 50$ Hz.

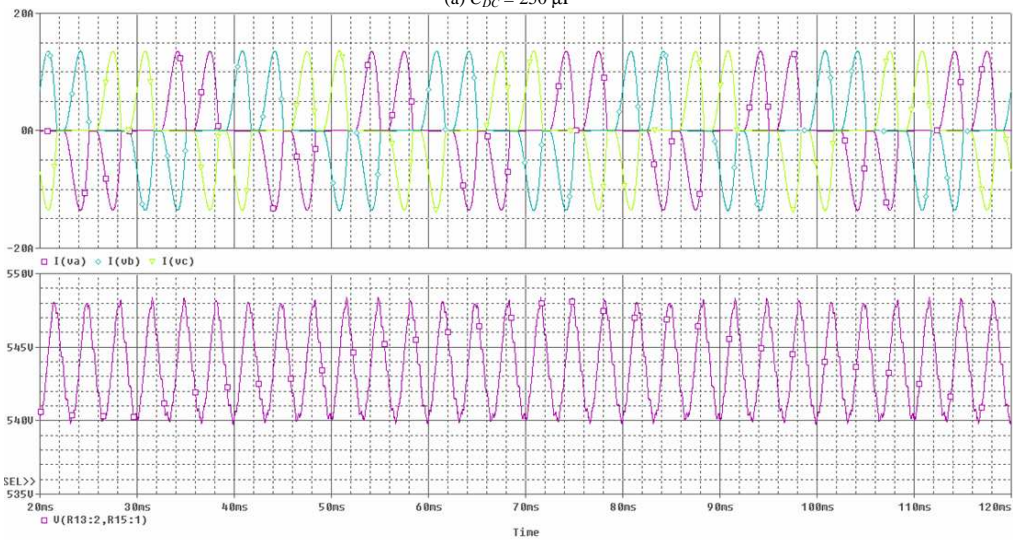
Diode rectifier: $L_{series} = 1$ mH.

Initial condition of the DC-bus capacitor: 565 V (except for $C_{DC} = 476.2$ mF, in which 542 V is used).

Simulation period larger enough to reach steady state.



(a) $C_{DC} = 250$ μF



(b) $C_{DC} = 1000$ μF

Fig. A4.82. Simulated VSD input currents (upper graphs) and DC-bus voltages (bottom graphs) for different DC-bus capacitance values.

Considering capacitors with 2.7 V and 1 F (capacity 100 times lower than common super-capacitors), 210 capacitors should be connected in series to reach 567 V, yielding an overall capacity of 4762 μF . Considering a price per unit of 1 €, therefore, for the 210 units the cost is 210 €. Therefore, to increase the typical capacity of a 3.7-kW 2-level inverter, which is about 250 μF , a total capacitance of 5012 μF is reached. A reduction of 10.57 p.p. in the input current *THD*, as well as the improvement of the output voltage waveforms, can be important argues to justify the investment, simultaneously with the major advantage of extending the VSD ride-through capability.

A4.9 Motor Deceleration

After the tripping of the VSD, the IM will simply continue to slow down until its speed gets out of the range acceptable for the process. In case the electrical part of the VSD is able to withstand the sag, the drop in system voltage will cause a drop in voltage at the motor terminals.

For balanced sags, all the three phase voltages drop the same amount. Assuming that the voltages at the motor terminals are equal to the supply voltages, the sag at the motor terminals is exactly the same as the sag at the rectifier terminals, if no compensation is made by the VSD. The DC-bus capacitor will somewhat delay the drop in voltage at the DC bus and thus at the motor terminals. The drop at the motor voltage leads to a drop in its torque and, consequently, in its speed. The drop in the motor speed can disrupt the production process requiring an intervention by the process control. The speed of the motor is governed by the energy balance equation (A4.45), where J_{sys} is the inertia of the system (motor plus load) and ω is the system angular speed. In an approximate form, the motor torque can be expressed by (A4.46). Assuming the motor running at steady state and $T_N = T_{\text{load}}$, (A4.45) can be combined with (A4.46), yielding (A4.47). The motor slip is given by (A4.48). The load torque for elementary loads can be expressed by (A4.49), where $k = 0$ represents a constant torque load, $k = 1$ a linear torque load, and $k = 2$ a quadratic torque load. Combining (A4.47), (A4.48) and (A4.49), yields (A4.50), which is a first-order differential equation. In Fig. A4.83, the simulated results of (A4.50) for a 3-kW, 400-V, 50-Hz motor with a nominal torque $T_N = 20.5$ N.m and a nominal slip $s_N = 0.065$, considering different system inertia and motor terminals voltage, are presented.

$$\frac{d}{dt} \left(\frac{J_{\text{sys}} \cdot \omega^2}{2} \right) = \omega \cdot (T_{\text{mtr}} - T_{\text{load}}) \quad (\text{A4.45})$$

$$T_{\text{mtr}} \approx \left(\frac{U}{U_N} \right)^2 \cdot \frac{s}{s_N} \cdot T_N \quad (\text{A4.46})$$

$$\frac{d}{dt} \left(\frac{J_{syst} \cdot \omega^2}{2} \right) \approx \omega \left(\left(\frac{U}{U_N} \right)^2 \cdot \frac{s}{s_N} \cdot T_N - T_{load} \right) \quad (\text{A4.47})$$

$$s = \frac{\omega_{sync} - \omega}{\omega_{sync}} \Leftrightarrow \omega = \omega_{sync} (1 - s) \quad (\text{A4.48})$$

$$T_{load} = K \cdot \omega^k = K \cdot \omega_{sync}^k (1 - s)^k \quad (\text{A4.49})$$

$$\frac{ds}{dt} = \frac{K \cdot \omega_{sync}^{k-1} \cdot (1-s)^k}{J_{syst}} \cdot \frac{U^2 \cdot s \cdot T_N}{U_N^2 \cdot s_N \cdot J_{syst} \cdot \omega_{sync}} \quad (\text{A4.50})$$

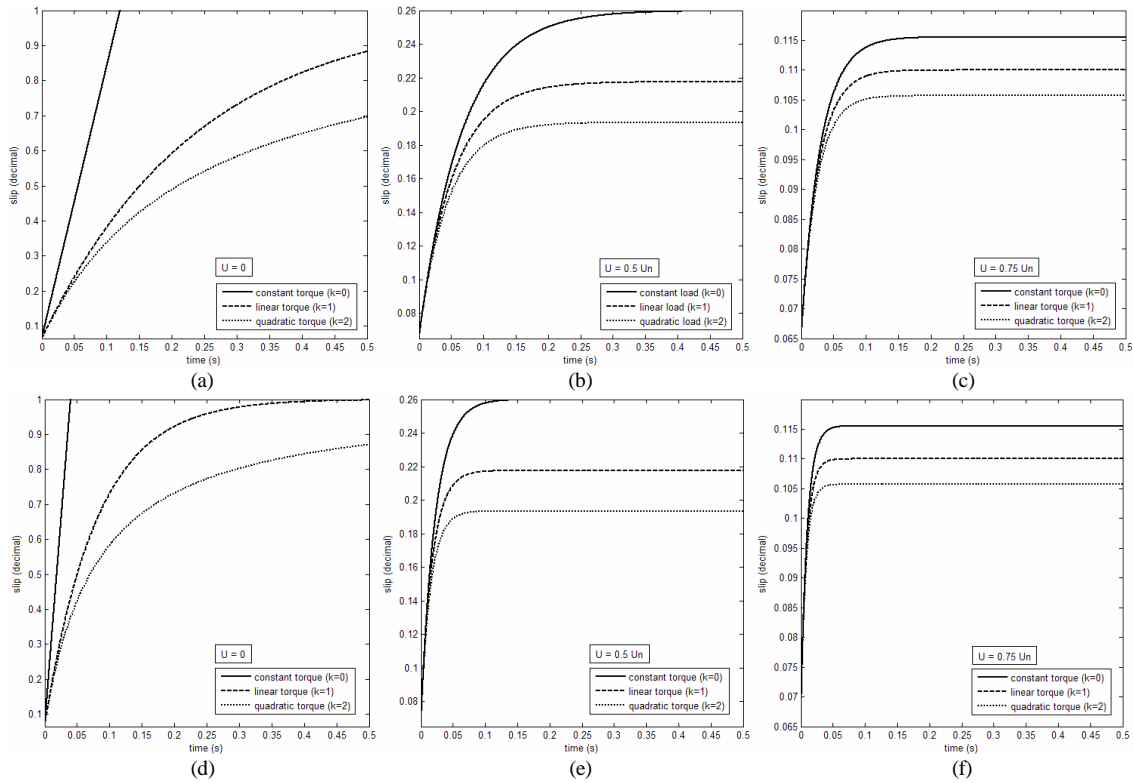


Fig. A4.83. Simulated slip increase during a balanced voltage drop (or sag) for a 3-kW, 400-V, 50-Hz, 4-pole IM, with a rotor inertia $J_{rtr} = 0.0056 \text{ kg}\cdot\text{m}^2$, a nominal slip $s_n = 0.065$, and a nominal torque $T_N = 20.5 \text{ N}\cdot\text{m}$: (a) $U = 0 \text{ V}$ & $J_{syst} = 3J_{rtr}$; (b) $U = 200 \text{ V}$ & $J_{syst} = 3J_{rtr}$; (c) $U = 300 \text{ V}$ & $J_{syst} = 3J_{rtr}$; (d) $U = 0 \text{ V}$ & $J_{syst} = J_{rtr}$; (e) $U = 200 \text{ V}$ & $J_{syst} = J_{rtr}$; (f) $U = 300 \text{ V}$ & $J_{syst} = J_{rtr}$.

Based on Fig. A4.83, it is possible to state that, large inertia systems have naturally higher immunity to voltage sags. Additionally, constant torque loads have higher sensibility to voltage sags since the deceleration can be very high. For moderate sags, quadratic loads, with a relatively high inertia, can maintain the motor slip within tolerable values.

Therefore, the efforts on ride-through capabilities should be focused on constant torque loads, or on loads with a relevant constant-torque component (static friction).

Nevertheless, it should be noted that most modern VSDs control the motor slip, limiting it to a maximum value, by means of properly adjusting the synchronous speed to the rotor speed.

The results presented in this section are also important to Chapter 5, regarding the deceleration during automatic stator-winding connection-mode transition periods.

A4.10 Considerations on Mitigation Methods

The most commonly used mitigation method is to disable the operation of the inverter, so that the motor no longer loads the VSD. This prevents damage due to overcurrents, overvoltages, and torque oscillations. After the voltage recovers the VSD is automatically restarted. The disadvantage of this method is that the motor load slows down more than needed. When synchronous restart is used, the drop in speed can be somewhat limited, but non-synchronous restart leads to very large drops in speed or even standstill of the motor. An important requirement for this type of VSD is that the controller remains active. During the sag, the controllers can be powered from the DC-bus capacitor or from separate capacitors or batteries. Alternatively, the kinetic energy of the mechanical load can be used to power the DC-bus capacitors during a sag or interruption [31], [32], [33].

The voltage-tolerance problem of drives is ultimately an energy problem. In many applications the motor will slow down too much to maintain the process. Adding additional capacitors or a battery block to the DC bus can solve this problem, as previously discussed. Also, the installation of a motor generator set feeding into the DC bus will give the required energy.

A large amount of stored energy is needed to ensure tolerance against three-phase sags and short interruptions. For sags due to single-phase and phase-to-phase faults, which are the most common ones, only a limited amount of stored energy is needed as at least one phase of the supply voltage remains at a high value. Since super-capacitors are now available for a relatively low price, they can be used to increase the ride-through capability of VSD-IM systems. This appears to be the easiest way of improving the voltage tolerance for the majority of sags.

The use of diode rectifiers is cheap but makes control of the DC-bus voltage difficult. The moment the AC voltage maximum drops below the DC-bus voltage, the rectifier stops supplying energy and the motor is powered from the capacitors. Using a controlled rectifier consisting of thyristors, gives some control of the DC-bus voltage. When the AC-bus voltage drops, the firing angle of the thyristors can be decreased to maintain the DC-bus voltage. However, with such strategy, poor power factor is expected. For unbalanced sags different firing angles are needed for the three phases that could make the control rather complex. Additional disadvantages are that the control system takes a few cycles to react and that the firing-angle control makes the VSD sensitive to phase-angle jumps. Another option is to use some additional power electronics to draw more current from the supply during the sag. A kind of power electronic current source is installed between the diode rectifier and the DC-bus capacitor (as referred in Chapter 3). This current can be

controlled in such a way that it keeps the voltage at the DC-bus constant during a voltage sag [33]. The DC-voltage control is also possible, by using rectifier consisting of self-commutating devices (e.g., IGBTs). Algorithms have been proposed to keep the DC-voltage constant for any unbalance, drop, or change in phase angle in the AC voltages [34], [35], [36]. An additional advantage is that these IGBT-based rectifiers enable a quasi-sinusoidal input current, solving a lot of the harmonic problems caused by VSDs. The main limitations of all these methods are that they have a minimum operating voltage and will certainly not operate for an interruption.

In order to provide constant motor torque, it is also proposed the use of commercial versions or redesigned motors to operate in star connection at full load. If the DC-bus voltage drops dramatically, the stator windings can be changed to delta connection, thus allowing the motor to be fed at nominal voltage that can actually be produced by the inverter with a low amplitude modulation index, m_a . Of course the power switches must be able to draw roughly 1.75 times the normal current in order the motor be able to produce nominal torque at nominal speed, which inherently lead to an inverter with extra power and, therefore, more expensive. Another proposed solution is the (re)design of the motor winding for a voltage lower than the nominal, allowing the inverter to match that lower voltage operated at reduced m_a (here, again, extra current drawing capacity has to be provided, increasing the inverter cost). However, for a given power, the reduction of the motor voltage can lead to a slight reduction in motor efficiency. Of course, this solution has to be accomplished by proper measures to avoid inverter tripping as a function of DC-bus voltage level or the current drawn by the motor. If a sag happens, the m_a can be progressively increased to compensate the DC-bus average voltage drop. The proposed winding change can be done in damaged motors during rewinding or in healthy motors driving critical applications.

Instead of controlling the DC-bus voltage, it is also possible to control the motor terminal voltage. Normally, the speed controller assumes a constant DC-bus voltage and calculates the switching instants of the inverter from this. We saw earlier that the effect of this is that the DC-bus voltage is amplitude modulated (by SPWM technique) on the desired motor terminal voltages. This effect can be compensated by considering the DC-bus voltage in the algorithms used to calculate the switching instants, in order to compensate the reference voltage (e.g., $U_{ref} := U_{ref}/U_{DC}$, U_{DC} in p.u.). The drawback of this approach is that it can result in additional harmonic distortion (due to the possible overmodulation, see Chapter 3), particularly if the output voltage is already near the nominal value, and has a minimum voltage below of which it will no longer work properly (in the limit of the overmodulation region, meaning square-wave region).

A4.11 Conclusions

This appendix presents a rather extensive overview of voltage supply anomalies and their effect on the performance and operating limits of IMs, including torque ripple. Both individual and combined effects of *VMD*, *VUF*, *HVF* and *ATD* are discussed.

The most important tool which was used for the presented analysis is a model based on motor per-phase equivalent circuit that includes several important factors such as skin effect impact on rotor effective leakage inductance and resistance, frequency dependent core loss resistance, and thermal compensation of the resistive parameters. A correction for the thermal asymmetry in IMs under unbalanced voltages and currents was also considered. It was shown that loss-based derating gives fair but underestimated results in some situations, and could be a reasonable option for IMs whose thermal model is not known.

A methodology to evaluate individual impact of the referred PQ parameters is proposed, separating clearly the *VUF* and *VMD* impact. This is particularly important because most studies make no distinction, mixing voltage unbalance and voltage magnitude deviation, including NEMA derating curves.

Shortcomings of VU standards, definitions or limits were indicated. The *VUF* is particularly dangerous for the motor and should be monitored in the field. Particular combinations are quite dangerous for the motor, such as *VUF-HVF* acting simultaneously. The actual pattern of the voltage distortion and voltage unbalance has a significant influence on their impact on motor performance. The voltage amplitude deviation can increase significantly the impact of the previous referred voltage supply anomalies.

In short, it is recommended the inclusion of *VMD*, *VUF* (complex or scalar value), U_p (or U_n), *HVF*, and frequency deviation, as PQ-related limits in IM-related standards.

It is demonstrated that the motor power derating curves, as a function of *LVUR* and *HVF*, recommended by NEMA MG-1 standard, can lead in some cases to an overderating.

The influence of motor rated power (or power range), pole-number, rotor type (or torque-speed curve shape), efficiency class, and frame type on motor derating curves was evidenced, demonstrating that the motor power derating should be performed as a function of multiple variables, including those motor features, *VUF*, *HVF*, *VMD*, and *ATM*. However, extensive experimental validation of the results is required.

A multiple input, feed-forward ANN-based approach providing a mathematical description for motor power derating is proposed. Further testing and improvements on the ANN are required. Once the ANN is optimally trained with experimental results, it can be a useful tool for motor systems design and maintenance.

Regarding energy-efficiency or high-efficiency motors, it was demonstrated that as low as the rotor bars resistance, the lower the impact of the VU on the motor efficiency, power factor and winding temperature increase. This is can be an extra argument to invest in improved motors.

Motors designed for high starting torque are more susceptible to the unbalance effects due to the higher resistant torques created by the negative-sequence harmonics or by the inverse or negative-sequence component of an unbalanced system. Therefore, the NEMA rotors of design A or B, as well as, in general, the high-efficiency motors, are more immune to the VU. However, that immunity is slightly attenuated due to the skin effect in the rotor bars, which have a larger cross section in the case of aluminium-cage high-efficiency motors.

An important conclusion is that, for the same percentage value, the *VUF* and/or *VMD* impact on the motor performance is significantly stronger than *HVF*. Therefore, from the perspective of motor efficiency, the user should invest first on the voltage magnitude and unbalance correction, before looking at the *HVF*. Moreover, the stator winding adaptation to the actual motor voltage (or average voltage during the motor highest load periods) during repair/rewinding operations is also recommended for motors operating a large number of hours. This is important to convert the undervoltage unbalance situations to overvoltage or rated voltage unbalance situations, since they are considerably less dangerous for the motor. Of course, if other undervoltage correcting measures can be implemented, they should be the first step to solve the problem.

It is strongly suggested that the temperature rise, power derating curves, and other related regulations/standards regarding the VU should consider, at least, both *VUF* and positive-sequence voltage magnitudes to reflect the true system condition

In general, on the basis of the information presented in this appendix and in Appendix 3, it can also be said that, the higher the distribution factor of the stator winding, the higher immunity to the voltage unbalance, from a thermal perspective. Moreover, the single layer windings are the worse, due to the fact that they do not allow heat exchanges between phases.

The discussion on power derating is very important in the scope of in-field motor load estimation, and proper adjustments should be made in methods described in Chapter 4.

One important conclusion is that, when evaluating the technical and economical benefits of VSDs, the typical concept that those devices act as a sort of “full voltage unbalance insulator” is actually false. In fact, voltage unbalance and/or under/overvoltages present in most plants can ride through VSDs (without DC-bus voltage compensation capability), and the unbalance level and type depends on the capacitance and on the output fundamental frequency. Investing in extra DC-bus capacitance can be a cost-effective choice for critical systems, extending ride-through capability and improving input current and output voltage waveforms power quality of VSDs, including the attenuation of the input unbalanced power supply effect on DC-bus voltage and

output voltage waveforms. Reducing the output voltage unbalance and improving output waveform quality (lower harmonics) avoids extra losses and performance loss of motor. For a strongly unbalanced system, the use of such measures to attenuate the voltage unbalance effects can be cost effective for medium/large motors or large groups of small motors, operating a large number of hours per year, and/or driving critical applications. The increase of the motor lifetime should also be taken into account in the technical and economical evaluation.

In short, it can be concluded that the higher the capacitance, the higher the immunity of the VSD to supply short-duration perturbations/anomalies, improving the ride-through capability and performance of the system. Therefore, a trade-off has to be made. If a slip tolerance is defined (process requirement) the increase of the DC-bus capacitance allows extending the sag-duration tolerance, even without considering DC-DC regulation stages between capacitors and the DC bus, that allows to use more of the overall energy stored in the capacitors. Moreover, as referred, besides the ride-through capability improvement, the investment in additional capacitance can be a way of improving input and output waveforms power quality in VSD units.

Lastly, in the case of elastic transmission, care must be taken to ensure that no dangerous/undesirable oscillations occur during starting period, and the effect including the effect of voltage unbalance on motor torque should be taken into account.

A4.12 References

- [1] Dugan, R.; McGranaghan, M.; Beaty, H.: *“Electric Power Systems Quality”*, McGraw-Hill, 1996.
- [2] Driesen, J.; Craenenbroeck, T.: *“Guia de Aplicação da Qualidade de Energia – Perturbações de Tensão – Secção 5.1.3: Introdução ao Desequilíbrio”*, LPQI, Maio de 2002.
- [3] Souto, O.; Oliveira, J.; Ribeiro, P.: *“Power Quality Impact on Performance and Associated Costs of Three-Phase Induction Motors”*, 8th IEEE Inter. Conf. on Harmonics and Quality of Power, Conf. Proc., Vol. 2, pp. 791-797, 14-16 Oct. 1998.
- [4] Chapman, D.: *“Guia de Aplicação de Qualidade de Energia – Afundamentos de Tensão”*, LPQI, Abril de 2002.
- [5] IEEE Std. 519, 1992: *“Recommended Practices and Requirements for Harmonic Control in Electric Power Systems”*.
- [6] Agamloh, E.; Wallace, A.; Jouanne, A.; Anderson, K.; Rooks, J.: *“Assessment of Nonintrusive Motor Efficiency Estimators”*, IEEE Trans. on Ind. Applic., Vol. 41, No. 1, pp. 127-133, Jan./Feb. 2005.
- [7] Wiendebrug, E.; Ramme, A.; Mehteson, E.; Jouanne, A.; Wallace, A.: *“Modern on-line testing of Induction Motors for Predictive Maintenance and Monitoring”*, IEEE Pulp and Paper Industry Technical Conf., Conf. Record, pp. 163-168, 18-22 June 2001.
- [8] IEC 60034-1, Ed. 11, 2004: *“Rotating electrical machines - Part 1: Rating and performance”*.
- [9] *“Optimizing your motor-driven system”*, Motor Challenge, Fact Sheet, www.motor.doe.gov.
- [10] Jeong, S.: *“Representing Line Voltage Unbalance”*, 37th Industry Applications Conf., IEEE-IAS Annual Meeting, Conf. Record, Vol. 3, pp. 1724-1732, Oct. 2002.
- [11] Lee, C.; Chen, B.; Lee, W.; Hsu, Y.: *“Effects of Various Unbalanced Voltages on the Operation Performance of an Induction Motor under the Same Voltage Unbalance Factor Condition”*, IEEE Industrial and Commercial Power Systems Tech. Conf., Conf. Record, pp. 51-59, 11-16 May 1997.
- [12] Pillay, P.; Hofmann, P.; Manyage, M.: *“Derating of Induction Motors Operating With a Combination of Unbalanced Voltages and Over or Undervoltages”*, IEEE Trans. on Energy Conversion, Vol. 17, No. 4, pp. 481-491, Dec. 2002.
- [13] Siddique, A.; Yadava, G.; Singh, B.: *“Effects of Voltage Unbalance on Induction Motors”*, IEEE Inter. Symp. on Electrical Insulation, Conf. Record, pp. 26-29, USA, Sept. 2004.
- [14] Souto, O.; Oliveira, J.; Neto, L.: *“Induction Motors Thermal Behaviour and Life Expectancy Under Non-Ideal Supply Conditions”*, 9th IEEE Inter. Conf. on Harmonics and Quality of Power, Vol. 3, pp. 899-904, 1-4 Oct. 2000.
- [15] C. De Capua, C. Landi: *“Quality Assessment of Electrical Drives with Strongly Deformed Supply Waveform”*, Elsevier, Measurement 30, pp. 269-278, 2001.
- [16] Sen, P.; Landa, H.: *“Derating of Induction Motors Due to Waveform Distortion”*, IEEE Trans. on Industry Applications, Vol. 26, No. 6, pp.1102-1107, Nov./Dec. 1990.
- [17] Roy, D.; Mukhopadhyay, S.; Pal, S.; Bose, S.: *“Novel Thermal Model Aided Motor Derating Under Waveform Distortion”*, IEEE Inter. Conf. on Power Electronics and Drive Systems, Conf. Proc., Vol. 2, pp. 829-833, May 1997.

- [18] Mukundan, T.; Kundu, P.: “*Method of Reducing the Effect of Supply Unbalance on Induction Motors*”, IEEE Power Engineering Review, pp. 70-71, May 2000.
- [19] Manz, L.: “*Applying Adjustable-Speed Drives to Three-Phase Induction NEMA Frame Motors*”, IEEE Trans. on Industry Applications, Vol. 33, No. 2, pp. 402-407, March/April 1997.
- [20] Vamvakari, A.; Kandianis, A.; Kladas, A.; Manias, S.; Tegopoulos, J.: “*Analysis of Supply Voltage Distortion Effects on Induction Motor Operation*”, IEEE Trans. on Energy Conversion, Vol. 16, No. 3, pp. 209-213, Sept. 2001.
- [21] Eren, L., Devaney, M.: “*Power Factor Measurement For Rotating Machines Under System Unbalance*”, 16th IEEE Instrumentation and Measurement Techn. Conf., Conf. Proc., Vol. 2, pp. 1138-1141, 24-26 May 1999.
- [22] Grainger, J.; Stevenson, W.: “*Power System Analysis*”, McGraw-Hill International Editions, Electrical Engineering Series, New York, 1994.
- [23] Beaty, H.; Kirtley, J.: “*Electric Motor Handbook*”, McGraw-Hill Handbooks, New York, 1998.
- [24] Emanuel, A., “*Estimating the Effects of Harmonic Voltage Fluctuations on the Temperature Rise of Squirrel-Cage Motors*”, IEEE Trans. on Energy Conv., Vol. 6, No. 1, pp. 162-168, March 1991.
- [25] Cummings, P.: “*Estimating Effect of System Harmonics on Losses and Temperature Rise of Squirrel-Cage Motors*”, IEEE Trans. on Industry Applications, Vol. IA-22, No. 6, pp. 1121-1126, Nov./Dec. 1986.
- [26] Cummings, P., Dunki-Jacobs, J., Kerr, R.: “*Protection of Induction Motors Against Unbalanced Voltage Operation*”, IEEE Trans. on Ind. Applic., Vol. IA-21, No. 4, pp. 778-792, May/June 1985.
- [27] Bollen, M.: “*Understanding Power Quality Problems – Voltage Sags and Interruptions*”, IEEE Press Series on Power Engineering, Wiley-Interscience, John Wiley & Sons, New York, 2000.
- [28] Strangas, E.; Wagner, V.; Unruh, T.: “*Variable Speed Drives Evaluation Test*”, IEEE Industry Applications Magazine, Vol. 4, No. 1, pp. 53-57, January 1998.
- [29] Conrad, L.; Little, K.; Grigg, C.: “*Predicting and Preventing Problems Associated With Remote Fault-Clearing Voltage Dips*”, IEEE Trans. on Ind. Applic., Vol. 27, No. 1, pp. 167-172, Jan. 1991.
- [30] Mansoor, A.; Collins, E.; Morgan, R.: “*Effects of Unsymmetrical Voltage Sags on Adjustable-Speed Drives*”, 7th IEEE Int. Conf. on Harmonics and Quality of Power (ICHQP), Las Vegas, NV, pp. 467-472, October 1996.
- [31] Holtz, J.; Lotzhat, W.; Stadfeld, S.: “*Controlled AC Drives with Ride-Through Capacity at Power Interruption*”, IEEE Trans. on Industry Applic., Vol. 30, No. 5, pp. 1275-1283, Sept. 1994.
- [32] Pumar, C.; Amantegui, J.; Torrealday, J.; Ugarte, C.: “*A Comparison between DC and AC Drives as Regards their Behaviour in the Presence of Voltage Dips: New Techniques for Reducing the Susceptibility of AC Drives*”, Int. Conf. on Electrical Distribution (CIRED), Birmingham, U. K., June 2-5, 1997, pp. 9/1-5.
- [33] Benson K.; Chapman, J.: “*Boost Converters Provide Power Dip Ride-Through for AC-Drives*”, Power Quality Assurance Magazine, July 1997.
- [34] Moran, L.; Ziogas, P.; Joos, G.: “*Design Aspects of Synchronous PWM Rectifier-Inverter Systems Under Unbalance Input Voltage Conditions*”, IEEE Trans. on Industry Applications, Vol. 28, No. 6, pp. 1286-1293, Nov. 1992.
- [35] Wiechmann, E.; Espinoza, J.; Rodriguez, J.: “*Compensated Carrier PWM Synchronization: A Novel Method to Achieve Self-Regulation and AC Unbalance Compensation in AC Fed Converters*”, IEEE Trans. on Power Electronics, vol. 7, No. 2, pp. 342-348, April 1992.
- [36] Rioual, P.; Pouliquen, H.; Louis, J.: “*Regulation of a PWM Rectifier in the Unbalanced Network State Using a Generalized Model*”, IEEE Trans. on Power Electronics, Vol. 11, No. 3, May 1996, pp. 495-502.
- [37] David, A.; Maire, J.; Dessoude, M.: “*Influence of Voltage Dips and Sag Characteristics on Electrical Machines and Drives: Evaluation and Perspective*”, 3rd Int. Conf. On Power Quality: End-Use Applications and Perspectives, Amsterdam, The Netherlands, October 1994.
- [38] NEMA MG-1 Standard, 2006: “*Motors and Generators*”; and NEMA Standards Publication: “*Information Guide for General Purpose Industrial AC Small and Medium Squirrel-Cage Induction Motor Standards*”, 2002.
- [39] Fitzgerald, A.; Kingsley, C.; Umans, S.: “*Electric Machinery*”, 6th Ed., McGraw-Hill Higher Education, New York, 2003.
- [40] Dugan, R.; McGranaghan, M.; Beaty, H.: “*Electric Power Systems Quality*”, McGraw-Hill, New York, 1996.
- [41] Ferreira, F.; de Almeida, A.; Baoming, G.: “*Three-Phase Induction Motor Simulation Model Based on a Multifrequency Per-Phase Equivalent Circuit Considering Stator Winding MMF Spatial Harmonics and Thermal Parameters*”, 17th Inter. Conf. on Electric Machinery, Conf. Proc., Greece, September 2006.
- [42] Souto, O.; Oliveira, J.; Ribeiro, P.: “*Power Quality Impact on Performance and Associated Costs of Three-Phase Induction Motors*”, 8th IEEE Inter. Conf. on Harmonics and Quality of Power, Conf. Proc., Vol. 2, pp. 791-797, Oct. 1998.
- [43] Deprez, W., et al.: “*The Combined Effect of Practical Operating Conditions and Material Choice on the Performance of Induction Machines*”, 5th Inter. Conf. on Energy Efficiency in Motor Driven Systems, Conf. Proc., Beijing, China, June 2007.
- [44] Sen, P.; Landa, H.: “*Derating of Induction Motors Due to Waveform Distortion*”, IEEE Trans. on Industry Applications, Vol. 26, No. 6, pp. 1102-1107, Nov./Dec. 1990.
- [45] Ferreira, F.; de Almeida, A.; Baoming, G.: “*Comparative Study on 2-Level and 3-Level Voltage-Source Inverters*”, 5th Inter. Conf. on Energy Efficiency in Motor Driven Systems (EEMODS’07), Conf. Proc., Vol. II, pp. 581-602, Beijing, China, 2007.
- [46] Ferreira, F.; de Almeida, A.: “*Method for In-Field Evaluation of the Stator Winding Connection of Three-Phase Induction Motors to Maximize Efficiency and Power Factor*”, IEEE Trans. on Energy Conv., Vol. 21, No. 2, June 2006, pp. 370-379.
- [47] Ferreira, F.; de Almeida, A.: “*Novel Multi-Flux Level, Three-Phase, Squirrel-Cage Induction Motor for Efficiency and Power Factor Maximization*”, IEEE Trans. on Energy Conversion, Vol. 23, No. 1, pp. 101-109, March 2008.
- [48] Ferreira, F.; de Almeida, A.; Deprez, W.; Belmans, R.; Baoming, G.: “*Impact of Steady-State Voltage Supply Anomalies on Three-Phase Squirrel-Cage Induction Motors*”, Inter. Aegean Conf. on Electric Machines, Power Electronics (ACEMP’07) and Electromotion Joint Conf., Conf. Proc., pp. 607-615, Bodrum, Turkey, 10-12 Set. 2007.
- [49] Pietilainen, K.; Harnefors, L.; Petersson, A.; Nee, H.: “*DC-Link Stabilization and Voltage Sag Ride-Through of Inverter Drives*”, Trans. on Industrial Electronics, Vol. 53, No. 4, pp. 1261-1268, Aug. 2006.
- [50] Bonnet, A.; Boteler, R.: “*The Impact that Voltage Variations have on AC Induction Motor Performance*”, pp. 301-315, typographical notes not available.
- [51] “*Análise do Impacto das Perturbações na Qualidade da Energia Eléctrica na Unidade Industrial – Santos Barosa*”, Relatório síntese dos períodos de monitorização, N.º LEA-PQ-SB-15/2005, ISR-University of Coimbra, Dezembro de 2005.

- [52] Patrão, C.: “*Tratamento de Dados de Monitorização da Qualidade de Energia*” e “*Telemonitorização da Qualidade e Continuidade da Tensão em Clientes MT e AT*”, Relatório de Estágio Curricular – Direcção de Normalização e Tecnologia (DNT) da EDP Distribuição, Grupo de Actividade de Inovação Tecnológica (NTPI), Ano lectivo 2003/2004.
- [53] EN 50160 standard, 2000: “*Voltage characteristics of public distribution systems*”.
- [54] IEC 61800-2 standard, 1998: “*Adjustable speed electrical power drive systems – Part 2: General requirements – Rating Specifications for low voltage adjustable frequency a.c. power drive systems*”.
- [55] Hsu, J.; Kueck, J.; Olszewski, M.; Casad, D.; Otaduy, P.; Tolbert, L.: “*Comparison of Induction Motor Field Efficiency Evaluation Methods*”, IEEE Trans. on Industry Applications, Vol. 34, No. 1, pp. 117-125, Jan./Feb. 1998.
- [56] Leonhard, W.: “*Control of Electric Drives*”, 2nd Edition, Springer-Verlag, Berlin, 1997.
- [57] Jackson, D.: “*Low Voltage Insulation System Endurance Against Electronic Waveform and Cable Length*”, IEE Colloquium on Effects of High Speed Switching on Motors and Drives, Ref. No. 1999/144, pp. 6/1-6/7, June 1999.

Appendix 5 – Reliability of Motor-Driven Systems

Overview – In this appendix, EMODS reliability related issues are addressed, with the focus on IMs. A methodology to optimize the investment to increase EMODS reliability is proposed. Due to its present relevance and impact on IMs lifetime, bearing currents and voltage transients associated with VSD-fed IMs are discussed. In fact, nowadays, the incidence of failures in motor bearings due to the current activity is quite significant. The conditions leading to the circulation of currents through the bearings are analyzed from a comprehensive perspective, with special focus on the VSD-fed IMs, being addressed a number of solutions for their mitigation. In fact, bearing currents activity in electrical machines and the respective mitigation techniques have been widely discussed, but not fully understood, being this appendix a contribution on this topic. For example, safety limits for the voltage between inner and outer bearing rings and the effectiveness of local insulation-based mitigation techniques (e.g., insulation layers and ceramic spheres) need further investigation, being analysed in this appendix. An electrostatic shield concept for common-mode currents mitigation is also proposed and analyzed. The motor insulation system degradation depends upon electric, thermal, chemical and mechanical wear factors, which, acting individually or together, cause different failure modes. The causes and effects of the voltage transients on low-voltage IMs are addressed, with the focus on IMs fed by voltage-source inverters, and several mitigation techniques are discussed. Part of the information presented in this appendix was published in [10], [16] and [51].

A5.1 Introduction

Ageing is a process that governs the failure rate of a component as it degrades with age. It can be used in a slightly more general sense as being dependent on the actual age of the component and on the time since the last repair or maintenance intervention. Typically, to quantify the dependence of the failure rate on the age of a component, the well-known bathtub curve is used (Fig. A5.1), being the lifetime divided into three periods. The period between 0 and t_1 is called the wear-in period (also known as “infant mortality”), and the period after t_2 is called the wear-out period. The period between t_1 and t_2 is known as the useful life (also called “normal life period”) being a period of random failures, in which the failure rate is approximately constant (flat part of the curve). Useful life period is typically dominant, representing most of the operating time. In the first interval (0- t_1), the failure rate can be high in the initial phase, which can be explained by the fact that there may be undiscovered defects in the item, due to poor quality control. The defects can appear when the item is activated. In the second interval (t_1 - t_2), the failure rate stabilizes at a level where it remains for a certain amount of time. In the last interval ($> t_2$) the item begins to wear out and the failure rate begins to increase. The bathtub curve is only a stylized version of what can be a complex function of time. The actual failure rate as a function of time can be of completely different shape, although it is likely to contain, at least, an initial wear-in period and an overall increasing failure rate for older components. In the useful life period, the failure rate is assumed to be constant [1], [9]. In general, higher reliability leads to lower downtime and maintenance costs.

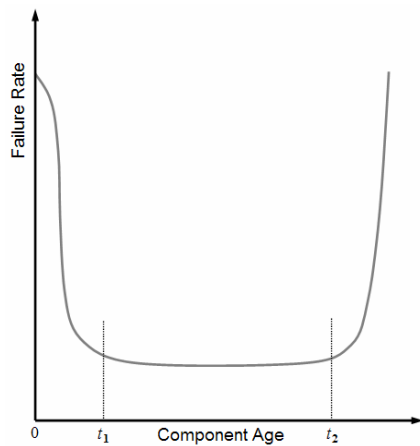


Fig. A5.1. Bathtub curve: component failure versus age.

Particularizing to the scope of this thesis, two systems are considered: the electric motor driven system (EMODS) and the motor itself. In the first case, the motor is considered a component and, in the second case, the parts integrating the motor are the components.

Regarding costs of interruption associated with the motor failure, they should also be considered during design and exploration of motor systems. The inconvenience due to interruptions needs to be quantified by one way or another. Any serious quantification requires a translation of the inconvenience into an amount of money. Typically, the costs associated with interruptions can be expressed as a function of reliability. In turn, the reliability is a function of the capital investment. The idea is that a more reliable system is more expensive to build and operate, but the costs associated with interruptions (either over the lifetime of the system or per year) are lower. The total exploration cost, or life-cycle cost, as a function of the capital investment, is typically a U-shape curve with a minimum corresponding to the optimum point of investment on reliability and/or efficiency, as it can be seen in Fig. A5.2. If the system operating cost curve were reciprocal of the investment (and continuous curve), the optimum investment point (maintaining the total cost) would be at the intersection point of both investment and system cost curves (Fig. A5.2, left). Considering a system with high downtime costs (e.g., continuous process industries), an extra investment analysis on reliability increase can be much as shown in Fig. A5.2 (right), in which the optimum investment is evidenced. Actually, the represented curves are discrete and less smooth since, in practice, the investment and the associated benefits are typically defined by steps. Even if we assume that both cost functions can be determined exactly, the curve still has some serious limitations, and should only be used as a qualitative demonstration of the cost-benefit trade-off. In some cases, additional investment does not always give a more reliable system¹.

Anyway, in general, the user is able to establish to each system the associated cost when it fails. But the establishment of a curve that relates the failures rate with the investment is rather complex. It is proposed first to establish the optimal proportion of investment in each component, and then it

¹ E.g., integrating a VSD in the EMODS can reduce system reliability due to the introduction of an additional series module in the system, which is sensible to power quality related anomalies.

is relatively easy to express the effect that the investment has on the overall failure rate. This proposed approach ensures the right proportion of investment in each module of a system.

Reliability is not a single-dimensional quantity, both number and duration of the interruption associated with the system failure influence the interruption costs. There is no sliding scale of reliability and cost, and the system designer can choose between a limited number of design options (sometimes there are just two options available). The two cost terms cannot simply be added since one term (building and operating costs) has a small uncertainty, and the other term (interruption costs) has a large uncertainty due to the uncertainty in the actual number and duration of interruptions.

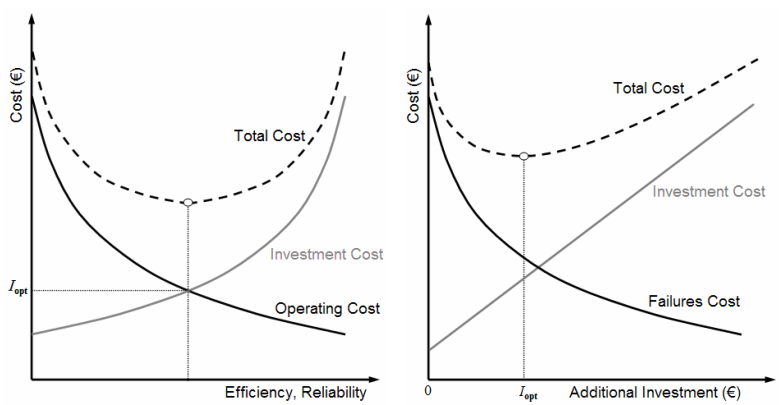


Fig. A5.2. (left) Approximate curve of the total system cost as a function of reliability and/or efficiency; (right) Approximate curve of the total system cost as a function of the extra investment.

The cost of a system operation interruption consists of a number of terms. Each term has its own difficulty in being assessed. Again, simply adding the terms to obtain the total costs of an interruption is not the right way, but due to the lack of alternatives it is often the only feasible option.

Direct costs are the costs that are directly attributable to the interruption of the system operation. For example, for domestic customers, if the motor of the refrigerator fails, the loss of food is a direct cost. For industrial customers, the direct costs consist, among others, of lost raw material, lost production, and salary costs during the non-productive period. When assessing direct costs, the savings in, for example, energy and raw materials should be discounted.

Indirect costs are must complex to evaluate, and, in many cases, they cannot be simply expressed in amount of money. A company can loose future orders when an interruption in the productive process leads to delay in delivering a product order.

The direct and indirect costs associated with an EMODS depend on the importance and dependency that main production lines have on it. For example, if the motor driving the ventilation system of the offices of an industrial plant fails, the production will not stop, thus it is not a critical system. However, if an EMODS integrated in a continuous transformation process stops, all the process will stop, and that is critical in terms of production-loss costs. Each particular EMODS

have to be classified according to its importance in order to allow the establishment of proper maintenance programs (preventive, periodic, or curative maintenance).

Unless modern diagnosis tools to predict motor failures (preventive or predictive maintenance) are used to determine when the motor will fail with a relatively high accuracy, most in-operation IMs can be considered as a stochastic component. In Appendix 6, basic theoretical principles on reliability are provided.

A5.2 Motor and Motor-Driven Systems Reliability

Typically, IMs have an overall lifetime in the range 12-20 years² (Table A5.1), and they are repaired up to 4 times during that period (the average is 2-3 times).

Table A5.2 presents a summary of the results of a number of studies carried out by the North American institutes EPRI³ and IEEE⁴ and by a large German industrial plant on the share of failures in electric motors. It should be noted that, as previously demonstrated, IMs represent more than 90% of the electrical motors, thus being well represented by the study. It can be concluded that, together, the motor failures associated to bearing and stator winding failures represent about $\frac{3}{4}$ of the total registered failures, as the motor failures associated with rotor failures represent about $\frac{1}{10}$ of total registered failures. On average, the bearing related failures represent more than $\frac{1}{2}$ of the total failures. In fact, the most recent study (of those presented) identified that more than $\frac{3}{4}$ of the total failures are associated with bearing failures. The main causes of IM failure in inside/indoor environments are the manufacturing defects and inadequate maintenance⁵. The inadequate motor operation or use represents a modest factor. As motor reliability is indeed important to minimize the cost associated with driven process interruptions and motor repair/maintenance, and even to minimize the energy consumption associated with the repair process (e.g., transport and repair process related energy), strategies to increase the reliability of the motor itself and of the motor-driven system, should be a goal.

TABLE A5.1
AVERAGE OVERALL LIFETIME OF INDUCTION MOTORS [2].

Rated Power Range	Average Overall Lifetime
[0.75 kW 7.5 kW]	12 yr
]7.5 kW 75 kW]	15 yr
> 75 kW	20 yr

From the foregoing discussion, it can be stated that IMs reliability depends mainly on the individual reliability of the bearings and stator windings.

² Typically, VSDs have a mean time to failure (MTF) of around 10 yr (for an ambient temperature lower than 40°C), depending on the failure rate of its components, such as fans, capacitors, and IGBTs [115].

³ Electrical Power Research Institute.

⁴ Institute of Electrical and Electronics Engineers.

⁵ Includes rewinding, reimpregnation, cleaning, bearing lubrication or replacement, etc.

TABLE A5.2
SHARE OF FAILURES IN ELECTRICAL MOTORS [5], [6], [8], [10], [114].

Induction Motor Part	EPRI ⁶ (1983)	EPRI ⁷ (1985)	IEEE ⁸ (1983)	IEEE ⁹ (1984)	IEEE (year n.a.) ¹⁰	Hüls AG ¹¹ (1990)	Average of all studies
Bearings	41%	41%	50%	60%	51%	76%	53.2%
Stator windings	37%	36%	25%	25%	16%	6%	24.2%
Rotor	10%	9%	9%	1%	5%	4%	6.3%
Other parts	12%	14%	16%	14%	28%	14%	16.3%

Table A5.3, presents a summary of a number of studies carried out by EPRI and IEEE on the main causes of IM failures. On the basis of Table A5.3, it can be concluded that the inadequate or poor maintenance has a very significantly impact on the IM reliability.

The concepts previously presented can be particularized for the case of IMs and EMODS. The IM is an electromechanical system integrating several components, which can be considered series connected stochastic components. In IMs, redundancy¹² in its components is extremely rare, being eventually found in motors for extremely critical applications. Actually, in critical motor systems, the redundancy can be obtained by using parallel-connected motors, becoming the motor a stochastic component of the system. This kind of applications is quite rare. Therefore, that kind of systems is not addressed, being only considered motors and motor systems without redundancy, i.e., when a component fails there are no components that can replace it in the operation. In other words, from the reliability theory perspective, only system series-connected components are considered for the IM and EMODS.

TABLE A5.3
MAIN CAUSES OF FAILURES IN ELECTRICAL MOTORS [5], [6], [8].

Motor Failure Causes	EPRI ¹³ (1983)	EPRI ¹⁵ (1984)	IEEE (1983)	IEEE (1984)	IEEE ¹⁴ (1986)	IEEE ¹⁵ (1986)	Average of all IEEE studies
Inadequate or poor maintenance	--	--	21%	23%	17%	25%	22%
Manufacturing deffects	33%	31%	20%	20%	23%	21%	21%
Other causes	67%	69%	59%	53%	60%	54%	57%

The main IM operation-related components are the stator windings (including terminal lead connections), the rotor, and the bearings. The other components can be partially damaged, but the motor can still operate, although inefficiently, as for the case of damaged iron core and/or external fan, in the case of TEFC-type motors, affecting indirectly the motor lifetime and efficiency due to the consequent additional losses and heating. Since the bearing- and winding-related failures

⁶ 4797 electrical motors, with rated power higher than 75 kW.

⁷ 6312 electrical motors.

⁸ 1141 electrical motors.

⁹ 1141 electrical motors (due to poor motor maintenance only).

¹⁰ Survey/study year not available.

¹¹ From a distribution of long-time study on failures at a large chemical plant (Fa. Hüls AG, 1990).

¹² Redundancy is the provision of more than one means of achieving a function.

¹³ In this study, inadequate or poor maintenance is integrated in "Other causes".

¹⁴ Outside/outdoor installations.

¹⁵ Inside/indoor installations.

represent about ¾ of the total motor failures, and since they represent the most critical components, for the sake of simplicity, the network for reliability analysis of an IM can be represented as in Fig. A5.3. Therefore, the mean time to failure, $MTTF$, of an IM can be described approximately by (A5.1), where subscripts “ wdg ” and “ brg ” denote the stator windings and bearings, respectively [8]. Note that the $MTTF_{brg}$ includes both bearings, and it can be easily calculated by (A5.2). The $MTTF_{wdg}$ can be calculated by (A5.3).

The main causes of stator-winding failures are related with, for example, insulation system disruption and terminal-leads contact breaking (single-phasing), which, in turn, depend on insulation material ageing, excessive heating, voltage stress (overvoltages or transients), partial discharge occurrence, overload, excessive mechanical vibration, poor terminal-leads contact, poor repair, etc. [8]. The main causes of bearing failure are the mechanical overload, heating, chemical contamination, poor lubrication, stray currents, electric discharges, etc. [8].

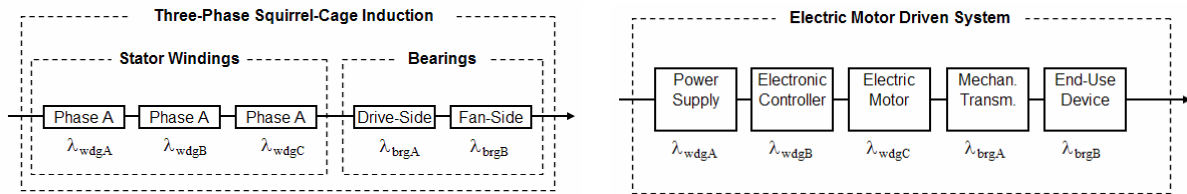


Fig. A5.3. Basic reliability network for the IM and EMODS.

$$MTTF_{mr} \approx \frac{1}{\lambda_{wdg} + \lambda_{brg}} = \frac{MTTF_{wdg} \cdot MTTF_{brg}}{MTTF_{wdg} + MTTF_{brg}} \quad (A5.1)$$

$$MTTF_{brg} = \frac{1}{\lambda_{brg1} + \lambda_{brg2}} = \frac{MTTF_{brg1} \cdot MTTF_{brg2}}{MTTF_{brg1} + MTTF_{brg2}} \quad (A5.2)$$

$$MTTF_{wdg} = \frac{1}{\lambda_{wdg1} + \lambda_{wdg2} + \lambda_{wdg3}} = \frac{MTTF_{wdg1} \cdot MTTF_{wdg2} + MTTF_{wdg2} \cdot MTTF_{wdg3} + MTTF_{wdg3} \cdot MTTF_{wdg1}}{MTTF_{wdg1} \cdot MTTF_{wdg2} \cdot MTTF_{wdg3}} \quad (A5.3)$$

It should be noted that, typically, when one of the bearings fails, since the other is, in principle, significantly worn-out, both bearings are replaced (to save money on transport, man-hour, process overtime, disassemble/reassemble, etc.), and, in some cases, even old but operational windings can also be replaced in the same repair operation. If both bearings are equal and are both replaced when one of them fails, (A5.2) can be simplified to (A5.4). Applying the same principle to the per-phase winding, (A5.3) can be simplified to (A5.5).

$$MTBF_{brg} = \frac{1}{\lambda_{brg1,2}} = MTBF_{brg1,2} \quad (A5.4)$$

$$MTBF_{wdg} = \frac{1}{\lambda_{wdg 1,2,3}} = MTBF_{wdg 1,2,3} \quad (A5.5)$$

In the cases where windings are replaced every time a bearing fails, windings can be ignored in the reliability analysis, since the bearing will fail first when considering both windings and bearings “as good as new” after the repair. However, this situation is more unlikely to happen.

IM operation is only possible if all the windings and bearings are healthy. Any evolutionary¹⁶ or catastrophic¹⁷ failure in one or both of these components leads to the evolutionary or catastrophic failure of the motor. Typically, the failures in the IMs are evolutionary but, since preventive or predictive maintenance is typically not carried out for most small/medium motors, the effective failure is only detected when it actually occurs, becoming catastrophic since the motor cannot operate anymore. Data obtained from a number of motor manufacturers and repair shops indicate that, in Industry, typically, the $MTTF_{brg}$ of small/medium motors is within 3.4 to 8.2 yr (considering 2 shifts or 16 h/day, 365 day/yr, yielding 5840 h/yr, and that bearings are typically designed for a nominal useful life of 20000 h at 100% load and 48000 h at 75% [114]) for line-fed IMs, and within 2.5 to 6.5 yr for VSD-fed IMs (see Chapter 3). The $MTBF_{wdg}$ is typically within 8 to 12 yr for line-fed IMs and within 5 to 10 yr for VSD-fed IMs. These values depend mainly on motor rated power, motor type/class, motor manufacturer, periodic maintenance (cleaning, lubrication, etc.) and on the operating conditions (power quality, surrounding environment, load profile, etc.) [8].

Since the $MTTF_{brg}$ is typically lower than the $MTTF_{wdg}$, the increase of the $MTTF_{brg}$ ¹⁸ is actually more effective to extend the $MTTF_{mtr}$ rather than increasing the $MTTF_{wdg}$. The most advantageous option is pushing $MTTF_{brg}$ to higher values close to $MTTF_{wdg}$, instead of pushing up $MTTF_{wdg}$ far away from the $MTTF_{brg}$ ¹⁹, as it can be seen in Fig. A5.4.

This can be proved mathematically as follows. Simplifying In order to simplifying the notation, (A5.1) can be written as in (A5.6), where $x = MTTF_{brg}$, $y = MTTF_{wdg}$, and $z = MTTF_{mtr}$. In Fig. A5.5, the three-dimension plot of (A5.6) is presented.

It is possible to conclude that, in terms of $MTTF$, the best option is to push up and equalize the $MTTF$ of the two components considered. For example, considering $x = y = 0.5$, if $\Delta_x = 0.5$ and $\Delta_y = 0$, then $z = 0.5$, but if $\Delta_x = \Delta_y = 0.25$, then $z = 0.5625$. Assuming equal cost to Δ_x and Δ_y , the last solution is the most advantageous.

¹⁶ The evolutionary failures are characterized by a gradual development and, initially, affect the operation only partially.

¹⁷ The catastrophic failures are characterized by a sudden occurrence, leading to the total and immediate operation stopping.

¹⁸ E.g., incorporating heavy-duty bearings and oil seals, which increase motor protection against dust and water.

¹⁹ E.g., if $MTTF_{brg} = 8$ yr and $MTTF_{wdg} = 12$ yr, then $MTTF_{mtr} = 4.8$ yr. Extending the $MTTF_{wdg}$ for 15 yr, the $MTTF_{mtr}$ is extended to 5.2 yr. However, if instead of extending the $MTTF_{wdg}$, the $MTTF_{brg}$ is extended to 11 yr, the $MTTF_{mtr}$ is extended to 5.7 yr, being the last option more advantageous.

$$z = \frac{x \cdot y}{x + y} \quad (\text{A5.6})$$

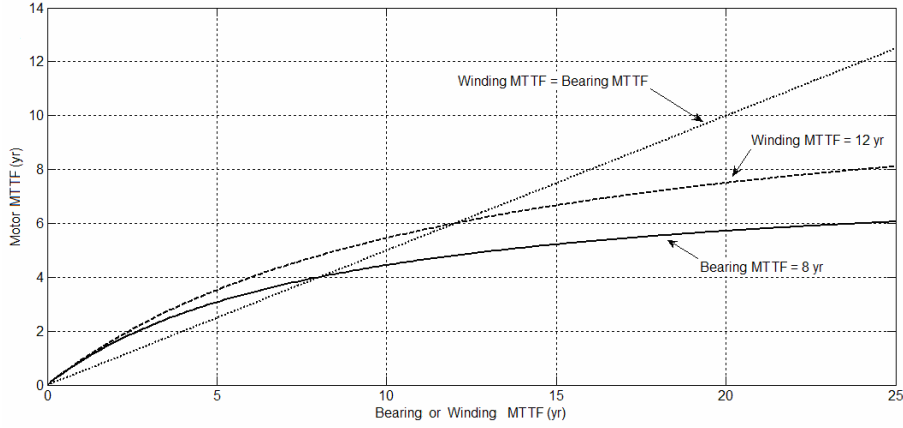


Fig. A5.4. Motor *MTTF* as a function the bearing and winding *MTTF*: (dotted line) Winding *MTTF* equal to bearing *MTTF*; (dashed line) Winding *MTTF* equal to 12 yr (fixed); (solid line) Bearing *MTTF* equal to 8 yr (fixed).

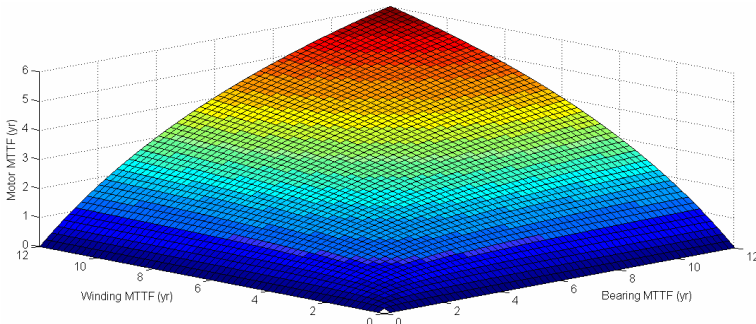


Fig. A5.5. Motor *MTTF* as a function of winding and bearing *MTTF*.

Assuming now that the cost to increase the *MTTF* of the bearing and winding is a and b (in €/yr, assumed as constants), the base *MTTF* is x_0 and y_0 , and the increase of the base *MTTF* is Δ_x and Δ_y , respectively, the total additional cost to increase the *MTTF* of the motor, Δ_{cost} , is given by (A5.7), the increase in the motor *MTTF*, Δ_{mttf} , is given by (A5.8), and the cost increase per additional year of *MTTF*, c_{mttf} , is given by the quotient between the additional investment and the additional increase in the motor *MTTF*, as expressed by (A5.9).

$$\Delta_{cost} = \Delta_{cost_x} + \Delta_{cost_y} = a \cdot \Delta_x + b \cdot \Delta_y \quad (\text{A5.7})$$

$$\Delta_{mttf} = \frac{(x_0 + \Delta_x) \cdot (y_0 + \Delta_y)}{(x_0 + \Delta_x) + (y_0 + \Delta_y)} - \frac{x_0 y_0}{x_0 + y_0} \quad (\text{A5.8})$$

$$c_{mtf} = \frac{\Delta_{cost}}{\Delta_{mtf}} = \left[\frac{(x_0 + \Delta_x) \cdot (y_0 + \Delta_y)}{(x_0 + \Delta_x) + (y_0 + \Delta_y)} - \frac{x_0 y_0}{x_0 + y_0} \right]^{-1} \cdot (a \cdot \Delta_x + b \cdot \Delta_y) \quad (A5.9)$$

In Fig. A5.6, the plot of (A5.9) for $a = 1$ €/yr and $b = \{1, 0.25\}$ €/yr, and $x_0 = 8$ yr and $y_0 = \{8, 12\}$ yr, is presented, showing the importance of the cost-benefit analysis to identify the optimum investment strategy. The minimum value of c_{mtf} corresponds to the optimum increase of the base $MTTF$, Δ_x and Δ_y , and to the optimum additional investment in each component, Δ_{cost_x} and Δ_{cost_y} .

In most practical cases, costs a and b are not constant (which means that the cost of a component does not increase linearly with the $MTTF$) and, therefore, they can be defined as a function of the $MTTF$, i.e., $a = f_a(MTTF_{brg})$ and $b = f_b(MTTF_{wdg})$. For the minimum value of $MTTF$ there is a corresponding offset value for a and b curves as a function of $MTTF$. The functions can be, for example, linear, quadratic, cubic, etc., and, for the sake of simplicity, they can be linearized as follows. Considering that a_i is the cost per each additional year of $MTTF_i$ ($a_i = f_{a_i}(MTTF_i)$), for the i^{th} component, and that two points A and B of that function are known (e.g., representing an step-increase in the quality or lifetime of the product or component, with the inherent cost increase), the additional investment, Δ_{cost_i} , is given by (A5.10), where the function $a_i = f_{a_i}(MTTF_i)$ is given by (A5.11), and $a_i(MTTF_{i_A})$ and $a_i(MTTF_{i_B})$ represents the a_i value for the $MTTF$ in points A and B, respectively. The total investment cost, C_i , associated with the component i is given by (A5.12).

$$\Delta_{cost_i} = a_{i_B} \cdot MTTF_{i_B} - a_{i_A} \cdot MTTF_{i_A} \quad (A5.10)$$

$$a_i = f_{a_i}(MTTF_i) = \frac{(a_{i_B} - a_{i_A})}{MTTF_{i_B} - MTTF_{i_A}} \cdot (MTTF_i - MTTF_{i_A}) + a_{i_A} \quad (A5.11)$$

$$C_i = f_{C_i}(MTTF_i) = a_i(MTTF_i) \cdot MTTF_i \quad (A5.12)$$

Generalizing, the total additional investment, Δ_{cost_syst} , for an overall $MTTF$ increase, Δ_{mtf_syst} , in a system with m components i is given by (A5.13) and (A5.14), respectively. The cost per additional year (or other time constant) in system $MTTF$ is given by (A5.15), which has to be minimized by properly choosing the investment share. The total system cost, C_{syst} , is given by (A5.16).

$$\Delta_{cost_syst} = \sum_{i=1}^m \Delta_{cost_i} \quad (A5.13)$$

$$\Delta_{mtf_syst} = \left(\sum_{i=1}^m \frac{1}{MTTF_i + \Delta_{mtf_i}} \right)^{-1} - MTTF_{syst_0} \quad (A5.14)$$

$$C_{mtf_syst} = \frac{\Delta_{cost_syst}}{\Delta_{mtf_syst}} \quad (A5.15)$$

$$C_{syst} = \sum_{i=1}^m C_i \quad (A5.16)$$

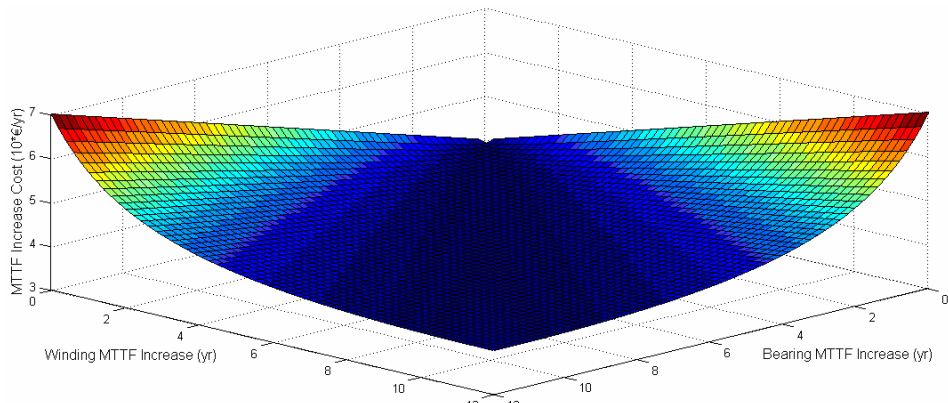
The total cost per year associated with the system failure, F_{syst} , can be expressed by (A5.17), where q_{syst} is the average system downtime cost per time unit (e.g., hour, day, or week), λ_{syst} is the system failure rate, r_{syst} is the average repair or operation reestablishment time (quantified by $MTTR$), Δt is the period of the analysis, and m_{syst} is the average cost per repair intervention in the system. The cost q_{syst} can be defined as a function of the duration of failure (or downtime) and failure rate (that dependency actual exists in most industries), yielding $q_{syst} = f_q(\lambda_{syst}, r_{syst})$. The extra system failure cost, Δ_{F_cost} , is given by (A5.18).

$$F_{syst} = (q_{syst} \cdot r_{syst} + m_{syst}) \cdot \lambda_{syst} \cdot \Delta t \quad (A5.17)$$

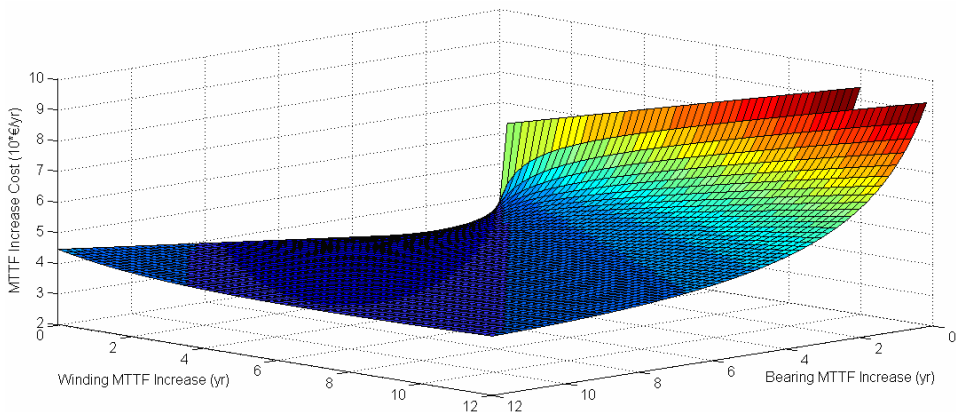
$$\Delta_{F_syst} = (q_{syst} \cdot r_{syst} + m_{syst}) \cdot (\lambda_{syst} + \Delta \lambda_{syst}) \cdot \Delta t - F_{syst} = (q_{syst} \cdot r_{syst} + m_{syst}) \cdot (MTTF_{syst} + \Delta_{mtf_syst})^{-1} \cdot \Delta t - F_{syst} \quad (A5.18)$$

Excluding the energy consumption costs, the total undiscounted cost variation associated with the system, for the period Δt , is given by the summation of (A5.13) and (A5.18).

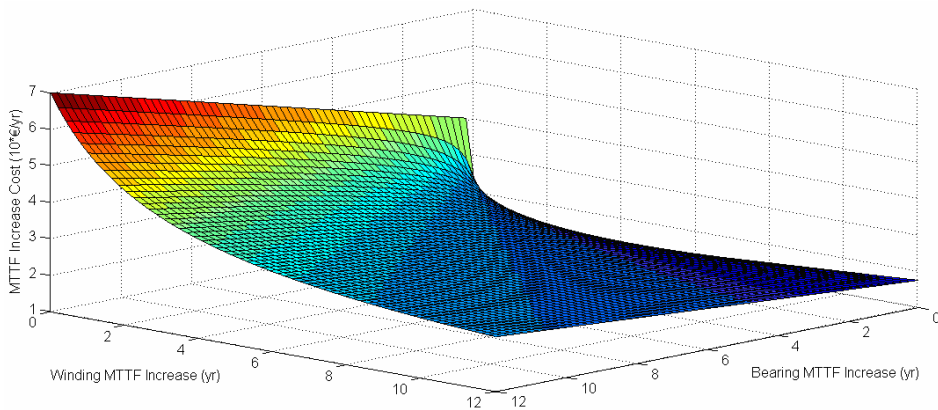
It can be concluded that the user can optimally share the investment among all system components on the basis of the $MTTF$ of each component and the cost associated with its increase. In short, the minimum of (A5.9) can be calculated to define the optimum share of the investment per component, the total investment variation can be calculated by (A5.13), and the total cost associated with the system failure can be calculated by (A5.18). The optimum investment for the minimum value of the total cost variation, given by the sum of the two previously referred costs, can be estimated mathematically or graphically. This principle can be applied during the purchasing, the maintenance or the repair of each component of the motor system or of the motor itself.



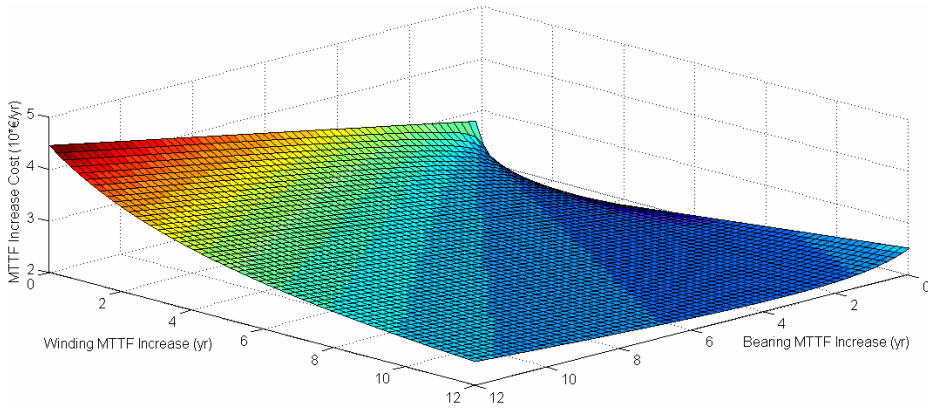
(a) $x_0 = 8$ yr; $y_0 = 8$ yr; $a = 1$; $b = 1$.



(b) $x_0 = 8$ yr; $y_0 = 12$ yr; $a = 1$; $b = 1$.



(c) $x_0 = 8$ yr; $y_0 = 8$ yr; $a = 1$; $b = 0.25$.



(d) $x_0 = 8$ yr; $y_0 = 12$ yr; $a = 1$; $b = 0.25$.

Fig. A5.6. Motor *MTTF* increase cost as a function of the winding and bearing *MTTF*.

Particularly in situations where the IM failure leads to high process downtime costs, measures should be taken to approximate the $MTTF_{brg}$ to the $MTTF_{wdg}$ by means of, for example, using high-robustness bearings (e.g., with silicon-nitride spheres), correct lubrication, improved seals, proper alignment between motor and load, and mitigation of the bearing-crossing currents. In the following sections, several issues on bearing and windage reliability are discussed.

Considering now an EMODS without redundancy, in which all the devices are connected in series, the $MTTF$ of such system is given by (A5.19), where λ_{pwr} is the power supply (including contactors, protection, cables, etc.) failure rate, λ_{ec} the electronic controller failure rate, λ_{mtr} the motor failure rate, λ_{trs} the mechanical transmission failure rate, and λ_{dvc} the end-use device or load failure rate. In such systems, the principles previously proposed for optimum investment can be applied. Therefore, the user should share the investment in a balanced or optimum way to increase the reliability of all components, instead of invest in one or two components alone to increase dramatically their reliability. The unbalance degree of investment should be dictated by the cost per $MTTF$ increase of each individual component.

$$MTTF_{\text{sys}} = \frac{1}{\lambda_{\text{sys}}} = \frac{1}{\lambda_{pwr} + \lambda_{ec} + \lambda_{mtr} + \lambda_{trs} + \lambda_{dvc}} \quad (\text{A5.19})$$

For example, considering typical values for the $MTTF$ of EMODS components, the mechanical transmission is in general the component having the lowest $MTTF$, which, in most cases, can be increased at a moderate additional investment, thus justifying an increased effort to maximize lifetime of that component. For some critical systems, incorporating belts and chains, redundancy can be considered, since the additional investment is, in principle, moderate.

A5.3 Considerations on Bearing Currents

As discussed in the previous section, the $MTTF$ of IMs strongly depends on the bearings $MTTF$ and, therefore, they are a key part of the motor in the reliability scope. Nowadays, an increasing amount of low-voltage IMs are fed by VSDs and, due to a number of phenomena that will be addressed next, the bearings of such motors are prone to have their lifetime shortened.

In a simplified form, considering only mechanical wear, the bearing useful lifetime, t_{lf} , can be defined by (A5.20), where ξ is the quotient between actual and rated loads of the bearing (related to the axial and radial forces), K_1 and K_2 constants, and ω the angular speed [12], [111]. Equation (A5.21) gives the relation between useful lifetime for different conditions, being useful to estimate the lifetime decrease in relation to a reference or original situation.

$$t_{lf} = K_1 \cdot \omega^{-1} \cdot \xi^{-K_2} \quad (\text{A5.20})$$

$$\frac{t'_{lf}}{t''_{lf}} = \frac{\omega'' \cdot (\xi'')^{K_2}}{\omega' \cdot (\xi')^{K_2}} = \frac{\omega''}{\omega'} \cdot \left(\frac{\xi''}{\xi'} \right)^{K_2} \Leftrightarrow t''_{lf} = t'_{lf} \cdot \frac{\omega'}{\omega''} \cdot \left(\frac{\xi'}{\xi''} \right)^{K_2} \quad (\text{A5.21})$$

The constant K_1 depends on the materials of the bearing and on its operating conditions (equal to a correction factor depending on greasing conditions, typically equal to $2 \times 10^6 / 60$, considering angular speed in r/min [47]). The constant K_2 depends on the type of bearing, being equal to 3 for standard steel ball bearings [12], [111]. Although not included in (A5.21), the lubricant temperature also influences strongly the bearing lifetime, particularly those lubricated for life. For modern high quality bearings the nominal or base life can deviate significantly from the actual service life in a particular application, depending the latter on a variety of influencing factors including lubrication, degree of contamination, misalignment, proper installation and environmental conditions, as well as bearing currents activity, being the latter extremely important [111]. Therefore, it would be desirable to include in (A5.20) the major aspects influencing the bearings lifetime, besides the mechanical wear.

It can be assumed that bearings of low/medium-power motors are typically designed for a nominal useful lifetime, t_{lf} , of 20000 h, according to (A5.20) [8], [47]. The partial loading (i.e., $\xi < 1$) increases useful lifetime by the power of three (in the case of standard steel ball bearings), therefore, for a typical motor with 75% average load, the useful lifetime can be approximately extended up to 2.4 times (i.e., 48000 h) [8], [47], [111]. In reality, this is a little more complex as ξ depends on both axial and radial forces and for part-load operation only the radial forces decrease [8], [47]. In principle, considering the same radial load, the angular speed duplication leads to the bearing lifetime reduction to half.

Typically, bearings overall lifetime (taking into account the off-operation periods) in industrial applications is within 4 to 8 yr, depending on a number of factors, such as bearing type and quality, lubricant used, maintenance, annual operating hours, and operating conditions²⁰, including actual angular speed and load [8], [12], [13], [14]. On average, 16% of the bearing premature failures are due to inadequate mounting, 36% to inadequate lubrication, 14% to contamination and 34% to excessive wear [111].

Although the vast majority of the bearing failures in IMs be caused by phenomena of mechanical, thermal and chemical nature (e.g., shaft misalignment, excessive mechanical stress,

²⁰ E.g., bearing speed and load (radial and axial), motor power supply (line/mains or VSD), motor eccentricities, load/motor vibration, mechanical transmission type and alignment, operating temperature, surrounding environment, etc.

excessive operating temperature²¹, excessive mechanical vibration and shock pulses, overspeed, inadequate lubrication, lubricant contamination and overheating, manufacturing defects, etc.) the electrical current crossing the bearings is another type of phenomenon (of electrical nature) that can occur in rotating electrical machinery (AC or DC), including motors and generators, which can contribute significantly to the bearing failure [5], [8], [14], [15].

The circulation of electrical currents through bearings is associated with the existence of a voltage between the motor shaft ends or between the shaft and stator/frame²², which results mainly from motor electromagnetic asymmetries²³ and/or power supply distortion and/or unbalance, in the case of line-fed IMs, and high-frequency²⁴ common-mode voltages (CMVs) and voltage transients²⁵ in the case of VSD-fed IMs [5], [8], [14], [48]. The high rate of voltage rise/variation, du/dt , is responsible for adverse effects in the form of motor insulation stress, EMI, and bearing and leakage currents [48]. It should be noted that power supply unbalance effects can actually propagate through VSD to motor (as it is discussed in Appendix 4), potentially leading to the circulation of currents similar to those that can exist in line-fed IMs. Additionally, power network voltage transients can also occur (due to atmospheric discharges, power network manoeuvring, etc.), causing bearing current circulation in a similar way to that in VSD-fed IMs. Any of these conditions can occur independently or simultaneously to produce stray (or parasitic) bearing currents of different natures.

In IMs fed by IGBT-based inverters, the bearing high-frequency current circulation can exist in almost all power and voltage ranges, and a number of recent studies confirm that, nowadays, they are becoming a significant cause of premature bearing failure [16], [109], [110], [111]. At this stage, it is important to distinguish bearing currents from leakage currents, which are those currents flowing from stator winding to frame, without passing through bearings, stressing the stator winding insulation and, when returning to the ground path combined with bearing currents (the total ground current can itself be called leakage current), originate EMI problems either by conduction or radiation [8], [16], [48].

Low-frequency bearing currents are likely to appear only in the line-fed, high-power and/or high-voltage motors [5], [8], [13], [14], [15], [16], [22]. Additionally, electric discharges can occur due to the electrostatic charging effect in the rotor from the driven devices (e.g., electrostatic charging generated by the friction and shock of particles in pump blades) [5], [8].

²¹ Excessive operating temperature is particularly dangerous since it changes the mechanical stress between the bearing components (which suffer a dimension change depending on the temperature gradient), which can increase the mechanical friction and wear, in turn contributing to the overheating. Moreover, the lubricant experiences a reduction in its lifetime and lubricating properties.

²² It is considered that the stator/frame is the motor ground, connected to the inverter ground and to the earth.

²³ For example, motor magnetic circuit asymmetry due to stator-rotor eccentricities.

²⁴ Typically between 2 and 20 kHz.

²⁵ Voltage-pulse overshoot at the motor terminals created by fast-switching IGBTs, causing high voltage rate (du/dt).

NEMA-MG 1, Part 31 (definite-purpose inverter-fed polyphase motors) [98], is an industry-accepted standard defining what is a VSD compatible motor. This standard addresses, in part, the motor capability with respect to temperature, torque, insulation, and operating limitations (excess current, line-to-line voltage, etc). It also addresses “shaft voltages that can result in the flow of destructive currents through motor bearings”, concluding with the following statement: “At this time, there has been no conclusive study that has served to quantify the relationship of peak voltage from inverter operation to bearing life or failure. There is also no standard method for measuring this voltage. Because of that, the potential for problems cannot consistently be determined in advance of motor installation”. Due to the phenomenon’s rarity and unpredictability, most manufacturers do not include warnings or recommendations in their literature or operation and maintenance manuals. Amidst the unpredictable cases of bearing current damage, industry experts have identified some factors that exacerbate the occurrence and promote damaging effects, such as the high switching frequency and inadequate grounding [109].

As a short introduction, the high-frequency bearing currents circulation in VSD-fed IMs, have two main different modes, but the same primary cause, which is the CMVs generated in the VSD output due to the instantaneous unbalance of the output PWM voltage waveforms. The first current mode is a consequence of the generated voltage between the shaft and the ground due to the motor stray capacitances. The presence of a shaft-ground high frequency voltage leads to the circulation of capacitive- and resistive-nature high frequency currents through both bearings, constituting the first circulation mode. The second high frequency current mode is a consequence of the voltage between the shaft ends, induced by the circulation of high-frequency common-mode currents from windings to the frame. The presence of a voltage between the shaft ends leads to the circulation of a capacitive and resistive high frequency current through the closed circuit formed by both bearings, shaft and frame. In both current modes, the constant circulation of resistive- and capacitive-nature currents, although its low amplitude, leads to the accelerated degradation of the lubricant, balls and races. If instantaneous electric contact occurs between the balls and races of one or both bearings, and a significant voltage exists between the shaft ends or between the shaft and ground, an electric discharge (characterized by a high current density) occurs, leading to severe damages in the balls and races surfaces (pitting and fluting), due to electric discharge machining (EDM) when the voltage accumulated in the shaft discharges through the bearing. The described effects can be worse if voltage transients occur in the voltage waveforms applied to the motor. In short, due to the existence of the IM stray capacitances between the windings and frame, windings and rotor, rotor and frame, and inside the bearings, high-frequency currents can circulate in the bearings of VSD-fed IMs. These currents can significantly decrease the lubricant and bearing

lifetime, and will eventually cause catastrophic motor bearing failure. These phenomena are analyzed in the following sections.

A5.3.1 Bearing Electrical Model and Lifetime

The advances in metallurgy processes and lubricants led to the reduction of the oil/grease film between the spheres (or balls) and the races of the bearings (reduced tolerances), to the improvement of their performance, and to the extension of their useful lifetime. In general, the impedance of the bearings is mainly resistive for speeds lower than 100 r/min but, for higher speeds (most of the motors operate with speed above 1000 r/min), the spheres movement on the lubricant (oil or grease) creates an insulating film (hydrodynamic film operation zone), with a thickness varying from 0.1 to 1 μm (typically in the range of 0.2-0.3 μm) and the impedance of the bearing becomes mainly capacitive²⁶, with an associated stray (or parasitic) capacitance. In these circumstances, the ohmic resistance can achieve values in the order of $\text{M}\Omega$. The higher the speed is, the higher the possibility of bearing stray capacitance existence will be. However, in some instants, random electric contacts between the spheres and races can occur due to imperfections in the races and spheres surface and/or high radial loads, leading to a sharp decrease of the bearing impedance to very low values [14]. The dielectric breakdown of the lubricant film²⁷, which occurs when its dielectric capability is exceeded by the shaft-ground voltage (electric charge accumulation in the rotor assembly), leads to a similar effect [8], [10], [14], [15]. In Fig. A5.7, an approximate equivalent circuit for a typical steel ball bearing is presented, in which the random electric contact between the races and spheres is represented by a switch.

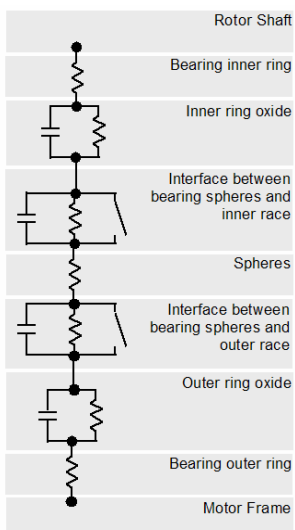


Fig. A5.7. Approximate equivalent circuit of a steel bearing [8], [10], [51].

²⁶ The lubricant film acts like a dielectric in a capacitor.

²⁷ For a sinusoidal voltage, the electric disruption occurs typically for peak values of 2-3 V. For a PWM voltage switched at $f_s > 1$ kHz the electric disruption occurs for peak values of 3-30 V [5], [8], [10], [12], [13], [14], [15], [51].

The lubricant (oil or grease) film thickness decreases with the increase of the lubricant temperature (due to the reduction of the viscosity), leading to the reduction of the breakdown voltage²⁸ and to the increase of the bearing capacitance (in the case of uninsulated bearings). The bearing temperature depends on load, speed, mechanical stress, motor internal temperature, ambient temperature, lubricant type, and parasitic bearing currents circulation. As previously referred, an increase of 10°C in the mineral lubricant temperature leads to a reduction of approximately 35% in their lifetime [8]. The semi-synthetic and synthetic lubricants lifetime decrease with the temperature increase is less pronounced [8]. Special greases are also available with increased thermal, electrical and chemical robustness [111].

The bearing temperature increase leads to the increase of the operating temperature of the lubricant. Thus, in order to avoid the bearing lifetime decrease, the operating temperature increase requires an increase in the lubrication frequency.

When a bearing is crossed by currents, accelerated degradation of the lubricant and of the races and spheres surface (pitting and fluting) occurs, which depends, in part, on the current density value, leading to the premature failure of the bearing. The expected lifetime of a bearing operating within nominal conditions, but experiencing electrical currents activity, can be typically described by the lifetime-current density curve presented in Fig. A5.8. If the current density is maintained below 0.8 A/mm² (peak value), the bearing lifetime is not significantly affected, being mainly limited by mechanical factors [8], [13], [14], [10]. For a current density higher than 2 A/mm² the expected bearing lifetime is 300 hours. Therefore, the recommended operating zone goes up to 0.8 A/mm². Note that, the severity of the damages caused by electric discharges depends upon the current density and not upon the current amplitude [10], [13], [14].

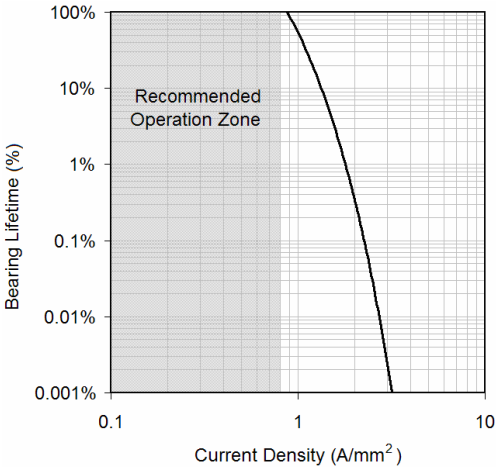


Fig. A5.8. Expected bearings lifetime as a function of current density peak value [10], [51].

²⁸ For operating temperatures significantly higher than normal (> 90°C) the breakdown voltage can decrease down to 1/3 of the normal values [5], [8], [10], [12], [13], [14], [15], [51].

The typical dielectric strength of the lubricant film is between 10 and 15 V/ μm , although it decreases with the increase of the duration of the peak value²⁶.

The lubricant viscosity reduction can accelerate the bearing wear. The increase of the lubricant viscosity reduces the heat transfer between the inner and outer rings [3] and increases the viscous friction losses of the bearing. The joint action of those factors leads to the increase of the temperature of the bearing and accelerates the lubricant degradation.

The electric current discharges²⁹, resulting both from the spheres-races contact and lubricant dielectric breakdown, are responsible by the most significant damages in the races and spheres, as electroplating, micro-craters, pitting and fluting³⁰, due to frequently repeated flash-over current, lubricant degradation and metallic particles production. The joint action of those effects leads to the accelerated degradation of the bearings [8], [14], [48]. For radial bearings (which represent the vast majority), the higher the radial force imposed by the load, the higher the contact area associated with surface irregularities and, due to the reduction of the current density associated with electric discharges, the lower the damages inflicted by them [14].

The premature lubricant degradation and, at a later stage, the additional mechanical wear of the races and spheres, leads to the increase of the friction and to the reduction of the bearing lifetime. Ultimately, those effects result in the reduction of the reliability and efficiency of the IMs.

A5.3.2 Motor High-Frequency Electrical Model and Lifetime

When IMs are excited by voltages and currents with high-frequency harmonic components (as those produced by VSDs, associated with the switching frequency and with the high du/dt of the voltage transients at the motor terminals), their stray capacitances (electrostatic coupling) become relevant, and must be considered if a high-frequency analysis is to be made. In Fig. A5.9, the stray capacitances are represented. In the high-frequency domain, the inductances can be neglected, and the major lumped stray capacitances of the motor are: stator winding-stator core capacitance (C_{WS})³¹, rotor-stator core capacitance (C_{RS}), stator winding-rotor capacitance (C_{WR}), and bearings capacitance (C_B). It is assumed that the motor frame is in contact with the stator core. There are also capacitances between windings of different phases (C_{WW}) and capacitances between winding coils and turns (C_{TT}). In Fig. A5.10, the typical values for C_{WS} , C_{RS} , C_{WR} and C_B are presented.

²⁹ This phenomenon as a similar effect to the machining of metal parts by means of electric discharge, being known as electric discharge machining, EDM [8], [48], [111].

³⁰ The deterioration will appear as fluting (groves) in the bearing race for motors running at relatively constant speeds and as frosting on the race surfaces for motors operating over a wide speed range [48].

³¹ The stray capacitance between the stator windings and stator core is typically the highest stray capacitance in the motor.

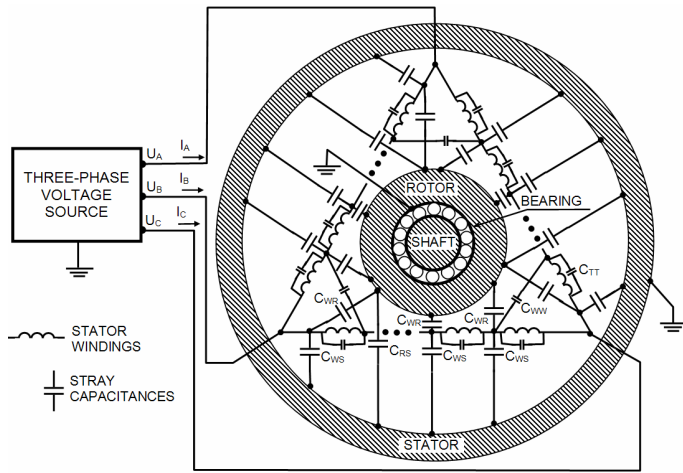


Fig. A5.9. Representation of the major stray capacitances in a delta-connected three-phase induction motor [10], [51].

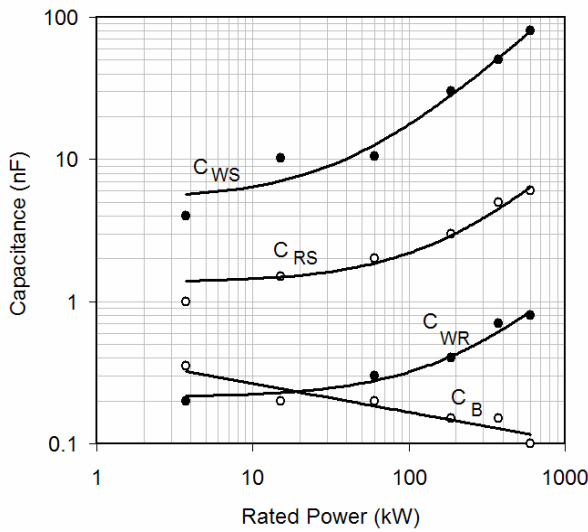


Fig. A5.10. Approximate values for the lumped stray capacitances in three-phase induction motors, as a function of the rated power [5], [12], [13], [14], [15], [10], [51].

A5.3.3 Motor Eccentricities

Several factors related either to manufacturing and repair/maintenance of rotating electrical machines, or to operating conditions, can cause stator-rotor eccentricities. Two different types of eccentricities can be defined – static and dynamic [5], [8] (Fig. A5.11).

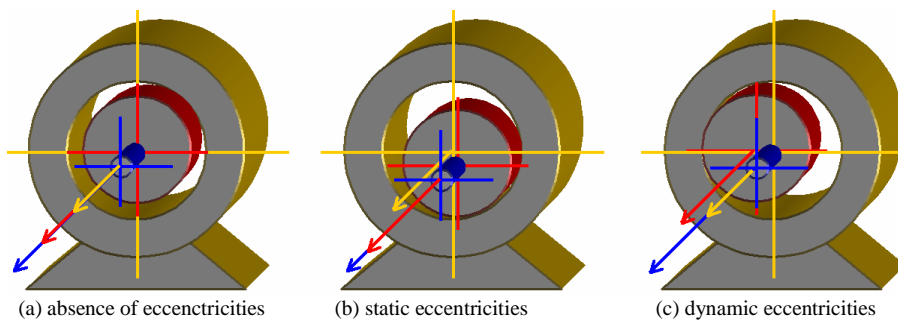


Fig. A5.11. Types of eccentricities in motors [8].

In the absence of eccentricities, the rotor symmetry axis (rotor geometric centre) is coincident with the stator symmetry axis (stator geometric centre) and with the rotor rotation centre. If the

rotor symmetry axis coincides with the rotor rotation centre, but does not coincide with the stator symmetry axis, a static eccentricity situation occurs. In this situation, the position corresponding to the minimum air-gap radial width is constant in space and time. The presence of this type of eccentricities is related with dimensional tolerances in the manufacturing process of the different motor parts (end-shields, bearings, stator core, frame, shaft, rotor core, etc.), incorrect mounting of end-shields and/or bearings, damaged and/or defective bearings, stator deformations, misaligned couplings, etc. [5], [8]. When the rotor symmetry axis does not coincide neither with stator symmetry axis nor with the rotor rotation centre, a dynamic eccentricity situation occurs. In this situation, the position corresponding to the minimum air-gap width (radial distance between rotor outer surface and stator inner surface) rotates along the stator inner perimeter, varying as a function of space and time. This kind of eccentricities is associated with manufacturing defects, rotor dynamic unbalance, as well as shaft and/or rotor core deformations due to the overheating or to the presence of high thermal gradients and high centrifugal forces existence and/or air-gap radial magnetic forces unbalance [5], [8].

In IMs, asymmetries in the air-gap space resulting from stator-rotor eccentricities lead to the magnetic flux asymmetric distribution and, consequently, to the air-gap radial magnetic forces unbalance [5], [8], [12]. The latter effect contributes to the increase of the mechanical vibration and can cause mechanical deformations in the rotor/shaft, which, jointly, lead to the accelerated mechanical degradation of the bearings and to the increase of the eccentricity itself³². In limit situations, catastrophic effects can occur as a result of the contact between rotor and stator surfaces.

The asymmetrical magnetic flux distribution, besides the referred effects, also leads to the increase of motor losses, mechanical vibration and acoustic noise [5], [8].

A5.3.4 Common-Mode Bearing Currents

The bearing common-mode currents³³ (noncirculating-type bearing currents, denoted by CMC or I_{CM}) in VSD-fed IMs are associated with the existence of a voltage between the shaft and the frame (normally grounded), U_{RS} , which results from the excitation of the motor stray capacitances (Figs. A5.12 and A5.13) by high-frequency common-mode voltages (denoted by CMV or U_{CM}) generated by the inverter³⁴ [8], [10], [48]. CMCs return path is through the connection between the IM ground and inverter ground, and/or even through the VSD power source neutral-ground path (if star connection is used), when the neutral is earthed/grounded. In most cases, the inverter ground (which should be earthed) corresponds to the input DC-link middle point, or a point between two

³² For a specific point if the air-gap decreases the reluctance decreases and, consequently, the magnetic induction increases. The attraction force between rotor and stator in that point will be higher than that of the antipodal point. Thus, a magnetic radial force unbalance situation is created, which can lead to severe physical effects.

³³ Also called shaft ground currents.

³⁴ The PWM voltage system generated by inverters can be decomposed in high-frequency components of differential mode and common mode [19].

series-connected, equal-value, small capacitors. It should be noted that the middle point of the main large capacitors in the DC-link forms a floating reference or ground of the inverter, usually not accessible externally. Basically, the high-frequency currents circulate in the closed circuit VSD-IM-ground. CMCs can also circulate through the devices mechanically coupled with the motor. The analysis of the CMCs circulation is based on an approximate representation of the distributed stray capacitances in a lumped-parameter motor model.

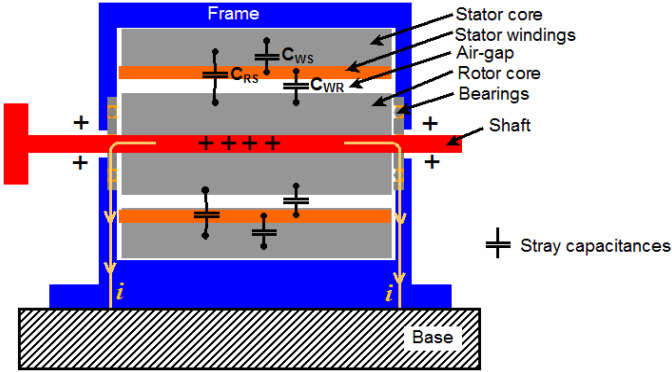


Fig. A5.12. Approximate representation of common-mode currents in induction motors [8], [51].

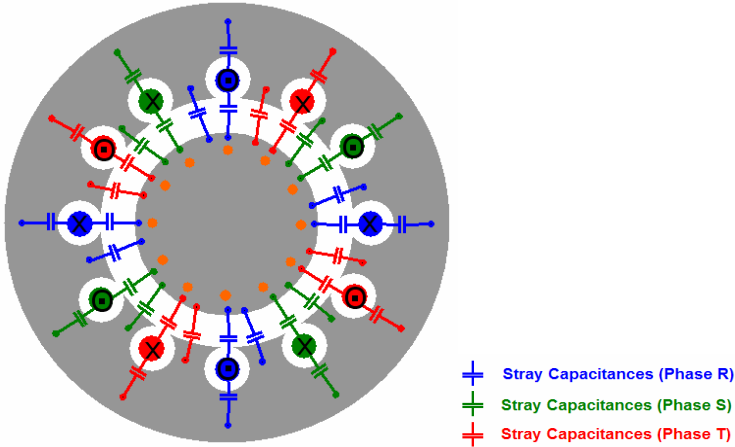


Fig. A5.13. Approximate representation of the stray capacitances in induction motors [8], [51].

For a motor fed by a typical two-level VSD, the CMV results from the instantaneous unbalance of the PWM three-phase voltage waveforms, which oscillates in relation to the ground, between $+\frac{1}{2}U_{DC}$ and $-\frac{1}{2}U_{DC}$, assuming constant DC-bus voltage (between positive and negative poles and between them and the ground), no stray capacitances between windings and ground, and no voltage reflection effect at the motor terminals. The CMV can be calculated by (A5.22), where $u_{Ag, Bg, Cg}$ are the instantaneous line-ground voltages (see Chapter 3). In star-connected loads, (A5.22) corresponds to the neutral-to-ground voltage. Equation (A5.22) can also be used to compute the CMVs in delta-connected motors (which represent the vast majority), since there is no neutral point. The most significant CMV harmonic has a frequency equal to the PWM switching

frequency and maximum amplitude equal to about $\frac{1}{3}$ of U_{DC} . In Fig. A5.14, the CMV simulated³⁵ waveform and spectrum is shown. In Fig. A5.15, the simulated CMV waveform, rotor-frame voltage and capacitive rotor-ground current are shown, considering stray capacitances, C_{WS} , C_{WR} , and C_{RS} . It should be noted that the winding-frame stray capacitance actually act as a low-pass filter, reducing the neutral-ground voltage.

$$u_{CM} = \frac{1}{3}(u_{Ag} + u_{Bg} + u_{Cg}) \quad (\text{A5.22})$$

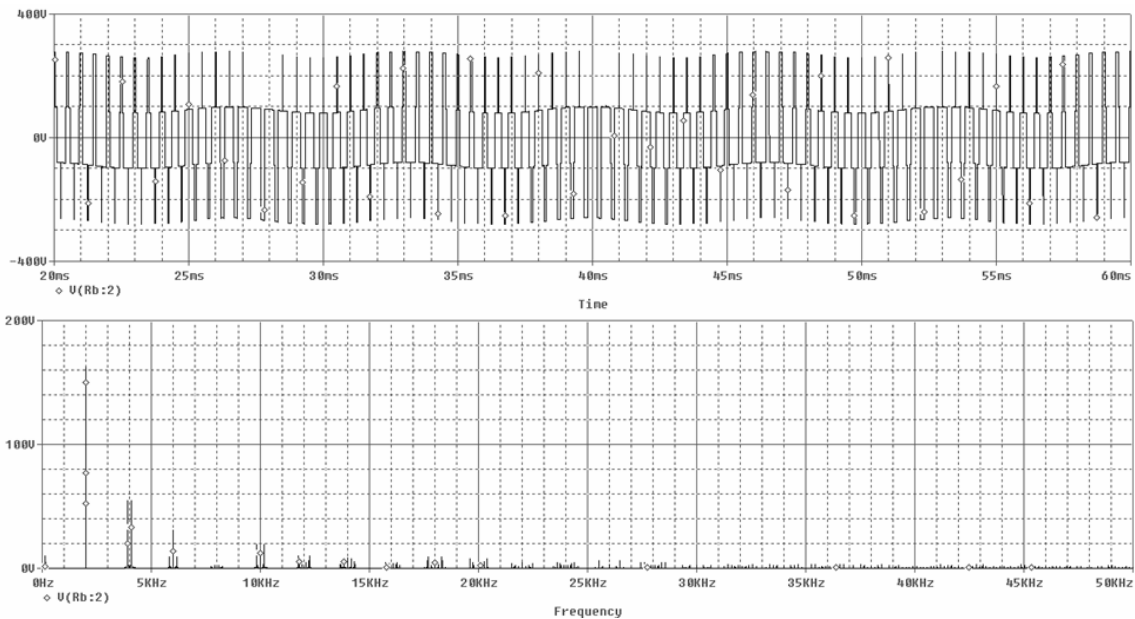


Fig. A5.14. Simulated CMV (in relation to ground) waveforms and the respective FFT for a VSD (diode rectifier plus DC-link plus 2-level inverter) feeding a fixed RL-series load ($L = 52.28$ mH, $R = 21.89 \Omega$), with a 2-kHz switching frequency and 540-V DC-bus mean voltage. Inverter output fundamental frequency equal to 27 Hz. 5-M Ω source-neutral-ground impedance to reduce 3rd and 9th harmonics in load neutral-ground voltage.

In short, shaft-ground voltages are associated with zero-sequence harmonics (e.g., triplen harmonics), stray capacitance three-phase system asymmetry (leading to fundamental and harmonics zero-sequence components existence), and fundamental and harmonic voltages unbalance. The neutral-ground voltages are associated with zero-sequence harmonics, winding asymmetry (e.g., unequal per-phase impedance), and fundamental and harmonic voltages unbalance.

In order to study the common-mode and shaft-ground voltages, several experimental tests were carried out with low-voltage inverters (2-level and 3-level inverters, see Chapter 3) and 3-kW and 7.5-kW motors (connected in both star and delta modes), at different voltages, fundamental frequencies and switching frequencies. The motors were prepared with a shaft contact brush to

³⁵ Simulations performed with PSPICE software tool.

allow the voltage measurement between shaft and ground. All instantaneous quantities were obtained with an oscilloscope with serial communication with a computer, and processed with MATLAB software (several scripts were written for FFT generation and voltage waveform characterization, e.g. distribution of instantaneous voltage levels per voltage range). Due to the huge number (more than 1000) of data sets obtained, only part of them are presented, but the conclusions are based on the analysis of all data obtained.

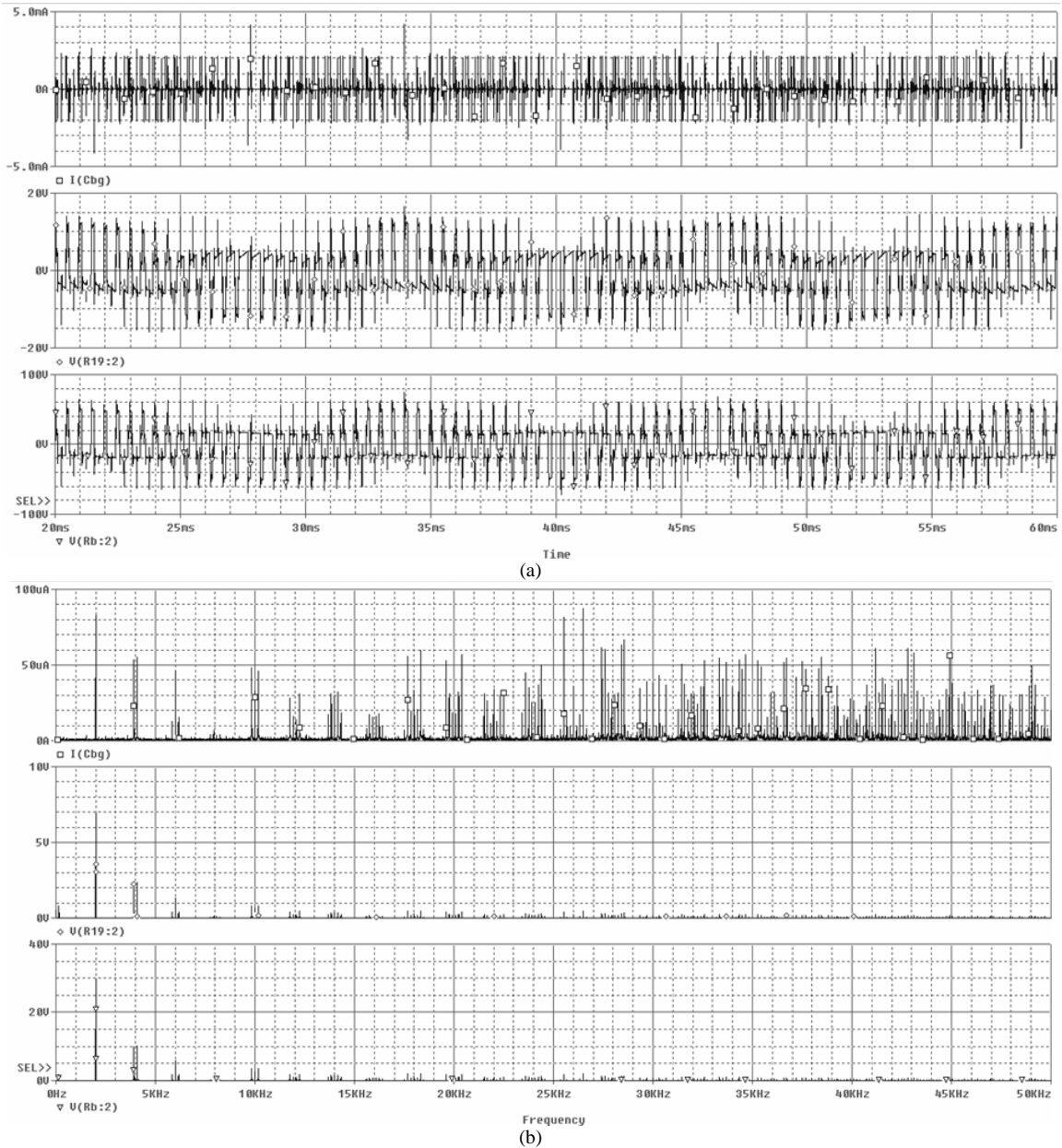


Fig. A5.15. Simulated CMV (in relation to ground) waveforms (a) and the respective FFT (b) for a VSD feeding a RL-series load ($L = 26.14 + 26.14$ mH, $R = 21.89 \Omega$) at 27 Hz fundamental frequency, with a 2-kHz switching frequency and 540-V DC-link mean voltage, considering stray capacitances between windings-middle point and frame (2 nF/phase), windings-middle point and rotor (0.1 nF/phase) and between rotor and frame (1 nF): (top, (a) and (b)) capacitive rotor-frame current; (middle, (a) and (b)) rotor-frame voltage; (bottom, (a) and (b)) CMV.

For the 7.5-kW and 3-kW IMs, both 400-V, 50-Hz, 4-pole motors, in one of the experimental setups, the line-ground voltage, U_{ag} , the star-neutral-ground voltage, U_{ng} , and the shaft-ground voltage, U_{sg} , as well as the ground current (by means of a clamp-on current probe around the three phases conductors, representing the total leakage current³⁶), I_g , were all acquired and processed. For the direct line/mains supply case (base case), U_{ng} and U_{sg} were found to be negligible, demonstrating a fair electromagnetic symmetry of the motors being tested. In the case of inverter-based supply, 2-, 5-, and 8-kHz switching frequencies were used. The setup is enough to analyze the most relevant spectrum of the considered waves.

Part of the results is presented in Figs. A5.16-A5.23. First, regarding the low-frequency harmonics and zero-sequence or homopolar components, observing Fig. A5.16, for star-connected winding, a significant 3rd order harmonic is found in the neutral-ground voltage as a consequence of the phase-ground voltage distortion, containing a significant 3rd order harmonic. This neutral-ground zero-sequence voltage harmonic component becomes significant when the inverter operates in the nonlinear or overmodulation region ($m_a > 1$), being maximized for the square-wave or six-step operation. In the latter case, assuming a 50-Hz, square wave, oscillating between $\pm \frac{1}{2}U_{DC}$, and a star connected winding, the 3rd-order, zero-sequence component, present in the neutral, has 3 times the square-wave fundamental frequency and $\frac{1}{3}$ of the square wave amplitude, i.e. $\pm \frac{1}{6}U_{DC}$, having also a square shape. Curiously, the 3rd order harmonic is very low in the shaft-ground voltage, being dominated by a fundamental frequency zero-sequence component (according to Fig. A5.16, the amplitude of the shaft-ground fundamental component reach more than 4 V, for the case of $f_s = 5$ kHz), which can result from supply voltage unbalance (e.g., due to the voltage unbalance impact on the VSD output voltage) and/or from unbalance three-phase stray-capacitance system, which can be considered as connected in star (actually two capacitive impedance stars can be considered – stray capacitance system between windings and frame, and stray capacitance system between windings and rotor, being the frame and rotor the respective neutral points). Since the supply voltage unbalance lead to a zero-sequence fundamental component in the winding star neutral, which is not the case, an explanation to the 3rd order harmonic in the shaft-ground voltage is the stray capacitance system unbalance (related to physical asymmetries). Although not important, the combination of low- and high-frequency shaft-ground voltage components, can lead to the increase of the absolute maximum shaft-ground peak values, and therefore to the intensification of the bearing currents activity, particularly those associated with the electric discharges. That fact is a strong argument to also mitigate the low-frequency shaft-ground and winding-ground CMVs.

³⁶ The capacitive leakage current pulses are characterized by a damped ringing effect.

It is important to distinguish the harmonics in respect to the line fundamental voltage and in respect to the inverter output fundamental voltage. In the output voltage of a three-phase full-wave or six-pulse diode rectifier, fed by a star-connected power supply with a reduced impedance between neutral and earth (or ground), and feeding a 2-level inverter, triplen harmonics (particularly the 3rd), in respect to the line frequency, are generated in the positive or negative DC-bus poles in relation to ground, as well as the 6th order harmonic in the positive-to-negative DC-bus voltage, which is the typical ripple. Increasing the impedance between supply neutral and ground, the odd triplen harmonics (in relation to the line frequency) are strongly attenuated, particularly the third harmonic.

In these conditions, due to the DC-bus voltage ripple, the line-to-line voltage produced by the VSD has harmonics corresponding to the frequencies $f = 6f_{1(line)} \pm f_{1(out)}$ (e.g., in relation to the output voltage, 11th and 13th harmonics for 25 Hz, 10.1th and 12.1th inter-harmonics for 27 Hz and 5th and 7th harmonics for 50 Hz, as shown in Appendix 4). When the output frequency is equal to the line frequency, these harmonics can be increased or decreased when interacting with odd non-triplen harmonics associated with the output PWM voltage waveforms (5th, 7th, 11th, ... harmonics, in relation to the output frequency, become significant for $m_a > 1.0$), depending on the time (displacement) for the same order harmonics.

Furthermore, the neutral-ground voltage or CMV, besides the switching frequency related harmonics, have also odd, triplen harmonics (in relation to line frequency), associated with the positive or negative DC-bus poles to ground voltages, and the odd, triplen harmonics associated with the output PWM voltages waveform. The shaft-neutral voltage has a similar spectrum to that of the CMV, but strongly attenuated, as it can be seen in the presented figures. The output line-to-ground voltages include the odd, triplen harmonics (in relation to the output voltages, for overmodulation), and the odd, triplen line-related harmonics (see Table A4.10 in Appendix 4).

Although the presented experimental leakage or ground current waveforms include both the winding-frame/ground and bearing common-mode currents, a relation between the ground current and the shaft-ground voltages can be noted, allowing to identify the most significant bearing current peaks. In fact, the ground current peaks observed in the experimental waveforms could either result from total or partial discharges in the stator windings or in the bearings. Careful correlation between instants in which shaft-ground voltage modulus is abruptly forced to a lower value close to zero and leakage current peaks occur allows the bearing current peaks identification (this is clearly evidenced in Fig. A5.24), resulting from lubrication film breakdown or contact between bearing spheres and races, assuming that no winding-ground current peaks occur simultaneously. Actually, since direct bearing current measurement is impracticable (only feasible in laboratory environment using special setups), for monitoring and predictive maintenance

purposes, it is proposed the acquisition of the shaft-ground voltages (and, for large motors the shaft-ends voltage) and the total leakage or ground common-mode current (clamp-on current probe embracing the three phases conductors), and correlation algorithms to extract the current pulses associated with electric discharges in bearings. This correlation has to take into account the time derivative of the voltage and current wave to identify steep variations. Further considerations on this subject can be found in [90].

Regarding high-frequency components of the inverter output voltage, the most significant component of neutral-ground and shaft-ground voltages are those corresponding to the switching frequency and respective side bands, as well as their multiples, typically characterizing the line-to-ground voltage waveform, as it can be seen in Figs. A5.16-A5.21. The output line-to-line voltages have a different spectrum, being the frequency of the most relevant high-frequency component two times the switching frequency [52]. Star-connection-case shaft-ground voltages at 50-Hz were limited roughly between ± 10 V. For the 7.5-kW motor the switching frequency component amplitude is more than 50 times lower than that of the neutral-ground voltage reaching near 2 V, reflecting the effect of the voltage divider formed by the stray capacitance. The increase of the overmodulation level can lead to the increase of the 3rd harmonic (in relation to the output voltage fundamental frequency) of the shaft-ground voltages, potentially increasing the maximum peak values³⁷ (this phenomenon is evidenced in Figs. A5.21, A5.22, and A5.23). The higher the motor load is, the higher the number of bearing current peaks will be (as it can be seen in Fig. A5.19). Moreover, the increase of the switching frequency increases the number of current discharges (per time unit) through the motor insulation system and through the bearings (as it can be seen in Fig. A5.16). Additionally, the higher the switching frequencies, the higher the amplitude of the leakage current, due to the lower impedance associated with the stray capacitances.

In short, comparing 2-level and 3-level inverters (full comparison presented in Chapter 3), it is clear that the latter leads to a lower magnitude common-mode and shaft-ground voltages and, therefore, the leakage current is, in general, lower. It should be noted that the du/dt associated with neutral-ground voltage is higher when voltage transients occur, increasing the bearing and leakage currents magnitude.

³⁷ The high-frequency homopolar components are modulated by the low-frequency homopolar components.

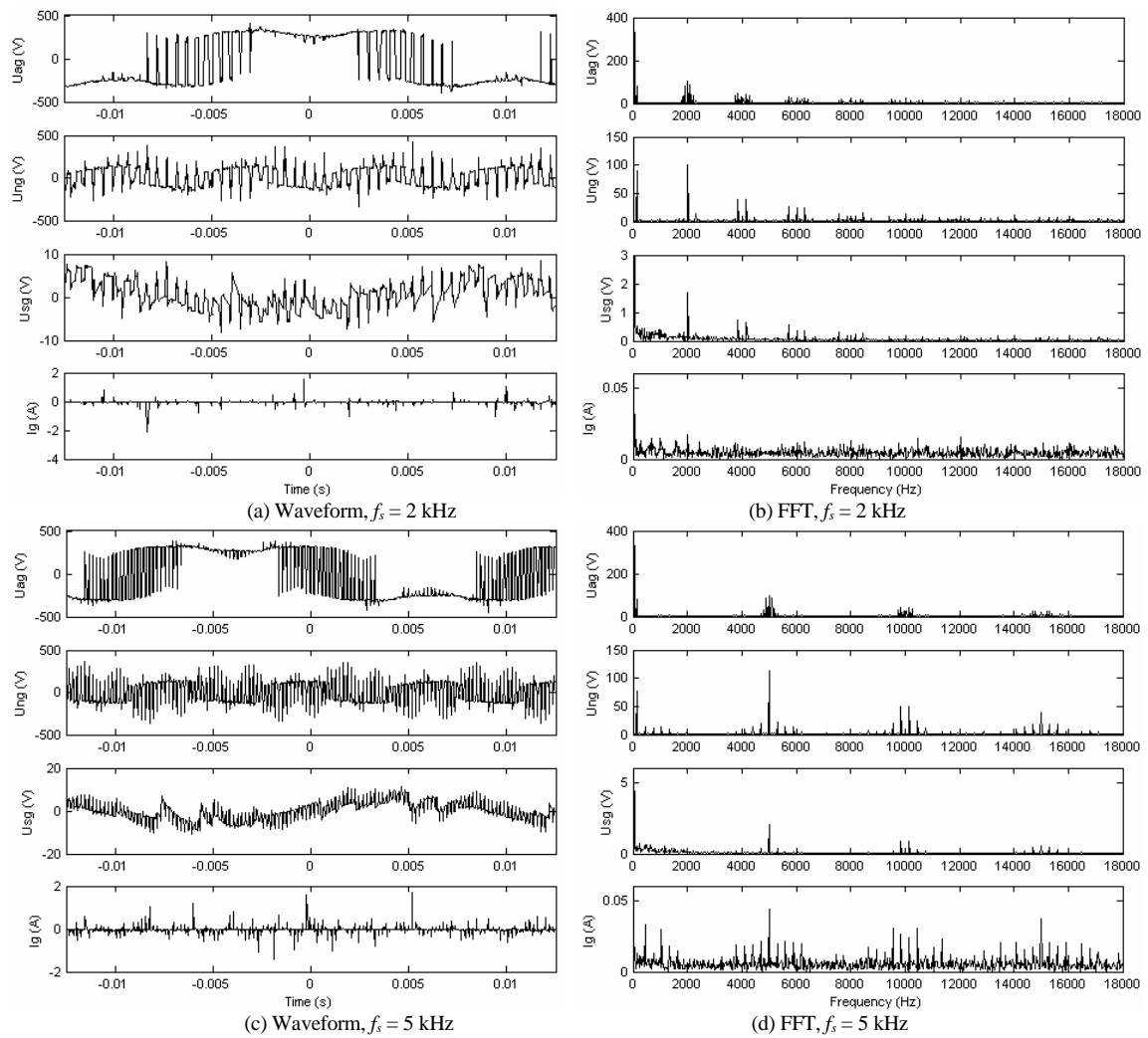


Fig. A5.16. Phase-to-ground, neutral-to-ground, shaft-to-ground (U_{sg}) and leakage current (I_g) for a 7.5-kW, 4-pole, 400-V, 50-Hz, star-connected (U_{ag}) IM, no-load. Motor fed by a 2-level VSD, generating a 50-Hz fundamental line-to-line voltage approximately equal to 400 V.

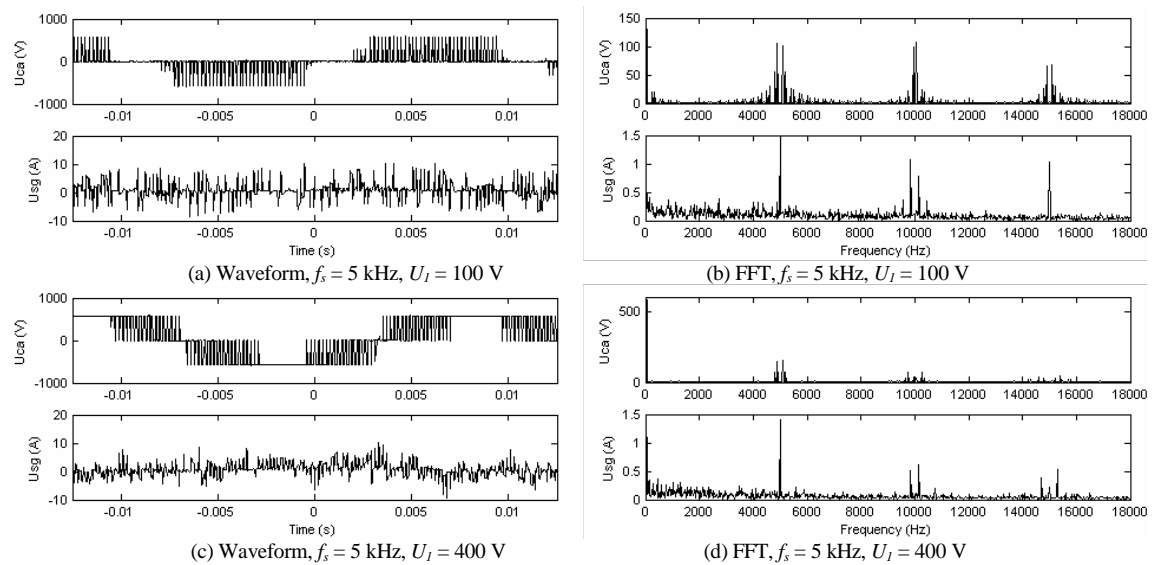


Fig. A5.17. Phase-to-phase and shaft-ground for a 7.5-kW, 4-pole, 400-V, 50-Hz, star-connected winding IM, no-load. Motor fed by a 2-level VSD, generating a 50-Hz fundamental line-to-line voltage approximately equal to 100 and 400 V.

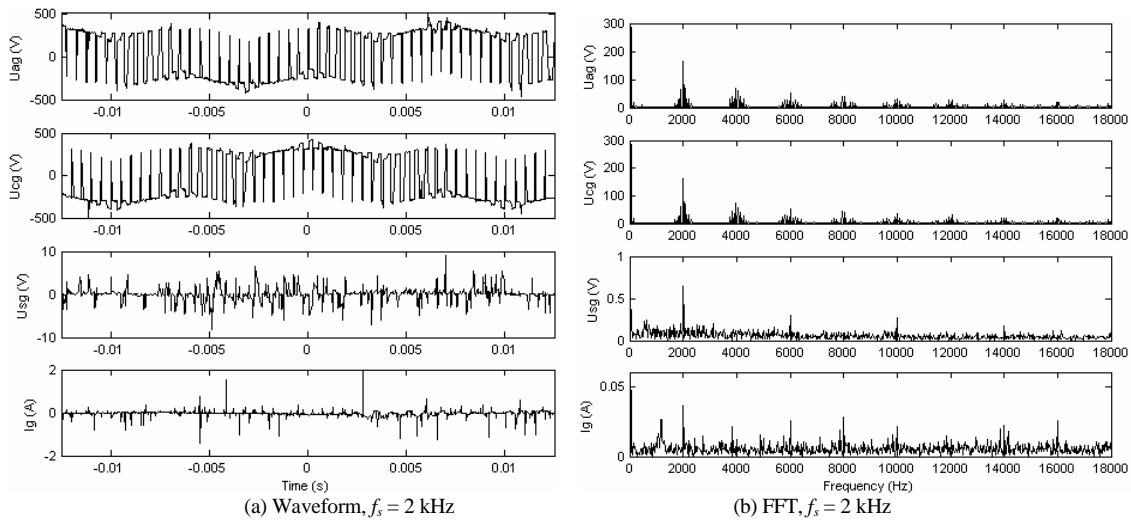


Fig. A5.18. Phase-ground, neutral-ground, shaft-ground and leakage current for a 7.5-kW, 4-pole, 400-V, 50-Hz, delta-connected winding IM, no-load. Motor fed by a 2-level VSD, generating a 50-Hz fundamental line-to-line voltage lower than 400 V.

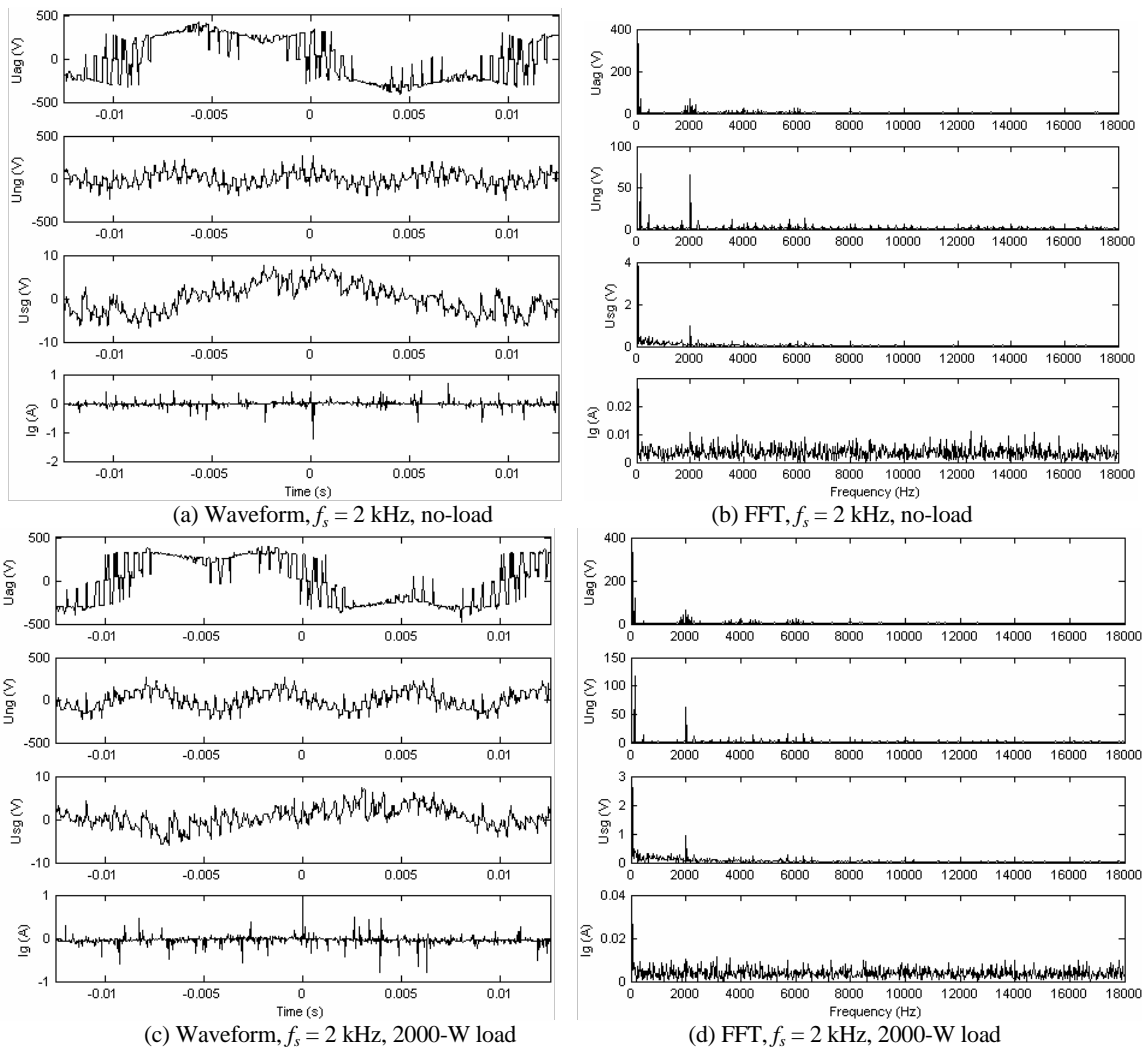


Fig. A5.19. Phase-ground, neutral-ground, shaft-ground and leakage current for a 7.5-kW, 4-pole, 400-V, 50-Hz, star-connected winding IM. Motor fed by a 3-level VSD, generating a 50-Hz fundamental line-to-line voltage approximately equal to 400 V.

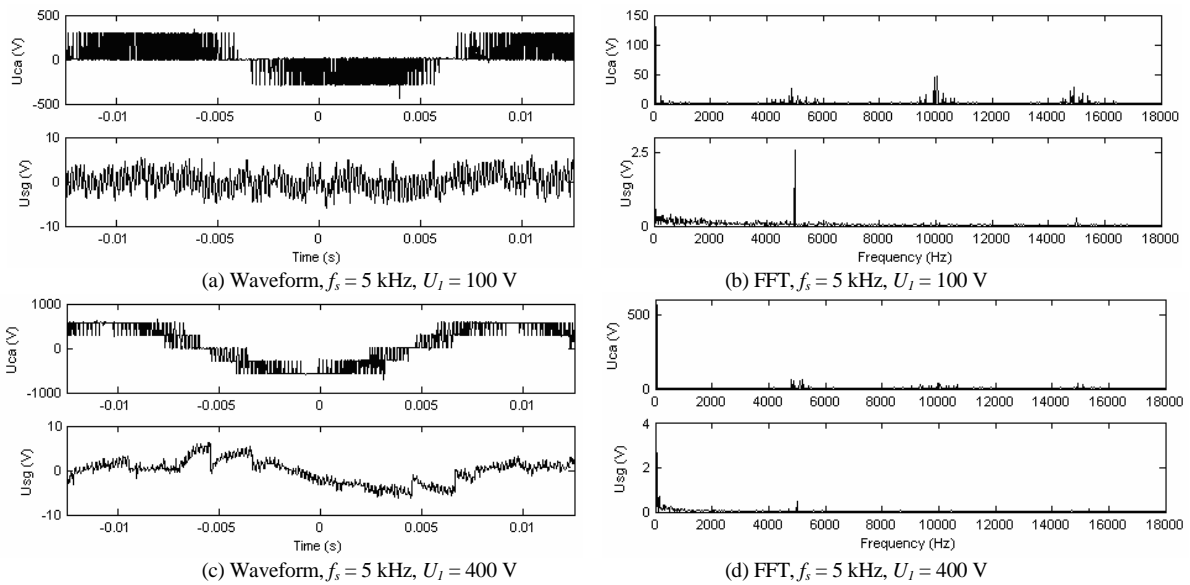


Fig. A5.20. Phase-to-phase and shaft-ground for a 7.5-kW, 4-pole, 400-V, 50-Hz, star-connected winding IM, no-load. Motor fed by a 3-level VSD, generating a 50-Hz fundamental line-to-line voltage approximately equal to 100 V.

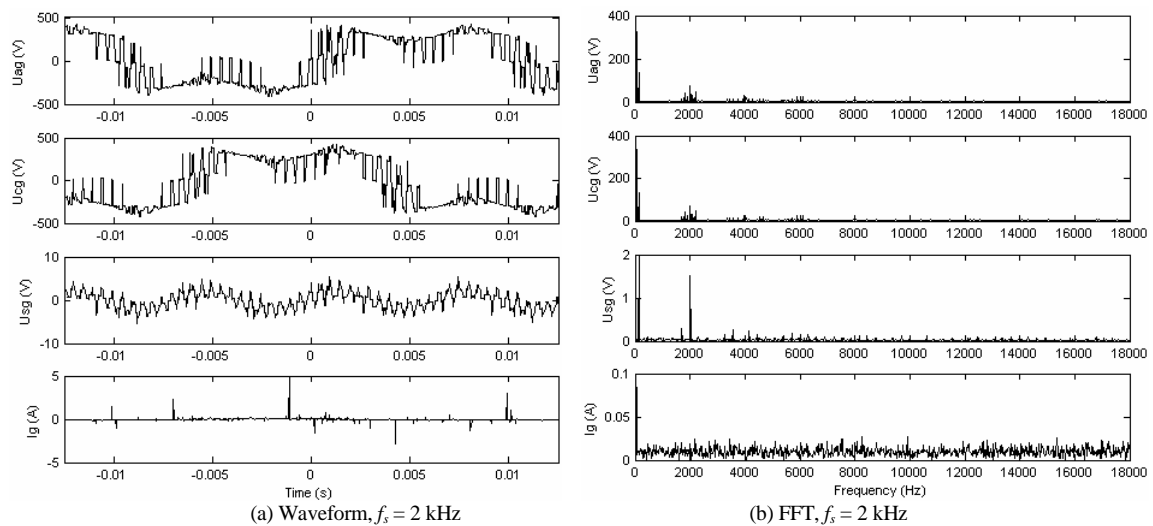


Fig. A5.21. Phase-ground, neutral-ground, shaft-ground and leakage current for 7.5-kW, 4-pole, 400-V, 50-Hz, delta-connected winding IM. Motor fed by a 3-level VSD, generating a 50-Hz fundamental line-to-line voltage approximately equal to 400 V.

Comparing delta and star connections, the delta increases the amplitude of the ground or leakage currents over the spectrum. In delta-connected windings, the triplen voltage harmonics and fundamental zero-sequence component become concentrated in the shaft-ground voltage (which does not happen in star-connected windings, since neutral point can actually concentrate part of the zero-sequence harmonic and fundamental components). When the 7.5-kW motor was fed directly by the line/mains, a 50 Hz component between the shaft and ground was found, evidencing unbalanced stray capacitance system.

Fig. A5.25 shows experimental shaft-ground voltages and bearing currents in a 5-hp, 460-V motor [48]. In fact, due to both CMV and electrostatic coupling between windings and rotor and rotor and frame, the motor shaft voltage is enabled to build up, as it can be seen in Figs. A5.26 and A5.27.

The waveforms of CMV in relation to the ground, U_{CM} , the voltage between the shaft ends, U_{SHAFT} , and the voltage between rotor shaft and stator, U_{RS} , can be approximately represented as in Fig. A5.27, which does not include low- and high-frequency oscillations that actually can exist in the CMV waveform, as it was evidenced experimentally, and assumes that neither electric contact between the bearing spheres and races nor the disruption of the lubricant film occurs. The amplitude and du/dt of CMV pulses can be both increased (typically up to 2 times the normal value [48]) due to the voltage wave reflection phenomenon at the motor terminals (addressed in next section) [8], [15], [48].

Regarding delta circulating currents, they are, in part, associated with motor electromagnetic asymmetries/unbalances and stator core saturation. Delta homopolar circulating currents, when associated to magnetic circuit asymmetries can increase the circulating bearing currents [8].

The common-mode currents (CMCs or I_{CM}) circulate in the circuit consisting of inverter-motor-ground/earth. In the motor, the CMCs circulate through both bearings. Recent studies and technical reports confirm that the low-voltage, inverter-fed, lifetime IMs can be significantly affected by bearing currents activity.

Currents resulting from electric discharges can also occur due to electrostatic charging of the rotor (building up the shaft-ground voltage), caused by the driven devices (e.g., electrostatic charge generated by the friction and collision of particles in pump blades), as previously referred.

In line-fed IMs, if the power supply is unbalanced and/or distorted (with odd, triplen harmonics in relation to ground), thus having homopolar or zero-sequence components, and/or the stray capacitance three-phase system between windings and rotor is unbalanced, a CMV between rotor/shaft and stator/ground, U_{RS} ($= U_{sg}$) is generated³⁸ (as shown before), leading to the CMC circulation through both bearings. However, only the high-power, line-fed motors are able to generate an U_{RS} with amplitude high enough to originate a significant CMC.

In Fig. A5.28, a simplified circuit to explain the CMCs circulation is presented, in which the random electric contacts (which originate electric discharges) and partial discharges in the lubricant film between the spheres and races are represented by switches. Due to the existence of a series of stray capacitances (C_{WR} in series with $C_{RE} // C_{B1} // C_{B2}$, forming a voltage divider) it is build

³⁸ For low-voltage, line-fed IMs, the voltage between the rotor and the stator (connected to the earth), U_{RS} , can reach peak values up to 1-2 V, but it is typically maintained within hundreds of μV [5], [8], [12], [13], [14], [15].

up a voltage, U_{RS} , between the shaft and stator (connected to the earth and VSD ground), as it can be seen in Fig. A5.28³⁹.

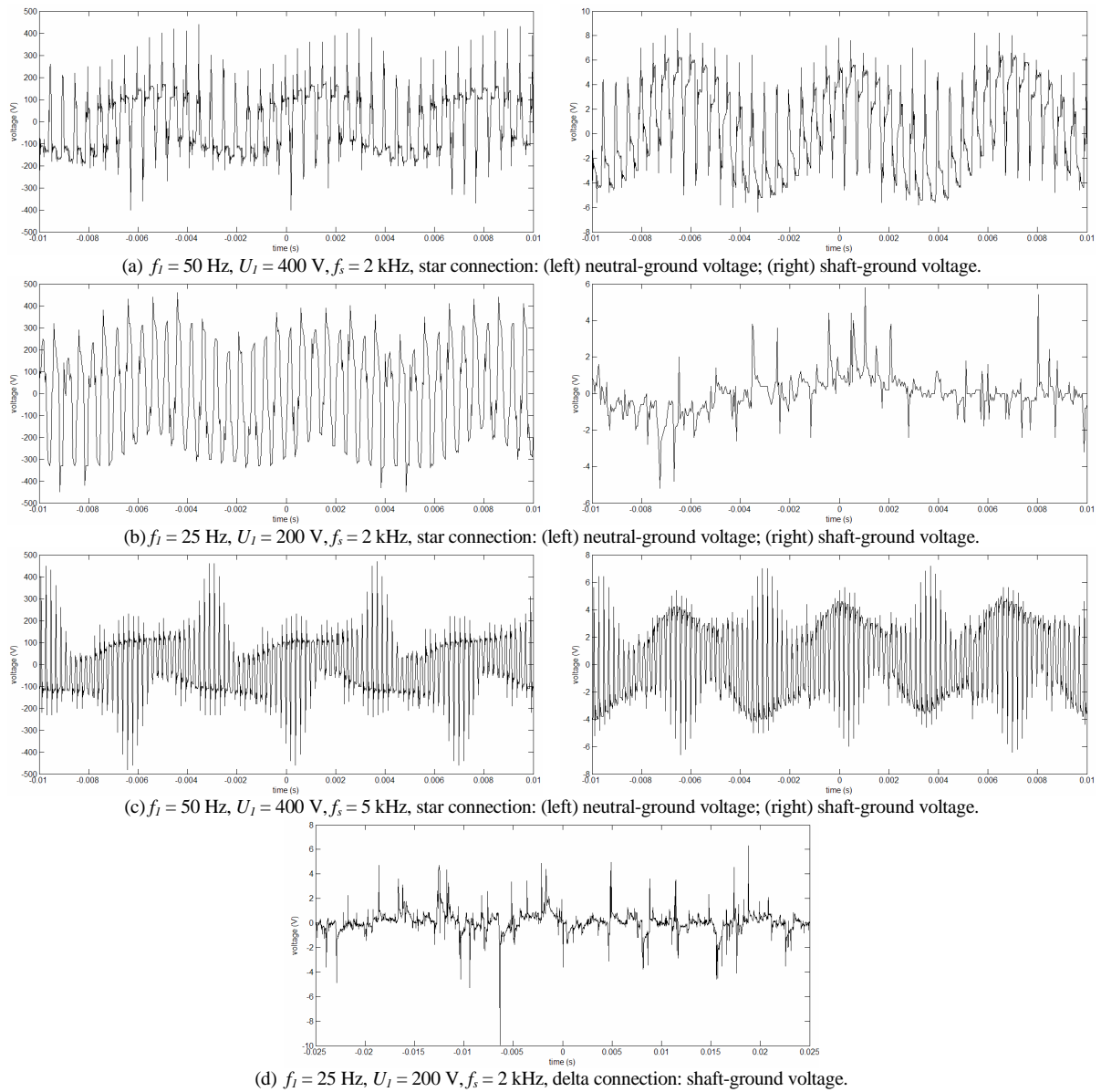


Fig. A5.22. Neutral-ground voltage (in the case of star connection) and shaft-ground voltages, for a 3-kW, 4-pole, 400-V, 50-Hz IM. Motor fed by a 2-level VSD, by means of a 12-m cable.

³⁹ In the low-voltage inverter-fed IMs ($f_i > 1$ kHz) the voltage between the shaft and stator, U_{RS} , reach peak values in the range of 10-20 V ($\approx 1/50$ of the DC voltage at the inverter input), being these values dependent upon the stray capacitances value [8], [10], [14], [48], [51].

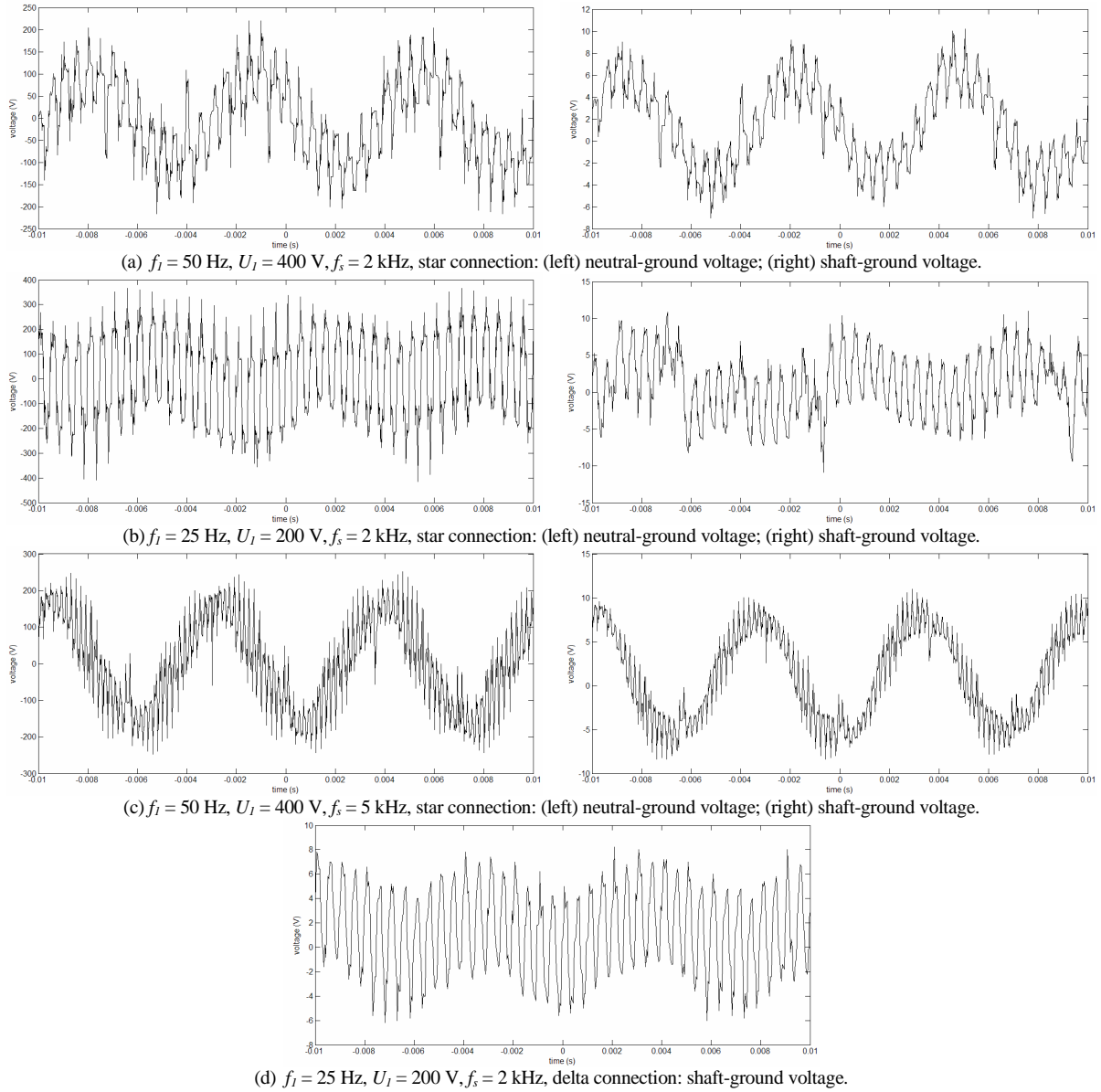


Fig. A5.23. Neutral-ground voltage (in the case of star connection) and shaft-ground voltages, for a 3-kW, 4-pole, 400-V, 50-Hz, motor fed by a 3-level VSD, by means of a 12-m power cable.

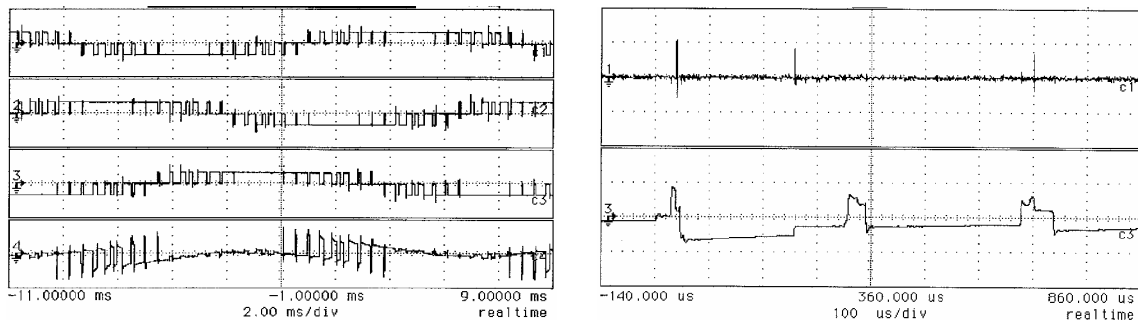


Fig. A5.24. Experimental results for a 5-hp, 460-V IM (extracted from [48]): (left) Line-to-line input voltages of a 5-hp/460-V motor (Chs. 1–3, 500 V/div) and the shaft-ground voltage (Ch. 4, 10 V/div); (right) bearing current (Ch.1, 50 mA/div) and shaft-ground voltage (Ch. 3, 10 V/div).

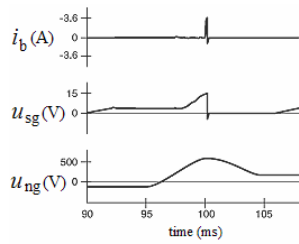


Fig. A5.25. Experimental bearing current (i_b), shaft-ground voltage (u_{sg}) and neutral-ground voltage (u_{ng}), evidencing the relationship during a bearing electric discharge for a large motor [109].

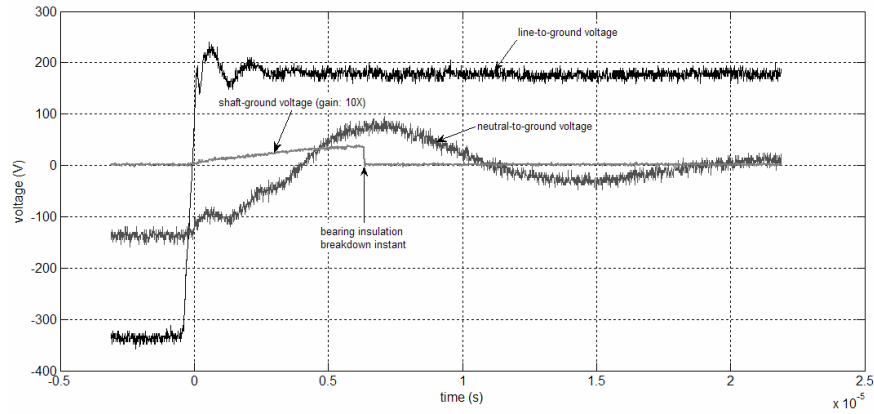


Fig. A5.26. Experimental expanded waveform of line-to-ground, shaft-to-ground neutral-to-ground voltages for a 7.5-kW motor at no-load and fed by a 2-level inverter ($f_s = 2$ kHz).

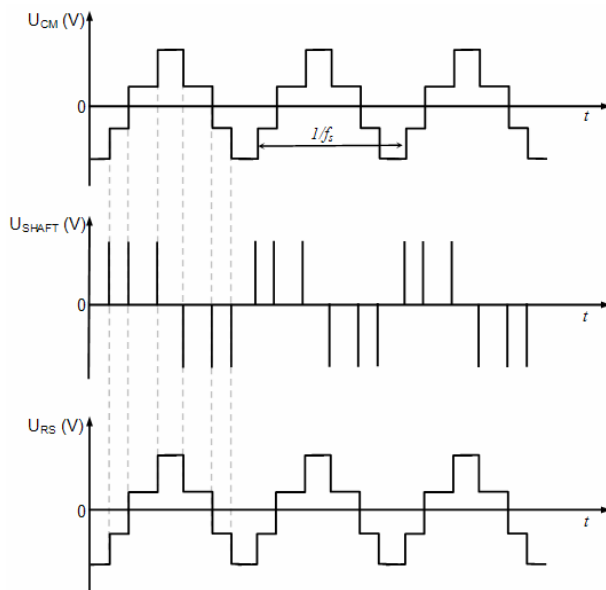


Fig. A5.27. Approximate representation of the waveform of CMVs between the windings and stator, voltage between shaft ends, and voltage between the shaft and stator, assuming that no electric contact between spheres and races and no disruption in the lubricant film occur [10], [51].

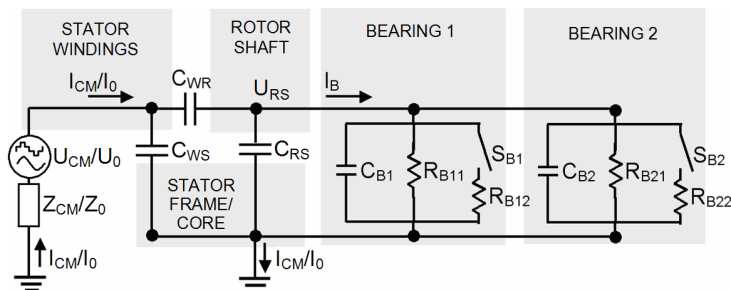


Fig. A5.28. Approximate circuit to explain the common-mode or homopolar current circulation (denoted by I_{CM}/I_0) [10], [51].

On the basis of Fig. A5.28, three types of CMCs can be considered: electric full or partial discharge currents, i_{CMD} , given by (A5.23), capacitive currents, i_{CMC} , given by (A5.24), and ohmic/resistive currents, i_{CMR} , given by (A5.25), for one of the bearings. The magnitude of the different CMC types strongly depends on the relation between the different stray capacitances, as it can be seen in Fig. A5.28, in which the symbols used in (A5.23), (A5.24) and (A5.25) are identified.

$$i_{CMD}(t) = R_{B12}^{-1} \cdot u_{RS}(t) \quad (A5.23)$$

$$i_{CMC}(t) = C_{B1} \cdot \frac{du_{RS}(t)}{dt} \quad (A5.24)$$

$$i_{CMR_B1}(t) = R_{B11}^{-1} \cdot u_{RS}(t) \quad (A5.25)$$

The CMCs are particularly dangerous when they result from electric full or partial discharge between the bearing races and spheres (or rolling elements), leading to the accelerated wear of those parts (as previously referred, due to pitting and fluting, both resulting from EDM phenomenon) and to the accelerated electrochemical degradation of the lubricant (dissociation of the oil or grease components). In fact, when the voltage between the rotor shaft and ground builds up to a sufficient level, it can discharge a current to ground through the bearings. Shaft voltage accumulates on the rotor until it exceeds the dielectric strength of the motor bearing lubricant or contacts between spheres and races occur, then the voltage discharges in a short current pulse to ground through the bearing. This is a random, frequent phenomenon. After discharge, the voltage again accumulates on the shaft and the cycle repeats itself. Initially, these discharges create a “frosted” or “sandblasted” effect, and usually the first symptom of bearing current damage is the audible noise created by the rolling elements riding over these pits in the bearing race. Over time, this deterioration causes a groove pattern in the bearing race (fluting effect), as it can be seen in Fig. A5.30, which is a sign that the bearing has sustained severe damage. Eventually, the deterioration will lead to complete bearing failure [109]. It should be noted that constant-speed operation can increase the risk and accelerate bearing damage.

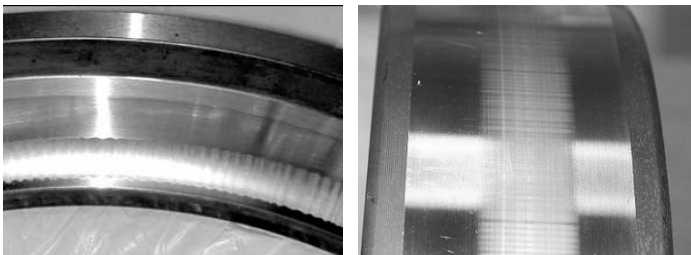


Fig. A5.29. Electrical erosion or fluting in the bearing rings races due to EDM [109], [111].

The capacitive and resistive CMCs are more regular but due to their low amplitude are less dangerous. Nevertheless, they can still contribute to the lubricant degradation and to the races and spheres fluting effect.

The capacitive-type CMCs (CMCCs), result from the presence of a voltage varying in time between the inner and outer bearing rings (U_{RS}). CMCCs amplitude is limited by the bearing parasitic capacitance, winding-rotor parasitic capacitance and by the common-mode or homopolar impedance⁴⁰ (Z_{CM} or Z_0 in Fig. A5.28). CMCCs have relatively low magnitude, being the instantaneous value proportional to the du/dt , as expressed in (A5.24). In the case of VSD-fed motors, the CMCCs circulate in all CMV amplitude transition instants. In the line-fed IMs, the CMCC components have the same frequency and waveform of the homopolar components of the source voltage (which can include triplen harmonic components in the presence of distortion).

As previously referred, in the line-fed IMs, if the power system is distorted or unbalance and/or the stray capacitance system between the stator windings and the rotor (C_{WR}) is unbalanced, there is a voltage between the shaft and stator/frame with frequency and waveform identical to the homopolar voltages between the windings and ground (or earth) [14]. The shaft-stator voltage amplitude, which depends on C_{WR} , C_{RS} , C_{B1} , and C_{B2} values, leads to the current circulation (with waveform and frequency identical to the voltages originating them) from the shaft to the stator or ground, through both bearings.

The discharge-type CMCs (CMCDs), flowing when an electric current discharge occurs, which can happen if the bearings are subjected to a voltage between the inner and/or outer rings (U_{RS}) and an electric contact occurs between the spheres and both rings, or the voltage is high enough to disrupt the lubricant film. That situation corresponds to closing the switch in the Fig. A5.28 of one or both bearings (represented by S_{B1} and S_{B2}). The instantaneous value of CMCDs is expressed by (A5.23). Since the ohmic resistance associated with the spheres races⁴¹ (R_{B12} and R_{B22}) is very low, the CMCDs can reach very high values. Note that the voltage responsible for the electric discharge only exists when the stray capacitances of both bearings (C_{B1} and C_{B2} in Fig. A5.28) exist simultaneously. The CMCDs produce pitting and fluting of the races and spheres, and, consequently, metallic particles. They also accelerate the lubricant degradation. The joint action of those effects translates in the accelerated degradation of the bearings [5], [8], [14].

At the instants in which the contacts between spheres and races (due to imperfections) and/or the lubrication film disrupts, the CMCDs can reach relatively high values (up to 5 A for contact instants, about 20 times higher than CMCCs, and typically in the order of 200 mA for disruption instants) and are characterized by a high current density, originating microscopic cavities and flutes

⁴⁰ The homopolar or common-mode impedance represents the impedance between the motor ground and the common-mode or homopolar voltage supply. It is associated to the ground-DC bus impedance of VSDs and/or to the ground-neutral impedance of star-connected power supplies (feeding the VSD input rectifier).

⁴¹ The stator/frame equivalent resistance can also be included in that resistance.

randomly distributed in the spheres and races of the inner and outer rings. The frequency of CMCDs caused by contacts between spheres and races is independent of the switching frequency, having a random behaviour. However, CMCDs caused by disruption have a more regular behaviour [8], [48]. The switching frequency has a significant influence in the bearing degradation since it influences the potential number of current discharges.

The ohmic/resistive-type CMCs (CMCRs), result from the presence of a time-varying voltage between the inner and outer rings of the bearings. CMCRs have frequency and waveform similar to the voltage waveform and the resistive impedance of the bearing limits their magnitude. The resistive impedance is mainly associated to the lubricant (R_{B1I} or R_{B2I} in Fig. A5.28). The instantaneous value of CMCRs is expressed by (A5.25). The CMCRs have extremely low amplitude (in the order of μA). However, although in an almost negligible way, CMCRs contribute to the lubricant degradation.

However, in the line-fed IMs, only the high-power motors are able to develop shaft-ground voltages high enough to originate CMCCs, CMCRs and CMCDs⁴² with significant magnitudes. In this kind of motors even CMCDs can exist due to the disruption of the lubricant film, which is unlikely to happen in the low-power and/or low-voltage line-fed IMs.

In Fig. A5.30, the approximate waveforms of the bearing currents, I_B , and of the rotor-stator (or shaft-ground) and shaft-ends voltages, U_{RS} and U_{SHAFT} , can be seen, considering that electric contacts between the spheres and races of the bearings and the disruption of the lubricant film occur. The voltage U_{RS} leads to the circulation of the different types of CMCs [8], [14]. The shaft-ends voltage is related with the bearing circulating-type currents, addressed in the following section.

As the inverter output voltage is characterized by high-frequency, high- du/dt pulses, CMCCs reach significant peak values (up to 200 mA, but typically lower than that value [8], [14]) and have a wide high-frequency spectrum, including the switching frequency related components. CMCCs are typically of low amplitude but, although not causing damages of the same magnitude of those caused by CMCDs, can lead to the dissociation of the lubricant grease and, consequently, to the degradation of the lubrication capability/quality, as well as to slight fluting effects in the races.

⁴² This kind of currents can reach 15 mA (peak) in a line-fed low-voltage IM.

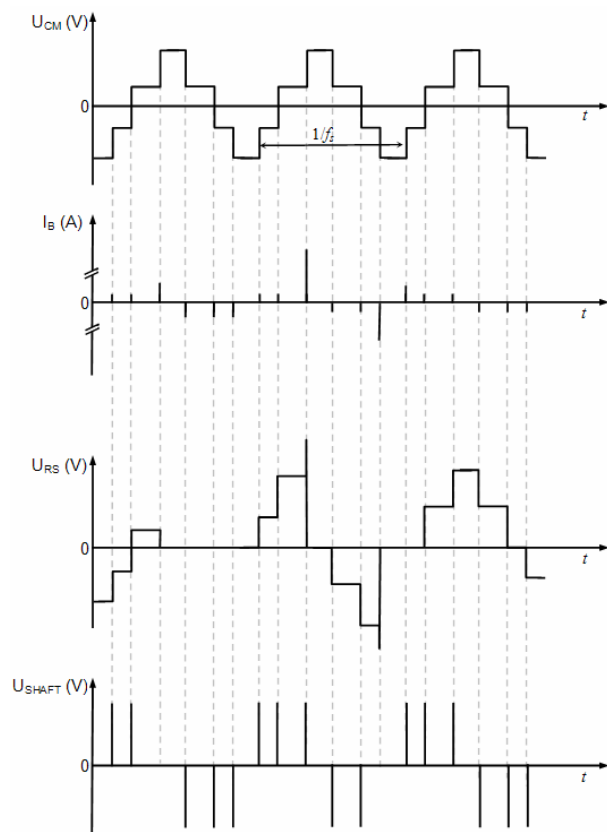


Fig. A5.30. Approximate representation of the waveforms of CMVs between windings and stator, U_{CM} , voltage between the shaft ends, U_{SHAFT} , voltage between shaft and stator, U_{RS} , and bearing currents (ohmic/resistive currents not represented), I_B , considering that electric contacts between the spheres and races and the disruption of the lubricant film occur [51].

A5.3.5 Circulating Bearing Currents

The bearing circulating currents (denoted by CRC or I_{CR}) include all the currents that circulate in the closed-loop circuit consisting of shaft, bearings and frame, when a voltage is induced in that circuit by stray magnetic fluxes rotating around the shaft (Figs. A5.31 and A5.32) [5], [8], [22].

To analyse the origin of low-frequency CRCs ($f < 500$ Hz) associated with line-fed IMs it is considered the motor model without stray capacitances, being only necessary to consider them to explain the origin of the high-frequency CRCs ($f \geq 1$ kHz) associated with inverter-fed motors.

In the low-frequency analysis it is considered only the relation between the stator winding currents and the associated magnetic fluxes. In the high-frequency analysis only the stray capacitances and the inductive coupling between stator winding and rotor are considered.

Low-frequency CRCs are widely reported and well understood for medium- and high-voltage, line-fed motors. In this case, the U_{SHAFT} is originated by motor electromagnetic asymmetries (e.g., due to the stator-rotor eccentricities and/or winding asymmetries) and/or distortion and unbalance of the three-phase power supply, which lead to the unbalance of the three-phase magnetic fluxes in the core. However, such currents are only significant for high-power, high-voltage motors.

High-frequency CRCs can also exist as a result of high-frequency CMCs circulation, in the case of inverter-fed motors, as it can be seen in Fig. A5.33. In fact, CMCs generate a stray flux around

the shaft, which induces a high-frequency voltage in the shaft ends⁴³ (inductive coupling), originating high-frequency CRCs. In fact, considering a diametral coil or turn of one phase, with a leakage path for high-frequency leakage common-mode currents, i_{CM} , flowing from winding to ground through both coil sides, the input current, flowing into the coil, is $i + i_{CM}$ and the returning current, flowing out from the coil, is $-i + i_{CM}$. This situation leads to a different current amplitude in the in-slot coil sides and, therefore, a magnetic flux unbalance in both coil sides occurs, leading to a stray flux around the motor shaft, in which an EMF is induced (inductive coupling).

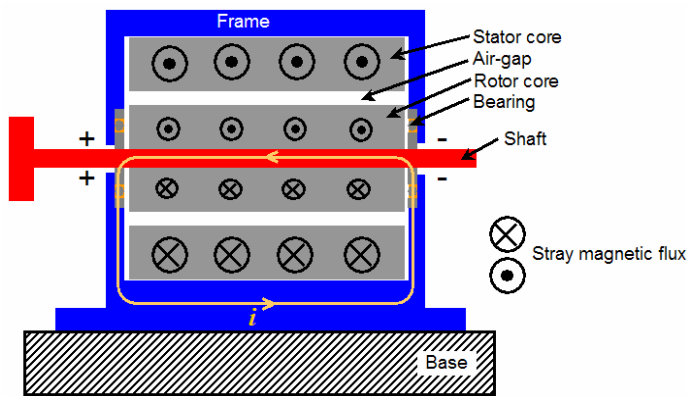


Fig. A5.31. Approximate representation of circulating currents in the induction motors [8], [51].

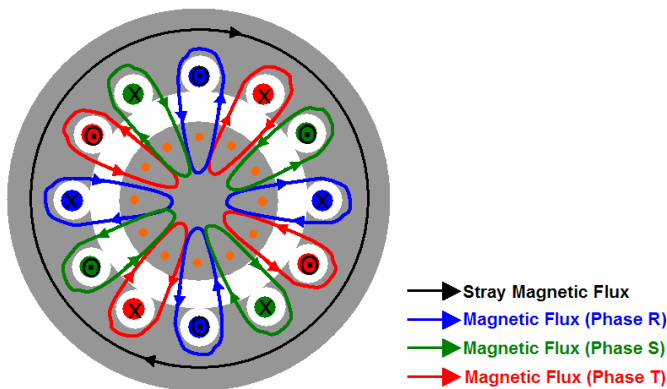


Fig. A5.32. Approximate representation of the stray magnetic flux in induction motors [8], [51].

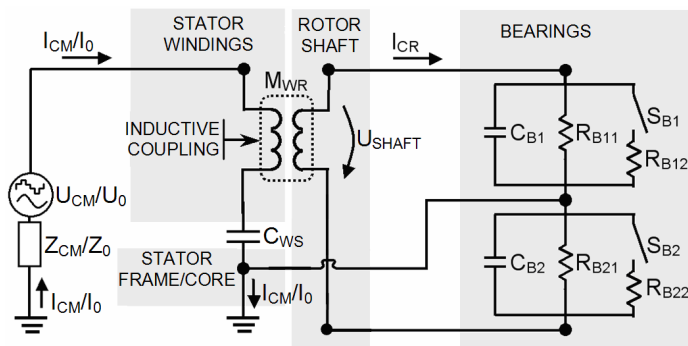


Fig. A5.33. Approximate circuit to explain the high-frequency circulating currents (denoted by I_{CR}) [10], [51].

⁴³ In the low-voltage, inverter-fed motors ($f_s > 1$ kHz), U_{SHAFT} can reach peak values of 1-2 V [5], [8], [12], [13], [14], [15].

On the basis of Fig. A5.33, three types of circulating stray bearing currents can be considered: full or partial discharge currents, i_{CRD} , described by (A5.26), capacitive currents, i_{CRC} , described by (A5.27), and ohmic/resistive currents, i_{CRR} , described by (A5.28).

$$i_{CRD}(t) = (R_{B12} + R_{B22})^{-1} \cdot u_{SHAFT}(t) \quad (A5.26)$$

$$i_{CRC}(t) = (C_{B1} + C_{B2}) \cdot \frac{du_{SHAFT}(t)}{dt} \quad (A5.27)$$

$$i_{CRR}(t) = (R_{B11} + R_{B21})^{-1} \cdot u_{SHAFT}(t) \quad (A5.28)$$

CRCs are particularly dangerous when they result from full or partial electric discharge phenomenon. The capacitive and resistive CRCs are more regular but, due to their low amplitude, have modest impact in the bearings lifetime.

Capacitive-type CRCs (CRCCs), result from the presence of a time-varying voltage between the inner and outer rings (associated with the u_{SHAFT}), producing the circulation of a current with frequency equal to that of the voltage, and, ignoring the series resistances, with an amplitude limited by the sum of the capacitive impedances of both bearings. The instantaneous value of CRCCs is expressed by (A5.27). CRCCs have relative low amplitude.

Discharge-type CRCs (CRCDs) occur when a voltage between the shaft ends exists and electric contacts occur between spheres and rings simultaneously in both bearings, or the voltage magnitude is high enough to originate the disruption of the lubricant film simultaneously in both bearings, leading to an electric discharge that provoke similar damages to those inflicted by CMCDs. The instantaneous value of CRCDs is expressed by (A5.26). Since the sum of R_{B12} and R_{B22} is very low, CRCDs can reach very high values. Note that severe electric discharge potential exists only if at least one of the stray capacitances (C_{B1} or C_{B2} in Fig. A5.33) exists or is not null due to electric contact between bearing rings.

Ohmic/resistive-type CRCs (CRCRs) result from the presence of a time-varying voltage between the inner and outer rings. This kind of currents has a frequency and waveform equal to that of the voltage and amplitude limited by the resistive impedance of the circuit composed by bearings, shaft and frame. For the sake of simplicity, only the resistances associated to the lubricant film, R_{B11} and R_{B21} in Fig. A5.33, are considered. The instantaneous value of CRCRs is expressed by (A5.28). The CRCRs have very low amplitude.

When CMCs return to the VSD and/or power supply ground (connected to the earth and/or to the motor ground) circulate through the C_{WS} (stator/frame connected to the earth and/or to the inverter ground), which presents itself as a low-impedance path for high du/dt . Therefore, the circulation of

CMCs is possible in delta-connected and star-connected (with or without neutral connection) windings, as it can be seen in Fig. A5.34.

As explained before, CMCs circulation in stator windings generates a stray magnetic flux around the shaft, which, induces high-frequency voltages between shaft ends⁴⁴ (inductive coupling), causing the CRCs circulation in the closed circuit composed by shaft, bearings, and stator, which can be added or subtracted to CMCs.

High-frequency CRCCs and CRCRs are typically of low amplitude (less than 20 mA, in the order of μA) and circulate at the CMV amplitude variation instants. Their effects are not significant, but contribute slightly contributing to the lubricant degradation.

High-frequency CRCDs are of medium amplitude (between 200 mA and 500 mA) and, as they depend on the existence of stray capacitances in both bearings, have a random behaviour [8], [14]. Nevertheless, CRCDs can produce fluting in the races.

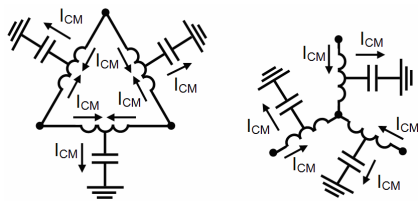


Fig. A5.34. High-frequency common-mode currents in the stator windings: (left) star connection; (right) delta connection [51].

Low-frequency CRCs are associated with line-fed motors and result from the presence of induced U_{SHAFT} . As it is illustrated in Fig. A5.32, if the per-phase magnetic fluxes in stator core are unbalanced, the resultant flux around the shaft (stray flux) becomes nonzero. Thus, by the Faraday's law, it is induced an EMF between the shaft ends and, by the Ohm's law, a current circulates in the closed circuit composed by the shaft, bearings and frame (Fig. A5.31), with an amplitude limited, in part, by the bearings impedance [5], [8], [51].

As previously referred, the asymmetrical distribution of the magnetic flux is mainly associated with asymmetries of the magnetic circuit resulting, for example, from stator-rotor eccentricities and/or stator core deformations (i.e., motor asymmetries) [5], [8], [14], [48]. This phenomenon can be aggravated by the existence of homopolar currents and/or asymmetrical distribution of currents in both the stator or rotor, resulting from asymmetries in stator windings, fractured/broken bars, stator core saturation, and unbalanced and/or distorted power supply [8].

Note that, considering very low stray capacitances, the circulation of significant zero-sequence currents, I_0 , including fundamental and/or triplen harmonic homopolar currents is only possible if the stator windings were connected in delta or in star with neutral connection (Fig. A5.35).

⁴⁴ In low-voltage inverter-fed IMs ($f_s > 1 \text{ kHz}$) the voltage between the shaft ends reaches peak values of 1-2 V ($\approx 1/500$ of the DC bus voltage), being these values dependent upon the stray capacitances value [14].

The induced voltage, between the shaft-ends is sinusoidal and its frequency is that of the fundamental voltage if only electromagnetic unbalance exists. In the presence of harmonic distortion or core saturation, components with frequencies corresponding to triplen harmonics can exist.

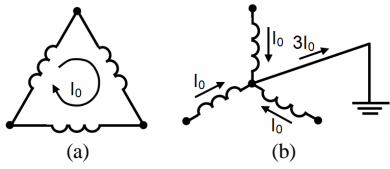


Fig. A5.35. Low-frequency homopolar or zero-sequence currents in the stator windings: (a) delta connection; (b) star connection with neutral [51].

Low-frequency CRCRs have typically low-amplitude (less than 50 mA, peak) and frequency equal to that of the homopolar voltages. In the medium/high-voltage and/or high-power motors, the CRCRs can reach higher values. However, they are negligible for the low-voltage line-fed IMs, but contribute to the degradation of the lubricant and to the races fluting (less severe than that produced by electric discharges).

The low-frequency CRCCs are negligible (in the order of μA), even for high-voltage high-power machines. The CRCDs can reach significant values ($> 1 \text{ A}$) due to the contact between spheres and rings. However, for line-fed motors, only those of high power ($> 100 \text{ kW}$) can develop voltages between the shaft ends with amplitudes high enough to originate significant bearing currents. In those motors, it is also possible to exist CRCDs due to the lubricant film disruption (which, in principle, it is unlikely to happen in low-voltage and/or low-power IMs).

A5.3.6 Bearing Current Diagnosis

If the user suspect of electrical activity in the bearings, a diagnostic should be carry out (pre-failure or post-failure) in order to identify clues of electric current circulation. The damages from bearing currents lead to increased acoustic noise and heat levels, reduced effectiveness of the lubricant, excessive vibration, and possible bearing failure. If the problem is not handled properly, the service life of the bearing will be drastically reduced.

In-service detection of damages associated with electric current activity (EDM) can be done using, for example, mechanical vibration and/or input current spectral analysis-based techniques (or simply using the acoustic noise) [5], [20]. In fact, the first symptom of deterioration is often an abnormal acoustic noise caused by increased vibration. Moreover, in degraded bearings, the friction increases and metal particles are liberated into the lubricant, increasing wear and temperature. In a general way, the bearing state can be evaluated by means of its temperature⁴⁵ [8]. Unfortunately, by the time the bearing noise is apparent, EDM damage has already occurred and

⁴⁵ The bearing temperature should be measured after thermal stabilization ($\Delta\theta_{10 \text{ min}} < 1^\circ\text{C}$) in no-load operation: $\leq 80^\circ\text{C}$ – normal value; 90°C high value; $\geq 100^\circ\text{C}$ failure indicative value. Among all possible causes for excessive operating temperature, it can be referred the poor mechanical adaptation/fitting, bearing defects, poor lubrication, misalignment between bearing and shields, etc. [8].

deterioration has developed to the point that complete bearing failure is probably not far behind. This can lead to the bearing destruction within a few months, being a critical issue, particularly in VSD-fed IMs [48].

Currently, there are three common non-destructive methods used in Industry to detect bearing currents and bearing current damage: vibration analysis, shaft-to-ground voltage analysis, and current analysis. As referred before, correlation between shaft-ground voltage and input common-mode or leakage current⁴⁶ can also be a good approach for identification of bearing currents.

While the referred methods can be implemented to either confirm or deny bearing current activity suspicions, they should be incorporated to establish a base or reference state for comparison purposes and monitoring. This can provide early detection of possible problems. It can also be useful to evaluate whether or not any installed protection methods are effective. It is important to emphasize that the referred test methods require deep expertise to operate the specialized equipment and analyze the data [109].

Vibration analysis can be particularly useful to confirm the existence of bearing fluting damage caused by EDM⁴⁷. The vibration spectrum of a bearing in the early stages of fluting damage will exhibit a mound of energy in the 2-4 kHz frequency range, as it can be seen in Fig. A5.36.

In the preventive maintenance scope, for a user-friendly and fair accurate diagnosis, it is proposed the use of combined current and vibration spectral analysis, using artificial neural networks, as described in [50] and in Appendix 6, which can be much improved for bearing diagnosis purposes if the shaft-ground voltage (and eventually shaft-ends voltage) and common-mode leakage input current is added to the analyzed data sets, and properly correlation is made. The shaft-ends and shaft-ground voltages measurement requires special probes due to the movement of the shaft.

Since all motors have some level of shaft-frame voltage, it is necessary to determine at what levels is cause for alarm. Unfortunately, there are no specific voltage limits that accurately evidence if or not a motor is experiencing EDM damage, since there are several variables that can affect the measured data, i.e., bearing lubrication, measurement equipment and method, running speed, etc. The referred methods of predicting EDM-related damages are not yet an exact science, and further research is needed. Different experts have different opinions on safe shaft-ends or shaft-ground voltage levels, depending on their individual experiences. Many experts, however, agree that trending this data can be most helpful in identifying deviations that can indicate the beginning or worsening of EDM-related damage, or even the bearing failure. Nevertheless, if the

⁴⁶ Measured by instantaneous summation of the line currents, by means of a clamp-on current probe around the three line conductors.

⁴⁷ As EDM damages continue and bearing degradation progresses, the fault-related energy spikes will migrate into regular bearing fault frequencies. Continuous monitoring of the vibration levels starting shortly after initial installation operation/start-up can provide important indications of vibration spectrum increasing or changing. There are commercially available simple diagnosis systems based on the vibration analysis, which record the spectrum for a healthy base case and detect significant changes in the vibration spectrum signature, alerting the user for an anomalous operation, being designed for bearing condition monitoring [52].

referred voltages were significant and present a specific pattern, there is a high certainty level of electric currents being flowing through the bearings.

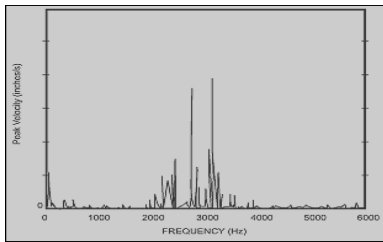


Fig. A5.36. Example of vibration spectrum due to the bearing fluting effect [109].

Obviously, after the failure and demounting of the bearing, the electric current circulation can be identified by the existence of pitting, fluting and/or frosting in the races and spheres, as well as by the discoloration (darkening), increase of the viscosity (suggesting chemical composition changes) and presence of small metal particles (bearing parts pull-out during electric discharges) in the lubricant [8], [51].

A5.3.7 Bearing Current Mitigation Techniques

The best solution to extend the bearing lifetime integrates the control off all the variables that can affect it, namely, mechanical, thermal, chemical and electrical, being the latter the aim of this section. Examples of mitigation techniques for bearing currents include shaft grounding, insulated bearings and journals, ceramic bearings, conductive grease, electrostatic (or Faraday) shield, and/or filtering techniques to eliminate common-mode voltages [8], [48], [49]. For the common-mode currents, the principle of these techniques is resumed in Table A5.4.

Among all the possible/proposed techniques to mitigate bearing currents in VSD-fed IMs, e.g., common-mode/homopolar voltages and voltage transients mitigation using active or passive filters between the inverter and motor (such as sine-wave filters and chokes⁴⁸), use of special cables (appropriate in terms of type and size), proper selection of switching frequency⁴⁹ [21], special inverter topologies (such as three-level inverters [7] and four-leg inverters [45]), electronic common-mode voltage cancellation modules between the inverter and motor [19], implementation of a well designed grounding system, etc., only the mitigation techniques based on shaft-ground connection with a contact brush, bearing insulation, and electrostatic shield installation, are analyzed in detail.

⁴⁸ Their installation should be done near the inverter output and, for that purpose, the conductors of the 3 phases and the ground conductor (connecting the inverter ground to the motor ground/frame) are wound (same wise, 3 to 5 turns) around the ferrite toroidal ring.

⁴⁹ The increase of the switching frequency leads to the reduction of the acoustic noise and improves the current waveform, but some manufacturers recommend its reduction in order to attenuate the bearing degradation and EMI problems (it is recommended 2 to 4 kHz) [21].

TABLE A5.4

TYPICAL TECHNIQUES TO MITIGATE COMMON-MODE BEARING CURRENTS [8], [10], [51].

Schematic and Principle of Operation	Description and Implementation	Advantages, Disadvantages and General Notes	
	<p>Insulation between the outer or inner bearing rings and motor frame in both bearings, by means of insulated bearings (insulated inner or outer ring) or sleeves in bearing housings (shaft or end-shields).</p>	<ul style="list-style-type: none"> - Insulated bearings: medium cost; direct replacement; inner-ring insulation more effective; proper insulation thickness should be provided to block high-frequency currents. - Hybrid bearings: very expensive; direct replacement; effective. - Insulating sleeves: expensive; require housing machining; allow use of conventional uninsulated bearings; insulation thickness typically enough to block high-frequency currents. - General note: should be complemented with insulated mechanical coupling between motor and load or motor shaft-ground brush, to avoid current to circulate through other equipments. 	
<p>C_A – Bearing insulation capacitance. Blocking or attenuation of the bearing currents.</p>		<p>Electrostatic (or Faraday) shield between the stator windings and rotor, by means of conductive film or paint in the stator core inner surface, connected to the ground. Can also be implemented partially in the slot openings.</p>	<ul style="list-style-type: none"> - Full electrostatic shield: medium/high cost; impracticable; effective; can experience significant losses. - Partial electrostatic shield: not expensive; easily feasible; effective; negligible losses. - General notes: avoids the need of insulated mechanical coupling or shaft-ground brush.
<p>$C_{WA} + C_{AR}$ – Electrostatic shield capacitances. Deviation of the currents directly to the ground, without passing through the rotor.</p>		<p>Shaft-ground connection by means of a contact brush or conductive grease.</p>	<ul style="list-style-type: none"> - Contact brush: low/medium cost (depending on the motor rating); effective; requires mechanical adaptation and maintenance; avoid the need of insulated mechanical coupling; not recommended. - Conductive grease: potentially not expensive; easy implementation; increased wear; short period of effectiveness; maybe a good solution in the future if new improved additives were developed.
<p>Minimization of the shaft-ground voltage. Deviation of the currents from rotor directly to the ground, without passing through the bearings.</p>		<p>Input low-pass filter by means of a star-connected capacitor bank with the neutral connected to the ground or shielded cables with shield connected to the ground. Deviation of the common-mode currents to the ground before entering the motor windings.</p>	<ul style="list-style-type: none"> - Low/medium cost; moderate effectiveness (depending on the design); recommended as a complementary solution.
<p>C_F – Input filter insulation capacitance. Deviation of the common-mode currents to the ground before entering the motor windings.</p>		<p>Insulation between motor and ground or increase of the return path or inverter ground to DC-link impedance (typically capacitive).</p>	<ul style="list-style-type: none"> - Motor ground insulation: medium/high cost; effective; impracticable due to the need of connecting the motor frame to the ground for protection purposes; not recommended. - Inverter ground to DC-link impedance increase: not expensive; moderate effectiveness (depending on the design); requires the reduction of the ground to DC-link capacitances in the inverter.
<p>C_A – Motor-ground insulation capacitance or inverter-ground to DC-link impedance increase. Attenuation of the leakage currents (including bearing currents) magnitude.</p>			

The mitigation of the CRCs can be made easily by using one insulated bearing in the non-drive end. In this case, the insulation has no particular requirements, providing that their thickness is

large enough to withstand the expected voltages (in some cases, a resin based coat is enough, but typically, an aluminium-oxide layer is used).

In the case of high-frequency CMCs four passive solutions can be considered: insulated bearings, electrostatic shield between stator windings and rotor and shaft-ground connection with a contact brush, all represented in the schematics of Table A5.4 by an additional capacitance or a shunt (identified in grey colour). In the case of insulated bearings, there are different types: with inner or outer ring insulation, and with ceramic spheres. In Figs. A5.37-A5.38, the outer ring insulation is represented. A FEM-based analysis of the insulated bearings is presented in next section.

Regarding CRCs, resulting from the voltage induced between shaft ends, one of the techniques to mitigate them is the interruption of the path using one insulated bearing in the nondrive-end⁵⁰. For that, bearings covered with an insulating layer (Figs. A5.37 and A5.38) or with ceramic spheres, commonly known as hybrid bearings (Fig. A5.39), or even the bearing housing (in shaft and/or frame) insulation introducing insulating sleeves, can be an effective solution. The last technique is quite effective, although expensive and time consuming since the bearing housing in shaft or frame have to be changed/adapted.

Instead of installing insulated or hybrid bearings, the user can request to the motor manufacturer the insulation of the bearing housing (in the end-shields and/or shaft) during the manufacturing process, but the cost typically precludes this application for motors smaller than 150 kW [48].

Bearing electric discharges can also be attenuated using conductive grease (incorporating electrically conductive additives, such as graphite) in order to minimize the capacitive effect and provide a low-impedance path through the bearing lubricant, preventing the shaft-ground voltage build up, therefore avoiding high flash-over currents [8]. Unfortunately, grease with enough metallic elements to provide conduction, without causing wearing bearing damage itself, is yet to be found [48]. In fact, due to the extra wear associated with the particles added to the lubricant (due to the abrasive effect, the mechanical wear can increase up to 60%, reducing the bearing useful lifetime) and to the short time of effective conducting, this technique is not recommended, although its potential low cost and easy implementation. However, it should be noted that improved greases to extend electric motors bearing lifetime are being provided by some bearing manufacturers [111].

Regarding insulated bearings, the external surface of their inner and/or outer steel rings is typically covered by a thick aluminium oxide insulation layer in the outer or inner steel rings. It can be a good solution to interrupt the passage of the low-frequency circulating currents, but, if the thickness is too low, they can be ineffective in the mitigation of high-frequency currents (common-

⁵⁰ If only the drive-end bearing is insulated, the currents can circulate through the mechanically coupled devices. As a way to maintain the current values within the safety limits, the RMS value of shaft-ends voltage should be lower than 1 V [5], [8], [15], [51].

mode and/or circulating currents). In fact, their effectiveness in blocking the circulation of high-frequency currents depends on the insulation thickness but, in general, is low due to the relatively high capacitance (i.e., low capacitive impedance) associated with the insulating film. For an effective mitigation of the high-frequency currents, it is recommended the application of a layer in the inner ring with a thickness equal or higher than 100-150 μm , depending on the material being used and on the current frequency range [10], which is a common thickness provided by manufacturers. The associated capacitance is 50 and 500 times higher than that associated with lubricant film. Theoretically, the insulated bearing method is only effective if the new capacitance associated to the insulation (C_A in Table A5.4) is significantly lower than the stray capacitance associated with the bearing, in order to reduce the voltage drop associated to the last one, ensuring an effective attenuation of the CMCs. Electrically insulated bearings have a longer service life compared with other standard uninsulated bearings. In general, they also have a high reliability, since they are not at all prone to damages caused by electric current activity. Leading manufacturers of electrical machinery and traction motors are installing an insulated bearing in the nondrive-end when the voltage between shaft ends exceeds 200 mV (RMS value). For a 100- μm layer, they can withstand voltages from 500 to 1000 V, but the breakdown voltage limit is being improved by manufacturers [111]. Actually, tests carried out by bearing manufacturers show that electrical breakdown of the insulating layer occurs above 3 kV (DC) [44], [109], [110], [111]. Insulated bearings with an aluminium-oxide layer up to 300- μm thickness on the bearing outer ring are available on request [44], [109], [110], [111]. The aluminium-oxide layer provides effective protection against AC and DC currents. The minimum ohmic resistance is 50 $\text{M}\Omega$ ⁵¹ at 1 kV (DC). Insulated bearings provide an electrical insulation insensitive to heat, moisture and chemicals. The insulated bearing performance and running accuracy are identical to standard non-insulated bearings and no additional mounting precautions are needed. This is a convenient and very reliable solution for low frequency currents. This type of bearings tend to be rather expensive, costing 3 to 4 times more than standard or conventional bearings (steel, uninsulated), and can replace them without any mechanical adaptation/change (they have the same standard dimensions), therefore, they can be considered a low-medium cost solution considering only the price premium over the standard bearing [8]. Typically, insulated bearings have substantial lead-times from suppliers.



Fig. A5.37. Bearings with insulated outer ring [44], [111], [110].

⁵¹ The electric resistance of insulated bearings should be measured with a megaohmmeter of 50 V and the value should be $\geq 50 \text{ M}\Omega$ [8].



Fig. A5.38. Bearing with insulated outer ring installed in a rotor shaft.

Regarding hybrid ball bearings, they have steel rings/races and ceramic spheres, typically of silicon nitride⁵² (Si_3N_4), whose properties are shown in Table A5.5. In Fig. A5.39, hybrid bearings and the respective ceramic balls are shown. They have a highly effective electric insulation due to the excellent insulating property of the silicon nitride. The impedance for a hybrid bearing is high, even for very high frequencies, providing an excellent protection against ring-to-ring voltages with high peak values and/or high frequency, since currents are effectively blocked. Even for small hybrid bearings equipped with a steel sheet reinforced contact seal of acrylonitrilebutadiene rubber (NBR), reinforced with a steel sheet, the voltage level for arcing occurrence through the seal/bearing contact is beyond 2.5 kV DC. Due to the high capacitive impedance and the high dielectric strength associated with hybrid bearings (the dielectric is essentially composed by the spheres), they allow an excellent mitigation/blocking of all sort of bearing currents, having a significantly extended lifetime in relation to conventional steel uninsulated bearings in VSD-fed IMs, and provide effective protection against flash-over damage to the grease and raceways caused by both AC and DC currents.

Additionally, this type of bearings can operate with higher speeds than those supported by standard bearings because the centrifugal forces generated by ceramic spheres are 40% of those generated by steel spheres (silicon nitride density is only 40% of the steel density) and the surface characteristics of silicon-nitride balls are much improved. As a result, less bearing cage stress or wear and reduced raceway wear during fast starts/stops and significantly lower friction losses⁵³ are expected in hybrid bearings, leading to lower operating temperatures, particularly at high speeds (> 8000 r/min) as it can be seen in Fig. A5.40. A lower operating temperature leads to an extended lubricant/lube lifetime, being the corresponding lubrication interval 3 to 5 times lower than that for

⁵² Silicon nitride (Si_3N_4) was developed in 1960-1970 in a search for fully dense, high strength and high toughness materials. A prime driver for its development was to replace metals with ceramics in advanced turbine and reciprocating engines to give higher operating temperatures and efficiencies. Although the ultimate goal of a ceramic engine has never been achieved, silicon nitride has been used in a number of industrial applications, such as engine components, bearings and cutting tools. Silicon nitride has better high temperature capabilities than most metals, combining retention of high strength and creep resistance with oxidation resistance. In addition, its low thermal expansion coefficient gives good thermal shock resistance compared with most ceramic materials. The wear resistance, low friction and high stiffness of fully dense silicon nitride improve the performance of high temperature unlubricated roller and ball bearings.

⁵³ The silicon-nitride-to-steel coefficient of friction is 30% of that for steel-to-steel, i.e., the internal bearing friction is 30% lower.

equivalent standard bearings requiring periodic lubrication. The material stiffness, lightweight, and inertness lead to lower bearing heat generation, while providing stiffer and higher speed bearing capabilities. The improved surface finishing (almost perfectly smooth⁵⁴) and geometry of silicon nitride balls, associated with their lower weight, also lowers significantly the bearing vibration levels (2 to 7 times lower than those for conventional steel ball bearings) and acoustic noise, as well as extending the speed limits and life of the bearing. They also present a higher corrosion resistance compared to conventional steel bearings. In fact, silicon nitride has a higher hardness and higher modulus of elasticity than steel, resulting in increased bearing stiffness and longer bearing service life in contaminated environments. Due to the unique properties of silicon nitride, ceramic balls drastically reduce the predominant cause of surface wear in conventional bearings (metal rings/metal balls). In conventional bearings, microscopic surface asperities on balls and races will “cold weld” or stick together even under normal lubrication and load conditions. Since ceramic balls will not cold weld to steel rings, wear is dramatically reduced. The fact that wear particles generated by adhesive wear are not present in hybrid bearings, also contributes to the lubricant life extension. Silicon nitride rolling elements have a lower thermal expansion than steel rolling elements of similar size, leading to increased robustness to excessive thermal magnitudes and gradients, since the size of ceramic balls changes less than that of the steel balls.

For normal operating conditions, all the referred factors lead to a service life for this type of bearings up to 5 times longer than that for conventional bearings [44], [109], [110], [111]. In severe operating conditions, including high amplitude and/or frequency shaft-ground and shaft-ends voltages, high temperatures and chemical contamination, significant mechanical shocks, poor lubrication, etc., due to the inherent high electrical, mechanical, thermal and chemical robustness, the useful lifetime of hybrid bearings can be up to 6-10 times longer than that of the conventional bearings. The associated maintenance cost reduction alone can be also significant [8].

To guarantee maximum electrical insulation in this type of bearings, seals/shields are typically made of rubber (as previously referred), which can actually increase slightly the bearing friction [8].

Hybrid bearings are typically expensive (10-20 times more than the conventional bearings [8], [111]), with long lead times [48], but the motor will run with higher efficiency (due to the lower friction) and longer *MTTF* (particularly for the case of inverter-fed motors), leading to lower total operating costs. Therefore, in some cases, this solution can be cost-effective, particularly when the cost associated with the motor downtime is high. They also allow the direct replacement of conventional bearings (have the same standard dimensions).

⁵⁴ Microstructure of silicon nitride can be uniformly engineered to sub-micron grain size, and the surface of a silicon nitride ball can have a better finishing and much lower roundness tolerance.

Fig. A5.41 presents the experimental common-mode bearing current mitigation (which becomes negligible) after the installation of hybrid bearings, evidencing their effectiveness.

TABLE A5.5
COMPARISON OF BEARING STEEL AND SILICON NITRIDE PROPERTIES.

Property	Steel	Silicon Nitride
Density (g/cm ³)	7.8	3.2
Elastic or Young's Modulus (×10 ⁹ N/m ²)	≈ 207	≈ 310
Hardness	R _c 60	R _c 78
Coefficient of linear thermal expansion @ 20°C (×10 ⁻⁶ /°C)*	≈ 12	≈ 3
Coefficient of friction	0.42 dry	0.17 dry
Poisson's ratio	0.3	0.26
Maximum Operating Temperature (°C)	327	1093
Chemically inert	No	Yes
Electrically non-conductive	No	Yes
Non-magnetic	No	Yes

Note: *Parts per million per Celsius degree.



Fig. A5.39. Hybrid bearings and ceramic balls [44], [111], [110].

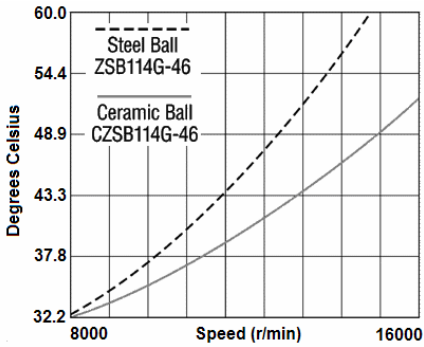


Fig. A5.40. Running temperature of steel-ball bearing and ceramic-ball bearings [111].

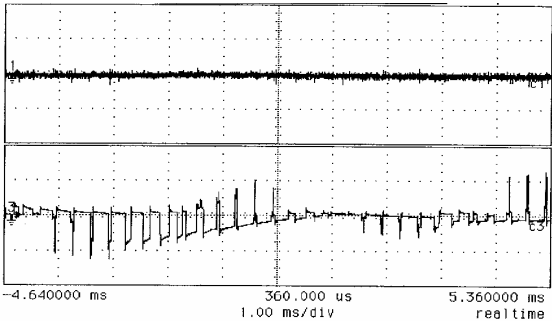


Fig. A5.41. Experimental results for a 5-hp, 460-V IM, with hybrid bearings (extracted from [48]): bearing current (Ch. 1, 200 mA/div) and shaft voltage (Ch. 3, 4 V/div).

A FEM-based analysis on insulated and hybrid bearings is presented in the next section.

Insulating only one bearing is not recommended for the CMCs produced by CMVs generated between the shaft and frame, because all the CMCs will circulate through the other bearing (aggravating their effects), being necessary to insulate both bearings.

Since the insulation of both bearings (either using insulated or hybrid bearings) does not eliminate shaft-ground voltages, being the rotor electrically insulated from the stator, the CMCs search the lowest impedance path to ground (or earth). This can potentially cause a problem if the path happens to be through conductive devices coupled mechanically to the IM and connected to the ground (e.g., tachometer shafts, electronic encoders, gear boxes, etc.), which can be damaged. Due to the referred reasons, in order to mitigate the shaft-ground voltage, a shaft-grounding device and/or insulated mechanical coupling can be installed. It should be avoided the connection to earth of sensible devices mechanically coupled to the IM. Obviously, this combination is better than one or the other independently, but at a much higher cost. Careful risk and cost analysis can help determine the protection most appropriate for a given application.

Low-frequency CRCs can also be attenuated connecting the windings in star mode without neutral connection, in order to block the homopolar circulating currents (e.g., due to saturation). For VSD-fed IMs, star connection also reduces the high-frequency leakage currents, thus reducing high-frequency CRCs. For that, if the motor is designed to operate with star connection at full load, the neutral should not be connected (as usually). If the motor is designed to operate in delta mode, when it fails, the conversion to star connection during rewinding should be evaluated, if no starting problems exist.

To avoid the increase or introduction of eccentricities and asymmetries (which produce low-frequency CRCs) during motor repair, among other aspects, it should be avoided: (a) frame distortion/deformation (particularly if it is of an aluminium league) resulting from the application of excessive temperatures during the winding stripping-out process; (b) the presence of rests of resin in the housing surfaces after impregnation (since they can introduce misalignments); (c) end-shields distortion/deformation (if they are made of aluminium league) caused by the use of excessive force during the screw or fitting tightness during assembling process [8].

The most effective and potentially cheaper solution is the electrical connection between the shaft and ground by means of a brush-based contact installation (grounding device or brush, as it can be seen in Fig. A5.42), providing that a good contact is maintained and a proper low-impedance cable⁵⁵ connecting the brush to the ground is used, otherwise the effectiveness of this technique is reduced. There are some grounding kits that are just now becoming commercially available to install as part of the whole system. Early testing and patent applications of such kits claim to eliminate CMVs from the system altogether. The disadvantage of this solution is the need for frequent maintenance, increasing the overall cost [8], but it is simple, effective and its cost is relatively low [44]. The shaft grounding can be an alternative or complementary measure to

⁵⁵ Since the common-mode currents are of high frequency, in the brush-ground connecting system multiwire conductors should be use to mitigate the skin effect.

mitigate significantly the CMCs effect, providing an alternative low-impedance path from the motor shaft to the motor frame/ground.

This technique can override the problem of electric discharge current resulting from electrostatic charging of rotor, since a low path is established to ground, effectively channelling or deviating the CMCs (or static charges flow to earth) away from the bearings [5], [8], [14]. The effectiveness of this technique for CMCs attenuation is clearly evidenced in Fig. A5.43, in which it is possible to observe that it significantly reduces the shaft-ground voltage (it become negligible), by not allowing the voltage to build up on the rotor, and, therefore, the bearing currents.

Grounding brushes can be custom fit to any motor shaft, are self-contained for use in clean-room environments, and can be retrofit to existing installations. They do, however, require replacement every few (two or three) years depending on the shaft rotating speed, brush contact pressure, and motor duty cycle. Nevertheless, the grounding brush is a reliable mean of protecting the motor bearings from damaging bearing currents.

To attenuate CRCs, the same principle can be used, but two shaft brushes, in both shaft ends, connected each other (providing a closed-loop circuit) and one of them also connected to the ground, should be implemented, otherwise shaft grounding becomes ineffective for CRCs [44].

However, its effectiveness can be minimized due to the action of a number of brush-shaft contact degradation factors, such as wear, dirty, oxidation, vibration, human interference, etc. [5], [22]. Therefore, in a number of situations, due to the significant installation (mechanical adaptation/fitting) and maintenance costs, this solution can become non-cost-effective.

Protecting motor bearings from unpredictable occurrence of bearing currents is not an exact science, but rather a process of risk assessment and cost analysis. There are certain measures that can be taken to reduce the risks, but not without additional cost. Since the occurrences are unpredictable, the user has to weigh the cost of protection against the cost associated with the motor downtime due to bearing failure. For example, installing a shaft grounding assembly in 75-kW motors driving a fan-system critical for the operation of a continuous industrial process would be much cheaper than replacing their bearings three months after starting them. However, waiving the extra cost of shaft grounding assemblies in smaller motors driving noncritical applications, the application of such strategy might not be the right decision, from the economical perspective.

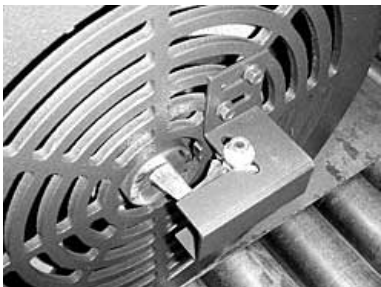


Fig. A5.42. Grounding brush installed in the non-drive end of a rotor shaft.

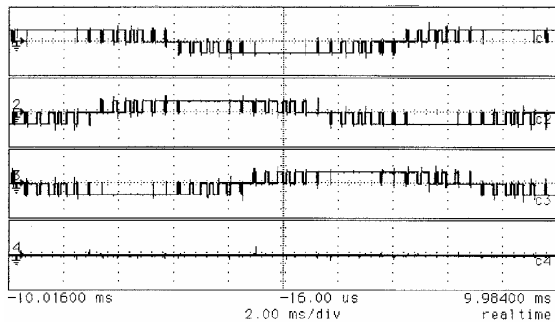


Fig. A5.43. Experimental results for a 5-hp, 460-V IM with shaft grounding system (extracted from [48]): line-to-line input voltages of a 5-hp/460-V motor (Chs. 1–3, 500 V/div) and the shaft-ground voltage (Ch. 4, 4 V/div).

At higher switching frequencies, the motor will generally run quieter, but the inverter output voltages become more destructive to the motor insulation and bearings. In fact, the higher the switching frequency of the PWM is, the higher the number of possible current discharges will be, and, therefore, the faster the damage caused by EDM. Most experts recommend that the switching frequency should be adjusted to a value as low as possible, without creating unacceptable audible noise levels, and the avoidance of frequencies above 6 kHz. Accordingly, it is generally a good idea to specify and install a VSD that has an adjustable switching frequency by means of relatively small increments (i.e., 1 kHz increments) to allow a fine tuning to the lowest acceptable level. Here, 3-level VSDs have advantage over 2-level VSDs since the noise produced in the motor is lower for a given switching frequency and, therefore, the switching frequency can be pushed down to lower levels (see Chapter 3).

More complex solutions have been proposed based on new inverter-motor topologies. For example, in [49], a 4-leg inverter topology is proposed to reduce the CMVs, with very promising results, but require special inverter topologies and control, being potentially expensive. In [39], a dual-bridge inverter (DBI) approach to eliminate CMVs and CMCs is proposed. The DBI is designed to generate balanced excitation of the IM and, therefore, it does not generate CMVs. Therefore, a significant attenuation of the shaft voltages and bearing currents occurs, as it can be seen in Fig. A5.44. However, shaft-ground voltages can be generated by asymmetrical high-magnitude, high- du/dt phase-to-ground voltage transients (e.g., in one phase), and the mitigation of the CMVs does not mitigate all bearing current modes. Moreover, the DBI requires a dual-voltage motor and the cost of the overall system is estimated to be high. In principle, the DBI provides a significant reduction of the conducted EMI and a minor reduction of the radiated EMI [48].

CMCs can also be reduced with the increase of the impedance between the inverter ground (typically corresponding to the middle point between two small capacitors in the DC-link) and the inverter DC-bus positive and negative poles, since part of the closed-loop path impedance for CMCs is increased. Of course, the CMCs also circulate through closed-loop composed by the ground of the power supply, the VSD, and the IM (connected to the ground).

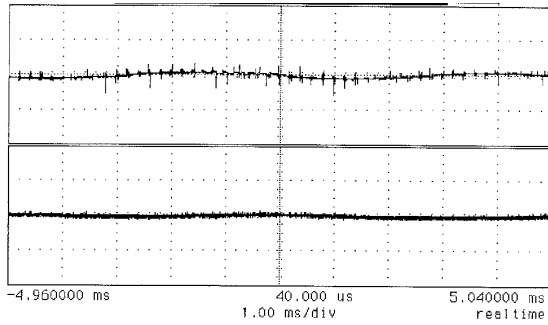


Fig. A5.44. Experimental results for a 5-hp, 460-V IM with a DBI-driven motor (extracted from [48]): shaft-ground voltage (top, 4 V/div) and bearing current (bottom, 200 mA/div).

In previous works, an air-gap electrostatic shield (or Faraday shield) along the inner stator core surface was proposed to reduce the shaft-ground CMVs, thus reducing/mitigating bearing CMCs (however, CRCs are not mitigated). It is a promising solution, already successfully tested in laboratory. In fact, tests performed have shown that this technique is quite effective since it leads to a strong attenuation of the shaft-ground voltages in the order of 90-98% [14], [28].

The principle is to minimize the stray capacitive coupling (or electrostatic coupling) between the stator windings (including coil heads) and the rotor, by means of the installation of an electrostatic shield (ES) connected to the ground (grounded conductive material in-between the rotor and the stator), such as copper foil tape or conductive paint applied to the stator length. This method reduces the parasitic capacitive currents crossing the motor air gap, minimizing the motor shaft-ground voltage. One drawback associated with the ES is that the construction methods to obtain the desired benefits are very precise, which potentially result in a significant motor extra cost [8], [14], [48].

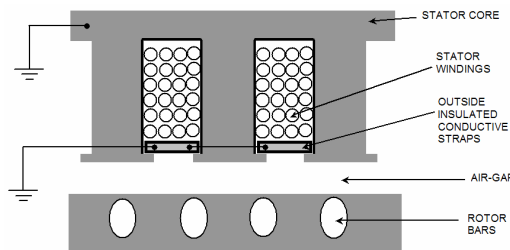


Fig. A5.45. Novel proposed electrostatic partial shield concept in the slot-openings [8].

The ES insertion into the air-gap has to be made without short-circuiting the stator laminations or bridging the air-gap [48]. This method does not affect the motor torque, but the conductive material can experience losses due to induced currents [14], [28]. Presently, motors with an ES are not commercially available [48].

Based on the same principle, an electrostatic partial shield is proposed in [10], considering only outside-insulated conductive straps⁵⁶ in the slot-openings or slot stick covers, all connected to the

⁵⁶ Insulation material straps with a conductive thick film in one of the surfaces can also be used, e.g., copper foil tape covered by a resin or varnish coat to avoid short-circuits between stator core sheets.

ground (as it can be seen in Fig. A5.45), thus simplifying the implementation and avoiding induced currents and losses in the shield. Moreover, since the stray capacitances between the stator windings and the rotor are related with the in-slot conductors and coil heads, it is proposed the installation of a shield covering the slot opening and, for a better attenuation, also covering the coil heads (e.g., insulated and covered with conductive tape), which is by far enough and effective to prevent the CMC circulation through the bearings of the motor and/or coupled devices. It should be noted that the use of a thick conductive film in the slot opening or in the slot stick covers do not lead to negligible induced currents⁵⁷ because the main magnetic flux induction will not cross orthogonally the shield surface since it is concentrated in the stator teeth. By itself, the slot (or slot stick covers) covering with a conductive film connected to the ground attenuates significantly the capacitive coupling between the stator windings and the rotor, being a fair measure. The introduced capacitance (see Table A5.4) can slightly aggravate the high-frequency CRCs due the increase of the winding-frame CMC circulation. In Tables A5.6 and A5.7, some experimental results on the use of the referred shield in a VSD-fed 11-kW IM, are presented. A FEM-based analysis of the proposed ES is presented in next section. The conductive film can be either of copper or aluminium, being the last more appropriate due to the higher resistivity.

TABLE A5.6
EFFECTIVENESS OF THE ELECTROSTATIC SHIELD FOR AN 11-kW VSD-IM SYSTEM [28].

	U_{RS} (V peak)	I_{CMC} (mA peak)	I_{CMD} (A peak)
VSD-fed IM without ES	10	500	3.5
VSD-fed IM with ES	2.2	17	None

TABLE A5.7
ESTIMATED BEARING LIFETIME FOR AN 11-kW VSD-IM SYSTEM [28].

Shaft radial load	IM without ES		IM with ES	
	Rotor weighth only (no-load)	3 times the rotor weighth	Rotor weighth only (no-load)	3 times the rotor weighth
I_{CMD} (A peak)	2.2	2.2	0	0
$A_{contact}$ (mm ²)	0.62	1.29	0.62	1.29
J (A/mm ² peak)	3.5	1.7	0	0
t_{if} estimated (h)	<10	1570	>10000	>100000
I_{CMC} (peak)	0.2-0.5 A	0.2-0.5 A	0.05 A	0.05 A
$A_{contact}$ (mm ²)	0.62	1.29	0.62	1.29
J (A/mm ² peak)	0.32-0.8	0.15-0.38	0.08	0.04
t_{if} estimated (h)	>100000	>100000	>100000	>100000

A5.3.8 Finite-Element Method-Based Analysis

Two different analyses were made: bearing insulation types and conductive slot-opening straps used as an electrostatic shield. For the FEM-based analysis, the FEMLAB software [96] was used. The “Small In-Plane Currents” submodule in the “Electromagnetics Module - Quasi-Statics” was selected, which is indicated for quasi-statics analysis of conducting and dielectric materials with

⁵⁷ Nevertheless, in order to reduce the Foucault currents, if any, the conductive zone can be divided in several small width strips short-circuited in one of the sides.

small in-plane currents and a negligible coupling between the electric and magnetic fields. This tool has time-harmonic analysis. The subdomain equation is given by (A5.29), where U is the electric potential, ω is the frequency, σ is the electrical conductivity and ϵ is the dielectric constant (permittivity).

$$-\nabla \cdot (\sigma \cdot \nabla U + j\omega \epsilon_0 \epsilon_r \cdot \nabla U) = 0 \tag{A5.29}$$

The selected element type was “Lagrange-Quadratic”. In the models, typical values for the dielectric constant and conductivity were assumed for the considered materials: air, steel, oil, aluminium oxide and silicon nitride, for the bearing analysis, and air, Teflon®, epoxy resin, enamel and copper, for the electrostatic shield analysis.

A5.3.8.1 Bearing Insulation Analysis

Three different types of commercially available deep-groove ball bearings were evaluated: conventional bearings, hybrid bearings (with silicon nitride spheres) and insulated bearings, as it can be seen in Fig. A5.46. Particularly for the insulated bearings, it is evaluated the most effective solution to block the currents - inner or outer insulation. Although 3-D analysis is the most appropriate for the purpose, simplified 2-D models (radial and axial cuts, Fig. A5.47) were used, which allow to analyze the worse cases in terms of electric field and require much less computation.

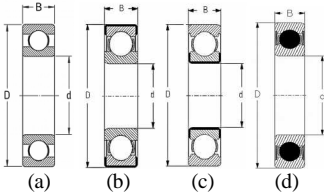


Fig. A5.46. Radial cut of deep groove ball bearings: (a) conventional; (b) with outer insulation; (c) with inner insulation; (d) with silicon nitride spheres. Simulated model size: $d = 19.2$ mm; $D = 35$ mm; $B = 8$ mm [10].

In the following analysis, the 2-D models presented in Fig. A5.47 were used in the simulations. The inner ring (shaft ring) and outer ring (frame ring) are located in the bottom and in the top parts of the models, respectively. The results can be also applied to the roller bearings, which can be described by the axial cut. Depending on the insulation system, 10 submodels were considered (Table A5.8), denoted by A-J letters. A mineral oil lubricant film of 1 μ m was considered. In relation to the inner and outer insulation layer technology, aluminium-oxide coats of 30, 60, 150 and 300 μ m were considered separately - manufacturers typically use the last two. The spheres have a diameter of 4.8 mm, the model width is 8 mm, and the races groove has a depth of 0.85 mm. The considered dimensions are normal for a typical small bearing. Due to the roughly

proportional increase of all dimensions for larger bearings the results are expected to remain valid. For the sake of simplicity, the models were solved only for 50 Hz for the sake of simplicity (moreover, the results can be easily estimated for higher frequencies). An electric potential in the shaft side ring of 1 V was used, being the frame ring grounded. The results can be easily extended to higher voltages.

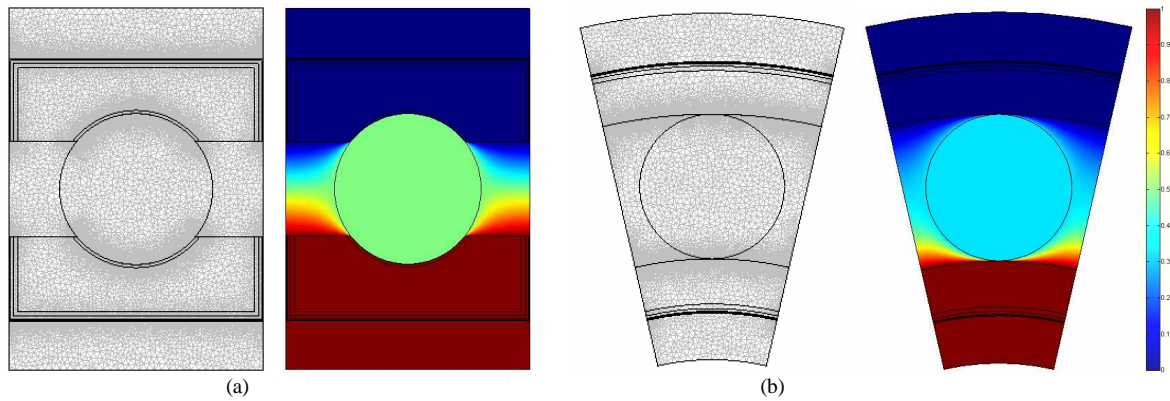


Fig. A5.47. 2-D models with mesh and electrical potential: (a) radial cut; (b) axial cut [10].

Firstly, on the basis of the obtained simulated results, it can be concluded that maximum electric field amplitudes are achieved in the sharp zones (e.g., interface air near the contact narrow region between the spheres and races), as expected (see Fig. A5.48). Moreover, even with the considered voltage (1 V), the values achieved in those points, exceed the dielectric strength of the air (3.2 V/ μm), as it can be seen in Fig. A5.49b. Therefore, partial discharges are expected in those zones, which can accelerate the lubricant degradation.

In Fig. A5.50, the electric potential variation along the vertical symmetry line can be seen for both radial and axial cuts, in which the voltage drop is deviated from the oil film to the insulation layers. In terms of voltage drop deviation, the ceramic sphere insulation is the most effective solution, as expected, and the inner ring insulation leads to better results than the outer ring insulation (see Fig. 50b).

TABLE A5.8
SUBMODELS FOR BOTH RADIAL AND AXIAL CUTS [10].

Submodel	Description
A	without insulation
B	with ground-side outer insulation: 30 μm of thickness
C	with ground-side outer insulation: 60 μm of thickness
D	with ground-side outer insulation: 150 μm of thickness
E	with ground-side outer insulation: 300 μm of thickness
F	with phase-side inner insulation: 30 μm of thickness
G	with phase-side inner insulation: 60 μm of thickness
H	with phase-side inner insulation: 150 μm of thickness
I	with phase-side inner insulation: 300 μm of thickness
J	with silicon nitride spheres (ceramic spheres)

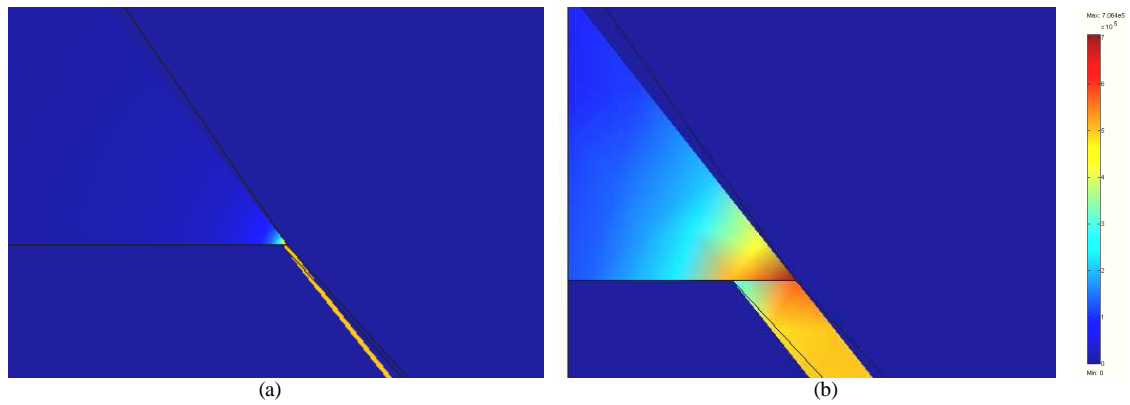


Fig. A5.48. Electric field in the interface between the sphere and inner race for the submodel A of the radial cut: (a) overview; (b) zoom [10].

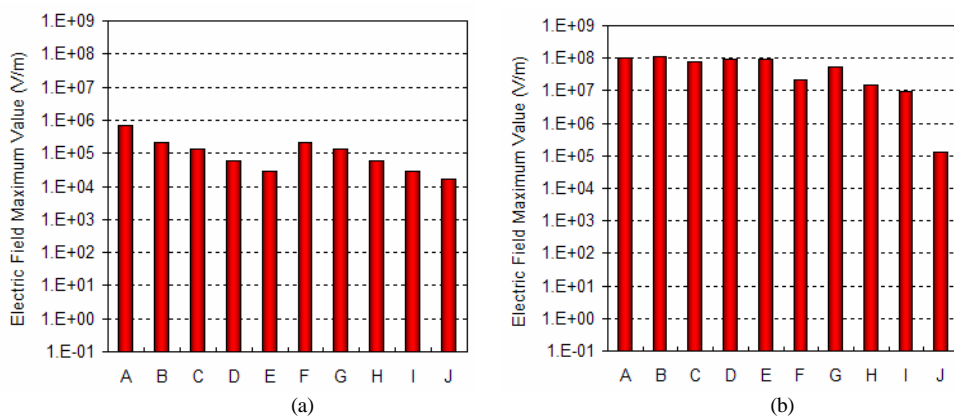
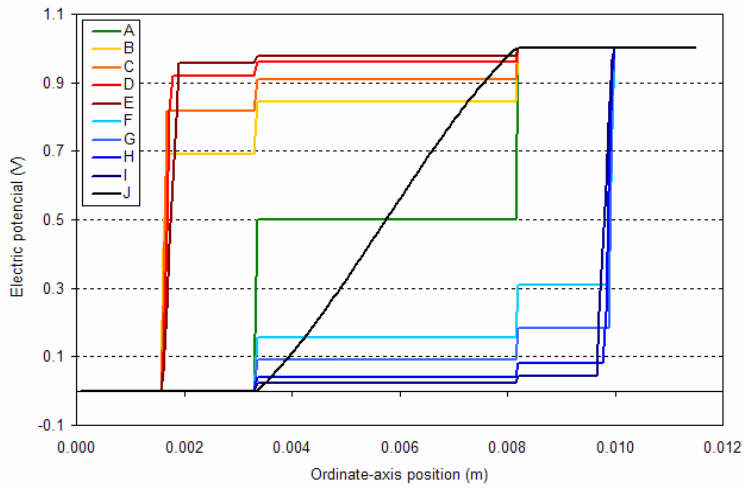


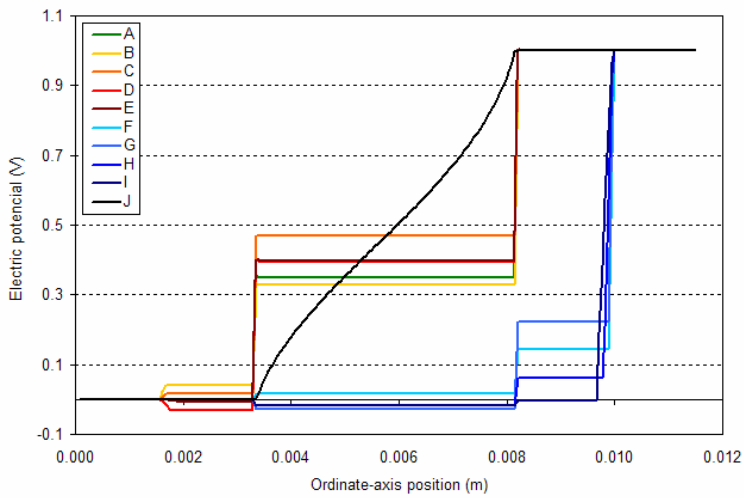
Fig. A5.49. Maximum value of electric field: (a) radial cut; (b) axial cut [10].

In Fig. A5.51, the electric field maximum value in the phase-side and ground-side lubricant film is presented. The mineral oil has a dielectric strength of approximately $7.87 \text{ V}/\mu\text{m}$ (depending on the type of oil or grease, it can vary between 7 and $15 \text{ V}/\mu\text{m}$). On the basis of Fig. A5.51, the estimated voltage safety limits can be established for the considered oil film thickness ($1 \mu\text{m}$), being presented in Fig. A5.52. If a different thickness is to be considered, the obtained limits can be rearranged (e.g., for the uninsulated bearing model, considering a oil film thickness of $0.2 \mu\text{m}$ (5 times lower than $1 \mu\text{m}$), the voltage limits can be divided by 5, which become according to previous reported limits). The frequency does not influence the presented limits.

In principle, even for the expected maximum values between the inner and outer rings, the dielectric breakdown of the insulation layers does not occur, since the aluminium oxide has a dielectric strength of approximately $16.9 \text{ V}/\mu\text{m}$. The silicon nitride has a dielectric strength of $15.0 \text{ V}/\mu\text{m}$.

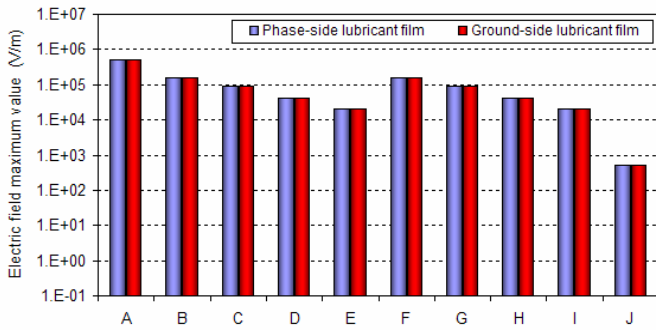


(a)

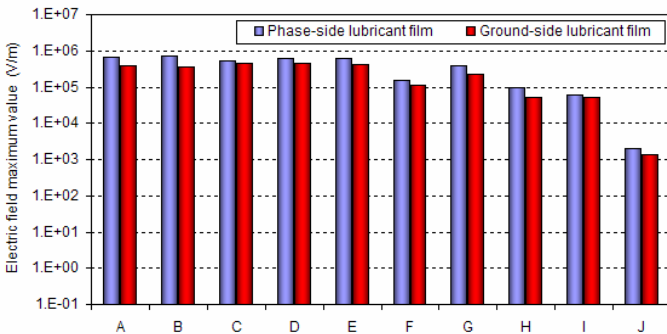


(b)

Fig. A5.50. Electric potential variation along the vertical symmetry line (absciss origin corresponds to the model upper limit): (a) radial cut; (b) axial cut [10].



(a)



(b)

Fig. A5.51. Electric field maximum value in the lubricant films for the considered conditions: (a) radial cut; (b) axial cut [10].

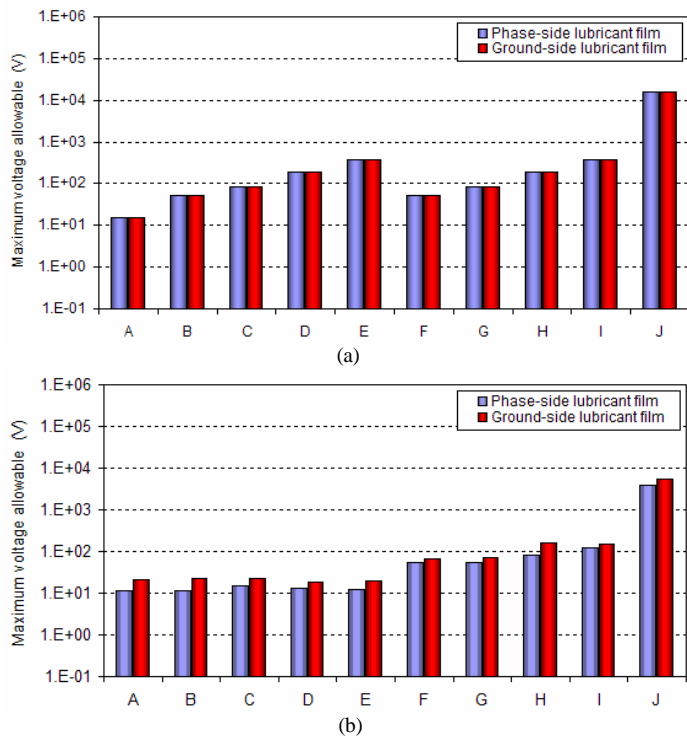


Fig. A5.52. Maximum voltage allowable between inner and outer rings for the considered conditions: (a) radial cut; (b) axial cut [10].

The higher the capacitive impedance is, the higher the current mitigation will be, which is the aim of the insulation-base techniques.

In Fig. A5.53, the result of the integration of the current density along the outer ring interface with frame is shown. The lower the current flowing into the ground is, the higher the capacitive impedance of the models being considered.

From the capacitive impedance perspective, the insulation in the inner ring is more effective than the insulation in the outer ring. Furthermore, the ohmic resistance, for a given insulation thickness, is also higher when covering the inner ring, since the corresponding surface is lower. Therefore, the overall resistive and capacitive impedance is more effective when the inner ring is insulated.

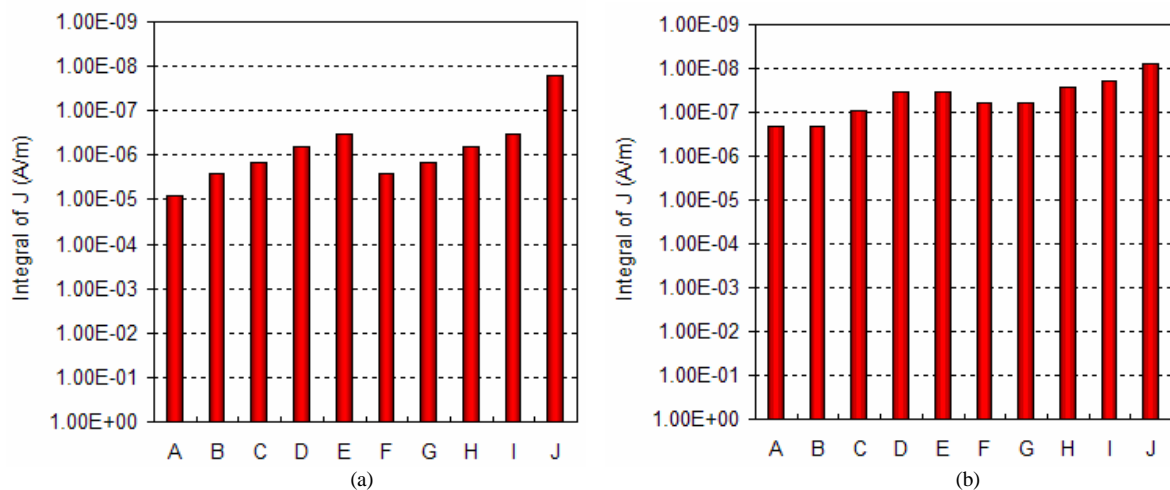


Fig. A5.53. Integral of current density along the outer ring interface with frame: (a) radial cut; (b) axial cut [10].

A5.3.8.2 Electrostatic Shield Analysis

To analyze the proposed partial electrostatic shield, the model presented in Fig. A5.54a was used with two different types of slot-opening insulation straps: with and without conductive surface grounded. The models were solved for 50 Hz. An electric potential in all slot conductors of 1 V was used, being the rotor and slot surfaces grounded. In Figs. A5.54 and A5.55, the electrical potential and electrical field magnitudes are presented, respectively. The maximum electric field magnitude between conductors and the rotor decrease from 55 V/m to ≈ 0 V/m, denoting a sharp decrease of the capacitive coupling between those parts. It can be concluded that the proposed solution is quite promising for the mitigation of the stray capacitance between the stator windings and the rotor, and, in principle, can be easily implemented.

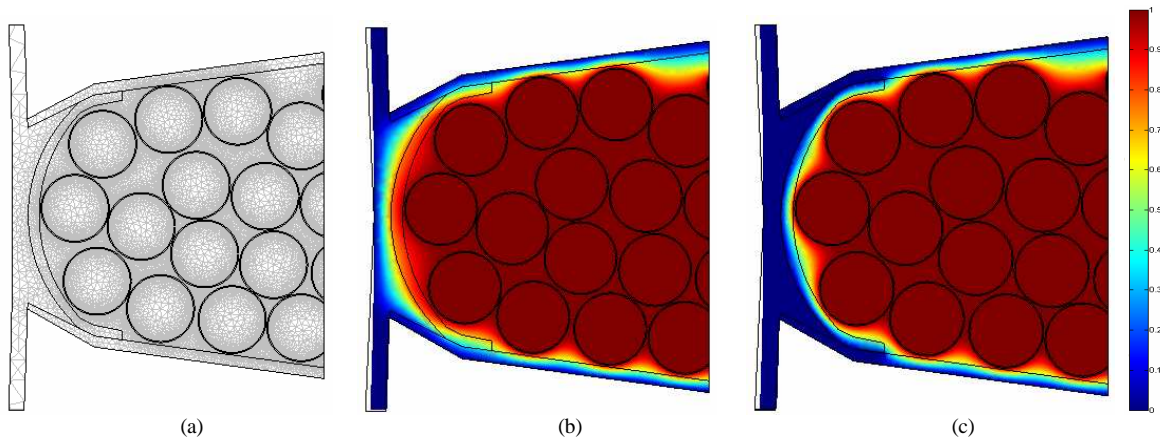


Fig. A5.55. Electrostatic shield analysis: (a) 2-D model; (b) electric potential without electrostatic shield; (c) electric potential with electrostatic shield [10].

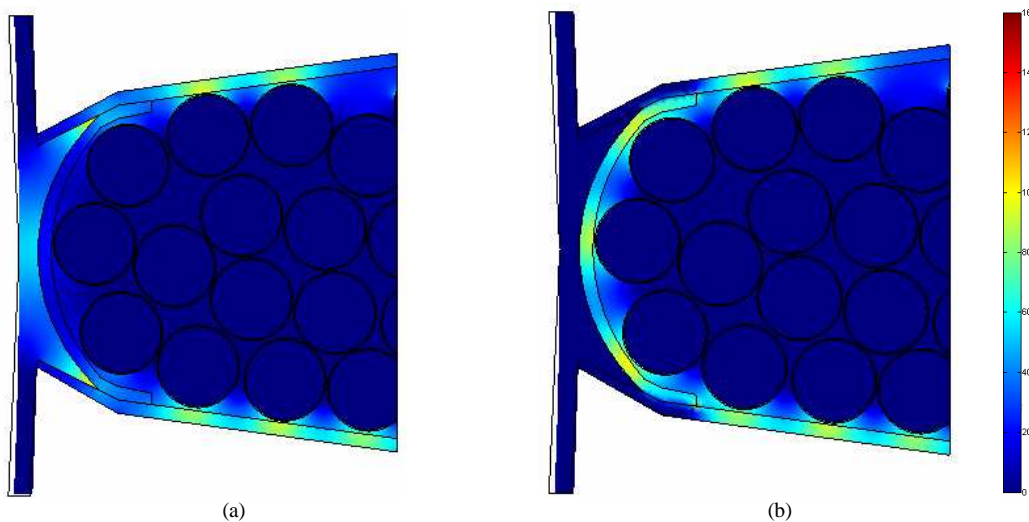


Fig. A5.56. Electric field: (a) without electrostatic shield; (b) with electrostatic shield [10].

A5.4 Considerations on Voltage Transients

As previously referred, in EU, the use of VSDs is growing fast in industrial and tertiary sectors, being sold in 2002 about 1.8 millions of units, 76% of which with power between 0.75 kW and 4 kW (see Chapter 3). The market is by far dominated by VSDs integrating voltage-source inverters with pulse-width modulation, which is the technology considered in the following discussion.

IMs are being improved continuously by manufacturers, and tend to be smaller, more powerful, more efficient and more reliable. Those improvements are achieved by means of optimized design and the use of better quality materials, including improved electrical insulation systems. However, VSD-fed IMs can experience, in short term, an insulation system breakdown, particularly in the cases in which the insulation system is old, weak, and/or is not appropriate to withstand PWM voltages [8], [16], [43]. In fact, according to a number of users and manufacturers, VSD-fed IMs can fail more frequently than those fed directly by the line/mains or by quasi-sinusoidal voltage systems [8], [16], [43].

As previously referred, roughly $\frac{1}{4}$ of the IM failures are due to the stator winding insulation system faults. The stator winding insulation system wear is related to electrical⁵⁸, thermal⁵⁹, chemical⁶⁰ and mechanical⁶¹ factors which, acting individually or together, lead to the degradation and occurrence of different failure modes [5], [8], [16], [54], [60]. Considering only thermal ageing, the stator winding failure (and thus the number of rewindings) depends on operating hours (or useful lifetime) and loading (here meaning operating temperature, which depends, in part, on actual motor load) [114]. In the stator winding, short-circuits between turns of the same phase, between turns of different phases or between turns and ground (or iron core), are examples of failures that can frequently occur due to the insulation system failure, mainly in the coil-heads base [8]. The probability of short-circuit occurrence between phases is higher when coils of different phases share the same slot [8].

One of the main electrical phenomena responsible for the accelerated degradation of the stator-winding insulation system is the voltage transients⁶² (VTs) occurrence at windings terminals [5], [8]. VTs are also a major factor responsible for bearing currents circulation, discussed previously. In fact, as previously referred, the VT mitigation techniques are also effective for bearing currents and EMI mitigation, and an integrated approach of these 3 issues is recommended to optimize effectiveness and costs. In the following sections, the main causes and effects of VTs associated

⁵⁸ E.g., high voltages, partial discharges, etc.

⁵⁹ Arrhenius law, e.g., excessive ambient temperature, motor loss increase, etc.

⁶⁰ E.g., winding contamination resulting from infiltration of moisture, oil, sand, corrosive products, etc., or from the accumulation of dust, rust, various residues, etc.

⁶¹ E.g., mechanical vibration, conductor flexion, etc.

⁶² Commonly known as voltage spikes or overvoltages.

with the VSD-fed, low-voltage IMs are discussed, and a number of solutions (design, manufacturing, repair and exploration) for their mitigation are proposed.

A5.4.1 Main Causes of Voltage Transients

Line-fed IMs can experience VTs associated with atmospheric electric discharges, high-voltage network control or switching manoeuvres, and motor protection and/or command equipment operation, being these issues discussed since 1930 [5], [8], [56], [57], [62], [69]. However, in the last decades, VTs become also associated with the use of VSDs, being a serious threat to the stator winding insulation system integrity [16], [54]-[78].

In fact, due to the nature of VSD output PWM voltage waveforms, characterized by step-shape-front pulses (travelling through the cable from inverter to motor) with high du/dt and the difference between motor and cable impedances, voltage wave reflection effects occur in the power cable⁶³ between the VSD and the motor, originating VTs (characterized by the maximum magnitude and rise time or du/dt) at the motor terminals due to the consequent superposition of the output and reflected⁶⁴ (at the motor terminals) voltage, as it can be seen in Fig. A5.56, in which it is possible to observe that the described phenomena lead to an accentuated difference between the PWM voltage waveforms at the inverter output and at the motor input [54]-[80], [82], [83], [86], [87]. VTs depend on the cable length and characteristic impedance and on the motor characteristic impedance (higher than that of the cable), and may occur even with relatively short cables (≈ 5 -m length). Additionally, the number of VTs is a function of the number of PWM pulses generated per fundamental period, which depends on the switching frequency (typically 2 to 20 kHz, for IGBT technology [8], [82]). In low-voltage (400-460 V) VSDs with fast-switching IGBTs, the pulse rise time (as well as the fall time) is typically 0.05-0.2 μ s (in order to reduce the inverter losses) and the steep slopes have typically a du/dt of 2.5-9.5 kV/ μ s (6 kV/ μ s is common for most IGBT-based inverters) [8], [81], [82], [86], [87]. However, each inverter has a different output voltage slope, depending on the IGBTs used.

After reflection effect, VTs are typically characterized by a magnitude up to 2 times the normal pulse magnitude⁶⁵ at the inverter output and a rise time lower than 0.2 μ s rise time, particularly in the sharp zones of the wave [8], [82], [83], [64]. Therefore, a du/dt of 4-14 kV/ μ s can occur [8], [87]. Therefore the motor insulation is heavily loaded and may breakdown [87]. Solutions to the VT occurrence problem are thus of great practical importance. It should be noted that 400-V line-fed motors withstand a line-to-ground peak voltage of $231 \cdot \sqrt{2}$ equally distributed over the

⁶³ Either in new or retrofit applications, VSD and motor are at separate locations, thus requiring long motor leads.

⁶⁴ The voltage reflection is a function of inverter output du/dt and of the length of the cable, which behave as a transmission line for the inverter output pulses [82].

⁶⁵ The VTs magnitude can be slightly higher than 2 times the DC-bus voltage if significant overshooting occurs in the IGBTs turn-on instants, increasing the pulse front magnitude at the inverter output, or if polarity reversals and dwell time are insufficient [5], [70], [71], [82], [83]. The overshoot is due to the DC-bus capacitors discharge when the transistor (e.g., IGBT) turns on [70], [71].

winding, and, in inverter-fed motors, this value can be pushed up to 565-600 V at the first turns of the winding.



Fig. A5.56. Experimental line-to-line voltage waveforms at the inverter output (bottom trace) and at the motor terminals (top trace) for long motor leads (> 25 m) [8], [78], [79].

In order to analyse the VT phenomenon at the motor terminals, preliminary experiments were carried out with a 5.5-kW, 4-pole IM fed by a commercial 2-level VSD (using a 7.5-m power cable) at two different switching frequencies (8 kHz and 16 kHz). The main results are presented in Fig. A5.57, which evidences the difference between the voltage waveforms at the VSD output and at IM input, and shows that the number of VTs increases with the switching frequency but its magnitude is independent of it. Additionally, more experimental results were obtained for a 3-kW, 4-pole IM fed by a 2-level VSD, shown in Figs. A5.58 and A5.59.

In Figs. A5.61 and A5.62, these VTs can be seen for a 3-kW motor fed by a 2-level and a 3-level VSD, by means of a 12-m non-shielded cable. As expected, the VTs have lower amplitude when the 3-level VSD is used due to the reduced du/dt (as referred in Chapter 3).

The damped high-frequency ringing effect at the motor terminals⁶⁶, which can occur in the both ascendant or descendent voltage variation instants of a pulse, is characterized by a high-frequency oscillation (1.5 MHz in the experimental results presented in Fig. A5.60), resulting in overvoltage and in the motor stray capacitances excitation, including those formed by air cavities or gaps in the insulation system, causing small capacitive currents to circulate through those paths, contributing to stress the motor insulation or ageing process. Besides the adverse effects on motor insulation, they also contribute to the capacitive currents circulating in the bearings [8], [82].

At this stage, it is important to distinguish the voltage between windings and ground and between winding parts. The former voltage is associated with the phase-to-ground voltages, and the latter voltage is associated with the phase-to-phase voltage (the difference of the respective waveforms can be seen in Figs. A5.58 and A5.59).

⁶⁶ The damped high-frequency ringing effect at the motor terminals is due to the distributed nature of the cable leakage inductance and coupling capacitance.

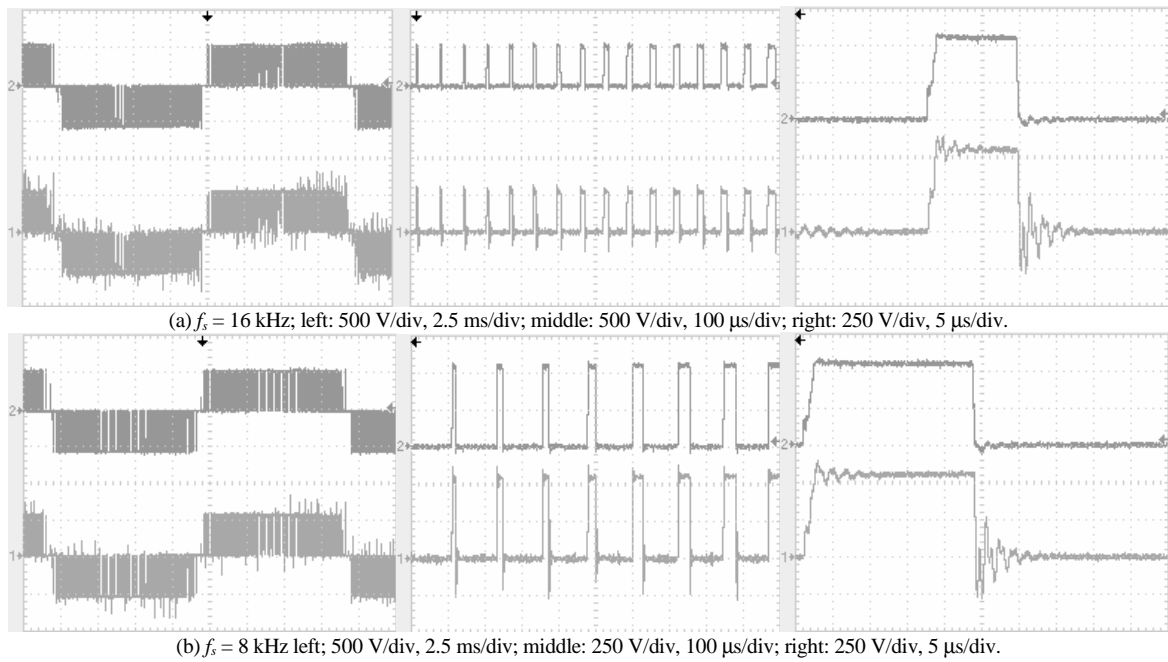


Fig. A5.57. Experimental line-to-line voltage at the inverter and motor terminals (5.5-kW, 4-pole IM fed by a 2-level inverter, by means of a 7.5-m power cable): voltage at the motor terminals (top waveforms, Ch. 2); voltage at the inverter terminals (bottom waveforms, Ch. 1).

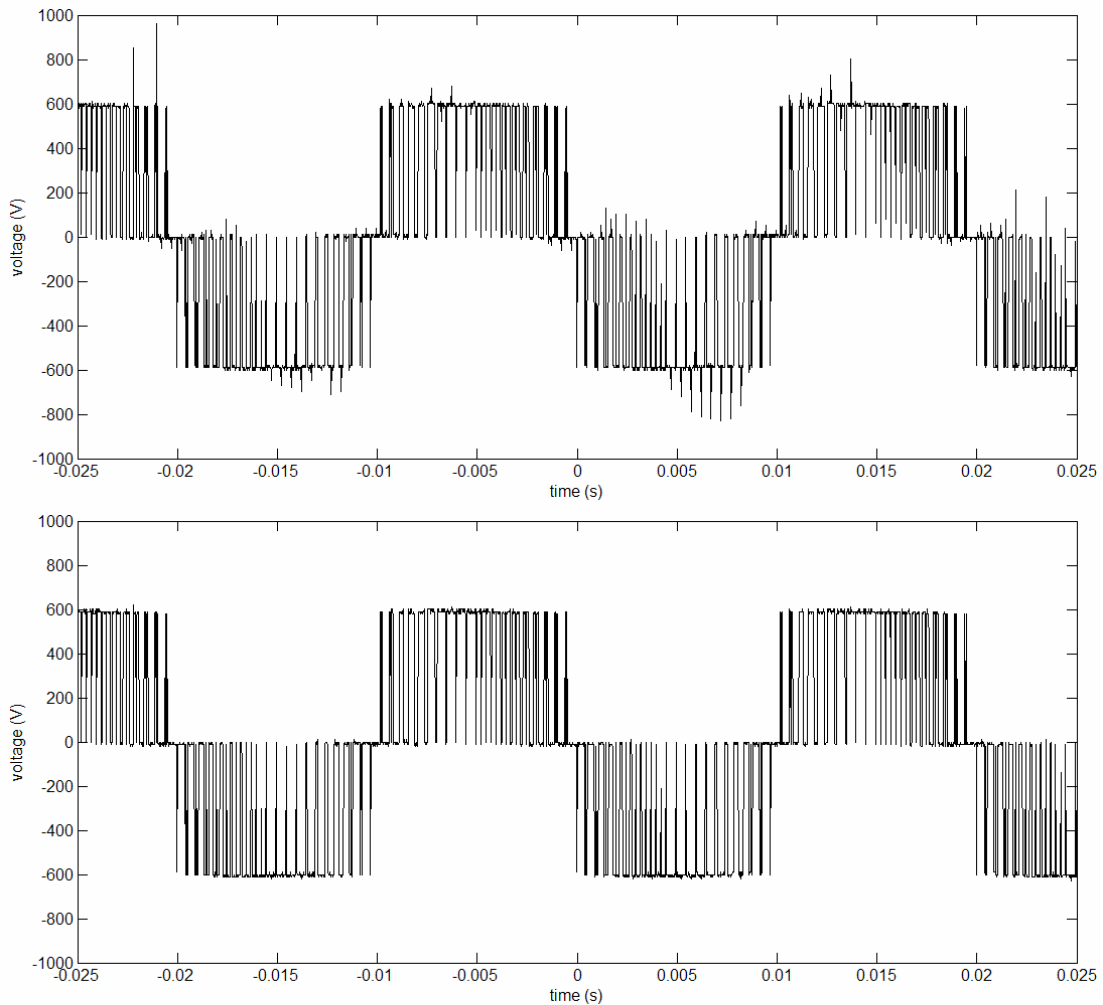


Fig. A5.58. Experimental line-to-line voltages for a 3-kW motor fed by a 2-level VSD by means of a 12-m power cable ($U_l = 400$ V, $f_l = 50$ Hz, $f_s = 2$ kHz): at the motor terminals (top); at the inverter terminals (bottom).

Regarding the theory behind voltage wave reflection, a short introduction is now presented [8], [82], [85], [86], [87], [88], [108]. When a voltage pulse front of a PWM wave travels from the inverter to the motor, a transmission line effect occurs. Forward-travelling waves, or PWM pulses, travel from the inverter to the motor, while backward-travelling waves move toward the inverter due to the voltage reflection. This voltage front sees an impedance mismatch at the motor terminals producing a reflection. The reflection mechanism can be viewed as a mirror that produces a reflected wave, u_r , which is a replica of the incident wave, u_i , that is flipped around such that all points on the u_r waveform are the corresponding points of the u_i waveform multiplied by the reflection coefficient. At the inverter, the reflected forward-travelling wave has the same shape as the incoming backward-travelling wave but with corresponding points reduced by the voltage reflection coefficient at the inverter [82]. Neglecting the purely resistive component (typically, very low), the characteristic impedance (or surge impedance) of the cable, Z_{cbl} , is given by (A5.30), where L_{cbl} is the distributed inductance of the cable (H/m) and C_{cbl} is the distributed capacitance of the power cable (F/m) [71], [82], [88]. Considering a motor characteristic impedance, Z_{mtr} , and the inverter characteristic impedance, Z_{vsd} , the voltage reflection coefficients in the motor, Γ_{mtr} , and in the inverter, Γ_{vsd} , are given by (A5.31) [71], [82], [86], [88].

$$Z_{cbl} = \sqrt{\frac{L_{cbl}}{C_{cbl}}} \quad (\text{A5.30})$$

$$\Gamma_{mtr} = \frac{Z_{mtr} - Z_{cbl}}{Z_{mtr} + Z_{cbl}} \quad \Gamma_{vsd} = \frac{Z_{vsd} - Z_{cbl}}{Z_{vsd} + Z_{cbl}} \quad (\text{A5.31})$$

The motor characteristic impedance, which is dominated by winding inductance for small motors, can be 10 to 100 times larger than the characteristic impedance of the cable⁶⁷ [48], [82] (Table A5.9). The motor characteristic impedance presents an effective open circuit to the incidental voltage wave at the end of the cable [48]. This results in large reflection causing the voltage peak increase at the motor terminals, as referred. In fact, the incident wave voltage is reflected back toward the inverter, and the voltage amplitude at the terminals of the motor approximately doubles. In general, the higher the motor power, the lower the voltage reflection coefficient at the motor terminals (e.g., $\Gamma_{mtr_{18.5kW}} = 0.8-0.9$ and $\Gamma_{mtr_{300kW}} = 0.5$ [48], [82], [86]), since the decrease of the motor characteristic impedance with the rated power is higher than the decrease of the respective cable characteristic impedance. This produces a reflected voltage at the

⁶⁷ The characteristic impedance of bundled cables is usually 80-190 Ω . Long lead cables commonly used for inverter-fed low-voltage IMs are of the type THHN-THWN, 14AWG (bare, soft annealed copper conductors), 600 V, gasoline and oil resistant (or equivalent), with the following characteristic impedance values: $C_{cbl} = 3.28 \times 10^{-2}$ nF/m, $L_{cbl} = 1.18$ μ H/m, $R_{cbl} = 19.69$ m Ω /m [82].

end of the cable approximately equal in magnitude and with the same sign, resulting in almost twice the magnitude of the incident voltage at the motor terminals.

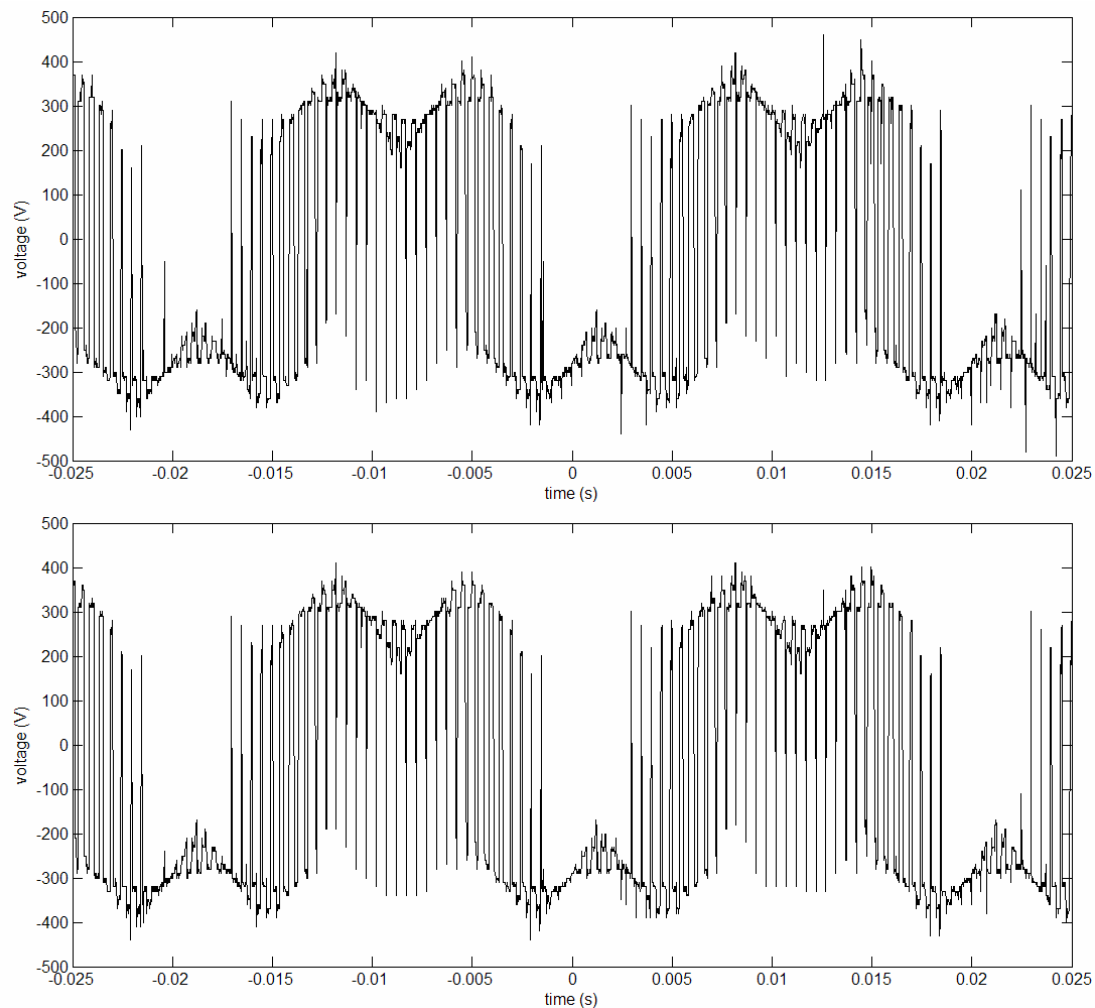


Fig. A5.59. Experimental line-to-ground voltages for a 3-kW motor fed by a 2-level VSD by means of a 12-m power cable ($U_l = 400 \text{ V}$, $f_l = 50 \text{ Hz}$, $f_s = 2 \text{ kHz}$): at the motor terminals (upper); at the inverter terminals (bottom).

TABLE A5.9
CHARACTERISTIC IMPEDANCE OF THREE-PHASE INDUCTION MOTORS WITH DIFFERENT RATED POWERS [48].

Motor Rating (kW)	Characteristic Impedance (Ω)
18.5	1500
37	750
75	375
150	188
300	94

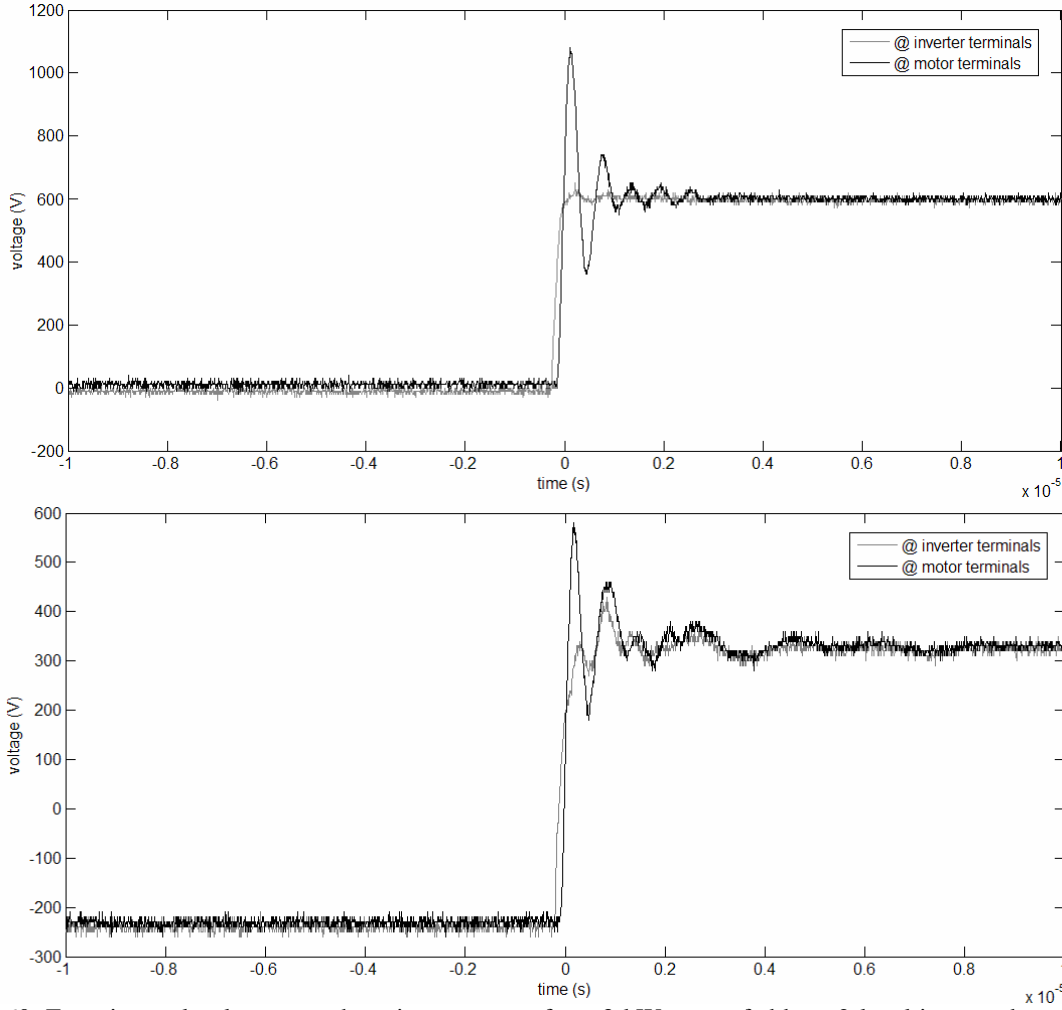


Fig. A5.60. Experimental voltage overshoot instant zoom for a 3-kW motor fed by a 2-level inverter by means of a 12-m power cable (D connection; $U_l = 200$ V; $f_l = 50$ Hz; $f_s = 2$ kHz): (top) line-to-line; (bottom) line-to-ground.

The critical cable length, l_{cr} , representing the minimum cable length after which voltage doubling occurs at the motor terminals, is given by (A5.32), where v is the pulse velocity (in m/s), and t_r is the pulse rise time (in μ s) [71]. The PWM pulses travel at approximately half the speed of light [82]. The critical cable length becomes shorter with lower inverter output pulse rise time. In Table A5.10, examples of critical cable lengths for different pulse rise times are presented. The du/dt depends on the voltage maximum value and on the t_r . The time the voltage pulse requires to travel from the inverter to the motor (propagation time of the voltage wave over the cable), t_t (in μ s), through a cable with length l_{cbl} , is given by (A5.33) [48], [82].

$$l_{cr} = \frac{v \cdot t_r}{2} = \frac{t_r}{2\sqrt{L_{cbl} \cdot C_{cbl}}} \quad (\text{A5.32})$$

$$t_t = \frac{l_{cbl}}{v} \quad (\text{A5.33})$$

If $t_t \geq t_r$, the voltage at the motor terminals almost doubles, and the t_r is no longer a parameter of the reflected voltage (for a finite-length, open-circuited cable and infinite du/dt , the voltage at the motor terminals actually doubles [82]). After the travel time, the forward-travelling inverter output pulse is reflected at the motor terminals, and the resulting backward-travelling wave, moving toward the inverter, will have an amplitude given by (A5.34), where U_{DC} is the DC-bus voltage of the inverter [82], [86]. The backward-travelling wave will then be reflected at the inverter terminals in the same manner, however, now as a function of the reflection coefficient of the inverter (or power supply). On the basis of (A5.31), it can be said that, for a typical low-impedance supply, the voltage reflection coefficient approach to -1 , and the resulting reflected wave travelling back toward the motor will be negative in amplitude.

$$\begin{cases} t_t < t_r : u_{mtr}(t_t) = t_t \cdot U_{DC} \cdot \Gamma_{mtr} \cdot t_r^{-1} \\ t_t \geq t_r : u_{mtr}(t_t) = U_{DC} \cdot \Gamma_{mtr} \end{cases} \quad (\text{A5.34})$$

After three transitions on the cable, the increasing motor terminal voltage will be reduced by this negative reflected wave, after it travelled back and reached the motor. Therefore, the peak voltage can be found by determining the total voltage due to reflections at the motor terminals, after three transitions in the cable, and adding this to the incident voltage wave magnitude, U_{DC} , according to (A5.35), which allows the critical rise time to be computed by properly setting the maximum desirable voltage overshoot.

$$\begin{cases} t_t < \frac{1}{3}t_r : u_{ll(peak)} = U_{DC} \cdot (3 \cdot l_{cbl} \cdot \Gamma_{mtr} \cdot v^{-1} \cdot t_r^{-1} + 1) \\ t_t \geq \frac{1}{3}t_r : u_{ll(peak)} = U_{DC} \cdot (\Gamma_{mtr} + 1) \end{cases} \quad (\text{A5.35})$$

A travel time lower than $\frac{1}{3}$ of the rise time means a high rise time and, for this situation, to avoid or minimize overvoltage the relation $3 \cdot l_{cbl} \cdot \Gamma_{mtr} \cdot v^{-1} \cdot t_r^{-1} \ll 1$ should be verified. For example, for a maximum overshoot of 0.2 p.u., the rise time should be $t_r = 5 \cdot 3 \cdot l_{cbl} \cdot \Gamma_{mtr} \cdot v^{-1}$, i.e., for a VSD with $U_{DC} = 565$ V, the allowable peak voltage would be 1.2 times 565 V, yielding 678 V. For the typical cable parameters $v = 160.63$ m/ μ s and, for a 30.5-m cable and $\Gamma_{mtr} = 0.9$, the rise time for a maximum overshoot of 0.2 p.u. is $t_r = 2.5$ μ s. Therefore, for $t_r < 2.5$ μ s, an overvoltage at the motor terminals within 20% to near 100% is expected. If, for example, $t_r < 2t_t$ the superposition effect can

lead to VTs with maximum amplitude twice the step front value (which corresponds to the DC-bus voltage in the case of the 2-level inverters, if no major overshoot effects occur).

TABLE A5.10
MINIMUM CABLE LENGTH AFTER WHICH VOLTAGE
DOUBLING OCCURS AT THE MOTOR TERMINALS FOR DIFFERENT PULSE RISE TIMES [82].

PWM Pulse Rise Time	Minimum Cable Length
0.1 μs	5.8 m
0.5 μs	29.6 m
1.0 μs	59.4 m
2.0 μs	118.9 m
3.0 μs	178.3 m
4.0 μs	237.7 m
5.0 μs	297.2 m

Assumptions: $\Gamma_{mr} = 0.9$; $C_{cbl} = 3.28 \times 10^{-2}$ nF/m, $L_{cbl} = 1.18$ $\mu\text{H/m}$, $R_{cbl} = 19.69$ m Ω /m; $v = 160.63$ m/ μs .

Therefore, VT peak values depend on the motor reflection coefficient, cable length, pulse travelling velocity, and inverter output pulse rise time. In general, the longer the cable and the higher the du/dt are, the higher the VT magnitude will be. The number of VTs (or PWM pulses generated) over a fundamental period (or VT occurrence frequency) depends on modulation strategy, switching frequency, and amplitude modulation index. Depending on the referred factors, VTs may occur 20-100 times per period (50 Hz). Experimentally, no differences in VTs amplitude and rise time were found when using different switching frequencies, as expected. In general, the lower the rise time, the lower the cable length should be [8], [70]. In general, VTs phenomenon can be particularly serious if the length of cable between the VSD and motor exceeds 12 to 30 m [8], [16].

More experimental results on the reflection of voltage pulses in the power cables between the inverter and the motor, using a 3-kW, 4-pole IM, are presented in Figs. A5.61-A5.68. The 3-wire power cables between inverter and motor have a total length of 12 m. The motor ground was connected to the inverter ground by a separate wire. The aim of these tests is to compare both 2- and 3-level technologies from the perspective of voltage reflection in cables and voltage peak generation, and, as it was already referred in Chapter 3, higher VTs at motor terminals are expected for the 2-level inverter.

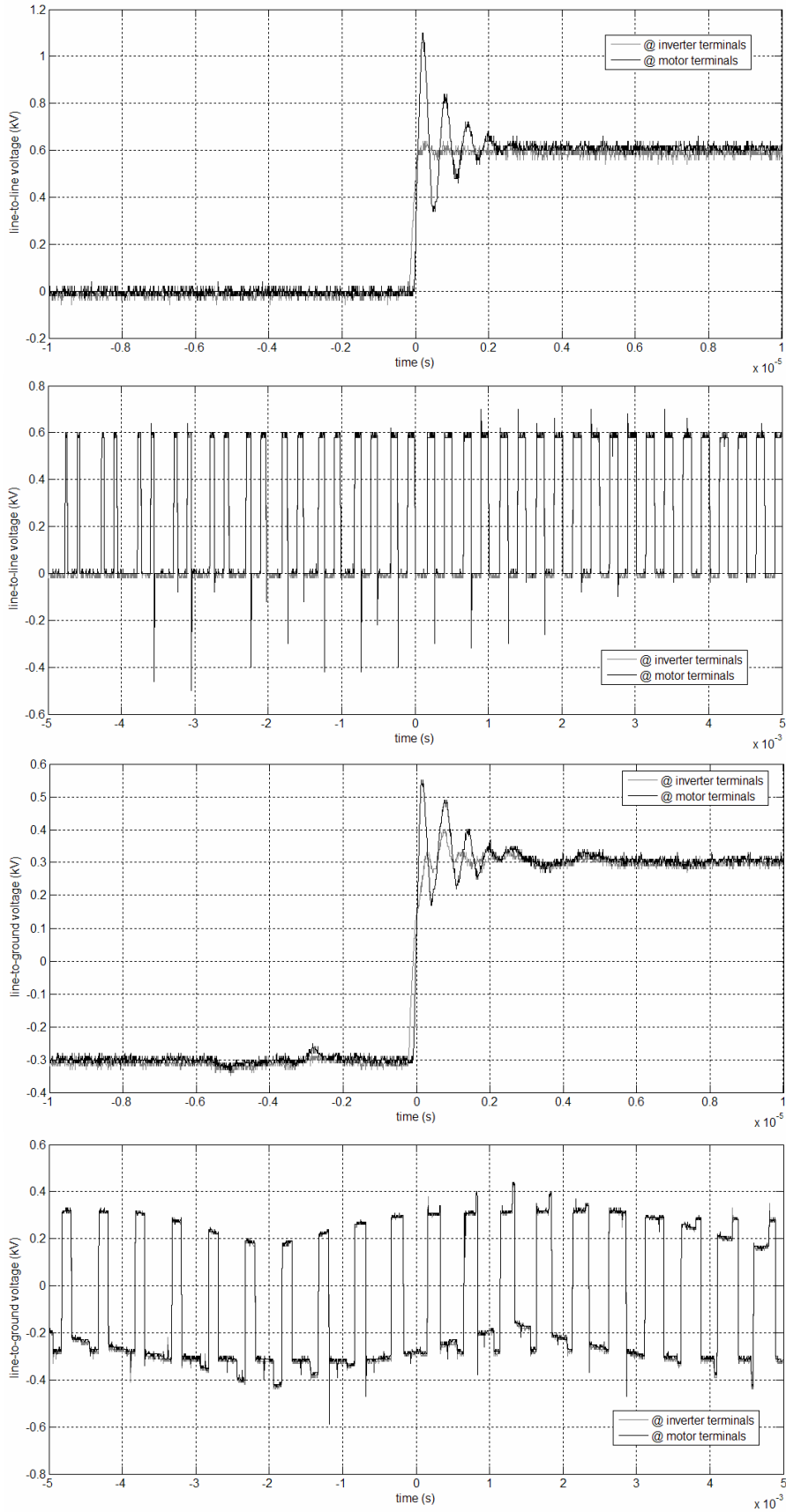


Fig. A5.61. Experimental voltage wave reflection effect at the motor terminals, for a 3-kW, 4-pole star-connected motor fed by a 2-level VSD, at no-load, by means of a 12-m cable.

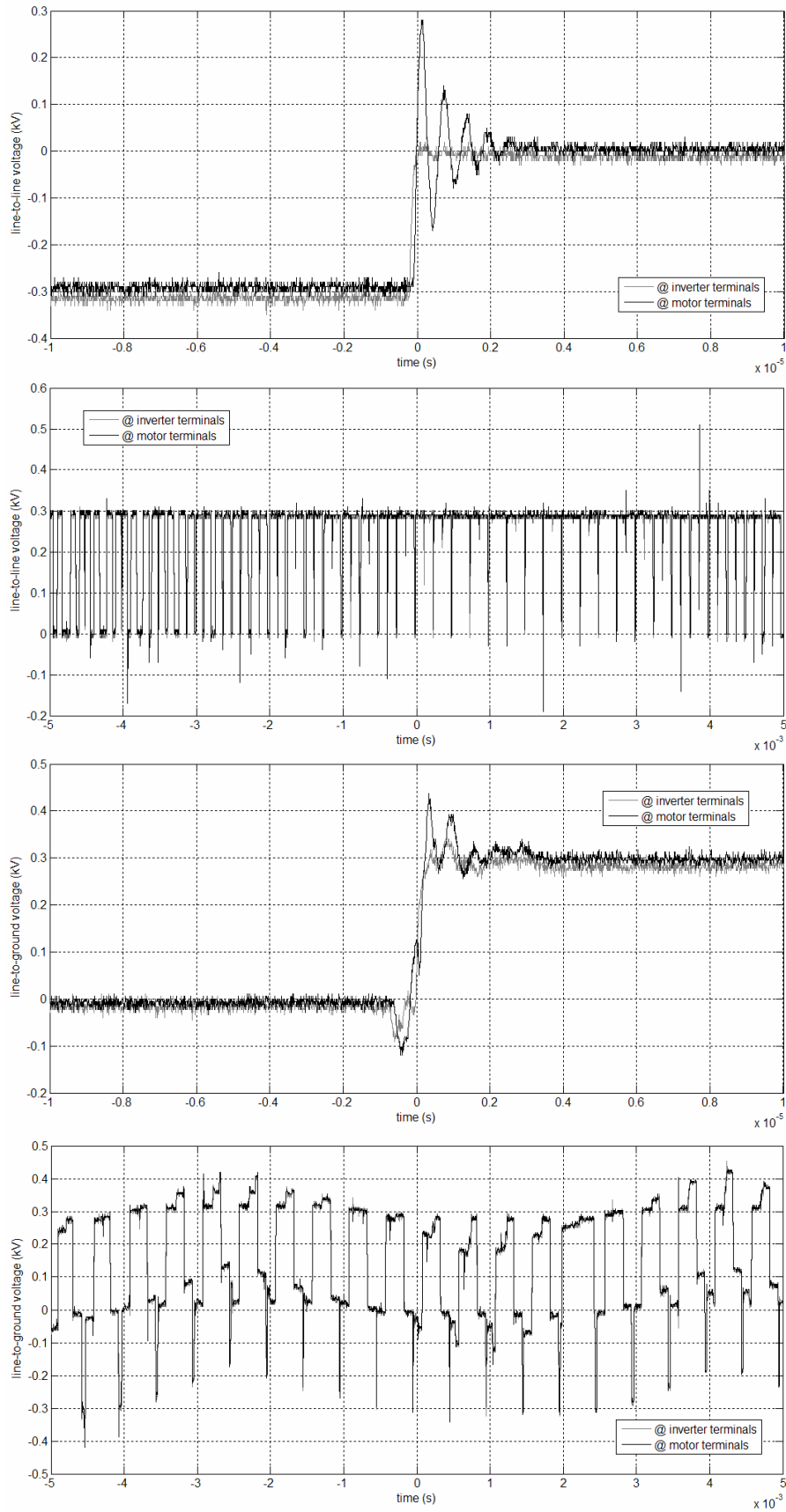


Fig. A5.62. Experimental voltage wave reflection effect at the motor terminals, for a 3-kW, 4-pole star-connected motor fed by a 3-level VSD, at no-load, by means of 12-m cable.

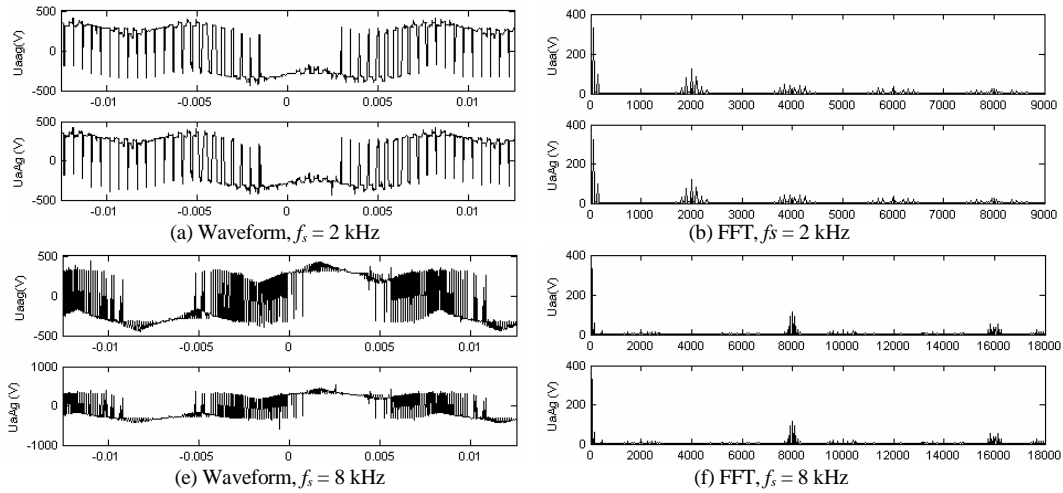


Fig. A5.63. Experimental winding-ground voltages for a star-connected, 3-kW IM fed by a 2-level inverter ($U_l = 400$ V, $f_l = 50$ Hz, no-load): (top traces) inverter terminals; (bottom traces) motor terminals. The figures for $f_s = 5$ kHz are presented in Appendix 6.

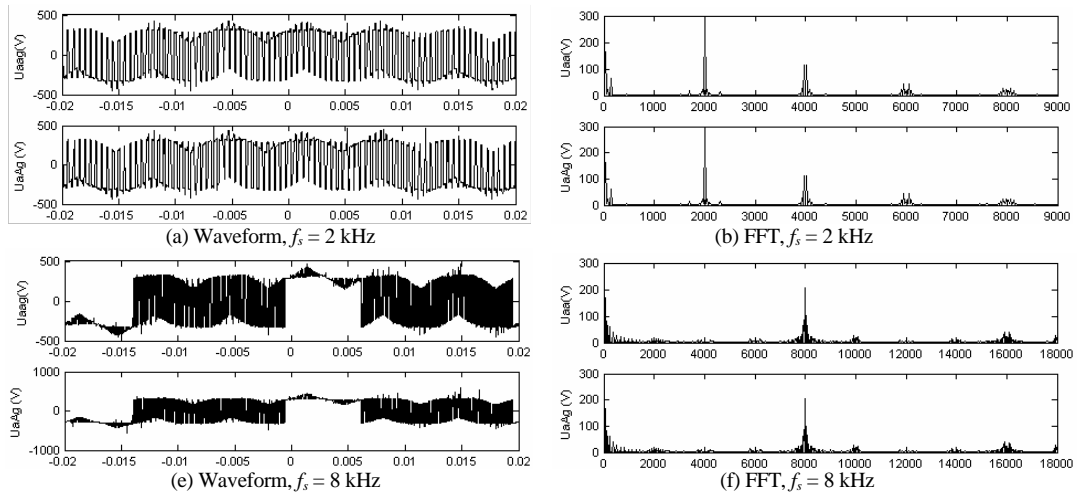


Fig. A5.64. Experimental winding-ground voltages for a star-connected, 3-kW IM fed by a 2-level inverter ($U_l = 200$ V, $f_l = 25$ Hz, no-load): (upper traces) inverter terminals; (lower traces) motor terminals. The figures for $f_s = 5$ kHz are presented in Appendix 6.

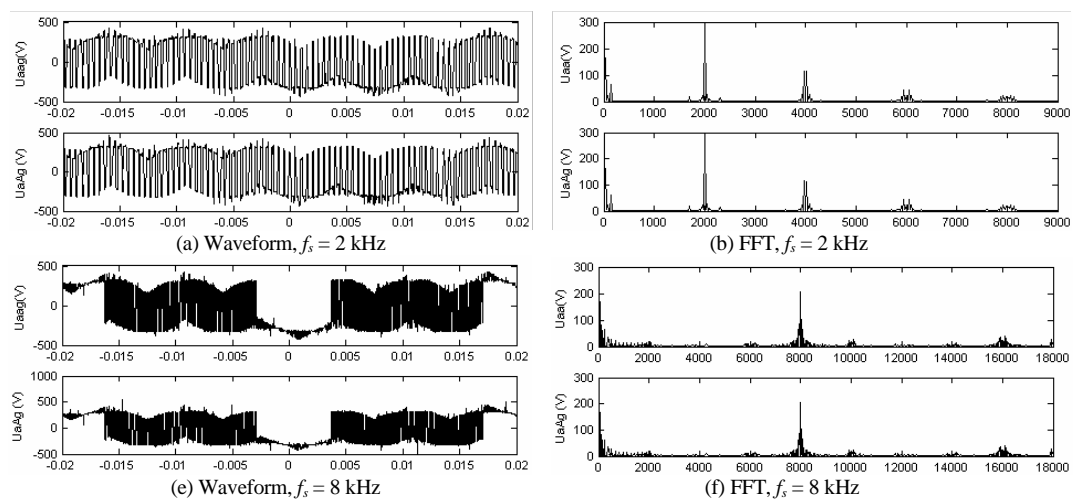


Fig. A5.65. Experimental winding-ground voltages for a delta-connected, 3-kW IM fed by a 2-level inverter ($U_l = 200$ V, $f_l = 25$ Hz, no-load): (top traces) inverter terminals; (bottom traces) motor terminals. The figures for $f_s = 5$ kHz are presented in Appendix 6.

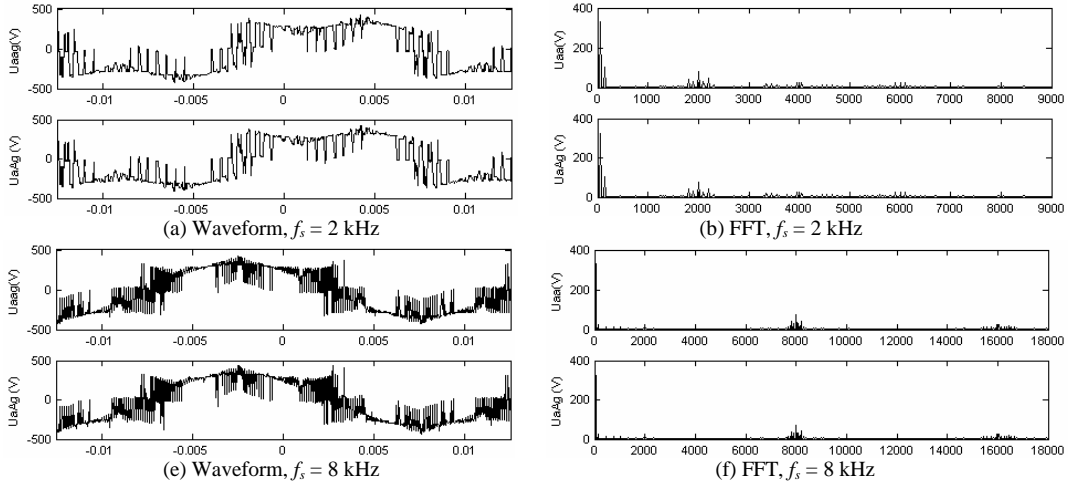


Fig. A5.66. Experimental winding-ground voltages for a star-connected, 3-kW IM fed by a 3-level inverter ($U_l = 400$ V, $f_l = 50$ Hz, no-load): (top traces) inverter terminals; (bottom traces) motor terminals. The figures for $f_s = 5$ kHz are presented in Appendix 6.

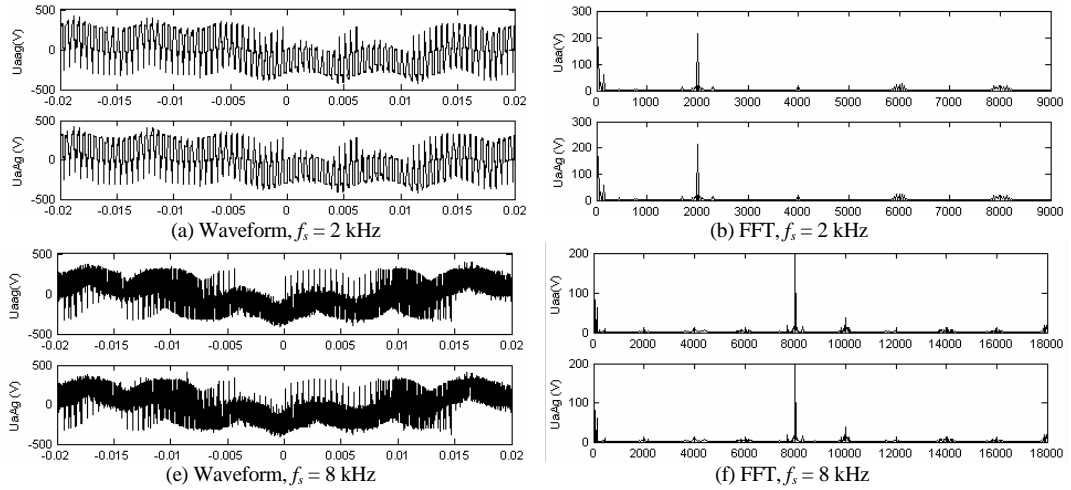


Fig. A5.67. Experimental winding-ground voltages for a star-connected, 3-kW IM fed by a 3-level inverter ($U_l = 200$ V, $f_l = 25$ Hz, no-load): (top traces) inverter terminals; (bottom traces) motor terminals. The figures for $f_s = 5$ kHz are presented in Appendix 6.

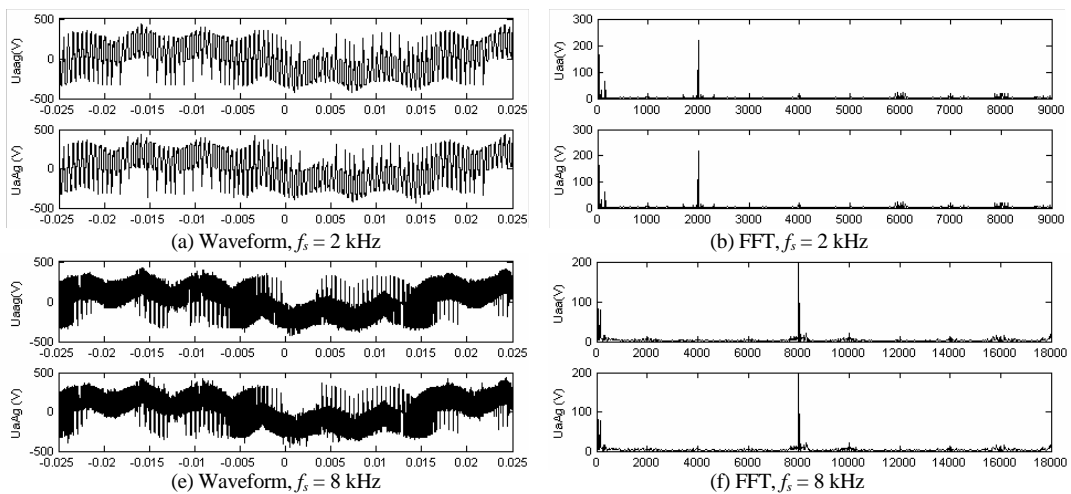


Fig. A5.68. Experimental winding-ground voltages for a delta-connected, 3-kW IM fed by a 3-level inverter ($U_l = 200$ V, $f_l = 25$ Hz, no-load): (top traces) inverter terminals; (bottom traces) motor terminals. The figures for $f_s = 5$ kHz are presented in Appendix 6.

A5.4.2 Main Effects of Voltage Transients

Due to the reduced rise time characterizing the VT-pulse front and to the presence of a distributed stray capacitance between stator windings and ground (stator core), the VT voltage distribution over the stator windings results significantly nonlinear, becoming concentrated in the initial turns and, therefore, high-amplitude instantaneous voltages can occur in those zones, which become vulnerable [8], [79], [80], [84], [85].

The voltage in the initial turns can reach half of the VT peak value at the terminals (with $t_r \approx 50\text{-}70$ ns). It should be noted that, when a winding is excited by a sinusoidal voltage supply, all the turns support approximately the same voltage (e.g., if the winding has 100 turns, each turn supports 1% of the applied voltage). The lower the t_r is, the higher the percentage of the total voltage applied to the initial turns will be, and more dangerous the VT will be to the insulation associated with those turns [79], [80].

Therefore, the effect of VTs is critical in the initial turns of the windings. In order to demonstrate the nonlinearity of the voltage distribution, as well as the pulse front changing over the winding, experimental tests were carried out in a 7.5-kW motor with a special tapped stator winding with access to 4 intermediate points (4 coil sets per phase, 3 series coils per coil set). The motor was fed by 2- and 3-level VSDs and connected in delta and star modes. The results for $f_s = 2$ kHz are presented in Figs. A5.69-A5.71, evidencing the highest du/dt at the first coil as well as a du/dt reduction roughly to half for the 3-level inverter. Moreover, higher du/dt values are expected for intermediate points for the delta connection⁶⁸. Additional experimental results on the 7.5-kW motor are presented in Figs. A5.73-A5.81.

Regarding winding-ground voltages, the switching frequency has low impact on the amplitude of switching frequency related harmonics at the winding leads and intermediate points. Nevertheless, in general, the higher the switching frequency, the higher the winding insulation voltage stress and the higher the leakage and bearing currents.

In [80], an increase of voltage between the first coil terminals from 13% to 61% for a cable length increase from 2.3 to 33.5 m, respectively, was verified, evidencing the influence of the cable length. In fact, since VTs can have components up to 5 MHz in the most sloped zones, the distributed capacitance between the windings and the ground are excited, leading to the majority of the voltage fall over the initial turns or coils of the winding⁶⁹ [62]. In [59], several experimental results on the voltage distribution over the winding turns are presented, being evidenced the

⁶⁸ Four differential voltage probes were used to acquire the voltage at the intermediate points of one phase of the 7.5-kW, 400-V, 50-Hz, 4-pole, IM. All the partial voltages over the phase winding, U_{ag} , U_{a1g} , U_{a2g} , and U_{a3g} , were acquired using a digital oscilloscope and processed using MATLAB software (e.g., FFT). For the line supply case and for the inverter with $f_s = 2$ kHz and $f_s = 5$ kHz, a 40 ms/2500 points window was used (sampling frequency equal to 50 kHz). For the inverter with $f_s = 8$ kHz a 20 ms/2500 points window was used (sampling frequency equal to 100 kHz). The acquisition and processing set-up is enough to analyse the relevant spectrum of the considered signals.

⁶⁹ Depending on several factors, the voltage amplitude in the initial turns of the windings can reach 30-60% of the VT amplitude [62].

dependency of it on the du/dt . For a rise time between 0.05 and 0.5 μs , 40% to 60% of the VT amplitude is concentrated in the first coil, and 40% to 70% of the voltage in the first coil is concentrated in the first turns [64], [69], [80], [85]. According to [86] and [87], as much as 85% of the VT peak magnitude can be found across the first turn of the first coil of the motor windings, and that percentage increases with the decrease of the voltage pulse rise time. However, those percentages depend on the measurement instant, as it is evidenced in Figs. A5.69-A5.71, explaining the differences between the stated values.

It is particularly interesting to compare the winding-to-ground peaks over the winding when the motor is fed directly by the line (Fig. A5.73) and by a 2-level inverter (Fig. A5.74). For the star-connected motor, the winding-to-ground voltage peaks decrease progressively from winding lead to neutral point (\approx zero voltage to ground for balanced systems), reaching a maximum of $\approx 231 \cdot \sqrt{2}$ V at the lead point and roughly half of that value at the middle point. For the inverter-fed motor, the winding-to-ground voltage peaks reach 375-400 V over all winding points, representing a significant increase of the winding electrical stress. Moreover, the third harmonic is significant (particularly for $m_a > 1.0$), potentially increasing leakage currents and shaft-ground voltage peaks, as explained earlier in this appendix.

Comparing the delta and star connections, it is possible to conclude that star connection leads to a significant reduction in the switching frequency related harmonics.

Regarding stator winding connection, delta connected motors will experience extra winding-ground stress over all phase turns, as it can be seen in Figs. A5.74 and A5.77, and, consequently, extra shaft-ground voltages and common-mode leakage and bearing currents, as previously discussed. In fact, the resultant fundamental voltage stress between the windings and the ground is much higher for the delta connection (60% higher), not depending on the number of turns (the same does not apply to voltage between turns or coils). Fig. A5.82 shows the theoretical winding-ground fundamental voltage amplitude variation, in different winding points for delta and star connections, evidencing the difference. This applies to inverter-fed and line-fed motors. Triplen harmonics are maintained constant along the winding either for the delta or star connection.

Comparing the 2-level and the 3-level inverters in terms of winding-ground voltage distribution, it is possible to observe that the voltage pulses toward to the neutral point have a significantly higher magnitude for the 2-level inverter. Additionally, the voltage spectrum is extended to higher frequencies for the 2-level inverter, as expected. The harmonic content is considerable lower for the 3-level inverters, being expected lower high-frequency leakage and bearing currents (see also Chapter 3). The propagation of the switching frequency related harmonics and along the winding happens without significant attenuation. The voltage stress is obviously higher for the 2-level inverter. The 3rd harmonic propagates as expected.

It is also important to evaluate the coil-to-coil or turn-to-turn voltage stress. Figs. A5.78-A5.81 show the voltage between the coil sets. The voltage peaks are significantly higher (almost twice) in the first coil set. There is also an increase of the voltage peaks in the last section. This phenomenon is aggravated with the increase of the switching frequency. This is why the reinforcement of the windings should be made, at least, in the first coils. When comparing the 2-level and the 3-level inverters, the latter one leads to significantly lower voltage peaks in the first coil set (roughly half the value) - this was experimentally verified for all the switching frequencies. When comparing the delta and star connections, the voltage peaks between coil sets are higher (almost twice) for the delta connection, as expected. The fundamental and switching frequencies components are distributed quasi-equally in the different sections, for the 2-level and 3-level inverters, regardless the motor stator winding connection (delta or star). However, in the case of the delta connection, both the first and last sections have higher voltage peaks (although this is less significant for the motor fed by the 3-level inverter), leading to higher voltage stress along the winding and, therefore, the reinforcement of the coils insulation should be made in the beginning and end of the phase winding (although increasing the cost of the winding, it can extend significantly the motor lifetime).

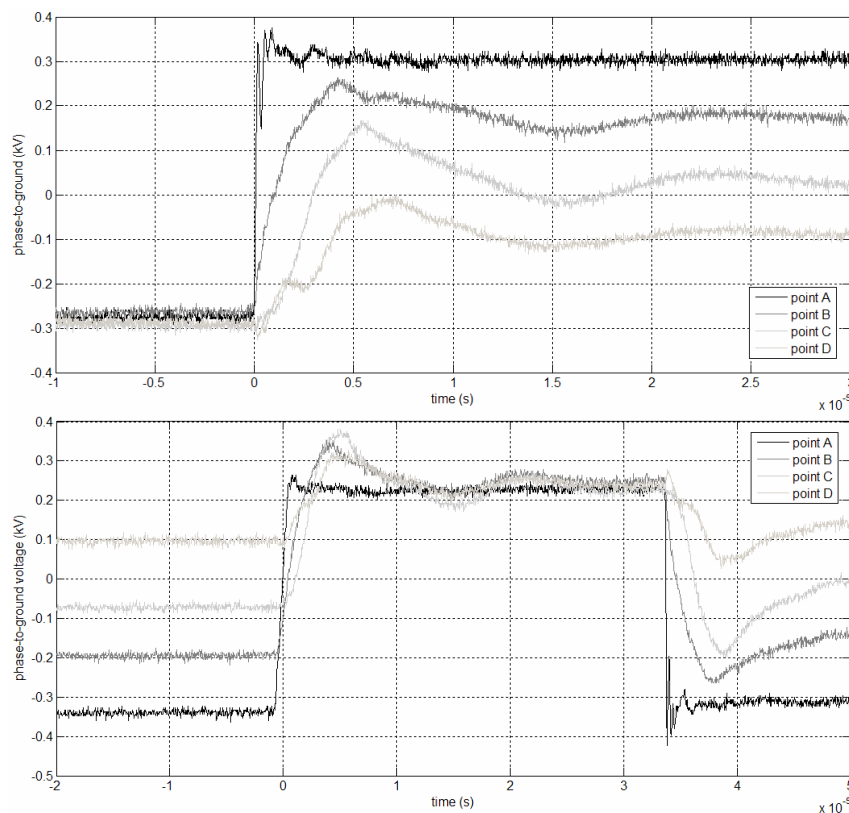


Fig. A5.69. Experimental instantaneous phase-to-ground voltage distribution in the phase-coils (winding divided in 4 parts, which were monitored by means of 4 intermediate points A (lead), B, C, and D, plus the grounded point) for a 7.5-kW, 4-pole, delta-connected motor fed by a 2-level VSD with a 2-kHz switching frequency.

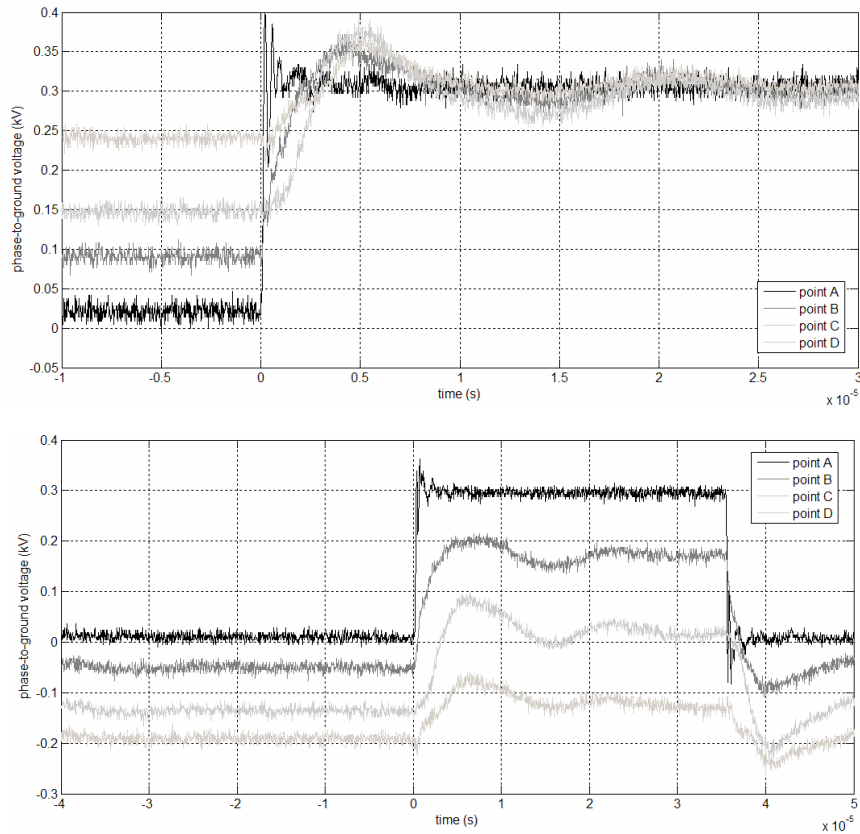


Fig. A5.70. Experimental instantaneous phase-to-ground voltage distribution in the phase-coils (winding divided in 4 parts, which were monitored by means of 4 intermediate points A (lead), B, C, and D, plus the grounded point) for a 7.5-kW, 4-pole, delta-connected motor fed by a 3-level VSD with a 2-kHz switching frequency.

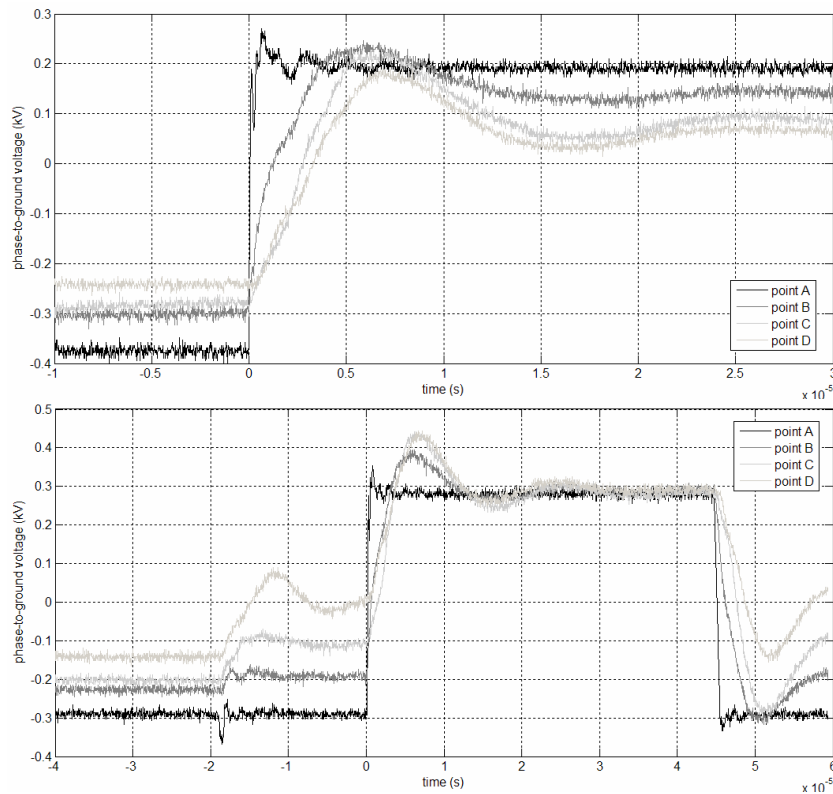


Fig. A5.71. Experimental instantaneous phase-to-ground voltage distribution in the phase-coils (winding divided in 4 parts, which were monitored by means of 4 intermediate points A (lead), B, C, and D, plus the grounded point) for a 7.5-kW, 4-pole, star-connected motor fed by a 2-level VSD with a 2-kHz switching frequency.

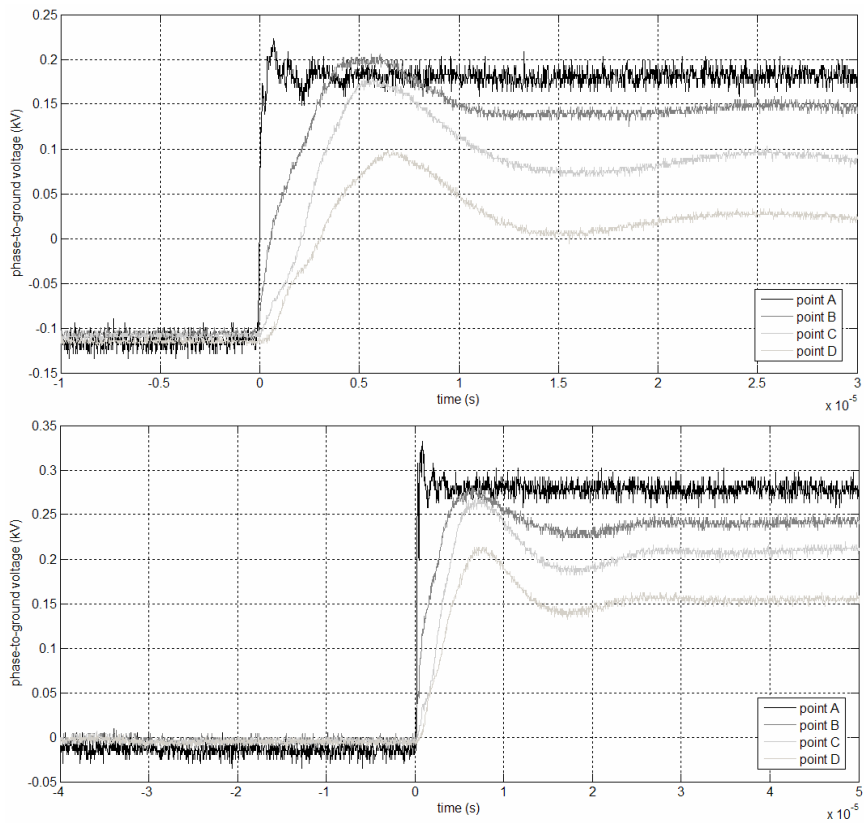


Fig. A5.72. Experimental instantaneous phase-to-ground voltage distribution in the phase-coils (winding divided in 4 parts, which were monitored by means of 4 intermediate points A (lead), B, C, and D, plus the grounded point) for a 7.5-kW, 4-pole, star-connected motor fed by a 3-level VSD with a 2-kHz switching frequency.

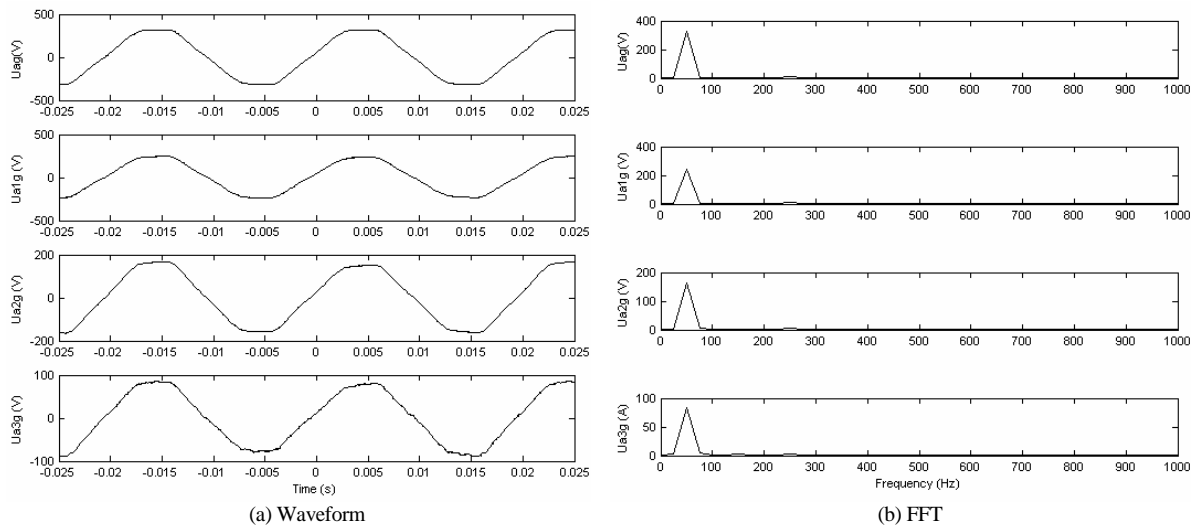


Fig. A5.73. Experimental winding-ground voltages for a line-fed, star-connected, 7.5-kW IM (400 V, 50 Hz, no-load).

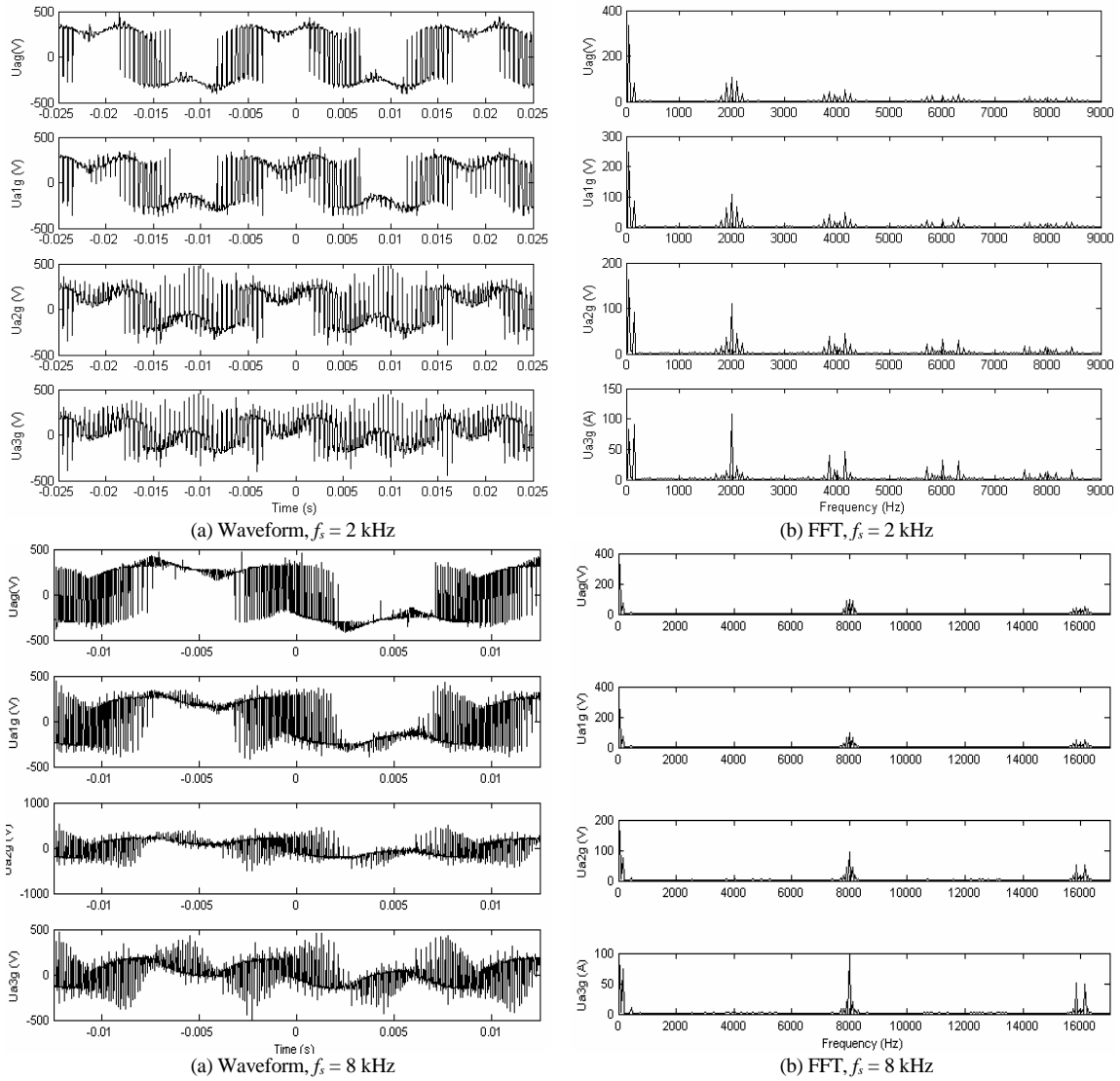


Fig. A5.74. Experimental winding-ground voltages for a star-connected, 7.5-kW IM fed by a 2-level inverter ($U_l = 400$ V, $f_l = 50$ Hz, no-load). The figures for $f_s = 5$ kHz are presented in Appendix 6.

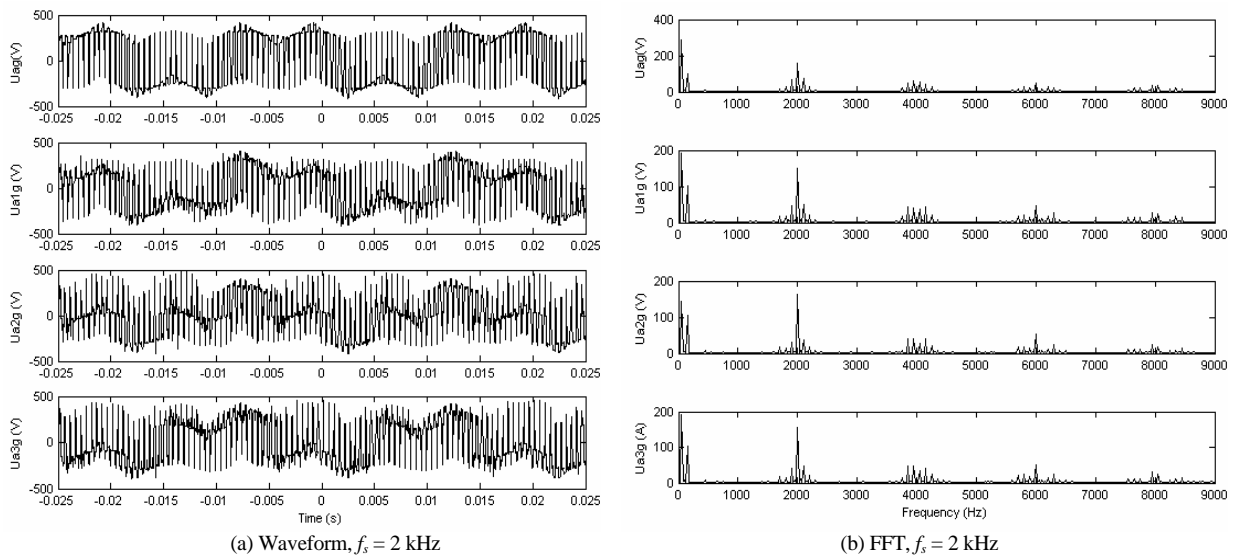


Fig. A5.75. Experimental winding-ground voltages for delta-connected, 7.5-kW IM fed by a 2-level inverter ($U_l = 400$ V, $f_l = 50$ Hz, no-load).

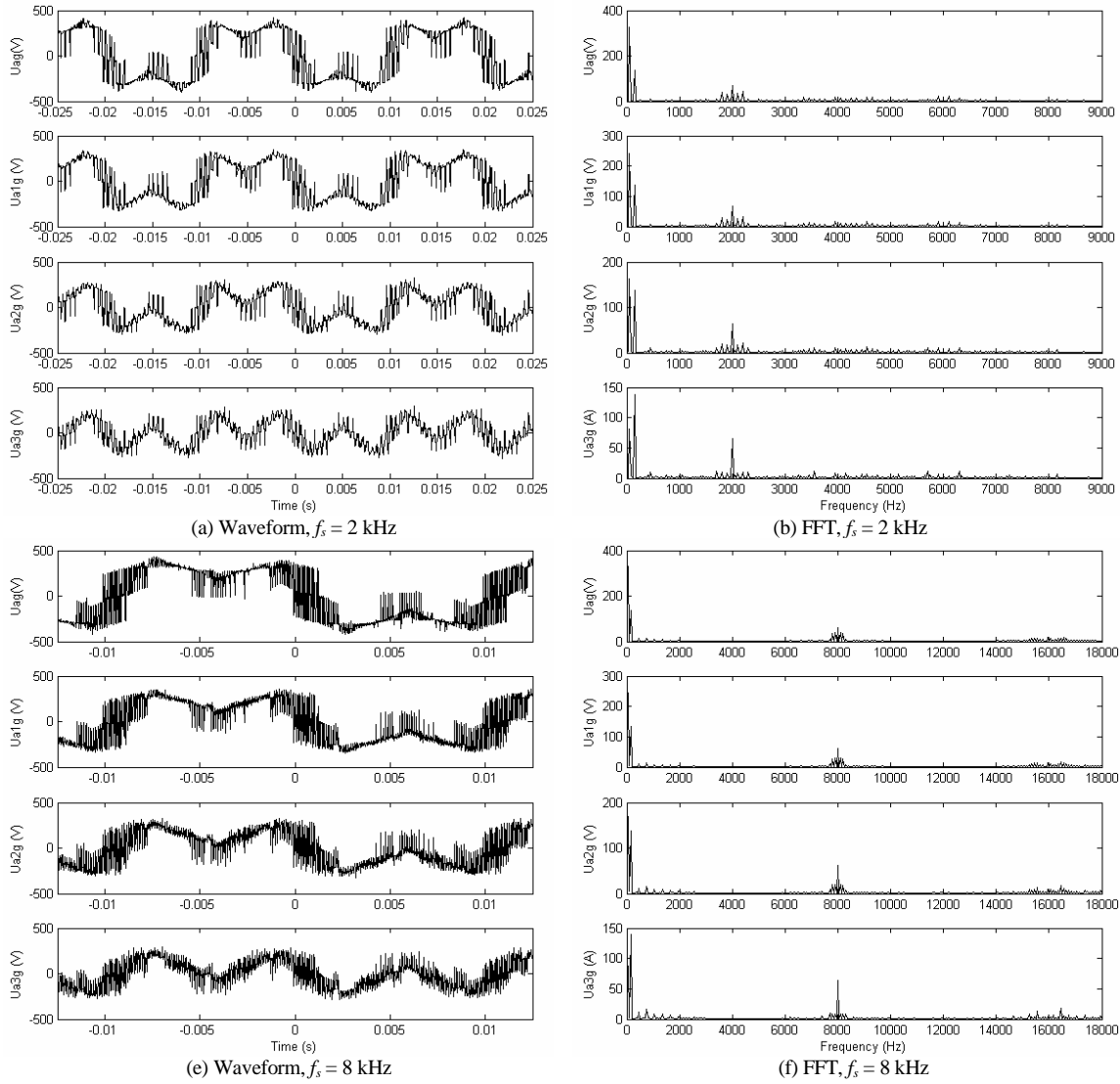


Fig. A5.76. Experimental winding-ground voltages for a star-connected, 7.5-kW IM fed by 3-level inverter ($U_l = 400$ V, $f_l = 50$ Hz, no-load). The figures for $f_s = 5$ kHz are presented in Appendix 6.

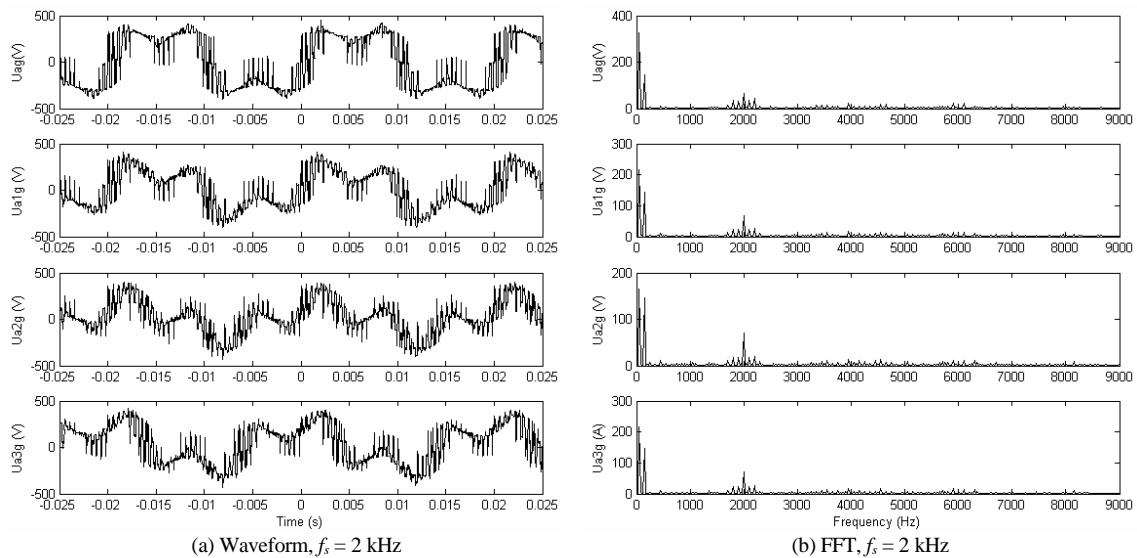


Fig. A5.77. Experimental winding-ground voltages for a delta-connected, 7.5-kW IM fed by a 3-level inverter ($U_l = 400$ V, $f_l = 50$ Hz, no-load).

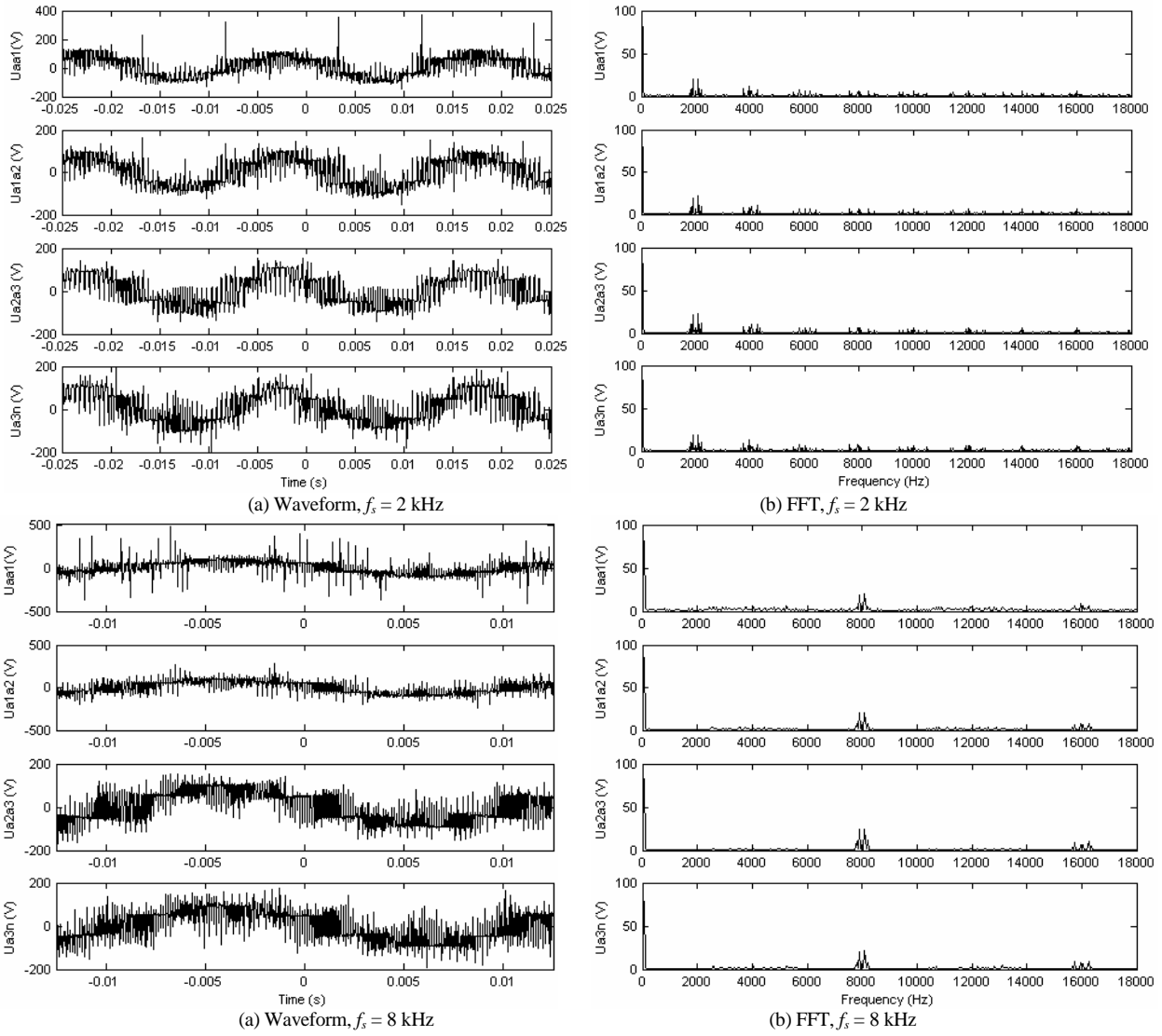


Fig. A5.78. Experimental voltages between coil sets for a star-connected, 7.5-kW motor fed by a 2-level inverter ($U_l = 400$ V, $f_l = 50$ Hz, no-load). The figures for $f_s = 5$ kHz are presented in Appendix 6.

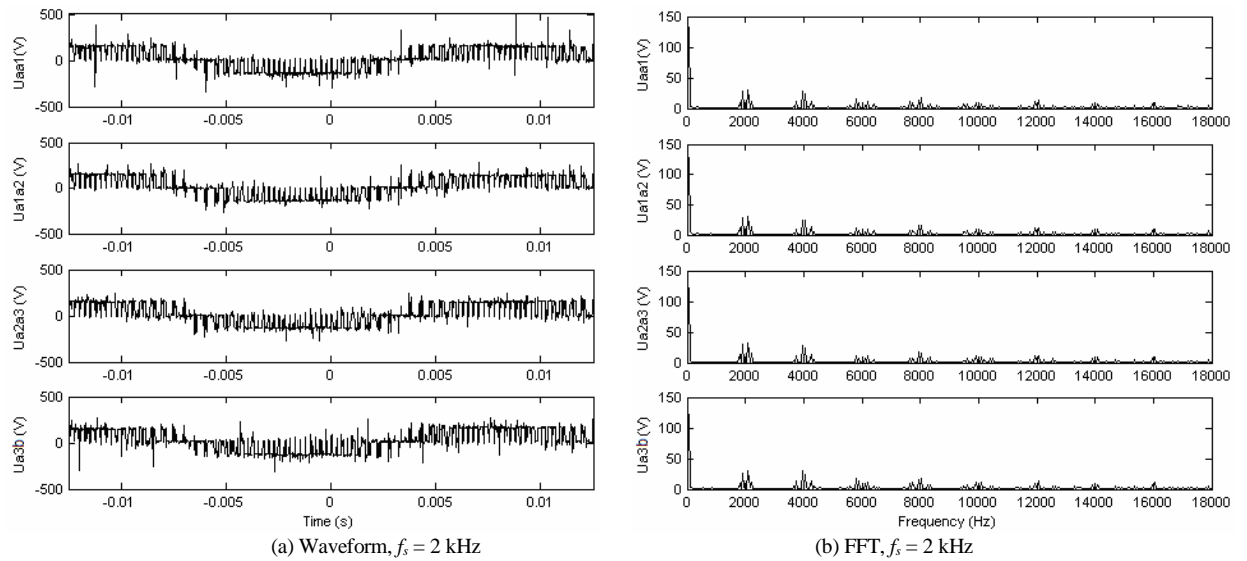


Fig. A5.79. Voltages between coil sets for a delta-connected, 7.5-kW motor fed by a 2-level inverter ($U_l = 400$ V, $f_l = 50$ Hz, no-load).

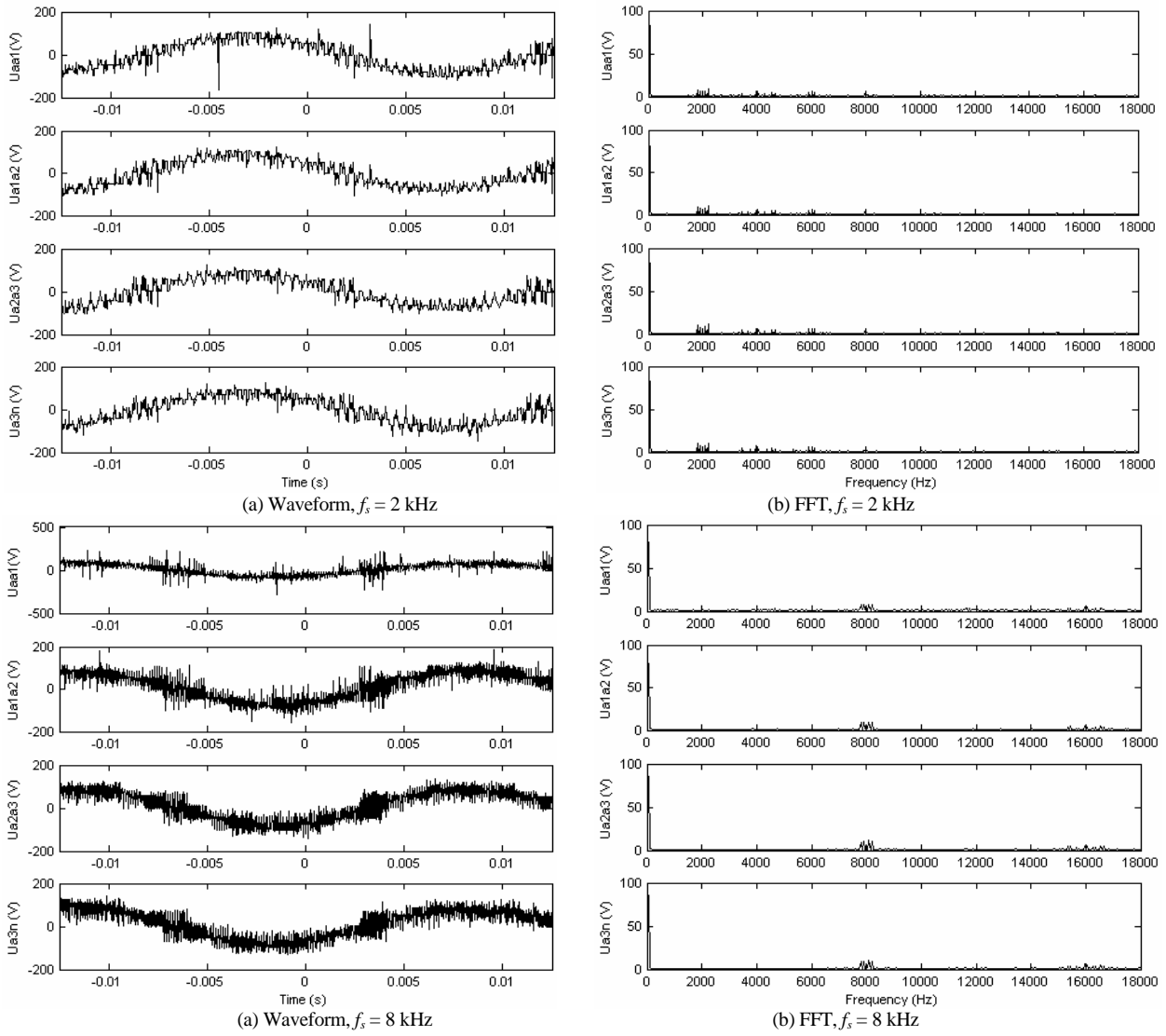


Fig. A5.80. Experimental voltages between coil sets for a star-connected, 7.5-kW motor fed by a 3-level inverter ($U_l = 400$ V, $f_l = 50$ Hz, no-load). The figures for $f_s = 5$ kHz are presented in Appendix 6.

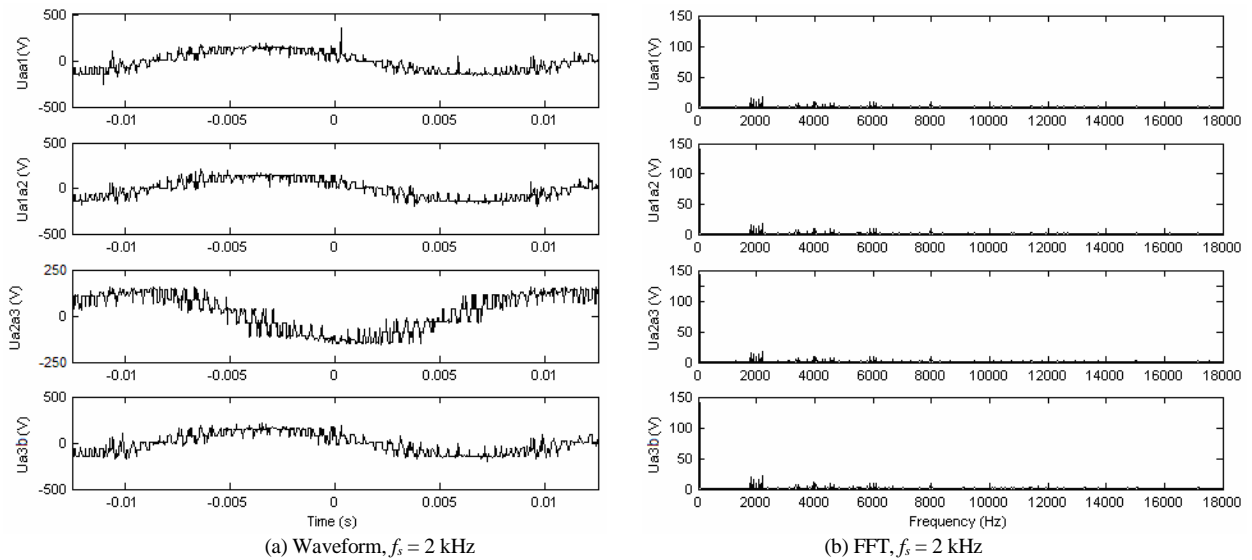


Fig. A5.81. Experimental voltages between coil sets for a delta-connected, 7.5-kW motor fed by a 3-level inverter ($U_l = 400$ V, $f_l = 50$ Hz, no-load).

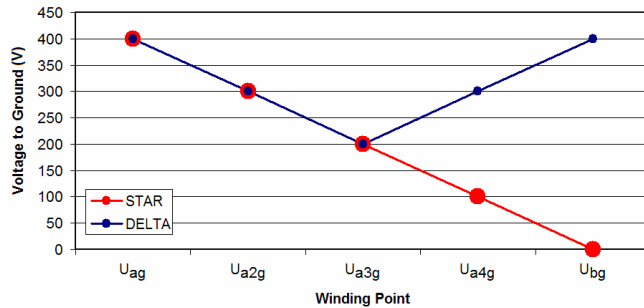


Fig. A5.82. RMS value of the fundamental voltage between stator winding and ground in different points, for delta and star connections.

VTs can cause full electric discharges⁷⁰ (EDs) and partial electric discharges⁷¹ (PDs), as well as an increase of the insulation voltage or electrical stress, which, when combined, can accelerate significantly the degradation of the motor insulation system [8], [54]-[78], [82], [83], [86], [87]. EDs and/or PDs occur when the VTs generated exceed the maximum value of the tolerated du/dt and/or of the dielectric strength of the insulation system [5], [8], [54]-[60]. Therefore, the higher the switching frequency is, the accelerated the insulation ageing will be.

The number of EDs and PDs occurring in the insulation system depends on the number, rise time and magnitude of VTs [62], as well as on the condition state of the insulation system.

Regarding PDs caused by VTs, they occur mainly in small air cavities or gaps⁷² (Fig. A5.83) existing in the stator winding insulation system, particularly those localized in the varnish/resin between conductors or between these and the ground (or stator-core slot surfaces), contributing to the insulation system deterioration, being inclusively used to diagnose its deterioration degree [59]-[62], [64]. PDs accelerate the insulation system⁷³ normal ageing process, and, in the worst case, form a fixed channel, eventually causing major insulation failure [86]. The air cavities will increase, and the insulation system becomes weaker until permanent failure occurs (electric contact or bridging between conductors and other metal parts). If VTs exceed the insulation dielectric strength, a full disruption can occur possibly leading to a permanent insulation system failure. Additionally, even ignoring the reflection effects in the conductors, the du/dt can stress the insulation because it allows the circulation of high-frequency capacitive parasitic currents through the insulation, including the air cavities, contributing to the electric deterioration of the overall insulation system, particularly between turns [8]. It is unlikely that the inter-turn insulation of the motor fails at the first surge. However, damaging effects are accumulated over a period of time.

⁷⁰ In full electric discharges, the total disruption or dielectric breakdown of the insulation occurs. In general, dielectric breakdown occurs when an electrical potential build-up exceeds the electrical limit or dielectric strength of a material. The negatively charged electrons are pulled in one direction and the positively charged ions in the other. When electrons are removed from a nucleus, it becomes positively charged.

⁷¹ In electric partial discharges, only the disruption of the air cavities or gaps of the insulation occurs. They are commonly known as corona or partial discharges [8].

⁷² In general, PDs can occur in spots of the insulation system contaminated by impurities with a lower permittivity and dielectric strength.

⁷³ Particularly in older motors fed by VSDs and with long cable runs, the lifetime of the insulation may experience a significant reduction due to the combined effect of the additional thermal stress (or operating temperature increase), PD activity and voltage stress.

Due to the nonlinear distribution of VTs, it is very likely that PDs occur in the ending region of the winding.

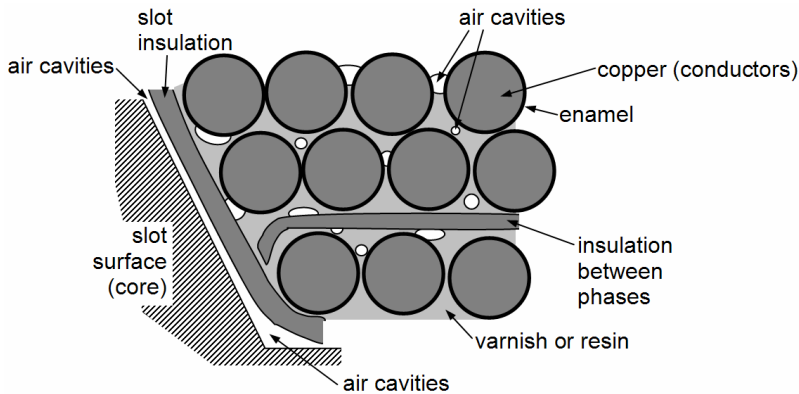


Fig. A5.83. Approximate representation of air cavities in the stator winding insulation system, where PDs can occur [8].

The disruption of the stator winding insulation system occurs when it is submitted to an electric field, E , with a value capable of perforate it, being this limit denominated by dielectric strength (DS). Considering only the part of the motor insulation system composed by solid materials, therefore its disruption is irreversible, lying permanently damaged. However, the insulation system disruption occurs in a gaseous-mean part (such as in the small parasitic air cavities or gaps), causing a PD, it can recover back to quasi-normal characteristics after the electric field magnitude decrease to values lower than the DS. In the latter case, the disruption voltage is commonly known as corona inception voltage or partial discharge inception voltage [8]. The earlier degradation of the insulation system also results from the capacitive current circulation between turns and between turns and the ground (stator core), due to the excitation of stray capacitances by the high du/dt (Fig. A5.84) [8].

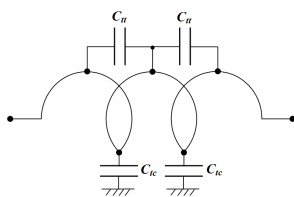


Fig. A5.84. Stray capacitances between turns and between turns and ground [8].

In order to explain PDs, it is important to explain the dielectric or electrical breakdown occurrence in a gas, as well as the subsequent effects. This kind of electrical discharges are denominated by “partial” because the VTs amplitude is not high enough to disrupt the solid insulation system between conductors (enamel⁷⁴ and varnish/resin) or between them and the core (slot insulation and varnish/resin), but is enough to disrupt the air cavities or gaps⁷⁵. This phenomenon is typical in medium-high voltage motors (rated voltage equal or higher than 6 kV)

⁷⁴ E.g., polyurethane, polyester, polyimide, etc. [91].

⁷⁵ The air disruption causes a visible light.

but, nowadays, it is extended to low-voltage IMs, in which it is experimentally demonstrated the occurrence of PDs and its contribution to the insulation system earlier failure [8], [16], [54]-[80]. The electrical breakdown within a gas (or mixture of gases, such as air) occurs when the dielectric strength of the gas(es) is exceeded. Regions of high electrical stress can cause nearby gas to partially ionize and begin conducting. Although air is normally an excellent insulator, when stressed by a sufficiently high voltage (an electric field strength of about⁷⁶ 30 kV/cm), it can begin to breakdown, becoming partially conductive (air molecules become ionized, providing a flow path for electric charges). If the voltage is sufficiently high, complete electrical breakdown of the air will culminate in an electrical spark or arc that bridges the entire gap. Before breakdown, there is a nonlinear relation between voltage and current as shown in Fig. A5.85, in which 4 different zones are identified. In zone 1, there are free electrons that can be accelerated by the electric field, establishing a current, which, after a certain voltage level, becomes constant, within zone 2. Zones 3 and 4 are caused by electron avalanche, as explain by the Townsend discharge mechanism⁷⁷. Partial breakdown of the air occurs as a corona discharge between the points with the highest electrical stress [93], [95].

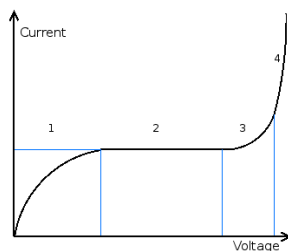


Fig. A5.85. Nonlinear relation between voltage and current before breakdown of an insulation gas.

The PD phenomenon in the air cavities between two conductors is schematically represented in Fig. A5.86 (approximate representation).

Considering the zone 2 indicated in Fig. A5.86a, corresponding to a block integrating conductors, enamel, varnish and air, in electrical terms, this corresponds to a capacitor with 3 different materials (dielectric means), as it can be seen in Fig. A5.86c. Ignoring the enamel between the conductors and assuming that the impregnant is an epoxy varnish, since the electrical permittivity of the air is 3.5 times lower than that of the varnish⁷⁸, the electric field in the air is 3.5 times higher than that in the varnish. Therefore, since the DS of the air is 13.3 times lower than that of the varnish⁷⁹, the air disrupts first. If, hypothetically, a 800-V instantaneous voltage between conductors occurs due to a VT, and the thickness of the air cavity, a , and of the varnish, e , were a

⁷⁶ Its exact value varies with the shape and size of the electrodes and increases with the pressure of the air.

⁷⁷ The Townsend discharge is a gas ionization process where an initial very small amount of free electrons, accelerated by a sufficiently strong electric field, gives rise to electrical conduction through a gas by avalanche multiplication. When the number of free charges drops or the electric field weakens, the phenomena ceases.

⁷⁸ The typical values of the dielectric constant of the air and of the epoxy varnish are $\epsilon_{air} = 1$ F/m and $\epsilon_{varnish} = 3.5$ F/m, respectively.

⁷⁹ The typical values for the dielectric strength or disruption electric field, E_{dis} , of the air and epoxy varnish are, respectively: $E_{dis,air} = 3$ kV/mm (some references state 3.2 kV/mm) and $E_{dis,varnish} = 40$ kV/mm (actually it can vary between 39-122 kV/mm, depending on the type of varnish or resin).

$= e = 0.2$ mm, the electric field in the air cavity would be approximately 3.11 kV/mm, while in varnish would be 0.89 kV/mm; since the electric field in the air cavity is higher than its dielectric strength, a PD would occur in the air. The same principle can be applied to the zone 1 indicated in the Fig. A5.86a (the equivalent scheme is presented in Fig. A5.86b) where, neglecting the enamel and assuming that the slot insulation has a permittivity and dielectric strength identical to that of the varnish, a voltage peak between the conductor with voltage U_A and the ground (stator core) would lead to an electric field in air 3.5 times higher than that of the slot insulation and, therefore, a PD would occur before the insulation disruption be reached. The considered varnish permittivity can actually be different if other than epoxy varnishes are used, or considering the different materials in the slot insulation, increasing the electric field in the air cavities. It should be noted that the insulators dielectric constant and strength depend on the frequency (or du/dt) of voltage applied and on the temperature⁸⁰ [99], [100], [101].

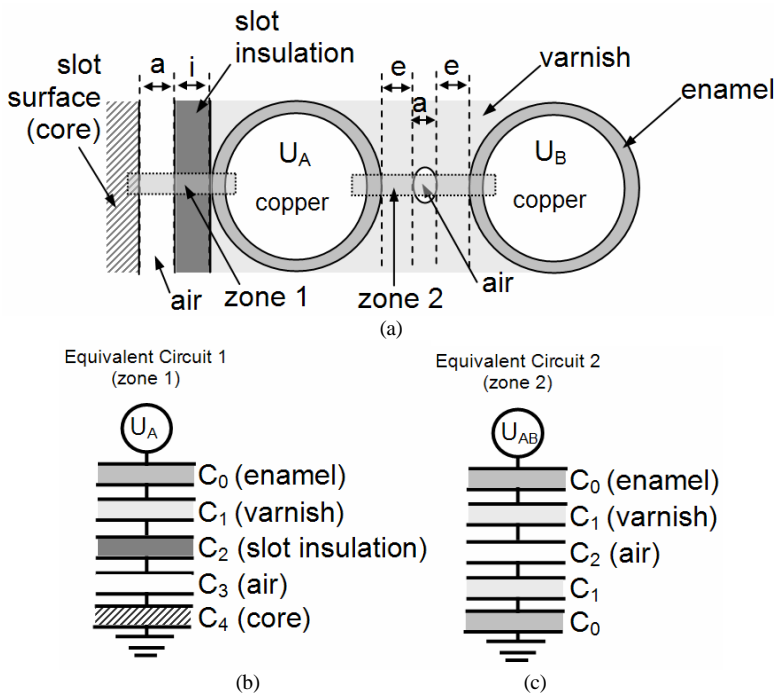


Fig. A5.86. Approximate representation of PD process in air-cavities between conductors with different potentials and varnish impregnation [8].

Due to the ozone production⁸¹ after the air disruption and the direct action of the electric discharge itself, the PDs deteriorate the insulation system by means of electrochemical processes (air cavity inner surfaces electrical corrosion and ozone chemical reaction⁸²), leading to earlier failures. The formation of ozone from molecular oxygen can be represented by the relation (A5.36) [89]. The ozone can be generated when a gas with oxygen is subjected to a corona electrical discharge, according to (A5.37), where $M = O_2$ or $M = N_2$ [89]. Actually, the electric discharge

⁸⁰ In fact, the temperature increase leads to the thermal conductivity increase, dielectric constant increase, dissipation factor increase, dielectric strength decrease, and resistivity decrease. The last four characteristics also depend on relative humidity.

⁸¹ The ozone is a gas composed by 3 oxygen atoms (O_3), and reacts with a number of types of organic compounds, including varnishes and resins, resulting in its accelerated deterioration.

⁸² Some types of impregnants and insulation materials are more resistant to PD [100].

dissociates the molecular oxygen through electron impact. According to the reaction scheme described by (A5.37), ozone generation increases with the increasing activities of corona discharge in air cavity. Ozone concentration increases until the optimum condition of corona discharge is achieved and then, due to the heat from the intense discharge in the air gap, the generated ozone dissociates, according to (A5.38), which is valid for dry air [89].



The phenomena above described result in the electrical degradation of the insulation system due to the high du/dt and/or high-amplitude of VTs, in a gradual (PDs and/or electrical stress⁸³) or abrupt (material disruption or EDs) way, particularly in the region between the turns of the same phase, where the insulation system is generally weaker⁸⁴ [8], [63]-[73]. The typical wire insulation (enamel) used in low-voltage IMs, supports a maximum du/dt of 500-750 V/ μ s. Moreover, the NEMA and IEC standards recommend that du/dt should not exceed 500 V/ μ s at the output of low-voltage (400-460 V) VSDs [8], [75], [72].

In the coils, the conductors are against each other, or very close to each other, being the insulation between them the enamel that covers them, as it can be seen in Fig. A5.87. The insulation separating them has twice the typical thickness of one conductor. Typically, for a conventional enamelled wire, with a 1.0236-mm copper section diameter (ref. 18 AWG), the insulation thickness is 0.0711 mm and the DS is about 84.4 kV/mm [91], i.e., two conductors against each other can withstand a maximum voltage of 12 kV (considering no thermal ageing and $du/dt \approx 0$). Varnish or resin can also exist between the enamel of both conductors, increasing the maximum voltage supported. Disruption voltage is a major factor influencing the motor insulation system lifetime.

⁸³ Insulation materials suffer an ageing process related to the amplitude and frequency of the electric field applied, commonly known as electrical stress.

⁸⁴ Between turns of different phases or between turns and ground, this phenomenon is not critical due to the reinforced insulation.

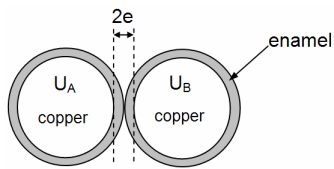


Fig. A5.87. Insulation between two enameled conductors (enamel thickness equal to e) [8].

The high electric field associated with the VTs does not affect significantly the insulation system if its magnitude does not exceed the DS or the maximum du/dt tolerated by the solid insulation parts. However, the VTs accelerate the natural (or thermal) ageing process (or the reduction of the DS decrease rate over the time) of the insulation system, which can lead to its early failure. The phenomena involved are related with the occurrence of EDs and PDs, particularly between turns of the same phase (typically, the weaker spot of the insulation system), including short-circuits or channelling between turns (contact by fusion), between phases and/or phases and ground, inevitable leading to the IM failure [8], [66]-[68], [70].

The insulation system failure between turns can result in closed loop circuits of extremely reduced impedance which, when crossed by time-varying magnetic fluxes, are crossed by high currents which, in turn, lead to the overheating and eventual copper fusion. The resulting high temperatures, can lead to the destruction of the adjacent conductors insulation, as well as of the phase-to-phase and phase-to-ground in-slot and coil-heads insulation. Eventually, the iron core interlaminar insulation destruction can also occur in those zones near the short-circuited turns. All the failures above described, due to their destructive nature, are irreversible.

In order to illustrate the PD phenomenon in heterogeneous means, a slot with enameled conductors and insulation straps, filled by epoxy resin, was studied by means of the finite-element method, using the FEMLAB software package, being the results presented in Figs. A5.89-A5.93. The electric field norm colour scale was limited between zero and the typical air dielectric strength (3 kV/mm). Therefore, the white parts represent the spots where the air dielectric strength is possibly exceeded. Each conductor has a different voltage in order to represent a more realistic situation. Based on the obtained results, it is possible to conclude that there is a strong possibility of PD occurrence in low-voltage motors experiencing VTs with up to 2 times the maximum rated voltage. Moreover, considering the same voltages in the windings, the smaller the motor, the higher the probability of the PD occurrence, since the electric field is on average higher due to the smaller distances between conductors, and probably smaller air cavities and gaps. This also justifies why PDs are also a problem in small/medium-power, low-voltage IMs.

Additionally, an increase in the temperature leads to the reduction of the permittivity of the air and to the increase of the permittivity of the resin or varnish, potentially resulting in the increase of the PDs occurrence [8], [100]. Moreover, the higher the VTs amplitude and du/dt , the lower the necessary number of VTs necessary to cause the insulation disruption.

It should be referred that ohmic/resistive and capacitive⁸⁵ leakage currents can circulate (named as sub-corona currents) in the air cavities, also contributing for the accelerated ageing of the insulation system.

It is clear that VTs occurrence can lead to the earlier or immediate failure of the insulation system of IMs, particularly if it is old. Short-circuits or channelling processes can also occur when the insulation between conductors become weaker due to moisture in the unimpregnated cavities, justifying the need to maintain the dryer as possible the insulation.

The insulation system degradation due to the PDs is gradual in grid-fed high-voltage IMs. However, it can be quite accelerated in inverter-fed, low-voltage IMs due to the high frequency of occurrence of VTs.

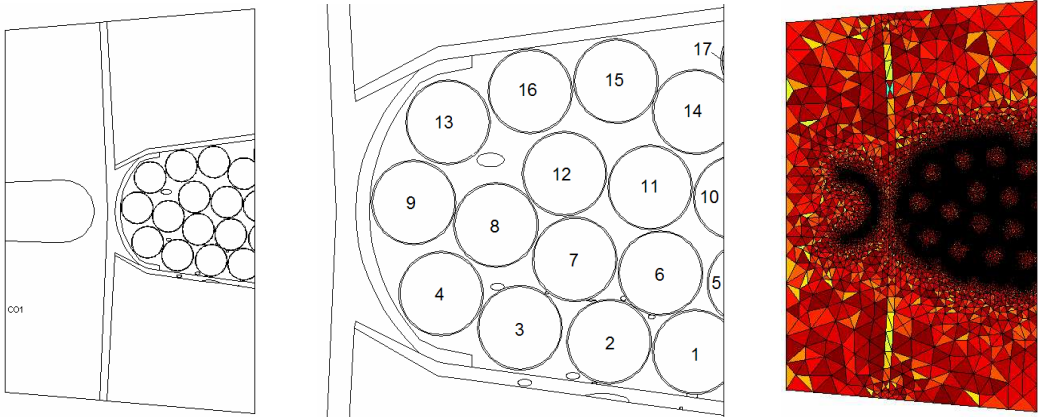


Fig. A5.88. Finite-element model used for simulations: (left) outline; (middle) outline zoom on conductors; (right) finite elements. The following voltages per conductor were used: 1 – 566 V; 2 – 556 V; 3 – 546 V; 4 – 536 V; 5 – 466 V; 6 – 456 V; 7 – 446 V; 8 – 436 V; 9 – 426 V; 10 – 366 V; 11 – 356 V; 12 – 346 V; 13 – 336 V; 14 – 266 V; 15 – 256 V; 16 – 246 V; 17 – 276 V.

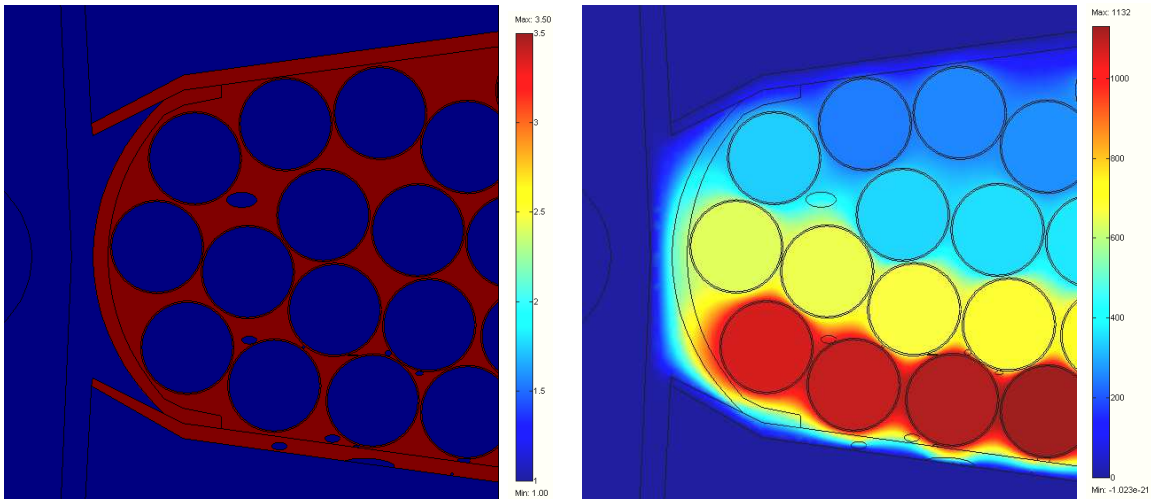


Fig. A5.89. Dielectric constant and electric potential.

⁸⁵ The capacitive leakage currents are of high frequency and circulate through the stray capacitances between air cavities extremes, between conductors, or between conductors and the ground.

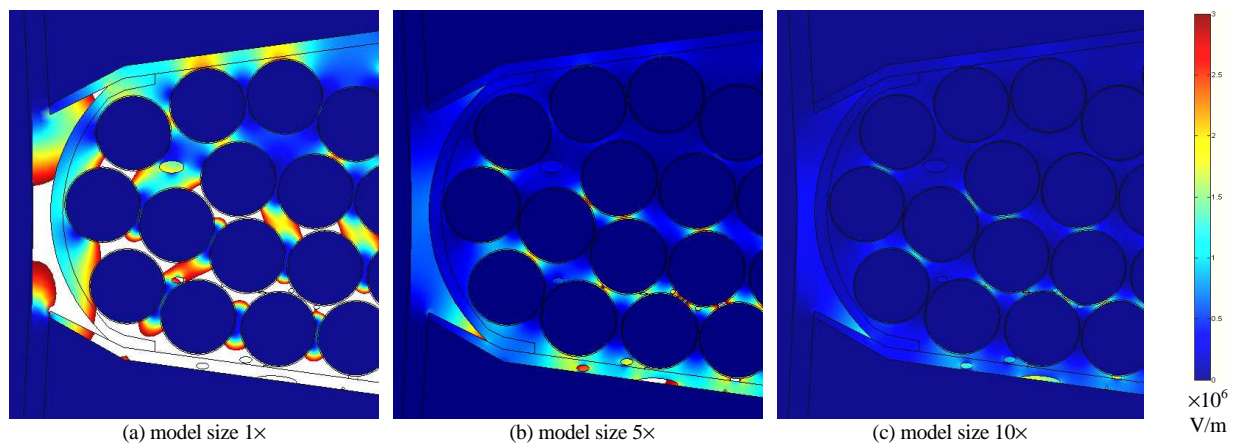
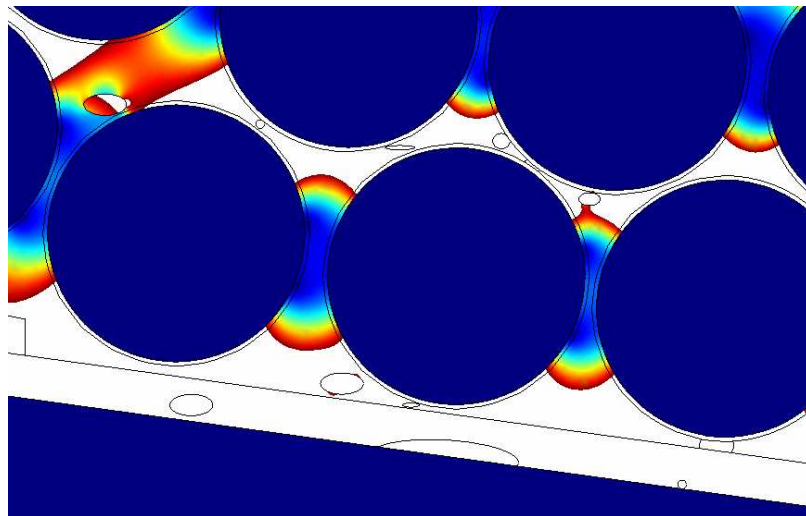


Fig. A5.90. Electric field norm for different model sizes corresponding to: (a) very small motor; (b) small motor; (c) medium motor.

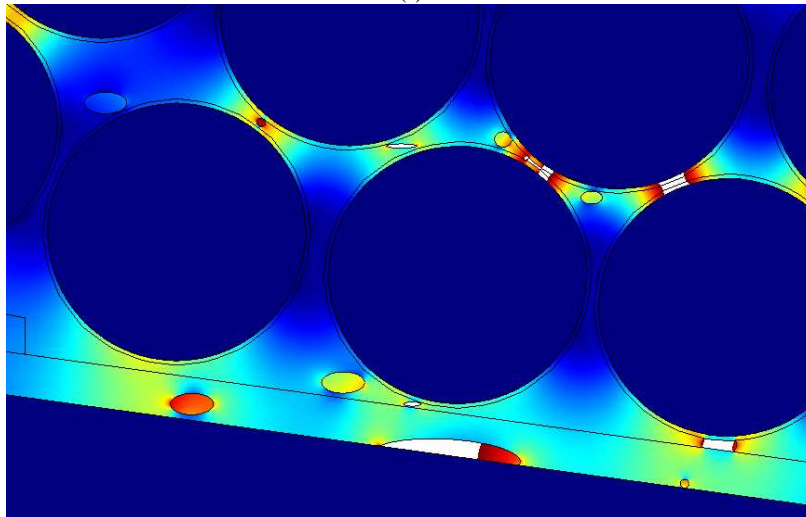
In fact, the PD occurrence is a symptom of insulation system deterioration (ageing degree), and the PD activity quantification can be used in predictive maintenance, as a way to evaluate the evolution of its state and estimate its remaining life.

Regarding DS variation with time, for example, in a brand new 400-V IM, the insulation system DS is very high (at least 10 times the rated voltage: 4-5 kV) but, over the time, decrease, as it can be seen in Fig. A5.93. When the ED and PD occurrence begin in the windings, the DS deteriorates exponentially with time. Typically, from the moment in which the DS of the insulation system of low-voltage motors is equal or lower than $2 \cdot U_N + 1000$ (in normal operating conditions, insulation system can last up to 12 yr until reach that state) the probability of occurrence of a total failure after 3-4 months is high [8], [54]. In fact, the DS decrease as a function of time is accelerated with the action of VTs (due to PDs, EDs and electrical stress). The experimental results presented in [66], in which “twisted pairs” were tested, shown that, increasing the voltage frequency from 50 Hz (sinusoidal) to 10 kHz (sinusoidal, unipolar PWM, and bipolar PWM waves were applied⁸⁶), the DS decrease rate becomes significantly higher (after 2 hours, the DS decreased to 3 kV for 10 kHz, and to more than 12 kV for 50 Hz). Therefore, depending mainly on the increase of the occurrence frequency, magnitude, and du/dt of the VTs, an accelerated degradation occurs (in relation to the natural ageing) of the insulation system, which leads to the motor earlier failure [8], [67], [91]. In the case of VSD-fed IMs, the increase of the switching frequency accelerates the DS decrease over time.

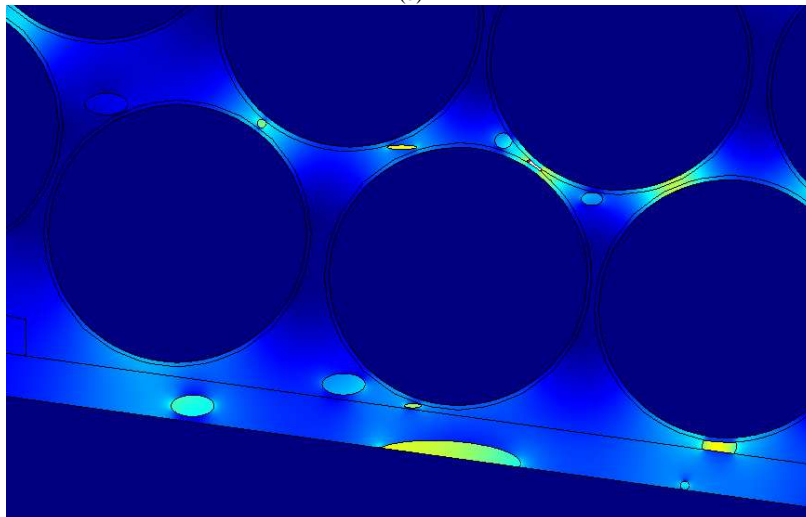
⁸⁶ The major difference between unipolar and bipolar is the du/dt , which doubles for the bipolar commutation. This test only imposes interturn (or turn-to-turn) stress, being the turn-to-ground stress not evaluated.



(a)

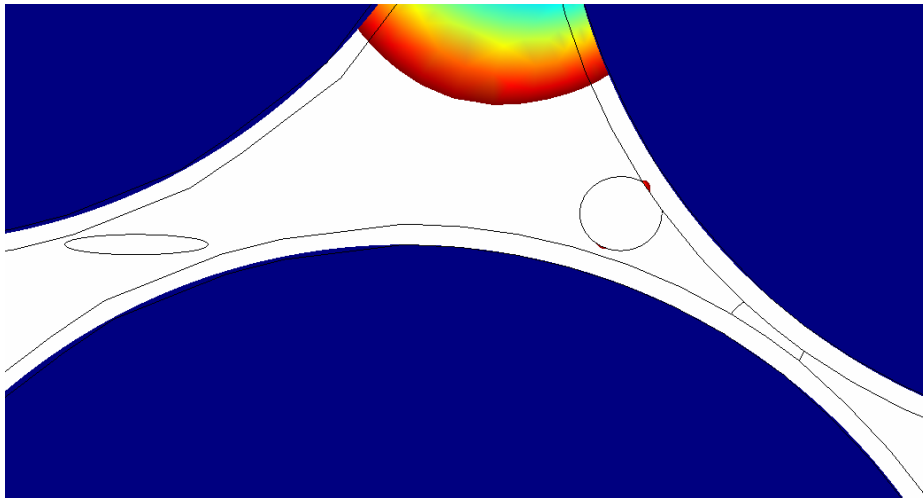


(b)

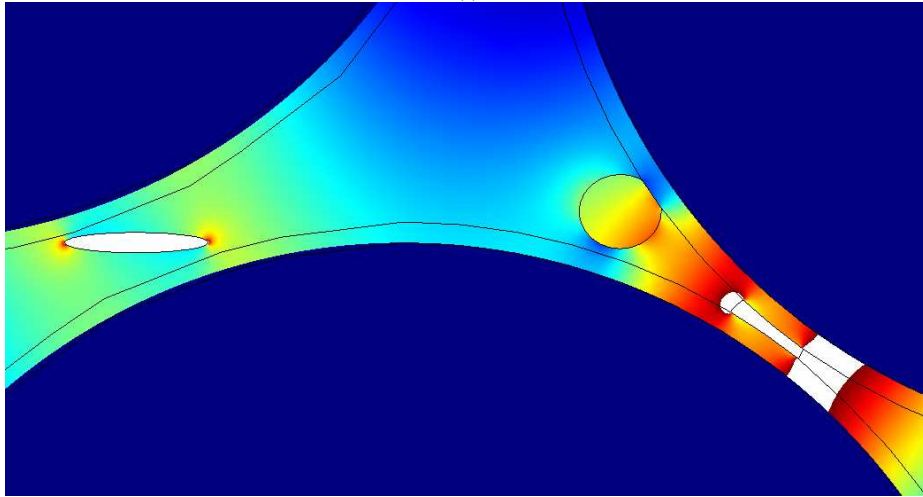


(c)

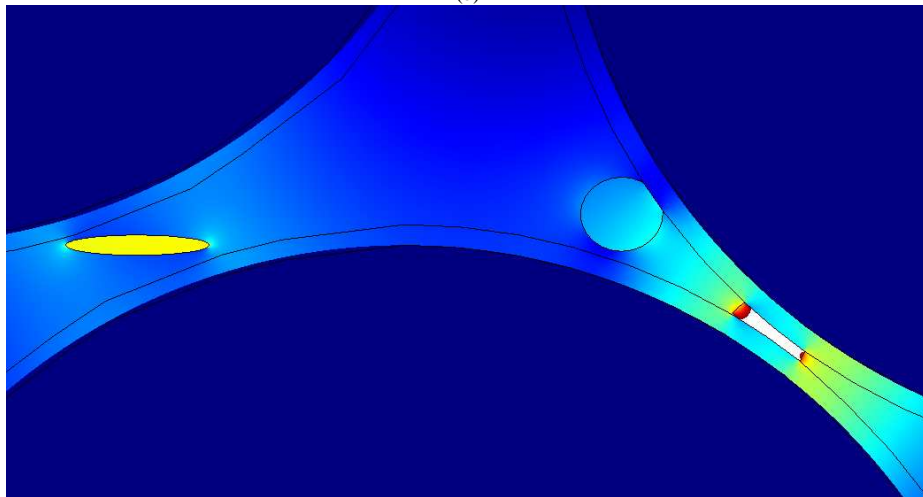
Fig. A5.91. Zoom of Fig. A5.90.



(a)



(b)



(c)

Fig. A5.92. Zoom of Fig. A5.91.

If a VSD-fed IM, with a lifetime imposed by Arrhenius law of t_{lf0} , its new lifetime, t_{lf} , can be approximately estimated by (A5.39), where K_1 , K_2 and K_3 are constants associated with the IM windings (typically, $K_2 > K_1 > K_3$), f_s is the switching frequency, f_1 is the reference fundamental frequency, t_r is the voltage rise time, U_p is the peak value of the applied voltage wave, U_{pN} is the peak value of the rated voltage and τ is equal to 2 and $2\sqrt{2}$ for the unipolar and bipolar voltage commutation (single-phase inverters), respectively [66].

$$\ln t_{lf} = \ln t_{lf0} - K_1 \cdot \ln\left(\frac{\tau \cdot \sqrt{f_s/t_r}}{2 \cdot \pi \cdot f_1}\right) - K_2 \cdot \ln\left(\frac{U_p}{U_{pN}}\right) - K_3 \cdot \ln\left(\frac{U_p \cdot \tau \cdot \sqrt{f_s/t_r}}{U_{pN} \cdot 2 \cdot \pi \cdot f_1}\right) \quad (\text{A5.39})$$

It is proposed to consider τ equal to $2\sqrt{2}$ and 2 for 2-level and 3-level voltage-source inverters, respectively, since the du/dt is roughly reduced to half in latter case⁸⁷. The proposed reduction of the constant τ for the 3-level inverters to $2/\sqrt{2}$, which is particularly indicated when there are long periods of operation with $m_a \leq 0.5$, is based on the turn-to-turn or coil-to-coil voltage stress reduction to roughly half in part of the fundamental period for $m_a > 0.5$ and over all fundamental period for $m_a \leq 0.5$. Of course, further experimental analyses are required on this subject.

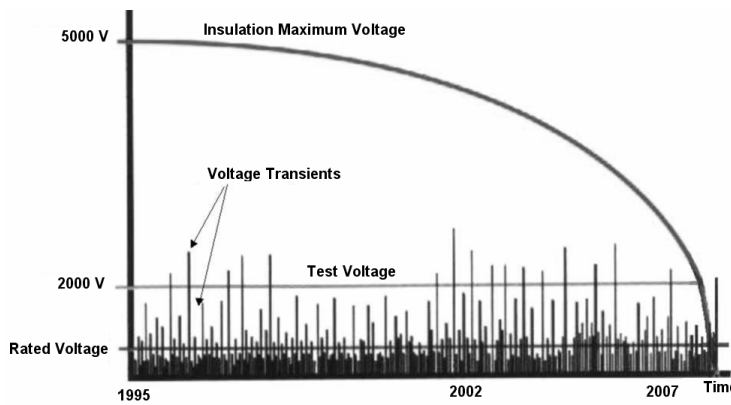


Fig. A5.93. Typical insulation system dielectric strength degradation over time for a 460-V IM [70]. The curve can be approximately described as $U_{max} = A \cdot \log(t-B) + C$, where t is the time, U_{max} is the maximum supported voltage, and A, B, and C are constants.

A5.4.3 Mitigation Techniques

In this section, several techniques to mitigate VTs occurrence and effects, which can be implemented by users and/or manufacturers, are addressed. The use of motor terminal filters, inverter output filters, and/or series reactors, as well as the reinforcement of the motor insulation system are typical examples of such techniques [16], [48], [73], [74].

⁸⁷ The du/dt reduction is valid for interturn, intercoil, and winding-ground voltages.

A5.4.3.1 Power Cable

The power cable between the inverter and the motor is typically selected by the user, being an important part of the motor system.

Regarding cable parameters, in [87] the results of tests performed with different cable lengths and types are presented. Experimental results presented in [86] evidence the influence of the cable length and type (shielded, unshielded, single-core, multi-core, etc.) and conductors cross-section, being part of the results summarized in Figs. A5.94 and A5.95. Without any filter between inverter and motor, the increase of the cable (shielded and unshielded) length up to a specific value (named as the critical length; in Fig. A5.94 corresponds to 50 m) leads to the increase of the VTs magnitude (maximum or peak value) but, from that value onwards, the VTs magnitude (related to the voltage reflection effect) remain roughly constant, while the rise time increases due to the higher damping effect, which depends on the cable type. For example, it was verified that, for a 50-m cable, replacing a regular cable by a ferrite cable (special high-damping cable), a reduction of the du/dt from 8 kV/ μ s to 3.5 kV/ μ s occurs. In fact, the maximum overvoltage is reached when the cable length exceeds the critical value, being recommended not to exceed that value. However, the longer the cable length is, the lower the du/dt will be. When shielded cables are used, the VTs magnitude is lower, due to the damping effect associated with the shield. The number of oscillations is a function of the reflection coefficient, and the respective period is a function of the cable length. Whether or not the shield is grounded, does not influence the voltage values. Regarding the cable conductors cross-section, it was verified that, when increasing it, the voltage slope at the motor terminals increases due to the lower damping effect⁸⁸, therefore affecting significantly the du/dt . A similar but slighter effect is noticed when replacing single-core by multi-core cables. Therefore, although oversized cross-sections can be used to reduce the cable voltage drop, they can aggravate the VTs at the motor terminals.

It is recommended the use of shielded cables (properly grounded to the inverter and motor) as well as the minimization of the cable length, because, in general, the higher the length, in order to reduce the VTs magnitude at the motor terminals. Moreover, introducing a filter at the inverter output, the VTs magnitude and du/dt are strongly reduced in long cables, being an effective solution. A filter at the motor terminals can become ineffective after a certain cable length, depending on the filter design.

⁸⁸ Since the value of the resistance decreases with the cross-section increase, yields a lower damping factor.

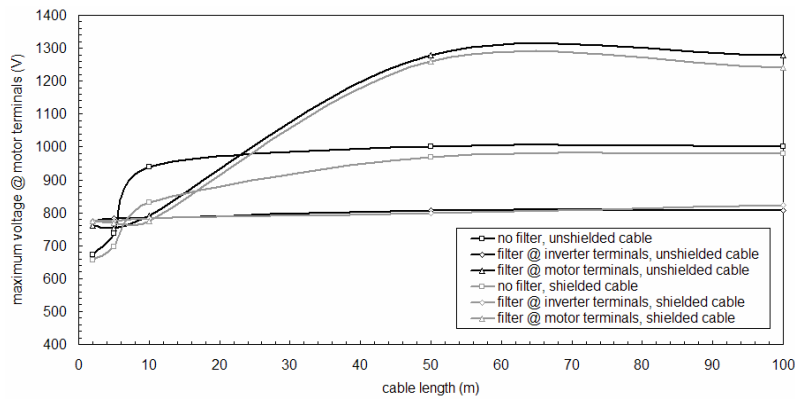


Fig. A5.94. Experimental maximum voltage at the motor terminals for a 15-kW, low-voltage motor. Data extracted from [86].

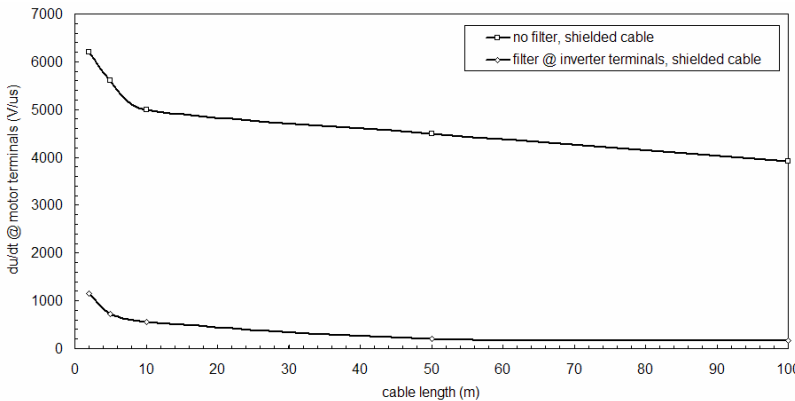


Fig. A5.95. Experimental du/dt at the motor terminals for a 15-kW, low-voltage motor. Data extracted from [86].

A5.4.3.2 PWM Waveforms

As previously referred, the higher the switching frequency is, the higher the VTs occurrence per time unit (or rate) will be, accelerating the motor insulation ageing. For a given switching frequency, the amplitude modulation index or the inverter operation zone (linear, nonlinear, or square-wave operation zones) also influences the number of VTs per time unit, since it strongly influences the number of PWM voltage pulses per fundamental period. Operating the inverter in the nonlinear zone reduces the number of pulses generated in relation to the linear zone. However, it is desirable to operate the motor within the linear region to improve voltage waveforms and motor performance. In general, when possible, the switching frequency reduction is recommended (e.g., down to 2 kHz), as explained before.

A5.4.3.3 Inverter Topology

There are commercially available VSDs integrating 3-level inverters (with a different topology from the conventional 2-level inverters), which lead to a significant reduction of the du/dt [16], as it is discussed in Chapter 3, and, therefore, significantly reducing the VTs magnitude. Moreover, using 3-level inverters, the investment in filters can be avoided, as well as the associated losses. This is an advantage that should also be taken into account when comparing 2-level and 3-level inverters.

A5.4.3.4 Filters and Reactors

Filters and reactors between inverter and motor are another solution for VTs slope (or du/dt) and magnitude reduction [8], [48], [74], [87]. A number of filters can be referred, namely LC-type filters (sine filter⁸⁹ or inverter output filter), LC-filter with insulated capacitor⁹⁰, and load-reactors (series-reactor motor filters⁹¹). RC filters (also named snubber networks or circuits) at the motor terminals⁹² can also be used. In [48], a motor terminal filter was connected in shunt at the motor terminals (RC-series star-connected filter, as it can be seen in Fig. A5.96), designed to match the motor characteristic impedance with that of the cable. In Table A5.11, the losses associated with different filter schemes are presented.

All the referred filters can reduce the VT peak value, but for the VT front slope reduction at the motor terminals, the load- or series-reactor gives the best solution [87]. Clearly, only the series-reactor is a valuable solution to reduce the du/dt without significantly increasing the losses, acting as a current limiting device and filtering the PWM waveform, therefore reducing the du/dt and the alternating electrical noise, as it can be seen in Figs. A5.97 and A5.98. Typically, a 5% reactance is used, which can be bulky and affect the transient performance of the drive and reduce the motor fundamental voltage [48].

Regarding the introduction of series inductances at the inverter terminals, associated with a RC filter, the effectiveness of such solution in reducing the VT magnitude and du/dt is shown in Fig. A5.97.

The main disadvantages associated with the series-inductances are the introduction of a voltage drop (3 to 5%), causing the motor torque to decrease (if no compensation is made), and the extra power losses, which, although small, are not negligible, and increase with the switching frequency [87].

The effectiveness in the VT mitigation (in terms of magnitude and du/dt) of the inverter output filter is evidenced in Fig. A5.97 (as well as in Figs. A5.94 and A5.95). The design depends on cable length, and the power losses depend on motor drive system rated power [48].

⁸⁹ Typically, sine filters integrate an inductance in series with the cable and a RC-series star-connected branch after inductances [48]. They are connected directly to the inverter output terminals and designed to reduce the du/dt below the critical value. The PWM output voltage becomes nearly sinusoidal. Attention has to be given to the switching frequency when the filter is used. The switching frequency has to be less than the filter resonance frequency, otherwise the filter or inverter could be damaged. The high cost of the filter is a disadvantage.

⁹⁰ Similar to the sine filter, but uses a three-winding transformer to supply the capacitors. High capacitance values can be used since the transformer reduces the capacitor current towards the primary side. The voltage waveform is similar to the one of the basic LC filter, but the voltage drop is smaller and, therefore, the system performance is better. The high cost is a disadvantage [87].

⁹¹ These filters reduce the voltage amplitude to 1 kV and the slope to 75-200 V/ μ s. Better results are obtained when the reactor is placed at the inverter terminals. The cable impedance is increased, resulting in a lower mismatch between cable and motor impedances. If the reactor is placed at the motor terminals, there are still reflections in the cable. Resulting overvoltages appear across the first windings of the filter and cannot be eliminated completely by the filter towards the motor. Another disadvantage of this configuration is that steep slopes cross the cable before being reduced (which can lead to EMI problems).

⁹² The RC snubber, or motor terminal filter, consisting of resistors and capacitors, is a simple and cheap solution. The RC snubber circuit is typically installed at the motor terminals and works as an impedance matching network. When the impedance matching is complete, there is no reflection and no overvoltages. For cable lengths up to 150 m, the design for a given cable type is independent of cable length, and the losses are mainly fixed for a given inverter-cable-motor system with varying load. In comparison to other types of filters, the effect on the motor voltage waveform is minimum, since there is no voltage drop and, consequently, no reduction of the motor torque. However the dissipation losses are relatively high and, since it is an additional attachment to the motor terminals, it is not possible to place a filter on the motor terminals in some manufacturing settings [48] (e.g., submersible pumps).

It should be noted that the motor terminals filter, the inverter output filter, and the series reactor, have all no significant impact on shaft-to-ground voltage and provide only a minor reduction in the radiated EMI.

Additional experimental results are shown in Table A5.12, with and without filters, evidencing the significant decrease in the voltage peak and du/dt across the first coil, reducing the inter-turn voltage stress. Moreover, during the coil winding insertion process, the first and last turns within a coil have a good chance to cross over or lie adjacent to each other in the stator slot and, therefore, the insulation is likely to experience an increased stress, at the proximity points, particularly in the first coils of the winding. Therefore, the application of proper filters and/or reactors to reduce the VTs magnitude and du/dt at the motor terminals can contribute to improve significantly the reliability of VSD-fed IMs, being a recommended measure for critical applications.

TABLE A5.11
FILTER SCHEMES FOR VSD-IM SYSTEMS WITH CABLES UP TO 30.5 m [48].

Filter Components	Inverter Output L+RC	Motor Terminal RC	Series Reactor L
<i>R</i>	190 Ω	65 Ω	--
<i>C</i>	0.075 μF	0.075 μF	--
<i>L</i>	0.2 mH	--	5 mH
Total losses (460-V, 5-hp IM)	90 W	78 W	10 W

Notes:
Cable characteristics. THHN, 14 AWG, $Z_{cbl} = 190 \Omega$.
Switching frequency: 2 kHz.

TABLE A5.12
EXPERIMENTAL VOLTAGE ACROSS THE FIRST COIL OF A 3-kW VSD-FED IM [82].

Voltage Across 1 st Coil (with 55 turns)			Type of Filter
u_{peak}	Overshoot	du/dt	
480 V	788%	800 V/μs	None
140 V	159%	155 V/μs	RC at the Motor Terminals
70 V	30%	Negligible	RCL at the Inverter Terminals

Notes:
3-kW, 230-V random-wound IM with specific taps in the winding (55 turns/coil & 6 coil/phase). VSD input line-to-line voltage: 208 V; VSD input DC-link voltage: 280 V; Cable length: 30.5 m. Voltage peak across the 1st coil with sinusoidal supply: 54 V/coil.

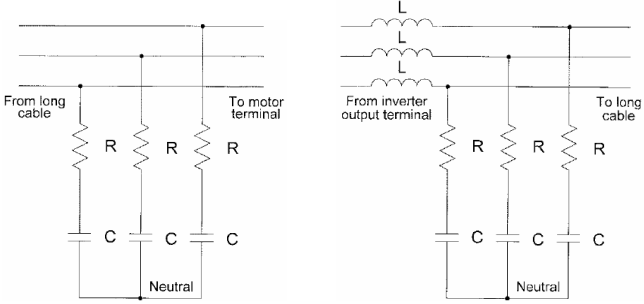


Fig. A5.96. Filters schematic: RC-series star-connected filter (first-order RC filter) at motor terminals (left) and L+RC-series filter (low pass filter) at inverter terminals (right) [48], [82].

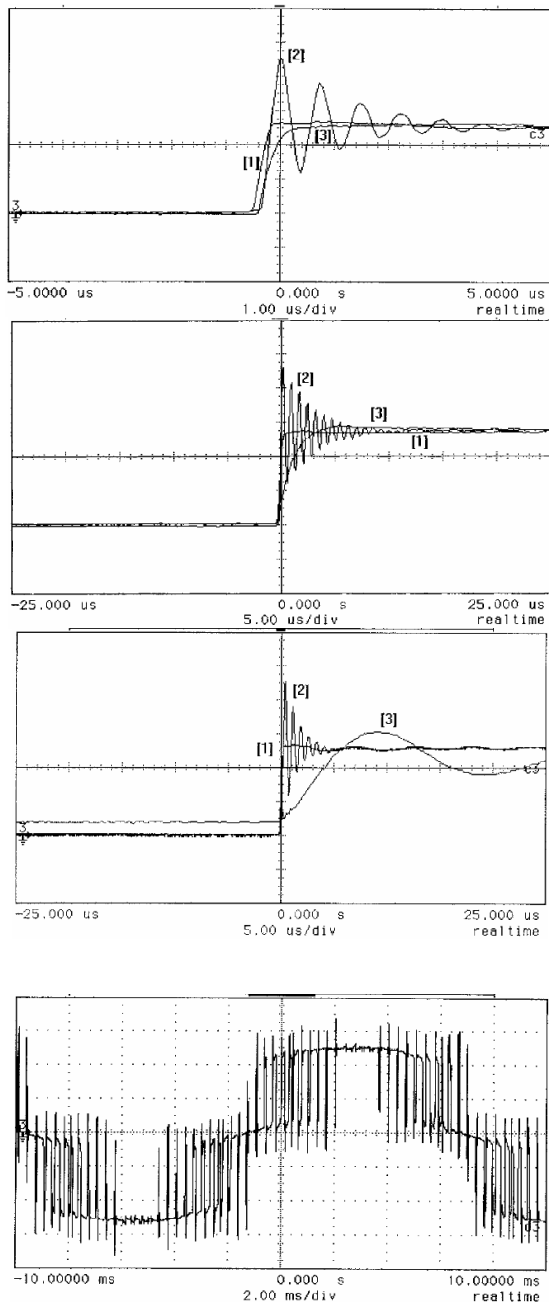


Fig. A5.97. Experimental motor terminal voltage waveforms for a VSD-fed 5-hp/460-V IM with motor terminal filter (top), inverter output filter (middle), and series-reactor (bottom): (trace 1, 250 V/div) voltage leading edge at inverter output; (trace 2, 250 V/div) voltage at motor terminal without filter or reactor; (trace 3, 250 V/div) voltage at motor terminal with filter or reactor [48].

Fig. A5.98. Experimental motor terminal voltage waveforms for a VSD-fed 5-hp/460-V IM with series reactor (250 V/div) [48].

A5.4.3.5 Insulation System Reinforcement and Winding Implementation

From the manufacturers and repairers point of view, the increase of the VSD-fed IMs robustness to VTs requires basically the reinforcement and quality improvement of the insulation system⁹³, including, for example, proper combination of wire enamel coat, slot and phase-to-phase insulation straps, and winding impregnating varnish or resin [8], [99]. Since 1995, the voltage rise time of power electronic devices has reduced by an order of magnitude (in part, the device switching losses) and the peak voltage handled has increased [67]. This led to changes in standards, as it can be seen in Fig. A5.99, in order to ensure adequacy of the insulation system for inverter-fed motors.

⁹³ The reinforcement of the insulation system means increasing the electrical, mechanical, thermal and chemical robustness.

Insulation materials of high quality, either in slots surface or in coil-heads, particularly between phases, should be used [8], [100]. In general, high-quality insulation materials means reduced thickness (slot insulation), high thermal conductivity, high dielectric strength, high resistance to PDs, and, inherently, extended lifetime. In principle, low-thickness slot insulation materials leads, by it self, to the improvement of the motor thermal dissipation capacity, but, to provide proper voltage disruption level, are characterized by high dielectric strength. Examples of high-quality insulation materials are Nomex^{®94}, Teflon[®], Kapton[®] (polyimide film), and Mylar[®] [100], [101], [102].

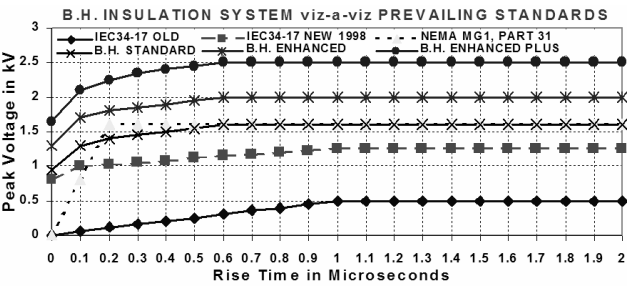


Fig. A5.99. Insulation system capability⁹⁵ [67].

Insulation between phases⁹⁶ is one of the most important aspects since it separates the higher potential differences between coils or conductors, either in heads or within slots, and, therefore, should be a priority. The reinforcement of the insulation of the conductors connecting the windings to the terminal box (by using insulating sleeves or straps) is also important since the insulation system failure in those zones is common in the VSD-fed IMs, explained, in part, by the nonlinear distribution of the voltage, as previously discussed.

The use of reinforced enamelled wire is also a measure than can increase significantly the motor robustness to VTs. The manufacturers developed reinforced enamelled wires⁹⁷ which, in order to increase the disruption voltage, the mechanical robustness and the endurance to electrochemical corrosion associated with PDs, have additional enamel layers (or increased thickness) and/or with special covers, which integrate organic or inorganic composites (e.g., metal oxides) [8], [55], [61]-[65], [68], [71], [73], [76]-[78], [91], [92]. It should be referred that the increase of the enamel operating temperature leads to the reduction of its disruption voltage. Moreover, although the simple increase of the thickness can itself lead to the increase of the voltage disruption, the addition of special composites can also contribute significantly to the that purpose [8]. For

⁹⁴ Used in conductor wrap, coil wrap and interleaving, slot liners, wedges, mid- and top-sticks, phase insulation, end-laminations, lead insulation, etc. [101].

⁹⁵ IEC 60034-17 Standard, Rotating Electrical Machines - Guide for the application of cage induction motors when fed from converters. Several considerations on the insulation system capability can also be found in the NEMA MG-1 Standard, Part 31, Definite purpose inverter motors [97].

⁹⁶ VTs between phases have typically higher magnitude than the VTs between phases and ground.

⁹⁷ There are different types of enamelled conductors/wires (commonly known as magnet wires), reinforced with a double, triple or quadruple layers and/or different enamel compositions (known as reinforced, heavy-built, double-bounded, triple-built, quadruple-built, inverter-rate, inverter-duty, inverter-grade, ultra-shielded, corona-resistant, etc.) [8]. The enamel can be polyurethane, polyester, polyimide, etc., with or without overcoats [91]. In [98], a new magnetic wire insulation was developed with an improved wire film/coat that has been tested against standard insulation with an accelerated wire life test using twisted pairs fed by a 20-kHz, 1500-V (peak), 0.05- μ s rise time and 50% duty-cycle voltage source. Additional protection was achieved without increasing significantly the insulation thickness.

example, the enamel thickness duplication leads to the increase of the disruption voltage in 30% and, for windings exposed to the same voltage magnitude and temperature, inverter rated-type conductors (with composites) last about 5 times more than the quadruple-built conductors (with 4 enamel layers). Additionally, in relation to the conventional enamelled conductors, the reinforced enamelled conductors withstand higher du/dt and are more resistant to the thermal degradation. It should be emphasized that the simple increase of the insulation thermal class can extend significantly its lifetime [67], since it compensates the accelerated ageing due to VTs. In fact, the simple increase of the enamelled wire thermal class can be a good option without significant increase in the winding cost (e.g., from F to H class, the cost increase is about 10-15%).

Although the improved enamelled wire can contribute to extend significantly the insulation lifetime, on average, for a given thermal class, the reinforced insulation wires cost more than 20-30% than the conventional wires. In order to reduce the winding cost, the reinforced wire can be used only in the first coil (for star-connected windings) or first and last coils (for delta-connected windings), which are the most critical, as discussed previously.

Impregnation processes (including the curing process) minimizing the air cavities in the insulation system, and the use of high-quality impregnants (resin or varnish) with a high DS and a viscosity adequate to the impregnation and curing processes, should be used [8], [100]. The most used impregnants are the polyester⁹⁸ and the epoxy, but improved special impregnants for special applications are also available in the market [8], [99], [100]. Independently of the wire enamel nature, the insulation system disruption voltage increases when the impregnation is carried out, being the better, the smaller the number of air cavities (with possibility of ionizing or ozone production) in it. In general, the minimization of the air cavities in the insulation system extends its lifetime, since it contributes to the increase of the respective electrical and mechanical robustness, as well as to the increase of the thermal dissipation capability, leading to the reduction of the motor internal temperature, with the consequent increase of its insulation life. Obviously, the impregnation process quality depends on the effective filling of the cavities or gaps (strongly related to the techniques and equipments used) and with the impregnant retention degree in the windings and slots (related with the used insulating materials and with the conductors number and diameter [8]) during the polymerization or curing process, which can itself significantly influence the retention degree (e.g., stator rotation during curing increases the retention degree). For low-voltage IMs, it is recommended the use of an impregnant with thermal class immediately higher than the motor thermal class (but not lower than F class) and the use of the trickle impregnation (with stator rotation) or of the dip-and-bake impregnation, repeated twice [8]. Alternatively, a motor insulation system experiencing VTs should be derated to reach the original lifetime.

⁹⁸ Synthetic plastic polymer in which constituting units are connected by ester groups.

Regarding impregnation techniques, some specialists refer that the vacuum pressure impregnation (VPI) is not effective for IMs with random windings since, although the impregnant fills effectively the winding cavities, after the impregnation, the impregnant tends to drop out before polymerization, leading to a final result equal or worse than that obtained by rotary trickle or dip-and-bake impregnation⁹⁹. It was experimentally demonstrated¹⁰⁰ that, for the same enamelled wire, the impregnated windings by the dip-and-bake, repeated twice, have higher voltage disruption level in relation to those impregnated by VPI, proving that the latter technique has moderate effectiveness for low-voltage and/or low-power IMs (≤ 90 kW) [8]. However, a number of specialists claim that if impregnants with proper viscosity¹⁰¹ are used and the stator is properly rotated during curing process, VPI can result, in most cases, in a high-quality impregnation. Moreover, if a proper combination of insulation materials and impregnants is used, for high-power motors with form-wound stator windings, VPI is the only method eliminating effectively the air cavities from the windings. After the impregnation and polymerization process the final quality of the insulation system should be tested by means of high potential and surge tests [8].

Since the insulation system breaking occurs mainly at the winding heads base, an excellent impregnation should be guaranteed in that zone, particularly in IMs with a high start/stop rate and/or driving loads with high torque variation rates.

It should be referred that there are commercially available inverter-duty IMs, which are provided with an improved winding insulation¹⁰² [73], [87]. These motors have also a better. NEMA Std. MG-1, Part 31, specifies that stator winding insulation systems for definite purpose inverter-fed motors with base rating voltages equal or lower than 600 V should be designed to resist to a peak voltage up to 1600 V with rise times as low as 100 ns ($du/dt = 16$ kV/ μ s), as it can be seen in Table A5.13 [97]. A number of additional considerations on VSD-fed IMs can be found in NEMA-MG1, Part 30 & 31. However, motor manufacturers report that voltages equal or higher than 1000 V can exceed the dielectric strength of standard in-field motors, resulting in early failures [48].

For conventional IMs fed by a VSD, after a failure, the repairers can upgrade the insulation system to increase their lifetime, by means of the referred modifications (see also Appendix 3).

TABLE A5.13
NEMA STANDARD MG-1, PART 31: MOTOR INSULATION CAPABILITY [97].

Motor Type	Peak Voltage	Rise Time	du/dt
Conventional Design B	1000 V	$> 2 \mu$ s	500 V/ μ s
Inverter-Duty Design B	1600 V	$> 0.1 \mu$ s	16000 V/ μ s

⁹⁹ Which is strongly related to the presence of air cavities in the insulation system.
¹⁰⁰ In this study, 26 IMs, divided in 6 groups with different enamelled wire and impregnated with different methods, fed by VSDs (integrating IGBTs) were tested [13].
¹⁰¹ A resin should be used (instead of varnish), due to its relatively high viscosity.
¹⁰² In these motors, the initial part of the winding has a higher insulation level because of the nonlinear voltage distribution, and the phase-to-phase insulation is improved [87].

Building the motor and the inverter is one apparatus is an elegant way to reduce the cable length, solving the VT problem [8], [16], [67]. In fact, the reflection phenomenon can be attenuated by means of integrating the inverter into the motor frame (typically at the terminal/conduit box), since the conductors' length is minimized. The slopes are still high but they are not destructive when the motor is provided with an improved insulation system. Presently, there are several manufacturers offering this solution in the market.

The turns/conductors crossing, during the coils construction and their insertion in the slots, can contribute to the reduction of the electrical robustness of the insulation system. In fact, for most cases, a high number of crossing points in the conductors can actually exist, being the voltage between them higher than that expected between uncrossed conductors (as it can be seen in Fig. A5.100) and, consequently, in the presence of VTs, this situation can increase the possibility of PDs, EDs, and short-circuits occurrence.

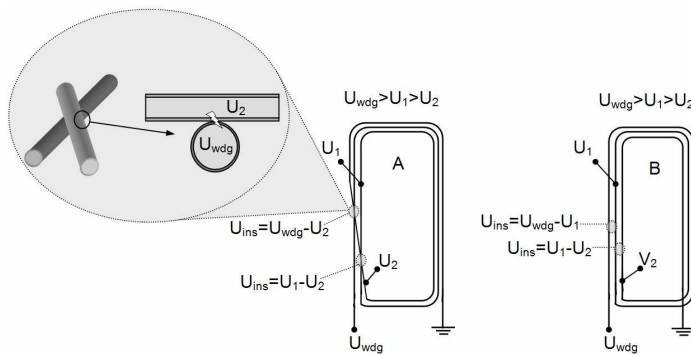


Fig. A5.100. Effect of crossing turns in coils [8].

To avoid such situations, the coils should be wound in a methodical manner (e.g., using an automatic or semi-automatic machine), in order to avoid the conductors crossing, with the lead or initial turn as far as possible from the last turn. This procedure facilitates the introduction of the coils in the slots and allows, in some cases, increasing the slot-filling factor (see Appendix 3).

Furthermore, positioning the initial turns in the centre of the coil section can also contribute to mitigate the DP occurrence, since it reduces the electric potential difference between conductors or between them and the core. This can be achieved by a careful, methodical construction.

The use of parallel conductors, can be a good option since it leads to the reduction of the high-frequency additional losses in the copper, the increase of the slot-filling factor, the increase of the varnish/resin retention during the impregnation, and to the increase of the coils flexibility (facilitating their introduction in the slots and the reduction of the coil-heads length). The reduction of the coil-heads mean length and the increase of the slot-filling factor can contribute to the decrease of the reflection coefficient at the motor terminals due to the reduction of the leakage inductance and winding resistance [8], [71].

The use of parallel conductors of reduced section also contributes to the skin effect reduction in the stator windings, leading to the reduction of the IM impedance to high-frequency currents and, therefore, contributing to the reduction of the reflection coefficient and high-frequency winding losses [8]. The reflection coefficient can also be minimized by means of reducing the average coil pitch, since it leads to the reduction of their mean length, and therefore the leakage inductance. The coils-heads decrease also improves motor efficiency. When parallel conductors are intended to be used, and for that purpose separated coils are constructed to be connected in parallel, it should be avoided the approximation between the ending and initial turns, since, as previously referred, that increases the voltage difference between turns, contributing to the occurrence of PDs, EDs, and short-circuits, during the VTs occurrence.

During the coils insertion (particularly in the VSD-fed IMs) it is also important to avoid damages (e.g., scratches) in enamelled wire during the construction process and stator coils, since they contribute to the PDs, EDs, and short-circuits occurrence [8].

Moreover, in order to increase the robustness of the VSD-fed IMs to the VTs, if possible, winding configurations without coils of different phases in the same slot should be implemented (see Appendix 3).

A5.5 Conclusions

Firstly, it is important to emphasize that users should invest carefully in the motor systems and in the motor repair or maintenance, in order to maximize the benefit obtained with that investment. Improving the reliability of only one of the modules of the EMODS is clearly a wrong strategy if the aim is to maximize the overall system reliability. The estimation of costs to increase the reliability of each module is required to establish a function that allows the optimum investment share to be determined. Integrated studies, including simultaneous reliability and efficiency analysis, can obviously give much better results in terms of investment share decision, since the reliability is related with the efficiency. After establishing the optimum share of investment in each system component, the users have to take into account the cost associated with the system failure (downtime cost) and, on the basis of that information, decide which is the most advantageous total investment. In the reliability scope, the investment should be directed to the minimization of the repair time (including reinstallation and restarting) and failure rate. An example is when inverters trip (which can be considered a failure) frequently in continuous processes requiring a complex restart (extending significantly the downtime), becoming the component with the lower *MTTF*, therefore justifying, in some cases, the investment in extra DC-bus capacitance or other sort of ride-through capability improvement measure.

The circulation of currents in the motor bearings is a problem extensible to almost all IMs, but particularly to those fed by inverters. Bearing currents related problems in the line-fed IMs are only significant for high-power motors, because it is only in those cases that a voltage between shaft ends with a magnitude high enough to disrupt the lubricant film in the bearings is developed. The bearings failure implies the motor stop, which, in some cases, can lead to high downtime costs, particularly in continuous process industries. However, there are cost-effective solutions easily implemented and others more sophisticated that, in the future, can be effective, feasible and cost-effective. On the basis of the main world and author research on these issues, in this appendix, the main causes and effects related to the circulation of bearing currents were discussed, and several solutions to its mitigation were addressed. An assessment of passive, easy-to-implement, low-cost mitigation techniques was presented, including the shaft to earth/ground connection by means of a electric contact brush (shaft grounding device), use of insulated or hybrid bearings (the latter have a number of extra advantages over standard bearings) and the introduction of a partial electrostatic shield connected to the ground in the slot openings, being the latter proposed by the author. Moreover, in some cases, extra/complementary solutions to protect the sensible mechanically coupled devices using, for example, an insulated coupling system and/or a shaft-ground connecting brush.

When and where bearing currents will become a problem is still unpredictable, although things such as VTs, electromagnetic asymmetries, high-switching frequency, and constant-speed operation, just to name a few, can increase the risk and accelerate bearing damage. It is important to consider the entire system and all of the possible current paths, in order to predict where problems would be most likely to occur, as well as to identify and correct existing trouble areas.

The installation of filters and/or the use of improved inverter topologies to attenuate the common-mode voltages and currents can be an alternative or complementary solution to those previously referred. It is important to emphasize that the cost-effectiveness evaluation of such solutions should take into account the benefits in terms of voltage transients mitigation (which stress the stator winding) and conducted and radiated EMI problems. In fact, in order to optimize results and costs, the solutions for bearing and leakage currents, voltage transients and EMI mitigation in inverter-fed motors should be addressed from an overall perspective, since they relate each other.

As far as the author knows, a new approach for bearing currents analysis was used. It seems that the FEM-based analysis can be used to study the current activity in the bearings, allowing the establishment of safety limits for the voltage between the inner and outer bearing rings. On the basis of the above-presented results, it can be concluded that the bearing inner ring insulation (shaft side) is more effective than the outer ring insulation (frame/ground side), since the associated

capacitive impedance and ohmic resistance will be higher than those associated with the outer ring, considering the same insulation thickness. A thickness equal or higher than 100 μm is recommended for the bearing inner ring insulation layer. Moreover, the hybrid bearings (with ceramic spheres) are the best solution, as expected, although much more expensive.

A partial electrostatic shield consisting of slot-opening outside-insulated conductive straps or sticks (or insulation material straps or sticks with a conductive thick film in one of the surfaces properly covered by an insulating coating) connected to the ground, appears to be an effective solution to mitigate the shaft-ground voltage and, therefore, the common-mode bearing currents.

With the increasing use of inverters, these issues will require further attention, and improved constructive and/or electronic solutions to mitigate the bearing currents should be developed. For that purpose, it is necessary to develop mathematical models for IMs that allow the analysis in the high-frequency domain.

Suspicious of EDM damage in the bearing races can be verified by means of special vibration analysis techniques. Determining the likelihood of EDM damage in an existing application can be assisted by special combined shaft voltage and total leakage/ground current analysis to find possible damaging bearing current activity. If bearing currents become a problem in an installation, or if the calculated risks are high enough, the equipment can be protected by using the above-referred methods, either independently or in combination.

For every VSD application, the switching frequency should be minimized (at least to less than 6 kHz, being desirable a VSD with a resolution equal or lower than 1 kHz for adjustment purposes to allow fine tuning) and the cable should be as short as possible (in order to reduce the voltage reflection effect). For motors smaller than 20 kW, shaft-grounding devices are recommended, if the required maintenance is not a major barrier. For larger motors, insulated/hybrid bearings or a partial electrostatic shield are recommended, since they require negligible maintenance and a higher level of protection. If necessary, they can be combined with shaft grounding devices. When long power cables between inverter and motor are used, filters are recommended, requiring individual tuning to each application. If the access to the motor is difficult, insulated/hybrid bearings or a partial electrostatic shield are recommended, in order to avoid high labour costs for motor maintenance/replacement.

The 3-level inverter minimizes intercoils/interturns and windings-to-ground voltage stress and reduces the possibility of bearing currents. The star connections can increase motor reliability, as well as the efficiency (avoiding circulating currents).

As future work, it is suggested that the inclusion in the bearing lifetime equation defined by (A5.20) of the effect of current activity (number of current peaks higher than a specified value in a time period), and the development of a monitoring system correlating common-mode

leakage/ground current and the shaft-ground voltage waveforms and spectra using, for example, artificial neural networks for the final diagnosis. Additionally, at this stage, the proposed partial electrostatic shield for common-mode bearing currents mitigation requires experimental validation in different motors, which should be carried out in the future.

Regarding the VTs occurrence at the terminals of the VSD-fed IMs, the respective main causes and effects were reviewed. In fact, only a few parameters have major influence on VT-related ageing in VSD-fed IMs: voltage rise time, switching frequency, cable characteristic impedance (related with cable length, cross-section, and type), motor characteristic impedance (related with motor rating), and insulation system quality (related with thermal class, materials, and air-cavities existence). The fundamental factors for the PDs occurrence, which is an important insulation system-ageing factor in IMs, are the VTs occurrence and the presence of air cavities or gaps in the impregnating varnish or resin between enamelled conductors or between them and the slot surfaces.

Several techniques to mitigate the occurrence and effects of VTs were addressed, including the increase of the robustness of the motor insulation system and winding design improvement, inverter topology, filters, and cable characteristics. If the proposed procedures were applied in the motor during either the design/manufacturing- or the use-phase (including motor repair/maintenance), its useful lifetime, can be significantly extended.

A5.6 References

- [1] Bollen, M.: *“Understanding Power Quality Problems – Voltage Sags and Interruptions”*, IEEE Press Series on Power Engineering, Wiley Interscience, John Wiley & Sons, Inc., 2000.
- [2] de Almeida, A., *et al.*: *“Actions to Promote Energy-Efficient Electric Motors”*, ISR-University of Coimbra, European Commission, S.A.V.E., Motors Study Group, 1996.
- [3] Anderson, R.; Neri, L.: *“Reliability-Centered Maintenance: Management and Engineering Methods”*, Elsevier Applied Science, London, 1990.
- [4] Smith, D.: *“Reliability and Maintainability in Perspective”*, 2nd Edition, John Wiley & Sons, New York, 1985.
- [5] Cardoso, A.: *“Diagnóstico de Avarias em Motores de Indução Trifásicos/Three-Phase Induction Motors Failure Diagnosis”*, Coimbra Editora, Portugal, 1991.
- [6] Joksimovic, G.; Penman, J.: *“The Detection of Inter-Turn Short Circuits in the Stator Winding of Operating Motors”*, IEEE Trans. on Ind. Electronics, Vol. 47, No. 5, pp. 1078-1084, Oct. 2000.
- [7] Abreu, J.; Emanuel A.: *“Induction Motor Thermal Ageing Caused by Voltage Distortion and Imbalance: Loss of Useful Life and Its Estimated Cost”*, IEEE Trans. on Industry Applications, Vol. 38, Issue 1, pp. 12-20, Jan./Feb. 2002.
- [8] Ferreira, F.: *“Técnicas Avançadas de Manutenção Curativa e Reabilitação de Motores de Indução Trifásicos de Baixa Tensão/Advanced Methods for Curative Maintenance and Rehabilitation of Low-Voltage, Three-Phase, Induction Motors”*, Tese de Mestrado/Master Science Thesis, Universidade de Coimbra/University of Coimbra, 2002.
- [9] Yu, L.: *“Fault Tree Analysis and Reliability Assessment of Auxiliary Power Supply system for an HVDC Plant”*, Master Thesis, written at KTH, the Royal Institute of Technology, School of Electrical Engineering, 2007.
- [10] Ferreira, F.; Pereirinha, P.; de Almeida, A.: *“Study on the Bearing Currents Activity in Cage Induction Motors using Finite-Element Method”*, 17th Inter. Conf. on Electric Machinery (ICEM’06), Conf. Proc., September 2006.
- [11] Modares, M.; Kaminskiy, M.; Krivtsov, V.: *“Reliability Engineering and Risk Analysis – A Practical Guide”*, Marcel Dekker, Inc., New York, 1999.
- [12] Hodowanec, M.: *“Satisfactory Motor Bearing Service Life: A Review of Often Overlooked Design Considerations”*, Pulp & Paper Industry Tech. Conf., Conf. Record, pp. 170-177, June 1995.
- [13] Busse, D.; Erdman, J.; Kerkman, R.; Schlegel, D.; Skibinski, G.: *“Bearing Currents and Their Relationship to PWM Drives”*, IEEE Trans. on Power Electronics, Vol. 12, No. 2, March 1997.
- [14] Busse, D.; Erdman, J.; Kerkman, R.; Schlegel, D.; Skibinski, G.: *“Characteristics of Shaft Voltage and Bearing Currents”*, IEEE Industry Applications Magazine, Vol. 3, No. 6, pp. 21-32, Nov./Dec. 1997.

- [15] Hodowanec, M.: "External Loading and Bearing Problems in Direct Connected Motors", 43rd Annual Petroleum and Chemical Industry Conf., Conf. Record, IEEE Incorporated Industry Applications Society, pp. 153-162, Sept. 1996.
- [16] de Almeida, A.; Ferreira, F.; Both, D.: "Technical and Economical Considerations to Improve the Penetration of Variable-Speed Drives for Electric Motor Systems", IEEE Trans. on Industry Applications, Vol. 41, No. 1, pp. 188-199, Jan./Feb. 2005.
- [17] Lawson, J.: "Motor Bearing Fluting", Pulp & Paper Industry Tech. Conf., Conf. Rec., June 1993.
- [18] Bell, S. et al.: "Experience With Variable-Frequency Drives and Motor Bearing Reliability", IEEE Trans. on Industry Applications, Vol. 37, No. 5, pp. 1438-1446, Sept./Oct. 2001;
- [19] Xiang, Y.: "A Novel Active Common-Mode-Voltage Compensator (ACCom) for Bearing Current Reduction of PWM VSI-Fed Induction Motors", 13th Annual Applied Power Electronics Conf. and Exposition (APEC'98), Conf. Proc., Vol. 2, Feb. 1998.
- [20] Schoen, R. et al.: "Motor Bearing Damage Detection Using Stator Current Monitoring", IEEE Trans. on Industry Applications, Vol. 31, No. 6, pp. 1274-1279, Nov./Dec. 1995.
- [21] Chen S.; Lipo T.; Fitzgerald, D.: "Source of Induction Motor Bearing Currents Caused by PWM Inverters", IEEE Trans. on Energy Conversion, Vol. 11, No. 1, pp. 25-32, March 1996.
- [22] Lipo, T.; Chen, S.: "Circulating Type Motor Bearing Current in Inverter Drives", IEEE Industry Applications Magazine, Vol. 4, No. 1, pp. 32-38, Jan./Feb. 1999.
- [23] Saylor, S.: "Motor Bearing Failure from VFD Induced Shaft to Ground Voltages in HVAC Applications", IEEE Technical Applications Conference and Workshops (Northcon95), 10-12 Oct. 1995, p.p. 212, 1995.
- [24] SEW-Eurodrive: "Drive Engineering Practical Implementation", Volume 1, 5, 7, 8, 9, 1995-1998.
- [25] Polovjadof, M.; Amor, A.: "Application: Numerical Results of a Study of the Electromagnetic Noise in Induction Motors with Effects of Rotor Eccentricity", Inter. Conf. on Electrical Machines, Conf. Proc., Vol. I, Sept. 1996.
- [26] Jouanne, A.; Enjeti P.; Gray W.: "Application Issues for PWM Adjustable Speed AC Motor Drives", IEEE Industry Applications Magazine, Vol. 2, No. 5, pp. 10-18, Sept./Oct. 1996.
- [27] Erdman, J.; Kerkman, R.; Schlegel, D.; Skibinski, G.: "Effect of PWM Inverters on AC Motor Bearing Currents and Shaft Voltages", IEEE Trans. on Ind. Appl., Vol. 32, No. 2, Mar/Apr 1996.
- [28] Busse, D.; Erdman, J.; Kerkman, R.; Schlegel, D.; Skibinski, G.: "An Evaluation of the Electrostatic Shielded Induction Motor: A Solution for Rotor Shaft Voltage Buildup and Bearing Current", IEEE Trans. on Industry Applications, Vol. 33, No. 6, pp. 1563-1570, Nov/Dec 1997.
- [29] Chen, S.; Lipo, T.; Fitzgerald, D.: "Modelling of Motor Bearing Currents in PWM Inverter Drives", IEEE Trans. on Industry Applications, Vol. 32, No. 6, pp. 1365-1370, Nov./Dec. 1996.
- [30] Chen, S.; Lipo, T.: "Bearing Currents and Shaft Voltages of an Induction Motor Under Hard- and Soft-Switching Inverter Excitation", IEEE Trans. on Ind. Appl., Vol. 34, No. 5, pp. 1042-1048, Sep./Oct. 1998.
- [31] Rendusara, D.; Enjeti, P.: "A Method to Reduce Common Mode & Differential Mode dv/dt at the Motor Terminals in PWM Rectifier/PWM Inverter Type Adjustable Speed Drive Systems", 13th Annual Applied Power Electronics Conf. and Expo. (APEC'98), Conf. Proc., Vol. 2, Feb. 1998;
- [32] Wang, F.: "Motor Shaft Voltages and Bearing Currents and their Reduction in Multilevel Medium-Voltage PWM Voltage-Source-Inverter Drive Applications", IEEE Trans. on Ind. Applic., Vol. 36, No. 5, 1336-1341, Sept./Oct. 2000;
- [33] Wood, S.: "The Design of Large Machines for Variable Speed Drives", IEE Colloquium on Design, Operation and Maintenance of High Voltage (3.3 kV to 11 kV) Electric Motors for Process Plant (Ref. No. 1999/178), Sept. 1999;
- [34] Habetler, T.; Naik, R.; Nondahl, T.: "Design and Implementation of an Inverter Output LC Filter Used for dv/dt Reduction", IEEE Trans. on Power Electronics, Vol. 17, No. 3, pp. 327-331, May 2002.
- [35] Zawadzki, M.; Judson, B.: "Case History of Shaft Currents on a 1500 hp Motor on PWM Supply", Pulp and Paper Industry Technical Conf., Conf. Record, June 1999.
- [36] Zhang, H.; Jouanne, A.; Dai, S.: "A Reduced-Switch Dual-Bridge Inverter Topology for the Mitigation of Bearing Currents, EMI, and DC-link Voltage Variations", IEEE Trans. on Ind. Appl., Vol. 37, No. 5, pp. 1365-1372, Sept./Oct. 2001.
- [37] Bhattacharya, S.; Resta, L.; Divan, D.; Novotny, D.: "Experimental Comparison of Motor Bearing Currents with PWM Hard- and Soft-Switched Voltage-Source Inverters", IEEE Trans. on Power Electronics, Vol. 14, No. 3, May 1999.
- [38] Halkosaari, T.; Tuusa, H.: "Reduction of Conducted Emissions and Motor Bearing Currents in Current Source PWM Inverter Drives", Annual IEEE Power Electronics Specialists Conf. (PESC 99), Vol. 2, June 1999.
- [39] Jouanne, A.; Zhang, H.: "A Dual-Bridge Inverter Approach to Eliminating Common-Mode Voltages and Bearing and Leakage Currents", IEEE Trans. on Power Electronics, Vol. 14, No. 1, January 1999.
- [40] Link, P.: "Minimizing Electric Bearing Currents in ASD Systems", IEEE Industry Applications Magazine, Jul/Aug 1999.
- [41] ABB Motors: "Technical Notes: Bearing Currents in Modern Drive Systems", 1999;
- [42] Barker, S.: "Avoiding Premature Bearing Failure with Inverter-Fed Induction Motors", Power Engineering Journal, August 2000.
- [43] de Almeida, A.; Ferreira, F.; Fonseca, P.; Chretien, B.; Falkner, H.; Reichert, J.; West, M.; Nielsen, S.; Both, D.: "VSDs for Electric Motor Systems", European Commission, DG TREN, SAVE II Programme, 2001.
- [44] SKF: "Rodamientos híbridos para maquinaria eléctrica", publicación 5128 Sp, 2002;
- [45] Ollila, J.; Hammar, T.; Iisakkala, J.; Tuusa, H.: "On the bearing currents in the medium power variable speed AC drives", ISBN 0-7803-3946-0/97, IEEE, 1997;
- [46] Sohler, A.: "The Unseen Truth Behind Motors fed by Inverters", WEG New Zealand, June, 1998;
- [47] Martin Doppelbauer, Expert opinion, SEW-Eurodrive, 2007.
- [48] Jouanne, A.; Zhang, H.; Wallace, A.: "An Evaluation of Mitigation Techniques for Bearing Currents, EMI and Overvoltages in ASD Applications", IEEE Trans. on Industry Applications, Vol. 34, No. 5, Sept./Oct. 1998, pp. 1113-1122.
- [49] Julian, A.; Oriti, G.; Lipo, T.: "Elimination of Common-Mode Voltage in Three-Phase Sinusoidal Power Converters", IEEE Trans. on Power Electronics, Vol. 14, No. 5, Sept. 1999, pp. 982-989.
- [50] Santos, F.; Trovão, J.; Ferreira, F.; Coelho, D.: "Three-Phase Induction Motor Condition Evaluation by means of Combined Current and Vibration analysis Using Artificial Neural Networks", 2nd Inter. Conf. on Electrical Engineering (CEE'07), Conf. Proc., November 2007.

- [51] Ferreira, F.; Sá, C.; Carvalho, J.: “*Análise e Técnicas de Atenuação da Passagem de Correntes Eléctricas nos Rolamentos dos Motores de Indução Trifásicos*”, Revista Kéramica, N.º 271, Março/Abril de 2005 & Revista Manutenção, N.º 91, 1.º Trimestre, 2007.
- [52] Mohan, N.; Undeland, T.; Robbins, W.: “*Power Electronics - Converters, Applications, and Design*”, 2nd Edition, John Wiley & Sons, Inc., New York, 1995.
- [53] de Almeida, A.; Bertoldi, P.; Falkner, H.: “*Energy Efficiency Improvements in Electric Motors and Drives*”, Springer-Verlag, Berlin, 2000.
- [54] Kemp, I.: “*Partial Discharges in Solid Insulation*”, IEE Colloquium on Advances in HV Technology (Digest No. 1996/173), pp. 5/1-5/8, 1996.
- [55] Lebey, T.: “*Influence of some voltage waveform characteristics on the partial discharge patterns: application to PWM power supply*”, IEEE Electrical Insulation Conf. and Electrical Manufacturing & Coil Winding Conf., Conf. Proc., pp. 627-630, October 1999.
- [56] Dymond, J.; Stranges, N.; Younsi, K.: “*Stator Winding Failures: Contamination, Surface Discharge Tracking*”, Trans. on Industry Applications, IEEE, Vol. 38, No. 2, pp. 337-344, March/April 2002.
- [57] Campbell, S.; Stone, G.: “*Examples of stator Winding Partial Discharge due to Inverter Drives*”, IEEE Inter. Symposium on Electrical Insulation, Conf. Rec., Anaheim, CA USA, pp. 231-234, 2-5 April 2000.
- [58] Müller, K., et al.: “*An Approach for Measuring Partial Discharge in PWM Inverter Driven Induction Machines*”, IEEE Inter. Symposium on Electrical Insulation, Conf. Rec., Anaheim, CA USA, 2-5 April 2000.
- [59] Neacsu, C.; Bidan, P.; Lebey, T.: “*Off Line Measurements of Partial Discharges in Turn Insulation of Low Voltage Rotating Machines*”, IEEE Inter. Symposium on Electrical Insulation, Conf. Rec., Anaheim, CA USA, pp. 235-237, 2-5 April 2000.
- [60] Casale, M.; Schifani, R.: “*Partial Discharge Tests Using CIGRE Method II*”, IEEE Trans. on Dielectrics and Electrical Insulation, Vol. 7, No. 1, pp. 133-140, February 2000.
- [61] Watson, J.: “*The Use of Line Current as a Condition Monitoring Tool for Three Phase Induction Motors*”, IEE, Savoy Place, London, 1999.
- [62] Stone, G., et al.: “*New Tools to Determine the Vulnerability of Stator Windings to Voltage Surges from IFDs*”, Inter. Conf. on Electric Machines and Drives (IEMD'99), Conf. Proc., pp. 149-153, May 1999.
- [63] Beeckman, R., et al.: “*Studies on Magnet Wire Degradation with Inverter Driven Motors*”, IEEE Electrical Insulation Conf. and Electrical Manufacturing & Coil Winding Conf., Conf. Proc., pp. 383-387, 1997.
- [64] Kaufhold, M.; Auinger, H.; Berth, M.; Speck, J.; Eberhardt, M.: “*Electrical Stress and Failure Mechanism of the Winding Insulation in PWM-Inverter-Fed Low-Voltage Induction Motors*”, IEEE Trans. on Industrial Electronics, Springer-Verlag, Vol. 47, No. 2, pp. 396-402, April 2000.
- [65] Gao, G. et al.: “*Studies on the Insulation Life of Adjustable Speed Drive (ASD)-fed Motors Under Accelerated Aging Conditions*”, Conf. on Electrical Insulation and Dielectric Phenomena, Conf. Proc., pp. 581-584, 1999.
- [66] Cavallini, A., et al.: “*Voltage Endurance of Electrical Components Supplied by Distorted Voltage Waveforms*”, IEEE Inter. Symp. on Electrical Insulation, Conf. Rec., Anaheim, USA, April 2000.
- [67] Jackson, D.: “*Low Voltage Insulation System Endurance Against Electronic Waveform and Cable Length*”, IEE Colloquium on Effects of High Speed Switching on Motors and Drives, Ref. No. 1999/144, pp. 6/1-6/7, June 1999.
- [68] Schump, D.: “*Winding Tests for Drive Duty Induction Motor Stators*”, Electrical Insulation Conf. and Electrical Manufacturing & Coil Winding Conf., Conf. Proc., pp. 623-625, October 1999.
- [69] Stone, G., et al.: “*Methods to Determine which Inverter Drives need Upgraded Motor Stator Windings*”, Pulp and Paper Industry Technical Conf., Conf. Rec., pp. 212-216, June 2000.
- [70] Baker Instrument Company: *Measure of Quality*, 2001.
- [71] Penrose, H.: “*Repair Specification for Low Voltage Polyphase Induction Motors Intended for PWM Inverter Application*”, 2nd Edition, Book 2 of the MotorDoc™ Series, 2001.
- [72] Penrose, H.: *Variable Frequency Drives Theory, Application, and Troubleshooting*, University of Illinois at Chicago, Energy Resource Center, 2001.
- [73] Jackson, D.: “*Reliability through Increased Safety Insulation Systems - The effect on high-speed switching on the motor insulation system*”, Power Engineering Journal, pp. 174-181, August 2000.
- [74] Steinke, J.: “*Use of an LC Filter to Achieve a Motor-friendly Performance of the PWM Voltage Source Inverter*”, IEEE Trans. on Energy Conversion, Vol. 14, No. 3, pp. 649-654, Sept. 1999.
- [75] Habetler, T.; Naik, R.; Nondahl, T.: “*Design and Implementation of an Inverter Output LC Filter used for dV/dt Reduction*”, IEEE Trans. on Power Electronics, Vol. 17, No. 3, pp. 327-331, May 2002.
- [76] Beeckman, R.: “*Inverter Drive Issues and Magnet Wire Responses*”, Electrical Insulation Conf. and Electrical Manufacturing & Coil Winding Conf., Conf. Proc., pp. 139-141, October 1999.
- [77] Wood, S.: “*The Design of Large Machines for Variable Speed Drives*”, IEE, Savoy Place, London, 1999.
- [78] Leeson Electric Corporation: “*LEESON's IRIS™ - Inverter Rated Insulation System*”, 2002.
- [79] Al-Ghubari, F.; Jouanne, A.; Wallace, A.: “*The Effects of PWM Inverters on the Winding Voltage Distribution in Induction Motors*”, Electric Power Components and Systems, Taylor & Francis, Vol. 29, pp. 447-458, July 2001.
- [80] Oyegoke, B.: “*Voltage Distribution in the Stator Winding of an Induction Motor Following a Voltage Surge*”, Electrical Engineering Research Journal, Vol. 82, No. 3-4, March 2000.
- [81] Bose, B.: “*Power Electronics and Variable Frequency Drives - Technology and Applications*”, IEEE Press, USA, 1996.
- [82] Jouanne, A.; Enjeti, P.; Gray, W.: “*Applications Issues for PWM Adjustable Speed AC Motor Drives*”, IEEE Industry Applications Magazine, Vol. 2, No. 5, pp.10-18, Sept./Oct. 1996.
- [83] Suresh, G.; Toliyat, H.; Rendusara, D.; Enjeti, P.: “*Predicting the transient effects of PWM Voltage Waveform on the stator Windings of Random Wound Induction Motors*”, IEEE Trans. on Power Electronics, Vol. 14, No. 1, January 1999.
- [84] Oyegoke, B.: “*Voltage distribution in the stator winding of an induction motor following a voltage surge*”, Electrical Engineering Research Journal, Vol. 82, No. 3-4, pp. 23-30, March 2000.
- [85] Al-Ghubari, F.; Jouanne, A.; Wallace, A.: “*The Effects of PWM Inverters on the Winding Voltage Distribution in Induction Motors*”, Electric Power Components and Systems, July 2001.

- [86] Devos, B.; Desmet, J.; Belmans, R.; Hameyer, K.: "A practical approach to the influence of long cables on inverter supplied induction motors", typographical notes not available.
- [87] Desmet, J.; Devos, B.; Stockman, K.; Belmans, R.: "Influencing parameters on overvoltages at the terminals of inverter supplied induction motors", typographical notes not available.
- [88] Hayt, W.: "Engineering Electromagnetics", McGraw-Hill Inter. Ed., Eng. Series, 5th Ed., 1989.
- [89] Boonseng, C.; Kinnares, V.; Apriratikul, P.: "Harmonic Analysis of Corona Discharge Ozone Generator Using Brush Electrode Configuration", IEEE Power Engineering Society Winter Meeting, Vol. 1, pp. 403-408, 23-27 Jan. 2000.
- [90] Ferreira, F.; Trovão, J.; de Almeida, A.: "Motor Bearings and Insulation System Condition Diagnosis by Means of Common-Mode Currents and Shaft-Ground Voltage Correlation", 18th Inter. Conf. on Electrical Machines (ICEM'08), Vilamoura, Portugal, Sept. 2008.
- [91] Divljakovic, V.; Vooren, E.; Vekic, B.; Vojnovic, B.: "Dielectric Strength of Magnetic Wire Coatings Exposed to Simultaneous Thermal and Radiation Aging", IEEE Electrical Insulation and Dielectric Phenomena Conf., Annual Report, pp. 793-798, 18-21 Oct. 1992.
- [92] Zalewski, E.: "A Comparison of Class H Polyesterimide Compared to Class H Polyester", 1989 Report on Dual Coated Magnetic Wire, IEEE, 1989, pp. 158-160.
- [93] Young, H.; Freedman, R.; Ford, A.: "Electric Potential", Sears and Zemansky's University Physics, 11th Ed., San Francisco, 2004.
- [94] Rigden, J.: "Macmillan Encyclopedia of Physics", Simon & Schuster Macmillan, 1996.
- [95] Kuffel, E.; Zaengl, W.; Kuffel, J.: "High Voltage Engineering Fundamentals", 2nd Ed., Butterworth-Heinemann, 2004.
- [96] FEMLAB3 Multiphysics Modelling, FEMLAB 3.0a, 2004.
- [97] NEMA Standard MG1-Part 31 & 30, Revision 2, *Motors and Generators*, April 1995.
- [98] Yin, W.; Bultemeier, K.; Barta, D.; Floryan, D.: "Dielectric Integrity of Magnetic Wire Insulations under Multi-Stresses", Phelps Dodge Magnet Wire Company Fort Wayne, IN, release.
- [99] Von Roll Isola France, Division Resins: "Electrical Insulating Materials – Insulating Liquids", Technical Brochure, March 2003.
- [100] Teinser, "Aislamientos Eléctricos", Teinser – Técnicas Industriales Serra, S.A., Grupo Isovolta, Austria.
- [101] Dupont: "Setting the Standard for Electrical Insulation – NOMEX[®]", Technical Brochure, 2002.
- [102] Dupont: "Dupont High Performance Films - Kapton[®]", "Kapton – Summary of Properties", Technical Brochures, 1998-2000.
- [103] Bruning, A., et al.: "Effect of Cavity Sub-Corona Current on Polymer Insulation Life", IEEE Trans. on Electrical Insulation, Vol.26, No. 4, pp. 826-836, Aug. 1991.
- [104] Bulington, E.; Abney, S.; Skibinski, G.: "Cable Alternatives for PWM AC Drive Applications", Copyright Material IEEE, Technical Paper No. PCIC-98, <http://bwcecom.belden.com/college/techpprs>, April 24, 2003.
- [105] Hwang, D., et al.: "Analysis of Insulation Characteristics of Low-Voltage Induction Motor Driven by IGBT PWM Inverter", 2000 IEEE Inter. Symposium on Electrical Insulation, Conf. Rec., Anaheim, CA USA, pp. 17-202-5, April 2000.
- [106] Jenkins, J.; Hall, W.: "Stressing Insulation in Motor Repair Testing", IEEE Electrical Insulation Magazine, Vol. 6, No. 5, pp. 13-19, Sept./Oct. 1990.
- [107] Jiancheng, S.; Heng Kun, X.; Yonghong, C.: "Study on UWB Frequency Characteristics of Partial Discharge as a Criterion of Aging Degree of Stator Winding Insulation", 6th Inter. Conf. on Properties and Applications of Dielectric Materials, Conf. Proc., Xi'an Jiatong University, Xi'an, China, pp. 181-184, 21-26, June 2000.
- [108] Laggate, D., et al.: "Reflected Waves and Their Associated Current", IEEE Industry Applications Society, St. Louis, MO, October 12-16, 1998.
- [109] www.greenheck.com, 2007.
- [110] www.bardenbearings.com, 2007.
- [111] www.skf.com, 2006.
- [112] www.fag.com, 2007.
- [113] www.sew-eurodrive.pt, 2007.
- [114] Doppelbauer, M., *Expert opinion/Notes from*, SEW-Eurodrive, 2007.
- [115] Reinert, J.; Karlsson, P.: "Improving performance and energy consumption of industrial processes by using variable speed drives", Emotron – Dedicated Drive, European Center for Power Electronics e.V. (ECPE) Seminar, "Towards Energy Gain and Savings – Emerging Drives and Generator Systems", Warsaw, Poland, 15-16 April 2008.

Appendix 6 – Complementary Notes and Figures

Previous Note: In this appendix, for the sake of simplicity, in each subsection (or Section A6.*.*), the figures, tables and equations are numbered starting from number 1. However, the references have only one counting, as usual. The information presented should be intended as complementary to that included in chapters 1-5 and appendixes 3-5 of this thesis, and, besides important background information, it also includes novel information resulting from on-going research work.

A6.1 Complement to Chapter 1

A6.1.1 Section 1.1

A. World Primary Energy Demand

Regarding the world primary energy demand, in Fig. 1 a reference scenario is presented. Global demand is expected to grow by more than 50% over the next quarter of a century, with coal use rising most in absolute terms [102].

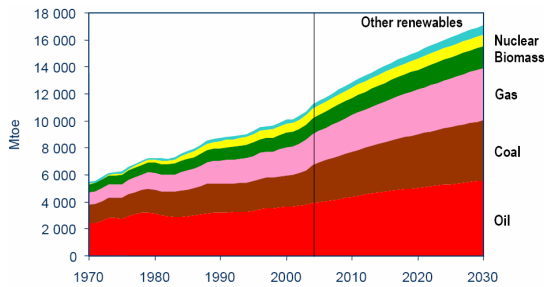


Fig. 1. Reference scenario for the world primary energy demand [102].

B. Electricity Consumption in the EU-15

Regarding motor electricity consumption and installed capacity in the EU-15, for the industrial and tertiary sectors, additional information is presented in Figs. 2-4.

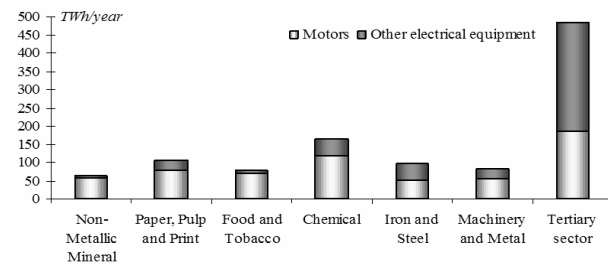


Fig. 2. Motor electricity consumption in each industrial sector and in the tertiary sector, for the EU-15, 2001 [3].

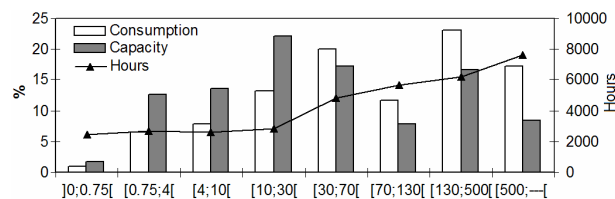


Fig. 3. Installed motor capacity, electricity consumption and average operating hours by power range in the industrial sector, for the EU-15, 2001 [3].

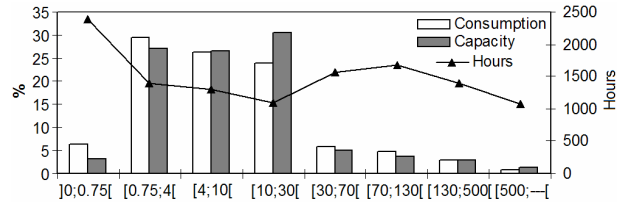
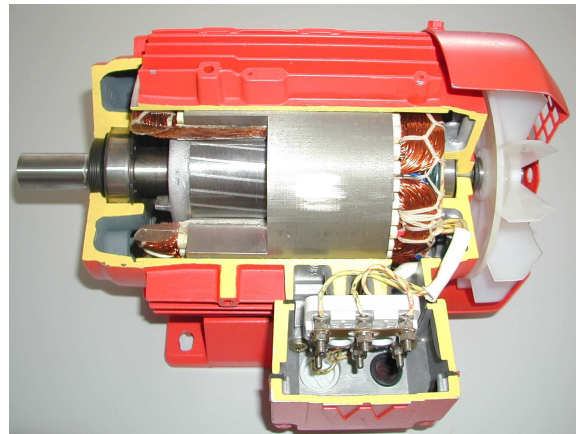


Fig. 4. Installed motor capacity, electricity consumption and average operating hours by power range in the tertiary sector, for the EU-15, 2001 [3].

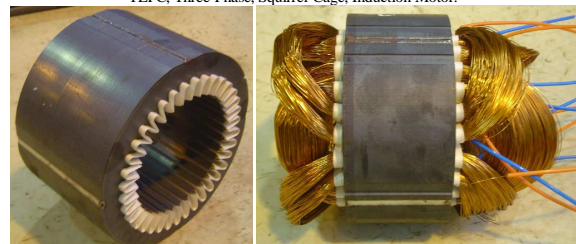
A6.1.2 Section 1.2

A. Three-Phase, Squirrel-Cage, Induction Motors

In Figs. 1 and 2, the different parts of IMs can be seen. In Figs. 3 and 4, the torque-speed curves for IMs with different rotor-bar shapes and the typical efficiency-load curves, according to the NEMA MG-1 standard, can be seen.



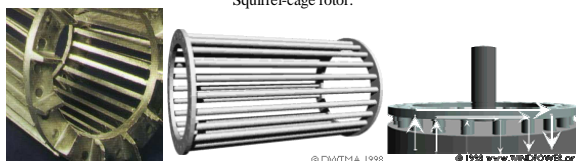
TEFC, Three-Phase, Squirrel-Cage, Induction Motor.



Stator core with slot insulation and windings.



Squirrel-cage rotor.



Squirrel-cage (bars and end-rings).

Fig. 1. Different parts of three-phase squirrel-cage induction motors.

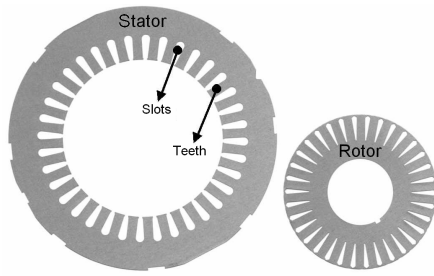


Fig. 2. Magnetic steel sheets of the stator and rotor core.

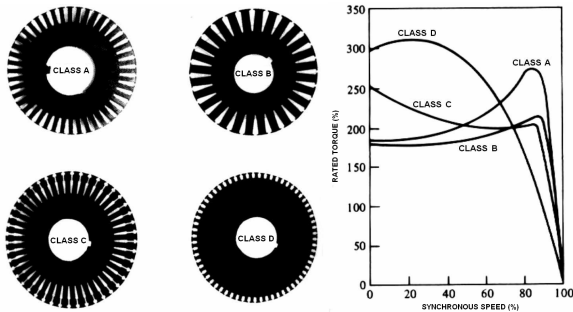


Fig. 3. Torque-speed curves for IMs with different rotor-bar shapes, according to the NEMA MG-1 standard [96].

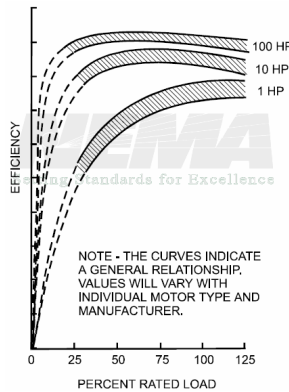


Fig. 4. Motor efficiency as a function of the load, for different rated power levels, according to the NEMA MG-1 standard [96].

B. Other Electric Motors

Regarding the other relevant motor technologies. Some short general notes are presented next.

Conventional DC motors (DCMs) are designed to operate from a direct voltage source. Typically, they have excitation windings in the stator, which produce a magnetic field when an external voltage is applied to them, and a rotating armature, which has several separate windings, fed through brushes which make contact with a rotary switch called a commutator. This device enables to switch the electric current in the several armature windings in order that the magnetic field of the stator and armature are permanently misaligned to generate maximum torque. The stator can also use permanent magnets. The basic operating principle is still the same. Traditionally, DCMs with windings are classified as shunt, series or compound, which reflects the way the field and armature circuits are connected. Complete information on this sort of motors can be found, for example, in [13]–[28]. These configurations date back to the time before the developments of power electronics, and a strong association built-up between one or other type of DCM and a particular application. The main characteristics of DCMs are the relative high construction

complexity (and, therefore, high cost), low reliability, high maintenance requirements (brushes and commutator wear), low efficiency, large volume, high EMI¹, and, perhaps, the only advantage, speed and/or torque control easiness, requiring inexpensive electronics. Traditionally DCMs with brushes have been used in industrial applications requiring accurate torque and/or speed control (e.g., servo drives, traction) and/or where only DC power is available. The developments in power electronics in the last decades allowed IMs to achieve the same torque/speed performance of DCMs in high demand applications, but with much higher reliability leading to a strong decline in market share of DCMs [29].

The so-called permanent magnet (PM) motors integrate permanent magnets² in the rotor. Brushless PM motors are rapidly becoming one of the most popular motor types. They differ from brushed permanent magnet DCMs in that the magnets are in the rotor instead of the stator, and in the commutation method, which is electronically controlled. Brushless PM motors, therefore, avoid the use of a commutator and brushes, inherently having higher efficiency and reliability. The stator can incorporate salient poles and concentrated windings in the case of the brushless DC motors (BLDCs) or distributed windings (similar to those used in IMs) in the case of the PM synchronous motors (PMSMs) [18], [28], [30], [31]. The rotor is reliable, but high magnetic fields and/or high temperatures can demagnetize it. A cross-section drawing of those technologies is presented in Figs. 4 and 5. In both cases an electronic controller³ is necessary, except in the case of the PMSMs incorporating an auxiliary squirrel-cage in the rotor for line-start capability. The latter motor type has the main advantages of both IMs and PM motors, and is commonly known as hybrid motor⁴ or line-start PM motor (LSPM). Additional information on this type of motors can be found in [97]–[100].

A PWM-VSD for the PMSM is required, being possible sensorless speed control. For the BLDC control, the rotor position is typically detected using sensors (optical or magnetic), encoders or resolvers. This type of motors can easily replace the IMs. These motors are still highly customized without suitable standards (e.g., dimensions, mounting, power, torque specifications, etc.) to allow a commodity market to develop. Due to the mass production for specialized applications, their cost has been decreasing and may become a key player, particularly in the low power range. They have a large savings potential [29]. Their main advantages are the relative high efficiency (up to 95%), high reliability (no brush and commutator wear), reduced maintenance, long lifetime, good thermal dissipation (no electrical or magnetic losses in the rotor), high power density, high

¹ Brushes-commutator interaction creates transients, sparks and ozone.

² Typically, the rotor magnets are made of ferrite or rare-earth alloys, e.g., neodymium-ferrite-boron (Nd₂Fe₁₄B₁). New alloys are being investigated to reduce the size of the rotor.

³ PM motors are also known as electronically controlled/commutated motors (EC motors).

⁴ Some HVAC systems and fans manufacturers are already incorporating LSPM motors (incorporate an auxiliary squirrel-cage for starting), which operate at synchronous speed after reaching the steady state. It should be noted that LSPM motors have been presented since 1955. However, the lack of high-energy PMs in the past and their high prices later on, lead to an uneconomical situation for mass production of LSPM motors. In recent years, by the introduction of high-energy PMs with reasonable prices, many attempts have been carried out to make this sort of motors feasible and economical. In relation to IMs, they have significantly higher efficiency and power factor in all power ratings and frame size.

torque/size ratio, excellent torque-speed curve, excellent dynamic response (since the rotor is light, the torque/inertia ratio is high, allowing high accelerations), silent operation (due to the smaller cooling fan), and high speed range capability. The main disadvantage is the relatively high cost (depending on magnet materials⁵). In general, this type of motors is applied in applications where high efficiency, low maintenance and/or high power density is required. Nowadays, PM motors are used widely in automotive industry (e.g., fuel pumps, assisted wheeling, traction, etc.), aerospace industry (e.g., robotics, centrifuges, pumps, high performance mechatronic systems, etc.), general industry (e.g., automation, CNC machines, fans, pumps, compressors, etc.), medical equipment, domestic and commercial equipment (e.g., washing and drying machines, HVAC, etc.), computer peripheral equipment (e.g., cooling fans), high performance elevators with direct drive, etc. From the energy-efficiency perspective, they are a good alternative to VSD-fed IM. A comparison of efficiency-load curves for PMSMs and IMs is presented in Fig. 6. The typical efficiency levels for PMSMs are presented in Fig. 7, evidencing the excellent performance of such motors in relation to IMs, particularly for low power ranges.

The reluctance motors have solid steel salient-pole rotor, therefore, they are reliable and cheap to produce. If the stator has salient poles they are called switched reluctance motors (SRMs), being one of the most recent entrances in the motor market, and if the stator has a distributed winding they are called synchronous reluctance motors (SyRMs) [18], [28], [30], [32], [33]. An auxiliary squirrel-cage in the rotor can be used to allow line-start capability. If no auxiliary cage is used in the rotor, an electronic controller is needed. The manufacturing of the rotor is cheap but high-precision equipment is required due to the very small air-gap. The most relevant losses are in the stator windings and core but core losses also occur in rotor (high speed motors). However the rotor heating is not significant. The low rotor inertia, associated with the high starting torque, allows fast dynamic responses. The main advantages are the high efficiency (equal or higher than that of the high-efficiency IMs) for wide load and speed ranges, the high speed (up to 100000 r/min) and/or acceleration capability, superior torque capability (high torque at low speed), high power density (reduced volume and weight), high reliability, reduced maintenance, long lifetime, construction simplicity, operation flexibility, low manufacturing cost, low-cost electronic controller for the SRM (half the power switched are needed since there is no need to invert the windings current) and the diversity of the size and shape. SyRMs require a PWM-VSD-based control. The main disadvantages of SRMs are the non-smooth torque and the high acoustic noise due to the vibration in the audible range due to the torque and radial forces variation generated over the operation. In the SyRMs, the vibrations and acoustic noise are strongly attenuated, being presently a promising technology for industrial purposes, although the relatively lower power

⁵ However, in the last decade the magnets price has decreased due to large production of magnet in China. For example, the average price of sintered Nd₂Fe₁₄B₁ has decreased by 40% from 1998 to 2003 [117].

factor [32]. However, manufacturers are improving these aspects. Moreover PMs can be added to improve SyRMs performance (including power factor improvement), being this sort of motors known as magnet assisted synchronous reluctance motors (PMASRMs) [31]. The reluctance motors power range is up to 75 kW and their applications include laboratorial centrifuges, compressors, washing machines, vacuum cleaners, vacuum pumps, HVAC, industrial variable-speed drives, machine-tools, automation, office equipment, traction, etc. [18]. They are also indicated to special environments (e.g., high temperature).

In the scope of high-efficiency motors, the PM and reluctance technologies have to be considered, having a significant saving potential ranging from 5 to 10% [2]. However, these technologies are not analysed in this thesis. Therefore, no further consideration will be made on this sort of motors.

As the name suggests, single-phase induction motors operate with a single-phase power supply. In single-phase induction motors, there is a stator main winding and an auxiliary winding for starting purposes. The rotor is of the squirrel-cage type. When the motor is connected to a single-phase power supply, the main winding carries an alternating current, which produces a pulsating magnetic field. Due to induction, the rotor is energized. As the main magnetic field is pulsating, the torque necessary for the motor rotation is not generated. This will cause the rotor to vibrate, but not to rotate. Hence, the single-phase induction motor is required to have a starting mechanism that can provide the starting kick for the motor to rotate. This is accomplished by the auxiliary stator winding, which normally is connected in series with a capacitor. The combination of the two windings creates a rotating magnetic field and the motor torque is generated in the rotor. After starting, a centrifugal switch may be used to disconnect the auxiliary winding. In relation to the equivalent three-phase IMs, they have a slightly higher construction complexity due to the extra capacitor and centrifugal switch, a higher cost, a slightly lower reliability, a lower efficiency, similar EMI, and can also be fed directly from AC line or from VSDs. Single-phase motors are mainly used in household appliances, and rarely exceeding a few kilowatts. The most relevant electric household appliances are subject of efficiency assessment regulation, in which the efficiency of the whole equipment is regulated. Other integral single-phase motors can be found⁶, mostly in the residential sector, in applications such as submersible pumps and machine tools. In general terms, single-phase motors are used when a three-phase power supply is unavailable.

Synchronous motors (SyMs) are similar to IMs in that they both have similar stator windings to produce a rotating magnetic field. However, the synchronous motors rotor field current is supplied by a separate DC power supply. Conventionally, the rotor was fed through slip rings and brushes, but more recent versions use a

⁶ For example, there are also some fractional horsepower single-phase motors called shaded-pole motors, with have a very low efficiency ($\approx 15-20\%$), used to drive fans of refrigeration systems. Some manufacturers are now providing low-power PMSMs with embedded converter, which can be fed directly from single-phase supply and have a much higher efficiency ($\approx 60-70\%$) but cost 3-4 times more than the shaded-pole motors. Since the frame and shaft size and shape is equivalent, the replacement can be made directly without extra mechanical adaptation [107].

brushless DC generator to supply the rotor. In SyMs, the rotor locks into step with the rotating magnetic field and rotates at synchronous speed. There is no slip in a SyMs, that is, the rotor always moves at exactly the same speed as the rotating stator magnetic field. The speed is thus determined by the number of poles of the motor and frequency of the power supply. The speed will remain constant, even with wide variations in the load. In order to accelerate the motor up to synchronous speed an auxiliary device is needed. Usually, this is accomplished by adding an auxiliary squirrel-cage into the rotor (known as damper winding), allowing the motor to start as an IM. When the motor speed reaches approximately 97% of nameplate speed, the DC-field current is applied to the rotor producing a pull-in torque and the rotor will pull-in-step and synchronize with the rotating magnetic flux field in the stator. SyMs are somewhat more complex than IMs and, hence, are more expensive. In relation to the equivalent three-phase IMs, they have a slightly higher construction complexity due to the windings of the rotor and slip rings/brushes or brushless DC generator, lower reliability (particularly if slip rings/brushes are used), a higher efficiency, similar EMI, and a higher cost. Additionally, they have two advantages over IMs, which are the possibility of power factor regulation and the very accurate speed. Synchronous motors represent only 5% of the volume of electric motor revenues (even much less in terms of sales volume) with their use confined to high power ratings (typically above 500 kW) and are typically used because of their slightly higher efficiency and capabilities for power factor control. SyMs are also used in specialized customized applications in which very accurate speed control is required.

The universal motor is a rotating electric machine similar to a DC series wound motor but designed to operate either from direct current or single-phase alternating current. The stator and rotor windings of the motor are connected in series through the rotor brushes/commutator. Therefore the universal motor is also known as an AC series motor or an AC commutator motor. In relation to the equivalent three-phase IMs, they have a slightly higher construction complexity due to the higher construction complexity, lower reliability (similar to DCMs, if operated at high speeds) and very limited lifetime, lower efficiency, and higher EMI (similar to DCMs). They can operate with both AC and DC current and have a good power to weight ratio⁷, but their maximum output is limited and motors exceeding one kilowatt are not common. Although they were used in traction applications [19], nowadays they are mainly used in household appliances, such as vacuum cleaners (main appliances are regulated for the overall performance) and portable appliances such as power and garden tools having a small number of operating hours.

⁷ However, IMs have a much higher power density per volume or mass. This can be exemplified by comparing two main line traction motors. A proven design AC commutator or universal motor (rating: 1230 kW, 7730 N.m @ 1520 r/min; max. torque (over 5 min): 8530 N.m; max. speed: 1600 r/min; mass: 3550 kg; inertia: 120 kg.cm²; outer length: 870 mm; outer diameter: 1200 mm) operated for many years in intercity locomotives, voltage controlled by transformer tap changer. Nowadays VSD-fed IMs are used (rating: 1428 kW, 9155 N.m @ 1490 r/min; max. torque (over 5 min): 11600 N.m; max. speed: 4200 r/min; mass: 2660 kg; inertia: 22 kg.cm²; outer length: 920 mm; outer diameter: 850 mm), being superior in every aspect. As a result, a locomotive containing 4 VSD-fed IMs can produce similar traction force as the former much heavier with a 6-universal-motor driving system, the torque of which is pulsating at double the supply frequency [19].

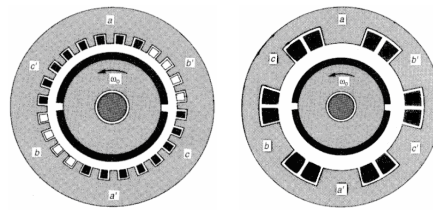


Fig. 4. Cross-section view of a three-phase permanent-magnet motor with 2-pole stator and 2-pole rotor: (left) synchronous permanent-magnet motor (also known as electronically controlled motor, EC); (right) brushless DC motor (BLDC).

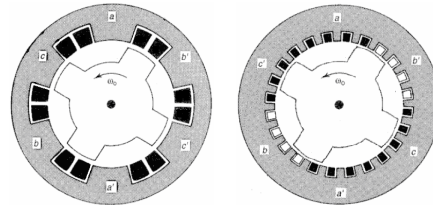


Fig. 5. Cross-section view of a three-phase reluctance motor: (left) switched reluctance motor (6-pole stator and 4-pole rotor); (right) synchronous reluctance motor (2-pole stator and 4-pole rotor).

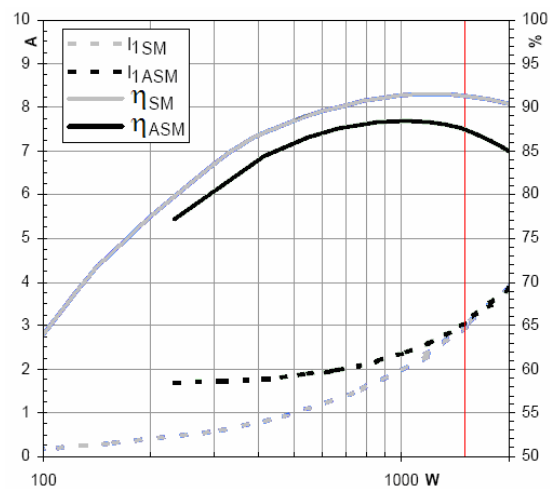


Fig. 6. Comparison between efficiency-load curves for two different 1.1-kW motors: ASM = IM; SM = PMSM [2].

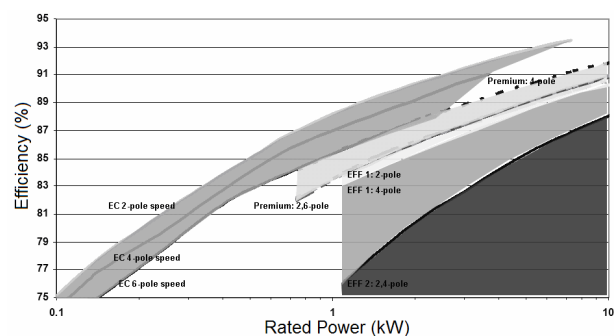


Fig. 7 Full-load efficiency limits of EC/PM motors (source: EBM-Papst, 2007).

C. Some Economic-Analysis Related Definitions

Simple payback, SPB , is given by (1), where C is the investment (or additional investment) and the S is the savings in a given period (e.g., month or year).

$$SPB = \frac{C}{S} \quad (1)$$

Discount rate, r_d , is a financial concept based on the future flow in lieu of the present value of the cash flow. For every discount rate there is a corresponding interest rate, r_i , and vice versa, according to (2) and (3).

$$r_d = \frac{r_i}{1+r_i} \quad (2) \quad r_i = \frac{r_d}{1-r_d} \quad (3)$$

Net present value, NPV , is a standard method for the financial appraisal of a long-term project, and it is given by (4), where NCF is the net cash flow, t is the time of the cash flow, C_0 is the capital outlay (investment or additional investment) at the beginning of the investment time ($t = 0$).

$$NPV = \sum_{t=1}^n \frac{NCF_t}{(1+r_i)^t} - C_0 \quad (4)$$

Rate of return, ROR , corresponds to the r_i in (4) that leads to $NPV = 0$.

Payback period, PB , is the time required for the cash inflows to equal the original outlay.

A cost-benefit analysis is an alternative capital budgeting method, which includes issues other than cash, such as time saving, technical advantages, etc.

Note that, in some equations, the discount rate corresponds to the interest rate minus inflation rate, being this denoted as r_{ii} . In this thesis it is assumed an interest rate of 4% and an inflation rate of 2%, therefore the considered discount rate is $r_{ii} = 2\%$. In some cases two values are used, 2% and 10%. The first value reflects a social perspective whereas the higher value represents a typical perspective of an industrial or commercial consumer.

The expression to calculate the cost of the conserved energy, CCE , or cost of the saved energy, CSE , is given by (5), where $c(t)$ is the flux of the measure costs (€/h), and $p(t)$ is the flow of power savings (kW), and r_{ii} the continuous discount rate (interest rate minus inflation rate). However, (5) is not practical.

$$CCE = \frac{PV(c(t))}{PV(p(t))} = \frac{\int_0^{\infty} c(t) \cdot e^{-r_{ii}t} dt}{\int_0^{\infty} p(t) \cdot e^{-r_{ii}t} dt} \quad (5)$$

Assuming small discount rates and that the energy is saved at constant rate (kWh/yr), (5) can be simplified to (6), where n is the lifetime of the conservation measure, S the annual energy savings, and AC is the annualized cost of the investment.

$$CCE = \frac{AC}{S} \quad (6)$$

The annualized cost for a system over a period with n years can be calculated by means of the summation of all the annualized costs of the present values of all the investments made in the considered period, including annual constant investments, for example, in maintenance. Regarding discounting, the initial investment, C_0 , occurs in the present, thus no discounting is necessary. For constant annual investments, C , and one-

time investment in the year t , C_t , the present discounted value, PDV , is given by (7) and (8), respectively.

$$PDV = C \cdot \frac{[1 - (1+r_{ii})^{-n}]}{r_{ii}} \quad (7)$$

$$PDV = C_t \cdot (1+r_{ii})^{-t} \quad (8)$$

The total present discounted value is given by (9).

$$PDV_{total} = C_0 + \sum_{j=1}^n PDV_j \quad (9)$$

In calculating the service life of a system, the irregular cash flow over the entire service life is transformed into an annuity (constant annual value paid every year) for the same service life. The annualized cost is given by (10). Annualise cost equation is designed to give the annual, year-end payment that would be necessary to repay the initial investment over a write-off period of n years.

$$AC = PDV_{total} \cdot \frac{r_{ii}}{1 - (1+r_{ii})^{-n}} \quad (10)$$

Combining (10) and (6) yields (11).

$$CCE_{syst} = \frac{PDV_{syst} \cdot r_{ii}}{S_{syst} \cdot \left[1 - \frac{1}{(1+r_{ii})^n} \right]} \quad (11)$$

In order to assess the cost-effectiveness of high-efficiency components or systems, the CCE_{syst} or CSE_{syst} (in €/kWh) can be calculated using (11), where PDV is the present extra cost of the improved component(s) or system (in €), S_{syst} the energy savings (in kWh/yr) per year originated by the high-efficiency component(s) or system, and n the lifetime period of the component(s) or system (in yr). If CSE is lower than the electricity cost the investment is cost-effectiveness, otherwise is not cost effectiveness. In general, (11) can be applied to a system, considering that all components are replaced by equal components, and the extra cost in relation to the technology with lower efficiency is constant. Some exceptions can occur as when replacing a V-belt by a timing belt, in which it necessary to invest in the replacement of the pulley only initially. Therefore, proper application of (11) is necessary to avoid calculation errors. In [3], the cost-effectiveness analysis is based on CCE defined by (11), where PDV_{syst} is the cost of the equipment plus the installation and r_{ii} is considered equal to 10%.

The energy cost savings for a system with n components can be calculated using (12).

$$\begin{aligned} S_{yr} &= P_{out_eq} \cdot N_{h/yr} \cdot C_{kWh} \cdot \left(\frac{1}{\eta_{syst}} - \frac{1}{\eta_{syst} + \Delta\eta_{syst}} \right) = \\ &= P_{out_eq} \cdot N_{h/yr} \cdot C_{kWh} \cdot \left(\frac{1}{\prod_{i=1}^n \eta_i} - \frac{1}{\prod_{i=1}^n (\eta_i + \Delta\eta_i)} \right) \end{aligned} \quad (12)$$

For variable load motors with m different periods, the annual savings are given by (13), where i is a period with approximately constant output power, efficiency, and electricity cost, and motor B has an efficiency higher than that of the motor A.

$$S_{yr} = \sum_{i=1}^m \left[\left(\frac{P_{outA-i}}{\eta_{A-i}} - \frac{P_{outB-i}}{\eta_{B-i}} \right) \cdot N_{h/yr-i} \cdot C_{kWh-i} \right] \quad (13)$$

A6.2 Complement to Chapter 2

A6.2.1 Section 2.1

A. Motor Related Definitions

Efficiency of the drive system is the ratio of the power delivered by the motor shaft to the total power drawn from the input power supply, and is usually expressed as a percentage. Efficiency of the complete drive module is the ratio of the total output power delivered by the inverter to the motor and auxiliaries (motor ventilation fan, etc.) to the total power drawn from the input power supply, and is usually expressed as a percentage [12]. Motor efficiency, η , in power, is given by (14), where T is the torque, ω is the speed, P_{elec} is the real or active input power, and P_{mech} is the mechanical, shaft or useful output power.

$$\eta = \frac{P_{mech}}{P_{elec}} = \frac{T \cdot \omega}{P_{elec}} \quad (14)$$

Motor efficiency, in energy, is given by (15), where t is the duration of the operating period.

$$\eta = \frac{\int_t P_{mech} dt}{\int_t P_{elec} dt} \quad (15)$$

In a balanced, undistorted, three-phase system, the motor power factor is given by (16), where S is the apparent power or absolute value of complex power.

$$\lambda = \frac{P_{elec}}{S} = \frac{\sqrt{3} \cdot U \cdot I \cdot \cos \varphi}{\sqrt{3} \cdot U \cdot I} \quad (16)$$

In a balanced, three-phase system, with current distortion but sinusoidal voltage, the motor power factor is given by (17) [12].

$$\lambda = \frac{\sqrt{3} \cdot U \cdot I_1 \cdot \cos \varphi_1}{\sqrt{3} \cdot U \cdot I} = \frac{I_1}{I} \cos \varphi_1 \quad (17)$$

Motor load, ζ , is given by (18), and motor load factor, ζ_{avg} , is given by (19) where P_N is the motor rated power.

$$\zeta = \frac{P_{mech}}{P_N} \quad (18)$$

$$\zeta_{avg} = \frac{1}{P_N} \cdot \frac{1}{\Delta t} \int_t^{t+\Delta t} P_{mech}(t) dt = \frac{\sum_{i=1}^n \Delta t_i \cdot \zeta_i}{\sum_{i=1}^n \Delta t_i} \quad (19)$$

B. Complementary Figures on SLLs Study

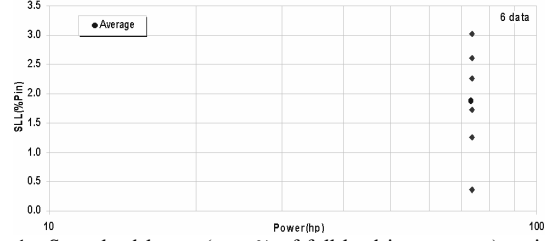


Fig. 1. Stray load losses (as a % of full-load input power) variation with motor rated power, for 6-pole, 50-Hz motors [1].

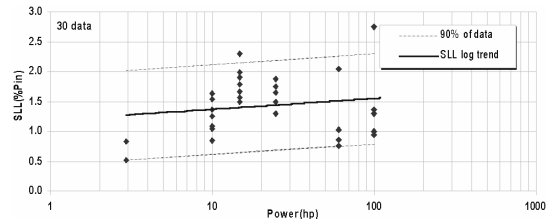


Fig. 2. Stray load losses (as a % of full-load input power) variation with motor rated power, for 4-pole, 50-Hz motors [1].

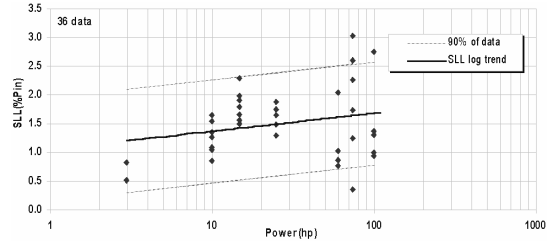


Fig. 3. Stray load losses (as a % of full-load input power) variation with motor rated power, for 6- and 4-pole, 50-Hz motors [1].

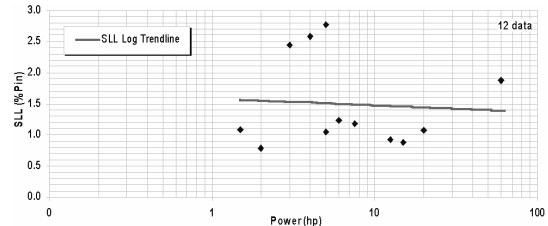


Fig. 4. Stray Load Losses (as a % of full-load input power) variation with motor rated power, for 8-pole, 60-Hz motors [1].

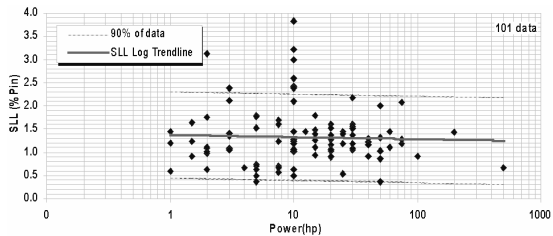


Fig. 5. Stray Load Losses (as a % of full-load input power) variation with motor rated power, for 6-pole 60-Hz motors [1].

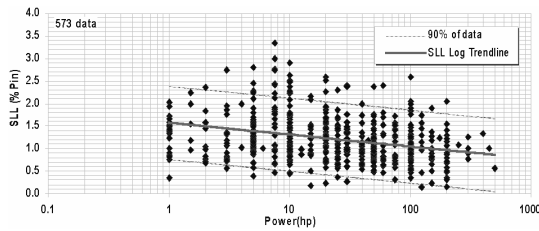


Fig. 6. Stray load losses (as a % of full-load input power) variation with motor rated power, for 4-pole 60-Hz motors. There are three additional 1-hp motors with SLL of 4.1%, 4.5% and 5.3%, which are not shown [1].

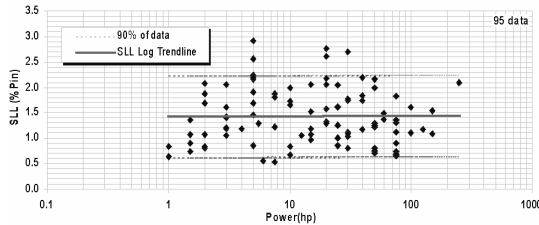


Fig. 7. Stray load losses (as a % of full-load input power) variation with motor rated power, for 2-pole 60-Hz motors [1].

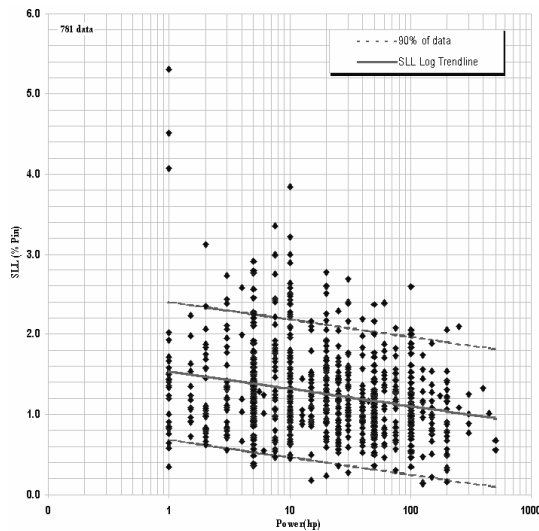


Fig. 8. Stray load losses (as a % of full-load input power) variation with motor rated power, for 8-, 6-, 4-, and 2-pole, 60-Hz motors [1].

A6.2.2 Section 2.2

A. Additional Information on Efficiency Improvement by Means of Number of Phases Increase

TABLE 1
ESTIMATED LOSSES AND EFFICIENCY FOR A 22-kW,
4-POLE, 50-HZ IM WITH DIFFERENT NUMBER OF PHASES [105].

Phases	Stator Joule Losses	Rotor Joule Losses	Total Losses	Loss Reduction	Efficiency
3	1901.0 W	1608.3 W	2659.3 W	--	89.2%
6	1773.7 W	589.0 W	2512.7 W	5.5%	89.8%
12	1743.4 W	588.6 W	2482.0 W	6.7%	89.9%

Assumptions:
Iron losses plus friction & windage losses equal to 150 W; Sinusoidal excitation; same fundamental air-gap flux; fixed stator-core design; Rated output power and speed; Stator coils do not change; Series-connected windings.

TABLE 2
COMPARISON BETWEEN THREE-PHASE AND SIX-PHASE INDUSTRIAL IMs [105].

Poles	Rating	Motor Efficiency	
		3-Phase	6-Phase
2	1.1	83.8%	85.4%
	7.5	88.6%	90.2%
	22	91.7%	92.9%
	90	95.1%	96.0%
4	1.1	79.8%	81.3%

7.5	88.6%	89.8%
22	92.3%	93.5%
90	94.3%	95.5%

B. Additional Considerations on Copper-Cage Rotors

In fact, in addition to a number of aspects that can be fine tuned for better motor performance, the main improvement comes from using more and/or better active materials, such as the die-cast copper-cage rotors that have recently reached a commercial state of development, which is the most recent introduction in the high-efficiency IM manufacturing.

While the use of more material certainly makes motors heavier, it not necessarily leads to a different frame size for a given rated power. In most cases only core is slightly longer and this can be compensated, in part, by using a smaller fan, as the thermal losses to be dissipated are lower. The outer diameter can also be increased slightly without shaft-base distance changes, preserving same frame size. The use of better quality materials allows increasing efficiency preserving frame size. For example, the difference between the outer stator core diameter in EPAct and NEMA Premium aluminium-cage rotor motors (Fig. 1) could be avoided by using copper-cage rotor technology.

Die-cast copper-cage rotor technology was introduced in the market firstly by a European manufacturer (which also introduced in the first half of 2008 a second generation of copper-rotor IMs, in the 1.1-200 kW range), but it is now being produced around the world, including China. Copper-cage rotors allow improving motor efficiency maintaining the same dimensions (or considering reduced platform variances), or, alternatively, maintain the same efficiency and reduce the rotor and motor sizes. In the first case, even considering the higher (and increasing) copper commodity prices, the aluminium-cage versus copper-cage rotors, is, nowadays, in favour of the latter option [104].

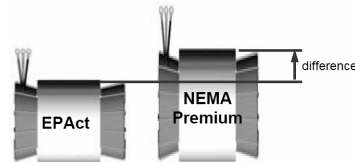


Fig. 1. Difference between the stator core outer diameter for EPAct and NEMA Premium IMs [104].

In Fig. 2, the extra aluminium-cage rotor inertia problem associated with HEMs can be seen. In general, an increase between 30% and 90% in the rotor inertia is expected for aluminium-cage EFF1-class over EFF2-class IMs, up to 30 kW. As a result, the per-hour start/stops number is considerable lower for EFF1-class IMs. That drawback can be overcome using die-cast copper-cage rotors. The result is, for the same efficiency, a better dynamic response. The potential for efficiency improvement by means of incorporating copper-cage (combined with the other efficiency-optimization factors) is so great that it can actually justify the introduction of a wholly new efficiency class, as it can be seen in Figs. 3 and 4, which show the efficiency-load curves comparison for copper- and aluminium-cage rotors. In fact, for identical design IMs, the simple change from aluminium

to copper rotor increases significantly motor efficiency over all load range.

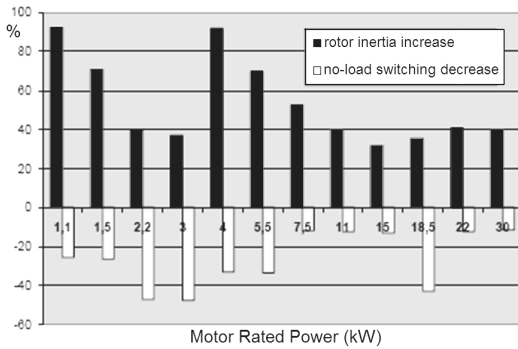


Fig. 2. Comparison between aluminium-cage rotor, EFF1-class and EFF2-class motors: rotor inertia and number of permissible start/stops per hour at no load [2], [81].

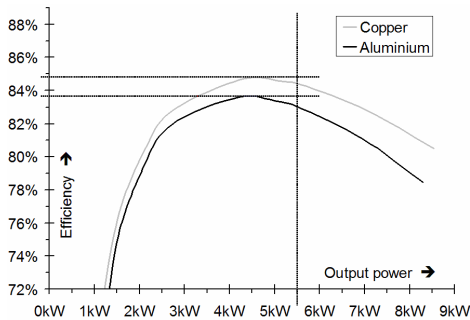


Fig. 3. Comparison of the efficiency of an aluminium and a copper rotor in an otherwise identical 5.5-kW motor [82].

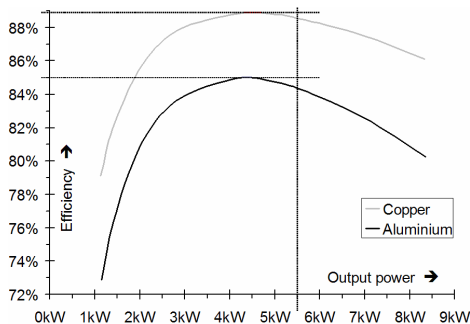


Fig. 4. Comparison of the efficiency of a simple standard (old EFF 3 class) 5.5-kW motor with that of an efficiency-optimized 5.5-kW motor containing a copper rotor [82].

Until recently, aluminium was the material of choice for die-cast cage-rotors in industrial IMs because it melts at 660°C, whereas copper, which was for a long time considered only a theoretical alternative, melts at 1083°C [82], [104]. However, as the conductivity of copper is about 60% higher than that of the aluminium, considerable effort was made over a number of years to develop a casting die that would have an economically viable lifetime⁸ when used at the much higher temperatures needed to cast copper [104]. This has been achieved with strengthened nickel-based alloy die, operated at elevated temperature [104]. The first motors with these novel rotors were exhibited at industrial equipment expositions in 2003 [82]. Most motor manufacturers are now able to produce this technology,

⁸ Die-cast copper rotors had not been economical to manufacture due to short die life, related with the higher copper melting temperature, which leads to loss of die strength, decarbonisation and oxidation of die steels, thermal shocks, and rapid thermal fatigue.

and European motor manufacturers achieved economical production of copper rotors, being done routinely. Fig. 5 shows copper-cage rotor motors from different manufacturers. Obviously, the better conductivity of the copper helps to reduce motor power losses and improve efficiency. In general, copper-cage rotors have reduced heat losses and have lower additional losses. They also provide improved control characteristic in VSD-fed IMs due to the stiffer torque-speed curve in the quasi-linear region.

In Table 3, the improvements in an 11-kW, 4-pole motor by means of replacing the aluminium-cage rotor by a copper-cage rotor are shown. Percentage rotor loss reduction with such material change is more significant for smaller motors [104]. It should be noted that the reduction of starting torque (and the consequent starting current increase) could be compensated by proper redesign of bar shape (e.g., can be used a double cage, as it can be seen in Fig. 5). In fact, complex conductor bar shape can only be made by die casting, which is a significant advantage over mounted copper bars (in medium-high power motors).

Moreover, for commercial scale production, EPAct/IE2 compliant general purpose IMs, similar operating characteristics and efficiency IMs, data on materials usage and costs from six motor manufacturers (averaged), copper-cage rotor motors redesigned to optimally use the high-conductivity cage, current⁹ metal prices, and excluding overhead burdens, copper-cage rotors benefit from weight reduction, e.g., for 7.5- and 15-hp motors (89.6% and 91.1% motor efficiency, respectively), a copper-cage rotor is 21.5% and 18.3%, lighter, respectively, than the aluminium-cage rotor design at the same motor efficiency, leading to materials cost savings of about 17.9% and 14.3%, respectively [104].

TABLE 3
CHARACTERISTICS OF AN 11-kW, 4-POLE IM WITH AN ALUMINIUM- AND COPPER-CAGE ROTOR (DIRECT REPLACEMENT MAINTAINING THE FRAME SIZE) [104].

Feature	Rotor Material		Variation	
	Aluminium	Copper	Absolute	%
Rated Rotor I ² R Losses	262 W	157 W	+104 W	-40%
Rated Efficiency	89.5%	90.7%	+1.2 p.p.	+1.4%
Rated Temp. Rise	64°C	59.5°C	-4.5°C	-7.0%
Rated Slip	2.22%	1.37%	-0.85 p.p.	-38%
Rated Speed	1760 r/min	1775 r/min	+15 r/min	+0.85%
Rated Power Factor	0.815	0.790	-0.025	-3.0%
Starting Torque	58.2 N.m	37.0 N.m	-21.2 N.m	-36%
Breakdown Torque	152 N.m	125.9 N.m	-26.1 N.m	-17%

One of the issues associated with copper-cage rotors was the effect that the high casting temperatures in rotor laminations. The Curie point¹⁰ of iron is at 770°C and if the magnetic sheet steel is heated above that temperature there might well be permanent consequences. As explained in [82], based on experimental results, performed to measure a number of different parameters of untreated iron and of iron that had been annealed at various temperatures, it was found that iron losses decrease and the magnetization improves, if the annealing temperature does not exceed a certain limit. Subsequent investigations showed that the high temperature does not penetrate the steel to any great depth, as it can be seen in

⁹ April, 2007.

¹⁰ The temperature at which the material loses its ferromagnetic properties.

Fig. 6-8. As the thermal conductivity of steel is about $\frac{1}{8}$ that of copper, the copper is able to conduct the heat to the outside faster than the heat can penetrate the steel-sheet core.



Fig. 5. Copper-cage rotors of different shape and size, from different manufacturers.

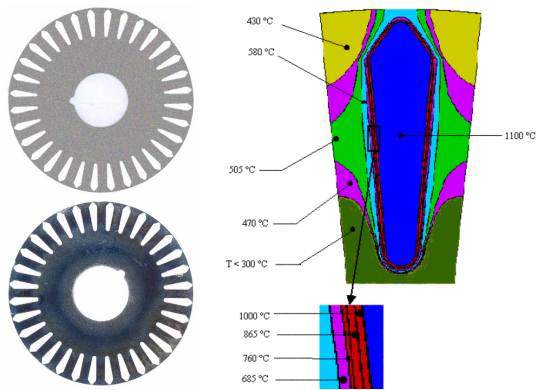


Fig. 6. View of a rotor lamination (left-top) before assembly and (left-bottom) after die-casting with copper; (bottom) Temperature distribution during die-casting [82].

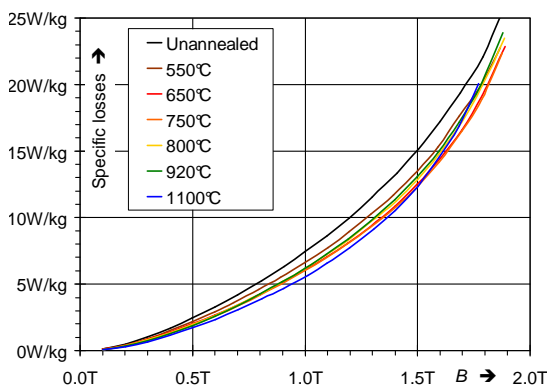


Fig. 7. Influence of the higher casting temperature for copper on the rotor lamination [82].

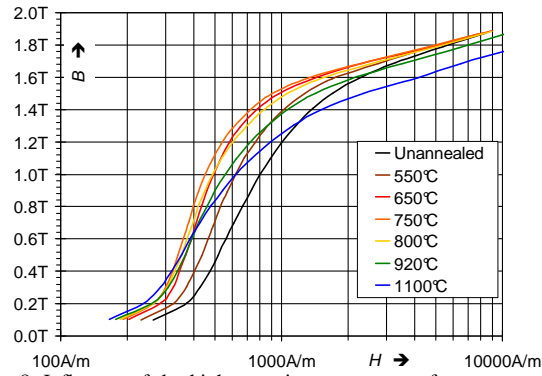


Fig. 8. Influence of the higher casting temperature for copper on the magnetization curve [82].

It is well known that the starting torque in copper-cage rotor IMs is significantly smaller than the maximum torque (see Figs. 9-11), which is achieved just at a speed very close to the nominal speed. In general, those characteristics are accentuated with the motor rated power, which have lower ohmic losses¹¹. As the motor accelerates to steady-state speed, the frequency of the rotor current and reactance decreases accordingly. The relative significance of the rotor ohmic resistance component, whose absolute magnitude remains constant (ignoring skin effect), increases as a result, and the torque increases, despite the decreasing current in the stator and rotor windings. At the rated operating point, the frequency of the rotor current decreases to very low values (e.g., for a 50-Hz, 2-pole, 2940-r/min motor, the rated slip is 60 r/min, corresponding to 1-Hz rotor frequency). At this frequency, the rotor reactance is negligible and, although the force resulting from rotor and stator fields interaction becomes lower (as a result of the lower current), it acts almost entirely tangentially, with practically the entire magnetic force being converted into mechanical torque. A certain amount of resistance in the rotor-cage is therefore required. Consequently, using copper in place of aluminium in the rotor cage leads to lower resistance and lower starting torque, accordingly. An experimental measurement performed on a 5.5-kW motor showed a starting torque reduction from 90 N.m to 85 N.m (5.6% decrease). If this small drop in the starting torque is unacceptable, the shape of the rotor slots will need to be modified so that skin effect during starting limits the effective cross-sectional area of the cage conductor bars, increasing the respective. Once the motor is running at close to full speed, the frequency will be so low that the skin effect is no longer relevant and the entire conductor cross-section can be used to carry the rotor current. If the resistance in the squirrel-cage rotor is smaller, the starting current will be higher. In the previously referred 5.5-kW motor, the experimental starting current/rated current ratio increased from 6.5 to 7.5 times for the die-cast aluminium-cage and copper-cage rotors (15% increase), respectively, as expected, since starting current is mainly

¹¹ It should be noted that if the rotor resistance is null, the angle between the rotating magnetic fields of the stator and rotor would be exactly 180° and the force between these two magnetic fields would act purely radially, i.e., its tangential component would be zero, and this purely "reactive" or "wattless" force would contribute nothing to the motor torque. Therefore, a certain ohmic resistance component is necessary, inherently resulting in power loss.

limited by the reactance, which is practically independent of the conductive material used.

Based on the foregoing discussion, for the same rotor design, replacing the aluminium by copper has, in practical terms, a moderate impact on the starting current and torque-speed curves, although in a number of applications this changes can have significant impact. Whereas the torque is smaller when the rotor is stationary due to the greater conductivity of copper¹², it is by far larger for a given steady-state speed in the quasi-linear region of torque-speed curve. It is possible to effectively choose whether to benefit from higher torque or from higher rotational speed, as it can be seen in Fig. 11. The advantage of using copper-cage rotors is that it leads to both power losses reduction and power density increase, i.e., the same output power from a smaller motor (improved dynamic response) or more output power from the same sized motor (improved efficiency). However, the benefit of using a copper-cage rotor will be the lower slip at the same current and power input levels, leading to higher motor efficiency levels. The higher mass rotor is indicated for continuous operation with a few switching cycles, in which starting losses compared with continuous losses are negligible.

The EFF1/IE2 and Premium equivalent motors are clearly cost-effective for most of the applications. However, care should be taken on the replacement of EFF3-class or EFF2-class IMs by EFF1-class IMs, since, in some cases, the improvement in efficiency can not overcome the increase in the mechanical power required by the load due to the speed increase, i.e., slip reduction, as it is represented in Figs. 9 and 10. In fact, a typical strategy to increase motor efficiency is reducing rotor resistance. However, it leads to the increase of the slope of the quasi-linear zone of the motor torque-speed curve (Figs. 9 and 10). Except for constant power loads, the power required by the load can increase significantly. This should be taken into account when calculating the savings.

Although copper with a copper conductivity rating is a better conductor than aluminium by a factor of about 60%, a higher conductivity factor can be found in copper-cage rotors due to the fact that die-cast aluminium-cage rotors tends to contain cavities and defects that are absent in the die-cast copper-cage rotors [82]. Also, the aluminium used for casting is usually an alloy containing only 99.5% aluminium. This alloy is used as it offers improved mechanical strength, but its conductivity is lower because the other alloying elements are effectively impurities [82]. An additional disadvantage of using aluminium is that the defects in the die-cast cage mentioned above can also lead to rotor unbalance. When a copper-cage rotor is used, the cooling fins can be removed (slightly reducing windage losses), since there is less heat to be dissipated, and the rotor does not need to be balanced for normal speeds (e.g., up to 3000 r/min). The much simpler design of a copper-cage rotor compared to an aluminium-cage rotor is evidenced in Fig. 5, contributing to compensate, to some degree, for the

additional costs of using what is a substantially more expensive conducting material.

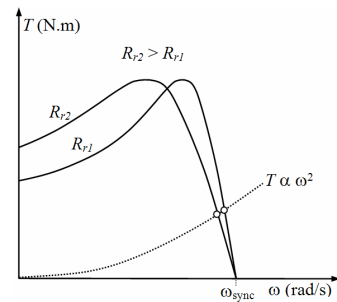


Fig. 9. Simplified torque-speed curves for IMs with different rotor resistances.

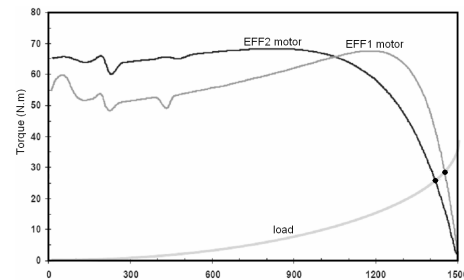


Fig. 10. Torque-speed curves for EFF1 and EFF 2 motors, showing the effect of the spatial harmonics [81].

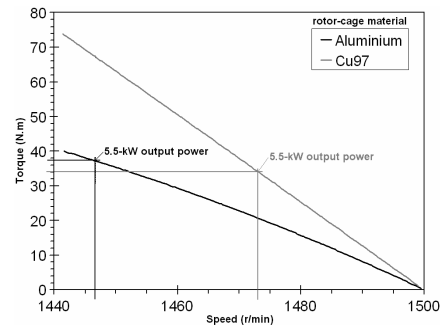


Fig. 11. Experimental operating points in the quasi-linear region of the torque-speed curve for the same output power (5.5 kW) for copper-cage and aluminium-cage rotors [82].

Once it has reached the end of its service life, such equipment is not treated as waste but as a highly sought-after source of secondary raw materials. With a density of $8.96 \text{ g}\cdot\text{cm}^{-3}$ copper belongs to the class of heavy metals, whereas aluminium has a density of only $2.70 \text{ g}\cdot\text{cm}^{-3}$ (3.3 times lower than copper density) and is classified accordingly as a light metal. When copper-cage rotor technology is used for efficiency improvement purposes, since the cross-sectional area of the rotor conductors, and hence its volume, is in principle maintained, the greater density of copper means that a copper-cage rotor will have a much greater mass and, as the kilogram price of copper is significantly larger than that of the aluminium, material costs will be substantially higher. Assuming equal size and motor efficiency improvement, a copper-cage rotor is thus significantly heavier than an aluminium-cage rotor (e.g., 33.5% higher assuming that $\frac{2}{3}$ of the rotor is composed by steel with a density of $8 \text{ g}\cdot\text{cm}^{-3}$) and its moment of inertia is greater too, as the extra mass is located around the periphery of the rotor. Therefore, if the load inertia is low, the increase in the rotor inertia can

¹² It is assumed Cu97, i.e., copper with a conductivity that is 97% of the IACS value. The casting method, which involves pre-filling the slots of the iron rotor core with a special powder that vaporizes or decomposes during casting, guarantees that the final conductivity is not lower than this assumed value.

increase significantly the starting time frame and thus the rotor losses during that period.

This may need to be taken into account when adjusting the control response of VSDs and, in extreme cases, for some applications, it may well mean that the copper-cage rotor cannot be used. An example of such application is machine tools, typically demanding that rotor is stopped or reversed extremely frequently, possibly even every second, therefore simply not possible to decelerate and re-accelerate the rotor fast enough. And even if it is possible with special control strategies, it wastes the energy saved associated with the copper rotor usage.

However, if the aim is to have the same efficiency level and the same motor frame size, copper bars allow decreasing the rotor inertia, which can be a significant advantage in the dynamic performance of the systems, but also in terms of energy savings in the case of motor with a high ON/OFF cycling rate, even without any special dynamic response requirement. In the last case, copper rotors lead to the decrease of the mechanical time constant during starting, leading to significant decrease of the rotor losses over that period.

When maximizing efficiency, the greater mass of the copper-cage rotor is beneficial, as the motor can be overloaded for longer during thermal transient periods. Despite the fact that aluminium has a significantly larger heat capacity ($900 \text{ kJ.kg}^{-1}.\text{K}^{-1}$) than copper ($380 \text{ kJ.kg}^{-1}.\text{K}^{-1}$), when expressed relative to material volume, the order of the heat capacities reverses: $2.43 \text{ kJ.l}^{-1}.\text{K}^{-1}$ for aluminium compared to $3.39 \text{ kJ.l}^{-1}.\text{K}^{-1}$ for copper. Considering same rotor size and shape, using copper for the squirrel-cage rotor therefore provides an overload capacity about 40% greater (the rotor thermal constant is higher). In this context, overload occurs during starting period (starting current rises to 5-10 times the rated current) and can occur during relatively short period over duty-cycle. In fact, during starting period, the Joule losses can be 25 to 100 times higher than that at the rated operating point. This can cause problems in some medium-large power applications, as a motor with an aluminium rotor that was switched off (possibly due to an unscheduled shutdown) and is still warm can only be switched on again after being allowed to cool for a specified period, and this can prove to be very costly in tightly scheduled production environments. Here, the copper rotor is able to store better the excess heat loss during restarting without suffering or causing damage and to gradually dissipate this thermal energy once the motor is back up and running. However, the linear dilatation coefficient difference in relation to steel is higher in the case of copper, potentially leading to higher mechanical stress during overheating periods.

Additionally, the introduction of the die-cast copper rotor has, for instance, made possible manufacturing certain fully encapsulated IMs. If such motors were to be totally immersed in water and only operated in this state, improved cooling conditions are naturally provided, and no special rotor is, in principle, required. However, if those motors were not necessarily nor exclusively to be used under water, the heat dissipation through the encapsulation can be seriously impeded. In fact, a manufacturer of such motors found that aluminium-cage

rotor IMs had stator windings rotor 5°C and 15°C hotter, respectively, than copper-cage rotor IMs, and the last solution was used [82]. This had obvious consequences on IM lifetime (lifetime roughly halved for every 10°C increase in temperature). This effect can prove to be decisive when planning the deployment of this sort of expensive and potentially hard-to-replace motor.

As already mentioned, HEMs can also be manufactured using aluminium-cage rotors and this has in fact been the norm so far but, as discussed, in general, copper-cage rotors are advantageous over aluminium-cage rotors when: (a) the electrical energy is significantly expensive; (b) the supply of electrical energy is highly restricted; and (c) there are unusual difficulties in dissipating power loss as heat.

Any proposal to save energy by using more material is always accompanied by the objection that extra energy is used in making the extra material required. Obviously, this energy has to be included in the energy balance. As end-of-life products are increasingly being recycled and fed back into the production cycle, the higher scrap value must also be subtracted from the additional cost of procurement. Manufacturing copper from ore¹³ and scrap requires about 50 and 30 GJ/t of primary energy, respectively. As most products incorporating significant copper amounts enjoy an average 15- to 30-yr long service life, and as the copper market 15 and 30 years ago was about $\frac{3}{4}$ and $\frac{1}{2}$ of present market, respectively, the estimated rate of recovery and reuse of the copper used at those times is estimated to be about 60 and 90%, respectively [82]. However, recovery and reuse rate should be expressed relative to present production levels and, on the basis of the previous values, presently, it is estimated that approximately 45% of the copper produced in Germany is from reprocessed scrap [82] but, for the sake of simplicity, it can be assumed as 50%, resulting in an average energy consumption for copper manufacturing of 40 GJ/t. Assuming an overall efficiency for the generation and distribution of electric power of 33% (i.e., per each kWh of electricity saved in the motor, 3 kWh of primary energy are saved [82]), which approximately reflects the situation in Germany, the resulting primary energy loss relationships can be estimated, being presented in Fig. 12. For example, if the current density is equal to 3 A/mm^2 , copper power losses of 17.64 W/kg (Fig. 12, left) are generated, and it will take approximately 206 h of full-load operation to equalize the motor copper losses to the primary energy spent to produce the copper (Fig. 12, middle). Alternatively, for a given current, considering 10 A/mm^2 and 1 kg of copper as the base case, it will take roughly 270 h to save the energy (by means of loss reduction) necessary to produce the additional used copper ($3.33 \text{ kg} - 1 \text{ kg} = 2.23 \text{ kg}$) to reduce the current density to 3 A/mm^2 (Fig. 12, right), providing the same conductor length. It is interesting to note that there is an optimum value for the current density, which minimizes the time period to recovery additional energy spent on the extra copper production, as it is evidenced in Fig. 12, right). This time period can be interpreted as an environmental payback period and is clearly very short, significantly shorter than the already

¹³ An ore is a volume of rock containing components or minerals.

short financial payback period. However, the environmental payback period strongly depends on the target motor efficiency level. If the desired efficiency improvement is small, then the required amount of material (in this case, copper) is also small.

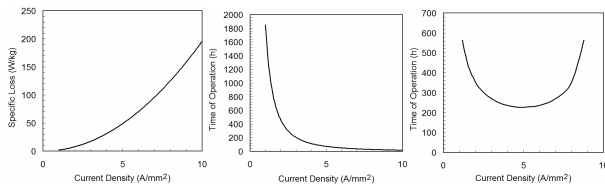


Fig. 12. Energetic payback from using more copper considering full-load motor operation: (left) specific copper losses as a function of current density; (middle) time of operation to equalize losses and copper production primary energy as a function of current density; (right) operating time to recovery the additional primary energy spent to produce the additional copper, as a function of current density, assuming 10 A/mm² current density and 1 kg copper as the reference or base case.

As shown, the IMs performance can be improved through the use of more and better materials and improved design. If these improvements are implemented, practically all motors operating a large number of hours per year will, over their extended lifetime (due to lower losses and operating temperature), yield savings equivalent to the purchase of several new motors. Additionally, for a given torque, the angular speed of HEMs is in general higher due to the lower rotor resistance. In loads with a cubic relation between power and speed (e.g., centrifugal pumps and fans), this can lead to extra energy consumption, attenuating the potential savings associated with the efficiency improvement. For such loads, increasing the motor speed by, for example, 1% (of the nominal value) leads to an increase in output power of almost 3% (of the nominal value) that more than overrides the reduction in losses. In fact, some users have registered an increase rather than a decrease in energy consumption due primarily to the smaller slip that accompanies the use of low-resistance rotors. Whether or not this additional input power, which is delivered to the motor shaft as additional mechanical output power, is regarded as a loss depends on the specific application. In VSD-fed IMs, this problem does not exist. Problems with the higher starting current and longer starting period (due to the higher rotor inertia) can also occur, requiring in some cases resizing of power supply and of protection and command devices.

This demonstrates the need of an overall motor management programme in the industrial plants. For example, less efficient IMs can be readapted to low operating hours applications, and replaced by new HEMs. In general, from an economical point of view, it is cost-effective to invest in HEMs: (a) for new applications, (b) when a standard IM fails, and (c) when the in-operation standard IM is strongly oversized. The replacement of a healthy, well-sized standard IM is rarely a good option, since the extra cost corresponds to the overall HEM cost. For new applications, payback times can vary between 0.8 yr and 2-3 yr for the 0.75-70 kW power range and 4000 h/yr of operation. For most industrial applications, even if the standard motor is free, its LCC is higher than that of a high-efficiency or premium-efficiency motor. It should be noted that, as the motor rated power increases,

in the replacement of an EFF2-class by an EFF1-class motor, although the percentage energy savings decrease, the absolute energy savings costs increase, as it can be seen in Fig. 13.

Experimental tests were carried out for EFF1- and EFF2-class motors (main characteristics shown in Table 4). The EFF1-class motor integrates copper-cage rotor. Both motor were commercially available. They have different weights, but represent the typical situation for which it is necessary to evaluate the savings and payback for a given application.

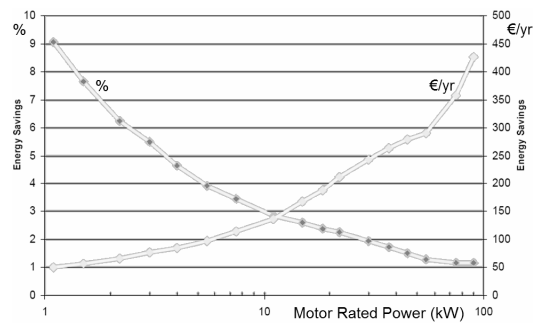


Fig. 13. Energy saving potential of replacing an EFF1-class by an EFF2-class motor (3840 h/yr, 100% load, 0.1 €/kWh)[81].

TABLE 4
NAMEPLATE DATA OF TWO 400-V, 50-Hz,
4-POLE 1.1-kW IMs OF DIFFERENT EFFICIENCY CLASSES.

Relevant Characteristics	Standard Motor	High-Efficiency Motor
Rotor Cage	Aluminium	Copper
Efficiency Class	EFF2	EFF1
Cooling Type	TEFC	TEFC
Rated Speed	1400 r/min	1460 r/min
Rated Power Factor	0.77	0.78
Rated Current	2.8 A	2.45 A
Weight	16 kg	19 kg
List Price (year 2002, no discounts)	135 €	170 €

The tested motors have the characteristics shown in Table 5. The main results are presented in Figs. 22-27.

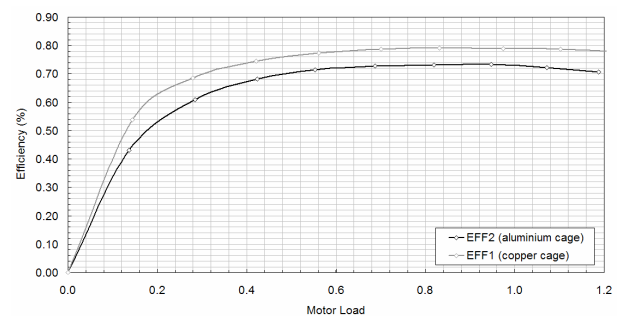


Fig. 14. Experimental efficiency-load curves (1.1-kW, 4-pole IMs).

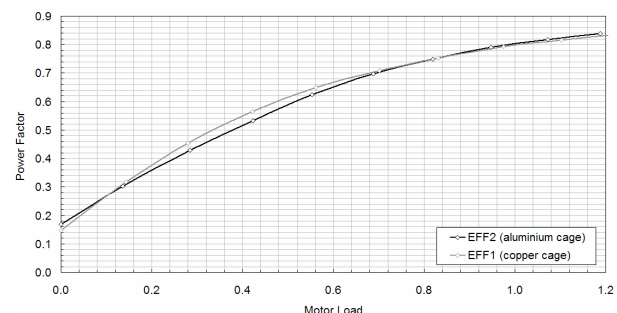


Fig. 15. Experimental power factor-load curves (1.1-kW, 4-pole IMs).

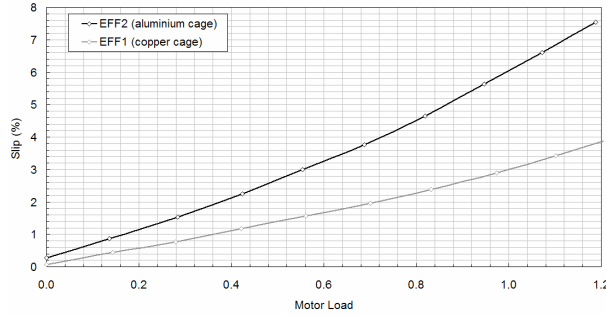


Fig. 16. Experimental motor slip-load curves (1.1-kW, 4-pole IMs).

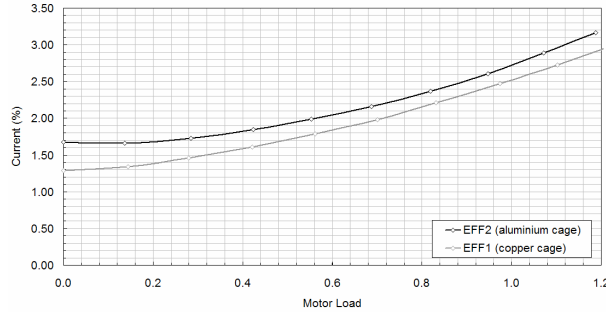


Fig. 17. Experimental motor current-load curves (1.1-kW, 4-pole IMs).

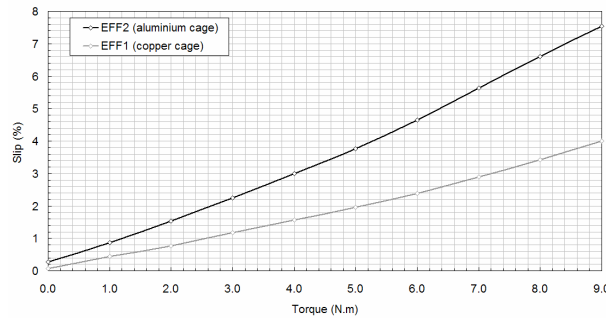


Fig. 18. Experimental motor slip-torque curves (1.1-kW, 4-pole IMs).

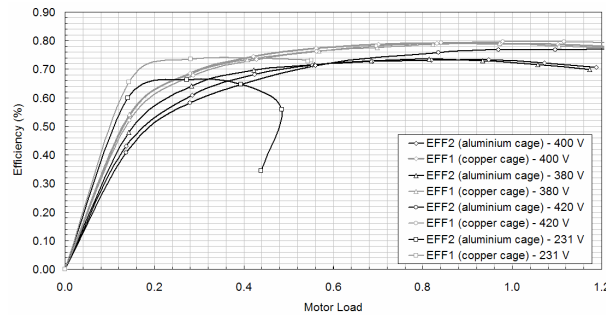


Fig. 19. Experimental efficiency-load curves (1.1-kW, 4-pole IMs).

An example of application of the tested motors is analysed next. The payback time is given by the quotient between the cost difference and the savings. It is considered a centrifugal fan, 8000 h/yr and 0.06 €/kWh. The operating point for a centrifugal fan will be different due to the lower slip of the copper rotor motor. For the considered application, the EFF2-class IM will operate with 94.1% load and the copper-cage rotor motor will operate with 98.6% load, due to the increased speed. The annual savings are

$$S_{€/yr} = \left(\frac{1.035}{0.735} - \frac{1.085}{0.785} \right) \cdot 8000 \cdot 0.06 \approx 12.5 \text{ €/yr,}$$

and the simple payback for the additional investment (35 €) is 2.8 yr, which is attractive. Additionally, due to the lower temperature, an extended lifetime and a lower motor maintenance cost are expected.

Considering a repair scenario, a 1% decrease in the EFF2-class motor efficiency after repair and a repair cost of 40% of the new standard motor price (54 €) can be assumed, yielding

$$S_{€/yr} = \left(\frac{1.035}{0.725} - \frac{1.085}{0.785} \right) \cdot 8000 \cdot 0.06 \approx 21.8 \text{ €/yr,}$$

and the simple payback is 5.3 yr, which is much less attractive.

Considering replacing the in-operation EFF2-class motor by the EFF1-class motor, the payback would be 13.6 yr, which is not an economical option, unless the replaced motor is used in other application (with reduced number of operating hours), leading to a 2.8-yr payback.

Typically, for new applications, the payback time for the extra cost of high-efficiency over standard motors is up to 3 yr, and it decreases with the increase of the power rating, the number of operating hours and the electricity price. Since the typical useful lifetime of an IM is about 12 to 20 yr, it can be concluded that, in general, high-efficiency motors are a good option for new well-designed applications, even considering the slight increase in the motor speed (for VSD-fed IMs this aspect can be ignored).

D. Notes and Examples on EMODS Overall Optimization

Conveyor Systems - As a source of motion, a conveyor consists in a belt adapted to continuously carry a load between two points. Conveyor systems are widely used in Industry to handle materials or packages. They can also be found in many services, such as baggage handling in airports (see Appendix 7). The escalator systems are very similar to elevating conveyor systems. The main components are the motor, the mechanical transmission, the conveyor and, eventually, a VSD. In order to illustrate the overall system optimization, an example is presented, based on a case study presented in [106]. It is considered the implementation of a new 0.75-kW horizontal conveyor system to handle mineral rocks in an extraction plant, which operates 8000 h/yr. The average electrical energy is assumed to be 0.07 €/kWh. In order to reduce the power required by the conveyor, it is operated at $\approx 60\%$ of rated speed. It is considered a 155-N.m steady-state torque and a 235-N.m starting torque (1.52 times the steady-state torque during 1% of the overall operating time). The conveyor input is 0.45 kW, since it is operating at 60% of rated load, due to the speed reduction.

For a helical-worm geared system, with a 0.75-kW 4-pole motor (73% load) and a VSD, the system efficiency is:

$$\eta_{conv-systA} = \eta_{vsd} \cdot \eta_{mtrA} \cdot \eta_{gearA} = 0.96 \cdot 0.72 \cdot 0.82 = 0.567.$$

For a helical-bevel geared system, with a 0.55-kW 4-pole motor (86% load) and a VSD, the system efficiency is:

$$\eta_{conv-systB} = \eta_{vsd} \cdot \eta_{mtrB} \cdot \eta_{gearB} = 0.96 \cdot 0.69 \cdot 0.95 = 0.629.$$

Note that the 0.55-kW motor is still able to provide the required starting torque. It should be noted that 0.55-kW

and 0.75-kW motors have the same frame size. The improved system leads to savings of 44.17 €/yr.

Additionally, the investment is lower for the most efficient system due to the motor power reduction and gear cost reduction. This is a win-win choice.

During starting period gear unit B has a low efficiency due to the friction between the crown wheel and the worm lead, and a nominal steady-state efficiency of 64% to 96%. During starting, gear unit A has efficiency very close to the steady-state nominal, which is 95%. However, the consumed energy during starting period is negligible in relation to the steady-state consumption. Only transient torque overloads should be taken into account, in order to size properly the motor starting torque.

In general, a 10% energy saving potential can be stated for this sort of systems, considering only system efficiency improvement, but much more savings can be obtained if the conveyor speed is reduced and, simultaneously, the handled quantity over the conveyor is increased.

Compressed-air systems - Compressed-air is a frequently used energy source in industry. In compressed-air systems, an electrical motor drives a compressor, and the compressed-air is stored, treated (dry, filtered, etc.), and distributed, though a network of pipes, all over the production site to the end-use devices (car industry robots, high-pressure spraying pistols, etc.). System performance depends on the performance of each element, yet overall system design and operation have an even greater influence on performance. In Portugal, pump systems use about 19% of the electrical energy in Industry (2.9 TWh/yr). European studies demonstrate that approximately 75% of the exploitation costs are for the consumed energy, 12% for maintenance and 13% for the capital investment. In most cases the system efficiency is about 10%. This form of energy (compressed air) is expensive (0.006 to 0.03 €/N.m³) and should be well controlled. Together with the use of HEMs and VSDs, the following technical measures could improve the overall performance of a compressed air system: (a) optimal choice of the type of compressor for specific end-use applications; (b) improvement of compressor technology (e.g., multi-stage compressors); (c) use of sophisticated control systems, including speed variation; (d) recovery of heat for use in other functions; (e) improvement of air treatment (e.g., drying, filtering); (f) improvement of overall system design, including the introduction of multi-pressure systems; (g) improvement of air flow in pipe-work to reduce the pressure losses caused by friction; (h) reduction of air leaks; (i) optimization of specific end-use devices; and (j) input air cooling.

According to a number of studies, the saving potential in compressed-air systems is on average 25%, but can be up to 33% when HEMs, VSDs and air leakage reduction are considered simultaneously.

Pumping systems - Pumps are machines with rotary blades used to maintain a continuous flow of liquids. There is a very wide range of pumping applications, from industrial dishwashers to large pumps in the cooling circuit of power stations. This wide use produces a broad

spectrum of available pump types. The improvement of pumping systems efficiency is achieved mainly by selecting the correct pump for the application and working conditions. Important factors are the design of the section head of the pump, the pump flow, the design of the pump impeller, the properties of the fluid, and the motor speed selected. In a pumping system, the replacement of the existing motor by a high-efficiency or premium motor, integration of a VSD for flow control, removing throttle valve, replacement of typical pipes by low-friction pipes, and replacement of the pump by a better one, significant savings can be obtained.

In Portugal, they use approximately 16% of the electrical energy in Industry and 25% of the worldwide consumption. A saving potential of 40% can be achieved considering an average period of 15 to 20 years. The main pump types are the centrifugal and the positive displacement. The centrifugal pumps, sharing approximately 85% of the market, represent a high saving potential, since 60% to 70% of the pumping system are oversized, many of them in more than 20%. Typically, the consumed energy cost represents 85% of the life-cycle cost, being the remaining 15% associated with maintenance (10%) and initial investment (5%).

In [2], a case study is presented on pumping system optimization, identifying a total saving potential of about 44%. In the considered system, for a specific operating point, the original efficiency, considering the motor, pump and throttle-based flow regulation was:

$$\eta_{pump-systA} = \eta_{transf} \cdot \eta_{mtr-IE1} \cdot \eta_{pump} \cdot \eta_{throttle} = .$$

$$= 0.986 \cdot 0.943 \cdot 0.604 \cdot 0.625 = 0.351$$

Optimizing this system, i.e., incorporating speed control with a VSD removing output throttle, and taken into account the potential motor efficiency decrease due to the extra losses associated to PWM-power supply and the potential transformer efficiency increase, the resulting efficiency was:

$$\eta_{pump-systB} = \eta_{transf} \cdot \eta_{vsd} \cdot \eta_{mtr-IE1} \cdot \eta_{pump} = .$$

$$= 0.988 \cdot 0.962 \cdot 0.934 \cdot 0.704 = 0.625$$

The resulting 44% savings are very significant. However, for this sort of system, since there is a flow regulation over overall duty cycle, the energy savings should be made over the entire duty cycle period, and the corresponding energy efficiency (or average power efficiency) should be obtained, considering all operating points. This demonstrates the complexity of the evaluation and optimization, but, above all, shows the significant potential associated with speed variation.

Moreover, in pump systems, case studies demonstrate that, for example, in a 250-m pipe, increasing diameter from 50 mm to 80 mm, the respective efficiency increases from 37% to 83%, and a reduction in power of 2.19 kW is obtained (3.95 kW to 1.76 kW), corresponding to a saving potential of about 55%.

For more complex systems, e.g., incorporating water storage, as water utilities, other factors should be taken into account as the possibility of deviate and extend the pumping period to the reservoirs, in order to match as much as possible the off-peak power periods, in which the electricity is generally cheaper, and reduce the fluid speed, in order to decrease the friction losses in the piping

system. These strategies may require the increase of the reservoirs capacity and, therefore, additional investment.

According to [101], in large pumping stations requiring output pressure/flux soft-starters and VSDs should be used, to optimize the investment without losing control capability (e.g., 6 pumps with soft-starting and 1 pump with speed control allow continuous output pressure/flux control, avoiding the investment in 7 pumps with speed control for the same purpose).

Ventilation systems - Fans are machines with rotary blades used to maintain a continuous flow of gas, typically air. The most common types are the axial and the centrifugal fans. They range from very small ones used to cool electronic components of computers, to very large ones such as combustion air fans used in power stations. The opportunities for reducing energy consumption of fan systems, in addition to the application of HEMs and VSDs, include: (a) choosing a high-efficiency fan, primarily influenced by blade geometry and casing shape; (b) designing the ventilation system for minimum loss during the required duty, including the length, cross-section, position, and bending of ducts¹⁴; (c) choosing the best fan for the application; (d) choosing the best type of control to regulate the fan speed.

In Portugal, the consumption of the fans represents, on average, 12% of the energy consumption in industrial plants. Energy savings from 5% to 30% are possible in most installations, with a typical payback up to 2 years.

For example, in a centrifugal fan system integrating a VSD, a 5-kW IM, a V-belt transmission, and a centrifugal fan, ignoring the air-conduit output system, the efficiency for a specific load point (fixed speed) is given approximately by:

$$\eta_{fan-systA} = \eta_{vsd} \cdot \eta_{mtr-IE1} \cdot \eta_{v-belt} \cdot \eta_{fan} = 0.96 \cdot 0.85 \cdot 0.94 \cdot 0.81 = 0.62,$$

meaning 62% energy efficiency (relation between useful fan energy and input energy).

Replacing the IE1-class motor by one of IE2-class and the smooth-V belt by a cogged-V belt, the efficiency can be improved to:

$$\eta_{fan-syst} = \eta_{vsd} \cdot \eta_{mtr-IE2} \cdot \eta_{v-belt-cog} \cdot \eta_{fan} = 0.96 \cdot 0.89 \cdot 0.98 \cdot 0.81 = 0.68,$$

meaning a 6 p.p. efficiency improvement.

If speed variation is considered instead of throttling for airflow regulation, the energy efficiency of the overall centrifugal fan system can be significantly improved, being this issue addressed in Section A6.3.

Refrigeration systems - In Portugal, The industrial refrigeration represents 4% of the electrical energy in industry, which is equivalent to 1.4% of the overall electrical consumption in Portugal. It is estimated that 80% of the 0.63 TWh consumed by the refrigeration systems is associated with agro-alimentary sector. The saving potential is estimated to be 20%, meaning approximately 0.13 TWh/yr in Portugal. Here, pump, fan and compressor rules apply, but additional considerations should be referred as cooling production as a function of the actual needs, installation of heat recovery system in

¹⁴ In [118], it is demonstrated by a case study that increasing conduits diameter from 0.9 m to 1 m in an industrial ventilator leads to a saving potential of 34%, and increasing conduit bending radius from 0.25 m to 0.5 m leads to a saving potential of 37.5%.

the main compressor, improvement of the thermal insulation of the cooling circuit, control of the cooling fluid flow, regulation of the air flow in the condensers, and integrated continuous control of all variables as a function of the temperatures, just to name a few. Case studies on cold production demonstrate that replacing a pump with conventional speed control (constant head) by a pump with optimized speed control, the system power can be reduced in 38% (saving potential).

Belt conveyor systems – It is considered now that a belt conveyor is required in a plant to convey 6 m³ of dry sand (about 10 t) per hour. The conveyor belt has 1.2-m wide belt and runs on rollers, the transport line is 14-m long, and the lifting height is 2.5 m. A geared motor drives one of the two driving pulleys. The shaft power demand is 0.8 kW. The plant is to run 15 h/day, 230 day/yr. Assuming 0.08 €/kWh, for a 0.8-kW worm-gear based system, the gear, motor and system efficiency are 72%, 75% and 54%, respectively, being the motor rated power of 1.5 kW, leading to a running cost of 414 €/yr. For a 0.8-kW bevel-gear system, the gear, motor and system efficiency are 95%, 71% and 67%, respectively, being the motor rated power of 1.1 kW, leading to a running cost of 304 €/yr. The acquisition cost for both systems is approximately 500 €. Therefore, 110 €/yr savings can be obtained with the bevel-gear system in the new construction of the plant. Even the replacement of an old gear system will pay off after ≈ 3 years [103].

Elevators/Lifts – In [101], an energy saving of 77% (31 Wh/trip to 7 Wh/trip) in a 1250-kg, 1-m/s elevator is referred after replacing a 2-speed IM based system (installed in year 1970) by a VSD-fed geared IM (with regeneration capability).

More examples of energy savings obtained in EMODS with the use of VSDs can be found in [103].

A6.2.3. Section 2.5

A. Automatic Systems for Motor Efficiency Measurement

For the direct-method-based standards, the calculations require the load test and the no-load test with different voltage levels to estimate the iron losses and windage and friction losses. The main modules of the system are (Fig. 1): dynamometer (Magtrol, model HD-815-8NA), auto-transformer (Slidac, 230-295V, 20A), automated Voltage Regulator (Powerex), DC sources (HP, model E3631A), Pentium PC, data acquisition board (National Instruments, PCI-MIO 16E-4), power analyzer (Yokogawa, WT1030M), GPIB board and signal conditioning electronics.

Regarding power quality control, the automatic voltage regulator (AVR) ensures that supply voltage unbalance does not exceed 0.5%. Harmonic distortion can increase steeply the losses of electrical motors and therefore decrease the efficiency values of the motors being tested. The total harmonic distortion of the 3-phase supply is (and should be) under 1%. If a test facility has nearby factories with arc furnaces, large variable speed drives or other significant non-linear loads, power quality may be low. In these cases, there may be a need to install

harmonic filters to reduce voltage harmonic distortion to less than 1%.

The speed and torque measurement is provided by the dynamometer optical encoder and load cell, respectively. These signals are processed by the power analyzer, which automatically calculates the mechanical power.

The computer data acquisition board analogue output is connected to a power operational amplifier, which feeds the dynamometer winding. Therefore it is possible to use the computer to control the load torque from minimum residual to maximum torque given by the dynamometer. The maximum power that can be handled continuously by the dynamometer is 5.5 kW.

The motorized autotransformer¹⁵, connected after the AVR, allows the voltage amplitude variation from zero to 127% of line voltage (max.: 511 V, line-to-line). The incorporated motor is controlled by solid-state relays connected to the data acquisition card analogue output. Therefore it is possible to use the computer to fully control the amplitude of the voltage applied to the motor.

The operating temperatures are measured by thermocouples and thermistors connected to the data acquisition card analogue inputs. The system has capacity to read simultaneously the temperature in 5 points. The distributed motor internal temperature is estimated from the stator winding electrical DC resistance measurement. In this process the line voltage must be disconnected and the motor stopped, and a DC voltage is applied to the windings (by means of a relay). The resultant current, after its conversion to a proportional voltage, is acquired with the data acquisition board and processed.

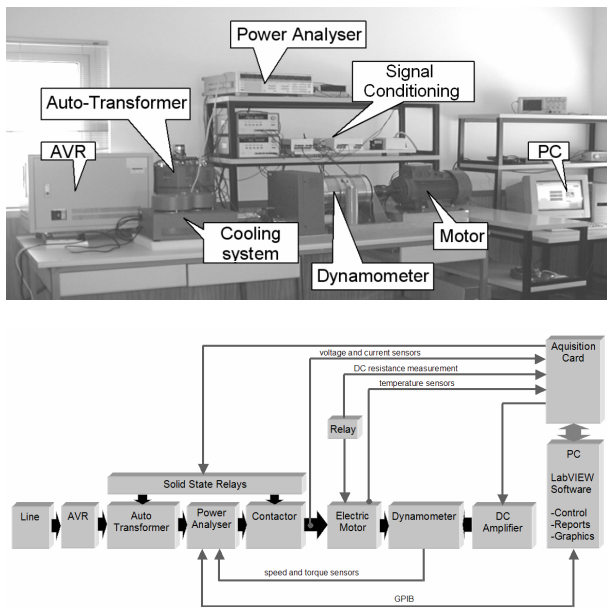


Fig. 1. Testing facility photograph and block diagram .

The voltage, current, power factor, active power, reactive power, apparent power, harmonics, total harmonic distortion and frequency are measured directly by the three-phase power analyzer which has data communication with the PC. The instantaneous voltages and currents values are measured by voltage and current sensors, connected to the acquisition board (these

¹⁵ The autotransformer use can be avoided if the motor load setup is able to drive the motor under test at synchronous speed (e.g., using a VSD-fed IM as load).

measurements are not needed for efficiency measurement purposes).

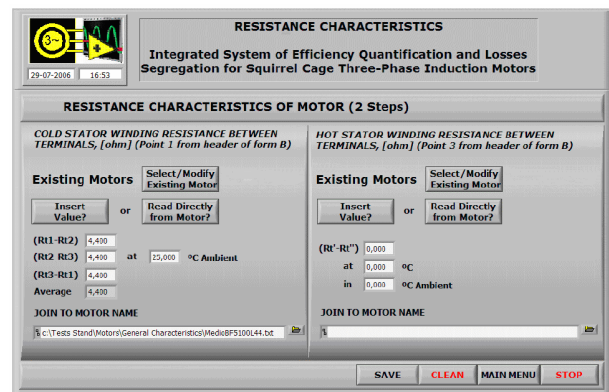
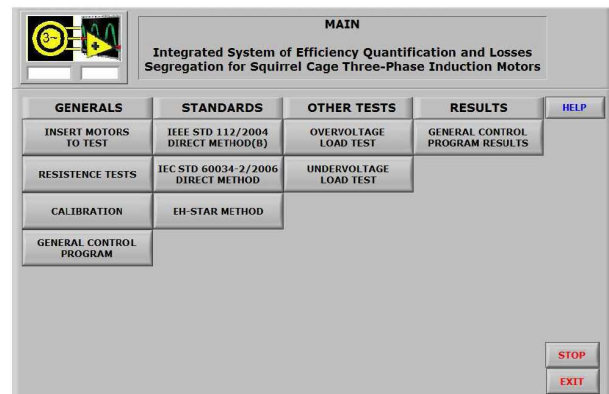
The user-friendly developed software interface (LABVIEW environment, Fig. 2) can generate automatically the efficiency and power factor curves as a function of the load, allowing an easy analysis of results and measurements. The software controls the equipment and data acquisition and performs mathematical operations and allows the visualization of results in tables and graphs.

As an example of application, a comparison of the performance of low-power, low-voltage, die-cast copper-cage rotor 4-pole, 400-V, 50-Hz, 1.1-kW IMs with die-cast aluminium-cage rotor IMs was carried out, using IEEE 112-B.

For both motors 2 tests were performed. One is the load test with different 6 load points, decreasing from approximately 150% to 25% of nominal torque. The other is the no-load test for iron losses as well as for friction and windage losses calculation, with voltages decreasing from 125% of the rated voltage to the point where voltage reduction starts to increase significantly the current. After the load and no-load tests, the user can automatically visualize (and print) the results in table and graphical forms, including the efficiency, power factor and the losses.

In Fig. 3 the losses distribution variation with the load is presented for the aluminium squirrel cage induction motor (1.1 kW, 4 poles) and for the copper squirrel-cage induction motor (1.1 kW, 4 poles). In Fig. 4 the efficiency and load factor variation with load can be seen for both motors.

The efficiency and power factor of the copper squirrel-cage motor is significant higher (at all load points).



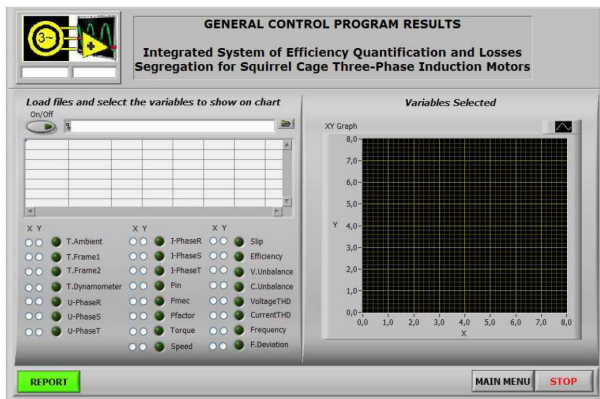
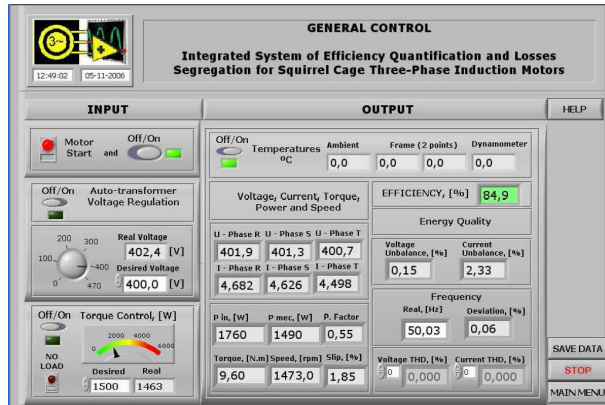
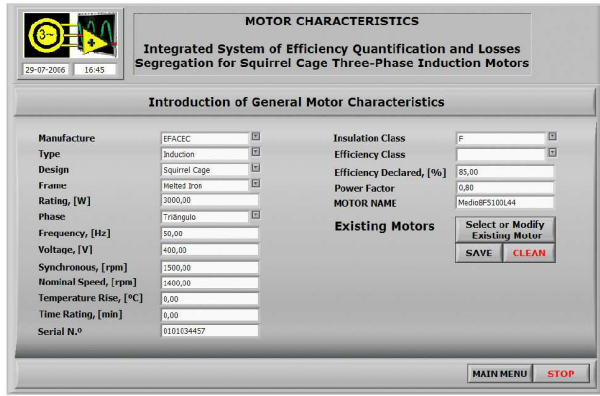


Fig. 2. Main control panels of the software developed to control the motor test bench shown in Fig. 1.

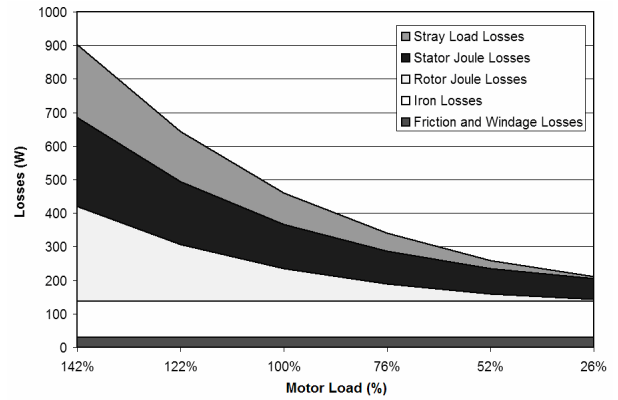
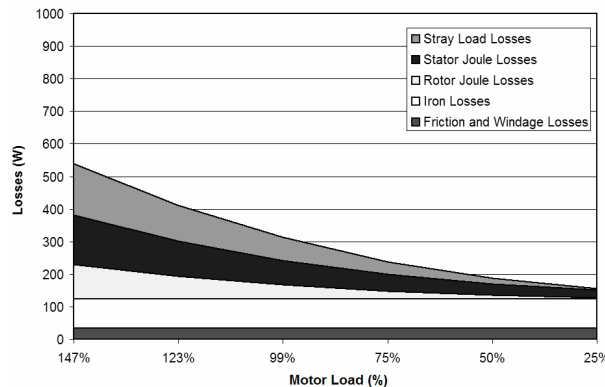


Fig. 3. Variation of losses with load in a 1.1-kW, 4-pole IM: (top) copper-cage rotor; (bottom) aluminium-cage rotor.

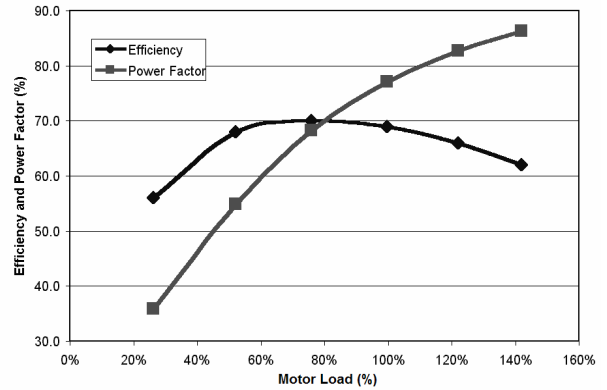
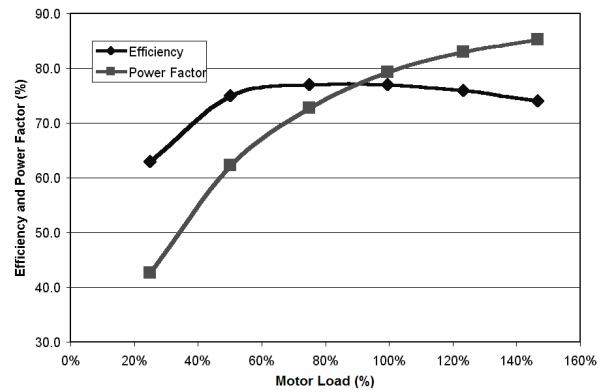


Fig. 4. Variation of efficiency and power factor with load in a 1.1-kW, 4-pole IM: (top) copper-cage rotor; (bottom) aluminium-cage rotor.

A6.3 Complement to Chapter 3

A6.3.1 Section 3.1

A. Harmonics Related Definitions

Harmonic content is the quantity obtained by subtracting from an alternating quantity its fundamental component. From a practical approach and with inter-harmonics neglected, the RMS value of the harmonic content, Q_h , is given by (1), where h is the harmonic order, Q_h is the RMS value of harmonic component of order h , and Q can represent either current, voltage or other alternating quantity [12]. Load-side harmonic content is a function of the inverter waveform and load reactance.

$$Q_h = \sqrt{\sum_{h=2}^{h=n} Q_h^2} \quad (1)$$

Total harmonic distortion, THD , is relative to the fundamental component of the considered quantity and the total harmonic factor, THF , is relative to the RMS value of the considered quantity, being defined by (2) and (3), where Q_1 and Q are the fundamental and total RMS values [12].

$$THD = \frac{\sqrt{Q^2 - Q_1^2}}{Q_1} \quad (2)$$

$$THF = \frac{\sqrt{Q^2 - Q_1^2}}{Q} \quad (3)$$

The difference between THD and THF can be significant for both voltage and current. It is important to note that these definitions include inter-harmonics¹⁶. When inter-harmonics are present, the waveform is no longer periodical, which can produce more complex effects than those produced by harmonics. If inter-harmonics are negligible, the equations (2) and (3) can be simplified to (4) and (5).

$$THD = \frac{\sqrt{\sum_{h=2}^{h=40} Q_h^2}}{Q_1} \quad (4)$$

$$THF = \frac{\sqrt{\sum_{h=2}^{h=40} Q_h^2}}{Q} \quad (5)$$

The summation is extended to and includes order 40, according to IEC common practice [12]. For particular use, the highest frequency content of THD (order h from 14 to 40 inclusive) is named partial harmonic distortion coefficient, PHD , and the even content (where order h is only even) is named even harmonic distortion coefficient, EHD , given (6) and (7), respectively.

$$PHD = \frac{\sqrt{\sum_{h=14}^{h=40} Q_h^2}}{Q_1} \quad (6)$$

$$EHF = \frac{\sqrt{\sum_{h=2, \text{even}}^{h=40} Q_h^2}}{Q_1} \quad (7)$$

A6.3.2 Section 3.2

A. Considerations on Harmonics Associated with VSDs

The effect of one or more harmonic sources on a power system depends primarily on the system frequency response characteristics. The nonlinear devices or loads¹⁷ can be represented generally as current harmonic sources. Therefore, the harmonic voltage distortion on the power system depends upon the impedance versus frequency characteristics seen by those current sources. This phenomenon is illustrated in Fig. 1, where the behaviour

of a rectifier with capacitive load connected to the power supply is shown, evidenced the effect of a nonsinusoidal line current flow in the voltage in the supply impedance, resulting in voltage distortion at the rectifier terminals.

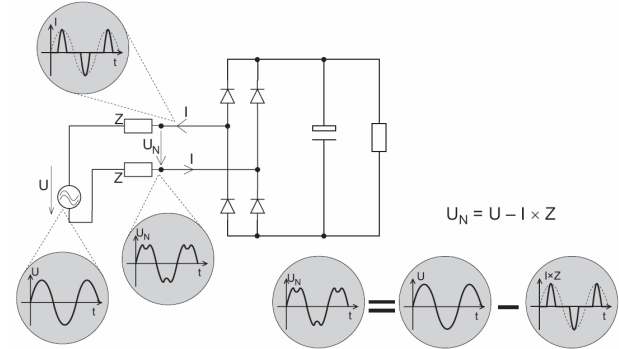


Fig. 1. Supply system-connected rectifier with capacitor [71].

The system frequency response characteristics are affected by a number of factors, which have to be considered when analysing a specific system. The system short-circuit capacity¹⁸ is an indication of the fundamental frequency system impedance at a certain point. For quasi-pure inductive power sources, this is also a measure of the system impedance for each particular harmonic frequency, when multiplied by the harmonic order¹⁹. In relation to weaker systems (small short-circuit capacity), stiffer systems (large short-circuit capacity) have lower voltage distortion for a given harmonic current content [59], [60].

Capacitor banks (e.g., used for power factor improvement) and insulated cables are major components that affect system frequency response characteristics. The connection of capacitors can cause resonance conditions that can magnify harmonic levels. Usually, capacitor banks are dominant in industrial and overhead distribution systems.

As power electronics are proliferating, AC-DC rectifiers are playing an increasingly important role. There is a large growth of diode and thyristor converters on utility systems, including those used in VSDs (3-phase, full-wave rectifiers), leading to line current and voltage harmonic distortion, poor power factor, EMI (by radiation or conduction), line and equipment harmonic current loading (supplementary losses and increased heating or temperature rise), accelerated ageing, tripping, communication interference and meter inaccuracy (errors and poor measurements) in sensible loads connected to the same supply or nearby the equipment producing EMI, etc. [57]. In fact, current harmonics at the VSD input stage can feed back into the power bus grid, and can disrupt other types of equipment on the premises.

Among all elements in the supply system, the common victims of the harmonics generated by VSDs and rectifiers are motors (increased losses, speed fluctuations), transformers (increased losses and heating,

¹⁶ Harmonic voltages are sinusoidal voltages with a frequency equal to an integer multiple of the fundamental frequency of the supply voltage. Inter-harmonic voltages are sinusoidal voltages with frequency between the harmonics (not an integer multiple) [12].

¹⁷ Sources of supply system harmonics: AC/AC and AC/DC converters (in general), soft-starters, frequency inverters, servo controllers, speed controllers, arc furnaces, induction furnaces, fluorescent tubes (including those with power factor correction), saturated magnetic circuits (e.g., saturated transformers, motors and chokes), household appliances such as radio, TV, and computer, etc. [70].

¹⁸ Capacity of the utility system with the respect to the fundamental-frequency volt-ampere of the load: I_{sc}/I_1 , $I_{sc} = U_{ff}/(\sqrt{3}\omega_1 L_s)$. If the short-circuit current, I_{sc} , increases, the capacity of the system at the point of common coupling (PCC) increases. The internal impedance, L_s , is often specified in terms of I_{sc} at the PCC. On a per-phase basis, I_{sc} is the per-phase RMS current supplied by the AC source to the faults if all 3 phases are shorted to ground at PCC: $I_{sc} = U_s/(\omega_1 L_s)$ [59].

¹⁹ That is why in standards the maximum allowable harmonic current ratio I_h/I_1 decreases, although not linearly, with increasing value of the harmonic order h [59].

saturation phenomena may occur), cables (increased resistive and dielectric losses), capacitor banks (heating, ageing, resonance phenomena), converters, computers, regulators, relays, circuit breakers, or/and no-volt trip devices (nuisance tripping), measuring and control devices (measuring errors, limitation of functions, loss of function), etc. [71].

Additionally, harmonic currents may cause additional harmonic losses in the utility system, may excite electrical resonances leading to large overvoltages, and overload circuit wiring²⁰.

In the case of three-phase diode rectifiers being used in the input stage, the negative-sequence harmonics (5th, 11th, ...) are particularly worrying in terms of losses increase.

In Fig. 2 the harmonic currents, i_h , of input current, i_c , of a VSD as an electric load, affects the voltage, $u(t)$, in the point of common coupling (PCC). The voltage distribution at the PCC depends on the internal impedance of the AC source and on the magnitude and order of the injected current harmonics.

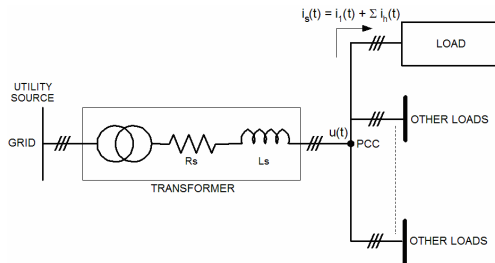


Fig. 2. Electric three-phase network with a load injecting current harmonics into the power network, with upstream transformer and other downstream loads.

Theoretically assuming perfectly continuous DC output current of a three-phase diode rectifier, the harmonic current frequency at the input has a value h times higher than fundamental frequency (50 Hz or 60 Hz), where the harmonic order, h , is given by (1)²¹, where $k = 1, 2, 3 \dots$ and p is the rectifier pulsation index (for a full-wave or six-pulse diode rectifier $p = 6$) [8]. The current h^{th} order harmonic amplitude, I_h , is calculated on the basis of (2) [8].

$$h = k \cdot p \pm 1 \quad (1)$$

$$I_h = I_1 \cdot h^{-1} \quad (2)$$

The power factor, λ , is defined by the quotient between the real power, P , and the apparent power, S . For nonsinusoidal signals, the power should be computed taking into account the harmonics, as in (3), where U_h and I_h are given by (4).

$$\lambda = \frac{P}{S} = \frac{\sum_{h=1}^{\infty} U_h I_h \cos(\theta_{u_h} - \theta_{i_h})}{\sqrt{U_1^2 I_1^2 + U_1^2 I_{h(\text{total})}^2 + U_{h(\text{total})}^2 I_1^2 + U_{h(\text{total})}^2 I_{h(\text{total})}^2}} \quad (3)$$

²⁰ E.g., for a 400-V, 100-A electrical circuit it is possible to provide 4-kW at $\lambda = 1$ but only 2-kW at $\lambda = 0.5$.

²¹ The theoretical current harmonic spectrum, assuming $L_s = 0$, is 20%, 14%, 9%, 8%, 6%, 5%, 4%, and 4% for the 5th, 7th, 11th, 13th, 17th, 19th, 23rd and 25th order harmonics, resulting in a power factor of $3/\pi = 0.955$ (note that, in this case, there is a unity displacement power factor).

$$U_{h(\text{total})} = \sqrt{\sum_{h=2}^{\infty} U_h^2} \quad I_{h(\text{total})} = \sqrt{\sum_{h=2}^{\infty} I_h^2} \quad (4)$$

It is assumed that the voltage supply is sinusoidal or with a very low distortion, yielding (5) [59], where λ_θ is the displacement λ , i.e., the power factor associated with the displacement between voltage and current fundamental components, and THD_i is the current total harmonic distortion (equal to $I_{1(\text{rms})}/I_{\text{total}(\text{rms})}$), defined according to [8].

$$\lambda = \frac{P}{S} = \frac{\cos(\theta_{u_1} - \theta_{i_1})}{\sqrt{1 + THD_i^2}} = \frac{\lambda_\theta}{\sqrt{1 + THD_i^2}} = \frac{I_{1(\text{rms})}}{I_{\text{total}(\text{rms})}} \quad (5)$$

Due to the relation between λ and THD_i , the efficiency of the electrical energy use is influenced by the voltage and current harmonic distortion. It should be emphasized that in three-phase, 6-pulse, diode rectifiers (Fig. 4) the power factor is a function of rectifier load, as it can be seen in Fig. 3. In VSDs with such rectifiers, at light loads (up to 30-50%), the line-side current only flows when the voltage output value of the diode rectifier is above to that of the DC-link capacitor voltage, becoming discontinuous between each two pulses over half cycle. As the load on the VSD increases, the line-side current can become continuous between each two pulses over half cycle (seven waveforms presented in Fig. 4). The point at which the current becomes discontinuous depends on the size of the line-side and DC-link inductances (L_s and L_{dc} , as shown in Fig. 6), as it can be seen in Fig. 5, in which the results of several simulations are presented.

One way to improve input current waveform is increasing the AC-side inductance (between the rectifier and the utility), L_s , as it can be seen in Fig. 5. The inductance at the DC-bus, L_{dc} , has to be of 2 times the per-phase AC-side inductance, for the same effect in line current (but in AC-side 3 inductances have to be used).

It should be noted that the increase of the L_s and/or L_{dc} also contributes to the reduction of the common-mode currents circulating in the close-loop motor-ground-power source-VSD-motor, due to the increase of the common-mode impedance. This can lead to the bearing currents mitigation.

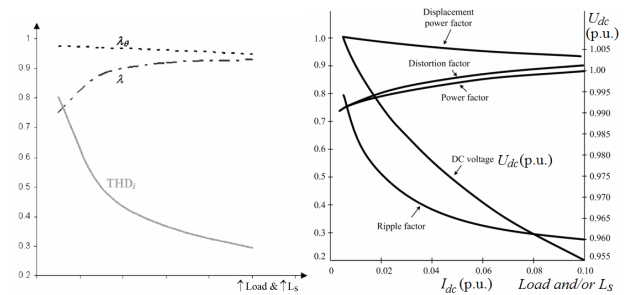


Fig. 3. (left) Power factor variation as a function of load in a three-phase, six-pulse, diode rectifier, assuming sinusoidal voltages and constant DC voltage (in the absciss axis, it can be considered increasing I_d/I_{sc}) [57], [59], [60]; (right) Performance characteristics of a 3-phase, 6-pulse, diode, bridge rectifier with parallel-RC load ($C_{dc} \rightarrow \infty$). Not in scale [57].

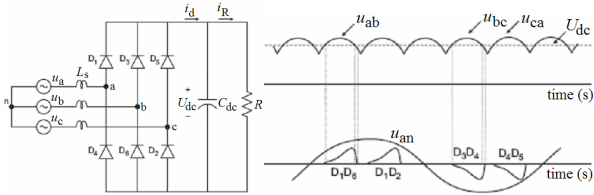


Fig. 4. Three-phase, 6-pulse, diode, bridge rectifier with parallel-RC load ($C_{dc} \rightarrow \infty$) [57]: (left) Schematic; (right) Voltage and current waves.

However, the increase of L_s leads to the decrease of the rectifier output average voltage, which is a disadvantage since, for a given output fundamental voltage, the m_a inverter has to be higher (if the inverter is operating near the unitary m_a , it can be increased up to the nonlinear or overmodulation region, producing more low-order harmonics).

Nowadays, there are several strategies to reduce harmonic distortion. The most obvious is the use of equipments with low harmonic pollution level. The power network impedance can also be reduced, by means of changing the installation or a number of equipments. Filtering equipment installation-based solutions can also be adopted.

Structural modifications can include the reinforcement of the power system (short-circuit power/capacity), the use of VSDs with 12-pulse (or more) rectifiers or controlled rectifiers, and/or improvement of VSD input filtering.

In Fig. 6, the points where an EMODS can be changed to improve the power quality, including the power network, from the harmonic distortion point of view, are identified. The current harmonics vary according to the EMODS configuration and voltage harmonics, which, in turn, affect the distributed voltage waveform and result from both current harmonics circulation and impedance of the grid.

The short-circuit power increase leads to the decrease of the voltage distortion in the PCC of nonlinear loads, due to the total impedance reduction upstream the load. However, there is no attenuation at harmonic current level. Being the transformer a fundamental element in the transport and distribution of the electrical energy, it has a major role in minimizing harmonic distortion. The higher the short-circuit capacity and/or the lower the overall series impedance, the lower the voltage distortion will be. In general, the harmonic currents circulation in industrial power networks can be strongly attenuated with the introduction of a relatively large inductance upstream the polluting load [8], [60], [61].

In general, the following measures can be used to reduce supply system harmonics: (a) suitable power factor correction equipment; (b) line filter connected in series with the supply; and (c) supply via an isolating transformer [71].

In most low-medium power VSDs, full-wave, six-diode (or six-pulse) rectifiers are typically used with a capacitor at the output DC link and, in some cases, with an inductance (L_{dc}), forming together a low-pass filter, which contributes to the linearization of the DC-bus current and voltage. This sort of rectifier, of simple conception and reduced investment, generates high-amplitude input current harmonics of low order (mainly

5th, 7th, 11th, and 13th order harmonics). The typical input current wave is presented in Fig. 7 [8], [60], [61]. If most of the loads of an industrial plant include this sort of rectifiers, the respect for normative/standard requirements becomes difficult to fulfil, and the power transformer should be oversized. In most cases, it is necessary to use additional filtering techniques.

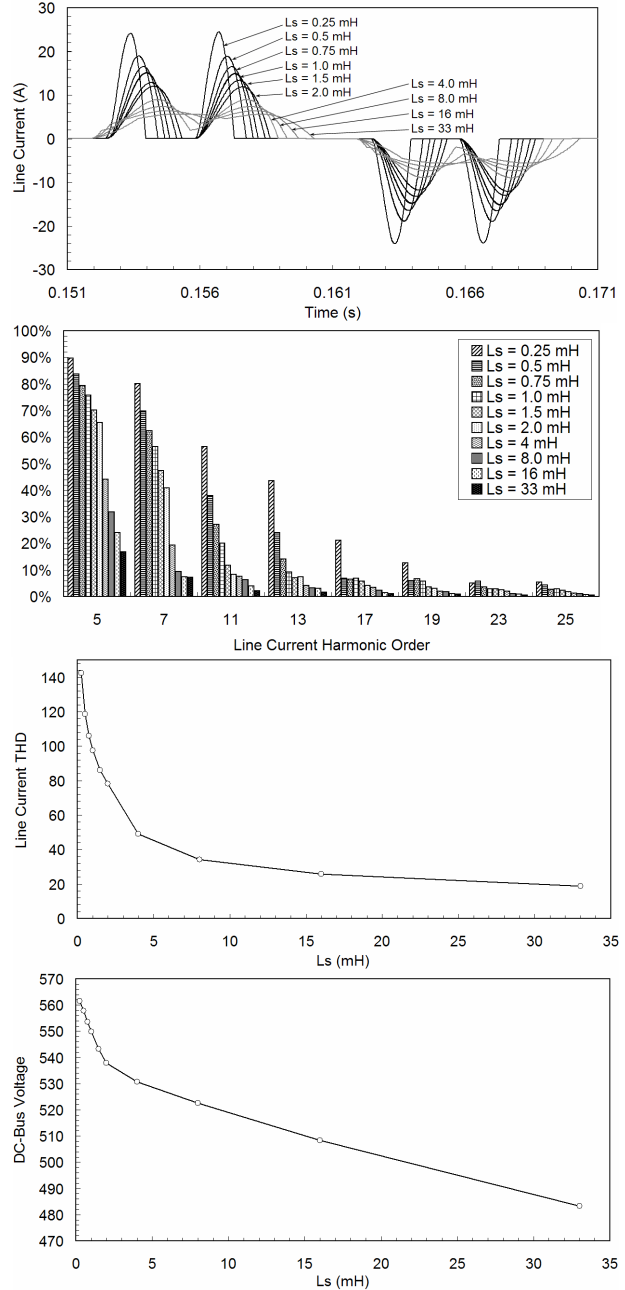


Fig. 5. Simulated AC-side inductance (L_s) influence on the rectifier input current and on the DC-bus voltage (3-phase, 6-pulse, diode rectifier, fed by a star-connected power source, $U_{an} = U_{bn} = U_{cn} = 326.7$ V, 50 Hz, with $R_{ng} = 1$ Ω , feeding a DC-bus with a $C_{dc} = 250$ μ F with a PWM inverter operating with $f_1 = 50$ Hz and $f_s = 2$ kHz and a RL-series load with $L = 52.28$ mH and $R = 21.89$ Ω).

The twelve-pulse rectifier is obtained from two six-pulse rectifiers connected in parallel. Therefore, the two rectifiers are fed by one 3-winding transformer (one primary and two secondary) or by two 2-winding transformers (Fig. 7) [61]. In both cases, the secondary three-phase voltage systems of both transformers should have a time displacement of 30° [61]. This solution results

in the attenuation of some harmonic components of low order at the primary side. The major disadvantage results from the use of special-design transformers, which can be significantly expensive, in relation to commonly used transformers.

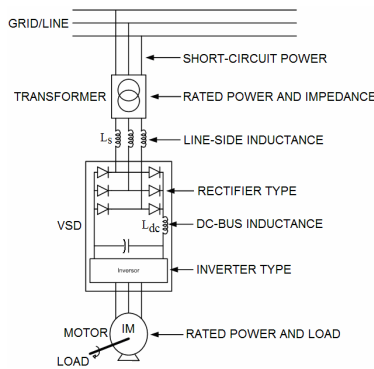


Fig. 6. Main points where the harmonic distortion can be influenced in an EDMOS [60].

The 24-pulse rectifier consists in the use of two 12-pulse rectifiers in parallel, with the respective transformers with three windings, being the primary windings displaced by 30° (Fig. 7) [61]. This rectifier leads to an input current practically without low-order harmonics, but the cost is significantly higher than that of the 12-pulse rectifier. However, when the installation has a high-power EMODS or several medium-power EMODS, this solution can represent one of the most economic and effective solutions for harmonic distortion mitigation.

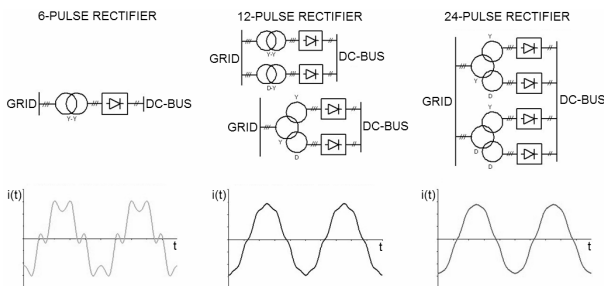


Fig. 7. Input current waveform for different types of rectifiers [60].

A controlled rectifier is obtained replacing the 6-pulse rectifier diodes by thyristors or IGBTs. Thyristor-based rectifiers or phase-controlled rectifiers (Figs. 8 and 9)²² present a number of problems associated with the introduction of switching-related notches in the voltage waveforms, depending on the firing angles of thyristors and affecting directly the voltage waveform quality of the power network. The resulting power factor is relatively low. Typically, this sort of rectifiers is not used in voltage-source inverters with PWM technique. They are used, for example, in square-wave or six-step inverters, requiring DC-bus voltage regulation.

Fully controlled IGBT-based rectifiers (or active front-ends) are bidirectional in terms of power flow, allowing rectification and regeneration, as well as the DC-bus voltage level and the power factor control over all load range (e.g., within 0.95 to 1.0 range [62]). They also

²² Phase-controlled rectifiers are characterized by low conduction losses, negligible switching losses, soft switching with zero current, high efficiency (typically 98%), simple control, generation of line frequency related harmonics in load and source, lagging line power factor, EMI production. In such rectifiers, it is possible fuse protection and fault current suppression by gate control [57].

act as an active front-end or active harmonic filter, typically limiting the current total harmonic distortion up to 5%, independently of the current direction [61]. Therefore, the compensation of power factor and harmonic currents of parallel-connected loads is possible. With proper control, the input current can result approximately sinusoidal, with low-amplitude low-order current harmonics and high-amplitude high-order current harmonics, being the last much easier to filter. The main disadvantage of this sort of rectifiers is the high cost, mainly associated with the supplementary filter and the use of six extra IGBTs.

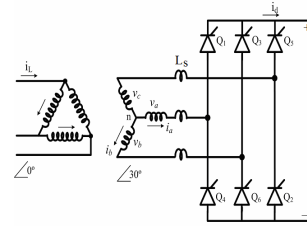


Fig. 8. Schematic of a 3-phase, 6-pulse, thyristor bridge converter [57].

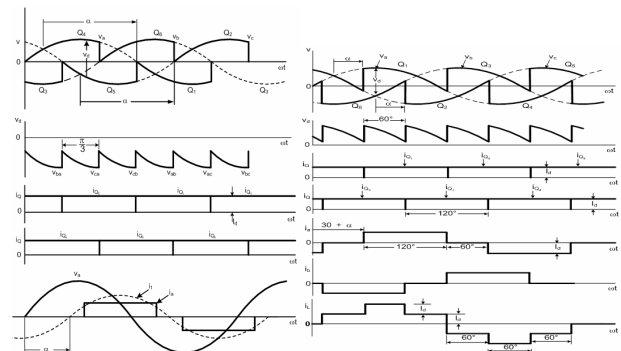


Fig. 9. Voltage and current waveforms of a 3-phase, thyristor, 6-pulse bridge converter, in inverting mode: (left) $\alpha = 150^\circ$, mode C; $\alpha = 40^\circ$, mode A [57].

Six-pulse diode rectifiers without downstream or upstream inductances (L_{dc} or L_s), independently of power, inject typically harmonic components of 5th, 7th, 11th, 13th, 17th and 19th order (most relevant), with amplitudes in relation to fundamental commonly around 63%, 54%, 10%, 6.1%, 6.7% and 4.8%, respectively, which are considered here as reference. Considering the simple diode rectifier and the associated transformer costs the base or reference investment, if a typical downstream inductance L_{dc} is introduced, that cost increases roughly 10-20%, but amplitudes of dominating harmonics are decreased to approximately 30%, 12%, 8.9%, 5.6%, 4.4% and 4.1% of fundamental, respectively [60]. For a 12-pulse rectifier plus required special transformer(s) (two secondary windings transformer or two conventional transformers), the investment is 1.5-2 times higher, but the amplitudes of the referred harmonics are strongly reduced to 3.6%, 2.6%, 7.5%, 5.2%, 1.2% and 1.3% of fundamental, respectively. For a 24-pulse rectifier plus required two special transformers, the investment is 3-4 times higher, being the spectrum similar to that of the 12-pulse rectifier, except for the 11th and 13th order harmonics, which are strongly attenuated to approximately 1% and 0.7% of fundamental, respectively. The rectifier with IGBTs (active front-end) can cost up to 2.5 times the diode rectifier, although it is not so

significant if energy regeneration potential is taken into account, and its harmonic spectrum includes components of same order but with amplitudes as low as 2.6%, 3.4%, 3%, 0.1%, 2.1% and 2.2%, respectively [60], and power factors near unit can be achieved with proper control [67].

As previously referred, although input current harmonics in a VSD (VSI type) can be strongly reduced by introducing an inductance large enough in the AC-side and/or DC-bus-side [8], [61], the tendency is to reduce its value or even take it out in order to reduce the VSD size and price. Commonly, it is recommended the use of external filters with an inductance of value equal to 100 mH divided by the motor useful power in kW, e.g., for a 100-kW motor an 1-mH inductance is recommended, resulting in a strong THD_i reduction [60]. When new VSDs are acquired, the DC-link and/or AC-side inductances should be properly designed in order to fulfil power quality requirements in the most relevant related standards²³.

The filtering strategy is commonly used as a corrective measure in existing installations where the harmonic distortion increase becomes critical. In general, it is a good solution for new or in-operation industrial plants. Three techniques can be distinguished: passive, active and hybrid filtering.

The passive filtering principle is illustrated in Fig. 10, being appropriated for global compensation. This sort of filtering technique has to be tuned for a harmonic frequency or frequency range (e.g., 5th, 7th and 11th order harmonics) to be mitigated and, typically, it is syntonized over the 5th order harmonic, and integrates a set of series-connected inductances and capacitors, connected between the line and ground. The recommended spot for installation is near the loads generating harmonics [63], [64]. This technique is rarely used in new installations. A set of filters can also be used, where each one is syntonized over a different frequency or range of frequencies (band-pass filter), allowing improved harmonic mitigation. Typically, only low-order harmonics are filtered ($h \leq 25$) [63], [64].

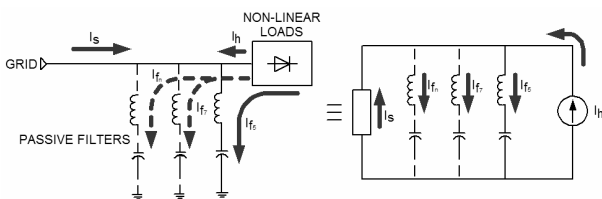


Fig. 10. Passive filtering principle [60].

Passive filtering requires special attention since its performance depends on grid impedance and is not adaptable to load changes, requiring careful design to avoid resonance effects (e.g., due to interaction between

²³ Relevant power quality related standards: IEC 61000-2-2; IEC 61000-2-4; IEC 61000-3-2; IEC 61000-3-3; IEC 61000-3-4; IEC 61000-3-5; EN 50 160:1994; IEEE Std. 519-1992. Basically, IEC 61000 standards regard electromagnetic compatibility (EMC), including the harmonic distortion control at common entry point. IEC 61000-4-7 regards testing and measurement techniques, and defines new methods for the measurement of harmonics and interharmonics in power supply systems [70]. It should be referred that, besides the IEC and IEEE standards, there are also other standards related to EMI such as EN (equivalent to IEC), CISPR, VDE, FCC, as well as military standards that specify the maximum limit on conducted EMI. For the FCC and VDE standards, the conducted noise has to be measured by means of a specific impedance network called line impedance stabilization network (LISN). Standards on radiated EMI are also specified by the referred agencies.

the filtering and capacitor banks for power factor correction), which can amplify the harmonics not covered by the filter [60].

Using electronic systems it is possible to control the harmonic distortion actively, being denominated this technique by active filtering, whose principle is presented in Fig. 11. Active filtering compensates instantaneously harmonic components injected into the grid, by means of introduction of harmonic components of the same order but in opposite-phase, as it can be seen in Fig. 12 [63], [64]. Active filtering is the most suitable solution to installations with a large number of low-power VSDs, but is expensive in relation to other passive techniques (the cost is 1.5 to 2.5 times higher) and, although the continuous improvements in this field, the commercial available rated power is still quite limited nowadays. Active filtering is more flexible than passive, and, therefore, it is typically seen as a dedicated solution to each load and it is recommended for dynamic loads.

It is also possible to implement hybrid filtering, as it is shown in Fig. 11, leading to improved filtering over passive filtering, since resonance and overload risk is lowered and, at the same time, allowing compensation of harmonics existing in the power grid.

The briefly described strategies to attenuate harmonics at EMODS and installation levels have specific advantages and disadvantages, and require investment in additional equipment and/or the power supply system upgrade. The most appropriate strategy should be chosen as a function of total load, installation power system, and permitted or desirable harmonic distortion level. Strategies requiring power system upgrade or restructuring are complex and require a large investment (e.g., the power transformer represents a significant part of the overall electrical installation investment).

The change of an in-operation EMODS is typically difficult, but the selection of a new equipment should be made taking into account the presented considerations.

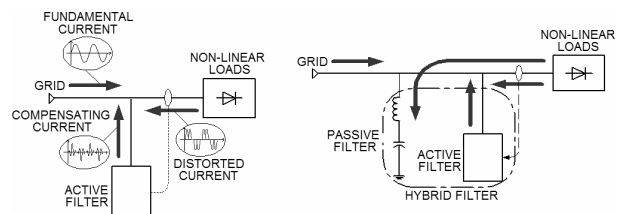


Fig. 11. Principle of active (left) and hybrid (right) filtering [60].

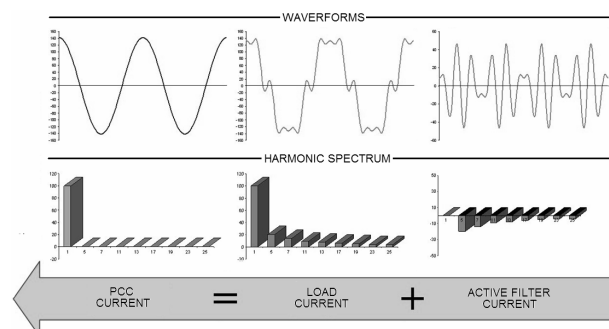


Fig. 12. Current waves and spectrum in an active filtering system [60].

Regarding harmonic and common-mode components injected into the motor, as well as interference associated with electromagnetic radiation produced by the cable

between the inverter and the motor, according to [65], electromagnetic compatibility (EMC) measures to reduce those undesirable factors at the motor side are shielded VSD-IM cables, output chokes²⁴ near VSD, and output filters. Alternatively to the shielding, an output choke can be used for the motor cable to achieve the desirable electromagnetic interference limit value. The shield should be connected by the shortest possible route and earthed over a wide area at both ends²⁵. For double-shielded cables, the outer shield should be grounded at the inverter and inner shield at the motor. Earthed sheet-metal ducts or metal pipes can also be used to shield the cables. High-frequency compatible grounding should be provided for the inverter and all additional units. These issues are addressed in the following section.

B. EMI Associated with VSDs

Regarding electromagnetic interference (EMI) issues, VSDs generate both conducted noise in line-to-inverter power cables and high-frequency airborne radiated EMI in the inverter-to-motor power cable. The high IGBT switching speed causes oscillatory currents with a frequency range from hundreds of kilohertz to several megahertz, causing wide-band radiated EMI, which can interfere with surrounding control circuits and other electronic equipment. Furthermore, the high du/dt can couple through the capacitance between the motor stator windings and motor frame, causing high-frequency currents to flow (leakage currents) in the return ground conductors, which can cause tripping of ground current relays or circuit breakers installed for protection. Traditionally, filters and metallic conduits or shields have been used to suppress EMI emissions. More recently, alternative mitigation techniques have been suggested to reduce EMI and common-mode voltages, such as common-mode inductors and transformers and the addition of line or grounding capacitors. It should be noted that common-mode EMI filters have no significant effect on the shaft voltage (see Appendix 5). To reduce the conducted EMI, filters and common-mode transformers can be placed between the line and the inverter, and between the inverter and the motor. Table 1 shows the impact of a number of mitigation techniques on the conducted EMI reduction at the VSD input, summarizing the information presented in [66]. In [66], no significant difference was observed when using either short (≈ 3 m) or long (≈ 300 m) cables, when using metallic conduit/shield, or whether or not the ground conductor is bundled with the phase conductors. A significant reduction in the conducted EMI occurs when a common-mode choke is applied at the VSD input. The application of a common-mode transformer, also effectively reduces the conducted EMI. The losses for both the common-mode choke and common-mode transformer are about 7 W, for the tested system [66]. The most significant reduction in the conducted EMI is achieved after applying multiple common-mode filters between the line and the VSD, in addition to line-to-line capacitors [66]. In [65], a line filter (close to inverter) is

recommended to reduce conductive EMI, in order to comply the system with standard limits²⁶ defined in [70].

Regarding radiated EMI, Table 2 shows the impact of a number of different mitigation techniques on the radiated EMI reduction of the output of VSDs. The National Electric Code²⁷ (NEC) requires that the equipment-grounding conductor be routed with the phase conductors if a non-metallic conduit is used. If a metallic conduit is used the conduit may act as the grounding conductor (note that flexible metallic conduit requires a separated ground conductor) [66]. Bundling of the grounding conductor or using the grounded metallic conduit or (electrostatic shield) leads to a substantial radiated EMI reduction. Since this technique requires modest investment, it is strongly recommended. However, common practice is to simply run the three-phase conductors without including a ground wire.

As it can be seen in Table 2, a significant reduction from base case is obtained when applying a common-mode transformer or a common-mode choke between the inverter and the motor, being the latter more effective and, in principle, cheaper.

The most significant reduction in radiated EMI is achieved when common-mode choke and a differential-mode filter connected between the inverter and the motor are implemented (no bundled ground conductor). If the last measure is associated with the first referred, the radiated EMI is reduced to very low values, completely avoiding interference with surrounding equipments.

For industrial purposes, the simplest solution for critical applications interfering with surround sensitive equipment is to use a 3-conductor shielded cable, or, at least, a 4-conductor cable, with the fourth conductor being used as ground conductor. Additional information on this scope can be found in technical manuals from inverter manufacturers (e.g., [65]).

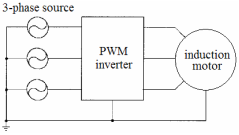
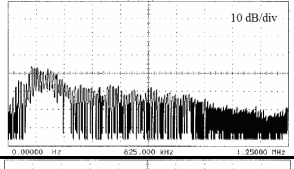
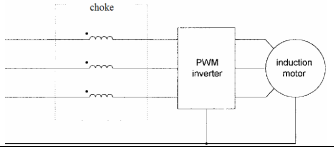
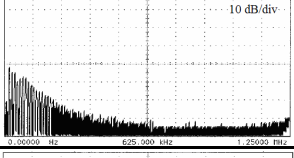
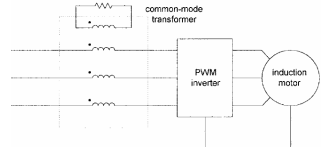
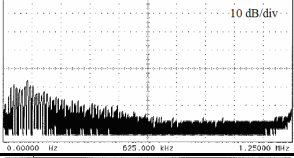
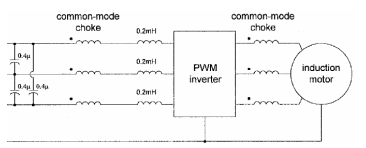
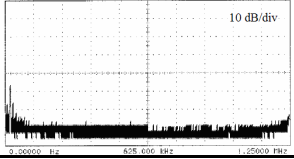
²⁴ Routing all 3 phases together through the output choke, but not the earth/ground conductor.

²⁵ Using metal shield clamps or metal cable glands.

²⁶ No EMC limits are specified for interference emission in voltage supply systems without earthed star point (IT systems). The effectiveness of input filters in IT systems is severely limited [65], [68].

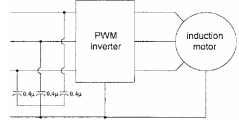
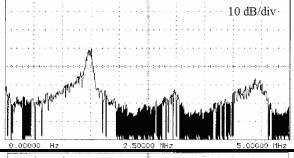
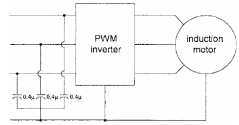
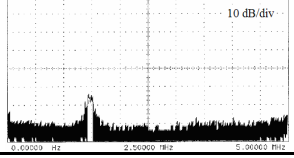
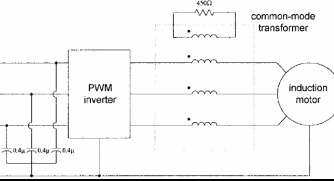
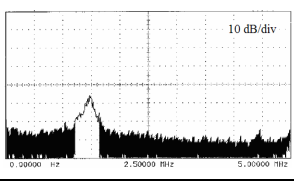
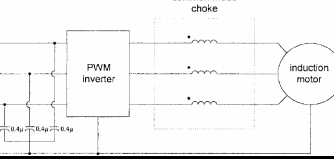
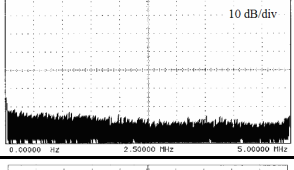
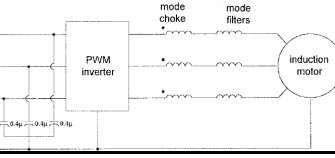
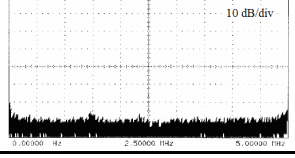
²⁷ The National Electrical Code (NEC), or NFPA 70, is a U.S. standard for the safe installation of electrical wiring and equipment.

TABLE 1
DIFFERENT MITIGATION TECHNIQUES FOR CONDUCTED EMI AT THE INPUT OF VSDs [66].

Schematic	Description	Result (line current spectrum, dB)
	No mitigation measures. Base or reference case.	
	Common-mode choke. Winding inductance ≈ 5 mH.	
	Common-mode transformer. Winding inductance ≈ 3.9 mH.	
	Multiple filters.	

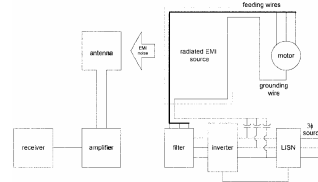
Notes: 230-V, 5-kVA VSD system, no-load, 12-kHz switching frequency, 3.05-m motor lead. The drive used in the test has a DC-link inductor, which is used to reduce the current harmonics injected back to the AC power grid. This inductor, together with the DC-bus snubber capacitor, also helps to reduce the differential-mode conducted EMI.

TABLE 2
DIFFERENT MITIGATION TECHNIQUES FOR RADIATED EMI AT THE OUTPUT OF VSDs [66].

Schematic	Description	Result (receiver signal spectrum, dB)
	No mitigation techniques. Lead wires and grounding wire form a loop. No bundled ground conductor. Base or reference case.	
	No mitigation techniques. Lead wires and grounding wire bundled. The results of using the grounded metallic conduit are the same as when bundling the ground conductor with the phases.	
	Common-mode transformer. Lead wires and grounding wire form a loop. No bundled ground conductor.	
	Common-mode choke. Lead wires and grounding wire form a loop. No bundled ground conductor.	
	Common-mode choke and a differential mode filter. Lead wires and grounding wire form a loop. No bundled ground conductor.	

Notes:
230-V, 5-kVA VSD system, no-load, 12-kHz switching frequency, 3.05-m motor lead. Radiated EMI measured using a square loop antenna (0.093 m²) and a high-bandwidth amplifier (500 Hz to 5 MHz at an amplification ratio of 100). The source of radiation was the cable connecting the motor to the PWM inverter. Cables in the test are mounted onto a wooden frame (0.686 m \times 0.915 m), which is displaced 1.22 m from the antenna (the basis for this setup was the German Std. VDE 0871 Class A).

Setup schematic (lead wires and grounding wire form a loop):



A6.3.3 Section 3.7

A. Economical Advantages Associated with VSDs

Whether or not the VSD is a good investment depends in part on its cost-effectiveness. Whether energy conservation is being used as the sole or partial justification for installing the VSD, accurate savings values are required to ensure the rate of return of the additional capital cost of the VSD installation is properly calculated. Several benefits are associated with VSDs, such as energy savings²⁸, smoother operation, acceleration and deceleration control, compensate for changing process variables, adjust the rate of production, allow accurate positioning, control torque or tension, just to name a few. This section emphasizes the energy savings potential associated with VSD (and to speed control in general) in a number of important loads or systems. In general, loads can be characterized as a function of speed, and described as a combination of constant torque, linear torque, and quadratic torque load components. Constant power loads can also be found but are relatively rare. For the sake of simplicity, it is normally considered only the dominant torque-speed behaviour for economical evaluation purposes.

In steady-state, i.e., null acceleration, four main elementary load behaviours can be defined as a function of speed by (1) and (2), where K_k is a constant and k is 0 for constant power load, 1 for constant torque load, 2 for linear torque load, and 3 for quadratic torque load. However, real loads can only be correctly described using a combination of the mentioned elementary loads, but can, in most cases, be approximately described by the dominant behaviour without major errors. Generally, a load can be mathematically described in steady-state operation by (3) and (4). For example, in a fan, if the friction in the fan bearings is not considered, $K_0 = K_1 = K_2 = 0$ and $K_3 \neq 0$. Note that, for elevating applications (conveyors, escalators, lifts, etc.), the gravity effect is described by a constant torque component for steady-state operation (constant speed), corresponding to $k = 1$. In general, for horizontal conveyors (essentially a static-friction load) $k = 1$, for industrial mixers, machine-tools and reciprocating/piston compressors (viscous friction), it can be considered $k = 2$, and for centrifugal pumps and fans, it can be considered $k = 3$.

For transient analysis the mass and inertia of all moving parts of a system have to be taken into account. The mass of linear movement loads can be converted into an equivalent inertia, which can be added to the rotary parts inertia.

$$T = K_k \cdot \omega^{k-1} \quad (1)$$

$$P_{mech} = K_k \cdot \omega^k \quad (2)$$

$$T = \sum_{k=0}^3 K_k \cdot \omega^{k-1} \quad (3)$$

$$P_{mech} = \sum_{k=0}^3 K_k \cdot \omega^k \quad (4)$$

²⁸ According to [101], 50% of all industrial motor driven processes can experience a significant reduction in energy consumption with speed regulation. About 15% of the installed industrial motor power in Europe is already driven by VSDs. For the remaining 35%, an average energy reduction of 35-40% is estimated [101].

Considerations on pumps - In pumps²⁹, it is more efficient to regulate the flow of fluid by regulating the speed of the motor rather than by restricting the flow using a throttle device (e.g., valve). Pump formulas that are used to determine the savings are simple, but they are easily misapplied, leading in most cases to overestimated energy savings [72], [73]. The result can be a bad investment decision. The process system must be mathematically modelled so that the pump hydraulic formulas can be properly applied, describing the curves presented in Fig. 1. This modelling is simple, but necessary to achieve accurate results. With the pump operating at a fixed speed, at any given flow rate the pressure or head, required by the process, typically expressed in meters³⁰, is lower than the pressure developed by the pump. The only exception is at the natural operating point, where the system and pump curves intersect (see Fig. 1).

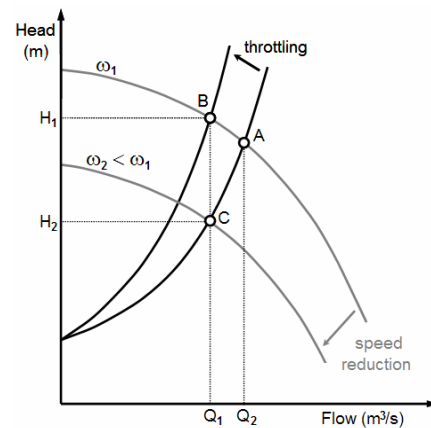


Fig. 1. Centrifugal pump and system characteristics, for different flow control methods, assuming that pump suction pressure never change [14], [69], [72], [103].

To match the pressure and flow requirement of the process, control valves can be used to either directly or indirectly drop the pump pressure. Direct pump discharge pressure dropping, requires output throttling, by means of valves inserted between the pump discharge and the process (Fig. 2, left). A device that drops pressure and has flow through it, consumes power. Obviously, this power has to be supplied by the electric motor driving the pump. Indirect pump discharge pressure dropping, require a by-pass controlled by a valve, which recycles additional flow through the pump (Fig. 2, right), taking advantage of the fact that there is an inverse relationship between pump discharge pressure and flow. With recycling or by-pass, the valve controls the flow through the pump body to a point where the pump discharge pressure matches that required by the system. Both output pressure throttling and recycling are extremely inefficient, but, of the two, recycling is the worst. Affinity laws govern the relationship between the speed of the impeller, head (or

²⁹ Roughly 73% of the pumps are rotodynamic, and 27% are of positive displacement. On average, 80% of the pumps LCC is associated with energy consumption, 8% associated with initial cost (purchase), and 12% associated with maintenance.

³⁰ The advantage of using head pressure in meters is that the differential head developed by a pump and the head loss due to flow through a pipe becomes independent of specific gravity.

pressure) developed by the pump, and the respective input power required. However, careful application of these laws is required when static head exists, to avoid overestimated savings [73]. The brake horsepower (BHP), or mechanical power required by the pump, has a proportional relationship to flow, so the electric motor must supply this additional power associated with throttle device pressure drop. BHP of a pump is given by the quotient between hydraulic power and pump efficiency (which varies with flow) for the operating point under consideration.

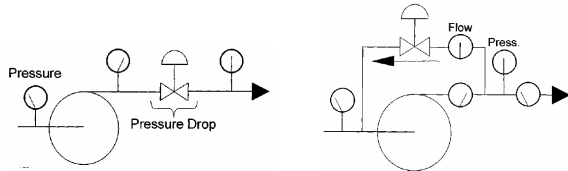


Fig. 2. Different throttling methods for flow and pressure control in a centrifugal pump: (left) output pressure throttling; (right) recycling or throttled by-pass.

As it can be seen in Fig. 1, the process system requires less pressure for reduced flow, while the pump discharge pressure increases at reduced flow. As the flow requirement is reduced, there is an increasing overpressure. With a fixed-speed pump, the methods that deal with this overpressure, in order to force pump and system curves intersection for a required flow, waste power (from point A to point B in Fig. 1). However, this intersection could be achieved at any flow rate without the power wastage associated with the overpressures by changing the pump impeller speed (from point A to point C in Fig. 1), using a VSD. As it is evidenced in Fig. 1, ignoring pump efficiency, since the pump BHP is proportional to H times Q , it is obvious that the difference in head pressure for throttling-based and VSD-based flow control techniques, for a given flow, leads the pump to require a significantly higher power in the first case. In short, for centrifugal pumps, the least efficient flow regulation technique is the by-pass (required power maintained approximately constant), followed by the output throttling, the ON/OFF cycling, the magnetic coupling and the VSD (or other sort of direct motor speed control, e.g., poles change), as it can be seen in Fig. 5 and 6 [73], [103].

If only one fixed speed head-flow curve is known for a pump, as well as the corresponding pump efficiency as a function of flow, it is necessary to project the final operating point for variable speed into the fixed speed curve using affinity laws, and the corresponding efficiency is also the efficiency of the final operating point. An important issue is the inverter and motor efficiency variation with frequency, voltage and load, when load speed varies [74], and the dependency of the overall efficiency of the pumping system on the efficiency of each of its components. Obviously, the efficiency drop in those components has a minor impact in system overall savings associated with speed control³¹. However, it is important to emphasize that pump efficiency-flow curve

is quite different whether considering fixed (with throttling) or variable speed flow control (as it can be seen in Fig. 3), and IMs operating at reduced frequency and load have reduced efficiency (see [74] and Figs. 3.54-3.57 of Chapter 3), both factors contributing to reduce the energy savings associated with speed-based flow control. VSD efficiency also varies slightly with frequency and load. These efficiency variations have to be considered to avoid gross errors (for rigorous calculation, power transformer efficiency can also be taken into account) in the energy savings estimations, particularly when large investments are being evaluated.

Examples of modelling are presented in [72]. Pumps are often connected in series or in parallel, being relatively simple to model these systems by representing the multiple pumps as one pump with new characteristics [72]. Basically, in series-connected pumps, the differential head is additive at any given flow and the total BHP is the sum of the BHP of individual pumps. In pumps in parallel, the flow rate capability is additive at any given head and the BHP is the sum of the BHP of individual pumps. The effects of the specific gravity have also to be taken into account. In fact, the BHP requirement of a pump is directly proportional to the specific gravity of the fluid being pumped. For example, given a pump delivering the same flow of water ($g_e = 1.0$) versus crude oil ($g_e = 0.85$), pumping water would require 17.6% more horsepower than pumping crude oil.

In steady-state, i.e., null acceleration, centrifugal fans and pumps respect affinity laws, given by (5)-(8), where H is the discharge head, Q the discharge flow rate, ω is the impeller speed, P_{hydr} is the hydraulic or pump/fan shaft input (or required) power, and the subscripts "1" and "2" denote the initial and final conditions, respectively. In the case of the pumps, equations (5)-(8) assume that no static pressure head exists. Considering static pressure head, and an angular speed, ω , higher than that for $H = H_0$, ω_0 , yields (9)-(11), as illustrated in Fig. 6. The hydraulic power required by a pump (BHP) is given by (12), where g_e is the specific gravity (ratio of density of liquid to that of water) and K is a constant depending on the metric system ($K = 6.5120 \times 10^{-9}$ for the international system).

In process lines the flow versus pressure curves can be represented by the polynomial equation (13), where a , b , and c are constants. Practically, in both characteristics b can be considered zero.

In pump discharge lines, a corresponds to the static head of the system. To find c , one head-flow rate has to be known.

The pump flow versus head characteristic, corresponding to the "shut-in" pressure developed at the pump discharge at a given suction pressure and at zero flow, can be represented by (14), where d has to be set properly to achieve the "best fit" with the manufacturer curve.

$$\frac{Q_1}{Q_2} = \frac{\omega_1}{\omega_2} \quad (5)$$

$$\frac{H_1}{H_2} = \left(\frac{\omega_1}{\omega_2} \right)^2 \quad (6)$$

³¹ Typically, the VSD losses are by far overshadowed by the energy savings associated with the speed adjustment. Additionally, bypassing the VSD when the output and input fundamental frequencies are equal can be a cost-effective measure [74].

$$\frac{H_1}{H_2} = \left(\frac{Q_1}{Q_2}\right)^2 \quad (7)$$

$$\frac{P_{hydr_1}}{P_{hydr_2}} = \left(\frac{\omega_1}{\omega_2}\right)^3 \quad (8)$$

$$\frac{Q_1}{Q_2} = \frac{\omega_1 - \omega_0}{\omega_2 - \omega_0} \quad (9)$$

$$\frac{H_1}{H_2} = \frac{H_0 + K_1 \cdot Q_1^2}{H_0 + K_1 \cdot Q_2^2} \quad (10)$$

$$\frac{P_{hydr_1}}{P_{hydr_2}} = \frac{H_0 \cdot (\omega_1 - \omega_0) + K_1 \cdot (\omega_1 - \omega_0)^3}{H_0 \cdot (\omega_2 - \omega_0) + K_1 \cdot (\omega_2 - \omega_0)^3} \quad (11)$$

$$P_{hydr} = H \cdot Q \cdot g_e \cdot K \quad (12)$$

$$H = a + b \cdot Q + c \cdot Q^2 \quad (13)$$

$$H = a + c \cdot Q^d \quad (14)$$

As an example of pump system modelling, it is considered one pump and two different lines, as represented in Fig. 4. Assuming the characteristic curves presented in Fig. 3, the pump can be modelled as

$$H_{pump} = 4000 - 4049 \cdot 10^{-5} \cdot Q_1^2$$

The line A (between constant pressure bus and pump suction) has a pressure drop of 200 ft (1 ft = 0.3048 m) at a flow of 4000 gal/min (1 gal/min = 0.2271 m³/h = 6.31×10⁻⁵ m³/s), therefore it can be modelled as

$$H_A = 1.56 \cdot 10^{-5} \cdot Q_1^2$$

The suction pressure is, therefore, dependent upon the pump flow.

The line B has a pressure drop of 861 ft at a flow of 4000 gal/min, therefore it can be modelled as:

$$H_B = 1000 + 5.38 \cdot 10^{-5} \cdot Q_2^2$$

The line C has a fixed flow of 500 gal/min and 0 ft head ($H_C = 0$). In this example, there is a difference from the natural operating point presented in Fig. 1, in which it is assumed that pump suction pressure never change.

It is known that

$$\sum_{i=1}^m Q_i = 0$$

meaning,

$$Q_1 = Q_2 + Q_3$$

Additionally,

$$\sum_{i=1}^m H_i = 0$$

therefore the overall equation yields

$$H_{in} - H_A + H_{pump} - H_B - H_C = 0$$

Solving the previous equations it is possible to calculate Q_2 , being 5263 gal/min [72].

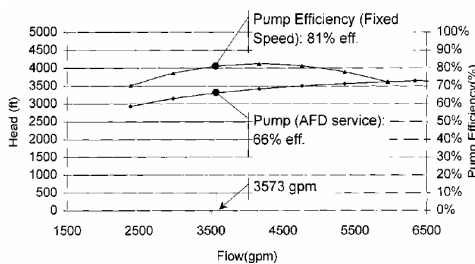


Fig. 3. Pump efficiency for fixed and variable speed [72].

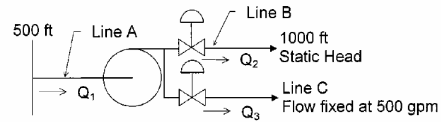


Fig. 4. Process configuration for mathematical modeling examples.

The example given assumes an upstream pressure bus that never changes, a single pump, and looking for a solution at only one flow point. However, there are series and parallel configurations of pumps and lines and solutions at multiple flow points must be found. In general, process lines, pump pressure-flow curves, and pump BHP-flow curves can be modelled as polynomial equations. The individual formulas that determine the flow versus pressure relationship for the lines and pumps are applied to give an overall equation of the pressure and flow for the process system.

In general, for economical evaluation purposes, several steps are required for both fixed- and variable-speed systems, for example, assessment of pump BHP for each of the flow rates, estimation of input real power (taken into account the overall system efficiency), multiplication of input real power by the annual percentage of time for each flow rate, computation of electricity savings, etc. The average savings per year, during use-phase period or economic life, can be obtained by summing annual savings (future value) and dividing that value by the number of years. The future value of savings differs from the present values by the annual interest rate. When the differential capital cost of the VSD versus fixed-speed throttled technique is determined, this savings number can be used to determine the rate of return (ROR) and net present value (NPV) of the VSD investment. If ROR is higher than the discount rate, it is an advantageous option. Most companies establish a minimum ROR as a major criterion for investment acceptance [72].

For centrifugal pumps without lift or static head (e.g., closed-loop circuit), respect the cube power law, i.e., the consumed power is proportional to the cube of the speed, as shown in Fig. 5. If the user wants to reduce the flow in the process, valve control can be used or, alternatively speed control can be applied using a VSD. Although both techniques fulfil the desired objective, the consumed energy is significantly higher when valve throttle control is used, according to the foregoing discussion.

Assuming that is necessary to vary the pump flow to 60%, using a VSD instead of throttling the pump output, reduces the required mechanical power to about 65% (Figs. 5 and 6).

If there is a system head associated with providing a lift to the fluid in the pumping system, the pumps must overcome the corresponding static pressure, as shown in Fig. 6. According to [73], the mathematical expressions (Darcy's formula) typically used to express friction losses (or loss of head), as being proportional to the square of the flow or speed, can be different for a number of equipments [73]. The friction head loss, H_{ft} , is given by (15), where a is the Moody friction factor, l the length of the pipe or duct, d the diameter of the pipe or duct, v the average fluid velocity in conduit, g the acceleration of gravity, and K is a constant depending on used units.

$$H_p = K \cdot a \cdot l \cdot v^2 \cdot d^{-1} \cdot g^{-1} \quad (15)$$

In these pumping systems the mechanical energy is used to overcome the friction in the pipes, plus the mechanical work associated with lifting the fluid against the gravity. If the percentage of the power associated with overcoming the pipe friction is relevant, energy savings can still be achieved although typically less than in systems without static pressure head (closed circulation systems).

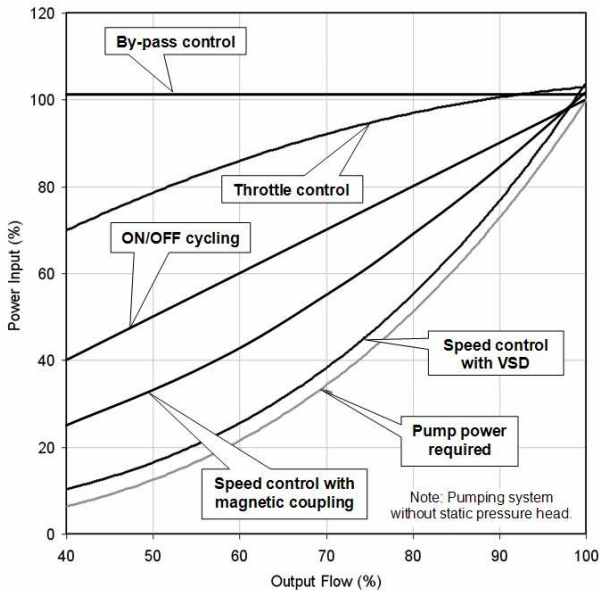


Fig. 5. Input power for different flow control methods of a centrifugal pump without static pressure head [14], [73], [75], [103].

For pumping systems with static pressure head, it should be ensured that minimum speed for the desired flow is enough for the pump to provide the required head, since it is proportional squared speed.

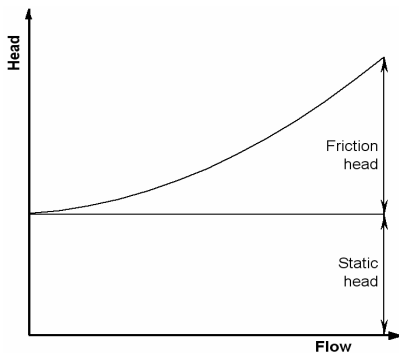


Fig. 6. Total system resistance from frictional losses plus static head losses [75].

Fig. 7 illustrates an example of the power absorbed by a pump system with different components. For the same output flow, the inefficient system absorbs more than twice the power absorbed by the optimised system, showing the importance of integrated motor systems design. In fact, by means of replacing a standard by an energy efficient motor (EEM), increasing the coupling efficiency (e.g., by means of improved shaft alignment), integration of a VSD for flow control removing throttle valve, installation of low friction pipes, and replacing the

pump by one having a better efficiency, significant savings can be obtained.

Assuming that the system is described by the Fig. 7, and the system operates 50% of the time at 100% of the flow and 50% of time at 70% of the flow, it can be verified that, in relation to the original system, the consumption for the improved system can be reduced to 49% as it can be seen in Fig. 8.

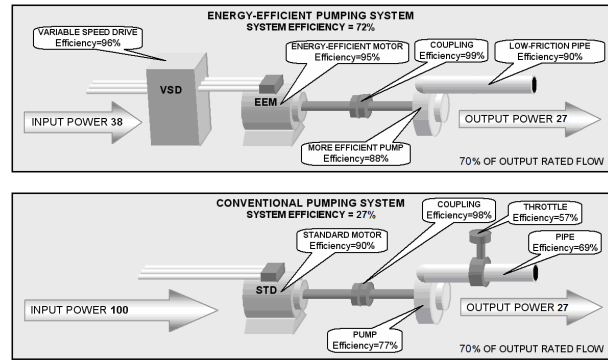


Fig. 7. Two pumping systems providing 70% of output rated flow: (top) Conventional system, with poor efficiency; (bottom) Energy-efficient pumping system combining efficient technologies [75].

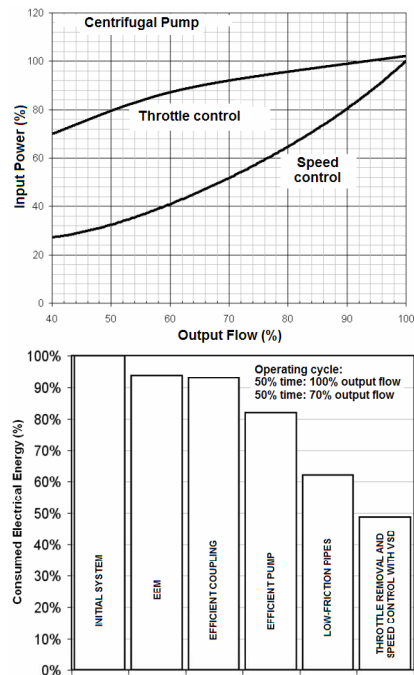


Fig. 8. (top) Input mechanical power required for different flow control methods of a centrifugal pump with static pressure head. (bottom) Electrical energy savings in a pumping system after integrating efficient technologies, considering constant efficiencies equal to those presented in Fig. 7.

If the original system input were on average 10 kW and operate 4000 h/yr, the user, through its improvement could save up to 1122 €/yr (assuming 0.055 €/kWh). This demonstrates the significant savings associated with the energy efficient technologies and speed-based flow control, in pumping systems. Obviously that the longer the low-flow periods the larger the savings associated with speed control. The presented concepts also explain why it is important to avoid excessive head and piping systems angles, in order to avoid extra losses. Note that, if

the power required by proper speed regulation is taken into account, the required rated power of the IM and VSD may be lower, reducing the investment.

In many pumping applications several pumps are used in parallel to produce the required flow. Operating all pumps at reduced speed rather than cycling the pumps ON/OFF according to the demand, significant energy savings can be reached. For example, in a low static head two pump system, with independent piping circuits, operating both pumps at 50% of the rated flow requires approximately 25% of the power required for a single pump operating at 100%, and in both cases 50% of system rated flow is provided. The associated saving potential is 75%. Other advantages are that pumps stay warm (no condensation in the windings), seals stay wet and alive, and high-shock starts on system are eliminated [75]. Fig. 9 illustrates this situation. Also it is possible to control the "water-hammer"³² effect, which degrades the pipes by controlled acceleration/deceleration using VSDs.

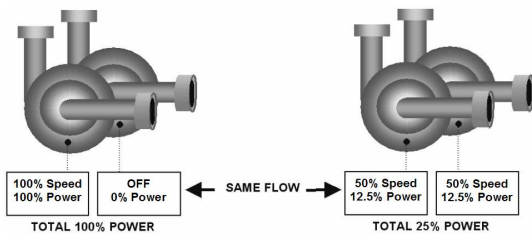


Fig. 9. Pumping plant: Useful relationship to consider with closed loop circulating independent systems where "head" is not a major factor [75].

To show an example of a more complex system, it is now presented a case study, presented in [72], on the integration of VSDs in a crude-oil shipping system, shown in Fig. 10, with 10 storage tanks, six 600-hp booster pumps configured in 3 trains of 2 parallel pumps each, six 5500-hp booster pumps configured in 2 trains of 3 parallel pumps each, and a system of 3 parallel pipelines. The flow demand and the pipeline configuration are constantly changing. Historical flow and pipeline availability was used to establish the process framework. For a 20-year period, the application of a VSD in the 5500-hp shipping pump motors in one or two of the two series trains was found to be cost-effective, with savings of 333 k€/yr and 600 k€/yr, respectively. This allows a maximum of 3150 k€ in extra capital to be spent to install the VSD equipment. In this case, the capital cost of retrofitting VSDs into this application was found to be very close to the extra capital maximum limit. Although the 5-year simple payback and 15-year period of savings, the economic interest is reduced for the company. If other projects with higher ROR are available, they should have precedence. This is an example that demonstrates the importance of taking into account the discount rate and ROR in the economic analysis. In modern companies this is the main decision factor between competitive projects.

Whether electrical energy savings is the sole or partial justification for installing VSDs, the savings calculations must be done correctly. Otherwise, the consequence may

³² Overpressure occurring in flowing fluid when the flow rate varies steeply or is stopped.

be a bad business decision. Simple formulas and "rules of thumb" for calculating energy savings usually overestimate them. The process system must be mathematically modelled to accurately determine the savings. The level of savings is mainly dependent upon the process configuration, being the motor and VSD efficiency of relative low importance in the overall economic calculations. The cost-effectiveness of VSDs for flow control is mainly dependent on the number of hours, required power, and actual flow in each period of the operating cycle. As previously referred, in each period, the lower the actual-to-rated flow, the higher the savings potential when using variable speed in relation to throttle.

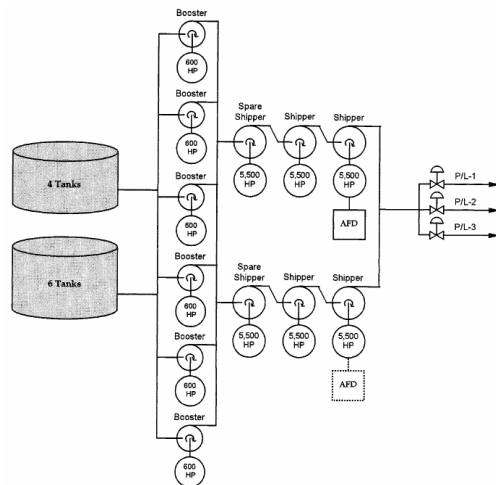


Fig. 10. Case study: crude-oil shipping system: 10 storage tanks, six 600-hp booster pumps configured in 3 trains of 2 parallel pumps each, six 5500-hp booster pumps configured in 2 trains of 3 parallel pumps each, and a system of 3 parallel pipelines [72].

In water utilities, with storage tanks, it is possible to save energy by means of reducing speed, which is possible increasing the pumping period if no head problems occur. Speed reduction leads to lower friction head related power losses. Since power reduction depends on the cube of the speed, for a given pumped water volume, if pumping period is extended 100%, the flow can be reduced to 50%, and the consumed hydraulic energy drops to 62.5%, considering a static head of 50% of the initial pressure head (friction plus static head, Fig. 6). Of course the pumping period should be within the off-peak hours where the electricity has a lower price, which can eventually require the increase of the tanks capacity.

In sewage lift stations, sewage usually flows through sewer pipes under the force of gravity to a wet well location. From there it is pumped up to a treatment process. When fixed speed pumps are used, the pumps are set to start when the level of the liquid in the wet well reaches some high point and stop when the level has been reduced to a low point. Cycling the pumps ON/OFF results in frequent high surges of electrical current to start the motors resulting in electromagnetic and thermal stresses in the motors and power control equipment, the pumps and pipes are subjected to mechanical and hydraulic stresses, and the sewage treatment process is forced to accommodate surges in the flow of sewage through the process. When VSDs are used, associated

with proper control, the pumps operate continuously at a speed that increases as the wet well level increases. This matches the outflow to the average inflow and provides a much smoother operation of the process.

Considerations on fan - When a fan is driven by a fixed-speed motor, the airflow may sometimes be higher than it needs to be. Airflow can be regulated by means of flow restricting methods (throttling), but it is more efficient to regulate it by means of speed variation. Most of the discussed concepts for single pumps without static pressure head apply to centrifugal fans. As in pumps, throttling and speed variation influence the fan efficiency. By efficiency decreasing order, the main flow control techniques are by-pass (required power maintained constant), discharge/outlet dampers, inlet vanes, ON/OFF cycling, magnetic coupling and VSDs [69], [73], [75]. In Fig. 11, power input for discharge/outlet dampers, inlet vanes, and VSD for a centrifugal fan is presented, being the first the worst of the represented methods. In Fig. 12, typical power input for flow regulation in an IM-driven fan by means of speed control using triac-based voltage regulation and combined two-speed IM (6/4 poles) plus by-pass, is shown. The energy consumption in these loads is so sensitive to the speed that the user can achieve large savings with even modest speed adjustments. For example, according to Fig. 11, for 60% output flow, the savings of speed variation over damper flow control methods can be roughly 80%.

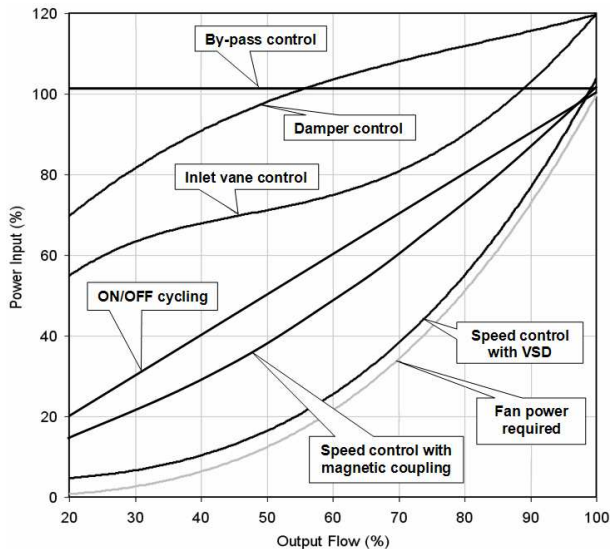


Fig. 11. Input power for different flow control methods of a centrifugal fan [14], [73], [75].

Typically, it is assumed that in airflow conduits the head pressure change in proportion to the square of flow rate. However, when modelling fan systems and estimating energy savings, the systems elements that change head pressure in proportion to less than the square of the flow rate or air speed should be identified. Examples of such system elements are HEPA filters³³ (head loss proportional to the speed), bag filters

³³ High-efficiency particulate air (HEPA) filter is a type of high-efficiency air filter. HEPA filters can remove at least 99.97% of airborne particles 0.3 μm in diameter. Particles of this size are the most difficult to filter and are thus considered the most penetrating particle size (MPPS). Particles that are larger or smaller are filtered with even higher efficiency.

(proportional to speed raised to 1.2), throwaway filters (proportional to the speed raised to 1.65), Air handler coils (proportional to speed), and disc type water meters (proportional to speed). If these relations are not taken into account in the savings calculation, overestimated savings can result [73].

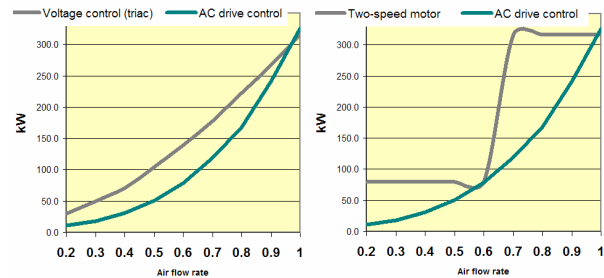


Fig. 12. Input power for different flow control methods of a centrifugal fan (fan: backward curved, 1-m³/s nominal flow, 1890-Pa total pressure increase, 70% efficiency; transmission: 100% efficiency; motor: IM, 3 kW, 400 V, 90% efficiency). Curves generated by the software FanSave 4.0.B Energy Saving Calculator for Fans, ABB, 2008.

When selecting a fan system the operating noise level usually plays a decisive role in most applications. Axial fans used in indoor refrigeration applications often have to operate in noise critical environments. In such applications manufacturers commonly recommend one of the following speed control systems: IMs fed by electronic voltage regulators (VRs, using phase-cut with anti-parallel thyristors [57], [59], with or without noise filter and/or by-pass), IMs fed by autotransformers³⁴, VSD-fed IMs (integrated or separated VSDs, with or without filters), and PM motors with or without integrated VSD [76]. In general, noise levels produced by systems with VR-based speed regulation are higher than those produced by systems with VSD-based speed regulation [76]. In installations, where noise level issues are highly critical and, in particular, when employing slow running fans, driven by 8-, 10- or 12-pole motors, it is recommended the use of VSDs. To control fans with higher speeds, driven by 4- or 6-pole motors, a VR-fed IM is an acceptable solution [76]. VRs (or slip-controlled drives) control the speed of an IM by increasing its slip. Since they are generally less efficient than VSDs, slip controlled drives have lost popularity and presently are mainly used in special situations (e.g., variable load, fixed speed applications or low-dynamics variable-speed applications such as refrigeration units). In fact, a number of applications can benefit with simple voltage regulation, either made by VRs or other techniques (see Chapter 5).

As previously referred, power consumption is a function of the motor design and the control system selected. For medium-high power fans, three major driving options can be referred: (a) IMs with “soft” speed-torque curve (or with relatively large rotor resistance), whose speed can be regulated by changing voltage and/or frequency; (b) IMs with “steep” speed-torque curve (or with relatively low rotor resistance) whose speed can be regulated by changing frequency and voltage; and (c) PM motors, requiring dedicated speed control units. The typical bandwidth of motor efficiencies for a 6-pole, 880-r/min, 1.5-kW motor driving an axial fan system, ignoring

³⁴ Including the solution “MEC”.

impeller and controller efficiencies, are 72-74% for the VR-fed IM (soft torque-speed curve), 78-80% for the VSD-fed IM (steep torque-speed curve), 83-86% for the PM motor with ferrite magnets, and 86-89% for PM motor with neodymium-iron-boron magnets [76]. Therefore, in general, for low power ranges, PM motors can lead to significant improvement of the fan system performance.

In Fig. 13 and Tables 1 and 2, a comparison between different variable-speed axial/helicoidal fan systems (1.05 kW, 8 poles, 630 r/min, 400 V), carried out by a large fans manufacturer, is presented.

Some experimental tests on a small helicoidal fan driven by different 0.5-kW motor systems were carried out, being the main results and conclusions presented in Section 3.8, and complementary results/curves presented in Figs. 14-21.

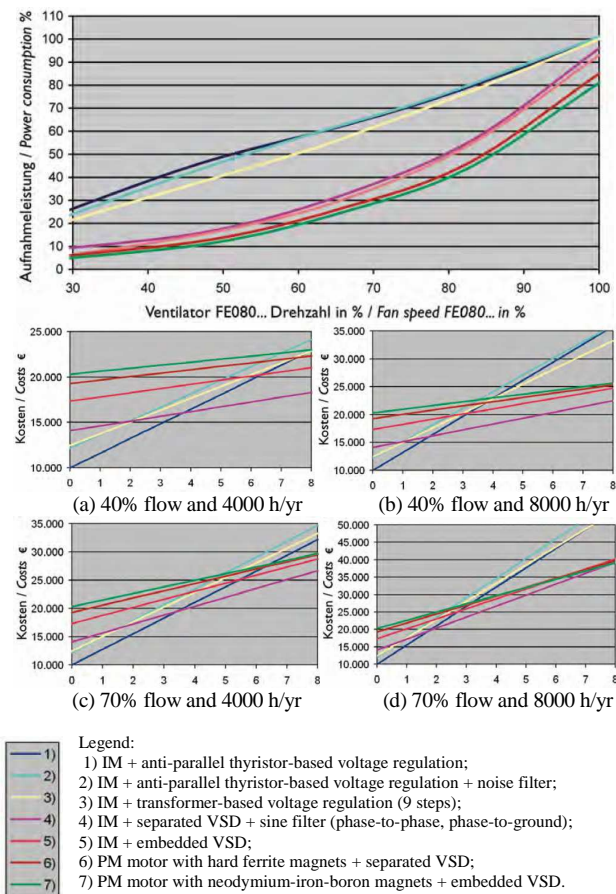


Fig. 13. Comparison of operating costs and power consumption for different variable-speed axial/helicoidal fan driving technologies (system with 10 fans of 1.05-kW) [76].

TABLE 1
COMPARISON OF COST FOR DIFFERENT VARIABLE-SPEED AXIAL FAN SYSTEMS (10 × 1.05-kW FANS, TYPE FE080-ADQ.6N.5) [76].

Technology	Investment with motor, control protection and wiring	Annual energy consumption and operating costs (0.1 €/kWh)			
		4000 h/yr 40% flow	8000 h/yr 40% flow	4000 h/yr 70% flow	8000 h/yr 70% flow
IM + anti-parallel thyristor-based voltage regulation	10000 €	16170 kWh 1617 €	32340 kWh 3234 €	27720 kWh 2772 €	55440 kWh 5544 €
IM + anti-parallel thyristor-based voltage regulation + noise filter	12200 €	14910 kWh 1491 €	29820 kWh 2982 €	28140 kWh 2814 €	56280 kWh 5628 €
IM + transformer-based voltage regulation	12450 €	13020 kWh 1302 €	26040 kWh 2604 €	26040 kWh 2604 €	52080 kWh 5208 €
IM + separated VSD + sine filter	14100 €	5250 kWh 525 €	10500 kWh 1050 €	15750 kWh 1575 €	31500 kWh 3150 €
IM + embedded VSD	17350 €	4620 kWh 462 €	9240 kWh 924 €	14280 kWh 1428 €	28560 kWh 2856 €
BLDC with hard ferrite magnets + separated VSD	19300 €	3780 kWh 378 €	7560 kWh 756 €	12810 kWh 1281 €	25620 kWh 2562 €
BLDC with neodymium-iron-boron magnets + embedded VSD	20300 €	3360 kWh 336 €	6720 kWh 672 €	11760 kWh 1176 €	23520 kWh 2352 €

TABLE 2
ADVANTAGES AND DISADVANTAGES OF DIFFERENT VARIABLE-SPEED MOTOR SYSTEMS FOR A HELICOIDAL FAN [76].

Technology	Investment cost	Efficiency	Profitability	Noise behaviour	Easy installation	Comments
IM + anti-parallel thyristor-based voltage regulation	+	-	+	-	+++	Lowest investment costs. Non critical noise application.
IM + anti-parallel thyristor-based voltage regulation + noise filter	+	-	-	+	+	Electromagnetic noise reduction. Complex installation (wiring)
IM + transformer-based voltage regulation (9 steps)	+	-	-	+++	+++	Optimal noise conditions. Large dimensions due to transformer.
IM + separated VSD	+	++	+++	+++	+++	Optimal performance/cost ratio, without electromagnetic noise. Possible to use standard fans.
IM + separated VSD + sine filter	+	++	++	+++	++	Not suitable for parallel operation of standard fans. High risk of malfunction for motor windings and bearings.
IM + embedded VSD	+	++	++	+++	++	Moderate investment costs with good performance/cost ratio, supplementary fitting possible.
PM motor with hard ferrite magnets + separated VSD	-	++	++	+++	++	High efficiency, special motor, no by pass possible in case of electronic failure.
PM motor with neodymium-iron-boron magnets + embedded VSD	-	+++	+++	+++	++	High efficiency, special motor, no by pass possible in case of electronic failure.

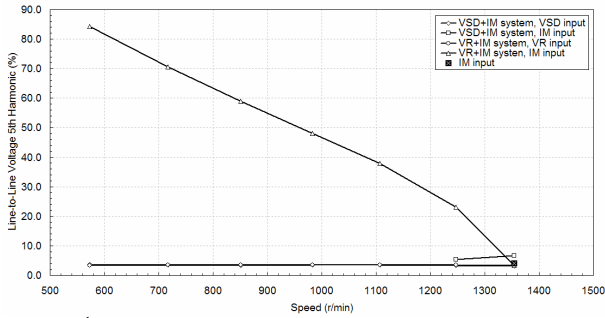


Fig. 14. 5th harmonic of the line-to-line voltage (0.5-kW, 4-pole IM).

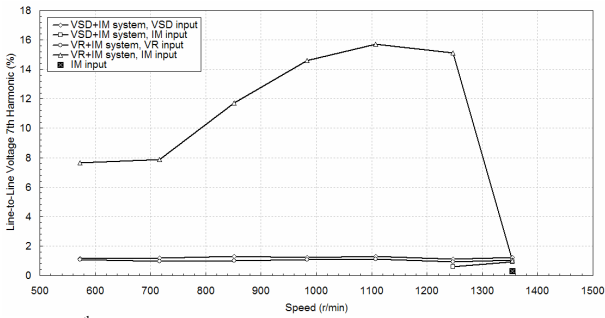


Fig. 15. 7th harmonic of the line-to-line voltage (0.5-kW, 4-pole IM).

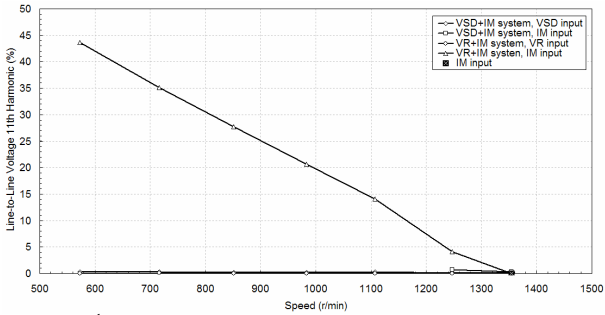


Fig. 16. 11th harmonic of the line-to-line voltage (0.5-kW, 4-pole IM).

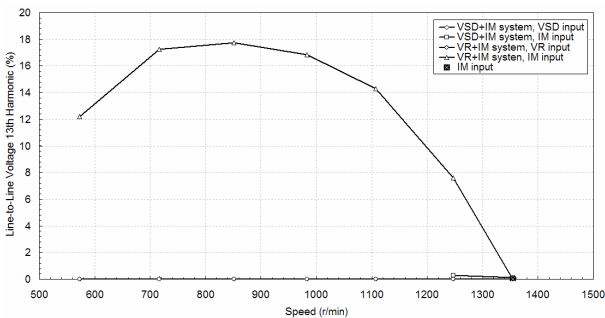


Fig. 17. 13th harmonic of the line-to-line voltage (0.5-kW, 4-pole IM).

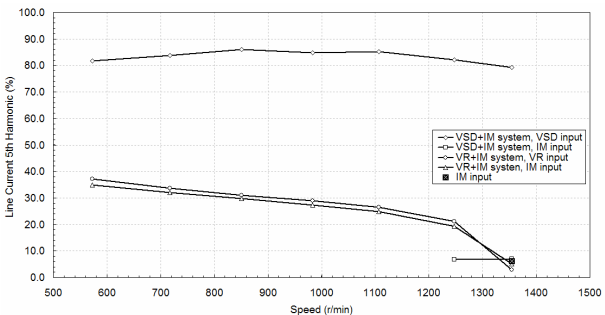


Fig. 18. 15th harmonic of the line current (0.5-kW, 4-pole IM).

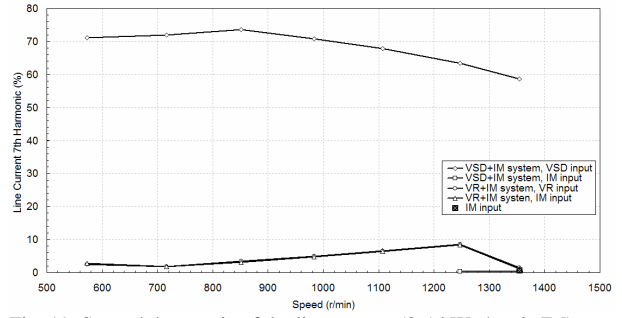


Fig. 19. Seventh harmonic of the line current (0.5-kW, 4-pole IM).

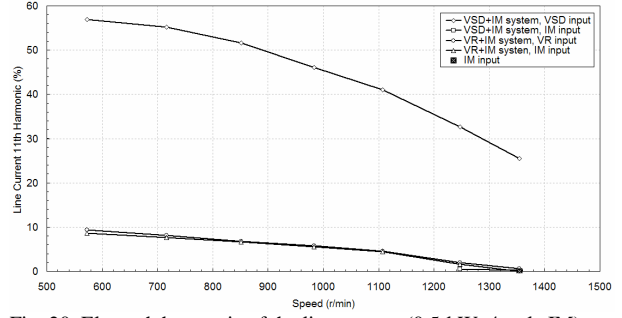


Fig. 20. Eleventh harmonic of the line current (0.5-kW, 4-pole IM).

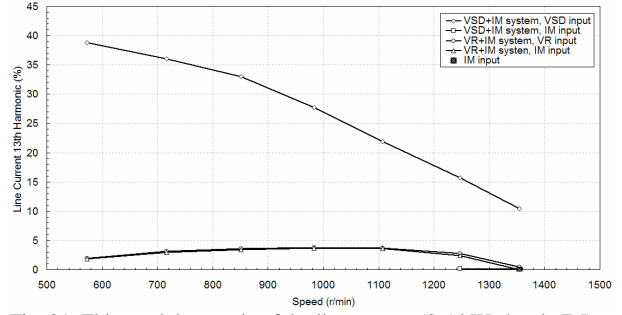


Fig. 21. Thirteenth harmonic of the line current (0.5-kW, 4-pole IM).

Considerations on combined fans and pumps - For example, in a roof top chiller system (Fig. 22), VSDs can be applied to modulate the pump speed, based on zone temperature control, and/or to control the fan speed, based on the coolant return temperature. The result, compared with ON/OFF cycling control, is a more stable temperature in the controlled space and more efficient operation, by typically decreasing the fan energy in the range 25-50%.

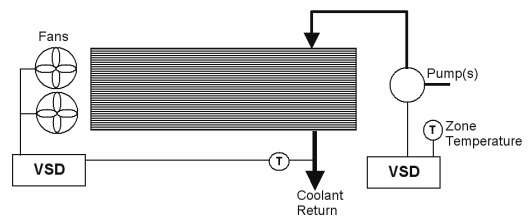


Fig. 22. Application of VSDs on a roof top chiller [75].

Considerations on compressors - Rotary screw and piston air-compressors (both positive displacement compressors) are essentially constant torque loads, which can also benefit from the application of variable-speed control. The savings associated with variable-speed control depend on the control system/technique that is being replaced. In Fig. 23 the energy savings achieved by fitting a VSD to a rotary screw compressed air unit,

compared to other methods of flow control at partial load, can be seen. In a compressor with modulating control, if the demand is 50% of the rated capacity, the energy savings associated with the VSD integration is about 30% [75].

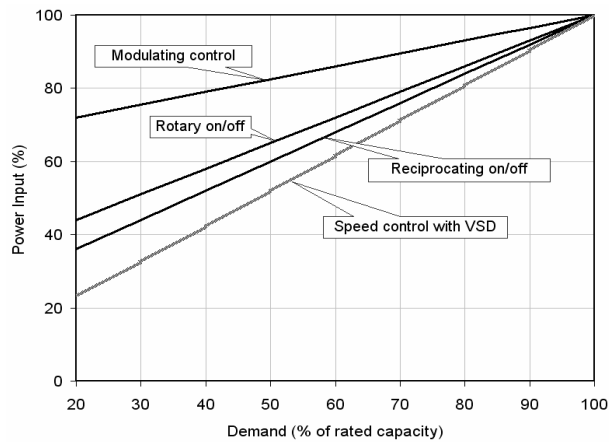


Fig. 23. Energy saved by using a VSD on a rotary screw air compressor [75].

Energy savings with constant torque loads is typically considerably less than with centrifugal pumps or fans, which obey the power cube law, and so to retrofit a VSD to a compressor it is less likely to be economic on the grounds of energy savings alone. Additionally, care needs to be taken to ensure adequate lubrication at reduced speeds. However, the introduction of screw compressors with integral speed control has enabled the additional price of variable speed control to be significantly reduced, leading to typical energy savings of 15-20%. These machines therefore deserve to be considered for all new applications with long running hours, when there is a widely varying demand. Further energy savings will also be achieved through improved pressure control, by reducing the mean generation pressure. Another example of VSD application in compressors is for refrigeration purposes. The use of VSDs for temperature control (floating head operation) in the refrigeration pumps/compressors (e.g., walk-in freezer, Fig. 24) can eliminate the ON/OFF cycling losses and decrease the temperature difference between the condenser and the evaporator, with large energy savings (typically 25%).

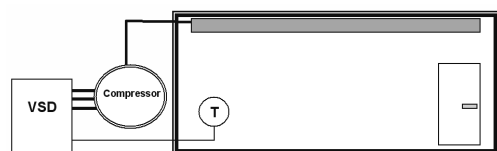


Fig. 24. Application of VSDs on a variable speed refrigeration compressor in a walk-in freezer [69], [75].

The temperature control can also be improved, in terms of differential between internal and external temperatures. It should be referred that a significant energy saving potential is also associated with other variables influencing temperature control strategies. For example, in industrial refrigerators or freezers, the use of “e-cubs” (extremely low-cost measure) in the inner temperature sensor to simulate the thermal inertia of the products being cooled, in order to avoid excessive or

useless activation of the compressor if the products still maintain the desired conservation temperature, even when the indoor/room temperature increases above that point [77].

Considerations on acceleration/deceleration and regeneration - New VSD topologies allow the braking energy to be injected back to the source/grid³⁵ - VSDs with regenerative capability [69], [75], [103]. This feature can be a way of saving a significant amount of energy in applications with frequent and/or long braking/decelerating operations, as for example lifts, hoists, industrial trolleys/trains, large rotary saws, flywheel presses, centrifuges, etc. This is only possible if the motor mechanical transmission allows this mode of operation.

In the case of the lifts, when they going down, and the load weight (people inside) is larger than the counterweight, then the motor torque is in opposite direction to the speed, i.e., the motor is braking. In the same way, when the lifts are going up unloaded, energy savings can be reached if the motor is controlled with a regenerative VSD (Fig. 25). In lifts, 44% of savings can be obtained with regeneration.

In Fig. 26, possible energy savings in lifts, using different technologies, can be seen. With the use of regenerative VSD system, and efficient transmission, the consumed energy can be reduced to 19%, when compared to a conventional system, using a pole changing drive. PM motors with direct drive (without gears) coupling and regenerative braking are also being introduced in new high-efficiency lifts [75], [69].

The same principles apply to hoists and cranes, except that there is no mobile counterweight, and regeneration is only possible when the materials handled going down.

In high-inertia loads (e.g., machine-tools, lathes, flywheel wheel presses and large rotary saws or high inertia wheel sheet saws) or/and high-speed loads (e.g., industrial centrifuges³⁶ machines and high-speed lathes with an automatic feeder), high-mass vertical, inclined or horizontal movement applications (e.g., lifts, hoists/cranes³⁷, trolleys, conveyors and escalators), with frequent accelerating/decelerating operation, it is also possible to save significant amounts of energy with regeneration. In fact, when running, this type of loads has a large amount of kinetic energy, which in a braking process, can be regenerated back to the grid, if a regenerating VSD is used. When high inertia or mass loads are running, the motor speed and torque are in the same direction, but when the operation ends, typically it requires a fast stop. To explore the energy saving potential, the braking energy can be re-injected into the grid instead of dissipating in a resistance.

³⁵ Instead of being converted in heat loss in a braking resistor. In systems with multiple inverters, the energy regeneration can be made using the DC-bus, providing that when some of the inverters are consuming energy, the other are regenerating [101], [106], [119].

³⁶ Industrial centrifuges are accelerated or decelerated in regular cycles. The acquisition and annual operating cost (for 6500 h/yr) of a conventional frequency converter with dynamic braking by means of a resistor (and cooling system) and frequency converter with active power recovery (regeneration capability), both with 50 kW rated power, are, 7400 € and 8750 €, and 7768€/yr and 7332 €/yr, respectively [103].

³⁷ Large crane applications (> 500 kW) represent the largest energy reduction potential through active front-end [101].

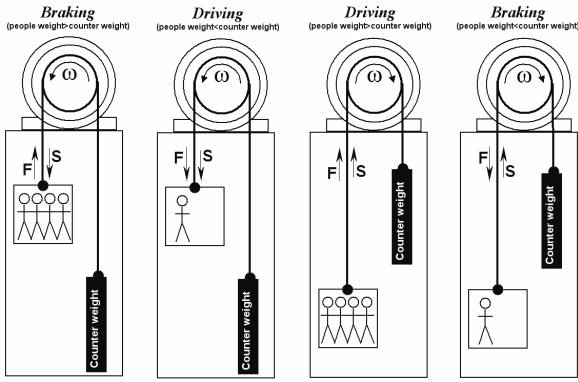


Fig. 25. Lift motor operating modes (F if the force wise applied to the lift cable by motor and S is lift movement; Power can be recovered in an “empty up” or “full down” trip) [75], [103].

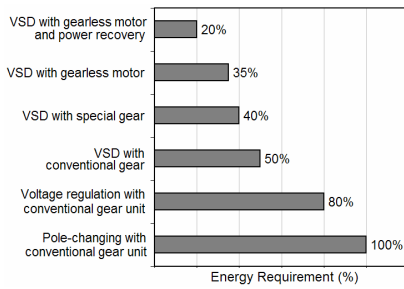


Fig. 26. Energy demand of a lift [75], [103].

Another important aspect is the acceleration process. As it can be seen in Fig. 27, if the motor is simply turned ON (situation (a)), without any speed control, the rotor losses will be higher than if is used a pole changeable motor (situation (b))³⁸. A more efficient acceleration technique uses a VSD (situation (c)) that will significantly reduce the energy consumption, compared to the other mentioned techniques. In fact, increasing progressively the voltage frequency, the slip can be controlled, reducing rotor losses during starting period, and extending motor lifetime. If no significant starting torque is required by the load, soft starting by means of voltage regulation, either using electronic regulation (VR or soft-starter³⁹) or by stator-connection change, can also decrease significantly the motor overall losses and starting current, extending motor lifetime (less heat is generated in the motor, which has positive effect on its service life).

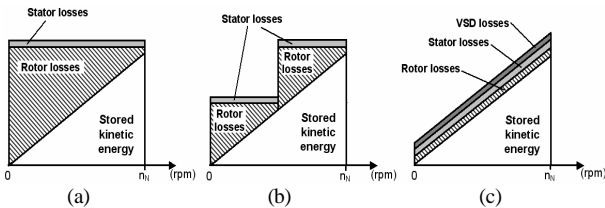


Fig. 27. Energy-consumption for an acceleration period: (a) standard motor; (b) two-speed motor; (c) VSD [75], [103].

Considerations on conveyors and escalators - In constant torque devices (e.g., horizontal conveyors, either for materials handling or people transportation in, for example, airports, Fig. 28), the torque is approximately independent of the transported load (is essentially friction

³⁸ A 3-speed motor can also be used, reducing even more the rotor losses during starting.

³⁹ Actually, VRs and soft-starters have typically the same topology, but power filters are incorporated in VRs to improve permanent operations.

dependent). Typically, the materials handling output of a conveyor is controlled through the regulation of input quantity, and the torque and speed are roughly constant. But, if the materials input to the conveyor is changed, it is possible to reduce the speed (the torque is roughly the same), and, as it can be seen in Fig. 29, significant energy savings will be reached, proportional to the speed reduction. For constant materials output, the relation between speed and handled materials weight or mass is constant. Therefore, to ensure the same (or to lower) materials output and reduce input power, the conveyor speed can be reduced and, to compensate, the materials quantity or load over the conveyor can be increased (or maintained).

Nowadays, elevating escalators (Fig. 30) are used in a number of commercial buildings (e.g., shopping centres) around the world and inclined/elevating conveyors are widely used in Industry.

In the case of elevating conveyors, the steady-state torque is also roughly constant, if load mass does not vary, but has a load mass-dependent component (associated with the load handled) and a speed-dependent component (associated with the system friction). The first component can be added to the second for descending applications and subtracted for lowering applications, assuming bidirectional mechanical transmission between motor and conveyor/escalator. In the second case, regeneration is possible, depending on the mechanical transmission and on the relation between friction component, average weight handled and slope of the conveyor/escalator. However, the following analysis is only for the elevating applications. In the transient state, the equivalent inertia should be taken into account. Considering a conveyor-belt driven by an IM by means of a belt-pulleys transmission system, the steady-state torque required to the motor is given in by (16), where α is the slope, η_{belt} is the belt-pulleys transmission efficiency, r_{pi} is input pulley radius, J_{pi} is the input pulley inertia, r_{po} is the output pulley radius, J_{po} is the output pulley inertia, r_c is the conveyor-belt cylinders radius, J_c is the conveyor-belt cylinders inertia, m is the handled materials mass, $T_{friction}$ is the conveyor-belt load torque component associated with static friction, $T_{gravity}$ is the conveyor-belt load torque component associated with gravity effect on handled materials, J_{mtr} is the motor inertia, ω_c is the conveyor-belt cylinders angular speed, and ω_{mtr} is the motor angular speed. In the transient state, considering an equivalent inertia depending on pulleys and rotor inertias and handled mass, J_{eq} (17) can be written, where T_{em} is the motor electromagnetic torque, and the motor mechanical losses (friction and windage losses) are ignored. The equivalent inertia to the motor, J_{eq} and the linear speed of the conveyor-belt, v_c , are given by (18) and (19), respectively. The output materials rate, q_{out} (in kg/s), is given by (20), where l_c is the conveyor-belt length. Assuming constant output materials rate $q_{out} = K_2$, the mechanical power required by the load, P_{mech} , is given by (21), where K_3 and K_4 are constants, and the speed-dependent and constant load components are evidenced. This can also be applied to escalators. Therefore, in inclined elevating conveyors and escalators, it is possible to conclude that, for a given fixed output quantity (materials or persons) per time unit and variable

handled quantity over the conveyor system, the speed reduction leads to a lower savings potential (in relation to that associated with equivalent horizontal conveyor systems) due to the load torque component associated with gravity, whose relative importance increases with the system slope.

$$T_{load} = \frac{r_{pi}}{r_{po} \cdot \eta_{belt}} (T_{friction} + T_{gravity}) = \frac{r_{pi}}{r_{po} \cdot \eta_{belt}} (K_{friction} + m \cdot g \cdot r_c \cdot \sin \alpha) \quad (16)$$

$$T_{em} - T_{load} = J_{eq} \frac{d\omega_{mtr}}{dt} \quad (17)$$

$$J_{eq} = J_{mtr} + J_{pi} + \left(\frac{r_{pi}}{r_{po}} \right)^2 \cdot (J_{po} + 2J_c + m \cdot r_c^2) \quad (18)$$

$$v_c = \omega_c \cdot r_c = \omega_{mtr} \cdot r_c \cdot \frac{r_{pi}}{r_{po}} \quad (19)$$

$$q_{out} = m \cdot l_c^{-1} \cdot v_c = K_1 \cdot m \cdot \omega_{mtr} \quad (20)$$

$$P_{mech}|_{q_{out}=K_2} = \omega_{mtr} \cdot T_{load} = K_3 \cdot \omega_{mtr} + K_4 \quad (21)$$

Reduced required power by means of speed reduction, leads to motor, transmission and VSD rated power needs, and, therefore, to a significant reduction in the investment.

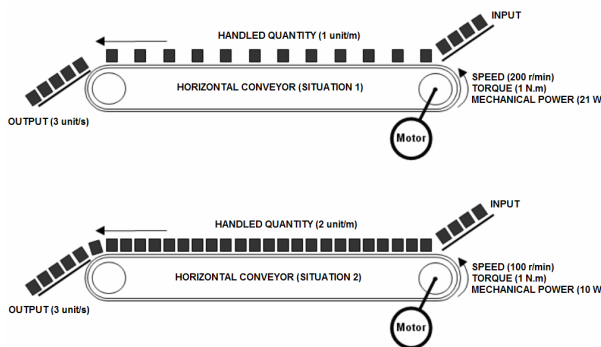


Fig. 28. Power required by an horizontal conveyor: (top) lower load, higher speed; (bottom) higher load, lower speed.

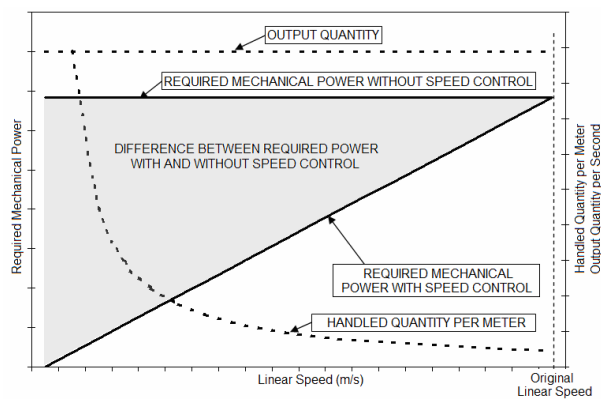


Fig. 29. Power required by a horizontal conveyor for constant and variable speed.

The application of VSDs in elevating conveyors and escalators has other benefits, namely, the controlled acceleration and deceleration, the speed reduction or stop when no material or no body is using the system (using proper external sensors), and the voltage amplitude regulation as a function of actual load, to maximize the

motor efficiency and power factor. In steady-state operation, the voltage amplitude regulation capability as a function of load is by itself a major benefit associated with VSDs.

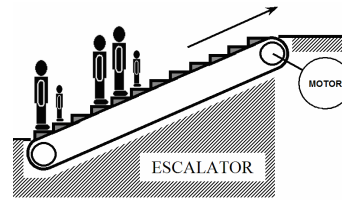


Fig. 30. Simplified representation of an escalator.

Another way to save energy by reducing speed in conveyor belts is to change the driving speed by increasing the driving-end pulley diameter. These strategy leads to the decrease of the mechanical power required and to the increase of the mechanical transmission efficiency due to the increase of the pulley diameter. If the original motor is maintained and no voltage regulation is provided, the slip decreases (due to the lower breaking torque), and, although the reduced absolute motor Joule losses, the motor power factor and efficiency decrease (actual motor load becomes roughly half), slightly attenuating the savings. If proper voltage regulation is made, the motor power factor and efficiency can be maintained at high values. The net benefit is a considerable reduction of the input real power in the system. The overall savings can also be slightly attenuated when, maintaining the same motor, a direct-coupling transmission is replaced by a new one with proper transmission ratio (belts or gears), since their losses and efficiency have also to be taken into account. In these cases, voltage regulation (e.g., either by changing voltage or winding-connection mode) of the oversized motor or, when it fails, its replacement by a smaller motor (preferably a HEM) should be considered. If the speed is to be reduced, the simple application of gears or belts, maintaining the motor power, will result in an oversized system (with poor efficiency), with extra available torque.

A6.3.4 Section 3.9

For the sake of completeness, a technology assessment of the most common mechanical transmission systems is presented in this section. Mechanical transmission transfers the mechanical power from the motor to the load, and can also be used to adapt the speed and torque. The efficiency of these system components vary typically from 60% to 99%, having a significant impact in the overall EMODS efficiency, as well on the maximum output driving torque. Mechanical transmission also affects the system mechanical transient response. The choice of the transmission system should depend on several factors, e.g., load type, speed and torque required, surrounding ambient temperature and contamination degree, acoustic noise, reliability, mechanical response, etc. In industrial and commercial sectors, the majority of the mechanical transmission systems can be divided into four major groups, namely direct coupling, gears, belts and chains, which will be individually discussed in the following sections.

In general, the transmission ratio and efficiency for a transmission system is given by (1), where ω , η_{trs} , T and P are angular speed, efficiency, torque and power, respectively, and the subscripts *in* and *out* refer to the input and output of the transmission system.

$$i = \frac{\omega_{in}}{\omega_{out}} = \frac{P_{in} \cdot T_{out}}{P_{out} \cdot T_{in}} = \frac{T_{out}}{\eta_{trs} \cdot T_{in}} \quad (1)$$

A. Direct Coupling

Direct coupling is the most used transmission type (about 50% of the applications). If the alignment of the motor and load is proper, has a very high efficiency, commonly up to 99.5%, and transmit the mechanical power without slippage. The use of the direct coupling is limited to applications where the load and motor speed is equal. If the motor and load shafts are misaligned (Fig. 1), beside the efficiency reduction (e.g. due to the friction increase), the motor and load bearings lifetime can be strongly shortened. Commercially available equipment for alignment (Fig. 2) is available at moderate cost. From the mechanical perspective, the direct coupling can be hard, semi-elastic, or elastic. From the electric perspective, direct coupling can be conductive or insulating. Depending on the coupling geometry and type, the maintenance is practically not required or very sporadic, but higher maintenance frequency is typically required when a damper ring (made of rubber or polymer) or insulation coats are used between both parts of the coupling, due to natural mechanical wear and temperature ageing, particularly if significant misalignment or vibration exists. A major disadvantage of this type of coupling is the possibility of mechanical vibration transmission from load to motor (or vice-versa), as well as the significant dependency that efficiency and acoustic noise have on the shafts alignment, which is rather difficult to guarantee in most industrial plants. Nevertheless, the user should first evaluate the possibility of using direct coupling in all applications (before considering other sort of mechanical transmissions), from the perspective of efficiency and reliability maximization.

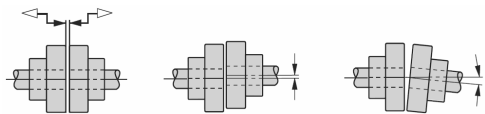


Fig. 1. Direct coupling: (left) proper alignment; (centre) parallel misalignment; (right) angular misalignment.



Fig. 2. Direct coupling and commercial equipment for shafts alignment.

B. Gears

Gears, which are typically used for speed reduction and/or torque increase purposes, transmit mechanical power without slippage, and are commonly used in loads

requiring low speed (up to 1200 r/min) and high torque. Depending on their construction and arrangement, geared devices can transmit forces at different speeds, torques, or in a different direction from the mechanical power source, which are important advantages in relation to direct coupling. In cases where motor and the driven equipment are in close proximity, gears also have an advantage over other non-direct coupling transmission devices in the reduced number of parts required (if only one gear stage is used). The major disadvantages are that gears are expensive to manufacture and their lubrication requirements may impose relatively high operating costs. There are several types of gears, being the most common the helical, bevel, spur, worm, crown, and planetary gears. A new type of gear was introduced by a large manufacturer of motor systems called “spiroplan”, described further. Combined units, integrating helical, bevel and/or worm-gear stages are widely used. In Table 1, examples of commercially combined gear units are shown (combined meshes can increase the efficiency of the group slightly for a given transmission ratio).

In gear-based mechanical transmissions, losses are associated with friction in the gears, bearings, seals, ventilation and lubricant viscosity. In general, the higher the transmission ratio and the number of stages, the lower the gearbox efficiency.

Spur gears are the simplest, and probably most commonly used in low-performance applications, since they have in general lower efficiency levels per stage (94-96%). Their general form is a cylinder with radially-projected spur-form teeth (straight-cut teeth), in which the leading edges of the teeth are aligned parallelly to the axis of rotation. These gears can only mesh correctly if they are fitted with parallel axes. With spur gears, when a pair of teeth meets, they immediately make line contact across their entire width. This causes mechanical impact stress and acoustic noise production. Spur gears make a characteristic whine at high speeds and cannot take as much torque as helical gears because their teeth are receiving significant mechanical impacts. Spur gears are used for low-speed applications running in environments where acoustic noise control is not a major problem.

Helical gears offer a refinement over spur gears. They have a typical efficiency per-stage in the range of 95-98% (roughly independent on system power, as it can be seen in Fig. 3). The leading edges of the teeth are not parallel to the axis of rotation, but are set at an angle. This angling causes the tooth shape to be a segment of a helix. The angled teeth engage more gradually than do spur gear teeth. With parallel helical gears, each pair of teeth first makes contact at a single point at one side of the gear wheel. A moving curve of contact then grows gradually across the tooth face. It may span the entire width of the tooth for a time. Finally, it recedes until the teeth break contact at a single point on the opposite side of the wheel. Thus, force is taken up and released gradually. This causes helical gears to run more smoothly and quietly than spur gears, which is a significant advantage. The use of helical gears is indicated when the application involves high speeds⁴⁰, for large power transmission, and/or when the acoustic noise abatement is important. Disadvantages

⁴⁰ The speed is considered to be high when the pitch line velocity (that is, the circumferential velocity) exceeds 25 m/s.

of helical gears are the relative higher price, the resultant thrust along the axis of the gear, which needs to be accommodated by appropriate thrust bearings (which are typically more expensive than radial bearings), and a higher degree of sliding friction (in relation to spur gears) between the meshing teeth, often addressed with specific additives in the lubricant. A commercial helical gear unit is shown in Table 1. Double-helical gears, also known as herringbone gears, overcome the problem of axial thrust presented by standard or single helical gears by having V-shape teeth, corresponding to two mirror-imaged single-helical gears stacked. This cancels out the thrust since each half of the gear thrusts in opposite direction. They can be directly interchanged with spur gears without any need for bearing replacement, attenuating the potential additional price associated with this type of gears.

Bevel gears are essentially conically shaped, although the gear does not extend all the way to the vertex (or tip) of the cone that bounds it. They have a typical efficiency in the range 95-98% per stage (roughly independent on the system power, as it can be seen in Fig. 3). With two bevel gears in mesh, the vertices of their two cones lie on a single point, and the shaft axes also intersect at that point. The teeth of a bevel gear may be straight-cut as with spur gears, or they may be cut in a variety of other shapes. Spiral-bevel gears have teeth that are both curved along their length and set at an angle, analogously to the way helical gear teeth are set at an angle compared to spur-gear teeth. Spiral-bevel gears have the same advantages and disadvantages relative to their straight-cut cousins as helical gears do to spur gears. Straight-bevel gears are generally used only at linear speeds below 5 m/s.

A crown gear is a particular form of bevel gear whose teeth project at right angles to the plane of the wheel. In their orientation the teeth resemble the points on a crown. A crown-gear can only mesh accurately with another bevel gear, although crown gears are sometimes seen meshing with spur gears.

A worm gear is a gear that resembles a screw. It is a sort of helical gear, but its helix angle is usually somewhat large (close to 90 degrees) and its body is usually fairly long in the axial direction. These attributes give it its screw like qualities. A worm is usually meshed with an ordinary disk-shaped gear, called “gear” or “wheel”. The prime feature of a worm-and-gear set is that it allows the attainment of a high gear ratio with few parts, in a small space. In worm-and-gear sets, since the worm helix angle is large, the sliding action between teeth is considerable, and the resulting frictional losses cause the efficiency of the gear to be typically in the 75-90% range, being the efficiency value considerably dependent on the system size, as it can be seen in Fig. 6. The distinction between worm and helical gears is made when at least one tooth persists for a full 360 degrees turn around the helix. If this occurs, it is a worm gear, if not it is a helical gear. A worm may have as few as one tooth. The usual screw nomenclature applies: a one-toothed worm is called “single-thread” or “single-start”. A worm with more than one tooth is called “multiple-thread” or “multiple-start”. In a worm-gear set, the worm drives the gear. However, if the gear attempts to drive the worm, it may or may not succeed, since the gear teeth may simply

lock against the worm teeth, because the force component circumferential to the worm is not sufficient to overcome friction. Whether this will happen depends on a function of several parameters. However, an approximate rule is that if the tangent of the lead angle is greater than the coefficient of friction, the gear will not lock. Worm-gear sets that do lock in the above manner are called “self-locking”. The self-locking feature can be an advantage, as for instance when it is desired to set the position of a mechanism by turning the worm and then have the mechanism hold in that position. This sort of braking system, can actually save energy, if it is used instead of an electromagnetic braking embedded or not in the motor. If medium to high power transmission is desired, the tooth shape of the gear is modified to achieve more intimate contact with the worm thread. A noticeable feature of most of such gears is that the tooth tops are concave, so that the gear partly envelops the worm. A further development is to make the worm concave (viewed from the side, perpendicular to its axis) so that it partly envelops the gear as well. This is called a cone-drive or Hindley worm. Commercial worm gear units are shown in Table 1.

In Fig. 4, typical list per-kW prices for different gear units are shown.

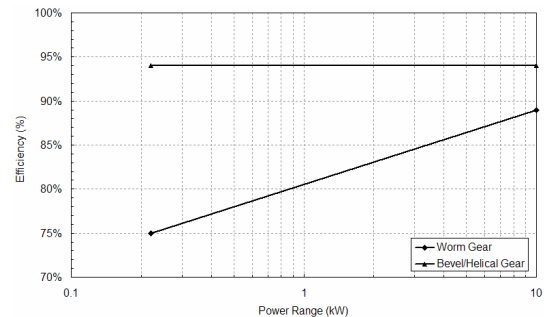


Fig. 3. Average efficiency comparison for worm and helical/bevel gears ($i = 30-60$, single-stage), as a function of power range [2].

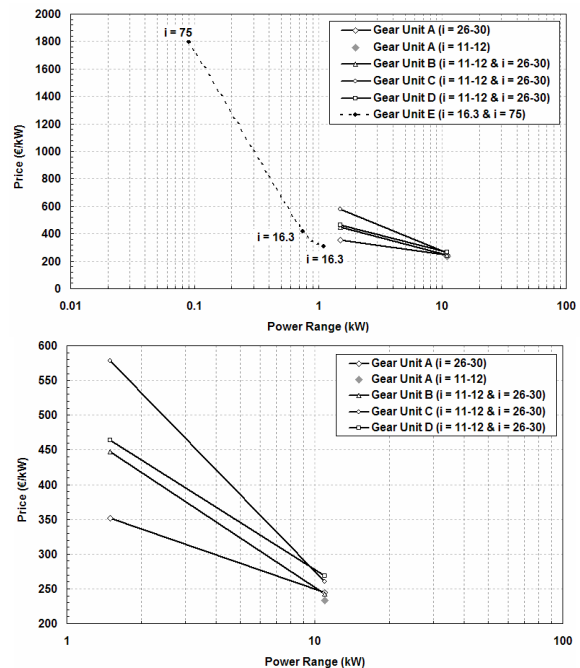


Fig. 4. Prices per kW of commercial gearbox units [106]: Gear Unit A – Helical; Gear Unit B – Helical with Parallel Shaft; Gear Unit C – Helical-Bevel; Gear Unit D – Helical-Worm; Gear Unit D – Spiroplan.

An epicyclical gear or planetary gear is a gear system that consists of one or more outer gears (or planet gears) meshing with a central gear (or sun gear) and an outer ring gear (or annulus), which meshes with the planet gears. Typically, the planet gears are mounted on a movable arm or carrier which itself rotate relative to the sun gear. A commercial planetary gear unit is shown in Table 1.

Multi-ratio systems can be used to improve the starting and stopping process of a mechanical system and allow maintaining the system efficiency in high levels, but they are not addressed in this thesis.

There are also commercially available cycloidal speed reducers (Fig. 5), in which the conventional toothed gears are replaced by discs and rollers rotating around a central eccentric bearing (rolling contact). In a rolling contact, all major torque transmitting components roll and experience compression, they do not slide or shear, contributing to minimize friction, wear, and heat generation, and consequently improve efficiency and reliability. Single-stage efficiency approaches 93%, and double-stage efficiency approaches 86%, meaning a good performance over worm gear reducers (with similar output capability). Unlike common gear mechanisms, which have only 1 or 2 teeth to absorb the entire shock load with possible gear teeth breakage, at least 66% of ring gear rollers and cycloidal disc lobes share the shock load under compression. Therefore, this technology withstands 500% shock overloads (in relation to rated torque) without damage and are very compact, having high torque to weight ratios (compared to worm, helical and planetary gears). They are available in the market from 0.12 kW to 55 kW, with output torques up to 60700 N.m. Additionally, they produce low noise level, have relatively high efficiency (compared to worm gears), and require very low maintenance (oil change interval within 2500 h of operation and easy-to-replenish oil lubrication) [78], [79]. In fact, regarding compactness, unlike helical speed reducers which require additional stages to achieve higher reduction ratio (increased size/weight, decreased efficiency, more bearings and gears to maintain), changing the ratio of cycloidal reducers (up to 87:1) involves only the changing of ring gear rollers, cycloidal disc lobes, and eccentric bearing. The external physical dimensions of speed reducers remain the same. The relatively lower losses and, consequently, the lower operating temperature (particularly in relation to worm gears), lead to a longer service life and energy savings in relation to equivalent worm gears [79].

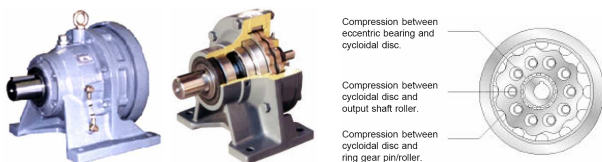


Fig. 5. Cycloidal gears: (left) picture; (right) operation principle.

Mechanical variable speed reducers or disco drives (Fig. 6) can also be referred, allowing speed regulation mechanically [79]. The input speed goes through the high-speed mechanism, and the speed reduction takes place with the contact among the inner sun disc, planet

discs, and outer ring, by means of viscous traction, and the speed variation is achieved by changing the radial position of the planet discs relative to the shaft center. The location of the inner sun and outer rings remains unchanged relative to the frame. Planet discs drive a slow speed carrier mechanism, which outputs the low speed. According to manufacturers, this system is characterized by an excellent load shock resistance at low output speed and low-speed starting capability with high load. The commercially available units have large output torque and fair efficiency at low and high speed (up to 85%, as it can be seen in Fig. 7), fully enclosed design, output speed variation within 0.1% (even at extremely low output speed range), compactness (eliminates tall cumbersome drive package and the low profile allows it to fit into a tight space) and lightweight, multiple mounting and configurations, simple speed variation control, low operating sound level, low inertia, very low vibration operation, simple installation and handling with in-line configuration (Fig. 6), and minimum maintenance.

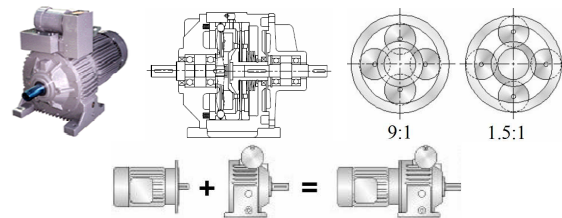


Fig. 6. Variable-speed reducer: (left) picture; (right) operation principle [79].

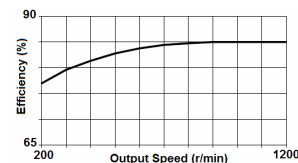


Fig. 7. Variable speed reducer efficiency-output speed curve [79].

Regarding maintenance cost of gear units, in general, it depends on the handled load (stop/start frequency, mechanical shock transients, inertia, acceleration, etc.), operating time to each load level, surrounding environment (temperature, humidity, corrosive substances, etc.), lubricant type⁴¹ and quantity, since it influences the gear efficiency. In short, the choice of a gear should depend upon the acquisition cost, operating cost including the maintenance and energy costs (depend upon reliability and efficiency as a function of load), and required gear ratio for the process.

The total energy saving potential associated with the replacement of worm gears by helical or bevel gears is in the range of 5 to 20%, being higher for low power applications, due to the larger difference in efficiency [81], [82]. In order to illustrate the typical simple payback, some examples are presented in the Table 2, assuming an electricity cost $C_{kWh} = 0.05-0.07$ €/kWh, a discount rate of 2%, a motor efficiency of 80%, and annual energy savings per kW calculated according to (2), where $N_{h/yr}$ is the number of operating hours per year. For a per-kW calculation base, both annualized cost and annual savings were divided by the output power. It should be noted the importance of the motor efficiency in

⁴¹ E.g., mineral oil typically last up to 5/3 times more than synthetic oil.

the savings calculations. Additionally, since the lower efficiency gear (worm gear) considered in the example, is more expensive than the others, the payback results null. In fact, the use of worm gears can only be justified if space/volume restrictions exist, since they are relatively more compact. Obviously, the lower the motor efficiency, the higher the savings associated with the gear efficiency improvement. Therefore, if HEMs are considered, the investment in high-efficiency gears can become, in some cases, non-cost-effective.

$$S_{\text{€/kW}\cdot\text{yr}} = S_{\text{€/yr}} \cdot P_{\text{out}}^{-1} = (\eta_{\text{irs_low}}^{-1} - \eta_{\text{irs_high}}^{-1}) \cdot N_{h/\text{yr}} \cdot C_{\text{kWh}} \cdot \eta_{\text{mtr}}^{-1} \quad (2)$$

An important advantage of gears over direct driving with frequency or pole-number change is the possibility of maintaining approximately constant the motor shaft power available, as well as the efficiency for very low speeds, as it can be seen in Fig. 8. Additionally, if fixed, low speed is required, choosing a motor with reduced pole number (e.g., 2 poles) and adapt a gear to reduce speed, can lead to a more efficient system (although lubricant leakage issues in gear units can limit the motor number of poles) when compared to a direct-coupled motor with a 6- or 8-pole motor, whose efficiency is, in general, relatively poor (see Section 3.9.6).

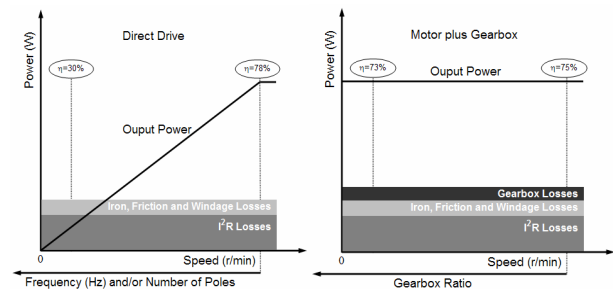


Fig. 8. Simplified comparison between the available output power and efficiency in direct driving and gearbox-based driving [81].

C. Belt-Pulley Sets

A belt is a looped strip of flexible material, used to mechanically link two or more rotating pulleys or shafts. The belts, besides they could act as mechanical fuses, allow a flexibility in the positioning of the motor in relation to the driving load, and, using pulleys (or sheaves) of suitable diameter, can decrease or increase speed (and torque) with a large number of possible speed ratios. When slip occurs, the transmission ratio varies as a function of load, which is a disadvantage in most applications. Belt-pulleys-based transmissions are used in about $\frac{1}{3}$ of the electric motor transmissions in Industry and in commercial buildings [83], coupling electric motors with a wide variety of loads. In order to ensure reliable performance and optimize the overall efficiency of motor drives, it is important to select the most suitable belt transmission for each particular application. A properly designed belt transmission system provides relatively high efficiency, cleanliness and low acoustic noise. Additionally, it does not require lubrication, and can have low maintenance requirements.

In this section, the characteristics of the main belt types are surveyed, with particular emphasis on their

energy efficiency, cost-effectiveness and application ranges. Among all sort of belts that can be found in market, they can be divided into three main groups, namely, smooth-V belts, cogged-V belts, flat belts and synchronous or timing belts, as shown in Table 3.

In general, cogged-V belts are more efficient than smooth-V belts. Cogged-V belts can be found with radial or longitudinal cogs, both solution reducing mechanical hysteresis losses. Longitudinal cogs allow a better position fixation in the pulley. The flat belts (thinner than V belts) are more efficient than cogged-V belts. Variable pitch drives are pulley and belt drives in which the pitch diameter of one or both pulleys can be adjusted.

The large majority of belt transmissions uses V belts, which are the cheapest belts and present an efficiency curve which drops rapidly when the load goes below or above the design load, as it can be seen in Fig. 13. The efficiency of V belts also degrades rapidly with use, requiring regular maintenance. V belts can successfully be replaced by other types of belts, which offer higher peak efficiency, flatter efficiency curves and lower maintenance requirements.

The V shape of the belt tracks in a mating groove in the pulley (or sheave), resulting in a reduced slip and correct positioning of the belt in relation to the pulley. The belt also tends to wedge into the groove as the load increases. The greater the load, the greater the wedging action, improving torque transmission and making the V-belt an effective solution. They can be supplied at various fixed lengths or as a segmented section, where the segments are linked (spliced) to form a belt of the required length. For high-power requirements, two or more V belts can be joined side-by-side in an arrangement called a multi-V, running on matching multi-groove sheaves. The strength of these belts is obtained by reinforcements with fibers such as steel, polyester or Aramid (e.g., Twaron). V-belts have efficiency in the 90-96% range, depending on elasticity, slip, belt tension, alignment and diameter of the pulleys. The misalignment (see Fig. 9) of the pulleys can affect significantly the lifetime and efficiency of the belt-pulley set, and should be particularly avoided. Excessive tension lead to accelerated wear of the belt, bearings, and shafts. Reduced tension lead to excessive slip and losses, which, consequently, lead to premature failure of the belt. This kind of mechanical transmission requires periodic tension adjustment. There are commercially available equipments to align pulleys and measure/adjust tension/strength (Figs. 10 and 11). The equipment for belt tension measurement⁴² (Fig. 11), allows reducing the acoustic noise emitted by the belt. Typically, it uses optical technology (infrared) and is very simple to use, being recommended for belts with a natural frequency between 30 Hz and 600 Hz. The sensor lead is placed at a 50-mm distance (no special care is needed with the angle between the sensor lead and the belt surface) from the in-operation belt, and after a few seconds, the natural frequency is computed.

⁴² This equipment measures the natural frequency of the vibration in the belts, directly related to the belt strength. If the belt strength increases, the vibration frequency also increases. This equipment is indicated for long belts vibrating at low frequencies (lower than 30 Hz). The measurement is made with the system off and still. By means of a stroke in the belt, it vibrates at the static auto-frequency, being the strength measured using LASER pulses.



Fig. 9. Belt-pulley systems installation: (left) torsional misalignment; (center) angular misalignment; (right) parallel misalignment.

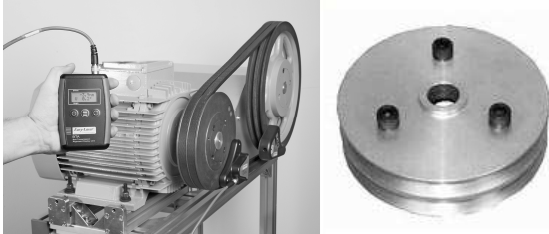


Fig. 10. (left) Two-V belt and double-groove pulleys transmission system and commercial system for belt-pulley systems alignment. (right) Double-groove pulley.



Fig. 11. Commercial systems for belt-pulley systems strength adjustment.

The belt losses are a combination of torque losses and speed losses. In order of decreasing importance, the torque losses can include hysteresis, friction, windage, slip, and creep losses.

Hysteresis losses are due to the belt bending and unbending around the pulleys, and occur mainly at the four flexing points (Fig. 12). This kind of losses is a function of the stress imposed on the belt materials, which is dependent on the belt thickness, pulleys diameter, and material damping factor.

Hysteresis losses can thus be decreased by decreasing the belt thickness (these losses are proportional to the cube of the belt thickness), by increasing the pulley diameter and by using better belt materials [83]. Hysteresis power loss for the same pulley size grows directly with the rotating speed and is basically independent of the load.

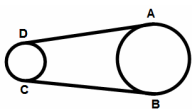


Fig. 12. Belt drive showing four flexing points: A, B, C, and D.

Frictional losses are associated with the friction between the sidewalls of the belt and the inside walls of the pulley. These losses occur whenever a V belt enters or leaves the pulley. These losses are significant in V belts, which rely on the grip between the pulley walls and the belt to transmit torque. In synchronous belts there are also small frictional losses associated with the entrance and the exit of the belt teeth into and out of the teeth of the sprockets. These losses also grow directly with the speed of operation and show little variation with the load. In flat belts the frictional losses are negligible.

Windage losses are associated with the kinetic energy, which is transferred to the surrounding air due to the belt motion. The smoother the belt surface, the smaller these losses will be. Cogged or toothed belts thus have higher windage losses. Although these losses grow steeply with the belt speed, they are comparatively small relative to other belt losses. Windage losses are essentially constant as a function of the load.

There are also the belt speed losses, which can be divided into slip and creep losses. Slip losses are due to the slippage that occurs in V belts and flat belts when there is not enough belt tension to provide static friction between the belt and the pulleys. With a properly tensioned belt, the slip is minimal. The tension of the belt has an optimum value. If the tension is too high, there will be premature wear of the bearings, whereas too little tension leads to slippage. Even a properly adjusted V belt will stretch with usage, leading to a decrease in belt tension and thus to increased slip losses. Creep losses are due to different belt elongation before entering and after leaving a pulley.

Due to increased tension in the section of the belt pulled by the driver pulley, a slightly longer, narrower belt section leaves the driven pulley. This small difference causes the belt to creep around the pulley, which reduces the speed of the driven shaft. In a well-designed V-belt drive, creep losses are typically in the range of 0.5-1% [83]. Creep losses are a function of the belt construction, the pulley diameter, load, and speed.

Fig. 13 shows the typical efficiency curve of a properly installed and maintained V belt. The efficiency drops significantly when the belt is operated below rated load because torque losses (hysteresis, friction and windage) are almost independent of the load and thus stay nearly constant, while the useful power delivered is reduced. A properly tensioned belt has negligible slip at or below rated load, but slips significantly when overloaded, causing the efficiency of a V belt to drop in an overload condition. As was already mentioned, V belts stretch with time and lose efficiency.

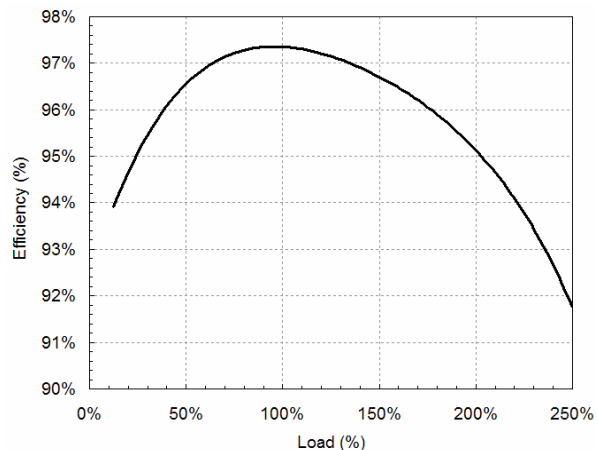
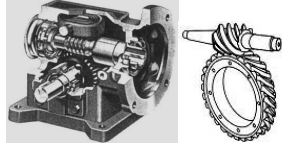
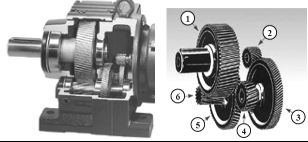
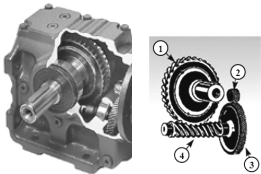
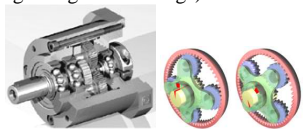


Fig. 13. Typical efficiency variation as a function of load for a V belt, considered constant input speed [83].

Picture & Designation	Description & Main Advantages of the Gear	Characteristics			
		Power Range	Gear Ratio and Speed Range	Torque	Efficiency Range
 <p>Worm-Gear Units (single-stage)</p>	<ul style="list-style-type: none"> - Low efficiency; - Low acoustic noise; - Low cost; - High torque. 	0.12-22 kW	Gear Ratio Range $i = 7-50$ Speed Range 0.1-500 r/min	10-100 N.m	50-96%
 <p>Helical-Gear Units (three-stage or two-stage)</p>	<ul style="list-style-type: none"> - Relatively high cost; - High efficiency; - Low acoustic noise; - Reduced backlash; - General purpose; - Compact. 	0.09-160 kW	Gear Ratio Range $i = 3-290$ $i_m = 90-27000$ Speed Range 0.05-809 r/min	31-18000 N.m	94-98%
 <p>Helical-Bevel Gear Units (three-stage or two-stage) 3-stage: 2-stage helical + 1-stage bevel 2-stage: 1-stage helical + 1-stage bevel</p>	<ul style="list-style-type: none"> - High efficiency; - Flat efficiency curve; - High endurance; - High-torque; - Wear free; - Long maintenance-free operation; - Reduced backlash (optionally). 	0.12-200 kW	Gear Ratio Range 3-stage units $i = 4-200$ $i_m = 94-32500$ 2-stage units $i = 3-40$ Speed Range 0.1-522 r/min	3-stage units 125-50000 N.m 2-stage units 40-1500 N.m	94-98%
 <p>Spiroplan®-Gear Units</p>	<ul style="list-style-type: none"> - Wear free; - Lubrication for service life; - Long maintenance-free operation; - Low acoustic noise; - Very compact. 	0.09-1.1 kW	Gear Ratio Range $i = 4-75$ Speed Range 8-329 r/min	12-70 N.m	50-90%
 <p>Helical-Worm-Gear Units (single-stage helical, single-stage worm)</p>	<ul style="list-style-type: none"> - Fair efficiency*; - Low acoustic noise; - Low cost; - High torque; 	0.12-22 kW	Gear Ratio Range $i = 7-288$ $i_m = 110-34000$ Speed Range 0.1-397 r/min	43-4000 N.m	75-90%
 <p>Planetary-Gear Units (single-stage or two-stage)</p>	<ul style="list-style-type: none"> - Very high power density; - High reliability; - Cost-effective; - High efficiency; - Low backlash; - Very compact; - High torque; - High overhung loads. 	1.1-5 kW	Gear Ratio Range $i = 3-10$ $i_m = 16-100$ Speed Range (N/A)	25-3000 N.m	95-98%

Notes: *Higher than that of the straightforward worm-gears.
 The symbol i_m means multi-stage transmission ratio. Additional characteristics per-stage and figures for spur and bevel gears:


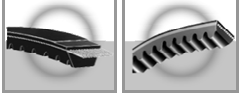
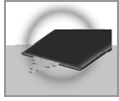


	Single-Stage Spur Gears Efficiency: 96-99% Maximum Gear Ratio: $i_{max} \approx 7$		Single-Stage Bevel Gears Efficiency: 96-99% Maximum Gear Ratio: $i_{max} \approx 5$
---	--	---	---

TABLE 2
 COST-EFFECTIVENESS OF COMMERCIAL GEARBOX UNITS WITH RATED POWER HIGHER THAN 10 kW.

Scenario	Annual Savings	Simple Payback	CSE, 2 yr
Helical ($\eta=98\%$) vs. Helical-Worm ($\eta=89\%$)*	55.0 to 91.7	0	-0.14 to -0.47
Spiroplan ($\eta=90\%$) vs. Helical-Worm ($\eta=89\%$)**	6.7 to 11.1	0	0
Planetary ($\eta=97\%$) vs. Helical-Worm ($\eta=89\%$)***	49.4 to 82.4	0	0

Assumptions:
 New application; 8000 h/yr; 0.05-0.07 €/kWh; Discount rate = 2%; Motor efficiency = 90%.
 *Price premium = -25 to -50 €/kW. **Price premium= 0 €/kW. ***Price premium = 0 €/kW.

TABLE 3
EXAMPLES OF COMMERCIAL BELTS [14], [103].

Picture & Designation	Description & Main Advantages of the Belt	Characteristics		
		Price Premium*	Max. Reduction	Efficiency
 Flat- or Smooth-V Belt	<ul style="list-style-type: none"> - Suitable for shock loads; - Periodic maintenance; - No change of pulleys required; - Low first cost; 	--	$i_{max} \approx 8$	90-96%
 Cogged-V Belt	<ul style="list-style-type: none"> - Suitable for shock loads; - Periodic maintenance; - No change of pulleys required when replacing V belts. - Easy to retrofit; - Small slip. 	1-2 €/kW	$i_{max} \approx 8$	95-97%
 Flat Belt	<ul style="list-style-type: none"> - Suitable for shock loads; - No periodic maintenance; - Change of pulleys required when replacing V belts (low cost); - medium-high speed; - Small slip; - Low noise. 	3-6 €/kW	$i_{max} \approx 5$	96-99%
 Synchronous or Timing Belt	<ul style="list-style-type: none"> - No suitable for shock loads; - No periodic maintenance; - Change of pulleys required when replacing V belts (high cost); - Low-medium speed; - Slipless; - Noisy. 	8-16 €/kW	$i_{max} \approx 8$	96-99%
 Chevron Pattern Timing Belt	<ul style="list-style-type: none"> - No suitable for shock loads; - No periodic maintenance; - Change of pulleys required when replacing V belts (high cost); - Slipless; - Low noise. 	9-17 €/kW	$i_{max} \approx 8$	97-99%

Note: *Price premium over V belts, without considering the pulley price premium.

Belt losses are converted to heat, which means that a high-loss belt will run warmer than a more efficient belt, leading to an accelerated ageing of the belt materials. Measuring the temperature difference of the belt in relation to ambient temperature is a good indicator of the belt efficiency. Typically, an efficient belt drive, immediately after shutdown, will be at moderate temperature, up to 40-50°C, depending on the ambient temperature. If the temperature is high than 60-70°C, the belt requires maintenance. Infrared cameras or sensor probes may be used to measure the temperature belts. Belt transmission losses are strongly dependent upon the mechanical power being transmitted. The higher the system rated output power the lower the belt-related losses as a percentage of the motor power output. Additionally, the higher the speed is, the higher the belt losses will be. For small loads, the belt losses represent a significant percentage of the power being transmitted. This fact is mainly due to the higher relative importance of the hysteresis losses in small drives, especially when using small pulleys. Independent tests, carried out with fan drives used in the exhaust fans in multifamily buildings, show that for small loads (less than 2.2 kW) the belt transmission losses can be as high as 30% [83].

Both smooth-V belts and cogged-V belts have a similar structure and run on the same pulleys. The tensile strength is provided by polyester cords and the body is made of neoprene or other synthetic rubber. Cogged-V belts can substantially reduce hysteresis losses, since the presence of the cogs results in less compression and decompression of the rubber material. The amount of the energy savings is highly dependent upon the pulley

diameters, with smaller pulleys providing higher savings. The use of sheaves with a diameter below the minimum recommended values is common due to space and first-cost constraints. Fig. 14 shows the relative performance of smooth-V belts and cogged-V belts. If the transmission ratio is to be maintained and there are no space restrictions, the user can actually increase the diameter of both pulleys, increasing the efficiency of the belt-pulleys system, assuming that pulleys diameter is near the minimum recommended diameter. However, this measure leads to extra cost, being necessary a cost-effectiveness evaluation.

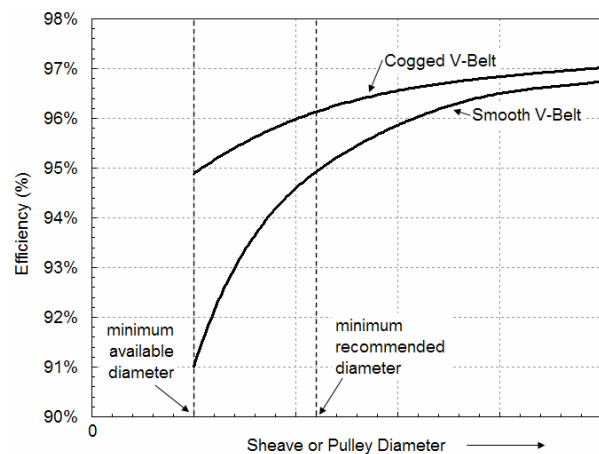


Fig. 14. Typical efficiency variation as a function of pulleys or sheaves diameter for cogged (molded-notch) and smooth (or conventional) V-belts at full load [83].

The pulleys diameter strongly affects the efficiency, especially of conventional or smooth V belts. During partial load operation, the efficiency gain of cogged-V belts over smooth-V belts is larger than at full load since the hysteresis losses are the most significant contribution to the total losses. While there is a wide range of efficiency improvement due to load and sheave diameter variations in specific applications, on average a 3% efficiency improvement can be expected by switching from smooth-V belts to cogged-V belts. Due to the lower losses and the better heat dissipation (larger surface and induced air turbulence), cogged-V belts run cooler, thus having a longer lifetime. Cogged-V belts also have a raw rubber edge, improving the friction coefficient between the belt and the sheaves. Some users complain that this improved friction factor leads to reduced pulley lifetime. By eliminating the cloth wrapping on the belt, more tensile cords can be used, increasing the belt load capacity.

In Fig. 15, the typical curves of the efficiency as a function of load are presented for V belts, flat belts and synchronous belts.

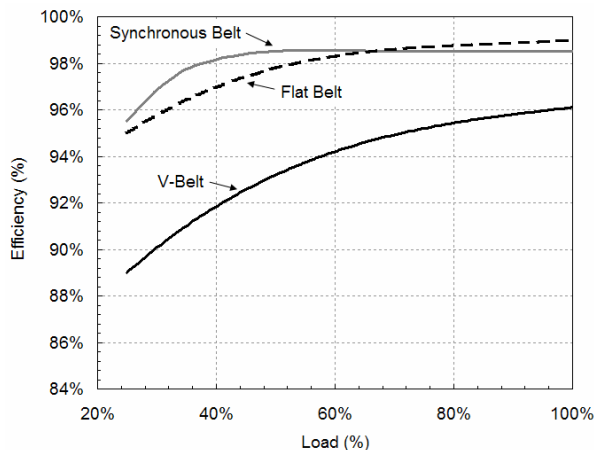


Fig. 15. Typical efficiency variation as a function of load for different belt-pulley sets, considering fixed speed [83].

Timing or synchronous belts, also known as toothed, notch or cog belts, are a positive-transfer belt and can track relative movement. These belts have teeth that fit into matching grooves of toothed pulleys (sprockets). When correctly tensioned, they have no slippage and are often used to transfer direct motion for indexing or timing purposes (hence their name). Synchronous belts are the most efficient, with a typical efficiency in the 97.5-98.5% range. Synchronous belts with a helical offset tooth design are also available. The helical offset tooth design forms a chevron pattern (Table 3) and causes the teeth to engage progressively. The chevron pattern design is self-aligning. The chevron pattern design does not make the noise that some timing belts make at idiosyncratic speeds, and is more efficient at transferring power (efficiency up to 98.5-99%). Belt acoustic noise can impact workers close to operations. Using synchronous belt-and-sprocket systems designed to reduce acoustic noise⁴³, the overall environment acoustic noise pollution can be reduced, which can be very important in sound-sensitive work

⁴³ Acoustic noise associated with the belt teeth slapping into sprockets and generating an impact noise, which is the typical whine sound at frequencies determined by tooth pitch and drive operating speed.

areas. Belt profiles that gradually roll each angled belt tooth through a sprocket, eliminating impact noise, should be used. Also, self-tracking tooth patterns eliminate the need for sprocket flanges, another source for irritating rubbing noises. A progressive tooth engagement design can be up to 19 decibels quieter than a synchronous belt with a conventional straight-tooth profile.

The initial generation of synchronous belts used stretch-free fiber-glass tensile cords with neoprene as the filling material. Most synchronous belts have a wear-resistant tooth facing material to protect the tooth surfaces. This material presents a low coefficient of friction to decrease the friction losses when the belt teeth enter and leave the sprocket teeth. The critical elements in these belts are the fiber-glass cords, which wear due to their repetitive flexing, leading to a typical belt lifetime of around 12000 hours. Several manufacturers have recently introduced high-performance synchronous belts, which use Kevlar tensioning cords and a polyurethane body. These belts have a substantially higher load carrying capacity, per unit of width, than the previous generation of belts. Additionally their lifetime is longer, typically around 24000 hours. Although these synchronous belts are more expensive than fiber-glass corded belts, they last longer, and use narrower and thus cheaper sprockets, so their total cost can be lower. Synchronous belts are stretch-free and can achieve higher efficiency than V belts due to lower hysteresis, power friction losses, and truly synchronous operation (no slip and no creep). The lower flexing losses result from the small thickness of the belt between the teeth. The absence of speed losses (slip and creep) is due to the positive mating of the teeth of the belt with the teeth of the sprockets. Due to the absence of speed losses, the synchronous belts have not only higher peak efficiency than V belts, but also a flatter efficiency curve. Synchronous belts are ideal for applications requiring accurate speed control of the load. As there is no slip, there is an exactly fixed ratio between the input and output speeds equal to the ratio of the number of teeth in the sprockets. They are not, however, suited for shock loads, where abrupt torque changes can shear belt teeth. Polyurethane synchronous belts feature higher resistance to shock loads than the previous designs that used neoprene rubber. With loads that show a strong relation between speed and power consumption it is very important not to waste the energy savings achieved with synchronous belt operation through the higher operating speed of the load. Common loads where this may happen are centrifugal fans and pumps where the power grows approximately with the cube of the speed. It is essential to choose the sprockets to take into account the absence of slippage in the synchronous belt transmission and thus drive the load at a speed no greater than required. With the exception of high-torque, very-low-speed applications, since they require less maintenance, synchronous belt systems are often selected to replace roller chain drives synchronous belts, with the efficiency similar to a well-maintained chain drive. Unlike metal chains, synchronous belts do not require regular lubrication and maintenance, and can also operate in dusty or wet (water or oil) environments.

Flat belts are a simple system of power transmission that was well suited to its time in History. Flat belt-pulley

sets need to be carefully aligned to prevent the belt from slipping off the pulley. Flat belts also tend to slip off the pulley face when heavy loads are applied. In practice, such belts were often given a half-twist before joining the ends, so that wear was evenly distributed on both sides of the belt. Flat belts have a middle layer, which is normally made of extruded polyamide tapes bonded together and is responsible for giving the belt its traction strength. The application speed and torque requirements determine the thickness of this layer and the belt width. Polyamide gives the belt a high and stable elastic modulus. For high tensile strength applications, Kevlar can be used in the central core. Polyamide fabric layers are bonded on both sides of the central layer contributing also to the belt strength. The outer layers are made of elastomers having high friction coefficients. Special synthetic leather covers can be used in applications with oil contamination. The efficiency of the flat belt, typically peaking at over 99%, is not only higher but the efficiency gap widens for light loads. In comparison with V belts, flat belts have lower losses due to the much lower hysteresis losses (for the same load, flat belts are much thinner), lower friction losses (flat belts sit on the surface of the flat pulleys and they do not have the friction losses of V-belts associated with wedging into and pulling out of the grooves) and lower slip losses (unlike V belts, flat belts do not stretch with age, keeping a constant tension, and thus avoid slippage losses and the need for regular maintenance). Polyamide flat belts are adjusted by imposing an elongation, typically between 2% and 2.5%, during installation. The elongation produces a tension that remains essentially constant during the belt lifetime. Normal shock loads are absorbed by the elasticity of the polyamides in the belt. Flat belts are typically used for linear speeds within 10 to 100 m/s. Due to their flat, symmetrical structure and vibration-damping elastomers, flat belts produce low noise.

Round belts are circular cross-section belts designed to run in pulleys with circular (or quasi-circular) groove. They are for use in low-power low-torque applications, but, in Industry, they are rarely used. Typically they have efficiency similar or lower to that of the smooth-V belts.

Besides efficiency, one of the key considerations in choosing a belt type is the need to deal with shock loads, as these can impose a large stress both in the belt and on the motor and driven equipment. Through slippage and elasticity, both V belts and flat belts can absorb shock loads, although the cyclic application of these loads contributes to the reduction of belt lifetime. In fact, uncontrolled motor starting subjects the driven equipment to a large and sudden mechanical stress, especially if high-inertia loads are driven. With IMs, which are the most common type of motor used in belt-drive applications, this means a sudden applied torque 2 to 3 times the rated value. The increasing penetration of VSDs, besides providing energy savings, also provides soft-starting and soft-stopping, decreasing the stress in the mechanical transmission. VSDs and other soft-start controls can thus enable the use of synchronous belts in applications where shock loads are due to motor starting and to sudden motor deceleration. Some applications produce shock loads due to the great inertia forces or due to very strong torque fluctuations, like rock crushers, grinders, beater mills, rolling mills, choppers,

reciprocating compressors, etc. Besides efficiency and the presence of shock loads, other factors that influence the belt choice are cost-effectiveness, speed of operation, acoustic noise, and environmental factors.

Regarding cost-effectiveness, some examples are presented. Cogged-V belts can be used in the same pulleys as the equivalently rated V belts. Thus in new applications and in retrofits (assuming the belt needs replacement anyway) the extra cost is only the cogged-V belt extra cost over smooth-V belt, which typically falls in the range 1-2 €/kW [83]. An average efficiency improvement of 3% is assumed. The design lifetime of V belts is typically 24000 hours, which implies a clean and cool environment, low start/stop cycling rate, optimum tension (which implies the need for regular maintenance), and absence of overloads. Most real-life applications involve a combination of factors, which accelerates the ageing process.

The installation of high-efficiency belt transmission systems can occur in the following scenarios: (a) in a new system; (b) in an existing system, when the belt transmission needs replacement; and (c) in an existing system, in which the belt transmission is working properly. The extra investment in high-efficiency belt systems is smaller in the first two cases, resulting in greater cost-effectiveness. Case (c), which is less likely to occur, but may still be cost-effective in many applications, especially when reduced maintenance is considered, or when other work being done on the system (such as a motor replacement) reduces the belt replacement cost. Table 4 shows the cost-effectiveness of cogged-V belts, for scenario (b), assuming 12000 hours lifetime (therefore, 2 belts are purchased over the considered 2 year period), for both smooth- and cogged-V belts, which is typical for fiber-glass corded belts⁴⁴. Cogged-V belts are very cost-effective, offering a CSE between 5 and 30 times cheaper than typical electricity rates. The calculations assumed identical lifetimes for both types of belts, although cogged-V belts should last longer due to their lower running temperature and higher tensile strength. The most sensitive factor for the cost effectiveness of motors and drives is the number of hours. It is assumed two different electricity prices, 0.06 and 0.1 €/kWh, corresponding to average prices for industrial and tertiary sectors, respectively. In the calculations the IM efficiency was assumed to be 90%, which is a typical value for medium size (about 20-60 kW) motors. If higher values (pertinent for large or high-efficiency IMs) were used, the savings would decrease a few percentage points. Conversely, greater savings result when low-efficiency motors are used. The cost savings associated with the longer lifetime brings the CSE to near zero or even to negative values (this means that the extra savings provided by lower efficiency belt replacement costs may be more than enough to offset the additional initial investment).

Synchronous belts require toothed pulleys (sprockets), which are more expensive than V belt pulleys. In a retrofit application, the additional investment required is the cost of the sprockets, plus the extra cost of the belts and of the installation. In the cost-effectiveness calculations it is

⁴⁴ For Kevlar-corded belts twice the lifetime should be considered.

assumed that those extra costs fall in the range 8-16 €/kW. This price variation strongly depends on the rating of the belt drive, with the large drives requiring a smaller price premium per kW. The sprockets typically cost 1.5-2 times the cost of the belts and depending on operating conditions last over 3 belt changes. Table 4 shows the CSE for the replacement of conventional V belts by synchronous belts, according to scenario (b), being assumed that there is an average 5% efficiency improvement and that the synchronous belt will last 16000 hours (therefore only 1 belt and 1 sprocket purchase over the considered 2-year period). With the exception of belt drives with a small number of operating hours per year, the retrofit of synchronous belts is very cost-effective. In Tables 4 the extra savings due to lower belt maintenance and replacement requirements, as well as the savings due to reduced downtime, were not considered. These savings alone, over the lifetime of the belt drive system, can often justify the extra investment. In a new installation (scenario (a)), synchronous belts are even more attractive, as the price premium is typically 30% smaller than in a retrofit application, due to avoidance of the full pulley costs.

The installation of flat belts requires special pulleys, but their cost is substantially smaller than the price of synchronous belt sprockets. Flat belts, like cogged-V belts, carry a modest price premium over smooth-V belts. In a retrofit installation, the extra cost of the flat belt plus

the full cost of its associated pulleys typically falls in the range 3-6 €/kW. Since the mechanical effort is more evenly distributed in flat-belt pulleys than in V-belt pulleys or than in sprockets, the flat belt pulleys last longer – typically over 50000 hours (four to five times more than belt life). Table 4 shows the cost-effectiveness of retrofitting flat belts (scenario (c)) when V belts need replacement, assuming that the flat belt lifetime is 12000 hours (therefore 1 pulley and 2 belts are purchased over the considered 2-year period, and second purchased belt at future time is thus discounted), and that there is an average efficiency improvement over conventional smooth-V belts of 5%.

As a conclusion, some final remarks concerning belt transmission can be made. Widespread use of energy-efficient belt transmissions in the motor drives of the industrial and tertiary sectors can produce substantial electricity savings, taking into account the huge amount of electricity consumed by EMODS and the fact that almost 1/3 of the them integrate belt-pulley transmission, as well as savings in terms of peak power, leading to additional savings for both the utility and the consumer. In drives using belt transmissions, energy-efficient belts can provide the same magnitude of energy savings as energy-efficient or high-efficiency motors, demonstrating its importance when optimizing EMODS. Belt-based driving systems thus deserve greater attention.

TABLE 4
COST-EFFECTIVENESS OF COMMERCIAL BELTS.

	Savings (€/kW)	Payback (yr)	CSE (€/kWh), 2 yr
Cogged-V belts ($\eta=96\%$) vs. Smooth-V belts ($\eta=93\%$)*	17.92-29.87	0.056-0.034	0.029-0.017
Timing belts ($\eta=98\%$) vs. Smooth-V belts ($\eta=93\%$)**	29.26-48.77	0.547-0.164	0.282-0.085
Flat belts ($\eta=98\%$) vs. Smooth-V belts ($\eta=93\%$ ***)	29.26-48.77	0.062-0.205	0.032-0.106

Assumptions:

Direct retrofit; 8000 h/yr; 0.06-0.1 €/kWh; Motor efficiency = 90% (typical for 20-60 kW); Discount rate = 2%.

* Price premium = 1 to 2 €/kW. ** Price premium = 8 to 16 €/kW. *** Price premium = 3 to 6 €/kW.

Conventional or smooth V belts, although they are the least efficient belt technology, are used in the vast majority of belt transmission applications. This is due to a combination of their initial lower cost, market inertia and lack of awareness of the more efficient alternatives. Energy-efficient belts are generally very cost-effective to retrofit V belts when they need to be replaced, leading to CSE significantly lower than electricity prices. In new installations, as the extra costs lower, the CSE is even lower. In many cases, they will even be cost-effective as a retrofit (replacing a working belt drive). Besides achieving substantial energy savings, the more efficient belt transmission technologies can also increase productivity, by decreasing downtime and maintenance requirements associated with replacement or adjustment of V belts. There are several technologies that can be used to improve the efficiency of the belt transmission. The optimum choice depends on several factors, namely the presence of shock loads, cycling rate and the starting method, speed of operation, torque and power, synchronous operation requirements (no slip or creep), noise constraints, number of operating hours per year, and the operating environment. Cogged-V belts can be retrofitted very inexpensively in most applications as they use existing pulleys and their extra cost over smooth-V

belts is small. Although cogged-V belts are the cheapest alternative, achieving a typical efficiency improvement of 3%, their efficiency is less than the high-performance alternatives and they require maintenance. Both synchronous and flat belts achieve higher efficiency improvements, typically around 5%, and are practically maintenance-free. Both types of belts require special pulleys to operate, with the synchronous belt pulleys being the most expensive. Synchronous belts provide slip-free synchronous operation, have a long lifetime, and can operate in wet and oily environments. Their operation can be noisy at high speed and their main weakness is the lack of capability to absorb shock loads. Flat belts have a small slip, can withstand shock loads, and produce little noise even at high speeds. They can be used at very high speeds (up to over 100 m/s). Since most of the literature available in this area is provided or is written by belt manufacturers, independent testing of the energy efficiency for the different belt types is required. Both the energy savings and the side effects (maintenance requirements, noise, lifetime of belt and pulleys) should be monitored over a sufficiently long period to allow the characterization of the real belt drive performance. Development of simple and inexpensive methods to monitor and measure belt efficiency, possibly based on infrared cameras or probes

to measure the belt temperature and on the optical measurement of speed losses. These techniques are potentially useful to detect maintenance and replacement requirements of V belts and of flat belts. Another possibility, suggested in [83], is the development of thermochromic coatings for the belts that would allow the detection of inefficient operation of the belts by simple visual inspection.

Moreover, the belts also have the advantage of attenuating or filtering mechanical vibrations from load to motor, contributing to extend motor lifetime, and facilitating motor mechanical vibration spectrum-based diagnosis, factors that should be taken into account in the technical analysis. However, torque pulsations can be amplified if they are equal or near resonant frequency of the mechanical system. Therefore, in belt-driven applications, relatively large load fluctuations (as much as 10% or more) at belt passing speed can occur. Further considerations on this issue are made in Section 3.9.5.

D. Chain-Sprocket Sets

Similarly to belt-pulleys units, chain-sprocket (also known as timing or roller chains, Fig. 16) allow flexibility in the relative positioning between motor and load and, using sprockets of different sizes, allow adjusting the speed of the load. Similarly to the synchronous belts, chains have no slip and are normally used in applications where reduced speed and high torque are required (typically, the maximum transmission ratio is around 6 [103]). They support high temperatures and high mechanical shocks or transients. With proper periodic maintenance (cleaning and lubrication), their lifetime is long and their efficiency is in the 95-98% range. Roller chain or bush roller chain is the type of chain most commonly used for transmission of mechanical power in industrial and agricultural machinery. It is simple, reliable, and efficient, but requires more attention to maintain than may be desired by potential owners. Therefore, there has been of late a tendency towards the use of other modes of mechanical transmission such as timing belts. The need for lubrication, not just to the outside of the chain but especially to the inner surfaces between the pins and bushings and to the bushings and rollers, is a source of aggravation for almost all users of roller chains. Owners of complex machinery using high speed chain drives, who have to use very expensive sophisticated lubrication systems to keep the chain lubricated, all the way up to the owners of large surface mining draglines and bucket-wheel excavators, struggle with the goal of giving their roller chains the cleanest, most continuous lubrication. Improper maintenance leads to additional friction, less efficiency, more noise and more frequent replacement. Many major roller chain manufacturers have developed low-maintenance roller chains such as with grease sealed into the joints (O-ring) and with an oil-impregnated sintered metal bushing ("Duralube" or "Lambda").

Replacement of chains by synchronous belt in applications operating with moderate-temperature environment is, in general, advantageous since it leads to significant maintenance reduction, efficiency improvement and noise reduction.



Fig. 16. Roller chains and sprockets.

Derailleur gears are a variable ratio transmission system commonly used on bicycles, consisting of a chain, multiple sprockets and a mechanism to move the chain from one sprocket to another (the set of rear sprockets is known as cassette or freewheel), properly adjusting its tension.

E. Other Types of Mechanical Transmission Systems

For the sake of completeness, in this section, the mechanical and electromechanical variable-speed systems are briefly addressed.

Hyrostatic transmissions transmit all power with hydraulics, having no solid coupling of the input and output. One half of the transmission is a hydraulic pump and the other half is a hydraulic motor, or hydraulic cylinder. Since positive displacement pumps and motors are used, one revolution of the pump or motor corresponds to a set volume of fluid flow that is determined by the displacement regardless of speed or torque, leading to an excellent control. Speed is regulated by regulating the fluid flow with a valve or by changing the displacement of the pump or motor. Many different design variations have been used. A swash plate drive employs an axial piston pump or motor in which the swash plate angle can be changed to adjust the displacement and thus adjust the speed. This sort of systems is used on excavators, lawn tractors, forklifts, winchdrive systems, heavy lift equipment, agricultural machinery, etc.

Hydrodynamic drives or fluid couplings use oil to transmit torque between an impeller on the constant-speed input shaft and a rotor on the adjustable-speed output shaft. The torque converter in the automatic transmission of a car is a hydrodynamic drive.

Hydroviscous drives consist of one or more discs connected to the input shaft pressed against a similar disc or discs connected to the output shaft. Torque is transmitted from the input shaft to the output shaft through an oil film between the discs. The transmitted torque is proportional to the pressure exerted by a hydraulic cylinder that presses the discs together.

Eddy current and hysteresis drives or clutches, which are electromechanical transmission or slip-controlled transmission system, consists of a fixed speed motor and a current-controlled clutch. The clutch contains a fixed speed rotor and an adjustable speed rotor separated by a small air-gap. A direct current in a field coil produces a magnetic field that determines the torque transmitted from the input rotor to the output rotor. Using speed feedback the controller provides closed-loop speed regulation by varying clutch current, only allowing the clutch to transmit enough torque to operate at the desired speed. This sort of systems has, inherently, poor efficiency. Power proportional to the slip speed times operating torque is dissipated as heat in the clutch. Nowadays, due to the system efficiency concerns, slip controlled drives have lost popularity and are only used in special situations.

Due to the restrict use, relatively high cost, and inherent low efficiency, of the mechanical and electromechanical variable-speed transmission systems presented in this section, they are rarely used in the typical EMODS operating in industrial and tertiary sectors.

A6.3.5 Section 3.9.5

In Figs. 1 and 2, additional results on the analysis of the elastic mechanical transmission on EEMODS fed by balanced and unbalanced power supply, presented in Section 3.9.5.

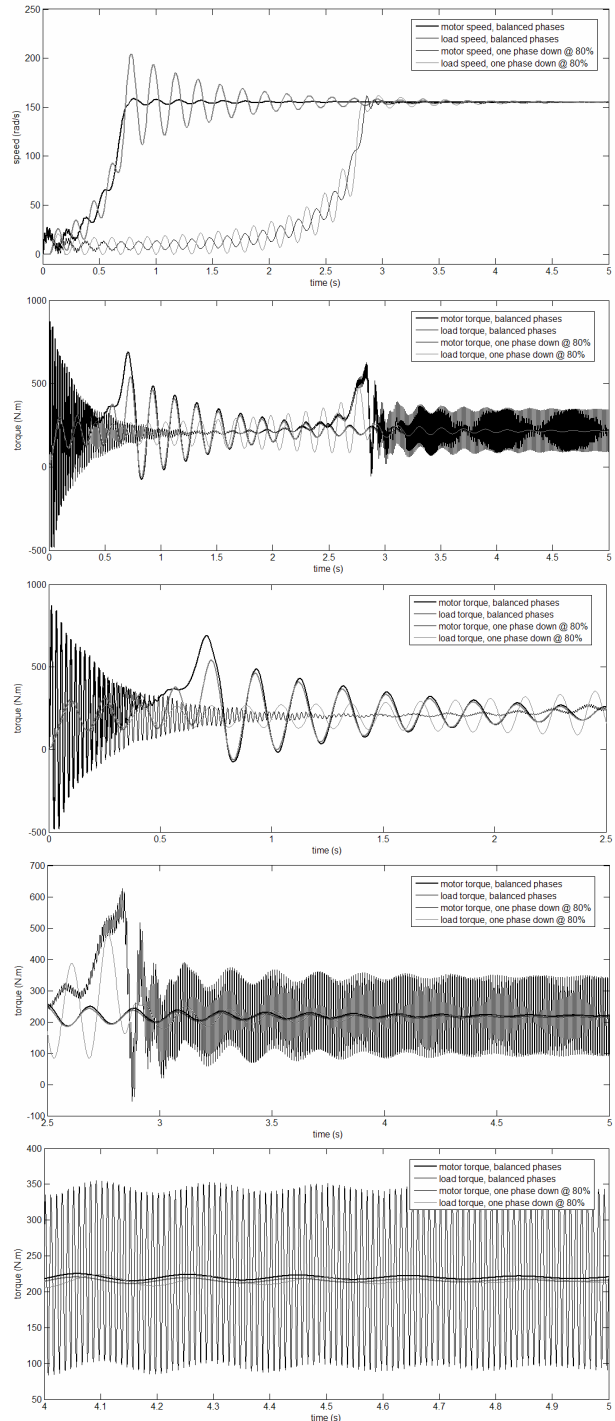


Fig. 1. Transient response (speed and torque) of an elastic transmission, considering $J_{load} = 0.5 \cdot J_{mr}$, $K_{ela} = 250$ N.m/rad, and $T_{load} = \text{sign}(\omega_{load}) \cdot (0.1|\omega_{load}| + 200)$ N.m.

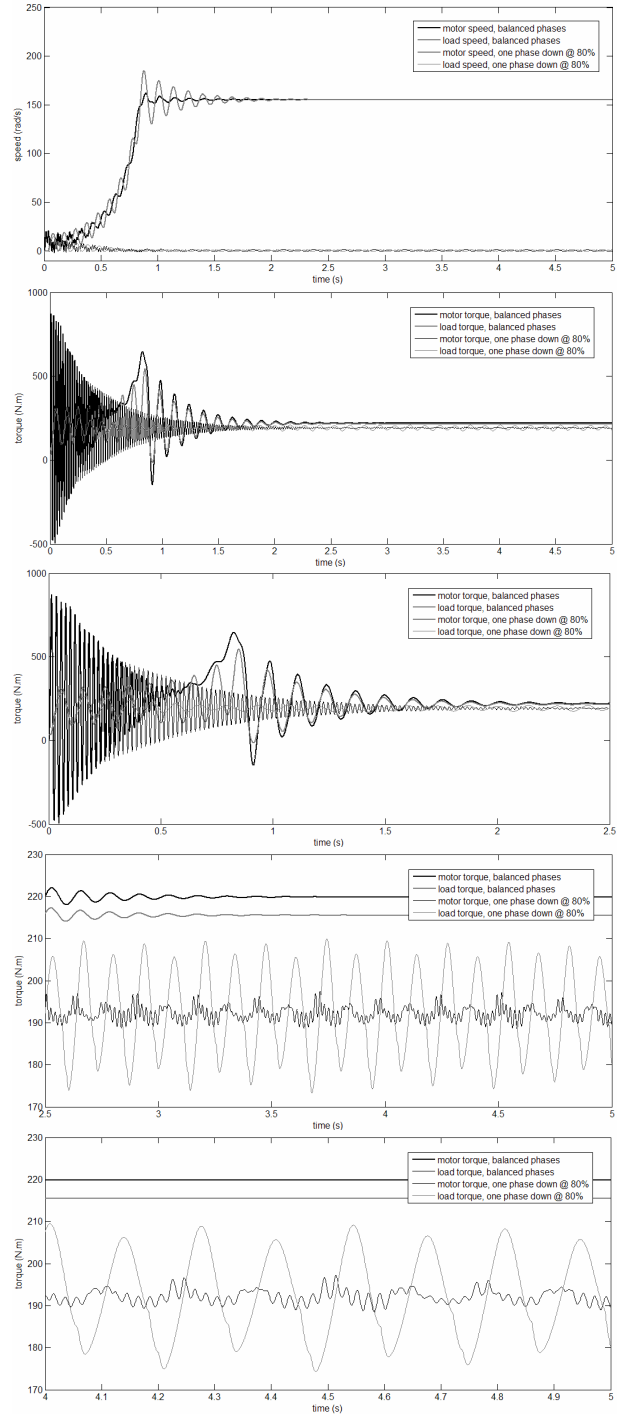


Fig. 2. Transient response (speed and torque) of an elastic transmission, considering $J_{load} = 0.5 \cdot J_{mr}$, $K_{ela} = 500$ N.m/rad, and $T_{load} = \text{sign}(\omega_{load}) \cdot (0.1|\omega_{load}| + 200)$ N.m.

A6.3.6 Section 3.10

A. Selection of IMs for Variable Speed Applications

The drive applications can be divided into six elementary categories: 1) constant torque or linear load-speed relation (e.g., conveyors); 2) linear torque or quadratic load-speed relation (e.g., mixers); 3) quadratic torque or cubic load-speed relation (e.g., centrifugal fan and pumps); 4) constant power loads (e.g., winding or coil drives); 5) dynamic load (e.g., trolleys/trains, torque demand for acceleration followed by a low load); 6) static load (hoists and lifts, mainly steady high static load with

overload peaks). Although the dominant load behaviour can be classified according to the previous categories, a combination of two or more behaviours characterizes most loads [65].

In category 5), the motor load in the dynamic periods determines the motor peak power according to which the dimensions are to be set. The thermal load determines the required continuous power to the motor. The thermal load is determined on the basis of travelling cycle. The load speed characteristic is a significant factor in determining the motor cooling system.

In category 6), approximately 70% to 90% of the rated motor torque is required assuming constant speed upwards or downwards. The highest operation torque is required for acceleration with maximum load in the upward direction.

Some basic recommendations are commonly made by manufacturers as the use of IMs with F- or H-class and 4 poles (this recommendation applies particularly to vertical mounted gear motor units that are operated with a high oil filling level) [65].

When selecting an IM for a certain application, several aspects have to be taken into account, related to surrounding environment, power supply and load profile. For example, IMs can be operated at low speed with rated torque without forced cooling if the operating condition differ from S1 operation (e.g., S3-type load profile), avoiding a too large motor selection, which, in some cases, can lead the inverter to trigger a short-circuit protection due to the small winding resistance [65].

As referred previously, the average load factor of motors operating in Industry and tertiary sector is roughly 57%, but in some power ranges can be as low as 25% [85]. Motor oversizing is a common situation in Industry, associated with systematic poor system design with high safety factors by OEMs, poor readaptation of motors different from original, overestimation of the mechanical power required by the load or its variation over the operating cycle or with time (process load change). Besides the extra and unnecessary capital investment, those situations result in the degradation of the efficiency and power factor of IMs, as referred in Chapters 2 and 4, although the decrease, in terms of efficiency, is attenuated for higher motor ratings or high efficiency class motors due to the inherent flatter efficiency-load curve. Nevertheless, the power factor and efficiency reduction leads, by itself, to the operation cost increase in relation to the optimum operation situation. The only advantage associated with the IM oversizing is the increase of the useful lifetime and the reliability, as a result of the lower operating temperature.

Inversely, IMs slightly undersized experience an increase in the power factor, but a reduction in the efficiency, an overheating, and, consequently, a reduction in the useful lifetime and reliability. IM overheating becomes particularly critical in applications for the so-called risk or dangerous environments (e.g., with atmospheres potentially explosive areas, identified with “Ex” mark⁴⁵), which can be found in a number of Industry types (e.g., petroleum, gas, chemical and pharmaceutical). In these cases, overheating is not admissible. In most

cases, the motor load should be within 75-100% load range.

The IM sizing has to respect the electromagnetic, thermal and mechanical motor limitations, in order to avoid the motor efficiency and reliability degradation. In this section, several issues related to the thermal and mechanical limitations associated with VSD-fed TEFC (equivalent to IP 55 protection degree) IMs are discussed, and a methodology for proper IM selection for variable-speed EMODS is proposed, focusing steady-state operation.

In the case of variable-speed EMODS with VSD-fed IMs, most of the considerations on the motor under or oversizing still valid. However, the corresponding power factor is considerable higher and varies less as a function of the motor load, as it can be seen in Fig. 1. Besides that, as previously referred, there are VSDs with quasi-unitary power factor and regenerative capability, and, in general, they can accelerate the degradation of IMs insulation system and bearings, reducing significantly its useful lifetime, particularly if the insulation system is old. The thermal degradation is responsible for the natural ageing of the insulating materials, according to the well-known Arrhenius law. The insulation materials lifetime is considered the period over which the insulation properties are maintained for a given voltage.

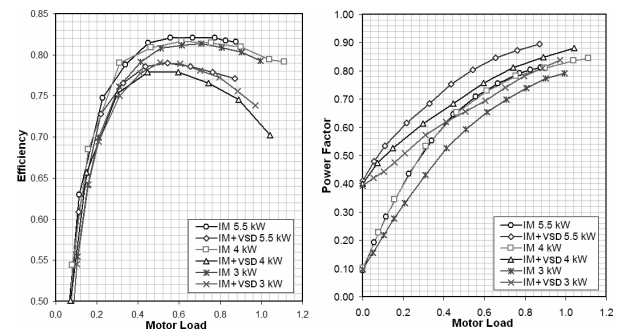


Fig. 1. Efficiency and power factor curves as a function of load for 4-pole, 3-, 4-, 5.5-kW IMs (400 V/50 Hz), with and without VSD (11 kVA, $U/f_s = 8$ kHz, $f_i = 50$ Hz, $U = 400$ V) [84].

If the load operation or profile is well known and fixed, the safety margin can be minimized, being maximized the load factor. However, if the load operation is not fully known, it is convenient to introduce a safety margin, or if the load varies significantly over the operating cycle, it is inevitable the motor to operate over the low-load period, leading both cases to the motor load factor (or average load) reduction. The mechanical transmission effect on motor loadability has also to be taken into account.

Simplifying, IMs thermal behaviour can be described by an equivalent circuit with a resistance (representing the equivalent thermal resistance) and a parallel capacitance (representing the equivalent thermal/heat capacity), as it can be seen in Fig. 2, with a 1st order system response (thermal time constant corresponding to point B). In Fig. 3, the experimental thermal response to stator winding losses is presented for a 3-kW IM. The voltage between the terminals of the circuit represents the different between the average internal and external (ambient) temperatures of the motor. The current represents the losses generated in the motor interior. Equivalent thermal

⁴⁵ In units, such motors represent less than 1% of the total low-voltage electric motor market.

resistance and capacity of an IM are both related with the materials (including air spaces) incorporating it, as well as the corresponding heat-transfer rate. The equivalent thermal resistance varies inversely with the heat transfer rate, which can be by conduction, convection (natural or forced) and by radiation, being the first two modes dominant in IMs [84], [86]. A more accurate motor thermal model is described in Appendix 2. The forced convection heat transfer mode depends on the internal and external air movement. For example, increasing the linear speed of the air in the external frame surface, the equivalent thermal resistance decreases according to curve indicated in Figs. 4 and 5.

The air linear speed is approximately proportional to the motor speed, as it can be seen in Fig. 6.

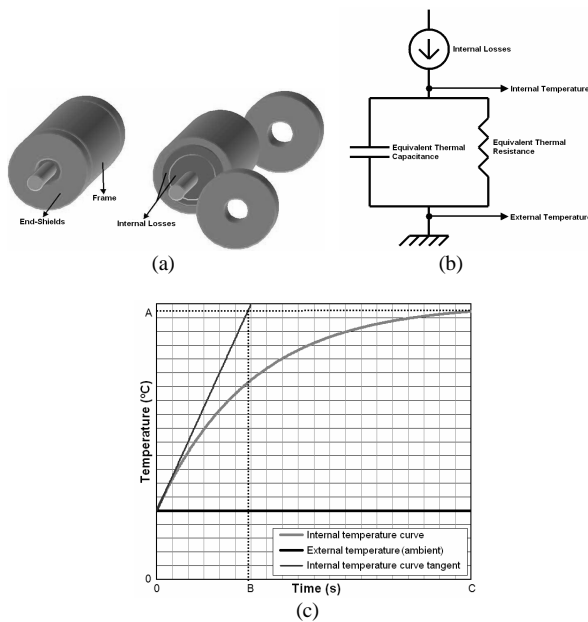


Fig. 2. (a) Simplified thermal model of an IM; (b) Equivalent thermal resistance and heat capacity of an IM; (c) Internal temperature variation of an IM after start [84].

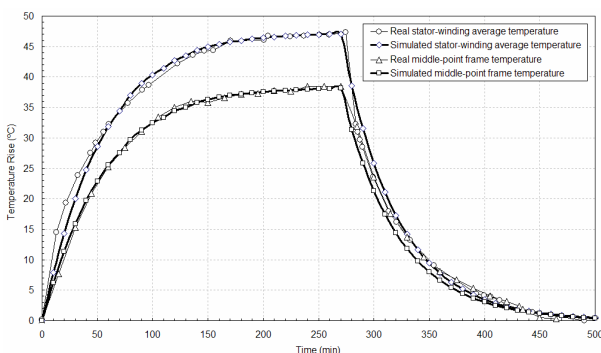


Fig. 3. Experimental thermal the stator winding and the ambient and between frame and ambient, for a TEFC, 4-pole, 3-kW IM. Values obtained with the DC test (stator windings fed by a DC power source).

An IM reaches its thermal steady state or equilibrium when the internal average temperature⁴⁶ stabilizes or becomes constant. In that state, the motor thermal/heat capacity does not influence the internal and external temperature difference, since the thermal equivalent

⁴⁶ Depending on the motor part, different temperatures can be found inside the motor. For example, in the TEFC IMs, the hottest spot in the stator windings can be found in the coil head opposite to the external fan side [127].

circuit impedance becomes only resistive [84], [86]. During the thermal transitory state, the internal temperature depends on the motor losses and on the equivalent thermal resistance and capacitance. This state occurs when motor speed, motor torque and/or ambient temperature varies. Starting/stopping periods are examples of transient states. In Fig. 2c, the thermal transient typical curve can be seen. For a given loss increase at the initial instant, the internal temperature increases up to a certain value, over a certain period, after which stabilizes, i.e., enters in the steady-state (after point C in Fig. 2c). The thermal time constant of the motor is given by point B, of Fig. 2c. For small TEFC motors, the thermal time constant is in the order of 15 minutes, but can be up to 2 hours or more for large motors.

During sizing process, the steady-state and the transient-state periods have to be taken into account, particularly when the motor torque is in the proximity of the admissible torque limits (or loadability, see curves in Appendix 2). For any fundamental frequency, when IMs are fed by VSDs their losses increase in relation to the purely sinusoidal feeding situation and, consequently, their internal operating temperature also increases. The motor loss increase is associated with the VSD output waveforms harmonic content, as referred previously [87]. The total losses can increase up to 15-20% and the motor efficiency can decrease 1-3% [87]. In these conditions, to ensure that rated temperature is not exceeded, most manufacturers recommend that the output shaft power should not exceed 90% of the power limit as a function of the fundamental frequency (for the rated frequency, this limit corresponds to motor rated power). This power limitation can be translated in an available torque limitation in the motor. Therefore, in order to maintain the rated temperature, VSD-fed IMs torque limit should be less than 10% of that of the line-fed IMs [75], [88], [89]. In [88] it is suggested that, for $f_s > 5$ kHz, no derating is needed, but for $f_s < 5$ kHz, a 10% derating is recommended. The approximate thermal steady-state (or equilibrium⁴⁷) torque-speed curves ensuring the rated temperature in a TEFC, 4-pole IM, are shown in Fig. 7. For short periods (1 minute every 10 minutes⁴⁸) and during starting, which depend on motor size and type, the torque limits can be much higher [88]. In reality, the curve lower than rated speed is smooth and continuous (see Fig. 3.5 in Chapter 3, and Appendix 2), but it was segmented in three parts in order to facilitate the analysis or mathematical description.

⁴⁷ It is assumed that the operating period, in each load point, is enough for the motor to reach thermal equilibrium (typically considered when $\Delta\theta < 2$ K/h), i.e., it is several times higher than motor thermal time constant.

⁴⁸ During starting the slip compensation can be set to 130-150%, and, consequently, the motor develops at most 130-150% of the rated torque [65]. This can also influence the motor selection. For example, for a trolley drive with 1.3-kW travel power, 13-kW maximum power, 270 r/min minimum speed and 2610 r/min maximum speed, assuming that the motor can provide 150% output during acceleration phase, the motor should have an 8.67-kW power capability, leading to a 9.2-kW rated power motor (delta as rated connection). For a hoist (high constant load with intermittent overload) drive with 26-kW maximum power, 20-kW sustained power, low speed only for positioning, brake applied when stationary, S3-load type (40% c.d.f.), the inverter can yield 150% of its rated current during acceleration. The solution is a 22-kW motor (star as rated connection) [65].

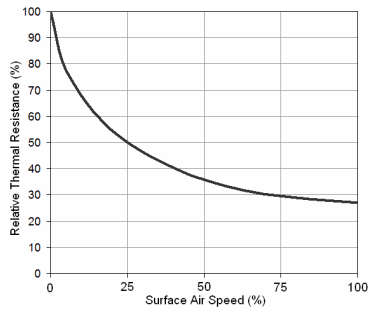


Fig. 4. Typical relative thermal resistance as a function of the external cooling air linear speed (depends on motor type and size) [18], [84].

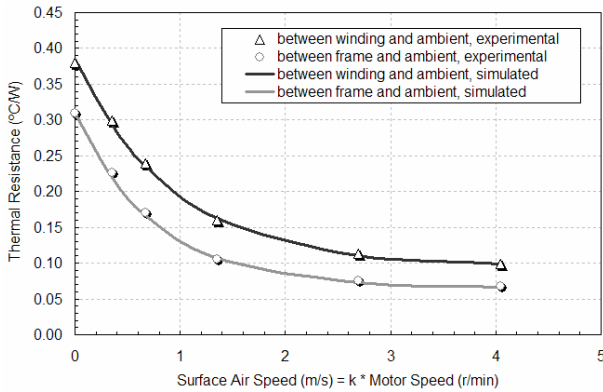


Fig. 5. Experimental thermal resistance between the stator winding and the ambient and between frame and ambient, for a TEFC, 4-pole, 3-kW IM. Values obtained with the no-load test.

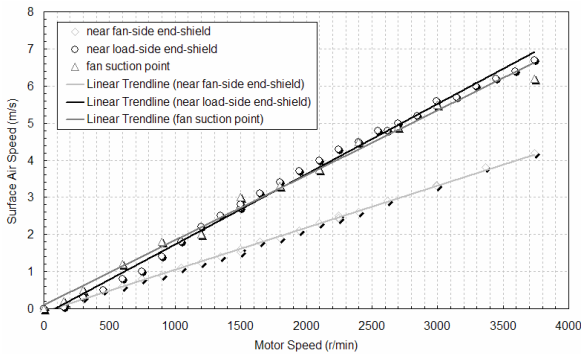


Fig. 6. Experimental frame surface air linear speed as a function of motor speed, for a TEFC, 4-pole, 3-kW IM.

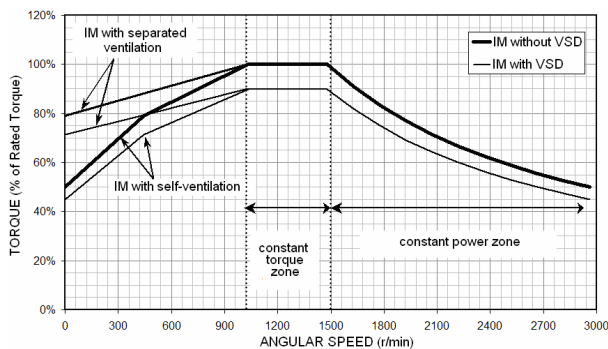


Fig. 7. Approximate steady-state torque-speed curves ensuring rated temperature (motor loadability), for a TEFC, 4-pole, IM [84], [88], [18], [59], [90].

In the zone between 0% and 65-70% of the nominal speed (or roughly the rated frequency), although the reduction of the friction and windage losses and core losses (assuming proper voltage regulation), the torque limit decreases significantly since thermal dissipation

capability decreases more than motor losses (stator-winding losses and rotor losses depend mainly on load, and its frequency dependency is very low for low frequency and slip ranges).

It should be noted that, in IMs with forced or separated ventilation, the available torque decreases because there is a decrease in the internal thermal dissipation by convection (blades/fins in the squirrel-cage end-rings), which is responsible by the convection-based dissipation of part of the heat generated by the coil heads. For self-cooled or self-ventilated IMs, this torque reduction is naturally aggravated: the heat transferred by convection depends on the fan air-flow output, which is proportional to the motor speed which, in turn, depends on the fundamental voltage frequency.

In the constant torque zone, although the equivalent thermal resistance decreases due to the speed decrease, the mechanical losses and core losses also decrease (assuming constant magnetizing flux⁴⁹) allowing the torque to be maintained practically constant for speeds between 65-70% and 100% rated speed.

Above rated speed, although the thermal dissipation capability increases (due to the fan air-flux output increase), assuming that the inverter output fundamental voltage cannot increase significantly above rated value⁵⁰, the maximum allowable torque curve starts to decrease due to the magnetizing flux decrease (torque roughly proportional to the squared magnetizing flux), and the motor enters in the so called field weakening⁵¹ operating region or zone. Additionally, the frequency increase leads to a higher stator winding voltage drop (due to the impedance increase), also contributing to the magnetizing flux decrease. That decrease is compensated by a slip increase (within the quasi-linear region of the torque-speed curve), which also balances the overall motor impedance increase with frequency, otherwise, the input current would be strongly limited. Therefore, core losses decrease (assuming fixed voltage), friction and windage losses increase, and rotor losses increase. In these circumstances, the output power has to be constant to avoid exceeding rated temperature, and, therefore, the torque is inversely proportional to the speed. The motor has a poor efficiency in this operating mode.

It should be noted that, if the voltage is increased in order to maintain the rated flux, the core losses increase for frequencies higher than rated, but a lower increase of the rotor losses occurs, since the slip will not increase so much. Therefore, since the dissipation capability increases, the motor can draw a slight higher torque.

After the constant power zone, whose limit occurs for the maximum admissible slip, the motor torque capability becomes inversely proportional to the squared speed (or frequency), and the power is inversely proportional to the

⁴⁹ The core losses can roughly be described by: $P_{fe} \approx U^2 \cdot (K_1 + K_2/f)$, where K_1 and K_2 are constants.

⁵⁰ The inverter output voltage is limited by the connected supply voltage. Considering the PWM overmodulation region, the VSD output fundamental voltage can be increased above input rated voltage, although with low-order harmonic content, which can increase significantly motor losses and contribute to the torque attenuation in relation to the harmonic free operation with the same fundamental voltage. The inverter output voltage can be higher than the motor rated voltage if the latter has a rated voltage lower than the power supply of the inverter. There are some PWM techniques that allow the fundamental voltage to be increased above input voltage.

⁵¹ The field weakening zone starts when the maximum output voltage of the inverter is reached (constant power with an inversely proportional decrease in torque).

speed (or frequency). Additionally, for most IMs, there are also speed limitations (typically 3000 r/min) associated with bearing speed limits and rotor dynamic balance tolerances. In fact, for speed above nominal, the bearings can overheat, leading to the accelerated degradation of their lubricants.

Ultimately, the aim of the presented limits is to ensure original useful lifetime of the motor. However, if a motor of B thermal class is rewound for F thermal class, the admissible temperature increases, pushing up the steady-state torque-speed capability curve.

Furthermore, it is also important to take into account the transient torque-speed curve in order to ensure that it is proper for driving the load (e.g., in terms of starting period), which is a critical issue in constant torque of high-inertia loads.

As previously referred, loads can be characterized as a function of the load profile. The type of load to be driven is very important to know. They can be typically described by one or more elementary relations between mechanical power or torque and speed, typically being dominant one of them, which is the one considered in the technical and economical analysis, for the sake of simplicity. Lifts, conveyors, trolleys/trains, machine-tools, piston compressors, are examples of cases where the combination of different characteristics is evident. Load torque-speed curve also gives the starting torque required. The load diagram defines speed, torque and power for the mechanical steady-state over a set of operating periods of the operating cycle. The load diagram can be approximately computed if the torque-speed and efficiency-speed curves of the load are known. All the overload periods over the operating cycle should be identified. In some cases a motor with lower rated power can be chosen if the overload duration is significant shorter than the motor thermal time constant, avoiding significant overheating. This principle is behind the duty types defined by IEC 60034-1 [88], in which different load profiles are classified (S1, S2, ... S11). The most commonly used motors are of S1-duty type.

The number of direct on-line start/stop operations limit over a time period is also standardized, and if those limits are exceeded, derating factors have to be applied [88]. Alternatively, soft-starting strategies can be implemented (soft-starters, VRs, VSDs, Y/D, etc.) to avoid derating [88].

When selecting an IM, several parameters have to be taken into account, such as the cooling type and rotation wise, protection degree, altitude and ambient temperature, minimum, rated and maximum speed for steady-state operation, start, rated and maximum torque, rated power, service factor, duty type, etc.

Regarding cooling type, typically, self-cooled IMs (IC 411, IEC 60034-6 Std.) can provide rated torque for speed between 65-70% and 100% of rated speed, without overheating. Below that speed it is necessary to use forced ventilation (either retrofitted or originally specified). However, an IM with forced ventilation is more expensive than a self-cooled IM, and, depending on a number of factors, it can be more cost-effective to use a self-cooled motor with higher power. However, it should be taken into account that, for larger motors, the load factor decreases and, consequently, the efficiency and

power factor also decrease. It should be also noted that most IMs have bidirectional fans, but some large IMs can incorporate unidirectional fans (more efficient), and the user should take that into account, when specifying rotation wise.

As concerns ambient temperature and altitude, a number of considerations can be stated. For ambient temperatures lower than 40°C, the power provided by the IM can be increased, without overheating. For altitudes higher than 1000 m, the power provided by the IM has to be decreased, in order to avoid overheating. Most manufacturers have tables with the relation between those two factors and the power that can be provided by the IM without overheating (Fig. 8). The protection degree should be chosen as a function of the ambient conditions where the IM operates. For dangerous environments special IMs of type “*ε*” should be used, as referred before.

Regarding speed, the motor rated, minimum and maximum steady-state speed should be chosen as a function of load. The maximum speed depends on the rotor dynamic balance and bearings. Typically, the motor speed can reach 1.2 times its rated speed without mechanical problems. Above that value it is necessary to ask manufacturer for a special adaptation. It should be mentioned that, for large frequencies (e.g., 100 or 200 Hz), there are special IMs incorporating amorphous steel in the core, with low iron losses [91].

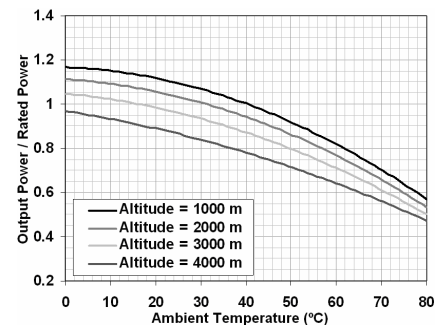


Fig. 8. TEFC IMs output power capability as a function of the ambient temperature, for different altitudes [92], [93].

Moreover, the number of poles should be, in general, minimized (if possible) since motor efficiency and power factor decrease with the increase of the number of poles, as it can be seen in Table 1, and as it is evidenced in Section 3.9.6.

TABLE I
EFFICIENCY AND POWER FACTOR OF 18.5-KW,
400-V, 50-HZ IMs, WITH DIFFERENT NUMBER OF POLES [93].

ω	p	$\eta_{4/4}$	$\eta_{3/4}$	$\eta_{2/4}$	$\lambda_{4/4}$	$\lambda_{3/4}$	$\lambda_{2/4}$
2945 r/min	2	92%	92%	91%	0.88	0.85	0.78
1475 r/min	4	92%	92%	90%	0.84	0.79	0.70
975 r/min	6	90%	91%	89%	0.84	0.78	0.70
735 r/min	8	90%	90%	88%	0.82	0.75	0.65

Starting, rated and maximum torque, as well as rated power, duty type, and service factor⁵² should be chosen as a function of load. As referred previously, if short overload periods occur with duration lower than motor

⁵² Service factor typically varies between 1.0 and 1.15. A service factor of 1.15 means that the motor can operate at 115% load without suffering a significant reduction in its lifetime.

thermal time constant, they should not be considered in the motor selection, providing that motor is able to handle those loads in terms of torque.

For VSD-fed IMs, the insulation system should be reinforced in order to increase robustness to voltage transients and partial discharges, as it is explained in Appendix 5. Of course, the motor bearings should be mechanically compatible with the characteristics of the coupling/load and mounting type (vertical, horizontal, etc.). Moreover, the predictable temperature increase can be compensated by upgrading thermal class. The bearings should be both insulated and/or the shaft connected to the ground, as explained in Appendix 5.

In the VSD selection, several aspects have to be analysed. For example, the VSD should not be chosen based on the motor nominal current. The rated current of the VSDs should be calculated on the basis of motor maximum current, including the overload periods, even if their duration is short. This is, in part, due to the fact that thermal time constant of the inverter power electronic components is, in most cases, significantly lower than that of the motor. It should be noted that the VSD integrated protections act when an overload occurs (in relation to the rated values) [59]. The type of start and stop required by the application should be specified, including regenerative aspects. Regarding switching frequency, common VSDs allow the user to chose 3 or 4 different switching frequencies. The switching frequency leads, for example, to the increase of EMI and inverter losses, and, up to a certain value, to the increase of the motor losses, as previously discussed in Chapter 3.

To properly select or optimize an IM to drive a variable-speed load, the pole number, rated power and mechanical transmission relation (if exists) have to be properly defined. For that, it is necessary, among other aspects, to know the load torque-speed curve, the maximum and minimum values for speed and torque, as well as the operating periods for each load level (load profile).

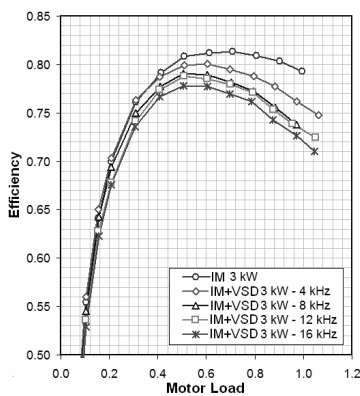


Fig. 9. System efficiency as a function of the load for a 3-kW, 400-V, 50-Hz, IM, with and without VSD, 11 kVA, U/f , three-phase, diode rectifier, $f_s = 4, 8, 12$ and 16 kHz. Test conditions: $f_i = 50$ Hz; $U = 400$ V. Efficiency measured by direct method [84].

The deliberated inclusion of mechanical transmission systems to adapt speed and/or torque, is not, in general, an economically advantageous option, due to the introduction of more losses in the system and higher maintenance requirements. However, the use of non-direct transmission systems allows the choice of the

desirable transmission relation, providing a more accurate speed and/or torque regulation in relation to the pole number options, being, in some cases, an option technically inevitable, from the torque required perspective. Therefore, the inclusion of mechanical transmission should be technically and economically evaluated.

IM sizing should ensure its compatibility in terms of torque-speed curve (TSC), in order to guarantee that the operating temperature of the motor stays equal or lower than the motor rated temperature, for steady-state, as well as the compatibility between motor and load torque-speed curves for both the transient and steady-state modes.

The torque thermal limit approximate curve (TTL) for VSD-fed IMs, can be divided into 4 different regions (A, B, C and D) for self-cooled/ventilated IMs (denoted as SV) and 3 different regions (A, B and E) for forced-ventilation IMs (denoted as FV), as it can be seen in Fig. 10. In region A, the power is assumed to be constant; in region B, the torque is assumed to be constant; in regions C, D and E, the torque is assumed to be variable. It is assumed a 10% derating due to the motor additional losses associated with the inverter output PWM voltages.

The TTL curve is defined approximately in Table 2, where ω_N is the rated speed (r/min), ω is the actual speed (r/min), f_N is the rated frequency (Hz) and P_N is the rated power (W) of the motor.

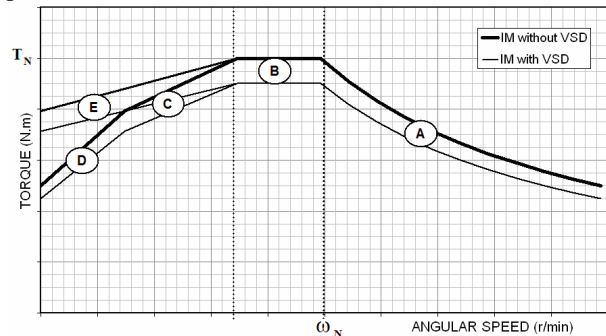


Fig. 10. IM loadability for different operating regions considering sinusoidal voltage supply and PWM-voltage supply [84].

The basic condition for the thermal compatibility between a VSD-fed IM and load is the nonintersection between the load TSC and the TTL, assuming that, for the maximum load speed, the input power required by the load is lower than 90% of the motor rated power and, for the load minimum speed, the torque required by the load is lower than 90% of the torque corresponding to the thermal limit of the motor.

TABLE 2
LOADABILITY OR TORQUE THERMAL
LIMIT APPROXIMATE CURVE (TTL) FOR VSD-FED IMs.

Region	Speed (r/min)	Self-Ventilation (SV)	Forced Ventilation (FV)
D, E	$0 \leq \omega < 0.3 \cdot \omega_N$	Eq. (1)	Eq. (3)
C, E	$0.3 \cdot \omega_N \leq \omega < 0.7 \cdot \omega_N$	Eq. (2)	
B	$0.7 \cdot \omega_N \leq \omega < \omega_N$	Eq. (4)	
A	$\omega \geq \omega_N$	Eq. (5)	

$$T = \left(0.02 \cdot \frac{f_N}{\omega_N} \cdot \omega + 0.5 \right) \cdot T_N \cdot 0.9 \quad (1)$$

$$T = \left(0.01 \cdot \frac{f_N}{\omega_N} \cdot \omega + 0.64 \right) \cdot T_N \cdot 0.9 \quad (2)$$

$$T = \left(0.006 \cdot \frac{f_N}{\omega_N} \cdot \omega + 0.79 \right) \cdot T_N \cdot 0.9 \quad (3)$$

$$T = 0.9 \cdot T_N \quad (4)$$

$$T = 0.9 \cdot \frac{60}{2\pi} \cdot \frac{P_N}{\omega} \quad (5)$$

In Table 3, a methodology for adaptation of IMs to the load in steady state is shown.

An IM is considered well designed if its rated power is minimized and no intersections occur between TSC and TTL. Moreover, depending on the level of motor overload, if the duration of those intersections is shorter than the motor thermal time constant, they are admissible.

Based on the foregoing discussion, a methodology for proper sizing of VSD-fed IMs is proposed in Table 4.

TABLE 3
METHODOLOGY FOR ADAPTATION OF IMs TO THE LOAD (STEADY STATE).

TSC ≥ TTL in region:	TSC < TTL in region:	Measure:
A	Indifferent	↑ P_N
B	Indifferent	↑ P_N and/or ↑ p
C, D	A or B	↑ p or FV
E	A or B	↑ p
--	A, B, C, D and E	Admissible Solution

TABLE 4
METHODOLOGY FOR PROPER SIZING OF VSD-FED IMs.

Step	Action/Measure
1 st	Selection of an IM with rated power equal or immediately higher than maximum input power required by the load in the specified speed range.
2 nd	Calculation of TTL (on the basis of Table 2) and TSC.
3 rd	Identification of the intersection points between TSC and TTL, for each operating region.
4 th	Specification of the most appropriate measures (on the basis of Table 3).
5 th	Verification of motor starting torque suitability for driving the load.
6 th	Specification of the most appropriate measures (on the basis of Table 3).

In Fig. 11 the TTL curves for different EMODS and the TSC curves for two different loads (Load I: horizontal conveyor; Load II: centrifugal fan), are shown. In Table 5, the TTL curve for the EMODS I and the curves TSC for Loads I and II, are shown, being similar the TTL curves calculation for the other EMODS. In Fig. 12, the TTL curves for different transmission relations taking into account the transmission efficiency (considered constant and equal to 97%) are shown.

It is also assumed that, for calculation purposes, the load has 5 different operation periods, with equal duration, for a 16-hour operation cycle (960 min), as it can be seen in Table 6.

The corresponding weighted average motor load over the operating cycle for each EMODS is presented in Table 7.

As referred before, due to the possibility of significant motor losses and speed variation when varying supply

frequency (as shown in Chapter 3), which influences motor loadability, the motor nominal parameters become untuned when IMs are fed by VSDs.

TABLE 5
TSC AND TTL CURVES FOR EMODS I AND FOR LOADS I AND II.

Electric Motor-Driven System	T (N.m)	ω (r/min)
EMODS I with SV	$158996/\omega$	[1480 2960]
	107.46	[1036 1480]
	$0.0363 \cdot \omega + 68.77$	[444 1036]
EMODS I with FV	$0.0726 \cdot \omega + 53.73$	[0 444]
	$158996/\omega$	[1480 2960]
	107.46	[1036 1480]
Load I	$0.0218 \cdot \omega + 85.08$	[0 1036]
	95.5	[300 1500]
Load II	$0.000016 \cdot \omega^2$	[300 2500]

Applying the proposed methodology, the optimal solution can be identified for Loads I and II, being the results presented in Table 8 (application of the methodology presented in Table 4 to the examples being analysed).

For the Load I, the use of the 18.5-kW VSD-fed IM (EMODS I in Fig. 11) to feed the Load I is not recommended since, although the IM rated power exceeds the conveyor rated power, the fact that the IM is being fed by a VSD leads to a decrease of 10% of its rated power (yielding 16.7 kW) and, for speeds below rated, the curves TSC and TTL intersect each other, even considering forced cooling. Therefore, this solution is not appropriate. One of the hypotheses is increasing the 22-kW IM power maintaining the number of poles (EMODS II in Fig. 11). However, for a self-ventilated 22-kW IM, curves TSC and TTL still intersect each other, not being a satisfactory solution for steady-state operation. However, for a 22-kW IM with forced ventilation, curves TSC and TTL do not intersect each other, being a safe solution, but not the optimum one: the IM rated power exceeds largely the load rated power, decreasing the corresponding average motor load (see Table 7). The two previous solutions, although in accordance with the common practice in Industry, are not the most advantageous. If a self-cooling IM is to be used, the motor rated power should be increased to 30 kW, ensuring that curves TSC and TTL do not intersect each other. This solution is totally unrecommended, due to the inherent increase of the system cost (the IM would have twice the power required by the load) and average load reduction (32%, Table 7), leading to poor motor average efficiency and power factor over the operating cycle. According to Table 8, the most convenient solution is the SV, 6-pole, 18.5-kW IM (EMODS IV in Fig. 11), being the TSC and TTL curves intersection eliminated. Besides that, for an 18.5-kW, 6-pole IM, the average motor load is 52%, yet existing a safety margin. However, it is necessary to ensure that bearings and rotor dynamic calibration are adequate for the maximum speed required by the load (1.53 times the motor rated speed). If a 15-kW, 6-pole IM is used, assuming that the rated power decrease 10% when it is fed by a VSD, a 5% overload occurs.

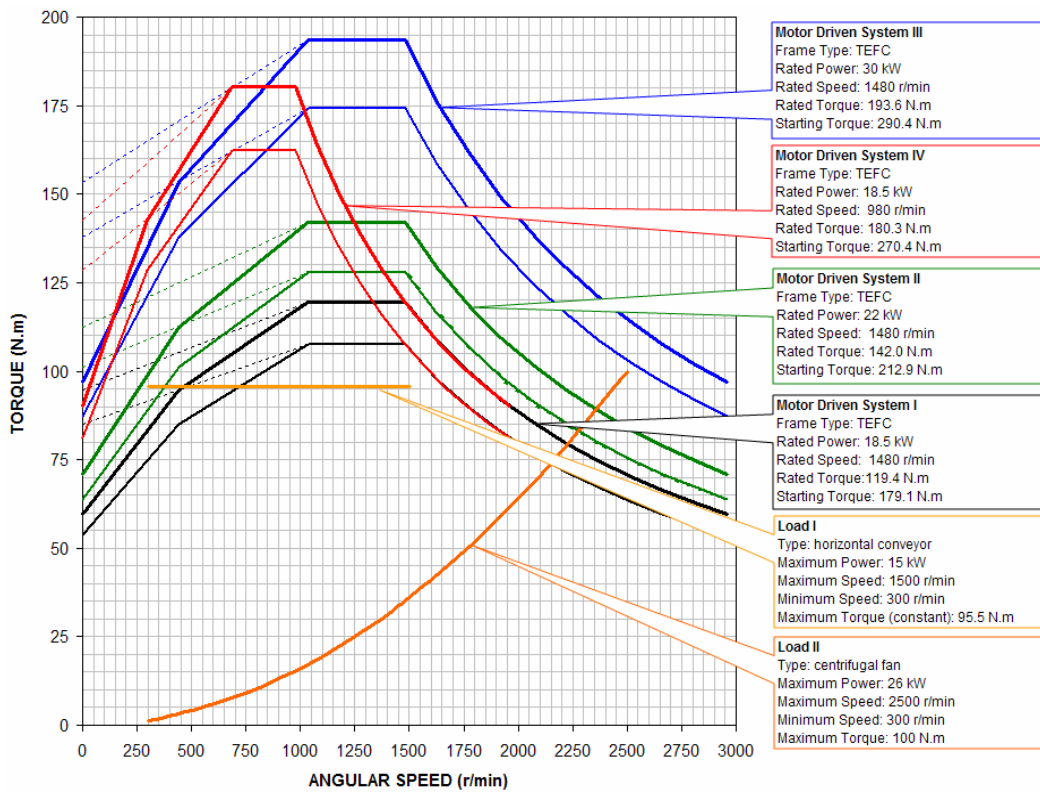


Fig. 11. Motor loadability for different motor driven systems without gears, at different speeds [84].

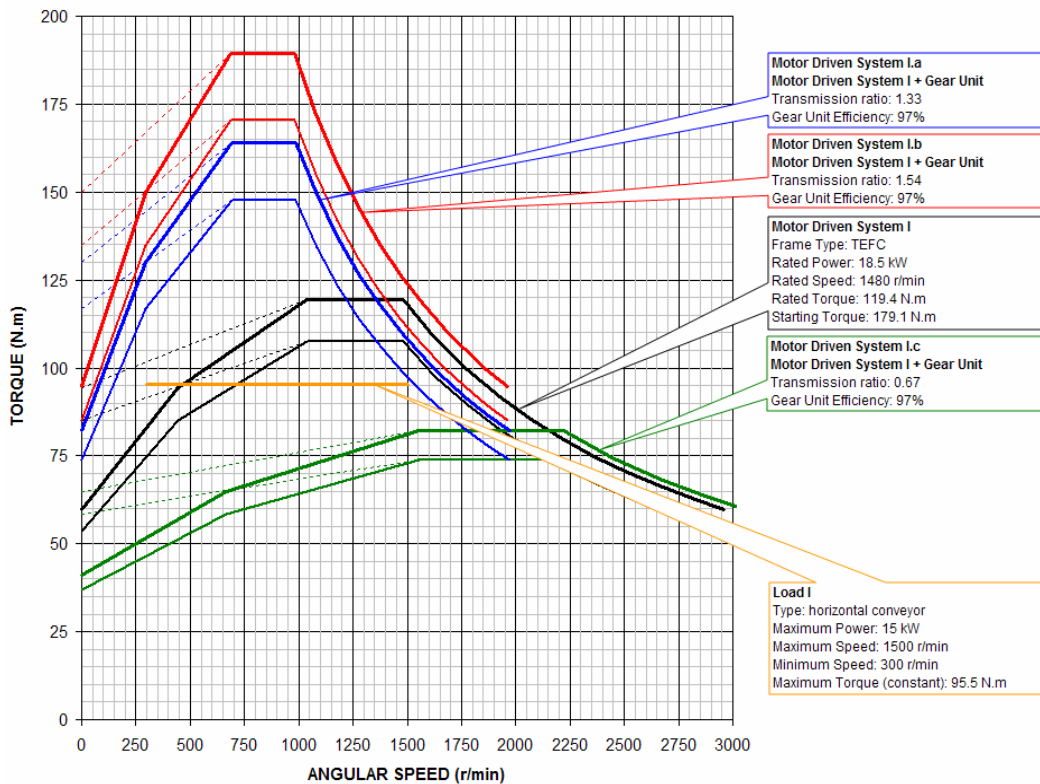


Fig. 12. Motor loadability for different motor driven systems with gears, at different speeds [84].

In the case of Load II, the most proper solution is to use a 4-pole 30-kW IM, leading to a motor load factor of 31%, which is considerably low. The motor would have to operate between 20 and 167% rated speed to satisfy load requirements. A bipolar 30-kW IM is not an admissible solution since its typical rated torque at 2938-2940 r/min is 98-100 N.m (fed by a VSD would be 88.2-90 N.m. The latter solution can only be considered if the

maximum (or in the proximity of maximum) load period is very short. A 2-pole, 37-kW IM (speed of 2930 r/min for a rated torque of 120 N.m) operates between 10 and 83% of rated speed, satisfying the torque requirements for maximum speed and ensuring a higher safety margin. But, in this situation, the average load factor would be 25%.

TABLE 6
OPERATING CYCLE FOR THE CONSIDERED EMODS [84].

Load	Period	ω (r/min)	ω (rad/s)	T (N.m)	Time (min.)	P_N (kW)
Load I Conveyor	1	300	31.42	95.5	192	3.0
	2	750	78.54	95.5	192	7.5
	3	1000	104.7	95.5	192	10
	4	1250	130.9	95.5	192	12.5
	5	1500	157.1	95.5	192	15
Load II Centrifugal Fan	1	300	31.42	1.44	192	0.045
	2	1000	104.7	16.0	192	1.68
	3	1500	157.1	36.0	192	5.66
	4	2000	209.4	64.0	192	13.4
	5	2500	261.8	100	192	26.2

TABLE 7
AVERAGE MOTOR LOAD FOR THE CONSIDERED EMODS [84].

EMODS	IM	Average Motor Load Over the Operating Cycle	
		Load I	Load II
I	18.5 kW / 4 poles	52%	51%
II	22 kW / 4 poles	44%	43%
III	30 kW / 4 poles	32%	31%
IV	18.5 kW / 6 poles	52%	51%
V	30 kW / 2 poles	--	31%
VI	37 kW / 2 poles	--	25%

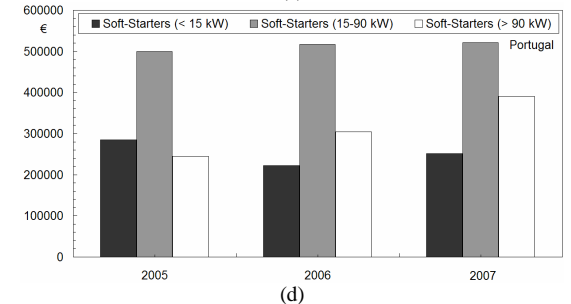
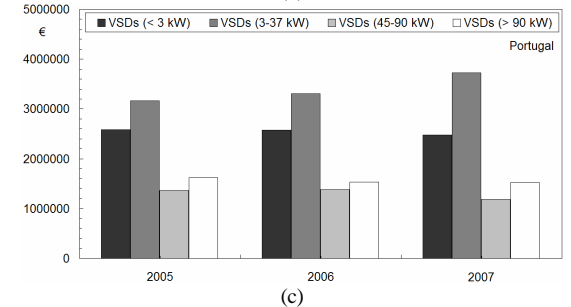
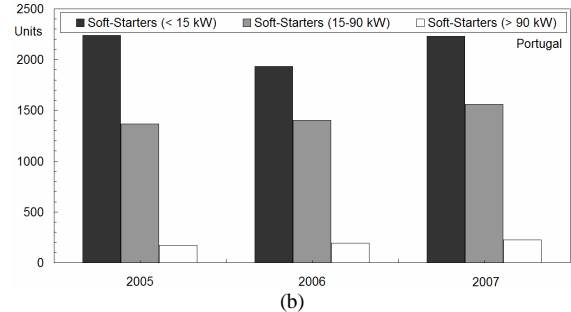
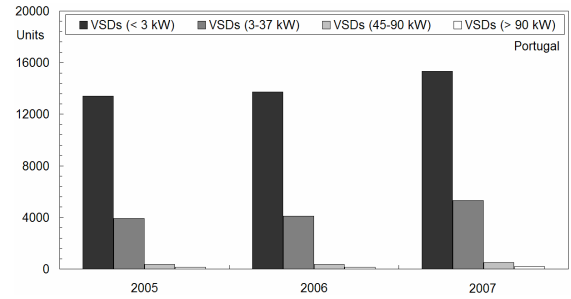
TABLE 8
EVALUATION ACCORDING TO TABLE 3.

Load	MDS	Step	Cooling	Region	TTL intersects TSC ?	Load torque is higher than motor torque?	Measure to be taken:	Starting torque is proper ?	Doable solution ?	Solution maximizes motor load factor ?	Optimal solution ?
Load I	EMODS I	1 st	SV	A	No	No	---	Yes	No	---	---
				B	No	No	---				
		C	Yes	---	FV or $\uparrow p$	No	---	---			
		D	No	Yes	---						
		FV	A	No	No	---	Yes	---			
			B	No	No	---					
	EMODS II	2 nd	SV	A	No	No	---	Yes	No	---	---
				B	No	No	---				
		C	No	No	---	Yes	Yes	No			
		D	Yes	---	FV or $\uparrow p$						
		FV	A	No	No	---	Yes	Yes	No		
			B	No	No	---					
EMODS III	2 nd	SV	A	No	No	---	Yes	Yes	No	---	
			B	No	No	---					
	C	No	No	---	Yes	Yes	No				
	D	No	No	---							
	FV	A	No	No	---	Yes	Yes	No			
		B	No	No	---						
EMODS IV	3 rd	SV	A	No	No	---	Yes	Yes	Yes	Yes	
			B	No	No	---					
	C	No	No	---	Yes	Yes	Yes				
	D	No	No	---							
	FV	A	No	No	---	Yes	Yes	Yes			
		B	No	No	---						
EMODS III	1 st	SV	A	No	No	---	Yes	Yes	Yes	Yes	
			B	No	No	---					
	C	No	No	---	Yes	Yes	Yes				
	D	No	No	---							
	FV	A	No	No	---	Yes	Yes	Yes			
		B	No	No	---						
E	No	No	---	Yes	Yes	Yes					
F	No	No	---								

Finally, it should be referred that, in the case of the Load I, assuming that a reducing mechanical transmission system, with a transmission ratio $i = 1.33$ (EMODS Ia, Fig. 12) to adapt the EMODS I to the load is integrated in the system, it would be an alternative solution to be considered. However, the overall efficiency of the EMODS Ia would be, in principle, slightly lower than that of the EMODS IV due to the transmission efficiency (95-98%), even considering that, in general, motor efficiency decreases slightly with the pole number increase (Table 1), and system cost would increase. Nevertheless, careful studies on transmission and motor number of poles are required, as discussed in the Section 3.9.6.

A6.3.7 Section 3.10

A. Portuguese Market Information on VSDs and Soft-Starters



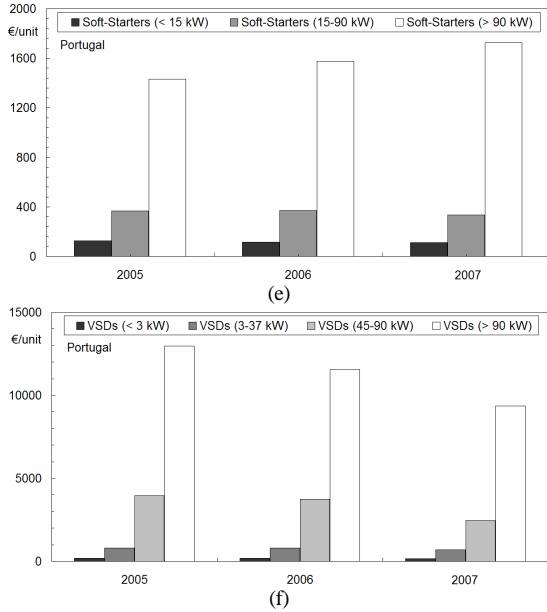


Fig. 1. Portuguese market information (70-80% representativeness) on VSDs and Soft-Starters per power range (Source: Survey AGEFE, 2008).

A6.4 Complement to Chapter 4

A6.4.1 Sections 4.11 and 4.12

A. Air-Gap Torque Method [9], [10]

The air-gap torque method for motor efficiency field assessment is a new method developed at the Oak Ridge National Laboratory. This is a high-intrusion method. Table 1, is a self-explanatory tabulation for motor losses and efficiency. As indicated, the basis losses are rotor copper loss, stator copper loss, friction and windage loss, core loss, and the stator and rotor stray losses (or stray-load losses). The rotor copper loss for IMs depends on the slip.

The output power of a motor is the product of the shaft angular speed and the shaft output torque. This output torque is the air-gap torque less the torque losses associated with friction, windage, and stray losses (mainly caused by rotor currents).

A significant difference between the air-gap torque method and the IEEE 112 Standard method E1, is that it considers the losses associated with the negative torques produced by the negative-sequence excitation components, which result from unbalanced and/or distorted voltages. The air-gap torque method has a unique advantage over the method E1 for efficiency field assessment.

TABLE I
MOTOR LOSSES AND EFFICIENCY.

Stator input power	Stator input power = Rotor intake power + Stator total loss
Stator total loss power	Stator total loss = Stator copper loss + Core loss + Stator stray loss
Rotor intake power	Rotor intake power = (air-gap torque times speed) + Rotor total loss
Rotor total loss power	Rotor total loss = Rotor copper loss + Friction & windage + Rotor stray loss
Output power	Output power = stator input power – stator total loss – rotor total loss
Efficiency	Efficiency = output power/stator input power

The instantaneous input power of an IM is the summation of products of the instantaneous phase

voltages, u_a , u_b , u_c , and phase currents, i_a , i_b , and i_c , as in (1).

$$p_{in} = u_a i_a + u_b i_b + u_c i_c \quad (1)$$

A portion of this instantaneous power includes the charging and discharging of the energy stored in the windings. Therefore, this instantaneous power cannot represent the instantaneous torque even at a constant speed after subtracting the losses. However, the average value of instantaneous power at full load represents the input power of the motor for the efficiency calculation. The conventional single-frequency power equation using power factor, RMS current and voltage is a special case of the average instantaneous power.

Air-gap torque equations have been known for several decades. They can be traced worldwide in various publications. Equation (2) is valid for the three-phase stator windings, where Ψ_a , Ψ_b , and Ψ_c are the flux linkages of windings a , b and c , respectively, and R_{ph} is the phase resistance. Substituting (2) in (1) yields (3).

$$\begin{cases} u_a = \frac{d\Psi_a}{dt} + R_{ph} \cdot i_a \\ u_b = \frac{d\Psi_b}{dt} + R_{ph} \cdot i_b \\ u_c = \frac{d\Psi_c}{dt} + R_{ph} \cdot i_c \end{cases} \quad (2)$$

$$p_{in} = i_a \left(\frac{d\Psi_a}{dt} + R_{ph} \cdot i_a \right) + i_b \left(\frac{d\Psi_b}{dt} + R_{ph} \cdot i_b \right) + i_c \left(\frac{d\Psi_c}{dt} + R_{ph} \cdot i_c \right) \quad (3)$$

From (2), the flux linkages can also be given as (4).

$$\begin{cases} \Psi_a = \int (u_a - R_{ph} \cdot i_a) dt \\ \Psi_b = \int (u_b - R_{ph} \cdot i_b) dt \\ \Psi_c = \int (u_c - R_{ph} \cdot i_c) dt \end{cases} \quad (4)$$

Subtracting the copper losses and the terms pertinent to the energy stored in the windings, the air gap torque equation can be written for the line data as indicated in (5), where p is the pole-pairs, i_A , i_B , and i_C the line currents, and R the half of the line-to-line resistance value. The integrals in (5) represent flux linkages.

$$T_{ag} = \frac{p}{\sqrt{3}} \left\{ \begin{aligned} & (i_A - i_B) \cdot \int [u_{CA} - R(i_C - i_A)] dt \\ & - (i_C - i_A) \cdot \int [u_{AB} - R(i_A - i_B)] dt \end{aligned} \right\} \quad (5)$$

From the definition of R , $R = R_{ph}$ for star-connected motors, and $R = R_{ph}/3$ for delta-connected motors. Equation (5) is associated with certain assumptions and approximations. First, the degree phase leakage reactances of motor are linear and identical. Second, the negative sequence winding spatial components (not the time harmonics) are negligible. Third, the torque components produced by sources that are not dependent on the armature winding currents, such as permeance cogging torque in a permanent-magnet motor, are not considered. Fourth, the instantaneous magnetic

unbalances for three phases are ignored. Fifth, the effect of DC components in flux linkages is neglected.

When using either three leads for star-connected motors without a neutral connection or three leads for delta-connected motors, (5) can be further simplified using the relation (6).

$$i_A + i_B + i_C = 0 \quad (6)$$

The above equation can be rewritten to the known format that uses only two line voltages, two line currents, and one-half of line-to-line resistance as the input data for the calculation of the air-gap torque.

Regarding the numerical evaluation of integrals, if the time increment between data points is small enough (e.g., sample rate of 5 kHz) a simple trapezoidal method can be used. Other methods using Simpson's rule or Gauss's rule for numerical evaluation of integrals can also be used.

As mentioned earlier, the shaft output power is calculated from the shaft speed (r/min) and shaft torque, as in (7), where T_{mtr} is the shaft torque, given in N.m and ω is the angular speed, given in rad/s. The shaft torque is the difference of air-gap torque, T_{ag} , and torque losses corresponding to mechanical loss and stray loss produced by rotor current, as in (8).

$$P_{out} = T_{mtr} \cdot \omega \quad (7)$$

$$T_{mtr} = T_{ag} - P_{f\&w} \cdot \omega^{-1} - P_{SLL} \cdot \omega^{-1} \quad (8)$$

From (7) and (8), the motor efficiency is computed using (9).

$$\eta = \frac{\omega \cdot T_{ag} - P_{f\&w} - P_{SLL}}{P_{in}} \quad (9)$$

The air-gap torque method requires the acquisition of the voltage and current waveform data so that these waveforms may be used in the integrations described above. It is best the waveform data may be acquired over a period of several cycles, preferably even one second so that oscillations in the load may be averaged. The waveforms must be acquired with a reasonably high sampling rate so that a high accuracy of the waveforms shape may be achieved.

In addition to the voltage and current waveforms, a measurement of no load power into the motor must be made. To do this, the motor must be uncoupled and a power meter used to measure the power input. The motor speed must also be measured, which can be done with a stroke light (stroboscope) while the motor is in normal service. The motor resistance must also be measured, requiring motor disconnection for this measurement.

Until the method has been developed into a package unit that performs both the data acquisition analysis, the waveform data will have to be acquired with a recording device and converted into a digital file, then this data, along with the speed, stator resistance and no-load power would be used as input to software that performs the calculation.

B. Ontario Hydro Modified (OHM) Method [9], [10]

The method developed as a medium intrusion method is a modification of the Ontario Hydro version of IEEE 112 Method E Segregated Loss Method. The method will be referred to as the Ontario Hydro Modified (OHM) method. Although this method has been selected for the category of medium intrusion, it has actually been found to provide quite reasonable accuracies. It can provide accuracies within two or three percentage points when the empirical factors used in estimating the losses are selected based on test results for a representative population of motors. The method becomes less reliable as loads approach 50% because it uses an approximation for no-load losses, and the impact of this approximation when determining losses becomes more significant at low loads.

Ontario Hydro uses an empirical value of 3.5% to find the no-load losses rather than actually performing no load testing. A factor of 0.035 is multiplied times the full load watts into the motor to estimate the no load watts loss. This value was revised for motors less than 50 hp by using the same ratio as is used in the table of stray load loss approximation provided in IEEE Standard 112. This revision results in an empirical factor of 0.042. As a further refinement, this value could be optimized by testing samples of motors at different horsepower levels. The stray load loss is estimated simply using the method provided in IEEE 112. Since the input power at full load is not known, this value is estimated using the nameplate current and voltage with a power factor of 0.8. The stator resistance at load is estimated based on a simple approximation using the motor current to estimate the temperature rise.

The only measurements needed are the voltage, current, power factor, speed, and cold stator resistance. The motor does not have to be disconnected to measure the stator resistance. The total resistance of the motor and feeder may be measured from the motor control center (MCC), and then the feeder resistance estimated based on the length of the cable run and wire gauge. The feeder resistance would then be subtracted from the total resistance to find the motor resistance. This technique will not result in unacceptable errors. For a 7.5-hp IM, an error of 100 feet in estimating the feeder length would result in an error in determining motor efficiency of about 1%. Thus, all measurements except motor speed may be taken from the MCC bucket. In the event that the motor is inaccessible, even the motor speed may be determined from an analysis of the motor current waveform.

A MATHCAD or MATLAB program can be developed to produce the load and efficiency estimate using the data previously described. The algorithm can include the following steps:

1. Measurement and recording of motor current, voltage, power factor and motor speed;
2. Calculation of the input power;
3. Calculation of the no-load losses;
4. Calculation of the SLLs;
5. Calculation of the Joule losses;
6. Calculation of the temperature-corrected slip and rotor losses;
7. Calculation of the motor efficiency ($\eta = 1 - P_{loss} \cdot P_m^{-1}$).

The no-load losses are assumed to be the sum of the friction and windage and core loss. If the no-load power input cannot be measured, the no-load losses can be set to

4.2% of the motor input power at rated load, as explained above. If the power input at rated load is not known, the rated current and voltage and a power factor of 0.8 can be used.

The SLLs are assumed to be 1.8% of the motor input watts for motors smaller than 125 hp. This is in accordance with Table 2 of IEEE Standard 112. The SLL at loads less than rated is corrected by the square of the ratio of motor current to rated current.

The Joule heating loss in the stator is found by multiplying the stator winding resistance by the square of the motor current. The motor winding resistance is corrected as a function of an approximate temperature. The approximate temperature is determined by using the ratio of change in motor current above no-load to the rated change times the rated temperature rise. If the resistance with the temperature rise is measured and used in this calculation, the temperature correction should not be used.

The power in the rotor is the power into the motor minus the sum of the no-load losses, SLLs and the Joule heating losses. The rotor losses are found by multiplying the temperature corrected slip times the power into the rotor. The temperature corrected slip is found using a rotor corrected slip times the power into the rotor. The temperature corrected slip is found using a rotor conductor temperature with the same approximate temperature as discussed above.

The rotor losses are added to the no-load losses, the stray load loss and the Joule heating losses to find the total losses. The efficiency is simply the ratio of the input watts minus the total losses to the input watts.

C. Nameplate Equivalent Circuit Method [9], [10]

A modified version of IEEE Std. 112 method-F has been used. This is a low intrusion method. In it, an extra resistance has been added to the rotor circuit to account for stray losses since they are mostly dependent on rotor current. Once the value of each of the equivalent circuit components is known accurately, as shown below, efficiency may be obtained from the measurement of motor speed. Two low-intrusion approaches can be followed to determine the values of the seven components of the per-phase equivalent circuit. Both rely on the motor's nameplate data and NEMA standards. The first approach requires the measurement of stator resistance (r_1) at rated load temperature. The second approach estimates r_1 using generic relationships based on the number of poles ($2p$), horsepower rating (P_N), and rated line voltage (U_N) of the motor. Equation (10) applies to design B motors.

$$r_1 = 1.1 \cdot 10^{-4} \cdot (2p)^{0.52} \cdot P_{N(hp)}^{-1.26} \cdot U_N^2 \quad (10)$$

Thus, this second approach does not require any measurements specific to the motor interest: all motors with the same nameplate data will be found to have the same Equivalent Circuit. Consequently, their efficiency in the field will be estimated differently only if their speed is different. It is this approach that is used in the NEQ method. Once r_1 is known the rest of the parameters are found as follows. Nameplate's rated horsepower, voltage, current and either power factor or efficiency allow the

computation of the rated power input and overall motor impedance Z_T and efficiency or power factor respectively. From the rated power input and IEEE 112 standard information, the load-dependent SLLs can be estimated as a percentage ($SLL_{\%}$) of the output power at rated load. Thus, the equivalent loss resistance $r_{2(SL)}$ in series with the rotor circuit is a constant given by (11).

$$r_{2(SL)} = SLL_{\%} \cdot \frac{P_{out(N)}}{3I_{rotor}^2} \quad (11)$$

Note that $SLL_{\%} = 1.8\%$ for motors of less than 125 hp, and that the rotor current at rated conditions can be initially estimated to be a factor (i.e., 80%) of the nameplate rated stator current. Once the equivalent circuit parameters are defined, if the resulting factor is far from the initial guess, the computations can be repeated using the newly obtained value. The friction and windage losses are taken as a constant percentage ($FW_{\%}$) of the rated output power, as in (12), where $FW_{\%} = 1.2\%$ for 4 pole motors below 200 hp. This loss allows the appropriate raw-efficiency for the equivalent circuit of the motor, at rated conditions, to be determined as in (13).

$$P_{f\&w} = FW_{\%} \cdot P_{out(N)} \quad (12)$$

$$\eta_{N(raw)} = \eta_N + P_{f\&w} \cdot P_{in(N)}^{-1} \quad (13)$$

The nameplate NEMA Class - A, B, C, or wound rotor - provides a value for the ratio between the stator and rotor leakage reactances (x_1 -to- x_2 ratio) - 1.0, 0.67, 0.43, 1.0, respectively. The nameplate NEMA Code letter - D, E, ... L - brackets the value of the locked rotor current - from 5 to 12.5 times horsepower rating. It was decided to use the mid point of the range corresponding to the motor's Code letter. This, together with the rated voltage, allows the computation of the magnitude of the motor's impedance under locked rotor conditions ($|Z_{l(s=1)}|$). The rated slip, s_N , overall resistance and reactance, x_1 -to- x_2 ratio, and magnitude of the locked rotor impedance can then be used to iteratively find the values of x_1 , x_2 , r_2 and Z_m that yield the raw efficiency for the rated conditions and satisfy the locked-rotor current condition simultaneously. Finally, the magnetizing impedance Z_m yields readily the values of its constituents: the core resistance (r_0) and the magnetizing inductance (x_m). The values of the equivalent components found above: r_1 , x_1 , r_0 , x_m , r_2 , x_2 , and r_{2SL} can then be used to compute the motor's raw efficiency, η_{raw} , at any load and voltage from the measurement of motor speed only by means of (14), where s is the slip corresponding to measured speed and the Z parameters are complex numbers related to the motor equivalent circuit parameters as shown in Figs. 1 and 2.

$$\eta_{raw}(s) = \frac{\left| \frac{\bar{Z}_g}{\bar{Z}_2 + R_L} \right|^2 \cdot \frac{R_L}{\text{Re}\{\bar{Z}_T\}}}{\quad} \quad (14)$$

The net efficiency, η , is found by subtracting the friction and windage losses from the motor's raw power output. Net efficiency is thus computed by subtracting from the raw efficiency the ration of the friction and

windage losses to the power input using (15), when power input to the motor is known.

$$\eta(s) = \eta_{raw}(s) - P_{f\&w} \cdot P_m^{-1} \quad (15)$$

Alternatively, the efficiency can be computed by (16), where U_{ll} is the motor terminal line-to-line voltage, or, if unavailable, the nameplate voltage.

$$\eta(s) = \eta_{raw}(s) - P_{f\&w} \cdot \left(3 \cdot \frac{|U_{ll}|^2}{|Z_T|^2} \cdot \text{Re}\{\bar{Z}_T\} \right)^{-1} \quad (16)$$

Using, for example, the LABVIEW software package a virtual instrument self-standing code (i.e., the user does not need to have LABVIEW on the computer), can be developed to apply the nameplate Equivalent Circuit Method, requiring nameplate information as input. This should include: number of phases and poles, motor size (in horsepower), phase-to-phase voltage, and full-load current, speed, and power factor. In addition, the user inputs the NEMA design class and code. Once this information has been entered, the code calculates the equivalent circuit. Estimation of motor efficiency and load require only the motor speed, which can be measured using an optical tachometer.

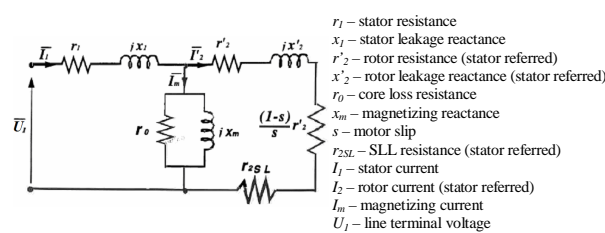


Fig. 1. Schematic of the per-phase equivalent circuit [9].

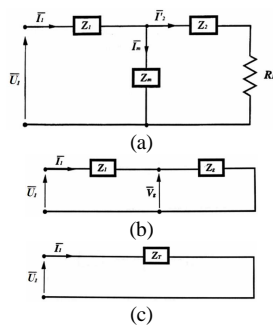


Fig. 2. Schematic of per-phase equivalent circuit condensed to [9]: (a) basic functional impedances; (b) stator and gap impedances; (c) single impedance.

A6.4.2 Section 4.13

A. Circle Diagram [6]

Considering the per-phase approximate equivalent circuit (AEC) for IMs, shown in Fig. 1, which is the base of the approximate circle diagram, shown in Fig. 2, the stator current is given by (1).

$$I_1 = \frac{E_1}{\left(R_1 + \frac{R_2}{s} \right) + j(X_1 + X_2)} \quad (1)$$

It is evident from that equation that if the impressed voltage E_1 (for the AEC, $U_1 = E_1$) is fixed and the primary current is calculated for a series of motor speed, the locus

of the tip of the phasor, I_1 , will form an arc of a circle. This diagram is very convenient for visualization purposes, but it is based on several approximations. The usual form of the approximate circle diagram assumes a constant air-gap field at all speeds, i.e., it lumps the primary and secondary impedances on the secondary side of the magnetizing current, as shown in Fig. 1, and, additionally, ignores the saturation level variation (particularly when estimating starting current by means of locked-rotor test). The data necessary to construct circle diagram are the magnitude of the no-load current, ON, and the locked-rotor current, OS, and their phase angles with reference to the line voltage, OE. A circle with its centre on the line NU at right angles to OE is drawn to pass through N and S. Each line on the diagram can be measured directly in A, but also represents VA or power, when multiplied by the phase voltage times the number of phases. The line VS drawn parallel to OE represents the total motor input rotor, and scale VT represents primary I^2R loss. The ST represents the power at standstill, which, divided by the synchronous speed, gives the starting torque. At any load point A, OA is the primary current, NA the secondary current, and AF the motor input. The motor output is AB, the torque times the synchronous speed is AC, the secondary I^2R loss is BC, the primary I^2R loss is CD, and the no-load copper loss plus core loss is DF. The maximum power factor point is P, located by drawing a tangent to the circle from O. The maximum output and maximum torque points are similarly located at Q and R by tangent lines parallel to NS and NT, respectively. The diameter of the circle is equal to the voltage divided by the standstill reactance, or equal to the locked-rotor current value on the assumption of zero resistance in both windings.

Besides the error previously mentioned due to assuming constant air-gap voltage at all loads, other errors occur in the approximate circle diagram, resulting from variations in reactance and in secondary resistance (skin effect) over the speed range, due to changes in the magnetic saturation (as previously referred) and secondary frequency. The diagram does, however, afford a convenient means of checking the overall performance of a motor with a minimum of test data.

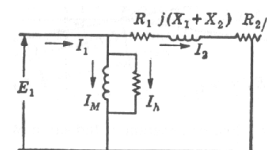


Fig. 1. Approximate per-phase equivalent circuit of an IM.

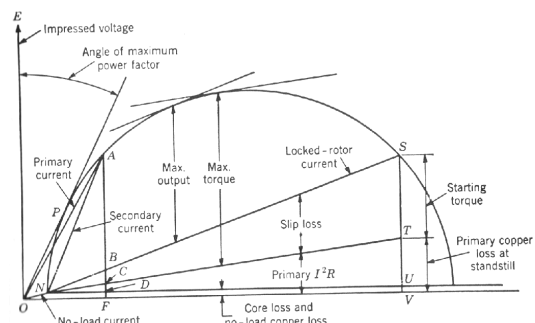


Fig. 2. Approximate circle diagram (on the basis on the approximate per-phase equivalent circuit) of an IM.

A6.5 Complement to Chapter 5

A6.5.1 Section 5.2

A. Additional Curves for Y/D Connection Change

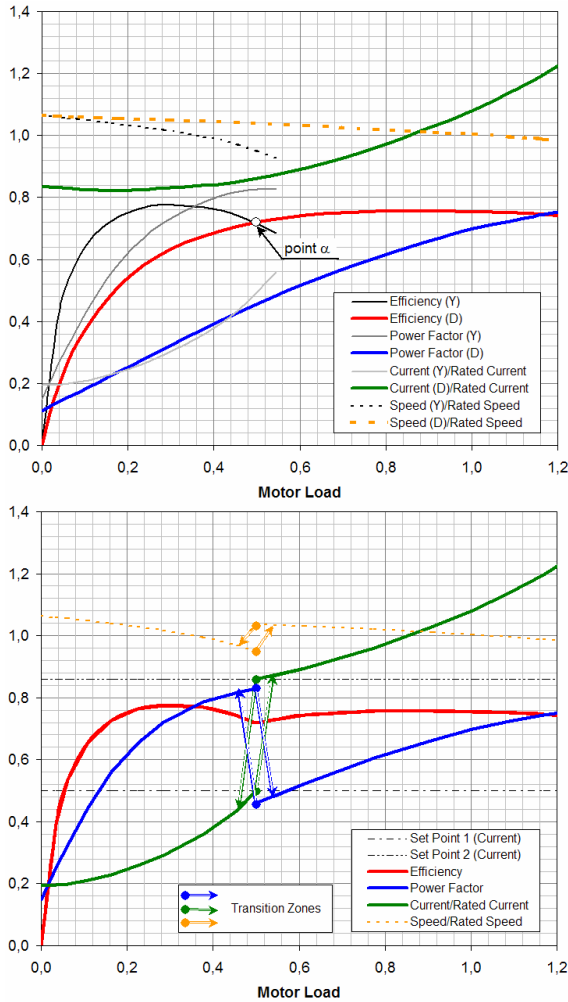


Fig. 1. Efficiency, power factor and current as a function of the load for a 2.2-kW, 4-pole motor: (top) with fixed delta connection; (bottom) with automatic change of the winding connection.

B. First Prototype of the Smart-Switch

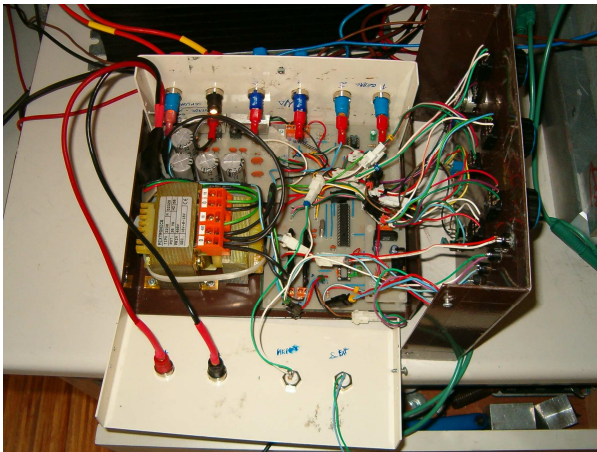


Fig. 2. First prototype of the electronic device (*Smart-Switch*) for automatic management of the stator winding connection as a function of the line current.

C. Motor Line Current and Torque for Different Starting Methods

Fig. 3. Line current (RMS value) and average torque for an IM using different starting methods: direct-on-line (D.O.L.) starting, starting with Y/D connection change, and starting with a soft-starter device (anti-parallel thyristor electronic voltage regulator, see Fig. 2 of Section A6.5.3).

A6.5.2 Section 5.3

A. Generalized MMF Space Harmonics and Performance Analysis of Combined Multiple-Step, Star-Delta, Windings Applied to IMs

In this section, a generalized MMF space harmonics and performance analysis of combined multiple-step, star-delta, three-phase windings applied on IMs is presented. The combined star-delta three-phase windings are very old. As far as authors know, the first reference on this topic is the patent of Korthals [34], issued in 1918, where two-winding system, incorporating one star-connected winding and one delta-connected winding, combined together, in a three-phase induction motor. Both windings are manufactured with same number of poles, but spatially displaced by 30° , and the delta-connected

winding has a number of turns $\sqrt{3}$ times larger than the star-connected winding. Star-delta three-phase windings are actually used in some two-pole IMs driving high-inertia loads, requiring high-starting torque, in order to allow magnetizing flux regulation and starting current limitation. However, such windings can they could be used also for saving energy in variable-load induction motors [35], and for terminal-voltage adjustment in synchronous generators [36].

As sometimes happens, the novelty is not fully true where it is claimed. Examples of such situations are the papers of Hughes [37] and Chen [38] or even the patent of Gjota [39] where the first reference of the patent of Korthals [34] is not at all cited. This is why it is to be underlined that the present paper will not bring any news on the combined star-delta winding principles, but offers a general method of analysis as a function of number of turns and relative spatial position of the two windings, taking into account the spatial harmonics of the resultant magnetomotive force (*MMF*) depending on the per-winding *MMF* waveform space harmonics.

The calculation results are verified on a new developed motor, wound in order to allow experimental analysis of different situations regarding the constitution of the star and delta windings, leading to discrete steps in the air-gap flux density level.

MMF Analysis - It is supposed that the single-layer or double-layer winding of an IM have the coils divided in two parts (or separated windings), being the first part connected in delta and the second one connected in star. The two separated windings can be connected in parallel or in series, being the parallel connection conditioned to more restrictions regarding the number of turns [37], [38]. The series connection has no restrictions excepting the spatial symmetry [35], [36], [38]. Depending on the constitution and on the manner in which the coils of each phase are divided between the star and delta systems, the whole system can be characterized as being a three- or a six-magnetic axis.

In Fig. 1, it is represented a series-connected three-phase combined star-delta system of windings. Both the star and delta components are symmetrical, and the star component is connected between the supply and the inner delta. As the magnetic axes is concerned, the magnetic axes of the star connected phases can be characterized by an angle α , assumed to be in the range $[-\pi/6 + \pi/3]$, related to a reference axis perpendicular to that of the opposite phase of the delta branch, as it can be seen in Fig. 1.

If $\alpha = 0$, which is the case considered in the patent of Korthals [34], the analysis may be performed as in the Chen's paper [38], applied to a semi-six-phase system. As it is clear, this case can be obtained from any normal phase winding having 60° (electrical) distribution, connecting one part of the coils in the delta system and the remaining coils in the star system, considering the phase coils series connected in their natural order.

If $\alpha = -\pi/6$, there are only three magnetic axis for both star and delta winding parts. This case is representing the situation where, the phase of a normal machine is divided into two parts, as, for example, two parallel paths, whose magnetic axis are the same. It is clear that, in this case, the partial windings have larger space harmonics, and the

manner of establishing the parallel path is an interesting subject with possibility for optimization [42]. In [43], the performance of a 4-pole induction motor using this configuration (among other) is experimentally analysed, from the motor steady-state performance perspective.

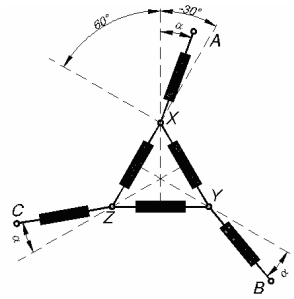


Fig. 1. Relative spatial displacement of the star and delta windings in a combined star-delta winding.

The $\alpha = \pi/3$ case, as it is shown in the paper, represents a possible limit situation, leading to an intermediate step in the air-gap flux density adjustment.

If the combined star and delta windings are both regular, it means that there are symmetrical integer windings, and the time variation of the instantaneous currents in the star system will be balanced as in (1).

$$\begin{cases} i_{AX} = I\sqrt{2} \sin \omega t \\ i_{BY} = I\sqrt{2} \sin(\omega t - \frac{2}{3}\pi) \\ i_{CZ} = I\sqrt{2} \sin(\omega t - \frac{4}{3}\pi) \end{cases} \quad (1)$$

The Kirchoff's theorem applied in the connection points between the star and delta systems leads to the phasorial equations in (2), whose phasorial diagram is presented in Fig. 2.

$$\begin{cases} \bar{I}_{XY} = \bar{I}_{YX} \cdot e^{j\pi} = \frac{1}{3}(\bar{I}_{BY} - \bar{I}_{AX}) \cdot e^{j\pi} = \frac{\bar{I}_{AX}}{\sqrt{3}} \cdot e^{-j\frac{2}{3}\pi} \cdot e^{j\pi} = \frac{\bar{I}_{AX}}{\sqrt{3}} \cdot e^{+j\frac{1}{3}\pi} \\ \bar{I}_{YZ} = \bar{I}_{ZY} \cdot e^{j\pi} = \frac{1}{3}(\bar{I}_{CZ} - \bar{I}_{BY}) \cdot e^{j\pi} = \frac{\bar{I}_{AX}}{\sqrt{3}} \cdot e^{+j\frac{2}{3}\pi} \cdot e^{j\pi} = \frac{\bar{I}_{AX}}{\sqrt{3}} \cdot e^{-j\frac{1}{3}\pi} \\ \bar{I}_{ZX} = \bar{I}_{XZ} \cdot e^{j\pi} = \frac{1}{3}(\bar{I}_{AX} - \bar{I}_{CZ}) \cdot e^{j\pi} = \frac{\bar{I}_{AX}}{\sqrt{3}} \cdot e^{-j\frac{1}{3}\pi} \cdot e^{j\pi} = \frac{\bar{I}_{AX}}{\sqrt{3}} \cdot e^{+j\frac{2}{3}\pi} \end{cases} \quad (2)$$

Currents defined by (2) are valid whatever would be the relative spatial position between the star and delta windings. Using (1) and (2), the time variation of the instantaneous currents in the delta winding can be expressed by (3).

$$\begin{cases} i_{XY} = I\sqrt{\frac{2}{3}} \cdot \sin(\omega t + \frac{1}{6}\pi) \\ i_{YZ} = I\sqrt{\frac{2}{3}} \cdot \sin(\omega t - \frac{2}{3}\pi + \frac{1}{6}\pi) \\ i_{ZX} = I\sqrt{\frac{2}{3}} \cdot \sin(\omega t - \frac{4}{3}\pi + \frac{1}{6}\pi) \end{cases} \quad (3)$$

Defining N_Y , N_D as the number of series connected turns and K_{wYs} , K_{wDs} as the winding factors for the s^{th} order spatial harmonic, in the star and delta windings, respectively, the *MMF* produced by the two windings can be written taking into account the classical theory of producing the rotating waves by fixed currents. For the star winding yields (4), and, in the same manner, considering the time and space relative situation, for the delta winding yields (5).

The number of turns and winding factors of both windings depend on how the winding of each phase is distributed in the star and delta components. Typically, due to the smaller number of distributed coils in each part, the winding factors of each component are larger than the winding factor of the equivalent full winding having the number of turns $N_t = N_Y + N_D$. Using the following notation for the p.u. number of turns of the star and delta part, expressed by (6), the resultant clockwise (CW) MMF given by the combined winding, using (4) and (5) is given by (7), where was noted the phase displacements of the D component, φ_s , as in (8).

$$MMF_Y(\theta, t) = \frac{3N_Y I \sqrt{2}}{\pi} \left(\sum_{s=1,7,13,\dots} \frac{K_{wYs}}{s} \cos(\omega t - s\theta) + \sum_{s=5,11,17,\dots} \frac{K_{wYs}}{s} \cos(\omega t + s\theta) \right) \quad (4)$$

$$MMF_D(\theta, t) = \frac{3N_D I \sqrt{2}}{\pi \sqrt{3}} \left(\sum_{s=1,7,13,\dots} \frac{K_{wDs}}{s} \cos\left[\omega t + \frac{\pi}{6} - s\left(\theta + \frac{\pi}{6} - \alpha\right)\right] + \sum_{s=5,11,17,\dots} \frac{K_{wDs}}{s} \cos\left[\omega t + \frac{\pi}{6} + s\left(\theta + \frac{\pi}{6} - \alpha\right)\right] \right) \quad (5)$$

$$\begin{cases} N'_Y = N_Y \cdot (N_Y + N_D)^{-1} \\ N'_D = N_D \cdot (N_Y + N_D)^{-1} \end{cases} \quad (6)$$

$$MMF_{\Sigma CW}(\theta, t) = \frac{3N_t I \sqrt{2}}{\pi \sqrt{3}} \left(N'_Y \sqrt{3} \sum_{s=1,7,13,\dots} \frac{K_{wYs}}{s} \cos(\omega t - s\theta) + N'_D \sum_{s=1,7,13,\dots} \frac{K_{wDs}}{s} \cos(\omega t - s\theta + \varphi_s) \right) \quad (7)$$

$$\varphi_s = s \cdot \alpha + \frac{\pi}{6}(1 - s) \quad (8)$$

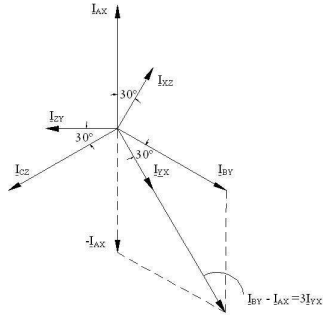


Fig. 2. Current time-phase displacement in the star and delta winding parts of a combined star-delta winding.

Equation (7) may be written, after restriction of the same order terms, as in (9),

$$MMF_{CW}(\theta, t) = \frac{3N_t I \sqrt{2}}{\pi \sqrt{3}} \left(\sum_{s=1,7,13,\dots} \frac{K_{wseq}}{s} \cos(\omega t - s\theta) \right), \quad (9)$$

where the resultant equivalent winding factor K_{wseq} is given by

$$K_{wseq}^2 = 3N'_Y{}^2 K_{wYs}^2 + N'_D{}^2 K_{wDs}^2 + 2\sqrt{3}N'_Y N'_D K_{wYs} K_{wDs} \cos \varphi_s \quad (10)$$

Similarly, the counter-clockwise (CCW) component will be exactly as in (9), but applied to negative-sequence space harmonic orders, yielding (11).

$$MMF_{CCW}(\theta, t) = \frac{3N_t I \sqrt{2}}{\pi \sqrt{3}} \left(\sum_{s=5,11,17,\dots} \frac{K_{wsc}}{s} \cos(\omega t + s\theta) \right) \quad (11)$$

It is obvious from (8) that, for the particular case when there is either star ($N'_Y = 1, N'_D = 0$) or delta ($N'_Y = 0,$

$N'_D = 1$) component exclusively, it will lead to the values of the winding space harmonic order as in (4) or (5), respectively.

Analysis of an Integer Winding with $q = 3$ – The combined star-delta winding was applied and verified on a particular 4-pole IM with a 36-slot stator core, and an integer⁵³, single-layer, eccentric winding. In order to have more possibilities of verification, the per-phase winding was divided in three series-connected parts, according to Fig. 3. For example, for the phase “A” the first portion is A-M_A, the second is M_A-N_A, and the third is N_A-X.

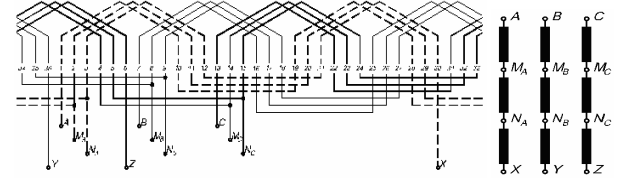


Fig. 3. Winding setup for a 36-slot, 4-pole IM: (left) winding diagram; (right) winding connections.

In Table 1, the connections defined in order to verify the theory, starting from full delta up to full star, are described. It is considered that the motor is supplied from line at the terminals A, B, C, in all the considered cases.

TABLE 1
POSSIBLE CONNECTIONS OF THE WINDING PRESENTED IN FIG. 3.

Case	Winding Connection	Symbol	α	N'_Δ	N'_Y	K_{wD}	K_{wY}
1	X-B, Y-C, Z-A	D	-	1	0	0.9598	--
2	X-M _B , Y-M _C , Z-M _A	Dy-I	0	2/3	1/3	0.9848	1
3	X-M _C , Y-M _A , Z-M _B	Dy-II	$\pi/3$	2/3	1/3	0.9848	1
4	X-N _C , Y-N _A , Z-N _B	Yd-I	$\pi/3$	1/3	2/3	1	0.9848
5	X-N _B , Y-N _C , Z-N _A	Yd-II	0	1/3	2/3	1	0.9848
6	X-Y-Z	Y	--	0	1	--	0.9598

In cases 2 to 5, it is possible to observe that one of the windings is concentrated ($K_w = 1$) and the other has $q = 2$ (2 slots per pole and phase) with winding factor $K_w = \cos(10^\circ)$. The independent air-gap MMF created by these two cases is presented as calculation in the Fig. A6.5.4.

In Table 2, the calculated values for $\cos \varphi_s$, according to (8), necessary to calculate the space harmonics winding factors using (10), are presented. If $\alpha = 0$ (case 2 and 5 in Table 1), K_{wdeq} is given by (12). This fundamental equivalent winding factor defines the amplitude of the resultant rotating field in the air gap of the motor.

$$K_{wseq} = \left| \sqrt{3}N'_Y K_{wYs} + N'_D K_{wDs} \right| \quad (12)$$

If full D is the rated connection, the ratio between the magnetizing flux for each possible connection and that of rated connection, is given by the ratio of full delta fundamental winding factor to the equivalent fundamental winding factor in each connection, according to (13). It is obvious that the field coefficient k_ϕ is in the range $[1 \ 1/\sqrt{3}]$.

⁵³ Integer number of slots per pole and phase, q .

$$k_\phi = \frac{\phi_{mag}}{\phi_{magD}} = \frac{K_{w1D}}{K_{w1eq}} \quad (13)$$

TABLE 2
CALCULATED VALUES FOR $\cos\phi_s$ AS A FUNCTION OF α AND S .

$\alpha \backslash S$	1	5	7	11	13	17	19
$-\frac{\pi}{6}$	$\frac{\sqrt{3}}{2}$	0	$\frac{\sqrt{3}}{2}$	0	$\frac{\sqrt{3}}{2}$	0	$\frac{\sqrt{3}}{2}$
0	1	$-\frac{1}{2}$	-1	$\frac{1}{2}$	1	$-\frac{1}{2}$	-1
$\frac{\pi}{3}$	$\frac{1}{2}$	-1	$-\frac{1}{2}$	1	$\frac{1}{2}$	-1	$-\frac{1}{2}$

Considering only fundamental waves, the expected approximate values for the magnetizing flux, iron losses and derated output power for the nominal efficiency level, are presented in Table 3. It should be emphasized that the derated output power steps are quite balanced among all connection modes.

TABLE 3
THEORETICAL AIR-GAP FLUX DENSITIES FOR THE POSSIBLE CONNECTIONS ($\alpha=0$) OF THE WINDING PRESENTED IN FIG. 3.

Case	Winding Connection	Symbol	ϕ_{mag} (p.u.)	P_{fe} & P_{out}^* (p.u.)	ΔP_{out}
1	X-B, Y-C, Z-A	D	1	1	--
3	X-M _B , Y-M _C , Z-M _A	Dy-II	0.8976	0.8057	-19.4%
2	X-M _C , Y-M _A , Z-M _B	Dy-I	0.7778	0.6050	-24.9%
4	X-N _C , Y-N _A , Z-N _B	Yd-I	0.7187	0.5165	-14.6%
5	X-Y-Z	Yd-II	0.6527	0.4260	-17.5%
6	X-N _B , Y-N _C , Z-N _A	Y	0.5774	0.3333	-21.8%

* Approximate derated output power for the nominal efficiency level, approximately proportional to the square of the magnetizing flux.

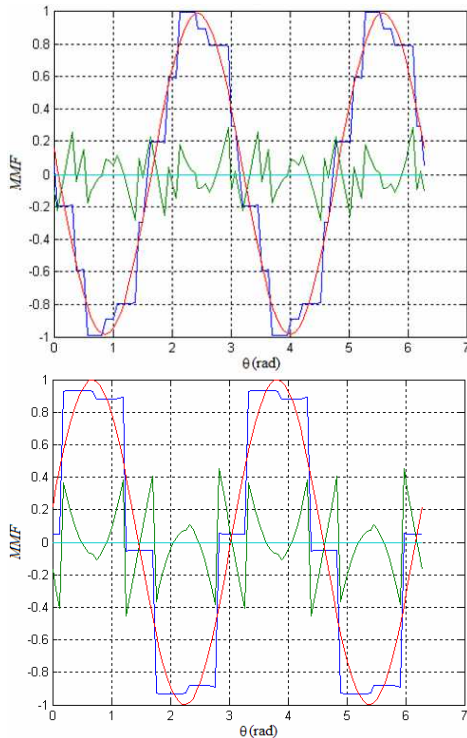


Fig. 4. Calculated independent air-gap MMF created by the two considered winding parts: (top) $q = 2$ ($K_{w1} = 0.9848$); (bottom) $q = 1$ (right, $K_{w1} = 1$). MMFs (fundamental, resultant, differential) are calibrated in the phase reference system.

For example, a 10 kW IM, would operate at nominal efficiency providing 10 kW, 8 kW, 6 kW, 5 kW, 4 kW and 3 kW, if the D, Dy-II, Dy-I, Yd-I, Yd-II and Y connection modes, respectively.

Experimental Results – In order to carry out experimental tests, the winding diagram in Fig. 3 was implemented in a 4-kW, 4-pole, 112-frame IM incorporating two test-coils, one on a polar pitch and other on a tooth pitch in order to have an experimental value for the EMF. No-load tests were performed in order to measure the no-load current and losses, as well as to segregate the no-load stator Joule, iron/core and mechanical losses. The motor worked properly (with the same rotation direction) in all the possible connections allowed for the winding arrangement (with the same rotation direction).

In Table 4 the experimental and calculated results are compared. The calculated fundamental field coefficient, k_ϕ , should be compared with the per-unit (p.u.) values of the experimental induced voltage, U_{ind} , in the 10-turns polar pitch test coil, measured using a true-RMS voltmeter. The iron losses, P_{fe} , and the linear value of the no-load current, $I_{nl(linear)}$ (obtained by extending the linear portion of the no-load current dependence versus line voltage up to the rated line voltage). A fair agreement between the calculated and measured values was obtained.

Additional simulations and experiments are being performed, and will be published and interpreted in detail. In the future, experimental steady-state efficiency-load, current-load, and torque-speed curves will be carried out, in order to evaluate the energy savings potential of such motor if a special connection management equipment is provided. Load stator Joule losses and thermal issues will be also evaluated in the future.

TABLE 4
COMPARISON BETWEEN THE CALCULATED AND MEASURED VALUES FOR THE MOTOR UNDER TEST.

Winding Connection	Calculated Values			Measured Values			
	K_{w1eq}	k_ϕ	$(k_\phi)^2$	$\frac{U_{ind}}{U_{rated}}$ (V)	I_{nl} (p.u.)	$I_{nl(linear)}$ (p.u.)	P_{fe} (p.u.)
D	0.9598	1	1	14.5	1	1	1
Dy-II	1.0693	0.8976	0.8057	13.0	0.8965	0.797	0.863
Dy-I	1.2339	0.7778	0.6050	11.5	0.7931	0.637	0.608
Yd-I	1.3354	0.7187	0.5165	10.1	0.6965	0.542	0.529
Yd-II	1.4705	0.6527	0.4260	9.4	0.6483	0.437	0.417
Y	1.6624	0.5773	0.3333	8.4	0.5793	0.322	0.333

Conclusion on the Presented Results – The proposed combined star-delta three-phase winding can be used in a motor with a specially designed stator winding, allowing multi-step air-gap flux regulation. It can be applied in some 2-pole IMs driving hard-starting and/or high-inertia systems, in order to allow magnetizing flux regulation and starting current limitation, as well as for saving energy in variable-load IMs and for synchronous generator in order to adjust the terminal voltage. Additional information on this topic can be found in [128].

B. Experimental Core Losses For the MFLIM_E

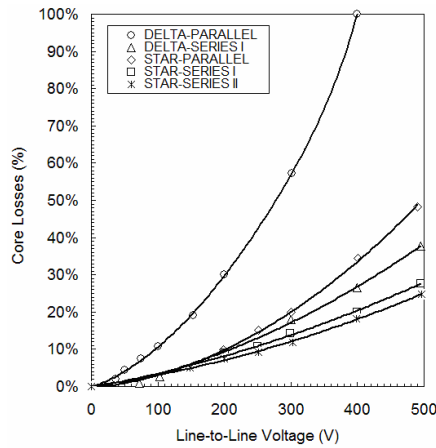


Fig. 5. Experimental core losses as a function of the line-to-line voltage for the multi-connection IM presented in Chapter 5 (MFLIM_E).

C. Combined VSD and Connection-Mode Change Use

In this section, some academical considerations are presented, being only discussed in a preliminary basis.

Another potential advantageous approach is the fusion of the presented multi-connection concept with the control provided by two-level VSIs using SPWM, helping to maintain the m_a as close as possible to 0.8-1.0 range. As referred in Chapter 3, for such devices, in the linear modulation ($m_a \leq 1$), large amplitude sideband harmonics centered around the frequencies of harmonics associated with switching frequency and its multiples are the most significant, and, although without significant impact on motor torque, are responsible for most harmonic core losses.

Overmodulation ($m_a > 1$) can be used, appearing more sideband harmonics centered around the frequencies of harmonics m_f and its multiples, but with relatively low amplitude, and, thus the associated with harmonic core losses are lower than for linear modulation and lower inverter switching losses are expected. However, the low-order harmonics (5th, 7th, 11th, 13th, etc.) start to increase, which are responsible for torque pulsations, torque-speed curve degradation, slip increase and additional losses, particularly those resulting from the negative sequence harmonics (5th, 11th, etc.).

Moreover, in the typical inverters, the fundamental amplitude can only be increased (theoretically) up to 1.2745 times (beginning of square-wave operation, $m_a > 3.2-3.5$, in which the low-order harmonics are higher than for overmodulation) in relation to $m_a = 1$ [59]. For the 400 V grid connected inverters, the DC-bus voltage is 540 V (however, average values up to 566-585 V can be found, depending on the actual grid line-to-line voltage, DC-bus capacitance, and inverter actual load). For a $m_a \approx 1.0$, at 50 Hz, the expected line-to-line fundamental voltage of the motor is 331-358 V, and for a 400 V fundamental voltage, a $m_a \approx 1.3-1.4$ (overmodulation) is needed, creating significant low-order harmonics, inevitably. One way to solve this problem is designing the reference winding to that value. The flux regulation can also be used when significant voltage fluctuations (particularly for long voltage dips) are expected either for line- or inverter-fed motors.

It should be referred that, in general, Y-type connections also contribute to a better phase voltage and current waveform.

On the other hand, due to the need of flux regulation to maximize the efficiency, either as a function of frequency and/or load, the proposed magnetizing flux regulation concept is suitable to improve the quality of the inverter output voltage waveforms at low or high than rated speed, due to the possibility to approximate the m_a to the unity, which leads to a low voltage THD, as shown in Fig. 6, improving the motor system performance, either considering synchronous (constant m_f , encouraged for $m_f \leq 21$, providing it is multiple of 3 and odd integer [59]) or asynchronous (constant switching frequency, encouraged for $m_f > 21$ [59]). The asynchronous PWM is a typical strategy in general-purpose inverters.

In fact, as discussed in Chapter 3, for low switching frequencies (say equal or lower than 2 kHz) a significant increase on the motor core losses (either harmonic eddy loss and harmonic minor-loop hysteresis loss components) can occur with the decrease of m_a below unit (for a 50-Hz, 400-V, 7.5-kW motor, the increase of m_a from 0.50 to 0.86 can lead to a decrease of more than 30% in the core losses [108]). The motor additional losses increase depends on the fundamental voltage and frequency, motor load, m_f and m_a , as explained in Chapter 3.

In Fig. 7, middle graph, the expected m_a using several connections can be seen, which become considerably higher than the single-connection operating mode, for speeds (or frequencies) lower than nominal.

To demonstrate the described effects, a multi-connection 7.5-kW motor (MFLIM_E) was fed by a two-level inverter, and a no-load test was performed for a fundamental frequency of 50 Hz and a carrier frequency of 2 kHz (fixed). The external fan was removed to ensure minimum slip (the obtained slip was very near to zero), and thermal equilibrium was guaranteed. The experimental results are shown in Fig. 8. It was verified that the no-load harmonic losses decrease with the increase of m_a . However, for a m_a higher than 1.0 (overmodulation), although the verified lower harmonic no-load losses, the fundamental load losses will be higher at load conditions, as previously referred.

Additional experimental results were carried out in a 4-pole, 3-kW IM, for Y and D connections, at 100% and 83% of rated magnetizing flux ($m_a \approx 1.3$ and 0.6 for 100% flux and $m_a \approx 0.9$ and 0.5 for 83% flux), and an 86% and 67% decrease in the harmonic no-load losses occurred, respectively, after increasing the m_a and, simultaneously, changing the connection from D to Y.

Nevertheless, it is clear that simple solutions to minimize inverter output harmonics can be used, such as filters and increased switching frequency, although introducing extra losses and extra EMI, respectively.

If the two-speed multi-flux motor concept is adopted, say a 2/4-pole motor, the operation can be divided in two main zones - high-torque, poor-efficiency zone and low-torque, improved-efficiency zone. In the low-torque zone, the 2-pole mode, combined with proper flux level, should be used with frequencies up to 50 Hz (plus slip compensation). The 4-pole mode, combined with proper flux level, should be used with frequencies up to 100 Hz.

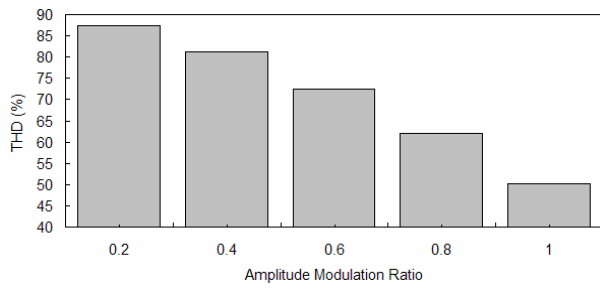


Fig. 6. Theoretical total harmonic distortion (THD, according to IEC standards), as a function of m_a , for a 3-phase voltage source inverter with PWM output voltage, assuming $m_f > 9$, odd and multiple of 3, and considering only harmonics with significant amplitudes up to $4m_f \pm 1$ [59].

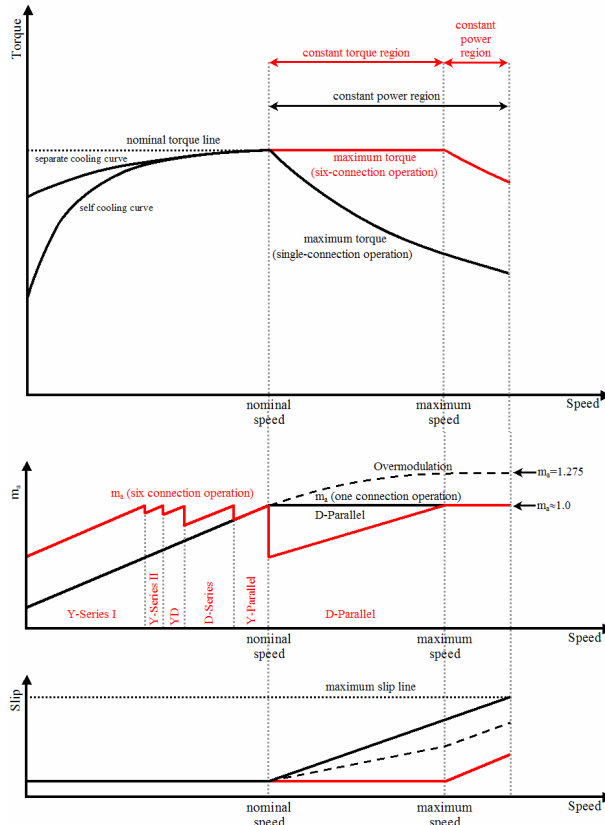


Fig. 7. Motor torque capability curves for constant operation without exceeding the thermal limit (top) and the corresponding amplitude modulation ratio (middle) and slip (bottom), assuming a typical constant U/f control, with a boost for zero speed, and considering two different approaches: single connection (DP) and multiple connections (YP as reference).

Due to the minimization of fundamental frequency and the possibility of using a m_a with a value in the range 0.8-1.0, the 2-pole mode is better in terms of efficiency, and the 4-pole mode is better for high torque demand periods. In the latter case, the efficiency, although lower, can be maximized using proper flux regulation. Again, the inverter has to be properly oversized to withstand the additional current.

The discussed concepts can be hypothetically used in IM-driven electric vehicles (variable-load, variable-speed application), in which the user selects the most appropriate connection according to the power or torque demand, and the reference connection is designed for the most used frequency and torque.

For example, if the vehicle is running at steady state in a horizontal road at medium speed, a low flux connection can be selected. But, if the vehicle is fully loaded, and has to run at higher speeds in a road with positive slope, a boost connection can be selected. In Fig. 7, the load/current limits for the different winding types should be taken into account.

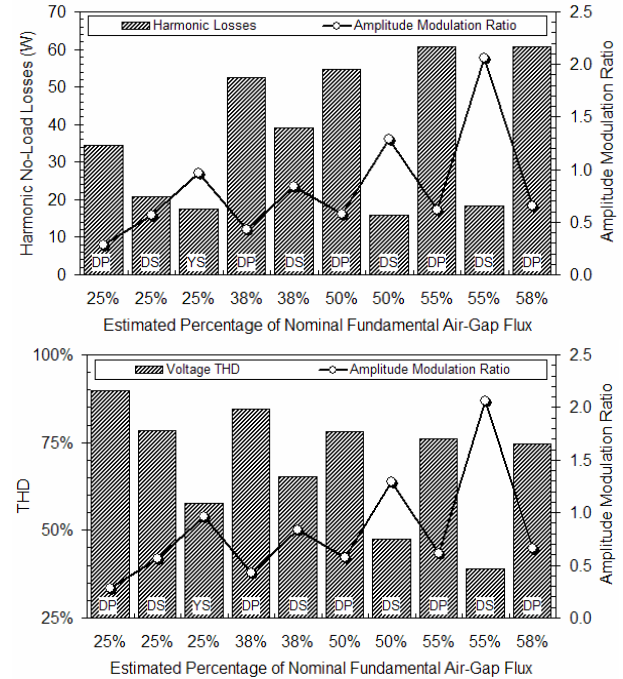


Fig. 8. No-load harmonic losses, line-to-line voltage total harmonic distortion (THD, according to IEC standard), and amplitude modulation ratio for the MFLIM_E (7.5-kW multi-connection motor), without external fan (to minimize the slip), for different fundamental air-gap flux levels (estimated on the basis of fundamental voltage) and connections (DP, DS and YS1). The motor was fed by a two-level VSI-PWM-based VSD, with fixed $f_s = 2$ kHz and $f_i = 50$ Hz.

Furthermore, a boost connection can be useful to transient high peak load or torque demands, as it was already referred, increasing torque capability over the field-weakening operation zone (for speeds or frequencies higher than nominal), as it can be seen in the Fig. 2, in which the efficiency of the motor decreases due to the higher slip. In fact, in situations requiring a fundamental frequency higher than nominal frequency, it can be useful to connect the motor in DP connection in order to guarantee that constant magnetizing flux is generated to maintain available torque. Otherwise, the inverter, due to voltage limitations, cannot increase the voltage at the motor terminals for higher frequencies leading to the typical constant power torque-speed capability curve. This concept also applies when considering only Y/D (or DS/YP) connection management, provided that the low-flux connection Y (or DS) is the nominal connection. Of course, this is only possible if the inverter is properly oversized to withstand the additional current.

Moreover, if a voltage decrease in the DC-bus of the inverter occurs, the flux boosting could also be used for compensation, instead of using a boost DC-DC converter. This can be useful in the scope of ride-through capability during low voltage sags.

In the case of permanent magnet synchronous motors, the voltage regulation in the stator winding can be used to

boost the voltage in generating and braking operations, particularly for low speeds.

Another advantage associated to the use of the low flux winding connections, when convenient, is the reduction of the inter-turn insulation voltage stress, which can lead to the increase of the motor lifetime.

Lastly, the automatic pole change and/or flux regulation can also be used to reduce significantly the rotor losses during starting period.

D. Simple Strategy to Recovery Energy During Stopping Period in Large High-Inertia Line-Fed Induction Motor Driven Systems

In this section, some academical considerations are presented, being only discussed in a preliminary basis.

Nowadays, energy recovering during deceleration or braking periods is a well-explored technique in IMs fed by VSDs, incorporating special rectifier/inverter input stages, allowing energy to be injected back into the power grid. However, for line-fed IMs, during the stopping or deceleration period, after disconnecting the power supply, the energy stored in the system inertia is, in general, not recovered, due to obvious technical reasons, and can be significant in high-inertia rotary saws, sheet saws driven by high-inertia wheels, rock crushers and grinders with flywheels, centrifuges, presses with flywheel, just to name a few high-inertia applications (Fig. 9). The rotor inertia itself is also significant in large IMs, significantly contributing to the overall inertia of the system. There are also applications with a large number of start/stop cycles per minute, such as industrial heavy trains with reciprocating movement feeding large sheet saws with round logs of wood, allowing part of the kinetic energy to be recovered before using mechanical brakes in the proximity of the trail-end when the train is returning.

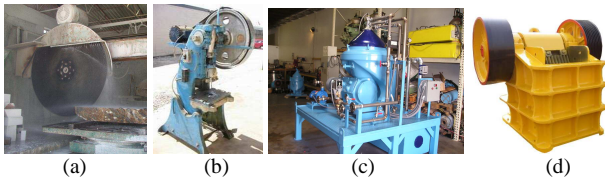


Fig. 9. Examples of high-inertia loads: (a) large marble rotary saws; (b) fly-wheel presses; (c) industrial centrifuges; (d) rock crushers.

In this paper, a novel principle to recovery energy during stopping period in line-fed multi-speed IMs is proposed based on the motor connection change from a lower pole-number mode(s) to a higher pole-number mode(s). The principle is described and a connection-management strategy is proposed, on the basis of preliminary simulations.

The automatic pole change and/or magnetizing flux regulation, is commonly used to reduce significantly the rotor losses during starting period. It is proposed now the application of the pole change principle, using a 2- or 3-speed IM, or even a pole-amplitude modulation (PAM) IM [6], [13], [23], as a way to recovery energy during motor stopping period. In fact, for a conventional line-fed IM operating at its nominal speed, there is no way to recovery energy during stopping period, unless a VSD with a regenerative module or bidirectional front-end, is used, which is a very expensive solution, only be justified

if very large amounts of energy can be recovered over all the stopping or decelerating period and variable speed and/or torque is also required by the process. Line-fed IMs can operate as generators if its speed exceeds the synchronous speed. Assuming that it is possible to increase the number of poles during stopping period, it is theoretically possible to force the motor to behave as a generator for a specific part of the stopping period (see Fig. 10), since the synchronous speed is reduced (e.g., changing from 2 poles to 4 poles reduces the synchronous speed to half). When a motor is operating near rated speed, it is typically stopped by simply disconnecting it from the mains power supply. However, if during the stopping period the motor is first reconnected to the power supply with a higher number of poles, the new synchronous speed is half of the initial value, and the rotor speed becomes about twice the synchronous speed, operating as a generator until the rotor speed becomes equal to the new synchronous speed. With the proposed approach, the stopping time is shortened and energy recovery is possible. This is proposed for the first time in this paper, but further research is needed regarding current behaviour and impacts on motor lifetime of such procedure.

For the sake of simplicity, in order to discuss the proposed principle, it is considered a common 2-speed IM (consequent-pole technique [43]), in which it is possible to change the pole number from 2 to 4 during the stopping process. Of course, to optimize the motor operation, the stator winding should be designed to maximize efficiency with the lower pole number, obviously reducing the generator-mode efficiency associated with the higher pole number operation, decreasing the energy recovering potential.

In order to illustrate that principle, a simulation was made for a 2-pole, 400-V, 50-Hz, 2980-r/min, 200-kW IM, whose equivalent circuit parameters were obtained experimentally, driving a high-inertia load with viscous friction (the viscous friction torque at steady-state equal to 213.7 N.m, corresponding to $\frac{1}{3}$ of nominal torque). The motor equivalent circuit parameters considered in the SIMULINK simulation model were obtained experimentally, and are $R_s = 5.5 \text{ m}\Omega$, $L_s = 0.13369 \text{ mH}$, $R_r = 4.8 \text{ m}\Omega$, $L_r = 0.57296 \text{ mH}$, and $L_m = 0.01019 \text{ H}$. The motor rotor plus load inertia is $J_{mtr} = 5 \cdot 2.1 = 10.5 \text{ kg}\cdot\text{m}^2$ (motor rotor inertia equal to $2.1 \text{ kg}\cdot\text{m}^2$) and the viscous friction component is $T_{load} = 0.6817 \cdot \omega$. During generation region, the motor is forced to operate with 4 poles in the model by simply changing the pole number, maintaining the same equivalent circuit parameters (actually, no major differences exist between the parameters for a 2-pole and for a 4-pole IM, except the rotor inertia). Two different simulations were carried out, considering the initial condition for speed 313.46 rad/s (or 2993.3 r/min, corresponding to a slip of -0.9955 for the 4-pole mode), which represents the speed that would be achieved if the motor were operating with 2 poles before entering in the stopping process. In the first simulation, it is assumed that the motor is connected to the grid since the beginning of the stopping process (without optimum control). In the second simulation, it is assumed that the motor is connected to the grid only during the regenerating period (with optimum control), i.e., real power flows from the

motor to the grid, which was previously identified as within the [277 157] rad/s speed range. The results are presented in Figs. 11 and 12, being possible to conclude that with optimum control of connection/disconnection of the motor from power supply during stopping period, it is possible to recovery more energy.

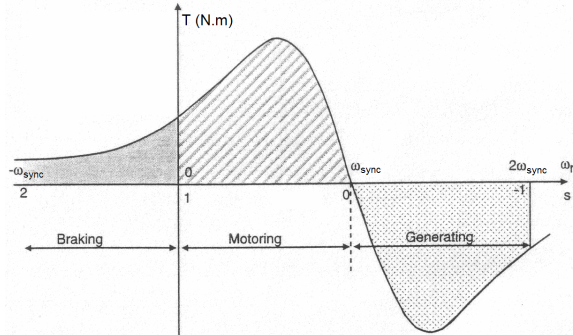


Fig. 10. Average torque vs. slip curves with constant voltage supply in an IM, evidencing the motoring, braking and generating operation regions.

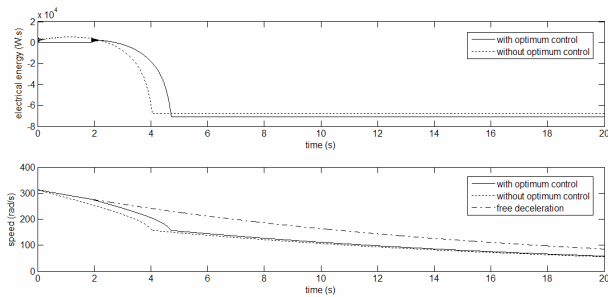


Fig. 11. Simulation of a 200-kW, 2/4-pole IM: electrical energy and speed considering energy recovering during stopping period.

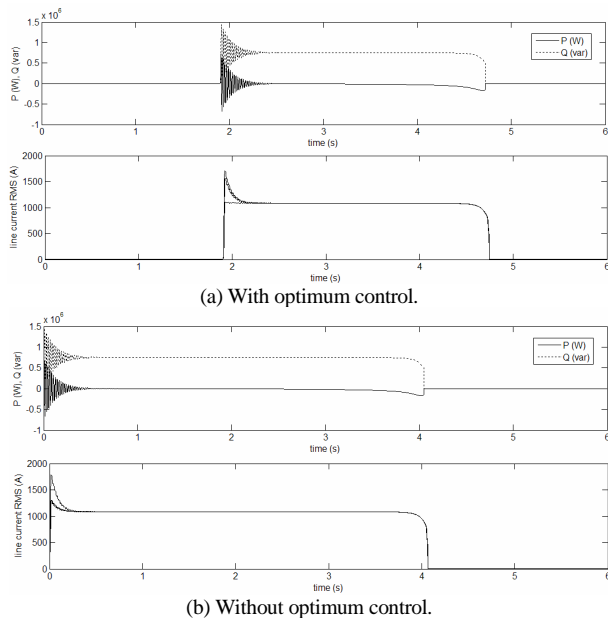


Fig. 12. Simulation of a 200-kW, 2/4-pole IM: real power, reactive power and line current RMS value considering energy recovering during stopping period.

The total kinetic energy stored is given by (14), and the energy regeneration/recovering potential (without considering the losses in the motor) is given by (15). The percentage kinetic energy regeneration/recovering

potential over the total kinetic energy available in the beginning of the stopping process is given by (16).

$$E_{kin} = \frac{1}{2} \cdot J \cdot \omega_0^2 \quad (14)$$

$$E_{rec} = \frac{1}{2} \cdot J \cdot (\omega_i^2 - \omega_f^2) \quad (15)$$

$$E_{rec\%} = (\omega_{i_rec}^2 - \omega_{f_rec}^2) \cdot \omega_0^{-2} \cdot 100\% \quad (16)$$

For the example given, considering an initial speed of $\omega_0 = 314.16 (1-0.002233) = 313.46$ rad/s (0.2233% slip, $\frac{1}{3}$ the rated slip), $\omega_i = 277$ rad/s and $\omega_f = 157$ rad/s, the energy recovering potential (without considering the energy losses associated with the system friction) is about 53% of the total kinetic energy stored in the system.

From the simulated results, which take into account the friction losses, an energy efficiency (mechanical to electrical energy conversion) of 41.4% and 32.1% and a recovered energy of 70.74 kJ and 67.81 kJ over the regenerating stopping, with and without optimum control, respectively, were obtained. Considering all the equivalent circuit parameters 4 times higher, the recovered energy is 46.42 kJ and 45.52 kJ, with and without optimum control, respectively, and a significant decrease occurs in the current RMS value during the energy recovering period, which is extended. Considering 15 stops per hour, 6000 h/year operating time, 0.1 €/kWh electricity price, and 70 kJ (or 0.0194 kWh) of recovered energy in each stop (with optimum control), yields 174.6 €/year of annual savings. In a system with more inertia, the savings potential increases proportionally. Other 2-speed motors can be also considered (e.g., 4/6 poles), or even 3-speed motors (e.g., 4/6/8 poles), in which the results can be even better from the energy recovery perspective. For motor with pole changing for smoother starting, the proper control (line power connection/disconnection as a function of the estimated motor speed using an electronic device [3]) during stopping process represents negligible cost for large machines, and the recovery energy can be significant, particularly if they are driving very high-inertia loads and frequent stops occur. Proper pole-switching system has to be studied (either using thyristors and/or contactors) in order to reduce the reconnection current and voltage transients. Additional information on this topic can be found in [126].

As far as the authors know, the proposed strategy for energy recovering during stopping period in line-fed, high-inertia, IM driven systems is novel, and can have a significant energy savings potential. Besides that, the inherent low cost makes it very attractive, justifying further research, particularly considering the motor adaptation during rewinding process or even the use of two-speed commercial motors. The control device and stator winding arrangement required for the application of the proposed principle can also be used to optimize the motor starting process and steady-state operation as a function of the motor actual load, increasing the associated cost-effectiveness.

At this stage, experimental tests are required to evaluate, for example, voltage and current transients during pole changing and motor line power reconnection, as well as the energy savings during

deceleration/stopping periods. Stator winding design optimization issues should also be analysed further in detail, regarding MMF waveforms and losses in both low- and high-speed modes.

Additional information on this topic can be found in [126].

A6.5.3 Section 5.4

A. Motor Energy Controller (MEC)

The Motor Energy Controller (MEC) with voltage regulation capability. A commercial unit picture and the basic topology and input and output voltages are shown in Fig. 1.

The MEC is a device designed to optimize efficiency and save energy in IMs during starting transient period and steady-state operation. It integrates a controller that combines soft-starting, power factor correction and energy saving capabilities. Additionally, it displays kW, kWh, power factor, current, voltage, and date/time counting (e.g., it has a counter for the working time in saving and bypass modes). The MEC enables dynamic/automatic optimization of line-to-line voltage to assure that the only required energy is delivered to the controlled motor, but it can also operate in manual mode. When it detects a load lower than 60%, the voltage decreases approximately 25%, otherwise it is maintained with the rated value, using a bypass contactor.

The voltage regulation is made by means of the combination of 3-phase voltage vectors and angles (VVC – Voltage Vector Combination). It provides two pure sine voltage levels according to motor load, therefore, no harmonics or EMI/RFI are produced. It also incorporates RS-232 and Modbus (SCADA) communication capability. According to the manufacturer, the efficiency is 99.5% in saving mode, and the input current THD is less than 1%.

The MEC starts the motor at reduced voltage to reduce start up current. Then, after 10 seconds, full voltage is supplied to the motor thereby ensuring the completion of the start up. If the motor load is below a set level, as configured by the user, reduced, sinusoidal voltage will be supplied to the motor. If the motor load increases above the set level, full voltage will be supplied to the motor.

In addition to direct energy savings, the MEC reduces start-up current to 1.8-2.2 times the nominal, reducing motor wearing and extending its life expectancy, and eliminates the need for installation of soft-starters and reduces the size power factor correction devices.

This device also allows connection of capacitors in parallel to the motor, standard short circuit current protection, and complies with EMC standards (no harmonics), even during start-up.

Transforming only the unnecessary voltage allows voltage control with pure sine, but with a power 7 times smaller than that for full power transformation. Different steps and voltage combinations allow different output voltage levels, depending on the application and product model. Therefore, the device weights approximately 7 times less than an equivalent autotransformer (e.g., the

weight for a 7.5, 75, and 150 kW device is 19, 70, and 153 kg, respectively).

According to the manufacturer, this patented technology is in use in more than 10000 installations world wide, since year 2000.

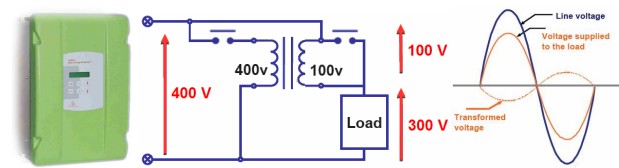


Fig. 1. Motor Energy Controller (MEC): (left) Commercial device unit; (right) Operation principle. Source: Power Electronics Systems Ltd., www.pe-sys.com [56].

The manufacturer claims that, on average, the real power can be reduced up to 18%, the apparent power and line current can be reduced up to 30-50%, the reactive power can be reduced up to 15-75%, the conduction losses in the power cables can be reduced up to 51-75%, the motor LCC can be significantly reduced and the motor lifetime extended (due to the lower losses and the consequent reduced operating temperature) [56].

This device is recommended for IMs operated at constant speed and variable load. Examples of applications are: process industry, food and beverage production, mining, quarries, conveyors, escalators, HVAC, fans, plastic moulding injection, pumps, compressors, grinders, crushers, chippers, mixers, etc.

B. Anti-Parallel Thyristor Electronic Voltage Regulator

Regarding electronic voltage regulators, in Fig. 2, the basic topology for a three-phase full-wave device with anti-parallel thyristors is shown. In Fig. 3, the voltage and current waveforms and characteristic curves considering a resistive load and a firing angle $\alpha = 90^\circ$ are shown.

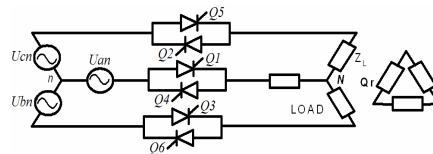


Fig. 2. Basic topology of an anti-parallel thyristor electronic voltage regulator [57].

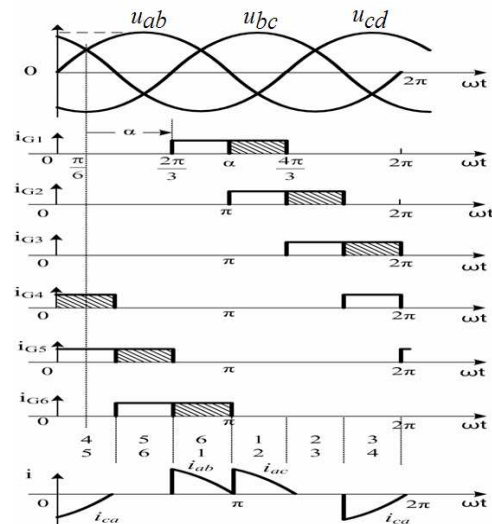


Fig. 3. Voltage and current waveforms for a firing angle $\alpha = 90^\circ$ [57].

In Fig. 4, the characteristic curve of the line current RMS value as a function of the firing angle α for different loads (defined by the respective fundamental displacement angle, ϕ , of the load) is shown.

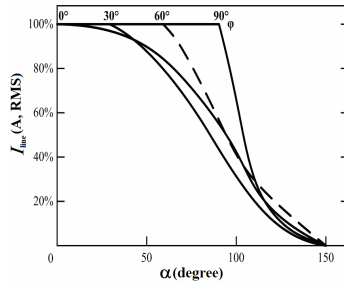


Fig. 4. Line current as a function of α for different types of loads [57].

C. Comparison between YY/D Connection Change and Electronic Voltage Regulator

According to [94], 80% of IMs are light loaded (load $\leq 70\%$) and delta connected. With YY/D connection change (here, YY symbol means Y parallel connection, which is the reference connection, and D symbol means D series connection), significant efficiency improvements are only possible at less than 40-50% load. The YY/D connection change as a function of the load (load point for connection change can be within 65% and 85%, but typically $\approx 75\%$).

For loads equal to or higher than 60%, thyristor-based voltage regulators (phase-cutting devices) have a negative impact on the system performance due the losses in thyristors, low power factor, high current distortion (THD_i up to 25% at no-load), ultimately leading to additional losses and accelerated ageing of transformers and motors.

In Table 1, an experimental comparison in terms of system loss reduction between an autotransformer (AR), an electronic voltage regulator (EVR), and YY/D connection change strategy is presented, for a 5.5-kW, 4-pole IM, in relation to the fixed YY connection case.

TABLE 1
SYSTEM LOSS REDUCTION
WHEN USING DIFFERENT VOLTAGE REGULATION STRATEGIES
IN RELATION TO FIXED YY CONNECTION IN A 5.5-kW, 4-POLE IM [94].

Load (%)	0	10	20	30	40	50	60	70	80	90	100
VR**	30.5	28.7	23.4	16.7	14.3	10.4	6.7	4.1	1.9	0.6	0
EVR	20.5	18.7	13.4	6.7	4.3	0.4	-1.3	-2.1	-3.1	-3.4	-2.1*
D Conn.	13.9	13.7	13.1	12.1	10.7	8.9	6.7	4.1	1.1	-2.3	-6.1

* Approximately zero in the case of using by-pass contactor.
** Losses in the autotransformer not taken into account.

D. Torque-Speed Curves for Delta and Star Connection

In Fig. 5, the starting problems that, in some cases, can occur when the star connection is used (assuming delta as rated connection) are evidenced – the reduction of the accelerating torque leads to a longer starting period.

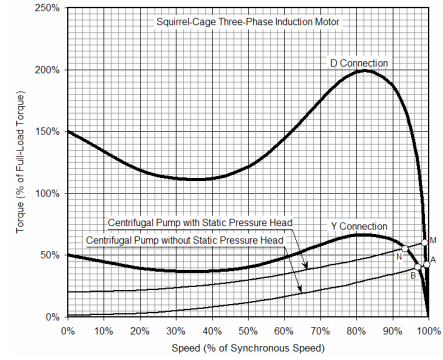


Fig. 5. Torque-speed curves of an IM for start and delta connection, and the corresponding operating points for a centrifugal pump with and without pressure head.

A6.6 Complement to Appendix 3

A6.6.1 Section A3.2

A. Method for Minimization of Space Harmonics in Double-Layer Concentric Windings

The main reference for the proposed method is [7]. The proposed method is applicable to some regular windings where the concentric groups of coils from adjacent poles have the magnetic axis at 180° (electrical). Windings with a q (slot/pole/phase) equal to an integer and equal to an integer plus 0.5 (e.g., $q = 1.5, 2.5$, etc.) fulfil this condition. The difference is that the integer windings have the two groups of coils under the adjacent poles with identical constitution as pitches, and in case of $q = k.5$ (fractional) the group under a pole has different number of coils and pitches compared to the group of coils under the adjacent pole. Fig. 1 shows the simplest case with one coil under a pole (N_1 turns) and another coil under the adjacent pole (N_2 turns), having 180° between the magnetic axes and connected together observing the rule *return-return*. If N_{1+2} is the total number of turns of two coils and N'_1 and N'_2 are the correspondingly p.u. number of turns per each coil, the resulting *MMF* created by the group of two coils is given by (1).

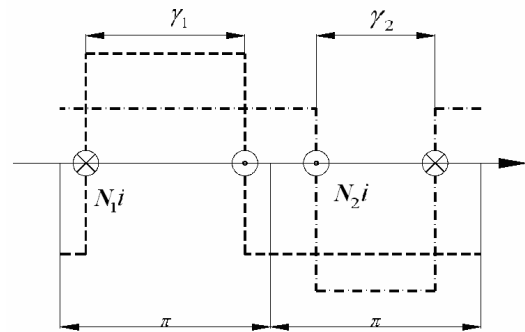


Fig. 1. Simplest case with one coil under a pole (N_1 turns) and another coil under the adjacent pole (N_2 turns), having the 180° between the magnetic axes and connected together observing the rule *return-return*.

$$MMF_{1+2}(\theta, t) = \frac{2i(t)N_{1+2}}{\pi} \sum_{s=1}^{\infty} \frac{1}{s} \left[N_1 \sin\left(\frac{s\gamma_1}{2}\right) - (-1)^s N_2 \sin\left(\frac{s\gamma_2}{2}\right) \right] \cos(s\theta) \quad (1)$$

Applying the superposition rule, if there are m concentric coils under the first pole with pitches γ_m (in degrees) and n concentric coils under the next pole with pitches γ_n (in degrees) the resulting *MMF* is given by (2).

The term within square brackets is the winding factor of the group of coils, K_{ws} . It is representing, as always in the concentric coils, where the $MMFs$ of all the coils are in phase (no distribution factor), the weighted average of the pitch factors of all the coils.

$$MMF_{total}(\theta, t) = \frac{2i(t)N_{total}}{\pi} \sum_{s=1}^{\infty} \frac{1}{s} \left[\sum_m N'_m \sin\left(\frac{sY_m}{2}\right) - (-1)^s \sum_n N'_n \sin\left(\frac{sY_n}{2}\right) \right] \cos(s\theta) \quad (2)$$

In integer windings the two groups of coils are identical, and, therefore, all the even space harmonics are null. If $q = k.5$, there will be even and odd space harmonics. In this case, taking into account that the triplen space harmonics will disappear in the resulting wave, it is necessary to impose only the cancellation of space harmonics or order 2, 4, 5, 7, 8, 10, 11, etc. Since double-layer concentric windings are being considered, there are exactly $2k + 1$ coils in the two groups and the unknowns N'_i , as in (3). The bottom equation in (3), sum of the turns, is needed for calibration of the total number of turns in order to fulfil the per-phase magnetizing flux condition.

$$\begin{cases} \sum_i N'_i \sin\left(\frac{sY_i}{2}\right) = (-1)^s \sum_j N'_j \sin\left(\frac{sY_j}{2}\right), & s = 2, 4, 5, \dots \\ \sum_{i=1}^{2k+1} N'_i = \sum_i N'_i + \sum_j N'_j = 1 \end{cases} \quad (3)$$

The system defined in (3) may be solved for each particular case. It is interesting to note that it has an analytical solution in simple trigonometrically functions, yielding the number of turns per coil, in order of increasing the coil pitch, given by (4), where $t = 1, 2, 3, \dots, 2k + 1$ [7].

$$N'_t = 4 \cdot \sin\left(\frac{\pi}{6}\right) \cdot \sin\left(\frac{(2t-1)\pi}{6}\right) \quad (4)$$

It can be verified that the solution lead to cancelling of all space harmonics excepting the $3k$ order and $Zp \pm 1$ (slotting space harmonics). Using the solution (4) the fundamental winding factor, K_{w1} , is given by (5).

$$K_{w1} = (2k + 1) \cdot \sqrt{3} \cdot \sin\left(\frac{\pi}{6}\right) \quad (5)$$

In order to verify the proposed strategy, some examples are analyzed. First, it is considered a fractional winding with $k = 1$ (9 slots, 2 poles, $q = 1.5$), whose diagram is represented in Fig. 2. Applying (3) yields (6).

$$\begin{cases} N'_2 \sin\left(\frac{s \cdot 2\pi}{2}\right) - (-1)^s \left[N'_1 \sin\left(\frac{s \cdot 4\pi}{2}\right) + N'_3 \sin\left(\frac{s \cdot 8\pi}{2}\right) \right] = 0, & s = 2, 4, 5, \dots \\ N'_2 + N'_1 + N'_3 = 1 \end{cases} \quad (6)$$

Using the (4), the result is: $N'_2 = 0.3473$; $N'_3 = 0.5321$; $N'_1 = 0.1206$. In order to verify that, for example, the 2nd order spatial harmonic is minimized, i.e.,

$$\begin{aligned} 0.3473 \cdot \sin\left(\frac{2 \cdot 2\pi}{2}\right) - 0.1206 \cdot \sin\left(\frac{2 \cdot 4\pi}{2}\right) - 0.5321 \cdot \sin\left(\frac{2 \cdot 8\pi}{2}\right) &= 0 \Leftrightarrow \\ \Leftrightarrow 0.3008 - 0.1188 - 0.1820 &= 0 \end{aligned}$$

The same can be done for the other harmonics.

Considering now another fractional winding with $k = 2$ (15 slots, 2 poles, $q = 2.5$), whose diagram is represented in Fig. 3, the result for the number of turns is: $N'_1 = 0.0437$; $N'_3 = 0.209$; $N'_5 = 0.3383$; $N'_4 = 0.2798$; $N'_2 = 0.1292$.

General results for $k = 1, 2, 3$, and 4 are summarized in Table 1.

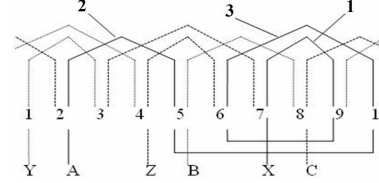


Fig. 2. Winding diagram for a 9-slot, 2-pole, double-layer concentric winding ($q = 1.5$).

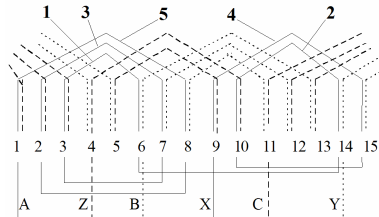


Fig. 3. Winding diagram for a 15-slot, 2-pole, double-layer concentric winding ($q = 2.5$).

TABLE 1
FUNDAMENTAL WINDING FACTOR AND NUMBER
OF TURNS FOR SINUSOIDAL FRACTIONAL WINDINGS, $q = k + 0.5$.

k	K_{w1}	N'_1	N'_2	N'_3	N'_4	N'_5	N'_6	N'_7	N'_8	N'_9
1	0.9023	0.1205	0.3473	0.5321	--	--	--	--	--	--
2	0.9052	0.0437	0.1292	0.2090	0.2798	0.3383	--	--	--	--
3	0.9061	0.0223	0.0665	0.1092	0.1495	0.1864	0.2191	0.2470	--	--
4	0.9064	0.0135	0.0404	0.0667	0.0921	0.1163	0.1389	0.1596	0.1782	0.1943

For the case of integer windings, it is now considered a 48-slot, 4-pole winding ($q = 4$), whose diagram is presented in Fig. 4. Since there is symmetry, (3) can be applied only to one group of coils and even harmonic are inherently zero, yielding

$$\begin{cases} N'_1 \cdot \sin\left(\frac{s \cdot \pi}{2}\right) + N'_2 \cdot \sin\left(\frac{s \cdot 5\pi}{12}\right) + N'_3 \cdot \sin\left(\frac{s \cdot \pi}{3}\right) + N'_4 \cdot \sin\left(\frac{s \cdot \pi}{4}\right) = \\ s = 5, 7, 11 \\ N'_1 + N'_2 + N'_3 + N'_4 = 0.5 \end{cases}$$

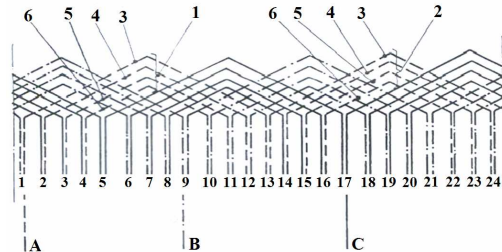


Fig. 4. Winding diagram of half of a 48-slot, 4-pole, double-layer concentric winding ($q = 4$).

The solution for the optimum number of turns is $N'_1 = 0.114$; $N'_2 = 0.1862$; $N'_3 = 0.1317$, $N'_4 = 0.0681$, and the winding factor is $K_{w1} = 0.9121$. The resulting MMF is shown in Fig. 5. The TSHD is 0.67%. Of course, the slot

filling factors are not constant, existing non-uniformity in using the space of the slots.

For a 36-slot, 4-pole winding ($q = 3$), whose diagram is shown in Fig. 6, since there is symmetry, (3) can be applied only to one group of coils and even harmonic are inherently zero, yielding

$$\begin{cases} N_1' \sin \frac{s \cdot \pi}{2} + N_2' \sin \frac{s \cdot 7\pi}{18} + N_3' \sin \frac{s \cdot 5\pi}{18} = 0, \\ s = 5, 7 \\ N_1' + N_2' + N_3' = 0.5 \end{cases}$$

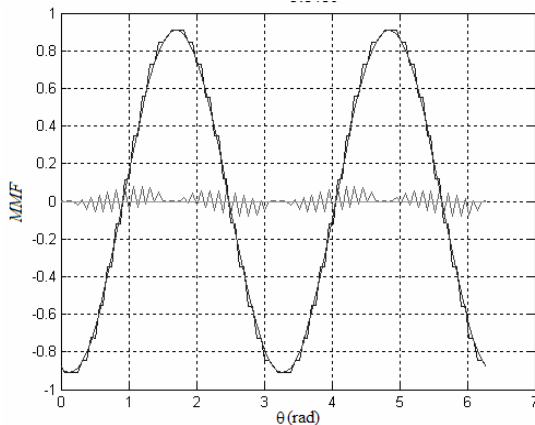


Fig. 5. Resulting MMF for a 48-slot, 4-pole, double-layer concentric winding.

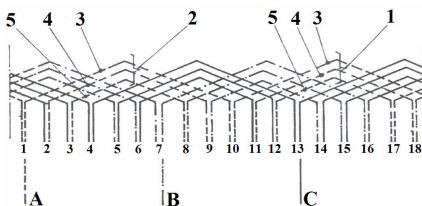


Fig. 6. Winding diagram for a 18-slot, 2-pole, double-layer concentric winding ($q = 3$).

The solution for the optimum number of turns is $N_1' = 0.1527$; $N_2' = 0.2267$; $N_3' = 0.1206$. Fundamental winding factor is $K_{w1} = 0.9162$. The resulting MMF is presented in Fig. 7. The TSHD is 1%.

It can be concluded that the method is correct and simplifies the optimization of double-layer concentric windings.

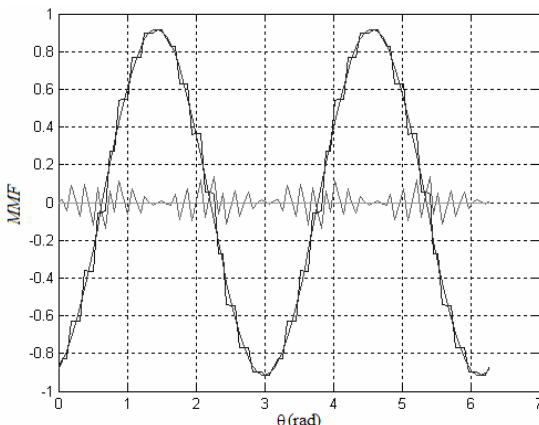


Fig. 7. Resulting MMF for a 36-slot, 4-pole, double-layer concentric winding.

B. BOBISOFT Software – Additional Figures and Application Examples

In the following figures, some additional panels of the software BOBISOFT are shown, as well as examples of stator winding redesigns carried out by some of the users.

Regarding the typical values for air-gap induction, air-gap thickness and conductor current density, used for the alert messages given by BOBISOFT, they were provided by a Portuguese induction motor manufacturer, and shortly presently next. For [1.1→160] kW power range, the air-gap induction varies within [0.8→0.5] T for EFF2-class, 2-pole IMs, within [1.0→0.72] T for EFF3-class, 4-pole IMs, and within [0.9→0.68] T for EFF2-class, 4-pole IMs; the air-gap thickness varies within [0.25→1.7] mm for EFF2-class, 2-pole IMs, within [0.25→0.9] mm for EFF3-class, 4-pole IMs, and within [0.28→1.0] mm for EFF2-class, 4-pole IMs; the current density varies within [9.0→3.5] A/mm² for EFF2-class, 2-pole IMs, within [1.0→5.5] A/mm² for EFF3-class, 4-pole IMs, and within [7.5→4.1] A/mm² for EFF2-class, 4-pole IMs.

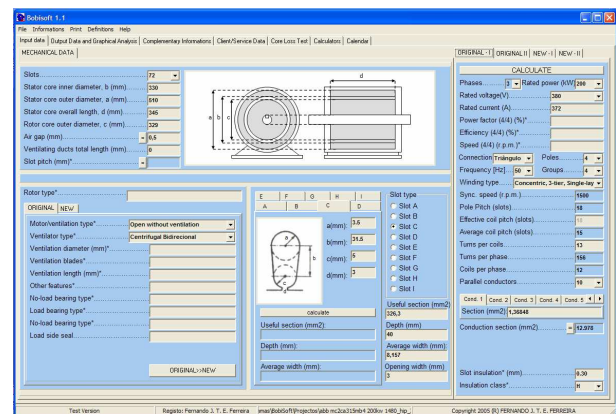


Fig. 8. Panel to insert electrical and mechanical data.

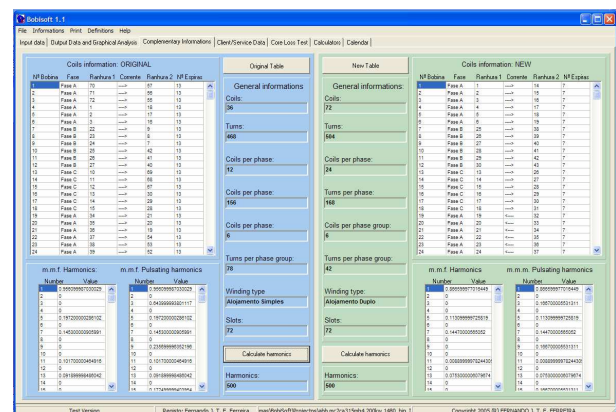


Fig. 9. Panel for numerical visualization of the spatial harmonics.

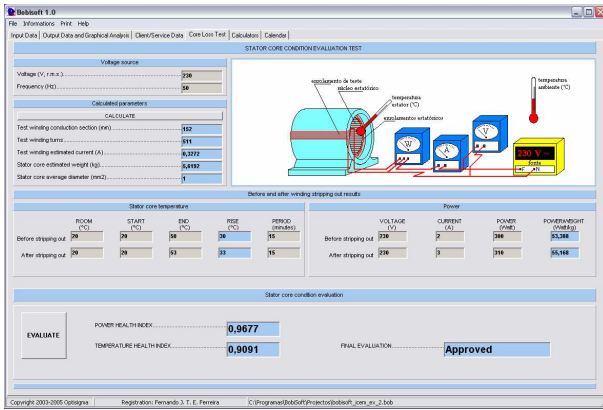


Fig. 10. Core loss evaluation test panel.

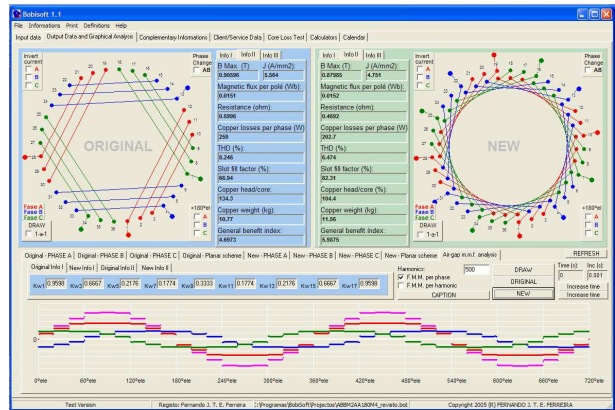


Fig. 13. Panel to visualize the main results (example 3).

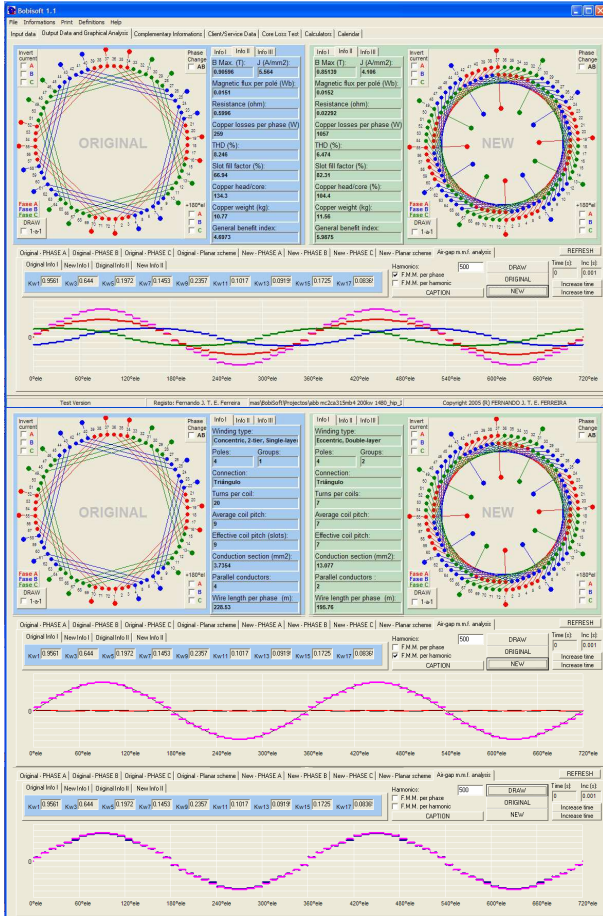


Fig. 11. Panel to visualize the main results (example 1).

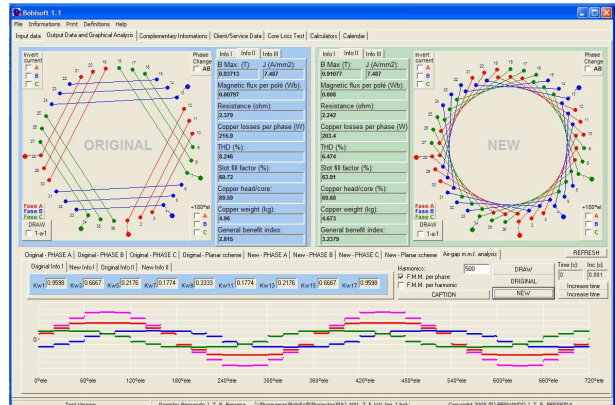


Fig. 14. Panel to visualize the main results (example 4).

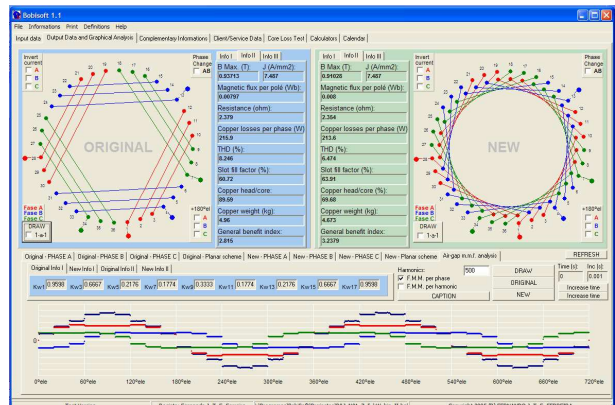


Fig. 15. Panel to visualize the main results (example 5).

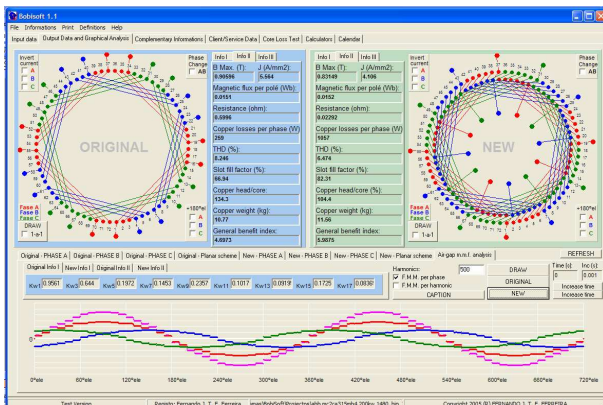


Fig. 12. Panel to visualize the main results (example 2).

C. Motor Condition Diagnosis

Regarding the motor condition diagnosis system proposed in Section A3.5, some complementary information is now presented.

The stator currents were measured on two phases with two current probes (voltage output proportional to the measured currents), being the third current computed using the other two. The radial vibrations were measured with a high-sensitivity, magnetic piezoelectric accelerometer, with a frequency range from 2 Hz to 10 kHz. The data was collected with a data acquisition card that is connected to a PCI slot of a personal computer. The acquired signals were properly filtered to remove undesirable high-frequency components, which can produce aliasing of the sampled signal. In order to correctly identify the proposed faulty conditions, a proper frequency resolution is required, being necessary a high-resolution spectrum (considered 0.1 Hz) and a frequency

range from 0 to 1 kHz. To obtain data with those characteristics, the data acquisition module was set to acquire 20000 samples at a sampling frequency rate of 2 kHz, resulting in a 10-second acquisition window for each signal. When the acquiring process is complete, the system saves all the acquired signals in a text file.

The implementation of the preprocessor was made using MATLAB. It converts the sampled signal to the frequency domain using an FFT algorithm. The spectrum generated by this transformation includes only the magnitude information about each frequency component. However, a main disadvantage of the classical spectral estimation is the impact of side-lobe leakage due to the inherent windowing of finite data sets (spectral leakage) [45]. To reduce these effects it was used a Hanning window [58]. At the end of the preprocessing phase a large number of frequency components, from 0 to 1 kHz (with a resolution of 0.1 Hz) were obtained.

The data selection process was made using MATLAB, because it is one of the few programs that can work with large sets of data. The preprocessing stage generates 10000 points of data for each case. This amount of data is too large to be processed by typical computers, therefore it is necessary to make a criteria selection of specific frequency components. In order to reduce the large amount of spectral information to usable levels, the frequencies that can be calculated by the equations indicated in [45]-[47] for the stator currents and the frequencies indicated in [44] for the vibrations signal were selected. These frequencies correspond to a number of condition states, as broken bars, bearing damage, dynamic eccentricity, etc. The frequency harmonics were selected to integrate this group of data, leading to a reduction from 10000 data points to around 100 data points, for each case. At the end of this stage four groups of frequencies (three, for the stator currents and one for the vibrations) were obtained. Data limits were properly converted to [-1 1] range, because it is a requirement for neural networks input [51]. Since there were not negative magnitude values, all the data is analysed to find the maximum value of the magnitudes of the frequencies of each example. Then, when the maximum value of each case is found, all the respective values are divided by the maximum value, resulting in a practical [0 1] data range. Normally the maximum value corresponds to the magnitude of the electrical fundamental frequency.

For the analysis of spectral patterns, ANNs may be used for classification. To perform classification, it is necessary to attach to each pattern a label that describes the operational state of the induction motor at the time of collecting the pattern. The ANN input vector is a pattern and the output is the class label [53].

In this case, a healthy condition according to data achieved through data acquisition card corresponds to "0" output. Consequently, the output "1" corresponds to an abnormal condition.

The ANN algorithm module was implemented using MATLAB. A Feed Forward Neural Network (FFNN) with one input layer, one hidden layer, and one output layer, is used for this purpose. Since four groups of data are being considered, four identical FFNN were created. The created FFNN have been trained to identify the presence or not of a specific type of fault in induction

motors. There is no theory or training algorithm to determine the exact number of neurons to solve a given problem. Currently, the design of network configurations is still a trial and error process [54].

For this system three layers were used, the magnitude of the characteristic frequencies are the inputs, the hidden layer has 20 neurons (obtained by iteratively to minimize simultaneously error and computing efforts) and 10 output neurons, corresponding each one to a different type of fault.

Since the outputs of the ANNs are between 0 and 1, then the output layer should use a sigmoid transfer function. The sigmoid function is the most popular activation function because it resembles the behaviour of biological neurons [54]. In this type of neural network, every neuron is connected to all neurons in adjacent layers with no lateral connections. During training, the information flows forward from the input layer to the output layer and the error is propagated backward through weights to calculate the weight adjustments. Training involves the modification of the weights until the error is reduced to an acceptable limit. The first layer receives the input, modifies it using the set of weights, and passes it to the hidden layers; each hidden layer in turn propagates the modified inputs to the layer above and, eventually, to the output layer where the overall error is calculated. The hidden layers are used to represent the nonlinear characteristics of the data [55].

There are several methods that can be used to adjust the weights in the FFNN. However, there is no way to tell beforehand which learning approach will work best for a given application. The learning approach that was used is based upon the back-propagation training algorithm Levenberg-Marquardt that has been shown to produce good results for this type of problems because it has a good training speed and can work with reduce memory systems [55]. In Fig. A3.39, ANN architecture is shown.

Experimental tests were carried out using four 0.75-kW, 220/380-V, 3.34/1.93-A, 50-Hz, 4-pole, delta-connected, three-phase squirrel-cage induction motors, with 22-bar rotors. The data was obtained under full-load condition. The mechanical load was provided by a magnetic power brake. One of the motors is normal (healthy condition), which is considered as reference for comparing with faulty motors. In the other three motors damages were inflicted: two motors with partially broken rotor bars, and one motor with rotor unbalance and eccentricity. Before inflicting damages on motors, all of them were previously tested to demonstrate their similitude (negligible differences were found). After the acquisition process, the acquired signals were properly processed. At the end of the entire processing phase the system returns the diagnosis for each case. For the sake of completeness, and to confirm the diagnostic of the system, the spectrums of one stator current and of the vibrations are presented in Figs. 16-24. The stator current spectrums for each case are shown in Figs. 16, 18, 20, and 22, respectively. Since the main characteristic frequencies appear in the range of 0 to 100 Hz, it was only plotted the spectrum to this specific range, instead of the all frequency range (0-1 kHz). With this scale, the presence of specific types of faults can be easily detected. Despite the fact that motor failure can be detected by mechanical

vibration spectrum analysis, the vibration is a second order effect compared to the current components, and in many cases the fault has to be severe enough to be detected by vibration analysis [44]. The vibration spectra for each case are shown in Fig. 17, 19, 21, and 23, respectively. Therefore, the vibration spectra obtained for the tested motor are difficult to understand in cases of absence or low severity (since the motor as a reduced power), and the vibration index is very low at the characteristic frequencies. So the only significant features for this type of cases are the frequency harmonics. The detection of this type of faults is a quite complex task for a common user, but the ANNs can easily manage it. For example, only in the case of the motor with two partially broken rotor bars, it is clearly visible the appearance of new frequency components that are not present on healthy states or low severity cases. In the case of the healthy motor there are some low magnitude frequency components that appear on the side lobes of the current spectrum caused by the load effects. The vibration spectrum only has frequency components relative to the harmonics. In Figs. 16 and 18, the current and vibration spectra are presented. In this case, no faults were reported, as expected.

In the case of the motor with two partial broken rotor bars there are two side lobes around the fundamental frequency. These frequency components associated with rotor broken bars can be determined by the expressions indicated in [45]-[47]. The vibration spectrum has the usual frequency components relative to the fundamental harmonics and some characteristic frequencies, like the frequency of the rotor. In Figs. A3.45 and A3.46, the corresponding spectra are shown. In this case, the system reported the presence of broken rotor bars fault, as expected.

For the case of the motor with rotor eccentricity there are two side lobes around the fundamental frequency. These frequency components can be determined by the corresponding air gap eccentricity expressions indicated in [45]-[47]. The vibration spectrum has only frequency components relative to harmonics. In Figs. 20 and 21, the spectra are presented. In this case, the system reported the presence of eccentricity, as expected.

In the case of the motor with unbalanced rotor there are multiple frequency sidebands around the fundamental frequency that correspond to the detection of dynamic eccentricity. These frequency components can be determined by the corresponding dynamic eccentricity expressions indicated in [45]-[47]. The vibration spectrum has only frequency components relative to harmonics. In Figs. 22 and 23, the spectra are presented. In this case, the system reported the presence of mechanical rotor unbalance and indicates possible presence of eccentricity.

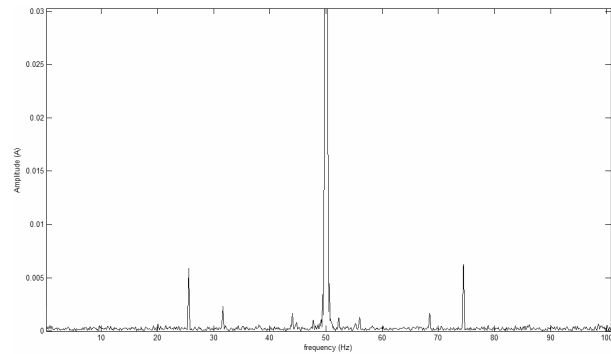


Fig. 16. Stator current spectrum of a healthy induction motor at full load.

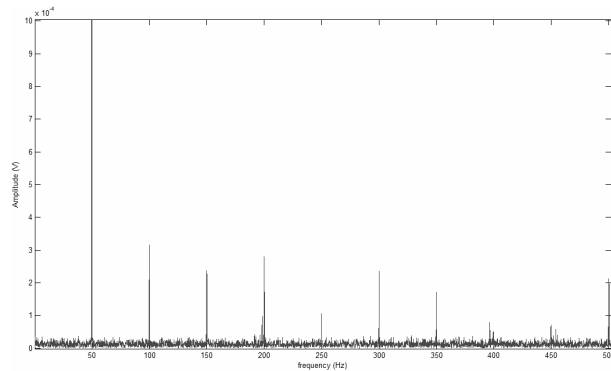


Fig. 17. Vibration spectrum of a healthy induction motor at full load.

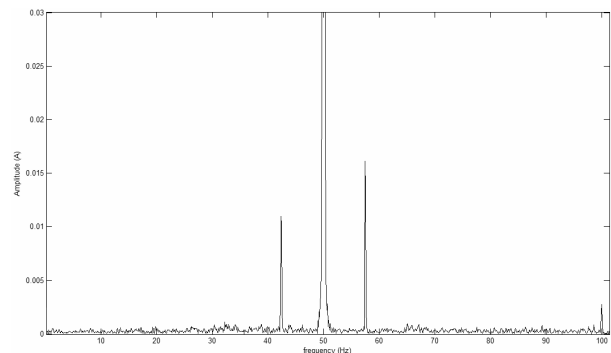


Fig. 18. Stator current spectrum of an IM with two partially rotor broken bars.

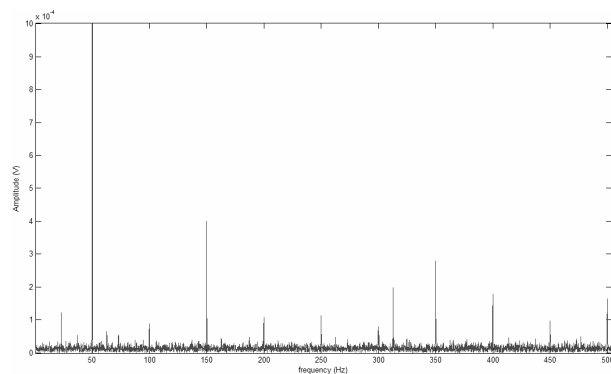


Fig. 19. Vibration spectrum of an IM with two partially broken rotor bars.

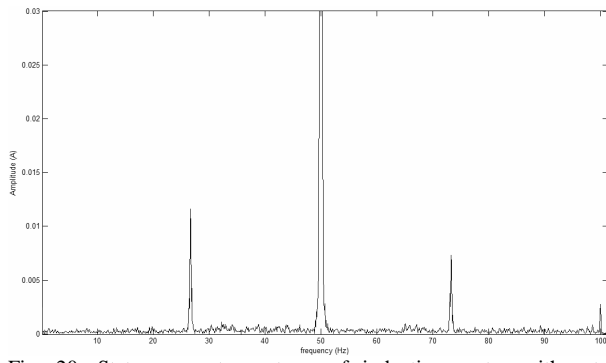


Fig. 20. Stator current spectrum of induction motor with rotor eccentricity.

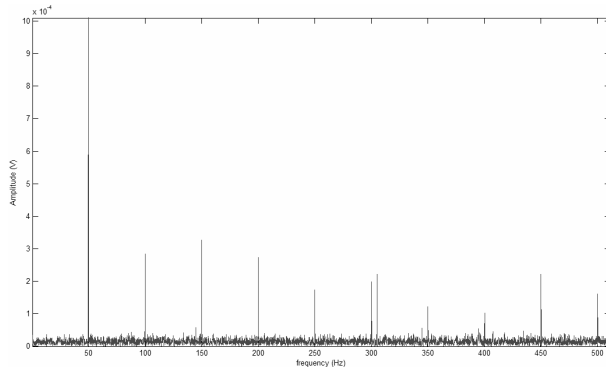


Fig. 21. Vibration spectrum of induction motor with rotor eccentricity.

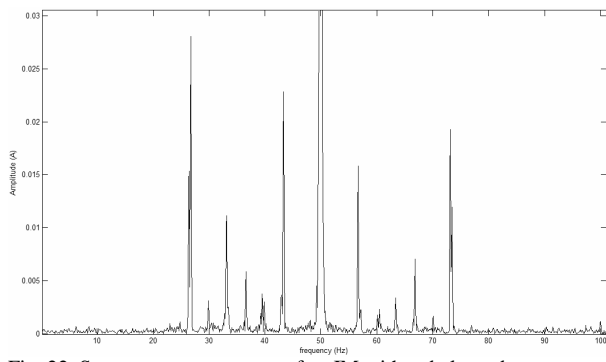


Fig. 22. Stator current spectrum of an IM with unbalanced rotor.

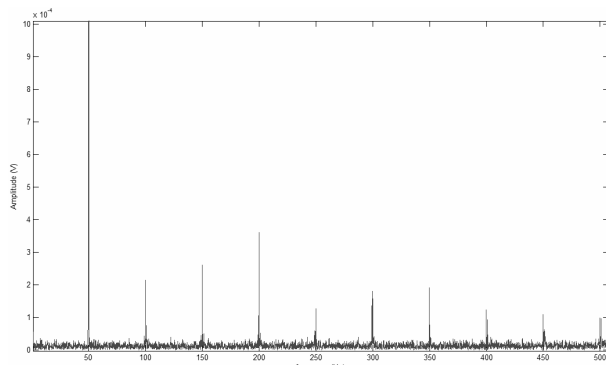


Fig. 23. Vibration spectrum of an IM with an unbalanced rotor.

D. Motor Bearings and Insulation System Condition Diagnosis by Means of Common-Mode Currents and Shaft-Ground Voltage Correlation

Nowadays, an increasing amount of IMs is fed by voltage-source inverters with pulse-width modulation. The mean time to failure (MTTF) of the IMs depends mainly on bearings and stator insulation system MTTF.

In fact, more than three-fourths of the total motor failures are due to bearing and/or stator winding failures. In inverter-fed IMs, bearing actually account for more than half of the motor failures. Unexpected motor failures, and the consequent downtime, can be critical in some industries, as those of continuous process, leading in most cases to huge production and profit losses. Therefore, the motor condition or health-state diagnosis is clearly an important issue in the industrial scope.

Low-frequency circulating bearing currents are widely reported and well understood for medium- and high-voltage line-fed motors, and they are mainly related with asymmetries of the electromagnetic system of the motor (e.g., due to eccentricities). However, due to their very low amplitude, this kind of currents is typically harmless for low-voltage, low-power line-fed motors.

Nevertheless, studies carried out in last decade confirm that, the low-voltage, inverter-fed IMs with rated power up to 90 kW (which represent the majority of the in-use IMs) are also affected by bearing currents activity, which is responsible for a significant decrease of the bearings lifetime. These high-frequency currents are different from the previous described, and include circulating and common-mode types. The common-mode currents are the most dangerous, particularly when they result from electric full- or partial-discharge between the inner and outer rings and the spheres of the bearings. These phenomena lead to the lubricant or grease electrochemical degradation and to the accelerated wear of the ring races and spheres (due to the microscopic groves and fluting that result from electric discharge machining) of the bearings. The common-mode capacitive and resistive/ohmic currents, although less dangerous, are more regular and contribute to the heating of the bearings, which leads to the decrease of the lubricant and seals lifetime. The common-mode bearing currents result mainly from the existing parasitic capacitances between stator-winding and stator, stator-winding and rotor, and rotor and stator, which are excited by the high du/dt of the PWM voltage waveforms produced by the voltage-source inverters.

The analytical and experimental analysis of the problem is well explored (see [109]-[111], [75]), and the study of the safe limits of voltage and frequency between inner and outer bearing rings and the effectiveness of local insulation-based mitigation techniques (e.g., insulation layers or films and ceramic spheres) is investigated in [112].

Common-mode leakage currents flowing from stator windings to motor frame or ground is also a phenomenon associated with both line-fed and inverter-fed motors, but it is accentuated critical in the last case due to the high-frequencies components present in the inverter output voltage waveforms. In general, the frequency and intensity of the leakage current peaks, as well as the respective spectral content, can be a good indicator of the insulation system integrity, since those factors are related with current components of capacitive and resistive/ohmic nature and with current peaks

resulting from partial discharge activity.

Since the sum of the instantaneous values of the three line currents flowing into the motor windings is equivalent to both common-mode leakage and bearing currents, it is possible to analyse the activity of such currents by monitoring the line instantaneous currents sum waveform. Moreover, the common-mode electric discharge currents occurring in the bearings (due to random electric contact between races and spheres or dielectric/lubricant film disruption) can be also identified by means of shaft-ground voltage monitoring, as it can be seen in Fig. 24. On the basis of Fig. 24, it is possible to identify the correlation between shaft-ground voltage and bearing currents resulting from electric discharge, which was actually evidenced in [112]. Therefore, the common-mode leakage current peaks associated with the bearing currents can be easily identified, and, therefore, the peaks associated with the stator-winding partial discharges or momentary shunts to ground can be separated. This principle allows separating both phenomena and provides information for separated insulation system and bearings condition diagnosis.

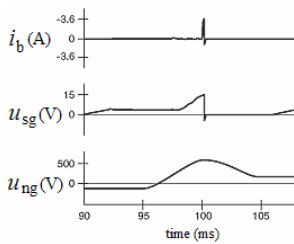


Fig. 24. Experimental bearing current (I_b), shaft-to-ground voltage (u_{sg}) and neutral-to-ground voltage (u_{ng}), relationship during a bearing electric discharge.

Of course the acquired and analysed quantities can also be used for diagnosing other motor anomalies. Since the number and magnitude of the electrical discharges in bearings and between the winding and the ground/frame are an indicator of the respective level of degradation, that sort of information can be used effectively to evaluate the condition of those motor parts. The continuous leakage current from winding to ground also allows evaluating the general state of the insulation system.

In this section, a novel motor condition diagnosis methodology is proposed with the focus on bearings and insulation system condition is proposed based on the correlation of the instantaneous input currents sum and on the shaft-ground voltage. It can potentially be also used to other kind of diagnosis, such as to detect significant electromagnetic asymmetries. A user-friendly system for acquiring and processing the data using artificial neural-networks is proposed, similar to that described in [113], but properly modified for the new diagnosis strategy. The proposed method should be intended as a complementary technique to other well-known methods for winding and rotor faults diagnosis using instantaneous line currents and mechanical vibration.

The structure of this system is divided into two main modules: the data acquisition module (hardware and

software) and the data analysis module (software). The latter includes four sub-models, namely, pre-processor, data selection, ANN algorithm and post-processor, as it can be seen in Fig. 25.

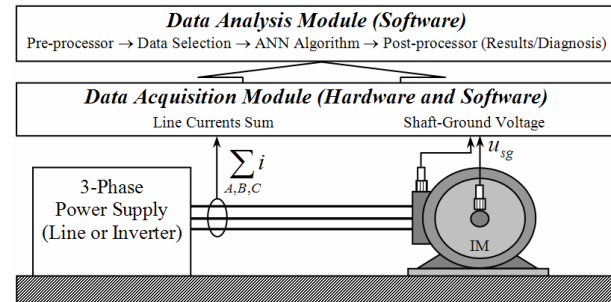


Fig. 25. Diagram of the proposed diagnosis system.

The data acquisition module acquires the motor total leakage/ground current (line currents sum) and the shaft-ground voltage, by means of interface software developed in LABVIEW, data acquisition card (NI 6040E PCI-MIO-16E-4) connected to a PCI slot of a computer, and some hardware probes. The line currents sum is simply measured using a Hall-effect clamp-on current probe embracing the three line conductors, therefore inherently giving the instantaneous currents sum. The shaft-ground instantaneous voltage is measured using a differential voltage probe with a special contact lead for the shaft potential acquisition, being the other lead trivially connected to the motor frame. The acquired signals were properly filtered to remove undesirable high-frequency components, which can produce aliasing of the sampled signal.

In order to correctly identify the proposed faulty conditions, a good frequency resolution is required, being necessary a high-resolution spectrum (considered 0.1 Hz) and a frequency range from 0 to 1 kHz. To obtain data with those characteristics, the data acquisition module was set to acquire 20000 samples at a frequency rate of 2 kHz, resulting in a 10-second acquisition window for each signal. When the acquiring process is complete, the system saves all the acquired signals in a text file.

The implementation of the pre-processor was made using MATLAB. It converts the sampled signal to the frequency domain using an FFT algorithm. The spectrum generated by this transformation includes only the magnitude information about each frequency component. At the end of the pre-processing phase a large number of frequency components, from 0 to 1 kHz (with a resolution of 0.1 Hz) were obtained. However, the most significant time-domain transients (high d/dt) of the currents sum waveform and of the shaft-ground voltage are also identified (by means of signal variation and peak amplitude), selected and recorded (with the respective time instant of occurrence), for further analysis and correlation.

The pre-processing stage generates 10000 points of data for each case. In order to reduce the large amount of spectral information to usable levels, specific well-known frequency-domain components and time-domain

transients for both currents sum and shaft-ground voltage were selected, corresponding to certain condition states or events related to the rotor speed, switching frequency (in the case of inverter-fed motors), voltage unbalances, stator winding unbalances, rotor-stator eccentricities, bearing damages, insulation system degradation, bearing electric-discharge currents, etc. The frequency harmonics were selected to integrate this group of data, leading to a reduction from 10000 points to around 100 points of data, for each case.

Experimental data is presented in Fig. 26, where it is possible to observe the correlation between common-mode current and the shaft-ground voltage⁵⁴, as well as the low-frequency component (50 Hz) in the shaft-ground voltage, associated with motor eccentricities or electromagnetic asymmetries. Basically, when a high time-derivative is simultaneously identified in the shaft-ground voltage and in the common-mode current, the probability of bearing electric discharge occurrence is high, particularly if the instantaneous shaft-ground voltage modulus is forced to a lower value close to zero. High current peaks without accentuated shaft-ground decrease are associated with stator winding to frame currents, which can be related to partial discharges.

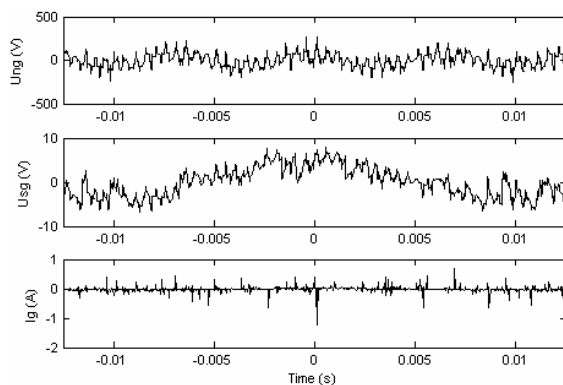


Fig. 26. Neutral-to-ground (U_{ng}), shaft-to-ground (U_{sg}) and common-mode leakage current (I_g) for 7.5-kW, 4-pole, 400-V, 50-Hz, star-connected winding IM, ≈ 400 -V fundamental voltage, 50-Hz fundamental frequency. Motor fed by a 3-level inverter-based VSD at 2-kHz switching frequency.

As far as the author knows, the proposed approach for motor diagnosis, in terms of electrical quantities used, is novel, being characterized by the simplicity and low cost of the acquisition system, since only one current probe and one voltage probe is used. Consequently, the processing task is also lighter in relation to conventional methods, since it requires less information.

Besides the main target of the proposed system, which is the insulation system (leakage currents and partial discharges) and bearings (damages and currents activity) health-state evaluation, it is also possible to diagnose voltage unbalances, stator winding unbalances, rotor-stator eccentricities, etc. By itself, the indirect bearing current activity detection and evaluation is very important to help user to decide whether or not they should, for example, install insulated bearings and/or

⁵⁴ In Fig. A5.24 (Appendix 5), the correlation between bearing current and shaft-ground voltage can be seen.

shaft-ground contact brushes. Correlating the results of the proposed strategy with those of the conventional diagnosis methods using vibration and individual line currents analysis, it is possible to improve significantly the motor condition evaluation methods effectively.

In the future, experimental tests will be carried out, in order to evaluate the effectiveness of the proposed system. Additional information on this topic can be found in [125]. The work presented should be intended as a kick-off, requiring further research.

E. Extra Pictures on Motor repair



Fig. 27. Windings burning-out process using a gas torch.

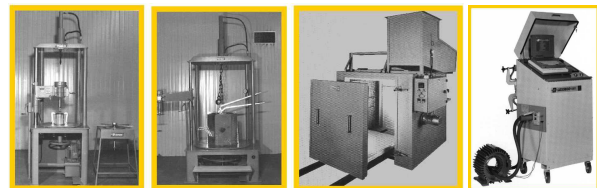


Fig. 28. Recommended winding stripping-out methods: (a) End-winding cutting machine (*Thumm* technique); (b) Winding pull-out machine (*Thumm* technique); (c) Oven to heat the windings. If burning-out process were performed with temperatures on average above 360°C the core losses will increase significantly. That limit depends on the type of core and the size of the motor. It is important to note that the temperature of the core is normally higher than the programmed in the oven.



Fig. 29. Bearing handling: (left) manual bearing extractor open; (centre) hydraulic extractor; (right) induction bearing heater.



Fig. 30. Impregnation: (left) vacuum pressure or VPI; (centre) manual trickle; (right) automatic trickle.

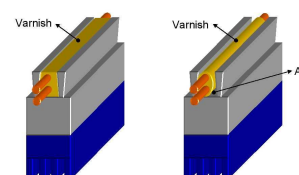


Fig. 31. Impregnation: (left) good quality; (right) poor quality.

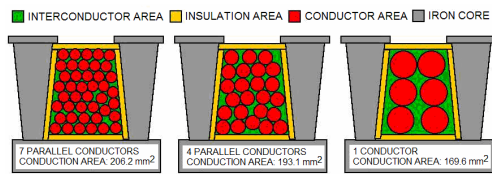


Fig. 32. Influence of conductors gauge on the slot-filling factor.

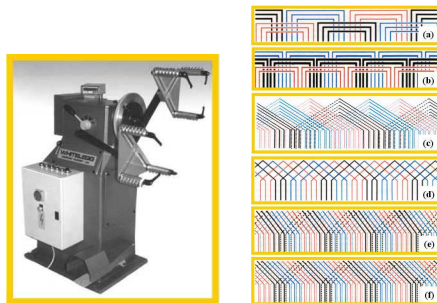


Fig. 33. (left) Semi-automatic coil winding machine; (right) Typical winding configurations: (a) two-tier, concentric winding; (b) three-tier, concentric winding; (c) double-layer, short-pitched, concentric winding (d) single-layer, lap winding (e) double-layer, short-pitched, lap winding; (f) double-layer, full-pitch, lap winding.

A6.7 Complement to Appendix 4

A6.7.1 Section A4.2

A. Additional Notes on PQ Causes and Effects

Voltage distortion means that voltage, and, consequently, the current waveforms assume non-sinusoidal shape. The distorted waveform corresponds to the sum of different sine waves with different magnitude and phase, having frequencies that are multiples of power-system frequency.

Classic sources of voltage distortion are electric machines working above the knee of the magnetization curve (magnetic saturation), arc furnaces, welding machines, rectifiers, and conventional DC brush machines. Modern sources of voltage distortion are all nonlinear electric loads, such as power electronics equipment including static power converters (AC-DC converters or rectifiers, and DC-AC converters or inverters), data processing equipment and high-efficiency lighting. Static power converters represent the main nonlinear loads used in Industry for a wide kind of applications, e.g., electrochemical sources, switched-mode power supplies, VSDs and UPSs [8]. In the vicinity of large single-phase loads (e.g., induction and arc furnaces), and in rural areas particularly on mixed industrial and domestic systems, supplies may be distorted beyond the recommended limits. Some of the main consequences are the increased probability of occurrence of resonance, neutral overload in three-phase systems, overheating of all cables and equipment, loss of efficiency in electric machines, electromagnetic interference with communication systems, errors in measuring devices, and nuisance tripping of thermal protections, just to refer a few.

The voltage notching of the AC voltage wave is caused by the commutating action of the rectifier. Traditionally, the current wave shape is used as the basis for harmonic analysis, and voltage notching is calculated from the voltage drops caused by the current harmonics.

The depth of the notch at points nearer to the power source is proportional to the system impedance up to that point. The width of the notch is the commutation angle [8].

Typically, AC line harmonics are generated by three-phase bridges. The characteristic harmonics produced by static power converters require balanced impedances in the AC system and equal firing of the thyristors in the converter. If the firing circuits do not operate symmetrically so that the commutation of each device is not correct, noncharacteristic harmonics are produced. These normally are small, but with a parallel resonance at one of them, they can be amplified to a value that could cause problems.

The harmonics produced by electric arc furnaces used for the production of steel are unpredictable because of the cycle-by-cycle variation of the arc, particularly when boring into new steel scrap. The arc current is aperiodic, with a continuous spectrum of harmonic frequencies of both integer and noninteger orders. However, harmonic measurements have shown that integer-order harmonic frequencies, particularly low-order starting with the second and ending with the seventh, predominate over the noninteger ones [8]. They have also shown that the amplitude decreases with order. As the pool of molten metal grows, the arc becomes more stable, resulting in much steadier currents with much less distortion and less harmonic activity. The current becomes symmetrical around the zero axis, thus eliminating the even harmonic orders and noninteger harmonics. It must be emphasized that other furnaces will exhibit somewhat different patterns of harmonic current, but the referred values may be useful in harmonic studies if more specific data for a particular furnace is not available [8]. In a typical arc furnace application in which unbalanced conditions prevail during unstable arc periods, some triplen harmonics will appear in the line currents.

Where phase currents are unbalanced, the individual phase harmonics will appear in the line currents as phasor sums of the phase harmonics in their own harmonic domain.

The emergence of renewable, alternate energy sources has resulted in the use of many varied topologies as power conditioners or inverters for utility tied operations. These inverters are available in single- and three-phase units, and their outputs may be very clean sinusoids with near unity power factor, or may contain various characteristic and noncharacteristic harmonics and power factors that may cause unacceptable PQ on the electric utility grid or interfere with its controls or relays. These inverters may act as current sources attached to the electric utility or as voltage sources tied to the electric utility through a series impedance, usually an inductor, to limit the current between the inverter and the electric utility grid.

The single-phase inverters for dispersed generation generally are rated for less than 10 kW and typically would cause no problems for a utility in small numbers. As their use increases, however, large numbers of inverters tied to the same feeder may cause problems if the inverter's harmonics are excessive.

Three-phase inverters for dispersed generation are typically rated at 10 kW through 1 MW and are more likely, at least in the short term, to cause unacceptable

utility waveforms if the inverters' output waveforms contain high percentages of harmonics. As with the single-phase inverters, the three-phase inverters may be line-commutated or self-commutated (sometimes called force-commutated) topologies. Also, as with the single-phase inverters, the output harmonics are dependent upon many variables. The DC operating voltage level for these inverters varies over a wide range for most renewable energy sources. These variations are dependent upon weather, time of day, temperature, tracking algorithms, ageing of collectors, and many other uncontrolled factors. Additionally, AC electric utilities may have undesirable effects on the output of the inverter. Variables such as ambient utility harmonics, unbalanced line voltages, unequal phase displacement, high and low levels of AC voltage, and line impedances are several variables that affect the output harmonics of the inverters.

Control of power to loads by phase control of thyristors will create harmonic currents. The thyristor-based controlled rectifier (TCR) is simply a special case of electronic control wherein the power factor is very low. Heating loads, which have nearly unity power factor, sometimes are controlled by phase control of thyristors, being produced odd-order harmonics.

The expressions for cycloconverter current harmonics are extremely complex. They vary as a function of the frequency ratio of the cycloconverter. The first term in the equation represents six-pulse converter components and the second term denotes the converter's sideband characteristic frequencies.

Most recent electronic equipment uses a switch mode power supply to provide the voltage to the equipment. This is an economical power supply that is not affected by minor voltage changes in the power system. It feeds a capacitor that supplies the voltage to the electronic circuitry. Since the load is a capacitor as seen from the power system, the current to the power supply is discontinuous. That is, current flows for only part of the half-cycle, therefore, becoming distorted.

The voltage level variation at the motor terminals can be related to voltage sags, swells, fluctuations, and voltage drops in power cables, as it can be seen in Fig. 1, which shows various kinds of interference in the low frequency (LF) range that can occur in low-voltage supply systems. Equipment operating from such a supply must have sufficient interference immunity to ensure trouble-free operation. On the other hand, the low voltage supply system must have a minimum quality that must be assured by the operator [71].

Voltage interruptions⁵⁵ are typically caused by switching of large transformers, motors, and capacitors, and the effects include the drop-out and chattering of relays, deactivation of motor brakes, etc. [71].

Voltage dips⁵⁶ or sags are a decrease of the normal voltage level in the three phases between 10 and 90% of the nominal RMS voltage at the power frequency, for duration of half cycle to 1 minute. It is mainly caused by faults in the transmission or distribution network (problems related to the system itself, e.g., failures of

duration ≤ 1 s), most of the times on parallel feeders, as well as faults in consumer installations (e.g., short-circuits in the supply system) and connection/switching of heavy loads (electric heating, electric furnaces) and start-up of large motors or loads (several seconds or tens of seconds, low depth), including IMs, whose starting current can be several times higher than nominal current⁵⁷. The main consequences are the malfunction of information technology equipment, namely microprocessor-based control systems (PCs, PLCs, VSDs, etc.) that may lead to a process stoppage, and tripping of contactors and electromechanical relays, as well as disconnection and loss of efficiency and torque fluctuations in electric rotating machines.

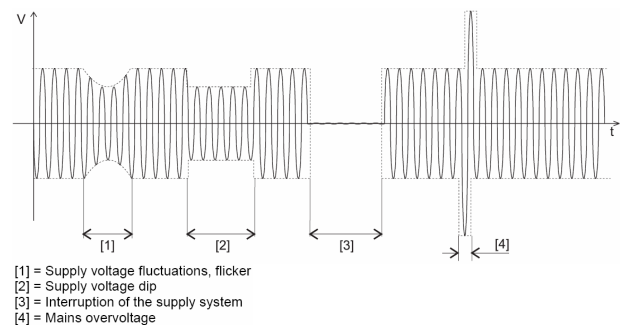


Fig. 1. Disturbances in the low-voltage supply system [71].

Voltage swells or overvoltages (transients) are a momentary increase of the voltage, at the power frequency, outside the normal tolerances, with duration of more than one cycle and typically less than a few seconds. The possible causes are switching operations in the medium-voltage supply system, thunderstorms, start/stop of heavy loads, badly dimensioned power sources, badly regulated transformers (mainly during off-peak hours), switching of power factor correction equipment without inductors, etc. The main consequences are the, malfunctioning, data loss, flickering of lighting and screens, stoppage or damage of sensitive equipment, and destruction of electronic equipment if the voltage values are too high.

Voltage fluctuations are oscillations of voltage value, amplitude modulated by a signal with a frequency up to 30 Hz. The main causes are the arc furnaces, welding equipment, heavy-load fluctuations (oscillating loads) such as lifts and presses, and frequent start/stop of electric motors. The consequences are common undervoltages. The most perceptible consequence is the flickering of lighting (fluctuations in intensity of lights) and screens, giving the impression of unsteadiness of visual perception. Fluctuations also happen as a function of the period of the day, namely, during peak hours. In some industrial installations, although the regulations, the voltage drop in the power cables feeding motors far from the command and protection boards, exceeds by far the established limits, leading to significant and constant reductions in the voltage at the motor terminals.

The motor voltage should be kept as close to the nameplate value as possible, with a maximum deviation

⁵⁵ According to [95], supply voltage reduction to less than 1% (prearranged: execution of scheduled works; accidental: long interruption or short interruption).

⁵⁶ According to [95], supply voltage reduction to 90% and 1% (duration 10 ms to 1 s).

⁵⁷ In these cases, since the power cables are sized to the steady-state current, the high magnitude of the starting current results in a large voltage drop in the power grid and electric installations. The magnitude of this effect depends on the grid short-circuit power and on the installation impedance.

of 5%. Although motors are designed to operate within $\pm 10\%$ of nameplate voltage, large variation significantly reduces efficiency, power factor, and service life. When operating at less than 95% of design voltage, motors typically lose 2 to 4 points of efficiency, and service temperatures increase up to 20°C, greatly reducing insulation lifetime. Running a motor above its design voltage also reduces power factor and efficiency. Since the voltage decreases with distance from the step-down transformer, all voltage measurements should be taken at the motor terminal box. Note that low power factor reduces the efficiency of the electrical distribution system both within and outside of your facility. Low power factor results when IMs are operated at less than full-load. Many utilities charge a penalty if power factor dips below 0.93-0.95. Installing single capacitors or banks of capacitors either at the motor or at the motor control centers (MCC) addresses this problem [122].

Power cables that supply motors running near full load for many hours should be oversized in new construction or during rewinding. This practice minimizes line losses and voltage drops [122].

Curiously, the majority of industrial motors in the USA are designed for 460-V operation, yet the utility distribution system is designed for 480 V. The rationale here is that the cable voltage drop allows the proper voltage of 460 V at the motor terminals [123].

In the EU, motors are designed for 400-V operation matching the utility distribution system voltage. Yet, most of the in-service old motors were designed to 380 V.

Measurements carried out in the EUA have shown that in spite of the cable drop, the motor terminal voltages can be substantially higher than rated voltage in stiff industrial systems, while it may be well below the nominal voltage, when the system is heavily loaded in weak commercial or industrial systems [123].

Besides the overvoltage or undervoltage problem existing in the power system, the supply is never perfectly balanced.

According to ANSI C84-1 Std., the magnitude of long voltage fluctuations should be within the $U \pm 10\%$ range [120]. This type of abnormality is associated with problems related to the system itself (e.g., failures, less than one second) but also to the start of large loads (several seconds or tens of seconds, low-depth), including the IMs, whose starting current can be several times higher than nominal current.

According to the point 7.3 of the IEC60034-1 [121], voltage and frequency variations during operation, for AC machines rated for use on a power supply or fixed frequency supplied from an AC generator (whether local or via a supply network), combinations of voltage variation and frequency variation are classified as being either zone A or zone B, in accordance with Fig. 2 for motors.

A machine shall be capable of performing its primary function (i.e., developing rated torque, in the case of IMs), continuously within zone A, but need not comply fully with its performance at rated voltage and frequency (see rating point in Fig. 2), and may exhibit some deviations. Temperature rises may be higher than those at rated voltage and frequency.

A machine shall be capable of performing its primary function within zone B, but may exhibit greater deviations from its performance at rated voltage and frequency than in zone A. Temperature rises may be higher than those at rated voltage and frequency, and most likely will be higher than those in zone A. Extended operation at the perimeter of zone B is not recommended. In practical applications and operating conditions, a machine will sometimes be required to operate outside the perimeter of zone A. Such excursions should be limited in value, duration and frequency of occurrence. Corrective measures should be taken, where practical, within a reasonable time, for example, a reduction in output (or derating). Such action may avoid a reduction in machine life from temperature effects. The temperature-rise limits or temperature limits in accordance with standard IEC 60034-1 apply at the rating point and may be progressively exceeded as the operating point moves away from the rating point. For conditions at the extreme boundaries of zone A, the temperature rises and temperatures typically exceed the limits specified in this standard by approximately 10 K. An AC motor will start at the lower limit of voltage only if its starting torque is adequately matched to the counter-torque of the load, but this is not a requirement. For starting performance of design N motors, see IEC 60034-12.

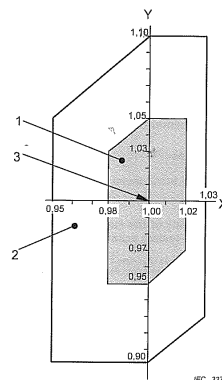


Fig. 2. Voltage and frequency limits specified in the standard IEC 60034-1 [121]:

- 1) Zone A;
- 2) Zone B (outside zone A);
- 3) Rating point.

Voltage levels above rated value, introduce larger magnetizing current components, while reducing the overall current level to a loaded motor. Operating efficiency of IMs is commonly mildly increased. This very small increase of efficiency is obtained at the expense of a severe decrease of operating power factor. Also, mild over-voltage condition will create a steeper torque-slip profile of the motor, effectively increasing the operating speed. Conversely, a lower than ideal (or rated) operating voltage causes a rather severe increase of stator current, which introduces a very rapid increase of the resistive I^2R losses generating a temperature increase and efficiency drop. Prolonged higher than normal operating temperatures is the most significant cause for insulation failure for low-voltage motors. Obviously, the nameplate displays the voltage level at which the motor should be run, since it is the motor designer's specification. At rated load, significant overvoltages represent negligible additional insulation stresses yet severely decrease power factor, while undervoltage conditions are the source of a steep temperature increase and a noticeable efficiency drop of the motor [124].

B. Deduction of Equations (A4.8), (A4.9), and (A4.10)

Equation (A4.8) is obtained as follows. Assuming (1), (2) and (3), one can write (4).

$$HVF = \frac{1}{U_R} \cdot \sqrt{\sum_{h=5,7,11,13} \frac{U_h^2}{h}} \quad (1)$$

$$U_h = d \cdot \frac{U_1}{h} \quad (2)$$

$$U_1 = U_R \quad (3)$$

$$HVF = \frac{1}{U_1} \cdot \sqrt{\sum_{h=5,7,11,13} \frac{\left(d \cdot \frac{U_1}{h}\right)^2}{h}} = d \sqrt{\sum_{h=5,7,11,13} \frac{1}{h^3}} \quad (4)$$

On the basis of (4) the distortion constant d can be defined as in (5).

$$d = HVF \cdot \left(\sqrt{\sum_{h=5,7,11,13} \frac{1}{h^3}} \right)^{-1} \quad (4)$$

Replacing (4) in (2), yields (5), which is the equation (A4.8).

$$U_h = \frac{U_1}{h} \cdot HVF \cdot \left(\sqrt{\sum_{h=5,7,11,13} \frac{1}{h^3}} \right)^{-1} \quad (5)$$

Equation (A4.9) is obtained as follows. Assuming (1), (3) and (6), one can write (7).

$$U_h = U_5 = d \cdot \frac{U_1}{5} \quad (6)$$

$$HVF = \frac{1}{U_1} \cdot \sqrt{\sum_{h=5,7,11,13} \frac{\left(d \cdot \frac{U_1}{5}\right)^2}{h}} = d \sqrt{\sum_{h=5,7,11,13} \frac{1}{5^2 \cdot h}} \quad (7)$$

On the basis of (7) the distortion constant d can be defined as in (8).

$$d = HVF \cdot \left(\sqrt{\sum_{h=5,7,11,13} \frac{1}{5^2 \cdot h}} \right)^{-1} \quad (8)$$

Replacing (8) in (6), yields (9), which is the equation (A4.9).

$$U_h = \frac{U_1}{h} \cdot HVF \cdot \left(\sqrt{\sum_{h=5,7,11,13} \frac{1}{h^3}} \right)^{-1} \quad (9)$$

Equation (A4.10) is obtained as follows. Assuming (1), (3) and (10), one can write (11).

$$U_5 = d \cdot \frac{U_1}{5} \wedge U_{7,11,13} = 0 \quad (10)$$

$$HVF = \frac{1}{U_1} \cdot \sqrt{\frac{\left(d \cdot \frac{U_1}{5}\right)^2}{5}} = d \sqrt{\frac{1}{5^2 \cdot 5}} \quad (11)$$

On the basis of (11) the distortion constant d can be defined as in (12).

$$d = HVF \cdot \left(\sqrt{\frac{1}{5^2 \cdot 5}} \right)^{-1} \quad (12)$$

Replacing (12) in (10), yields (13), which is the equation (A4.10).

$$U_5 = \frac{U_1}{5} \cdot HVF \cdot \left(\sqrt{\frac{1}{5^2 \cdot 5}} \right)^{-1} = \sqrt{5} \cdot U_1 \cdot HVF \quad (13)$$

B. Additional Simulated Results on the effect of DC-Bus Capacitance on the System Susceptibility to Voltage Unbalance

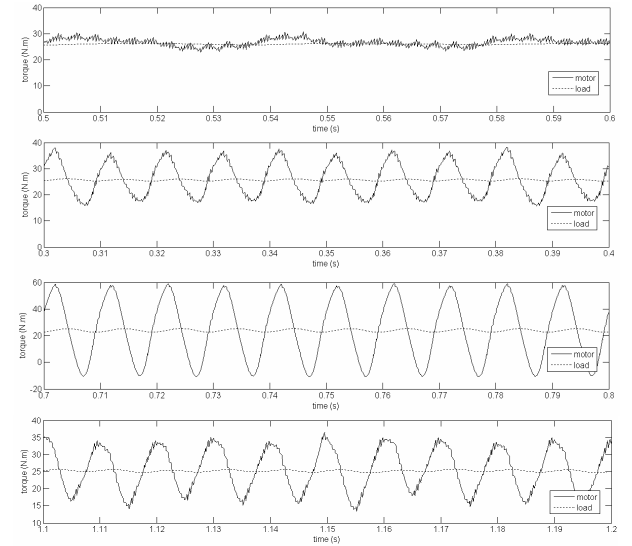


Fig. 3. Time zoom of torque for the motor and load ($C_{DC} = 250 \mu\text{F}$, $f_{1(mr)} = 50 \text{ Hz}$, $m_a = 1.8$).

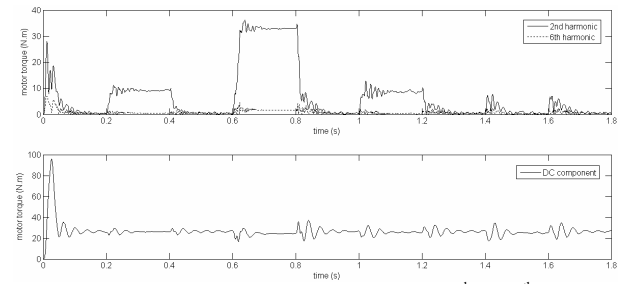


Fig. 4. Average value (or DC equivalent value), 2nd and 6th harmonic components (50-Hz base frequency) of the motor torque ($C_{DC} = 250 \mu\text{F}$; $f_{1(mr)} = 50 \text{ Hz}$; $m_a = 1.8$).

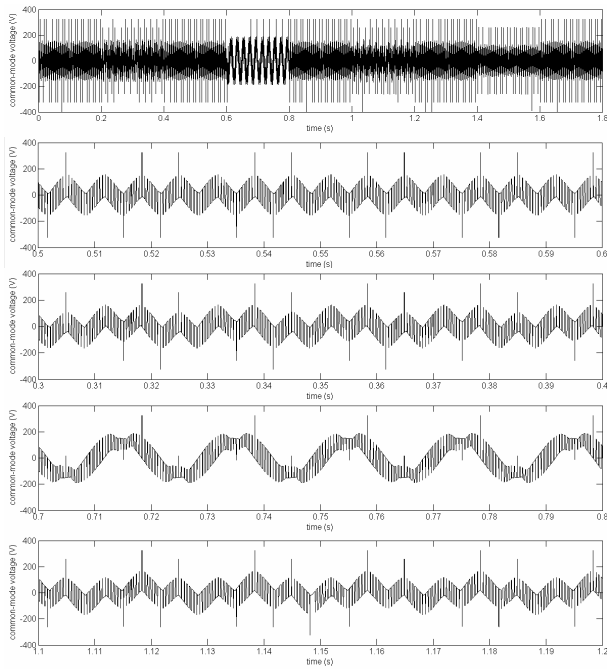


Fig. 5. Common-mode voltage (summation of phase-to-ground voltages divided by 3), ($C_{DC} = 2500 \mu\text{F}$; $f_{i(mtr)} = 50 \text{ Hz}$; $m_a = 1.8$).

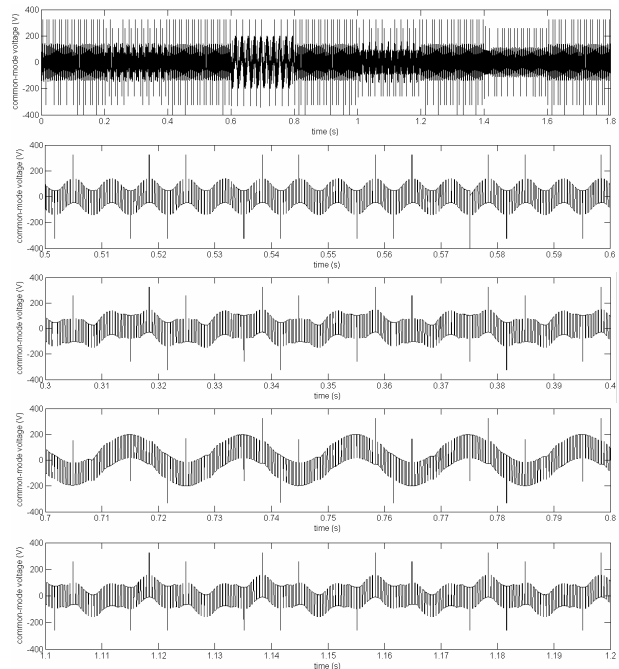


Fig. 8. Common-mode voltage (summation of phase-to-ground voltages divided by 3), ($C_{DC} = 25000 \mu\text{F}$; $f_{i(mtr)} = 50 \text{ Hz}$; $m_a = 1.8$).

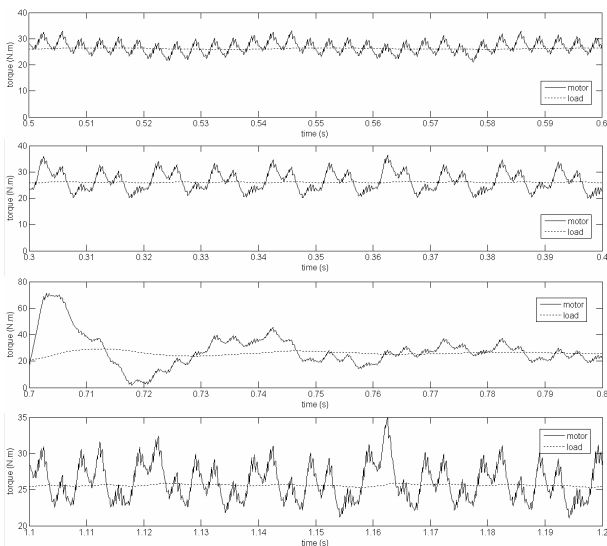


Fig. 6. Time zoom of the torque for the motor and load ($C_{DC} = 2500 \mu\text{F}$; $f_{i(mtr)} = 50 \text{ Hz}$; $m_a = 1.8$).

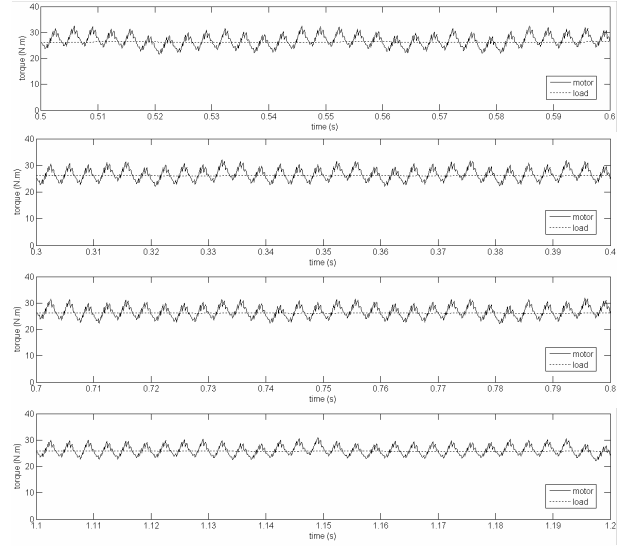


Fig. 9. Time zoom of the torque for the motor and load ($C_{DC} = 25000 \mu\text{F}$; $f_i = 50 \text{ Hz}$; $m_a = 1.8$).

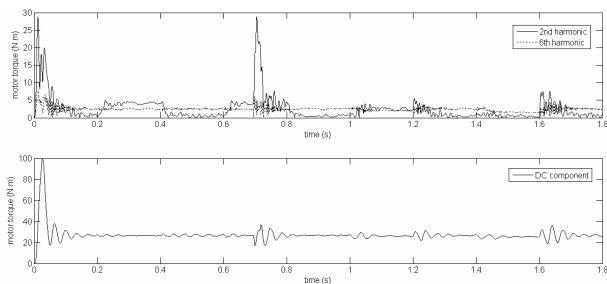


Fig. 7. Average value (or DC equivalent value), 2nd and 6th harmonic components (50 Hz base frequency) of the motor torque, ($C_{DC} = 2500 \mu\text{F}$; $f_{i(mtr)} = 50 \text{ Hz}$; $m_a = 1.8$).

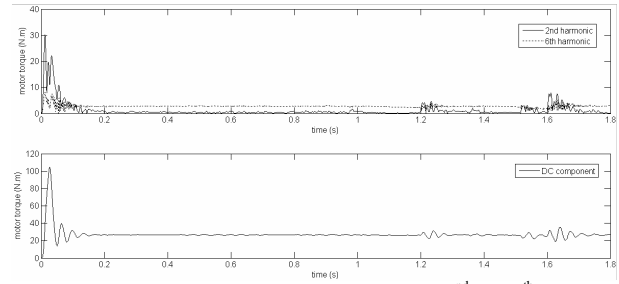


Fig. 10. Average value (or DC equivalent value), 2nd and 6th harmonic components (50-Hz base frequency) of the motor torque ($C_{DC} = 25000 \mu\text{F}$; $f_i = 50 \text{ Hz}$; $m_a = 1.8$).

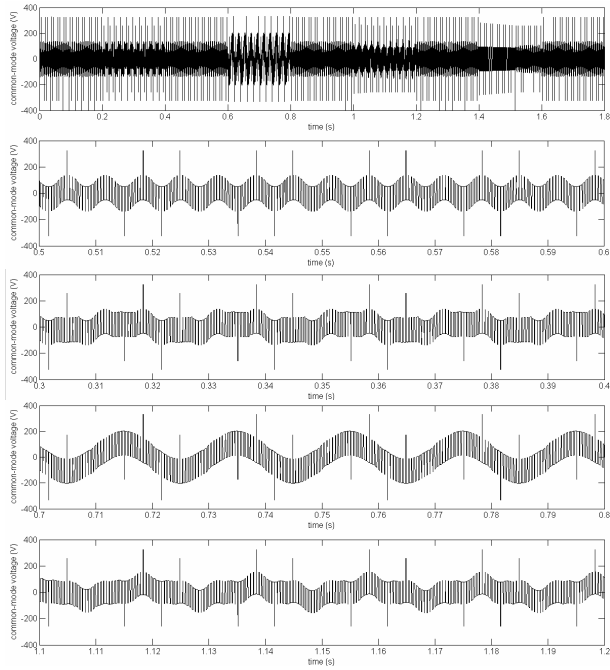


Fig. 11. Common-mode voltage (summation of phase-to-ground voltages divided by 3), ($C_{DC} = 25000 \mu\text{F}$; $f_i = 50 \text{ Hz}$; $m_a = 1.8$).

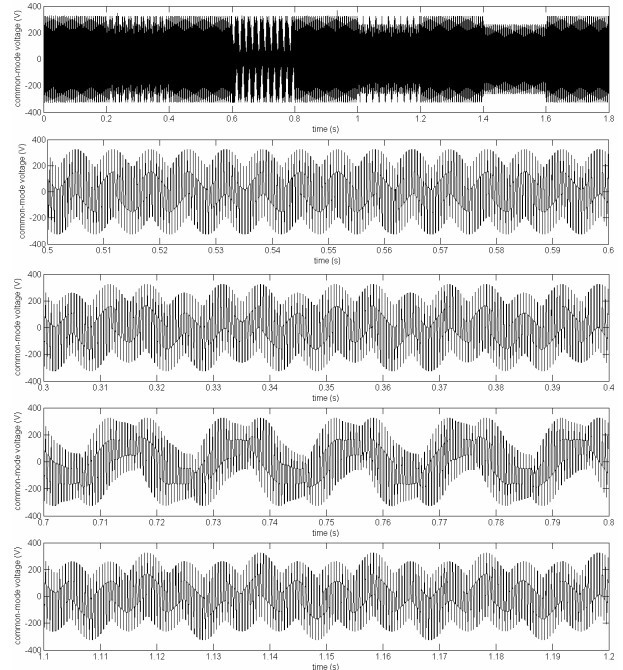


Fig. 14. Common-mode voltage (summation of phase-to-ground voltages divided by 3), ($C_{DC} = 250 \mu\text{F}$, $f_i = 40 \text{ Hz}$, $m_a = 0.95$).

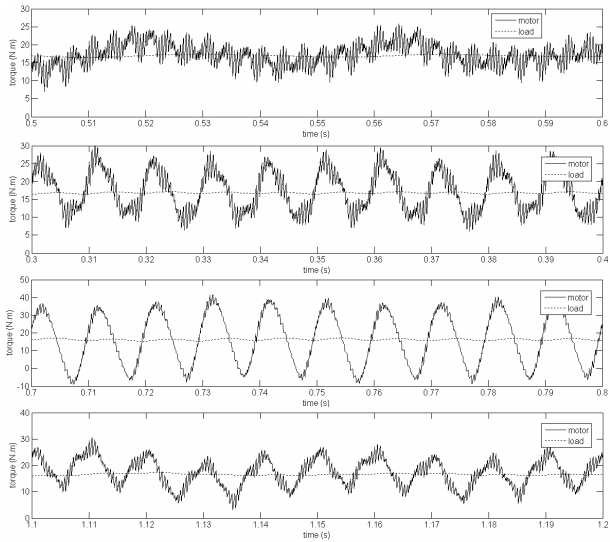


Fig. 12. Time zoom of the torque for the motor and load ($C_{DC} = 250 \mu\text{F}$; $f_i = 40 \text{ Hz}$; $m_a = 0.95$).

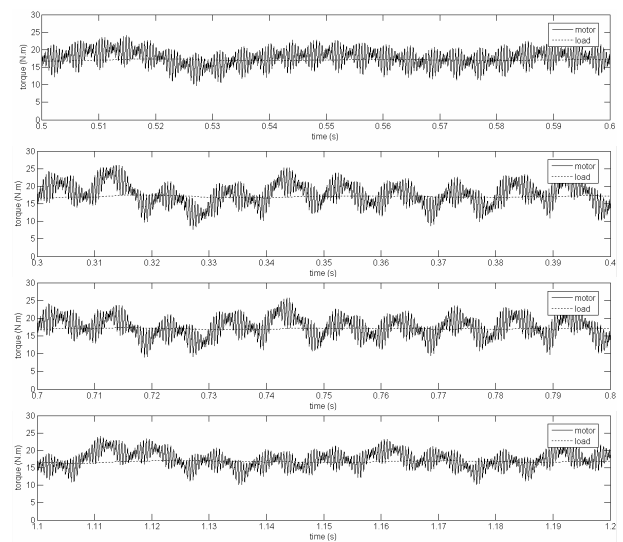


Fig. 15. Time zoom of the torque for the motor and load ($C_{DC} = 2500 \mu\text{F}$; $f_i = 40 \text{ Hz}$; $m_a = 0.95$).

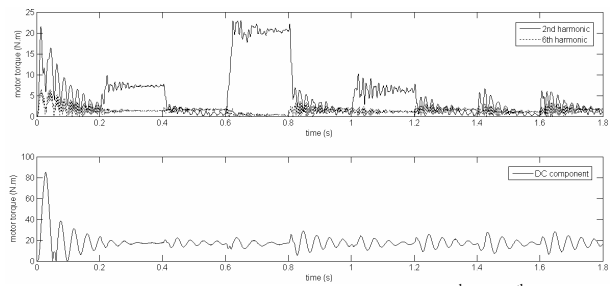


Fig. 13. Average value (or DC equivalent value), 2nd and 6th harmonic components (50 Hz base frequency) of the motor torque, ($C_{DC} = 250 \mu\text{F}$; $f_i = 40 \text{ Hz}$; $m_a = 0.95$).

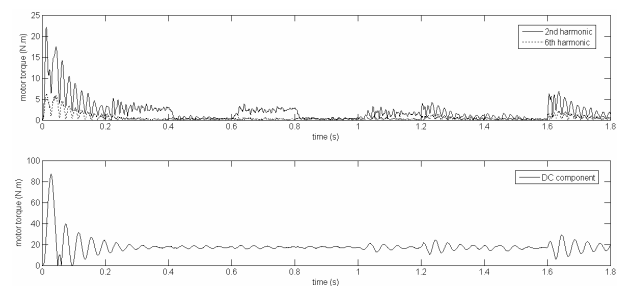


Fig. 16. Average value (or DC equivalent value), 2nd and 6th harmonic components (50-Hz base frequency) of the motor torque, ($C_{DC} = 2500 \mu\text{F}$; $f_i = 40 \text{ Hz}$; $m_a = 0.95$).

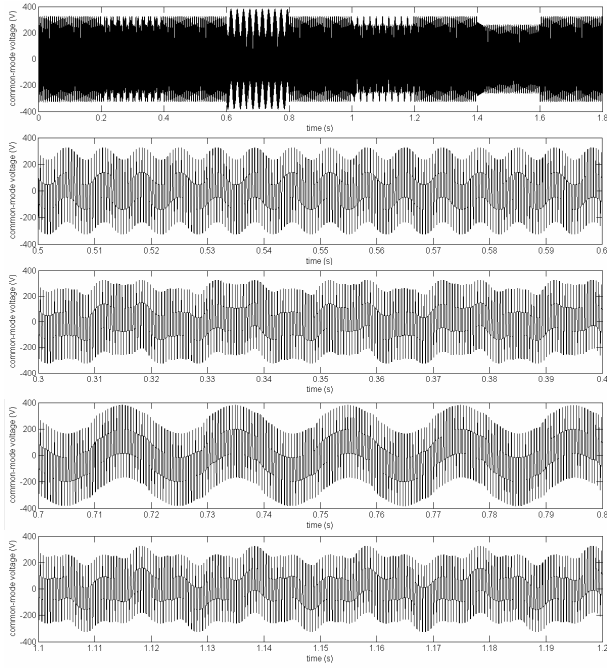


Fig. 17. Common-mode voltage (summation of phase-to-ground voltages divided by 3), ($C_{DC} = 2500 \mu\text{F}$; $f_l = 40 \text{ Hz}$; $m_a = 0.95$).

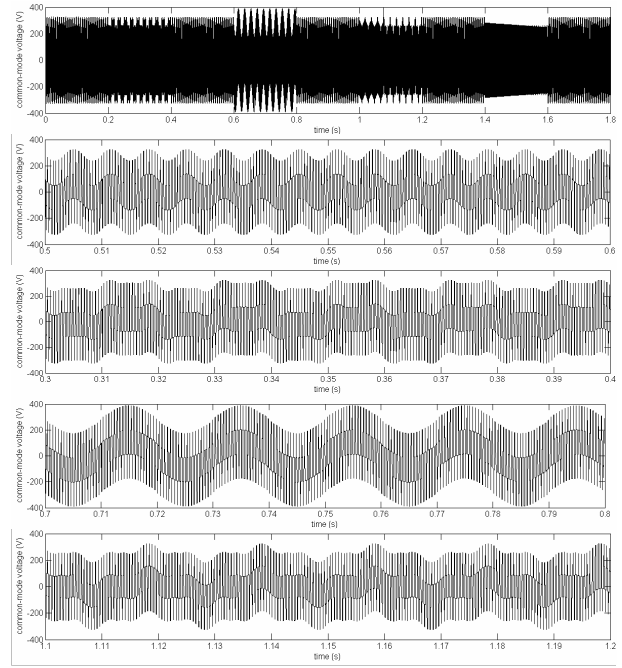


Fig. 20. Common-mode voltage (summation of phase-to-ground voltages divided by 3), ($C_{DC} = 25000 \mu\text{F}$; $f_l = 40 \text{ Hz}$; $m_a = 0.95$).

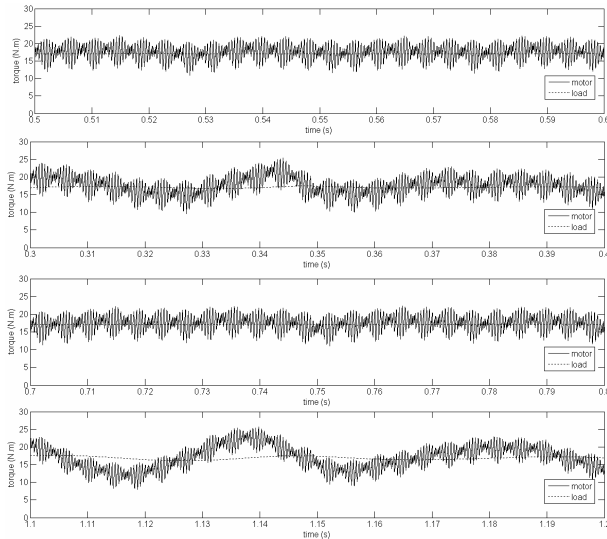


Fig. 18. Time zoom of the torque for the motor and load ($C_{DC} = 25000 \mu\text{F}$; $f_l = 40 \text{ Hz}$; $m_a = 0.95$).

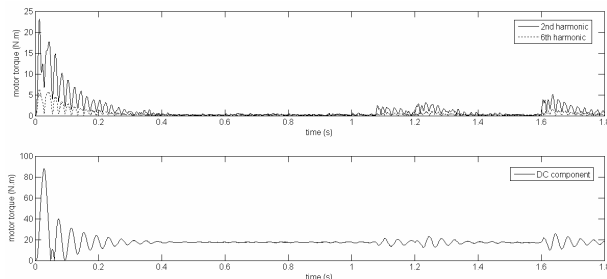


Fig. 19. Average value (or DC equivalent value), 2nd and 6th harmonic components (50-Hz base frequency) of the motor torque, ($C_{DC} = 25000 \mu\text{F}$; $f_l = 40 \text{ Hz}$; $m_a = 0.95$).

A6.7.2 Section 7.7

A. Influence of DC-Bus Capacitance on DC-Bus and Inverter Output Line-to-Line Voltages

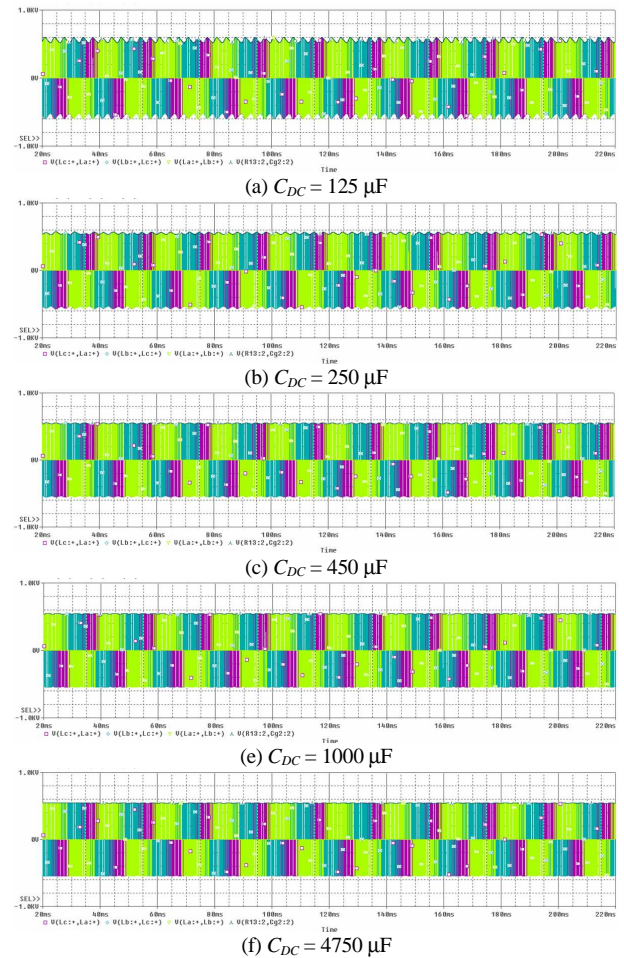
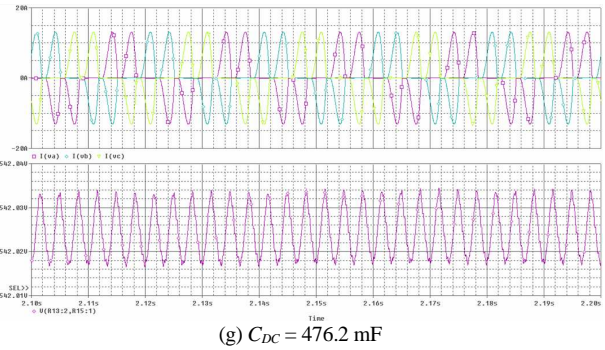
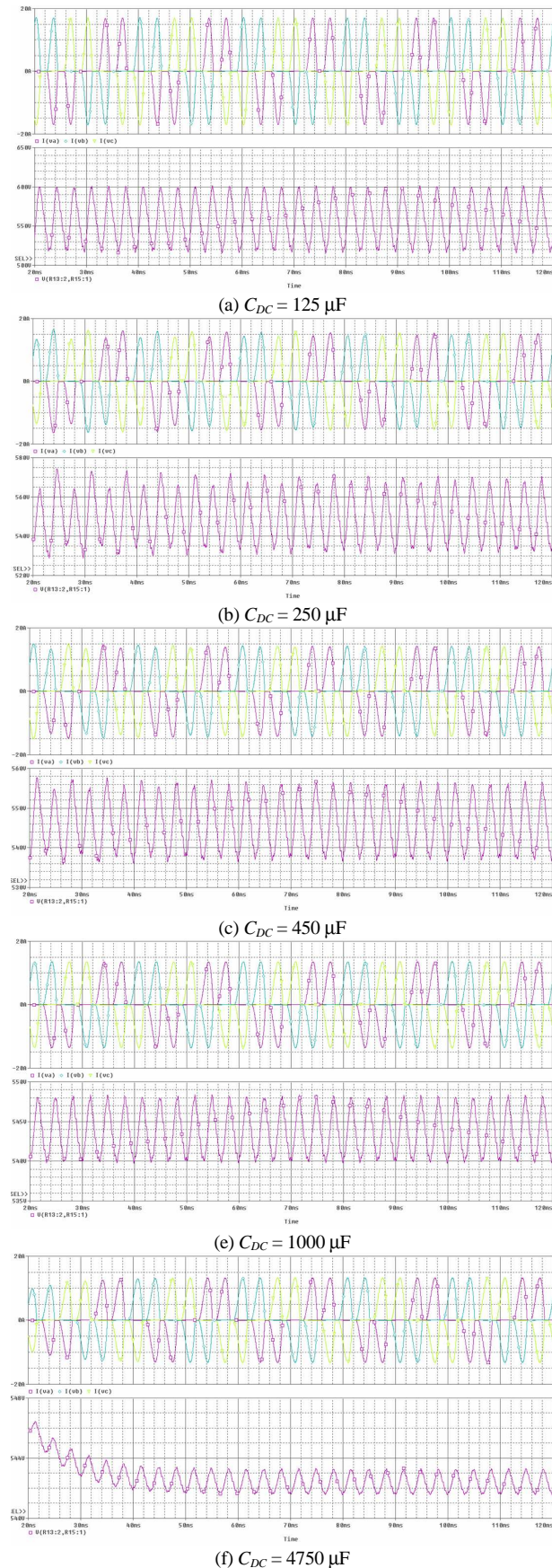


Fig. 1. DC-bus and inverter output line-to-line voltages for different DC-bus capacitance values.

A6.7.3 Section 7.8

A. Influence of DC-Bus Capacitance on Input Current Distortion



(g) $C_{DC} = 476.2 \text{ mF}$
 Fig. 1. VSD input currents (upper graphs) and DC-bus voltages (bottom graphs) for different capacitance values.

A6.8 Complement to Appendix 5

A6.8.1 Section A5.1

A. Basic Principles on Reliability [86], [114], [115], [116]

Two quantities are normally used to describe the behaviour of a stochastic component⁵⁸: the failure rate and the expected or average repair time (time the component resides in the non-healthy state).

The failure rate, λ , gives the average probability that the component will fail in the next small period of time, Δt , according to (1).

$$\lambda = \lim_{\Delta t \rightarrow 0} \frac{\Pr(\text{failure in period } \Delta t)}{\Delta t} \quad (1)$$

A more practical way of defining λ is through the number of failures, n , in a population with N units, during a useful lifetime period Δt , according to (2).

$$\lambda = \frac{n}{\Delta t \cdot N} \quad (2)$$

The two definitions are equivalent under a number of assumptions, being the most important the repair possibility after every failure within a short time. Typically, (2) is obtained from observed failures, being easily calculated from field data. Due to the lack of observed data, component reliability determination may require use of generic failure data adjusted for the various factors that influence the failure rate for the component under analysis. Generally, these factors are: environmental factors, which affect the failure rate due to the extreme mechanical, electrical, nuclear, and chemical environments (e.g., high vibration environment, would lead to high stresses that promote failure of components), design factors, which affect the failure rate due to the quality of material used and workmanship, material composition, functional requirements, geometry, and complexity, and operating factors, which affect the failure rate due to the applied stresses resulting from operation, testing, repair, and maintenance practices, etc.

⁵⁸ Stochastic, from the Greek "stochos" or "aim, guess", means of, relating to, or characterized by conjecture and randomness. A stochastic component or process is one whose behaviour is non-deterministic in that a state does not fully determine its next state.

Accordingly, the failure rate can be presented by (3), where λ_a is the actual failure rate, λ_b is the base or generic failure rate, K_E , K_D , and K_O are correction factors for the environment, design, and operation, respectively. It is possible to subdivide each of the correction factors to their contributing subfunctions accordingly. For example, $K_E = f(k_a, k_b, \dots)$ when k_a and k_b are factors such as vibration level, moisture, and pH level. These factors may be different types of components. The failure rate of a component can be obtained from a table with typical values, and then they are multiplied by the applicable adjusting factors for the type of component, being analysed.

$$\lambda_a = \lambda_b \cdot K_E \cdot K_D \cdot K_O \quad (3)$$

Generally, λ_b is obtained from an empirical model called the Arrhenius model. An indicator often used to quantify the reliability of a component, equipment or system is the mean (or expected) time to failure, $MTTF$ ⁵⁹, i.e., the time between consecutive failures, excluding the time associated with the operation reestablishment or the mean operation time between consecutive failures of a component. For a period in which n failures occur, and an operation time until the failure, OT , the $MTTF$ can be defined by (4), provided that a sufficient number of failures have occurred in the analysed period [116]. Operation time depends on the motor maintenance and operating conditions, as well as on the intrinsic motor quality. The mean (or expected) time to repair, $MTTR$, can be defined by (5). In relation to the motor systems, it can be defined the downtime, DT , which includes the time to assembly/disassembly, repair, transportation, etc., i.e., corresponds the period between the failure and the restarting of the system. It is important to guarantee a reduced $MTTR$ since, although spare motors can exist for immediate replacement, there is in most cases an inherent cost to the service or production stoppage. The mean (or expected) time between failures, $MTBF$, is equal to the sum of $MTTF$ and $MTTR$.

$$MTTF = \frac{\sum_{x=1}^n OT_x}{n} \quad (4)$$

Since typically $MTTR \ll MTTF$ ($MTTF$ typically less than 1% of $MTTR$ for industrial low-medium power motors), $MTBF$ can be considered approximately equal to $MTTF$, i.e., the $MTTR$ can be neglected.

$$MTTR = \frac{\sum_{x=1}^n (DT_x)}{n} \quad (5)$$

$MTTF$ is equal to the reciprocal of λ (expressed by (2)), according to (6). $MTTF$ is typically defined in the constant failure rate period of the bathtub curve, considering only useful life.

$$MTTF = \lambda_{ff}^{-1} \quad (6)$$

It should be noted that over 95% of reliability evaluation studies use the simple model with a single failure rate and a single repair rate, which assumes both repair and lifetime exponentially distributed, according to (7), where $F(t)$ is the probability distribution function of the lifetime (probability that the component fails before it reaches an age t), $R(t)$ is the reliability, i.e., the probability of a component succeed during its intended mission over time t .

$$F(t) = 1 - e^{-\lambda t} \quad (7)$$

For example, if the failure rate of a component is $\frac{1}{8} \text{ yr}^{-1} = 0.125 \text{ yr}^{-1}$, the probability of a failure before reaching 8, 10, and 12 years is 63.21%, 71.35%, and 77.69%, respectively. The $MTTF$ can be defined by (8).

$$MTTF = \int_0^{\infty} R(t) dt \quad (8)$$

There are several reasons why this distribution is almost the only one used, but one of the most important is that most components in use are in they useful operating time. They have passed the wear-in period and have not yet reached the wear-out period, assuming that the failure rate of a component versus time can be described through a bathtub curve. However, in most cases, the exponential model is not correct for the repair time, because there are several variables that can influence that time.

Considering a network approach, in which the stochastic behaviour of a system is represented graphically by means of a number of network blocks, connected in parallel or in series. Each block refers to a stochastic component of the system. The considered model is such that the system is healthy as long as path through the network exists. This method is very suitable to get an overview of the reliability of a system. When the reliability is quantified by using a stochastic network, several mathematical approximations are needed. The calculations assume that the repair time and the useful lifetime are exponentially distributed for all components. Each block is characterized by a failure rate and an expected repair time r .

For the sake of completeness, it is also defined the availability and unavailability. For each element an average availability, α , and an average unavailability, υ , can be defined by (9) and (10). The availability is the ability (either in active operation or that it is able to operate if required) of an item (under combined aspects of its reliability, maintainability, and maintenance support) to perform its required function at a stated instant of time or over a stated period of time. The average availability denotes the mean proportion of time the item is functioning, and in (9) it is assumed that the item is repaired to an "as good as new" condition every time it fails. The average unavailability denotes the mean proportion of time the item is not functioning.

⁵⁹ This concept only applies to equipment that can actually be repaired.

$$\alpha = \frac{\sum_{x=1}^n (OT_x)}{\sum_{x=1}^n (OT_x + DT_x)} = \frac{MTTF}{MTTF + MTTR} = \frac{MTBF - MTTR}{MTBF} \quad (9)$$

$$\nu = 1 - \alpha = \frac{MTTR}{MTTR + MTTF} = \frac{MTTR}{MTBF} \quad (10)$$

In order to increase the availability of the motors, the repair shops and/or maintenance teams should use techniques, equipments and materials, which simultaneously lead to the *MTTF* maximization and *MTTR* minimization. For systems with significant costs associated with interruptions, it is likely to be advantageous to pay more for the repair to accelerate the process, if no spare motor is available, i.e., the amount of additional cost to repair that can be spent should be calculated as a function of the cost associated to the system failure.

The reliability of a system with series connected components is the probability of the m components or items succeed during its intended mission time t . A series connection represents the situation where each component failure leads to the system failure. Thus, probabilistically, the system reliability $R_{\text{sys}}(t)$ from independent blocks is obtained from (11).

$$R_{\text{sys}}(t) = \prod_{i=1}^m R_i(t) = 1 - F_{\text{sys}}(t) \quad (11)$$

The hazard rate (instantaneous failure rate), λ_{sys} , for a series system is, assuming a constant failure rate model for each stochastic component (e.g., assuming an exponential time to failure for each component), $\lambda_i(t) = \lambda_i$, is given by (12).

$$\lambda_{\text{sys}} = \sum_{i=1}^m \lambda_i \quad (12)$$

The *MTTF* is defined by (8). Using (8) and (14), the *MTTF* of the system is (15).

$$R_i(t) = e^{-\lambda_i t} \quad (13)$$

$$R_{\text{sys}}(t) = \exp\left(-t \sum_{i=1}^m \lambda_i\right) = e^{-\lambda_{\text{sys}} t} \quad (14)$$

$$MTTF_{\text{sys}} = \frac{1}{\lambda_{\text{sys}}} \quad (15)$$

For a parallel system (16) and (17) are valid. A parallel connection represents redundant components, where the system does not fail until all of the components fail.

$$R_{\text{sys}}(t) = 1 - F_{\text{sys}}(t) = 1 - \prod_{i=1}^n (1 - R_i(t)) \quad (16)$$

$$MTTF_{\text{sys}} = \int_0^{\infty} R_{\text{sys}}(t) dt \quad (17)$$

After proper mathematical transformation, described in [114], and assuming that all m units are identical with a constant failure rate (e.g., in an active redundant system), λ , the reliability can be described by (18). Therefore, yields (19).

$$R_{\text{sys}}(t) = 1 - (1 - e^{-\lambda t})^m \quad (18)$$

$$MTTF_{\text{sys}} = MTTF \left(1 + \frac{1}{2} + \dots + \frac{1}{m}\right) \quad (19)$$

It can be concluded that the design of active redundant systems, the *MTTF* of the system exceeds the *MTTF* of an individual unit. However, the contribution to the *MTTF* of the system from the second unit, the third unit, and so on, would have a diminishing return as m increases. This means that, there would be an optimum number of parallel blocks (units) by which a designer can maximize the reliability and, at the same time, minimize the cost of the component in its life cycle.

Considering spare components that can replace the faulty components, the repair time is reduced to the replacement time, which should be very low. Some system spent a time to reach the steady-state operation, i.e., time until start to execute the associated tasks. In such systems, after the replacement of one or more components, the repair time or downtime includes the transient phase or restarting duration.

In Fig. 1, a four state component model is shown. The component or system cannot fail while in maintenance, but the maintenance can start while the component or system is being repaired. A faulty component or system will be first repaired before it becomes healthy again. These principles apply to motors and motor driven systems.

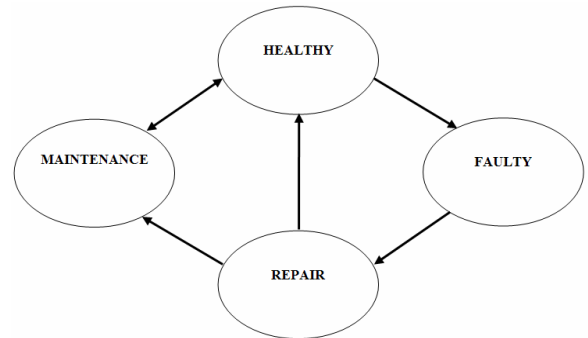


Fig. 1. Four-state component model.

B. Arrhenius Law for Insulation Materials and Lubricants

In Fig. 2, the impact of the temperature increase on the insulation and mineral lubricant lifetime is shown [86], [127].

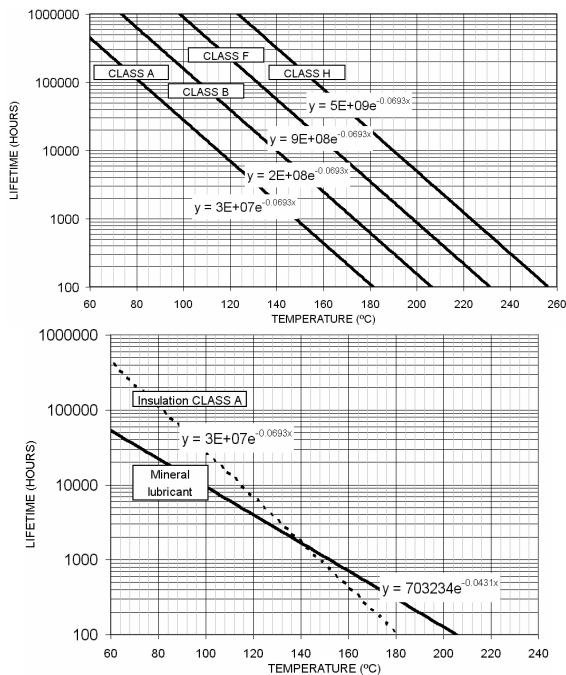


Fig. 2. Impact of the temperature increase on the insulation and lubricant lifetime [86], [127].

A6.8.2 Section A5.4.2

In Figs. 1-10, additional experimental results for a 7.5-kW motor fed by 2- and 3-level inverters are shown.

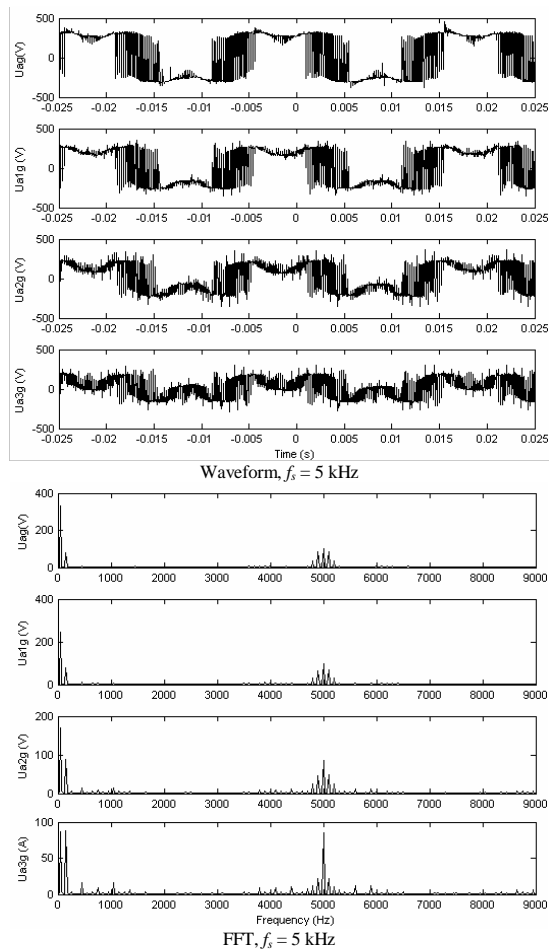


Fig. 1. Experimental winding-ground voltages for a star-connected, 7.5-kW IM-fed by a 2-level inverter ($U_l = 400$ V, $f_l = 50$ Hz, $f_s = 5$ kHz, no-load).

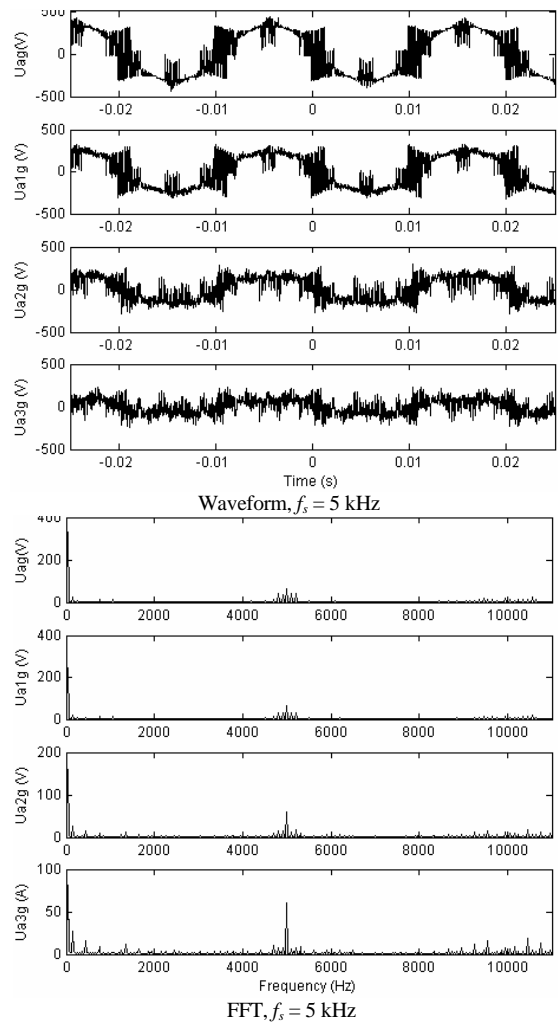
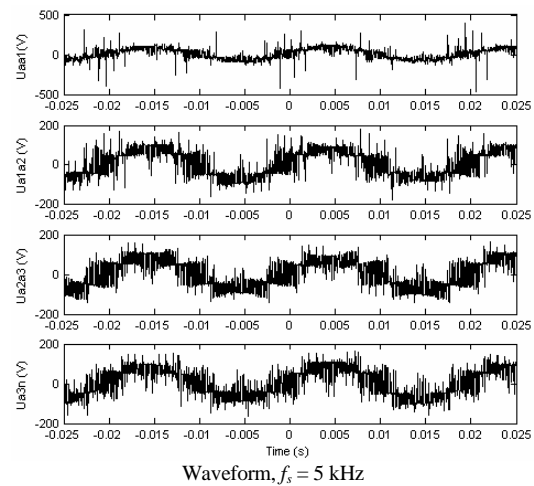


Fig. 2. Experimental winding-ground voltages for a star-connected, 7.5-kW IM-fed by 3-level inverter ($U_l = 400$ V, $f_l = 50$ Hz, $f_s = 5$ kHz, no-load).



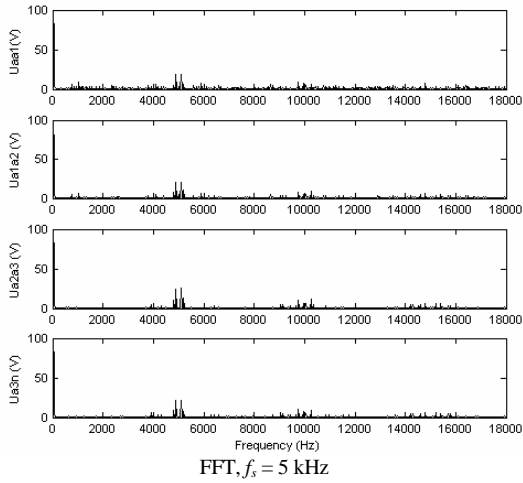


Fig. 3. Experimental voltages between coil sets for a star-connected, 7.5-kW motor fed by a 2-level inverter ($U_l = 400$ V, $f_l = 50$ Hz, $f_s = 5$ kHz, no-load).

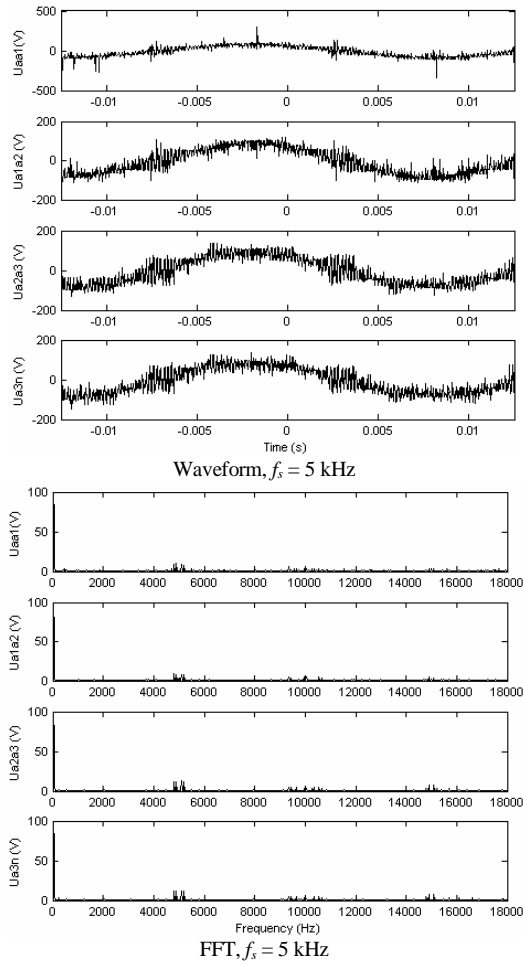


Fig. 4. Experimental voltages between coil sets for a star-connected, 7.5-kW motor fed by a 3-level inverter ($U_l = 400$ V, $f_l = 50$ Hz, $f_s = 5$ kHz, no-load).

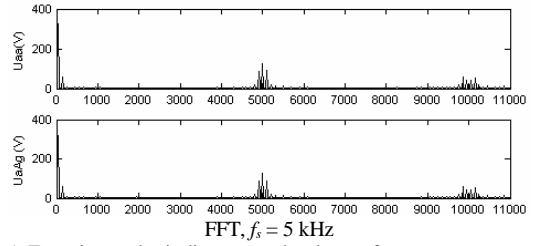
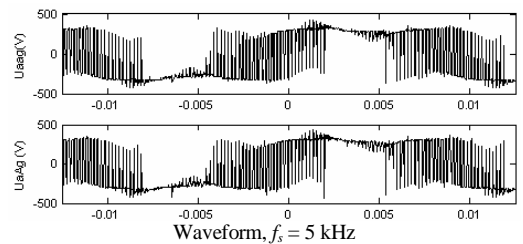


Fig. 5. Experimental winding-ground voltages for a star-connected, 3-kW IM fed by a 2-level inverter ($U_l = 400$ V, $f_l = 50$ Hz, $f_s = 5$ kHz, no-load): (upper traces) inverter terminals; (lower traces) motor terminals.

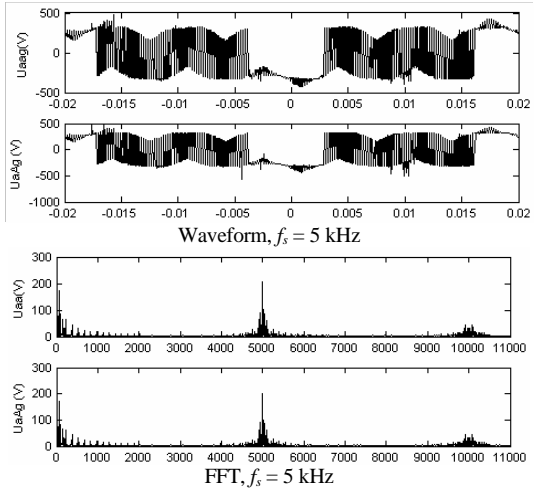


Fig. 6. Experimental winding-ground voltages for a star-connected, 3-kW IM fed by a 2-level inverter ($U_l = 200$ V, $f_l = 25$ Hz, $f_s = 5$ kHz, no-load): (upper traces) inverter terminals; (lower traces) motor terminals.

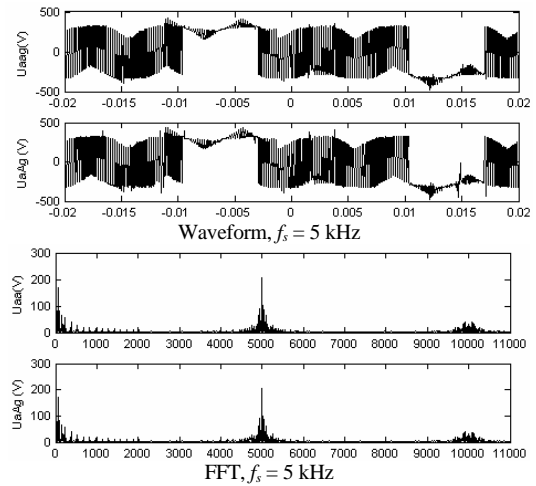
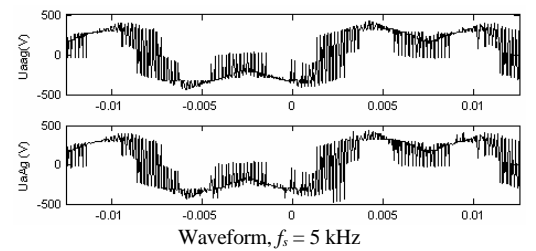


Fig. 7. Experimental winding-ground voltages for a delta-connected, 3-kW IM fed by a 2-level inverter ($U_l = 200$ V, $f_l = 25$ Hz, $f_s = 5$ kHz, no-load): (upper traces) inverter terminals; (lower traces) motor terminals.



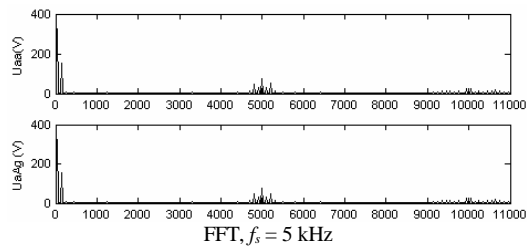


Fig. 8. Experimental winding-ground voltages for a star-connected, 3-kW IM fed by a 3-level inverter ($U_l = 400$ V, $f_l = 50$ Hz, $f_s = 5$ kHz, no-load): (upper traces) inverter terminals; (lower traces) motor terminals.

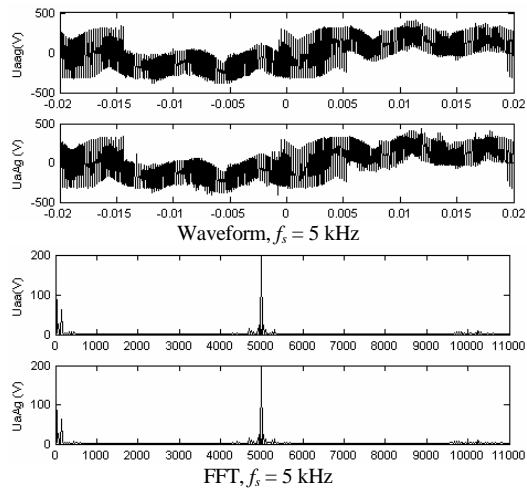


Fig. 9. Experimental winding-ground voltages for a star-connected, 3-kW IM fed by a 3-level inverter ($U_l = 200$ V, $f_l = 25$ Hz, $f_s = 5$ kHz, no-load): (upper traces) inverter terminals; (lower traces) motor terminals.

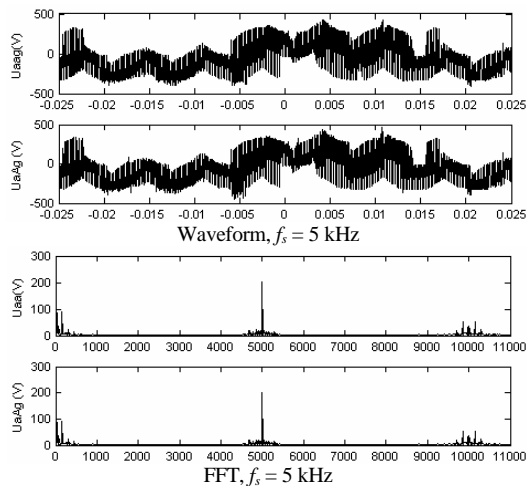


Fig. 10. Experimental winding-ground voltages for a delta-connected, 3-kW IM fed by a 3-level inverter ($U_l = 200$ V, $f_l = 25$ Hz, $f_s = 5$ kHz, no-load): (upper traces) inverter terminals; (lower traces) motor terminals.

A6.9 References

[1] de Almeida, A.; Ferreira, F.; Busch, J.; Angers, P.: "Comparative Analysis of IEEE 112-B and IEC 34-2 Efficiency Testing Standards Using Stray Load Losses in Low-Voltage Three-Phase, Cage Induction Motors", IEEE Trans. on Industry Applications, Vol. 38, No. 2, pp. 608-614, March/April 2002.

[2] Doppelbauer, M.: "Saving Energy and Costs in Electrical Drive Systems", SEW-Eurodrive, 2007.

[3] de Almeida, A., et al.: "Improving the Penetration of Energy-Efficient Motors and Drives", Prepared for the European Commission, DGTE, SAVE II Programme, 2000.

[4] Stoft, S.: "The Economics of Conserved-Energy "Supply" Curves", University of California Energy Institute, Workable Energy Regulation (POWER), April 1995.

[5] Balvanyos, T.; Lave, L.: "Economic Analysis Methods", Carnegie Mellon University, Pittsburgh, Pennsylvania.

[6] Alger, P.: "Induction Machines – Their Behavior and Uses", Gordon and Breach Publishers, 3rd Edition, 1995.

[7] Lacroux M.: "Les harmonique de champ produit par les enroulements concentrique", RGE, 66, 3, pp.145-151, 1957.

[8] IEEE Std. 519, 1992: "Recommended Practices and Requirements for Harmonic Control in Electric Power Systems".

[9] Kueck, J. et al.: "Assessment of Methods for Estimating Motor Efficiency and Load Under Field Conditions", Prepared by Oak Ridge National Laboratory, Managed by Lockheed Martin Energy Research Corp., for U.S. Dep. of Energy, Contract DE-AC05-96OR22464, January 1996.

[10] Hsu, J. et al.: "Comparison of Induction Motor Field Efficiency Evaluation Methods", IEEE Trans. on Industry Applications, Vol. 34, No. 1, pp. 117-125, Jan./Feb. 1998.

[11] Stoft, S.: "The Economics of Conserved-Energy "Supply" Curves", University of California Energy Institute, Workable Energy Regulation (POWER), April 1995.

[12] IEC 61800-2, 1998: "Adjustable speed electrical power drive systems – Part 2: General requirements – Rating specifications for low voltage adjustable frequency a.c. power drive systems".

[13] Chapman, S.: "Electric Machinery Fundamentals", 4th Edition, McGraw-Hill, New York, 2004.

[14] Nadel, S.; Shepard, M.; Greenberg, S.; Katz, G.; de Almeida, A.: "Energy-Efficient Motor Systems – A Handbook on Technology, Program, and Policy Opportunities", American Council for an Energy-Efficient Technology, Washington D.C., 2nd Ed., 2002.

[15] Chalmers, B.; Williamson, A.: "A.C. Machines – Electromagnetics and Design", John Wiley & Sons Inc., New York, 1991.

[16] Guru, B.; Hizirolu, H.: "Electric Machinery and Transformers", 3rd Edition, Oxford University Press, New York, 2000.

[17] Alger, P.: "Induction Machines – Their Behavior and Uses", Gordon and Breach Publishers, 3rd Edition, New York, 1995.

[18] Hughes, A.: "Electric Motors and Drives", 2nd Edition, Newnes, Oxford, 1993.

[19] Leonhard, W.: "Control of Electric Drives", 2nd Completely Revised and Enlarged Edition, Springer-Verlag, Berlin, 1997.

[20] de Almeida, A.; Bertoldi, P.; Leonhard, W.: "Energy Efficiency Improvements in Electric Motors and Drives", Springer-Verlag, Berlin, 1997.

[21] Beaty, H.; J. Kirtley: "Electric Motor Handbook", McGraw-Hill, New York, 1998.

[22] de Almeida, A.; Bertoldi, P.; Falkner, H.: "Energy Efficiency Improvements in Electric Motors and Drives", Springer-Verlag, Berlin, 2000.

[23] Fitzgerald, A.; Kingsley, C.; Umans, S.: "Electric Machinery", 6th Edition, McGraw-Hill Higher Education, New York, 2003.

[24] Sen, P.: "Principles of Electric Machines and Power Electronics", 2nd Edition, New York, John Wiley & Sons, 1997.

[25] Slemon, G.: "Electric Machines and Drives", Addison-Wesley Publishing Company, 1992.

[26] Chatelain, J.: "Machines Électriques", Tome I & II, Presses Polytech. Romandes, Dunod, 1983.

[27] Hindmarsh, J.: "Electrical Machines and their Applications", Butterworth-Heinemann; 4th Edition, 1995.

[28] Dubey, G.: "Fundamental of Electrical Drives", 2nd Edition, Alpha Science, New York, 2008.

[29] de Almeida, A.; Ferreira, F.; Fong, J.; Fonseca, P.: "EuP Lot 11 Motors, Ecodesign Assessment of Energy Using Products - Final Report for the European Commission", Institute of Systems and Robotics, University of Coimbra, February 2008.

[30] Bose, B.: "Modern Power Electronics and AC Drives", Prentice Hall PTR, New Jersey, 2005.

[31] Trevisiol, L.; Rossi, T.: "Permanent Magnet Synchronous Motor for Pump Application", Inter. Conf. on Energy Efficiency in Motor Systems (EEMODS'07), Conf. Proc., Beijing, China, June 2007.

[32] Boglietti, A.; Pastorelli, M.: "Energetic Comparison between Induction Motors and Synchronous Motors", Inter. Conf. on Energy Efficiency in Motor Systems (EEMODS'07), Conf. Proc., Vol. II, pp. 475-482, Beijing, China, June 2007.

- [33] Bartos, F.: "Forward to the Past' with SR Technology", Control Engineering Inter., Nov./Dec. 1999.
- [34] Kothals-Altes, W.: "Motor winding", US Patent 1,267,232, issued May 21, 1918.
- [35] Taylor, Noel R.; Taylor, Paul A.: "Automatic load seeking control for a motor", US Patent 4,691,155 issued Sep.1, 1987.
- [36] Fogarty, J.: "Combined delta-wye armature winding for synchronous generators and method", US Patent 6,704,993, issued Mar. 16, 2004.
- [37] Hughes, A.: "New 3-phase winding of low mmf harmonic content", Proc. of IEE, Vol.117, No. 8, pp.1657-1666, Aug. 1970.
- [38] Chen, Y.; Chen, Z.: "Investigation of a new AC electrical machine winding", IEE Proc.-Electr. Power Appl., Vol. 145, No. 2, pp.125-132, March 1998.
- [39] Gjota, R.: "Winding arrangement of a stator and/or rotor of a three phase generator or electromotor with improved performances", US Patent 4,710,661, issued Dec. 1, 1987.
- [40] Cidambaram, P.; Subbiah, M.; Krishnamurthy, M.R.: "Generalized theory for the performance of three phase induction motor with star-delta winding", Electric Machines and Power Systems, 12, pp. 383-396, 1987.
- [41] Klingshirn, E.: "High phase order induction motors. Part I-Description and theoretical considerations", IEEE Trans. on PAS, Vol PAS-102, No.1, pp. 47-53, Jan. 1981.
- [42] Sarbu, M; Cistelescan, M.; Wang, S., Demeter, E.: "Part-winding starting of the three-phase squirrel cage induction motor: air gap magnetic field analysis", 11th Inter. Symposium on Electromagnetic Fields in Electrical Engineering (ISEF'03), Maribor, Slovenia, Sept. 18-20, pp.143-148, 2003.
- [43] Ferreira, F.; de Almeida, A.: "Novel Multi-Flux Level, Three-Phase, Squirrel-Cage Induction Motor for Efficiency and Power Factor Maximization", IEEE Trans. on Energy Conversion, Vol. 23, No. 1, pp. 101-109, March 2008.
- [44] Finley, W.; Hodowanec, M.; Holter, W.: "An analytical approach to solving motor vibration problems", IEEE Trans. on Industry Applications, Vol. 36, No. 5, pp. 1467-1480, 2000.
- [45] Benbouzid, M.: "A review of induction motors signature analysis as a medium for faults detection", IEEE Trans. on Industrial Electronics, Vol. 47, No. 5, pp. 984-993, Oct. 2000.
- [46] Cusido, J., et al.: "New fault detection techniques for induction motors", Electrical Power Quality and Utilisation, Magazine, Vol. II, No. 1, pp. 39-46, 2006.
- [47] Thomson, W.; Fenger, M.: "Current signature analysis to detect induction motor faults", IEEE Trans. on Industry Applications, Vol. 7, pp. 26-34, 2001.
- [48] National Instruments: "LabVIEW User Manual", April 2003.
- [49] Gani, A.; Salami, M.: "A LabVIEW based data acquisition system for vibration Monitoring and analysis", Student Conf. on Research and Development, Conf. Proc., Malaysia, pp. 62-65, 2002.
- [50] Nehrbass, J., et al.: "Interfacing PC-based MATLAB Directly to HPC Resources", HPCMP Users Group Conf. (HPCMP-UGC'06), 2006.
- [51] Attia, J.: "Teaching Electronics with MATLAB", FIE '96, Conf. Proc., 1996.
- [52] Demuth, H.; Beale, M.; Hagan, M.: "Neural Network Toolbox 5 User's Guide for MATLAB", Mathworks, 2006.
- [53] Nejari, H.; Benbouzid, M., "Monitoring and diagnosis of induction motors electrical faults using a current Park's vector pattern learning approach", Electric Machines and Drives Inter. Conf. (IEMD'99), 9-12 May 1999, pp. 275 - 277, 1999.
- [54] Chow, M.; Sharpe, R.; Hung, J.: "On the application and design of artificial neural networks for motor fault detection", IEEE Trans. on Ind. Electronics, Vol. 40, No. 2, pp. 181-188, April 1993.
- [55] Alguindigue, I.; Loskiewicz-Buczak, A.; Uhrig, R.: "Monitoring and diagnosis of rolling element bearings using artificial neural networks", IEEE Trans. on Ind. Electronics, Vol. 40, Issue 2, pp. 209-217, April 1993.
- [56] "Motor Energy Controller", Power Electronics Systems Ltd., www.pe-sys.com, 2007.
- [57] Bose, B.: "Power Electronics and Motor Drives – Advances and Trends", Elsevier, Academic Press, New York, 2006.
- [58] Barros, J.; Fiego, R.: "On the Use of the Hanning Window for Harmonic Analysis in the Standard Framework", IEEE Trans. on Power Delivery, Vol. 21, No. 1, pp. 538-539, January 2006.
- [59] Mohan, N.; Undeland, T.; Robbins, W.: "Power Electronics - Converters, Applications, and Design", 2nd Ed., John Wiley & Sons, Inc., New York, 1998.
- [60] Trovão, J.; Ferreira, F.: "Distorção Harmônica no Sector Industrial - Causas, Efeitos e Soluções", Revista Manutenção, N.º 88, 2006.
- [61] Mohan, N.: "Power Electronics, Circuits, Devices, and Applications", New Jersey, Prentice-Hall, Inc., 1996.
- [62] "A Gremlin Called Harmonic Distortion", Vector, pp. 25, Nov./Dec. 2003.
- [63] Dugan, R.; McGranaghan, M.; Wayne, H.: "Electrical Power Systems Quality", McGraw-Hill, New York, USA, 1999.
- [64] Deflandre T.; Murras, P.: "Les Harmoniques sur les Reseaux Electriques", Eyrolles, Paris, France, 1998.
- [65] SEW-Eurodrive: "Movidrive MDX60B/61B Drive Inverters – System Manual", Edition 06/2005, 11323728/EN.
- [66] Jouanne, A.; Zhang, H.; Wallace, A.: "An Evaluation of Mitigation Techniques for Bearing Currents, EMI and Overvoltages in ASD Applications", IEEE Trans. on Industry Applications, Vol. 34, No. 5, Sept./Oct. 1998, pp. 1113-1122.
- [67] Jezernik, K.: "VSS Control of Unity Power Factor", IEEE Trans. on Industrial Electronics, Vol. 46, No. 2, pp. 325-332, April 1999.
- [68] IEC Std. 61000-4-7, 2002: "Electromagnetic Compatibility (EMC) – Part 4-7: Testing and Measurement Techniques – General Guide on Harmonics and Interharmonics Measurement and Instrumentation, for Power Supply Systems and Equipment Connected Thereto".
- [69] Almeida, A., et al.: "VSDs for Electric Motor Systems", Prepared for the European Comm., DG TREN, SAVE II Programme, 2001.
- [70] IEC 61800-3, 1998: "Adjustable Speed Electrical Power Drive Systems - Part 3: EMC requirements and specific test methods".
- [71] SEW-Eurodrive: "EMC in Drive Engineering", Edition 08/2002, Drive Engineering - Practical Implementation 10530 41X/EN.
- [72] Carlson, R.: "The Correct Method of Calculating Energy Savings to Justify Adjustable-Frequency Drives on Pumps", IEEE Trans. on Ind. Applic., Vol. 36, No. 6, pp.1725-1733, Nov./Dec. 2000.
- [73] Maxwell, J.: "How to Avoid Overestimating Variable Speed Drive Savings", Industrial Energy Technology Conference (IETC), <http://txspace.tamu.edu/handle/1969.1/5621>, 2005.
- [74] Rooks, J.; Wallace, A.: "Energy Efficiency of VSDs", IEEE Industry Applications Magazine, May/June 2004, pp. 57-61.
- [75] Almeida, A.; Ferreira, F.; Both, D.: "Technical and Economical Considerations to Improve the Penetration of Variable Speed Drives for Electric Motor Systems", IEEE Trans. on Industry Applications, Vol. 41, No. 1, pp. 188-199, Jan./Feb. 2005.
- [76] Ziehl-Abegg: "Speed Control of Fans for Refrigeration and Air Conditioning – A Comparison of Different Systems for Speed Control", Motor Challenge, 2007.
- [77] "E-Cube", Greenchoice Ltd., www.greenchoiceltd.com, 2008.
- [78] "Cycloidal Speed Reducers", Vector, Drives & Switchgear, Sept. 2003, pp. 32.
- [79] www.durali.com, Dec. 2007.
- [80] www.michelin.com, Dec. 2007.
- [81] Doppelbauer, M.: "Energy Efficient Electric Drives", VEM Meeting, 2007.
- [82] Fassbinder, S.: "Saving Energy with High-Efficiency Motors", Briefing paper, Leonardo Energy, Sept. 2007, available on-line: www.leonardo-energy.org.
- [83] de Almeida, A.; Greenberg, S.: "Technology assessment: energy-efficient belt transmissions", Energy and Buildings, No. 22, pp. 245-253, Elsevier Science, 1995.
- [84] Ferreira, F.; Sá, C.: "Considerações sobre a Seleção de Motores de Indução Trifásicos para Accionamentos de Velocidade Variável", Revista Kéramica N.º 277, Março/Abril 2006;
- [85] Ferreira, F.; de Almeida, A.: "Method for In-Field Evaluation of the Stator Winding Connection of Three-Phase Induction Motors to Maximize Efficiency and Power Factor", IEEE Trans. on Energy Conversion, Vol. 21, No. 2, pp. 370-379, June 2006.
- [86] Ferreira, F.: "Técnicas Avançadas de Manutenção Curativa e Reabilitação de Motores de Indução Trifásicos de Baixa Tensão/ Curative Maintenance and Rehabilitation Advanced Methods for Low-Voltage, Three-Phase, Induction Motors", Tese de Mestrado/Master Science Thesis (available in Portuguese only), Universidade de Coimbra/University of Coimbra, 2002.
- [87] Haring, T.: "Design of Motors for Inverter Operation", in "Energy Efficiency Improvements in Electric Motors and Drives", Springer-Verlag, Berlin, Heidelberg, 2000.
- [88] ABB Motors: "Basic Motor Technology", Finland, 1996.
- [89] Swardt, H.: "Hazardous areas – "E" Motors with VSDs", Drives & Switchgear, Vector, Nov/Dec 2003, pp. 23-24.
- [90] Palma, J.: "Accionamentos Electromecânicos de Velocidade Variável", Fundação Calouste Gulbenkian, Lisboa, 1999.

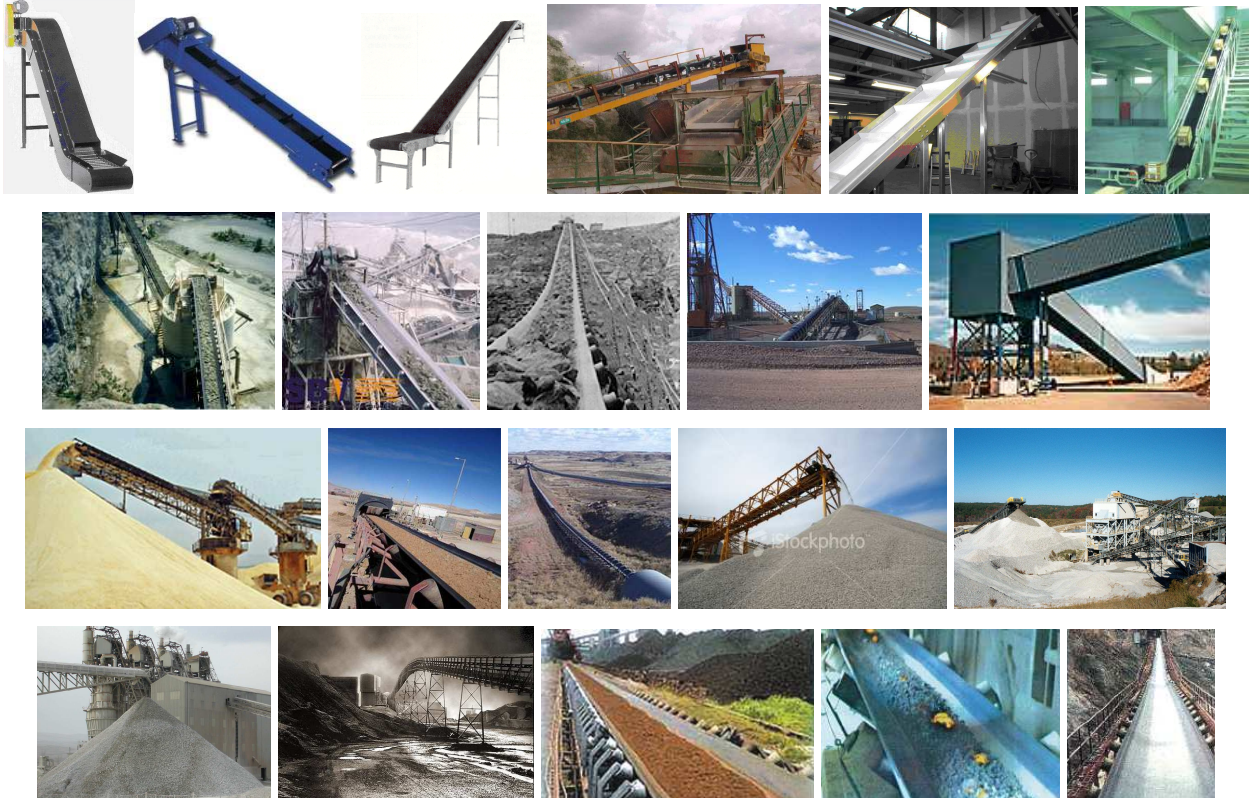
- [91] Dems, M.; Komez, K.; Wiak, S.; Stec, T.; Kikosicki, M.: "Application of circuit and field-circuit methods in designing process of small induction motors with stator cores made from amorphous iron", The Inter. Journal for Computation and Mathematics in Electrical and Electronic Eng., Emerald Group Publishing Limited, Vol. 25, No. 2, pp. 283-296, 2006.
- [92] EFACEC: "Catálogo de Motores de Indução com Rotor em Curto-Circuito", 2001.
- [93] VEM Catalogue: "Three-Phase High-Voltage Asynchronous Motor – 140-8000 kW", 2007.
- [94] Kostić, M.; Janda, Ž.; Radaković, J.; Miskolci, L.: "Induction Motors with YY/ Δ Connection Change for Efficiency and Power Factor Increasing at Loads up to 75-85%", XVI Inter. Conf. on Electrical Machines (ICEM'04), Conf. Proc., 2004.
- [95] EN 50160, 2000: "Voltage characteristics of public distribution systems".
- [96] NEMA MG 1 Standard, 1998: "Motors and Generators".
- [97] Kiurihara, K.; Rahman, M.: "High-efficiency line-start interior permanent magnet synchronous motors", IEEE Trans. Ind. Appl., Vol. 40, May/June 2004, pp. 789-796.
- [98] Yang, B., et al.: "Comparison of dynamic characteristics of the line start permanent magnet motor and the induction motor", KIEE Int. Trans. EMECS, Vol. 2-B, pp. 90-94, 2002.
- [99] Miller, T.: "Synchronization of line-start permanent-magnet ac motors", IEEE Trans. Power Appar. Sys., Vol. PAS-103, pp. 1822-1828, July 1984.
- [100] Rahman, M.; Little, T.: "Dynamic performance analysis of permanent magnet synchronous motor", IEEE Trans. Power Appar. Sys., Vol. PAS-103, pp. 1277-1282, June 1984.
- [101] Reinert, J.; Karlsson, P.: "Improving performance and energy consumption of industrial processes by using variable speed drives", Emotron – Dedicated Drive, European Center for Power Electronics e.V. (ECPE) Seminar, "Towards Energy Gain and Savings – Emerging Drives and Generator Systems", 15-16 April 2008, Warsaw, Poland.
- [102] Waide, P.: "The Global Energy Consumption of Electric Motor Systems – Challenges and Opportunities", Inter. Conf. on Energy Efficiency in Motor Systems (EEMODS'07), Plenary Session, Presentation Slides, Beijing, China, June 2007.
- [103] "Saving Energy with Electrical Drives", German Electrical and Electronic Manufacturers' Association, Division Automation/Electric Drive Systems (ZVEI-Automation), Frankfurt, April 2006.
- [104] Fuchsloch, J.; Noltman, J.; Peters, D.; Brush, E.; Cowie, J.: "Systematic Design Approach for a New Series of Ultra-NEMA Premium Copper Rotor Motors", Inter. Conf. on Energy Efficiency in Motor Systems (EEMODS'07), Conf. Proc., Beijing, China, June 2007.
- [105] Williamson, S.; Smith, S.; Barnes, M.; Apsley, J.: "Efficiency Gains in Multi-Phase Induction Motor Drives", 5th Inter. Conf. on Energy Efficiency in Motor Driven Systems (EEMODS'07), Conf. Proc., Beijing, 2007.
- [106] SEW-Eurodrive, Mealhada, Portugal, *Experts opinion, technical & economical data, and presentation slides*, 2008.
- [107] Bertolazzi, G., Wellington Italia Srl., *Expert opinion*, 2008.
- [108] Boglietti, A.; Ferraris, P.; Profumo, F.: "Effects of Different Modulation Index on the Iron Losses in Soft Magnetic Materials Supplied by PWM Inverter", IEEE Trans. on Magnetics, Vol. 29, No. 6, pp. 3234-3236, Nov. 1993.
- [109] Busse, D. et al.: "Bearing Currents and Their Relationship to PWM Drives", IEEE Trans. on Power Electr., Vol. 12, No. 2, pp. 243-252, March 1997.
- [110] Busse, D.; Erdman, J.; Kerkman, R.; Schlegel, D.; Skibinski, G.: "Characteristics of Shaft Voltage and Bearing Currents", IEEE Industry Applications Magazine, Vol. 3, No. 6, pp. 21-32, Nov./Dec. 1997.
- [111] Lipo, T.; Chen, S.: "Circulating Type Motor Bearing Current in Inverter Drives", IEEE Industry Applic. Magazine, Vol. 4, No. 1, pp. 32-38, Jan./Feb., 1998.
- [112] Ferreira, F.; Pereirinha, P.; de Almeida, A.: "Study on the Bearing Currents Activity in Cage Induction Motors using Finite-Element Method", XVII Inter. Conf. on Electric Machinery (ICEM2006), Conf. Proc., Sept. 2006.
- [113] Santos, F.; Trovão, J.; Ferreira, F.; Coelho, D.: "Three-Phase Induction Motor Condition Evaluation by means of Combined Current and Vibration analysis Using Artificial Neural Networks", 2nd Inter. Conf. on Electrical Engineering (CEE'07), Conf. Proc., Oct. 2007.
- [114] Anderson, R.; Neri, L.: "Reliability-Centered Maintenance: Management and Engineering Methods", Elsevier Applied Science, London, 1990.
- [115] Smith, D.: "Reliability and Maintainability in Perspective", 2nd Edition, John Wiley & Sons, New York, 1985.
- [116] Yu, L.: "Fault Tree Analysis and Reliability Assessment of Auxiliary Power Supply system for an HVDC Plant", Master Thesis, written at KTH, the Royal Institute of Technology, School of Electrical Engineering, 2007.
- [117] Benecki, W.: "Magnetics Industry Overview: 2004 China Magnet Symposium Highlights Recent Industry Trends", Technical Report, 2004. Available on-line: <http://www.walbenecki.com>.
- [118] Witt, M., WiH & Sohn AG, Fachvortrag VEM Fachtagung, Juni 2003.
- [119] Karlsson, P.: "Small-Signal Modelling and Analysis of DC Distributed Power Systems", EPE Journal, No. 2, pp. 49-58, Jun. 2007.
- [120] Dugan, R.; McGranaghan, M.; Beaty, H.: "Electric Power Systems Quality", McGraw-Hill, 1996.
- [121] IEC 60034-1, Ed. 11, 2004: "Rotating electrical machines - Part 1: Rating and performance".
- [122] "Optimizing your motor-driven system", Motor Challenge, Fact Sheet, www.motor.doe.gov.
- [123] Pillay, P.; Hofmann, P.; Manyage, M.: "Derating of Induction Motors Operating With a Combination of Unbalanced Voltages and Over or Undervoltages", IEEE Trans. on Energy Conversion, Vol. 17, No. 4, pp. 481-491, Dec. 2002.
- [124] Wiendebrug, E.; Ramme, A.; Mehteson, E.; Jouanne, A.; Wallace, A.: "Modern on-line testing of Induction Motors for Predictive Maintenance and Monitoring", IEEE Pulp and Paper Industry Technical Conf., Conf. Record, pp. 163-168, 18-22 June 2001.
- [125] Ferreira, F.; Trovão, J.; de Almeida, A.: "Motor Bearings and Insulation System Condition Diagnosis by Means of Common-Mode Currents and Shaft-Ground Voltage Correlation", 18th Inter. Conf. on Electrical Machines (ICEM'08), Conf. Proc., Vilamoura, Portugal, Sept. 2008.
- [126] Ferreira, F.; Cistelean, M.; Baoming, G.: "Simple Strategy to Recovery Energy During Stopping Period in Large High-Inertia Line-Fed Induction Motor Driven Systems", 18th Inter. Conf. on Electrical Machines (ICEM'08), Conf. Proc., Vilamoura, Portugal, Sept. 2008.
- [127] Jackson, D.: "Low Voltage Insulation System Endurance Against Electronic Waveform and Cable Length", IEE Colloquium on Effects of High Speed Switching on Motors and Drives, Ref. No. 1999/144, pp. 6/1-6/7, June 1999.
- [128] Cistelean, M.; Ferreira, F.; Cosan, B.: "Generalized MMF Space Harmonics and Performance Analysis of Combined Multiple-Step, Star-Delta, Three-Phase Windings Applied on Induction Motors", 18th Inter. Conf. on Electrical Machines (ICEM'08), Conf. Proc., Vilamoura, Portugal, Sept. 2008.

Appendix 7 – Extra Pictures on Motor Applications

A7.1 Examples of Horizontal Belt Conveyors (or Conveyor Belts)



A7.2 Examples of Inclined Belt Conveyors



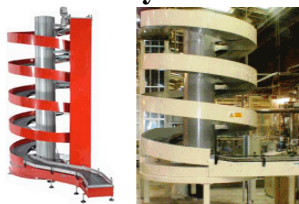
A7.3 Examples of Horizontal Chain Conveyors



A7.4 Examples of Roller Conveyors



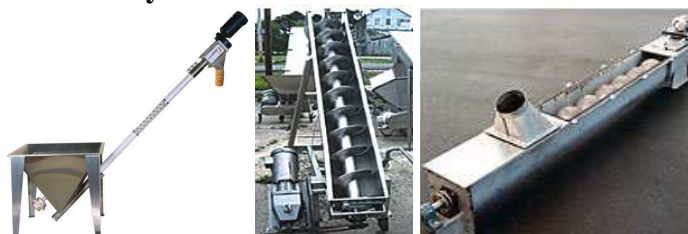
A7.5 Examples of Vertical, Spiral Belt Conveyors



A7.6 Examples of Vertical (Elevators) and Horizontal Chain/Bucket Conveyors



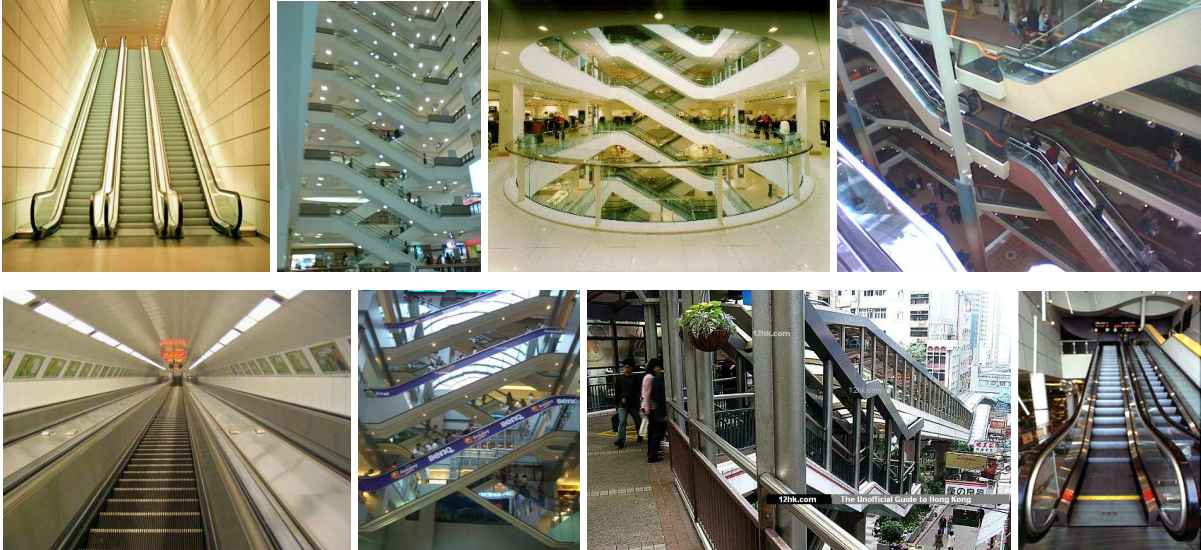
A7.7 Examples of Screw Conveyors



A7.8 Examples of Aero-Mechanical or Disc Conveyors



A7.9 Examples of Straight Escalators



A7.10 Example of a Spiral Escalator



A7.11 Examples of Lifts



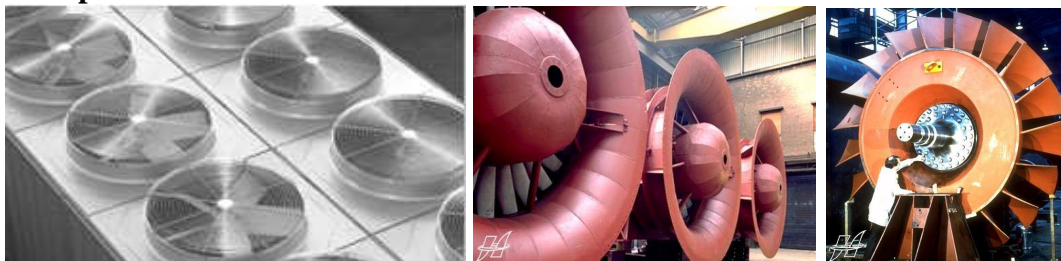
A7.12 Example of a Large Crane



A7.13 Examples of Centrifugal Fans



A7.14 Examples of Axial Fans



(Left) Chiller fans; (Middle) Mine fans; (Right) 600-MW power station fan.

A7.15 Examples of Industrial Centrifugal Pumps



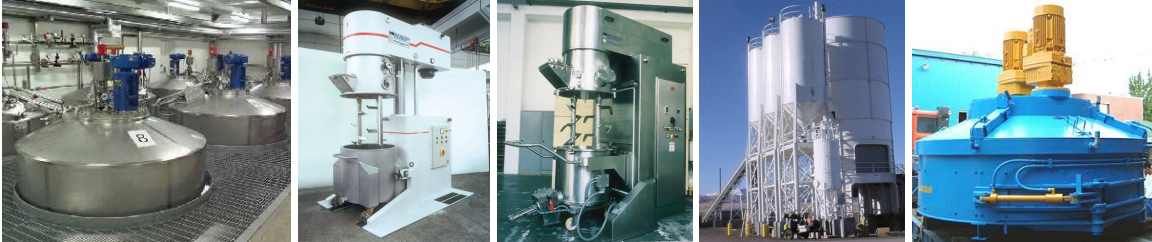
A7.16 Examples of Piston Reciprocating Compressors



A7.17 Examples of Rotary Screw Compressors



A7.18 Examples of Vertical Industrial Mixers



A7.19 Examples of Horizontal and Inclined Industrial Mixers



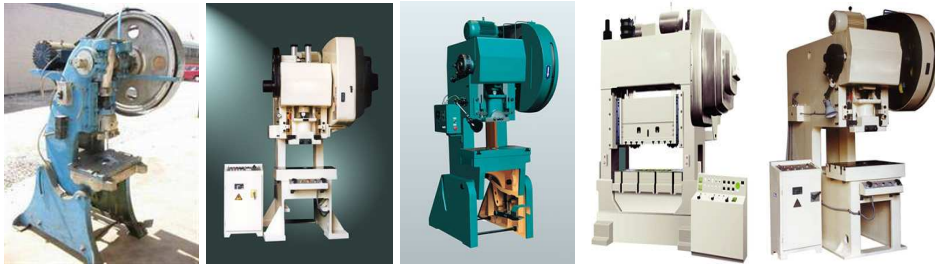
A7.20 Examples of Sheet Saws



A7.21 Examples of Rotary Saws



A7.22 Examples of High-Inertia Wheel Presses



A7.23 Examples of Vertical Centrifuges



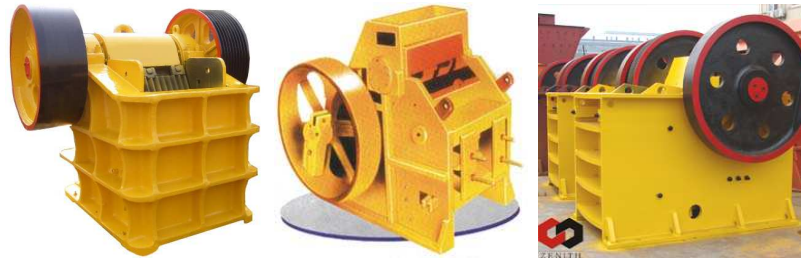
A7.24 Examples of Horizontal Centrifuges



A7.25 Example of a High-Precision Industrial Lathe



A7.26 Examples of Rock Crushers



A7.27 Examples of Industrial Beater Mills



A7.28 Example of a Rolling Mill



A7.29 Examples of Bucket-Wheel Excavators



A7.30 Examples of Pumpjacks



A7.31 Examples of Medium-Size Walk-In Freezers



A7.32 Examples of Large Roof-Top Chillers



A7.33 Example of a HVAC Unit in a Commercial Building

